FEB - FRESENIUS ENVIRONMENTAL BULLETIN
Founded jointly by F. Korte and F. Coulston
Production by PSP - Vimy Str. 1e, 85354 Freising, Germany in
cooperation with PRT-Parlar Research & Technology
Vimy Str 1e, 85354 Freising
Copyright© by PSP and PRT, Vimy Str. 1e, 85354 Freising, Germany
All rights are reserved, especially the right to translate into foreign language or other processes - or convert to a machine language, especially for data processing equipment - without written permission of the publisher. The rights of reproduction by lecture, radio and television transmission, magnetic sound recording or similar means are also reserved.
Printed in Germany-ISSN 1018-4619

FEB-EDITORIAL BOARD

CHIEF EDITOR:
Prof. Dr. Dr. H. Parlar
Parlar Research & Technology-PRT
Vimy Str.1e
85354 Freising, Germany

MANAGING EDITOR:
Dr. P. Parlar
Parlar Research & Technology
PRT, Vimy Str.1e
85354 Freising, Germany

CO-EDITORS:

Environmental Spectroscopy
Prof. Dr. A. Piccolo
Universita di Napoli "Frederico II"
Dipto. Di Scienze Chemica Agrarie
Via Universita 100, 80055 Portici, Italy

Environmental Biology
Prof. Dr. G. Schuurmann
UFZ-Umweltzentrum
Sektion Chemische Ökotoxikologie
Leipzig-Halle GmbH,
Permoserstr.15, 04318
04318 Leipzig, Germany
Prof. Dr. I. Holoubek
Recetox-Tocoen
Kamenice126/3, 62500 Brno, Czech Republic
Prof. Dr. M. Hakki Alma
Kahramanmaras Sutcu Imam University
Avsar Kampusu, 46100 Kahramanmaras, Turkey

Environmental Analytical Chemistry
Prof. Dr. M. Bahadir
Lehrstuhl für Ökologische Chemie
und Umweltanalytik
TU Braunschweig
Lehrstuhl für Ökologische Chemie
Hagenring 30, 38106 Braunschweig, Germany
Dr. D. Kotzias
Via Germania29
21027 Barza(Va), Italy

Environmental Management
Dr. K. I. Nikolaou
Env.Protection of Thessaloniki
OMPEPT-54636 Thessaloniki
Greece

Environmental Toxicology
Prof. Dr. H. Greim
Senatkommision – DFG / TUM
85350 Freising, Germany

Environmental Proteomic
Dr. A. Fanous
Halal Control GmbH
Kobaltstr. 2-4
D-65428 Rüsselsheim, Germany

Environmental Education
Prof. Dr. C. Bayat
Esenyurt Üniversitesi
34510 Esenyurt, Istanbul, Turkey

Advisory Board
K. Bester, K. Fischer, R. Kallenborn
DCG. Muir, R. Niessner,W.Vetter,
A. Reichlmayr-Lais, D. Steinberg,
J. P. Lay, J. Burhenne, L. O. Ruzo

Marketing Manager
Cansu Ekici, B. of B.A.
PRT-Research and Technology
Vimy Str 1e
85354 Freising, Germany
E-Mail: parlar@wzw.tum.de
parlar@prt-parlar.de
Phone: +49/8161887988

Fresenius Environmental Bulletin is abstracted/indexed in:
Biology & Environmental Sciences, BIOSIS, CAB International, Cambridge Scientific abstracts, Chemical Abstracts, Current Awareness, Current Contents/Agriculture, CSA Civil Engineering Abstracts, CSA Mechanical & Transportation Engineering, IBIDS database, Information Ventures, NISC, Research Alert, Science Citation Index (SCI), Scisearch, Selected Water Resources Abstracts

CONTENTS

ORIGINAL PAPERS

HIGH-SPEED RAILWAY EMBANKMENTS STABILIZATION BY USING A PLANT BASED BIOPOLYMER 7626
Huseyin Suha Aksoy, Mesut Gor

ARSENIC REMOVAL FROM AQUEOUS SOLUTIONS USING IRON OXIDE COATED SEPIOLITE 7634
Sedef Arikan, Deniz Dolgen, M Necdet Alpaslan

HEALTH RISK ASSESSMENT OF TOXIC HEAVY METALS IN WHEAT CROP GROWN UNDER DOMESTIC WASTEWATER IRRIGATION 7643
Kafeel Ahmad, Zafar Iqbal Khan, Robina Kaukab, Kinza Wajid, Naunain Mehmood,Hira Muqaddas, Tassawur Abbas, Muhammad Fahad Ullah, Mohamed Soliman Elshikh, Abdulaziz Al Sahli, Mohamed El-Zaidy, Ijaz Rasool Noorka, Shahzadi Mahpara, Hazoor Ahmad Shad, Muhammad Ayub

UNNOTICED MICROORGANISMS IN DISINFECTION OF SWIMMING POOLS: FREE- LIVING AMOEBA 7651
Zuhal Zeybek, Busra Demir, Miray Ustunturk Onan

SENSITIVITY OF BETA-GLUCOSIDASE TO SOIL CONTAMINATION WITH ZINC, COPPER, NICKEL, CADMIUM AND LEAD 7658
Karol Wieczorek, Jan Kucharski, Jadwiga Wyszkowska

BIOCHAR-MOREL PROMOTES WHEAT SALINE RESISTANCE BY INCREASING ROOT/SHOOT RATIO 7667
Zhongdong Yu, Phonepaserd Phanpadith, Shuai Zhang, Dan Yu, Minglei Li, Yongxiang Kang

ENVIRONMENTAL EFFECTS OF T-SHAPED GROINS BUILT ON THE EASTERN BLACK SEA COAST ON SHORE PROTECTION 7674
Veli Sume

MULTIPLE TIME-SCALE PROPERTIES OF AIR POLLUTION INDICES: A CASE STUDY OF LANZHOU, CHINA 7681
Zuhan Liu, Linan Sun, Jiayao Wang, Lili Wang, Kai Shi, Chunqiong Liu

SPATIAL VARIABILITY IN SOIL FERTILITY RELATED TO THE "FERTILE ISLANDS" EFFECT OF VITEX NEGUNDO 7687
He Zhao, Yong Zhao*, ZhiMing Zhang, Guo Dong, XiaoKe Yuan

THE RELATIONSHIP OF VERTICILLIUM WILT AND SEED SURFACE MICROFLORA WITH GOSSYPOL LEVEL IN COTTON (GOSSYPIUM SPP.) 7695
Oktay Erdogan, Hulya Ozgonen-Ozkaya, M Erhan Gore

VISUAL QUALITY ASSESSMENT OF TOWNSCAPES: A STUDY FOR NIKSAR TOWN (TOKAT) OF TURKEY 7703
Pervin Yesil

IN VITRO PROPAGATION OF SEA DAFFODIL (*PANCRATIUM MARITIMUM* L.) USING SEEDLING EXPLANTS 7710
Ugur Sirin, Elif Kanmaz

EVALUATION OF DROPLET SIZE SPECTRA FOR AGRICULTURAL PESTICIDE APPLICATIONS USING WATER SENSITIVE PAPER AND IMAGE ANALYSIS TECHNIQUES 7717
Abdullah Beyaz, Metin Dagtekin, Ibrahim Cilingir, Dilara Gerdan

Fe-BASED IONIC LIQUIDS SYNTHESIZED BY ULTRASONIC HEATING CIRCUMFLUENCE: CHARACTERIZATION AND DESULFURIZATION 7724
Dan-ni Yang, Jia-xiu Guo, Fa-ming Liao, Hua-qiang Yin, De-ming Luo

ENHANCED DEGRADATION EFFICIENCY OF THREE DIMENSIONAL GRAPHENE-TiO2 HYDROGEL BASED ON COMMERCIAL TITANIUM(IV) OXIDE 7734
Xiangfei Wei, Mingliang Chen

BIOSORPTION AND SEPARATION/PRECONCENTRATION OF LEAD AND NICKEL ON RHODOCOCCUS RUBER BIOMASS 7740
Esin Kiray, Cigdem Er, Ergin Kariptas, Harun Ciftci

COMPARISON OF THE PHYSICOCHEMICAL PROPERTIES OF CHITOSAN EXTRACTED FROM SHRIMP SHELL WASTE WITH DIFFERENT DEACETYLATION DEGREES 7750
Aygul Kucukgulmez, A Eslem Kadak, Ladine Celik, Afsin Farivar, Mehmet Celik

DYES WASTEWATER TREATMENT VIA ELECTROCHEMICAL OXIDATION 7756
Qiong Li, Yanbo Wang

REMOTE SENSING AND GIS BASED VIEWSHED ANALYSIS FOR WATER VISIBILITY FROM SETTLEMENTS OF A MEDITERRANEAN CITY 7760
Mehmet Akif Erdogan

THE INFLUENCE OF VS/TS RATIO OF A-SLUDGE ON ANAEROBIC CO-DIGESTION OF KITCHEN WASTE WITH A-SLUDGE 7769
Renjun Ruan, Jiashun Cao, Fang Fang, Chao Li, Lei Qi, Changshuang Zhao

ASSESSMENT OF SALT TOLERANCE ACCESSIONS OF SESBANIA SESBAN (L.) MERRIL USING SOME MORPHOLOGICAL AND BIOCHEMICAL PARAMETERS 7780
Mohamed Tarroum, Fahad Al-Qurainy, Salim Khan, Mohammad Nadeem, Aref Alshameri, Abdel-Rhman Z Gaafar, Saleh Alansi

EVALUATION OF FACTORS RELATED TO WELL-BEING EFFECTS OF URBAN GREEN SPACES ON USERS 7789
Serap Yilmaz, Tugba Duzenli, Deryanur Dincer

CYANOBACTERIA BLOOM MITIGATION USING CALCIUM HYDROXIDE AND AN ILLITE COMPOSITE ALGICIDE 7801
Hongqiang Wang, Anna Zhang, Lieyu Zhang

LEVELS OF HEAVY METALS IN TWO FISH SPECIES IAGO OMANENSIS AND AUXIS THAZAR FROM THE GULF OF AQABA, RED SEA 7806
Tariq Al-Najjar, Mwaffaq Al Khushman, Maroof Khalaf, Mohammad Wahsha, Khalid Abu Khadra

A MODIFIED GIS-BASED WATER-SEDIMENT-ADSORBED PHOSPHORUS COUPLING MODEL AND ITS APPLICATION IN A TYPICAL WATERSHED OF SEMIARID REGIONS 7815
Lei Wu, Shanshan Qiao, Xia Liu

FILTRATION RATE, OXYGEN CONSUMPTION, PHOSPHOROUS AND NITROGENOUS EXCRETION OF MYTILUS GALLOPROVINCIALLIS AND EFFECT IN AQUEOUS ENVIRONMENT 7825
Kostas Katsoulis

GREEN SYNTHESIS OF COPPER OXIDE NANOPARTICLES USING OCIMUM BASILICUM EXTRACT AND THEIR ANTIBACTERIAL ACTIVITY 7832
Melda Altikatoglu, Azade Attar, Fatih Erci, Corina Marilena Cristache, Ibrahim Isildak

EVALUATION OF HEAVY METALS UPTAKE BY WHEAT GROWING IN SEWAGE IRRIGATED SOIL: RELATIONSHIP WITH HEAVY METAL IN SOIL AND WHEAT GRAINS 7838
Zafar Iqbal Khan, Sana Iqbal, Fauzia Batool, Kafeel Ahmad, Mohamed Soliman Elshikh, Abdulaziz Al Sahli, Mohamed El-Zaidy, Humayun Bashir, Ijaz Rasool Noorka, Muhammad Sher, Ahmad Muneeb, Aima Iram Batool, Shahzadi Mahpara, Mumtaz Akhtar, Naunain Mehmood, Hazoor Ahmad Shad, Yunus Dogan, Hira Muqaddas, Muhammad Ayub

ECOSYSTEM SERVICE EVALUATION OF STREAMS FOR NUTRIENT AND BACTERIA PURIFICATION IN A GRAZED WATERSHED 7849
Theodoros Chalazas, Ourania Tzoraki, David Cooper, Maria Adamantia Efstratiou, Vasileios Bakopoulos

AN EVALUATION OF SEDIMENT YIELD EVOLUTIONS FOR DIFFERENT SUB-CATCHMENTS AND LAND USE TYPES IN THE YANHE RIVER WATERSHED, LOESS PLATEAU 7860
Lei Wu, Mengling Peng, Xia Liu

PROBABILITY WEIGHTED MOMENTS AND THEIR EFFECTS ON THE RAINFALL DEPTH–DURATION–FREQUENCY CURVES 7874
Omer Levend Asikoglu, Ertugrul Benzeden

IMPROVEMENT OF WATER USE PRODUCTIVITY THROUGH THE SRFR MODEL IN BORDER STRIP IRRIGATION OF WHEAT ACROSS HAMIDIYEH FARMS (KHUZESTAN, IRAN) 7885
Arash Tafteh, Mohammad Reza Emdad

PROTECTIVE CHARACTERISTICS OF CAFFEIC ACID PHENETHYL ESTER(CAPE) ON NEURODEGENERATIVE EFFECTS OF ORGANOPHOSPHATE INSECTICIDE IN RATS 7893
Lacine Aksoy, Omer Hazman, Ahmet Buyukben

PERFORMANCE ANALYSIS OF A BETA TYPE STIRLING ENGINE WITH REGENERATIVE DISPLACER 7900
Yasar Onder Ozgoren

PREDICTING POLLUTANT EMISSIONS OF A 300MW CFBB USING BIDIRECTIONAL LEARNING MACHINE 7906
Guo-Qiang Li, Lu Zhang, Keith C C Chan, Jun-Nan Zou, Li-Zhuang Xu

DETERMINATION OF HEAVY METAL BIOAVAILABILITY IN ATMOSPHERIC DUST COLLECTED FROM COAL MINING AREAS AND HEALTH RISK ASSESSMENT 7914
Yafen Han, Xiaoxing Wei, Qi Li, Jieyun Liu, Na Liu

LATEWOOD PROPORTION INSIDE GROWTH RINGS BY BALD CYPRESS STEMS IN SERBIA 7925
Dusan Jokanovic, Dragica Vilotic, Vesna Nikolic, Marina Nonic, Jovana Devetakovic, Dragica Stankovic

ASSESSMENT OF THE IMPACTS OF INDUSTRIAL EFFLUENT DISCHARGES ON THE EPILITHIC DIATOMS COMMUNITY AND WATER QUALITY OF SAHNAHAN STREAM, MALATYA, TURKEY 7931
Betul Celik, Vesile Yildirim

THE ASSESSMENT OF LANDSCAPE FRAGMENTATION IN AN AGRICULTURAL ENVIRONMENT: DEGRADATION OR CONTRIBUTION TO ECOSYSTEM SERVICES 7941
Derya Gulcin, K Tuluhan Yilmaz

APPROXIMATION MODEL FOR CARBON DIOXIDE INCREASING LEVEL AND IMPACT OF VENTILATION SYSTEM IN A UNIVERSITY CLASSROOM 7951
Wannawit Taemthong

ANTI-BIOFILM ACTIVITY OF BENZYL SUBSTITUTED HEXAHYDROIMIDAZO [1,5-a] PYRIDINIUM BROMIDE SALTS AGAINST SOME PATHOGENIC MICROORGANISMS 7957
Nur Ceyhan-Guvensen, Hayati Turkmen

COMPRESSIVE PROPERTIES ANALYSIS FOR CONCRETE MATERIALS UNDER ACID-FREEZING RAIN ACTION 7967
Yinlei Sun, Liansheng Tang

EFFECT OF DIFFERENT WAVELENGTHS OF LIGHT ON GROWTH, PIGMENT CONTENT AND PROTEIN AMOUNT OF *CHLORELLA VULGARIS* 7974
Gokce Kendirlioglu, A Kadri Cetin

STUDY ON OLS CORRELATION ESTIMATION OF FARMERS' ENTHUSIASM FOR GRAIN PRODUCTION AND GRAIN PRODUCTION CIRCULATION UNDER THE BACKGROUND OF URBANIZATION CONSTRUCTION IN OLS 7981
Bangxi Li, Jingdong Luan

RESPONSE OF MICROBIAL ACTIVITY TO ADDITION OF NERIUM OLEANDER L. LEAVES IN SOIL UNDER DIFFERENT MOISTURE CONDITIONS 7992
Sahin Cenkseven, Burak Kocak, Secil Berna Kuzu, Hatice Korkmaz Guvenmez, Cengiz Darici

RAINFALL-TRIGGERED LIMITED DATA-BASED ANALYSIS OF LANDSLIDES IN TRABZON PROVINCE, TURKEY 8001
Ebru Eris

THE TURKISH SURVEYING PRIVATE SECTOR 8008
Okan Yildiz, Yakup Emre Coruhlu

IN VITRO EFFECTS OF SOME PESTICIDES ON GLUTATHIONE-S TRANSFERASE ACTIVITY 8023
Mehmet Emin Diken, Serap Dogan, Mehmet Dogan, Yasemin Turhan

RESEARCH ON THE METHOD OF NEW GENERATION OF MULTI-SENSOR INFORMATION FUSION TECHNOLOGY TO PROMOTE THE DEVELOPMENT OF WISDOM AGRICULTURE IN 'INTERNET +' MODE 8030
Zhen Zhang, Xueping Xiong

THE LONG-TERM CHANGES OF MAIN SURFACE-DWELLING ARTHROPOD GROUPS WITH TIME SINCE FIRE IN *PINUS BRUTIA* FORESTS OF SOUTHWESTERN ANATOLIA 8041
Burcin Yenisey Kaynas

ASSESSMENT OF HEAVY METAL CONTAMINATION AND ACCUMULATION PATTERNS IN THE COASTAL AND DEEP SEDIMENTS OF LAKE SALDA, TURKEY 8047
Huseyin Caldirak, Bedri Kurtulus, Mustafa Can Canoglu, Evren Tunca

EFFECT OF FLOCCULANT ON THE SETTLEMENT OF IRON TAILINGS 8062
Hongzheng Zhu, Jinbo Zhu, Alejandro Lopez Valdivieso, Hainan Wang, Zhengyan Zhou

STUDY ON THE INFLUENCE OF COPPER AND NICKEL IONS ON THE HYDROLYSIS-MBR PROCESS 8069
Guangzhi Wang, Likun Huang, Zhi Xia

COMPARISON OF DAMAGE MECHANISM FOR TC4 BLADE OF STEEL BALL AND SAND SHOCK 8078
Zhu Guanfang, Zhang Zhongping, Gao Pengpeng, Li Chunwang, Kang Yifan, Liu Jing, Gao Pengpeng

RESEARCH ON THE REVERSE LOGISTICS MANAGEMENT OF MEDICAL WASTE BASED ON THE RFID TECHNOLOGY 8084
Hao Liu, Zhong Yao

PUBLIC PERCEPTION OF ENVIRONMENTAL RISK IN TURKEY 8093
Ayla Bilgin, Selim Latif Sanin

STUDY ON CONTROL MECHANISM OF LOOSE COAL WORKING FACE SURROUNDING ROCK AND APPLICATION UNDER HIGH GAS COAL SEAMS 8100
Jia-zhuo Li, An-ying Yuan, Chuan-qi Zhu

GHOST FISHING EFFECTS OF LOST BOTTOM TRAMMEL NETS IN A STORM: A SIMULATION 8109
Caner Enver Ozyurt, Ferhat Buyukdeveci, Volkan Baris Kiyaga

ISOLATION AND UTILIZATION OF A TRICLOPYR DEGRADING BACTERIUM, *BACILLUS CEREUS TR*-13 8119
Jiangwei Zhu, Kun Xie, Yan Zhao

ANALYSIS OF WELLBORE STABILITY OF SHALE GAS RESERVOIR DRILLING 8125
Ni Weijun, Li Qi, Song Xiaomei

EXPERIMENTAL STUDY OF PETROCHEMICAL OILY WASTEWATER TREATMENT FOR REUSE 8131
Hai-Xiang Zhang, Yang Li, Zhan-Dong Li, Gui-tong Dong, Peng Wang, Wei Li

EVALUATION THE EFFECT OF GREEN SPACE ON AIR POLLUTION DISPERSION USING SATELLITE IMAGES AND LANDSCAPE METRICS: A CASE STUDY OF ISFAHAN CITY 8135
Zahra Bagheri, Mozhgan Ahmadi Nadoushan, Maryam Foroughi Abari

EFFICIENCY OF PHEROMONE WATER TRAPS AND LIFE CYCLE OF *TUTA ABSOLUTA* (LEPIDOPTERA: GELECHIIDAE) IN DIYARBAKIR PROVINCE, TURKEY 8146
Yunus Bayram, Mehmet Duman, Musa Buyuk, Cetin Mutlu

MODEL PREDICTIVE CONTROL OF WIND TURBINE WITH DOUBLY FED INDUCTION GENERATOR 8154
Jing Zhang,Peijia Yu, Bowen Li, Bangsong Shi

CONSUMER TRENDS FOR ORGANIC PRODUCTS: THE CASE OF THE MARMARA REGION IN TURKEY 8160
Sule Turhan, Hasan Vural, Ibrahim Ak, Burcu Erdal

EXPERIMENTAL STUDY ON THE MECHANICAL PROPERTIES OF ROCK SLOPE COLLAPSE 8166
Qian Zhang, Weigang Zhao,Yang Gao, Xinzhi Li, Yifang Li, Xiaoran He

RESERVOIR CHARACTERISTICS AND PORE STRUCTURE CLASSIFICATIONS OF CHANG 6 MEMBER OF YANCHANG FORMATION OF TRIASSIC IN JIYUAN OILFIELD OF ORDOS BASIN, CHINA 8176
Ye Tao, Dazhong Ren, Shi Shi, Zhaohua Zhou, Shuwei Ma, Zhang Qian

REACTIVE DYE DEGRADATION USING Fe-LOADED BENTONITE AS A FENTON-LIKE CATALYST: FROM PROCESS OPTIMIZATION TO EFFLUENT ACUTE TOXICITY 8184
Milena Becelic Tomin, Aleksandra Kulic, Djurdja Kerkez, Miljana Prica, Sanja Rapajic, Dragana Tomasevic Pilipovic, Vesna Pesic

CONTAMINATION ASSESSMENT OF HEAVY METALS IN STREET DUST OF CHENGDU, SW CHINA 8199
Bin Zhang, Jiao Yue, Jia Deng, Xinqiang Ning, Yanhua Cai, Di Wu

THE RETROSPECTIVE INVESTIGATION OF POISONING CASES APPLIED TO AN EDUCATIONAL RESEARCH HOSPITAL IN TURKEY 8207
Gulten Kucukal, Itir Erkan

EFFECTS OF DIFFERENT IRRIGATION LEVELS ON MEDITERRANEAN CORN BORER (*SESAMIA NONAGRIOIDES* LEFEBVRE) POPULATIONS AND EFFECTS OF FATTY ACIDS IN CORN BORER PREFERENCES 8211
Ali Beyhan Ucak, Cevdet Kaplan, Behcet Inal, Serpil Gencoglan

PHYLOGENETIC ANALYSIS OF *URTICA* SPP. BY THE INTERNAL TRANSCRIBED SPACER (ITS) OF 18S-26S rDNA IN ORDU PROVINCE OF TURKEY 8221
Onur Koloren, Secil Eker

ULTRASOUND EXTRACTION OF TOTAL FLAVONOIDS FROM TORREYA FARGESII FRANCH. AND ITS ANTIOXIDANT ACTIVITY BASED ON RESPONSE SURFACE METHODOLOGY (RSM) 8226
Jin Shang, Jianhua Wang, Xianrong Zhou, Bo Jiang, Mingyi Qin

GLUCOSINOLATES IN HEADS AND SPROUTS OF GREEN, WHITE AND ROMANESCO CAULIFLOWER 8233
Golge Sarikamis, Begum Aydın, Merve Yavuz

THE EFFECTS OF CO-CULTIVATION IN WHEAT(TRITICUM SP.) AND FLAX (LINUM USITATISSIMUM L.) ON SHOOT REGENERATION CAPACITY OF EXPLANTS 8239
Ramazan Beyaz, Mustafa Yildiz

ACCUMULATION CHARACTERISTICS AND HEALTH RISK OF HEAVY METALS IN SOIL AND PLANT:A CASE STUDY FROM HUAIBEI COALFIELD,CHINA 8246
Dawei Huang, Herong Gui, Manli Lin, Weihua Peng

EFFECTS OF LOW TEMPERATURE STRESS ON THE PHYSIOLOGICAL PROPERTIES OF 'DAWUXING' YOUNG LOQUAT FRUIT 8255
Ronggao Gong, Wei Yang, Mingan Liao, Zhihui Wang, Qunxian Deng, Yong Zhang

SOIL CARBON SEQUESTRATION POTENTIAL OF DIFFERENT LAND USE AND LAND COVER SYSTEMS IN EASTERN PLATEAU AND HILLS AGROCLIMATIC ZONE OF INDIA 8263
Anita Mohanty, Chandan Sahu, Hemendra Nath Nayak, Sanjat Kumar Sahu

INFLUENCE OF Al^{3+} DOSAGE ON THE FLOCCULATION PERFORMANCE OF ACTIVATED SLUDGE AND ITS MECHANISM 8270
Haisong Li, Jia Zhou, Xiaolei Chen, Dongjin Wan, Wenning Mai

USE OF PERMEABLE REACTIVE BARRIER FOR GROUNDWATER REMEDIATION AT ONE WASTEWATER TREATMENT PLANT SITE 8278
Qingshan Ma, Zujiang Luo

ESTIMATING RECOVERABLE FUEL WOOD BIOMASS FROM SMALL DIAMETER TREES IN BRUTIAN PINE (*PINUS BRUTIA* TEN.) STANDS 8286
Mehmet Eker, Ramazan Ozcelik

EVALUATION OF ECO-FRIENDLY LEMON OIL AGAINST THE GREEN PEACH APHID *MYZUS PERSICAE* SULZER (HOMOPTERA: APHIDIDAE) USING FOUR SOLVENTS 8298
Tawfiq M Al-Antary, Idres H Belghasem, Salah Eddin A Araj

DETERMINATION OF THE VISUAL PREFERENCE LEVELS AND PERCEPTUAL DIFFERENCES IN THE APPEARANCE OF CERTAIN TAXA IN DIFFERENT SEASONS 8304
Emine Tarakci-Eren, Tugba Duzenli

ANTIBIOTIC RESISTANCE RATIO OF *ACINETOBACTER BAUMANNII* AGAINST TO TEN ANTIBIOTICS AND MULTIDRUG RESISTANCE INDEX 8316
Nur Ceyhan-Guvensen, Dilek Keskin, Funda Sankur

THE SEASONAL VARIATIONS OF HEAVY METAL ACCUMULATION IN THE TENCH (*TINCA TINCA*, L., 1758) AND PIKE (*ESOX LUCIUS*, L., 1758) OF ASARTEPE DAM LAKE, TURKEY 8321
Pınar Karacakaya, M Borga Ergonul, Sibel Atasagun

THE IMPACTS OF THE BIOCHAR ADDITION IN DIFFERENT DOSES ON YIELD AND NUTRIENT UPTAKE OF THE CHICKPEA PLANT (CICER *ARIETINUM* L.) UNDER THE CONDITIONS WITH AND WITHOUT INCUBATION 8328
Ahmet Demirbas, Tolga Karakoy, Hasan Durukan, Halil Erdem

BARLEY POWDERY MILDEW (*BLUMERIA GRAMINIS* F. SP. *HORDEI*) VIRULENCE GENE SPECTRUM IN THE SOUTHAEGEAN REGION OF TURKEY 8337
Elif Dalgic, Ahmet Zeybek

HOT SPOTS OF NO_X EMISSION FROM THE CEMENT FACTORY MAIN STACKS 8345
Majid Farhadi, Pierre Sicard, Alessandra De Marco, Mohammad Khoshgoftar, Adewale M Taiwo, Mohammad Javad Mohammadi, Shahram Sadeghi, Shirin Esmaeili, Abdeltif Amrane[10], Bahram Kamarehie, Yusef Omidi Khaniabadi

© by PSP Volume 26 – No. 12A/2017 pages 7626-7633 Fresenius Environmental Bulletin

HIGH-SPEED RAILWAY EMBANKMENTS STABILIZATION BY USING A PLANT BASED BIOPOLYMER

Huseyin Suha Aksoy*, Mesut Gor

Civil Engineering Department, Engineering Faculty, Firat University, Elazig, Turkey

ABSTRACT

Astragalus is a biopolymer, obtained from a plant that grows mostly in Turkey, Iran, Turkmenistan, Iraq, China, Korea, Japan, Syria, Mongolia and North Africa etc. In this study, the availability of Astragalus as an additive in the rail road fills is researched with regards to durability and strength parameters. A bump grows up when there is differential settlement between a bridge abutment and an approach embankment. The allowable differential settlement should be nearly equal to zero at high speed train railway embankments. For determining the proportion of Astragalus needed for reaching the maximum strength parameters, ten different soil samples were prepared with Astragalus content ranging from 0% to 10% by weight. The optimum moisture content (w_{opt}), maximum dry density and strength parameters are figured out for all mixtures. Nowadays, the high resilience modulus (M_R) fills are commonly used in high speed rail roads. These fills have a high energy absorption capacity and strength. The M_R value can be determined through CBR (California Bearing Ratio) tests. According to the experimental studies, adding 1 % of Astragalus to the sandy soils was deemed suitable in terms of strength parameters, economy and CBR values.

KEYWORDS:
Railway embankment design, biopolymer, strength parameters, resilience modulus, Astragalus, unconfined compression test.

INTRODUCTION

Astragalus is a plant based biopolymer that grows in Turkey, Iran, Turkmenistan, Iraq, China, Korea Japan, Syria, Mongolia and North Africa etc. Thousand tons of Astragalus is produced in these countries [1]. It is possible to purchase Astragalus lower than 6 $/kg in global markets. Chemically, it is a complex mixture of acidic polysaccharides, mostly present as calcium, magnesium and potassium salts. Astragalus swells quickly in water to form highly viscous colloidal sols or semi-gels, which act as protective colloids and stabilizing agents. Unlike many other gums, solutions of Astragalus have a very long shelf life without loss of viscosity [2]. Astragalus has been used commercially for well over 2000 years and is currently widely used as an emulsifier and thickener in emulsion systems in food, pharmaceutical and cosmetic industries [3]. In literature, numerous studies can be found about chemical and mechanical properties of Astragalus [3-4].

People have been building roads and houses by using soil as building and base material for ages. A road embankment should be built with a certain load-bearing capacity and resistant to volumetric changes. Besides, the fill settlements must not go over the limits; the embankment slope should be preferred in appropriate gradient or the strength must be increased via proper techniques such as geotextile, soil nailing and anchorage. The engineering properties of a fill can be enhanced in two ways: making compaction or adding additives such as lime, cement, fly ash and natural resin.

Since the fills are continuously under the effect of dynamic external forces like traffic, their dynamic characteristics such as the modulus of elasticity and the resilience modulus must be known. The resilience modulus of the sub-ground material is determined with the Eq. (1) below by using the CBR test results [5].

$$M_R = 1500.CBR \quad (1)$$

where M_R is the modulus of resilience (psi).

The earthworks of a road can be ranked as base, sub-base and the sub-grade layers. The qualities of sub-grade materials for fills are divided into 5 categories depending on their CBR values (very poor, poor to fair, fair, good and excellent) [6]. The CBR values of sub-grade materials are between 0-7% and these rank in very poor and poor to fair classes. Besides, the unconfined compressive strength (25 - 100kN/m^2) of sub-grade is classified as soft and mid. These kinds of soils are recognized as unstable and needed to be stabilized in road constructions.

The existing soil may not be suitable for the construction of supporting fill. Therefore, low-cost, harmless and natural additive materials must be used for the purpose of soil stabilization. Cement, bituminous materials, lime, fly ash, resins and chloride can be used as additives [7]. Gopal et al. [8] used some different natural resins for stabilizing sandy soil (dune sand). They determined that natural resins, Rosin and Terminalia alata tannins could reliably be

used in the soil. They examined the effect of compaction on the strength to determine the optimum stabilized layer thickness in roads and the helipads that are to be constructed in arid and dune regions. Besides, they analyzed the effects of temperature and bacteria on stabilized samples. Several researchers used various biopolymers and polymers (gellan gum, agar gum, glucan, xanthan gum, guar gum, modified starches etc.) to improve strength parameters of soils [9-16]. Levacic and Bravar [17] determined the properties of soil samples prepared by mixing the urea formaldehyde resin with soil. They prepared soil samples added different proportions of resins. The investigation of various parameters showed that resin significantly improved the geotechnical parameters of soil. They, consequently, determined that urea formaldehyde was suitable for soil stabilization. On the other hand, some investigators used chemical resin for improving the geotechnical parameters of dunes. These chemical products consist of melamine, urea, sodium carbonate and sulphuric acid. They determined that the compression strength increased to the value of 2.4 N/mm^2, in case 2% of sulfonated urea-melamine formaldehyde and 0.25% of sodium chloride were used. Researchers indicated that this resin had nutritious effects for the plants. Thus, improving dunes with these materials would have positive effects on the environment [18]. Galan-Marin et al. [19] used natural polymer (alginate) for the stabilization of clayey soil. The compressive strength of clayey soils increased from 2.23 to 3.77 MPa. Maghchiche et al. [20] utilized polymers and biopolymers (polystyrene, polyacrylamide and cellulose) in order to improve water retaining properties and stabilization of arid and semiarid lands. In several studies, researchers analyzed the settlement of high speed train embankments by using finite element method. Both researches showed that the total differential settlements provided only high strength subgrade layer [21-22]. Tayfur and Egeli [23] analyzed the total differential settlements of railway embankments. They used different water-cement ratios. By using finite element analysis results, researchers used artificial neural networks to predict the main stiffness specifications of cement-stabilized high speed railway embankment layers.

The cross sections of the road structures are ranked as base, sub-base and the sub-grade layers [24]. The base and sub-base layers are the two main layers ensuring the load bearing capacity of roads. The base and sub-base layers consist of the mixture of crushed stone, the particle diameter of which reaches up to 19mm, and the clay material. These layers should transmit the load weight to the ground without permanent deformation. Settlement and expansion are the main problems for these layers. The basic components of a rail road can be seen in the Fig. 1.

MATERIALS AND METHODS

With the purpose of determining the effects of Astragalus on the geotechnical properties of sandy soil, laboratory works are carried out in accordance with ASTM E1266-12 [25], Standard Practice for Processing Mixtures of Lime, Fly Ash, and Heavy Metal Wastes in Structural Fills and Other Construction Applications standard. In the lab works; the sieve analysis is performed in accordance with the ASTM C136 / C136M-14 [26], Standard Test Method for Sieve Analysis of Fine and Coarse Aggregates standard and in line with these analyses, the classification is made according to the Unified Soil Classification System (USCS). Right after these classification works, standard compaction test is implemented to the mixtures and the optimum moisture content and the maximum dry density are determined correspondingly ASTM D698-12e1 [27], Standard Test Methods for Laboratory Compaction Characteristics of Soil Using Standard Effort (12 400 ft-lbf/ft^3 (600 kN-m/m^3). The samples are prepared as ten different mix proportions of Astragalus from 0% to 10%. All the samples are prepared in the optimum moisture content and the shear box tests are carried out in accordance with the ASTM D3080 / D3080M-11 [28], Standard Test Method for Direct Shear Test of Soils Under Consolidated Drained Conditions standard. Unconfined compressive strength of samples which contained 1% to 10% Astragalus are determined (according to ASTM D2166 / D2166M-13 [29], Standard Test Method for Unconfined Compressive Strength of Cohesive Soil). The CBR values are determined in accordance with the ASTM D1883-14 [30], Standard Test Method for California Bearing Ratio (CBR) of Laboratory-Compacted Soils.

The index tests. A sandy soil, received from Turkish city of Elazig, is used as the embankment material in the tests performed. The relevant laboratory test results can be seen in the Table 1 and Fig. 2. In the result of the hydrometer tests and sieve analysis, the clay, silt, sand, and gravel rates of the soil are found to be 2.0%, 9.9%, 85.5% and 2.6% respectively. Consequently, the soil class is defined as SW-SM (well-graded Sand with Silt) in USCS and A-1-b (excellent to good) in AASHTO soil classification systems.

Astragalus (a biopolymer) is used as the additive. Astragalus is grinded as it is seen in Fig.3. After this grinding process, the Astragalus material is sifted by the sieve 177µm. Then, the sifted Astragalus is added to the soil from 1% to 10% and Proctor tests were performed on these mixtures.

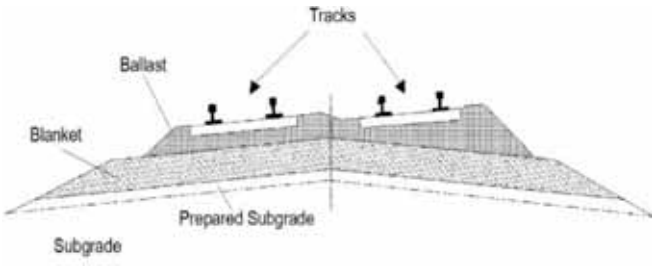


FIGURE 1
Typical cross-sections of road.

TABLE 1
Soil properties

Specific Gravity	2.68
Optimum Water Content (%)	12.0
Max. Dry Density (kN/m^3)	18.9
Content of Fines (%)	11.9
Internal Friction Angle (˚)	41.5
Cohesion (kN/m^2)	26.0
CBR value	14.0
Soil Classification (USCS), (AASHTO)	SW-SM, A-1-b

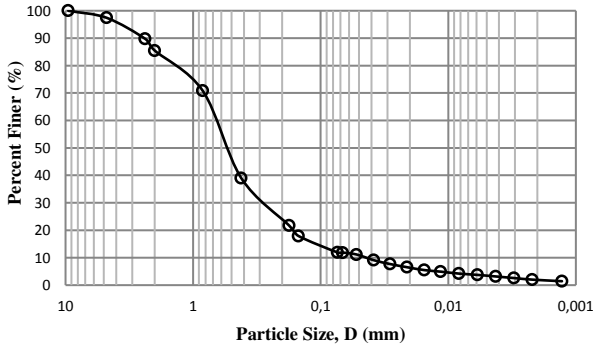


FIGURE 2
Particle size distribution of soil



FIGURE 3
Astragalus
(before and after granulation and sieve process)

TABLE 2
Results of the Proctor tests

Resin ratio (%)	Max. dry density (kN/m^3)	Optimum Moisture Content (%)
0	19.0	12.0
1	18.0	14.5
2	17.5	15.0
3	16.9	16.5
4	16.2	16.5
5	15.9	17.0
6	15.0	18.0
7	14.8	18.5
8	14.6	18.5
9	14.5	19.0
10	14.6	19.0

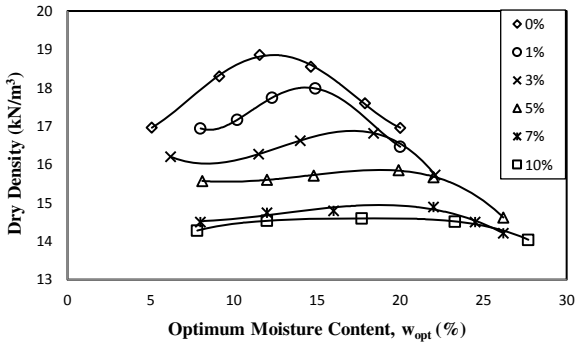


FIGURE 4
Results of the Proctor tests



FIGURE 5
Shared test specimen

TABLE 3
Results of shear box test

Resin ratio (%)	Internal friction angle (°)	Cohesion (kN/m²)
0	41.5	26.0
1	37.0	38.0
2	27.5	44.0
3	20.0	48.5
4	19.5	51.5
5	18.5	52.5
6	18.2	51.5
7	18.3	47.5
8	18.0	45.0
9	17.5	41.0
10	18.5	35.5

RESULTS AND DISCUSSION

Proctor tests. The values of optimum moisture contents and maximum dry density are determined in the result of the Proctor tests for each mixture. The data obtained as a result of the tests were summarized in Table 2 and Fig. 4. In this study, samples prepared at the Proctor density and optimum moisture content are used in all tests.

Shear box tests. Various ratios of Astragalus (1% to 10%) are added to the sandy soil and compacted to Proctor density. After this, the shear box tests are performed on the prepared soil samples. The samples are sheared at a constant rate of 0.5mm/min. The results of the shear box test are provided in Table 3. The final state of the sample in the shear box test is seen in Fig. 5.

Unconfined compression tests (UCS). Unconfined compression tests are conducted on the soil samples containing Astragalus (1% to 10%). The samples are sheared at a constant rate of 0.5mm/min. Fig.6. shows the results of the unconfined compression tests. In the figure, it is clearly seen that the ductility of soil samples increases with increasing Astragalus content. Therefore, in UCS tests load-displacement readings after reaching peak strength are not ceased, until limitations of test system.

Increase in Astragalus content decreases the unconfined compression strength and elasticity (tangent) modulus. Maximum compressive strength value is obtained from the 1% Astragalus samples. Increasing Astragalus content caused barrel type failure like cohesive soils in UCS tests (Fig.7.).

CBR tests. The CBR test consists of measuring the necessary load for ensuring a piston in standard sizes to penetrate in the soil sample in a definite speed. This load is divided by the load needed for the piston to penetrate into the same depth in a standard crushed rock sample and the result obtained multiplied by 100 and so the CBR value is found. Usually, 2.5 and 5mm of depths are used, but the depth values of 7.5 - 10 and 12.5 mm can be used too, if required. The penetration loads relating to crushed rock were standardized too. The CBR values are developed for measuring the bearing capacity of the soil for road construction [31]. The CBR tests are performed on the samples with optimum moisture content, in Proctor density and by adding increasing amounts of resin (0% to 10% by weight). CBR test results can be seen in Fig. 8.

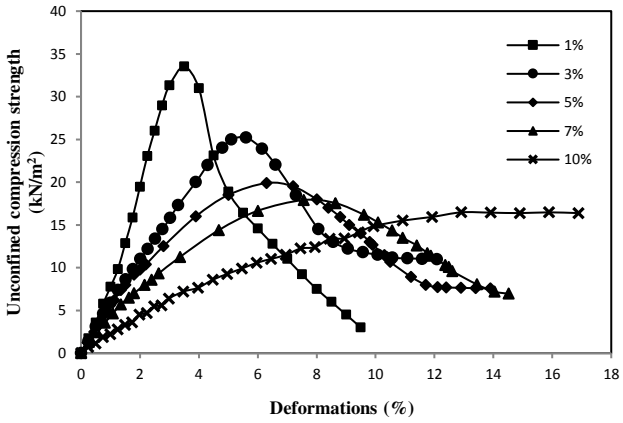


FIGURE 6
Results of the UCS tests

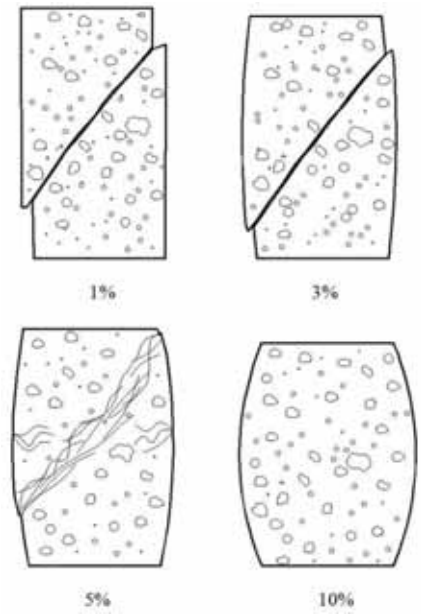


FIGURE 7
Detail of soil samples after the UCS tests

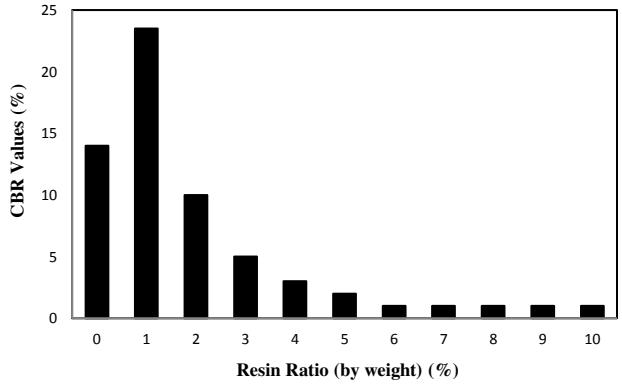


FIGURE 8
CBR values vs. resin ratio



FIGURE 9
Soil sample with 10% Astragalus after CBR test

Especially for samples which contain 10% Astragalus, soil spurted out from CBR mould and some heave of soil is observed (Fig.9.). Increasing Astragalus content caused plastic-like behavior of the samples.

Astragalus can be used as a soil additive in small quantities. Increasing its amount increases the optimum moisture content. For instance, when comparing additive-free soil (0% Astragalus) and soil containing 5% Astragalus, it is observed that the optimum water content increases from 12 to 17 %. Moreover, it is also observed that the dry density decreased from 18.9kN/m^3 to 15.9kN/m^3, after adding 5% of Astragalus.

Increase in Astragalus content not only decreases the angle of internal friction, but also results in higher cohesion values. For instance, when comparing additive-free soil and soil samples containing 5% of Astragalus, the angle of internal friction decreases from 41.5˚ to 18.5˚ with a decrease of 55%, and the cohesion value increases to 52.5kN/m^2 from 26kN/m^2 with an increase of 100%.

While the maximum cohesion is obtained with the addition of 5 % Astragalus, it is seen that the angle of internal friction declines sharply. This decline in the angle of internal friction and increase in the cohesion separate the behavior of the embankment soil from the properties of the cohesionless soils and causes them behave like the cohesive soils.

Even as the angle of internal friction is 41.5˚ in the additive-free samples, it becomes 37˚ with a decrease of 11% after the addition of 1 % Astragalus. Besides, the cohesion value of the additive-free samples has been determined as 26kN/m^2. With the addition of 1% Astragalus, it increased 45% and iss determined as 38kN/m^2.

As indicated above, the increase in the rate of Astragalus increases the dry density of the soil. When the previous studies are analyzed, it is observed that the resilience modulus (and the CBR value) was affected too much by the density of the soil [32-33]. In these studies, it was reported that the resilience modulus decreased as a result of the decrease in dry density. As a result of the experiments carried out, the increasing percentage of Astragalus decreased the dry density. However, it is determined that the unconfined compressive strength and CBR value peaked in 1 % of Astragalus and then decreased sharply. It is considered that this was caused by Astragalus to constitute adhesion among the soil grains then soil samples pretend to be cohesive soils.

CONCLUSIONS

Astragalus is a “green” material which can be used in soil as a stabilizer. With the addition of 1% Astragalus, the CBR results and UCS of sandy soil reaches a maximum value. It is seen that the carrying capacity of the soil decreased rapidly when the Astragalus content exceeded 1% by weight.

Furthermore, adding Astragalus in the increasing rates causes a decrease in soil strength. It is determined that 1% is the most suitable rate of Astragalus addition in sandy soils in terms of economy, strength parameters, and the CBR values.

The immobilization of Astragalus in the ground using soil stabilisation treatment is emerging as a viable and economical way of stabilization because of its advantages over other containment and soil stabilization methods.

In the laboratory observations, it is seen that the strength of the soils with Astragalus additive considerably increased after they lose their water content. Therefore, the effects of the changes of water content on the behavior of soils with Astragalus additive can be researched in the future studies.

REFERENCES

[1] Coppen J.J.W. (1995) Gums, resins and latexes of plant origin, (Non-wood forest products 6). Food and Agriculture Organization (FAO), Rome, 152p.

[2] Abtahi, S.M., Bagherzadeh, K., Esfahan, E.Z. (2015) Investigating the effects of number and frequency of incisions on production and survival of Astragalus keyserlingii. Journal of Rangeland Science. 5(3), 242-250.
[3] Gavlighi H.A., Meyer A.S., Zaidel D.N.A., Mohammadifar M.A. and Mikkelsen J.D. (2013) Stabilization of Emulsions by Gum Tragacanth (Astragalus spp.) Correlates to the Galacturonic Acid Content and Methoxylation Degree of the Gum. Food Hydrocolloids. 31(1), 5-14.
[4] Balaghi S., Mohammadifar M.A. and Zargaraan A. (2010) Physicochemical and Rheological Characterization of Gum Tragacanth Exudates from Six Species of Iranian Astragalus. Food Biophysics. 5(1), 59-71.
[5] The Asphalt Institute (1969) The Asphalt Institute Manual Series No.1, The Asphalt Institute, Maryland, 94p.
[6] Bowles J.E. (1992) Engineering Properties of Soil and Their Measurements. Mcgraw-Hill Boston, 4th Edition, 480p.
[7] Mitchell, J.K. (1981) Soil Improvement (State of the Art Report), X. Soil Mechanics and Foundation Eng. Conference, Stockholm, Sweden. 4, 509-565.
[8] Gopal, R., Singh, J. and Das, G. (1983) Chemical Stabilisation of Sand Comparative Studies on Urea-Formaldehyde Resins as Dune Sand Stabiliser and Effect of Compaction on Strength (Part IV). Indian Soc. Desert Tech. Univ. Cen. of Desert Studies Trans. 8(2), 13-19.
[9] Kavak, A., Bilgen, G. and Mutman, U. (2010) In-situ modification of a road material using a special polymer. Scientific Research and Essays. 5(7), 2547-2555.
[10] Chang, I. and Cho, G. C. (2012) Strengthening of Korean residual soil with β-1, 3/1, 6-glucan biopolymer. Construction and Building Materials. 30, 30-35.
[11] Chen, R., Zhang, L. and Budhu, M. (2013) Biopolymer stabilization of mine tailings. Journal of Geotechnical and Geoenvironmental Engineering. 139(10), 1802-1807.
[12] Khatami, H. and O'Kelly, B. (2013) Improving Mechanical Properties of Sand Using Biopolymers. Journal of Geotechnical and Geoenvironmental Engineering. 139(8), 1402–1406.
[13] Chen, R., Lee, I. and Zhang, L. (2014) Biopolymer stabilization of mine tailings for dust control. Journal of Geotechnical and Geoenvironmental Engineering. 141(2), 04014100, 1-10.
[14] Chang, I., Prasidhi, A. K., Im, J., Shin, H. D. and Cho, G. C. (2015) Soil treatment using microbial biopolymers for anti-desertification purposes. Geoderma. 253, 39-47.
[15] Chang, I., Im, J., Prasidhi, A. K. and Cho, G. C. (2015) Effects of Xanthan gum biopolymer on soil strengthening. Construction and Building Materials. 74, 65-72.
[16] Chang, I., Prasidhi, A.K., Im, J. and Cho, G.C. (2015) Soil strengthening using thermo-gelation biopolymers. Construction and Building Materials. 77, 430-438.
[17] Levacic, E. and Bravar, M. (1990) Soil Stabilization by Means of Lendur-EH Ureaformaldehyde. Rudarsko Geolosko Naftni Zbornik. 2, 137-143.
[18] Lahalih, S.M. and Ahmed, N. (1998) Effect of New Soil Stabilizers on The Compressive Strength of Dune Sand. Construction and Building Materials. 12(6-7), 321-328.
[19] Galán-Marín, C., Rivera-Gómez, C. and Petric, J. (2010) Clay-based composite stabilized with natural polymer and fibre. Construction and Building Materials. 24(8), 1462-1468.
[20] Maghchiche, A., Haouam, A. and Immirzi, B. (2010) Use of polymers and biopolymers for water retaining and soil stabilization in arid and semiarid regions. Journal of Taibah University for Science. 4, 9-16.
[21] Egeli, I. and Usun, H. (2012) Designing High-Speed Train Railway Embankments Using Finite Element Analysis. Arabian Journal for Science and Engineering. 37(8), 2127-2136.
[22] Connolly, D., Forde, M.C., Giannopoulos, A. and Woodward, P.K. (2012) The Effect of High Speed Railway Embankment Conditions on Vibration Levels in the Near and Far Field. RRUKA Annual Conference, London, United Kingdom, 1-5.
[23] Tayfur, G. and Egeli, I. (2013) Railway Embankment Design Based on Neural Networks. Gradevinar. 65(4), 319-330.
[24] Erel, A. (2006) Standarts for Trakia Railways and Rehabilitation (in Turkish), Yuksel Project Press, Istanbul, 480p.
[25] ASTM E1266-12. (2012) Standard Practice for Processing Mixtures of Lime, Fly Ash, and Heavy Metal Wastes in Structural Fills and Other Construction Applications, ASTM International, West Conshohocken, PA.
[26] ASTM C136 / C136M-14. (2014) Standard Test Method for Sieve Analysis of Fine and Coarse Aggregates, ASTM International, West Conshohocken, PA.
[27] ASTM D698-12e1. (2012) Standard Test Methods for Laboratory Compaction Characteristics of Soil Using Standard Effort (12 400 ft-lbf/ft^3 (600 kN-m/m^3)), ASTM International, West Conshohocken, PA.
[28] ASTM D3080 / D3080M-11. (2011) Standard Test Method for Direct Shear Test of Soils Under Consolidated Drained Conditions, ASTM International, West Conshohocken, PA.
[29] ASTM D2166 / D2166M-13. (2013) Standard Test Method for Unconfined Compressive Strength of Cohesive Soil, ASTM International, West Conshohocken, PA.

[30] ASTM D1883-14. (2014) Standard Test Method for California Bearing Ratio (CBR) of Laboratory-Compacted Soils, ASTM International, West Conshohocken, PA.
[31] Powell W.D., Potter J.F., Mayhew H.C. and Nunn M.E. (1984) The Structural Design of Bituminous Roads LR 1132, Transport and Road Research Laboratory Report, Berkshire, England, 62p.
[32] George, K.P. (2004) Prediction of Resilient Modulus from Soil Index Properties FHWA/MS-DOT-RD-04-172, Federal Highway Administration, U.S. Department of Transportation, Washington, D.C., 72p.
[33] Gudishala, R. (2004) Development of Resilient Modulus Prediction Models for Base and Subgrade Pavement Layers from In Situ Devices Test Results, MS Thesis. Louisiana State University College of Engineering, India. 122 p.

Received: **12.12.2016**
Accepted: **24.10.2017**

CORRESPONDING AUTHOR

Huseyin Suha Aksoy
Civil Engineering Department,
Engineering Faculty,
Firat University,
Elazig – Turkey

e-mail: saksoy@firat.edu.tr

© by PSP Volume 26 – No. 12A/2017 pages 7634-7642 Fresenius Environmental Bulletin

ARSENIC REMOVAL FROM AQUEOUS SOLUTIONS USING IRON OXIDE COATED SEPIOLITE

Sedef Arikan*, Deniz Dolgen, M Necdet Alpaslan

Dokuz Eylül University, Department of Environmental Engineering, 35160, İzmir, Turkey.

ABSTRACT

In this research, adsorption of arsenic As(V) by iron oxide coated sepiolite (IC-SEP) was studied. Sepiolite which has significant deposits in Turkey and as a low cost natural material, was used as adsorbent after coating with iron oxide. Material characterization study as well as adsorption data affirmed that iron oxide was successfully coated onto sepiolite. Optimum adsorption parameters were determined by batch experiments. As(V) removal was best achieved at neutral pH range. Results showed that removal percentage of As(V) could be over 94% in the conditions of IC-SEP dosage 5.0 g/L, contact time 4 h, and initial concentration of 110 µg/L As(V). Bicarbonate was detected as a major anion possibly interfere As(V) adsorption. Langmuir isotherm model well fitted to equilibrium data; and maximum adsorption capacity was calculated as 0.501 mg/g which is larger than that of several other adsorbents. Kinetics study showed that As(V) adsorption was well described by pseudo second-order model. Results suggested that IC-SEP is an easily available and low-cost adsorbent, and can effectively be used to reduce As(V) concentration below the standards, i.e.10 µg As/L.

KEYWORDS:
Adsorption, arsenic, sepiolite, iron oxide coating, low-cost adsorbent

INTRODUCTION

Arsenic is a heavy metal and accumulates in the body so can be toxic or cancerogenic depending on dosage [1]. In view of the toxicity to humans, the contamination limit of arsenic in drinking water is reduced from 50 to 10 µg/L by the World Health Organization - WHO [2, 3]. The European Commission (EC) and USEPA maximum admissible concentrations for arsenic in drinking water have also been reduced to 10 µg/L [4]. Various technologies are being used for removal of arsenic from water. Adsorption, membrane processes, oxidation- filtration and ion exchange are most preferred advanced methods for arsenic removal from water [5,6,7,8,9]. However, they have relatively high investment, operational and maintenance costs; and thus their wide application are limited due to the economic constraints. Adsorption is such a system which can remove arsenic efficiently, with sludge-free operation and it can be low-cost alternative provided that regional available adsorbents are used [10,11,12, 13]

Natural affinity of arsenic to iron(hydro)oxides is a well-known issue and makes this material attractive in adsorption process [14,15]. Several studies were done by using iron based materials in order to improve their adsorption capacity such as ferrous based red mud sludge [16], bead cellulose loaded with iron(oxy)hydroxide [17], iron based biomass-silica gel composites [18], iron oxide coated sponge [19], iron oxide coated natural rock [20], iron oxide coated cement [21], Fe-exchanged natural zeolite [16], iron oxide coated perlite [22], modified activated carbons with iron hydro(oxide) nanoparticles [23], iron–manganese binary oxide (FeMnOx/RGO) [24]. The responsible mechanism for the removal of arsenic is adsorption on iron modified adsorbents, which refers to the formation of surface complexes between soluble arsenic species and the surface hydroxyl groups, as arsenic connects with the iron sites of the material [25].

Sepiolite is a natural clay mineral with large surface area and porosity which provides excellent adsorption capacity. Main deposits of sepiolite are located in Anatolia in Turkey, Ceelbuur in Somalia, South-central China and Spain, and commercially available [26]. The abundance and availability of sepiolite mineral reserves as raw material sources and the relatively low cost of sepiolite guarantee its continued utilization in the future [27]. These advantages make sepiolite a unique adsorbent to use it in arsenic treatment. Iron modified sepiolite was effectively used to remove heavy metals like chromium(VI) and lead(II) from ground water and cobalt(II) ions from aqueous solutions [28, 29]. Sepiolite has been recently researched by [30] and [31] in order to evaluate arsenic sorption. For an effective adsorption, surface area is one of the critical parameter and it depends on particle size [32]. Because of the lack of this important detail in the literature as well as material characterization and competing anions in the water, this study presents a comprehensive approach for arsenic adsorption by iron oxide coated sepiolite. In this scope, surface

morphology, phase structure, surface area and pore volume data were investigated for both raw sepiolite and iron oxide coated sepiolite. Further, high arsenic bearing groundwater, supplied from Balıkesir, in the west part of Anatolia, where arsenic was measured up to 1000 µg/L, was also tested for competing ions interference on arsenic adsorption.

MATERIALS AND METHODS

Reagents. All chemicals were of reagent grade and used without further purification. The water used in this study was deionized water. A standard 1,000 mg/L As(V) solution (Merc, Germany) was used for preparation of diluted solutions. 0.1 M NaOH and HCl solutions were used for pH adjustment. Arsenic bearing groundwater was also experienced in order to investigate competing ions effect on the adsorption efficiency.

Preparation of iron oxide coated sepiolite (IC-SEP). Raw sepiolite (SEP) was provided from Eskişehir region, Turkey. It was crushed and sieved in the range of 300-1000 µm, washed with deionized water and dried in an oven at 105^0C. Then, 20 g of this material, was soaked in 50 mL of 0.5 M ferric nitrate solution at pH 10, at room temperature. The mixture was homogeneously stirred by mechanical shaker for 2 hours, and dried again at 200^0C in an oven for overnight. After that, iron oxide coated material was repeatedly washed in deionized water until the supernatant was clear. The material was dried in an oven and stored in capped bottles for further use.

Characterization of the adsorbents. The particle morphology of raw sepiolite (SEP) and iron oxide coated sepiolite (IC-SEP) were measured by scanning electron microscopy (SEM, Japan, JEOL JSM6060). Elemental analyses of SEP and IC-SEP was carried out by EDX connected to the SEM. X-ray diffraction pattern was taken from X-ray diffractometer (Rigaku D/Max 2200PC diffractometer with Ni-filtered Cu Kα radiation) to identify the components. The specific surface area and pore volume of adsorbents were measured by BET method on a Micromeritics Gemini apparatus.

Batch experiments. Batch experiments were carried out in Erlenmeyer flasks in order to obtain rate and equilibrium data. Two parallel experiments were conducted using SEP and IC-SEP. 50 mL As(V) solutions and adsorbent were put in Erlenmeyer flasks and shaken in a mechanical shaker with speed of 100 rpm. The effects of pH, contact time, initial As(V) concentration, adsorbent dose, particle size, competing anions were studied. Influent and effluent arsenic concentrations were measured by an inductively coupled plasma-optical emission spectrometry (HG-ICP-OES) (Optima 2100 DV).

Adsorption kinetic study. Adsorption kinetics of the selected adsorbent (IC-SEP) were identified by batch experiments. Three different initial arsenic concentrations, i.e., 100.8, 494 and 1503 µg/L, were reacted with 5 g/L of adsorbent during 8 hours. Samples were taken 15, 30, 60, 120, 240 and 480 minutes time intervals and arsenic concentrations were measured. The pH was kept as 7 and the experiments were conducted at room temperature. The obtained data were fitted to the first-order, pseudo first-order, second-order and pseudo second-order reaction kinetics models.

The equation to define the first order reaction mechanism is presented as [33];

$$-(dC_t)/dt = kC_t \quad (1)$$

In this equation, C_t is the concentration at a contact time (mg/L), C_o is the initial concentration (mg/L) and k is the first order adsorption rate constant. When integrating equation for the boundary conditions (t =0 to t and C=C_o to C_t), the linearized form of model is obtained as;

$$lnC_t = lnC_o - kt \quad (2)$$

In pseudo-first order reaction model, the rate (dq_e/d_t) is proportional to the difference between the amount of adsorption at time t and the adsorption capacity of adsorbent ($q_e - q_t$). The pseudo-first order reaction equation is generally expressed as follows;

$$(dq_t)/dt = k_1 (q_e - q_t) \quad (3)$$

In the equation, q_e and q_t define the adsorption capacity at equilibrium time and any time, and k_1 is the adsorption rate constant. Integrating equation at the boundary conditions (t =0 to t and q_t=0 to q_t) gives the linearized form of model and it can be presented as:

$$\ln(q_e - q_t) = lnq_e - k_1 t \quad (4)$$

Second order reaction model is based on steady state concentration and widely used for the adsorption process [34, 35]. The mathematical expression of the second order reaction mechanism is expressed as;

$$-(dC_t)/dt = k_2 C_t^2 \quad (5)$$

In the equation, C_t defines the concentration at a contact time (mg/L), C_o the initial concentration (mg/L), and k_2 is the second order adsorption rate constant. Integrating equation at the boundary conditions (t =0 to t; C_t=0 to C_t), linearized form of model is written as;

$$1/C_t - 1/C_0 = k_2 t \quad (6)$$

Finally, pseudo-second-order reaction model which is based on the adsorption capacity [35] is presented as;

$$dq_t/d_t = k_{p2}(q_e - q_t)^2 \quad (7)$$

In the equation, q_t is the adsorption capacity of any time (mg/g), q_e is the adsorption capacity at equilibrium time (mg/g) and k_{p2} is the pseudo second order adsorption rate constant. Integrating the equation at boundary conditions (t =0 to t and q_t=0 to

q_t) gives the linearized form of model as;

$$t/q_t = 1/(k_{p2}{q_e}^2) + (1/q_e)\,t \qquad (8)$$

Adsorption isotherm study. Adsorption capacity of iron-oxide coated sepiolite (IC-SEP) was found through isotherm study. For this purpose, batch experiments were performed with 50 mL of As(V) solutions at initial concentrations ranging from 100 to 10,000 µg/L. Experiments were conducted at pH 7, at room temperature and 4 h of contact time. Effluent arsenic concentrations were measured by ICP-OES. Obtained data were used in arsenic equilibrium studies fitting them to Langmuir model (Eq.9) and Freundlich model (Eq.10). The linearized Langmuir isotherm equation is given as follows [36]:

$$1/q_e = 1/q_m + 1/(bq_m)\,(1/C_e) \qquad (9)$$

Where q_e is the amount of arsenic adsorbed at equilibrium (mg/g), C_e is the equilibrium concentration (mg/L), $q_m$is the adsorption capacity (mg/g), b is the adsorption energy (L/mg).

Freundlich isotherm is an empirical equation and commonly used for adsorption processes [37], as well. Linearized form of Freundlich isotherm is expressed as:

$$lnq_e = lnk_f + 1/n\,(lnC_e) \qquad (10)$$

Where $k_f$is the adsorption capacity (mg/g), q_e is amount of adsorbate adsorbed per unit mass of adsorbent (mg/g) and C_e is equilibrium concentration and *1/n* is affinity coefficient.

TABLE 1
Elemental analysis of SEP and IC-SEP

	SEP	IC-SEP
Element	**Weight (%)**	
Si	59.06	60.71
O	21.99	22.57
Mg	16.86	10.63
Ca	0.89	0.33
Al	1.18	2.32
Fe	-	3.44

RESULTS AND DISCUSSION

Adsorbent characterization. Surface morphologies of adsorbents (SEP, IC-SEP) were identified by SEM analyses, and chemical compositions by EDX. The original pictures of the materials and the images obtained from SEM analysis were given in Fig. 1. The SEM images in Fig. 1 indicate that SEP and IC-SEP particles has quite porous surface. The chemical compositions of adsorbents are listed in Table 1. EDX analyses showed that SEP is primarily a mixture of Si, O, Mg, and Al and major constituent of sepiolite was silicate. Iron content was not detected in SEP, while the iron content IC-SEP particles were 3.44 % by weight. This is relatively low value and most likely attributed to surface sensitive characteristics of EDX analyses. As sepiolite has porous structure, iron coating could be penetrated into deeper parts *via* pores resulting lower iron content in the samples.

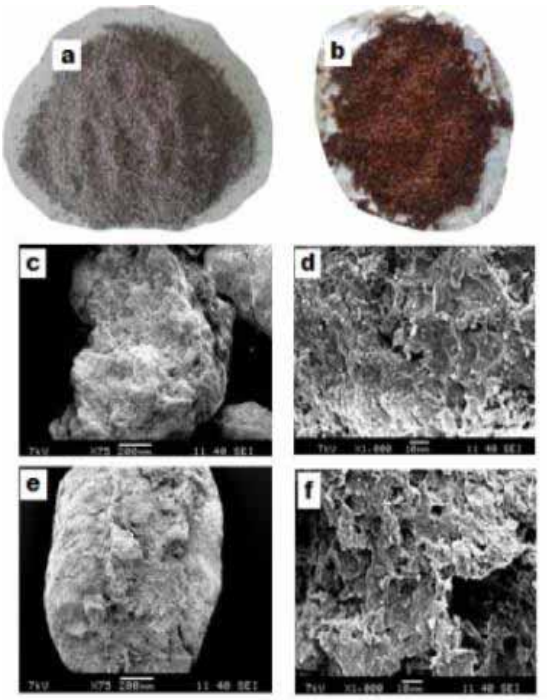


FIGURE 1
Photographs and SEM images a Photo of SEP, b Photo of IC-SEP, c 75x magnification of SEP, d 1000x magnification of SEP, e 75x magnification of IC-SEP, f 1000x magnification of IC-SEP

In addition to EDX analysis, XRD analyses were also conducted, and phases of SiO_2, MgO, CaO, Al_2O_3, and Fe_2O_3 have been detected in IC-SEP. These results indicate that iron oxide coating on raw sepiolite was successfully achieved. BET surface area, pore volume and average pore size of adsorbents were presented in Table 2. Ironoxide coating process caused decrease in surface area of IC-SEP. The surface area of SEP was 197.3 m^2/g, whereas after coating with iron oxide, it decreased to 183.2 m^2/g. Similarly, total pore volume of SEP was 0.41cm^3/g and it decreased to 0.39 cm^3/g for IC-SEP. Reduction on pore volumes after coating might be explained iron impregnating into pores. On the other hand, for coated material, decrease in particle size was resulted insignificant reductions in surface area, pore volumes, and average pore size (see Table 2). Those reductions might be attributed to destroying pores during the crushing of raw materials.

TABLE 2
BET analyses of SEP and IC-SEP

Material	Surface Area (m^2/g)		Pore Volume (cm^3/g)		Avg. Pore Size (Å)
	BET	Micropore Area	Total	Micropore Volume	
SEP (710-1000 µm)	197.28	46.33	0.41	0.0195	82.35
IC-SEP (710-1000 µm)	183.24	33.92	0.39	0.0139	85.72
IC-SEP (425-710 µm)	177.01	34.38	0.37	0.0142	84.14
IC-SEP (300-425 µm)	188.80	35.11	0.38	0.0144	81.48

Adsorption experiments. Effect of pH on adsorption. Three different pH values of the influent, namely acidic (4), neutral (7) and basic (10) were experienced and As(V) removal efficiencies were found as 72%, 79% and 48% for IC-SEP (see Fig 2). However, SEP did not give any significant removal efficiency for varied pH levels. Figure 2 shows that pH values higher than 7 negatively affect As(V) removal efficiency. As reported by [38], decrease in adsorption of As(V) on iron oxide surface could be attributed to an increase in competing OH^- for adsorption sites with increasing pH. Maji [39] reported that, the neutral (H_3AsO_4), the monovalent ($H_2AsO_4^-$), the divalent ($HAsO_4^{2-}$) and the trivalent (AsO_4^{3-}) ions are stable at the pH ranges of 0–2, 3–6, 7–11, and 12–14, respectively. In our experiments, As(V) bearing water having pH value 7 was used. Monovalent and divalent arsenate oxyanions (stable at the pH ranges 3–6 and 7–11, respectively) might be present in the water and adsorb onto the positive surfaces of coated materials via ion exchange/ion attraction.

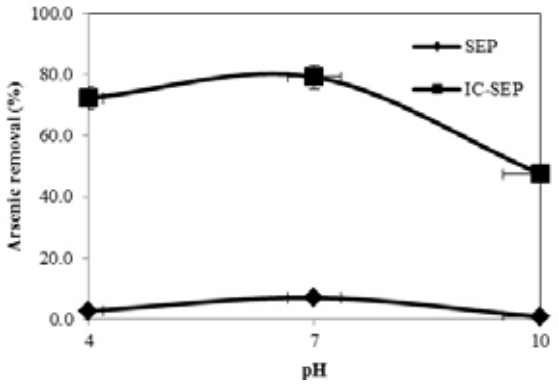


FIGURE 2
Effect of pH on arsenic removal for SEP and IC-SEP (initial As(V) concentration 110 µg/L, 2 hours contact time 5 g/L adsorbent dose)

Effect of contact time on adsorption. The effect of contact time on As(V) adsorption is demonstrated in Figure 3. Arsenic removal rate increased and reached to 82.5% at the end of two hours contact time, as shown in Fig. 3. Maximum removal efficiency of 90% was achieved within 4 hours, and remained fairly constant up to the end of the experiment (8 hours). Thus, four hours contact time was selected for the experiments. Figure 3 further indicates that arsenic removal by SEP was negligible and also time-independent. This result also shows that As(V) adsorption occurs only on positively charged iron coated sites of sepiolite, IC-SEP, and SEP without coating does not have adsorption capacity under the defined experimental conditions.

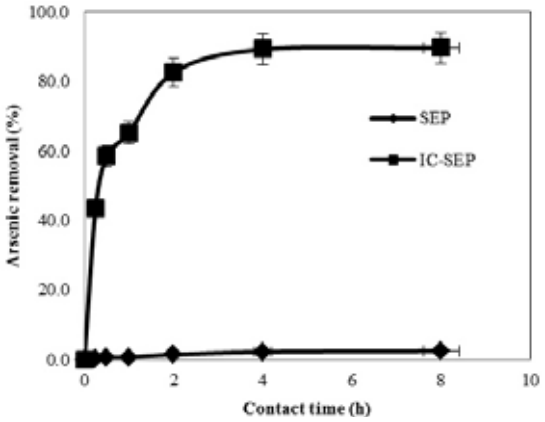


FIGURE 3
Effect of contact time on SEP and IC-SEP (initial As(V) concentration 110 µg/L, 5 g/L adsorbent dose)

Effect of initial arsenic concentration. IC-SEP could treat As(V) in water over 90% efficiency up to 538 µg/L initial As(V) concentration. Beyond this concentration, removal rate decreased and was 80% for 1613 µg/L. Above 1613 µg/L, removal efficiency was nearly stable and up to 9961 µg/L initial arsenic concentrations, removal rate decreased only approximately 8%. The reason for the decrease in As(V) adsorption efficiency at higher initial arsenic concentration might occur due to the adsorbent sites eventually became saturated with adsorbed arsenic. Those findings are illustrated in Figure 4. IC- SEP has a large adsorption capacity and it showed great performance to remove arsenic from water for high arsenic bearing water. Large surface area and pore volume of IC-SEP provide to hold As(V) anions not only onto surface, into the pores, as well. Raw sepiolite had almost no adsorption capacity in any As(V) concentrations as expected.

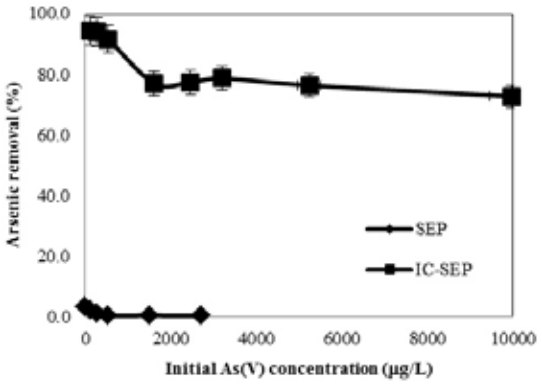


FIGURE 4
Effect of initial As(V) concentration on SEP and IC-SEP (5 g/L adsorbent dose)

Effect of adsorbent dose. The relationship between adsorbent dose and As(V) adsorption is depicted in Figure 5. Arsenic removal rapidly increased with an increase of IC-SEP dosage up to 5 g/L. For 1 g/L and 2 g/L adsorbent doses, removals were around 35% and 55%, respectively. Adsorption efficiency was reached to 95% for 5 g/L. For further doses, As(V) removal did not significantly change, app. 97% of initial As(V) could be treated for 25 g/L and 50 g/L doses. The rapid increase up to 5 g/L doses might be attributed to the fact that with an increase in the adsorbent dose, more adsorbent surface is available for the As(V) to be adsorbed.

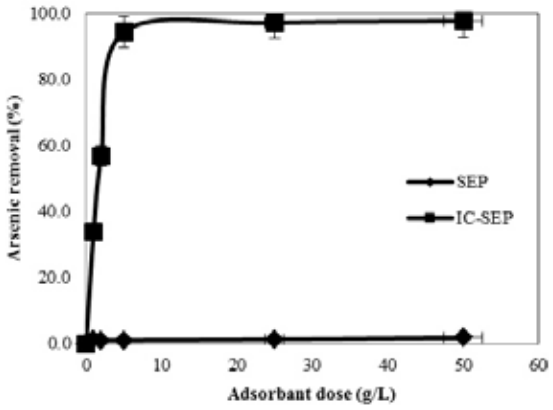


FIGURE 5
Effect of adsorbent dose on SEP and IC-SEP (initial As(V) concentration 110 µg/L, 4 hours contact time)

As a result of experiments, 5 g/L adsorbent dose was found capable to decrease arsenic concentration under desirable limit (i.e. 10 µg/L). Under 5 g/L, active surface site was not enough for satisfactory arsenic adsorption. Nearly 95% arsenic in the solution could be held by 5 g/L adsorbent dose and more. For this reason, 5 g/L adsorbent dose was used in the further experiments.

Effect of particle size. The effect of particle size on adsorption is presented in Figure 6 both SEP and IC-SEP. Negligible arsenic removal occurred for all size ranges, for SEP as expected. However, IC-SEP had lower performances in the smaller size ranges as seen in Fig.6. In the range of 300-425 µm and 425-600 µm, removal rates were nearly same and were obtained 85% and 88%, respectively. For 710-1000 µm size range, 94% removal was achieved. This situation can be caused from disappearing the pores in sepiolite when crushing to smaller sizes. Also, it can be interpreted that adsorption occurs into pores more than surface. Therefore, 710-1000 µm size range of modified sepiolite was found suitable to remove arsenic below 10 µg/L.

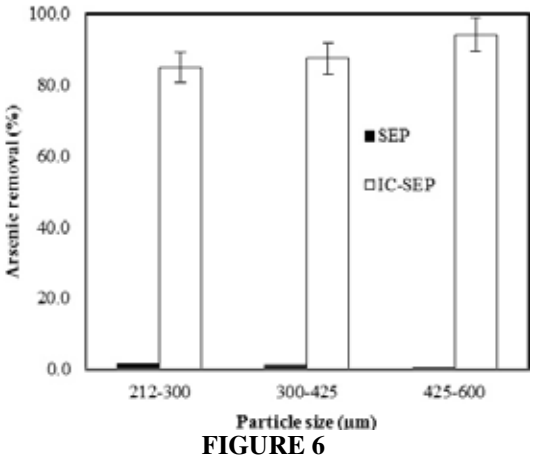


FIGURE 6
Effect of particle size on SEP and IC-SEP (initial As(V) concentration 110 µg/L, 5 g/L adsorbent dose)

Effect of competing anions in groundwater on adsorption. In groundwater sources several anionic components might exist, which could compete with arsenic for the available adsorption sites [40]. Sulfate (SO_4^{2-}), phosphate (PO_4^{3-}) and bicarbonate (HCO_3^-) are the major co-existing anionic components usually present in groundwater and affect arsenic removal undesirably. Therefore, in order to determine the effect of competing ions on As(V) removal, arsenic bearing groundwater (300 µg/L) from Balıkesir region, Turkey, was used in the study. Major anions in the groundwater used in the experiments were HCO_3^-, NO_3^2, SO_4^{2-} and Cl^- (Table 3).

TABLE 3
Concentration of anions in groundwater before and after adsorption tests

Anions (mg/L)	Before treatment	After Treatment by IC-SEP
Chloride	5.9	5.1
Nitrate	18.1	12.1
Sulphate	10.4	6.2
Bicarbonate	402.6	244.0
Phosphate	not available	not available

TABLE 4
Kinetic equations for IC-SEP

Kinetic of reaction	Initial concentration(µg/L)	Equation of reaction	R^2
First order	100.8	lnC_t=-0.251t-2.9802	0.707
	494	lnC_t = -0.2833t - 1.4314	0.7475
	2605	lnC_t = -0.1641t + 0.2264	0.5479
Pseudo-first-order	100.8	$ln(q_e-q_t)$= -1.2768t-4.184	0.9898
	494	$ln(q_e-q_t)$ = -0.2833t - 1.4314	0.9619
	2605	$ln(q_e-q_t)$ = -0.7556t - 1.569	0.8254
Second-order	100.8	$1/C_t$=11.324t+20.961	0.8339
	494	$1/C_t$ = -0.2833t - 1.4314	0.8749
	2605	$1/C_t$ = 0.2035t + 0.88	0.7477
Pseudo-second-order	100.8	t/q_t=52.942t+16.357	**0.9993**
	494	t/q_t = 10.535t + 3.1607	**0.9993**
	2605	t/q_t = 2.2554t+ 0.4808	**0.9997**

The groundwater sample was diluted to 100 µg As/L±5 with deionized water in order to compare the results with experiments by synthetic As(V) containing water. All the other parameters (pH, contact time, adsorbent dose) remained constant. Results revealed that competing anions in real arsenic bearing water resulted with interference; and thus arsenic removal efficiency decreased. Due to high adsorption capacity of IC-SEP (0.501 mg/g), the reduction of percent removal was only 17±5%. For the same experimental conditions, arsenic removal rate was obtained 94% for synthetic water and 77% for groundwater sample (Fig.7).

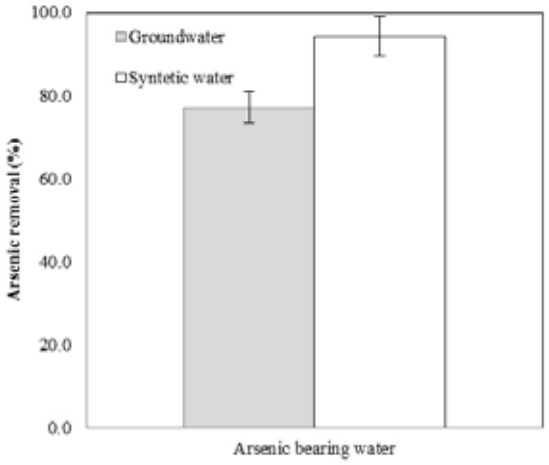


FIGURE 7
Effect of existing ions on arsenic adsorption (initial As concentration 110 µg/L, 4 hours contact time, pH 7)

As it presented in Table 3, following the adsorption experiments, the concentrations of HCO_3^- ,NO_3^-, SO_4^{2-} and Cl^- were measured as 244.0, 6.2, 12.1 and 5.1 mg/l, respectively. HCO_3^- concentration, as major anion, decreased dramatically after treatment and this situation also resulted by decreasing removal efficiency of As(V) for the groundwater sample (Table 3). However, removal efficiencies of other anions were quite low. Gao [41], studied existing anions on arsenic adsorption and observed an increase of 56 µg/L of arsenic concentration with initial bicarbonate content up to 1500 mg/L. They reported that desorption of arsenic by bicarbonate is significant, even at relatively low concentration levels. Stachowicz [42], observed that the presence of HCO_3^- increased the arsenate as well as arsenite concentration in solution, particularly evident in the pH range relevant for Bangladesh groundwater. They obtained from the experiments, the As(III) concentration increased about 10 times at the lowest pH value due to the presence of 0.01 M bicarbonate. HCO_3^- also enhances dramatically the adsorption of both pesticides on alpha-Al_2O_3 and clay [43].

Adsorption kinetic study. The adsorption kinetics of IC-SEP were studied using first order, pseudo first order, second order, and pseudo second order reaction mechanisms. The equations and coefficient of determination values (R^2) for all reaction models are presented in Table 4.

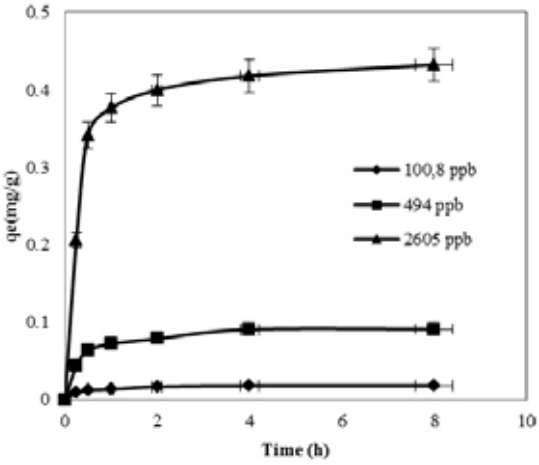


FIGURE 8
Adsorption kinetics of IC-SEP

TABLE 5
Langmuir and Freundlich isotherm constants for IC-SEP

Adsorbent	Adsorbent dose (g/L)	Langmuir			Freundlich		
		q_{max} (mg/g)	b (L/mg)	R^2	n	k_f (mg/g)	R^2
IC-SEP	5	0,501	6,909	**0,9958**	1,528	0,644	0,9860
	10	0,164	21,03	**0,9857**	1,65	0,351	0,9890
	20	0,102	44,85	**0,9912**	1,82	0,242	0,9819

The kinetic data could be best described by the pseudo-second-order kinetic equation which was based on the assumption that the rate limiting step may be chemical sorption or chemisorptions involving valency forces through sharing or exchange of electron between adsorbent and adsorbate [44, 45]. In chemisorption, the metal ions bind to the adsorbent surface by forming a chemical (usually covalent) bond and tend to find sites that maximize their coordination number with the surface [48]. Experimental data correlate excellent to the pseudo second order reaction model with a high co-efficient of determination value (R^2) as 0.9993. The rate constant k_{p2} is 172.87 g/mg.h. Similar results for arsenic removal obtained by [22, 47]. Figure 8 shows adsorption kinetics of IC-SEP during 8 hours contact time.

Adsorption isotherm study. The equilibrium adsorption isotherms have primarily importance to evaluate arsenic adsorption capacity. In order to determine the optimum isotherm model according to coefficient of determination values, both Langmuir and Freundlich models were applied to the adsorption experimental results as given in Table 5.

The co-efficient of determination value (R^2) is obtained as R^2=0.9958. High (R^2) value revealed that the Langmuir model was more suitable to explain the results than Freundlich model. Langmuir isotherm assumes monolayer adsorption onto a homogeneous surface with limited number of identical sites [49]. Thus, it can be implied that As(V) ions formed a monolayer on the adsorbent surface. The Langmuir constant and maximum adsorption capacity was calculated as 6.909 L/mg and 0.501mg/L, respectively. IC-SEP has higher adsorption capacity than most of the iron modified natural materials in the literature such as iron oxide coated sand 0.02857mg/g [6], iron oxide coated perlite 0.39 mg/g [22], iron coated zeolite 0.68mg/g [48] and iron oxide coated rock 0.36 mg/g [49].

CONCLUSIONS

In this research, adsorption mechanism of As(V) was studied by using iron oxide coated sepiolite (IC-SEP) *via* batch experiments. BET results suggested that raw sepiolite has higher surface area than IC-SEP, however, it has no adsorption capacity due to negatively surface charged. EDX and XRD analyses indicated that iron was successfully coated onto sepiolite (IC-SEP). As(V) was removed 94% within 4 hours at an initial concentration of 110 µg/l with 5 g/l of IC-SEP dosage. The adsorption of As(V) had highest efficiency at around neutral pH values that are typical for natural waters, therefore no pH adjustment would be required in application phase. This makes IC-SEP also easily-used and cost-effective material. In the existence of bicarbonate, as competing anion in ground water, may reduce the adsorption efficiency of IC-SEP, due to the competitively adsorption of HCO_3^- and As(V) onto IC-SEP. As(V) adsorption onto IC-SEP well defined by Langmuir isotherm and adsorption kinetic of IC-SEP revealed good with pseudo-second order reaction model. Results show that IC-SEP can be used as a low-cost and highly efficient adsorbent in order to treat arsenic bearing water.

ACKNOWLEDGEMENTS

The authors gratefully acknowledge Dokuz Eylül University, Scientific Research Project Program (BAP 2013.KB.FEN.030) for the financial support to this work.

REFERENCES

[1] Nilsson, R., Jha, A.N., Zaprianov, Z., Natarajan, A.T. (1993) Chromosomal aberrations in humans exposed to arsenic in the Srednogorie area Bulgaria. Fresen. Environ. Bull. 2, 59–64.

[2] WHO (1993) Guidelines for drinking-water quality. World Health Organization. 2nd Edition - Volume 1 – Recommendations, Geneva.

[3] WHO (2011) Guidelines for drinking-water quality.World Health Organization. (4th ed.).

[4] Vaclavikova, M., Gallios, G.P., Hredzak, S., Jakabsky, S. (2008) Removal of arsenic from water streams: an overview of available techniques. Clean Techn Environ Policy. 10, 89–95.

[5] Alpaslan, M.N., Dölgen, D., Boyacıoğlu, H., Sarptaş, H., (2010) Arsenic removal from drinking water by cheical methods. tüdergisi/e su kirlenmesi kontrolü. 20(1), 15-25.(in Turkish).

[6] Gupta, V.K., Saini, V.K., Jain, N. (2005). Adsorption of As(III) from aqueous solutions by iron oxide-coated sand. J Colloid Interface Sci. 288, 55-60.
[7] Jian-Gang, H., Di-Wu, F., Xiu-Zhi, L., Yong-li, Z., Sajjad, A. (2016) Mechanism of Cr^{6+}, Mn^{2+}, Cu^{2+} and Cd^{2+} adsorption by a low-cost rice husk-derived biochar in aqueous solutions. Fresen. Environ. Bull. 25(8), 2736-2744.
[8] Balci, B. (2016) Basic textile dye adsorption from aquous solution and synthetic dye bath wastewater by modified *eucalyptus* barks, Fresen. Environ. Bull. 25 (12a), 6124-6131.
[9] Selvaraj, A., Prabu1,P., Mohan, K., Kumaravel, I., Rajendran, V., (2016) Efficiancy of bacterial biopolymeric (eps) liganded silver mesocage complexes for hexavalent chromium adsorption**.** Fresen. Environ. Bull. 25 (12a), 6030-6037.
[10] Hassani, G., Alinejad, A., Rezaei, S., Jamshidi, A., Farsani, S.F., Zare1, M.R., (2016) Optimization of the removal of acid blue 25 from aqueous media by recyclable nano magnetic manganese ferrite, Fresen. Environ. Bull. 25 (8), 2919-2927.
[11] Shams, M., Nabipour, I., Dobaradaran,S., Ramavandi, B., Qasemi, M. and Afsharnia, M., (2013) An Environmental friendly and cheap adsorbent (municipal solid waste compost ash) with high efficiency in removal of phosphorus from aqueous solution. Fresen. Environ. Bull. 22(3), 723-736.
[12] Khosravi, R., Zarei, A., Fazlzadeh, M., (2017) Investigation of TiO_2 and ZnO nanoparticles coated on raw pumice for efficient removal of ethidium bromide from aqueous solutions. Fresen. Environ. Bull. 26, 1352-1358.
[13] Kavak, D. (2017) Adsorptıon of Cr(III) from aqueous medium by hazelnut shell and batch design. Fresen. Environ. Bull. 26,1784–1790.
[14] Razzouki, B., Hajjaji, S.E., Azzaoui, K., Errich, A., Lamhamdi, A., Berrabah,M., Li,Y.R., Wang,J., Luan, Z.K., Liang, Z., (2010). Arsenic removal from aqueous solution using ferrous based red mud sludge. J Hazard Mater.177, 131-137.
[15] Razzouki,B., Hajjaji, S., Azzaoui, K., Errich, A., Lamhamdi, A., Berrabah, M., Elansari, L.L. (2015) Physicochemical study of arsenic removal using iron hydroxide. J. Mater. Environ. Sci. 6 (5) (2015) 144-1450.
[16] Li, Z.H., Jean, J.S., Jiang,W.T., Chang,P.H., Chen,C.J., Liao,L.B. (2011) Removal of arsenic from water using Fe-exchanged natural zeolite. J Hazard Mater.187, 318-323.
[17] Guo, X.J., Du, Y.H., Chen, F.H., Park, H.S., Xie, Y.N. (2007) Mechanism of removal of arsenic by bead cellulose loaded with iron-oxyhydroxide (beta-FeOOH): EXAFS study. J.Colloid Interface Sci. 314, 427-433.
[18] Martinez-Cabanas, M., Carro, L., Lopez-Garcia, M., Herrero, R., Barriada, J.L., Vicente, M.E.S. (2015) Achieving sub-10 ppb arsenic levels with iron based biomass-silica gel composites. ChemEng J. 279, 1-8.
[19] Nguyen, T.V.,Vigneswaran, S., Ngo H.H., Kandasamy, J. (2010) Arsenic removal by iron oxide coated sponge: Experimental performance and mathematical models. J Hazard Mater. 182, 723-729.
[20] Maji, S.K., Kao, Y.H., Wang, C.J., Lu,G.S., Wu, J.J., Liu, C.W. (2012) Fixed bed adsorption of As (III) on iron-oxide coated natural rock (IOCNR) and application to real arsenic-bearing groundwater. Chem Eng. J. 203, 285-293.
[21] Kundu, S., Gupta, A.K. (2007) Adsorption characteristics of As(III) from aqueous solution on iron oxide coated cement (IOCC). J Hazard Mater. 142, 97-104.
[22] Mostafa, M.G., Chen, Y.H., Jean, J.S., Liu, C.C., Lee, Y.C. (2011) Kinetics and mechanism of arsenate removal by nanosized iron oxide-coated perlite. J Hazard Mater. 187, 89-95.
[23] Vitela-Rodriguez, A.V., Rangel-Mendez, J.R. (2013) Arsenic removal by modified activated carbons with ironhydro(oxide) nanoparticles. J Environ Manage. 114, 225-231.
[24] Zhu, J., Lou, Z., Liu, Y., Fu, R., Baigab, S.A., Xu, X. (2015) Adsorption behavior and removal mechanism of arsenic on graphene modified by iron–manganese binary oxide (FeMnOx/RGO) from aqueous solutions, RSC Adv. 5, 67951–67961
[25] Edwards, M. (1994) Chemistry of arsenic removal during coagulation and Fe-Mn oxidation. J Am Water Works Ass. 86(9), 64-78.
[26] Hrenovic, J., Tibljas, D., Ivankovic, T., Kovacevic, D., Sekovanic, L. (2010) Sepiolite as carrier of the phosphate-accumulating bacteria Acinetobacterjunii. Appl Clay Sci. 50(4), 582-587.
[27] Balci, S., Dincel, Y. (2002) Ammonium ion adsorption with sepiolite: use of transient uptake method. Chem. Eng. Process. 41(1), 79-85.
[28] Fu, R.B., Yang, Y.P., Xu, Z., Zhang, X., Guo, X.P., Bi, D.S. (2015) The removal of chromium (VI) and lead (II) from groundwater using sepiolite-supported nanoscale zero-valent iron (S-NZVI). Chemosphere. 138, 726-734.
[29] Lazarevic, S., Jankovic-Castvan, I., Potkonjak, B., Janackovic, D., Petrovic, R. (2012) Removal of Co^{2+} ions from aqueous solutions using iron-functionalized sepiolite. ChemEng Process. 55, 40-47.
[30] Oztel, M. D., Akbal, F., Altas, L. (2015) Arsenite removal by adsorption onto iron oxide-coated pumice and sepiolite. Environ Earth Sci. 73(8), 4461-4471.

[31] Ilic, N.I., Lazarevic, S.S., Rajakovic-Ognjanovic, V.N., Rajakovic, L.V., Janackovic, D.T., Petrovic, R.D. (2014) The sorption of inorganic arsenic on modified sepiolite: the effect of hydrated iron(III) oxide. J Serb Chem Soc. 79(7), 815-828.
[32] Arıkan, S. (2016) Investigation of arsenic adsorption performance of the modified natural materials, PhD Thesis, Dokuz Eylul University, Graduate School of Natural And Applied Sciences, Environmental Engineering Department, Izmir, Turkey.
[33] Lagergen, S. (1898) About the theory of so-called adsorption of soluble substances. Kungliga Svenska Vetenskapsa-akademiens, Handlinger. 24(4), 1-39.
[34] Ho, Y.S. (2004) Citation review of lagergren Kinetic raet equation on adsorption reactions. Scientometrics. 59(1) 171-177.
[35] Ho, Y.S., McKay, G. (2000) The kinetics of sorption of divalent metal ions onto sphagnum moss peat. Water Research. 34 (3), 35-42.
[36] Langmuir, I. (1918) The adsorption of gases on plane surfaces of glass, mica and platinum. Am Chem Soc. 40 (9), 1361–1403.
[37] Freundlich, H.M.F. (1906) Over the adsorption in solution. J Phys Chem. 57, 385-470.
[38] Manna, B.J., Dey, S., Debnath, S., Ghosh, U.C. (2003). Removal of arsenic from groundwater using crystalline hydrous ferric oxide (CHFO). Water Qual. Res. J. Canada. 38(1), 193–210.
[39] Maji,S.K., Pal,A., Pal,T., Adak,A. (2007) Sorption kinetics of arsenic on laterite soil in aqueous medium. J EnvironSciHealth-A. 42, 989–996.
[40] Wilkie, J.A., Hering, J.G. (1996) Adsorption of arsenic onto ferric hydroxide: effects of adsorbate/adsorbent ratios and co-occurring solutes. Colloid. Surf. 107, 97–110.
[41] Gao, X.B., Wang, Y.X., Hu, Q.H., Su, C.L. (2011) Effects of anion competitive adsorption on arsenic enrichment in groundwater. J Environ Sci Health Part A Toxic/Hazard Subst Environ Eng. 46, 471-479.
[42] Stachowicz, M., Hiemstra, T., Van Riemsdijk, W.H. (2007) Arsenic-bicarbonate interaction on goethite particles. Environ Sci Technol. 41, 5620-5625.
[43] Stathi,P., Christoforidis, K.C., Tsipis, A., Hela, D.G., Deligiannakis, Y. (2006) Effects of dissolved carboxylates and carbonates on the adsorption properties of thiuramdisulfate pesticides. Environ Sci Technol. 40, 221-227.
[44] Yao, S.H., Liu, Z.R., Shi, Z.L. (2014) Arsenic removal from aqueous solutions by adsorption onto iron oxide/activated carbon magnetic composite. J Environ Health Sci Eng. 12, 58.
[45] Ho, Y.S,. McKay, G. (2000) The kinetics of sorption of divalent metal ions onto sphagnum moss peat. Water Res. 34, 735-742.
[46] Atkins, P.W. (1995) Physical Chemistry, (Fifth ed.) Oxford.
[47] Attinti, R., Sarkar, D., Barrett, K.R., Datta, R. (2015) Adsorption of arsenic(V) from aqueous solutions by goethite/silica nanocomposite. Int J Environ Sci Technol. 12, 3905–3914.
[48] Jeon, C.S., Baek, K., Park,J .K., Oh, Y.K., Lee, S.D. (2009) Adsorption characteristics of As(V) on iron-coated zeolite. J Hazard Mater. 163(2-3), 804-808.
[49] Maji, S.K., Kao, Y.H., Liu, C.W. (2011) Arsenic removal from real arsenic-bearing groundwater by adsorption on iron-oxide-coated natural rock (IOCNR). Desalination. 280 (1-3), 72-79.

Received: **01.07.2016**
Accepted: **22.06.2017**

CORRESPONDING AUTHOR

Sedef Arikan
Dokuz Eylül University, Department of Environmental Engineering, 35160, İzmir, Turkey.

e-mail: sedef.arikan@deu.edu.tr

© by PSP Volume 26 – No. 12A/2017 pages 7643-7650 Fresenius Environmental Bulletin

HEALTH RISK ASSESSMENT OF TOXIC HEAVY METALS IN WHEAT CROP GROWN UNDER DOMESTIC WASTEWATER IRRIGATION

Kafeel Ahmad[1], Zafar Iqbal Khan[1*], Robina Kaukab[1], Kinza Wajid[1], Naunain Mehmood[2], Hira Muqaddas[3], Tassawur Abbas[4], Muhammad Fahad Ullah[4], Mohamed Soliman Elshikh[5], Abdulaziz Al Sahli[5], Mohamed El-Zaidy[5], Ijaz Rasool Noorka[6], Shahzadi Mahpara[7], Hazoor Ahmad Shad[8], Muhammad Ayub[9]

[1]Department of Botany, University of Sargodha, Sargodha, Pakistan
[2]Department of Zoology, University of Sargodha, Sargodha, Pakistan
[3]Department of Zoology, the Women University, Multan, Pakistan
[4]Department of Earth Sciences, University of Sargodha, Sargodha, Pakistan
[5]Department of Botany and Microbiology, College of Science, King Saud University, Saudi Arabia
[6]Department of Plant Breeding and Genetics, University College of Agriculture, University of Sargodha, Pakistan
[7]Department of Plant Breeding & Genetics, Faculty of Agricultural Sciences, Ghazi University, Dera Ghazi Khan
[8]Department of Chemistry, University of Sargodha, Sargodha, Pakistan
[9]Govt. College University Faisalabad, Pakistan

ABSTRACT

Dietary intake of contaminated crops with heavy metals causes serious human health risks. The current study focused on the atomic absorption analysis of Zn, Cu, Co, Pb, Mn, Fe, Cd, and Cr in the wheat grains and soil using pot experiment conducted in Sargodha, Pakistan. Results showed that the Zn concentration in wheat grains increased with continuous wastewater utilization. Except cadmium, mean concentration of other heavy metals was within permissible limits in the soil. A significant and positive correlation was also observed for Cu, Pb, and Cr between soil and crop. The application of wastewater for longer period of time caused enrichment factor and health risk index to be increased considerably suggesting that proper management is required for treating domestic wastewater to prevent potential health risks via dietary intake of crops contaminated with heavy metals.

KEYWORDS:
wastewater irrigation, heavy metals, health risk index, soil.

INTRODUCTION

Wastewater is widely used all over the world for irrigation [1,2,3,4].The application of wastewater, whether treated or untreated, is increasing at an alarming rate, irrigating about 20 million ha of agricultural land in the world. The industrial and household wastewater irrigation normally contains non-essential heavy metals in small amounts but this causes bioaccumulation of noxious metals in the plants transferring them via food chain [5,6].

Wastewater irrigation can provide water and nutrients and in this way it can be a useful practice of nutrient recycling [7,8,9]. Different soil properties such as pH, texture, type of the oxyhydroxides and amount of organic matter generally determine the transport of trace metals and essential components (carbonates, phosphates and clay) thereby trans-locating heavy metals from soil to plants [10].Some investigations have confirmed that after 50 to 100 years, the level of toxic heavy metals in the soil would surpass the maximum permissible limits if irrigated with reclaimed sewage water and this could have devastating effects on the environment [11].

From the nutritional point of view, wheat crop is very important and main constituent of diet all over the world and especially in Pakistan. Throughout the world, wheat (*Triticum aestivum* L.) is an essential crop preceding rice and other cereals. In Pakistan, wheat is widely grown over about 8,069,000 ha. Per capita usage of wheat is 120 kg per year that is quite high if compared with other countries of the world [12].

Major environmental issues arise from the deposition of heavy metals in the plants as these are toxic and can also cause harm to both plants and animals. Present study was conducted in order to determine heavy metal toxicity in soil and wheat grown using wastewater and to investigate associated health risk and the enrichment pattern of irrigating wastewater to the soil.

MATERIALS AND METHODS

Experimental Design. The study was carried out in Botanical Garden of University of Sargodha, Sargodha, Pakistan. Sargodha is an agricultural city

TABLE 1
Tolerable daily intake limits of different heavy metals

Heavy metals	Co	Cu	Zn	Pb	Mn	Fe	Cr	Cd
TDI (mg kg^{-1} day^{-1})	3.01[a]	3[b]	60[b]	0.214[b]	0.5[c]	45[d]	105[e]	0.07[e]

Source: [a] Food and Nutrition Board [21]; [b] FAO/WHO [22]; [c]FAO/WHO [23]; [d]USEPA [20]; [e]USEPA [24]

TABLE 2
Oral reference dose of different heavy metals

Heavy metals	Co	Cu	Zn	Pb	Mn	Fe	Cr	Cd
R_fD [a] (mg kg^{-1} day^{-1})	0.043	0.04	0.3	0.0035[b]	0.041	0.70	1.5	0.001

Source: [a]USEPA [24]; [b] WHO [25]

TABLE 3
Reference values of different heavy metals in grain and soil

Reference Value of Heavy metals (mg kg^{-1})								
Heavy metals	Co	Cu	Zn	Pb	Mn	Fe	Cr	Cd
In Crop	50[a]	73.3[a]	99.4[a]	3[b]	500[a]	425.5[a]	2.3[a]	0.2[a]
In Soil	5.23[c]	8.39[d]	44.9[d]	8.15[d]	46.7[d]	56.9[e]	9.07[d]	1.49[d]

Source: [a]FAO/WHO [26]; [b]WHO [25]; [c]Shad *et al*. [27]; [d]Singh *et al*. [28]; [e]Dosumu *et al*. [29]

TABLE 4
Results of analysis of variance for heavy metal concentrations in grains and soil

	Mean Squares							
Heavy metals	Co	Cu	Zn	Pb	Mn	Fe	Cr	Cd
Grains	0.02***	0.16^{ns}	10.1^{ns}	0.06^{ns}	0.5**	1.9***	0.03^{ns}	0.01***
Soil grown with wheat	0.01**	0.2^{ns}	0.4^{ns}	0.1^{ns}	0.06^{ns}	25.5^{ns}	0.003**	0.12^{ns}

ns= not-significant; *** = Level of significance at 0.001; ** = Level of significance at 0.01

known for citrus fruit. Using four different treatments of domestic wastewater, healthy seeds of wheat variety ''Galaxy" were sown in Nov, 2015 and harvested in April, 2016. Plastic pots were filled with about 2.5 kg of soil with two replicates of every treatment and then labeled accordingly. 8 seeds were sown in each plastic pot. The treatments were: T-I (GWI), T-II (50% GWI+50% WWI), T-III (25% GWI+75% WWI), and T-IV (WWI). The positions of pots were also changed regularly to ensure suitable environmental conditions.

Sample Preparation. Seed samples were drawn from each pot after harvest. Samples of soil were collected from upper 3-5 cm soil profile. After drying in air, samples were oven-dried at 72°C for 4 days. Furthermore, the seed samples were powdered with grinder and digested following Allen *et al*. [13].

Digestion. Taking 15 ml mixture of H_2SO_4, HNO_3 and $HClO_4$ (1:5:1), 1 gram of both seed and soil samples were separately heated at 80°C to attain colorless solution. After cooling, the samples were filtered and finally 50 ml volume of each sample was maintained by addition of distilled water.

Determination of Metals and Metalloids. To analyze concentration of different metals (Co, Pb, Cu, Cd, Mn, Zn, Fe, and Cr) in digested samples, atomic absorption spectrophotometer was used. Calibration curve was drawn for each metal and metalloid.

Statistical Analysis. The data were statistically examined using software package SPSS 16. To assess soil-plant interaction, Pearson's correlation coefficient was calculated. One-way ANOVA was employed for obtained data of concentration of heavy metals in soil and wheat. The statistical analysis for grain and soil was carried at different probability levels of 0.001, 0.01, and 0.05 [14].

Daily Intake of Metals. DIM was computed according to Sajjad *et al*. [15]. The average body weight was taken as 55.9 kg and daily intake of metal in wheat as 0.318 kg/person/day respectively [16,17].

Enrichment Factor. Enrichment factor was calculated using Buat-Menard and Chesselet [18].

Health Risk Index. HRI was worked out by dividing daily metal intake value by its R_fD (oral reference dose) [19]. HRI value greater than 1 considered serious health risks for consumers [20].

Table 1-3 show tolerable daily intake limit, oral reference doses, and reference values of different heavy metals in soil and grain, respectively.

RESULTS

The results revealed that analysis of variance has non-significant effect ($p>0.05$) of treatments on

TABLE 5
Mean concentrations for physico-chemical characteristics of soil

Physico-chemical parameters	pH	EC (dS m^{-1})	OM (%)	Avail. P (mg kg^{-1})	Avail. K (mg kg^{-1})	Textural class
T-I	8.03±0.16	9.33±0.17	0.83±0.08	8.10±0.47	2.35±0.38	Loam
T-II	7.80±0.13	1.02±0.29	0.75±0.19	1.39±0.23	3.06±0.67	Loam
T-III	8.13±0.30	6.64±0.21	1.13±0.14	1.32±0.07	3.45±0.83	Loam
T-IV	7.80±0.50	1.12±0.74	1.27±0.12	1.62±0.03	3.61±0.16	Loam
Mean squares	0.085^{ns}	0.901^{ns}	1.935^{ns}	3.455^{***}	1.672^{**}	

*** = Level of significance at 0.001; ** = Level of significance at 0.01; ns= not-significant

TABLE 6
Mean concentration of heavy metals (mg kg^{-1}) in soil under study

Heavy metals	T-I	T-II	T-III	T-IV	PML[a] (mg kg^{-1})
Co	0.185±0.1	0.22±0.11	0.313±0.1	0.36±0.15	50
Cu	0.82±0.19	1.05±0.23	1.06±0.28	1.38±0.25	73.3
Zn	4.653±0.2	8.293±0.2	8.413±0.3	8.28±0.35	99.4
Pb	0.11±0.1	0.13±0.11	0.13±0.12	0.42±0.18	0.2[b]
Mn	0.81±0.09	1.17±0.12	1.43±0.16	1.82±0.25	500
Fe	0.72±0.23	1.38±0.31	1.65±0.36	2.64±0.34	425.5
Cr	0.54±0.1	0.63±0.22	0.58±0.25	0.78±0.16	2.3
Cd	1.55±0.19	1.67±0.28	1.68±0.21	1.73±0.26	0.2

Source: [a] FAO/WHO [26]; [b] FAO/WHO [32]; PML= Permissible Maximum Limit

TABLE 7
Mean concentration of heavy metals (mg kg^{-1}) in wheat grains

Heavy metals	T-I	T-II	T-III	T-IV	PML (mg kg^{-1})
Co	0.77±0.16	0.79±0.12	0.87±0.17	0.896±023	9.1[a]
Cu	0.83±0.2	1.32±0.18	1.38±0.15	1.50±0.21	8.39[b]
Zn	0.99±0.15	0.301±0.1	0.64±0.09	1.12±0.12	44.19[b]
Pb	0.331±0.1	0.408±0.14	0.43±0.16	0.79±0.19	350[c]
Mn	0.55±0.17	0.65±0.12	0.70±0.13	0.89±0.18	46.75[b]
Fe	3.13±0.27	3.66±0.2	2.97.±0.31	3.26±0.23	56.9[d]
Cr	1.29±0.19	1.33±0.16	1.35±0.11	1.36±0.14	9.07[b]
Cd	1.93±0.2	2.06±0.24	2.11±0.27	2.41±0.2	1.49[b]

Source: [a]VROM [30];[b] Singh *et al*. [28]; [c] MEPC [31]; [d]Dosumu *et al*. [29]; PML= Permissible Maximum Limit

Cu, Pb, Fe, Cd, Mn and Zn concentrations in the soil whereas significant effect on the concentrations of Cr and Co. A non-significant effect ($p>0.05$) of treatments on Cr, Pb, Cu and Zn concentrations while significant effect ($p<0.05$) was seen on concentrations of Mn, Fe, Cd and Co in wheat grains (Table 4).

Physico-chemical characteristics of soil. The texture of the soil used for growing wheat was loam. Soil of all treatments was found basic with pH ranging from 7.80-8.13. The mean concentration of EC (dS m^{-1}) in treatments I, II, III, and IV was 9.33, 1.02, 6.64, and 1.12 respectively, while that of organic matter (%) was 0.83, 0.75, 1.13, and 1.27, respectively. The range of available phosphorus and potassium (mg kg^{-1}) was 1.32-8.10 and 2.35-3.61, respectively (Table 5).

Metals and metalloids (mg kg^{-1}) in soil. The concentration of heavy metals in soil grown with wheat at T-I showed following order: Fe>Cd>Cr>Zn>Cu>Co>Mn>Pb. At T-II, the order of heavy metals concentration was observed as: Fe>Cd>Cr>Cu>Co>Mn>Pb>Zn. The trend of concentration of heavy metals recorded at T-III as: Fe>Cd>Cu>Cr>Co>Mn>Zn>Pb while decreasing order ofmetals concentration was seen at T-IV as: Fe>Cd>Cu>Cr>Zn>Co>Mn>Pb. Of all the treatments, the mean concentration of Fe in soil was highest (Table 6).

Metals and metalloids (mg kg^{-1}) in grains. Among four different treatments, the mean values of Zn and Cd was found to be highest in wheat grains. The decreasing trend of heavy metals concentration reported at T-I was: Zn>Cd>Mn> Cu>Fe>Cr>Co>Pb. The same sequence of metals and metalloids was observed at T-II and T-III while at T-IV, the metals and metalloids were seen as: Zn>Fe>Mn>Cd>Cu>Cr>Pb>Co (Table 7).

Correlation between soil and wheat grains. In present study, Co, Mn, and Cd showed positive significant correlation, whereas Zn and Fe observed negative non-significant correlation, while Cu, Pb and Cr exhibited positive non-significant correlation between soil and wheat grains (Table 8).

TABLE 8
Correlation between heavy metal concentrations in soil and wheat grains

Heavy metals	Soil-Grain
Co	0.908**
Cu	0.513
Zn	-0.193
Pb	0.009
Mn	0.762**
Fe	-0.213
Cr	0.444
Cd	0.647*

** = Level of significance at 0.01; * = Level of significance at 0.05

Daily Intake of Metals (DIM). At T-I, daily metal intake was of the following order: Zn>Cd>Mn>Cu>Fe>Cr>Co>Pb.At T-II almost similar trend was seen differing only in concentrations of Fe, Mn and Cu. Similar trend was observed at T-III and T-IV; observed order was: Zn>Cd>Fe>Mn>Cu>Cr>Co>Pb. Among four treatments, the highest DIM was found in the case of Zn(Table 9).

Enrichment Factor (EF). The highest enrichment factor in all the treatments was obtained for Cd and Zn while lowestEF was reported for Co. The decreasing order of EF at T-I and T-IV was seen as: Cd>Zn>Cr>Pb>Mn>Cu>Fe>Co while those at T-II and T-III as: Zn>Cd>Cr>Pb>Mn>Cu>Fe>Co (Table 10).

Health Risk Index (HRI). Among the examined metals, Cd showed the highest HRI value in all treatments during present study. The trend of HRI at T-I and T-II was the same as: Cd>Pb>Mn>Cu>Zn>Co>Fe>Cr. T-III followed the decreasing order of HRI of different metals as: Cd>Mn>Pb>Cu>Zn>Co>Fe>Cr. T-IV followed the order as: Cd>Pb>Mn>Cu>Zn>Co>Fe>Cr (Table 11).

TABLE 9
DIM of heavy metals via intake of crop

Treatments	Co	Cu	Zn	Pb	Mn	Fe	Cr	Cd
I	0.0011	0.0046	0.0265	0.0006	0.0047	0.0041	0.0030	0.0088
II	0.0013	0.0059	0.0472	0.0007	0.0067	0.0079	0.0036	0.0095
III	0.0018	0.0063	0.0479	0.0008	0.0082	0.0094	0.0033	0.0096
IV	0.0021	0.0079	0.0471	0.0024	0.0103	0.0150	0.0045	0.0098

TABLE 10
Enrichment factor for heavy metals in edible parts of crop

Treatments	Co	Cu	Zn	Pb	Mn	Fe	Cr	Cd
I	0.02513	0.11308	2.23548	0.9028	0.13755	0.03076	1.65751	5.9831
II	0.02911	0.09105	12.4453	0.86561	0.16812	0.05042	1.86795	6.0396
III	0.03763	0.08792	5.93787	0.82132	0.1908	0.07429	1.69424	5.9317
IV	0.04203	0.1083	3.335	1.4443	0.191	0.10504	2.262	5.348

TABLE 11
HRI of heavy metals via intake of crop

Treatments	Co	Cu	Zn	Pb	Mn	Fe	Cr	Cd
I	0.027	0.126	0.078	0.194	0.153	0.006	0.002	9.572
II	0.032	0.162	0.138	0.226	0.219	0.012	0.003	10.35
III	0.045	0.164	0.140	0.226	0.268	0.015	0.004	10.36
IV	0.053	0.213	0.138	0.732	0.339	0.023	0.003	10.64

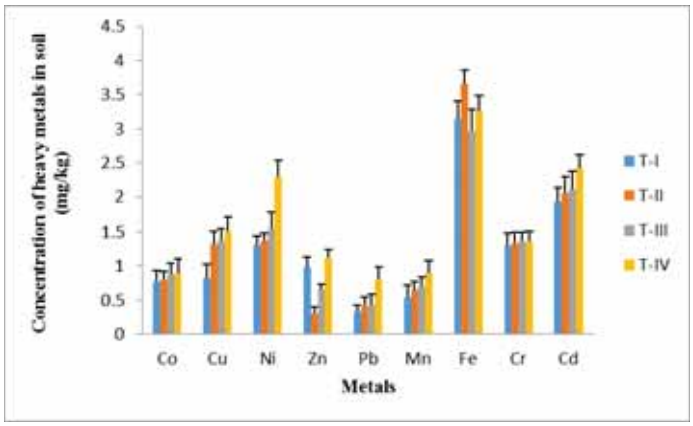


FIGURE 1
The variation of heavy metal concentration in soil

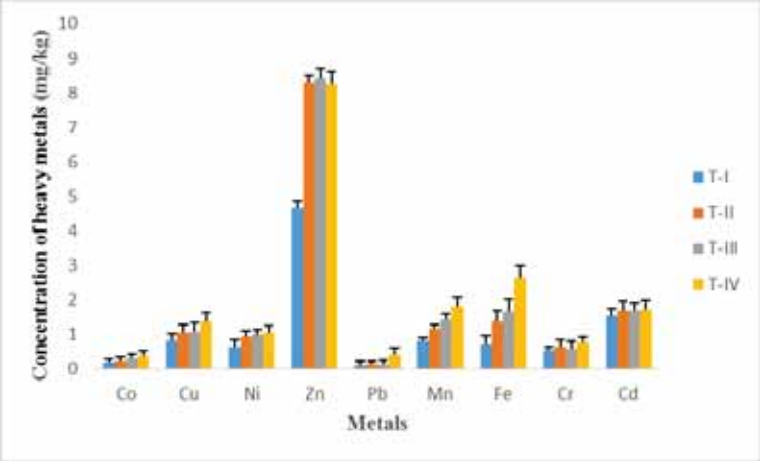


FIGURE 2
The variation of heavy metal concentration in grains of *T. aestivum*

DISCUSSION

When pH is usually higher than 6.5, metals are less likely to be available to the plants [33]. The activity of the soil microorganisms is affected due to the high amount of salts accumulated in the upper soil layers [34]. Soil salinity is measured in terms of electrical conductivity. Salakinkop and Hunshal [35] reported lower value of pH but higher value of EC as compared to the current findings. The organic matter (OM) contents of the soil frequently increased with the increasing application of wastewater. OM can be an important source of providing carriers for some heavy metals (Ni, Cu, Zn and others) in the soil [36].

All heavy metals were considerably higher in wastewater irrigated soil in comparison to all other treatments in current study. Yadav *et al*. [37] observed higher values of Fe and Mn but lower concentrations of Cu and Pb. In soil, the mean metal concentrations except cadmium were within the standard limits delineated by different public health organizations. Continuous use of wastewater might be the major cause of increasing concentration of toxic metals in soil as reported by other researchers [38].

The observed value of cobalt in wheat grains in current study was lower than the recommended limit of FAO/WHO [26]. Present Co concentration was almost similar to Tegegne [39].The copper concentration observed by Yu *et al*. [40] was much higher than the present values. An early finding of Feizi and Rastghalam [41] was much higher than current investigation in case of Cu. The present observed value of Zn in wheat was higher as compared to Pang *et al*. [42].Current work showed lower values of lead from the reported value of Han [43] but it was in accordance with Zhang [44] and Li *et al*. [4]. Concentration of manganese reported by Karatas *et al*. [45] was higher than present investigation. Current value was also higher than the findings of Al-Othman *et al*. [46]. Lower concentration of Fe and Cd was analyzed in current research in comparison to the observations of Kahlown *et al*. [47].Khan *et al*. [48] observed very high value of Fe as compared to the current value. The value of chromium observed in the present research was lower by the value of Han and Ma [49]. The values of Cr and Cd analyzed by Wang *et al*. [50] were higher than the analyzed values. The Cd concentration in wheat was also higher than the standard values given by FAO/WHO [26].

Pearson's correlation was used in order to analyze relationship of various elements between soil and plant. Except Zn and Pb, all other metals had positive correlation level among soil and grains depicting the absorption of metals.

The present DIM values of every treatment were below the tolerable daily intake (TDI), suggesting no human health risks. This finding was similar to Radwan and Salama [51].

If EF is greater than 1, it allows more bioavailability of metals in the soil using wastewater irrigation [52]. The current EF values were lower than the values of Fytianos *et al*. [53].

Metal concentrations in the cereal crops (like rice and wheat) are comparatively less than vegetables suggesting larger proportion of cereals in daily human diet [28]. HRI was worked out to evaluate subsequent risk from heavy metals contaminated crops grown on sewage irrigated soil. Current values displayed no such sign except for Cd which had HRI>1.

CONCLUSION

The current findings concluded that continuous wastewater irrigation causes toxic heavy metals to accumulate in the edible parts of crop. Except cadmium, all the metals in the wheat grains were found within respective permissible limits. The examined DIM values of different metals and metalloids were

within tolerable daily intake limits. Health Risk Index value of Cd was above 1, suggesting serious health risks to the consumers. The increasing population might be the reason of increasing heavy metal concentration in the domestic wastewater to manifold. Therefore, treated wastewater should be used for irrigating agricultural crops. Various remediation techniques can be applied to avoid heavy metal contamination of soil to some extent like engineering remediation and bioremediation etc.

ACKNOWLEDGEMENT

The Higher Education Commission, Pakistan is acknowledged for providing the financial support through the research project # 20-3546/NRPU/R&D/14/536 to the fourth author. The author thanks all the supporters of this project and the referees for their constructive comments.

REFERENCES

[1] Rattan, R.K., Datta, S.P., Chhonkar, P.K., Suribabu, K. and Singh., A.K. (2005) Long-term impact of irrigation with sewage effluents on heavy metal content in soils, crops and groundwater-A case study. Agriculture, Ecosystems and Environment. 109(3), 310-322.

[2] Mapanda, F., Mangwayana, E.N., Nyamangara,J. and Giller, K.E. (2005) The effect of long-term irrigation using wastewater on heavy metal contents of soils under vegetables in Harare, Zimbabwe. Agriculture, Ecosystems and Environment. 107(2): 151-165.

[3] Rothenberg, S.E., Du, X., Zhu,Y.G. and Jay, J.A. (2007) The impact of sewage irrigation on the uptake of mercury in corn plants (Zea mays) from suburban Beijing. Environmental Pollution. 149(2), 246-251.

[4] Liu, H., Probst, A. and Liao, B. (2005) Metal contamination of soils and crops affected by the Chenzhou lead/zinc mine spill (Hunan, China). Science of the Total Environment. 339, 153-166.

[5] Vaca-Paulin, R., Esteller-Alberich, M.V., Lugo-de la Fuente, J. and Zavaleta-Mancera, H.A. (2006) Effect of sewage sludge or compost on the sorption and distribution of copper and cadmium in soil. Waste Management. 26(1), 71-81.

[6] Yusufa, A.A., Arowolo, T.A. and Bamgboseb, O. (2003) Cadmium, copper and nickel levels in vegetables from industrial and residential areas of Lagos city, Nigeria. Food and Chemical Toxicology. 41(3), 375-78.

[7] Pereira, B.F., He, Z.L., Silva, M.S., Herpin, U., Nogueira, S.F., Montes, C.R. and Melfi, A.J. (2011) Reclaimed wastewater: Impact on soil-plant system under tropical conditions. Journal of Hazardous Materials. 192(1), 54-61.

[8] Gwenzi, W. and Munondo,R. (2008) Long-term impacts of pasture irrigation with treated sewage effluent on nutrient status of a sandy soil in Zimbabwe. Nutrient Cycling in Agroecosystems. 82(2), 197-207.

[9] Baddesha, H.S., Rao, D.L.N., Abrol, I.P. and Chhabra, R. (1986) Irrigation and nutrient potential of raw sewage waters of Haryana. Indian Journal of Agricultural Sciences. 56(8), 584.

[10] Marcussen, H., Holm, P.E., Strobel, B.W. and Hansen, H.C.B.. (2009). Nickel sorption to goethite and montmorillonite in presence of citrate. Environmental Science and Technology. 43, 1122-1127.

[11] Smith, C.J., Hopmans, P. and Cook,F.J. (1996) Accumulation of Cr, Pb, Cu, Ni, Zn, and Cd in soil following irrigation with treated urban effluent in Australia. Environmental Pollution. 94, 317.

[12] PARC. Pakistan Agricultural Research Council. (1989) Wheat Research and Development in Pakistan, Islamabad.

[13] Allen, S., Grimshaw, H. and Rowland, A. (1986) Chemical analysis, Moore PD, Chapman SB, Methods in Plant Ecology, Blackwell Scientific Publications, Oxford. pp. 285-344.

[14] Steel, R.G.D and Torrie, J.H. (1980) Principles and procedures of statistics. A Biometrical Approach, 2. McGraw-Hill, New York.

[15] Sajjad, K., Farooq, R., Shahbaz, S., Khan, M.A. and Sadique, M. (2009) Health risk assessment of heavy metals for population via consumption of vegetables. World Applied Science Journal. 6(12), 1602-1606.

[16] Wang, X., Sato, T., Xing, B. and Tao, S. (2005) Health risks of heavy metals to the general public in Tianjin, China via consumption of vegetables and fish. Science of the TotalEnvironment. 350, 28-37.

[17] Ge, K.Y. (1992)The status of nutrient and metal of Chinese in the 1990s. Beijing People's Hygiene Press. pp. 415–434.

[18] Buat-Menard, P. and Chesselet. R. (1979) Variable influence of the atmospheric flux on the trace metal chemistry of oceanic suspended matter. Earth and Planetary Science Letters. 42(3), 399–411.

[19] Cui, Y.J., Zhu, Y.G., Zhai,R. H.,Chen, D.Y., Huang, Y.Z., Qiu,Y. and Liang,J.Z. (2004) Transfer of metals from soil to vegetables in an area neara smelter in Nanning, China. Environment International. 30(6), 785-791.

[20] USEPA. US Environmental Protection Agency. (2002) Region 9. Preliminary Remediation Goals.

[21] Food and Nutrition Board. (2004) Dietary Reference Intakes [DRIs]: Recommended Intakes for Individuals. National Academy of Sciences, Washington, DC, USA.
[22] FAO/WHO. (2007) Joint FAO/WHO Food Standard Programme Codex Alimentarius Commission 13th Session. Report of the Thirty Eight Session of the Codex Committee on Food Hygiene, Houston, United States of America, ALINORM 07/ 30/13.
[23] FAO/WHO. (1994) Joint FAO/WHO Food Standard Programme. Codex Alimentarius Commission. 24th Session of Codex Committee on Food Additives and Contaminants. 2-7 July. Geneva Switzerland.
[24] USEPA (2010) Risk-based Concentration Table. United State Environmental Protection Agency, Washington, DC.
[25] WHO. (1996) Permissible limits of heavy metals in soil and plants (Geneva: World Health Organization), Switzerland.
[26] FAO/WHO. (2001) Report on the 32nd Session of the Codex Committee on Food Additives and Contaminants ALINORM 01/12, Beijing. China.20-24 March 2000.
[27] Shad, H.A., Ahmad, K., Khan, Z.I., Rizwan, Y., Tahir, H.M., Noorka, I.R., Dogar, M.Z.H., Zafar, A. and Zill-e-Huma. (2014) Comparative study of macro elements accumulated in different wheat varieties, irrigated with domestic sewage water. Agric. appl. Sci. 6, 48–56.
[28] Singh, A., Sharma, R.K., Agrawal, M. and Marshall, F.M. (2010) Health risk assessment of heavy metals via dietary intake of foodstuffs from the wastewater irrigated site of a dry tropical area of India. Food and Chemical Toxicology. 48(2), 611-619.
[29] Dosumu, O.O., Abdus-Salam, N., Oguntoye, S. and Afdekale, F.A. (2005) Trace metals bioaccumulation by some Nigerian vegetables. Centrepoint. 13,: 23-32.
[30] VROM. (2000) Circular on target values for soil remediation. Annex A, Dutch Ministry of Housing Spatial Planning and Environment (VROM). The Hague, The Netherlands.
[31] MEPC. (1995) GB15618, Soil Environmental Quality Standards in China. Beijing, RPC: Ministry of Environmental Protection of China.
[32] FAO/WHO. (1984) Codex Alimentarius Commission on contaminants. Joint FAO/WHO Expert Committee for Food Additives (JECFA)
[33] Harrison, P. and Waites, G. (1998) The Cassell Dictionary of Chemistry, Cassell, London.
[34] Garcia, C. and Hernandez, I. (1996) Influence of salinity on the biological and biochemical activity of a calciorthird soil. Plant Soil. 178(2), 255-263.
[35] Salakinkop, S.R. and Hunshal, C.S. (2014) Domestic sewage irrigation on dynamics of nutrients and heavy metals in soil and wheat (*Triticum aestivum* L.) production. International Journal of Recycling of Organic Waste in Agriculture. 3(3), 1-11.
[36] Lin, C., Negev, I., Eshel, G. and Banin, A. (2008) In situ accumulation of copper, chromium, nickel, and zinc in soils used for long-term wastewater reclamation. Journal of Environmental Quality. 37, 1477-1487.
[37] Yadav, A., Yadav, P.K., Srivastava, S., Singh, P.K., Srivastava, V. and Shukla, D.N. (2014) Profitability and health risk estimation of rice cultivation under wastewater irrigation from natural drainage. International Journal of Science and Research Publications. 4(3).
[38] Ghosh, A.K., Bhatt, M.A. and Agrawal, H.P. (2012) Effect of long-term application of treated sewage water on heavy metal accumulation in vegetables grown in northern India.Environmental Monitoring and Assessment. 184(2), 1025-1036.
[39] Tegegne, W.A. (2015) Assessment of some heavy metals concentration in selected cereals collected from local markets of Ambo City, Ethiopia. Journal of Cereals and Oilseeds. 6(2), 8-13.
[40] Yu, X., Wang, Z., Lynn, A., Cai, J., Huangfu, Y., Geng, Y., Tang, J. and Zeng, X. (2016) Heavy metals in wheat grown in sewage irrigation: A distribution and prediction model. Polish Journal of Environmental Studies. 25(1), 413-418.
[41] Feizi, M and Rastghalam, Z.S. (2012) The effect of treated wastewater irrigation on accumulation of heavy metals in selected plants. The Ist International and The 4th National Congress on Recycling of Organic Waste in Agriculture.
[42] Pang, Y., Tong, Y.A., Liang, L.Y., Ji, P.H. and Tang, X.W. (2015) Assessment of heavy metal pollution in soil-crop system on sewage irrigated farmland. Transactions of the Chinese Society for Agricultural Machinery. 4, 148-154.
[43] Han, B. (2000) Study on the influence of sewage irrigation on yield of Baiyin environmental quality of farmland and wheat. Gansu Agricultural Science and Technology. 6, 46-47.
[44] Zhang, N.M and Li,Y.H. (2005) Study on the absorption and accumulation characteristics of sewage irrigation area soil crop system on three kinds of heavy metals. In: The First National Symposium on Agricultural Environmental Sciences. Changsha, China. China Agricultural Ecological Environment Protection Association.

[45] Karatas, M., Dursun, S., Guler, E., Ozdemir, C. and Argun, M.E. (2006) Heavy metal accumulation in wheat plants irrigated by wastewater. Cellulose Chemistry and Technology. 40(7), 575-579.
[46] Al-Othman, Z.A., Ali, R., Al-Othman, A.M., Ali, J. and Habiba, M.A. (2013) Assessment of toxic metals in wheat crops grown on selected soils, irrigated by different water sources. Arabian Journal of Chemistry.1-8.
[47] Kahlown, D.M.A., Ashraf, D.M., Hussain, D.M., Salam, H.A. and Bhatti, A.Z. (2006) Impact assessment of sewerage and industrial effluents on water resources, soil, crops and human health in Faisalabad. PCRWR, Islamabad.
[48] Khan, Z.I., Ahmad, K., Ashraf, M., Akram, N.A., Rizwan, Y., Shaheen M., and Arshad, F. (2013) Assessment of potential toxicological risk for public health of heavy metals in wheat crop irrigated with wastewater: A case study in Sargodha, Pakistan. Asian Journal of Chemistry. 25(17), 9704-9706.
[49] Han, J.X and Ma, J.H. (2004) Polluting, transferring and accumulating of heavy metals in soil-wheat system in sewage irrigation region: A case study in Huafei river in Kaifeng. Ecology and Environment. 13(4), 578-580.
[50] Wang, Z., Zeng, X., Geng, M., Chen, C., Cai, J., Yu, X., Hou, Y. and Zhang, H. (2015) Health risks of heavy metals uptake by crops grown in a sewage irrigation area in China. Polish Journal of Environmental Studies. 24(3), 1379-1386.
[51] Radwan, M.A and Salama, A.K. (2006) Market based survey for some heavy metals in Egyptian fruits and vegetables. Food and Chemical Toxicology. 44(8), 1273-1278.
[52] Kisku, G.C., Barman, S.C. and Bhargav, S.K. (2000) Contamination of soil and plants with potentially toxic elements irrigated with mixed industrial effluent and its impact on the environment. Water, Air and Soil Pollution. 120, 121-137.
[53] Fytianos, K., Katsianis, G., Triantafyllou, P. and Zachariadis, G. (2001) Accumulation of heavy metals in vegetables grown in an industrial area in relation to soil. Bulletin of Environmental Contamination and Toxicology. 67(3), 423-430.

Received: **09.10.2016**
Accepted: **09.04.2017**

CORRESPONDING AUTHOR

Zafar Iqbal Khan
Department of Botany, University of Sargodha, Sargodha, Pakistan

e-mail: zikhan11@gmail.com

© by PSP Volume 26 – No. 12A/2017 pages 7651-7657 Fresenius Environmental Bulletin

UNNOTICED MICROORGANISMS IN DISINFECTION OF SWIMMING POOLS: FREE- LIVING AMOEBA.

Zuhal Zeybek[1], Busra Demir[2], Miray Ustunturk-Onan[1,*]

[1]Istanbul University Faculty of Science, Department of Biology, Fundamental and Industrial Microbiology, Istanbul, Turkey.
[2]Istanbul University Science Institute, Istanbul, Turkey.

ABSTRACT

The presence of free-living amoebae (FLA) in swimming pools has become an issue of increasing concern in recent years on account of their pathogenicity and their capacity to host other microorganisms. Effective disinfection doses for neutralizing bacteria in swimming pools are specified in the guideline (15.11.2011) put out by the Turkish Ministry of Health; however, this guideline does include any information about FLA. This study aims, therefore, to investigate the effect of different concentrations (1, 3, 5 mg/L) and contact times (0, 30, 240 minutes) of NaClO against trophozoites of FLA isolated from swimming pool waters in Turkey. Experiments were conducted using the most probable number (MPN) method. Maximum log reductions were determined to be 1.764, 2.165, and 3.388 for 1, 3, and 5 mg/L of NaClO, respectively, at 240 minutes of contact time. *A. castellanii* (ATCC 50373) cysts showed little log reduction (0.017) against 5 mg/L of NaClO, which has a cytotoxic effect against 3T3 cells. Thus, we recommend that new disinfection strategies be developed to try to control the presence of FLA in swimming pools.

KEYWORDS:
Swimming pool, free- living amoeba, Acanthamoeba, NaClO, disinfection.

INTRODUCTION

Although used for sport and leisure, swimming pools contain various microorganisms, including pathogenic ones, such as bacteria, viruses, fungi and protozoa, which can threaten the health of swimmers. *Escherichia coli, Pseudomonas aeruginosa, Salmonella sp., Shigella sp., Staphylococcus sp., Mycobacterium sp.,* and *Legionella sp.*are the most common bacterial pathogens in such aquatic environments. Other less common pathogens potentially found in these environments include *Giardia sp., Cryptosporidium sp. ,* and free-living amoebae (FLA) [1, 2, 3].

FLA are a heterogeneous group of protozoa found in natural environments, such as water and soils, with *Acanthamoeba*, *Hartmannella* and *Naegleria* being the most common genera, and others, like *Balamuthia, Vahlkampfia, Willaertia* and *Nuclearia*, detected more rarely in these environments. Most FLA can exist in two forms, a vegetative trophozoite one, able to feed, move and divide, and an inactive dormant cyst form [4, 5]. Some FLA are pathogenic for humans and responsible for keratitis. Some FLA cause infections of the central nervous system such as granulomatous amoebic encephalitis (GAE), a fatal disease [6, 7, 8] often in immunocompromised patients.

Furthermore, FLA have been described as reservoirs for several pathogenic bacteria, such as coliform bacteria, *Legionella*, *Mycobacterium* and *Chlamydia*. Although FLA actually ingest bacteria through phagocytosis, some bacteria are able to resist amoebal phagocytosis and consequently survive within FLA. Moreover, these bacteria become resistant to disinfectants and can lyse their host and spread through the aquatic environments. Recently, FLA have been described as by-passes, due to their ability to protect bacteria from water treatments. [9, 10, 11, 12, 13]. It is therefore important that effective disinfection methods for FLA in man-made water systems, such as swimming pools, are employed to protect human health.

The most common means of providing protection in swimming pool waters is the use of chlorine residual. The use of effective levels of chlorine concentration for the disinfection of swimming pools results in the death of free floating pathogenic bacteria, but these levels may not have the same effect on FLA [14, 15]. So, it is necessary to know the effective concentration of chlorine against FLA in order to eliminate both pathogenic FLA and their intracellular bacteria.

In Turkey, the water qualities considered to be healthy for swimming pools are indicated in a guideline issued (15.11.2011) by the Ministry of Health.. However, the current guideline fails to include any mention of FLA, despite the risks they present on account of their pathogenicity and capacity to host bacteria. For this reason, this study has aimed to investigate the effects of different concentrations and contact times of NaClO against FLA in order that preventative measures might be formulated.

MATERIALS AND METHODS

The disinfection effects of NaClO against FLA at different concentrations (1, 3, 5 mg/L) and contact times (0, 30, 240 min) were investigated in this study.

Preparation of disinfectant. The disinfectant, NaClO (Fastchlor), commonly used for the disinfection of swimming pools, was used in the experiments. After chlorine solutions were freshly prepared, the DPD method was applied immediately before each of the experiments to measure the 1 and 3 mg/L free chlorine concentration values, while a chlorine measurement kit (Norateks) was used to measure the 5 mg/L disinfectant. A 0.1M sterile solution of sodium thiosulfate (Merck) was used as neutralizer.

Amoeba strains. One standard strain of *Acanthamoeba castellanii* (*A. castellanii*) ATCC 50373 and four environmental *Acanthamoeba* strains (A10, A13, A14, A20) were used for the study. These environmental amoeba strains were isolated and selected from different swimming pools in Istanbul in a previous study [16].

All strains were thawed from -86 ºC before experiments and were re-grown on non-nutrient agar (NNA) spread with a dense suspension of heat- inactivated *Escherichia coli* (*E.coli*) ATCC 8739, which was prepared in Page saline. All NNA Petri dishes were incubated at 28 ºC and routinely examined with inverted microscope (x 100) until FLAs were able to be observed.

Get the trophozoites of amoeba cells. The amoeba cells were grown in an axenic culture on 75 cm^2 tissue culture flasks which contained 30 mL of protease peptone-yeast extract glucose (PYG) broth supplemented with 100 µg/mL Penicilline G and 100 µg/mL Streptomycine, and then incubated at 30 ºC for 3-7 days. After incubation, the PYG medium was replaced with Page's Amoeba Saline (PAS), and flasks were shaken vigorously to detach trophozoites adhering to the base of the flasks. Next, these trophozoite suspensions were transferred to a sterilized centrifuge tube. The number of viable trophozoites were adjusted to 10^6 cells/mL using a hemocytometer and the trypan blue method. Trophozoite suspensions were freshly prepared prior to conduct the experiments.

Get the cysts of amoeba cells. Cysts were produced from the culture of trophozoites. Mature cysts of each of the strains were obtained from cultures that had been aged in flasks for up to 6 weeks at 30 ºC. After incubation, cysts were directly transferred to a sterilized centrifuge tube and centrifuged at 3000 rpm for 10 min. The supernatant was removed, and the pellet was washed twice (3000 rpm for 5 min) by resuspension in PAS. After a final wash, the cysts were resuspended in PAS and viable cyst numbers were adjusted to a final concentration of 10^6 cells/mL using a hemocytometer and the trypan blue method. Cyst suspensions were used within 2 days.

Antiamoebal Activity Assay. For investigation of the effect of NaClO against amoeba cells, the most probable number enumeration technique described by Beattie et al. [17] was carried out. As can be seen the Figure 1, aliquots (0.1 mL) of trophozoite or cyst suspensions were added to three different sterile tubes, each containing 9.9 mL of NaClO solutions (1, 3, 5 mg/L), and to the control solution (PAS). The tubes were incubated at room temperature throughout tested contact time (0, 30, 240 min). At the end of each contact time, the tubes were vigorously shaken, and 1 mL aliquots were removed from test tubes and control solution. Aliquots taken from test tubes were placed in 9 mL of sodium thiosulfate (1:10 dilution) and permitted to stand for 15 min at room temperature for disinfectant neutralization. Aliquots taken from control tubes were placed in 9 mL of PAS. A 1-in-100 dilution was prepared in PAS from these 1-in-10 dilutions, and from these dilutions, five aliquots, each of which were of 1, 0.1, and 0.01 mL, were inoculated onto NNA plates seeded with heat-killed E. coli ATCC 8739. Flat-bottom 6-well tissue-culture plates were used for inoculation of 1 mL aliquots, and flat-bottom 12-well tissue-culture plates were used for inoculation of 0.1 mL and 0.01 mL aliquots. All plates were incubated at 30 ºC for 14 days.

Amoebic growth in each well was scored as 1, while no growth was scored as 0. Thus, the score for each of the 10-fold dilutions (i.e. 1, 0.1, and 0.01 mL) yielded one 3-digit number value. This number was entered into the most probable number (MPN) table to generate the MPN of amoebae per milliliter of each chlorine concentration, or control solution, at each time interval. Additionally, five 1-mL aliquots of the 1-in-10 dilution prepared in sodium thiosulfate were inoculated onto 90-mm Petri dishes containing NNA seeded with heat-killed *E. coli*. These plates were checked to ensure that there was no amoebic growth in the aliquots taken from the 1-in-100 dilution.

All experiments were done in triplicate. The average log reductions were calculated using the MPN of trophozoites or cysts per mL of chlorine concentration at the designated time points. The following formula was used to calculate the log reductions:

Log (viable cell at 0) – log (viable count at each time interval)

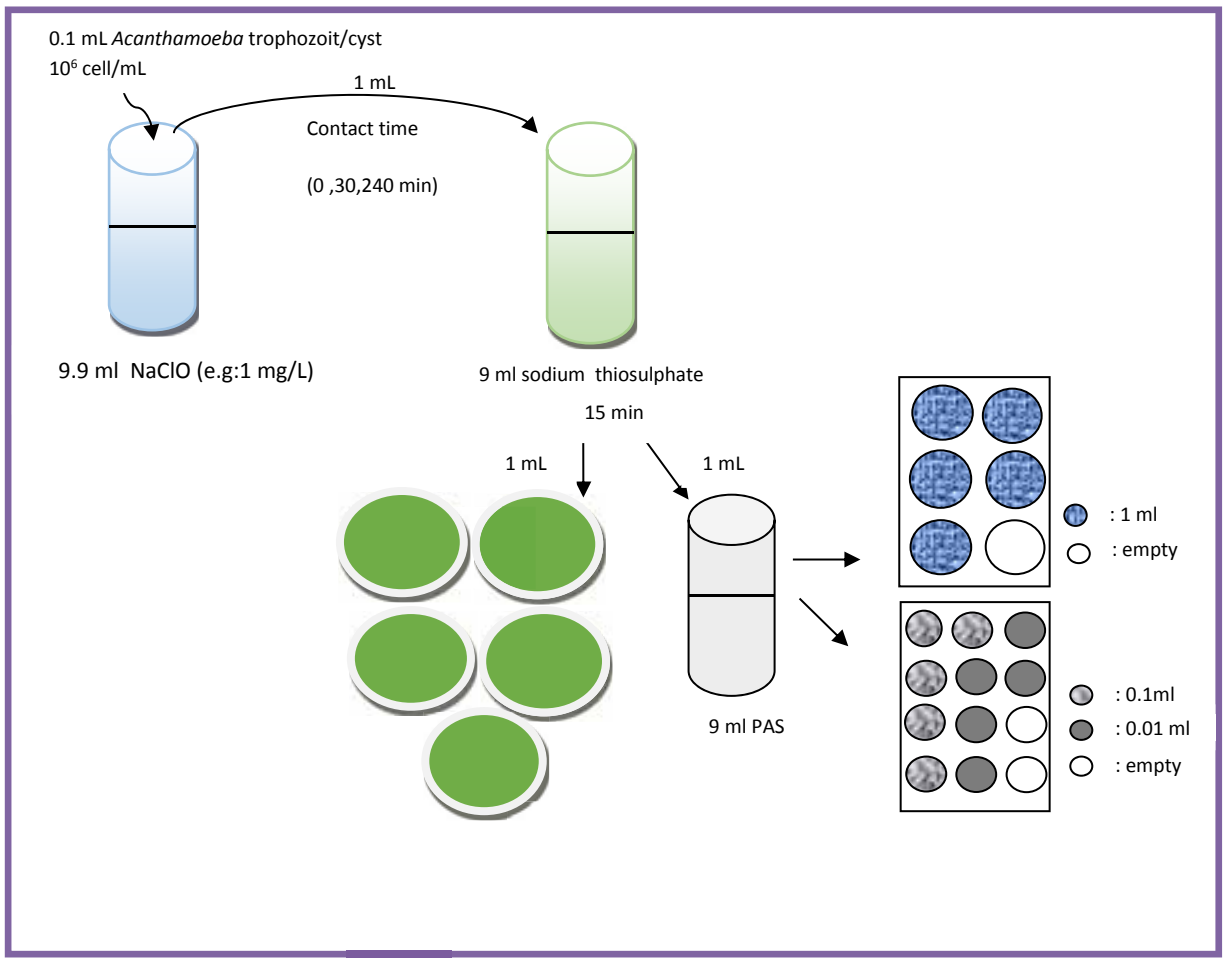


FIGURE 1
Antiamoebal Activity Assay

TABLE 1
The effect of 1 mg/L of NaClO against tested FLA strains.

Contact time (minute)	ATCC 50373 cyst		ATCC 50373 trophozoite		A10 trophozoite		A13 trophozoite		A14 trophozoite		A20 trophozoite	
	Avg. Log $_{10}$ counts	Log reductions	Avg. Log $_{10}$ counts	Log reductions	Avg. Log $_{10}$ counts	Log reductions	Avg. Log $_{10}$ counts	Log reductions	Avg. Log $_{10}$ counts	Log reductions	Avg. Log $_{10}$ counts	Log reductions
0	4.255	0	4.156	0.099	4.156	0.099	4.156	0.099	3.576	0.679	4.255	0
30	4.255	0	3.87	0.198	3.477	0.778	3.644	0.611	3.088	1.167	3.545	0.710
240	4.255	0	4.057	0.385	3.477	0.778	3.025	1.23	2.549	1.706	2.491	1.764

Cytotoxicity assay. An MTT assay was used to investigate whether different concentrations of NaClO (1, 3, 5 mg/L) generated cell proliferation on 3T3 cells (embryonic rat fibroblast) at 30 and 240 minutes [18, 19]. Statistical significance was determined by Student's *t* test. The *p*-Values <0.05 were considered significant.

RESULTS

Evaluation of Antiamoebal Activity of 1mg/L of NaClO. The effect of 1mg/L of NaClO against tested Acanthamoeba strains is shown in Table 1. Also presented in Table 1 are the average $\log_{10}$ counts of amoeba cells at the start of the experiment

TABLE 2
The effect of 3 mg/L of NaClO against tested FLA strains.

Contact time (minute)	ATCC 50373 cyst		ATCC 50373 trophozoite		A10 trophozoite		A13 trophozoite		A14 trophozoite		A20 trophozoite	
	Avg. Log $_{10}$ counts	Log reductions	Avg. Log $_{10}$ counts	Log reductions	Avg. Log $_{10}$ counts	Log reductions	Avg. Log $_{10}$ counts	Log reductions	Avg. Log $_{10}$ counts	Log reductions	Avg. Log $_{10}$ counts	Log reductions
0	4.255	0	3.985	0.27	3.465	0.79	3.647	0.608	3.045	1.21	3.729	0.526
30	4.255	0	3.606	0.649	2.869	1,386	2.300	1.955	2.549	1.706	2.771	1.484
240	4.255	0	2.245	2.01	2.207	2.048	2.173	2.082	2.299	1.956	2.090	2.165

TABLE 3
The effect of 5 mg/L of NaClO against tested FLA strains.

Contact time (minute)	ATCC 50373 cyst		ATCC 50373 trophozoite		A10 trophozoite		A13 trophozoite		A14 trophozoite		A20 trophozoite	
	Avg. Log $_{10}$ counts	Log reductions	Avg. Log $_{10}$ counts	Log reductions	Avg. Log $_{10}$ counts	Log reductions	Avg. Log $_{10}$ counts	Log reductions	Avg. Log $_{10}$ counts	Log reductions	Avg. Log $_{10}$ counts	Log reductions
0	4.255	0	3.572	0.683	2.427	1.828	2.299	1.956	2.489	1.766	3.507	0.748
30	4.255	0	2.546	1.709	2.084	2.171	1.796	2.459	1.866	2.389	2.204	2.051
240	4.255	0.017	1.401	2.854	1.698	2.557	0.867	3.388	0.867	3.388	1.812	2.443

(0 min) and after each contact time (30, 240 min), as well as the average log reduction for trophozoites and cysts after each contact time. Although this dose of free chlorine did not affect *A. castellanii* (ATCC 50373) cysts, it did cause a significant decrease, at various rates, in the number of trophozoite cells of both *A. castellanii* (ATCC 50373) and other tested environmental isolates. Maximum log reduction (1.764) was detected against trophozoites of the A20 strain after 240 minutes of contact time.

Evaluation of Antiamoebal Activity of 3 mg/L of NaClO. The effect of 3mg/L of NaClO against tested Acanthamoeba strains is shown in Table 2. A concentration of 3 mg/L of free chlorine did not inhibit *A. castellanii* (ATCC 50373) cysts, yet it did cause a decrease, at various rates, of trophozoite cell numbers of both *A..castellanii* (ATCC 50373) and other tested environmental isolates. Maximum log reduction (2.165) was detected against trophozoites of the A20 strain after 240 minutes of contact time.

Evaluation of Antiamoebal Activity of 5 mg/L of NaClO. The effect of 5mg/L of NaClO against tested Acanthamoeba strains is shown in Table 3. Unlike other free chlorine doses used in the experiments, the 5mg/L of free chlorine concentration led to a slight decrease (0.017) in log reduction on *A. castellanii* (ATCC 50373) cysts. On the other hand, the trophozoite form of all tested strains were generally inhibited much more with 5 mg/L of free chlorine concentration than with 3 mg/L of free chlorine concentration. Maximum log reduction (3.388) was detected against trophozoites of A13 and A14 strains.

From these results (Tables 1, 2, 3), it can be clearly seen that as free chlorine concentrations and contact times increased, the number of viable tested strains decreased.

When the effects of 1 and 3 mg/L of NaClO on 3T3 cell proliferation were investigated, it was found that none of these chlorine concentrations caused significant decrease of 3T3 cell proliferation at contact times of 30 and 240 minutes ($p > 0.05$). However, the highest dose used in the experiment, 5 mg/L of NaClO, was observed to significantly inhibit proliferation of these cells at an exposure time of 30 minutes ($p < 0.05$).

DISCUSSION

As swimming pools can harbor a wide variety of pathogenic microorganisms, their disinfection is very important. Chlorination is the predominant disinfection method applied in this type of aquatic environment. The guideline (15.11.2011) issued by the Ministry of Health in Turkey (http://www.resmigazete.gov.tr/eskiler/2011/12/20111215-13.htm) indicates that a free chlorine concentration of 0.3- 0.6 mg/L is necessary for swimming pools. This guideline also suggests limits on the number of indicator bacteria, such as total bacteria, total coliform bacteria, *Escherichia coli*, and *Pseudomonas aeruginosa*, but fails to include any information about FLA. Though a largely unnoticed microorganism, FLA could pose serious health threats due to both their pathogenicity and their capacity to host other pathogens. As they passes through water, FLA can cause rapidly progressing diseases, such as the fatal granulomatous amebic encephalitis (GAE), as well as amebic keratitis (AK), cutaneous lesions and sinusitis in swimmers. Moreover, FLA harboring bacteria can protect them from the effecst of biocides in swimming pools, even enabling these bacteria to grow more resistant to the biocides by harboring FLA [11, 6, 12]. Considering these risks, the control and elimination of FLA in swimming pools is necessary for the protection of public health.

The presence of FLA in swimming pools has been known for many years, with scientific research around the world being conducted to discover ways to eliminate them [20, 21]. However, this is the first study on this subject to be conducted in Turkey. In the study, the minimum inhibitor effect against tested strains was detected to be 1mg/l free chlorine, and the maximum log reduction was determined to be 1.764 against strain A20 (but not all), at a maximum exposure time of 240 minutes (Table 1). As this chlorine concentration is clearly higher than the chlorine concentration (0.3-0.6 mg/L) indicated in the guideline issued (15.11.2011) by the Ministry of Health in Turkey, the 1 mg/L of free chlorine concentration is believed to be insufficient for the elimination of FLA in swimming pool water. Similarly, Mogoa et al. found that free chlorine concentrations of 1 or 2 mg/L had no significant effect on the cultivability of *Acanthamoeba castellanii* (ATCC 30234) [22]. Critchley and Bentham observed that trophozoites of Acanthamoeba sp. were inhibited by a chlorine concentration of 1 mg/L but with an exposure time of 8 hours [23].

Disinfection can be defined as the killing of a large portion (but not necessarily all) of potential pathogenic organisms. As shown in Table 2, all tested amoeba trophozoites showed much more log reduction against 3 mg/L of free chlorine than against 1 mg/L at the same contact times, but none of them caused 3 log reduction. The most effective free chlorine concentration was 5 mg/L (Table 3). Two of the tested trophozoite strains (A13, A14) showed 3 log reduction at this dose. *A. castellanii* (ATCC 50373) cysts, however, were not inhibited with 3mg/L of free chlorine concentration at tested maximum contact time (240 minutes) and showed little log reduction (0.017) at 5 mg/L. Similar to the results from the present study, Mogoa found 3 log reduction for 5mg/L [22] and Jonckheere and Voorde reported virulent or avirulent Acanthamoeba strains to be insensitive to the chlorine concentrations used in tap water and swimming pools; a free chlorine concentration of 4 µg/mL did not destroy these strains after 3 h [21]. Bergmanson et al. demonstrated that 5mg/L killed *A. polyphaga* and *A. castellanii* within 24–48 h. The effective control of Acanthamoeba in water therefore requires a free chlorine residual of at least 5 mg/L [24].

The environmental strains (A10, A13, A14, A20) were detected to be generally more sensitive than *A. castellanii* ATCC 50373 against all tested doses of NaClO (Table 1, Table 2, Table 3), with the most sensitive strains being A20 for 1 mg/L of NaClO; A20 for 3mg/L of NaClO; and A13, A14 for 5mg/L of NaClO. These results reveal that the sensibilities of amoeba cells against free chlorine concentrations can change according to the specification of strains. As an illustration of this, Jonckheere and Voorde found that the pathogenic *A. culbertsoni* A-1 was more resistant to chlorine than the avirulent Acanthamoeba strain isolated from tap water [21]. However, Coulon et al. demonstrated that environmental strains had greater resistance than collection strains [25]. As the present study did not identify Acanthamoeba isolates at species-level nor investigate their pathogenicity, molecular studies have been planned for the future in order to conduct identification and pathogenicity tests of these strains that have been isolated from swimming pool waters in Turkey.

FLA trophozoites are known to be able to transform into cyst form under unfavorable conditions (e.g. chlorination) in aquatic environments (e.g. swimming pools), and thereby become more resistant [26]. Results from this study showed that *A. castellani*i (ATCC 50373) cyst growth was inhibited slightly (log reduction 0.017) with 5mg/L of free chlorine concentration at 240 minutes. It is quite clear from this that the elimination of the cyst form of FLA in swimming pools requires higher concentrations of chlorine and a longer time of contact. However, here it is important to note that studies concerning the potential health effects of chlorine on animals and humans have shown that even brief exposure to 1-3 mg/L of chlorine caused nose irritation and 5 mg/L caused eye irritation, while any amount higher than these concentrations caused chest pain, vomiting, lung injury and death [27]. In the present study, with the 5 mg/L concentration of free chlorine, significant reduction was observed in the proliferation of 3T3 cells, a 3 log reduction (not 100 % death) was determined on tested FLA trophozoites

and a minor inhibitor effect was detected (0.017 log reduction) on *A. castellanii* ATCC 50373 cysts. Just as FLA trophozoites can transform into cysts, the reverse can also occur, that is, FLA cysts can transform into trophozoites in suitable environmental conditions. Therefore, it necessary that FLA cysts, as well as their trophozoites, be eliminated to ensure the health and safety of swimmers in the swimming pools. On account of all the reasons presented in this paper, it is recommended that new, non-toxic, environment-friendly disinfectants, instead of chlorine, be tested against every form of FLA. In this way, it will be possible to eradicate both the trophozoite and cyst forms of these 'unnoticed' microorganisms.

In summary, Acanthamoeba spp., a natural inhabitant of swimming pools, is able to survive the free chlorine concentration used to ensure the microbial quality of these aquatic environments. The free chlorine concentrations used in this study were higher than the concentrations typically specified to control the environmental strains present in swimming pools in Turkey. According to this study's results, it was clearly shown that the Acanthamoeba strains isolated from swimming pool water in Turkey were unable to be destroyed by the applied amount of chlorine in these aquatic environments. Otherwise stated, the swimming pool disinfection procedures used in Turkey are not sufficient for preventing presumptive Acanthamoeba infections in human beings. Hence, first it is suggested that swimming pool water be comprehensively scanned for these 'unnoticed' microorganisms. Secondly, should these microorganisms be detected, treatment strategies specifically targeting FLA should be developed. Lastly, it is hoped that the data provided from this study shall serve to contribute to securing public health and raising awareness in public health authorities.

ACKNOWLEDGEMENTS

This study was supported by the Scientific Research Projects Coordination Unit of İstanbul University (Project No: 36146 and UDP - 57531). We would like to thank Dr. Serap Sancar and Dr. İdil Çetin for their assistance.

REFERENCES

[1] Burak, D.M., Zeybek, Z. (2011) Investigation of *Legionella pneumophila* and free living amoebas in the domestic hot water systems in Istanbul. Turk J Biol. 35, 679-685.

[2] Gianinazzi, C., Schild, M., Zumkehr, B., Wüthrich, F., Nüesch, I., Ryter, R., Schürch, N., Gottstein, B., Müller, N. (2010) Screening Of Swiss Hot Spring Resort For Potentially Pathogenic Free-Living Amoebae. Exp Parasitol. 126, 45-53.

[3] Görnik, K., Kuzna, G.W., (2004) Presence Of Virulent Strain Of Amphizoic Amoebae İn Swimming Pools of The City of Szczecin. Ann Agric Environ Med. 11, 233-236.

[4] Rodriguez-Zaragoza, S. (1994) Ecology of free-living amoebae. Crit Rev Microbiol. 20, 225–241.

[5] Thomas, J.M., Ashbolt, N.J. (2011) Do Free-Living Amoebae in Treated Drinking Water Systems Present an Emerging Health Risk. Environ Sci Tech. 45, 860-869.

[6] Marciano-Cabral, F., Cabral, G. (2003) Acanthamoeba Spp. As Agents of Disease in Humans. Clin Mic Rev. 16(2), 273-307.

[7] Dupuy, M., Berne, F., Herbelin, P., Binet, M., Berthelot, N., Rodier, M., Soreau, S., Héchard, Y. (2014) Sensitivity of free-living amoeba trophozoites and cysts to water disinfectants. Int J Hyg Env Health. 217, 335– 339.

[8] Visvesvara, G.S., Moura, H., Schuster, F.L. (2007) Pathogenic and opportunistic free-living amoebae: Acanthamoeba spp., Balamuthia mandrillaris, Naegleria and Sappinia diplodea. FEMS Microbiol and Med Microbiol. 50(1), 1-26.

[9] Cervero-Aragó, S., Rodríguez-Martínez, S., Puertas-Bennasar, A., Araujo, R.M. (2015) Effect of Common Drinking Water Disinfectants, Chlorine and Heat, on Free Legionella and Amoebae-Associated Legionella. Plos One. 10,1371.

[10] Greub, G., Raoult, D. (2004) Microorganisms Resistant to Free-Living Amoebae. Clin Mic Rev. 17(2), 413–433.

[11] King, C.H., Shotts, E.B.JR, Wooley, R.E., Porter, K.G. (1988) Survival of Coliforms and Bacterial Pathogens within Protozoa during Chlorination. Appl Env Mic. 54 (12), 3023-3033.

[12] Molmeret, M., Horn, M., Wagner, M., Santıc, M., Kwaık, Y.A. (2005) Amoebae as Training Grounds for Intracellullar Bacterial Pathogens. Appl Env Mic. 71(1), 20-28.

[13] Rowbotham, T.J. (1980) Preliminary report on the pathogenicity of *Legionella pneumophila* for freshwater and soil amoebae. J Clin Pathol. 33, 1179–1183.

[14] Bonnick, D.M. (2005) Swimming Pool Disinfection Tecniques & Pitfalls, Swimming Pools & SPA Baths- Effective Control of Water Quality and Public Health Conference.

[15] Thomas, V., Bouchez, T., Nıcolas, V., Robert, S., Loret, J.F., Levı, Y. (2004) Amoebae in Domestic Water Systems: Resistance to Disinfection Treatments and İmplication in Legionella Persistence. J Appl Mic. 97, 950-963.

[16] Türkmen, A (2012) The Microbiological Analysis of Water and Bıofilm Samples Taken from Swimming Pools in Istanbul. Master's thesis , Istanbul University Science Institute, Istanbul, Turkey.

[17] Beattie, T.K., Seal, D.V., Tomlinson. A., McFadyen. A.K., Grimason, A.M. (2003) Determination of amoebicidal activities of multipurpose contact lens solutions by using a most probable number enumeration technique. J Clin Mic. 41 (7), 2992–3000.
[18] Bugan, I., Karagoz, Z., Altun, S., Djamgoz, M.B. (2016) Gabapentin, an Analgesic Used Against Cancer-Associated Neuropathic Pain: Effects on Prostate Cancer Progression in an In Vivo Rat Model. Basic Clin Pharmacol Toxicol. 118 (3), 200-7.
[19] Grimes, J.A., Fraser, S.P., Stephens, G.J., Downing, J.E., Laniado, M.E., Foster, C.S., Abel, P.D., Djamgoz, M.B.A. (1995) Differential expression of voltage-activated Na+ currents in two prostatic tumour cell lines: contribution to invasiveness in vitro. FEBS Lett. 369,290–4.
[20] Init, I., Lau, Y.L., Fadzlun, A., Foead, A., Neilson, R.S. and Nissapatorn, V. (2010) Detection of free living amoebae, *Acanthamoeba* and *Naegleria*, in swimming pools, Malaysia. Trop Biomed. 27(3), 566–577.
[21] Jonckheere, J.D., Voorde, H., Van, D. (1976) Differences In Destruction of Cysts of Pathogenic and Nonpathogenic Naegleria and Acanthamoeba by Chlorine. Appl Env Mic. 31(2): 294-297.
[22] Mogoa, E., Bodet, C., Legube, B., Héchard, Y. (2010) Acanthamoeba castellanii: Cellular changes induced by chlorination. Exp Parasitol. 126, 97–102.
[23] Critchley, M., Bentham, R. (2009) The efficacy of biocides and other chemical additives in cooling water systems in the control of amoebae. J Appl Mic. 106 (3), 784-9.
[24] Bergmanson, J.P.G., Wang, E., Gire, A.I., Michael, S., Osato, M.S. (2011) In vitro effects of medium tonicity, nutrient concentration, and free chlorine, content on Acanthamoeba. Cont Lens & Ant Eye. 34, 164–168.
[25] Coulon, C., Collignon, A., McDonnell, G. and Thomas, V. (2010) Resistance Of *Acanthamoeba* Cysts To Disinfection Treatments Used İn Health Care Settings. J Clin Mic. 48(8), 2689–2697.
[26] Dupuy, M., Berne, F., Herbelin, P., Binet, M., Berthelot, N., Rodier, M., Soreau, S., Héchard, Y. (2014) Sensitivity of free-living amoeba trophozoites and cysts to water disinfectants. Int J Hyg Env Health. 217, 335– 339.
[27] Agency For Toxic Substances And Disease Registry, (2010) Toxicological Profile For Chlorine, U.S. Department Of Health And Human Servıces Public Health Service.

Received: **24.02.2017**
Accepted: **27.08.2017**

CORRESPONDING AUTHOR

Miray Ustunturk-Onan
Istanbul University Faculty of Science, Department of Bıology, Fundamental and Industrial Microbiology, Istanbul, Turkey.

e-mail: mirayustun@gmail.com

© by PSP Volume 26 – No. 12A/2017 pages 7658-7666 Fresenius Environmental Bulletin

SENSITIVITY OF BETA-GLUCOSIDASE TO SOIL CONTAMINATION WITH ZINC, COPPER, NICKEL, CADMIUM AND LEAD

Karol Wieczorek, Jan Kucharski, Jadwiga Wyszkowska*

University of Warmia and Mazury in Olsztyn, Faculty of Environmental Management and Agriculture, Department of Microbiology, Poland

ABSTRACT

In the experiment, loamy sand, sandy loam and sandy clay loam with a pH of 7.0 and 5.5 were contaminated with Zn^{2+}, Cu^{2+}, Ni^{2+}, Cd^{2+} and Pb^{2+} in the laboratory. The analyzed substrates differed in their chemical properties, and therefore they were contaminated with six different doses of each metal. Substrate samples were incubated for 30, 60 and 120 days, and the activity of β-glucosidase was determined at the end of each incubation period. The results were used to calculate the enzyme's resistance to soil contamination with heavy metals.

Enzyme activity in soil with natural levels of trace elements ranged from 0.539 mM PNP kg^{-1} h^{-1} DM in sandy clay loam with a pH of 7.0 to 0.247 mM p-nitrophenol (PNP) kg^{-1} h^{-1} DM in the same substrate with a pH of 5.5. The highest levels of β-glucosidase activity were noted in sandy clay loam, and the lowest in loamy sand. In acidic soils, enzyme activity increased after the first incubation period (30 days), whereas in neutral substrates, higher levels of β-glucosidase activity were observed after two successive incubation periods (60 and 120 days). β-glucosidase was most resistant to contamination with Cu^{2+} (RS=0.997) and least resistant to contamination with Zn^{2+} (RS=0.097).

KEYWORDS:
β-glucosidase, heavy metals, resistance, soil

INTRODUCTION

Cellulose is the main structural component of cell walls of terrestrial and aquatic plants. This biopolymer has linear structure, and is composed of thousands of glucose molecules joined by β-1,4-glycosidic bonds [1]. Cellulose differs from other natural polysaccharides in its rigid structure which imparts resistance to biodegradation [2]. β-glucosidase is an exoenzyme belonging to the group of cellulases. In the soil environment, β-glucosidase can be bonded to organic colloids [3]. The discussed enzyme participates in the final stage of cellulose decomposition [4–6]. It is responsible for catalytic hydrolysis of cellobiose molecules and short-chain oligosaccharides to glucose [7]. The enzyme's activity is limited by substrate availability and product content in the environment [8,9]. β-glucosidase is produced by various groups of organisms, including plants, animals, fungi and bacteria [10]. β-glucosidase is the one of the key indicators used in evaluations of soil organic matter and in soil biomonitoring [11]. β-glucosidase activity in soil indicates the of early changes in organic carbon content, which cannot be observed with the involvement of other analytical methods [3]. β-glucosidase is also sensitive to the soil pH, and can be used as an indicator of soil acidification [12].

The ability of microorganisms to adapt to a new environment is a vital mechanism of resistance to environmental pollution [13]. Microorganisms develop mechanisms that support transformation of metals into less toxic forms, immobilization of metals on the cell surface or in the form of intracellular polymers, precipitation and biomethylation of metals [14]. Enzymes secreted by soil-dwelling microorganisms are exposed to direct contact with heavy metal ions because they are not protected by cells capable of detoxifying metals [15]. β-glucosidase has been found to be sensitive to the presence of heavy metals in the soil environment [3].

The aim of this study was to determine the influence of heavy metals on β-glucosidase resistance and to evaluate the usefulness of β-glucosidase as an indicator of changes in soil contaminated with heavy metals.

MATERIALS AND METHODS

The experiment was performed in the laboratory. The experimental variables were: 1) soil type: loamy sand (LS), sandy loam (SL) and sandy clay loam (SCL); 2) pH_{KCl} of soil: 5.5 and 7.0 (Tab. 1); 3) type of heavy metal: Zn^{2+}, Cu^{2+}, Ni^{2+}, Cd^{2+}, Pb^{2+}; d) degree of soil contamination with heavy metals: 0°, I°, II°, III°, IV°, V° (Table 2); e) soil incubation time: 30, 60 and 120 days.

Natural soil samples were characterized by the following pH_{KCl} values: LS - 5.5, SL - 5.5 and 7.0,

TABLE 1
Physicochemical properties of soils used in experiment

Soil type*	Soil texture[grain diameter, mm]			C_{org}	pH_{KCl}	HAC	TEB	CEC	BS [%]
	2 – 0.05	0.05–0.002	< 0.002	[g kg^{-1}]					
	Content [%]					[mmol(+)kg^{-1} DM of soil]			
LS	80	12	8	5.05	7.0	10.50	55.00	65.50	83.97
	80	12	8	5.05	5.5	21.75	47.00	68.75	68.36
SL	72	21	7	7.05	7.0	8.00	111.0	119.0	93.28
	74	16	10	5.75	5.5	25.50	17.00	42.50	40.00
SCL	56	23	21	14.33	7.0	6.00	190.0	196.0	96.94
	56	23	21	14.33	5.5	12.75	107.0	119.7	89.35

*LS - loamy sand, SL - sandy loam, SCL - sandy clay loam
pH_{KCl} – pH of soil in 1M KCl, C_{org} – organic carbon content, HAC – hydrolytic acidity,
TEB - sum of exchangeable cations, CEC - cation exchange capacity, BS - base cations of percentage saturation

TABLE 2
Doses of heavy metals used in experiment, mg kg^{-1} DM of soil

Heavy metal	Soil contamination degree[1]					
	0°	I°	II°	III°	IV°	V°
Zn^{2+}	0	70	200	500	1500	5000
Cu^{2+}	0	25	50	80	100	500
Ni^{2+}	0	25	50	75	150	600
Cd^{2+}	0	0.5	1.5	3	5	10
Pb^{2+}	0	50	100	250	1000	5000

[1]0° - natural content, I° - elevated content, II° - weak contamination, III° - medium contamination, IV° - strong contamination, V° - very strong contamination

SCL - 7.0. Before the experiment, LS samples with a pH of 5.5 were alkalized with 1% aqueous suspension of $CaCO_3$ until the achievement of a pH of 7.0, and SCL samples with a pH of 7.0 were acidified with 1M aqueous solution of HCl until the achievement of a pH of 5.5. Both soil types were modified to stabilize pH levels in samples not contaminated with heavy metals.

Experimental design. 100 g air-dried soil samples were placed in 100 cm^3 glass beakers and combined with aqueous solutions of $ZnCl_2$, $CuCl_2$, $NiCl_2 \cdot 6\,H_2O$, $CdCl_2 \cdot 2^1/_2H_2O$ and $PbCl_2$. Metal doses were selected to prepare soil samples with various levels of contamination (Table 2) relative to Polish classes of soil suitability for agricultural and non-agricultural production, developed by the Institute of Soil Science and Plant Cultivation in Puławy, Poland [16]. The maximum allowable concentrations of heavy metals vary depending on their toxicity for living organisms. Soil contamination levels with heavy metals were discussed in greater detail by Wieczorek et al. [17]. Soil samples combined with heavy metal solutions were brought to 50% maximum water-holding capacity, covered with PE film and placed in an incubator set to the temperature of 25°C. Throughout the experiment (120 days), soil moisture levels were controlled once a week, and deionized water was added to compensate for moisture loss. The experiment was established in three series with three replications. The first series was discarded after 30 days of incubation, the second– after 60 days, and the third one – after 120 days.

Determination of β-glucosidase activity. On experimental days 30, 60 and 120, β-glucosidase activity (EC 3.2.1.21) in each sample was determined in three replications according to the method proposed by Alef and Nannipieri [18]. The substrate was 25 mM p-nitrophenyl-β-D-glucopyranoside (PNG) solution. Soil samples of 0.5 g were combined with 5 cm^3 of buffer with a pH of 6.0 and 1 cm^3 of PNG. The buffer was an aqueous solution containing 12.1 g of $C_4H_{11}NO_3$ (TRIS), 11.6 g of $C_4H_4O_4$, 14.0 g of $C_6H_8O_7$, 6.28 g of H_3BO_3 and 488 cm^3 of 1M NaOH, dissolved in water and poured into a 1 dm^3 measuring flask. 200 cm^3 of the buffer was diluted in deionized water, its pH was brought to 6.0 with 0.1 M HCl, and it was filled up to 1 dm^3. Samples were incubated for 1 hour at 37°C. After incubation, samples were combined with 1 cm^3 of 0.5 M aqueous solution of $CaCl_2$ and 5 cm^3 of TRIS with a pH of 12.0. The extinction of p-nitrophenol (PNP) was measured with the Perkin-Elmer Lambda 25 spectrophotometer (λ=400 nm). β-glucosidase activity was expressed in mM PNP kg^{-1} h^{-1} soil dry matter (DM).

Calculation of the β-glucosidase resistance (RS) index. β-glucosidase activity levels were used to calculate the enzyme's resistance to Zn^{2+}, Cu^{2+}, Ni^{2+}, Cd^{2+} and Pb^{2+} in soil based on the formula proposed by Orwin and Wardle [19]:

$$RS=1-\frac{2|D_0|}{C_0+|D_0|} \quad (1)$$

where:

C_0 – β-glucosidase activity in soil with naturally-occurring concentrations of heavy metals, D_0 – difference between β-glucosidase activity in soil

with naturally-occurring concentrations of heavy

TABLE 3
Content of heavy metals in mg kg^{-1}DM of soil

Heavy metal	Soil type[2]	pH	Soil contamination degree[1]					
			0°	I°	II°	III°	IV°	V°
			mg kg^{-1} DM of soil					
Zn^{2+}	LS	7.0	10.8	79.5	208.4	503.2	1450.3	4916.7
		5.5	10.8	81.2	212.6	513.3	1479.3	5015.0
	SL	7.0	16.6	81.7	209.0	504.1	1461.2	4920.6
		5.5	11.6	80.9	213.2	515.4	1485.6	5020.0
	SCL	7.0	13.0	82.8	213.8	503.2	1460.1	4921.5
		5.5	13.0	82.8	214.3	515.0	1484.3	5019.8
Cu^{2+}	LS	7.0	2.5	24.5	44.8	74.1	87.7	473.5
		5.5	2.5	24.9	45.9	77.3	93.4	487.9
	SL	7.0	3.8	25.8	46.1	75.4	89.0	474.8
		5.5	1.2	26.2	47.2	78.6	94.7	489.2
	SCL	7.0	3.6	25.6	45.9	75.2	88.8	474.6
		5.5	3.6	25.4	45.7	75.0	88.6	474.4
Ni^{2+}	LS	7.0	3.2	23.4	44.6	69.8	140.0	524.4
		5.5	3.2	24.3	46.8	71.2	151.2	567.6
	SL	7.0	4.6	24.6	45.8	71.0	141.2	525.6
		5.5	4.5	25.4	47.9	72.3	152.3	568.7
	SCL	7.0	3.7	24.1	45.3	70.5	140.7	525.1
		5.5	3.7	24.8	47.3	71.7	151.7	568.1
Cd^{2+}	LS	7.0	0.3	0.8	1.6	3.3	5.2	10.0
		5.5	0.3	0.8	1.7	3.4	5.3	10.2
	SL	7.0	0.3	0.8	1.7	3.2	5.3	10.4
		5.5	1.0	1.4	2.6	4.3	6.4	11.3
	SCL	7.0	0.2	0.7	1.6	3.1	5.2	10.3
		5.5	0.2	0.8	1.7	3.2	5.2	10.4
Pb^{2+}	LS	7.0	12.0	55.7	108.3	247.2	953.6	4921.0
		5.5	12.0	59.6	112.3	255.8	983.5	4978.5
	SL	7.0	16.0	59.2	111.8	250.7	957.1	4924.5
		5.5	9.3	62.8	114.5	259.0	986.7	4981.7
	SCL	7.0	11.9	63.4	114.0	254.9	961.3	4928.7
		5.5	11.9	65.3	114.9	259.8	997.2	4995.1

[1]explanation under Table 2
[2] LS - loamy sand, SL - sandy loam, SCL - sandy clay loam

TABLE 4
The proportion of variance η^2 in soil contaminated with Zn^{2+}, Cu^{2+}, Ni^{2+}, Cd^{2+} and Pb^{2+}

Factor[1]	Zn^{2+}	Cu^{2+}	Ni^{2+}	Cd^{2+}	Pb^{2+}
	[%]				
a	18.5	3.8	1.6	2.2	2.1
b	6.1	7.0	20.2	15.7	3.5
c	9.4	12.0	1.2	12.5	10.6
d	13.5	14.0	9.2	1.0	10.9
a⁒b	0.8	1.4	3.7	0.7	4.4
a⁒c	0.1	0.4	0.5	0.1	0.3
b⁒c	13.1	13.2	25.8	37.3	31.5
a⁒d	0.7	1.2	4.1	5.3	8.8
b⁒d	29.5	39.0	20.3	6.9	11.5
c⁒d	1.3	0.5	1.8	2.5	0.1
a⁒b⁒c	1.6	0.5	0.5	0.4	0.3
a⁒b⁒d	2.8	2.8	5.1	12.9	10.3
a⁒c⁒d	0.1	0.5	0.6	0.5	1.2
b⁒c⁒d	1.3	2.9	4.1	0.3	0.2
a⁒b⁒c⁒d	0.6	0.5	0.9	1.3	2.2
Error	0.6	0.3	0.5	0.5	2.1

[1]a – soil contamination degree, b – soil type, c - pH of soil, d – incubation time

metals and β-glucosidase activity in soil contaminated with heavy metals for 30 days.

The RS index can take on values in the range of -1 to +1. An RS index of +1 indicates an absence of contamination (full resistance). Lower values point to the presence of factors that disrupt the soil balance (lower resistance). The closer the value of the RS index to 0, the greater the drop in resistance. An RS index of 0 points to 100% disturbance, whereas negative values of the index are indicative of excessive levels of enzymatic activity. An RS index of -1 points to 200% disturbance caused by a disrupting factor.

Determination of the physicochemical properties of soil. The content of different soil fractions was determined based on the method proposed by Cassagrande and modified by Prószyński [20]. Hydrolytic acidity (HAC) and total exchangeable bases (TEB) were determined according to the method developed by Kappen [20]. Organic carbon (C_{org}) content was measured by Tiurin's quantitative method [20]. HAC and TEB values were used to calculate total cation exchange capacity (CEC) and base saturation (BS). Soil pH was determined potentiometrically with 1M KCl/soil, 1:2.5 [21,www.iso.org].

Determination of the heavy metal content of soil. The content of heavy metals in soil was determined by using atomic absorption spectrometry (AAS-30, Carl Zeiss Jena): Zn^{2+} at 214 nm, Cu^{2+} at 328 nm, Ni^{2+} at 232 nm, Cd^{2+} at 228 nm, and Pb^{2+} at 284 nm, after extraction with 1M HCl [22,23,www.pkn.pl] (Table 3).

Statistical analysis. Empirical data were processed statistically by ANOVA [24, www.statsoft.com]. Homogeneous groups were identified by Tukey's test at a significance level of p = 0.01. Pearson's coefficients of correlation were determined between β-glucosidase activity and the RS index vs. the degree of soil contamination with heavy metals. The proportion of variance η^2 was calculated in view of all experimental factors. β-glucosidase activity was presented in radar charts developed in Excel. Principal component analysis (PCA) of β-glucosidase resistance to heavy metals was performed in the Statistica application.

RESULTS

The experiment generated information about the effect of heavy metals on the activity and resistance of β-glucosidase. Effect size measurements (Table 4) indicate that the analyzed factors had a various influence. Regardless of the added heavy metal, the most important factors were soil type (10.51% on average), followed by incubation time (9.75% on average) and soil pH (9.12% on average).

TABLE 5
Activity of β-glucosidase in soil contaminated with Zn^{2+}, Cu^{2+}, Ni^{2+}, Cd^{2+} and Pb^{2+}, mM PNP kg^{-1} h^{-1} DM of soil

Soil type[2]	Soil pH	Soil contamination degree[1]						r
		0°	I°	II°	III°	IV°	V°	
Zn^{2+}								
LS	7.0	0.305^{a}	0.282^{a}	0.282^{a}	0.287^{a}	0.248^{b}	0.175^{c}	-0.570**
	5.5	0.343^{a}	0.308^{ab}	0.294^{bc}	0.258^{c}	0.210^{d}	0.052^{e}	-0.782**
SL	7.0	0.343^{a}	0.322^{a}	0.337^{a}	0.251^{b}	0.217^{b}	0.157^{c}	-0.334*
	5.5	0.348^{a}	0.297^{b}	0.308^{b}	0.224^{c}	0.214^{c}	0.152^{d}	-0.336*
SCL	7.0	0.539^{b}	0.548^{a}	0.534^{b}	0.478^{c}	0.435^{d}	0.285^{e}	-0.847**
	5.5	0.247^{ab}	0.255^{a}	0.226^{c}	0.242^{b}	0.203^{d}	0.098^{e}	-0.523**
Cu^{2+}								
LS	7.0	0.305^{a}	0.301^{a}	0.275^{b}	0.272^{b}	0.260^{b}	0.239^{c}	-0.551**
	5.5	0.343^{a}	0.276^{b}	0.269^{b}	0.258^{bc}	0.252^{bc}	0.238^{c}	-0.507**
SL	7.0	0.343^{d}	0.471^{a}	0.445^{b}	0.415^{c}	0.349^{d}	0.273^{e}	-0.160
	5.5	0.348^{b}	0.401^{a}	0.321^{c}	0.316^{c}	0.304^{c}	0.265^{d}	-0.171
SCL	7.0	0.539^{a}	0.533^{a}	0.515^{ab}	0.497^{b}	0.500^{b}	0.452^{c}	-0.665**
	5.5	0.247^{b}	0.268^{a}	0.247^{b}	0.233^{c}	0.209^{d}	0.204^{d}	-0.319*
Ni^{2+}								
LS	7.0	0.305^{a}	0.289^{b}	0.253^{c}	0.242^{c}	0.244^{c}	0.245^{c}	-0.565**
	5.5	0.343^{a}	0.304^{b}	0.299^{bc}	0.298^{bc}	0.301^{b}	0.273^{c}	-0.402**
SL	7.0	0.343^{d}	0.444^{a}	0.422^{ab}	0.408^{bc}	0.400^{bc}	0.378^{c}	0.011
	5.5	0.348^{d}	0.579^{a}	0.566^{ab}	0.540^{bc}	0.527^{c}	0.509^{c}	0.130
SCL	7.0	0.538^{a}	0.535^{a}	0.521^{b}	0.504^{c}	0.490^{d}	0.446^{e}	-0.615**
	5.5	0.247^{bc}	0.271^{a}	0.269^{ab}	0.248^{bc}	0.242^{c}	0.227^{c}	-0.258
Cd^{2+}								
LS	7.0	0.305^{a}	0.265^{b}	0.263^{b}	0.251^{bc}	0.233^{c}	0.233^{c}	-0.671**
	5.5	0.343^{a}	0.310^{b}	0.303^{bc}	0.283^{cd}	0.289^{bcd}	0.277^{d}	-0.447**
SL	7.0	0.343^{a}	0.346^{a}	0.333^{ab}	0.334^{ab}	0.330^{ab}	0.320^{b}	-0.085
	5.5	0.348^{a}	0.337^{ab}	0.320^{bc}	0.320^{bc}	0.310^{c}	0.310^{c}	-0.142
SCL	7.0	0.538^{b}	0.562^{a}	0.535^{b}	0.512^{c}	0.503^{c}	0.464^{d}	-0.493**
	5.5	0.247^{b}	0.266^{a}	0.263^{a}	0.263^{a}	0.244^{b}	0.238^{b}	-0.147
Pb^{2+}								
LS	7.0	0.305^{c}	0.303^{c}	0.357^{ab}	0.377^{a}	0.348^{ab}	0.329^{bc}	0.158
	5.5	0.343^{ab}	0.346^{ab}	0.356^{ab}	0.390^{a}	0.374^{ab}	0.324^{b}	0.011
SL	7.0	0.343^{ab}	0.354^{ab}	0.366^{a}	0.351^{ab}	0.330^{bc}	0.305^{c}	-0.132
	5.5	0.348^{ab}	0.395^{a}	0.369^{ab}	0.364^{ab}	0.349^{ab}	0.319^{b}	-0.137
SCL	7.0	0.538^{a}	0.422^{bc}	0.430^{bc}	0.441^{b}	0.393^{cd}	0.382^{d}	-0.575*
	5.5	0.247^{a}	0.165^{b}	0.142^{c}	0.147^{bc}	0.156^{bc}	0.136^{c}	-0.496*

**significant for p = 0.01, *significant for p = 0.05, n =53
The same letters in rows are assigned to homogenous groups (p<0.01)
[1] explanation under Table 2

[2] explanation under Table 3

β-glucosidase activity. Throughout 120 days of the experiment duration the β-glucosidase activity in soil varied from the soil type and, to a smaller extent, soil pH. In loamy sand with a pH of 7.0 and 5.0, the type of contaminant had a minor influence on β-glucosidase activity. In LS samples with a pH of 7.0, the highest levels of β-glucosidase activity were noted after 60 days of incubation. Higher activity was observed only in samples contaminated with Zn^{2+} (V°), Ni^{2+} (II°) and Cd^{2+} (IV° and V°) for 120 days. In LS samples with a pH of 5.5, the highest levels of enzyme activity were noted after 30 days of incubation, except for soil contaminated with Pb2+ (Tab. 5).

In SL samples with a pH of 7.0, β-glucosidase activity levels were highest in soil incubated with Zn^{2+} (up to IV°) and Pb^{2+} (up to IV°) for 30 days, and with Cu^{2+} (excluding IV°), Ni^{2+} and Cd^{2+} for 120 days. In SL samples with a pH of 5.5, the highest enzyme activity was observed after 30 days of incubation with Zn^{2+}, Ni^{2+} and Cd^{2+}, after 120 days with Cu^{2+}, after 30 days of contamination with Pb^{2+} (II°, III°, V°) and after 60 days with Pb^{2+} (I° and IV°) (Tab. 5).

In SCL samples with a pH of 7.0, β-glucosidase activity was considerably higher than in SCL with a pH of 5.5. The highest levels of enzymatic activity were observed in samples contaminated with Zn^{2+} and Cd^{2+} for 60 days (IV° and V° after 30 days), Cu^{2+} and Ni^{2+} for 120 days (IV° after 60 days), Pb^{2+} for 30 days (I° - III°) and 60 days (IV° and V°). Enzyme activity was substantially lower in SCL samples with a pH of 5.5 (Tab. 5).

Regardless of the soil contamination degree Zn^{2+} inhibited β-glucosidase activity by 15% (SCL with a pH 7.0) to 35% (LS with a pH of 7.0) on average, Cu^{2+} - by 6% (SCL with a pH of 5.5) to 25% (LS with a pH of 5.5), Ni^{2+} - by 7% (SCL with a pH of 7.0) to 16% (LS with a pH of 7.0), Cd^{2+} - by 3% (SL with a pH of 7.0) to 18% (LS with a pH of 7.0), and Pb^{2+} - by 23% (SCL with a pH of 7.0) to 40% (SCL with a pH of 5.5). Despite the above, soil contamination also stimulated enzyme activity. On average, β-glucosidase activity increased by 14% in soil samples contaminated with Cu^{2+} (SL with a pH of 7.0), by 20% (SL with a pH of 7.0) to 56% (SL with a pH of 7.0) in soil samples contaminated with Ni^{2+}, and by 3% (SL with a pH of 5.5) to 13% (LS with a pH of 7.0) in soil samples contaminated with Pb^{2+}.

TABLE 6
Resistance of β-glucosidase (RS) in soil contaminated with Zn^{2+}, Cu^{2+}, Ni^{2+}, Cd^{2+} and Pb^{2+}

Soil type	Soil pH	Soil contamination degree					r
		I°	II°	III°	IV°	V°	
Zn^{2+}							
LS	7.0	0.802[a]	0.854[a]	0.833[a]	0.801[a]	0.287[b]	-0.681[**]
	5.5	0.908[a]	0.988[a]	0.694[ab]	0.458[b]	0.097[ab]	-0.683[**]
SL	7.0	0.969[a]	0.896[a]	0.529[b]	0.504[b]	0.302[b]	-0.925[**]
	5.5	0.718[a]	0.705[a]	0.535[b]	0.562[b]	0.354[c]	-0.904[**]
SCL	7.0	0.894[a]	0.951[a]	0.779[b]	0.715[c]	0.397[d]	-0.871[**]
	5.5	0.884[a]	0.935[a]	0.898[a]	0.881[a]	0.294[b]	-0.693[**]
Cu^{2+}							
LS	7.0	0.974[a]	0.901[a]	0.995[a]	0.809[a]	0.755[b]	-0.764[**]
	5.5	0.660[a]	0.698[a]	0.672[a]	0.652[a]	0.537[b]	-0.716[**]
SL	7.0	0.827[a]	0.997[a]	0.813[a]	0.833[a]	0.480[b]	-0.720[**]
	5.5	0.858[a]	0.418[b]	0.422[b]	0.404[b]	0.315[b]	-0.768[**]
SCL	7.0	0.949[a]	0.923[a]	0.866[a]	0.893[a]	0.760[b]	-0.695[**]
	5.5	0.822[ab]	0.870[ab]	0.980[a]	0.717[b]	0.751[c]	-0.747[**]
Ni^{2+}							
LS	7.0	0.815[a]	0.681[a]	0.667[a]	0.631[a]	0.650[b]	-0.827[**]
	5.5	0.857[a]	0.768[ab]	0.725[b]	0.813[ab]	0.645[c]	-0.740[**]
SL	7.0	0.464[a]	0.459[a]	0.462[a]	0.452[a]	0.454[b]	-0.710[**]
	5.5	0.720[a]	0.715[a]	0.716[a]	0.628[a]	0.569[b]	-0.780[**]
SCL	7.0	0.860[a]	0.848[a]	0.733[b]	0.669[b]	0.632[c]	-0.860[**]
	5.5	0.737[a]	0.746[a]	0.682[a]	0.630[a]	0.568[b]	-0.808[**]
Cd^{2+}							
LS	7.0	0.844[a]	0.873[a]	0.800[a]	0.733[a]	0.685[b]	-0.788[**]
	5.5	0.894[a]	0.790[b]	0.705[c]	0.662[c]	0.663[d]	-0.877[**]
SL	7.0	0.468[a]	0.407[ab]	0.405[ab]	0.400[b]	0.388[c]	-0.859[**]
	5.5	0.511[a]	0.466[a]	0.438[a]	0.428[a]	0.408[b]	-0.871[**]
SCL	7.0	0.938[a]	0.816[b]	0.754[bc]	0.685[c]	0.578[d]	-0.884[**]
	5.5	0.811[a]	0.847[a]	0.768[a]	0.662[a]	0.607[a]	-0.816[**]
Pb^{2+}							
LS	7.0	0.686[a]	0.468[a]	0.605[a]	0.513[a]	0.553[b]	-0.758[**]
	5.5	0.749[a]	0.831[a]	0.609[ab]	0.969[a]	0.443[b]	-0.552[*]
SL	7.0	0.559[a]	0.581[a]	0.564[a]	0.528[a]	0.407[b]	-0.728[**]
	5.5	0.553[a]	0.540[a]	0.537[a]	0.476[a]	0.477[a]	-0.693[**]
SCL	7.0	0.844[a]	0.855[a]	0.816[a]	0.443[b]	0.601[c]	-0.899[**]
	5.5	0.367[a]	0.333[a]	0.400[a]	0.459[a]	0.347[a]	0.051

[*]significant for p = 0.01, [**]significant for p = 0.05, n = 14
The same letters in rows are assigned to homogenous groups (p<0.01)

[1] explanation under Table 2
[2] explanation under Table 3

Pearson's coefficients of correlation between β-glucosidase activity and soil contamination with heavy metals are presented in Table 5. In the vast majority of cases, the correlations were statistically significant, which implies that β-glucosidase activity is strongly linked with the amounts of Zn^{2+}, Cu^{2+}, Ni^{2+}, Cd^{2+} and Pb^{2+} present in the soil environment. A decrease in enzyme activity levels was observed in LS samples after 30, 60 and 120 days, in SL samples after 30 days, and in SCL samples after 30 and 60 days of the experiment.

β-glucosidase resistance. The highest average β-glucosidase resistance, regardless of the degree of contamination, was observed in LS with a pH of 7.0 exposed to Cu^{2+} (RS = 0.887), and the lowest – in SCL with a pH of 5.5 in soil contaminated with Pb^{2+} (RS = 0.381) (Table 6). Zn^{2+} reduced β-glucosidase resistance in the range of 1% in LS with a pH of 5.5 (II°) to 90% in LS (V°), Cu^{2+} - in the range of 1% in LS with a pH of 7.0 (III°) to 69% in SL with a pH of 5.5 (V°), Ni^{2+} - in the range of 14% in LS with a pH of 5.5 and in SCL with a pH of 7.0 (I°) to 55% in SL with a pH of 7.0 (IV° and V°), Cd^{2+} - in the range of 6% in SCL with a pH of 7.0 (I°) to 61% in SL with a pH of 7.0 (V°), and Pb^{2+} - in the range of 3% in LS with a pH of 5.5 (IV°) to 65% in SCL with a pH of 5.5 (V°). The influence of heavy metals on changes in β-glucosidase resistance varied across the analyzed soil types. Soil type was more likely to induce changes in the RS index than soil pH or contamination type. The values of correlation coefficients indicate that β-glucosidase resistance was most significantly inhibited by Cd^{2+}, followed by Ni^{2+}, Zn^{2+},Cu^{2+}, and that it was least affected by Pb^{2+} which did not significantly impair resistance in LS at a pH of 5.5 or 7.0 and in SCL with a pH of 5.5 (Table 6).

The principal components in PCA explained primary variables in 88.15% (Fig. 1). β-glucosidase resistance was most significantly inhibited by Cd^{2+}, followed by Ni^{2+}, Zn^{2+},Cu^{2+}, and it was least affected by Pb^{2+}. The most significant combined effect was exerted by Cu^{2+} and Cd^{2+} and by Cu^{2+} and Zn^{2+}, whereas the combined effect of Cu^{2+} and Pb^{2+} and of Zn^{2+} and Pb^{2+} was least significant. The highest degree of contamination (V°) had the most inhibitory effect on β-glucosidase activity in all soil types.

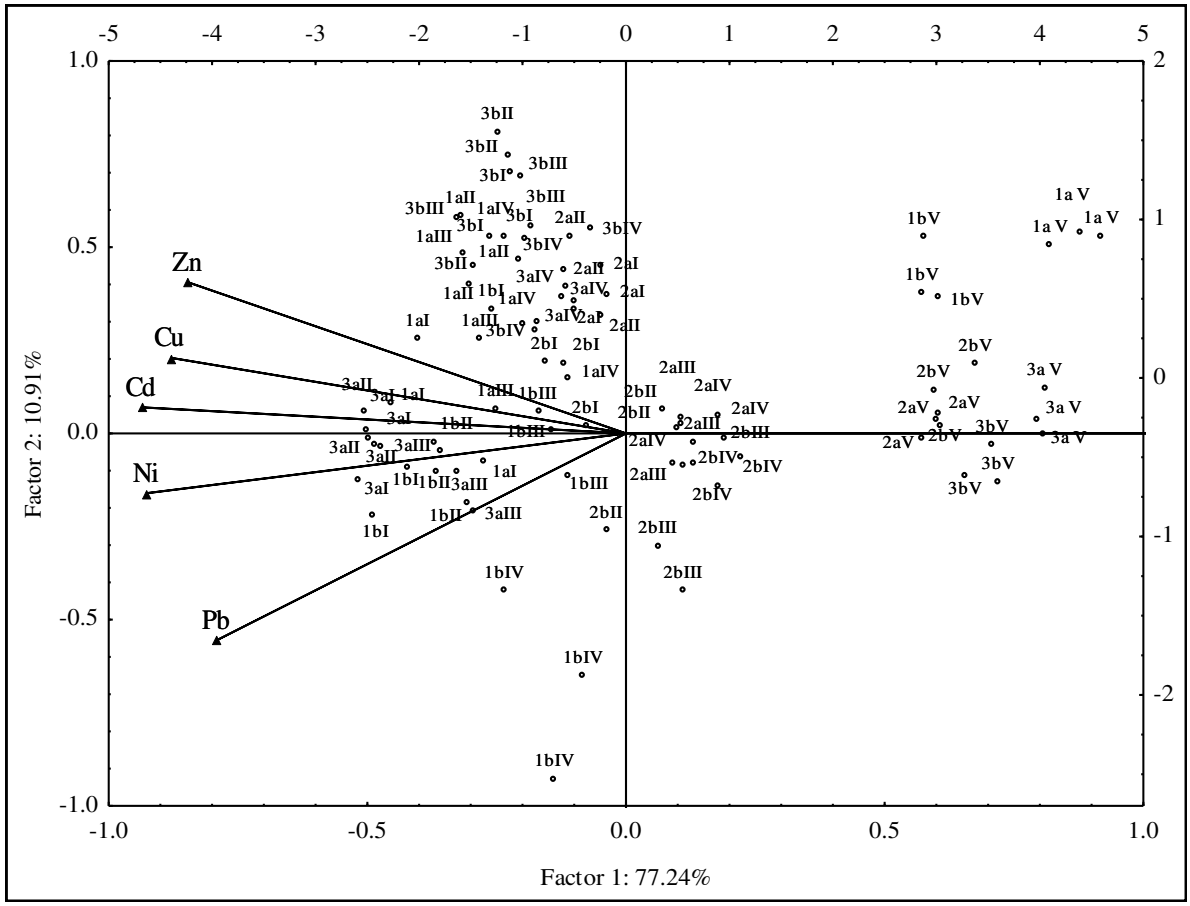


FIGURE 1
Resistance of β-glucosidase in soil contaminated with Zn^{2+}, Cu^{2+}, Ni^{2+}, Cd^{2+} and Pb^{2+} presented as Principal Component Analysis (PCA)

soil type: 1-loamy sand, 2-sandy loam, 3-sandy clay loam; soil pH: a-pH 7.0, b-pH 5.5;
soil contamination degree: 0-0°, I-I°, II-II°, III-III°, IV-IV°, V-V°
vectors of Zn, Cu, Ni, Cd and Pb refer to axes: X - bottom, Y - left; cases refers to axes: X - upper, Y – right).

DISCUSSION

Enzymes synthesized by soil microorganisms play an important role in biodegradation and organic matter transformation [24]. Products catalyzed by those compounds are used by other organisms and plants as a substrates necessary for growth and development [25,26]. They are also reliable indicators of changes induced by anthropogenic contamination in the soil environment [27].

β-glucosidase activity is highly correlated with the degree of heavy metal contamination in soil. Subject to the type of heavy metal and the degree of contamination, enzymes can respond positively or negatively to contamination stress [28]. Kuperman and Carreiro [29] demonstrated that the presence of As, Cd^{2+}, Cr, Zn^{2+}, Cu^{2+}, Ni^{2+} and Pb^{2+} in soil at concentrations of 7.2 to 48 mM kg^{-1} had an adverse effect on enzyme activity. Similar observations were made by Frederick et al. [30] in a study of soil samples from a defunct cement plant contaminated with Zn^{2+}, Cu^{2+}, Cr, Fe, Cd^{2+}, Pb^{2+}, Si^{4+} and Mn. The noted reduction in β-glucosidase activity resulted from simultaneous contamination with many metals whose individual concentrations were lower than in the present study. According to Dick and Tabatabai [31], some heavy metals - including Zn^{2+}, Ni^{2+}, Co^{2+} and Mn - act as cofactors and activators. Heavy metal levels tolerated by soil-dwelling organisms can contribute to an increase in enzymatic activity.

This study analyzed a broader spectrum of soil types, thus enabling a more detailed evaluation of contamination with Zn^{2+}, Cu^{2+}, Ni^{2+}, Cd^{2+} and Pb^{2+} as individual factors degrading the soil environment. Despite the above, more information is needed about the impact of heavy metals in various environmental conditions, in particular in environments exposed to the combined effect of several metals, and about mutual interactions between heavy metals in the biosphere.

β-glucosidase activity varies across different soil types. Wyszkowska et al. [32] demonstrated higher levels of enzymatic activity in sandy loam than in loamy sand, both contaminated and not contaminated with Cu^{2+}. β-glucosidase resistance decreased with an increase in Cu^{2+} concentrations, but greater changes in the RS index were observed in sandy loam than in loamy sand. In a study by Kucharski et al. [33], soil contamination with Ni^{2+} decreased β-glucosidase activity by 9% on average. In the current study, enzyme activity decreased by 15% on average in loamy sand. Unlike in sandy substrates, higher percentages of silt and clay contributed to the stability of the soil environment contaminated with Ni^{2+}. In the present study, β-glucosidase activity was clearly correlated with the content of different soil fractions. Differences were particularly visible when enzyme activity levels were compared in SCL with a pH of 7.0 and in SL and LS substrates with the same pH. In soils with a neutral pH, β-glucosidase activity increased considerably with increasing percentages of silt and clay, whereas in acidic soils, the above trend was not as profoundly expressed. In SCL with a pH of 5.5, enzyme activity was lower than in LS and SL with the same pH. Wyszkowska et al. [32], Kucharski et al. [33] and Lee et al. [34] demonstrated that the application of neutralizing substances or temporary cessation of agricultural activity on soils contaminated with heavy metals can stimulate β-glucosidase activity.

In this study, the application of the six-point scale of soil contamination, developed by the Institute of Soil Science and Plant Cultivation in Puławy, partially explains how the same levels of contamination with Zn^{2+}, Cu^{2+}, Ni^{2+}, Cd^{2+} and Pb^{2+} influence one of the most important and reliable biochemical indicators of soil quality. The use of non-homogeneous granulometric composition as a variable can expand our knowledge about the toxic effect of heavy metals on soil-dwelling microorganisms not only in direct interactions, but also in indirect interactions, including the acidification of contaminated soil, further inhibition of the growth of acid-sensitive microbes, and biochemical activity of soil.

CONCLUSIONS

β-glucosidase activity decreased with an increasing concentrations of Zn^{2+}, Cu^{2+} and Ni^{2+} in loamy sand and sandy loam and with an increase in Cd^{2+} and Pb^{2+} levels in sandy loam and sandy clay loam.

β-glucosidase activity was most significantly inhibited by Cd^{2+}, followed by Zn^{2+}, Cu^{2+}, Ni^{2+} and Pb^{2+}.

The type of soil substrate, soil pH and duration of the experiment were more likely to induce changes in β-glucosidase activity than the type and content of heavy metals in soil.

The physicochemical properties of soil contaminated with Zn^{2+}, Cu^{2+}, Ni^{2+}, Cd^{2+} and Pb^{2+} significantly differentiate the influence of those elements on β-glucosidase resistance. β-glucosidase activity was higher in sandy clay loam with a pH of 7.0 than in sandy loam and loamy sand with the same pH. In acidic substrates, the highest levels of β-glucosidase activity were noted in sandy loam, followed by loamy sand, and the lowest levels were observed in sandy clay loam.

The period during which β-glucosidase activity was inhibited in response to contamination with Zn^{2+}, Cu^{2+}, Ni^{2+}, Cd^{2+} and Pb^{2+} was shortened with

an increase in the silt and clay content of soil, relative to sandy substrates.

The effect of heavy metals on β-glucosidase activity over time was influenced by the pH of soil. In acidic substrates, enzyme activity was higher after 30 days, and in neutral soils – after 60 and 120 days.

ACKNOWLEDGEMENTS

The study was supported by research grant No. N N305 361839 from the Polish National Science Center and by the Ministry of Science and Higher Education funds for statutory activity.

REFERENCES

[1] Utobo, E.B. and Tewari, L. (2014) Soil ecosystem as bioindicators of soil ecosystem status. Appl. Ecol. Env. Res. 13(1), 147-169.
[2] Hon, D. (1994) Cellulose: a random walk along its historical path. Cellulose. 1, 1-25.
[3] Joachim, H.J. and Patrick, A.N. (2008) Selected Soil Enzymes: Examples of their Potential Roles in the Ecosystem. Afr. J. Biotechnol. 7(3), 181-191.
[4] Coughlan, M.P. (1985) Interscience. In: Russell, G.E. (Ed.) Biotechnology and Genetic Engineering Reviews. Newcastle-upon-Tyne. 3, 39-109.
[5] Verchot, L.V. and Borelli, T. (2005) Application of para-nitrophenol (PNP) enzyme assays in degraded tropical soils. Soil Biol. Biochem. 37, 625–633.
[6] Nam, K.H., Kim, S.J., Kim, M.Y., Kim, J.H., Yeo, Y.S., Lee, C.M., Jun, H.K. and Hwang, K.Y. (2008) Crystal structure of engineered beta-glucosidase from a soil metagenome. Proteins. 73(3), 788-793.
[7] Rapa, P. and Beerman, A. (1991) Bacterial cellulose. [in:] Biosynthesis and biodegradation of Cellulase. C.H. Haigler, P. J. Wiemer (eds), Marcel Dekker, New York. 535-599.
[8] Allison, S.D. and Vitousek, P.M. (2005) Responses of extracellular enzymes to simple and complex nutrient inputs. Soil Biol. Biochem. 37, 937–944.
[9] Allison, S.D., Weintraub, M., Gartner, T.B. and Waldrop, M.P. (2011) Evolutionary-economic principles as regulators of soil enzyme production and ecosystem function [in:] Soil enzymology. G. Shukla, A. Varma (eds), Springer-Verlag, Berlin. 229–243.
[10] Veena, V., Poornima, P., Parvatham, R. and Kalaiselvi, K. (2011) Isolation and characterrization of β-glucosidase Producing Bacteria from Different Sources. Afr. J. Biotechnol. 10(66),14907-14912.
[11] Ndiaye, E.L., Sandeno, J.M., McGrath. D. and Dick, R.P. (2000) Integrative biological indicators for detecting change in soil quality. Am. J. Alternative Agr. 15, 26-36.
[12] Acosta-Martínez, V. and Tabatabai, M.A. (2000) Enzyme Activities in a Limed Agricultural Soil. Biol. Fertil. Soil. 31, 85-91.
[13] Silver, S., Laddaga, R.A. and Misra, T.K. (1989) Metal-Microbe Interactions. In: Poolc, R.K. and Gadd, G.M. (Eds) Plasmid-determined resistance to metal ions. IRL Press, Oxford. 17-20.
[14] Doelman, P. (1986) Resistance of soil microbial communities to heavy metals. [in:] Microbial Communities in Soil, Elsevier Applied Science. V. Jensen, A. Kjoller, C.H. Sorensen (eds), Publishers, London. 33, 369-398.
[15] Baldrian, P. (2003). Interactions of heavy metals with white-rot fungi. Enzyme Microb. Tech. 32, 78-91.
[16] Siebielec, G., Smreczak, B., Klimkowicz-Pawlas, A., Maliszewska-Kordybach, B., Terelak, H., Koza, P., Hryńczuk, B., Łysiak, M., Gałązka, R., Pecio, M., Suszek, B., Miturski, T. and Hryńczuk, B. (2012) Absolute content of trace elements. In: Siebielec, G. (Ed.) Monitoring of the chemical composition of soil in Poland in 2010-2012. IUNG PIB, Puławy. 71-74.
[17] Wieczorek, K., Wyszkowska, J. and Kucharski, J. (2014) Influence of zinc, copper, nickel, cadmium and lead in soils on acid phosphatse activity. Fresen. Environ. Bull., 23(1A), 274-284.
[18] Alef, K., Nannipieri, P. and Trasar-Cepeda, C. (1998) B-glucosidase activity. [in:] Applied Soil Microbiology and Biochemistry. K. Alef, P. Nannipieri (eds), Academic Press. Harcourt Brace & Company Publishers, London. 350-352.
[19] Orwin, K.H. and Wardle, D.A. (2004) New indices for quantifying the resistance and resilience of soil biota to exogenous disturbances. Soil Biol. Biochem. 36, 1907-1912.
[20] Lityński, T., Jurkowska, H. and Gorlach, I. (1976) Chemical and agriculture analysis (in polish), PWN, Warszawa. 129-132.
[21] NF ISO 10390. (2005) Soil Quality, Determination of pH. AFNOR. 7.
[22] Polish Standard PN-92/R-04016. (1992) Agrochemical Soil Analyse, Determination of assimilated zinc contents, Polish Committee for Standarization (in polish). 4.
[23] Polish Standard PN-92/R-0401. (1992) Agrochemical Soil Analyse, Determination of assimilated copper contents, Polish Committee for Standarization (in polish). 4.
[24] StatSoft Inc. (2012) STATISTICA (Data Analysis Software System), TULSA, USA, version 10.0.

[25] Moreno, J.L., García, C. and Hernández, T. (2003) Toxic effect of cadmium and nickel on soil enzymes and the influence of adding sewage sludge. Eur. J. Soil Sci. 54, 377-386.
[26] Šiša, R. (1993) Enzymová aktivita půdy jako ukazateljeji biologickié aktivity. Rost. Vyroba. 39, 817-825.
[27] Masto, R.E., Chhonkar, P.K., Singh, D. and Patra, A.K. (2008) Changes in soil quality indicators under long-term sewage irrigation in a sub-tropical environment. Environ. Geol. 38, 1577-1582.
[28] Parisa, S., Hasan, S.V., Ahmad, H. (2008) Evaluation of some paddy soil properties on urease enzyme acivity. Conference on international Research on Food Security, Natio-nal Resources Management and Rural Development, Tropentag. 4.
[29] Kuperman, R.G. and Carreiro, M.M. (1997) Soil heavy metal concentrations, microbial biomass and enzyme activities in a contaminated grassland ecosystem. Soil Biol. Biochem. 29, 179-190.
[30] Frederick, O.O., Iroha, A.E. and Oswald, E.Ch. (2014) Evaluation of the concentration of selected heavy metals and the effects on soil enzymatic activities in abandoned cement factory Nigercem Nkalagu and its environs. Int. J. Biochem. Res. 4(1), 16-27.
[31] Dick, W.A. and Tabatabai, M.A. (1983) Activation of Soil Pyrophosphatase by Metal ions. Soil Biol. Biochem. 15, 59-363.
[32] Wyszkowska, J., Kucharski, M. and Kucharski, J. (2010) Activity of β-glucosidase, arylsulphatase and phosphatases in soil contaminated with copper. J. Elem. 15(1), 213-226.
[33] Kucharski, J., Boros, E. and Wyszkowska, J. (2009) Biochemical activity of nickel-contaminated soil. Pol. J. Environ. Stud. 18(6),1039-1044.
[34] Lee, I.S., Kim, O.K., Chang, Y., Bae, B., Kim, H.H. and Baek, K.H. (2002) Heavy metal concentrations and enzyme activities in soil from a contaminated Korean shooting range. J. Biosci. Bioeng., 94(5), 406-411.

Received: **01.01.2017**
Accepted: **28.09.2017**

CORRESPONDING AUTHOR

Jadwiga Wyszkowska
University of Warmia and Mazury in Olsztyn, Faculty of Environmental Management and Agriculture, Department of Microbiology, 10-727 Olsztyn, Pl. Lodzki 3, Poland,

e-mail: jadwiga.wyszkowska@uwm.edu.pl

© by PSP Volume 26 – No. 12A/2017 pages 7667-7673 Fresenius Environmental Bulletin

BIOCHAR-MOREL PROMOTES WHEAT SALINE RESISTANCE BY INCREASING ROOT/SHOOT RATIO

Zhongdong Yu[1,*], Phonepaserd Phanpadith[1], Shuai Zhang[1], Dan Yu[1], Minglei Li[2], Yongxiang Kang[1]

[1]College of Forestry, Northwest A&F University, Yangling, Shaanxi Province, 712100,China
[2]Institute of soil and water conversation, Chinese Academy of Science, Yangling, Shaanxi, 7121009, China

ABSTRACT

Water and soil with rich phosphate and salinization, as well as soil degradation, raise the requirement of adopting alternative methods for soil improvements. The potential use of symbiotic fungi and modern vector material agents as soil amendments increases the interesting of scientists world widely. To identify the role of biochar-morel agent for winter wheat growing in the salt stressed soil, winter wheat seeds were arranged in pot array after biaochar-morel agents were input to the soil, and growth index was dated and evaluated in green house. High performance liquid chromatography (HPLC) and histological dying after artificial inoculation were employed to detect the phytohormone secreted by morel in the liquid suspending and symbiosis structure, respectively, biochar was prepared in a optimized program from trimmed cedar in winter. Results showed seeds germinated highest at concentration 1.5% of this mixture. Without salt stress (namely, the positive control PC2), biochar-morel could improve seedlings root/shoot ratio significantly ($p<0.05$) at concentration 2.0%, 2.5%, with ratio of 0.469, 0.549, respectively. However, under 0.5% salt stress, the biochar-morel agent could improve root/shoot ration of seedlings significantly at tested concentration from 1.0% to 2.5% ($p<0.05$), with ratio of 0.515,0.653,0.573, 0.580, respectively, which are even higher than those results from positive control PC2. No significant difference was found on seedlings height, fresh weight, and biomass, but most of them are higher than the control except 0.5% tested concentrations whether under salt stress or not. Higher concentration showed higher improvement for wheat growth index. Averagely, salt stress can contribute 21% inhibition ratio for seeds germination, 21.8% for seedlings height, 36.3% for seedlings fresh mass, 12% for biomass, and 23.9% for root/shoot, respectively. However, biochar-morel can relieve salt stress at ratio 33.3% for seeds germination, 3% for height, 21% for fresh mass, 36.4% for biomass, and 471.4% for root/shoot ratio, respectively. Winter wheat improve itself salt resistance by enhancing root/shoot ratio. Morel in this study can secret phytohormons, IAA, SA and ABA, and so further stimulate the root system developing. Biochar in this agent can help reserving the activity of morel by concentrating nutrition and humidity around the morel mycelium, the interaction between morel and biochar gets a win-win result for wheat growing. This is a novel soil improving agent with potential application in practise.

KEYWORDS:
Biochar-morel agent, Winter wheat, Growth, Salt stress, Phytohormones

INTRODUCTION

In recent years, problems of soil salinization, water and soil rich phosphate and degradation in north China are getting very serious, seeking pollution-free bio-fertilizer and soil amendments has become a new trend of modern agriculture. Organic fertilizer, nanotechnology and high molecular polymer materials, and so on, have been implemented in soil improvement and environmental management [1],[2], in which the activated carbon material, because of its special micro porous structure and physicochemical properties[3], can help plants absorb nutrients, adjust the soil nutrients cycling, maintaining soil fertility, has been reported successfully applying for soil improvement in practise [4]. Soil effective microorganisms (EM), including rhizoidal, nitrogen-fixing bacteria [5], phosphorous bacteria [6],[7], mycorrhizal fungi [8], endophyte [7], which can establish good symbiosis relations with plant root system [9], and help plants absorb nutrients [10], [11], increase plant resistance by inducing the expression of resistant genes under biotic and abiotic stress [12],[13], or secreting plant pathogen antagonism for confronting pathogen infection[14], are so widely used as a novel agent instead of traditional chemical fertilizers and soil amendments. The synergistic from effective beneficial microorganisms (EM) and biological charcoal combination has created a new type of soil amendments with high efficacy, but also increase the sustainable adaptability of beneficial microbes in harsh environments [11].

In order to explore a comprehensive utilization of agricultural and forestry waste, we made those waste into biocharcocal, and optimized a cedar biochar for combining with an ascomycets, *Morchella crassipes*, collected from Chinese red pine stands

(*Pinus massoniana* Lamb.) in Mt. Qinling, we checked this agent in greenhouse and recorded the impact on winter wheat under a salt stress, so as to figure out a putative agent for soil improvement in north China, where soil salinization is prevail.

MATERIALS AND METHODS

Materials. Biochar material was prepared according to the method of Liang Xiao *et al,* [15]. Trimmed cedar branches were collected and dried to 50% fresh moisture content, cut into 10 cm of small section, and then put into the ceramic fibber muffle furnace in coking, according to the preset program within 80 min gradually from room temperature to 900 ℃ and back to room temperature, as the followings, 100 ℃ 10 min, then 200 ℃ 15 min, 400 ℃ 15 min, 600 ℃ 20 min, 800 ℃ 20 min, 900 ℃ 15 min, and then down to 800 ℃ 15 min, 300 ℃ 15 min, then decrease to 100 ℃ and powered off till it gets to room temperature naturally.

The branches after above program yielded a black biochar, with pH 8.17. It was crushed and sieved with 1 mm mesh size, and was left for the following processes.

Soil was collected from Yangling region in Shaanxi province, a typical farming soil under surface 5 ~ 10 cm depth , dried by natural wind and then sieved by a 1 mm mesh. Tested winter wheat varieties is Xiaoyan 6, which is widely planted in Yangling region, bought from Yangling Jin seed company. *Morchella crapsesis* was collected under the tree, *Pinus mossoniana* in Mt. Qinling , and identified by phylogen tree and morphology and kept in forest pathology lab in Northwest A&F University as no. NW-morel-003. When the morel was inoculated on PDA medium after 7 to 10 d culturing with sclerotium developed, it was scraped down gently from petridish surface and washed into sterilized water, a blender (PE, teck BTC - 329, USA) was then employed to prepare morel suspending liquid by 1 dish Φ (90 mm) per 100 mL sterilized water.

TABLE 1
Composition of the medium mixture

Composition	Cedar biochar	Corn cob powdery	agar	K_2HPO_4	$CaCl_2$
Ratio(%)	5	85	5	2.5	2.5

Preparation of biochar-morel agent. The culture medium mixture for the agent involved compositions as that in Table 1, per 100 gram mixture was pushed into one 150 mL triangle bottle for sterilization at 121 ℃ for 20 min. After cooling, Morchella suspending liquid of 30 mL was poured into each bottle, and then incubated in 25 ℃ chamber for 7-10 days so that the biochar-morel agent was developed.

Growth test by applying biochar-morel agent. Biochar-morel agent of weight ratio 0.5%, 1.0%, 1.5%, 2.0%, 2.5% per 800 gram soil, and 0.5% salt per 800 gram of pot soil , were blended carefully before putting them together into the pot as treatment groups with 3 repeats. A set of 3 repeats blanked with salt and biochar-morel was chosen as negative control group (abv. NC), and a set of 0.5% salt per pot without biochar-morel (abv. PC1) and without salt but biochar-morel (abv. PC2) were taken as positive control groups. Winter wheat seeds of 15 was planted into per pot and grow under 25℃ greenhouse with enough lighting. Dated germ ration by sprout seeds number dividing 15, and harvested shoot and root of seedlings 15 d later. Seedlings were dried at 105 ℃ for 2 h, and biomass of shoot and root was recorded. Average growth index under negative control and positive control, as well as under treatments (abv. TR) were then figured out and surveyed . The salt stress ratio (SSR) calculated as the formal, SSR = index of (NC - PC1) / NC * 100%; the relieved stress contributed by biochar-morel (abv. RSD) was calculated by formal, RSD = index of (TR-PC1) / PC1 * 100%; the putative promotion contributed (abv. PPD) by biochar-morel was calculated by formal; PPD1 = index of (PC2-NC) / NC * 100%; PPD2 = index of (TR-PC1) / PC1 * 100%.

Infection histological observation. Sampled root of winter wheat, washed in running tap water carefully, and then checked under the microscope in order to pick up the infected hair root. A freehand cutting was made and stained by cotton blue and acid fuchsin, respectively. Infection structures of root were checked and recorded under a microscope Leica 4000B.

Detection of Phytohormones. The *M. crassipes* strain was inoculated into liquid potato dextrose media at 25°C for at least 8 days to allow the fungus to secrete hormones such as indole-3-acetic acid (IAA), abscisic acid (ABA), jasmonate, salicylic acid (SA) and gibberellic acid. After filter sterilization, the media were analyzed and quantified using an LC-20AD high-performance liquid chromatography system (Shimadzu, Kinh Do, Japan) and an API 2000™ electro spray tandem mass spectrometer (Allen-Bradley, Milwaukee, WI, USA) per 8 days. Samples were separated within a Wondasil™ C18 column (5 µm, 4.6 × 150 mm; Shimadzu) as described by Shi et al. [16]. The amount of exogenous hormone was calculated from the peak areas of exogenous phytohormone compared with the corresponding standards.

Statistical Analysis. Microsoft Excel 2003 and IBM SPSS18.0 Statistics software were employed for data processing and statistical analysis, LSD method of the multiple comparison was used to judge the difference between treatments and controls.

TABLE 2
Effect of different concentrations of the mixture on the wheat seeds germination ratio

	Germination rate(%)	Height (cm)	Weight(g)	Biomass(g)	Root/shoot ratio
NC	76±0.031	20.82±0.002	0.21±0.021	0.03±0.009	0.42±0.082
PC1	60±0.0103	16.29±0.19	0.132±0.082	0.022±0.008	0.318±0.062
PC2	80±0.0285	21.4±0.63	0.21±0.013	0.03±0.0057	1.02±0.29
TR	62±0.091	16.78±1.57	0.16±0.39	0.03±0.0066	0.96±0.207
SSR	21.0526±0.33	21.7579±9.89	36.53846±2.9	12±0.111	23.92344±0.243
RSD	33.3333±2.19	3.00798±7.26	21.212±3.76	36.36364±0.18	471.4286±2.34
PPD1	5.26315±0.08	2.88461±0.13	0±0.38	20±0.367	142.8571±2.536
PPD2	3.33333±0.01	3.00798±0.02	21.2121±0.03	36.36363±0.11	201.88679±1.24

TABLE 3
Growth index of winter wheat under the biochar-morel applied (P＜0. 05)

concentration (%)	Height (cm)	Fresh mass (g)	Biomass per seedling (g)	Root-fresh weight (g)	Shoot-fresh weight (g)	Root/Shoot
0	20.82±1.82a	0.208±0.02a	0.035±0.04a	0.042±0.01a	0.166±0.01a	0.255±0.06a
5	20.11±0.56a	0.213±0.01a	0.024±0.04ab	0.054±0.00ab	0.160±0.02a	0.341±0.06a
10	21.93±1.52a	0.205±0.01a	0.029±0.05ab	0.049±0.00a	0.156±0.00a	0.313±0.02a
15	21.15±1.80a	0.191±0.03a	0.025±0.03ab	0.047±0.01a	0.144±0.01a	0.322±0.04a
20	21.65±1.70a	0.222±0.04a	0.039±0.02bc	0.072±0.02bc	0.151±0.02a	0.469±0.09b
25	20.84±1.12a	0.228±0.01a	0.033±0.01bc	0.081±0.01c	0.147±0.00a	0.549±0.09bc

Note: Different small letters in the same column mean significant difference (P＜0. 05).

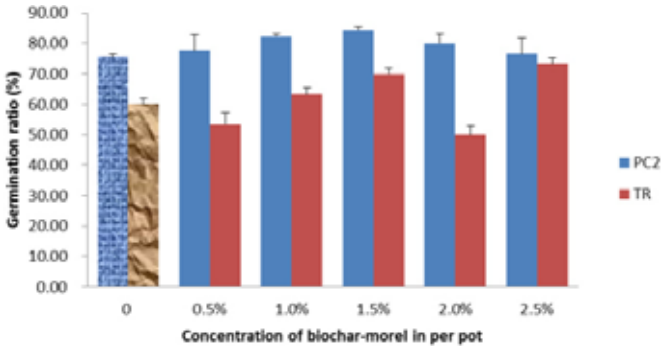


FIGURE 1
Seeds germination ratio under PC2 and TR

RESULTS AND ANALYSIS

Germination under biochar-morel agent applying. Compare the negative control NC, the seeds germination of the positive control PC1 is significantly lower than the NC, all positive control PC2, with application of biochar-morel only, improved averaged 9.86% germination rate of wheat seed comparing to PC1. At the concentration of 1.0% and 1.5% of the agent in PC2 group, seeds germination reached the highest rate of 84% and 70%, respectively (Figure 1), however, At 2.0% concentration point, germination rate getting down below the PC1. Under 0.5% salt stress, all groups showed lower seeds germination than NC, however, comparing to PC1, germination in treatment groups showed diverse style. concentration at 1.0%, 1.5%, 2.5% showed significantly higher germinated ratio than PC1 (P<0.05), the other two concentration, 0.5%, and 2.0% were significantly lower than the PC1(P<0.05), salt stress inhabited seeds average germ rate (SSR) 21.056%, Table 2 .

Seedlings growth by applying biochar-morel mixture. Different concentrations of biochar-morel can promote height of winter wheat seedlings, but there was no significant difference compared with the negative control. At concentration of 1.0%, wheat seedlings reached maximum height of 21.93 cm averagely; Biochar-morel can both promote the root weight and root/shoot ratio, when at concentration 2.0% and 2.5%, there is a significant difference from the negative control (p<0.05), Table 3, Figure 2. Fresh mass of seedlings showed no significantly difference among treatments, while biomass of seedling at 0.5% and 1.5% is significantly lower than the negative control, the other treated concentration showed no significant difference with the negative control. The low concentration of biochar-morel agent is not helpful for seedlings biomass accumulation, but helpful for height, root fresh weight and root/shoot ration, those index are slightly higher than the negative control. Table 3. The averaged promotion of biochar-morel for seedlings was 2.8% for height, zero for fresh mass, 20% for biomass,

142.8% for root/shoot ratio without salt stress, respectively, and 3% for seeds germination and height, 21% for fresh mass, 36% for biomass, 201% for root/shoot ratio under salt stress, respectively, Table. 2.

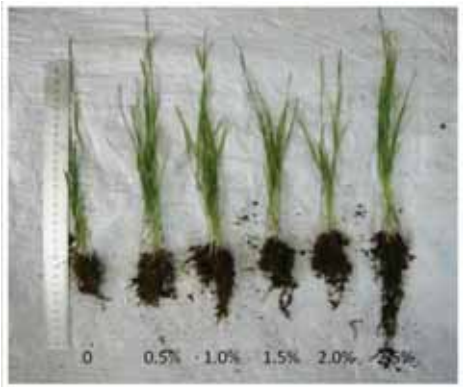


FIGURE 2
Winter wheat grow in pot with biochar-morel applying
Note: 0,0.5%,1.0%,1.5%,2.0%,2.5% represent biochar-morel concentration used

Salt resistance of wheat seedlings. Compared with NC, salt stress inhibited growth index of seedlings, too, Table 3. The inhibition ratio for height is 2.75%, 36% for fresh weight, 12% for biomass, 23% for root/shoot ratio, respectively. Compared with the positive control PC1, the biochar-morel can relieve salt stress (RSD) and promote each growth index (PPD), especially on root/shoot ratio. Biochar-morel can relieve salt stress ratio more than 4 fold that of the positive control PC1 (RSD=471%), and enhance root/shoot ratio 142% (PPD1) than the negative control PC2, 201.9% (PPD2) than the positive control PC1, Table 2. All treatment groups (TR) except at 0.5% biochar-morel, root/shoot ratio of 0.515, 0.653, 0.573, 0.580 under concentration 1.0%, 1.5%, 2.0%, 2.5%, were significantly higher than the positive control PC1, and at 1.5% concentration, root/shoot ratio reached the highest among all TR, Table 4. However, the height of seedlings was diverse and no significantly difference between the treatments (TR) and the positive control PC1. Except at 2.5% concentration, all treatment seedlings height is lower than the PC1. At concentration 1.0% and 1.5%, biomass showed significantly higher than the PC1, biomass of concentration 2.0% and 2.5% showed no difference with the PC1, and biomass 0.5% concentration is significantly lower than the PC1, this 0.5% concentration showed no help for biomass acumination whatever it is under salt stress or without salt stress, Table 3&4. Biochar-morel improve wheat salt stress and biomass by helping root system developed, the root/shoot ratio under salt stress and without salt stress are both higher than the negative control.

TABLE 4
Effect of the mixture on wheat seedlings growth under the stress of 0.5% NaCl (P＜0. 05)

Concentration (%)	Height (cm)	Fresh mass (g)	Biomass per seedling (g)	Root fresh weight (g)	Shoot fresh weight (g)	Root/Shoot
0	16.29±1.08a	0.124±0.01a	0.142±0.03a	0.037±0.01a	0.087±0.02a	0.420±0.04a
0.5	14.49±4.61a	0.112±0.11a	0.073±0.04ab	0.033±0.01a	0.079±0.02a	0.413±0.03a
1.0	16.23±0.17a	0.143±0.01a	0.191±0.02abc	0.049±0.01a	0.094±0.01a	0.515±0.05b
1.5	14.43±3.15a	0.138±0.00a	0.165±0.03abc	0.047±0.02a	0.091±0.01a	0.653±0.01c
2.0	16.12±1.27a	0.148±0.01a	0.148±0.02a	0.054±0.02a	0.094±0.01a	0.573±0.04bc
2.5	12.85±0.52a	0.158±0.04a	0.147±0.01a	0.058±0.01a	0.100±0.00a	0.580±0.03bc

Note, Different small letters in the same column mean significant difference (P＜0. 05).

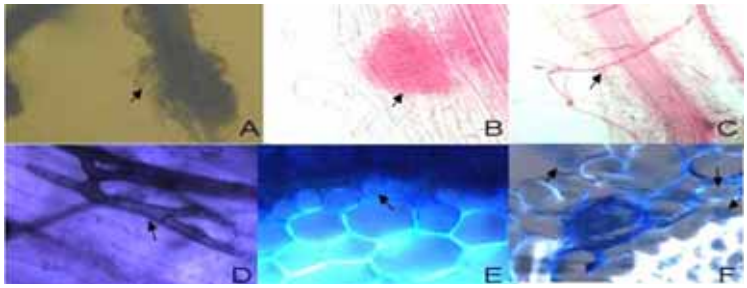


FIGURE 3
Colonization of *M. crass ipes* in the wheat root tissue
(Note, arrows refer to mycelia of infected morel)

A: the roots of infested, top enlargement, be full of hyphae circled the root surface; B: the hypha infection, induced root primordium (Fuchsin dyeing); C: the root surface with red mycelium (Fushin dyeing); D: the longitude mycelium in root epidemic (Cotton blue dyeing); E: Mycelium intra and inter epidermal cells and cells infected get enlarged (Cotton blue dyeing); F: the cortex cells, Casparian strip cells, pericycle cells infected by mycelium (Cotton blue dyeing).

Colonization of morel on the root of winter wheat. Roots infected by morel get swelled, and more adventitious roots and haired roots occurred whatever under salt stress or not. Infected hypha can be found both at root epidemic and primordial root , Figure 3 (A,B,C). Cross-section of cotton blue showed a mycelium sheath circled around the root, Figure 3D,E. Mycelia could be observed at the epidermal root layer, cortex layer (Figure 3E, F), Casparian strip cell and vessel cells in the pericycle (Figure 3F). Cortex cells infected with the mycelia became enlarger than those that were not infected (Figure 3E). Colonization of wheat roots by *M. crassipes* occurred both at the intercellular and intracellular levels (Figure 3E), forming an ectendomycorrhiza-like structure but without the ectomycorrhizal harting net, similar to that sweet corn[17].

Phytohormones secreted by biochar-morel. The functional endophytes ascribed to phytohormones secreted by themselves or induced from the host plant [18]. In this study, ABA, SA, and IAA could be stably detected after *M. crassipes* was inoculated into the liquid medium of potato and dextrose with concentration of 44.43 ng/mL, 36.55 ng/mL and 5.16 ng/mL at 24 dpi (Figure 4), respectively. Jasmonic acid and gibberellic acid 3 could not be detected by HPLC in this study. Further, none else of the phytohormones were found in the control samples.

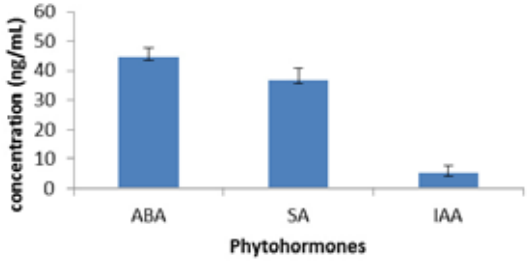


FIGURE 4
Phytohormones secreted by *M. crassipes* at 24 dpi

DISCUSSION

Generally, species of Morchella are symbiotically versatile; a strain of Morchella that was mycorrhizal with species of a Pinaceae species, was a non-mycorrhizal symbiont of *Arbutus menziesii* [19], a species of black morel can promote one European grass （*Bromus tectorum*） growth and its fire tolerance strongly, which was attributed to the seasonal forest fire in North America[20]. China is rich in Morchella species[21], most of them are explored as edibles, but they possess remarkable potential to be used for symbiotic associations in the agro-forestry system. We have collected another isolate morel, NW-morel-001, and we have found it can help crops and trees absorb nutrients, improve stress resistance and stimulate plant growth by secreting phytohormones[17]. In this study, SA and ABA secreted by morel were believed to be functional of water metabolism, stomata behaviour, biotic and abiotic resistance[22], IAA is in charged for improving wheat growth[23], the symbiosis histological checking also provide more clues for this kind of functional morel, more hair roots and swelled root tip were found if there is a morel colonized. Furthermore, exogenous abscise acid was reported to alleviate zinc uptake and accumulation in *Populus* × *canescens* when exposed to excess zinc[15], while, we still don't know whether those phytohormones we detected can help hold back the salt harm directly. Biochar in this study not only acted as a vector for morel survival under high salt stress environment, but also biochar itself can improve plant stress resistance by absorbing ambient humidity, changing iron motion and magnetic field around it, which interacts with morel symbiosis was proved more higher effective for winter wheat growth than sole using respectively (data not shown). Biochar-morel can increase root/shoot ratio significantly both under 0.5% salt stress and non-salt stress, which means root system developed well with this potential soil ameliorant, and the optimized concentration for using this biochar agent is from1.0% to 2.0% in greenhouse tests. Lower concentration than 0.5% in this study may not be helpful for morel-wheat symbiont construction, as that reported in mycorrhizal symbiont [24]. Fungi infection and salt harm may add up the burden for plant survival under a transformation soil, and an unfit higher concentration of biochar-morel can also accelerate the early infection and hence cause the seeds germinated badly and seedlings died quickly (data not shown). Growing winter wheat faced many challenges, including climate change[25] and rude tillage system[26], which seriously affect wheat yield in the world. This study first provided a novel symbiont soil amendment vectored by biocharcoal for winter wheat in greenhouse, however, the functional mechanism is still beyond understand, and need an intensive study in the future.

CONCLUSION

Winter wheat improve itself salt resistance by enhancing root/shoot ratio. Biochar-morel in this study can secret phytohormons and so further stimulate the root system developing. Although biochar-morel agent showed a diverse function on seeds germination, seedling heights, fresh mass and biomass, this novel agent can enhance root/shoot ratio stably and showed a potential application in field. Biochar-morel at concentration above 1.0% can help seeds germinate and root developing, increase root/shoot ratio significantly and so enhance winter wheat salt

resistance. Morel in the mixture can secret phytohormones, including IAA, SA and ABA, and form a special symbiosis with wheat, which is attribute to growth index promotion. Biochar as a functional vector in this study can help morel sustainably survival under stressed environment. This interact between biochar and morel got a win-win result for winter wheat, and showed a potential application in practise.

ACKNOWLEDGEMENTS

This study was supported by the national key research projects 2017YFD0600103-4-2 in China, Shaanxi Agricultural science and Technology Extension Project (2014NY124) and Forestry industry research special funds for public welfare projects (201404302).

The authors have declared no conflict of interest.

REFERENCES

[1] Downie, A., Crosky, A., Munroe, P. (2009) Physical properties of biochar [M]. In: Lehmann J, Joseph S (eds). Biochar for Environmental Management Science and Technology. ISBN:1849770557.

[2] Kurosaki, F., Koyanaka, H., Hata, T. (2007) Macroporous carbon prepared by flash heating of sawdust . Carbon. 45, 671-673.

[3] Chun, J., Xue, J.H., Jin, M.J. (2014). Review of researches on effects of biochar in reducing nitrogen and phosphorus losses with agricultural non-point source pollution. Journal of Ecology and Rural Environment. 30(4), 409-415.(in Chinese)

[4] Elmer, W.H., Pignatello, J.J. (2011) Effect of biochar amendments on mycorrhizal associations and Fusarium crown and root rot of Asparagus in replant soils. Plant Disease. 95(8), 960-966.

[5] Yang, Q., Chai, W.J., Zhang, C.L. (2013). Effects of a microbial fertilizer on *Sorghum bicolor* L. seeds germination, seeding growth and stress tolerance. Journal of Inner Mongolia Agricultural University. 34(6), 102-109.(in Chinese)

[6] Wei, W.,Wu, X.Q., Qiao, H. (2014) Screening and identification of phosphate-solubilizing fungi of Pinus massoniana rhizosphere and its application. Scientia Silvae Sinica. 50(9), 82-88. (in Chinese)

[7] Zhao, X.R., Lin, Q.M. (2001) A review of phosphate-dissolving microorganisms. Soils and Fertizers. 3, 7-11.(in Chinese)

[8] Brundrett, M., Bougher, N., Dell, B. (1996) Working with mycorrhizas in forestry and agriculture. Australian Centre for International Agricultura. 30(30),1947-1949.

[9] Wang, Y.F., Shen, T., Chen, X.S. (2014) Biological carbon mitigation hydroxybenzoic acid damage Malus seedlings role. Chinese Agricultural Sciences. 47(5), 968-976.

[10] Yoshizawa, S., Tanaka, S. (2008) Acceleration of composting of food garbage and livestock waste by addition of biomass charcoal powder. Asian Environmental Research. 1, 45-50.

[11] Wang, T. (2013) Efficient mutagenesis bacteria and biological carbon composites of heavy metal contaminated soil repair. Nankai University PHD Dissertation.(in Chinese)

[12] Abit, S.M., Bolster, C.H., Cai, P. (2012) Influence of feedstock and pyrolysis temperature of biochar amendments on transport of Escherichia coli in saturated and unsaturated soil . Environ. Sci. Technol. 46(15), 8097-8105.

[13] Yu, Z.D., Ren, Z.Z., Peng, S.B., Zhang, S. (2014) Effect of activate charcoals and a coupled biochar on growth of crops. Biomass Chemical Engineering. 48(3), 1-5.

[14] Warnock, D.D., Lehmann, J., Kuyper, T.W. (2007) Mycorrhizal responses to biochar in soil-concepts and mechanisms. Plant and Soil. 300:. 9-20.

[15] Liango, X., Yu, Z.D., Ma, J., Zhu, W.X., Zhao, C.J., Chen, L.M. (2013) Preparation and characterization of activated biocharcoal from different tree species. Chemistry and Industry of Forest Products. 33(3),125-130

[16] Shi, W.G., Li, H., Liu, T.X., Polle, A., Peng, C.H. (2015) Exogenous abscise acid alleviates zinc uptake and accumulation in Populus x canescens exposed to excess zinc. Plant Cell and Environment. 38, 207-223.

[17] Yu, D., Bu, F.F., Hou, J.J., Kang, Y.X., Yu, ZD. (2016). A morel improved growth and suppressed Fusarium infection in sweet corn. World J Microbiol Biotechnol. (2016) 32,192.

[18] Provorov, N.A., Vorobyow, N.I., Tikhonovich, I.A. (2009).Evolutionary genetics of plant-microbe symbioses. ISBN: 9781608768066

[19] Dahlstrom, J.L., Smith, J.E., Weber, N.S. (2000). Mycorrhiza-like interaction by Morchella with species of the Pinaceae in pure culture synthesis. Mycorrhiza. 9, 279-285.

[20] Baynes, M., Newcombe, G., Dixon, L., Castlebury, L., O'Donnell, K. (2012). A novel plant-fungal mutualism associated with fire. Fungal Biol.116, 133-144.

[21] Du, X.H., Zhao, Q., O'Donnell, K., Rooney, A. P. and Yang, Z.L. (2012) Multigene molecular phylogenetics reveals true morels (Morchella) are especially species-rich in China. Fungal Genetics and Biology. 49,455-469 .

[22] Waqas, M., Khan, A.L., Kamran, M. (2012). Endophytic fungi produce gibberellins and indoleacetic acid and promotes host-plant growth during Stress. Molecules.17(9),10754-73.
[23] Dat, J.F., Lopea-Delgado, H., Foyer, C.H. (1998). Parallel changes in H2O2 and catalase during the remote tolerance induced by salicylic acid or heat acclimation in mustard seedings. Plant physiol, 116(3), 1351-1357.
[24] Nina, K., Marie-Pierre, T., Ernst, E.H. (2009) Interactions between mycorrhizal fungi and mycorrhizosphere bacteria during mineral weathering: Budget analysis and bacterial quantification. Soil Biology & Biochemistry. 41(9), 1935-1942.
[25] Caldag, B., Saylan, L., Akatas, N., Bakanogullari, F., Ozgur, E. (2017). Investigation of the adaptation potential of winter crop to future climatic conditions in northwest of Turkey. Fresen. Environ. Bull. 26(1), 29-39.
[26] Taner, A., Arisoy, Z.R., Kaya, Y, Gultekin, I, Parigoc, F. (2015). The effects of various tillage systems on grain yield, quality paramenters and energy indices in winter wheat production under the rained conditions. Fresen. Environ. Bull. 24a,1463-1473.

Received: **08.01.2017**
Accepted: **10.10.2017**

CORRESPONDING AUTHOR

Zhongdong Yu
College of Forestry, Northwest A&F University, Yangling,712100 Shaanxi China

e-mail: yuzhongdong001@nwsuaf.edu.cn

© by PSP Volume 26 – No. 12A/2017 pages 7674-7680 Fresenius Environmental Bulletin

ENVIRONMENTAL EFFECTS OF T-SHAPED GROINS BUILT ON THE EASTERN BLACK SEA COAST ON SHORE PROTECTION

Veli Sume*

Department of Civil Engineering, Faculty of Engineering, Recep Tayyip Erdogan University, 53100, Rize, Turkey

ABSTRACT

The construction of the double highway on the Black Sea Coast was initiated in 1998, completed in 2000. During the construction, T-shaped groins where were built to protect the shore. In this article, the contribution of T-shaped groins to beach formation and their positive or negative effects on the change of coast and submarine topography were environmentally examined.

For this purpose, before the research on the map the groins were marked then the places where the groins would be constructed were levelled by taking soundings and their bathymetric maps were prepared. After the groins were built, the surrounds of the T-groins were determined by taking data with the echo sounders device and their bathymetric maps were prepared again.

Afterwards, these are whose construction was completed were observed at the beginning of winter, at the end of winter, at the beginning of summer, and at the end of summer. These observations investigated whether a beach was formed on the coast and the environmental effects conclusions were investigated. At the end of the study, the effects of the groins on submarine topography in terms of shore protection and the positive or negative environmental contributions to the shore were determined and the data were shown in graphs and figures.

KEYWORDS:
Environmental protection, T-head groin, Coastal protection, Eastern Black Sea, Sediment

INTRODUCTION

The coasts; the sediments dragged by the creeks, streams, and rivers, the coastal structures and coastal currents are effected of the wind and waves. As long as there is no invention, it will reach the state of equilibrium after a long period of time. Each intervention affects the coastal dynamics and contributes the movement to reach the state of equilibrium.

The impacts of wind, currents and the sediment transport should be taken into consideration in order to ensure that coastal structures do not disturb the coastal equilibrium.

The project designer should make a project with the best approach that will not disturb the balance by analysing these effects thoroughly. These works should be done before the project starts. After the start of the project, any new developments should be monitored and if necessary the balance of the coast should be protected through adjustments [1, 2].

Otherwise, the coastal balance can be quickly deteriorated and it may lead to a massive loss of property and life. The human factor should not be ignored while conducting these studies and the applications that help to establish human-coastal relations should be preferred.

For the establishment of a coastal-human relationship, the best way to protect the coast is to build sandbanks on the coast. The groins are the most important engineering constructions made within the scope of the coastal protection [3, 4].

The groins are coastal protection structures built generally perpendicular to the shore in order to create a shoreline along the coast that keeps the sediment and prevents the coastal erosion. It is built in the form of I, T, Y, r and L. They are constructed in a way that the intermediate distance will be 2-3 times of the length depending on the shape of the coast, the direction and amount of the sediment transport and the wave climate of the region [5-7].

In addition the groins also is awkward serve to hold the moving material on the shore, preserving the balance of the existing beach, keeping the large items on the upper part of the beach, preventing the harbour and the fishermen's shelters from being filled and ensuring a smooth beach formation.

The groins which are constructed as a result of the analysis of the coastal parameters ensure the formation of the beach in a short time and accelerate the coastal-human relationship. In addition, they meet the market's need for sand and gravel by holding the sediment carried by the rivers and taking them according to the engineering procedures [8, 9].

When coastal structures are to be constructed, the conditions of the region should be carefully examined. The direction of the dominant wave and accordingly the direction of the sediment transport along the coast should be determined. If there is a

structure on the shore, the upstream side of the structures which is affected by the sediment transport will start to be filled, while its downstream side will be subjected to erosion. This situation provides different results for the structures which are constructed in series [10, 11].

Again, according to the reviews it was found that exact results were not given about the length, space and heading lengths of the groins. When a coastal structure is built on any coast the followings factors affect the shoreline changes; the height of the wave (H), wave period (T), the angle of the wave (α), bottom slope (tan β), grain diameter (d_{50}), the size of the structure (L_x), the distance between the structures (L_g) and the amount of the sediment transport along the coastline (Q).

It is understood from the literature studies that when a structure is constructed along the shoreline, the balance of the shore changes and the shoreline is affected. If there is not any structure, the shore remains in balance [12, 13].

The groins built on coasts are coastal structures that are usually built upright on the shore to prevent coastal sediment should be movements, to reduce its amount, to prevent erosion occurring on the coast and to create a new shoreline or protective beach. They are also used to reduce the sediment movement on the upstream side and to prevent the port and the fishery shelters from being filled.

The interaction between the groins and the sediment transport along the shoreline has a very complex relationship. Therefore, the ability to set very precise guidelines for projecting can be only the requires long work results.

While constructing a groin, the connection of the groin to the coast should be strong and it should enter at least a 6 m. area. The groins should be placed in such a way, that the sediments moving towards the shore should not go beyond the angle of the structure. In this case, the most important factors to considered are the direction and development of the waves and the movement of the material.

The length of the groins varies from about 30 to 200 meters. The average angle is taken approximately as,

$$L_G = (1-3).L_X \quad (1)$$

The "T" groins hold the shore materials from both sides and provide better protection according to the straight groins. A series of T-groins, that work together in order to protect a long part of the shore is called the groin system. The T-groins are both functionally and structurally different from the breakwater. The breakwaters are made from heavier and larger components and therefore they are larger and higher. The length of a groin determines the amount of the coastal sediment transport and it is used to determine the gap between the groins. In the groins when the transport towards the shore increases, the transport towards the angle is decreased and the transport towards the downwards of the shore is protected. As a result the sand which was carried to the shore will form a hill. Although the groins which were examined in this study were made of stones, there are also groins type according to the types and function of the used materials. They can be classified in the following way.

According to the Type of the Used Material. Wooden groin, steel groin, concrete groin, asphalt and stone groins

According to the Function. Permeable, impermeable groins, high and low groins, fixed and adjustable groins

According to the Form. Plain (I) groins, T groins, L groins, Y groins, ┌ groins

MATERIALS AND METHODS

The wave climate of the Eastern Black Sea region; In the simplest sense, it can be said that wave is a mess that distorts and turns the balance of the hydraulic system upside-down. The waves seen in the seas, lakes and gulfs occur due to dependant forces such as tides and wind. They are named according to the name of the events they came from such as Tidal waves, wind waves etc. There are also waves which occur due to the volcanic eruptions and undersea earthquakes. Waves are classified according to the depths of the sea, the characteristics of the wave motions and the forces producing the wave.

Since the measurement of the wind wave is difficult and expensive, the observations are rather short. In Turkey, a regular wave measurement network has not been established yet. Therefore, the data which are required for the project estimated with the help of the wind records. The wind data which is used in the estimation of the wave is obtained from the meteorological wind data or from the synoptic wind maps [14-16].

Several methods have been developed to convert the wind data obtained from both sources into wave estimates. The most common of these is the SMB (Sverdrup Munk Bretschneider) method. The wind data used in this method is transformed into significant wave height and period.

The dominant wave direction of the shore region is N, NNW and NW and the significant wave heights vary between 1.5 m and 7.5 m. In some extreme values this can also reach 11.5 m. (At the storm which occurred in the region at the beginning of April 2002, a 200 kg heavy part of the lighthouse threw which was situated 12 meter high into the harbour).

Since the wave data obtained from the meteorological data are smaller than those obtained from

the synoptic maps, the data obtained from the SMB data were used for the safety of the structure.

The rivers in the Eastern Black Sea Regions are wild as their slopes are quite large due to the topographic structure of the region. Therefore, their flow rates are very high. This leads to significant sediment transport. This amount is estimated to be about 3-5 million tons / years [17-19].

The flow rate of the sediment carried by the stream depends on the flow conditions and the properties of the fluid and sediments.

$Q=f(v,\rho_s,\upsilon,d,\rho,h,R,j)$ (2)

(v: mean flow rate, ρ_s: specific weight of the sediment; υ: fluid viscosity; d: grain diameter; ρ: specific weight of the fluid; h: water depth; R: hydraulic radius; j: base slope of the river).

The general formula is given above. The general substance transport formula was developed by E. I..E.

$Q=14.153.101.26016.\log.A$ (3)

(A: basin area Km^2 ; Q: flow rate of the sediment tonnes/ year)

In addition, an equation was developed according to the data taken from the rivers in the Eastern Black Sea Region.

$Q = q, Q_{ort}$ (4)

a and b are regression coefficients, Q_{ort} is the daily average flow rate m^2/ sec. Q: the flow rate of the sediment transport tonnes / day.

The sediment transport made by the rivers in the Eastern Black Sea Region are estimated to be 3-5 million tonnes / year.

The sediment transport in the coast. The source of the sediment transport is the material which occurs as the result of the erosion of the land and the breakdowns of the rocks and is transported to the shore with the help of the rivers. The sediment which reaches the sea in this way is constantly moving in the coastal zone. This movement continues after adding the existing sediments. The movement of the sediments in the coasts is examined on the cross section of the coastal section of the unit width which is taken perpendicular to the shore and these sections are called the coastal profile. The coastal profiles are also classified according to the wave effects among themselves. The profile of the waves when they are small and less is called the "Normal Profile" or "Summer Profile" and when the waves are more and high then it is called the "Storm Profile" or "Winter Profile".

Although the main parameter which affects the coastal profile is the transport which is perpendicular to the coast, the effect of the parallel transport is also excessive. Here the effective factors are the settling velocity of the deep sea particle (w), mean wave stiffness (Ho/ Lo), and diameter of the sediment (d_{50}).

In addition, the sand- gravel which is taken randomly from the coast or from the coastal areas in improper manner can also change the coastal profile. The transport which is parallel to the shore is the transport caused by the coastal currents [20].

The impact of the groins onto the sediment distribution along the coast; T-groins are built along the route of the Black Sea Double Highway and are constructed to parallel the shore in most places where coastal protection is necessary according to the project criteria. The T-groins which have successfully been implemented in countries such as Japan, Britain, the USA and Israel have been constructed in groups in sequential order. Unlike the plain and L-groins they hold the sediment and do not leave it back during the transport which is upright or parallel to the shore.

The sand and gravel which constitutes the majority of the transport along the coast are kept by the groins built sequentially and as a result great sanding occurs on the shore. This new sanding creates a new shoreline and acquires a natural beach view. Thus, it contributes to the development of the coastal tourism and to the acceleration of the coastal-human relationship and allows people to benefit from the coast to the maximum extent.



FIGURE 1
The place and location of the T-groins

The sanding caused by the T-groins provides the opportunity to obtain a wide beach by continuing the coastal circulation. The coast ensures the balanced distribution of the sediment transport. The coast ensures the hydrodynamic balance as well as it helps to protect the highway from the wave effects and reinforcing the coastal-human relationship. It creates environmental health. On the other hand, the T- groins which are not built sequentially in a system along with the flat and L-groins may cause undesirable results such as damaging the shore. On the one hand, they fill the shore (by holding the sand-gravel), but on the other hand they may cause erosion (carving) [22].

Coastal erosion is one of the most frequent serious consequences that disrupt the coastal-human relations. The classic coastal protection structures which are made to prevent this are very large and expensive. Moreover, they completely disrupt the ecological balance of the place where they are built. They are causing environmental disasters.

The coastal engineers have started to look for effective solutions which can replace the classical coastal protection structures and which change the natural structure of the coast as little as possible. In this context, it can be easily said that the natural beaches are the best coastal protection structures. Therefore, the way to formation natural beach is to make T-groin.

This study examined the T-groins built on the coast of Trabzon Of - Soğukpınar for protection within the scope of the Black Sea Double Highway. The coast which was selected as the study area is a 1.7 km-long part of the Of coast whose total length is 11 km. There are 8 T-groins along the route (Figure 1). Also this route includes the port of Of, one fishery shelter and a boat yard.

The construction of the T-groins started in 2000 and in the same year all from this route were completed. They were constructed by combining them into groups. There are8 T-groins within the working area. In this study they are referred to as 1,2,3,4,5,6,7,8 from west to east [21].

All of the constructed groins are in the same size and the space between the groins (a) in the group is usually twice the size of the groin. Only the size of the No 3,4,5,6 groins along Soğukpınar is between 20 and 30 meters. The length of their headings (c) is half of the length of the groins (c= b/2). The size and the altitude are the same. The groin's height is b=75m, the length of the head is c=37.5 m, the space between the groins is a=150m, the width is 10 m, while the altitude of the groin is +1 m.

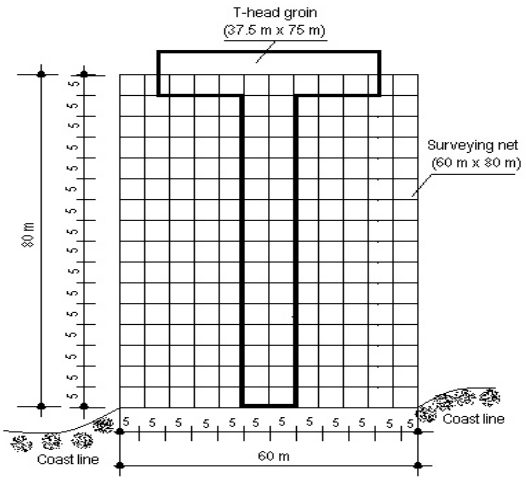
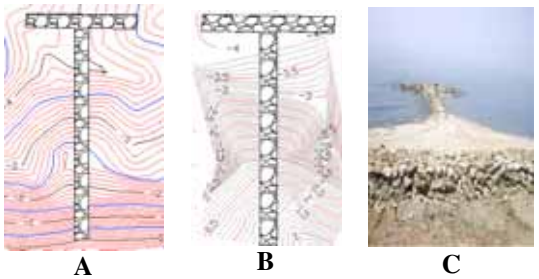


FIGURE 2
Measurement Grid

First of all visual inspections were performed on the constructed groins to determine whether there was any damage, filling or loss around the groin, if there was any sand-gravel accumulation around the heels. In addition, the groins are 60 m parallel to the sea and 80 m perpendicular to the sea. 5 x5 m grid sounding line capacity was realized on the area whose length is 60 x 80m (Figure 2).

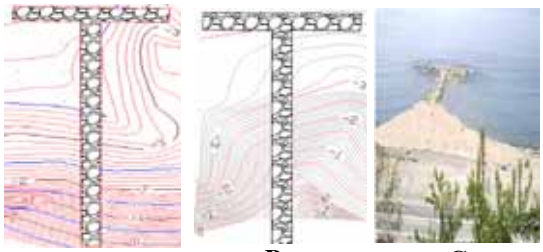
The contour lines of the groins were obtained by processing the obtained sounding values in a computer. This process was made separately according to the sounding values of the years between 2000 and 2016 and this gave the opportunity to compare the changes occurred within 16 years.

As a result; it was investigated whether there was material accumulation around the groins depending on the sediment motion and the groins were subjected to functional evaluation. The examination and evaluation was carried out 2 by 2 from west to east [23-28].



A **B** **C**

FIGURE 3
Soğukpınar T1 (A) July 2000, (B) July 2016, (C) Current view



A **B** **C**

FIGURE 4
Soğukpınar T3 (A) July 2000, (B) July 2016, (C) Current view

RESULT AND DISCUSSION

As a result of the research and investigation the groins were measured and evaluated 2 by 2 and the following results were obtained. In addition, the fullness % is according to the inside area of the T.

The transport which is parallel to the coast is also from west to east. So, the direction of the maximum transport dominant wave is north- west (NW). This means that the results of the investigation, measurement and observation are in agreement with

the theoretical information. This shows that the approach is correct. According to this: the T-head groins were constructed along the coast of Soğukpınar where there are 8 T-head groins in a group, an amount of material accumulated on the heel like sand, gravel et. on the No. T1, T2 and T3 groins. 33% fullness up to +2 altitudes has observed on the right heel of the Soğukpınar T4 groin (Figure 3-4 A-B-C).

There is a 35% fullness up to +2,5 altitudes on the heels of the Soğukpınar T5 and T6 groins. These groins which are filled with thin material are the groins that have had the most fullness so far. They are used as beache (Figure 5 A-B-C).

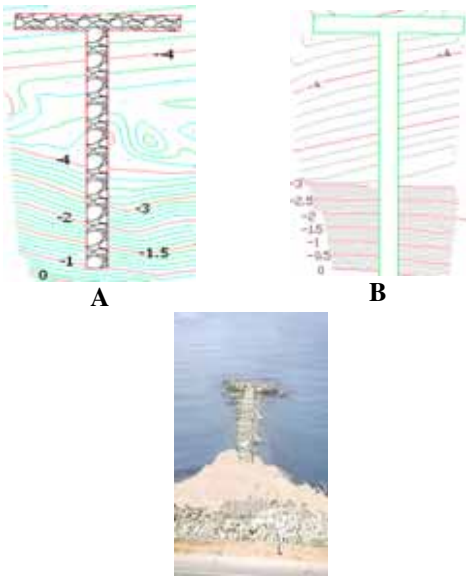
There is 50% fullness with fine material at the Soğukpınar T7 and T8 T-head groins. These overfilled T-head groins are used as beaches nowadays (Figure 6 A-B-C).

Their fullness rate is increasingly growing; they are used as beaches. There are 80% fullness with fine material at the Soğukpınar T7 and T8 T-head groins. These are the most filled groins according to the other T-head groins. They have very high environmental contribution and are used as beaches (Figure 3-4-5-6 A-B-C).

RESULS AND DISCUSSION

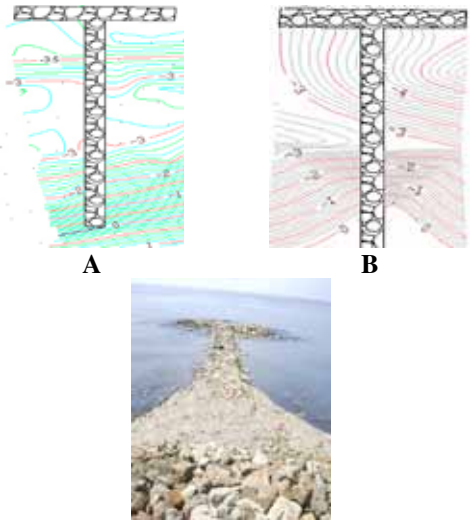
When the study area was investigated by walking along the coast, it was seen that the selection of the size was right, however the selection of the place was not done properly because, attention was not paid to the geometry of the groins and the altitude was too high (+1,5-2m). However, in some places on the beach T groin construction may be on agenda along the route until the end of the road construction. When these will be constructed in groups, it should be considered to calculate the distance between groins as 3 times of the length of the T and sufficient attention should be paid to the fishery shelters, boat yards and ports and the height of the construction should not exceed +0,5m. This allows the incoming waves to pass over the construction and reach the other T-groin, to release more materials and to speed up the filling.

Over time, the groins will be completely covered with sand and will disappear and a natural beach will be created. In this way, an environment will be occurred which can be used by the people more easily. In addition, the coastal changes should be monitored periodically, the occurred damages should be repaired, sand-gravel should be removed from the overfilled groins, and artificial filling can be done on some groins which need to be used as beaches. The coast must be monitored continuously and data bank should be established. It will be also useful to set up wave measurement stations at certain places along the coast in a region such as the Black Sea Region which provides too many values in this regard. In this way, data-based feedback will be ensured and the information reinforcement about the land and observation results will be realized. This data will increase the approach rate in the results after it is supported by empirical studies.



A B C

FIGURE 5
Soğukpınar T5 (A) July 2000, (B) July 2016, (C) Current view



A B

FIGURE 6
Soğukpınar T7 (A) July 2000, (B) July 2016, (C) Current view

REFERENCES

[1] Süme, V., Tansel, B. (2016) Capacity building for field inspections: A comprehensive assessment tool for monitoring structural integrity and sediment capture performance of T-head groins, Ocean & Coastal Management. 125, 20-28.

[2] Süme, V. (2014) Grain Size and Beach Formation Characteristic at the T-Head Groins System at Kiyicik, Turkey (Eastern Black Sea). J Civil Environ Eng. 4, 150.
[3] Güngördü, Ö., Otay, E.N. (1997) Kıyı şeridi değişiminin sayısal modellenmesi, inşaat mühendisliğinde gelişmeler III. Teknik Kongre, 701-710, Orta Doğu Teknik Üniversitesi (METU), Ankara, Turkey.
[4] CERC (1984) Shore protection manuel, fourth edition, US Army WES, Washington.
[5] CIRIA (1990) Groynes in Coastal Engineering: Data on Performance of Existing Groyne Systems. Construction Industry Research and Information Association (CIRIA), London, England. Technical Note 135.
[6] Süme, V. Önsoy, H., Yüksek, Ö. (1995) Dynamic Design of Breakwaters, 4.th. Int. Con. on Coastal and Port Eng. in Devel. Countries (COPEDEC IV), Rio de Janeiro, Brazil.
[7] Süme, V. (2002) Rize de İyidere-Çayeli arasında bulunan T-Mahmuzların kıyı koruma açısından incelenmesi, 4. Ulusal Kıyı Müh. Semp, Antalya, Turkey.
[8] Eslami Arab, S. (2009) A numerical study on design of normal and T-head groins. MSc-Report, Delft University of Technology, Delft, Netherlands.
[9] Özölçer, İ.H. (1997) Kıyı korunmasında mahmuzların etkilerinin araştırılması, Doktora Tezi (PhD Thesis), KTÜ, Fen Bil. Ens., İnş.Müh. Hidrolik ABD, Trabzon, Turkey.
[10] Önsoy, H., Yüksek, Ö. (1993) Doğu Karadeniz'de deniz erozyonuna karşı koruma ve yapay plajlar için kıyıya dik yapıların etüdü, K.T.Ü.-DPT Araştırma Projesi (Research Project), Trabzon, Turkey.
[11] Kraus, N.C., Hanson, H., Blomgren, S.H. (1994) Modern Functional Design of Groin Sytems, vol. 1327e1342. 24th ICCE, Kobe, Japan.
[12] Komar, P.D. (2011) Coastal erosion processes and impacts: the consequences of earth's changing climate and human modifications of the environment, reference module in earth systems and environmental sciences. Treatise Estuar. Coast. Sci. 3, 285-308.
[13] Özkan, E., Günbak, A.R. (1985) Introduction to Coastal and Harbour Engineering, Lecture Notes, METU, Ankara, Turkey.
[14] Saengsupavanich, C. (2012) Unwelcome environmental impact assessment for coastal protection along 7 km shoreline in Southern Thailand. Ocean & Coastal Management. 61, 20-29
[15] Uysal, K. (1995) Rüzgar verileri kullanılarak Doğu Karadeniz'de tasarım dalgası tahmini, Yük. Lis.Tezi (MsC Thesis), KTÜ, FBE, Trabzon, Turkey.
[16] Iskender, M.M., Frihy, O.E., El Ansary, A.E., Abd El Mooty, M.M., Nagy, H.M. (2007) Beach impacts of shore parallel breakwaters backing offshore submerged ridges, Western Mediterranean Coast of Egypt. Journal of Environmental Management. 85, 1109-1119.
[17] Çam, T. (1986) Doğu Karadeniz'de Dalga Tahmini ve Tasarım Dalgası Özelliklerinin Belilenmesi, Yük. Lis.Tezi (MsC Thesis), KTÜ, FBE, Trabzon, Turkey.
[18] Yüksek, Ö. (1992) Balıkçı Barınaklarının Dolma Sürecinin Araştırılması ve Uygun proje ölçütlerinin geliştirilmesi, Doktora Tezi (PhD), KTÜ, FBE Trabzon, Turkey.
[19] Van Rijn, L.C. (2011) Coastal erosion and control. Ocean & Coastal Management. 54, 867-887.
[20] Orhan, F. (1992) Doğu Karadeniz Akarsularında Sürüntü Maddesi Hareketi ve Miktarının Etüdü, Yük. Lis.Tezi (MsC Thesis), KTÜ, FBE, Trabzon, Turkey.
[21] E.İ.E. Genel Md. (1987) İnceleme, Türkiye Akarsularında Sediment Gözlemleri ve Sediment Taşıma Miktarları, Yayın No: 87.44, Ankara, Turkey.
[22] Önsoy, H. (1991) Batı Akdeniz'de Cezayir Kıyılarında Deniz Erozyonuna Karşı Korunma ve Yapay Plaj için Bir Etüd, DLH Bülteni, Ocak Sayısı, 2(5), 4-7.
[23] Hanson, H., Kraus, N.C. (2002) Chronic beach erosion adjacent to inlets and remediation by composite T-head groins. US Army Corps of Engineers, ERDC/CHL CHETN-IV-36.
[24] Doğuş Polat İnşaat (2002) Uygulama projeleri ve verileri, Rize, Turkey.
[25] Süme, V. (1998) Ölçme Bilgisi Kitabı, Bölüm 8, Hidrografik Ölçmeler, Derinliklerin ölçülmesi, İskandil alımı, Rize, Turkey, 317-342.
[26] US Army Corps of Engineers (1994) Hydrographic Surveying: Engineering and Design. Washington DC, US Army Corps of Engineers.
[27] Sane, M., Yamagishi, H., Tateishim, M., Yamagishi, T. (2007) Environmental impacts of shore-parallel breakwaters along Nagahama and Ohgata, district of Joetsu, Japan. Journal of Environmental Management. 82, 399-409.
[28] Bodge, K.R. (2003) Design aspects of groins and jetties. In: Mohan, R., Magoon, O., Pirrello, M. (eds.) Advances in Coastal Structure Design. American Society of Civil Engineers, Reston, VA. ISBN 0-7844-0689-8. 181-199.

Received: **23.01.2017**
Accepted: **28.09.2017**

CORRESPONDING AUTHOR

Veli Sume
Department of Civil Engineering
Faculty of Engineering
Recep Tayyip Erdogan University
53100, Rize – Turkey

E-mail: veli.sume@erdogan.edu.tr

© by PSP Volume 26 – No. 12A/2017 pages 7681-7686 Fresenius Environmental Bulletin

MULTIPLE TIME-SCALE PROPERTIES OF AIR POLLUTION INDICES: A CASE STUDY OF LANZHOU, CHINA

Zuhan Liu[1,2,3], Linan Sun[4], Jiayao Wang[5,6,*], Lili Wang[7], Kai Shi[3,8], Chunqiong Liu[8]

[1] Key Laboratory of the Education Ministry for Poyang Lake Wetland and Watershed Research, Jiangxi Normal University, Nanchang, China
[2]Jiangxi Province Key Laboratory for Water Information Cooperative Sensing and Intelligent Processing, Nanchang Institute of Technology, Nanchang, China
[3] Key Laboratory of Ecotourism in Hunan Province, Jishou University, Jishou, China
[4] College of Resources and Enviroment, Henan University of Economics and Law, Zhengzhou, China
[5] School of Resource and Environmental Sciences, Wuhan University, Wuhan, China
[6] Zhengzhou Institute of Surveying and Mapping, Zhengzhou, China
[7] School of Science, Nanchang Institute of Technology, Nanchang, China
[8] College of Biology & Environmental Sciences, Jishou University, Jishou, China

ABSTRACT

Based on the dynamics of air pollution in the Lanzhou from July 1, 2000 to June 30, 2015, the multi-scale characteristics of air pollution indices (i.e. SO_2, NO_2 and PM_{10}) are analyzed using the detrended cross-correlation analysis (DCCA). In the double logarithm curve $\log F^2(s)$~$\log s$, the long-range correlation of PM_{10} vs. NO_2 shows only one scaling regimes at the whole timescale which means their cross-correlation keep exhibiting long-term persistence with positive power-law in the scale-free interval of greater than 16 years; the long-range correlation of SO_2 vs. NO_2 shows two scaling regimes with two different scale indexes and a critical time scale of about one year; the long-range correlation of SO_2 vs. PM_{10} presents three scaling regime with three different scale indexes and with two critical time scales of about one year and 10 years. These results reflect the multi-scale response characteristics of the air pollution indices change on different time scales.

KEYWORDS:
Lanzhou, air pollution, multi-scale, power laws, long-range correlation

INTRODUCTION

Urban air pollution is one of the serious environmental issues that plagued the world. The impact of urban air pollution on human health has been also the focus of the public and governments [1, 2]. Air pollution forecast is in this context [3]. The so-called air pollution forecast is based on urban pollutant emissions and weather conditions, atmospheric diffusion, geographical and other factors to timely determine the next day the extent of air pollution in the region, and assess the impact and harm on the public daily activities. The air pollution forecast, providing conditions of future atmospheric environmental quality, can help the government to timely take effective measures to control the air pollution. In particular, serious pollution event is about to happen, relevant factory may be notified to limit production or traffic restriction may be released. People are advised to reduce outdoor activities to minimize the impact of urban air pollution on human body.

In recent years, research on atmospheric environmental change mainly focused on SO_2, NOx [4-6], and total suspended particulate [7, 8]and involved the organic compounds and heavy metals in PM_{10} and $PM_{2.5}$. The research employed mainly include analysis methods which combine investigation-sampling and physics-chemistry experiments [5, 9], pollution-load method [10, 11], Spearman's rank correlation coefficient method [12], environmental Kuznets curve model [13], gray neural network model [14], fuzzy mathematics method [15] and so on. The development of air pollution is a complex dynamic system, and the air pollution series itself is nonlinear and non-stationary. Hence, it is difficult to reveal the dynamic characteristics of air pollution using traditional methods and it cannot highlight the acts of nature.

The air pollution index (API), a referential parameter describing air pollution levels by many developed countries and regions in the world, provides information which could enhance the public awareness of air pollution. It could determine the pollution indices classification and corresponding pollutant concentration limits on the basis of environmental air quality standards and the influence of various pollutants on human health and ecological environment. Meanwhile, the API reporting in China requires converting monitored daily average air quality data into integer values, and then the report is released to the

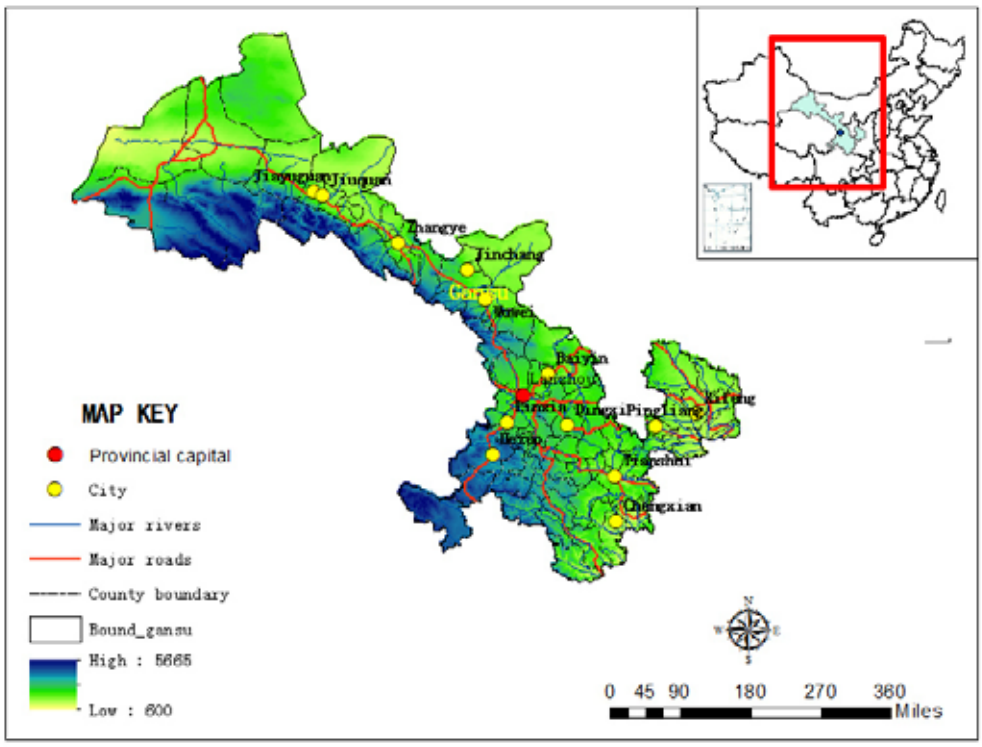


FIGURE 1
Topographic map of Lanzhou, northwest China

public. That is to say, though difficult to be understood in the single conceptual numerical form, the simplified air pollutants concentration (APC) can describe air quality and air pollution levels intuitively. Since June 2000, under the requirement of the State Environment Protection Agency of China, three major pollutants, including respirable particulate matter (PM_{10}), sulfur dioxide (SO_2) and nitrogen dioxide (NO_2) have been selected for API reporting in China. Temporal evolution of air pollutants is a complex phenomenon. It has to do with many factors, such as the movement and transformation of air pollutants, pollutants emission and climate condition [16]. Some previous studies indicate that some air pollutants exhibit nonlinearities, such as surface ozone [17], carbon dioxide (CO_2) emissions [18, 19], TSP and PM_{10} concentration [20, 21], just to name a few examples. Some studies focus on the methods and models for air quality assessment and the prediction of daily API time series.

Shi et al. [22] analyzed SO_2, NO_2 and PM_{10}, as well as the daily air pollution indexes (APIs) of Shanghai in China, and found that the temporal scaling behaviors in all the four series exhibit two different power laws. That is, SO_2, NO_2 and PM_{10}, have synchronization, however, their chemical characteristic and pollution mechanism are different from each other. Then, how are the scale-changes relationships among them implied? What are relationships among them? How does the change of one air pollution index affect the other one quantitatively? How to quantify the long-range correlation between factors? Although the three air pollution indexes have long memory, the article researched on relationship among them has not yet found. Therefore, further research on their relationship is necessary. Hence, the scale characteristics of the three air pollution indexes are studied by the Detrended Cross-Correlation Analysis (DCCA). And they, by now, have proved to be very useful to detect deep dynamical features.

STUDY AREA AND DATA

Overview of the study area. Lanzhou, the capital of Gansu Province in China, is located at the northeast edge of the Tibetan Plateau (102°30"-104°30"E, 35°5"-38°N). It has an urban area that is approximately 40 km long and 2 km to 8 km wide. It is a typical dumbbell-shaped valley city surrounded by the Tibetan Plateau in the west, Baita Mountain in the north, and Gaolan Mountain in the south (Figure 1). The special weather condition is controlled by the area's specific topographical features. Static wind frequency can reach 75%; during winter, the figure can be higher than 87%. An inversion layer has been in existence in the urban area for many years, particularly in winter. The height of this layer varies from 200 m to 600 m. The stability in the urban area is approximately 80% due to static wind and because the atmospheric stratification stability of the inversion layer and the basin is not conducive to the turbulent diffusion of pollutants [23, 24]. Lanzhou is

an industrial city known for petrol chemistry, metallurgy, and mechanical manufacturing. It consists of four districts (Figure 1), namely, Chengguan (metropolitan area), Xigu (large, heavy industrial area), and Qilihe and Anning (mix of residential areas, small factories, and farming areas). Hundreds of industrial plants are distributed throughout the four districts. The largest energy source in Lanzhou is coal (79.2%). The irrational energy consumption structure that relies mainly on the burning of coal triggers serious air pollution. The total SO_2 emission is 44.3 million kg, in which 21.5 million kg originates from industries in Lanzhou [25]. All of these factors render Lanzhou one of the most heavily polluted cities in China.

Data source and data preprocessing. The data source is the daily air quality index of Lanzhou offered on website of the Chinese Ministry of Environmental Protection (http://www.zhb.gov.cn/), and the data were obtained from July 1, 2000 to June 30, 2015. When the air pollution index data of 9 days were unavailable, we made up for it by the arithmetic average value of 2 days' data. If July 1, 2000 is set as number 1, then June 30, 2015 is set as 5477.

Moreover, other factors like time series length, edge effect and noise may also impact time-scaling property. To eliminate the boundary effect, the data were extended by cycle method [26, 27]. The method works on the hypothesis that a natural time series is a combination of both a low-dimensional dynamical system and a high-dimensional (random) noise. Unlike linear filters, nonlinear ones only remove those noisy data points. Those points can be then replaced by estimates computed from a nonlinear interpolation process [28, 29]. The Matlab7.6 and R softwares were adopted to accomplish the calculation.

DCCA METHOD

In order to quantify long-range cross correlations when nonstationarities are present, Podobnik and Stanley [30] propose a modification of standard covariance analysis which is called detrended cross-correlation analysis (DCCA). DCCA is also a generalization of detrended fluctuation analysis (DFA), but can be used to investigate the power-law cross-correlations between two simultaneously recorded time series. This method is very suitable to test the correlation of API time series with non-stationary characteristics. The specific algorithm of DCCA is as follows:

(1) Consider two time series $\{x_i\}$ and $\{y_i\}$, where i= 1,2,...N and N is the length of series:

$$x_k = \sum_{i=1}^{k}(x_i - \overline{x}) \quad y_k = \sum_{i=1}^{k}(y_i - \overline{y})$$

(2) Each of two time series x_k and x'_k is covered with N_s=int(N/s) nonoverlapping boxes of size s, i.e., each box contains s values. Since N may not be divisible by s, part data points in the tail of data series may not be able to enter the operation. In order to solve the problem, we can repeat the partitioning process from the tail of the data series, and a total of $2N_s$ boxes will be obtained accordingly.

(3) In each box, we can determine the "local trend", $\tilde{x}_{k,v}$ and $\tilde{x}'_{k,v}$, to be the ordinate of a linear least-squares fit. Next we calculate the covariance of the residuals in each box:

$$f^2(s,v) = \frac{1}{s}\sum_{k=1}^{s}(x_k - \tilde{x}_{k,v})(x'_k - \tilde{x}'_{k,v})$$

Where $f^2(s,v)$ is the covariance of residuals within the vth box of size s. $\tilde{x}_{k,v}$ and $\tilde{x}'_{k,v}$ are the fitted equation of the vth box.

(4) We calculate the detrended covariance by summing over all $2N_s$ boxes of size s as follows:

$$F^2(s) = \frac{1}{2N_s}\sum_{v=1}^{2N_s}(f^2(s,v))$$

(5) For $F^2(s)$ and s, they obey the power law in double logarithmic coordinates, that is:

$F^2(s) \sim s^{\lambda}$

which indicates that the series $\{x_i\}$ and $\{y_i\}$ there are long-range cross correlations. The λ is the scaling exponent of long-range cross correlations. λ>0.5 means that there are positive long-range cross correlations for the two series, that is, if there is a growing trend in one series, then the other series also shows an growing trend. While it is contrary when λ>0.5. The value of λ = 0.5 means there is no long-range cross-correlation, i.e., the change trend of one series has no effect on the change of the other one.

RESULTS AND DISCUSSION

Figures 2-4 gives the DCCA results of the three pollution indexes. There obviously are two or even three distinctly different intervals in the Figures. For the relationship between three pollution indexes in the same time interval, there are one, two, or even three scale-free intervals for the double logarithmic curve of $F(s)$ and s. Specifically, there is one scale-free interval for the PM_{10} vs. NO_2, two for the SO_2 vs. NO_2, and three for the SO_2 vs. PM_{10} and PM_{10} vs. NO_2; their scaling exponent λ is obtained by using a linear it in each scale-free interval. With s_c (s_{c1}=ln365≈5.9 and s_{c2}=ln3650≈8.2) as the two cut-off point, the corresponding time of location s_c is one year and 10 years, and this reflects the impact of natural year and interdecadal variations to the long-range correlation of climate factors.

In the first scale interval, for the scaling exponent λ of PM_{10} vs. NO_2, their scaling exponent λ =1.62 >1 at the whole timescale (up to 16 years at least), which means their cross-correlation keep exhibiting long-term persistence with positive power-law in the scale-free interval of greater than 16 years.

That is, the PM_{10} increased (decreased) with increasing (decreasing) NO_2, both have stronger synchronicity at the time scale of 16 years at least. For SO_2 vs. NO_2, their cross-correlation is similar to that of PM_{10} vs. NO_2. One thing it is not, there is a same trend, increasing or decreasing, for least one year ($s<s_{c1}$). While for SO_2 vs. PM_{10} , λ=0.99 is regarded as $1/f^{\beta}$ noise, which indicates that the cross-correlation of SO_2 and PM_{10} manifested as $1/f$ noise behavior with power law at a large temporal scale.

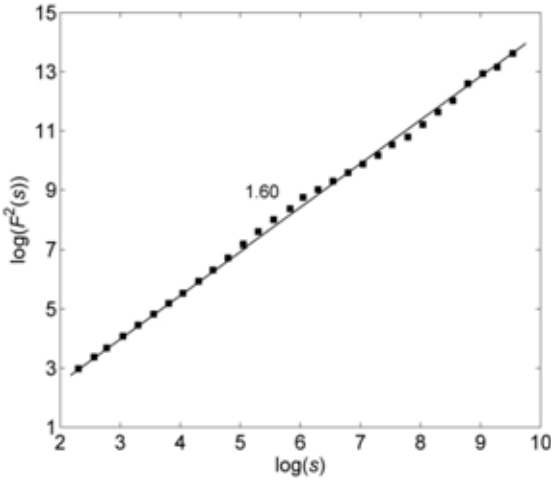


FIGURE 2
DCCA of PM_{10} vs. NO_2

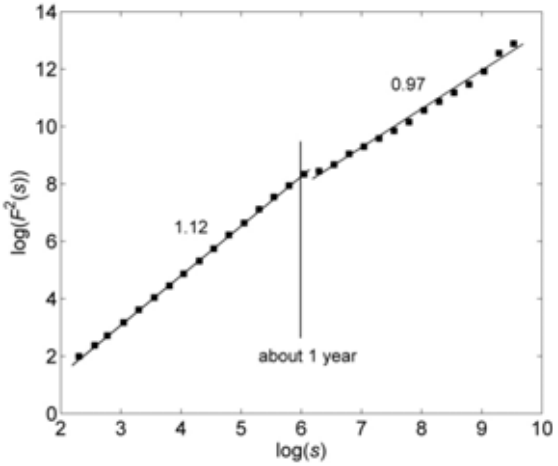


FIGURE 3
DCCA of SO_2 vs. NO_2

In the second scale-free interval, the same state of PM_{10} vs. NO_2 in temporal evolution still exist. While for SO_2 vs. NO_2, λ=0.97 means their cross-correlation keep exhibiting long-term persistence with positive power-law in the scale-free interval of greater than one year and up to 16 years at least, but performance is slow compared with the time scale of one year. Moreover, as to the SO_2 vs. PM_{10}, the scaling exponent λ=0.37<0.5 means their cross-correlation presents anti-persistence with negative power-law in the scale-free interval of greater than one year and less than 10 years.

In the third scale-free interval, the scaling exponent of SO_2 vs. PM_{10} is λ=1.62, their long-range cross-correlation changes to positive non-power-law as the time becomes longer.

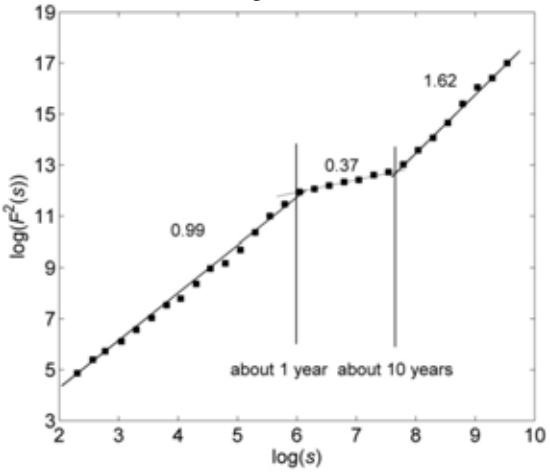


FIGURE 4
DCCA of SO_2 vs. PM_{10}

The scale-free intervals of the cross-correlation between SO_2, NO_2 and PM_{10} reflect the interaction, interdependence and change characteristics between them. In the whole 16 years, there is a strong positive long-range cross-correlation between PM_{10} vs. NO_2 all along. If the NO_2 pollution in Lanzhou increases (decreases) within one year, the PM_{10} also increases (decreases) over 16 years. But the cross-correlation of SO_2 vs. NO_2 and SO_2 vs. PM_{10} are clearly different from that of PM_{10} vs. NO_2, which can be reference Part 4. In a word, for the three pollution indexes of Lanzhou, the DCCA exponent quantitatively measures the cross-correlation of any two series in terms of long-term cross-correlation exists at the different time scale. The prevention and control of air pollution in Lanzhou should be developed towards regional jointly prevention and control in the planning and construction of Lanzhou and its surrounding towns.

CONCLUSIONS

In this paper, we collected the daily air pollution index data of Lanzhou from July 1, 2000 to June 30, 2015, which were analyzed by using the detrended cross-correlation analysis (DCCA) method. From the DCCA analysis results, we can find that there are two or even three scale-free intervals for the double logarithmic curve of $F(s)$ and s between three pollution indexes (SO_2, NO_2 and PM_{10}) in the whole 16 years. The two cut-off points s_{c1}=ln365≈5.9 and s_{c2}=ln3650≈8.2 of the cross-correlation reflect the impact of natural year and inter decadal variation. In the first scale-free interval, the scaling exponent λ of PM_{10} vs. NO_2 and SO_2 vs. NO_2 show positive power-law long-range cross-correlation; the scaling exponent λ of PM_{10} vs. SO_2 is close

1 between SO_2 vs. NO_2, which can be regarded as $1/f^{\beta}$ noise. In the second scale-free interval, days, the cross-correlation of PM_{10} vs. NO_2 exhibits continually long-term persistence. The cross-correlation of SO_2 vs. NO_2 changes to $1/f^{\beta}$ noise and that of SO_2 vs. PM_{10} changes to anti-persistence with negative power-law in the scale-free interval of greater than one year and less than 10 years ($s_{c1}<s<s_{c2}$). In the third scale-free interval, the cross-correlation of PM_{10} vs. NO_2 and SO_2 vs. NO_2 are similar to characteristic in the second scale-free interval, but that of SO_2 vs. PM_{10} is transformed into high long-term persistence with positive power-law.

These results correspond to atmospheric circulation and regional transport hypothesis. It suggests that in specific geographical and meteorological conditions, the atmospheric pollution type of Lanzhou may have changed from local pollution into regional pollution. The long range cross-correlation properties of air pollution in Lanzhou between the three pollution indexes helps to understand the nature of regional air pollution in the city.

ACKNOWLEDGEMENTS

This work was supported by the China Postdoctoral Science Foundation (NO. 2016M60 0515), the Opening Fund of Key Laboratory of Poyang Lake Wetland and Watershed Research (Jiangxi Normal University), Ministry of Education (NO. PK2017002), the Science and Technology Project of Jiangxi Provincial Department of Education (NO. GJJ161097), the Key Project of Jiangxi Provincial Department of Science and Technology (NO. 20161BBF60061), the National Natural Science Foundation of China (NO. 41603128 and 41465010) and the National Key Technology R & D Program (NO. 2015BAH50F0 0).

REFERENCES

[1] Ghose, M.K., Paul, R. and Banerjee, R.K. (2005) Assessment of the Status of Urban Air pollution And Its Impact on Human Health in the City of Kolkata. Environmental Monitoring & Assessment. 108,151-167.

[2] Silveira, C., Roebeling, P., Lopes, M., Ferreira, J., Costa, S., Teixeira, J.P., Borrego, C. and Miranda, A.I. (2016) Assessment of health benefits related to air quality improvement strategies in urban areas: an impact pathway approach. Journal of Environmental Management. 183, 694-702.

[3] Liu, Z.Z., Dong, P. and Wang, L. (2005) Urban air pollution forecast and environmental capacity control. Power System Engineering. 21, 17-19.

[4] Krotkov, N.A., Mclinden, C.A., Li, C., Lamsal, L.N. and Celarier, E.A. (2016) Aura OMI observations of regional SO_2 and NO_2 pollution changes from 2005 to 2015. Atmospheric Chemistry & Physics. 16, 4605-4629.

[5] Hamer, P.D. and Shallcross, D.E. (2007) Modelling the impact of oxygenated VOC and meteorology upon the boundary layer photochemistry at the South Pole. Atmospheric Science Letters. 8, 14-20.

[6] Sun, L.N., Liu, Z.H., Wang, J.Y., Wang, L.L., Bao, X.C., Wu, Z.M. and Yu, B. (2016) The evolving concept of air pollution: a small-world network or scale-free network? Atmospheric Science Letters. 17, 308-314.

[7] Larissi, I.K., Koukouletsos, K.V., Moustris, K.P., Antoniou, A. and Paliatsos, A.G. (2010) Pm10 concentration levels in the Greater Athens area Greece. Fresen. Environ. Bull. 19, 226-231.

[8] Sanchez-Reyna, G., Wang, K.Y., Gallardo, J.C. and Shallcross, D.E. (2005) Association between PM_{10} mass concentration and wind direction in London. Atmospheric Science Letters. 6, 204-210.

[9] West, L.J., Killworth, P.D., Cornell, V.C. and Challenor, P.G. (2005) Remote visualization of Labrador convection in large oceanic datasets. Atmospheric Science Letters. 6, 198-203.

[10] Zhang, R.B., Qian, X., Zhu, W.T., Gao, H.L., Hu, W. and Wang, J.H. (2014) Simulation and evaluation of pollution load reduction scenarios for water environmental management: a case study of inflow river of Taihu Lake, China. International Journal of Environmental Research & Public Health. 11, 9306-9324.

[11] Bhargava, A. and Gopani, N. (2016) Assessment and forecasting of automobile air pollution load in ahmedabad based on different methods. IJSRE 4, 5034-5045.

[12] Heo, S. and Lee, J.T. (2013) Study of environmental health problems in Korea using integrated environmental health indicators. International Journal of Environmental Research & Public Health. 10, 3140-3156.

[13] Xiao, Q., Gao, Y., Hu, D., Tan, H. and Wang, T.X. (2011) Assessment of the interactions between economic growth and industrial waste water discharges using co-integration analysis: a case study for China's Hunan Province. International Journal of Environmental Research & Public Health. 8, 2937 - 2950.

[14] Pasini, A. and Modugno, G. (2013) Climatic attribution at the regional scale: a case study on the role of circulation patterns and external forcings. Atmospheric Science Letters. 14, 301-305.

[15] Li, A. and Liu, J.Y. (2013) Efficient environmental air quality evaluation scheme based on the fuzzy mathematics method. In Informatics and Management Science, Du, W. (ed.) Vol. III. Springer: London, 645-651.
[16] Penrod, A., Zhang, Y., Wang, K., Wu, S.Y. and Leung, L.R. (2014) Impacts of future climate and emission changes on U.S. air quality. Atmospheric Environment. 89, 533-547.
[17] Tao, Z., Hewings, G. and Donaghy K. (2010) An economic analysis of Midwestern US criteria pollutant emissions trends from 1970 to 2000. Ecological Economics. 69, 1666-1674.
[18] Tunc, G.I., Türüt-Asik, S. and Akbostanci, E. (2009) A decomposition analysis of CO_2 emissions from energy use: Turkish case. Energy Policy. 37, 4689- 4699.
[19] Akbolat, D. and Şenyiğit, U. (2012) Short-term effect of different irrigation water levels on soil carbon dioxide (CO_2) emission. Fresen. Environ. Bull. 21, 3869-3872.
[20] Saarikoski, S., Sillanpaa, M., Sofiev, M., Timonen, H., Saarnio, K., Teinela, K., Karppinen, A., Kukkonen, J. and Hillamo, R. (2007) Chemical composition of aerosols during a major biomass burning episode over Northern Europe in spring 2006: Experimental and modeling assessments. Atmospheric Environment. 41, 3577-3589.
[21] Slini, T., Kaprara, A., Karatzas, K. and Moussiopoulos, N. (2006) PM_{10} forecasting for Thessaloniki, Greece. Environmental Modelling & Software. 21, 559-565.
[22] Shi, K., Liu, C.Q., Ai, N.S. and Zhang, X.H. (2008) Using three methods to investigate time-scaling properties in air pollution indexes time series. Nonlinear Analysis. 9, 693-707.
[23] Chu, P.C., Chen, Y.C., Lu, S.H. (2008) Atmospheric effects on winter SO_2 pollution in Lanzhou, China. Atmospheric Research. 89, 365–373.
[24] Chu, P.C. Chen, Y.C. Lu, S.H. Li, Z.C. and Lu, Y.Q. (2008) Particulate air pollution in Lanzhou China. Environment International. 34, 698-713.
[25] Jiang, J.H. and Peng X.D. (2002) Numerical study on air pollution concentration over Lanzhou in winter under complex terrain. Plateau Meteorology. 21, 1-7. (in Chinese with English abstract)
[26] Faiman, G.A. and Horovitz, A. (1996) On the choice of reference mutant states in the application of the double-mutant cycle method. Protein Engineering. 9, 315-316.
[27] Chavanne, T.J. and Jr, G.G.G. (1998) Variation in Risk Taking Behavior Among Female College Students as a Function of the Menstrual Cycle. Evolution & Human Behavior. 19, 27-32.
[28] Jazwinski, A.H. (1970) Stochastic processes and filtering theory. Academic Press, New York. 247.
[29] Harvey, A.C. (1989) Forecasting, structural time series models and the Kalman Filter. Cambridge University Press. 312.
[30] Podobnik, B. and Stanley, H.E. (2008) Detrended cross-correlation analysis: a new method for analyzing two nonstationary time series. Physical Review Letters. 100, 38-71.

Received: **07.02.2017**
Accepted: **19.09.2017**

CORRESPONDING AUTHOR

Jiayao Wang
School of Resource and Environmental Sciences, Wuhan University, Wuhan, China,

e-mail: jywang_wuhan@126.com

© by PSP Volume 26 – No. 12A/2017 pages 7687-7694 Fresenius Environmental Bulletin

SPATIAL VARIABILITY IN SOIL FERTILITY RELATED TO THE "FERTILE ISLANDS" EFFECT OF *VITEX NEGUNDO*

He Zhao, Yong Zhao*, ZhiMing Zhang, Guo Dong, XiaoKe Yuan

College of Forestry, Henan Agricultural University, Zhengzhou, Henan, China

ABSTRACT

Vitex negundo shrubs serve as both windbreaks and soil stabilizers and can aid in soil water retention and improve soil nutrients in the soils of arid and semi-arid regions. To reveal the factors underlying these functions of *Vitex negundo*, this study analyzes the total nitrogen, organic matter and available phosphorus contents of soil exposed to the “fertile islands” effect of *Vitex negundo* and investigates the correlating variability in spatial structure. The results show significant differences in soil nutrients at varying horizontal distances from the main stem of the shrub, and the richness of soil nutrients gradually declines with increased distance from the main stem. The results also demonstrate that total nitrogen and soil organic matter typically decrease from the surface to the lower levels. Analysis by Kriging interpolation indicates that soil strata nearer to the surface contain greater nutrient richness than deeper soil. Hence, the results indicate that *Vitex negundo’s* "fertile islands" effect causes great variability in spatial structure. Analyzing this variation will contribute to efforts to improve local ecological sustainability.

KEYWORDS:
Vitex negundo, "fertile islands", soil nutrient, horizontal and vertical distances

INTRODUCTION

"Fertile islands" is a phenomenon in which soil nutrients accumulate under shrubs as a result of complex interactions between soil and organisms [1-2]. The "fertile islands" effect is most dramatic in arid and semi-arid areas [3], and it appears that this phenomenon is due to the gathering of nutrients by various shrub species [4]. The "fertile islands" themselves are defined as areas that include the non-biological environment of shrubs and shrubs themselves, and beneath plants with more soil resources than the bare areas. And they practice tends to be seen as the results of a range of interacting physical and biotic concentrating mechanisms [5-7]. In recent years, an increasing number of studies have investigated the effects of "fertile islands." Much has been discovered about “fertile islands”; for instance, an increasing total N in the upper 15 cm of soil has been reported along with an increased density of plants under shrubs [8]. Changes in the soil nutrient profile at different soil depths in saline-alkaline soil as well as the higher soil nutrient accumulation ability of near-surface soil (defined as soil surface fertility) over deeper strata have also been explored [9-10].

In recent years, many analyses of "fertile islands" have been performed in China, where research concentrates on the northern part of Inner Mongolia, the grasslands of western Ningxia and the Xinjiang Desert. However, this phenomenon has rarely been studied in the central Chinese arid and semi-arid regions. In addition, research on the zonal concentration of nutrients has focused mainly on the shrub canopy. Studies on the effects of spatial zones, various horizontal distances from plants, various soil zones and shrubs facing different directions (i.e., the aspect of exposure) have yet to be reported. In terms of plant species, existing research concentrates on *Halostachys caspica*, *Haloxylon ammodendron*, *Tamarix ramosissima* and *Ammopiptanthus mongolicus*. Nutrient hoarding in the *Vitex negundo* shrub has received less attention. In general, “fertile islands” can been taken as sites for the regeneration of shrubs and herbaceous plants [11], it provided nutrients for the soil microbial populations and soil microfauna [7], and it also can effectively promote nutrient cycling [12]. Thus, through investigating *Vitex negundo’s* "fertile island" effect on the soils of the semi-arid Taihang Mountain will contribute valuable information for sustainability of the ecological environment.

SITE

Our study site is located on a low hill (112°28'–112°30'E, 35°01'–35°03'N) of approximately 337–342 m in elevation, near Jiyuan City, Henan Province, China. The test area has a temperate continental monsoon climate, with an annual average temperature of 14.3°C. The study area’s average active temperature exceeds 5°C, while the annual cumulative temperature is 50.610°C, and the area receives an average of 2370.5 h of sun annually. The inter-annual variation is between 1948 h and 2602 h. The average annual sunshine rate is 54%, for which the annual variation is between 44% and 50%. The study soil

type is cinnamon soil, with a pH value of 7.0–7.5 and parent rock composed mainly of sandstone and shale. The main plant community constituents are shrubs and trees; shrubs include *Vitex negundo L*, *Ziziphus jujube* and *Lespedeza bicolor*, while trees include *Quercus variabilis*, *Platycladus orientalis* and *Robinia pseudoacacia*. Dominant herbaceous plants of the study area include *Setaria viridis*, *Artemisia princeps*, *Pennisetum flaccidum*, *Heterophylla arthraxon* and *Rehmannia glutinosa*. Under the abovementioned climatic factors, the native *Vitex negundo* is resistant to drought and barren soil and is thus widely distributed in the study area.

MATERIALS AND METHODS

In March 2013, three *Vitex negundo* shrubs of similar size and location served as test subjects (Table 1). To avoid mutual interference between the individual shrubs selected, *Vitex negundo* subjects were more than 3 m from their nearest neighbors. Next, soil samples were collected from each of the four directions (north, south, east, and west) around the subject. Samples were chosen from earch horizontal direction, with distances from the shrub roots the crown of the main stem of 0–30cm, 30–60 cm, 60–90 cm, 90–140 cm and 140–190 cm. Additionally, three samples from the vertical strata were collected, at depths of 0–5 cm, 5–10 cm and 10–20 cm (Figure 1). In general, a total of 60 samples were tested for each shrub, which contains 20 samples at every earch horizontal direction and 3 samples in every depth. We considered each *Vitex negundo* soil sample to be one repeat, and soil samples from a given *Vitex negundo* specimen served as one data set, while data from three specimens were averaged to determine the soil nutrient content.

Soil chemical analysis. Total nitrogen (TN) was determined using the Kjeldahl nitrogen method. To determine the available phosphorus content (AP), the $NaHCO_3$ molybdenum stadium anti-mix reagent method was used, while soil organic matter (SOM) was determined using the potassium dichromate volumetric method. Sample distribution diagrams were prepared using Photoshop 7.0software, Data were elicited by means of the valid questionnaire called SPSS and analyzed with one-way ANOVA, and R-Studio software was used for Kriging interpolation maps.

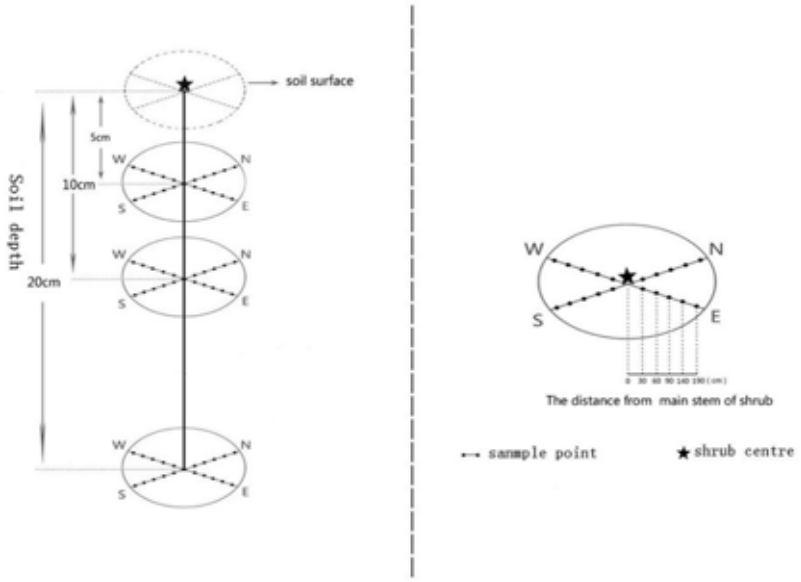


FIGURE 1
Diagram of soil sampling points.

TABLE 1
Basic characteristics of subject *Vitex negundo.*

Shrubs	GPS	Altitude/m	Height/m	Crown Size/m^2
1	35°01'N, 112°29'E	342	1. 70	1. 5 ×1. 2
2	35°02'N, 112°29'E	340	1. 40	1. 3 ×1. 4
3	35°01'N, 112°28'E	337	1. 65	1. 5 ×1. 6

TABLE 2
Variation in spatial structure of the total nitrogen content.

Direction	Soil depth (cm)	TN at different distances (g kg^{-1})									
		0–30 cm		30–60 cm		60–90 cm		90–140 cm		140–190 cm	
E	0–5	1. 38±0. 17	A a	1. 43±0. 16	A a	0. 97±0. 10	A ab	0. 95±0. 13	A ab	0. 62±0. 19	A b
	5–10	0. 61±0. 05	B a	0. 63±0. 09	B a	0. 56±0. 04	B a	0. 66±0. 43	B a	0. 75±0. 09	A a
	10–20	0. 58±0. 04	B a	0. 55±0. 05	B a	0. 63±0. 07	B a	0. 58±0. 04	B a	0. 67±0. 02	A a
W	0–5	1. 08±0. 12	A b	0. 82±0. 07	A b	1. 54±0. 21	A a	1. 01±0. 11	A b	0. 94±0. 11	A b
	5–10	0. 64±0. 05	B a	0. 58±0. 03	AB a	0. 63±0. 02	B a	0. 65±0. 03	B a	0. 61±0. 01	B a
	10–20	0. 478±0. 09	B a	0. 53±0. 09	B a	0. 49±0. 04	B a	0. 52±0. 08	B a	0. 55±0. 09	B a
S	0–5	1. 73±0. 32	A a	0. 92±0. 14	A b	1. 56±0. 19	A ab	1. 29±0. 23	A ab	1. 09±0. 12	A ab
	5–10	0. 70±0. 09	B a	0. 62±0. 06	AB a	0. 68±0. 08	B a	0. 72±0. 14	B a	0. 65±0. 04	B a
	10–20	0. 54±0. 11	B a	0. 57±0. 07	B a	0. 57±0. 02	B a	0. 52±0. 04	B a	0. 55±0. 03	B a
N	0–5	1. 00±0. 12	A b	1. 17±0. 12	A ab	1. 63±0. 18	A a	1. 20±0. 16	A ab	0. 90±0. 22	A b
	5–10	0. 63±0. 05	A a	1. 04±0. 36	A a	0. 89±0. 25	B a	1. 00±0. 22	A a	1. 22±0. 29	A a
	10–20	0. 72±0. 14	A a	0. 52±0. 09	A a	0. 57±0. 03	B a	0. 64±0. 08	A a	0. 64±0. 08	A a

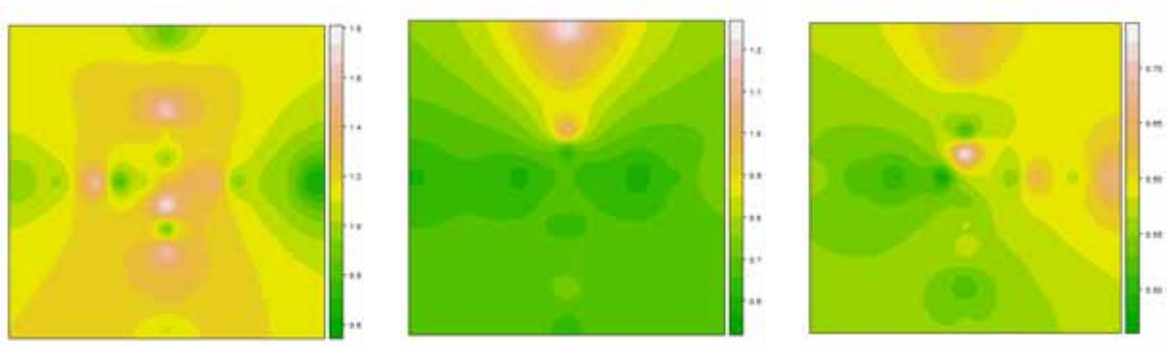
Note: In each table, E represents east, W represents west, S represents south and N represents north. Capital direction symbols indicate full 5% significance in each column, while lowercase letters represent a clear 5% significance in each row. TN is total nitrogen. AP is available phosphorus. SOM is soil organic matter.

RESULTS

Spatial variability in total nitrogen content. We analyzed the phenomenon of "fertile islands" from the perspective of spatial structure. In the horizontal direction, the total nitrogen content of the soil tended to decrease from the root crown toward the stem of the shrub drip line, but results vary in each direction (Table 2). To the east, total nitrogen content was greatest at 30–60 cm from the main stem at soil depths of 0–5 cm, reaching 1.43 g kg^{-1}. The second largest value was in the range of 0–30 cm from the main stem, and the smallest values were found at 140–190 cm. The values remained steady and without significant differences ($P<0.05$) at soil depths of 5–10 cm and 10–20 cm. To the west, the total nitrogen content was greatest at 60–90 cm from the main stem of the shrub at the 0–5 cm soil depth, reaching 1.54 g kg^{-1}. In this direction, the total nitrogen content also remained steady and without significant variation ($P<0.05$) at soil depths of 5–10 cm and 10–20 cm. To the south, the total nitrogen content was highest at 0 – 30 cm from the shrub's center in 0–5 cm of soil, reaching 1.73 g kg^{-1}. There were no significant differences in the total nitrogen values over the range of soils at 5–10 cm and 10–20 cm depths. To the north, total nitrogen content was highest at 60–90 cm from the shrub's center at soil depths of 0–5 cm, reaching 1.63 g kg^{-1}. There were no significant differences in total nitrogen at soil depths of 5–10 cm and 10–20 cm.

In the vertical direction, total nitrogen content followed a trend in which values at the 0–5 cm soil depth > values at 5–10 cm > values at 10–20 cm. To the east, within 0–140 cm from the shrub's center, the total nitrogen content at soil depths of 0–5 cm was significantly higher than that at depths of 5–10 cm and 10–20 cm. To the west and south, total nitrogen content values at 0–5 cm were significantly higher than those at 10–20 cm of soil. To the north, while the total nitrogen content tended to decrease from shallow to deep, the change values were not significant at the same distance and at different soil depths—except at the distance of 60–90 cm (Table 2).

The Kriging interpolation map shows that the total nitrogen content of the soil was significantly enriched under *Vitex negundo* at 0–5 cm of soil, and the values were higher in the center than outward to the north, the west and the south (Fig. 2). This phenomenon demonstrates the "fertility island" mechanism of nutrient concentration. Moreover, the enrichment effect in other directions was not obvious, except northward at a soil depth of 5–10 cm. At a soil depth of 10–20 cm, a weak nutrient concentration effect appeared to the north, with no obvious effect in other directions. These results indicate that the total nitrogen is higher under the shrub canopy than outside that area, and the total nitrogen content decreases from shallow to deep in the soil under the shrubs.



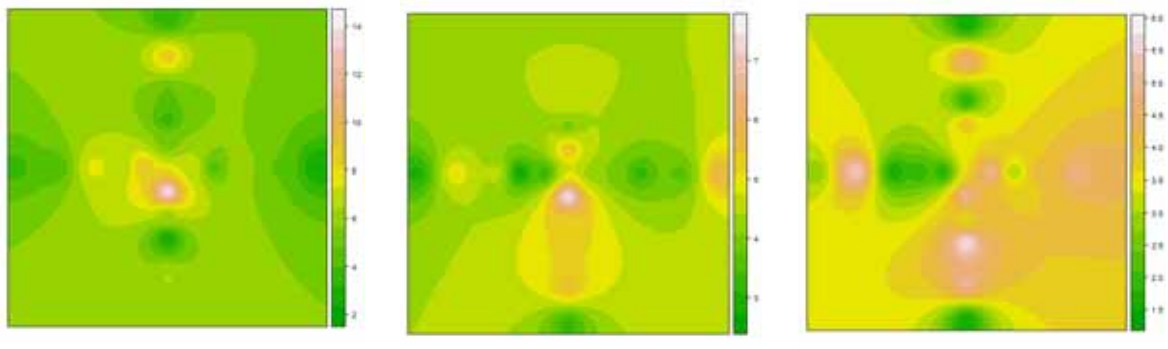
(a) **(b)** **(c)**

FIGURE 2
Kriging interpolation map of total nitrogen (g kg^{-1}) at (a) 0–5 cm, (b) 5–10 cm, and (c) 10–20 cm soil depth.

TABLE 3
Spatial variation of available P content.

Direction	Soil depth (cm)	AP at different distances (mg kg^{-1})														
		0–30 cm			30–60 cm			60–90 cm			90–140 cm			140–190 cm		
E	0–5	7. 06±0. 73	A	a	4. 50±0. 75	A	bc	6. 09±0. 72	A	ab	4. 72±0. 54	A	bc	2. 64±0. 35	A	c
	5–10	4. 26±0. 54	A	ab	3. 75±0. 86	A	ab	3. 26±0. 60	B	b	3. 65±0. 90	A	ab	5. 74±0. 25	A	a
	10–20	4. 91±1. 23	A	a	3. 08±0. 39	A	a	4. 02±0. 92	AB	a	4. 75±0. 67	A	a	4. 40±1. 55	A	a
W	0–5	8. 87±1. 76	A	a	9. 01±2. 03	A	a	7. 61±0. 08	A	a	4. 12±1. 93	A	a	3. 71±1. 05	A	a
	5–10	3. 26±0. 69	B	a	2. 73±0. 20	B	a	4. 54±1. 44	B	a	4. 96±1. 07	A	a	2. 96±0. 70	A	a
	10–20	1. 75±0. 34	B	b	1. 85±0. 25	B	b	1. 56±0. 23	C	b	5. 36±1. 89	A	a	2. 85±0. 89	A	ab
S	0–5	13. 89±1. 19	A	a	6. 23±0. 39	A	b	2. 57±0. 29	A	b	6. 49±2. 30	A	b	5. 77±0. 60	A	b
	5–10	7. 23±1. 25	B	a	5. 34±0. 67	AB	a	5. 25±2. 12	A	a	5. 51±0. 45	A	a	3. 28±1. 3	AB	a
	10–20	4. 90±2. 36	B	a	3. 64±0. 72	B	a	5. 75±2. 22	A	a	4. 92±1. 90	A	a	1. 48±0. 15	B	a
N	0–5	5. 14±1. 07	A	b	3. 54±0. 72	A	b	5. 58±1. 15	A	b	8. 46±0. 38	A	a	3. 36±0. 81	A	b
	5–10	5. 38±0. 89	A	a	4.00±0. 67	A	a	4. 67±1. 93	A	a	4. 54±1. 14	B	a	4. 17±0. 96	A	a
	10–20	3. 54±0. 22	A	ab	3. 86±1. 54	A	ab	1. 80±0. 30	A	b	4. 57±0. 77	B	a	1. 49±0. 47	A	b

Note: Explanation analogous to Table 2.



(a) **(b)** **(c)**

FIGURE 3
Kriging interpolation map of available P (mg kg^{-1}) at (a) 0–5 cm, (b) 5–10 cm, and (c) 10–20 cm soil depth.

Variability in the spatial structure of available P content. Collated findings from our test samples are presented here (Table 3). Along the surface and eastward, the available P content was highest at 0–30 cm from the main stem of the shrub and at the 0–5 cm soil depth, reaching 7.06 mg kg^{-1}. The second highest values were in the range of 60–90 cm from the main stem of the shrub, and the lowest were found at 140–190 cm. The available P content remained steady, without significant differences ($P<0.05$), at distances of 0–140 cm and at soil depths

of 5–10 cm and 10–20 cm. Westward, the available P content was highest at 30–60 cm from the main stem of the shrub and at the 0–5 cm depth, reaching 9.01mg kg^{-1}, followed by the values in the 0–30 cm range. The available P content remained steady in the westward direction, with insignificant differences ($P<0.05$) at the 5–10 cm depth. The available P content was highest in the range of 90–140 cm from the main stem of the shrub, at 10–20 cm of soil, reaching 5.36 mg kg^{-1}. To the south, the available P content was highest at 0–30 cm from the main stem of the shrub at soil depths of 0–5 cm, reaching 13.89 mg kg^{-1}. Differences to the south were insignificant ($P<0.05$) for available P among soil strata 5–10 cm and 10–20 cm deep. To the north, the available P content was highest at distances of 90–140 cm from the main stem of the shrub at soil depths of 0–5 cm and 10–20 cm. Samples at various distances showed insignificant ($P<0.05$) differences in available P values in 5–10 cm of soil.

In eastern vertical soil levels, available P values in 0–5 cm of soil were significantly higher than in 5–10 cm soil at distances from the main stem of the shrub of 60–90 cm. To the west and south, values for available P at the 0–5 cm soil depth were significantly higher than those at the 10 – 20 cm depth at a distance of 60–90 cm. Only at 90–140 cm northward from the shrub canopy core was the available P content in 0 – 5 cm of soil significantly higher than that at 5–10 cm and 10–20 cm depths (Table 3).

The Kriging interpolation map shows significant available P content enrichment of soil under *Vitex negundo* at soil depths of 0–5 cm, while in all directions, enrichment appears higher in the center and is higher than anywhere else (Fig. 3). Enrichment effects were not obvious elsewhere, except to the south at the 5–10 cm soil depth. In soil 10–20 cm deep, enrichment in all directions was not obvious except to the south, where there was a weak nutrient concentration effect. These results indicate that the content of available P in our samples exhibited the widely reported phenomenon in which critical soil elements are concentrated under the shrub canopy. Additionally, the value of available P decreased from the surface to deep soil.

Spatial variability of organic matter content. Along the soil surface, organic matter content varied in each direction (Table 4). To the east, organic matter content was highest at a distance of 0–30 cm from the shrub area and at the 0–5 cm soil depth, reaching 25.54 g kg^{-1}. Among the 0–90 cm values at the 5–10 cm and 10–20 cm depths, the organic matter content showed no significant change. To the west, the organic matter content at soil distances of 60–90 cm from the main stem of the shrub and at 0–5 cm soil depth was highest, reaching 26.24 g kg^{-1}, while values from soils at a distance of 0–30 cm were the second highest. Values for the organic matter content at the 5–10 cm and 10–20 cm depths did not vary significantly ($P<0.05$). The highest organic matter content to the south lay between the 0–30 cm and 0–5 cm soil depths, reaching 31.29 g kg^{-1}, a value significantly higher than that observed in other directions. No significant differences in the values of organic matter appeared laterally across the shrub canopy at depths of 5–10 cm and 10–20 cm. To the north, the organic matter content at distances of 30–60 cm from the stem of the shrub and at 0–5 cm soil reached 22.64 g kg^{-1}. The organic matter content at a depth of 5–10 cm of soil was not significantly different across the lateral plane. The highest organic matter content appeared at distances of 0–30 cm from the main stem of the shrub and at the 10–20 cm depth, reaching 10.89 g kg^{-1}.

Across soil depths to the east, organic matter values in 0–5 cm of soil were all significantly higher than those at depths of 5–10 cm and 10–20 cm. To the west, organic matter content at the 0–5 cm soil depth was significantly higher than the values from the 5–10 cm and 10–20 cm depths, except at 30–60 cm deep. To the south, the organic matter content at the 0–5 cm depth was significantly higher than the values at 10–20 cm deep and 0–140 cm from the main stem of the shrub. The organic matter contents northward at 0–5 cm depths were significantly higher than the values at 5–10 cm and 10–20 cm of soil and 0–140 cm from the main stem of the shrub (Table 4).

The Kriging interpolation map shows that the organic matter content of the soil was significantly enriched under *Vitex negundo* at 0–5 cm of soil depth, gradually decreasing outward in all directions (Fig. 4). Additionally, the enrichment effect was not dramatic, except at the 5–10 cm soil depth toward the south. At soil depths of 10–20 cm, the nutrient concentration was not dramatic, except to the east and north, where weak enrichment effects were detected. Therefore, the near-surface organic matter content results meet the expectation of concentrated nutrients under a shrub canopy. The depth sample results also show that the organic matter values at 0–5 cm were greater than those at the 5–10 cm and 10–20 cm depths.

DISCUSSION

The soil samples under *Vitex negundo* exhibited higher levels of total nitrogen, available P and organic matter content close to the base than at the shrub periphery. It is clearly observable that *Vitex negundo* shrubs function to gather soil nutrients; the shrubs absorb nutrients as an adaptation to arid and semi-arid environments [13-14]. These results are consistent with other studies showing that the contents of total nitrogen, nitrate and organic compounds in the shrub rhizosphere were higher than the contents outside that zone [15-19]. The reason for

this enrichment effect is that the shrub produces nutrients in the form of leaf detritus, which is then trapped by roots and sheltered by branches and stems; organisms associated with the plant also trap nutrients by ingesting detritus and excreting byproducts locally, preventing the solution and washing away of nutrients by rainfall [20]. In addition, shrubs serve as shelter and habitat for large fauna, whose dung contributes to the shrubs' "fertility island" effect [21]. The process of obtaining nutrients and metabolic secretions from plant roots may cause complex changes in the structure of nutrients [22], while the quantity and activity of microbiota around plant roots will affect the accumulation and transformation of soil nutrients [23].

In the vertical direction, the soil nutrients decrease with the depth from the surface, with soil nutrient content values at 0 – 5 cm higher than those at 5 – 10 cm, which in turn are higher than those at the 10 – 20 cm soil depth. This finding is consistent with the conclusions of previous studies [24-25]. This vertical heterogeneity exists because the shallow layer of soil receives shrub litter, where accumulated nutrients tend to remain concentrated.

In the horizontal plane, the effect of the nutrient enrichment of soil is more obvious in the 0 – 5 cm soil depth layer than that in the soil layers of 5 – 10 cm and 10 – 20 cm. This difference may be related to root development and shrub growth [26-28]. Additionally, fungi are known to fuse with the roots of many species in many genera of woody plants, and the shallow conditions may be more suitable for the growth of fungi. Fungal activities also can add soil nutrients that will make nutrients more easily accessible to shallow soil [29].

In each direction, the soil nutrients differ, even at the same distance from the main stem of the shrub and at the same soil depth. The soil enrichment effect varies according to plant aspect and conditions [30]. The nutrient enrichment effect in some directions is higher than in other directions, which may be related to the localized effect of wind, terrain conditions and other environmental factors; many studies show that plants grow roots very unevenly in accordance with such conditions [31]. Roots seek out moisture and are often stunted on the sunny side by heat and dryness but grow vigorously where some shade retains moisture. However, shrubs may be more vigorous on the sunny side given the specific conditions of heat and dryness extremes. Where extremes are weak, moisture remains available, and heat is not excessive, richer soil lies to the south and west due to increased biotic activity. Where heat and dryness dominate, the shaded side is often richer because biota have adapted to the heat and thrive in the sheltered directions [32].

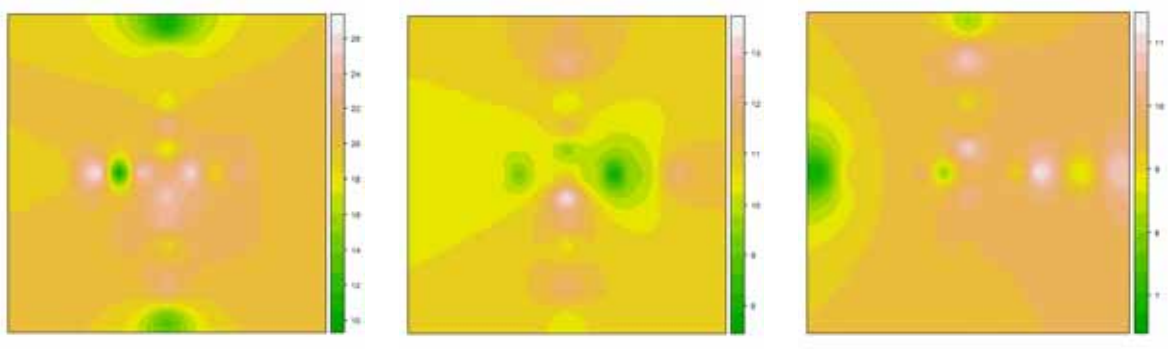
CONCLUSION

Our work indicates that the "fertile island" effect creates significant differences in the soil nutrients under *Vitex negundo* shrubs. Regardless of the slope aspect, the nitrogen, organic matter and available phosphorus content of soil follow the same trend in which the richness of soil nutrients gradually declines with increased distance from the main stem of the shrub. The "fertile island" also causes soil strata nearer to the surface to have greater nutrient richness than deep soil, and the enrichment effect reaches its highest concentration in shallow soil; it is much higher near the surface than in deep soil. Characterizing the spatial variation where "fertile islands" may significantly change the soil environment, this ability of *Vitex negundo.* Shrub will be beneficial for soil reclamation, plant restoration and increasing biodiversity in poor soil, with high ecological relevance in semi-arid areas.

TABLE 4
Variation in spatial structure of organic matter content.

Direction	Soil depth (cm)	SOM at different distances (g kg^{-1})																	
		0–30 cm			30–60 cm			60–90 cm			90–140 cm			140–190 cm				
E	0–5	25. 54±2. 21	A	a	18. 69±1. 21	A	b	22. 05±0. 70	A	ab	19. 50±0. 32	A	b	19. 62±2. 22	A	b		
	5–10	9. 94±0. 20	B	ab	7. 83±0. 42	B	b	9. 77±0. 52	B	ab	11. 84±1. 05	B	a	11. 16±1. 18	B	a		
	10–20	9. 89±0. 60	B	a	9. 07±0. 56	B	a	11. 15±1. 48	B	a	8. 66±1. 34	B	a	10. 83±0. 48	B	a		
W	0–5	24. 64±0. 17	A	a	11. 08±0. 68	A	c	26. 24±1. 57	A	a	18. 37±2. 53	A	b	18. 71±2. 41	A	b		
	5–10	10. 33±1. 14	B	a	9. 30±0. 79	A	a	10. 43±0. 92	B	a	10. 38±0. 75	B	a	10. 27±1. 33	B	a		
	10–20	8. 28±0. 22	B	a	9. 74±0. 55	A	a	9. 27±2. 36	B	a	9. 11±0. 50	B	a	6. 72±0. 20	B	a		
S	0–5	31. 29±3. 59	A	a	16. 81±3. 59	A	b	18. 86±1. 92	A	b	22. 35±2. 45	A	b	13. 55±1. 51	A	b		
	5–10	13. 34±1. 39	B	a	11. 97±1. 18	B	a	10. 48±0. 83	B	a	11. 81±1. 45	B	a	10. 33±0. 09	AB	a		
	10–20	10. 16±1. 12	B	a	9. 74±1. 17	B	a	9. 55±0. 17	B	a	9. 43±0. 75	B	a	9. 48±0. 69	B	a		
N	0–5	17. 48±2. 73	A	a	22. 64±3. 70	A	a	17. 78±1. 23	A	a	19. 45±1. 50	A	a	10. 40±0. 49	A	b		
	5–10	9. 63±2. 31	B	a	11. 32±1. 17	B	a	10. 30±0. 99	B	a	12. 17±0. 67	B	a	11. 40±1. 92	A	a		
	10–20	10. 886±1. 25	AB	a	9. 38±0. 68	B	a	9. 10±0. 50	B	a	10. 68±1. 63	B	a	8. 29±0. 28	A	a		

Note: Explanation analogous to Table 2.



(a) **(b)** **(c)**

FIGURE 4
Kriging interpolation map of organic matter (g kg^{-1}) at (a) 0–5 cm, (b) 5–10 cm, and (c) 10–20 cm soil depth.

ACKNOWLEDGEMENTS

This work was by supported by National Natural Science Foundation of China [number: 31270750]. We thank the Xiaolangdi Ecological Station in Henan Province, CHN, for providing soil and plant materials. We also thank the College of Forestry Laboratory (Henan Agricultural University, CHN) and Dr. Zhao Yong (Henan Agricultural University, CHN) for technical guidance.

REFERENCES

[1] Dunkerley, D. (2000) Hydrologic effects of dryland shrubs: defining the spatial extent of modified soil water uptake rates at an Australian desert site. Journal of Arid Environments. 45, 159-72.

[2] Eldridge, D.J. and Robson, A.D. (1997) Blade ploughing and Exclosure Influence Soil Properties in a Semi-Arid Australian Woodland. Journal of Range Management. 50, 191-98.

[3] Schlesinger, W.H., Reynolds, J.F., Cunningham, G.L., Huenneke, L.F., Jarrell, W.M. and Virginia, R.A. and Whitford, W.G. (1990) Biological feedbacks in global desertification. Science. 247(4946), 1043-8.

[4] Garner, W. and Steinberger, Y. (1989) A proposed mechanism for the formation of 'fertile islands' in the desert ecosystem. Journal of Arid Environments. 16, 257-62.

[5] Collins, H.P. and Cavigelli, M.A. (2003) Soil microbial community characteristics along an elevation gradient in the Laguna Mountains of Southern California. Soil Biology and Biochemistry. 35, 1027-37.

[6] Reynolds, J.F., Virginia, R.A., Kemp, P.R., Soyza, A.G.D. and Tremmel, D.C. (1999) Impact of drought on desert shrubs: effects of seasonality and degree of resource island development. Ecological Monographs. 69(1), 69-106.

[7] Stock, W.D., Dlamini, T.S. and Cowling, R.M. (1999) Plant induced fertile islands as possible indicators of desertification in a succulent desert ecosystem in northern Namaqualand, South Africa. Plant Ecology. 142(1-2), 161-167.

[8] Francopizana, J., Fulbright, T.E. and Gardiner, D.T. (1995) Spatial relations between shrubs and prosopis glandulosa canopies. Journal of Vegetation Science. 6(1), 73-78.

[9] Zhang, P., Yang, J., Zhao, L., Bao, S. and Song, B. (2011) Effect of Caragana tibetica nebkhas on sand entrapment and fertile islands in steppe–desert ecotones on the Inner Mongolia Plateau, China. Plant and Soil. 347, 79-90.

[10] Zhang, Y., Liang, A., Wang, P., Yang, G. and Zhang, X. (2010) Effect of different vegetation restoration models on soil fertility in zhifanggou watershed in gully region of loess region. Acta Agriculturae Boreali-Occidentalis Sinica. 19(9), 114-118.

[11] Xuehua, L.I., Jiang, D. and Luo, Y. (2010) Soil fertile islands of shrub canopy and impacts on vegetation in chronosequence of caragana microphylla. Journal of Liaoning Technical University. 49(4), 830–838.

[12] Rong, Q., Liu, J., Cai, Y., Lu, Z., Zhao, Z., Yue, W. and Xia, J. (2016) "Fertile island" effects of tamarix chinensis, lour. on soil n and p stoichiometry in the coastal wetland of laizhou bay, china. Journal of Soils & Sediments. 16(3), 864-877.

[13] Chaudhry, Q., Blom-Zandstra, M., Gupta, S. and Joner, E.J. (2005) Utilising the synergy between plants and rhizosphere microorganisms to enhance breakdown of organic pollutants in the environment. Environmental Science & Pollution Research International. 12(1), 34-48.

[14] Dieffenbach, A. and Matzner, E. (2000) In situ soil solution chemistry in the rhizosphere of mature Norway spruce (Picea abies [L.] Karst.) trees. Plant and Soil. 222, 149-61.

[15] Dong, L., Cao, J., Li, X., Dai, L. and Su, Y. (2011) Dynamic change of salt contents in rhizosphere soil of salt-tolerant plants. Acta Ecologica Sinica. 10, 2813-21.
[16] Hirobe, M., Ohte, N., Karasawa, N., Zhang, G.S., Wang, L.H. and Yoshikawa, K. (2001) Plant species effect on the spatial patterns of soil properties in the mu-us desert ecosystem, inner mongolia, china. Plant & Soil. 234(2), 195-205.
[17] Ruan, J. and Zhang, F. (2004) Effects of litter incorporation and nitrogen fertilization on the contents of extractable aluminium in the rhizosphere soil of tea plant (Camallia sinensis, (L.) O. Kuntze). Plant & Soil. 263(1), 283-296.
[18] Shi, W., Wang, X. and Yan, W. (2004) Distribution patterns of available p and k in rape rhizosphere in relation to genotypic difference. Plant & Soil. 261(1-2), 11-16.
[19] Turpault, M.P., Utérano, C., Boudot, J.P. and Ranger, J. (2005) Influence of mature douglas fir roots on the solid soil phase of the rhizosphere and its solution chemistry. Plant & Soil. 275(1-2), 327-336.
[20] Delgado-Baquerizo, M., García-Palacios, P., Milla, R., Gallardo, A. and Maestre, F.T. (2015) Soil characteristics determine soil carbon and nitrogen availability during leaf litter decomposition regardless of litter quality. Soil Biology & Biochemistry. 81, 134-142.
[21] Whitford, W.G., Anderson, J. and Rice, P.M. (1997) Stemflow contribution to the 'fertile island' effect in creosotebush, larrea tridentata. Journal of Arid Environments. 35(3), 451-457.
[22] Ruan, J.Y., Zhang, F.S. and Wong, M.H. (2000) Effect of nitrogen form and phosphorus source on the growth, nutrient uptake and rhizosphere soil property of camellia sinensis L. Plant & Soil. 223(1-2), 65-73.
[23] Hinsinger, P., Plassard, C. and Jaillard, B. (2006) Rhizosphere: a new frontier for soil biogeochemistry. Journal of Geochemical Exploration. 37(47), 210-213.
[24] Zhang, Q., Cheng, B., Yang, Z., Gao, C., Zhang, Y. and Zhang, L. (2006) Nutritional characteristics of Caragana jubata shrub and distribution patterns of soil nutrients in Luya Mountain. Chinese Journal of Applied Ecology. 17(12), 2287-2291.
[25] Zhao, H., Su, Y., Zhang, H., Zhao, L. and Zhou, R. (2007) Multiple effects of shrub on soil properties and understory vegetation in horqin sand land, inner Mongolia. Journal of Desert Research. 27(3), 385-390.
[26] Bhark, E.W. and Small, E.E. (2003) Association between plant canopies and the spatial patterns of infiltration in shrubland and grassland of the Chihuahuan Desert, New Mexico. Ecosystems. 6(2), 0185-0196.
[27] Schlesinger, W.H., Abrahams, A.D., Parsons, A.J. and Wainwright, J. (1999) Nutrient losses in runoff from grassland and shrubland habitats in southern New Mexico. I. rainfall simulation experiments. Biogeochemistry. 45(1), 21-34.
[28] Zhao, Y., Zhu, Y., Wang, Q., Chen, Z., Fan, W. and Yang, X. (2011) Effects of nitrogen absorption of vitex negundo in different nitrogen fertilization levels. Science of Soil & Water Conservation. 9(5), 110-114.
[29] Sariyildiz, T. and Anderson, J.M. (2003) Interactions between litter quality, decomposition and soil fertility: a laboratory study. Soil Biology & Biochemistry. 35(3), 391-399.
[30] Jones, M.D., Singleton, D.R., Carstensen, D.P., Powell, S.N., Swanson, J.S., Pfaender, F.K. and Aitken, M.D. (2008) Effect of incubation conditions on the enrichment of pyrene-degrading bacteria identified by stable-isotope probing in an aged, pah-contaminated soil. Microbial Ecology. 56(2), 341.
[31] Diacono, M. and Montemurro, F. (2010) Long-term effects of organic amendments on soil fertility. a review. Agronomy for Sustainable Development. 30(2), 401-422.
[32] Jobbágy, E.G. and Jackson, R.B. (2001) The distribution of soil nutrients with depth: global patterns and the imprint of plants. Biogeochemistry. 53(1), 51-77.

Received: **07.02.2017**
Accepted: **01.10.2017**

CORRESPONDING AUTHOR

Yong Zhao
College of Forestry,
Henan Agricultural University,
Zhengzhou, Henan – China

E-mail: zhaoyonghnnd@163.com

© by PSP Volume 26 – No. 12A/2017 pages 7695-7702 Fresenius Environmental Bulletin

THE RELATIONSHIP OF VERTICILLIUM WILT AND SEED SURFACE MICROFLORA WITH GOSSYPOL LEVEL IN COTTON (*GOSSYPIUM* SPP.)

Oktay Erdogan[1,*], Hulya Ozgonen-Ozkaya[2], M Erhan Gore[3]

[1]Nevsehir Haci Bektas Veli University, Faculty of Engineering and Architecture, Department of Biosystem Engineering, 50300, Nevsehir, Turkey
[2]Suleyman Demirel University, Faculty of Agriculture, Department of Plant Protection, 32260, Isparta, Turkey
[3]Abant Izzet Baysal University, Faculty of Agriculture and Nature Science, Department of Plant Protection, 14280, Bolu, Turkey

ABSTRACT

The aim of study was determined to relationship between on the seed surface microflora and reaction to Verticillium wilt of cotton cultivars with different gossypol levels. Thirteen cotton cultivars were examined gossypol level and the seed surface microflora of the cotton *in vitro*. Then, these cultivars were observed susceptibility to non-defoliating (Vd11 isolate) and defoliating (PYDV6 isolate) pathotypes of *Verticillium dahliae* Kleb. *in vivo*. Cultivars were significant at ($P \leq 0.05$) probability level for disease intensity values *in vivo* and gossypol values *in vitro*. While the highest gossypol value was determined in "Gloria" cultivar (*Gossypium hirsutum* L.) with a 1.669 µg $mL^{-1}$and resistant control "Giza 45" (*Gossypium barbadense* L.) with a 1.343 µg mL^{-1}, the lowest gossypol value was found in "Gossypolsüz Nazilli" (0.196 µg mL^{-1}) and susceptible control "Çukurova 1518" (0.484 µg mL^{-1}) of *G. hirsutum* L. While the lowest of disease intensity value was observed Vd11 isolate and PYDV6 isolate in the highest gossypol, resistant control "Giza 45" cultivar (0.30-1.11). The highest disease intensity values were found in the lowest gossypol, "Gossypolsüz Nazilli" cultivar (2.24-2.82) and susceptible control "Çukurova 1518" cultivar (2.00-2.63), respectively. Fungus species were isolated in high and low gossypol of cotton seeds at the same rate.

KEYWORDS:
Gossypol, *Verticillium dahliae* Kleb., disease intensity, cotton.

INTRODUCTION

Cotton, outside the textile industry is the raw material of approximately 50 industries such as oil, gunpowder and film material. Cotton oil is used in many areas such as soaps and detergents and animal feed. Cotton oil, as an alternative to petrol, is increasingly being used as raw material in bio-diesel production too [1]. About 34 million ha of cotton growing and obtained from approximately 24.8 million tons of lint yield from this area in the world. India, China, USA, Pakistan, Brazil, Uzbekistan and Turkey is one of the leading countries in cotton production [1, 2]. In Turkey, about 458.000 ha of upland cotton was grown and 738.000 tons lint yield was produced in the four main regions Southeastern Anatolia, Aegean, Çukurova and Antalya. Turkey's share in world cotton production is approximately 2.5 % and is ranked seventh [3].

Gossypol is a phenolic compound triterpenoid aldehyde or polyphenolic binaphthyl aldehyde in both plant and seeds in all types of cotton grown. This compound was synthesized by the epidermal cells in the roots, it is communicated to the interior decoration of transmission and here it is localized. Firstly, Gossypol defined in 1886 by Longmore and purified by Marchlewski in 1889 [4]. No gossypol plants were obtained by Michael for the first time in 1954. Smith [5] reported the lowest rate of gossypol on root and the highest rate of gossypol on seed in plant. Sotelo et al. [6] observed the amount of gossypol in the leave with 0.297 mg g^{-1}, in the seed with 0.847 mg g^{-1} of *G. hirsutum* L. Fidan et al. [7] concluded that gossypol concentration of the seed varies from 0.0 % to 9.0 %, but most commercial cotton varieties usually contain the compound from 0.6 % to 2.0 %. Gossypol not only to human and animals, but also can be active against pests, fungi and microorganisms. Many researchers reported that gossypol have antimicrobial, anticancer and antioxidant properties [8, 9, 10]. Also, the pigment glands of cotton plants includes derivatives with gossypol such as desoxyhemigossypol, hemigossypol, hemigossypolone and heliocide. These compounds are important in plant protection against pests and diseases [11].

V. dahliae Kleb. is one of the factors that negatively affect yield and quality in cotton growing, known worldwide as the most devastating and destructive, causing wilt in 160 families and 40 different plant species [12, 13]. Pathogen, invaded xylem, cause xylem occlusion, so major damage occurs on plant yield and quality [14, 15, 16, 17].

The losses of seed cotton yield due to Verticillium wilt were reported about 75 % in California, 8- 10 % in Russia and 4 % in Syria [18]. Verticillium wilt was responsible for significant yield losses (approximately 1.5 million bales) in the world cotton belt [19]. One of the most effective methods is used to resistant varieties without an economic chemical control in the control against the Verticillium wilt. Several authors reported that varieties lose resistance over time and development of resistant varieties studies should be made permanent [20, 21, 22]. Also, in Turkey, cotton is grown in different climatic conditions, causing damage to drought and heat, and this is effective in the selection of cotton varieties [23].

Today, the number of studies of susceptibility to Verticillium wilt containing of gossypol levels in cotton cultivars is very limited. Desoxyhemigossypol and hemigossypol synthesized in plants against pathogenic fungi such as *V. dahliae* and *Fusarium oxysporum* f.sp. *vasinfectum*, these pathogens were classified as phytoalexin, because they are also toxic [24]. Puckhaber et al. [25] carried out to determine the effect of gossypol on *Rhizoctonia solani* development of positive and negative in the studies, reported gossypol may equally positive and negative effect, whereas seen gossypol inhibition less than desoxyhemigossypol and hemigossypol, hemigossypol and desoxyhemigossypol has the most important fungicide. A positive gossypol was found better bactericide by negative gossypol [26].

The aim of study was determined to relationship between on the seed surface microflora and susceptibility to non-defoliating (ND) and defoliating (D) pathotypes of *V. dahliae* Kleb. of cotton cultivars with different gossypol levels.

MATERIALS AND METHODS

Materials. Plant materials. In the study, a total of thirteen cotton cultivars were used as control of three different cultivars (Carmen/tolerant-Bayer Crop Science AG, Leverkusen, Germany; Çukurova 1518/susceptible-Eastern Mediterranean Agricultural Research Institute, Adana, Turkey and Giza 45/resistant-Cotton Research Institute, Egypt) of different cotton species as material (Table 1).

Test microorganism. Isolated from cotton and a high virulence pathotypes, Vd11 isolate (ND pathotype, Nazilli Cotton Research Institute) and PYDV6 isolate (D pathotype, Adnan Menderes University, Faculty of Agriculture, Department of Plant Protection) used for an artificial inoculum [27].

Detection of gossypol level on cotton seeds. Cotton seeds of each cultivar were weighed 1 g in experiment, these were homogenized in 10 mL of 96 % ethanol. Extract was removed and the residue passed through two layers of cheesecloth. After filtration, the extracts were extracted three times with 1 volume diethyl ether (1:1, v:v). The ethanol was removed by rotary evaporator [28]. Extraction procedures were performed in three replications for each cotton varieties. Liquids containing various concentrations gossypol (0-2 ppm) were used for determining quantities of gossypol as standard. The resulting liquid UV visible spectrophotometer (T-80 Plus UV-VIS Spectrophotometer, PG Ins Ltd LA) was observed at 440 nm and quantitated by gossypol [29].

Pot trials. Conidial suspension technique was used to test the susceptible of cotton cultivars with different percentage levels of gossypol against *V. dahliae* Kleb. in pot trials. Experiment was established as randomised plot design with five replications in a growth room (at 24±1 °C; 50-70 % relative humidity; a 12 h light/12 h dark). A 33 % soil, 33 % sand and 33 % peat containing mixture was sterilized in autoclave at 121°C for one hour and was filled into 5 cm diameter plastic pots. Of the 4 seeds sown each plastic pots, only one left at cotyledonary stage and others were removed. *V. dahliae* cultures having high virulence isolates (Vd11 and PYDV6) were developed on Potato Dextrose media broth for inoculation. After two weeks, spore suspension in the flask were adjusted as 4 x 10^6 conidia mL^{-1} with a hemacytometer and 5 mL of adjusted suspension released to the bottom of each plastic pots and plants at the six-true-leaf stage were placed in the pots. Three-five weeks after inoculation, disease severity was assessed for each plant on a 0-to-4 rating scale according to the percentage of foliage affected by acropetal chlorosis, necrosis, wilt, and/or defoliation (0=healthy plant; 1=1–33 %; 2=34–66 %; 3=67–97 %; 4=dead plant) [30]. Disease Severity Index (DSI) was calculated using the formula and obtained data were subjected to Arcsin for transformation [31].

DSI=[(ax0)+(bx1)+(cx2)+(dx3)+(ex4)]/M

DSI: Disease severity index; a, b, c, d, e: The plant number with degree 0, 1, 2, 3, 4 respectively, M= Total plant number.

Detection of microflora on cotton seed surface. Seeds of each cultivar in order to determine microflora of cotton seed heated for 5 minutes in 5 % NaOH and a waiting period on sterile blotting excess moisture is received after washing twice with sterile distilled water. Seed surfaces after drying were cultured on Potato Dextrose Agar (PDA) media and the seeds were incubated at 25 ± 1°C for 10 days. 100 seeds were used for each genotype in this method. Growing colonies at the end of incubation period were counted to genus level and isolating ratios are calculated in the experiment. At the species level identification of isolated fungi were

carried out using macroscopic and microscopic methods [32, 33, 34, 35].

Statistical analysis. All data obtained in experiments were analysed statistically by using JMP statistical software program (5.0.1, SAS Institute, Cary, NC) for analysis of variance and means were compared using Fisher's protected least significance difference (LSD) test at 5 % probability level [36].

RESULTS AND DISCUSSION

Detection of gossypol level on cotton seeds. The levels of gossypol (µg mL^{-1}) in the seeds of cotton cultivars in the experiment were given in Table 2. The amounts of gossypol have varied according to the species and cultivars of the same species in cotton seeds. Cultivars were significantly ($P \leq 0.05$) different level for gossypol results. The lowest amount of gossypol was determined in "Gossypolsüz Nazilli" cv (*G. hirsutum*) with a 0.196 µg mL^{-1} and susceptible control "Çukurova 1518" cv (*G. hirsutum*) with a 0.484 µg mL^{-1} in the cotton seeds. While the highest amount of gossypol was observed in "Gloria" cv (*G. hirsutum*) with a 1.669 µg mL^{-1} and resistance control "Giza 45" cv (*G. barbadence*) with a 1.343 µg mL^{-1}, respectively and followed by "St-373" cv (1.090 µg mL^{-1}) and "GSN 12" cv (0.911 µg mL^{-1}). Other candidate cultivars had gossypol levels between 0.599 µg mL^{-1} and 0.850 µg mL^{-1} (Table 2). In a similar study, gossypol level was observed between 0.81 % - 1.04 % in *G. barbadense* L. and 0.64 % - 1.09 % in *G. hirsutum* L. in the seeds studies [37]. Gossypol level with 0.0 % type of *G. sturtian* Will. of Australian origin was determined more than 9.0 % type of *G. davidsonii* Kell. [38]. Gossypol level was found a 0.384 mg g^{-1} in "Mexico 72-69" (*G. barbadense* L.), a 0.218 mg g^{-1} in "SP-21" (*G. hirsutum* L.) [9]. The amount of gossypol in cotton plants and seeds which can vary across varieties [39]. The amount of gossypol was determined a 0.387 mg g^{-1} and a 6.780 mg g^{-1} in the leaves and seeds of

TABLE 1
Species and origins of cotton cultivars in the experiment.

Cultivar (cv)	Species	Origin
Gloria	*G. hirsutum*	Australian
Carmen (tolerant-control)	*G. hirsutum*	Australian
Nazilli DT-15	*G. hirsutum*	Nazilli-Turkey
Çukurova 1518 (susceptible-control)	*G. hirsutum*	Adana- Turkey
Flash	*G. hirsutum*	Hatay- Turkey
Maydos Yerlisi	*G. herbaceum*	Nazilli- Turkey
Giza 45 (resistant-control)	*G. barbadence*	Egypt
Gossypolsüz Nazilli	*G. hirsutum*	Nazilli- Turkey
NP Özbek 100	*G. hirsutum*	Nazilli- Turkey
BA 308	*G. hirsutum*	Hatay- Turkey
St-373	*G. hirsutum*	USA
GSN 12	*G. hirsutum*	Nazilli- Turkey
Cloudia	*G. hirsutum*	Australian

TABLE 2
Gossypol level of cotton seeds in the experiment (µg mL^{-1}).

Cultivar (cv)	Gossypol level (µg mL^{-1})[a]
Gloria	1.669 a
Carmen (tolerant-control)	0.599 ef
Nazilli DT-15	0.850 bcd
Çukurova 1518 (susceptible-control)	0.484 f
Flash	0.764 cde
Maydos Yerlisi	0.701 cdef
Giza 45 (resistant-control)	1.343 a
Gossypolsüz Nazilli	0.196 g
NP Özbek 100	0.722 cdef
BA 308	0.769 cde
St-373	1.090 b
GSN 12	0.911 bc
Cloudia	0.630 def

[a] Mean values with the same letter within a column are not significantly different at the 0.05 probability level by LSD.

TABLE 3
Disease intensity values of cotton cv inoculated with two pathotypes of *V. dahliae* isolates in pot trials.

Cultivar (cv)	Disease intensity values in pot trials	
	Vd11 isolate[a]	PYDV6 isolate[a]
Gloria	0.72 f	1.58 ef
Carmen (tolerant-control)	0.60 g	1.51 f
Nazilli DT-15	0.72 f	1.60 ef
Çukurova 1518 (susceptible-control)	2.00 b	2.63 b
Flash	0.70 f	1.57 ef
Maydos Yerlisi	0.60 g	1.51 f
Giza 45 (resistant-control)	0.30 h	1.11 g
Gossypolsüz Nazilli	2.24 a	2.82 a
NP Özbek 100	1.50 c	2.25 c
BA 308	0.89 d	1.79 d
St-373	0.70 f	1.56 ef
GSN 12	0.85 de	1.77 d
Cloudia	0.77 ef	1.65 de

[a] Mean values with the same letter within a column are not significantly different at the 0.05 probability level by LSD.

TABLE 4
Rates of fungi growing on the seed surface in PDA media (%).

Cultivar (cv)	Growing rates of fungi in seed (%)							
	Fs	Rh	Al	As	Tr	Rz	Ng	Others[a]
Gloria	18	5	39	24	2	1	5	10
Carmen	18	6	28	26	7	2	-	13
Nazilli DT-15	20	4	31	27	3	1	6	8
Çukurova 1518	19	8	33	26	2	2	-	10
Flash	18	3	33	33	3	1	-	9
Maydos Yerlisi	25	6	37	28	4	3	7	10
Giza 45	28	2	35	21	5	1	-	8
Gossypolsüz Nazilli	30	12	30	15	5	1	3	4
NPÖzbek 100	12	4	35	24	5	1	4	15
BA 308	35	6	20	29	1	1	6	2
St-373	28	7	31	25	2	4	-	3
GSN 12	25	4	35	26	2	3	-	5
Cloudia	22	3	33	30	3	3	3	3

Fs: Fusarium, Rh: Rhizoctonia, Al: Alternaria, As: Aspergillus, Tr: Trichotechium, Rz: Rhizopus, Ng; Nigrospora.
[a]Growing bacteria, yeast colonies in seeds on PDA media.

"Acala 1517-70"; a 6.780 mg g^{-1} and a 10.980 mg g^{-1} in the leaves and seeds of "OR-19", respectively [40].

Pot trials. Disease intensity index values of cotton cultivars in pot trials were given in Table 3. Differences between cultivars were significant at ($P \leq 0.05$) probability level for disease severity value in a pot experiment conducted in a growth room. In the pot experiments, disease resistant and high amount of gossypol, resistant control "Giza 45" cv with a 0.30 index value showed the lowest disease severity and followed by "Carmen" cv (0.60) and "Maydos Yerlisi" cv (0.60) for Vd11 isolate according to the disease severity index. The highest intensity of disease was observed in low amount of gossypol, "Gossypolsüz Nazilli" cv (2.24) and susceptible control "Çukurova 1518" cv (2.00). Other candidate cultivars had index values between 0.70 and 1.50. Resistant control "Giza 45" cv (1.11) was in the first place and followed by tolerant control "Carmen" cv (1.51) and "Maydos Yerlisi" cv (1.51). Again the highest intensity of disease was determined in "Gossypolsüz Nazilli" (2.82) and susceptible control "Çukurova 1518" cv (2.63) for PYDV6 isolate. Zaki et al. [41] reported the antifungal compounds determining in inoculated plants with *Verticillium albo-atrum*, these compounds could not detect in uninoculated plants. Also, vergosin and hemigossypol compounds were more effective than the antifungal agents and gossypol against *V. albo-atrum*. According to Mace and Stipanovic [42] found desoxyhemigossypol (6.1 µg ml^{-1} dose) in cotton roots and stems infected with *V. dahliae* reduced growth of the pathogen around 75 %. When used to different concentrations of some herbicides in cotton areas applied to cotton seed, haloxyfob and linuron have prevented to the mycelial growth of *F. oxysporum* f. sp. *vasinfectum* in solid and liquid culture. The amount of gossypol

increased compared to control in disease plants, which prevented to the mycelial growth of the pathogen *in vitro* [43]. The peptide components have isolated resistant to fungal pathogens and bollworm seeds of the eight cotton varieties and when capable of inhibition *V. dahliae* conidia, α-amylase and other peptides viewed, between fungicidal activity of peptides and resistance of cotton varieties determined a correlation [44]. Ten cotton varieties were inoculated with D and ND pathotypes (10^6 conidia mL^{-1}) in the growth chamber, As a result of the study, the lowest disease severity value was determined in the "Maydos Yerlisi" cv [45].

Detection of microflora on cotton seed surface. Rates of fungi growing on the seeds cultured on PDA medium were given in Table 4. *Alternaria* spp., *Fusarium* spp. and *Aspergillus* spp. isolated intensively both low levels of gossypol and high levels of gossypol on seed, respectively. *Alternaria* spp. were found the highest in "Gloria" cv (39 %), the lowest in "BA 308" cv (20 %). *Fusarium* spp. were determined the highest in "BA 308" cv (35 %) and "Gossypolsüz Nazilli" cv (30 %). In similarly, *Aspergillus* spp. were isolated between 15 % - 33 % in low and high gossypol of cultivars. Macroscopic and microscopic studies of carried out on cotton seed; Alternaria colonies were identified as largely *A. alternata*; *Fusarium* spp. were identified as *F. oxysporum*, *F. semitectum* and *F. solani*; *Aspergillus* spp. were identified as *Aspergillus niger*, *A. flavus* and *A. ochraceus*. Isolating rate of *Rhizoctonia* spp. was found between 2 - 12 % in low and high gossypol of cultivars (Table 4). Our results showed parallels with the other studies. Moore and Rollins [46] reported that outside capillary roots and seed coat of gossypol in the cotton plant, as the internal structure of seeds, leaves, stems, roots, branches, boll shell, stigma and the sytle in plant and flower parts. Klich [47] was isolated different filamentous fungi in delinted surface sterilized cotton seeds and there were no differences in fungal flora among cultivars. Of the seventeen taxa isolated, *Alternaria* spp. *Colletotrichum gossypii*, *Fusarium equiseti*, *F. pallidoroseum* (*F. semitectum*) were present more than 10 %. *F. semitectum* have isolated a sulfuric acid delint in the cotton seed by blotter method, but haven't determined a relationship with disease symptoms after the seed output in the autoclaved soil [48]. Arabsalmani [49] isolated that fungal species of different genus from seed coat and embryo parts on PDA medium after surface disinfection of seeds in the study. While *A. alternata* and *Fusarium* spp. were isolated from embryo portion of "Sahel" cv by 32.1 % and 33.3 % ratio, *A. macrospora* and *Fusarium* spp. were isolated from the seed surface by 25 % and 21.4 % ratio, respectively. The absence of a relationship between gossypol level and fungus developing on the seed surface may be attributed to environmental and climatic conditions. Similar results were reported by Baba [50].

CONCLUSION

In this study, the amount of gossypol in the cotton seed was determined different to species, the cultivars of the same species and origins. While the highest amount of gossypol determining both *G. barbadence* L. (tolerant control Giza 45 cv) and *G. hirsutum* L. (Gloria cv), the lowest amount of gossypol has been determined in "Gossypolsüz Nazilli" cv and susceptible control "Çukurova 1518" cv (*G. hirsutum* L.). In this context, gossypol content of the seed may vary according to species, variety, environmental conditions, plant growth and development stages. While the lowest disease severity against both pathotype of *V. dahliae* Kleb. was determined on the highest amount of gossypol in resistant control "Giza 45" cv, the highest intensity of disease was found on the lowest amount of gossypol in "Gossypolsüz Nazilli" cv. The disease intensity index values were obtained near the *G. barbadance* L. such as "Gloria", "Carmen" and "Claudia" cultivars with origin of Australian in upland cotton. Plant breeders will increase the chances of success in the resistance breeding studies against the Verticillium wilt, especially the use of cultivars with high gossypol in the cotton plant parts without an economic chemical control in the control against Verticillium wilt. Meanwhile, fungi were isolated on the seeds of low and high gossypol cultivar at the same level. Therefore, there was concluded any relationship between level of gossypol on the seed and species of fungi growing on the seed surface.

ACKNOWLEDGEMENTS

The authors would like to thank Prof. Dr. Kemal Benlioglu of University of Adnan Menderes, for kindly providing PYDV6 isolate.

REFERENCES

[1] USDA (United States Department of Agriculture Foreign Agricultural Service) (2016) Cotton Area, Yield, and Production. Online located at: https://www.fas.usda.gov/data/cotton-world.

[2] Gokdogan, O., Erdogan, O., Eralp, Ö. and Zeybek, A. (2016) Energy Efficiency Analysis of Cotton Production in Turkey: A Case Study from Aydın Province. Fresen. Environ. Bull. 25(11), 4959-4964.

[3] TSI (Turkish Statistical Institute) (2016) Agricultural structure and production. Government Statistic Institute of Prime Minister Publ. Online located at: http://www.tuik.gov.tr (in Turkish).
[4] Jones, L.A. (1991) Definition of Gossypol and its Prevalence in Cottonseed Products. Cattle Research with Gossypol Containing Feeds. National Cottonseed Products Association, Memphis.
[5] Smith, F.H. (1961) Biosynthesis of Gossypol by Excised Cotton Roots. Nature. 192, 888-889.
[6] Sotelo, A., Villavicencio, H., Montalvo, I. and Gonzalez, M.T. (2005) Gossypol Content on Leaves and Seeds from Some Wild Malvaceae Species. The African Journal of Traditional. 2(1), 4-12.
[7] Fidan, M.S., Bölek, Y., Oğlakçı, M. and Bardak, A. (2009) Gossypol in Cotton. Kahramanmaraş Sütçü İmam University Journal of Nature Science. 12(1), 93-101.
[8] Vroh Bi, I., Baudoin, J.P., Hau, B. and Mergeai, G. (1999) Development of High Gossypol Cotton Plants with Low Gossypol Seeds Using Trispecies Bridge Crosses and i*n Vitro* Culture of Seed Embryos. Euphytica. 106, 243-251.
[9] Cai, Y., Zhang, H., Zeng, Y., Mo, J., Bao, J., Miao, C., Yan, F., Bai, J. and Chen, F. (2004) An Optimized Gossypol High Performance Liquid Chromatography Assay and Its Application in Evaluation of Different Gland Genotypes of Cotton. Journal of Biosciences. 29(1), 101-105.
[10] Kline, M.P.S., Rajkumar, V., Timm, M.M., Kimlinger, T.K., Haug, J.L., Lust, J.A., Greipp, P.R. and Kumar, S. (2008) R (-) gossypol (AT-101) Activates Programmed Cell Death in Multiple Myeloma Cells. Experimental Hematology. 36, 568-576.
[11] Mellon, J.E., Zelaya, C.A., Dowd, M.K., Beltz, S.B. and Klich, M.A. (2012) Inhibitory effects of gossypol, gossypolone, and apogossypolone on a collection of economically important filamentous fungi. Journal of Agriculture and Food Chemistry. 60, 2740-2745.
[12] Pegg, G.F. (1984) The Impact of Verticillium Diseases in Agriculture. Phytopathology Mediterranean. 23, 176-192.
[13] Joaquim, T.R. and Rowe, R.C. (1990) Reassessment of vegetative compatibility relationships among strains of *Verticillium dahliae* using nitrate-nonutilizing mutants. Phytopatholgy. 80, 1160-1166.
[14] Beckman, C.H. (1987) The Nature of Wilt Diseases of Plants. APS Press, St Paul, Minnesota.
[15] Tjamos, E.C., Tsitsiyannis, D.I. and Tjamos, S.E. (2000) Selection and evaluation of rhizosphere bacteria as biocontrol agents against *Verticillium dahliae*. In: Tjamos, E.C., Rowe, R.C., Heale, J.B. and Fravel, D.R. (Eds.), Advances in Verticillium research and disease management, American Phytopathological Society (APS) Press, St. Paul, 244–248.
[16] Pegg, G.F. and Brady, B.L. (2002) Verticillium wilts. 1st ed. CABI Publishing. Wallingford.
[17] Rowe, R.C. and Powelson, M.L. (2002) Potato early dying: management challenges in a changing production environment. Plant Disease. 86, 1184-1193.
[18] Bejarano-Alcazar, J., Blanco, L.M.A., Melero, V. and Jimenez Diaz, R.M. (1996) Etiology, Importance and Distrubation of Verticillium Wilt of Cotton in Southern Spain. Plant Disease. 80(11), 1233-1238.
[19] Nemli, T. (2003) Cotton Disease and Control Methods. Cotton Training Seminar, 14-17 October, İzmir, 103-111.
[20] Wilhelm, S., Sagen, J.E. and Tietz, H. (1974) Resistance to Verticillium wilt in Cotton: source, techniques of identification, inheritance trends and Resistance potential of Multipline Cultivars. Phytopathology. 64, 924-931.
[21] El-Zik, K.M. (1985) Integrated control of verticilium wilt of cotton. Plant Disease. 69, 1025-1032.
[22] Onan, E. and Karcılıoğlu, A. (1998) Pathotypes of *V. dahliae* from cotton in Aegean Region and Review of Verticillium Wilt Tolerance in Nazilli 84 Cotton. J Turkish Phytopathology. 27, 113-120.
[23] Barutçular, C., Yıldırım, M., Koç, M., Akıncı, C., Toptaş, I., Albayrak, O., Tanrıkulu, A. and El Sabagh, A. (2016) Evaluation of Spad Chlorophyll in Spring Wheat Genotypes Under Different Environments. Fresen. Environ. Bull. 25(4), 1258-1266.
[24] Liu, J., Benedict, C.R., Stipanovic, R.D. and Bell, A.A. (1999) Purification and Characterization of S Adenosyl-L-Methionine: Desoxyhemigossypol-6-O Methyltransferase from Cotton Plants. An Enzyme Capable of Methylating the Defense Terpenoids of Cotton. Plant Physiology. 121, 1017-1024.
[25] Puckhaber, L.S., Dowd, M.K., Stipanovic, R.D. and Howell, C.R. (2002) Toxicity of (+) and (-) gossypol to the plant pathogen, *Rhizoctonia solani*. Journal of Agriculture and Food Chemistry. 50, 7017-7021.
[26] Aksoy, Y., Lim, M.C., Dowd, M.K., Wan, P.J., Klesius, P.H. and Shoemaker, C. (2004) *In vitro* inhibitory effect of gossypol from gossypol-acetic acid and (+) and (-) isomers of gossypol on the growth of edwardsiella ictaluri. Journal of Applied Microbiology. 97, 87-92.

[27] Erdoğan, O. (2009) Determination of Reactions of Some Cotton Breeding Lines against Cotton Wilt Disease Caused by *Verticillium dahliae* Kleb. Adnan Menderes University Journal of Faculty of Agriculture. 6(2), 9-16.
[28] Bell, A.A. (1969) Phytoalexin production and Verticillium wilt resistance in cotton. Phytopathology. 59, 1119-1127.
[29] Awadalla, O.A. and El-Refai, I.M. (1992) Herbicide-induced resistance of cotton to Verticillium wilt disease and activation of host cells to produce the phytoalexin gossypol. Canadian Journal of Botany. 70, 1440-1444.
[30] Bejarano-Alcazar, J., Blanco, L.M.A., Melero, V. and Jimenez Diaz, R.M. (1995) Influence of inoculum density of defoliating and nondefoliating pathotypes of *V. dahliae* on epidemics of Verticillium wilt of cotton in southern Spain. Phytopathology. 85, 1474-1481.
[31] Karman, M. (1971) General Information in Plant Protection Investigations, Evaluation and Performing of the Trials. Regional Agricultural Protection Institute, İzmir, 279p.
[32] Nirenberg, H.I. (1976) Untersuchungel Über Die Morphologische und Biologische Differenzierung in der Fusarium Sektion Liseola. Mitteilungen aus der Biologischen Bundesanstalt Für Lant- und Forstwirtschaft. 169, 1-117.
[33] Booth, C. (1977) *Fusarium* a Laboratory Guide to the ldentification of the Major Species. CMI, Kew Surrey.
[34] Samson, R.A., Hoekstra, E.S., Frisvad, J.C. and Filtenborg, O. (1995) Introduction to Food-Borne Fungi. Fourth Ed. Centraalbureau vo or Schimmelcultures, Netherlands.
[35] Leslie, J.F. and Summerel, B.A. (2006) The *Fusarium* Laboratory Manuel. Blackwell Publish, USA.
[36] Steel, R.G.D., Torrie, J.H. and Dickey, D.A. (1997) Principles and procedures of statistics: A biometrical approach. 3rd edition, McGraw Hill Book Co. Inc., New York. 400-428.
[37] Percy, R.G., Calhoun, M.C. and Kim, H.L. (1996) Seed Gossypol Variation with in *G. barbadense* L. Crop Science. 36, 193-197.
[38] Vroh Bi, I., Baudoin, J.P. and Mergeai, G. (1998) Cytogenetics of the Glandless Seed and Glanded Plant Trait from *Gossypium sturtianum* Willis Introgressed into Upland Cotton (*Gossypium hirsutum* L.). Plant Breeding. 117, 235-241.
[39] Stipanovic, R.D., Puchaber, L.S., Bell, A.A., Percival, A.E. and Jacobs, J. (2005) Occurrence of (+) and (-) gossypol in wild species of cotton and in *Gossypium hirsutum* marie galante (Watt) Hutchinson. Journal of Agriculture and Food Chemistry. 53(16), 6266-6271.
[40] Meyer, R., Vorster, S. and Dubery, I.A. (2004) Identification and Quantification of Gossypol in Cotton by Using Packed Microtips Columns in Combination with HPLC. Analytical and Bioanalytical Chemistry. 380(4), 719-724.
[41] Zaki, A.I., Keen, N.T. and Erwin, D.C. (1972) Implication of Vergosin and Hemigossypol in the Resistance of Cotton to *Verticillium albo-atrum*. Phytopathology. 62, 1402-1406.
[42] Mace**,** M.E. and Stipanovic, R.D. (1995) Mode of Action of the Phytoalexin Desoxyhemigossypol against the Wilt Pathogen, *Verticillium dahliae*. Pesticide Biochemistry and Physiology. 53(3), 205-209.
[43] Canıhoş, Y., Kurt, Ş. and Özgönen, H. (2000) Herbicide-induced Resistance to Fusarium Wilt in Cotton and Gossypol Production of Host Cells. Turkish J of Agriculture and Forestry. 24, 129-135.
[44] Abdurakhimov, R.S., Veshkurova, O.N., Uzbekov, V.V., Arzanova, I.A., Sultanova, E.M. and Salikhov, S. (2009) Effect of Cotton-Seed Biocidal Peptides and Gossypol on Resistance to Biotic Factors. Chemistry of Natural Compounds. 45(2), 213-216.
[45] Göre, M.E., Erdoğan, O. and Altın, N. (2017) Searching for resistance sources to Verticillium wilt of cotton in seedlings from *Gossypium* spp. Tropical Plant Pathology. 42, 28-31.
[46] Moore, A.T. and Rollins, M.L. (1961) New Information on the Morphology of the Gossypol Pigment Gland of Cottonseed. Journal of the American Oil Chemists Society. 38, 156-160.
[47] Klich, M. (1986) Mycoflora of Cotton Seeds from the Southern United States: A Three Year Study of Distribution and Frequency. Mycologia. 78(5), 706-712.
[48] Costa, M.L.N., Dhingra, O.D. and Da Silva, J.L. (2005) Influence of internal seedborne *Fusarium semitectum* on cotton seedlings. Fitopatologia Brasileira. 30(2), 183-186.
[49] Arabsalmani, M. (2015) Cotton seed borne disease in Golestan Province in Northern Iran. Cumhuriyet University Faculty of Science, Science Journal. 36(3), 2065-2070.
[50] Baba, H., Zumre, M. and Ozyigit, I.I. (2016) A Comparative Biogeographical Study of Myxomycetes ın Four Different Habitats of Eastern Mediterranean Part of Turkey. Fresen. Environ. Bull. 25(5), 1449-1460.

Received: **09.02.2017**
Accepted: **30.09.2017**

CORRESPONDING AUTHOR

Oktay Erdogan
Nevsehir Haci Bektas Veli University
Biosystem Engineering Department
50300 Nevsehir – Turkey

E-mail: oktaye@gmail.com

© by PSP Volume 26 – No. 12A/2017 pages 7703-7709 Fresenius Environmental Bulletin

VISUAL QUALITY ASSESSMENT OF TOWNSCAPES: A STUDY FOR NIKSAR TOWN (TOKAT) OF TURKEY

Pervin Yesil*

Department of Landscape Architecture, Faculty of Agriculture, Ordu University, 52200, Ordu, Turkey

ABSTRACT

Although Middle Black Sea region of Turkey harbors various natural and cultural aspects, the scientific researches about such a rich source of the region are still insufficient. The present study was conducted to assess the visual landscape quality of natural and cultural beauties of Niksar town and close surroundings and to investigate the effects of landscape components on visual quality. The type of landscape with the greatest visual quality value was identified as Rocky Habitat Landscape 2 (r=4.386) and it was followed respectively by Agricultural Landscape 5 (r=4.227) and Natural Landscape 3 (r=4.137). It was observed that all of the landscape parameters considered in this study (naturalness, variety, vividness, being interesting, harmony, originality, cultural value) significantly affected visual quality values. Besides, perceptibility also had significant effects on visual quality of the landscapes. Finally recommendations were provided for the future use of natural resources of the region.

KEYWORDS:
Visual quality, visual quality assessment, visual perception, aesthetic of landscape, Niksar, Turkey.

INTRODUCTION

The visual impact of a site is related to level of degradation, degree of naturalness, diversity of flora and fauna in natural landscapes and also related to physical attributes of the space like availability, accuracy in space setup, functionality and conventionality in cultural landscapes. Therefore visual quality studies deal not only with esthetic characteristics of the landscapes, but also with functional characteristics of those landscapes.

Identification, assessment, preservation and sustainability of visual quality of landscapes are among the essential topics of ecosystem management studies [1]. Landscape quality assessment constitutes a significant component of environmental management and planning works and it is also actively used in environmental perception researches [2]. High quality landscapes usually correspond to areas that are rich in water, oxygen, geomorphological formations, animal and vegetal species, and/or are interesting for educational or scientific purposes [3]. An environmental management system must necessarily include scenic beauty as a key component [4]. Though, it is not always easy to apply techniques for the assessment of landscape visual quality, this quality can be reasonably considered as a resource which has to be preserved in order to protect rural landscape diversity [5].

Visual landscape quality assessment has been emphasized and methodologically searched in recent studies [6-14]. Although physical approach model [15, 16] and psychological approach model [17] are used in visual quality assessment studies, psychophysical approach model [18-24] relating human preferences with environmental stimulants is the most common model used in visual quality assessments. The Scenic Beauty Estimation (SBE) Method is a well-known psychophysical technique for landscape visual quality evaluation [18]. In SBE researches, participant assessments based on photographic presentation of landscape images are used [4, 10, 18, 21, 23, 25-36].

The present study was conducted to put forth visual landscape quality of the selected sites, to determine the best representative landscape types and to determine the prominent sides of these landscape types and finally to provide future planning recommendations.

MATERIALS AND METHODS

Study area. The present research was conducted in Niksar town and close surroundings. Niksar is a town of Tokat province and located in Middle Black Sea section of Black Sea region. Niksar is established at the most strategic location of Silk Road extending along Kelkit Valley and also at significant and active routes of Turkey. It is located within Kelkit valley, which is an important natural site of Turkey. Kelkit valley is located in Black Sea region, but has Mediterranean microclimate, thus biome of the region harbors narrow and disconnected spreads. The mixture of European-Siberian and Mediterranean biomes is observed together within the valley. The important nature site has a mosaic landscape composed of oak forests,

red pine, scotch pine and black pine forests, residual cedar populations, agricultural lands, river-side plant communities and Mediterranean-specific maquis populations. The flora of Kelkit Valley includes a unique mixture of Mediterranean, Iran-Turan and Europe-Siberia floristic components which have never been seen in other cedar (*C. libani*) forests of the world. The flora of the site consists of 200 taxa, of which 13 are endemic to Turkey [37]. One of these cedar populations is located within the boundaries of Niksar town.

Selection of the photographs. In this study, the method used by Bulut and Yılmaz [23] in the town of Kemaliye was modified and applied to Niksar. Initially 600 photographs were taken from Niksar town and close surroundings. Then these photos were divided into 6 main groups based on represented landscape characteristics and 5 photos were selected for each group (a total of 30 photos). The main groups were as follows: Natural Landscape (NL), Urban Landscape (UL), Rural Settlements Landscape (RS), Rocky Habitats Landscape (RH), Agricultural Landscape (AS) and Plateau Landscape (PL).

Surveys. Selected photos were arranged as a Power Point presentation and presented to groups of 30 participants. The survey questions were asked to be replied along with this presentation. The main groups represented by these photos were pointed out and participants were asked to score accordingly. While presenting the photos into the screen, initially information was provided about the parameters.

The first section of the survey (questionnaire) form was composed of questions about demographic characteristics of the participants. In the second section, participants were asked to score each photo for relevant parameters [Naturalness (Na), Variety (Va), Vividness (Vi), Being interesting (I), Harmony (H), Originality (O), Cultural values (Cv) and Visual Landscape Quality (VLQ)] in a 1-5 scale (1 representing the lowest and 5 the highest score). Participants were undergraduate students of Ordu University Agricultural Faculty (92 people), Faculty of Education (62 people), Faculty of Science (61 people) and Ünye Faculty of Economics and Administrative Sciences (35 people) and graduate students (27 people). There were a total of 277 participant university students.

A scale was created by using some references [21, 29, 30] for the analysis of landscape characteristics. Landscape variables were determined on the basis of mean scores according to measurement scale by means of expert method [38]. This scale is composed of 13 landscape characteristics (Table 1).

SPSS 22 statistical software was used to evaluate the surveys applied for visual quality analysis. Mean values were taken into consideration and resultant data was subjected to correlation analysis.

TABLE 1
Scale for landscape parameters

Variables	Abbreviation	Scoring			
		0	1	2	3
Degree of naturalness	DN	Houses + roads + other = 0;	Few isolated elements	Crops without man-made elements	natural
Vegetation type	VT	No vegetation or unclear	Only grass, herbaceous	Grass and bushes	Mixed vegetation (grass, bushes and trees)
Percentage of land cover by vegetation	PLCV	%0-25	%25-50	%50-75	%75-100
Diversity of man-made elements	DME	none	1	2	3 or more
Presence of positive man-made elements (sights and typical houses)	PPME	%0-25	%25-50	%50-75	%75-100
Percentage of negative man made elements (roads, industries, power lines, etc.)	PNME	%0-25	%25-50	%50-75	%75-100
Type of topography	TT	almost flat	wavy	mountain	Very mountain
Type of dominant texture	TDT	smooth	medium	rough	
% area covered by dominant texture	ACDT	%0-25	%25-50	%50-75	%75-100
Colour diversity of natural elements	CDNE	none	1	2	3 or more
Colour diversity of man-made elements	CDME	none	1	2	3 or more
Perceptibility	PE	weak	medium	high	
Horizon type	HT	panoramic	semi-open	vista	



Picture NL3, average scoring: 4.137



Picture UL2, average scoring: 4.206



Picture RS1, average scoring: 3.931



Picture RH2, average scoring: 4.386



Picture AL5, average scoring: 4.227



Picture PL2, average scoring: 4.271

FIGURE 1
The photos with the greatest VLQ values

RESULTS AND DISCUSSION

Demographic characteristics of participants are commonly used to identify the interactions between demographic parameters and relevant traits. Since all the participants were composed of undergraduate and graduate students, participants exhibited a homogenous pattern with regard to education level and occupation-like criteria. Therefore, only the age and gender distributions were evaluated. Of the participants, 41.2% were female, 58.8% were male, 83.8% were younger than 24 years, 15.5% were between 25-39 and 7% were between 40-59 years.

The photos with the greatest VLQ values were identified as NL3 (4.137), UL2 (4.206), RS1 (3.931), RH2 (4.386), AL5 (4.227) and PL2 (4.271). Based on VLQ order, the photos with the greatest scores for each landscape type are presented in Figure 1. Among these photos, Rocky habitat

scenery (RH2) had the greatest score and it was respectively followed by Agriculture Landscape (AL5) and Natural Landscape (NL3) (Table 2).

Tokat province is prominent with rocky habitats and with this characteristic, it became the subject matter of the study of Acar et. al [38]. The present study also supported the idea that rocky habitats were among the most valuable attributes of the region.

Of the landscapes with the greatest average VLQ scores, NL3, UL2, RH2, AL5 and PL2 scenes had also the greatest naturalness scores in their groups (respectively with 4.566; 3.585; 4.498; 4.238; 4.375). The scenes RS1, RH2, AL5 and PL2 had the greatest variety scores (3.578; 3.978; 3.675; 3.632); RS1 and PL2 had the greatest vividness scores (3.708; 3.971); UL2, RS1, RH2 and PL2 had the greatest being interesting scores (3.347; 3.058; 3.581; 3.227); NL3, UL2, RS1, RH2, AL5 and PL2 had the greatest harmony scores (3.863; 3.758; 3.545; 3.960; 3.838); RS1, RH2 and PL2 had the greatest originality scores (3.625; 3.892; 3.606); UL2 and RS1 had the greatest cultural value scores (4.043; 3.578) and all these values supported the VLQ values of the photos. In this case, of the photos with the greatest scores, 83.3% were parallel to naturalness parameter, 66.7% variety, 33.3% vividness, 66.7% being interesting, 100% harmony, 50% originality and 33.3% cultural value parameter. Among all groups, the photo PL2 with the greatest VLQ value in its own group had the greatest average score from all parameters except for cultural value.

Only UL2 and RS1 differentiated from the others with regard to naturalness parameter and nonparallel increase in VLQ values of the photos of urban landscape (UL) and rural settlements (RS) groups with the degree of naturalness was an expected case. In other words, it is irrelevant to expect high naturalness degree from settlement areas.

According to Clay and Smith [26], cursory analysis does not provide sufficient evidence. Therefore, the relationships were also evaluated with correlation analysis. Initially correlations of VLQ with naturalness (Na), variety (Va), vividness (Vi), being interesting (İ), harmony (H), originality (O) and cultural value (Cv) parameters were investigated.

As it was seen in Table 3, there were quite strong significant correlations between VLQ and all parameters (p<0.01). The variable with the strongest linear relationship with VLQ was Vi (r = 0.931) and it was respectively followed by H (r = 0.922) and I (r = 0.907).

There were quite significant and positive correlations between landscape types (NL3, UL2, RS1, RH2, AL5 and PL2) and perceptional parameters (N, Va, Vi, H, O, Cv) (p<0.01). Current findings are parallel to findings of [38]. Considering the correlations between landscapes and perceptional parameters, the greatest correlations were observed between AL5 landscape and naturalness (r=0.626), variety (r=0.582) and vividness (r=0.636) parameters and between RH2 landscape and being interesting (r=0.460), harmony (r=0.585) and originality (r=0.540) parameters (Table 4).

The correlation analysis results presenting the relationships between landscape attributes and VLQ are provided in Table 5. The only variable with a significant correlation with VLQ was PE. In this case, a positive change was observed in visual quality level of the site with increasing perceptibility levels. Özhancı and Yılmaz [39] also reported increasing landscape score with increasing perceptibility of the images.

TABLE 2
Average VLQ scores of the photos

	Average VLQ	Standard Deviation		Average VLQ	Standard Deviation		Average VLQ	Standard Deviation
NL1	3.433	0.974	**RS1**	3.931	1.056	**AL1**	4.094	0.880
NL2	3.560	1.057	**RS2**	3.765	0.959	**AL2**	4.090	0.874
NL3	4.137	0.946	**RS3**	3.845	1.033	**AL3**	3.899	1.034
NL4	3.639	1.090	**RS4**	3.697	0.979	**AL4**	3.668	1.112
NL5	4.083	0.998	**RS5**	3.928	1.015	**AL5**	4.227	0.870
UL1	3.357	1.172	**RH1**	4.379	0.815	**PL1**	3.022	1.176
UL2	4.206	0.883	**RH2**	4.386	0.765	**PL2**	4.271	0.849
UL3	3.108	1.184	**RH3**	3.780	0.996	**PL3**	4.058	0.903
UL4	3.635	1.036	**RH4**	3.794	1.024	**PL4**	3.542	1.016
UL5	3.032	1.246	**RH5**	4.112	0.904	**PL5**	3.733	0.971

TABLE 3
Correlations between landscape elements and VLQ (N=277)

	VLQ	N	Va	Vi	İ	H	O
N	0.641						
Va	0.840	0.522					
Vi	0.931	0.742	0.816				
İ	0.907	0.488	0.838	0.758			
H	0.922	0.781	0.707	0.909	0.777		
O	0.871	0.764	0.677	0.834	0.808	0.925	
Cv	0.751	0.338	0.717	0.680	0.742	0.627	0.755

Correlation is significant at 0.01 level (2-tailed).

TABLE 4
Correlations between visual preference points and landscape parameters

	NL3	UL2	RS1	RH2	TAL5	PL2
N	0.454	0.368	0.527	0.529	0.626	0.565
Va	0.378	0.321	0.523	0.486	0.582	0.521
Vi	0.484	0.432	0.431	0.486	0.636	0.568
İ	0.351	0.370	0.420	0.460	0.404	0.360
H	0.323	0.473	0.469	0.585	0.533	0.511
O	0.311	0.411	0.470	0.540	0.408	0.398
Hv	0.333	0.384	0.433	0.456	0.326	0.369

Correlation is significant at 0.01 level (2-tailed).

TABLE 5
Correlations between landscape attributes and VLQ

	VLQ	DN	VT	PLCV	DME	PPME	PNME	TT	TDT	ACDT	CDNE	CDME	PE
DN	0.278												
VT	0.131	0.707											
PLCV	0.123	0.583	0.707										
DME	0.309	-0.783	-0.566	-0.367									
PPME	0.000	-0.783	-0.632	-0.224	0.894								
PNME	-0.131	-0.707	-1.000	-0.707	0.566	0.632							
TT	0.278	0.167	0.707	0.583	-0.033	-0.224	-0.707						
TDT	-0.679	-0.833	-0.707	-0.417	0.433	0.671	0.707	-0.417					
ACDT	0.555	0.633	0.141	-0.117	-0.433	-0.671	-0.141	-0.117	-0.733				
CDNE	0.131	0.707	1.000	0.707	-0.566	-0.632	-1.000	0.707	-0.707	0.141			
CDME	-0.034	-0.822	-0.775	-0.365	0.876	0.980	0.775	-0.365	0.730	-0.584	-0.775		
PE	0.926	0.300	0.141	-0.117	0.167	-0.224	-0.141	0.217	-0.733	0.733	0.141	-0.219	
HT	-0.393	-0.283	0.200	-0.283	-0.141	-0.316	-0.200	0.424	0.141	-0.141	0.200	-0.310	-0.141

Correlation is significant at 0.01 level (2-tailed).

The relationship between landscape attributes and VLQ were put forth with Spearman's correlation analysis. There were quite significant correlations between VLQ and PE (p<0.01). Besides, there was a negative correlation between PNME and VT (p<0.01). In other words, negative man-made elements in the photo effected vegetation type and reduce diversity. There was a significant relationship between CDNE and VT (p<0.01) and colour diversity of natural elements increased with increasing diversity in vegetation. There was a negative relationship between DN and TDT (p<0.05) and such a correlation indicated the relationship between increasing slope and degree of naturalness. Existence of a correlation between DME and PPME (p<0.05) indicated a relationship between man-made items and diversity. There was a significant correlation between DME and CDME (p<0.05) and quite significant correlations between CDME and PPME. There was quite negative correlations between PNME and CDNE (p<0.01) and increasing negative man-made elements decreased colour diversity of natural elements.

CONCLUSIONS

The present study was conducted to assess the perceived landscape values of a settlement located in Middle Black Sea Region of Turkey. Present results revealed rocky sites, agricultural lands and other natural attributes in Niksar town and close surroundings as significant and prominent resources. The region has a rich agricultural land-

scape and there are several sites potentially available for agro-tourism, highland tourism and ecotourism activities. However, natural preservation and transfer to future generations without distortions should be the basic target in future planning works.

It was observed in this study that naturalness, variety, vividness, being interesting, harmony, originality and cultural value parameters had significant roles in increase or decreases in visual quality level of the landscape. The more these parameters in the forefront, the higher the landscape beauty is. Besides, perceptibility of the landscape also significantly affected visual quality. Therefore, landscape visual quality and patterns should definitely be taken into consideration while preparing land use plans.

ACKNOWLEDGEMENTS

The authors are also grateful to Assoc. Prof. Dr. Zeki Gokalp (a Certified English Translator and an expert in Biosystems Engineering) for his critical reading and through syntactic corrections of the manuscript.

REFERENCES

[1] Erdönmez, M.Ö. and Kaptanoğlu, A.Y.Ç. (2007) Peyzaj Estetiği ve Görsel Kalite Değerlendirmesi. İstanbul Üniversitesi Orman Fakültesi Yayınları, Seri B. 58(1), 39-51.

[2] Daniel, T. and Meitner, M.M. (2001) Representational Validity of Landscape Visualizations: The Effects of Graphical Realism on Perceived Scenic Beauty of Forest Vistas. Journal of Environmental Psychology. 21(1), 61-72.

[3] Real, E., Arce, C. and Sabucedo, J.M. (2000) Classification of Landscapes Using Quantitative and Categorical Data, and Prediction of Their Scenic Beauty in North-Western Spain. Journal of Environmental Psychology. 20(4), 355-373.

[4] Meitner, M.J. (2004) Scenic Beauty of River Views in the Grand Canyon: Relating Perceptual Judgments to Locations. Landscape and Urban Planning. 68(1), 3–13.

[5] Angileri, V. and Toccolini, A. (1993) The Assessment of Visual Quality as a Tool for the Conservation of Rural Landscape Diversity. Landscape and Urban Planning. 24(1), 105-112.

[6] Wright, G. (1974) Appraisal of visual landscape qualities in a region selected for accelerated growth. Landscape Planning, 1, 307-327.

[7] Arthur, L.M., Daniel, T.C. and Boster, R.S. (1977) Scenic assessment: an overview. Landscape planning. 4, 109-129.

[8] Williamson, D.N. and Calder, S.W. (1979) Visual resource management of Victoria's forests: a new concept for Australia. Landscape Planning. 6(3-4), 313-341.

[9] Steinitz C. (1979) Simulating alternative policies for implementing the Massachusetts scenic and recreational rivers act: The North River Demonstration Project. Landscape and Planning. 6(1), 51-89.

[10] Dearden, P. (1981) Public participation and scenic quality analysis. Landscape Planning. 8(1), 3-19.

[11] Kaplan, R., and Talbot J.F. (1988) Ethnicity and preference for natural settings: A review and recent findings. Landscape and Urban Planning. 15(1-2), 107-117.

[12] Brown, T. (1994) Conceptualizing smoothness and density as landscape elements in visual resource management. Landscape and Urban Planning. 30(1-2), 49-58.

[13] Parsons, R. (1995) Conflict between ecological sustainability and environmental aesthetics: Conundrum, canärd or curiosity. Landscape and Urban Planning. 32(3), 227-244.

[14] Daniel, T.C. (2001) Whither scenic beauty? Visual landscape quality assessment in the 21st century. Landscape and urban planning. 54(1), 267-281.

[15] Ode, A.K., and Fry, G.L.A. (2002) Visual Aspects in Urban Woodland Management. Urban Forestry & Urban Greening. 1(1), 15-24.

[16] Tyrväinen, L., Silvennoinen, H. and Kolehmainen, O. (2003) Ecological and Aesthetic Values in Urban Forest Management. Urban Forestry & Urban Greening. 1(3), 135-149.

[17] Van den Berg, A.E. and Koole, S.L. (2006) New wilderness in the Netherlands: An investigation of visual preferences for nature development landscapes. Landscape and Urban Planning. 78(4), 362–372.

[18] Bergen, S.D., Ulbricht, C.A., Fridley, J.L. and Ganter, M.A. (1995) The validity of computer-generated graphic images of forest landscape. Journal of Environmental Psychology. 15(2), 135-146.

[19] Palmer, J.F. and Hoffman, R.E. (2001) Rating reliability and representation validity in scenic landscape assessments. Landscape and Urban Planning. 54, 149-161.

[20] Clay, G.R., and Daniel, T.C. (2000) Scenic landscape assessment: the effects of land management jurisdiction on public perception of scenic beauty. Landscape and urban planning. 49(1), 1-13.

[21] Arriaza, M., Cañas-Ortega, J.F., Canas-Madueno, J.A. and Ruiz-Aviles, P. (2004) Assessing the visual quality of rural landscapes. Landscape and urban planning. 69(1), 115-125.

[22] Sullivan, W.C. and Lovell, S.T. (2006) Improving the visual quality of commercial development at the rural–urban fringe. Landscape and urban planning. 77(1), 152-166.
[23] Bulut, Z. and Yılmaz, H. (2008) Determination of landscape beauties through visual quality assessment method: a case study for Kemaliye (Erzincan/Turkey). Environmental Monitoring Assessment. 141(1), 121–129.
[24] Özkan, U.Y. (2014) Assessment of Visual Landscape Quality Using IKONOS Imagery. Environmental Monitoring and Assessment. 186(7), 4067-4080.
[25] Habron, D. (1998) Visual perception of wild land in Scotland. Landscape and urban planning. 42(1), 45-56.
[26] Clay, G.R. and Smidt, R.K. (2004) Assessing the validity and reliability of descriptor variables used in scenic highway analysis. Landscape and Urban Planning. 66(4), 239-255.
[27] Acar, C., Kurdoğlu, B.C., Kurdoğlu, O. and Acar, H. (2006) Public preferences for visual quality and management in the Kackar Mountains National Park (Turkey). International Journal of Sustainable Development & World Ecology. 13(6), 499-512.
[28] Fuante de Val, G., Atauri, J.A. and de Lucio, J.V. (2006) Relationship between landscape visual attributes and spatial pattern indices: a test study in Mediterranean-climate landscapes. Landscape and urban planning. 77(4), 393-407.
[29] Acar, C. and Sakıcı, Ç. (2008) Assessing landscape perception of urban rocky habitats. Building and Environment. 43(6), 1153-1170.
[30] Bulut, Z. and Yılmaz, H. (2009) Determination of waterscape beauties through visual quality assessment method. Environmental Monitoring and Assessment. 154, 459–468.
[31] Cengiz, B., Smardon, R.C. and Memlük, Y. (2011) Assessment of river landscapes in terms of preservation and usage balance: A case study Black Sea Region, Turkey). Fresen. Environ. Bull. 20(7), 1673-1684.
[32] Islas, P.V. and Vergara, G. (2012) Perceived Visual Landscape Changes in a Fire Prone Environment: A Multi-method Approach. Journal of Environmental Psychology. 32(2), 144-157.
[33] Frank, S., Fürst, C., Koschke, L., Witta, A. and Makeschina, F. (2013) Assessment of Landscape Aesthetics—Validation of a Landscape Metrics-Based Assessment by Visual Estimation of the Scenic Beauty. Ecological Indicators. 32, 222-231.
[34] Cengiz, C., Bekci, B. and Cengiz, B. (2014) A comparative study of public green spaces in the changing urban texture in terms of preferences for ornamental plants and visual quality: The case of Bartın (Turkey). Fresen. Environ. Bull. 23(9a), 2326-2342.
[35] Junge, X., Schüpbach, B., Walter, T., Schmid, B. and Lindemann-Matthies, P. (2015) Aesthetic quality of agricultural landscape elements in different seasonal stages in Switzerland. Landscape and Urban Planning. 113, 67-77.
[36] Cengiz, B., Cengiz, C. and Bekci, B. (2016) Assessing the visual quality of rural highway landscape reclamation in the Western Black Sea Region of Turkey. Fresen. Environ. Bull. 25(3), 933-952.
[37] Eken, G., Bozdoğan, M., Isfendiyaroğlu, S., Kılıç, D.T. and Lise, Y. (2006) Türkiye'nin Önemli Doğa Alanlari. Ankara: Doğa Derneği.
[38] Acar, H., Eroğlu, E. and Acar, C. (2013) Landscape values of rocky habitats in urban and semi-urban context of Turkey: A study of Tokat city. Journal of Food, Agriculture & Environment. 11(2), 1200-1211.
[39] Özhancı, E. and Yılmaz, H. (2011) Rekreasyon Alanlarının Görsel Peyzaj Kalitesi Yönünden Değerlendirilmesi; Erzurum Örneği. Iğdır Üniversitesi Fen Bilimleri Enstitüsü Dergisi. 1(2), 67-76.

Received: **10.02.2017**
Accepted: **29.08.2017**

CORRESPONDING AUTHOR

Pervin Yesil
Department of Landscape Architecture,
Faculty of Agriculture,
Ordu University,
52200, Ordu – Turkey

E-mail: perviny48@gmail.com

© by PSP Volume 26 – No. 12A/2017 pages 7710-7716 Fresenius Environmental Bulletin

IN VITRO PROPAGATION OF SEA DAFFODIL (*PANCRATIUM MARITIMUM* L.) USING SEEDLING EXPLANTS

Ugur Sirin[1,*], Elif Kanmaz[2]

[1]Department of Horticulture, Faculty of Agriculture, Adnan Menderes University, Aydin, 09100, Turkey
[2]Republic of Turkey Ministry of Food, Agriculture and Livestock, Aydin, 09020, Turkey

ABSTRACT

Pancratium maritimum L. (*Amaryllidaceae*) is a native bulbous species which has a potential as an ornamental plant. It is in danger of extinction due to human activities and dense housing in coastal regions, which are its natural habitat. The aim of this research was to propagate *Pancratium maritimum* L. in tissue culture by using its seeds. In order to test the tissue culture, explants (part of (a) primary root (radicle) + hypocotyl and (b) epicotyl + cotyledon) from small seedlings of sea daffodils germinated from seeds in water + agar medium, were cultured in MS medium, which included 6.5 g/L agar, 30 g/L saccharose, and two different dosages of BAP (1.0-2.0 mg/L) and NAA (0.1-1.0 mg/L). In three different germination tests in water+agar medium, germination ratios of 58.74 %, 57.75% and 29.58 % were achieved at the end of the 21st day. However, contamination was observed in most of the seedlings which were grown from seeds germinated in the water + agar medium. Only the explants obtained from the seeds which were sown in the second germination test were transferred to MS nutrient medium. Callus formation was observed in the MS medium containing 1.0 mg/L BAP-0.1 mg/L NAA, but bulblet formation was not observed.

KEYWORDS:
Tissue culture, seed germination, bulblet formation, epicotyl, hypocotyl

INTRODUCTION

Turkey is rich in geophytes and there are about 600 species of bulbs in Anatolia [1]. *Pancratium* is a bulbous genus in the *Amaryllidaceae* family [2] and *P. maritimum* L. is one of the geophytic species which grows in Turkey. It has a perennial, tunicate bulb like a tulip, narcissus or hyacinth. The plants also have long strip-shaped greenish-bluish waxy leaves. Sea Daffodil plants grow to a height and spread of 30 cm and bear umbels of sweetly scented flowers in late summer [3], which in Turkey is from June to October. This species forms large, white, trumpet-shaped flowers like lilies on a flower stem with 3-15 flowers. Because it has showy scented flowers, this species has a potential for use as a cut flower, an outdoor plant in patios, or as a pot plant. In addition, the species contains a number of alkaloids, flavanoids and polyphenolic compounds such as pancratistatin, etanol, ungeremine and zefbetaine which are used in medical and pharmacological areas [4, 5, 6]. Also, extracts of *Pancratium maritimum* L. could be used as an insecticide and acaricide [7]. This species has a natural distribution in countries in the Mediterranean basin including Turkey, France, Spain, Italy, Greece, Lebanon and Israel, and on Cyprus and Crete [8].

Environmental factors have important implications for the germination and survival of Mediterranean plants since the climate is well characterized by its seasonality of temperature and precipitation [9]. Natural proliferation of sea daffodoils occurs by germination of seeds which are scattered around, and by the formation of bulblets. However, the seed distribution areas of sea daffoils are sand dunes, so that a lack of adequate abiotic conditions for germination and development in these areas prevents the spread of the plant. In a natural environment, the existence of sand dune vegetation is spatially and temporally influenced by environmental factors such as temperature, moisture deficiency, sand erosion, salinity and salt spray. Also, vegetation in coastal sites is destroyed by human activities, construction and tourism facilities. Man-made disturbances such as tourism and housing infrastructure and the heavy use of recreational activities may cause the destruction of habitats beyond the recovery limits of the ecosystem [10]. Also, Demir et al. [10] reported that Sea Daffodil populations are under threat because of intensive housing development and recreational usage in coastal areas. This causes a decline in the distribution of some plants such as sea daffodils which grow in dune areas, and this in turn further endangers this species by decreasing the number of plants [8]. At the same time, because this species is used for medical purposes, it is removed from its native growing habitats for its alkaloid content [1, 6]. Considering its medicinal, ornamental and ecological value, an appropriate conservation program is urgently needed to prevent further loss of these plants [11]. Because

of this and the medical importance of its secondary metabolites, plant biotechnology methods such as tissue culture, micropropagation and molecular cloning have been employed for the production of this species [12].

Because of the destruction of its natural distribution area, the population of this plant species is decreasing, growth parameters are weakening, and also a reduction in the size and number of organs such as leaves, shoots and flowers is taking place. Sea daffodil plants under stress conditions can lose their seed production capacity and bulblet formation performance. Also, because it is in the category of endangered species and because of the collection of bulbs from its native habitats, it is necessary to propagate this species from seeds. Although a germination rate of approximately 50% [13] has been obtained in the propagation of sea daffodils from seeds, it was necessary to use in vitro culture techniques instead of classical methods, because a long time is needed with production from seeds for the formation of a mature bulb and for it to reach the size for blooming. On the other hand, loss of seeds cultured in *in vivo* conditions, failure of embryo feeding because of insufficient endosperm, and technical faults in the propagation period prevented us from achieving the desired success. For these reasons, it has been stated that germinating the seeds in in vitro conditions might be more successful [14]. Furthermore, the germination rate remains low due to unsuitable abiotic conditions for seed germination in sand dune areas where the seeds of this species are naturally dispersed where, although seed germination occurred, the seedling did not form a bulblet.

When a scan was made of previous research on the propagation of *Pancratium* via tissue culture, it was realized that studies were mainly conducted using the bulb and pieces of the bulb such as scales [15, 16, 17, 18], as in many other species [19]. Therefore, the aim of the current study was to investigate the propagation and bulb formation possibilities of sea daffodils by using seeds in tissue culture techniques. Thus, this study aimed to propagate *Pancratium* by using parts of seedlings previously germinated. In order to achieve this, the research hypotheses were: 1) H_0 = It is possible to propagate bulblets by using (a) primary root (radicle)+hypocotyl and (b) epicotyl+cotyledon parts of a seedling of sea daffodil; 2) H_0 = BAP and NAA dosages in MS culture medium used in this study are suitable for bulblet formation using explants taken from seedlings obtained by seed germination. To our knowledge, there are no studies in which the explants used are directly taken from seedling parts such as primary root (radicle)+hypocotyl and epicotyl+cotyledon parts of sea daffodils.

If this method is successful, the time needed to obtain bulbs from seeds will be shortened and also the number of bulblets obtained from one seed will be increased. In addition, the results also will contribute to shortening the time for the improvement of new varieties [14].

MATERIALS AND METHODS

In this research, which was conducted from 2011 to 2013 at Adnan Menderes University, *Pancratium maritimum* L. seeds were used as plant propagation material. Naturally matured pods which had botanical seeds in them were collected from plants from a *Pancratium maritimum* L. patch growing in a wild habitat in the region of Alata (Erdemli), Mersin (in the Mediterranean region of Turkey) in October and November in 2011 and 2012. The seeds were not separated from the testa and were kept in room conditions in the black spongy protective testa which looks like a piece of coal [20] until germination.

Studies were conducted in two stages: in the first stage of the experiment, the seeds were germinated in water + agar medium; in the second stage, explants obtained from the germinated seeds were planted in enriched MS [21] culture medium with different dosages of NAA and BAP.

The first stage of the experiment was conducted as follows. For in vitro propagation of sea daffoils, seeds were first separated from the matured pods and then the coal-colored spongy seed testa was removed from the seed and the seeds were sterilized. After that, a water + agar culture was prepared for seed germination. For sterilization, the seeds were kept in 70% ethanol for 1-2 minutes, and after that they were sterilized by immersion for 20 minutes in a commercial sodium hypochlorite (NaOCl) (50%) solution which included 5% active Cl with the addition of 2-3 drops of Tween-80. Later, they were washed three times for five minutes each with sterilized deionised water [22]. Also, to prevent the development of fungi on the seeds, the fungicide Benomil (Benlate PM 50%, w/w, methyl 1-butylcarbamoyl-2-benzymidazol carbamate) was applied for 20 minutes at a 1% dosage. After sterilization, the seeds were transferred under aseptic conditions for germination in the water+agar medium, and the cultures were placed in an incubation chamber for 30 days.

The germination conditions in the incubator where the seeds were kept were 24 h darkness and a temperature of 23^{o}C until germination ended. The percentage of germinated seeds was determined every day for 21 days starting from the first germination date.

Preparation of water + agar medium. First, 8 g of agar was weighed and mixed with 1 L of sterile distilled water. The resulting solution that obtained after mixing water and agar, was sterilized at 121 °C

TABLE 1
NAA and BAP dosages in the MS culture medium used for planting explants obtained from germinated seeds

Treatment No	Dosages of NAA and BAP
1	0.1 mg.L^{-1} NAA- 1.0 mg.L^{-1} BAP
2	1.0 mg.L^{-1} NAA- 2.0 mg.L^{-1} BAP
3	0.1 mg.L^{-1} NAA- 2.0 mg.L^{-1} BAP
4	1.0 mg.L^{-1} NAA- 1.0 mg.L^{-1} BAP

TABLE 2
Germination percentages in water+agar medium and percentage of explants obtained from the seedlings

Treatment repetitions	Number of seeds cultured in water+agar	Number of germinated seeds (after 21 days)	Germination rate (%)	Infection on germinated seeds (%)	Number of explants obtained from seedlings	Percentage of explants obtained from seedlings (%)	Percentage of explants forming callus (%)
1	240	141	58.75 a	100.00	-	-	-
2	240	138	57.50 b	92.75	10	7.25	10
3	240	71	29.58 c	100.00	-	-	-
LSD%5			0.627**				



(a) **(b)**

FIGURE 1
(a) General view of *Pancratium maritimum* L. seeds in water +agar medium
(b) Germinated seeds in water+agar medium

for 40 min in an autoclave, and after sterilization, the mixture was poured into jars and allowed to dry.

In the second stage. The seedlings derived from the water + agar medium seed germination culture were separated into two parts: (a) primary root (radicle) + hypocotyl and (b) epicotyl + cotyledon. These two explant types were cultured for bulblet formation in aseptic conditions in MS [21] medium supplemented with 6.5 g.L^{-1} agar, 30 g. L^{-1} saccharose and various alternative concentrations of naphthaleneacetic acid (NAA) and 6-benzylaminopurine (BAP) [16, 23]. The MS medium used for explant planting contained two different dosages of NAA and BAP as shown in Table 1. The pH of the MS culture medium was optimized to 5.7. The MS culture medium was sterilized in an autoclave at 121 °C for 20 minutes [17], and afterwards the MS medium was decanted into sterile cups in sterilized cabins. Finally, the explants were cultured in this medium.

Both in the seed germination period and in the explant culture period, the cultures were kept at 23 ± 1 °C in a climate-controlled room. The seeds were cultured in water + agar medium and were maintained in dark conditions until germination ended, and the explants obtained by dividing the seedlings grown from the germinated seeds were maintained in 16/8 h light / dark photoperiod (3000 lux) conditions. During the study, the germination rate of the seeds sown in the prepared media (water + agar) was determined.

Experimental design and data analysis. At first stage of the experiment, a completely randomized experimental design was used and the germination experiment was conducted at three different

times with four replicates. In each repetition of germination tests twenty four jars were used and in each replication six jars were used that contains ten seeds in each jar. In a replication 60 seeds, totally 240 seeds were used in each germination tests. At the second stage; the research was conducted with three replicates using randomized plots in the factorial designs, and in each replicate two jar (one of the jar contains explants type of primary root (radicle)+hypocotyl and the second jar contains explants type of epicotyl+cotyledon) were used. In Arcsine transformation was performed for experimental data taken in percentages before statistical analysis. An analysis of variance (ANOVA) and LSD comparison of means test ($p \leq 0.05$) were performed.

RESULTS AND DISCUSSION

In this research, an attempt was made to develop a method for bulblet formation in tissue culture by using explants taken from seedlings obtained from germination of natural mature seeds of *Pancratium maritimum* L.

The results of the experiment showed that the germination rate of the seeds cultured in aseptic conditions (water + agar medium) was increased when healthy and mature seeds were used. However, the germination rates varied depending on the seed collection period. Germination tests were replicated three times and the highest germination rate was obtained in the first germination test while the lowest rate was found in the third test (Table 2, Figure 1).

In the first germination experiment, 141 seeds of 240 seeds planted in water+agar were germinated and a 58.75 % germination rate was obtained at the end of 21 days in tissue culture medium consisting of only water+agar (Figure 1), but because of the effect of certain phenolic components in the seeds, some contamination (blackout points) occurred on the seedlings before the explants were obtained. In a very short period the seedlings lost their vitality and the medium lost its usage properties. Therefore, the germinaton test was repeated and at the end of the second germination test 138 seeds of 240 seeds cultured in medium were germinated (57.50% germination rate). In order to increase the reliability of the results, the germination was repeated for a third time in the water + agar medium, and as a result a germination rate of 29.58% was obtained (Table 2). This percentage of germination is satisfactory as it is proportional to the percentage established by Nikopoulos and Alexopoulos [24]. However, higher germination rates (70-90%) were obtained in 70 days [24], but in the present study the seeds were germinated in the water + agar medium for only 21 days. The germination rates obtained at the end of this period are given in Table 2. No plant growth regulator was added to the water + agar medium used in the seed germination experiments. Similarly, Nikopoulos and Alexopoulos [24] advised that GA_3 should definitely not be added to the culture medium during seed germination. When the germination rates in the work of these researchers were analyzed, it was found that the germination rate was approximately 15-25 % in a 30 day period and that germination of the seeds was low at the beginning in relation to the increasing dosages of GA_3 in the culture medium.

At the end of the second seed germination experiment, two different explant types were obtained from the 7.25% of the seedlings which had grown from germinated seeds by dividing the seedlings into (a) primary root (radicle) + hypocotyl and (b) epicotyl + cotyledon. These explants were cultured in MS medium prepared by adding different doses of NAA and BAP (Figure 2). The desired development was not achieved in the explants planted in the culture medium and no bulblet formation took place. As seen in Figure 3, callus formation occured only on one primary root (radicle) + hypocotyl type explant in the MS medium which contained 1.0 $mg.L^{-1}$ BAP-0.1 mg. L^{-1} NAA. Likewise, as reported by Nikopoulos and Alexopoulos [24] low NAA concentration (0.1 $mg.L^{-1}$) also had a positive effect on bulblet development. In our research, no callus or bulblet formation was obtained in the culture medium which contained 1.0 $mg.L^{-1}$ NAA. This indicated that callus formations on explants occurred because of the effect of BAP rather than the NAA used in the culture medium. Thus, it was determined that the highest callus development on *Camelina sativa* L. explants occurred on root explants and in MS medium with 1.0 mg. L^{-1} BAP+ 1.0 mg. L^{-1} NAA added [25]. And it was reported that the best response of bulblet regeneration in both *F. imperialis* and *F. persica* was obtained from 1 mg/L BAP + 0.4 mg/L NAA+4 mg/L IAA (by Mohammadi-Dehcheshmeh et al. [23]). In our study also, callus development occurred on primary root (radicle) + hypocotyl type explants. In another study which included BAP in the culture medium, Nasırcılar et al. [19] obtained the highest bulblet formation rate on *Muscari* sp. in an MS medium that contained 4 $mg.L^{-1}$ BAP and 0.25 $mg.L^{-1}$ NAA. On the other hand, considering Nasırcılar et al.'s [19] study, the use of high BAP concentrations in the MS medium may increase bulblet formation. It is reported that the type, concentration and combination of plant growth regulators added to the culture medium affect the regeneration capacity of explants [26, 27, 28], and also that genotype may affect bulblet formation as mentioned by Marinangeli and Curvetto [29] in *Lilium* sp. propagation. For example, traumatic acid increased the number of bulblets per scale of *Lilium* in *in vivo* culture [29].

The most important problem in this experiment was the contamination that occured during seed germination and explant culture. As reported by Gümüş and Ellialtıoğlu [17] and Gümüş [35], the contamination rate was not succeeded to decrease below 40% in in vitro culture of this species. In order to

solve this problem, Nikopoulos and Alexopoulos [24] suggested the use of mycostatics, antibiotics or immersion of the bulbs in hot water for 1-3 hours before sterilization with sodium hypochlorite solution. In the study, even though all sterilization procedures were followed before culturing in medium, a high rate of contamination occurred on the explants, and in all cultures on all explants except one, contaminations occured and explants lost their vitality. However, Nikopoulos and Alexopoulos [24] stated that the sterilization process was easier and more effective using ripe seeds of *P. maritimum* obtained from closed pods rather than those collected from the ground and from opened pods. Likewise, difficulties were encountered in the sterilization process with other explant types such as twin scales in the production of tissue culture of this species, and these could not be effectively sterilized [30].

In conclusion, no bulblet formation occurred on any explants in this research, including the explant which formed a callus. Unlike Dragassaki et al. [15] who succeeded in bulblet formation by using scale explants in MS medium, bulblet formation did not occur in this research, which used a different explant type. Despite success in bulblet formation depending on the type of explants in work on numerous species such as *Muscari* sp. [19], *Galanthus elwesii* [31] and *Pancratium biflorum* Roxb. [32], in this study no bulblet formation took place because of the character of the explants used. For example, in MS medium with 4.0 mg/l BAP +1.0 mg/l NAA, *P. biflorum* Roxb. scale explants produced adventitious bulblets and also leaf segments produced a large number of adventitious bulblets on B5 medium supplemented with 1.0 mg/l NAA + 0.2 mg/l BAP [32]. At the same time, Genova et al. [33] reported that bulblets were regenerated directly from bulb scales as well as from leaves. In our study, callus development occurred on primary root (radicle) + hypocotyl type explants. Because the explants used in this study were different from bulb scales, bulb formation was not achieved, and only a callus was formed. On the other hand, achieving callus formation in the explants which were grown shows that bulblets can form if the length of time in MS medium is extended. Thus, Nesi et al. [34] obtained bulblets from bulb scales cultured in BA supplemented MS medium after 60 days of culture and obtained 4-6 bulblets per bulb after 6 months later.

Even though a 29.58 % germination rate was obtained in the third repetition of seed germination tests in in vitro culture, in this last repetition of germination tests all of the cultures were soon lost because of infection. Because of the infection problems which occurred during the trial, new procedures for sterilization must be developed in future studies on *P. maritimum* L. In addition, it was thought that the infection was not only related to the seed surface but may also have come from the seed structure. Gümüş and Ellialtıoğlu [17], who tried to propagate Sea Daffodils in in vitro conditions, mentioned that the main problem was infection when underground parts of the plants were used as explants, as in this study.

CONCLUSIONS

Pancratium maritimum L. is a native bulbous plant species which has a usage potential as a potted plant, a seasonal outdoor plant or as a cut flower. At the same time, some components of the bulbs that are used in the fields of pharmaceuticals and medicine increase the usefulness and importance of this species. The species can be propagated by using seeds under properly controlled conditions for germination. However, with the plants obtained in this manner, it takes a long time for them to grow and for the bulb to reach a sufficient size for flowering.



FIGURE 2
Explants cultured in MS mediums which included different NAA and BAP dosages

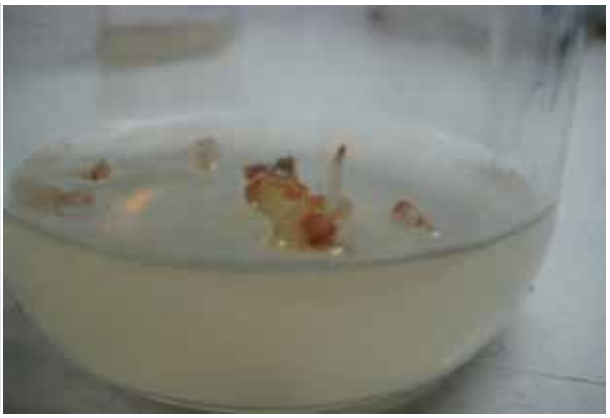


FIGURE 3
Callus formation on explant in MS medium containing 1.0 mg.L^{-1} BAP - 0.1 mg.L^{-1} NAA

Therefore, production of this species by biotechnological methods is gaining importance. Parts obtained from the developed bulb such as bulb scales have been used as explants in production by these techniques in in vitro conditions. Our results showed that the most important problem with in vitro production was the infections which developed on explants obtained from bulbs. On the other hand, it was observed that the potential for new bulblet formation from bulb scales was low. In this study explants obtained from plantlets grown from germinating seeds were used because it was thought that the infection rate might be low and their ability to regenerate might be high.

However, contamination was still an important problem both on the seeds germinated on water+agar medium and on the explants taken from the seedlings. At the end of research, the highest germination rate obtained was 58.75 %; explants were obtained from only 10 seedlings and callus formation occurred on only one of the explants. It is thought that extending the duration of seed germination, the development of new sterilization techniques against infection, and keeping the explants with calluses grown in MS culture medium for longer in the culture will enable the formation of bulblets.

ACKNOWLEDGEMENTS

This study was supported by the Adnan Menderes University Scientific Research Fund.

The authors have declared no confict of interest.

REFERENCES

[1] Arslan, N., Gürbüz, B., Sarıhan, E.O., İpek, A., Özcan, S., Parmaksız, İ., Mirici, S. and Gümüşçü, A. (2002) A study on cultivation of *Sterbergia fisheriana* (Herbert) rupr. Prooceedings of II. National Ornamental Plants Congress, Antalya, 78-84.

[2] Blamey, M. and Grey-Wilson, C. (1993) Mediterranean Wild Flowers. Haper Collins, Great Britain.

[3] Könemann (2004) Botanica: The Illustrated A-Z of Over 10000 Garden Plants and How to Cultivated Them. M. Ed.: Susan Page, Margaret Olds, Pub.: Gordon Cheers, ISBN: 3-8331-1253-0 633p.

[4] Pettit, G.R., Pettit III, G.R., Groszek, G., Backhaus, R.A., Doubek, D.L., Barr, R.J. and Meerow, A.W. (1995) Antineoplastic agents. An investigation of the *Amaryllidaceae* genus *Hymenocallis*. Journal of Natural Products. 58(5), 756-759.

[5] Youssef, D.T.A., Ramadan, M.A. and Khalifa, A.A. (1998) Acetophenones, a chalcone, a chromone and flavonoids from *Pancratium maritimum*. Phytochemistry. 49(8), 2579-2583.

[6] Berkov, S., Evstatieva, L. and Popov, S. (2004) Alkaloids in Bulgarian *Pancratium maritimum* L. Zeitschrift fur Naturforschung C-A J, Biosciences. 59, 65-69.

[7] Abbassy, M.A., El Gougary, O.A., El Hamady, S. and Sholo, M.A. (1998) Insecticidal, acaricidal and synergistic effects of soosan, *Pancratium maritimum* extracts and constituents. Journal of the Egyptian Society of Parasitology. 28(1), 197-205.

[8] Zahreddine, H., Clubbe, C., Baalbaki, R., Ghalayini, A.and Talhouk, S. N. (2004) Status of native species in threatened Mediterranean habitats: The case of *Pancratium maritimum* L. (Sea Daffodil) in Lebanon. Biological Conservation. 120, 11-18.

[9] Thompson, J.D. (2005) Plant evolution in the Mediterranean. Oxford University Press, Oxford.

[10] Demir, Z., Müderrisoğlu, H., Aksoy, N., Aydin, Ş.Ö., Uzun, S. and Özkara, H. (2010) Effects of second housing and recreational use on *Pancratium maritimum* L. population in western Black Sea region of Turkey. Journal of Food, Agriculture & Environment. 8(2), 890-894.

[11] Di Maio, A. and De Castro, O. (2013) Development and characterization of 21 microsatellite markers for *Pancratium maritimum* L. (*Amaryllidaceae*). Conservation Genetics Resources. 5, 911–914.

[12] Orhan, I., Koca, U. and Şener, B. (2008) Advances in Biotechnological Applications of Various Amaryllidaceae Plants. Floriculture, Ornamental and Plant Biotechnology Advances and Topical Issues, Global Science Books, Vol: V, 548-554.

[13] Ayanoğlu, F., Sarıhan, E.O., and Kaya, D.A. (1999) Determination of germination ability of Sea Daffodil (*Pancratium maritimum* L.) seeds, and the effect of different substrates on emergence. The proceedings of 3rd Fieldcrop Congress of Turkey, Adana, Vol II, 397-400.

[14] Pierik, R.L.M. (1987) In vitro Culture of Higher Plants. Martinus Nijhoff Publishers, Netherlands, 344p.

[15] Dragassaki, M., Economou, A.S. and Vlahos, J.C. (2003) Bulblet formation and in vitro survival extra vitrum in *Pancratium maritimum* L. Acta Horticulture. 616, 347-352.

[16] Stanilova, M., Bogdanova, Y., Berkov, S., Bosseva, Y. and Gussev, C. (2004) In vitro clonal propagation of *Leucojum aestivum* L. 3rd Conference on Medicinal and Aromatic Plants of Southeast European Countries, Book of Abstracts, Slovak Republic, p. 45.

[17] Gümüş, C. and Ellialtıoğlu, Ş. (2006) Possibilities of in vitro propagation of Sea Daffodil (*Pancratium maritimum*). Proceedings of III. National Ornamental Plants Congress, İzmir, 454-460.
[18] Georgiev V., Ivanov, I. and Pavlov, A. (2010) Obtaining and Selection of *Pancratium maritimum* L. In Vitro Cultures with Acetylcholinesterase Inhibitory Action. Biotechnology & Biotechnological Equipment. 24(sup1), 149-154,
[19] Nasırcılar, A.G., Mirici, S., Karagüzel, Ö., Eren, Ö. and Baktır, İ. (2011) In vitro propagation of endemic and endangered *Muscari mirum* from different explant types. Turkish Journal of Botany. 35(1), 37-43.
[20] Werker, E. and Fahn, A. (1975) Seed anatomy of *Pancratium* species from three different habitats. Botanical Gazetta. 136(4), 396-403.
[21] Murashige, T. and Skoog, F. (1962) A revised medium for rapid growth and bio-assays with tobacco tissue cultures. Physiol. Plant. 15, 473-497.
[22] Panayotova, L.G., Ivanova, T.A., Bogdanova, Y.Y., Gussev, C.V., Stanilova, M.I., Bosseva, Y. Zh., Stoeva, T.D. (2008) In vitro cultivation of plant species from sandy dunes along the Bulgarian Black Sea Coast. Phytologia Balcanica. 14 (1), 119 –123.
[23] Mohammadi-Dehcheshmeh, M., Khalighi, A., Ebrahimie, E., Sardari, M. and Naderi, R. (2006) Direct bulblet regeneration from mature embryo: A rapid, efficient and genotype-independent in vitro morphogenesis pathway for preservation of endangered wild populations of *Fritillaria imperialis* and *Fritillaria persica*. HortScience. 41(4), 1066-1066.
[24] Nikopoulos, D. and Alexopoulos, A.A. (2008) In vitro propagation of an endangered medicinal plant: *Pancratium maritimum* L. Journal of Food, agriculture & Environment. 6(2), 393-398.
[25] Göre, M. and Kurt, O. (2015) Research to establish effects of explant sources and plant growth regulators on camelina (*Camelina sativa* L. Crantz) tiller and plant induction. Anadolu Journal of Agr. Sci. 30, 268-274. ISSN: 1308-8750 (Print) 1308-8769 (Online).
[26] Molnár, Z. and Ördög, V. (2005) Microalgal and cyanobacterial extracts in the tissue cultures of higher plants (pea, tobacco, beet). Proceedings of the 8th Hungarian Congress on Plant Physiology and the 6th Hungarian Conference on Photosynthesis, Acta Biologica Szegediensis, 49(1-2), 39-40.
[27] D'Onofrio, C. and Morini, S. (2006) Somatic embryo, adventitious root and shoot regeneration in in-vitro grown quince leaves as influenced by treatments of different length with growth regulators. Scientia Horticulturae. 107, 194-199.
[28] Yemets, A.I., Yu, N.B., Shysha, E.N., Rakhmetov, D.B. and Blume, Y.B. (2013). Establishment of in Vitro Culture, Plant Regeneration, and Genetic Transformation of *Camelina sativa*. Cytology and Genetics. 47(3), 138-144.
[29] Marinangeli, P. and Curvetto, N. (1997) Bulb quality and traumatic acid influence bulblet formation from scaling in Lilium species and hybrids. HortScience. 32(4), 739-741.
[30] Slabbert, M.M., De Bruyn, M.H., Ferreira, D.I. and Pretorius, J. (1993) Regeneration of bulblets from twin scales of *Crinum macowanii* in vitro. Plant Cell Tissue and Organ Culture. 33(2), 133-141.
[31] Staikidou, I., Selby, C. and Hanks, G.R. (2006) Development of a medium for in vitro culture of *Galanthus* species based on the mineral composition of bulbs. The Journal of Horticultural Science and Biotechnology. 81(3), 537-545,
[32] Begum, S. and Hadiuzzaman, S. (1993) *In vitro* multiple shoot regeneration from bulb scale and leaf segments of *Pancratium biflorum* Roxb [in Bangladesh]. Plant Tissue Culture, Bangladesh. 3(1), 41-45.
[33] Genova, E., Bogdanova, J., Berkov, S. and Stanilova, M. (2004) In vitro micropropagation and acclimatization of *Leucojum aestivum* L. (Summer Snowflake) in Bulgaria. 3rd Conference on Medicinal and Aromatic Plants of Southeast European Countries, Book of abstracts. Slovak Republic, p.63.
[34] Nesi, B., Trinchello, D., Lazzereschi, S., Ruffoni, B. and Grassotti, A. (2009) Micropropagation of *Pancratium maritimum* from twin- and tri-scales. Società Ortoflorofrutticoltura Italiana, 136-138.
[35] Gümüş, C. (2015) A review of researches on Sea Daffodil (*Pancratium maritimum* L.) plant. Derim. 32(1), 89-105,

Received: **15.02.2017**
Accepted: **31.08.2017**

CORRESPONDING AUTHOR

Ugur Sirin
Adnan Menderes University,Faculty of Agriculture
Department of Horticulture,
09100 Aydin – Turkey

E-mail: usirin@adu.edu.tr

© by PSP Volume 26 – No. 12A/2017 pages 7717-7723 Fresenius Environmental Bulletin

EVALUATION OF DROPLET SIZE SPECTRA FOR AGRICULTURAL PESTICIDE APPLICATIONS USING WATER SENSITIVE PAPER AND IMAGE ANALYSIS TECHNIQUES

Abdullah Beyaz[1,*], Metin Dagtekin[2], Ibrahim Cilingir[1], Dilara Gerdan[1]

[1]Ankara University, Faculty of Agriculture, Department of Agricultural Machinery and Technologies Engineering, 06130 Aydinlikevler Ankara, Turkey
[2]Cukurova University, Ceyhan Technical College, Department of Agricultural Machinery, Ceyhan Adana, Turkey

ABSTRACT

This study aims to evaluate the average droplet size and range of droplet size, which affects agricultural pesticide quality using image analysis techniques.

In the study droplet diameters was measured by using 26 x 76 mm water sensitive paper produced by Ciba-Geigy with a little sprayer. A Nikon D300s camera body and a 105-mm macro lens were used for capturing images. Image J software was used for image evaluations, and Microsoft Excel software was used for evaluation of numerical data.

At the end of the study, number median diameter (NMD) was calculated as 75 µm, diameter surface (ds) was calculated as 31 µm, volume median diameter (VMD) was calculated as 300 µm, Sauter diameter (dv/s) was calculated as 37 µm, and VMD/NMD was found 4.00 from evaluations.

KEYWORDS:
Image processing, Image J, Droplet size, Water-sensitive card

INTRODUCTION

The primary objective of agricultural pesticide applications is to protect a variety of agricultural products from the diseases, reduce crop losses, and at the end, obtaining high-quality products. There are a lot of agricultural application types in the world such as physicomechanical applications, plant breeding, genetic applications, biological control, and cultural control. However, in Turkey, chemical control method is using as a common method. Chemical control is based on liquid chemicals and sprayers which deliver the liquid to the target surface.

Transmitting droplets to the target surface by carrying them with water or oil solutions is called the spraying treatment (spraying). The equipment used in plant protection with this method during these operations is called a sprayer.

As chemical applications, liquid applications are the most common. Liquid spraying is carried out with various types of the sprayer with different characteristics. Spraying the fluid is usually performed with a pump and a nozzle to use the pressure's energy for converting the fluid into droplets. Sprayer success depends on the selection of the appropriate type of purpose and accuracy of calibration. Spraying quality can be demonstrated by determining the drop diameter and drop distribution value. Droplet size uniformity is one of the most important parameters that determine the suitability of spraying for the purpose, while other characteristics may be listed as the average diameter and size ranges of droplets collected on the target surface, droplet frequency and coverage rate of the droplets.

Moreover, researchers who work on spraying technologies, sprayer sellers, growers and companies that produce pesticides want to compare spraying equipment and application parameters [6]. Therefore, determining the characteristics and evaluation of droplet distribution is very important.

In these kinds of studies, a micrometer microscope-based method generally use for conduct analyses in measurements, and they are more reliable. However, this measurement technique is complicated, and the measurement process takes too much time. It can be completed in a relatively short time if analysts use a computer with an image analysis program. By this way the characteristic values can be obtained on the entire surface of the water-sensitive paper. This provides a significant advantage over other measurement methods of droplet analysis. Therefore, particularly in recent years, the image analysis software has become widespread for droplet evaluations.

In this study; average droplet size, droplet size distribution and range of droplet sizes were evaluated using image analysis techniques. The results were analyzed statistically.



FIGURE 1
Water sensitive card



FIGURE 2
Small sprayer pump

MATERIALS AND METHODS

Material. The research took place in laboratory conditions. To collect droplets and analyze droplet sizes, 26 x 76 mm water sensitive cards used in the study which was produced by Ciba-Geigy. The role of these cards is to make spots where droplets fall visible. The diameter of droplets smaller than 10 microns can be measured with these cards (Fig. 1).

A small sprayer pump was used for carrying out the spraying in this study (Fig. 2). As a test liquid, water was used instead of pesticide in the laboratory for making the experiments easier.

Image analyses process covers topics of converting an image to a digital image and processing this image on a computer to make it easier to understand. The computer is required to analyze the image for image interpretation. The goal of image enhancement techniques is to convert the image into a suitable format for a more particular purpose than the original image.

'Image J' software for image processing system consists of the operations after getting image from a camera to perform all operations up to statistical analysis [1]. 'Image J' software was used for the image analysis, while 'Microsoft Excel' was used the numerical value analysis (Fig. 3). In the study, for capturing images, a Nikon D300s camera body was used which has a 12-megapixel CMOS sensor, was more reliable and precision for droplet diameter measurements on the water-sensitive cards with using a 105-mm macro lens (Fig. 4).

Method. For the measurement of droplet size, a small sprayer was used to spray the fluid onto the water-sensitive cards. During the trial, the spraying process was carried out from 15-cm high in normal walking speed. After spraying, the water-sensitive

cards were photographed with a professional Nikon D300s camera using a 105-mm macro lens. The images were captured in a JPEG file format. These photographs then analyzed with the help of the 'ImageJ' image processing software, and the droplet sizes were determined.

While the images were analyzed by the 'ImageJ' image processing software, the images of the water sensitive cards were opened using the open command in the ImageJ software, and then the image was converted to 8-bit – grayscale image by using the process menu, threshold sub-menu. 8-bit - gray color selection, followed by particle analysis. Perimeter and clear results were selected from the settings menu to obtain the desired particle analysis data (Fig. 5). Then, perimeter values converted to the diameter values.

Based on the periphery of the droplets that were measured, they were corrected with spreading factor coefficients, so the droplet diameter values which were measured from water-sensitive cards were converted into actual diameter values. Then the Excel data table was converted to plots (Table 1)

Diameter measurements showed a broad distribution range of drop diameters, depending on spraying. Diameter values and a wide distribution range of drop clusters are used for the evaluation of the quality of spraying [8]. The most characteristic droplet diameters used for assessing the quality of pulverization are; Volumetric Median Diameter (VMD), Number Median Diameter (NMD), Arithmetic Median Diameter (da), (ds), Diameter volume (dv), Sauter diameter (dv/s).



FIGURE 3
Nikon D300s camera body and 105-mm macro lens

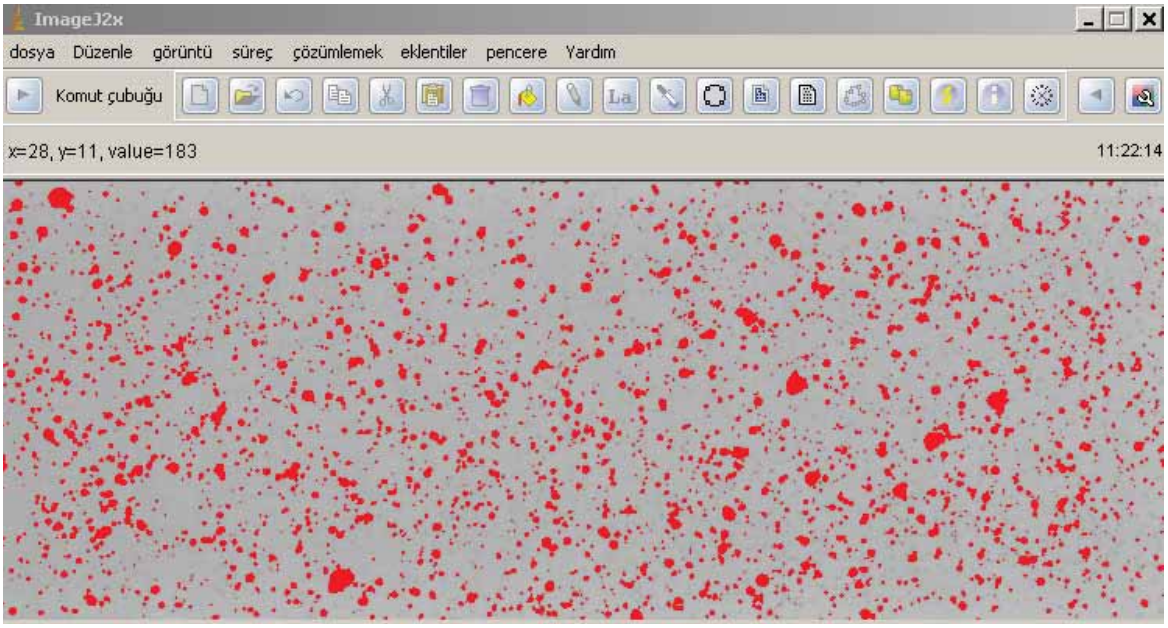


FIGURE 4
Image software interface

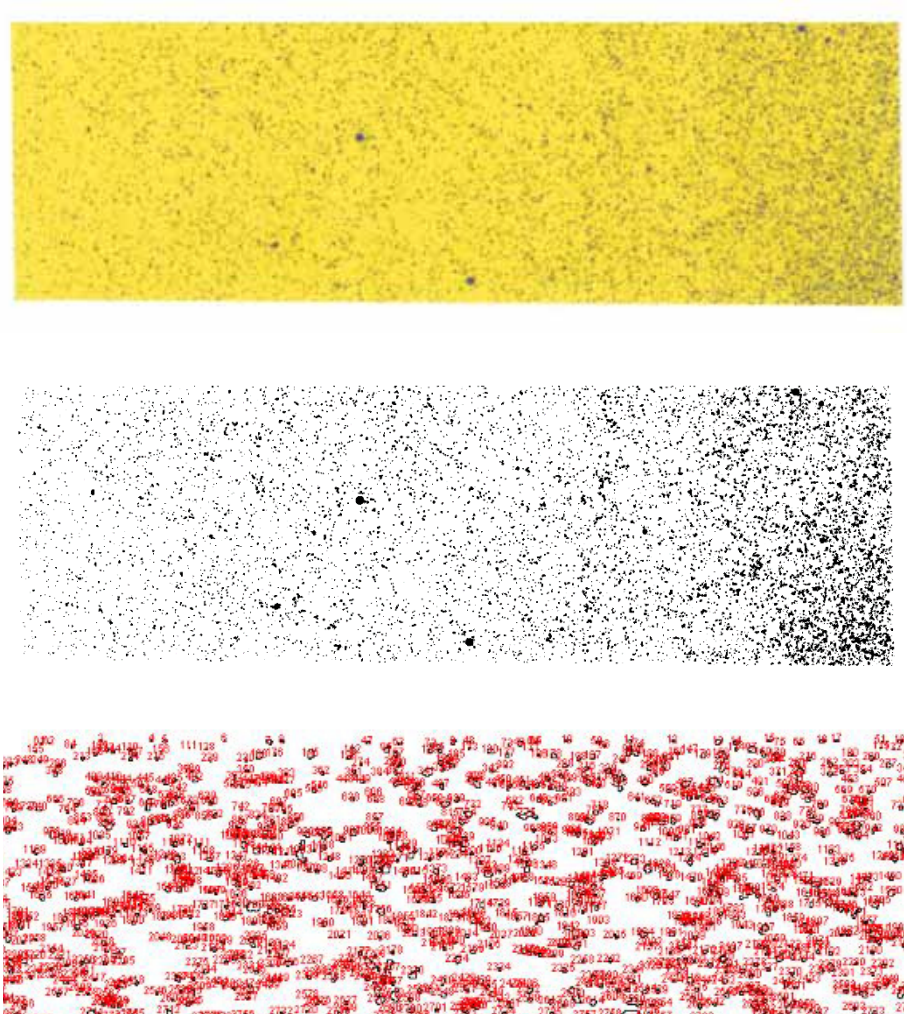


FIGURE 5
Image processing steps

TABLE 1
Spreading Factor

Droplet diameter (µm)	Spreading factor	Real droplet diameter (µm)
100	1.7	59
200	1.8	109
300	1.9	155
400	2.0	200
500	2.1	243
600	2.1	285

TABLE 2
Classifications of spraying based on the characteristic of drop diameter [5]

VMD (um)	Spraying term
10-30	Fog
31-50	Aerosol
51-100	Very small spraying
101-200	Small sprays
201-400	Medium size spraying
>400	Large size spraying

- Diameter surface (ds), which is the average diameter, the surface that could dampen was calculated from the $((\sum n_i * d_i^2 / n)^{1/2})$ formula,
- Sauter diameter (dv/s), which gives information about the surface coverage rate, was calculated from the $(\sum ni * d_i^3 / \sum ni * d_i^2)$ formula,
- The range of droplet size (VMD/NMD) also expresses the diameter closeness values among droplet diameters.

In the formulas; 'n' is the express droplet number and 'd' express droplet diameter.

Volume Median Diameter (VMD) separates the total volume values of the sprayed droplets into two equal parts. The volume formed by the smaller drops equal the volume formed by the larger diameter drops based on the VMD value. Briefly, this is the diameter value with 50% of the spray volume. This diameter value is expressed in different symbols like Dv0.5, D0.5 or V (0.5) [7]. Spraying commonly refers to the value of the average diameter, and it is named according to these diameter values (Table 2).

To ensure biological effectiveness, the target surface must have the appropriate number of droplets and droplet diameter. For each spraying application type, there are appropriate numbers of droplets and droplet diameters (Table 3).

Number median diameter (NMD) expresses the droplet diameter, which is equal to the limit value of the numbers of smaller and larger diameters.

The range of droplet size is important as well. Two different way may be used in the calculation of the coefficient for the range of droplet size. This value indicates significant changes based on the type of nozzle used. The range of droplet size coefficient of homogeneity (CH) was calculated to obtain the relevant data.

The obtained CH value showed that the spraying droplet diameters were getting closer. This value was higher than '1' and the values converging to '1' showed that the droplet diameters were becoming uniform. Drop formation affects the physical properties of the spray liquid, sprayer nozzle type and size, operating pressure, and factors like spraying pattern. A liquid pesticide resistance of flow varies based on its content. Another important factor that affects the size of droplets is working pressure. When we fix nozzle type and size the pressure increase and droplet sizes become smaller [3]. Homogeneity coefficient or drop range of droplet size changes according to the type of nozzle (Table 4).

TABLE 3
Optimum droplet size based on targets of spraying [5]

Target surfaces and type of spraying	Droplet diameter (VMD, µm)
Flying insects (insecticides)	10-50
Insects on the leaves (insecticide)	30-50
Leaf sprays (fungicide)	40-100
Ground spraying (herbicide)	250-500

TABLE 4
CH value according to the nozzle type

Nozzle type	CH
Range impingement jet nozzles	5... 10
Range jet slotted nozzles	2...7
Cone-beam nozzles	2...4
Rotary disc nozzles	1.20...1.60
Electrodynamic nozzles	1.08...1.30

TABLE 5
Number of droplets, and calculation of diameter range and other characteristics

Droplet number (n)	Diameter Range (µm)	Average range of group (µm)	ni.di (mm)	ni.di^2 (mm^2)	ni.di^3 (mm^3)	Number addition %	ni.Vi (mm^3)	Volume Addition (%)
1090	0-30	0.015	16.35	0.25	0.00	14.43	0.00	0.00
1429	30-50	0.01	14.29	0.14	0.00	33.35	0.00	0.34
3586	50-100	0.025	89.65	2.24	0.06	80.83	0.00	1.57
1271	100-200	0.05	63.55	3.18	0.16	97.66	0.00	11.42
163	200-400	0.1	16.3	1.63	0.16	99.81	0.00	90.16
14	400-500	0.05	0.7	0.04	0.00	100.00	0.00	100.00
7553			200.84	7.47	0.38	100.00	0.00	100.00

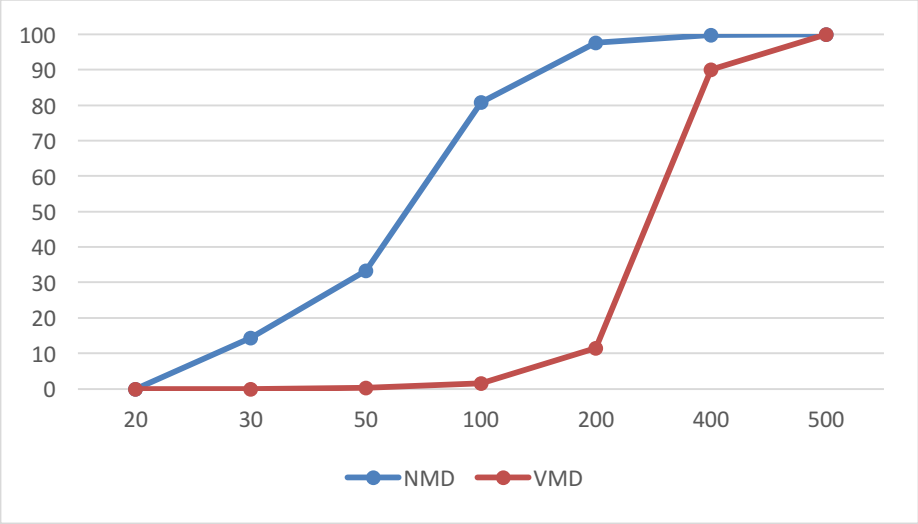


FIGURE 6
Graph of VMD and NMD

RESULTS AND DISCUSSION

For (VMD) and (NMD) evaluations, the droplet diameters were grouped within the 0-50 µm diameter range. The droplet numbers were evaluated in each group and exaluated in Excel tables (Fig. 4). After the diameter evaluations, VMD and NMD plots were drawn using the Excel software (Fig. 6).

The number of droplets was calculated in each group using the data in Table 5 and the results were as the following;

- Number median diameter (NMD) was calculated as 75 µm.
- Diameter surface (ds) was calculated as 31 µm
- Volume median diameter (VMD) was calculated as 300 µm.
- Sauter diameter (dv/s) was calculated as 37 µm.
- In the plot, the red line represents the VMD values, and the blue line represents the NMD values. Midlines on the plot can give us VMD and NMD values. According to these lines, the VMD value was calculated as 300 µm and the NMD value was calculated as 75 µm.
- The range of droplet size coefficient of homogeneity (CH = VMD/NMD) was calculated as 4.00.

Different researchers are studying different issues about spraying and quality improvements in spraying machines.

The main characteristics of spraying quality are;

- Spraying norm and dose (Calibration is very important for norm (Lt/ha) and dose (ml/ha).)
- Spraying coverage (It also means chemical coverage (ml/cm^2).)
- Droplet size spectra (µm)
- Range of droplet size (CH)
- Droplet density (number/cm^2)
- Droplet coverage (It also means that liquid coverage (%).)
- Drift

For this reason, a lot of studies have been conducted to observe different aspects of spraying applications. For example, Mangadoa et al. [4] studied measurement of pesticide treatment by image analysis. They used water-sensitive cards for determining spraying coverage and provided results of coverage for spraying regarding insignificant, under-dosing, ideal, excessive, overdosing spraying applications. In difference to Mangadoa, in this study, we provided different droplet size spectra such as Number median diameter (NMD), Volume median diameter (VMD), Diameter surface (ds) and Sauter diameter (dv/s) [4]. These droplet size spectra present the relationship between target surfaces and spraying types as seen in Table 3. Moreover, droplet coverage values are given in the results section of the study as seen in Fig. 6. Additionally, the CH factor was evaluated as 4.00 for determination of the appropriate nozzle type as seen in Table 4.

De Moor et al. worked on image analysis of water-sensitive paper as a tool for evaluation of spray distribution for orchard sprayers [2]. They determined a spraying machine's working quality for different distances and angles. They revealed relationships of velocity, distance, and angle as results for determining the spraying machine's working quality by using water-sensitive cards. Unlike De Moor, in this study, we used water sensitive cards for determining spraying characteristics using image analysis techniques as a reverse application for CH and droplet size spectra [2]. The CH and Droplet size spectra values that we obtained gave us a chance of determining the appropriate nozzle type and target

surfaces, as well as spraying type relationships as it is seen in Tables 3 – 4.

According to the study results, the small sprayer pump showed the characteristics of range impingement jet nozzles. We understand this from the 4.00 range of droplet size coefficient of homogeneity. This type of sprayer is used for herbicide applications, as well as for prevention from aerial effects.

According to the results, we may state that;

- Usage of an image processing technique is quick, easy and effective.
- Usage of an image processing technique is low-cost and directly usable.
- Effective digital data are obtained, and storage may provide an easy way to compare rates for other studies based the droplet analysis.
- The measurements of droplets that do not have a specific shape may be easily carried out by image processing techniques.
- When we compare the method to other methods like Microscopy, the process may be carried out easier in comparison to others.
- Considering the resolution of the images and the camera used in this study, one may obtain better results using the higher-quality equipment.

REFERENCES

[1] Cebeci, Z., Cengizler, I. and Gökçe, M.A. (1992) The possibilities of using digital image processing systems in water products engineering. Agricultural Engineering Week, Water Products Engineering Session. 25-29 May 1992, Eğirdir, Isparta, Turkey.

[2] De Moor, A., Langenakens, J. and Vereecke, E. (2000) Image analysis of water sensitive paper as a tool for the evaluation of spray distribution of orchard sprayers. Aspects of Applied Biology. 57, 2000.

[3] Dursun, E. and Çilingir, I. (1991) Sprayer characteristics and the factors affecting it. Ankara University, Faculty of Agricultural Publications: 1206, Associations: 49, Ankara, 34p.

[4] Mangadoa, J., Arazuria, S., Arnala, P., Jaréna, C. and Lópeza, A. (2013) Measuring the accuracy of a pesticide treatment by an image analyzer. Procedia Technology. 8, 498 – 502

[5] Matthews, G.A. (1992) Pesticide Application Methods. 2nd Edition, Longman, New York, 405p.

[6] Salyani, M. and Fox, R.D. (1999) Evaluation of spray quality by oil and water-sensitive paper. Transactions of the ASAE. 42(1), 37-43.

[7] Wolf, R.E., Gardisser, D.R. and Willams, W.L. (1999) Spray droplet analysis of air induction nozzle using WRK DropletScan technology. ASAE Paper No:991026, St. Joseph, Michigan, USA.

[8] Zeren, Y. and Bayat, A. (1999) Agricultural Struggle Mechanism. Çukurova University, Faculty of Agriculture, No: 233, Course Books Publication No: A-75, Adana.

Received: **22.02.2017**
Accepted: **24.09.2017**

CORRESPONDING AUTHOR

Abdullah Beyaz
Ankara University
Faculty of Agriculture
Department of Agricultural Machinery
and Technologies Engineering
Ankara –Turkey

E-mail: abeyaz@ankara.edu.tr

© by PSP Volume 26 – No. 12A/2017 pages 7724-7733 Fresenius Environmental Bulletin

FE-BASED IONIC LIQUIDS SYNTHESIZED BY ULTRASONIC HEATING CIRCUMFLUENCE: CHARACTERIZATION AND DESULFURIZATION

Dan-ni Yang[1], Jia-xiu Guo[1,2,*], Fa-ming Liao[1], Hua-qiang Yin[1,2], De-ming Luo[2]

[1]College of Architecture and Environment, Sichuan University, Chengdu 610065, China
[2]National Engineering Research Center for Flue Gas Desulfurization, Chengdu 610065, China

ABSTRACT

1-butyl-3-methylimidazolium chloride ([Bmim]Cl) was synthesized by ultrasonic heating circumfluence method and used as the intermediate for preparing Fe-based ionic liquids (Fe-ILs). By introducing the ultrasonic oscillation, the structure of [Bmim]Cl was unaffected but the reaction was shortened, achieving a good yield. The prepared [Bmim]Cl was mixed with $FeCl_3 \cdot 6H_2O$ at different mole ratios to synthesize Fe-ILs. The characteristic results showed that Fe-ILs have excellent thermal stability and $FeCl_4^-$ is the principal anion in Fe-ILs. A ternary desulfurization solution consisted of prepared Fe-ILs, water, and ethanol was applied for the flue gas desulfurization. Different compositions of desulfurization solution have great effects on the desulfurization efficiency and water is an indispensable component for SO_2 removal. Fe-ILs with different mole ratios of [Bmim]Cl to $FeCl_3 \cdot 6H_2O$ exhibit different SO_2 removal activities. When the mass ratio of Fe-ILs, water, and ethanol is at 1:2:4, Fe-IL1 has the highest SO_2 adsorption capacity of 69.35 mg/g while Fe-IL3 has the maximum SO_4^{2-} conversion rate of 42.3%, indicating that the prepared Fe-ILs have dual functions of adsorbent and catalyst and are able to catalytically oxidize SO_2 to form H_2SO_4 in the presence of O_2 and H_2O.

KEYWORDS:
Fe-based ionic liquids, Ultrasonic heating circumfluence method, Desulfurization, Catalyst

INTRODUCTION

Ionic liquids have many advantages, including extremely low vapor pressure, wide liquid range, high thermal and chemical stability, and excellent gas solubility [1-4]. Apart from being used as green solvents and catalyst carrier, ionic liquids are widely used for capturing CO_2, removing sulfides from fuel oil or pollutants in flue gas. Among diverse ionic liquids, Fe-ILs have attracted much attention due to the catalytic oxidation properties. It was reported that Fe-ILs combined with H_2O_2 could be utilized to catalytically oxidize and remove the organic sulfur in petroleum oil [5]. The mechanism of Hg^0 removal by Fe-based ionic liquids has shown that it involves with Hg^0 oxidation by the $FeCl_4^-$ anion and the regeneration of $FeCl_4^-$ anion [6]. A previous study [7] has found that Fe-ILs, ethanol and water could be composed of a ternary system for removing SO_2.

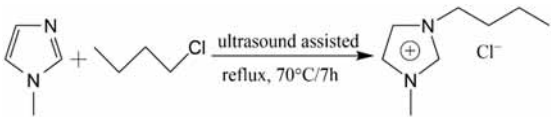
Fe-based ionic liquids were usually prepared by conventional heating method, involving two steps: Menschutkin quaternisation 1-methyl-imidazole by butylchloride, followed by the anion exchange with metal chloride [8, 9]. However, the conventional synthesis is quite time-consuming which requires as long as 72 h of reflux [7, 10] and uses large amounts of classical solvents. Thus, the separation and purification steps are crucial [11]. These drawbacks become the chief barriers to the large-scale production and application of ionic liquids. Therefore, it is necessary to introduce auxiliary means to shorten the synthesis time of ionic liquids. An efficient microwave-assisted method [12] was used to prepare 1,3-dialkylimidazolium tetrafluoroborate ionic liquids on a large scale in a closed vessel. It was found that the introduction of microwave shortens drastically the reaction time and achieves good yields. Ultrasonic irradiation can enhance dramatically the anion exchange for the preparation of 1-butyl-3-methylimidazolium salts from ammonium salts and [Bmim]Cl [11]. When an ultrasonic field was produced directly in the reaction vessel, a yield of 86% was able to get for [Bmim]Cl via the sonication of 1-chlorobutane and 1-methylimidazole within 2 h [13]. However, few studies have examined the effect of ultrasonic heating circumfluence on the [Bmim]Cl preparation. Furthermore, the improvement of ionic liquids synthetic method to make a rapid and inexpensive route is one of the great challenges for the wide application of Fe-ILs. Therefore, the objective of this study is to evaluate the impacts of ultrasonic oscillation on the structure and reaction time of [Bmim]Cl, especially $[Bmim]FeCl_4$, and more in-deeply, to investigate the influence of desulfurization reaction system of $[Bmim]FeCl_4$ on desulfurization activity.

In the present study, an ultrasonic heating circumfluence method was utilized to prepare [Bmim]Cl. The synthesis product was used as the precursor of $[Bmim]FeCl_4$. Initially, the effect of ultrasound bath on the reaction of 1-chlorobutane and

1-methylimidazole was investigated. Secondly, Fourier transform infrared (FTIR) spectroscopy, ^{1}H nuclear magnetic resonance (^{1}H-NMR), Raman spectroscopy, and thermogravimetric/differential thermal analysis (TG/DTA) were conducted to determine the chemical structures of prepared [Bmim]Cl and [Bmim]$FeCl_4$. Thirdly, the prepared ionic liquids were applied to the wet flue gas desulfurization and the influences of $FeCl_3 \cdot 6H_2O$ content in Fe-ILs as well as desulfurization solution composition on the desulfurization performance were investigated. Lastly, the content of oxidized SO_2 (SO_3 or SO_4^{2-}) in the products was measured to verify the catalytic oxidation ability of Fe-ILs.

MATERIALS AND METHODS

Material. 1-methylimidazole (AR) was provided by Chengdu Xiya Reagent Co. Ltd.. Butyl chloride (99%) was purchased from Changzhou Xinhua Active Material Research Institute. Hexahydrated ferric chloride ($FeCl_3 \cdot 6H_2O$), ethyl acetate, and ethanol were all of analytical grades reagent from Chengdu Kelon Chemical Reagents Factory. The pure nitrogen, oxygen, and liquid SO_2 were provided by Sichuan Xuyuan Chemical Co. Ltd.. All chemicals were used without further purification. The SO_2 gaseous with a concentration of 0.25% was diluted by N_2 from liquid SO_2.

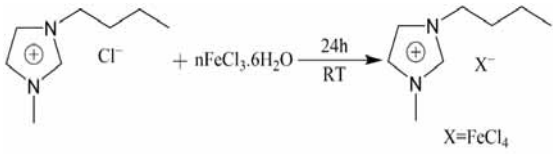


SCHEME 1

Preparation of Fe-based ionic liquids. Fe-ILs were synthesized by two steps according to a similar procedure as described in the previous report [7, 14].

(1) Synthesis of 1-butyl-3-methylimidazolium chloride. An improved preparation method was used to synthesize the intermediate of Fe-ILs, which is [Bmim]Cl, by ultrasonic heating circumfluence. Both 1-methylimidazole (500 mmol, 41.44 g) and 1-chlorobutane (600 mmol, 56.07 g) were placed in a 250 mL flask. The sonochemical reactions were carried out in an ultrasonic cleaning bath of frequency 40 kHz (KQ-100 E). The reaction mixture was refluxed for 7 h at 70 °C by ultrasonic irradiation assistance (Scheme 1). The mixture was cooled and washed with isovolumetric ethyl acetate for 3 times to remove unreacted starting materials. The [Bmim]Cl intermediate was obtained by drying the product under vacuum at 90 °C for 7 h and achieved a yield of 95%.

(2) Synthesis of [Bmim]$FeCl_4$. Fe-ILs were prepared by mixing [Bmim]Cl and $FeCl_3 \cdot 6H_2O$ at molar ratios of 1:1 (Fe-IL1), 1:2 (Fe-IL2), and 1:3 (Fe-IL3), respectively. These mixtures were stirred vigorously in air at room temperature for 24 h (Scheme 2). A two-phase system was achieved after centrifugation and the upper layer was so-called the Fe-ILs. Then the product was purified with distilled water and dried under vacuum at 90 °C for 10 h. A yield of 90% was achieved for Fe-ILs. The viscosity of the prepared Fe-ILs was measured by an Anton-Paar AMVn falling ball viscometer and was determined to be 19.52 mPa·s at 40 °C (in three measurements).



SCHEME 2

Characterizations. The chemical structures of synthetic ionic liquids were determined by FTIR, ^{1}H-NMR, and Raman spectroscopy. FTIR spectra were acquired with a Bruker TENSOR27 spectrometer (KBr film). Raman spectra were recorded on a Renishaw RM2000 spectrometer. The ^{1}H-NMR spectrum was measured by a Bruker Avance 400 Hz spectrometer with deuterated dimethyl sulfoxide (DMSO-d6) as the solvent, and tetramethylsilane (TMS) as the internal standard. The thermal behaviours of ionic liquids were investigated by TG/DTA using a Thermal Analyzer (EXSTAR 6000, Japan) under nitrogen atmosphere at a heating rate of 10 °C/min.

Activity evaluation. The experiments were carried out in a fixed bed reactor at ambient pressure and 40 °C. For all experiments, the flow rate of gas was 50 mL/min and the dosage of ionic liquids was 2 g. The simulated flue gas contained 0.25% SO_2, 10% O_2, and N_2 as the balance. The gas mixture was passed through a micro reactor (scrubber) containing the ionic liquids. The reactor was a U-shaped tube with a ball (2 cm in diameter) in the lower-middle part of the outlet. The ball was filled with some glass beads. They allow the ionic liquids to be contacted with gas to the maximum extent. The reactor was partly immersed in a water bath to control reaction temperature. The SO_2 concentrations in the gas stream were determined according to our previous study [15]. The desulfurization efficiency η was calculated by analyzing the SO_2 inlet and outlet concentrations:

$$\eta(\%) = \frac{SO_{2(inlet)} - SO_{2(outlet)}}{SO_{2(inlet)}} \times 100\%$$

According to the reported procedure [16-18], the content of SO_2 (SO_3 or SO_4^{2-}) oxidized by the Fe-ILs was measured on a spectrophotometer (UV-

TABLE 1
Comparison of synthetic methods

Entry	method	RX /mmol	MIM /mmol	Time	Temp. /°C	Yield /%	Power	Ref.
1	Conventional refluxing method	-	-	72 h	70	-	-	[7]
2	Conventional refluxing method	110	100	48 h	75	-	-	[6]
3	Conventional refluxing method	120	100	24 h	80	89	-	[21]
4	MW [a]	4	2	90 s [b]	80	76	240 w	[22]
5	MW(closed vessel)[c]	155	155	24 min	150	91	300 w	[12]
6	Probe system [d]	220	200	2h	80	86	20 Hz	[13]
7	Ultrasonic heating circumfluence	600	500	7 h	70	95	40 Hz	This study

a Microwave irradiation was used as the energy source by simple exposure of neat reactants in open containers. b The reaction was conducted by intermittent heating with a 10 s interval for mixing after each heating is completed, i.e. 90(s)=30+15+15+15+15 (s). c The reaction was conducted in a closed vessel under microwave irradiation. d An ultrasonic field is produced directly in the reaction vessel in probe system.

1100, Shanghai Meipuda Instrument Co. Ltd., China). Briefly, the sample was dissolved in deionized water. Polyvinyl alcohol, as the protect reagent, was added into the aqueous solution. Hydrochloric acid and barium chloride were then slowly added into the above solution with the blender running. Ten min later, the content of SO_4^{2-} was calculated by determining the absorbance of the aqueous mixture using the spectrophotometer at 422.5 nm.

RESULTS AND DISCUSSION

Effect of synthesis methods. The comparison of different preparation methods of 1-butyl-3-methylimidazolium chloride is shown in Table 1. The conventional method takes several hours to afford reasonable yields. It can be concluded that the reaction time could be reduced by using higher reaction temperature for the synthesis of [Bmim]Cl intermediate by conventional refluxing method (entries 1, 2, 3). For entry 4, microwave irradiation was used as the energy source, and this solvent-free method requires a reaction time of only a few minutes. However, it is not suitable for manufacture on a larger scale because of the hygroscopic nature of salts. In view of the irritant volatile alkyl halides and the corrosive and hygroscopic 1-methylimidazole, heating volatile materials in an open vessel in a microwave oven is redundant and hazardous. Therefore, in order to improve this method, Bhushan et. al. [12] has synthesized [Bmim]Cl on a larger scale in a closed vessel under microwave irradiation, and the yield reached 91%. In addition, the introduction of ultrasound irradiation can provide a relatively mild synthetic condition and expand the production scale during the [Bmim]Cl preparation process [13]. A probe system was used to produce an ultrasonic field directly in the reaction mixture for the preparation of [Bmim]Cl. After 1-chlorobutane and 1-methylimidazole have been oscillating for 2 h at 80 °C, the yield of [Bmim]Cl was 86%. Among all the methods in Table 1, the ultrasonic heating circumfluence achieved the highest yield of 95%. It could be a promising method for the synthesis of [Bmim]Cl which could greatly reduce the reaction time from 72 h to 7 h, compared to the conventional method at the same reaction temperature. This is because the ultrasound produces cavitation effect under the high-energy situation and forms the internal jet with strong impact force. The internal jet accelerates the formation and adiabatic collapse of the transient cavitation bubbles, which promotes the chemical reactions [19, 20].

Characteristic of [Bmim]Cl intermediate. FTIR and ^{1}H-NMR analyses were used to determine the chemical structure of [Bmim]Cl intermediate prepared by ultrasonic heating circumfluence. As shown in Figure 1a, C–H stretching vibration on the imidazole ring appears at 3395 cm^{-1}, and C–H stretching vibration on the line is observed at 2960 cm^{-1}. The peaks at 3080 and 3140 cm^{-1} can be assigned to the interaction of aromatic C–H with Cl^- [23, 24]. The region around 1630 cm^{-1} is assigned to C–H symmetric stretching vibration on the imidazole ring. Peaks at 1460 and 1380 cm^{-1} belong to the $–CH_3$ stretching vibration. A peak observed at 1170 cm^{-1} corresponds to the stretching vibration of C–N on the ring. The vibration of out-of-plane ring C–H bending appears at 755 cm^{-1}, and the stretching vibration of C–Cl is detected at 665 cm^{-1}. It suggests that the chemical structure of the ionic liquid contains alkyl and imidazolyl groups. In Figure 2a, the ^{1}H-NMR spectrum (DMSO-d_6, ppm) is composed of 0.91 (3H, $NCH_2CH_2CH_2C\boldsymbol{H}_3$), 1.29 (2H, $NCH_2CH_2C\boldsymbol{H}_2CH_3$), 1.82 (2H, $NCH_2C\boldsymbol{H}_2CH_2CH_3$), 3.95 (3H, $NC\boldsymbol{H}_3$), 4.27 (2H, $NC\boldsymbol{H}_2$), 7.92 (1H, $CHC\boldsymbol{H}N$), 8.01(1H, (CH_3) $NC\boldsymbol{H}CH$), 9.68 (1H, $NC\boldsymbol{H}N$). These peaks correspond to the hydrogen atoms from the [Bmim]Cl ionic liquid [25-28]. All the characterization results are consistent with the published data [6, 29], indicating that the ionic liquid prepared by ultrasonic assistance possesses the expected structure.

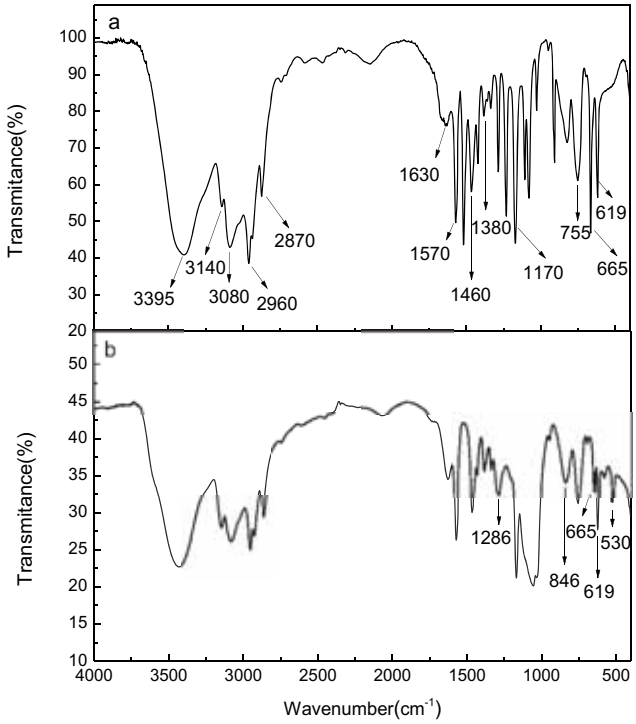


FIGURE1
FTIR spectra of fresh [Bmim]Cl (a) and recycled [Bmim]Cl (b)

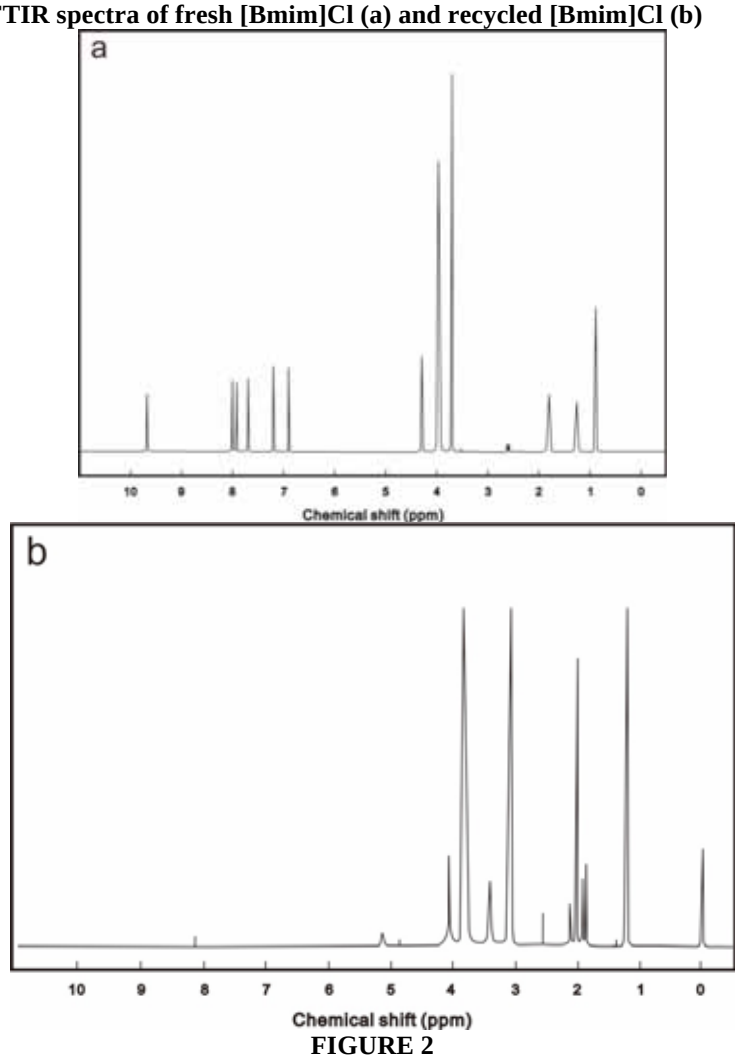


FIGURE 2
^{1}H-NMR spectra of the intermediate [Bmim]Cl (a) and Fe-IL2 (b)

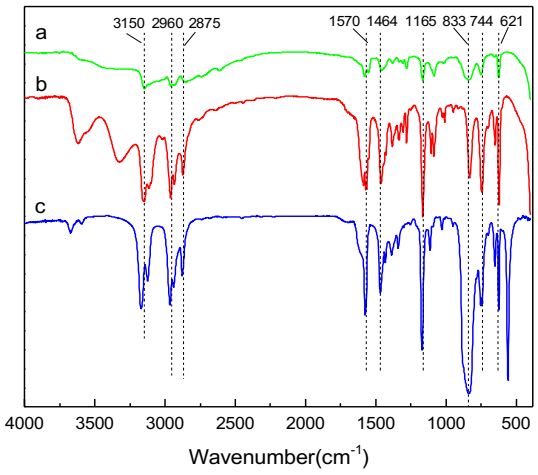


FIGURE 3
IR spectra of Fe-based ionic liquid [Bmim]$FeCl_4$: Fe-IL1 (a), Fe-IL2 (b) and Fe-IL3 (c)

Characterization of Fe-based ionic liquids. The FTIR spectra of samples with different [Bmim]Cl/$FeCl_3 \cdot 6H_2O$ molar ratios are shown in Figure 3. No remarkable peak is observed at the wave number greater than 3200 cm^{-1} in the spectrum of Fe-IL1. This is very different from those of Fe-IL2 and Fe-IL3. It illustrates these samples have different hydrophilic properties which change along with the component of the Fe-ILs. Instead, vibrations of hydroxyl are detected in the spectra of Fe-IL2 and Fe-IL3. The increased hydrophilic may be benefit for the catalytic oxidation of SO_2 because water is necessary when Fe-ILs are used as catalyst in the desulfurization of flue gas [7]. In addition, locations of other peaks in the spectra of the three samples are very close, but the peak strength increases with the increasing $FeCl_3 \cdot 6H_2O$ fraction. Peak at 3150 cm^{-1} is attributed to the C–H stretching vibration on the imidazole ring. Peaks at 2960 and 2875 cm^{-1} are assigned to the C–H stretching vibrations of the alkyl chain [30]. The C=N stretching vibrations of the imidazole ring are observed at 1570 and 1464 cm^{-1} [6, 31]. The peaks at 1165, 832, and 742 cm^{-1} correspond to the characteristic absorption peaks of ring stretching vibrations and plane vibration of the imidazole ring [32]. All the above bands are attributed to the adsorption of ionic liquids cation $[Bmim]^-$ [27, 33]. These characteristic absorption peaks are quite consistent with the spectrum of [Bmim]$FeCl_4$ reported in the literature [6]. However, compared to the spectrum of [Bmim]Cl, in Figure 1a, the disappearance peak in the range of 3000-3100 cm^{-1} can be attributed to the formation of new species, such as [Bmim]$FeCl_4$ and [Bmim]Fe_2Cl_7. This is because the interaction between C (2)–H and $FeCl_4^-$ or $Fe_2Cl_7^-$ is much weaker than that between C (2)–H and Cl^- [30].

Generally, there are various anionic Fe(III) species in the [Bmim]$FeCl_4$ such as Cl^-, $FeCl_4^-$, $Fe_2Cl_7^-$, and $Fe_3Cl_{10}^-$. The Raman spectra of Fe-ILs with different [Bmim]Cl/$FeCl_3 \cdot 6H_2O$ molar ratios were taken to further confirm their major anionic Fe(III) species. As shown in Figure 4, the peaks at 195.85 and 319.58 cm^{-1} in the spectrum of Fe-IL1 might be ascribed to [Bmim]Cl, and the peaks observed at 333.13 and 113.08 cm^{-1} are due to the symmetric Fe–Cl bond stretch vibrations of $FeCl_4^-$ [34]. This indicates that [Bmim]Cl is not fully formed Fe-ILs when the ratio of [Bmim]Cl to $FeCl_3 \cdot 6H_2O$ is at 1:1. The Raman spectrum of Fe-IL2 is similar to that of Fe-IL3 in 100~500 cm^{-1}. The peaks at 195.85 and 319.58 cm^{-1} disappear and Raman intensity of peaks at 113.08 and 333.13 cm^{-1} are enhanced, indicating that [Bmim]Cl is fully formed Fe-ILs when the ratios of [Bmim]Cl and $FeCl_3 \cdot 6H_2O$ are 1:2 and 1:3. The increased $FeCl_4^-$ content in Fe-ILs is very helpful for the catalytic oxidation of SO_2. According to the literatures [30, 35], when the molar ratio of [Bmim]Cl to $FeCl_3$ was one, $FeCl_4^-$ was the main anion; when the ratio was less than one, the anion $Fe_2Cl_7^-$ formed; and when the ratio exceeded one, some Cl^- are remained. However, in this study, some Cl^- are remained when the molar ratio of [Bmim]Cl/$FeCl_3 \cdot 6H_2O$ is 1:1, and the characteristic peak of $Fe_2Cl_7^-$ does not appear in the spectrum of Fe-ILs when the molar ratio of [Bmim]Cl/$FeCl_3 \cdot 6H_2O$ is 1:3. It indicates that the anionic structure of Fe-ILs is affected by the different raw materials because anhydrous $FeCl_3$ is used as the raw materials in the literatures [30, 35] while $FeCl_3 \cdot 6H_2O$ is used in this paper. Therefore, it demonstrates that Fe-ILs with different [Bmim]Cl/$FeCl_3$ molar ratios contain the same $[FeCl_4]^-$ anions and the chemical formula of Fe-IL2 and Fe-IL3 should be [Bmim]$FeCl_4$.

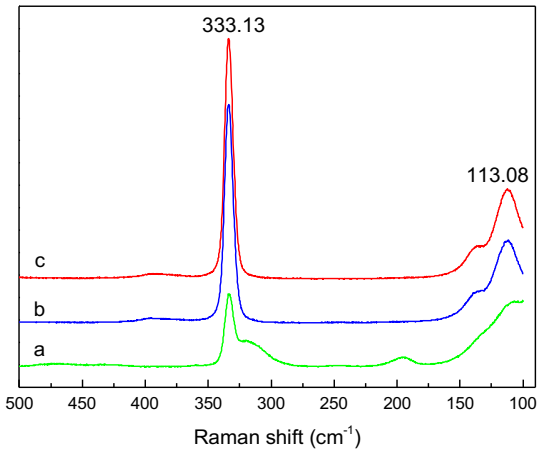


FIGURE 4
Raman spectra of Fe-based ionic liquid [Bmim]$FeCl_4$: Fe-IL1 (a), Fe-IL2 (b), and Fe-IL3 (c)

The NMR spectrum of [Bmim]$FeCl_4$ ionic liquids with molar ratio of [Bmim]Cl/$FeCl_3 \cdot 6H_2O$ at 1:2 is shown in Figure 2b. The ^{1}H-NMR spectrum data (DMSO-d_6, ppm) is 1.08 (3H,

$NCH_2CH_2CH_2C\boldsymbol{H}_3$), 1.85 (2H, $NCH_2CH_2C\boldsymbol{H}_2CH_3$), 2.12 (2H, $NCH_2C\boldsymbol{H}_2CH_2CH_3$), 3.10 (3H, $NC\boldsymbol{H}_3$), 3.85 (2H, $NC\boldsymbol{H}_2$), 5.2 (1H, NC***H***), and 8.11 (1H, NC***H***N). Because the magnetism of Fe-based ionic liquids can interfere the NMR measurement, the chemical shifts of 2H in imidazolium shift to downfield compared to the ^{1}H-NMR spectrum of [Bmim]Cl, and the peak shape changes are observed in the $–NCH_2$ and –NCH shift. It suggests that the anion of ionic liquids is combined with H atom on the imidazole ring through a hydrogen bond and the prepared Fe-based ionic liquids have the chemical molecular of [Bmim]$FeCl_4$.

The thermal stability strongly influences the technical conditions and industrial application prospects of ionic liquids. Thermogravimetric-differential thermal analysis of Fe-ILs with molar ratio of [Bmim]Cl to $FeCl_3{\cdot}6H_2O$ at 1:2 was used to investigate the thermal stability. As shown in Figure 5, there is no significant loss of mass from 25 to 300 °C with a slow rate in TG. When the temperature rises to 320.5 °C, the weight loss rate is increasing, indicating that Fe-IL2 begins to decompose. Two exothermic peaks at 375.6 and 390.4 °C appear on the DTA curve. The former peak is attributed to the pyrolysis temperature of 3-butyl group, and the latter one is due to the decomposition of the 1-methyl. The thermal analysis establishes that the Fe-ILs prepared by ultrasonic assistance is thermally stable up to 320.5 °C. Therefore, the Fe-ILs is stable under the experimental conditions (20~80 °C), and the absorption and regeneration experiments could be conducted at a higher temperature.

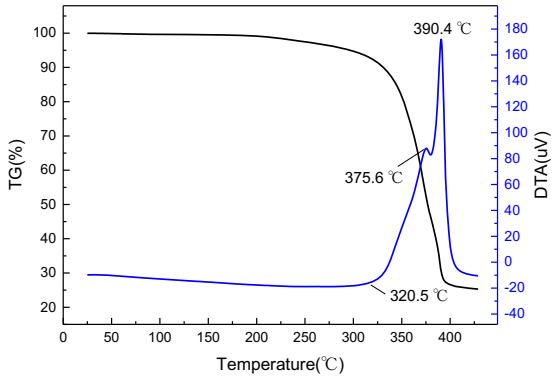


FIGURE 5
TG/DTA curves of Fe-IL2

Desulfurization performance of [Bmim]Cl intermediate. The desulfurization performance of the prepared intermediate was evaluated. During the desulfurization process, only 2 g of [Bmim]Cl ionic liquids were used without any other additives. The relationships between desulfurization efficiency and time of fresh [Bmim]Cl and recycled [Bmim]Cl are shown in Figure 6. Fresh [Bmim]Cl exhibits good SO_2 removal ability. A desulfurization efficiency of 100% can maintain 380 min, and then the desulfurization efficiency gradually decreases with the increase of reaction time. When the SO_2 removal efficiency decreases to 50%, the SO_2 adsorption capacity and reacting time of fresh [Bmim]Cl are 95.90 mg/g and 570 min, respectively. The sample after desulfurization was treated by a rotary evaporator at 90 °C for 4 h under 0.09 bar vacuum condition [29], and it was subsequently used to evaluate reusability performance. As shown in Figure 6, the recycling desulfurization performance of the treated [Bmim]Cl is far worse than that of fresh [Bmim]Cl. When the desulfurization efficiency decreases to 50%, the SO_2 adsorption capacity and reacting time of recycled [Bmim]Cl decrease to 25.96 mg/g and 180 min, respectively, indicating that [Bmim]Cl intermediate has poor reusability in SO_2 removal.

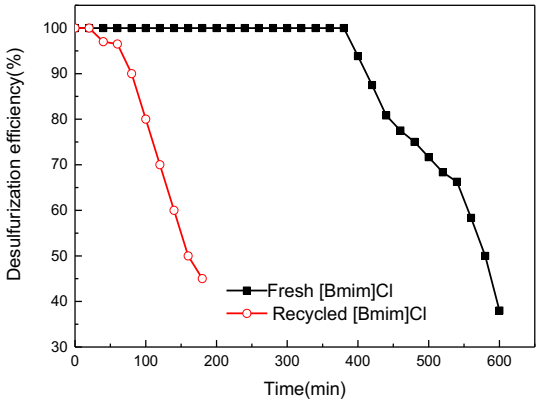


FIGURE 6
Comparison of desulfurization properties with time in fresh [Bmim]Cl and recycled [Bmim]Cl. 2 g of [Bmim]Cl ionic liquids was used in this test. Experimental conditions: SO_2: 0.25%, O_2:10%, flow rate: 50 mL/min, T = 40 °C.

The FTIR spectrum of recycled [Bmim]Cl was investigated to clarify the causation of the declined desulfurization performance, and the result is shown in Figure 1b. Compared with the spectrum of fresh [Bmim]Cl, a new weak peak at 1286 cm^{-1} in the spectrum of recycled [Bmim]Cl is observed, which is assigned to residual SO_2 after treatment under 0.9 bar vacuum condition. The sharp peak at 665 cm^{-1} is significantly weakened in the recycled [Bmim]Cl, which may be resulted from the substituted of –Cl by –S or $–SO_2$ during desulfurization. The weak C–S-C bond vibration at 530 cm^{-1} proves this point. They are the main reasons for the decreasing SO_2 removal capacity. The results also show that for the removal of SO_2, [Bmim]Cl mainly plays a role of adsorption.

The desulfurization performance of Fe-ILs. In this paper, a ternary desulfurization system was constructed for the wet flue gas desulfurization, which consisted of Fe-ILs, water, and ethanol with a mass ratio of 1:2:4. Simultaneously, the SO_4^{2-} conversion rate was investigated by the mass ratios of

oxidized SO_2 to total absorbed SO_2. The desulfurization performances of Fe-ILs with different molar ratios of [Bmin]Cl to $FeCl_3$·$6H_2O$ are given in Figure 7 and Table 2.

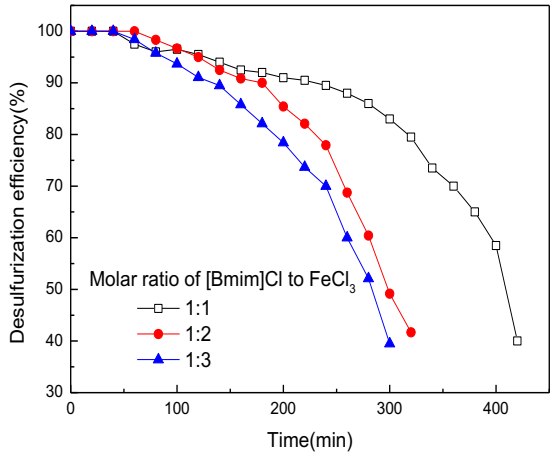


FIGURE 7
Effects of different molar ratios of [Bmim]Cl to $FeCl_3$·$6H_2O$ on the SO_2 removal. Experimental conditions: $m_{Fe\text{-}IL}$: m_{water}: $m_{ethanol}$=1:2:4, SO_2: 0.25%, O_2:10%, flow rate: 50 mL/min, T = 40°C

The molar ratio of [Bmim]Cl to $FeCl_3$·$6H_2O$ is found to be an important factor for the desulfurization performance. With the increase of reaction time, the desulfurization efficiencies of all samples decrease gradually. When the molar ratio of [Bmim]Cl to $FeCl_3$·$6H_2O$ is 1:1, the system has SO_2 absorption capacity of 69.35 mg/g and SO_4^{2-} conversion rate of 42.3%. When the $FeCl_3$·$6H_2O$ increases, the SO_2 absorption capacity of Fe-ILs decreases while SO_4^{2-} conversion rate increases. When the molar ratio of [Bmim]Cl to $FeCl_3$·$6H_2O$ changes from 1:1 to 1:3, the absorption capacity of SO_2 decreases to 48.37 mg/g while SO_4^{2-} conversion rate increases to 61.7%. This indicates that $FeCl_3$·$6H_2O$ plays an important role.

Decreased SO_2 removal activity might be ascribed to the changed acidities of ionic liquids resulted from the different molar ratios of [Bmim]Cl to $FeCl_3$·$6H_2O$. It is observed that the Lewis acidity of ionic liquids increases with the fraction of $FeCl_3$ [36, 37], following the order: [Bmin]Cl/$FeCl_3$ < [Bmin]Cl/2$FeCl_3$ < [Bmin]Cl/3$FeCl_3$. As SO_2 is an acid gas, it is logical to conclude that the Lewis acidity of the ionic liquids is unfavourable for the flue gas desulfurization. Besides, Lewis acidity is not the only factor to affect the desulfurization efficiency. It depends on both Lewis acidity and viscosity [5]. According to the literature [38], when the molar ratio of $FeCl_3$ to [Bmim]Cl exceeded 1.5 or 2, some $FeCl_3$ could not fully react with [Bmim]Cl and the ionic liquids were not really pure, causing the increase of viscosity. Therefore, the desulfurization efficiency of Fe-ILs follows the order of [Bmin]Cl/3$FeCl_3$·$6H_2O$ < [Bmin]Cl/2$FeCl_3$·$6H_2O$ < [Bmin]Cl/$FeCl_3$·$6H_2O$. The increased SO_4^{2-} conversion rate could be ascribed to the formation of more $FeCl_4^-$ with the increase of $FeCl_3$·$6H_2O$ in Fe-ILs, which is confirmed by the Raman results. The desulfurization experiments confirm that the prepared Fe-ILs have dual functions of absorbent and catalyst. By combining the absorption capacity of SO_2 and the mass ratios of oxidized SO_2 to total absorbed SO_2 of Fe-ILs, Fe-IL2 is selected to undergo the following experiments.

TABLE 2
The SO_2 absorption capacities and SO_4^{2-} conversion rates of [Bmim]Cl/n $FeCl_3$•$6H_2O$

Mole ratio of [Bmim]Cl to $FeCl_3$	SO_2 absorption capacity mg/g	SO_4^{2-} conversion rates
1:1	69.35	42.3%
1:2	52.75	52.8%
1:3	48.37	61.7%

Effects of solution composition on the desulfurization. The effects of solution composition on the desulfurization performance were investigated and the results are shown in Figure 8. Different compositions of desulfurization solution and component contents have great effects on the desulfurization efficiency of the ternary system. There is hardly any desulfurization efficiency when only Fe-IL2 exists in the system without water or ethanol, as well as in the binary system, e.g. Fe-IL2 and water or ethanol. Good desulfurization performance can be achieved only when the desulfurization system contains Fe-IL2, water, and ethanol with a certain ratio by weight.

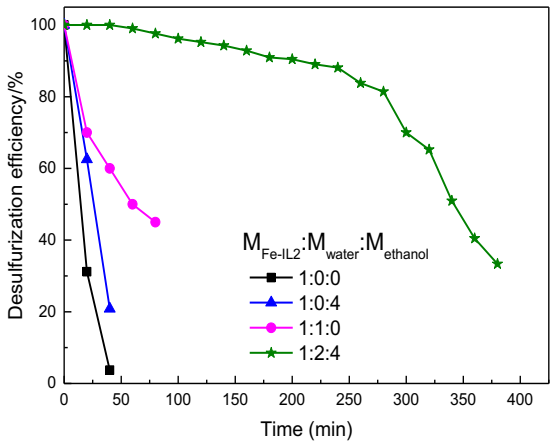


FIGURE 8
Effects of solution composition on the desulfurization performance. $M_{Fe\text{-}IL2}$: M_{water}: $M_{ethanol}$ is the mass ratio of Fe-IL2, water and ethanol. Experimental conditions: SO_2: 0.25%, O_2:10%, flow rate: 50 mL/min, T = 40 °C.

The prepared Fe-IL2 has a high viscosity value of 19.52 mPa•s at 40 °C, nearly 40 times the value of

water at 0 °C, causing that the interphase mass transfer between gas and Fe-IL2 becomes more difficult. This is due to that a single Fe-IL2 has hardly any desulfurization efficiency. For the binary systems of Fe-IL2 and ethanol or water, the desulfurization efficiency increases marginally compared with the single Fe-IL2. This is because the presence of hydroxyl group in desulfurization system can enhance the adsorption of SO_2 through H–bonding interaction and reduce the oxidation barrier [39]. In addition, water is very important for the SO_2 removal because of phase transfer between the gas phase and liquid phase. SO_2 must dissolve in the water to form SO_3^{2-} and HSO_3^-, and then can be catalytically oxidized by O_2 with Fe(III) catalyst [7]. Thus, in the binary systems of Fe-IL2 and water, Fe-IL2 has a certain capacity for SO_2 removal but it exhibits a poor performance. It is well accepted that pure imidazolium-based ionic liquids mixed with other molecular solvents should be better regarded as nanostructured aggregates with polar and nonpolar regions rather than homogeneous solvents [40]. A reasonable explanation for the poor performance is that it cannot form a homogeneous solvent in the binary system composed of Fe-IL2 and water, which limit the full contact between SO_3^{2-} and catalyst, causing the low removal efficiency of SO_2. When the desulfurization systems contain Fe-IL2, ethanol and water, desulfurization performance is significantly improved. This may be that ethanol molecules are capable of changing the interaction between cations and water, anions and water by introduction of C–H···O interactions with cations, as well as the strong hydrogen-bond interactions between the anions and the hydroxyls of the ethanol [41]. The introduction of ethanol into the desulfurization system contributes to form a homogenous solution and makes it easier for recycling Fe-IL2 by distillation ethanol from their aqueous diluted solutions [41]. The constructed ternary system can provide the water needed in the catalytic oxidation reaction, resulting in considerable removal efficiency. The removal of SO_2 by Fe-ILs catalytic oxidation probably can be described as the following chemical reactions [6, 7]:

$$SO_2 + H_2O \rightarrow H_2SO_3$$
$$H_2SO_3 \leftrightarrow H^+ + SO_3^{2-}$$
$$[Bmim][Fe^{3+}Cl_4] + SO_3^{2-} \rightarrow [Bmim][Fe^{2+}Cl_3] + SO_4^{2-}$$
$$[Bmim][Fe^{2+}Cl_3] + SO_2 + O_2 + H^+ \rightarrow [Bmim][Fe^{3+}Cl_4] + H_2SO_4$$

The overall reaction is as follows:

$$2SO_2 + O_2 + H_2O \rightarrow 2H_2SO_4$$

CONCLUSIONS

The introduction of ultrasonic oscillation doesn't change the structure of [Bmim]Cl, and the ultrasonic heating circumfluence method shortens reaction time and achieves a good yield. The chemical shifts of the hydrogen located in the cation of ionic liquids are sensitive to the composition of ionic liquids and $FeCl_4^-$ is the principal anion in Fe-ILs. Fe-ILs have excellent thermal stability of structure. Different compositions of desulfurization solution have great effects on the desulfurization efficiency, and water is an indispensable component for SO_2 removal. The prepared Fe-ILs have dual functions of adsorbent and catalyst, and Fe-ILs can catalytically oxidize SO_2 to form H_2SO_4 in the presence of O_2 and H_2O.

ACKNOWLEDGEMENTS

This work is financially supported by Sichuan Provincial Science and Technology Agency Support Projects (grant number 2016GZ0047).

REFERENCES

[1] Bhargava, B.L., Balasubramanian, S. (2005) Dynamics in a room-temperature ionic liquid: A computer simulation study of 1,3-dimethylimidazolium chloride. The Journal of Chemical Physics. 123, 144505.

[2] Hanke, C.G., Atamas, N.A., Lyndenbell, R.M. (2002) Solvation of small molecules in imidazolium ionic liquids: a simulation study. Green Chemistry. 4, 107-111.

[3] Tokuda, H., Tsuzuki, S., Susan, M.A.B.H., Hayamizu, K., Watanabe, M. (2006) How ionic are room-temperature ionic liquids? An indicator of the physicochemical properties. The Journal of Physical Chemistry B. 110, 19593-19600.

[4] Urahata, S.M., Ribeiro, M.C. (2004) Structure of ionic liquids of 1-alkyl-3-methylimidazolium cations: A systematic computer simulation study. Journal of Chemical Physics. 120, 1855-1863.

[5] Jiang, Y., Zhu, W., Li, H., Yin, S., Liu, H., Xie, Q. (2011) Oxidative desulfurization of fuels catalyzed by Fenton-like ionic liquids at room temperature. ChemSusChem. 4, 399–403.

[6] Cheng, G., Zhang, Q., Bai, B. (2014) Removal of Hg^0 from flue gas using Fe-based ionic liquid. Chemical Engineering Journal. 252, 159-165.

[7] Xie, M., Li, P., Guo, H., Gao, L., Yu, J. (2012) Ternary system of Fe-based ionic liquid, ethanol and water for wet flue gas desulfurization. Chinese Journal of Chemical Engineering. 20, 140-145.

[8] Lin, I.J.B., Vasam, C.S. (2005) Metal-containing ionic liquids and ionic liquid crystals based on imidazolium moiety. Journal of Organometallic Chemistry. 36, 3498-3512.

[9] Sitze, M.S., Schreiter, E.R., Patterson, E.V., Freeman, R.G. (2001) Ionic liquids based on $FeCl_3$ and $FeCl_2$. Raman scattering and ab initio calculations. Inorganic Chemistry. 40, 2298-2304.
[10] Wilkes, J.S., Levisky, J.A., Wilson, R.A., Hussey, C. L. (1982) Dialkylimidazolium chloroaluminate melts: a new class of room-temperature ionic liquids for electrochemistry, spectroscopy and synthesis. Inorganic Chemistry. 21, 1263-1264.
[11] Lévêque, J.M., Luche, J.L., Pétrier, C., Roux, R., Bonrath, W. (2002) An improved preparation of ionic liquids by ultrasound. Green Chemistry. 4, 357-360.
[12] Khadilkar, B.M., Rebeiro, G.L. (2002) Microwave-assisted synthesis of room-temperature ionic liquid precursor in closed vessel. Organic process research & development. 6, 826-828.
[13] Namboodiri, V.V., Varma, R.S. (2002) Solvent-free sonochemical preparation of ionic liquids. Organic letters. 4, 3161-3163.
[14] Wang, H., Yan, R., Li, Z., Zhang, X., Zhang, S. (2010) Fe-containing magnetic ionic liquid as an effective catalyst for the glycolysis of poly (ethylene terephthalate). Catalysis Communications. 11, 763-767.
[15] Guo, J.X., Qu, Y.F., Shu, S., Wang, X.J., Yin, H.Q., Chu, Y.H. (2015) Effects of preparation conditions on Mn-based activated carbon catalysts for desulfurization. New Journal of Chemistry. 39, 5997-6015.
[16] Hu, R.P., Wu, L., Yu, Y.H., Liao, H. (2009) Determination of sulfate in high-purity zinc phosphate by spectroscopic-turbidity method. Technology & Development of Chemical Industry. 38, 42-44.
[17] Zhang, L., Wang, C., Wang, W., Xu, W., Zhang, J. (2009) Determination method of trace amount SO_4^{2-} in electronic grade phosphoric acid. Inorganic Chemicals Industry. 41, 56-58.
[18] Ren, S., Hou, Y., Wu, W., Jin, M. (2011) Oxidation of SO_2 absorbed by an ionic liquid during desulfurization of simulated flue gases. Industrial & Engineering Chemistry Research. 50, 998-1002.
[19] Gaplovsky, A., Gaplovsky, M., Toma, S., Luche, J.L. (2000) Ultrasound effects on the photopinacolization of benzophenone. The Journal of Organic Chemistry. 65, 8444-8447.
[20] Rajagopal, R., Jarikote, D.V., Srinivasan, K.V. (2002) Ultrasound promoted Suzuki cross-coupling reactions in ionic liquid at ambient conditions. Chemical Communications. 6, 616-617.
[21] Sonkaria, S., Kim, H.T., Kim, S.Y., Kumari, N., Kim, Y.G., Khare, V., Ahn S.H. (2016) Ionic liquid-induced synthesis of a graphene intercalated ferrocene nanocatalyst and its environmental application. Applied Catalysis B: Environmental. 182, 326-335.
[22] Varma, R.S., Namboodiri, V.V. (2001) An expeditious solvent-free route to ionic liquids using microwaves. Chemical Communications. (7), 643-644.
[23] Dieter, K.M., Dymek, C.J., Heimer, N.E., Rovang, J.W., Wilkes, J.S. (1988) Ionic structure and interactions in 1-methyl-3-ethylimidazolium chloride-aluminum chloride molten salts. Journal of the American Chemical Society. 110, 2722-2726.
[24] Tait, S., Osteryoung, R.A. (1985) Infrared study of ambient-temperature chloroaluminates as a function of melt acidity. Inorganic Chemistry. 23, 4352-4360.
[25] Dharaskar, S.A., Wasewar, K.L., Varma, M.N., Shende, D.Z., Yoo C. (2016) Synthesis, characterization and application of 1-butyl-3-methylimidazolium tetrafluoroborate for extractive desulfurization of liquid fuel. Arabian Journal of Chemistry. 9, 578-587.
[26] Grishina, E.P., Ramenskaya, L.M., Gruzdev, M.S., Kraeva, O.V. (2013) Water effect on physicochemical properties of 1-butyl-3-methylimidazolium based ionic liquids with inorganic anions. Journal of Molecular Liquids. 177, 267-272.
[27] Lu, B., Cai, N., Sun, J., Wang, X., Li, X., Zhao, J., Cai, Q. (2013) Solvent-free oxidation of toluene in an ionic liquid with H_2O_2 as oxidant. Chemical Engineering Journal. 225, 266-270.
[28] Wang, J., Yao, H., Nie, Y., Zhang, X., Li, J. (2012) Synthesis and characterization of the iron-containing magnetic ionic liquids. Journal of Molecular Liquids. 169, 152-155.
[29] Tang, Y.X., Mao, W.K., Ma, N., Zhu, X.F., Hua, J., Yin, H.Q. (2010) Adsorption performances for sulfur dioxide using imidazole ionic liquids. Environmental Science. 31, 2582-2586.
[30] Ko, N.H., Lee, J.S., Huh, E.S., Lee, H., Jung, K.D., Kim, H.S., Cheong, M. (2008) Extractive desulfurization using Fe-containing ionic liquids. Energy & Fuels. 22, 1687-1690.
[31] Wang, F., Zhang, Z., Yang, J., Wang, L., Lin, Y., Wei, Y. (2013) Immobilization of room temperature ionic liquid (RTIL) on silica gel for adsorption removal of thiophenic sulfur compounds from fuel. Fuel. 107, 394-399.
[32] Xun, S., Zhu, W., Zheng, D., Zhang, L., Liu, H., Yin, S., Zhang, M., Li, H. (2014) Synthesis of metal-based ionic liquid supported catalyst and its application in catalytic oxidative desulfurization of fuels. Fuel, 136, 358-365.
[33] Chowdhury, A., Thynell, S.T., Lin, P. (2009) Confined rapid thermolysis/FTIR/ToF studies of tetrazolium-based energetic ionic liquids. Thermochimica Acta. 485, 1-13.

[34] Lin, I.J.B., Vasam, C.S. (2005) Metal-containing ionic liquids and ionic liquid crystals based on imidazolium moiety. Journal of Organometallic Chemistry. 690, 3498-3512.
[35] Yang, J.Z., Xu, W.G., Zhang, Q.G., Jin, Y., Zhang, Z.H. (2003) Thermodynamics of {1-methyl-3-butylimidazolium chloride + Iron (III) chloride. The Journal of Chemical Thermodynamics. 35, 1855-1860.
[36] Li, F.T., Liu, R.H., Wen, J.H., Zhao, D.S., Sun, Z.M., Liu, Y. (2009) Desulfurization of dibenzothiophene by chemical oxidation and solvent extraction with $Me_3NCH_2C_6H_5Cl•2ZnCl_2$ ionic liquid. Green Chemistry. 11, 883-888.
[37] Li, F.T., Liu, Y., Sun, Z.M., Chen, L.J., Zhao, D.S., Liu, R.H., Kou, C.G. (2010) Deep extractive desulfurization of gasoline with $xEt_3NHCl•FeCl_3$ ionic liquids. Energy & Fuels. 24, 4285-4289.
[38] Chen, X., Song, D., Asumana, C., Yu, G. (2012) Deep oxidative desulfurization of diesel fuels by Lewis acidic ionic liquids based on 1-n-butyl-3-methylimidazolium metal chloride. Journal of Molecular Catalysis A. Chemical, 359, 8-13.
[39] Zhang, H., Cen, W., Liu, J., Guo, J., Yin, H., Ning, P. (2015) Adsorption and oxidation of SO_2 by graphene oxides: A van der Waals density functional theory study. Applied Surface Science. 324, 61-67.
[40] Dupont, J. (2004) On the solid, liquid and solution structural organization of imidazolium ionic liquids. Journal of the Brazilian Chemical Society. 15, 341-350.
[41] Wu, B., Zhang, Y., Wang, H. (2009) Insight into the intermolecular interactions in [Bmim] BF_4/[Amim]Cl-Ethanol-Water mixtures by Near-Infrared Spectroscopy. The Journal of Physical Chemistry B. 113, 12332-12336.

Received: **03.03.2017**
Accepted: **01.10.2017**

CORRESPONDING AUTHOR

Jia-xiu Guo
College of Architecture and Environment, Sichuan University, Chengdu, 610065, P.R. China

e-mail: guojiaxiu@scu.edu.cn

© by PSP Volume 26 – No. 12A/2017 pages 7734-7739 Fresenius Environmental Bulletin

ENHANCED DEGRADATION EFFICIENCY OF THREE DIMENSIONAL GRAPHENE-TiO_2 HYDROGEL BASED ON COMMERCIAL TITANIUM(IV) OXIDE

Xiangfei Wei[1], Mingliang Chen[2,*]

[1]West AnHui University, Luan, Anhui, 237012, China
[2]Jiangnan Graphene Research Institute, Changzhou 213149, China

ABSTRACT

In general, graphene-TiO_2 composites as well as 3D hydrogels are almost prepared by using P25 or organic titanium. However, due to the valuableness of P25 and the toxic of organic titanium, the development of graphene-TiO_2 only limited to scientific research. Herein, we reported the development of three-dimensional graphene-TiO_2 hydrogels by a facile one-pot hydrothermal approach and explored its environmental applications as photocatalyst. During the hydrothermal reaction, the graphene nanosheets and TiO_2 particles self-assembled into 3D interconnected networks, in which the spherical nanostructured TiO_2 particles with uniform size were densely anchored onto the graphene nanosheets. We have shown that the resultant graphene-TiO_2 hydrogels displayed the synergistic effects of the assembled graphene nanosheets and TiO_2 particles and therefore exhibited a unique collection of physical and chemical properties such as increased adsorption capacities, enhanced photocatalytic activities.

KEYWORDS:
Graphene-TiO_2 hydrogels, Degradation efficiency, UV−vis absorption spectra

INTRODUCTION

Graphene, a single layer of carbon atoms patterned in a hexagonal lattice, has attracted great attention all over the world for its potential applications in catalysis [1], energy-storage devices [2], and environmental fields [3] due to its excellent mechanical, electronic, and thermal properties. As an important member of functionalized graphene materials, graphene based photocatalysts composite has been researched several years. In particular, P25-graphene composite is recently found to be a more efficient photocatalyst compared to P25 and P25-carbon nanotubes due to its giant 2D planar structure [4]. In this TiO_2-C composite, graphene could act as an acceptor for the photogenerated electrons from the UV light excited P25 and ensure fast charge transportation in view of its high conductive.

Moreover, previous studies have showed that graphene oxide (GO) can form a 3D hydrogel structure by various supramolecular interactions including hydrogen bonding, coordination, electrostatic interaction, and π-π stacking [5, 6]. Such graphene-based 3D macrostructures are electrically conductive, mechanically strong, and thermally stable. Therefore, 3D TiO_2-graphene composite is expected to be an efficient photocatalyst. On the other hand, the integration of nanostructured materials into macroscopic devices that can translate phenomena at the nanoscale to the macroscopic level proves the key to paving the way to realizing applications of nanomaterials [7]. Recently, macroscopic 3D P25-graphene materials such as P25 graphene hydrogels deserve special attention owing to their macroscopic scale and the more practical use as available devices, compared to 2D P25-graphene sheets [8, 9]. However, the P25 is very expensive and only applied to scientific research, which cannot be used in large doses for various applications. The 3D graphene based commercial titanium(IV) oxide has not been reported yet.

Herein, we prepared 3D graphene-TiO_2 hydrogels (GT) by incorporation of commercial titanium(IV) oxide powders via a facile one-step hydrothermal approach and explored its environmental applications as superior photocatalyst. The photocatalytic properties of 3D graphene-TiO_2 hydrogels are investigated by degrading methylene blue (MB) solution.

EXPERIMENT

Preparation of 3D graphene-TiO_2 hydrogels (GT). Graphene oxide (GO) was purchased from Suzhou Graphene Nanotechnology Co., Ltd. GT was prepared by adding 1 g of commercial titanium(IV) oxide powders (TiO_2, amorphous, 98%) into a certain amount of homogeneous GO aqueous dispersion (4 mg mL^{-1}) under sonication for about 2 h. After that, the mixture was sealed in a 50 mL Teflon-lined autoclave and maintained at 180°C for 12 h. The autoclave was naturally cooled in room temperature, and then, a black cylinder (i.e., GT) was obtained. The

size of GT can be freely adjusted by changing the volume of GO aqueous dispersion. The as-obtained GT samples were freeze-dried overnight for the following experiment and the samples code was listed in Table 1.

TABLE 1
Samples code and bandgap of the as-prepared samples.

Graphene oxide (mg)	Commercial TiO_2 (g)	Samples code	Band gap (eV)
0	1	GT-0	3.2
20	1	GT-2	2.9
40	1	GT-4	2.8
60	1	GT-6	2.6

Characterization of the sample. Scanning electron microscopy (SEM) images were obtained on a SEM instrument (Quanta 400 FEG FEI). X-ray powder diffraction (XRD) patterns were recorded using a Bruker AXS-D8 Advance powder X-ray diffractometer using Cu/Ka radiation (λ = 1.5406 Å) at a step size of 0.04° and a dwell time of 1.0 seconds. Raman spectroscopy was recorded at a LabRam HR800 UV NIR using a 633 nm laser excitation with working distances on a ×50 lens. Diffuse reflectance spectra (DRS) were recorded in the range from 100 to 2000 nm using the UV-vis spectrophotometer (Jasco V660).

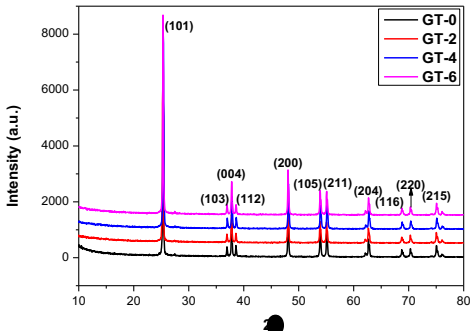
Photocatalytic experiments of the sample. The photodegradation of methylene blue (MB) dyes was observed based on the absorption spectroscopic technique. In a typical process, aqueous solution of the MB dyes (1×10^{-5} mol L^{-1}, 40 mL) and the photocatalysts (GT samples, 40 mg) were placed in a cylindrical quartz vessel. Under room conditions and stirring in dark for 2 h, the vessel was exposed to the visible light irradiation produced by a CHF-XM500 Xenon light source system (the average light intensity was 30 mW cm^{-2}) with the main peak at wavelength more than 400 nm. All other lights were insulated. At given time intervals, the photoreacted solution was analyzed by recording the maximum absorbance of MB at 660 nm with the UV-vis spectrophotometer (Jasco V660).

RESULTS AND DISCUSSIONS

Through the hydrothermal reaction, the synthesis and functionalization of graphene-TiO_2 hydrogels is realized. As shown in Fig. 1a, well-formed 3D gel-like cylinder can form from initial solutions containing GO and commercial TiO_2 powders. As well as, the color and size of cylinder is darken and enhanced with increasing the amount of GO. With the reduction proceeding, the π-conjugated structures of reduced GO sheets are increased which increases the amount of π-π stacking cross-links between graphene sheets. The partial overlapping or coalescing of flexible graphene sheets results in construction of the 3D structures. The residual oxygenated functional groups on the graphene sheets could entrap ample water into the graphene network and Ti-O-C bonds are formed between graphene sheet and TiO_2 powder, thus 3D graphene-TiO_2 hydrogels are formed.



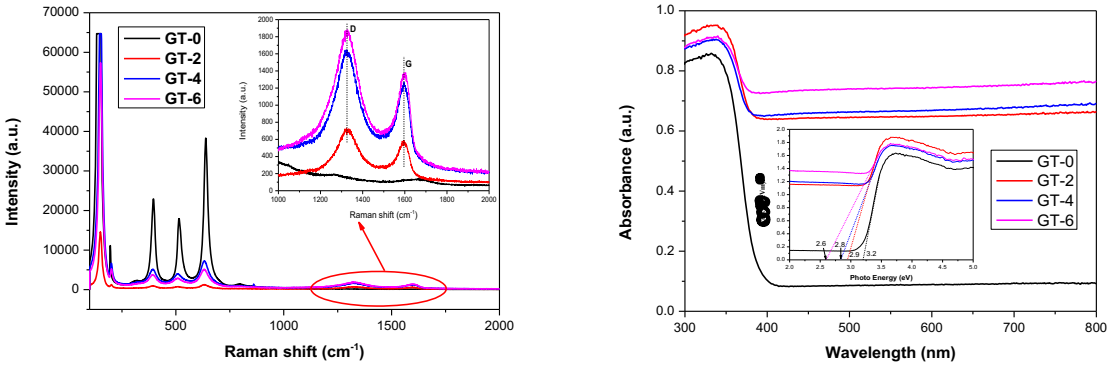
(a)



(b)

FIGURE 1
(a) Photographs the obtained hydrogels after hydrothermal reaction and (b) XRD patterns of the as-prepared samples.

Fig. 1b shows the XRD patterns of the as-prepared samples. In all graphene-based gel samples, (001) reflection peak of GO at around 2θ = 10.8° [10] disappeared, indicating the high-effective reduction of GO. On the other hand, 2θ values of diffraction peaks observed at 25.28, 37.01, 37.78, 38.64, 48.02, 53.92, 55.06, 62.72, 68.80, 70.36, and 75.12. These peaks were assigned to reflections from (101), (103), (004), (112), (200), (105), (211), (204), (116), (220), and (215) crystal planes, which mainly corresponds to anatase phase of TiO_2. The results indicate all of the amorphous TiO_2 powders are transformed to anatase phase after hydrothermal reaction at 180 ℃.



(a) **(b)**

FIGURE 2
(a) Raman spectra. (b) Diffuse reflectance spectra of the as-prepared samples.

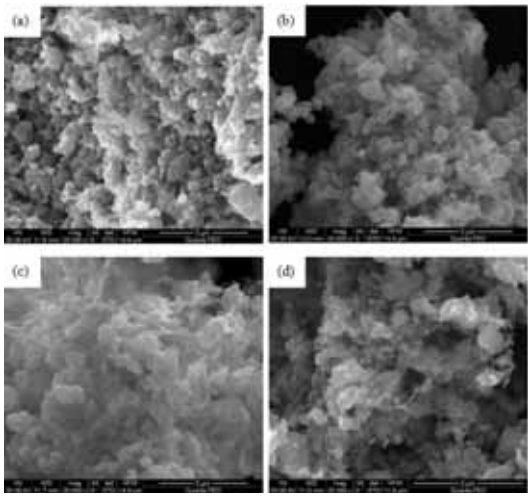


FIGURE 3
SEM images of the (a) GT-0, (b) GT-2, (c) GT-4 and (d) GT-6.

Raman spectroscopy is a powerful tool to characterize the crystalline quality of graphene. The Raman spectra of the series GT composites are presented in Fig. 2a. The specific vibration modes are located at 144 cm^{-1} (E_g), 396 cm^{-1} (B_{1g}), 512 cm^{-1} (B_{1g}+A_{1g}) and 631 cm^{-1} (E_g) indicating the presence of the anatase phase in all of these samples. The D bands located at 1324 cm^{-1} and G band at 1597 cm^{-1} are revealed in GT-2, GT-4 and GT-6 composites observably (Fig. 2a inset), which are E_{2g} vibrational mode in plane and A_{1g} breathing mode, respectively. With increasing amount of GO the intensity of both bands also increases. Moreover, the intensity ration of the D and G band (I_D/I_G) changes from 1.25 (GT-2) to around 1.35 (GT-6), indicating a decrease in the average size of the sp^2 domains upon the reduction of GO.

Fig. 2b presents the UV-vis absorption spectra of the series GT composites. The presence of different amounts of GO influences the optical properties of light absorption significantly. With increasing GO amount in the composites light absorption intensity in the UV region grows and a red shift to higher wavelength in the absorption edge at about 400 nm also observed [11]. Increased background in the area 400-800 nm is caused by incorporation of GO into the matrix of TiO_2 [12].

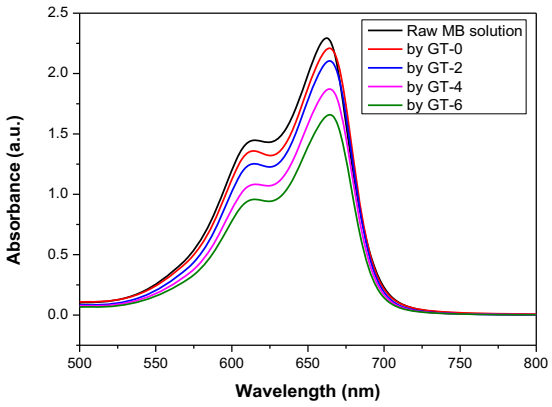
According to the equation for band gap:
$\alpha h\nu = B(h\nu - Ebg)^2$
where $\alpha = (1-R)^2/2R$, R is the reflectance of the "infinitely thick" layer of the solid [13], B is absorption coefficient and hν is the photon energy in eV. Fig. 2b (inset) plots the relationship of $(\alpha h\nu)^{1/2}$ versus photon energy ($h\nu = 1239/\lambda$) [14, 15], which shows that the band gap of pure TiO_2 is 3.20 eV [16], whereas the band gap of the GT composites has been reduced from value 2.9 eV (sample GT-2) to value 2.6 eV for sample GT-6. It can be considered that the introduction of graphene could reduce the bandgap of TiO_2 and extend the photo-activity of TiO_2 to visible light region.

The morphologies and microstructures of the series GT composite are investigated by SEM. As shown in Fig. 3a, after thermal treatment, the bare

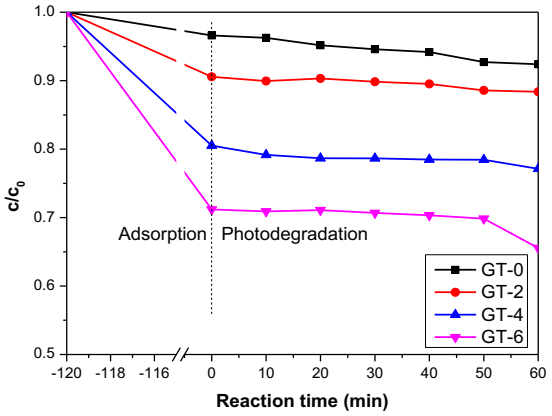
TiO_2 powder (sample GT-0) shows an irregular particulate morphology and has obvious agglomeration with particles size ~2 μm. After being modified by the graphene, the TiO_2 particles become uniformly. The phenomenon suggests that graphene can prevent the aggregation of the TiO_2 particles to a certain extent. The partial aggregated TiO_2 particles could be attributed to the weak adhere strength between the TiO_2 particles and the graphene. Meanwhile, the graphene sheet can be clearly observed in samples GT-2, GT-4 and GT-6. The pore sizes of the network are formed in the range of submicrometer to several micrometers and the walls consist of thin layers of stacked graphene sheets. Particularly, the pore sizes and numbers increase with an increase amount of graphene.

The potential application of 3D GT samples as a reusable organic pollutant scavenger is investigated by chosen MB as model probe. Before measurement, the same amount of the series GT samples was added into MB dye molecule solutions. After that, all suspensions were stirred for 90 min in the dark to achieve the adsorption and desorption equilibration. Then under irradiation, the TiO_2 were excited and the photogenerated carriers could transfer to the nearby MB and take part in the redox reactions, leading to the decomposition of MB into CO_2 and H_2O [17]. The UV-vis optical absorption of sample GT-6 is shown in Fig. 4a. In the presence of GT-6, the absorption intensity is almost 6, 3 and 1.5 times lower than that in the presence of bare TiO_2 powder (sample GT-0), GT-2 and GT-4, respectively, revealing that GT-6 possesses higher dye adsorption capacity in comparison with other GT samples and bare TiO_2 powder.

The photodegradation of MB is further investigated after MB is adsorbed on the surface of the series GT composites. The normalized temporal concentration changes (c/c_0) of MB during the decontamination were derived from the changes in the dye's absorption profile (λ= 660 nm) at a given time interval. Fig. 4b shows the time dependent absorption spectra of MB solutions during simulated visible light irradiation in the presence of different photocatalysts. The *Y*-axis is reported as c/c_0, where c_0 and c are the initial and actual concentration of MB at different reaction times, respectively. It is clear that the GT-6 sample shows significant progress in the decontamination of MB compared to bare TiO_2 powder (GT-0) and other GT samples. Under visible light irradiation, about 8% of the initial dyes were decomposed by GT-6 after 1 h. In contrast, only ~3% of the initial dyes were decomposed after the same time period for bare TiO_2 powder. More importantly, we found that the photocatalytic activities of GT samples enhanced with the increase of the amount of graphene. The phenomenon confirms that the photocatalytic activity of TiO_2 in visible light region could be improved by introduction of graphene.



(a)



(b)

FIGURE 4
(a) UV−vis absorption spectra of original MB solution, and the adsorptive MB solutions in the presence of sample GT-6 with different irradiation time of visible light; (b) Relative changes of the absorption peak intensity as a function of reaction time in the presence of the series GT composites.

The key advance of GT-6 with enhanced adsorptivity should first be assigned to the high adsorption capacity, which is a perquisite for good photocatalytic activity. As mentioned above that 3D GT-6 sample exhibits lots of pores with size of several micrometer, we believe that the adsorptivity originating from physical adsorption will contribute to the enhancement in the photocatalysis. Furthermore, considering the specific structure of the model organic aromatic pollutant MB, the enhanced adsorptivity should also be attributed to the selective adsorption of the aromatic dye on the aromatic regions of the graphene by π-π electron coupling [18, 19]. In addition, taking into account the chemically bonded TiO_2 particles and graphene in the 3D network of GT-6, graphene is recognized as an acceptor of the photogenerated electrons by TiO_2, which expands the light absorption range and ensures fast charge transportation (to suppress the electron-hole recombination) in

view of its high conductivity [20, 21]. Therefore, the electrons could transfer stereoscopically in GT-6 through the 3D graphene networks [22], leading to an improvement in photocatalysis of MB by GT-6 sample.

CONCLUSION

In summary, we demonstrated the synthesis of 3D graphene-TiO_2 hydrogels by using commercial TiO_2 powder and graphene oxide. The obtained GT hydrogels exhibited well-defined interconnected 3D porous microstructure. The spherical structured TiO_2 particles with a uniform size were densely decorated onto the graphene sheets. The resultant GT samples showed the synergistic effects of the self-assembly of graphene sheets and TiO_2 particles. For adsorption capacity and photodegradation, the incorporation of TiO_2 particles and graphene nanosheets not only increased the surface area of the hydrogel materials but also expanded the light absorption range and enabled fast charge transportation, which enhanced capacity of rapidly adsorbing and photodegrading organic dyes.

ACKNOWLEDGEMENTS

This work was supported by National Natural Science Foundation of China No. 11474310, Key projects of Anhui Provincial Department of Education (No. KJ2017A406, No. KJ2017A401, No. KJ2016A749, No. KJ2015A150), Quality Engineering Projects of Anhui Province (No.2015gkk015, No.2015jyxm284, No. 2016gxx153) and Program of West Anhui University.

REFERENCES

[1] Li, Y., Wang, H., Xie, L., Liang, Y., Hong, G. and Dai, H. (2011) MoS_2 nanoparticles grown on graphene: an advanced catalyst for the hydrogen evolution reaction. Journal of the American Chemical Society. 133(19), 7296-7299.

[2] Yin, S., Zhang, Y., Kong, J., Zou, C., Li, C.M., Lu, X., Ma, J., Boey, F.Y.C. and Chen, X.D. (2011) Assembly of graphene sheets into hierarchical structures for high-performance energy storage. Acs Nano. 5(5), 3831-3838.

[3] Chandra, V., Park, J., Chun, Y., Lee, J.W., Hwang, I.C., Kim, K.S. (2010) Water-dispersible magnetite-reduced graphene oxide composites for arsenic removal. ACS Nano. 4, 3979−3986.

[4] Zhang, H., Lv, X., Li, Y., Wang, Y. and Li, J. (2010) P25-graphene composite as a high performance photocatalyst. ACS Nano 4, 380-386.

[5] Xu, Y.X., Sheng, K.X., Li, C., Shi, G.Q. (2010) Self-assembled graphene hydrogel via a one-step hydrothermal process. ACS nano. 4(7), 4324.

[6] Gao, H.C., Xiao, F., Ching, C.B., Duan, H.W. (2012) High-performance asymmetric supercapacitor based on graphene hydrogel and nanostructured MnO_2. ACS applied materials & interfaces. 4(5), 2801-2810.

[7] Tang, Z., Shen, S., Zhuang, J. and Wang, X. (2010) Noble-metal-promoted three-dimensional macroassembly of single-layered graphene oxide. Angew. Chem. Int. Ed. 49, 4603-4607.

[8] Hou, C., Zhang, Q., Li, Y., Wang, H. (2012) P25-graphene hydrogels: Room-temperature synthesis and application for removal of methylene blue from aqueous solution. Journal of Hazardous Materials. 205-206, 229-235.

[9] Zhang, Z., Xiao, F., Guo, Y., Wang, S. Liu, Y. (2013) One-Pot Self Assembled Three Dimensional TiO_2-Graphene Hydrogel with Improved Adsorption Capacities and Photocatalytic and Electrochemical Activities. ACS Appl. Mater. Interfaces. 5, 2227−2233.

[10] Stankovich, S., Dikin, D.A., Piner, R.D., Kohlhaas, K.A., Kleinhammes, A., Jia, Y., Wu, Y., Nguyen, S.T., Ruoff, R.S. (2007) RS: Synthesis of graphene-based nanosheets via chemical reduction of exfoliated graphite oxide. Carbon. 45(7), 1558–1565

[11] Stengl, V., Popelkova, D., Vlacil, P. (2011) TiO_2 graphene nanocomposite as high performance photocatalysts. J Phys Chem C. 115(51), 25209–25218.

[12] Zhang, Y., Tang, Z.-R., Fu, X., Xu, Y.-J. (2010) TiO_2-graphene nanocomposites for gas-phase photocatalytic degradation of volatile aromatic pollutant: is TiO_2-graphene truly different from other TiO_2-Carbon composite materials. ACS Nano. 4(12), 7303–7314.

[13] Christy, A.A., Kvalheim, O.M., Velapoldi, R.A. (1995) Quantitative-analysis in diffuse reflectance spectrometry - a modified Kubelka-Munk equation. Vib Spectrosc. 9(1), 19–27.

[14] Reddy, K.M., Manorama, S.V., Reddy, A.R. (2003) Bandgap studies on anatase titanium dioxide nanoparticles. Mater Chem Phys. 78(1), 239–245.

[15] Tauc, J., Grigorov, R., Vancu, A. (1966) Optical properties and electronic structure of amorphous germanium. Phys Status Solidi. 15(2), 627–637.

[16] Serpone, N., Lawless, D., Khairutdinov, R. (1995) Size effects on the photophysical properties of colloidal anatase TiO_2 particles - size quantization or direct transitions in this indirect semiconductor. J Phys Chem. 99(45), 16646–16654.

[17] Oliveira, L.C.A., Coura, C.V.Z., Guimarães, I.R., Goncalves, M. (2011) Removal of organic dyes using Cr-containing activated carbon prepared from leather waste. J. Hazard. Mater. 192, 1094-1099.
[18] Xu, J., Wang, L. and Zhu, Y. F. (2012) Decontamination of bisphenol A from aqueous solution by graphene adsorption. Langmuir. 28(22), 8418-8425.
[19] Wang, J.F., Tsuzuki, T., Tang, B., Hou, X.L., Sun, L. and Wang, X.G. (2012) Reduced graphene oxide/ZnO composite: reusable adsorbent for pollutant management. ACS applied materials & interfaces. 4(6), 3084-3090.
[20] Chen, X. and Mao, S.S. (2007) Titanium dioxide nanomaterials: synthesis, properties, modifications and applications. Chem. Rev. 107(7), 2891-2959.
[21] Yuan, J., Li, Y., Qiu, F., Zhang, T., Xu, J. and Li, P. (2017) Preparation of graphene/carboxymethyl cellulose/TiO2 composites for the removal of malachite green. Fresen. Environ. Bull. 26, 4969-4979.
[22] Hou, C.Y., Zhang, Q.H., Li, Y.G., Wang, H.Z. (2012) P25–graphene hydrogels: Room-temperature synthesis and application for removal of methylene blue from aqueous solution. Journal of hazardous materials. 205, 229-235.

Received: **12.03.2017**
Accepted: **11.10.2017**

CORRESPONDING AUTHOR

Mingliang Chen
Jiangnan Graphene Research Institute,
Changzhou 213149 – China

E-mail: mlchen2011@aliyun.com

© by PSP Volume 26 – No. 12A/2017 pages 7740-7749 Fresenius Environmental Bulletin

BIOSORPTION AND SEPARATION/PRECONCENTRATION OF LEAD AND NICKEL ON *RHODOCOCCUS RUBER* BIOMASS

Esin Kiray[1], Cigdem Er[2], Ergin Kariptas[3], Harun Ciftci[4,*]

[1]Ahi Evran University, Faculty of Science and Arts, Department of Biology, Kirsehir, Turkey
[2]Ahi Evran University, Mucur Vocational Training School, Kirsehir, Turkey
[3]Ahi Evran University, Faculty of Medicine, Department of Microbiology, Kirsehir, Turkey
[4]Ahi Evran University, Faculty of Medicine, Department of Biochemistry, Kirsehir, Turkey

ABSTRACT

At the present time emphasis is given to the utilization of microorganisms because of their great ability to absorb metal ions from aqueous solution. Hence, in this study, Pb^{2+} and Ni^{2+} ions at trace levels were separated and preconcentrated on a column containing a bacterium, *Rhodococcus ruber* bacterial biomass (RrBB), as a new solid phase extraction technique prior to their flame atomic absorption spectrometry (FAAS) determination. The optimum experimental and analytical parameters such as pH of sample solution, volume and concentration of eluent, flow rate of sample solution and eluent, sample volume, effect of common matrix ions and capacity of biosorbent were investigated and optimized. Under the optimized conditions, the preconcentration factors for Pb^{2+} and Ni^{2+} were calculated as 150 and 100, respectively. The analytical detection limits for Pb^{2+} and Ni^{2+} were 0.32 µg L^{-1} and 0.24 µg L^{-1} respectively. The Langmuir monolayer adsorption capacity of biomass was estimated as 42.91 and 6.78 mg g^{-1} for Pb^{2+} and Ni^{2+}, respectively. Certified reference material (NIST SRM 1640a) was also used to confirm the accuracy of the method. The developed solid phase extraction method was applied successfully for the determination of Pb^{2+} and Ni^{2+} in various water samples.

KEYWORDS:
Preconcentration, Separation, Lead, Nickel, *Rhodococcus ruber*.

INTRODUCTION

There is high interest in the determinations of Pb^{2+} and Ni^{2+} ions in environmental, food and biological samples due to their being extremely toxic for human and animal health [1, 2]. It has been demonstrated that heavy metals may play a role in the pathogenesis of diseases of nervous system such as multiple sclerosis, amylotrophic sclerosis, and Alzheimer's [3].

In the recent years there has been great interest in the determinations of Pb^{2+} and Ni^{2+} ions in environmental, food and biological samples owing to their excessive toxic nature for human and animal health [1].

Lead is a pollutant that is present in all habitats and high levels of it typically associated with severe health effects such as pathophysiological changes, brain and kidney damage, infertility, miscarriage, hypertension, provokes irritability, anorexia, malaise and headache for human. The indiscriminate disposal of lead into wastewaters by industrial activities can contaminate the ecosystems and often cause diseases. During recent years that case has been increasing worldwide and this has been a major concern in developing countries [4, 5].

Nickel is found in soils, meteorities and on the ocean floor. This element is widely used in the manufacter of many alloys and products such as stainless steel, ceramic paint, computer components, surgical and dental prosthesis, magnetic tapes, jewelry, kitchen ware, batteries, textiles and coins [6, 7]. Nickel can enter a water supply by dissolution of rocks and soils, industrial and consumer waste, biological cycles, acidic rain breaking down soils, releasing heavy metals into streams, lakes, rivers, and groundwater.[6] Nickel and its many organic compounds are very toxic and known carcinogen. It has been reported that general short and longer terms effects of Nickel can include irritation of the skin, eye irritation, allergic reactions in the skin and respiratory tract and asthma, kidney diseases, gastrointestinal distress, inflammation of the lungs, cancer of the lung and nose, particularly the sinuses [7, 8, 9].

World Health Organization (WHO) established a provisional tolerable weekly intakes (PTWI) of Pb^{2+} as 25.0 µg kg^{-1} body weight (equivalent to 3.5 µg kg^{-1} of body weight per day) for all human groups on the basis that lead is a cumulative poison, and Ni^{2+} was updated by WHO, in 2007, as 11 µg kg^{-1} of body weight [10, 11].

Recent publication stress, the growing importance of sensitive and accurate determinations

of elements at trace level in the field of the analytical and environmental chemistry [12]. Determination of trace metal ion excisting at trace levels particularly in natural matrices are in need of removing interfering matrix components and efficient preconcentration step to satisfy its determination requirements by atomic spectrometry [13].

Separation and preconcentration procedures have a very vital role for the sake of sample preparation, removing process and inorganic and organic trace analysis for environmental and analytical purposes. In order to remove specific components of the sample which are commonly toxic metal ions and/or harmful organic compounds from various samples, solid phase extraction (SPE) has been one of the preferred procedures. It has some important advantages such as simplicity, versatility, rapid phase separation, reproducibility, high preconcentration factors, low cost (because of lower consumption of reagents), flexibility, high recovery and more importantly it is environmentally friendly [6, 14]. In the SPE process trace elements require solid sorbent materials, such as Amberlite and Duolite XAD resins, activated carbon, cellulose, modified silica gel, polymeric resin, nanomaterials and biomass [15].

Owing to their advantages of large surface area, low cost, availability, profitability and high efficiency biomass, have gained interest over other materials as the solid phase for SPE to improve the sensitivity of atomic spectrometry [16]. Variations in the cell wall composition among the different microorganisms sucn as bacteria, algae, cyanobacteria and fungi cause significant differences in the type and amount of metal ion binding to them [17, 18]. Heavy metal adsorption using Gram positive bacteria appear to be stronger compared to Gram negative bacteria [19].

R. ruber, is a gram positive non-pathogenic species of the genus *Rhodococcus,* which is a part of the phylogenetic group nocardioform actinomycetes. These widely occurring microorganisms are of considerable environmental, biotechnological and clinical due to their ability to catobolize a wide range of compounds, to produce bioactive substances including acrylamide, to metabolize harmful environmental pollutants including toluene and herbicides [20, 21]. Additionally, the genus *Rhodococcus* has cell walls of chemotype IV, which means that the only diamino acid in the peptidoglycan is meso-diaminopimelic acid and that the major sugars are arabinose and galactose [22, 23].

In this work, a preconcentration method was developed by using *Rhodococcus ruber* bacterial biomass (RrBB) for the determinations of Pb^{2+} and Ni^{2+} in various water samples by high-resolution continuum source flame atomic absorption spectrometry (HR-CS FAAS). RrBB was used for the first time as biosorbent, for separation and enrichment of Pb^{2+} and Ni^{2+} ions in different waters samples such as commerical drinking water, tap water, mineral water and wastewater. Various experimental and analytical parameters, such as pH of sample solution, sample volume, flow rate of sample solution and eluent, volume and concentration of eluent, amount of biomass, effect of other ions, and capacity of biosorbent were investigated. The proposed method was applied for the determination of trace amounts of Pb^{2+} and Ni^{2+} in various water samples and standard reference materials (NIST SRM 1640a) with satisfactory results.

EXPERIMENTAL

Apparatus. The analysis was performed by ContrAA 300, a HR-CS FAAS (Analytik Jena AG, Jena, Germany), equipped with a 50 mm burner head. An acetylene flame (C_2H_2) was used for atomization of Pb^{2+} and Ni^{2+}. All absorption lines of elements in the spectral range of 185–900 nm can be analytically evaluated by using a Xe short-arc lamp as a continuum lamp source [24]. The spectral background of the sample in the HR-CS FAAS was always corrected directly on the analysis line simultaneously and independently. The operating conditions for Pb^{2+} and Ni^{2+} by HR-CS FAAS are given in Table 1.

TABLE 1
The operating conditions for HR-CS AAS

Parameters	Pb	Ni
Wavelength, nm	217.0005	232.0030
Flow rate of C_2H_2-air, L h^{-1}	65	60
Burner height, mm	8	6
Evaluation Pixels, pm	3	3
Background correction	Simultaneous	Simultaneous

Reagents and solutions. All of the reagents used were of analytical grade. All aqueous solutions were prepared with ultrapure water that had been obtained by Milli-Qwater purification system (Millipore, Corporation, MA, USA). Standard solution of Pb^{2+} and Ni^{2+} with concentration of 1,000 µg mL^{-1} was purchased from (Merck). In the study buffer solutions (Merck) of sodium acetate-acetic acid (for pH 3–5), sodium monohydrogen phosphate–potassium dihydrogen phosphate (for pH 6–8), and ammonium chloride–ammonia (for pH 9) were used. Calibration standards of Pb^{2+} and Ni^{2+} were obtained by suitable dilutions of the stock solutions. The required pH adjustments were made by 0.1 mol L^{-1} NaOH or 0.1 mol L^{-1} HCI solutions.

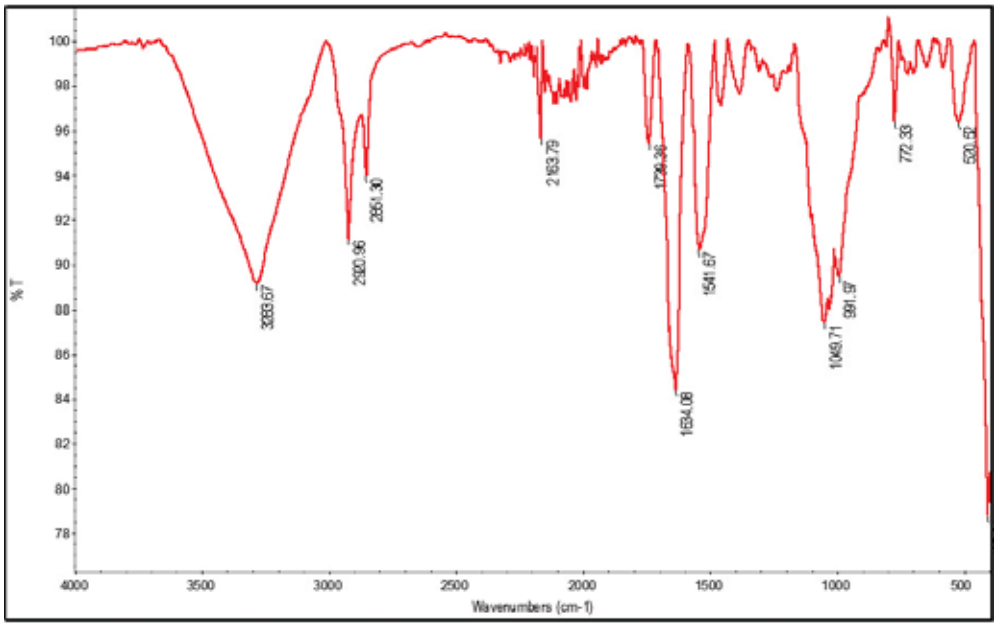


FIGURE 1
IR spectrum of RrBB

Growth of *Rhodococcus ruber.* Single colony isolates of *Rhodococcus ruber* JCM 0205 (JCM, Japanese Collection of Microorganisms) were grown up on GYEA streak plates at 30°C for 72 hours. These cultures were then used to inoculate sterile mineral salts medium (500 ml) in 2 L flasks, which were subsequently incubated at 30°C with shaking at 160 rpm in an orbital shaker. Cells were harvested at logarithmic phases by centrifugation at 9000 rpm for 20 minutes. The cells were stored by freezing them at -70°C, followed by freeze drying [25].

The FT-IR and SEM analysis. Fig.1. shows the FT-IR spectra of the RrBB (FT-IR, Model Nicolet 6700 FT-IR Spectrometer, Thermo Scientific). The broad band at 3283 cm^{-1} indicates the presence of hydroxyl groups. The peaks observed at 2920 cm^{-1} and 1634 cm^{-1} can be assigned to the C-H group and C=C stretching, respectively. The region between 1610 and 1500 cm^{-1} is associated with C-C stretching in aromatic rings found on the lignin structure. Elemental analysis of RrBB is shown in Table 2. (FLASH 200 CHNS/O Analyzers, Thermo Scientific)

TABLE 2
Elemental analysis of RrBB

Material	%C	%N	%H	%S
RrBB	49.7240	3.5560	7.6446	0.144

The morphology of the RrBB was assessed by scanning electron microscopy (SEM, Model–JSM-7600F) and the SEM patterns are shown in Fig. 2. The surface of RrBB is irregular, porous, and the surface honeycomb holes can reach micron scale about 5 microns. The porous structure of RrBB has a relatively large specific surface area, and this surface characteristic would substantiate high adsorption through mass transport inside the sorbent.

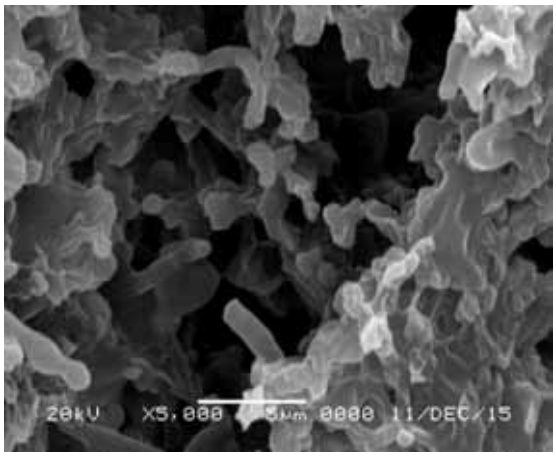


FIGURE 2
Scanning Electron Microscopy (SEM) image of RrBB

Column preparation. The glass column was 10 cm in length and 0.8 cm internal diameter. A small amount of glass wool was placed on the top and the bottom of the RrBB (0.3 g) to avoid disturbance during the sample passage. The biomass bed height in the column was approximately 2.0 cm. It was washed successively with water, 2 mol L^{-1} HCl and HNO_3 solutions, respectively. Before each cycle, the column was preconditioned by passing the blank solutions in working pH. The sample solution was permitted to flow through the column under gravity [26].

Separation/preconcentration procedure. The proposed procedure was tested with model solutions prior to the determination of Pb^{2+} and Ni^{2+} in real samples as off-line. The standard test solutions were prepared as follows: 1 mL of 5 mg L^{-1} of Pb^{2+} and Ni^{2+} standard solution added to 4 mL buffer solutions in a volumetric flask, and adjusted to a pH range of 3–9 with 0.1 mol L^{-1} of each HCl/NaOH.[6] Then, final volume was completed to 50 mL by deionized water. Before use, the column was preconditioned with the buffer solution for each working pH and then, the model solution was passed through the column at a flow rate of 4 mL min^{-1}. The adsorbed Pb^{2+} and Ni^{2+} ions on the column were eluted with 5 mL of 2 mol L^{-1} HCl solution that has a flow rate of 3 mL min^{-1}. The eluents were analysed for the determination of metal concentrations by HR-CS FAAS.

Preparation of water samples. Tap water was taken from Kırşehir water supply network while the river water was collected from Kızılırmak River. Commercial natural drinking water and mineral water were bought directly in a local supermarket in Kırşehir, Turkey. Wastewater sample was collected from the Organized Industrial Site in Kırşehir. For analysis, a 250 mL sample was placed in beaker and it was filtered through 0.45 μm cellulose nitrate membrane filters (Millipore) to remove suspended organic and other particles. An appropriate amount of buffer solutions and known amounts of analyte ions were mixed in a volumetric flask. Before use, the column was preconditioned by blank solution for each working pH. After the elution process, analyses of samples were performed according to the recommended preconcentration procedure.

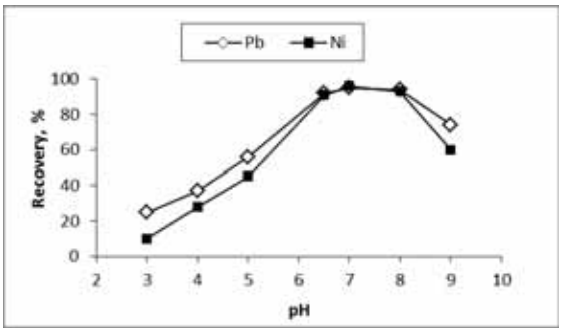


FIGURE 3
The effect of pH of sample solution on the recovery of Pb^{2+} and Ni^{2+}.

RESULTS AND DISCUSSION

Effect of Ph. The pH of the working solutions in the solid phase extraction is one of the critical parameters for quantitative recoveries of the analytes [27]. The determination of the recoveries of the analytes were set through the application of the preconcentration procedure by changing the pH of model solution in the range of 3.0–9.0. The effect of the pH value on therecovery values are given in Fig. 3. As shown in the figure, the adsorption percentage increases with the rise of pH and the highest recovery values were found in the pH ranging 6.5 - 8.0. The recoveries of Pb^{2+} and Ni^{2+} were found to decrease when the solutions pH is over 8.0 and less than 6.5. Therefore, pH 7.0 was selected as an optimum pH for adsorption and recovery of the analyte ions for subsequent studies.

Eluent effects: concentration, volume and flow rate. For the elution of the trace metals adsorbed on the biomass, dilute acid solutions with different concentrations and volumes were investigated. In order to choose the most effective eluent for desorbing, different concentration of HCl and HNO_3 solution were used for desorption. It has been found that particularly the hydrochloric acid solution provided higher recovery efficiency compared to the other solution. Thus, 5 mL of 2 mol L^{-1} HCI solution was used as eluent for desorption of metal ions from RrBB was used for subsequent measurements. The effects of various eluents on the recoveries of lead and nickel ions are summarized in Table 3.

The flow rate effect of eluent solution (5 mL of 2 mol L^{-1} HCl) on the recovery of Pb^{2+} and Ni^{2+} ions was examined in the range of 1.0–5.0 mL min^{-1} at optimum conditions. The recovery of analyte ions ranged between 95 and 100% at the eluent flow rates varying up to 3.0 mL min^{-1}. To decrease the analysis time, the eluent flow rate was chosen as 3.0 mL min^{-1} for Pb^{2+} and Ni^{2+}.

TABLE 3
The effect of eluent type on recovery of Pb^{2+} and Ni^{2+}

Eluent	Recovery (%) *	
	Pb^{2+}	Ni^{2+}
1 mol L^{-1} HCl, 5 mL	91±1	88±2
1 mol L^{-1} HCl, 10 mL	94±2	90±3
2 mol L^{-1} HCl, 5 mL	99±2	96±1
2 mol L^{-1} HCl, 10 mL	95±1	98±1
1 mol L^{-1} HNO_3, 5 mL	66±3	64±1
1 mol L^{-1} HNO_3, 10 mL	78±2	67±2
2 mol L^{-1} HNO_3, 5 mL	81±1	78±2
2 mol L^{-1} HNO_3, 10 mL	84±2	85±2

* Results are mean ± standard deviation of three replicate analyses.

Effect of flow rate of samples and sample volume. One of the characteristics of the flow rate of the sample in the adsorption process of Pb^{2+} and Ni^{2+} ions is that it determines the contact time of the sample solution with the solid phase adsorbent. The effect of the flow rate of sample solutions on the recovery of analytes was varied within the range of 1-7 mL min^{-1}. The optimum value for the flow rate of the sample solution was found to be up to 4 mL min^{-1}. Above this value, the recovery decreased

gradually which lead to the selection of the flow of 4 mL min^{-1} for Ni^{2+} and Pb^{2+} (Fig. 4). In the analysis of real samples, the sample volume or breakthrough volume is one of the most important parameters which has aninfluence on the enrichment factor [28]. For this purpose, aqueous solutions containing 5 µg Pb^{2+} and Ni^{2+} were preconcentrated from sample volumes in the range of 50 - 1000 mL. The recoveries of analyte were quantitative (>95%) for sample volumes up to 750 mL and 500 mL for Pb^{2+} and Ni^{2+}, respectively (Fig.5). The preconcentration factor (PF) is calculated by the ratio of the highest sample volume (750 mL for $Pb^{2+}$and 500 mL for Ni^{2+}) and the final lowest volume (5.0 mL). Maximum preconcentration factors for Pb^{2+} and Ni^{2+}were found to be as 150 and 100, respectively.

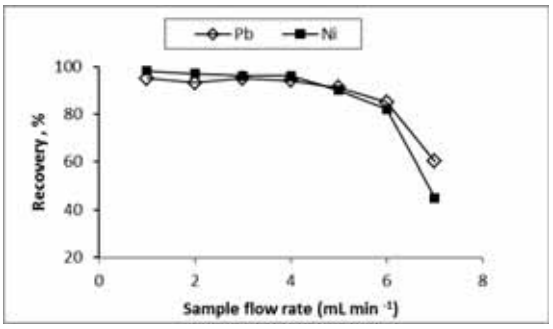


FIGURE 4
Effect of sample flow rate on the recovery of Pb^{2+} and Ni^{2+}.

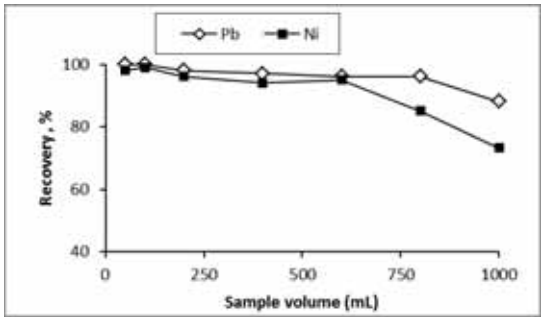


FIGURE 5
Effect of sample volume on the recovery of Pb^{2+} and Ni^{2+}.

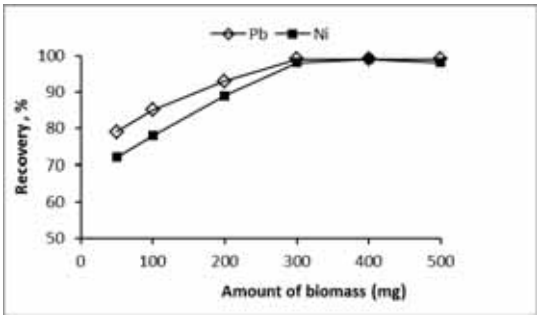


FIGURE 6
Effect of biomass amount on the recovery of Pb^{2+} and Ni^{2+}.

Effect of amounts of RrBB. The effects of amount of RrBB on the sorption of metal ions at optimum pH were found to be in the range of 50–500 mg. As seen in Fig. 6, the quantitative recoveries were obtained in range of 200–500 mg for Pb^{2+} and 300–500 mg for Ni^{2+}. Therefore, 300 mg of RrBB was selected for further studies.

Effect of interfering ion. Accompanying ions in various real samples, the effect of some foreign ions which interfere with the determination of the understudy ions was examined with the optimized conditions. In order to examine the selectivity of the method, the influences of some cations and anions on the solid phase extraction and determination of Pb^{2+} and Ni^{2+} were investigated. In these experiments, 50 mL solutions containing 5 µg of Pb^{2+} and Ni^{2+} ions and matrix ions were treated according to the preconcentration procedure. The recovery values given in Table 4 show no significant interferences up to 1000 mg L^{-1} of K^+, Ca^{2+} and Mg^{2+}, 2000 mg L^{-1} of Na^+, 10 mg L^{-1} of Zn^{2+} Cu^2, Co^{2+}, Cd^{2+}, Cr^{3+} and Fe^{3+} ions in the separation and determination of Pb^{2+} and Ni^{2+} ions at pH 7.0.

TABLE 4
Effect of matrix on the recovery of Pb^{2+} and Ni^{2+}

Foreign ions	Concentration (mg L^{-1})	Recovery (%) *Pb^{2+}	Recovery (%) *Ni^{2+}
K^+	1000	97±2	100±3
Na^+	2000	98±2	95±1
Ca^{2+}	1000	98±1	96±2
Mg^{2+}	1000	100±2	98±3
Zn^{2+}	10	98±2	96±3
Cu^{2+}	10	95±2	96±1
Co^{2+}	10	97±2	98±2
Cd^{2+}	10	98±2	98±2
Cr^{3+}	10	97±1	96±2
Fe^{3+}	10	96±3	100±3

* Results are mean ± standard deviation of three replicate analyses.

Capacity of the biomass. The adsorption isotherm models are normally used to describe the interaction between adsorbents and adsorbates, providing most important parameters for designing a desired adsorption system [29].

The obtainment of the adsorption capacity of biomass was ensured through batch experiments. For this purpose, 100 mg of biomass was added into a 250 mL flask containing 100 mL of model solution which has various concentrations of analyte ion under the optimum experimental conditions. After this procedure, The prepared solutions containing different amount of analytes were shaken for 2 h at 150 rpm at room temperature. Then, 10 mL of supernatant was taken from each solution and analytes ions in the solutions after dilution steps were determined by HR-CS FAAS.

In order to indicate the adsorption type and descrive the equilibrium isotherm, the Langmuir

adsorption model was applied.The linearized equation form of the Langmuir model used to evaluate maximum metal uptake is expressed by the following equation:

$C_e/q_e = C_e/q_{max} + 1/ K_L q_{max}$

In this equation, C_e is considered as the final metal concentrations in the solution at equilibrium (mg L^{-1}), q_e is the amount of sorbed metal ionsper gram of sorbent at equilibriums (mg g^{-1}), K_L is a constant related to the energy of adsorption/desorption (L g^{-1}) and q_{max} is the maximum adsorption capacity of sorbent (mg/g).

Langmuir model had been pointed out to fit the experimental data well, with the correlation coefficients (R^2) 0.913 and 0.876 for Pb^{2+} and Ni^{2+}, respectively. The Langmuir monolayer adsorption capacitys (q_{max}) were estimated as 42.91 and 6.78 mg g^{-1} for Pb^{2+} and Ni^{2+}, respectively. Constants of the energy (K_L) for Pb^{2+} and Ni^{2+}were calculated as 0.024 and 0.09 L g^{-1} respectively (Fig. 7, 8). High correlation coefficients indicate that the adsorption of Pb^{2+} and Ni^{2+} on the sorbent comply with the Langmuir adsorption isotherm. In other words, the solid surface displays a finite number of identical sites that are genetically uniform, and no interactions between adsorbed species, and a monolayer adsorption are established when the solid surface reaches saturation [30].

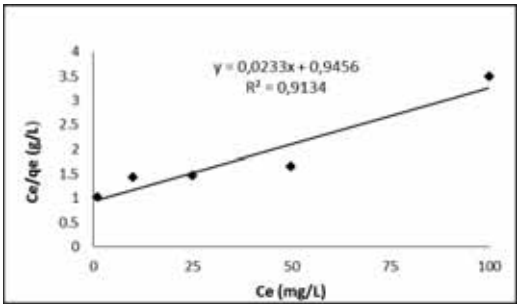


FIGURE 7
Adsorption isotherm of Pb^{2+} on RrBB

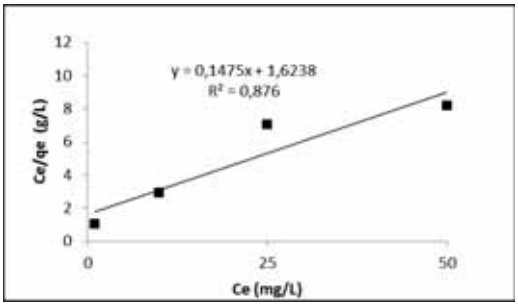


FIGURE 8
Adsorption isotherm of Ni^{2+} on RrBB

Analytical features. Under the optimum experimental conditions, linear dynamic ranges, correlation coefficients, limit of detections (LOD)s, precision and accuracy were examined. By using direct aspiration in HR-CS FAAS without applying the preconcentration system the linear dynamic ranges were obtained 0.10 –10.0 mg L^{-1} (R^2= 0.9998) and 0.05–5.0 mg L^{-1} (R^2= 0.9999) of lead and nickel, respectively. The limit of detection (LOD) is defined as three times of the mean values of standard deviation (SD) of blanks [31]. LODs were found as 0.32 µg L^{-1} for Pb^{2+} and 0.24 µg L^{-1} for Ni^{2+}. The precision of this procedure was examined by seven replicate measurements of 50 mL of sample solutions including 100 µg L^{-1} analytes ions. The mean recoveries for Pb^{2+} and Ni^{2+} were obtained as 98.6 % and 98.2 %, with the relative standard deviations (RSD) of 2.5 % and 2.1 %, respectively.

TABLE 5
Analytical performance and optimum condition of the proposed method for determination Pb2+ and Ni2+.

	Pb^{2+}	Ni^{2+}
pH	7.0	7.0
Amount of biomass (mg)	300	300
Eluent volume (2 mol L^{-1}HCl, mL)	5	5
Eluet flow rate (mL min^{-1})	3	3
Sample flow rate (mL min^{-1})	4	4
Maximum sample volume (mL)	750	500
Enrichment factor	150	100
Linear range (mg L^{-1})	0.10–10	0.05–5.0
Regressione quation (mg L^{-1})	A=0.0479xC+ 0.00029	A=0.0937xC+ 0.00058
Correlation coefficient (R^2)	0.9998	0.9999
Detection limit (µg L^{-1})	0.32	0.24
Precision (R.S.D, N=7) (%)	2.5	2.1

TABLE 6
Application of the present method to the standard reference material (NIST SRM 1640a, trace elements in water, 50 mL)

Element	Certified (µg L^{-1})	Found[a] (µg L^{-1})	Recovery (%)
b^{2+}	12.101 ± 0.050	11.65±0.03	96.3
Ni^{2+}	25.32 ± 0.14	24.68±0.10	97.5

[a] Results are mean ± standard deviation of three replicate analyses.

Under the optimum experimental conditions, linear dynamic ranges, correlation coefficients, limit of detections (LOD)s, precision and accuracy were examined. With the use of direct aspiration in HR-CS FAAS without applying the preconcentration system the linear dynamic ranges were obtained 0.10–10.0 mg L^{-1} (R^2= 0.9998) and 0.05–5.0 mg L^{-1} (R^2= 0.9999) of lead and nickel, respectively.The limit of detection (LOD) is defined as three times of the mean values of standard deviation (SD) of blanks. LODs were found as 0.32 µg L^{-1} for Pb^{2+} and 0.24 µg L^{-1} for Ni^{2+}. The precision of this procedure was examined by seven replicate measurements of 50 mL of sample solutions including 100 µg L^{-1}

analytes ions. The mean recoveries for Pb^{2+} and Ni^{2+} were reached as 98.6 % and 98.2 %, with the relative standard deviations (RSD) of 2.5 % and 2.1 %, respectively (Table 5). The accuracy of the procedure was confirmed by analyzing certified materials (NIST SRM 1640a, trace elements in natural water). Results were the average of three replicates. As can be seen in Table 6 the measured mean value is not significantly different from the certified value. The obtained recovery values for accuracy of the method were greater than 95%.

Analysis of real samples. In order to assess the applicability and feasibility of method for the analysis of real samples with different matrices, the proposed procedure was applied to the separation and recovery of ions from commerical drinking water, tap water, mineral water, and wastewater samples. The accuracy of the proposed method was also checked by analyzing spiked samples. The data acquired were presented in Table 7. There are satisfactory agreements between added and found levels of analytes for all samples.

Comparison to Other Procedure. A comparison of the proposed procedure with other reported preconcentration procedures was given in Table 8. Analytical characteristics obtained for this study are comparable to many procedures in the table. The present work has relatively low LODs and RSDs when compared to other methods. Another parameter, PF (150 and 100 for Pb^{2+} and Ni^{2+}) is found to be relatively high when compared to other methods. The adsorption capacity of biomass for lead is higher than those in studies of Soylak et al. [32], Tuzen et al. [33], Mendil et al. [34] and Duran et al. [35]. Besides that adsorption capacity of biomass for nickel is higher than those in studies of Tuzen et al. (2008) [33] and Mendil et al. [34].

The high sorption capacity is one of the most paramount specifications for metals ions biosorbents. According to the biosorption mechanisms, the way to enhance the sorption capacity may change. Cell wall functional groups play important roles in the biosorption process.The sorption process by dead biomasses or biomaterials is of physical nature because it is independent of metabolism. Metals biosorption mechanism is generally regarded as physicochemical interactions between metal ions and the functional groups present on the surface of biosorbent. This includes electrostatic interactions, ion exchange and metal ion chelation or complexation, microprecipitation and reduction [37, 38, 39].

TABLE 7
Levels of for Pb^{2+} and Ni^{2+} ions in various water samples

	Pb^{2+}			Ni^{2+}		
Sample	**Added** ($\mu g\ L^{-1}$)	**Found*** ($\mu g\ L^{-1}$)	**Relative Error (%)**	**Added** ($\mu g\ L^{-1}$)	**Found*** ($\mu g\ L^{-1}$)	**Relative Error (%)**
Commerical drinking	0	3.5±0.3		0	ND	
water	5.0	8.3±0.6	-2.3	5.0	5.2±0.5	4.0
Tap water	0	2.4±0.2		0	ND	
	10.0	12.8 ±1.3	3.2	10.0	9.6±0.7	-4.0
Mineral water	0	4.6±0.4		0	ND	
	20.0	24.2±1.5	-1.6	20.0	20.5±1.4	2.5
Wastewater	0	26.3±1.6		0	16.2±1.2	
	10.0	37.4±1.8	3.0	10.0	25.7±1.6	-1.9

ND: Not detected
*Mean and standard deviation from three determinations.

TABLE 8
A comparison of the proposed procedure with other reported preconcentration procedures

Analyte	**Material**	**Procedure**	**PF**	**Capacitiy of adsorban (mg g^{-1})**	**LOD ($\mu g\ L^{-1}$)**	**RSD (%)**	**Ref.**
Pb, Ni	*Aspergillus fumigatus* immobilized Diaion HP-2MG	FAAS	50	7.1, 6.8	0.52, 0.59	<7	[32]
Pb, Ni	*Pseudomonas aeruginosa* immobilized on multiwalled carbon nanotubes	AAS	50	6.07, 5.25	2.60, 1.30	<10	[33]
Pb, Ni	Penicillium italicum – loaded on Sepabeads SP 70	AAS	-	12.4, 6.67	2.70, 1.33	-	[34]
Pb, Ni	*Anoxybacillus gonensis* immobilized on Diaion HP-2MG	FAAS	50, 75	8.43, 6.80	2.0, 1.1	8.7, 5.6	[35]
Pb, Ni	*A. niger* immobilized on silica gel, column technique	FAAS	50	-	5.2, 1.6	<7	[36]
Pb, Ni	*Rhodococcus ruber* biomass	FAAS	160, 120	42.91, 6.78	0.32, 0.24	2.3, 3.5	Present paper

CONCLUSIONS

Rhodococcusruber bacterial biomass (RrBB) was used as a new biosorbent, further more a new analytical technique was developed for the separation and preconcentration of lead and nickel ions in various water samples. The developed SPE method provides a simple, rapid, accurate, and an economical procedure. Other advantages of The developed method are its reproducibility, high preconcentration factor and low detection limit. The system was successful in preconcentration of analytes from large sample volume (500 and 750 mL). This study offered a nonpolluting technique for the preconcentration and determination of trace metals.

REFERENCES

[1] Er, C., Senkal, B.F., Yaman, M. (2013) Determination of lead in milk and yoghurt samples by solid phase extraction using a novel aminothioazole-polymeric resin. Food Chem. 137, 55–61.

[2] Kaygusuz, M.K., Isik, N.O., Erden, K.E. (2017) The removal of Pb(II) from aqueous solutıons by strong and weak acidic catıon Exchange resıns. Fresen. Environ. Bull. 26, 3448-3454.

[3] Mishra, K.P. (2009) Lead exposure and its impact on immune system: a review. Toxicol in Vitro. 23, 969–972.

[4] Sayar, O., Zhad, H.R., Sadeghi, O., Amani, V., Najafi, E., Tavassoli, N. (2012) Pyridine-functionalized Fe_3O_4 nanoparticles as a novel sorbent for the preconcentration of lead and cadmium ions in tree leaf as a bioindicator of urban traffic pollution. Biol Trace Elem Res. 150, 403-410.

[5] Celebi, S.Z., Ekin, Z. (2017) Evaluation of plant metal content and biomass yield for the phytoextraction of Pb and Cd by hydroponically cultivated crop. Fresen. Environ. Bull. 26, 3309-3313

[6] Ciftci, H., Yalcin, H., Eren, E., Olcucu, A., Sekerci, M. (2010) Enrichment and determination of Ni2+ ions in water samples with a diamino-4-(4-nitro-phenylazo)-1H-pyrazole (PDANP) by using FAAS Desalination. 256, 48–53.

[7] Kulkarni, R.M., Shetty, K.V., Srinikethan, G. (2014) Cadmium (II) and nickel (II) biosorption by Bacillus laterosporus (MTCC 1628). J. Taiwan Inst.Chem. Engineer. 45, 1628–1635.

[8] Zarei, Z., Shemirani, F. (2012) Determination of Nickel in Food Samples by Flame Atomic Absorption Spectroscopy after Preconcentration and Microextraction Based Ionic Liquids Using Full Factorial and Central Composite Design. J Food Sci. 77, 1242-1248.

[9] Uncumusaoglu, A.A., Sengul, U., Akkan, T. (2016) Environmental contamination of heavy metals in the Yaglıdere Stream (Giresun), Southeastern Black Sea. Fresen. Environ. Bull. 25, 5492-5498.

[10] World Health Organization (WHO) (2011) Lead in Drinking-water Background document for development of WHO Guidelines for Drinking-water Quality. WHO/SDE/WSH/03. 04/09, Rev1 13-14.

[11] World Health Organization (WHO) (2007) English only Nickel in Drinking-water Background document for development of WHO Guidelines for Drinking-water Quality. WHO/SDE/WSH/07.08/55, 16.

[12] Topuz, B., Macit, M. (2011) Solid phase extraction and preconcentration of Cu(II), Pb(II), and Ni(II) in environmental samples on chemically modified Amberlite XAD-4 with a proper Schiff base. Environ Monit Assess. 173, 709–722.

[13] Pourjavid, M.R., Arabieh, M., Yousefi, S.R., Jamali, M.R., Rezaee, M. Hosseini, M.H., Sehat, A.A. (2015) Study on column SPE with synthesized graphene oxide and FAAS for determination of trace amount of Co(II) and Ni(II) ions in real samples. Mater Sci Eng C Mater Biol Appl. 47, 114-122.

[14] Mortada, W.I., Kenawy, I.M., Abdelghany, A.M., Ismail, A.M., Donia, A.F., Nabieh, K.A. (2015) Determination of Cu(2+), Zn(2+) and Pb(2+) in biological and food samples by FAAS after preconcentration with hydro-xyapatite nanorods originated from eggshell. Mater Sci Eng C Mater Biol Appl. 52, 288-296.

[15] Ciftci, H., Temuz, M.M, Ciftci, E. (2013) Simultaneous preconcentration and determination of Ni and Pb in water samples by solid-phase extraction and flame Atomic absorption spectrometry. E. J. AOAC Int. 96, 875-879.

[16] Yalçınkaya, Ö., Erdoğan, H., Çiftçi, H., Türker, A.R. (2012) Preconcentration of Aluminum on Nano ZrO2/B2O3 and Its Determination by Flame Atomic Absorption Spectrometry. Spectros. Lett. 45, 344–351.

[17] Javanbakht, V., Alavi, S.A., Zilouei, H. (2014) Mechanisms of heavy metal removal using microorganisms as biosorbent. Water Sci Technol. 69, 1775-1787.

[18] Nilanjana, D., Vimala, R., Karthika, P. (2008) Biosorption of heavy metals–An overview. Indian J. Biotech. 7, 159-169.

[19] Kulkarni, R.M., Shetty, K.V., Srinikethan, G. (2014) Cadmium (II) and nickel (II) biosorption by Bacillus laterosporus (MTCC 1628). J. Taiwan Inst.Chem. Engineer. 45, 1628–1635.

[20] Lopez, L.Y., Merma, A.G., Torem, M.L., Pino, G.H. (2015) Fundamental aspects of hematite flotation using the bacterial strain *Rhodococcus ruber* as bioreagent. Min. Engin. 75, 63–69.

[21] Chen, B., Otten, L.G., Resch, V., Muyzer, G., Hanefeld, U. (2013) Draft genome sequence of *Rhodococcus rhodochrous* strain ATCC 17895. Stand Genomic Sci. 9, 175–184.

[22] Larkin, M.J., Kulakov, L.A., Allen, C.C. (2005) Biodegradation and Rhodococcus-masters of catabolic versatility. Curr Opin Biotechnol. 16, 282-290.

[23] Dastager, S.G., Mawlankar, R., Tang, S.K., Krishnamurthi, S., Ramana, V.V., Joseph, N., Shouche,Y.S. (2014) *Rhodococcus enclensis* sp. nov., a novel member of the genus Rhodococcus. Int J Syst Evol Microbiol. 64, 2693-2699.

[24] Yilmaz, M., Teber, C., Akkan, T., Er, C., Kariptas, E., Ciftci, H. (2016) Determination of heavy metal levels in different tıssues of tench (*Tınca tınca* L., 1758) from Sıddıklı Kucukbogaz Dam Lake (Kırsehir), Turkey, Fresen. Environ. Bull. 25, 1972-1977.

[25] Kariptaş, E. (1998) Chemical Composition of *Rhodococcus ruber* with Different Growth Conditions, PhD, University of Newcastle upon Tyne, UK.

[26] Ciftci, H., Er, C., Ozkan, M. (2015) Determination of aluminum from water samples and dialysis fluids after separation/ preconcentration on Duolite XAD-761 polymericresin. Desal. and Water Treat. 57, 6916-6924.

[27] Daşbaşı, T., Saçmacı, Ş., Ülgen, A., Kartal, Ş. (2015) A solid phase extraction procedure for the determination of Cd(II) and Pb(II) ions in food and water samples by flame atomic absorption spectrometry. Food Chem. 174, 591–596.

[28] Pirouz, M.J., Beyki, M.H., Shemirani, F. (2015) Anhydride functionalised calcium ferrite nanoparticles: A new selective magnetic material for enrichment of lead ions from water and food samples. Food Chem. 1, 131-137.

[29] Barnabas, M.J., Parambadath, S., Mathew, A., Park, S.S., Vinu, A., Ha, C. (2016) Highly efficient and selective adsorption of In3+ on pristine Zn/Al layered double hydroxide (Zn/Al-LDH) from aqueous solutions. J. Solid State Chem. 233, 133–142.

[30] Bunluesin, S., Kruatrachue, M., Pokethitiyook, P., Upatham, S., Lanza, G.R. (2007) Batch and continuous packed column studies of cadmium biosorption by *Hydrilla verticillata* biomass. Journal of Bioscience and Bioengineering. 103, 509–513.

[31] Da Silva, P.A.B., De Souza, G.C.S., da S. Leotério, D.M., Belian, M.F., Silva, W.E., Paim, A.P.S., Lavorante, A.F. (2015) Synthesis and characterization of function-alized silica with 3,6-ditia-1,8-octanediol for the preconcentration and determination of lead in milk employing multicommuted flow system coupled to FAAS. J. of Food Compos. Analy. 40, 177–184.

[32] Soylak, M., Tuzen, M., Mendil, D., Turkekul, I. (2006) Biosorption of heavy metals on *Aspergillus fumigatus* immobilized Diaion HP-2MG resin for their atomic absorption spectrometric determinations. Talanta. 70, 1129–1135.

[33] Tuzen, M., Saygi, K.O., Usta, C., Soylak, M. (2008). *Pseudomonas aeruginosa* immobilized multiwalled carbon nanotubes as biosorbent for heavy metal ions. Bio Tech. 99, 1563–1570.

[34] Mendil, D., Tuzen, M., Soylak, M. (2008) A biosorption system for metal ions on *Penicillium italicum*-loaded on Sepabeads SP 70 prior to flame atomic absorption spectrometric determinations. J. Hazard. Mater. 152, 1171–1178.

[35] Duran, C., Bulut, V.N., Gundogdu, A., Soylak, M., Belduz, A.O., Beris, F.S. (2009) Biosorption of Heavy Metals by *Anoxybacillus gonensis* Immobilized on Diaion HP-2MG. Sep. Science and Tech. 335-358.

[36] Baytak, S., Koçyiğit, A., Türker, A.R. (2007) Determination of lead, iron and nickel in water and vegetable samples after preconcentration with *Aspergillus niger* loaded on silica gel. Clean, 35, 607 – 611.

[37] Rangabhashiyam, S., Suganya, E., Selvaraju, N., Varghese, L.A. (2014) Significance of exploiting non-living biomaterials for the biosorption of wastewater pollutants. World J Microbiol Biotechnol. 30, 1669-1689.

[38] Won, S.W., Kotte, P., Wei, W., Lim, A., Yun, Y.S. (2014) Biosorbents for recovery of precious metals. Bioresour Technol. 160, 203-212.

[39] Vazquez-Palma, D.E., Netzahuatl-Munoz, A.R., Pineda-Camacho, G., Cristiani-Urbina, E. (2017) Biosorptive removal of nickel(II) ions from aqueous solutions by Hass avocado (Persea americana Mill. var. Hass) shell as aneffective and low-cost biosorbent. Fresen. Environ. Bull. 26, 3501-3513.

Received: **13.03.2017**
Accepted: **29.07.2017**

CORRESPONDING AUTHOR

Harun Ciftci
Ahi Evran University, Faculty of Medicine, Department of Biochemistry, Kirsehir-Turkey

e-mail: harunciftci@yahoo.com

© by PSP Volume 26 – No. 12A/2017 pages 7750-7755 Fresenius Environmental Bulletin

COMPARISON OF THE PHYSICOCHEMICAL PROPERTIES OF CHITOSAN EXTRACTED FROM SHRIMP SHELL WASTE WITH DIFFERENT DEACETYLATION DEGREES

Aygul Kucukgulmez[1,*], A Eslem Kadak[2], Ladine Celik[3], Afsin Farivar[3], Mehmet Celik[1]

[1]Cukurova University, Faculty of Fisheries Department of Seafood Processing Technology, Adana, Turkey
[2] Kastamonu University, Faculty of Fisheries, Kastamonu, Turkey
[3]Cukurova University, Faculty of Agriculture, Department of Animal Science, Adana, Turkey

ABSTRACT

In this study chitosan with different degrees of deacetylation have been extracted from deep sea pink shrimp (*Parapenaeus longirostris*) shells not evaluated and discarded as waste products to investigate the effect of deacetylation on physicochemical properties of chitosan. In order to determine physicochemical characterization of the chitosans; moisture and ash contents, degree of deacetylation, molecular weight, apparent viscosity, water and fat binding capacities, Fourier Transform Infrared Spectroscopy, Scanning Electron Microscopy and X-ray diffraction analyses were applied. In addition, the physicochemical characteristics of the chitosan extracted from *P. longirostris* shells were compared to the commercial chitosan. Low degree deacetylated chitosan exhibited a higher molecular weight, higher viscosity and higher water and fat binding capacities compared to the high degree deacetylated chitosan. Study findings are considered to be useful for the economic use of shrimp wastes in Turkey and light the way for future studies on other crustacean species.

KEYWORDS:
Chitosan, Deacetylation degree, *Parapenaeus longirostris* Physicochemical properties

INTRODUCTION

Chitin (poly- β-(1,4)-2-asetamide-2-deoxi-β-D-glucopyranose) is known as the most available biopolymer after cellulose in the world. Firstly produced from fungi, in our day chitin is mostly extracted from shellfish (crab, shrimp, lobster) and insect skeletons [1]. Chitosan (poly-[β-(1,4)-2-amino-2-deoxi-β-D- glucopyranose) is the deacetylated form of chitin and because of its polycationic structure, it can be more easily dissolved compared to the chitin; and it has more superior features [2].

Chitosan has different reactive functional groups and the chemical modification of these groups enables chitosan to be a useful material in several different fields [3]. It is commonly used in different sectors including especially food, chemistry, biotechnology, agriculture, veterinary, cosmetic, medicine, dentistry, environmental protection, textile, paper making and packaging [4]. Physicochemical properties of chitosan significantly affect the use of chitosan in all these sectors. These physicochemical properties can be ranged as deacetylation degree, molecular weight, viscosity, solubility, and colour. The most important one among these is "Deacetylation Degree."

Deacetylation degree is the removal of acetyl group from aminoacetyl groups which are found in the structure of chitin. Thereby, only amine group remains behind. Deacetylation degree affects chitosan's physical, chemical, and biological qualities such as base and electrostatic characteristics, biodegradability, self-aggregation, and sorption properties [5]. Deacetylation degree varies in accordance with the source of chitin, extraction method, the duration of reaction, NaOH concentration, and the temperature of reaction [6, 7]. Determination of the qualities of chitosan acquired in different deacetylation degrees is significantly important in different usage areas of chitosan. For this reason, in the present study, chitosan with different degrees of deacetylation were prepared to investigate the effect of deacetylation on physicochemical properties of chitosan. In the characterization of the chitosan, deacetylation degree, moisture and ash content, molecular weight, apparent viscosity, water and fat binding capacity, fourier transform infrared spectroscopy, scanning electron microscopy and X-ray diffraction were measured. In addition, chitosan extracted from *P. longirostris* was compared to commercial chitosan.

MATERIALS AND METHODS

Materials. Fresh samples of deep sea pink shrimp (*Parapenaeus longirostris*) wastes were collected from a local shrimp processing factory. Shells were completely separated from these wastes in laboratory, washed in pure water and dried at 60ºC.

Two commercial chitosan (low and high deacetylation degree) of Sigma Chemical was used

as a control to compare with the extracted chitosan in this study.

Extraction of Chitosan. Chitosan was extracted by the method of Chang et al. [8]. Deproteinization and demineralization steps were carried out with 2.5 N NaOH at 65 ºC for 6 hours and 1.7 N HCl at 25 ºC for 6 h, respectively. The chitin residue was treated with 9 vol. of hydrogen peroxide and dried at 90 ºC for 2 h. Two different deacetylated chitosan (low and high degree) was prepared by alkali treatment of chitin using % 50 (w/v) NaOH in distilled water at 120 ºC (50 and 240 minutes). The reactants were filtered, washed with deionized water to neutral pH and dried at 90 ºC for 2 h. LDEC: Low degree deacetylated extracted chitosan, HDEC: High degree deacetylated extracted chitosan, LDCC: Low degree deacetylated commercial chitosan, HDCC: High degree deacetylated commercial chitosan.

Characterization of Chitosan. (1) Deacetylation Degree. Deacetylation degree of chitosan was determined by a potentiometric titration method. 250.0 mg portion of chitosan were dissolved in 10.0 ml of 0.30 M HCl and after being diluted to 50.0 ml with ultrapure water, it was titrated with 0.10 M NaOH [9].

(2) The moisture and ash contents. The moisture was determined after drying samples for 24 h at 105ºC, and ash content was determined by heating at 530ºC for 20 h.

(3) Molecular Weight Determination. The viscosity average molecular weight of chitosan was calculated from experimental intrinsic viscosity data by using the Mark-Houwink equation [10].

(4) Apparent Viscosity. Chitosan solution was prepared in 1% (v/v) acetic acid at 1% (w/v) concentration on a moisture-free basis. Viscosity of chitosan was determined with an AMVn Automated Micro Viscometer (Anton Paar, Graz, Austria). Results were averages of seven determinations and s were reported as centipoises units (cP).

(5) Water and fat binding capacity. Water binding capacity (WBC) and fat binding capacities (FBC) of chitosan were measured using a modified method of Wang and Kinsella [11]. Water and fat absorption were carried out by weighing a centrifuge tube containing 0.5 g of sample, adding 10 ml of water and mixing for 1 min to disperse the sample and centrifuged at 3500 rpm for 25 min. After the supernatant was decanted, the tube was weighed again. The same process was applied for fat binding capacity.

(6) Fourier Transform Infrared Spectroscopy (FTIR). The infrared spectrum (IR) was performed in a Perkin Elmer spectrometer (model 550 FT-IR/FIR/NIR Spectrometer Frontier, ATR), in the region 500-4000 cm^{-1}. The spectrum was obtained using sample of chitosan powder, previously dried in oven for 24 hours at temperature of 90°C.

(7) Scanning Electron Microscopy (SEM). SEM characterization was carried out using a Zeiss-Supra 55 type instruments. Prior to analysis, the dried chitosan powder was coated with platinum with automatic coating machine. Images of the samples surfaces were recorded at different areas and magnifications.

(8) X-Ray Diffraction (XRD). X-ray diffraction data were collected on a Rigaku-SmartLab diffractometer the voltage and the current used were 40 kV and 30mA, and 2θ with a scan angle from 4 to 45, respectively. Chitosan was prepared by compressing it in the cassette sample holder without any adhesive substances.

RESULTS AND DISCUSSION

The results of the physicochemical parameters (deacetylation degree, moisture, crude ash, molecular weight, apparent viscosity, water and fat binding capacities) of chitosan extracted from *P. longirostris* shells are shown in Table 1.

Deacetylation degree shows the amount of the number of deacetylated N-acetyl-D-glucosamine units in proportion to total unit number. Physicochemical properties of chitosan change in accordance with the deacetylation degree and deacetylation degree can be regulated with regard to the place of use in industry. In the present study, the deacetylation degree determined through the potentiometric titration method was measured as 72.86% in the low-degree group while it was determined to be 93.70% in the high deacetylation degree group. There are various methods available to increase or decrease the degree of deacetylation. In the deacetylation phase, NaOH concentration, and duration and temperature of the reaction are important factors on the deacetylation degree.

No statistical difference was observed in the moisture (1.52-1.80%) and raw ash (0.12-0.18%) contents of the chitosan with low and high deacetylation degree. High quality chitosan's raw ash content should be lower than 1% [12]. Hence, the moisture content of the both featured chitosan produced in this study is under this value. Similarly, Tajik et al. [12] determined the raw ash content of the chitosan acquired from Artemia to be between 0.19-0.51%.

TABLE 1
Physicochemical properties of chitosan extracted from *P. longirostris* with different deacetylation degrees

	Deacetylation Degree	
Parameters	**Low**	**High**
Deacetylation Degree (%)*	72.86±3.21	93.70±2.20
Moisture (%)	1.80±0.65	1.52±0.04
Crude ash (%)	0.12±0.01	0.18±0.07
Molecular weight (kDa)*	14.08±1.34	2.15±0.04
Apparent viscosity (cP)*	1450±141.42	150.00±43.58
Water binding capacity (%)*	808.17±10.44	654.16±23.32
Fat binding capacity (%)*	910.23±27.67	692.30±30.12

* indicates a significant difference between two groups ($p<0.01$)

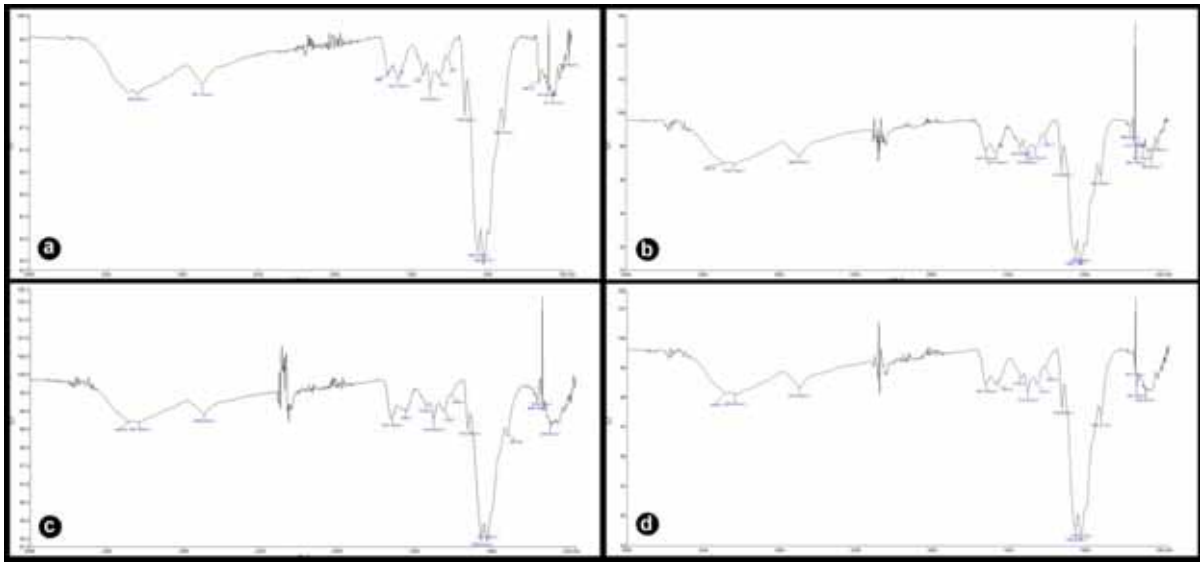


FIGURE 1
FTIR Spectra of Chitosan (a) LDEC (b) HDEC (c) LDCC (d) HDCC

TABLE 2
FTIR bands of chitosan with different deacetylation degrees

Functional Group/Wavenumber	**a**	**b**	**c**	**d**
C=O Amide I band	1655	1647,53	1647,48	1647,99
C=O-C-N	1587,70	1577,19	1550,70	1587,80
CH_2 vibration	1421	1420,20	1418,60	1416,30
CH-CH_3 vibration	1375,49	1376,38	1375,02	1375,22
Amide bands	1319	1320,21	1309,70	1314,30
NH	1261	1263,30	1263,30	1263,30
C-O-C	1150,42	1149,99	1151,68	1150,80
C=O	1062,97	1059,73	1065,51	1062,80
C=O	1026,37	1026,55	1027,22	1027,17
Fingerprint region, SH, PO_4 vibration	894,31	892,38	897,23	893,27

(a) LDEC (b) HDEC (c) LDCC (d) HDCC

In this study, it was detected that with the increasing deacetylation degree of the chitosan, there was a statistically important decrease in the viscosity value ($p<0.01$). Jeon et. al. [13] reported that the viscosity of the chitosan was closely related to the deacetylation duration; and in parallel with the present study's results, chitosan had the highest viscosity in the shortest deacetylation duration. In parallel with the viscosity values, molecular weight results also showed that chitosan with low deacetylation degree had higher values compared to the chitosan with high deacetylation degree. During chitosan production, several factors such as temperature rating, alkali concentration, duration of reaction, duration of

chitin acquirement, particle size, chitin concentration, and dissolved oxygen concentration may affect molecular weight [12].

Water and fat binding capacities of the chitosan group with high deacetylation degree were found to be lower (Table 1). Water and fat binding capacities of the both groups have shown similarities with the results of different studies carried out with different chitosan samples [12, 14, 15]. Similar to this study, Trung et al. [16] examined the functional qualities of chitosan with three different deacetylation degrees (75, 87, 96 %) in the same molecular weight (approximately 810 kDa) and reported that the chitosan with the lowest deacetylation degree had the higher water binding capacity. All these physicochemical properties of chitosan vary depending upon the source of chitin, isolation method, deacetylation degree, the duration of being processed with sodium hydroxide, concentration, and the temperature during the process.

FT-IR spectrums of the chitosan with low and high deacetylation degree, which were acquired from *P. longirostris*, and the commercial chitosan are demonstrated in Figure 1; and the details of spectrums are demonstrated in Table 2. As the deacetylation degree of the chitosan acquired from shrimp shell increased, 1655 peak in the group with low deacetylation feature was replaced by 1647 peak. In commercial chitosan groups, this value remained stable at 1647 peak. For both natural and commercial chitosan, it was seen in spectrum results that with the increase in the deacetylation degree, some functional groups moved away from the structure between 800-450 bands. As the deacetylation degree increased, 610 peak in the natural chitosan with low deacetylation degree was observed on 617 band. While this peak was not observed in commercial chitosan with low deacetylation degree, it was observed on 610.97 band in the high commercial. It was determined that with the increase in deacetylation degree, this peak became evident. In the general sense, it was observed that there were changes in the intensity of peaks between C=O Amide I band and Fingerprint region groups.

SEM pictures of the chitosan with different deacetylation degrees are presented in Figure 2. Chitosan's fibrillary structures are seen in the images, and it can be said that the acquired chitosan has a lamellar structure. Although generally a spherical structure is observed, particles comprising uneven shapes are also seen. It was determined that the group with high deacetylation had a more fibrillary structure compared to the group with low deacetylation.

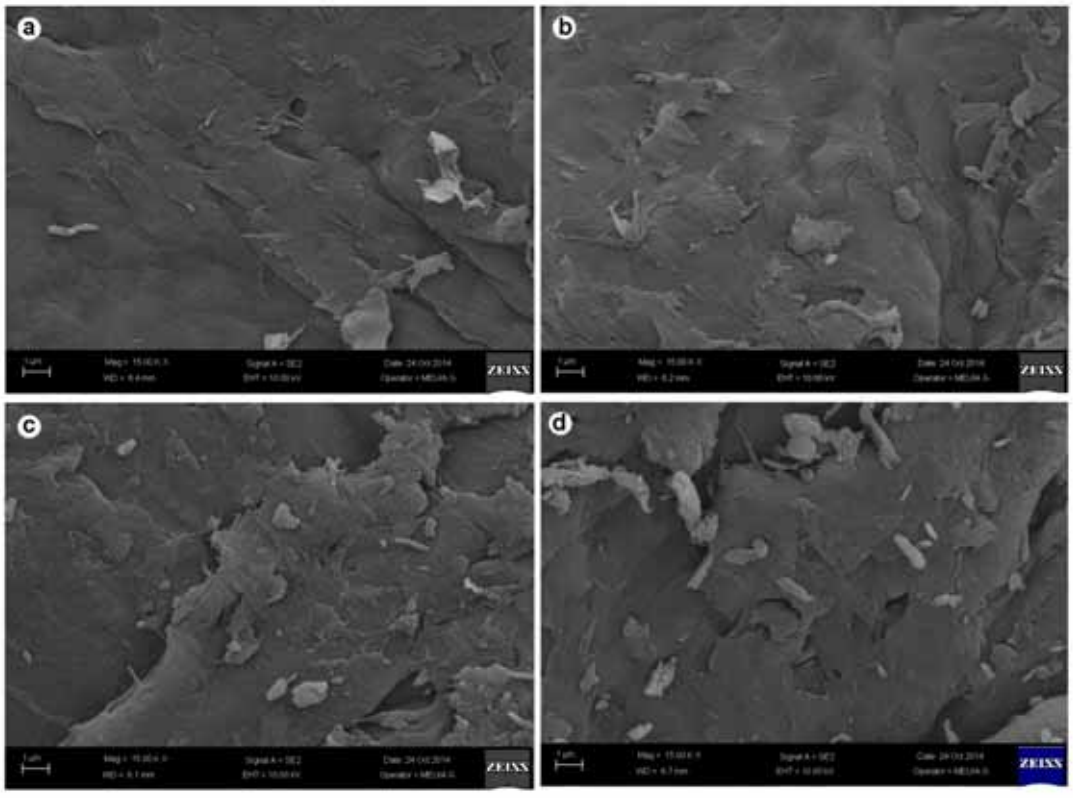


FIGURE 2
Scanning Electron Microscopy (SEM) of Chitosan at 15.00 KX
(a) LDEC (b) HDEC (c) LDCC (d) HDCC

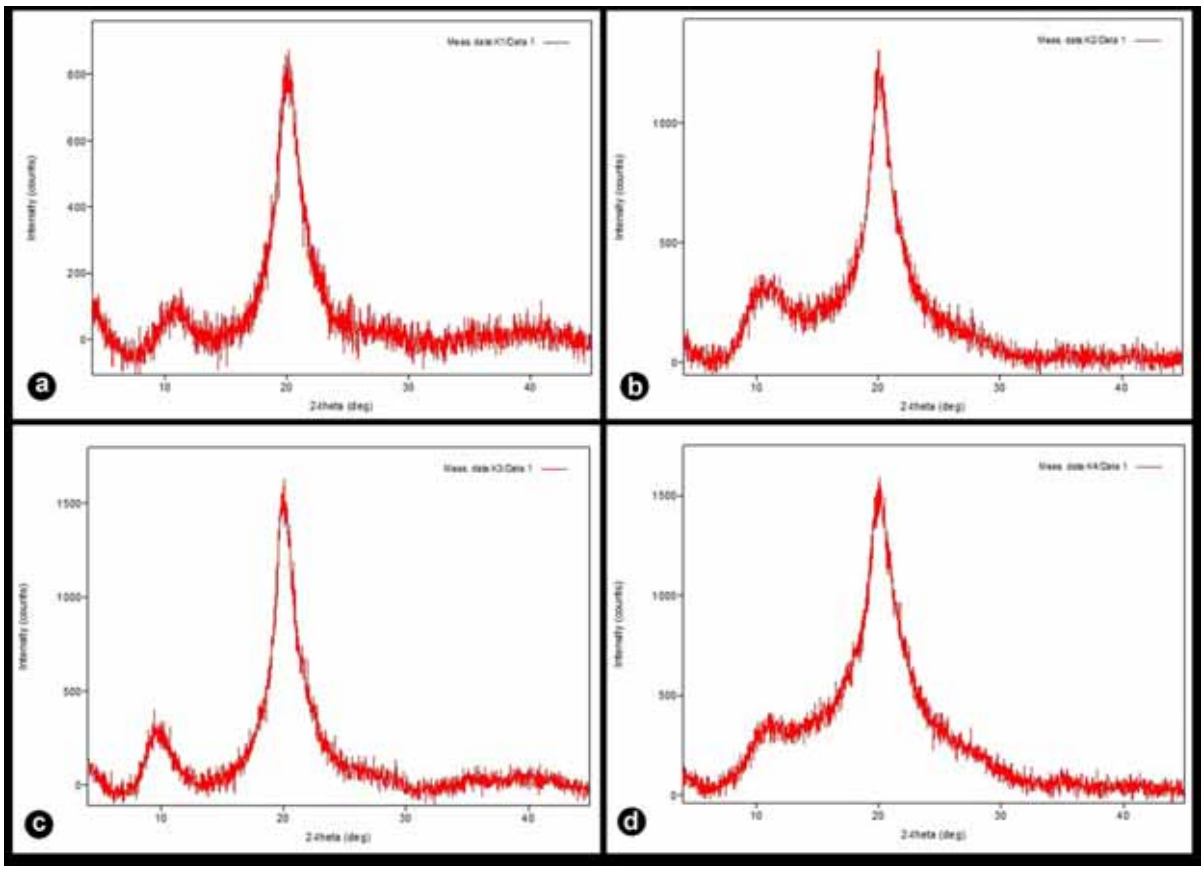


FIGURE 3
X-Ray Diffraction Patterns of Chitosan (a) LDEC (b) HDEC (c) LDCC (d) HDCC

XRD results of chitosan are shown in Figure 3. XRD results of chitosan extracted shrimp shell show two strong peaks 10.8 and 20.37° (low deacetylated), 10.01 and 20.04° (high deacetylated), respectively. XRD results of commercial chitosan show two strong peaks 9.56 and 19.82° (low deacetylated), 10.56 and 19.89° (high deacetylated), respectively. While teta-10 was under 200 in chitosan samples with low deacetylation quality, teta-20 was measured around 800. In the group with high deacetylation, the value of teta 10 was determined to be around 400 and the value of teta 20 was determined to be higher than 1000. With the increase in deacetylation, an increase was observed in both peaks.

In conclusion, with the development of shellfish processing technology, the recycling of wastes has become an important issue. Shellfish wastes, which are not utilized in factories in our country, have constituted a great potential. The utilization of wastes is an important topic both for aquaculture industry and public health. With the expansion in the usage possibilities of chitosan's different forms in different industries, the use of productions with no side effects particularly for human health will be enabled; and, it will be possible both to generate an income economically and to prevent the environmental pollution created by the wastes of processed shellfish.

REFERENCES

[1] Kumar, M. (2000) A review of chitin and chitosan applications. React. Funct. Polymers. 46(1), 1-27.
[2] Dutta, P.K., Dutta, J. and Tripathi VS. (2004) Chitin and chitosan: Chemistry, properties and applications. J. Sci. Ind. Res. 63(1), 20-31.
[3] Shahidi, F., Arachchi, J.K.V. and Jeon, Y.J. (1999) Food applications of chitin and chitosan. Trends Food Sci. Technol. 10, 37–51.
[4] Küçükgülmez, A., Celik, M., Yanar, Y., Sen, D., Polat, H. and Kadak, A.E. (2011) Physicochemical characterization of chitosan extracted from *Metapenaeus stebbingi* shells. Food Chem. 126, 1144–1148.
[5] Hussain, M.R., Iman, M. and Maji, T.K. (2013) Determination of degree of deacetylation of chitosan and their effect on the release behavior of essential oil from chitosan and chitosan-gelatin complex microcapsules. Int. J. Adv. Eng. App. 2(4), 4-12.

[6] Guo, X.F., Kikuchi, K., Matahira, Y., Sakai, K. and Ogawa, K. (2002) Water-soluble chitin of low degree of deacetylation. J. Carbohydr. Chem. 21(1-2), 149-161.
[7] Nemtsev, S.V., Gamzazade, A.I., Rogozhin, S.V., Bykova, V.M. and Bykov, V.P. (2002) Deacetylation of chitin under homogeneous conditions. Appl. Biochem. Microbiol. 38, 521–526.
[8] Chang, K.L.B., Tsai, G., Lee, J., and Fu, W-R. (1997) Heterogenous *N*-deacetylation of chitin in alkaline solution. Carbohydr. Res. 303, 327-332.
[9] Tolaimate, A., Desbrieres, J., Rhazi, M., Alagui, A., Vincendon, M. and Vottero, P. (2000) On the influence of deacetylation process on the physicochemical characteristics of chitosan from squid chitin. Polymer. 41, 2463-2469.
[10] Wang, Q.Z., Chen, X.G., Liu, N., Wang, S.X., Liu, C.S., Meng, X.H. and Liu, C.G. (2006) Protonation constants of chitosan with different molecular weight and degree of deacetylation. Carbohydr. Polymers. 65, 194-201.
[11] Wang, J.C. and Kinsella, J.E. (1976) Functional properties of novel proteins: Alfalfa leaf protein. J. Food Sci. 41, 286-292.
[12] Tajik, H., Moradi, M., Rohani, S.M.R., Erfani, A.M. and Jalali, F.S.S. (2008) Preparation of Chitosan from Brine Shrimp (*Artemia urmiana*) Cyst Shells and Effects of Different Chemical Processing Sequences on the Physicochemical and Functional Properties of the Product. Molecules. 13, 1263-1274.
[13] Jeon, Y.J., Kamil, J.Y.V.A. and Shahidi, F. (2002) Chitosan as an Edible Invisible Film for Quality Preservation of Herring and Atlantic cod. J. Agric. Food Chem. 50, 5167-5178.
[14] Cho, Y.I., No, H.K. and Meyers S.P. (1998) Physicochemical characteristics and functional properties of various commercial chitin and chitosan products. J. Agric. Food Chem. 46, 3839-3843.
[15] No, H.K., Lee, K.S. and Meyers, S.P. (2000) Correlation between physicochemical characteristics and binding capacities of chitosan products. J. Food Sci. 65, 1134-1137.
[16] Trung, T.S., Thein-Han, W.W., Qui, N.T., Ng, C.H. and Stevens, W.F. (2006) Functional characteristics of shrimp chitosan and its membranes as affected by the degree of deacetylation. Bioresource Technol. 97, 659-663.

Received: **28.03.2017**
Accepted: **13.10.2017**

CORRESPONDING AUTHOR

Aygul Kucukgulmez
Cukurova University
Faculty of Fisheries Department of
Seafood Processing Technology
Adana – Turkey

E-mail: akucukgulmez@cu.edu.tr

© by PSP Volume 26 – No. 12A/2017 pages 7756-7759 Fresenius Environmental Bulletin

DYES WASTEWATER TREATMENT VIA ELECTROCHEMICAL OXIDATION

Qiong Li, Yanbo Wang *

College of Chemistry and Chemical Engineering, Xinxiang University, 191 Jinsui Road, 453 003 Xinxiang, Henan, China

ABSTRACT

This paper deals with the degradation of dyes wastewater via electrochemical oxidation on a novel anode. The result showed that electrochemical oxidation is effective for dyes wastewater treatment. Under the optimum condition, the TOC removal reached 51.66%.

KEYWORDS:
Electrochemical oxidation, TOC removal, Acid Red B, wastewater treatment.

INTRODUCTION

Since dyes are considered as stable, stubborn, colorant, and potentially carcinogenic and toxic pollutants, their discharge will bring about serious environmental, aesthetical and health problems [1-5]. Therefore, the decontamination of dyes effluents from the textile and dyes industries should be effectively treated before they are discharged into the environment. Therefore, it is necessary to develop effective pretreatment technologies to remove/reduce the toxic substances before biological treatment. Some technologies have been developed for the potential application in the pretreatment of poor biodegradable and even toxic wastewater [6-8]. Electrochemistry has been used to pre-treat the wastewater containing methylene blue with its Bi improved by 16 times [9]. Anaerobic processes have been also applied to enhance the Bi of textile wastewater [10]. In addition, advanced oxidation technologies have been also employed to improve dyes wastewater treatment [11-13]. However, either removal efficiency and/or treatment cost have restricted the wide application of these pretreatment methods. Therefore, the dye was selected as a target pollutant in this study due to its biodegradable characteristics.

The electrochemical activity of PbO_2 electrodes is largely determined by the composition of the film [14]. Because of the easy deactivation of pure PbO_2, the stability and electrocatalytic activity of the PbO_2 anodes are expected to be improved to further satisfy the requirement of practical application [15-17]. But so far, to the best of our knowledge, there are few previously reported studies on rare earth oxides (Ce) co-doped into PbO_2 anode.

In this work, according to the degradation of dyes wastewater, the optimized doped molar ratio of Ce was also determined. The influence of parameters such as current density, electrolyte concentration and different Ce-doped molar ratio was investigated.

MATERIALS AND METHODS

Materials and chemicals. The dye used in the present work was purified from industrial Acid Red B (Dahai Chemical dyestuff Co. Ltd., China). The PbO_2 film of electrodes was prepared by the thermal decomposition and electro-deposition technique. Rare earth oxide ($Ce(NO_3)_3.6H_2O$) was added into the electroplating solution for the electrodeposition of the Ce-doped PbO_2 electrode.

Equipments and procedures. The samples were selected depending on the time duration of 0, 30, 60, 90 and 120 min. Total organic carbon (TOC) was detected by TOC automatic analyser (TOC-V CPH, Shimadzu, Japan).

The electrochemical oxidation system was mainly composed by two working electrodes (active area was 70 × 30 mm^2), and an electrolysis cell (working volume was 300 ml).

RESULTS AND DISCUSSION

Effect of current density. The effect of different current density (40, 60, 80 and 100 mA/cm^2) on the degradation of Acid Red B was investigated at 0.2 mol/l NaCl and suitable Ce-doped molar ratio (Pb : Ce = 200 mol : 0.6 mol). The result is shown in Fig. 1.

The TOC removal obtained with different current density conditions is shown in Fig. 1. The results showed that the degradation rate increased with current density increasing from 40 to 100 mA/cm^2. This also indicated that high current density could significantly promote the degradation rate.

Effect of concentration of electrolyte. Because conductivity of Acid Red B is low, strong electrolyte (NaCl) is added to promote the conductivity

of Acid Red B solution. Therefore, the effect of electrolyte concentration on degradation of Acid Red B should also be evaluated. In order to investigate the effect of electrolyte (NaCl) on degradation of Acid Red B, 0.05, 0.1, 0.2 and 0.4 mol/l NaCl is respectively tested by Ce-doped PbO_2 electrode (Pb : Ce = 200 mol: 0.6 mol). The results are shown in Fig. 2.

Figure 2 presents the TOC removal with the different electrolyte concentration in electrochemical oxidation system. After 120 min reaction, the TOC removal is 31.26, 44.87%, 47.51 and 51.66% at electrolyte concentration of 0.05, 0.1, 0.2 and 0.4 mol/l, respectively. This showed that an increase in electrolyte concentration could not always imply a promotion in the degradation efficiency.

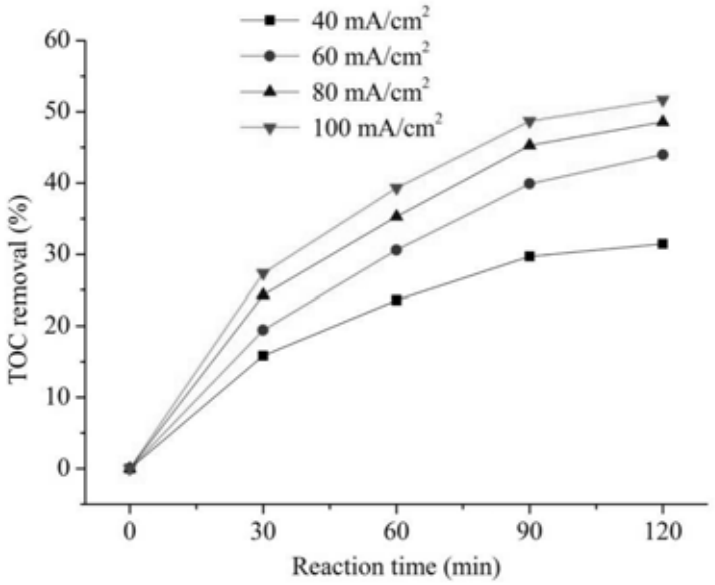


FIGURE 1
Effect of current density on degradation of Acid Red B

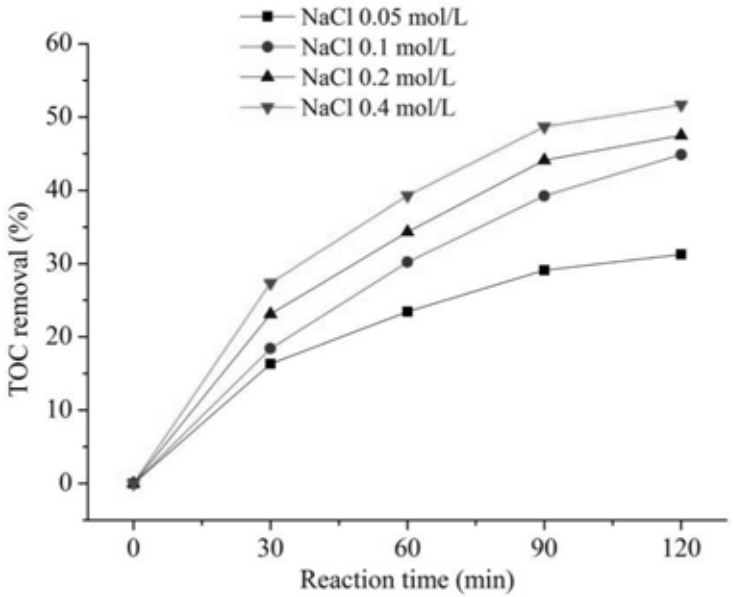


FIGURE 2
Effect of NaCl concentration on degradation of Acid Red B

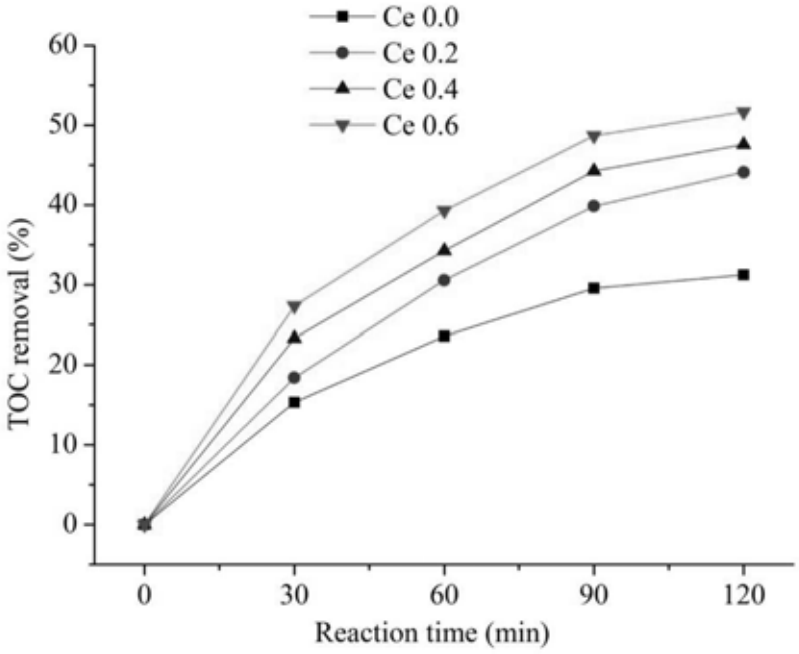


FIGURE 3
Effect of Ce-doped ratios on degradation of Acid Red B

Effect of Ce-doped molar ratio. The effect of different Ce-doped molar ratios (Pb (mol) : Ce (mol) = 200 : 0, 200 : 0.2, 200 : 0.4, 200 : 0.6) on the degradation of Acid Red B is investigated at 0.2 mol/l NaCl and 100 mA/cm^2 current density. The result is shown in Fig. 3.

As could be seen in Fig. 3, when the molar ratio was Pb : Ce = 200 : 0.6, the maximum TOC removal is achieved. The TOC removal by the co-doped electrode (Pb : Ce = 200 : 0.6) reached to 51.66%, which was higher than that of un-doped electrode (31.22%), after 120 min degradation. This suggested that suitable Ce-doped molar ratio has a positive influence on the catalytic activity of PbO_2 electrode. The Ce-PbO_2 electrode (Pb : Ce = 200 : 0.6) possessed an excellent degradation ability on TOC removal.

CONCLUSIONS

The PbO_2 electrode doped with Ce (Ce-PbO_2) is prepared by electrodeposition technique. The maximum degradation efficiency of Acid Red B is achieved by Ce-PbO_2 (Pb (mol) : Ce (mol) = 200 : 0.6) with 0.2 mol/l electrolyte (NaCl) and 100 mA/cm^2, in the electrochemical oxidation system. Under these conditions the maximum TOC removal reached to 51.66% after 120 min treatment.

REFERENCES

[1] Kabdasli, I., Konuk, K. and Tunay, O. (2017) Defluoridation of Drinking Water by Electrocoagulation with Stainless Steel Electrodes. Fresen. Environ. Bull. 26, 345-351.

[2] Rezaee, A., Kashi, G., Jonidi-Jafari, A., Khataee, A. and Nili-Ahmadabadi, A. (2011) Effect of Hydrogen Peroxide on Bacillus Subtilis Spore Removal in An Electrophotocatalytic System. Fresen. Environ. Bull. 20, 2750-2755.

[3] Li, W.D., Dai, Q.Z., Wang, J.D., Zhou, J.Z. and Chen, J.M. (2015) Study on Electro-catalytic Characterisation of Dye Wastewater via Gd and La Doped Lead Dioxide Electrodes. Oxid Commun. 38, 2253-2260.

[4] Muneer, M., Bokhari, T.H., Jamal, M.A., Khosa, M.K., Afzal, N., Adeel, S., Ullah, S., Iqbal, M. and Iqbal, M. (2015) Green Processes: Removal of Reactive Blue 19 by Gamma Radiation. Oxid Commun. 38, 2100-2106.

[5] Hadjltaief, H.B., Costa, P.D., Galvez, M.E. and Zina, M.B. (2013) Influence of Operational Parameters in the Heterogeneous Photo-Fenton Discoloration of Wastewaters in the Presence of an Iron-pillared Clay. Ind Eng Chem Res. 52, 16656-16665.

[6] Zou, X.L. (2015) Combination of Ozonation, Activated Carbon, and Biological Aerated Filter for Advanced Treatment of Dyeing Wastewater for Reuse. Environ Sci Pollut R. 22, 8174-8181.

[7] Uranga-Flores, A., de la Rosa-Juarez, C., Gutierrez-Granados, S., de Moura, D.C., Martinez-Huitle, C.A. and Hernandez, J.M.P. (2015) Electrochemical Promotion of Strong Oxidants to Degrade Acid Red 211: Effect of Supporting Electrolytes. J Electroanal Chem. 738, 84-91.

[8] Ju, Y.M., Liu, X.W., Li, Z.Y., Kang, J., Wang, X.Y., Zhang, Y.K., Fang, J.D. and Dionysiou, D. (2015) Environmental Application of Millimetre-scale Sponge Iron (s-Fe-0) Particles (I): Pretreatment of Cationic Triphenylmethane Dyes. J Hazard Mater. 283, 469-479.

[9] Elmolla, E.S. and Chaudhuri, M. (2011) Combined Photo-Fenton-SBR Process for Antibiotic Wastewater Treatment. J Hazard Mater. 192, 1418-1426.

[10] Yahiaoui, I., Aissani-Benissad, F., Madi, K., Benmehdi, N., Fourcade, F. and Amrane, A. (2013) Electrochemical Pre-treatment Combined with Biological Treatment for the Degradation of Methylene Blue Dye: Pb/PbO_2 Electrode and Modeling-optimization through Central Composite Design. Ind Eng Chem Res. 52, 14743-14751.

[11] Geilli, S., Piscitelli, D., Mattioli, D., Casu, S. and Spagni, A. (2011) Textile Wastewater Treatment in a Bench-scale Anaerobic-Biofilm Anoxic-aerobic Membrane Bioreactor Combined with Nanofiltration. J Environ Sci Heal A. 46, 1512-1518.

[12] Castro, E., Avellaneda, A. and Marco, P. (2014) Combination of Advanced Oxidation Processes and Biological Treatment for the Removal of Benzidine-derived Dyes. Environ Prog Sustain. 33, 873-885.

[13] Peternel, I., Biosic, D., Papic, S., Koprivanac, N. and Bozic, A.L. (2009) Investigation of the Photocatalytic Degradation of the Reactive Azo Dye (CI Reactive Red 45) in Aqueous Solution. Tekstil. 58, 433-436.

[14] Eremektar, G., Selcuk, H. and Meric, S. (2007) Investigation of the Relation between COD Fractions and the Toxicity in a Textile Finishing Industry Wastewater: Effect of Preozonation. Desalination. 211, 314-320.

[15] Li, X.L., Xu, H. and Yan, W. (2016) Fabrication and Characterization of PbO_2 Electrode Modified with Polyvinylidene Fluoride (PVDF). Appl Surf Sci. 389, 278-286.

[16] Chen, S.P., Hu, W.D., Hong, J.X. and Sandoe, S. (2016) Electrochemical Disinfection of Simulated Ballast Water on PbO_2/Graphite Felt Electrode. Mar Pollut Bull. 105, 319-323.

[17] Dai, Q.Z., Zhou, J.Z., Weng, M.L., Luo, X.B., Feng, D.L. and Chen, J.M. (2016) Electrochemical Oxidation Metronidazole with Co Modified PbO_2 Electrode: Degradation and Mechanism. Sep Purif Technol. 166, 109-116.

Received: **02.04.2017**
Accepted: **25.09.2017**

CORRESPONDING AUTHOR

Wang Yanbo
Xinxiang University,
191 Jinsui Road,
453 003 Xinxiang, Henan – China

E-mail: xxyanbo@163.com

© by PSP Volume 26 – No. 12A/2017 pages 7760-7768 Fresenius Environmental Bulletin

REMOTE SENSING AND GIS BASED VIEWSHED ANALYSIS FOR WATER VISIBILITY FROM SETTLEMENTS OF A MEDITERRANEAN CITY

Mehmet Akif Erdogan*

Cukurova University, Vocational School of Technical Science, Department of Architecture and City Planning, Division of Geographic Information Systems, 01310, Adana, Turkey

ABSTRACT

This study aims to determine the effect of water body visibility on preference of housing in the case of Adana City Dam Lake and its environment. The coast of water bodies are attractive spaces for human activities since the beginning of human history. Recently the uses of coastal areas are intensified due to the scenic value of water bodies. Viewshed analysis is the research of the relationships between a point data set and a single point. The visibility of water bodies which can be calculated spatially using viewshed analysis is becoming increasingly a common factor for land use/selection. As a result of this, viewshed analysis facilitates landscape planning in an appropriate way by considering scenic value of landscape features such as, water bodies. Viewshed analysis of Seyhan Dam Lake in Adana City with the support of remote sensing and Geographic Information Systems (GIS) provided accurate results and saved time, labour and cost. The study area is called Menekşe district in Adana located at the Eastern Mediterranean coast of Turkey and undergoing rapid population and urbanization due to agricultural capacity and industrialization which make this area ideal test-bed site for visibility analysis. This area is under pressure of urbanisation since introduction of city development plan in 2008. In this regard the visibility of Seyhan Dam Lake was modelled for Menekşe district to find out the effect of scenic value on land use preference. The outputs of this study will maintain more effective city development plans.

KEYWORDS:
Land use selection, visibility, water bodies, settlement, viewshed

INTRODUCTION

There is growing pressure on natural land use by the growing human population of the word to satisfy the need for additional housing [1, 2]. Therefore assessment of landscape, especially in an urban context, can be useful for policy planning and decisions to ensure optimal land use in case of settlement. At the landscape level, the main challenge is how to decide on the optimal allocation and management of the many different land use options [3]. In trying to cope with the problem of landscape abuse and destruction, one of the questions that natural resource planners frequently ask is: "Why is one landscape preferred more than another?" [4].

Scenic landscapes are a major source of human enjoyment and in some cases have been the object of direct public action to preserve their quality [5, 6, 7]. The public's sensitivity to scenery—how the landscape looks—was historically one of the first and is perhaps still one of the most important catalysts of environmental awareness and action [8, 9] Landscape perception assessments implies a causal link between landscapes changes made on the ground and the perception of scenic value [10].

The coast of water bodies are attractive spaces to create places for human activities since the beginning of human history. It is well known that the land areas adjacent to the water body shorelines are associated with large and growing concentrations of human population, settlements and socioeconomic activities, including many of the world's large cities [11]. Economic and transportation purposes are not the only drivers of the urbanization at coastal regions, water bodies visibility with aesthetic purpose is also one of the effective drivers.

With the development of land use planning, and its requirement for environmental data on which to base land use decisions, came an increased desire to elaborate valid means to quantify the scenic characteristics of landscapes [7, 12, 13]. The visibility of water bodies as a part of landscape which can be calculated spatially using viewshed analysis are increasingly getting one of the key factors for land use selection and planning [14, 15, 16, 17, 18]. Automated generation of landscape viewsheds and visible areas was one of the earliest applications of digital elevation models and GIS [19]. A viewshed is a spatial layer which identifies inter-visibility between specific locations in a landscape, and can encompass digital land surface models, as well as maps of land use [20, 21, 22]. This technique is particularly relevant to landscape assessment, given that landscape is first and foremost the appearance of the land.

Viewshed can be calculated from point locations using line of sight calculations and digital elevation models [23].

Landscape planning which determines the suitability of land use can be achieved in a more appropriate and accurate manner considering the fact of visibility of scenic valued landscape features such as water bodies. Viewshed analysis using remote sensing and Geographic Information Systems (GIS) has advantages such as saving time, labour and cost and also provide more accurate results.

Turkish Mediterranean city of Adana is a fast growing city as a result of agricultural capacity and industrialization [24, 25, 26, 27]. Menekşe district located at the east coast of Seyhan Dam Lake of Adana city became an important attraction following to city development plan in 2008. So this region is ideal test site for visibility analysis to find out the effect of scenic value on land use preference. In this respect, this study determined the effect of water body visibility on preference of landscape use in the case of Adana City Dam Lake.

STUDY AREA

The City of Adana is located at the eastern Mediterranean coast of Turkey represents a case of dense population and rapid urban changes. Dramatic changes took place as result of farming reform in 1950s. Immigration from neighbouring cities has been the main concern of city planners [24]. So the Menekşe district as a case study is one of the potential development area of Adana City (Figure 1). The study region has a total area of 1162 hectares and 27.5 km perimeter and 22 km coastline.

The Menekşe region, unlike other potential growth areas of Adana, is a peninsula surrounded by Seyhan Dam Lake. After establishment of municipality in 1992, thus urbanisation began in the form of low-rise buildings, due to the lake visibility value. Prior to this development, there was only Menekşe Village in the region as a rural settlement, with a population of 212.

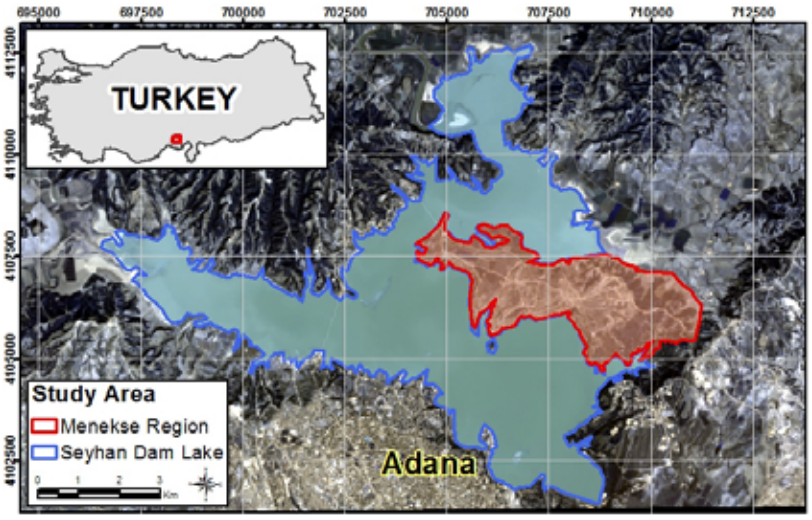


FIGURE 1
Location of the study area

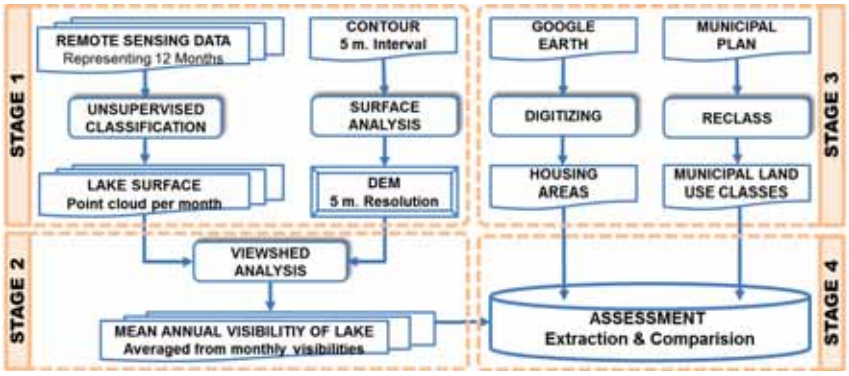


FIGURE 2
General flow diagram of the study

METHODOLOGY

The method of this study included four major section; (1) definition of viewshed components, (2) viewshed analysis, (3) pre-processing of ancillary data and (4) assessment of the results (Figure 2).

Definition of viewshed components. Remotely Sensed Data. The viewshed analysis creates a raster, recording the number of times each target area can be seen from the input locations. In this context; the spatial definition of the target area for which the visibility is to be calculated should be the first priority. Seyhan Dam Lake which is the target structure of visibility process has changeable surface areas depending on seasonal water levels. This means visibility of the lake is changing as a result of seasonality. In this study, the periodical surface areas of the lake for each month are extracted from 12 remotely sensed images, so that the time-varying visuality is calculated with higher accuracy.

GLOVIS database was searched for 12 up-to-date, cloud free LANDSAT satellite images which represent each month of the year.

Unsupervised Classification. Digital image classification techniques group pixels as classes to represent land cover features. There are two main image classification techniques: supervised and unsupervised. The unsupervised classification is first to group the spectral classes, based on numerical information and then match them to classes while supervised classification uses the homogeneous ground samples of the different surface cover types of interest to match the predefined classes.

Unsupervised classification was used for this study as only the lake surfaces were targeted from the each image. This saves labour and time in terms of collecting sample data for other classes. Thus, 12 LANDSAT images were classified using unsupervised classification technique of k-means to determine lake surface for each month.

The k-means classification begins with initializing k centroids (means), assigns each pixel to the cluster of the nearest centroid, then updates the cluster centroids, repeats the process until the k centroids are fixed. This is an iterative process for minimizing the sum of squared errors (SSE), hence it may not converge to a global optimum. Since its performance strongly depends on the initial estimation of the partition, a relatively large number of clusters are generally recommended to acquire as complete an initial pattern of centroids as possible. This technique is based on a simple clustering algorithm. Class counts were defined by the user and separated according to the spectral similarities [28].

Point Cloud. The lake surfaces are extracted from classified images. Monthly lake surfaces which are in raster format converted to 100x100 meters point vector data which are appropriate format for viewshed process representing monthly lake surface.

DEM Creation. In a GIS environment, terrain surfaces are often modelled by digital elevation model (DEM). DEM is rectangular grids in which elements are elevation measures of corresponding locations on the ground [29]. DEM can be obtained or created from remotely sensed data or readily available contours. 5 meters resolution DEM was created from 5 meter interval contours of the study area which was provided by Turkish General Command of Mapping.

Viewshed analysis. Viewshed analysis uses a Digital Elevation Model (DEM) that allows the analyst to inspect whether a source and a target are intervisible. The outcome of the analysis is usually a raster file whose cell values represent the level of intervisibility from an observer to the surrounding area [30].

According to Fisher [31, 32, 33], there are three main categories for viewshed techniques.

(1) *Binary viewshed* answers a basic query, namely, whether a target location can be seen from the viewing point. The cells take the value 0 in case of no inter-visibility or 1 otherwise.

(2) *Probable viewshed* was introduced in order to better simulate the inter-visibility between points. This technique uses the Monte Carlo method to create a perturbation of the results by introducing random errors. The raster cell values range between 0 and 1, while cells with values closer to 1 are more likely to be visible from the source.

(3) *Fuzzy viewshed* was introduced to calculate the decrease of inter-visibility between two points depending on factors such as weather conditions and distance.

In this study binary viewshed was used in GIS environment which identifies the cells in an input raster of study area that can be seen from one or more observation locations based on each points of monthly lake surface point cloud. Each cell in the output raster for each month receives a value that indicates how many observer points from point cloud of lake surface can be seen from each location of study area. Finally monthly lake visibility were spatially averaged to obtain mean annual visibility of Seyhan Dam Lake from Menekşe Region as observer location.

Pre-processing of ancillary data. Housing sites and municipal plan of the study area were taken into account as an ancillary data set for assessing the amount of lake visibility.

Housing sites are digitized by hand for each building from Google Earth. The garden borders of buildings are taken into account on digitizing process. Municipality plan which contains the study

area and was apporved in 1992. Study area is extracted from the plan and the detailed municipality land use types are grouped by reclassing according to main land use classes of the region like settlement, public facility, coast, forest, open green spaces, and rocky/hillside.

Assessment of the results. The values of mean annual visibility of the lake is extracted for the housing sites in the region. One sample t-tests are typically used to compare a sample mean to a known population mean. To assess differences in the strength of the associations between the visibility values for housing sites and the whole region, a one-sample t-test is used to find out whether the lake visibility is significant on settlement preferences. Also the mean annual lake visibility values are extracted for municipal land use types and compared each classes visibility values. The distribution of lake visibility as a natural resource will also be tested among the classes in terms of public rights and equality.

TABLE 1
Dates of selected Landsat image

Target month	Date (mm/dd/yyyy)	Target month	Date (mm/dd/yyyy)
January	01/19/2011	July	07/27/2013
February	02/04/2014	August	08/07/2012
March	03/24/2014	September	09/13/2013
April	04/01/2014	October	10/15/2013
May	04/29/2012	November	11/16/2013
June	06/25/2013	December	12/18/2013

RESULTS

12 LANDSAT image from GLOVIS database were listed in Table 1. The most appropriate remote sensing data set that meets the prevailing conditions are composed from six months at 2013, three months at 2014, two months at 2012 and one month at 2011.

As a result the k-means unsupervised classifier was a useful and successful technique to define distribution and location of single target class such as water body surfaces from multispectral satellite images such as Landsat [34].

ENVI 5.0 software package was used to implement K-Means unsupervised classification of selected Landsat images. Several K-Means variables such as number of classes, change threshold and maximum iteration number were tested to find the most accurate classification result. As a result of these tests number of classes, change threshold and maximum iteration were defined as 6, 2.0% and 6 respectively.

Classified images were reclassed to Boolean classes of water and non-water. Then the water bodies which are not belong to lake surface such as river or irrigation channels are removed from the water class. And also pixels that locate in lake area which are classified as non-water are assigned as water class to maintain lake integrity. This is resulted to final clear boolean data of lake and non-lake classes.

Accuracy assessment is conducted with randomly created ground truth point data which contains 100 samples for lake and non-lake data of each month. It is resulted that classification for May has the lowest accuracy of 92% among other months. And the K-Means classification performs the most accurate result for the image that represent lake surface for November with an accuracy of 97%.

The lake surfaces are extracted from processed lake and non-lake boolean classification results. Each monthly lake surfaces which are in raster format are converted to 100x100 meters gridded points vector data. The resulted point cloud data represent monthly lake surface as target structure of viewshed process. The all remote sensing process of the study that contains providing Landsat image, classification, and conversion to point cloud represent in Figure 3 as sample case months of May and November.

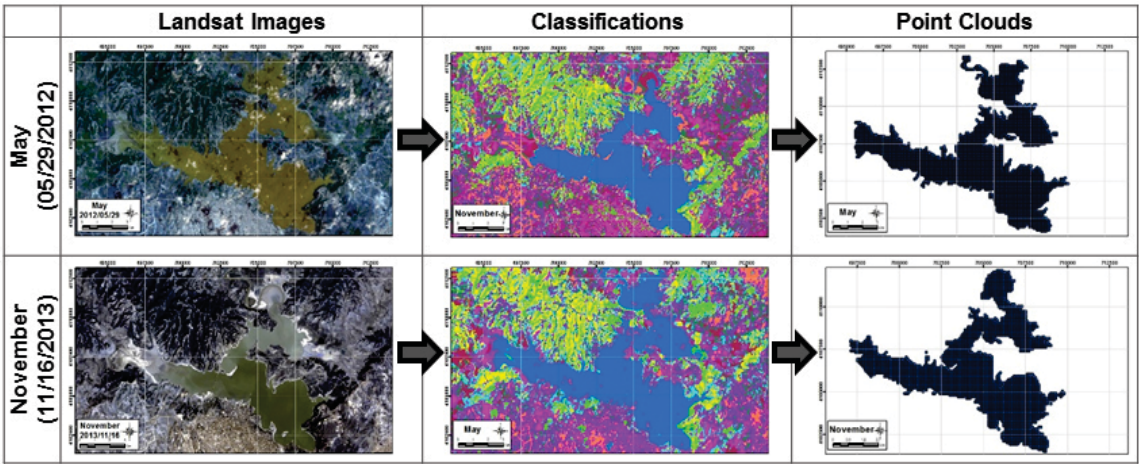


FIGURE 3
The remote sensing process: Sample cases of May and November.

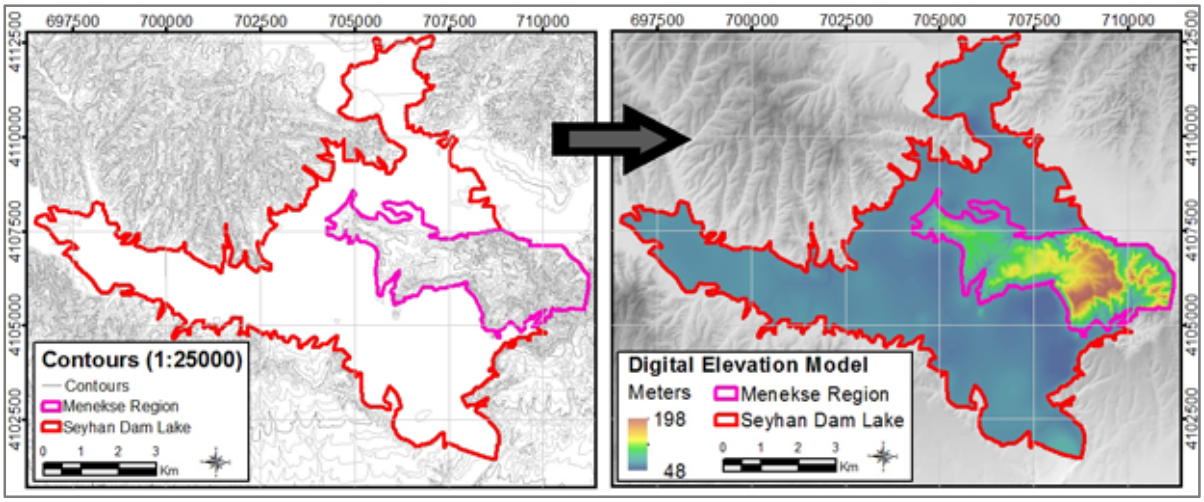


FIGURE 4
DEM creation process: Contour to DEM.

TABLE 2
Results of viewshed process

Target months	Total lake points	Visible Points		Visibility (%)		Target months	Total lake points	Visible Points		Visibility (%)	
		Max.	Mean	Max.	Mean			Max.	Mean	Max.	Mean
January	4298	3384	393,3	78	8,80	July	4178	3361	378,7	80	8,71
February	4452	3483	387,6	78	8,71	August	4299	3385	393,4	78	8,80
March	4503	3513	402,3	78	8,57	September	4254	3394	380,3	79	8,59
April	4953	3639	410,0	73	7,92	October	4256	3408	380,1	80	8,58
May	4970	3657	412,2	73	7,94	November	3853	3173	349,9	82	8,73
June	5159	3701	419,9	71	7,77	December	4200	3368	379,5	80	8,69

DEM was generated with the method developed by Michael Hutchinson [35, 36, 37] from digital contour lines spatial resolution of 5-m contour interval from a 1:25.000 scale topographic map which is obtained from Turkish General Command of Mapping (Figure 4).

Multiple viewshed calculations were done for assessing the seasonal lake visibility of each month. In viewshed analysis, visibility between a particular point and each of the pixels on a surface data is analysed to yield a binary (i.e., visible/non-visible) visibility map. Multiple viewshed analysis employs repeated calculations using multiple points and a single surface image. In this procedure, the number of viewshed calculations equals to the number of points of related months point cloud surface. Cell values of observer area in the final visibility map per month represent the sum of visible target points from the target feature as points from the lake surface. The lake visibility results as visible points for each month are proportional to related month's total point number of lake surface. Thus the monthly visibility are resulted as percent values (Table 2).

The viewshed process which is given in table 2 are assessed. The lake defined with maximum points of 5159 (5149 ha) at June which means lake reaches the largest surface at June in a season. On the contrary lake draws back to the smallest surface at November thus it was represented with a surface of 3853 points (3854 ha). These results show that with spring rains the lake starts to enlarge and reaches its largest surface at June. Just after irrigation of summer crops at lower plain the lake starts to shrink and reaches to the smallest surface area for the season.

Monthly lake visibilities indicate that the each month's maximum visible points at site are directly proportional to total number of point cloud of lake (R^2=0,97). The direct proportion also emerges between mean visible points and total number of point cloud of lake (R^2=0,88). Which directly affect one-to-one the mean visibility as percent. As a result of lake visibility as total number of visible points from study site reaches to the highest maximum value in June (3701 points) and minimum vales in November (3173 points) throughout the year. However this does not indicate that lake become most or least visible in terms of average visibility in the season because of variability on total number of point cloud of months.

The average visibility percentages represent that in January and August the lake was at the most visible period (8,8%) and lake come to the least visible status (7,8%) from June to December in the study site. These visibility variations over the months of a season are expected result of the unique

topographic structure of the study site and lake morphology. Topographic effect over the visibility was also discussed with several studies [38, 39, 40] and concluded with compatible results.

Mean annual visibility of Seyhan Dam Lake as a percentage for a season is calculated by spatially averaging each months visibility images (Figure 5). The result indicated that Seyhan Dam lake is 8,2% visible from Menekşe Region as average. The lake reaches to maximum visibility of 78% with standard deviation of 10,9 and also there are non-sighted locations in the region which means 0% visibility to lake. The aspects of southwest, west and south of the region are the most sighted locations respectively in terms of annual mean lake view (Table 3).

Buildings including their gardens of Menekşe Region were digitized by hand from Google Earth and imported in GIS environment as vector data (Figure 5). The total area of housing sites is 32,2 hectare which is 2,8% of the whole of Menekşe Region. When the mean annual visibility of Seyhan Dam Lake of housing sites are extracted from whole data, it represent that the mean lake visibility of housing sites is 15,8% with standard deviation of 10,4% and the values ranged from 0 to 53. This result suggested that the lake visibility has a strong effect on settlement selection in Menekşe region by residents.

The mean annual visibility of Seyhan Dam Lake is also extracted by the municipal land use classes of the Menekşe Region which are subsetted from main municipal plan of Adana City (Table 4). Rocky/hillside sites have the highest visibility to lake because of their slopes facing the lake towards southwest, west and south coasts of the region. Open green spaces, settlement, and public facility areas were extracted from municipality plan.

The one sample t-test determines whether the sample mean is statistically different from a known or hypothesized population mean by using the parameters of test variables and test value. In the test the test variable is compared against a test value, which is a known or hypothesized value of the mean in the population. In this case one sample t-test is arranged using building sites visibility values as test variable and the mean visibility of municipally defined settlement areas.

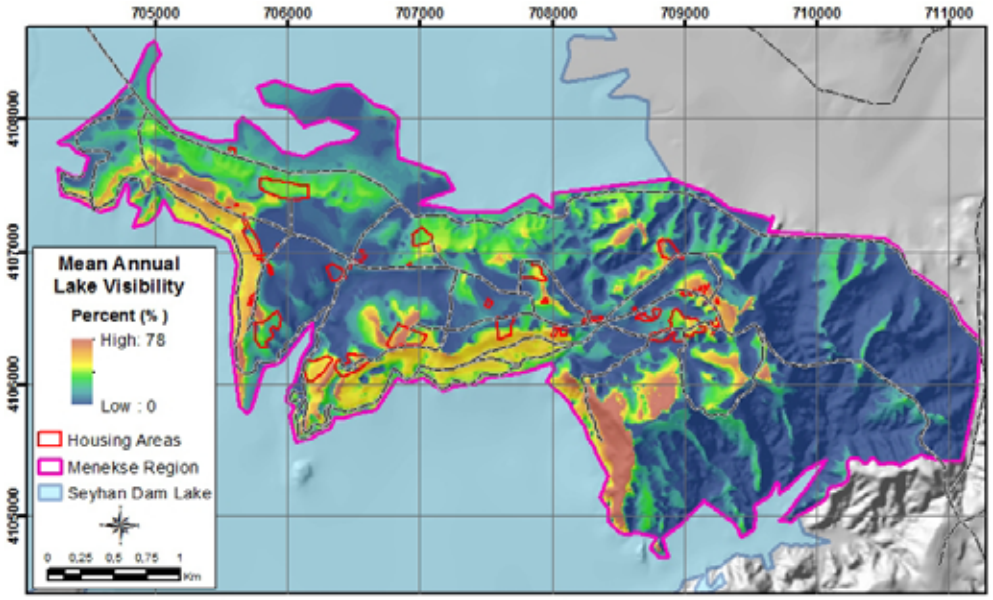


FIGURE 5
Mean annual visibility of Seyhan Dam Lake.

TABLE 3
Lake visibility of Menekşe Region according to aspects

Aspect	Area (ha)	Max. Visib.	Mean Visib.
North	162	53	7,48
Northeast	144	40	4,60
East	125	58	1,45
Southeast	133	54	5,25
South	153	59	10,80
Southwest	140	74	13,56
West	145	78	12,78
Northwest	161	72	8,83

TABLE 4
Lake visibility of municipal land use classes of Menekşe Region

Municipal Land Use Classes	Area (ha)	Annual Dam Lake Visibility		
		Max.	Mean	Std. Dev.
Rocky/Hillsides	71,3	78	21,5	15,3
Open Green Spaces	143,9	60	9,6	9,3
Settlement	347,6	74	9,4	11,1
Public Facility	11,2	39	8,3	10,0
Coast	84,0	58	8,1	8,6
Forest	313,0	52	2,4	6,0

One sample t-test of the means showed that the visibility difference between existing housing and municipal settlement areas are highly significant ($P<0.01$). This result highlights that the lake visibility is a significant factor for settlement selection at Menekşe Region. This deduction also emphasizes that water visibility as a landscape value will be effective on settlement selection in the sites where the housing is increasing.

DISCUSSION AND CONCLUSIONS

The aim of this study was to determine whether the water body visibility rate is significantly effecting the settlement location selection by residents. Although preliminary results showed that preference of housing location was closely related to direct visibility of water bodies regarding to the visual aesthetics. The relationship between water body visibilities and settlement selection was in line with the previous studies by Ayad [7] Zube et al. [8] and Zhang et al. [13].

Viewshed analysis uses a DEM that allows the analyst to inspect whether a source and a target are inter-visible [30]. The target features are generaly created by hand digitizing under GIS environment at several studies [14,15,16,17,18]. However proposed methodology with this study is unique in terms of using remotely sensed data and classifitation tecniques for the definition of seasonal lake surfaces as a target feature.

Multispectral satellite images such as Landsat that absorb of infrared wavelength region make such images an ideal combination for mapping the spatial distribution of land and water by its strong unique reflectance of water according to vegetation or soil [41]. These characteristics of water make use of the images that contain visible and infrared bands widely used for water surface mapping [42]. Thus in this study the classification of Landsat images (Landsat 7 and 8) with K-Means technique was integrated to viewshed process for spatial distribution of water surfaces. The classification accuracy of the outputs were examined, the results figure out that the specifications of Landsat image and K-Means method and also their combination provided accurate and quick output compare to digitizing by hand. This approach also performed adequately in terms of accuracy and sufficiency to define features for viewshed analysis. The resulted K-Means unsupervised classification of Landsat Images were also mentioned previously by the studies of Faber [43], Duda and Canty [44], and Jiang et al. [45].

The monthly assessment results of lake surface showed that the multi-temporal assessment rather than single time approach maintained more accurate estimation of seasonal lake visibility depending on changeable surface areas due to seasonal water levels. Secondly, the seasonal change and the most and least visible dates of the lake for Menekşe Region for a season are displayed. Annual lake visibility as a single layer was derived by averaging monthly viewshed results.

The mean annual lake visibility of housing sites is twice higher than whole region as the main finding of the study figure out the significance of lake visibility on settlement selection. However it is a reality that it is not possible to build houses legally to every location of the region. Thus it is needed to incorporate lake visibility on settlement, with respect to mean annual visibility and municipality plan. Depending on this consideration the mean visibilities of allowed settlement area and current housing sites are statistically compared using t-test. The result consolidate that the visibility difference between existing housing and municipal settlement areas were highly significant which means the effect of lake visibility is significantly effecting settlement selection on the Menekşe Region. This result statistically proved the argument of "The visibility of water bodies as a part of landscape are increasingly getting one of the key factors for land use selection and planning" by Litton et al. [14], Hagerhall et al. [15], Junker and Buchecker [16], Pfluger et al. [17], and Zhao et al. [18].

This paper highlights the presence of water body visibility effect on settlement selection by residents especially for regions which are located on coast of water surfaces and under rapidly growing settlement process such as Menekşe Region of Adana City. Moreover, the visibility of water bodies especially whose surfaces change seasonally such as lakes, can be calculated using viewshed analysis with the integration and support of time-series remotely sensed data, unsupervised classification within a GIS environment. Therefore, accurate quantitative information about the visibility of aesthetic

landscape resources such as water bodies would increase effectiveness of city development plans and would reward efforts to improve natural and built environments. Finally, our results can be of particular relevance in the context of land use and scenic value interaction, in a general manner and it can be used to assess the impact of the visibility of landscape components on land use/selection.

REFERENCES

[1] Baranzini, A. and Schaerer, C. (2011) A sight for sore eyes: Assessing the value of view and land use in the housing market. Journal of Housing Economics. 20, 191–199.

[2] Karakus, C.B., Kavak, K.S. and Cerit, O. (2014) Determination of variations on land cover and land use by remote sensing and geographic informatıon systems around the city of Sivas (Turkey), Fresen. Environ. Bull. 23, 667-677.

[3] de Groot, R.S., Alkemade, R., Braat, L., Hein, L. and Willemen, L. (2010) Challenges in integrating the concept of ecosystem services and values in landscape planning, management and decision making. Ecological Complexity. 7, 260–272.

[4] Shafer, E.L., Hamilton Jr., J.F. and Schmidt, E.A. (1969) Natural resources preferences: a predictive model. Journal of Leisure Research. 1, 1-19.

[5] Itami, R.M. (1989) Scenic Perception: Research and Application in U.S. Visual Management Systems. In: Landscape Evaluation: Approaches and Applications. P. Dearden and B. Sadler, (Eds.) University of Victoria. 211-241.

[6] Bishop, I.D. and Hulse, D.W. (1994) Prediction of scenic beauty using mapped data and geographic information systems. Landscape and Urban Planning. 30, 59-70.

[7] Ayad, Y.M. (2005) Remote sensing and GIS in modeling visual landscape change: A case study of the northwestern arid coast of Egypt. Landscape Urban Planning. 73, 307–325.

[8] Zube, E.H. (1980) Environmental Evaluation: Perception and Public Policy. In: Brooks/Cole Basic Concepts in Environment and Behavior Series. BrooKs/Cole Publishing Company.

[9] Nassauer, J. (1992) The appearance of ecological systems as a matter of policy. Landscape Ecology. 6, 239–250.

[10] Palmer, J.F. (2004) Using spatial metrics to predict scenic perception in a changing landscape: Dennis, Massachusetts. Landscape Urban Planning. 69, 201–218.

[11] Small, C. and Nicholls, R.J. (2003) A Global Analysis of Human Settlement in Coastal Zones. Journal of Coastal Research. 19, 584–599.

[12] Zube, E.H., Brush, R.O. and Fabos, J.Y. (1975) Landscape Assessment: Values, Perceptions, and Resources. Hutchinson and Ross Inc., Dowden.

[13] Zhang, Z., Tsou, J.Y. and Lin, H. (2000) GIS for visual impact assessment. In: Proceedings of the 21st Asian Conference on Remote Sensing, Taipei, Taiwan.

[14] Litton, R.B., Tetlow, R.J., Sorensen, J. and Beatty, R.A (1974) Water and Landscape: An Aesthetic Overview of Water in the Landscape. Water Info Center, Port Washington, New York.

[15] Hagerhall, C.M., Purcell, T. and Taylor, R. (2004) Fractal dimension of landscape silhouette outlines as a predictor of landscape preference. Journal of Environmental Psychology. 24, 247–255.

[16] Junker, B. and Buchecker, M. (2008) Aesthetic preferences versus ecological objectives in river restorations. Landscape and Urban Planning. 85, 141–154.

[17] Pflüger, Y., Rackham, A. and Larned, S. (2010) The aesthetic value of river flows: an assessment of flow preferences for large and small rivers. Landscape and Urban Planning. 95, 68–78.

[18] Zhao, J., Luo, P., Wang, R.and Cai, Y. (2013) Correlations between aesthetic preferences of river and landscape characters. Journal of Environmental Engineering and Landscape Management. 21, 123–132.

[19] Amidon, E. and Elsner, G. (1968) Delineating landscape view areas: A computer approach. Pacific Southwest Forest and Range Experiment Station, Berkeley, CA, USDA Forest Service (report RN PSW-180).

[20] Lake, I.R., Lovett, A.A., Bateman, I.J. and Langford, I.H. (1998) Modelling environmental influences on property prices in an urban environment. Computers, Environment and Urban Systems. 22(2), 121–136.

[21] Sander, H.A. and Manson, S.M. (2007) Heights and locations of artificial structures in viewshed calculation: How close is close enough? Landscape and Urban Planning. 82(4), 257–270.

[22] Yasumoto, S., Jones, A.P., Nakaya, T. and Yano, K. (2011) The use of a virtual city model for assessing equity in access to views. Computer Environment Urban Systems. 35, 464-473.

[23] Brabyn, L. and Mark, D.M. (2011) Using viewsheds, GIS, and a landscape classification to tag landscape photographs. Applied Geography. 31, 1115–1122.

[24] Akın, A., Erdogan, M.A. and Berberoğlu, S. (2013) The Spatiotemporal Land use cover Change of Adana City. ISPRS - International Archives of the Photogrammetry, Remote Sensing and Spatial Information Sciences. volume: XL-7/W2, 2013. 1-6.

[25] Akın, A., Clarke C.K. and Berberoğlu, S. (2014) The impact of historical exclusion on the calibration of the SLEUTH urban growth model. International Journal of Applied Earth Observation and Geoinformation. 27, 156-168.
[26] Berberoğlu, S., Akın. A. and Clarke, C.K. (2016) Cellular automata modeling approaches to forecast urban growth for Adana, Turkey: A comparative approach. Landscape and Urban Planning. 153, 11-27.
[27] Say, N., Okten, S.O., Aysu, A. and Yalcinkaya, N.M. (2017) Transformation of Land Use/Land Cover (LULC) Under Rapid Urbanization in Adana, Turkey. Fresen. Environ. Bull. 26, 3479-3485.
[28] Richards, J.A. and Jia, X. (1999) Remote sensing digital image analysis: an introduction, 3rd edition. Springer Verlag Berlin.
[29] Stucky, D. and Lee, J. (1998) On applying viewshed analysis for determining least-cost paths on Digital Elevation Models. International Journal of Geographical Information Science. 12, 891–905.
[30] De Montis, A. and Caschili, S. (2012) Nuraghes and landscape planning: Coupling viewshed with complex network analysis. Landscape Urban Planning. 105, 315–324.
[31] Fisher, P. (1992) First experiments in viewshed uncertainty simulating fuzzy viewsheds. Photogrammetric Engineering and Remote Sensing. 58(3), 345 352.
[32] Fisher, P. (1994) Probable and fuzzy models of the viewshed operation. In: Innovations in GIS, Worboys. M. (ed.) London: Taylor & Francis. 161-175.
[33] Fisher, P. (1995) An exploration of probable viewsheds in landscape planning. Environment and Planning B: Planning and Design. 22, 527-546.
[34] Satir, O., Berberoglu, S., Akca, E. and Yeler, O. (2016) Mapping the dominant forest tree distribution using a combined image classification approach in a complex Eastern Mediterranean basin. Journal of Spatial Science. 8596, 1–15.
[35] Hutchinson, M.F. (1996) A locally adaptive approach to the interpolation of digital elevation models. In: Proceedings, Third International Conference/Workshop on Integrating GIS and Environmental Modeling. Santa Barbara, CA: National Center for Geographic Information and Analysis.
[36] Hutchinson, M.F. and Gallant, J.C. (2000) Digital elevation models and representation of terrain shape. In: J.P. Wilson and J.C. Gallant (eds.) Terrain Analysis. Wiley, New York, 29–50.
[37] Hutchinson, M.F., Xu, T. and Stein, J.A. (2011) Recent Progress in the ANUDEM Elevation Gridding Procedure. In: Geomorphometry 2011, Hengel, T., Evans, I.S., Wilson, J.P. and Gould, M. (eds.) Redlands, California, USA, 19–22.
[38] Goodchild, M. and Lee, J. (1989) Coverage problems and visibility regions on topographic surface. Annals of Operations Research. 18, 175–186.
[39] Yokoyama, R., Shlrasawa, M. and Pike, R.J. (2002) Visualizing Topography by Openness: A New Application of Image Processing to Digital Elevation Models. Photogrammetric Engineering & Remote Sensing. 68, 257–265.
[40] Kim, Y.H., Rana, S. and Wise, S. (2004) Exploring multiple viewshed analysis using terrain features and optimisation techniques. Computers & Geosciences. 30, 1019–1032.
[41] Alesheikh, A.A., Ghorbanali, A. and Nouri, N. (2007) Coastline change detection using remote sensing. International Journal of Environmental Science and Technology. 4, 61–66.
[42] DeWitt, H. and Weiwen Feng, J.R. (2002) Semi-Automated construction of the Louisiana coastline digital land-water Boundary using landsat TM imagery, Louisiana's Oil Spill Research and Development Program, Louisiana State University, Baton Rouge, LA 70803.
[43] Faber, V. (1994) Clustering and the Continuous k-Means Algorithm. Los Alamos Science. 22, 138–144.
[44] Duda, T. and Canty, M. (2002) Unsupervised classification of satellite imagery: Choosing a good algorithm. International Journal of Remote Sensing. 23, 2193–2212.
[45] Jiang, H., Feng, M., Zhu, Y., Lu, N., Huang, J. and Xiao, T. (2014) An automated method for extracting rivers and lakes from Landsat imagery. Remote Sensing. 6, 5067–5089.

Received: **02.04.2017**
Accepted: **29.08.2017**

CORRESPONDING AUTHOR

Mehmet Akif Erdogan
Cukurova University,
Vocational School of Technical Science,
Department of Architecture and City Planning,
Division of Geographic Information Systems,
01310, Saricam, Adana – Turkey

e-mail: maerdogan@cu.edu.tr

© by PSP Volume 26 – No. 12A/2017 pages 7769-7779 Fresenius Environmental Bulletin

THE INFLUENCE OF VS/TS RATIO OF A-SLUDGE ON ANAEROBIC CO-DIGESTION OF KITCHEN WASTE WITH A-SLUDGE

Renjun Ruan[1,2,3], Jiashun Cao[2,3,*], Fang Fang[2,3] , Chao Li[2,3], Lei Qi[2,3], Changshuang Zhao[2,3]

[1]College of Civil Engineering and Architecture, Anhui Polytechnic University, Wuhu 241000, China
[2]Key Laboratory of Integrated Regulation and Resource Development on Shallow Lakes, Ministry of Education, Hohai University, Nanjing 210098, China
[3]College of Environment, Hohai University, Nanjing, 210098, China

ABSTRACT

Anaerobic digestion is a critical technology in the bio-based economy and can be applied to convert a wide range of organic substrates into methane. It can help us come true the carbon neutrality of wastewater treatment systems. Mono-digestion of kitchen waste often occurred with VFAs accumulation and ended in process failure. While the single digestion of sludge, with a limited biodegradability, result in poor anaerobic digestion performance. Considering that, a series of batch mesophilic co-digestion of kitchen waste (KW) with different ratio of VS/TS ('*f*') of A-sludge were performed to evaluate the effect of '*f*' on the co-digestion performance. A-sludge is produced during the highly loaded first stage of the two-phase 'Adsorptions-Belebungsverfahren' or A/B activated sludge system. We obtained A-sludge with different '*f*' (0.41, 0.55, 0.71) by controlling the parameters (HRT, OLR, SRT, DO) of A-stage of A/B process. The results revealed that co-digestion of appropriate fraction of kitchen waste with high '*f*' A-sludge could stimulate VS removal, total methane yield and total volumetric productivity, which increased by 1.40-fold, 2.38-fold, 3.30-fold as the ratio of '*f*' was increased from 0.41 to 0.71 without KW in the substrate, respectively. 1.36-fold, 2.16-fold and 2.93-fold correspond to 10 percent of KW in the substrate. The most optimal performance can be obtained in the 20 percent of kitchen waste with an 'f' value 0.55 of A-sludge in the substrate.

KEYWORDS:
Kitchen Waste, Co-digestion, Adsorption/Belebungsverfahren, Methane Yield, Volumetric Productivity

INTRODUCTION

Currently, there are around 2000 wastewater treatment plants (WWTPs) operating in China. Now, the goal of municipal wastewater systems has extended from protecting receiving water and human health to improving the system sustainability [1]. Municipal wastewater treatment plants consume large amounts of energy every year. It has been estimated that energy used in the WWTPs comprises around one fifth of a municipality's total energy use by public utilities, and it will continue to rise by 20% in the next 15 years with the increasing water consumption and more stringent regulations [2]. Various researches studied recover resources in wastewater for secondary uses in order to improve sustainability of WWTPs [3]. It might contribution to come true the carbon neutrality of wastewater treatment systems. Anaerobic digestion could be a method for energy recovery from low value organic by-products, such as waste activated sludge. The embodies energy is 9～10 folds as much as consumption energy in wastewater systems [4]. Therefore, it is a key technology in the bio-based economy and can be applied to come true 'Carbon Neutral' in wastewater treatment processes in future.

A wide range of organic substrates can be converted to biogas by means of anaerobic digestion. Kitchen waste (KW) is an available source of organic matter for anaerobic digestion [5]. Recently, the demands for reduction and utilization of municipal solid waste (MSW) have rapidly increased in China [6]. In 2006, the total amount of MSW collected and transported was 148 million tons, about 60% of which was food waste [7]. Food waste has a high content of moisture (70%～80%), high biodegradability (about 90%) and high energy content (0.7～1.1 kWh/L), and thus is an ideal substrate for anaerobic digestion [8]. The process of anaerobic digestion consists of four steps: hydrolysis, acidogenesis, acetogenesis, and methanogenesis [9]. Yet, digestion of single kitchen waste often results in process failure, because KW is a lipid-rich resource in which the lipid concentration is about 5.0 g/L [10]. The mono-digestion of kitchen waste would be problematic because of volatile fatty acids (VFAs) can be accumulated at high organic loading, resulting in the decrease of pH and even the failure of anaerobic di-

gestion [11-14]. Therefore, anaerobic mono-digestion of KW is mainly operated at low OLR (in the range of 1～3 g COD/ L.d) in order to avoid the accumulation of VFAs and subsequent process failure [15, 16]. Recently, anaerobic co-digestion, which mixes different wastes (solid or liquid organic wastes) with complementary characteristics in a single digester, has been widely used for production of biogas from various substrates. Several organic substrates have been successfully co-digested with kitchen waste, such as manure, wastewater, green waste and waste activated sludge [17-20]. A-sludge which is produced in the A-stage of A/B process is also a waste stream that might be suitable for co-digestion with kitchen waste.

'Adsorption-Belebungsverfahren' (A/B) process is one of a municipal wastewater treatment process. It is characterized for high-quality loading fluctuation resistance, avoiding flamentous bulking, especially, and generating large quantities sludge [21]. Large amounts of organics in wastewater are converted to waste activated sludge (WAS) during biological wastewater treatment. This technology is applied to many full scale WWTPs, for instance, Taian WWTP, Hedong Sewage Disposal Plant of Wulumuqi of China and the WWPTs of the Netherlands, Germany, Switzerland. The B-stage comprises a nitrogen treatment step by means of conventional nitrification/denitrification or oxygen-limited autotrophic nitrification/denitrification (OLAND) [22]. We focus on the highly loaded biological adsorption stage (A-stage) of this system. Anaerobic digestion of the huge volume excess of the A-sludge, greatly conduces to the parts of energy requirements or even energy self-sufficiency of the A/B process [23]. Sewage sludge (SS) characterized by relatively low C/N ratio and high buffer capacity [24, 25]. Therefore, it is able to stand co-substrates with high amounts of easily biodegradable organic matter and with low alkalinity values. Moreover, in many cases, co-digestion can also lead to the dilution of some undesired compounds present in SS such as heavy metals, pharmaceuticals and/or pathogens [26, 27]. Taking into account these facts, KW is very convenient co-substrate for A-sludge. Co-digestion of A-sludge with kitchen waste may not only enhance biogas production, but also improve the stability of the anaerobic digestion of kitchen waste, as A-sludge can provide the anaerobic digester with additional trace elements. Thus, it can satisfy the requirement of 'Carbon Offset' even 'Carbon Neutral' for WWTPs.

The previous studies mainly focused on optimizing the anaerobic digestion of sludge by adjusting external condition, such as temperature, pH, addition of zero of valent iron ect.. [28, 29]. Few studies realize the effect of internal property of sludge on the anaerobic digestion. It is generally known that process parameters have a great influence on the characteristics of waste activated sludge, VS/TS ratio of A-sludge is no exception. In this study, high 'f' A-sludge can be obtained by adjusting the important relevant control parameters of A-stage. The aim of this work is to evaluated whether co-digestion of high 'f' A-sludge and kitchen waste could obtain higher methane productivity and higher methane yield.

MATERIALS AND METHODS

Lab-scale A-stage reactor and influent. Lab-scale A-stage reactor of A/B process was designed and fabricated in the laboratory using perspex material. It used aeration and settling integration devices. It can cater to the need of sludge recirculation without return sludge pumps and reflux pipe. The aeration zone and settling zone of A-stage reactor has working/total volume of 3.75/4.32 L and 2.07/2.32 L, respectively (Fig. 1). The reactor was operated in continuous mode.

In order to stabilize the inlet water quality, the influent of A-stage was simulated wastewater. The components of simulated wastewater are showed in the following amount (in mg per L substrate): CH_3COONa: 200-500, NH_4Cl: 120, KH_2PO_4: 24, $MgSO_4.7H_2O$: 10, $CaCl_2.2H_20$: 15, H_3BO_3: 2, $FeCl_2.4H_2O$: 2, $ZnCl_2.4H_2O$: 0.4, $MnCl_2.4H_2O$: 0.8, $CuCl_2.2H_2O$: 0.2, $(NH_4)_6MoO_7.4H_2O$: 1.1, $NiCl_2.6H_2O$: 1.

Feedstock and inoculum. The kitchen waste (KW) was collected from the canteen of Hohai University and removed any non-food fraction (stone, bone, glass, wood chips). KW is composite in nature comprising uneaten food and food preparation leftovers which mostly comprising rice, vegetables, meat, fish, cooking oil. The moisture content of waste varied between 18% and 30%. The collected kitchen waste was masticated using blender and filtered through stainless steel sieve to remove coarse materials so as to avoid clogging problems and stored at 4℃. The A-sludge obtained from lab-scale A-stage reactor of AB process. The Characterisation of the Kitchen Waste (KW), A-sludge-0.41, 0.55, 0.71 are presented in Table 1.

The inoculum of A-stage origined from Jiangning Economic Development Zone WWPT of Nanjing. The inoculum of anaerobic reactors (An-inoculum) from an anaerobic fermentor of Jiangsu Chenjie Renewable Resources Science and Technology co., Ltd. Prior to use, the inocula were starved for 1 week and incubated at 35℃ to reactivate microbiological activity and remove the easily degradable VS. The Characterisation of the An-inoculum is also presented in Table 1.

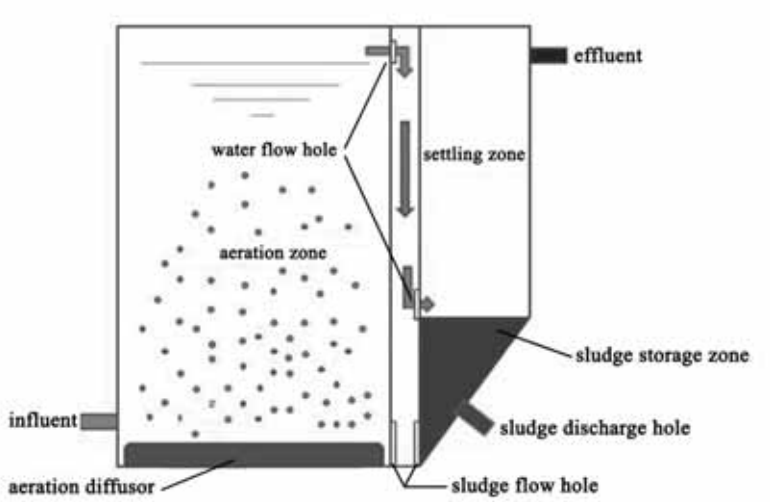


FIGURE 1
Device schematic of lab-scale A-stage reactor

TABLE 1
Characterisation of the Kitchen Waste (KW), A-sludge-0.41, 0.55, 0.71 and An-inoculum

Parameter	Units	KW	A-sludge-0.41[a]	A-sludge-0.55	A-sludge-0.71	An-inoculum
TS	g/L	164±5.2	35.7±0.021[c]	34.2±0.035	33.4±0.038	40.8±0.053
VS	g/L	152±4.9	20.5±0.028	24.3±0.031	28.7±0.024	23.5±0.047
TCOD	gO_2/L	214±6.7	22.3±1.1	27.1±2.3	32.1±0.9	ND
SCOD	gO_2/L	101±4.3	0.31±0.023	0.38±0.019	0.42±0.015	ND
TAN	mg/L	480±7	97±7.4	105±5.2	121±8.9	ND
TKN	mg/L	3812±67	1217±18	1282±21	1345±25	ND
VFAs	mg/L	6612±95	ND[b]	ND	ND	ND
Carbohydrates	g/L	102±5.7	ND	ND	ND	ND
Lipids	g/L	20.4±0.78	ND	ND	ND	ND
Proteins	g/L	21.6±1.1	ND	ND	ND	ND

[a]A-sludge-0.41, 0.53, 0.64 were the A-sludge with 'f' of 0.41, 0.55, 0.71, respectively.
[b]ND: not determined.
[c]All data were measured in triplicate.

TABLE 2
Relevant control parameters of A-stage of A/B process

parameters	Unite	Value
Hydraulic Retention Time HRT	min	15-60
Sludge Retention time SRT	day	0.5-2
Dissolved Oxygen DO	mg/L	0.2-1.5
Sludge Loading	kgCOD/(kgVSS.d)	2.27-5.67
Sludge Concentration	mg/L	3000

TABLE 3
The process parameters correspond to A-sludge of 'f' 0.41, 0.55, 0.71

f	HRT min	SRT day	DO mg/L	SL kgCOD/(kgVSS.d)	SC mg/L
0.57	15	2	1.5	3.405	3000
0.71	40	0.8	1.0	5.45	3000
0.86	25	0.5	0.75	5.67	3000

Experimental design and operation. A-stage operation with different control parameters. The A-sludge was obtained from the lab-scale A-stage reactor of A/B process. The ratio of VS/TS (volatile solid/total solid) of A-sludge can be changed by adjusting the relevant parameters of A-stage, such as sludge loading (SL), hydraulic retention time (HRT), sludge retention time (SRT), sludge concentration (SC) and dissolved oxygen (DO). The relevant control parameters of A-stage of A/B process are presented in Table 2. The A-sludge of VS/TS ratios 0.41, 0.55 and 0.71 were obtained when the process parameters of A-stage reactor were set as these three conditions (see Table 3). The waste sludge of A-stage was concentrated by settling at 24 h. To enhance the hydrolysis, the sludge was pretreated using alkaline method before the anaerobic fermentation according to the reference [30]. The pH of sludge was adjusted to 12 using 4 mol/L of sodium hydroxide, and then the sludge was stirred at 80 rpm for 6 h. After pretreatment, the pH of sludge was adjusted to 7 for anaerobic digestion. The sludge formed in A-stage with different 'f' values stored at 4℃ as substrate for subsequent anaerobic digestion.

A-sludge co-digestion with kitchen waste. The A-sludge of VS/TS ratios (0.41, 0.55 and 0.71) and percentage of kitchen waste (0%, 10%, 20%, 30% based on VS) in the feedstock on the performance of co-digestion was studied. Twelve of the same anaerobic lab-scale glass reactors with a total volume of 1L and a working volume of 800mL, and the mixing ratio of feedstock (A-sludge and kitchen waste) and inoculum was 1:1 (VS basis), which were operated for 30 days under mesophilic conditions (35±1℃). The inoculums-An, kitchen waste, and A-sludge were mixed by a Electric-stirrer for 15min. Well-mixed materials were loaded into the glass reactors and incubated for up to 30 days. All the experiments were conducted in triplicate. Inoculum without any feedstock addition was used as a control group. The twelve reactors were given different combinations of A-sludge and kitchen waste, i.e. 100%A-sldge (0.41), 100%A-sldge (0.55), 100%A-sldge (0.71); 90% A-sludge (0.41) and 10%KW, 90% A-sludge (0.55) and 10%KW, 90% A-sludge(0.71) and 10%KW; 80% A-sludge(0.41) and 20%KW, 80% A-sludge (0.55) and 20%KW, 80% A-sludge (0.71) and 20%KW; 70% A-sludge (0.41) and 30%KW, 70% A-sludge (0.55) and 30%KW, 70% A-sludge (0.71) and 30%KW (all of them based on VS).

Biogas generated was collected in a 5 L Tedlar gas bag (CEL Scientific, Santa Fe Springs, CA, USA). The volume and the percentage of methane in the biogas were measured once a day then converted to STP (standard temperature and pressure) condition during the 30 days. The initial pH of these reactors was adjusted to 7.2 and monitored without adjustment once a day in later. By the end of the trial, the VFAs, TS and VS were analysised. Methane yield expressed in mL/g$VS_{feedstock}$ was calculated as the volume of methane gas produced per g of VS loaded into the reactor at start-up, corrected by subtracting the methane yield obtained from the control reactor and adjusted linearly based on the amount of seed VS [31]. Methane productivity of feedstock is expressed in $V_{methane}/V_{work}$, which is the volume of methane gas produced ($V_{methane}$) per unit working volume of reactor (V_{work}), corrected by subtracting the methane yield obtained from the control reactor. TS reduction calculation was also corrected by subtracting the TS reduction obtained from the control reactor. The working volume of the reactor was taken as the maximum working volume after expansion had taken place.

Analytical methods. Analyses of the total fraction were performed directly on the raw samples. For analyses of the soluble fraction, the samples were centrifuged at 8000rmp for 10 min and then the supernatant was filtered through a nitrocellulose 0.45 mm filter. Total solids (TS), volatile solids (VS), total chemical oxygen demand (TCOD), soluble chemical oxygen demand (SCOD), total ammonia nitrogen (TAN) and total Kjeldahl nitrogen (TKN) were measured according to the standard methods. The pH was measured by HQ30d equipped with a standard electrode (PHC101). The concentration of volatile fatty acids (VFAs, calculated based on COD) was measured by a gas chromatograph (Agilent, GC-7890A, America) equipped with a flame ionization detector. The carrier gas was high purity nitrogen. The temperature of the column oven was initially programmed at 80 ℃ for 10 min, then elevated to 180 ℃ at 10℃/min and held for 1 min, eventually elevated to 220 ℃ and held for 5 min. The main components of biogas, CO_2 and CH_4, were analyzed with a gas chromatograph (Agilent, GC-7890A, America) equipped with a combined system of chromatographic column (SS-2m×2mm×13XMS, 60/80) and methanizer/flame ionization detector (FID). High purity nitrogen was used as a carrier gas at a flow rate of 3.0 mL/min. The separation column at 40℃, sample injector at 100℃ and FID at 300℃. The retention time of CH_4 and CO_2 were 2.2 min and 4.4 min, respectively. The lower detection limit for CH_4 and CO_2 were 0.2uLL^{-1} and 0.03uLL^{-1}, respectively. Protein was estimated by multiplying the organic nitrogen (TKN minus TAN) by 6.25 [32]. Lipids were analyzed following standard method. Carbohydrates were estimated by subtracting the amount of protein, lipids and VFA from VS.

RESULTS AND DISCUSSION

Volatile solid (VS) reduction of all reactors during the experimental period. As shown in Fig. 2, without KW in the substrate, the VS reduction during the experimental period was on average 26.7±1.3,

31.1±1.2 and 37.4±1.7% in the 100%A-sldge (0.41), 100%A-sldge (0.55) and 100%A-sldge (0.71), respectively. A 1.4-fold increase in volatile solid (VS) reduction was achieved with the increase in the 'f' value of A-sludge from 0.41 to 0.71. Mixing 10 percent of KW in the substrate, the 90% A-sludge (0.41) and 10%KW, 90% A-sludge (0.55) and 10%KW, 90% A-sludge (0.71) and 10%KW achieved average VS reduction of 32.7±1.6, 39.4±1.3 and 44.5±1.9%, respectively. A 1.36-fold increase in VS reduction was achieved by increasing the 'f' of A-sludge from 0.41 to 0.71 in the feedstocks. Higher VS removal efficiency was observed in reactor within certain limits amount of KW. This phenomenon was also observed by Dan and Li [33]. In contrast, the change trend were changed when 20 (or 30) percent KW was mixed in the feedstocks except for the case of the 'f' value of A-sludge ranged from 0.41 to 0.55 with 20 percent of KW in the substance. Kitchen waste posses the characteristic of extremely high biodegradability, with the hydrolysis of KW, total VFA concentrations increased greatly, the accumulation of VFAs led to irreversible acidification which inhibited methanogenic microorganisms' activities [34]. The problem will get worse if mixing high 'f' value of A-sludge with KW in the substrate. The highest VS reduction, 52.2%, was achieved at an 'f' value of 0.55 with 20%KW in the feedstocks. Small amounts of VS converted into other intermediate products throughout the entire experiment. This was the reason that we can observe the VS removal in the failed reactors.

Total methane yield of all reactors during the experimental period. The total methane yield of the anaerobic reactors is illustrated in Fig. 3. Without KW in the substrate, the average total methane yield at 'f' of 0.41, 0.55, 0.71 of A-sludge were 67.1±3.1, 108.4±5, and 159.7±6.8 mlCH_4/g$VS_{feedstock}$, respectively. The feature of 'f' (VS/TS) is associated with the complex composition of sludge, so as VS/TS to fresh leachate [35]. It should be noted that the improved methane yields were accompanied by the increased proportion of organics in sludge. Organic matter is effective constituent to produce methane. This effect was also seen at the percentage of kitchen waste increased from 0% to 10%, an average total methane yield of 94.3±4.3, 167.6±7.2 and 203.5±8.3 mlCH_4/g$VS_{feedstock}$. The methane yield increased 2.38-fold and 2.16-fold at the percentage of KW 0% and 10% in the substrate as 'f' increased from 0.41 to 0.71. The reactor, 80% A-sludge (0.55), exhibited the best performance which methane yield reached 244.1±11.3 mlCH_4/g$VS_{feedstock}$. The methane yield was highly correlated with the VS reduction (Fig. 2). Higher methane yield was observed in reactor with higher VS reduction. This phenomenon also can be seen by Dan and Li [32]. But when the 'f' further improved to 0.71 due to VFA inhibition slightly, which caused methane yield decreased from 244.1 ml CH_4/g$VS_{feedstock}$ to 183.3 ml CH_4/g$VS_{feedstock}$. For the reactors with 30% KW in the substrate because of an excessive amount of easily digestible matter which cause fatty acids accumulate severely. The methane yield reduced substantially (to a value of 8ml CH_4/g$VS_{feedstock}$), indicating severe process failure. This was also observed in a previous study where the methane yield decreased significantly with 50% or more dog food in the substrate [36].

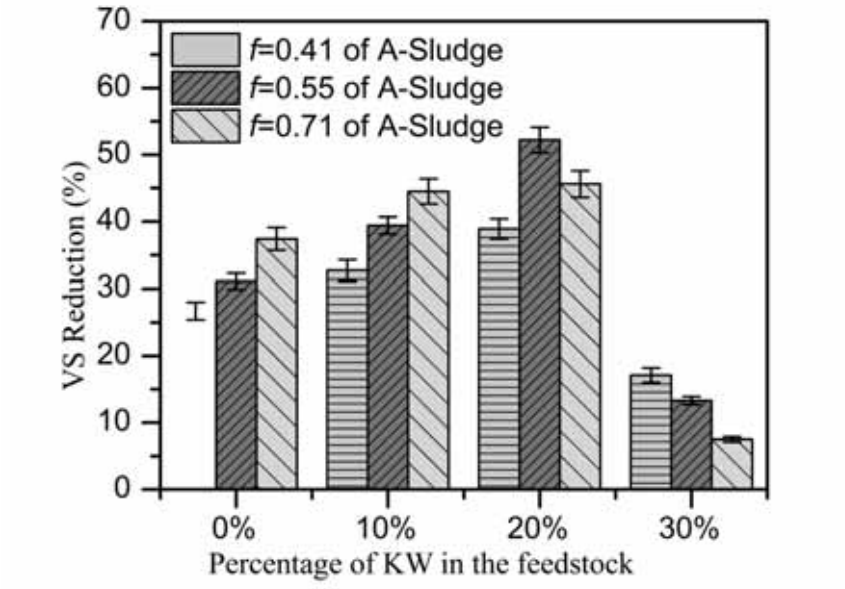


FIGURE 2
Reduction of volatile solids (%) during 30 days anaerobic co-digestion of KW with A-sludge of tested effluent–substrate compositions

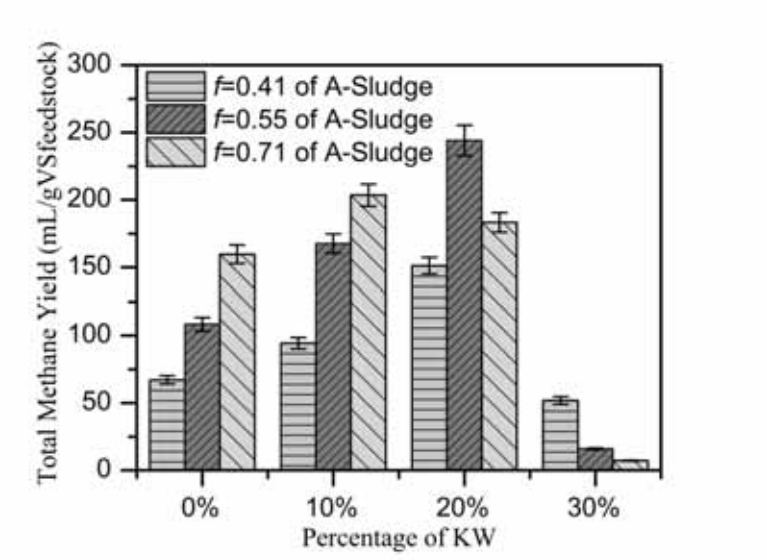


FIGURE 3
Methane yield during 30 days anaerobic co-digestion of KW with A-sludge of tested effluent–substrate compositions

Total volumetric productivity of all reactors during the experimental period. Total volumetric productivity of these anaerobic reactors is shown in Fig. 4. An average total volumetric productivity is 2.24±0.11, 4.21±0.17 and 7.47±0.24 $LCH_4/L_{work\ volume}$ in the 100% A-sludge (0.41), 100% A-sludge (0.55) and 100% A-sludge (0.71), respectively. And for 90% A-sludge (0.41) and 10%KW, 90% A-sludge (0.55) and 10%KW, 90% A-sludge(0.71) and 10%KW， the productivity is 3.85±0.11, 8.25±0.32, 11.32±0.39 $LCH4/L_{work\ volume}$, respectively. Volumetric productivity comparisons are correlated to those of the methane yield comparisons at the same percentage of KW. Increasing 'f' from 0.41 to 0.71 at 0 and 10 percent of KW increased the volumetric productivity 3.3-fold and 2.93-fold, respectively. The volumetric productivity at 20 percent of KW increased by 2.17-fold as the '*f*' was increased from 0.41 to 0.55. As the '*f*' further improved to 0.71, the volumetric productivity decreased to 10.45±0.42 $LCH4/L_{work\ volume}$. It is noted that the highest volumetric productivity (15.93±0.56 $LCH4/L_{work\ volume}$) was obtained in the reactor of 80% A-sludge (0.55) and 20% KW. However, when the portion of kitchen waste boost it to 30 percent, similar to the methane yield, the volumetric productivities also decreased significantly, which mainly resulted from the VFA accumulation (see Fig. 5). The VFA accumulation in these three digesters could lead to the imbalance between the rate of hydrolysis and acidogenesis and that of the generation of acetic acid and its consumption by methanogens for methane production [37].

The change trend of daily methane yield and pH during the experimental period. Fig. 6 represents the daily methane yield of all twelve reactors throughout the entire experiment. In the 100% A-sludge (0.41), 100% A-sludge (0.55) and 100% A-sludge (0.71) (Fig. 6 A) obtained a daily methane yield of 7.78, 8.67 and 9.91L/(kgVS*day), respectively. Improving the percentage of KW to 10 (Fig. 6 B), the three reactors obtained a value of 8.23, 9.34 and 13.54 L/(kgVS*day) respectively. Increasing the '*f*' of A-sludge from 0.41 to 0.71 at 0 and 10 percent of KW in the feedstock increased the maximum daily methane yield to 1.30-fold and 1.65-fold, respectively. However, it should be noted that the peak daily methane occurred with the '*f*' of 0.55 not 0.71 when 20% KW mixed in the feedstock (Fig. 6 C). It could be explained that, when the organic loading rate (OLR) increases, the methane yield increases to some extend but above the optimal OLR the volatile solids degradation and methane yield decreases due to overloading [38,39]. When the percentage of KW improved to 30 (Fig. 6 D), the easily digestible material content apparent severe overloading in the reactor (30%KW, 'f'=0.71), with excessive volatile fatty acids restrain the methanogens activity. Volatile fatty acids are not toxic themselves. However, their inhibiting effects could be indirect as they might lower the pH to undesirable level [40]. The methanogens will not be able to metabolise the acetate produced by the acetogenic organisms until the number of methanogenic organisms has increased sufficiently [41]. It was demonstrated that acetic acid content of >800 mg/L is a signal of digester failure [42]. From Fig.5, by the end of the trial, in the reactors of 70% A-sludge (0.55) + 30%KW and 70% A-sludge (0.71) + 30%KW, the accumulated VFAs reached 1449.2 mg/L and 1647.3mg/L, respectively. They were far exceeded 800 mg/L and ended up in failure.

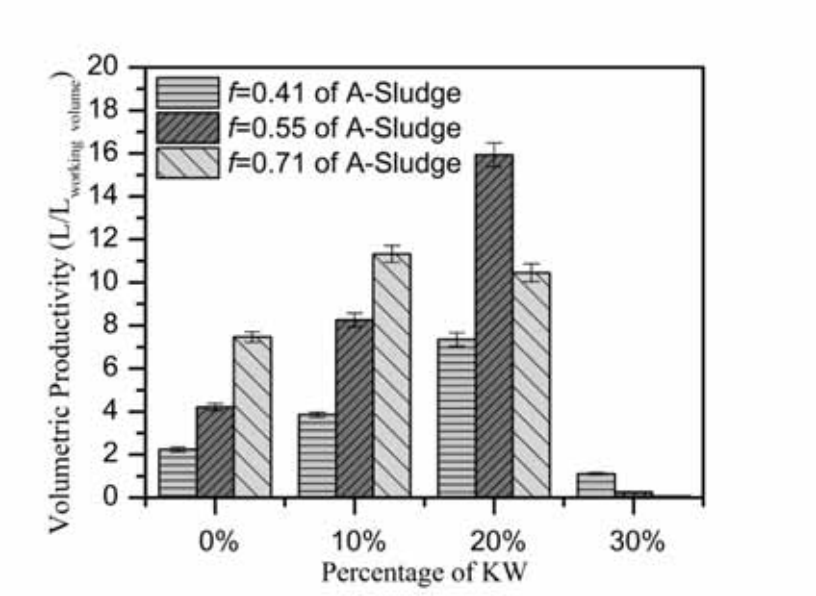


FIGURE 4
Volumetric Productivity during 30 days anaerobic co-digestion of KW with A-sludge of tested effluent–substrate compositions

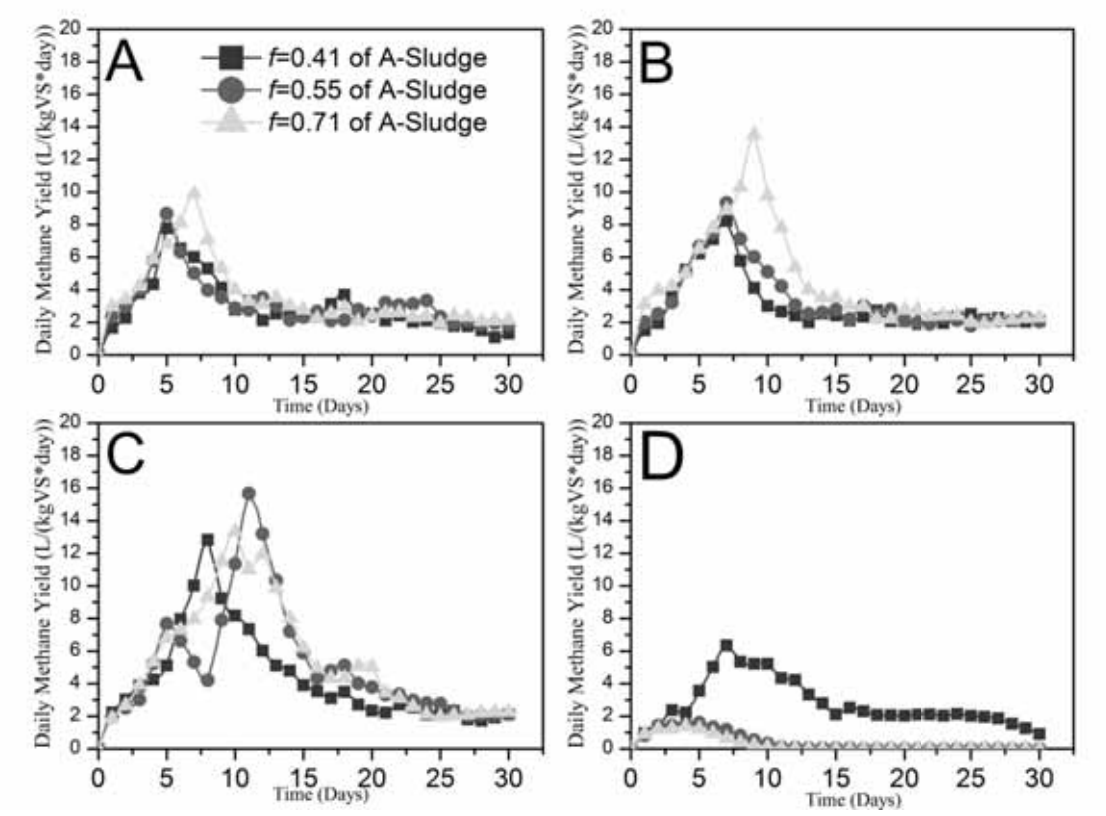


FIGURE 5
Daily methane yield profiles (A, B, C, D) during 30 days anaerobic digestion at the percentage of KW of 0, 10, 20, 30

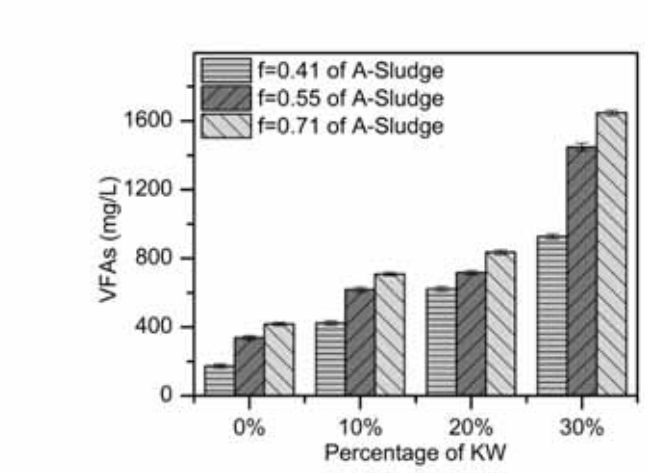


FIGURE 6
VFAs during 30 days anaerobic co-digestion of KW with A-sludge of tested effluent–substrate compositions

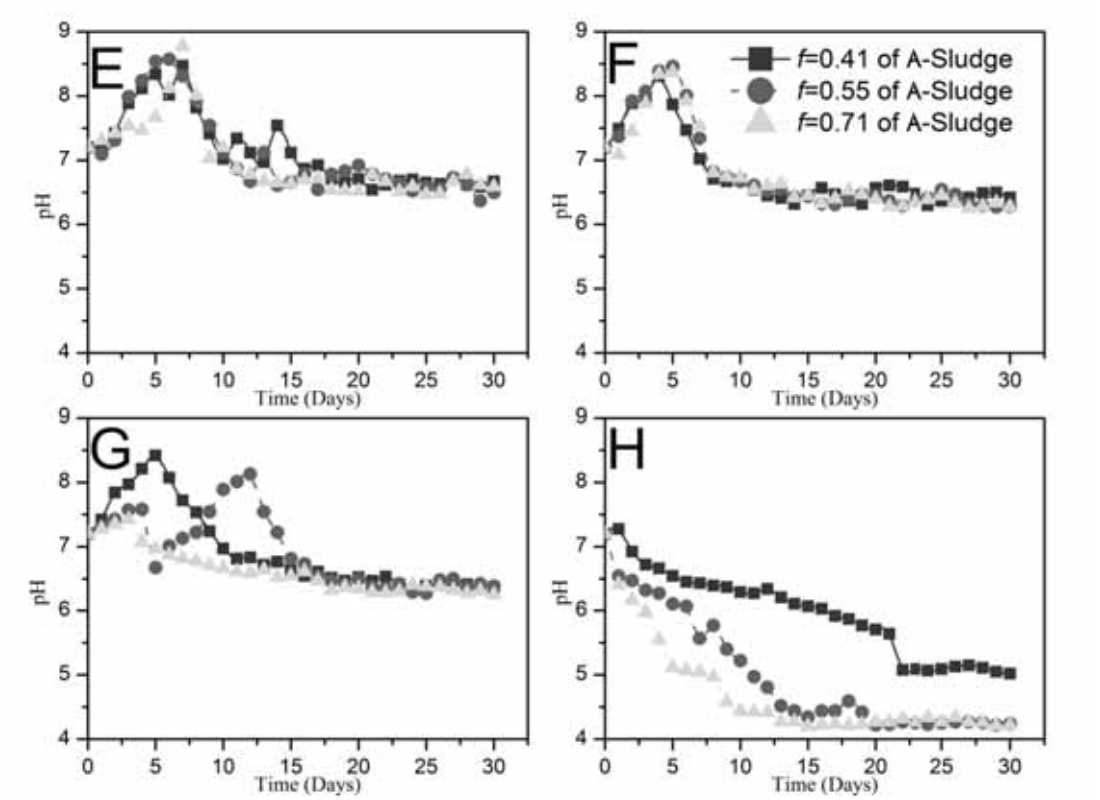


FIGURE 7
Change in the reactors pH (E, F, G, H) during 30 days anaerobic digestion at the percentage of KW of 0, 10, 20, 30

It can be seen from Fig. 7 (E, F, G) that the pH levels increased above 8.0 gradually at initial stage, then decreased below 6.5 gradually until the end. Instability of anaerobic digestion at higher value of pH and it caused rapid conversion rate of ionized ammonia nitrogen (AN) into free ammonia nitrogen (FAN). Increasing amount of FAN inhibited methanogens and resulted in accumulation of VFAs, which again leaded to decrease in pH and thereby declined the concentration of free ammonia nitrogen. The interaction among free ammonia nitrogen, VFAs and pH may lead to an 'inhibited steady state'. It's a condition where the process runs with a lower methane yield [43]. Improving the percentage of KW to 30 (Fig. 7 H), the pH levels decreased below 5.0 due to the hydrolysis/acidification bacteria can produce much VFAs from excessive substrate. The most favorable range of pH to achieve maximal biogas yield

in anaerobic digestion is 6.8–7.2. Methanogenic bacteria are extremely sensitive to pH fluctuations and prefer pH around 7.0 as the growth rate of methanogens is greatly reduced below pH 6.6. Acid-forming bacteria are less sensitive and tolerate pH in range of 4.0–8.5. The pH decrease mainly results from the accumulation of VFAs in the reactors. Increase of VFAs content may be caused by increased activity of the acidogenic bacteria coupled with inhibition of methanogens. Correlated with low methane yield even process failure.

CONCLUSIONS

The co-digestion of A-sludge with Kitchen waste was limited by the low 'f' of A-sludge. This study showed that the performance of anaerobic digestion can be improved by increasing the 'f' of A-sludge. In the WWTPs, high value organic by-product (WAS) can be obtained by adjusting process parameters. The potential energy stored in wastewater can be avoided consuming by the respiration of microbes in activated sludge and convert to stored in WAS. Therefore, the WWTPs require fewer extrinsic waste stream to come true energy self-sufficiency and effectively prevent the acidification which results from large amounts of extrinsic organic waste was loaded into anaerobic reactors. Obviously, this research provides a novel approach to co-treating and co-utilizing kitchen waste with A-sludge from WWTPs.

ACKNOWLEDGEMENTS

The authors would like to thank Ph.D. Oleyiblo Oloche James grammar guidance during the preparation of this paper. This work was supported financially by the China national Water pollution control and treatment science and technology major project (NO. 2012ZX07101-003-002).

REFERENCES

[1] Ardic, I. and Taner, F. (2005) Effects of thermal, chemical and thermochemical pretreativients to increase biogas production yield of chicken manure. Fresen. Environ. Bull. 14, 373-380.

[2] Kougias, P.G., Kotsopoulos, T.A. and Martzopoulos, G.G. (2010) Anaerobic Co-Digestion of Pig Waste with Olive Mill Wastewater Under Various Mixing Conditions. Fresen. Environ. Bull. 19, 1682-1686.

[3] Elnekave, M., Tufekci, N., Kimchie, S. and Shelef, G. (2006) Tracing the mixing efficiency of a primary mesophilic anaerobic digester in a municipal wastewater treatment plant. Fresen. Environ. Bull. 15, 1098-1105.

[4] Shizas, I. and Bagley, D. (2004) Experimental Determination of Energy Content of Unknown Organics in Municipal Wastewater Streams. J Eng. 130, 45-53.

[5] Ventura, J.R.S., Lee, J. and Jahng, D. (2014) A Comparative Study on the Alternating Mesophilic and Thermophilic Two-stage Anaerobic Digestion of Food Waste. J Environ Sci. 26, 1274-1283.

[6] Lin, J., Zuo, J.E., Gan, L.L., Li, P., Liu, F.L., Wang, K.J., Chen, L. and Gan, H.N. (2011) Effects of Mixture Ratio on Anaerobic Co-digestion with Fruit and Vegetable Waste and Food Waste of China. J Environ Sci. 23, 1403-1408.

[7] Zhang, D.Q., Tan, S.K. and Gersberg, R.M. (2010) Municipal Solid Waste Management in China: Status, Problems and Challenges. J Environ Manage. 91, 1623-1633.

[8] Jo, D.V., Lars, D.L., Willy, V. and Nico, B. (2013) High-rate Iron-rich Activated Sludge as Stabilizing Agent for the Anaerobic Digestion of Kitchen Waste. Water Res. 47, 3732-3741.

[9] De La Rubia, M.A., Raposo, F., Rincón, B. and Borja, R. (2009) Evaluation of the Hydrolytic–acidogenic Step of a Two-stage Mesophilic Anaerobic Digestion Process of Sunflower Oil Cake. Bioresour Technol. 100, 4133-4138.

[10] Zhang, C.S., Sun, H.J. and Tan, T.W. (2013) Batch and semi-continuous anaerobic digestion of food waste in a dual solid–liquid system. Bioresour Technol. 145, 10-16.

[11] Buyukkamaci, N. and Filibeli, A. (2004) Volatile Fatty Acid Formation in an Anaerobic Hybrid Reactor. Process Biochem. 39, 1491-1494.

[12] Palacio-Barco, E., Robert-Peillard, F., Boudenne, J.L. and Coulomb, B. (2010) On-line Analysis of Volatile Fatty Acids in Anaerobic Treatment Processes. Analytica Chimica Acta. 668, 74-79.

[13] Zhang, C.S., Xiao, G., Peng, L.Y., Su, H.J. and Tan, T.W. (2013) The Anaerobic Co-digestion of Food Waste and Cattle Manure. Bioresour Technol. 129, 170-176.

[14] Doğan, E. and Demirer, G.N. (2009) Volatile Fatty Acid Production from Organic Fraction of Municipal Solid Waste Through Anaerobic Acidogenic Digestion. Environ Eng Sci. 26, 1443-1450.

[15] Hecht, C. and Griehl, C. (2009) Investigation of the Accumulation of Aromatic Compounds during Biogas Production from Kitchen Waste. Bioresour Technol. 100, 654-658.

[16] Ma, J.X., Duong, T.H., Smits, M., Verstraete, W. and Carballa, M. (2011) Enhanced Biomethanation of Kitchen Waste by Different Pre-treatments. Bioresour Technol. 102, 592-599.

[17] Marañón, E., Castrillón, L., Quiroga, G., Fernández-Nava, Y., Gómez, L. and García, M.M. (2012) Co-digestion of Cattle manure with Food Waste and Sludge to Increase Biogas Production. Waste Manag. 32, 1821-1825.
[18] Zhang, L., Lee, Y.W. and Jahng, D. (2011) Anaerobic Co-digestion of Food Waste and Piggery Wastewater: Focusing on the Role of Trace Elements. Bioresour Technol. 102, 5048-5059.
[19] Kumar, M., Ou, Y.L. and Lin, J.G. (2010) Co-composting of Green Waste and Food Waste at low C/N Ratio. Waste Manag. 30, 602-609.
[20] Kim, H.W., Nam, J.Y. and Shin, H.S. (2011) A Comparison Study on the High-rate Co-digestion of Sewage Sludge and Food Waste using a Temperature-phased Anaerobic Sequencing Batch Reactor System. Bioresour Technol. 102, 7272-7279.
[21] Boehnke, B., Diering, B. And Zuckut, S.W. (1997) Cost-effective Wastewater Treatment Process for Removal of Organics and Nutrients. Water Eng Manag. 144, 18-21.
[22] Verstraete, W. and Vlaeminck, S.E. (2011) Zerowastewater: Shortcycling of Wastewater Resources for Sustainable Cities of the Future. Int J Sustain Dev World. 18, 253-264.
[23] Wett, B., Buchauer, K. and Fimml, C. (2007) Energy self-sufficiency as a feasible concept for wastewater treatment systems. In: IWA Leading Edge Technology Conference, Asian Water, Singapore.
[24] Astals, S., Esteban-Gutiérrez M., Fernández-Arévalo, T., Aymerich, E., García-Heras, J.L. and Mata-Alvarez, J. (2013) Anaerobic Digestion of Seven Different Sewage Sludges: A Biodegradability and Modeling Study. Water Res. 47, 6033-6043.
[25] Silvestre, G., Rodríguez-Abalde, A., Fernández, B., Flotats, X. And Bonmatí, A. (2011) Biomass Adaptation over Anaerobic Co-digestion of Sewage Sludge and Trapped Grease Waste. Bioresour Technol. 102, 6830-6836.
[26] Iacovidou, E., Ohangja, D.G. And Voulvoulis, N. (2012) Food Waste Co-digestion with Sewage Sludge—Realising Its Potential in the UK. J Environ Manag. 112, 267-274.
[27] Dai, X., Duan, N., Dong, B. and Dai, L. (2013) High-solids Anaerobic Co-digestion of Sewage Sludge and Food Waste in Comparison with Mono-digestions: Stability and Performance. Waste Manag. 33, 308-316.
[28] Appels, L., Baeyens, J., Degreve, J. and Dewil, R. (2008) Principles and Potential of the Anaerobic Digestion of Waste Activated Sludge. Prog Energy Combust. 34, 755-781.
[29] Feng, Y.H., Zhang, Y.B., Quan, X. and Chen, S. (2014) Enhanced Anaerobic Digestion of Waste Activated Sludge Digestion by the Addition of Zero Valent Iron. Water Res. 52, 242-250.
[30] Chu, L., Yan, S., Xing, X.H., Sun, X. and Jurcik, B. (2009) Progress and Perspectives of Sludge Ozonation as a Powerful Pretreatment Method for Minimization of Excess Sludge Production. Water Res. 43, 1811-1822.
[31] Angelidaki, I., Alves, M., Bolzonella, D., Borzacconi, L., Campos, J.L. and Guwy, A.J. (2009) Defining the Biomethane Potential (BMP) of Solid Organic Wastes and Energy Crops: A Proposed Protocol for Batch Assays. Water Sci Technol. 59, 927-934.
[32] Gali, A., Benabdallah, T., Astals, S. and Mata-Alvarez, J. (2009) Modified Version of ADM1 Model for Agro-waste Application. Bioresour Technol. 100, 2783-2790.
[33] Dan, B. and Li, Y.B. (2013) Solid State Anaerobic Co-digestion of Yard Waste and Food Waste for Biogas Production. Bioresour Technol. 127, 275-280.
[34] Liao, X.F., Zhu, S.Y., Zhong, D.L., Zhu, J.P. and Liao, L. (2014) Anaerobic Co-digestion of Food Waste and Landfill Leachate in Single-phase Batch Reactors. Waste Manag. 34, 2278-2284.
[35] Zhang, W.L., Zhang, L. and Li, A.M. (2015) Anaerobic Co-digestion of Food Waste with MSW Incineration Plant Fresh Leachate: Process Performance and Synergistic Effects. Chem Eng J. 259, 795-805.
[36] Xu, F. and Li, Y. (2012) Solid-state Co-digestion of Expired Dog Food and Corn Stover for Methane Production. Bioresour Technol. 118, 219-226.
[37] Montusiewicz, A. and Lebiocka, M. (2011) Co-digestion of Intermediate Landfill Leachate and Sewage Sludge as a Method of Leachate Utilization. Bioresour Technol. 102, 2563-2571.
[38] Rincón, B., Sánchez, E., Raposo, F., Borja, R., Travieso, L., Martín, M.A. and Martín, A. (2007) The Effect of Organic Loading Rate on the Anaerobic Digestion of Two- phase Olive Mill Solid Residue Derived from Fruits with Low Ripening Index. J Chem Technol Biotechnol. 82, 259-266.
[39] Babaee, A. and Shayegan, J. (2011) Effect of Organic Loading Rates (OLR) on Production of Methane from Anaerobic Digestion of Vegetables Waste. World renewable energy congress, Linköping/Sweden.
[40] Golueke, C.G., Oswald, W.J. and Gotaas, H.B. (1957) Anaerobic Digestion of Algae. Appl Microbiol. 5, 47-55.
[41] Ward, A.J., Hobbs, P.J., Holliman, P.J. and Jones, D.L. (2008) Optimisation of the Anaerobic Digestion of Agricultural Resources. Bioresour Technol. 99, 7928-7940.
[42] Ewa, K. and Jerzy, T. (2014) Process Characteristics, Inhibition Factors and Methane Yields of Anaerobic Digestion Process, with Particular Focus on Microalgal Biomass Fermentation. Renew Sust Energ Rev. 34, 491-500.

[43] Rajinikanth, R., Daniel, I.M. and Gursharan, S. (2013) A Critical Review on Inhibition of Anaerobic Digestion Process by Excess Ammonia. Bioresour Technol. 143, 632-641.

Received: **03.04.2017**
Accepted: **05.10.2017**

CORRESPONDING AUTHOR

Jiashun Cao
Key Laboratory of Integrated Regulation and Resource Development on Shallow Lakes
Ministry of Education
Hohai University
Nanjing 210098 – China

E-mail: 2461549690@qq.com

© by PSP Volume 26 – No. 12A/2017 pages 7780-7788 Fresenius Environmental Bulletin

ASSESSMENT OF SALT TOLERANCE ACCESSIONS OF *SESBANIA SESBAN* (L.) MERRIL USING SOME MORPHOLOGICAL AND BIOCHEMICAL PARAMETERS

Mohamed Tarroum*, Fahad Al-Qurainy, Salim Khan, Mohammad Nadeem, Aref Alshameri, Abdel-Rhman Z Gaafar, Saleh Alansi

Department of Botany and Microbiology, College of Science, King Saud University, Riyadh, 11451, Saudi Arabia

ABSTRACT

Salinity can negatively affect plant morphology and physiology. The impact of salt stress on plant biomass, total chlorophyll, proline, catalase (CAT), and superoxide dismutase (SOD) was assessed in eight accessions of *Sesbania sesban* (L.) Merrill, namely Sialkot, Khanewal 1, Chiniot, Bhowana 1, Khanewal 2, Sahianwala, Bhowana 2, and Shahpur. These accessions were grown in pots containing sand and peat moss (3:1). Treated plants were watered with 75, 150, and 200 mM NaCl, and untreated plants (control) were irrigated with tap water. A significant variation was noted in salinity tolerance among the accessions. The proline content and antioxidant enzyme activities increased at 75 and 150 mM and decreased at 200 mM NaCl. Khanewal 2, Bhowana 2, and Shahpur were the best-performing accessions, with greater biomass, proline accumulation and higher antioxidant enzyme activities. The Sialkot accession produced the lowest biomass and accumulated less proline with lower antioxidant enzyme activities than the other accessions. Clustering of salt stress responses using Hierarchical Cluster method revealed two major groups: the first comprised more tolerant accessions, and the second comprised moderately tolerant and salt sensitive accessions. Accessions with the highest salt tolerance could be recommended as forge crops in saline areas.

KEYWORDS:
Sesbania sesban (L.) Merril, salt stress, proline, superoxide dismutase (SOD), Catalase (CAT).

INTRODUCTION

Among abiotic stress factors, salt stress is one of the most serious threats to growth and crop productivity worldwide. Many previously published studies have explained the effects of salt-stress on plant parameters. According to Munns and Tester [1], high salinity inhibits plants in two phases: a rapid osmotic stress and a slow ionic phase. It was reported that salinity treatment led to a reduction of plant growth, net assimilation, leaf area, leaf water potential, and leaf photosynthesis. Furthermore, enzymatic activity, osmotic adjustment, protein synthesis, hormone balance transport of ions and water were affected by salt stress [2, 3]. Reactive oxygen species (ROS) are produced in living cells when plants are subjected to biotic or abiotic stress [4]. Thus, the ability of plant cells to maintain low cytosolic sodium concentrations is an essential process associated with their capacity to grow in high salt concentrations [5]. To survive in high salinity soils and mitigate the harmful effect of salt, plants exhibit various physiological and biochemical mechanisms, such as antioxidant enzyme activation and antioxidant compound synthesis, osmoprotectant and compatible solute biosynthesis, ion transport and uptake, ion homeostasis and compartmentalization, polyamine synthesis, and hormone modulation [6]. Previous findings indicated that plants exhibited better protection against the oxidative damage caused by NaCl owing to higher constitutive and induced activities of antioxidative enzymes, such as catalase (EC1.11.1.6, CAT) and superoxide dismutase (EC1.15.1.1, SOD) [7].

Sesbania sesban (L.) Merrill belongs to the subfamily Papilionoideae, family Leguminosae or Fabaceae. *S. sesban* is widely distributed and cultivated throughout tropical Africa and Asia, and has been introduced in tropical America [8]. *S. sesban* is a narrow-crowned, deep-rooting single or multi-stemmed plant that can be a shrub or small tree. In Arabic countries, such as Egypt, *S. sesban* is commonly known as "Egyptian sesban." The paripinnate leaves and tender branches of *S. sesban* are high in protein (20–25% crude protein) and with a high digestibility when consumed by ruminants, such as cattle and goats. The leaves of *S. sesban* have traditionally used as medicine for pain and inflammation. The flowers are arranged on racemes, and each raceme has between 2 and 20 flowers, which are yellow with purple or brown streaks [9]. According to Oosting, et al. [10], *S. sesban* is an exotic multipurpose fodder tree introduced to the Ethiopian highlands for livestock feed and soil conservation.

In the present study, we analyzed the effect of salt stress on plant biomass, total chlorophyll, proline, CAT, and SOD in *S. sesban* (L.) Merrill, to determine if these accessions could be cultivated as forge crops in salt-stressed conditions.

MATERIALS AND METHODS

The seeds of the eight accessions used in this study were obtained from the College of Agriculture, University of Sargodha, Pakistan. The experiment was conducted in the Department of Botany, College of Science, King Saud University. Seeds were sown in pots filled with sand and peat moss (3:1). The pots were maintained in a growth chamber under control conditions at a temperature of 23 ± 2°C, 16 h photoperiod, and 70% relative humidity. After germination, healthy seedlings were selected (one seedling per pot), and irrigated daily with tap water during the initial 3 weeks. After this growth period, pots were separated into four lots, and each lot contained four replications. Salt stress was induced by treating plants with saline solution at three concentrations of 75, 150, and 200 mM; and untreated plants were irrigated with tap water (control). After two months, plants were harvested, and the morphological parameters were determined. The samples were frozen in liquid nitrogen and kept at -80°C until biochemical parameters were measured.

Total chlorophyll estimation. The total chlorophyll (Chl) of leaves were extracted with acetone (80%, v/v) as described by Arnon [11]. The absorbance of the extract was read at 645 and 663 nm using a UV-1800 spectrophotometer (Shimadzu, Japan). The total chlorophyll contents were calculated using the following formula:
Total chlorophyll (µg/mL) = 20.2 (A645) + 8.02 (A663).

Proline levels. Proline was estimated by the method of Bates, et al. [12]. A total of 500 mg fresh leaves was homogenized in 10 mL 3% aqueous sulfosalicylic acid. After centrifugation, 2 mL supernatant was placed in a test tube, to which 2 mL ninhydrin and 2 mL glacial acetic acid were added. The mixture was then heated at 100°C for 1 h. After boiling, the reaction was stopped by placing the tubes in an ice bath for 5 min. Thereafter, 6 mL toluene was added to each reaction and mixed vigorously for 15 s. The absorbance of the upper phase was read at 520 nm using a UV-1800 spectrophotometer (Shimadzu, Japan). The proline values were expressed in µg/g fresh weight.

Antioxidant enzymes assays. Enzyme extractions were based on the methods of Jogeswar, et al. [13]. Leaf samples (100 mg) were ground in liquid nitrogen and dissolved in 100 mM sodium phosphate buffer (pH 7.4) containing 0.1 mM EDTA, 1% (w/v) PVP, and 0.5 % (v/v) Triton-X 100. The homogenate was centrifuged at 14,000 rpm for 20 min at 4°C, and supernatant was used to analyze the following antioxidant enzymes:

Catalase (CAT). CAT activity was measured following the method described by Claiborne [14]. The reaction mixture consisted of 1 mL 0.059 M H_2O_2 in 0.1 M sodium phosphate buffer (pH 7.4), 1.9 mL distilled water, and 100 µL enzyme extract. Catalytic activity was recorded spectrophotometrically by the decline of the absorbance at 240 nm owing to the disappearance of H_2O_2. CAT activity was expressed as units/g protein.

Superoxide dismutase (SOD). Pyrogallol indirect spectrophotometric assay has been developed for measuring SOD [15]. SOD activity was measured following the method of Marklund and Marklund [16]. The reaction mixture contained 1 mL 0.25mM pyrogallol, 1.9 mL 0.1 M sodium phosphate buffer (pH 7.4), and 100 µL enzyme extract. SOD activity (U/g protein) was defined as the amount of enzyme required to cause 50% inhibition of pyrogallol oxidation at 420 nm.

Statistical analysis. Results were statistically analyzed using IBM SPSS statistics 19 software. All values presented for data were the means of four replicates. Data from each parameter was subjected to a two-way analysis of variance (ANOVA); the Post Hoc of multiple comparisons for observed means were assumed by Duncan's test. P values at 0.05 were considered significant.

RESULTS AND DISCUSSION

Effect of NaCl treatments on morphological parameters. This study assessed the tolerance of eight accessions of *S. sesban* (L.) Merrill during salt stress at three levels of 75, 150, and 200 mM. We found a significant variation in the morphological traits (shoot weight, root weight, plant height, and leaf number) among accessions and treatments under both normal and salt stress conditions (Tables 1 and 2). The three NaCl concentrations led to a reduction of plant shoot weight, root weight, plant height, and leaf number in all accessions, and this reduction was more intense at high salt concentrations. Under control conditions, the highest shoot (25.5g) and root (3.3g) weights were recorded in Khanewal 2, whereas the Sialkot accession showed the lowest shoot (23.2 g) and root (2.2 g) weights. We also noted that there was a highly significant effect of both accessions and treatments on shoot and root weights. However, the effect of the interaction of accession and treatments was not significant in the mentioned parameters (shoot and root weights).

Moreover, a strong variation was also observed among accessions and among treatments regarding plant height. In the control conditions and under high NaCl concentrations (200 mM), the accessions Khanewal 2, Sahianwala, and Shahpur were the longest as compared with the other accessions. Concerning the number of leaves per plant, Khanewal 2 showed higher numbers in the control condition. Nevertheless, in the stress condition, the number of leaves of Khanewal 2, Sahianwala, and Bhowana 2 were convergent. The interaction between the treatments and accessions had no significant effect on all previously cited plant growth parameters (Table 2). These results concurred with the findings of several authors who reported that salt stress induced a reduction of plant morphological parameters. Abd_Allah, et al. [17] observed that salt stress drastically reduced the growth performance in *S. sesban*. When studying the effect of salt stress on growth and metabolic changes in nodules and other plant parts of two leguminous species (*Phaseolus vulgaris* and *Sesbania aculeat*e), Ashraf and Bashir [18] found that this stress caused a significant reduction in shoot length, root length, fresh and dry weights of shoots and roots. Patel, et al. [19] noted that shoot and root elongation, tap roots and lateral root tissues of *Delonix regia* (Fabaceae) seedlings were significantly decreased in response to soil salinization. As well for *Robinia pseudoacacia* seedlings, the root biomass, root length, root surface, stem and leaf biomass were decreased when the seedlings were subjected to salt stress [20].

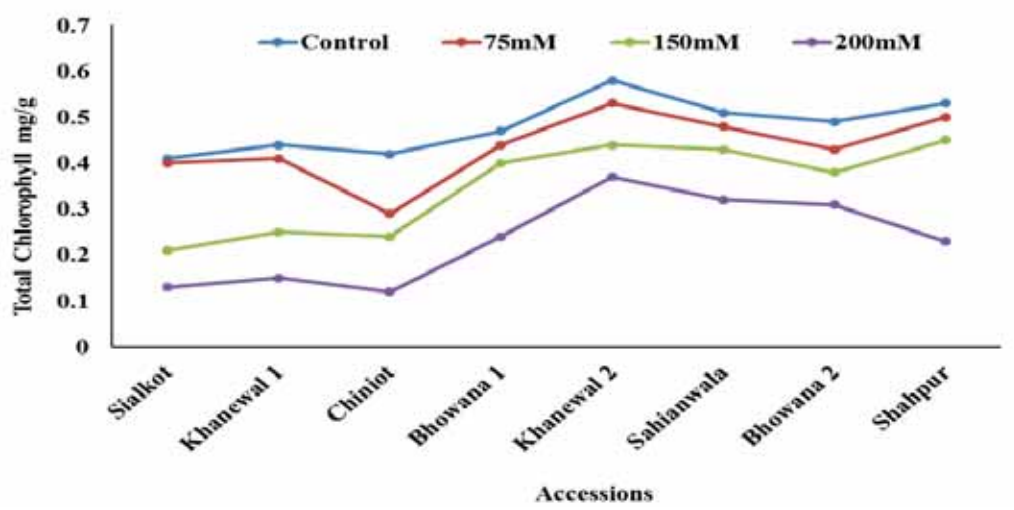


FIGURE 1
Change of total chlorophyll content in eight accessions of *Sesbania sesban* (L.) Merril grown under salt stress

TABLE 1
Effect of salinity on shoot weight, root weight, plant height and leaf number in eight accessions of *Sesbania Sesban* (L.) Merril. (The values are the mean of four replicates ± standard deviation)

	Shoot weight (g)				Root weight (g)			
	Control	75mM	150mM	200mM	Control	75mM	150mM	200mM
Sialkot	23.21 ± 1.19	19.83 ± 3.50	18.84 ± 1.50	13.42 ± 1.99	2.25 ± 0.58	2.1 ± 0.50	1.92 ± 0.47	1.45 ± 0.50
Khanewal 1	25.75 ± 0.34	24.84 ± 1.00	22.32 ± 0.73	15.97 ± 2.27	2.47 ± 0.48	2.44 ± 0.61	1.89 ± 0.88	1.82 ± 1.05
Chinot	27.59 ± 2.40	22.78 ± 1.25	22.46 ± 1.52	17.8 ± 0.92	2.62 ± 0.48	2.57 ± 0.50	1.94 ± 0.42	1.44 ± 0.05
Bhowana 1	25.66 ± 2.45	22.97 ± 1.79	21.95 ± 1.64	16.2 ± 1.30	2.77 ± 0.51	2.7 ± 0.05	2.32 ± 0.68	2.19 ± 1.05
Khanewal 2	29.5 ± 7.42	29.4 ± 6.63	25.49 ± 3.57	25.27 ± 1.76	3.38 ± 0.05	3.16 ± 0.14	2.84 ± 0.44	2.55 ± 0.60
Sahianwala	27.44 ± 0.68	24 ± 1.21	22.74 ± 1.71	22.39 ± 5.0	3.11 ± 0.58	2.98 ± 0.16	2.68 ± 0.70	2.16 ± 0.80
Bhowana 2	27.65 ± 0.24	22.67 ± 2.53	21.73 ± 0.81	20.71 ± 1.60	2.87 ± 0.35	2.79 ± 0.45	2.47 ± 0.52	2.57 ± 0.80
Shahpur	27.67 ± 2.39	26.16 ± 1.23	22.73 ± 1.32	18.13 ± 2.00	2.83 ± 0.38	2.81 ± 0.50	2.37 ± 0.63	2.18 ± 0.50
	Plant height (Cm)				**Leaf number**			
	Control	**75mM**	**150mM**	**200mM**	**Control**	**75mM**	**150mM**	**200mM**
Sialkot	75 ± 12.08	73 ± 2.88	63 ± 6.17	54 ± 9.00	22 ± 3.51	19 ± 2.00	16 ± 3.51	14 ± 5.00
Khanewal 1	87 ± 0.50	85 ± 5.50	72 ± 5.00	71 ± 4.50	23 ± 4.50	23 ± 0.57	22 ± 2.00	19 ± 1.00
Chinot	90 ± 4.00	88 ± 2.75	78 ± 4.00	67 ± 5.50	23 ± 0.57	22 ± 1.52	20 ± 0.00	17 ± 4.50
Bhowana 1	91 ± 8.50	85 ± 7.50	83 ± 7.50	71 ± 3.50	22 ± 1.00	21 ± 0.57	19 ± 1.00	18 ± 1.00
Khanewal 2	96 ± 6.00	86 ± 5.50	85 ± 9.00	74 ± 4.50	26 ± 1.00	25 ± 1.00	24 ± 1.00	22 ± 0.57
Sahianwala	97 ± 4.71	89 ± 10.00	87 ± 7.00	78 ± 6.50	24 ± 2.08	24 ± 0.00	22 ± 1.00	22 ± 1.00
Bhowana 2	101 ± 3.53	92 ± 7.50	92 ± 12.50	91 ± 5.00	24 ± 2.82	23 ± 3.00	23 ± 3.00	22 ± 3.51
Shahpur	98 ± 4.00	96 ± 2.50	94 ± 6.00	83 ± 7.00	23 ± 2.00	22 ± 0.57	21 ± 1.00	20 ± 0.57

TABLE 2
The Results of the P-values showing the effect of accessions, treatments and the interaction accessions - treatments in studied parameters.

	Shoot weight	Root weight	Plant height	Leaf number	Total chlorophyll	Proline	SOD	Catalase
Accessions	**0.000**	**0.000**	**0.000**	**0.000**	**0.000**	**0.000**	**0.000**	**0.000**
Treatment	**0.000**	**0.000**	**0.000**	**0.000**	**0.000**	**0.000**	**0.000**	**0.000**
Accessions -Treatments	0.596	1.000	0.237	0.754	**0.000**	**0.000**	**0.000**	**0.000**

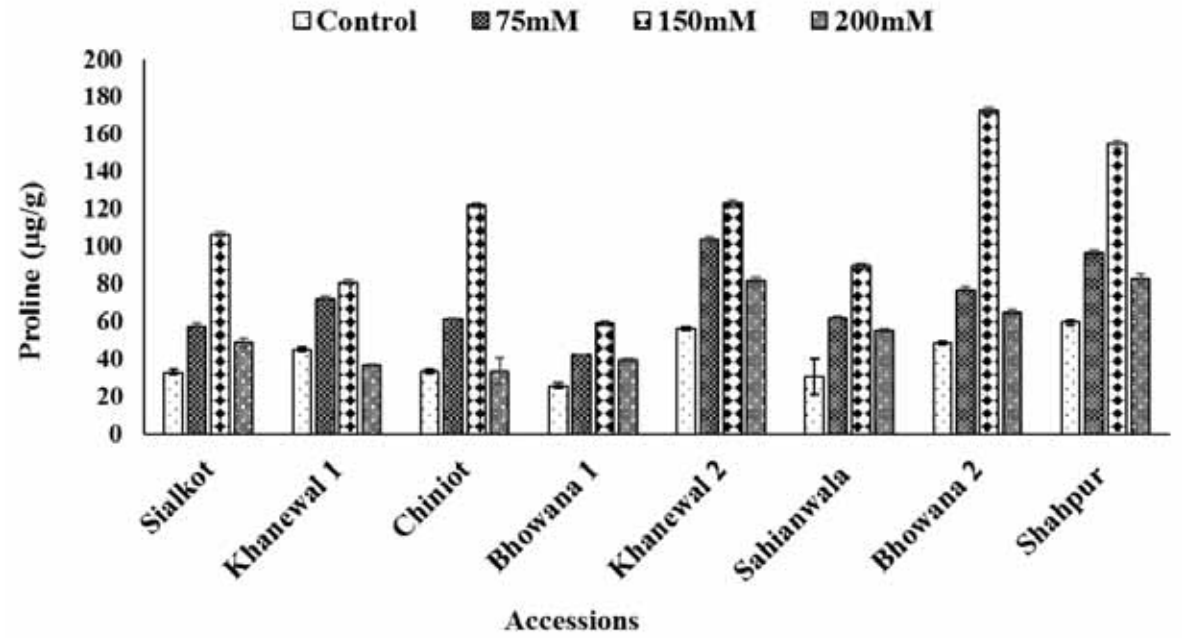


FIGURE 2
Proline accumulation in eight accessions of *Sesbania sesban* (L.) Merril grown under salt stress

Effect of NaCl treatments on total chlorophyll content. Chlorophyll is the main color agent responsible for photosynthesis. Under adverse circumstances, the chlorophyll level is a good indicator of the photosynthesis function [21]. Salt toxicity causes the degradation of pigment, thus a decrease in chlorophyll content owing to salinity stress is relatively common in salt sensitive plants. However, salt tolerant plants can protect themselves from deterioration resulting by the salinity stress effect [22].

In the present study the chlorophyll content of all accessions decreased with increased salt concentrations. Under 200 mM NaCl, the three accessions, Khanewal 2, Bhowana 2, and Sahianwala showed higher amounts of chlorophyll (0.37, 031, and 0.32 mg/g, respectively). However, lower amounts occurred in Shahpur, Sialkot, and Khanewal 1 (Figure 1). In addition to the significant difference between the treatments, it was noted that the total chlorophyll content was highly affected by accessions and by the interaction of accessions and treatments (Table 2). Our findings concur with the results of Taïbi, et al. [23], who noted that salt stress significantly decreased chlorophyll a and b in *Phaseolus vulgaris*. Misra and Gupta [24] also reported that chlorophyll content decreased with increasing NaCl concentrations in two high yielding genotypes of green gram. Several other researchers demonstrated that salinity reduced chlorophyll content in different species, e.g. sunflower [25], *Limoniastrum guyonianum* Boiss [26], *Lolium perenne* L [27] and *Atraphaxis bracteata* [28].

Effect of NaCl treatments on proline content. To cope with salinity, plants trigger different mechanisms that allow their adaptation and survival in saline environment [29]. Among these adaptation mechanisms, proline accumulation is frequently observed during the exposure of plants to adverse environmental conditions [30]. Our results of proline content (Figure 2) showed a significant variation among the accessions. In general, the different *Sesbania* accessions accumulated low proline levels in control conditions at a range of 25 to 59 µg/g. There was a significant increase of proline content in all accessions at 75 and 150 mM of NaCl treatments. However, at 200 mM NaCl concentrations, the proline content was diminished when compared to 75

and 150 mM NaCl. The highest proline content at 150 mM NaCl was detected in Bhowana 2 (172 µg/g) and Shahpur (154 µg/g), while the lowest proline contents were observed in Bhowana 1 (59.1 µg/g) and Khanewal 1 (80 µg/g). The results showed that besides the significant effect of salt treatments on proline accumulation, the proline content was highly affected by accessions and by the interaction between accessions and treatments (Table 2). Previous research of different plant species, such as blue panic grass [31], green gram [24], sunflower [32], and *Triticum aestivum* L. [33] indicated that proline biosynthesis could be stimulated in response to salt stress.

Effect of NaCl treatments on CAT and SOD activities. To grow in stress conditions, plants possess efficient enzymatic antioxidant defense systems, such as CAT and SOD, which work in combination to control uncontrolled oxidation and protect plant cells from oxidative damage by ROS scavenging [34]. In the present study, we analyzed CAT and SOD activities in control and stressed plants. Generally, we observed an increase of both enzymes activities in all accessions at 75 and 150 mM NaCl. However, 200 mM NaCl induced a reduction of enzyme activities when compared to previous treatments. The results of salt effect on CAT activities were summarized in Figure 3. Under the high level of NaCl (200 mM), Shahpur accession was ranked as superior with 65.73 U/g protein. Nevertheless, the lowest values were registered in Sahianwala, Sialkot, Khanewal 1 and Chiniot (25.5, 25.2, 23.5 and 13 U/g protein respectively). In Bhowana 1, Khanewal 2 and Bhowana 2, the moderate and convergent values of catalase activities were recorded.

As shown in Figure 4 all accessions treated with 75mM and 150 mM exhibited an enhancing activities of SOD when compared with their controls. Under 200 mM NaCl, the highest values of SOD activities (17.78, 17.6 and 17.3 U/g protein) were found in Bhowana 2, Chiniot and Bhowana 1 respectively. Whereas the low activity value (13.9 U/g protein) were presented in Sialkot accession. The differences between the effect of treatments and the effect of accessions on CAT and SOD activities were highly significant. The same results of p values (p= 0.000) were observed when studying the effect of interaction accessions and treatments on the activities of both enzymes (Table 2).

Previous studies indicated that NaCl stress could either stimulate or inhibit CAT and SOD activities. Our findings agree with the results of other researchers, such as Xu, et al. [35] and Yadav, et al. [36] , who found that salinity increased the SOD and CAT activities in turf grass and *Azolla*. According to Cavalcanti, et al. [37], CAT activity was dramatically decreased in cowpea leaves 1 day after 200 Mm NaCl treatment, whereas SOD did not change significantly in stressed plants. Studying the effect of salt stress on antioxidant enzyme activities in liquorice plants, Pan, et al. [38] concluded that SOD activity was upregulated, whereas CAT activity decreased owing to the oxidative stress induced by salt stress.

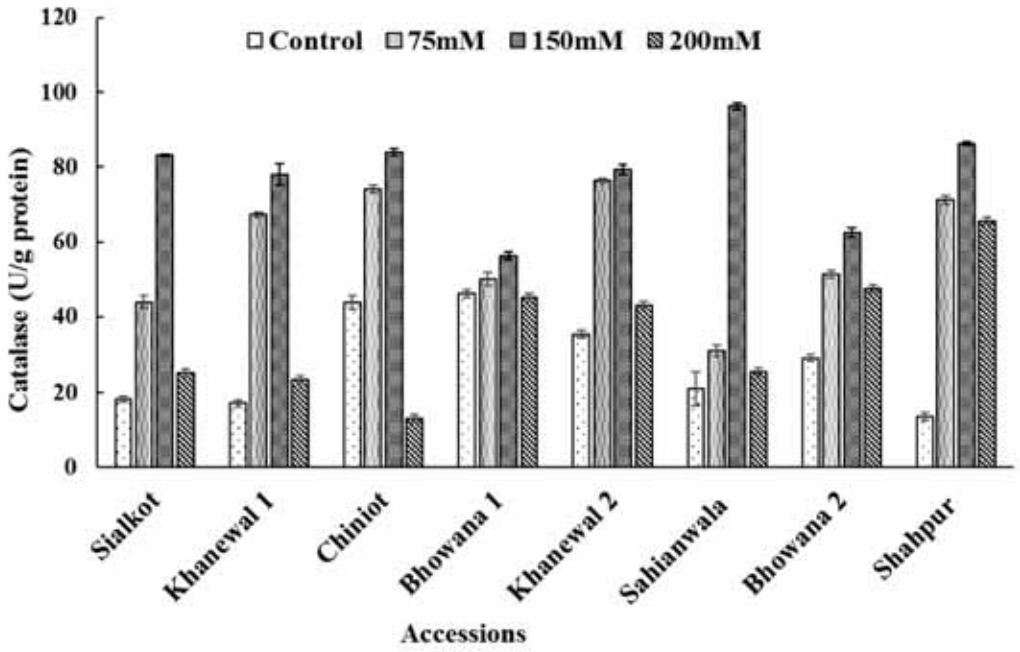


FIGURE 3
Catalase activity of eight *Sesbania sesban* (L.) Merril accessions grown under salt stress.

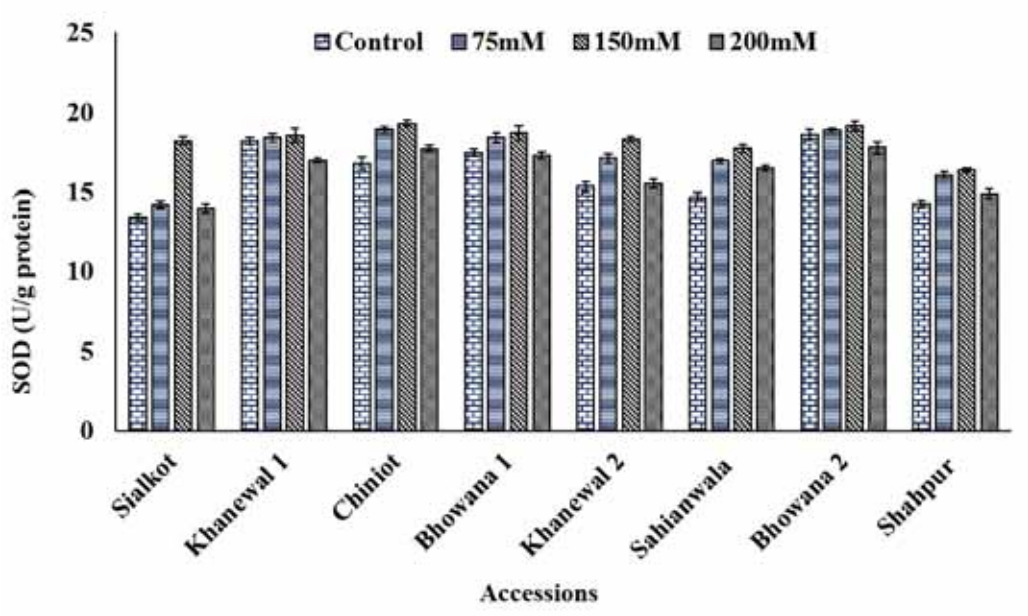


FIGURE 4
SOD activity of *Sesbania sesban* (L.) Merril accessions grown under salt stress.

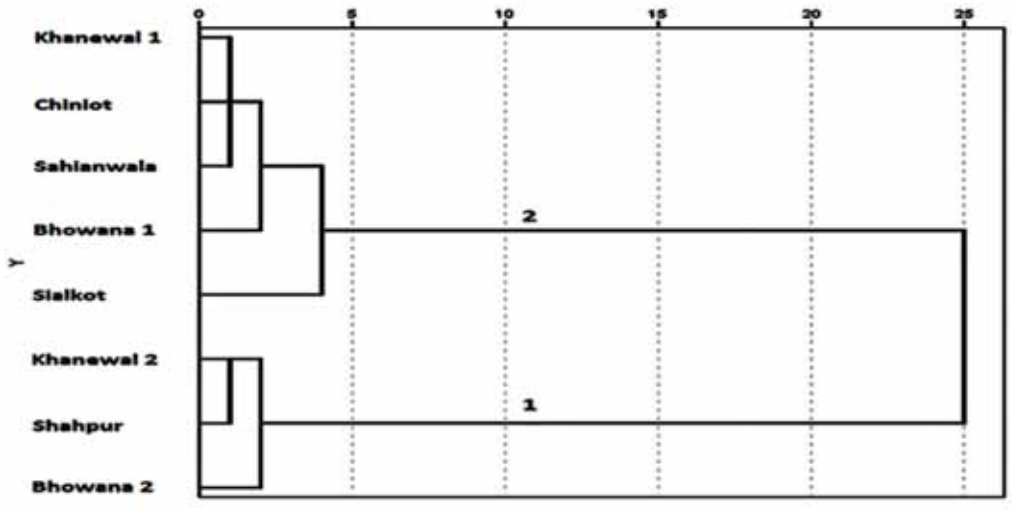


FIGURE 5
Dendrogram showing the relationship among eight *Sesbania sesban* (L.) Merril accessions based on shoot weight, dry weight, plant height, leaf number, total chlorophyll, proline, CAT and SOD in a Hierarchical cluster analysis.

The hierarchical cluster analysis using plant biomass, total chlorophyll, proline, CAT, and SOD activities was performed. It was noted that multivariate analysis distinguished *S. sesban* accessions into two clusters. The first cluster comprised the most tolerant accessions, which are Khanewal 2, Shahpur, and Bhowana 2. The second cluster comprised the accessions characterized as moderately and sensitive to salt stress as shown in Figure 5. Much research has previously used hierarchical cluster analyses to evaluate salt tolerance in rice [39], sugarcane [40], and buffel grass [41] .

CONCLUSION

In conclusion, it is suggested that morphological and biochemical parameters could be used to select salt-tolerant accessions of *S. sesban*. Considering the above-mentioned parameters, Khanewal 2, Bhowana 2, and Shahpur were found to be the best accessions, which could be recommended for use as a forge crop in saline areas.

ACKNOWLEDGEMENTS

The authors extend their appreciation to the Deanship of Scientific Research at King Saud University for funding through the Research Group Project No. RGP-014.

REFERENCES

[1] Munns, R., Tester, M. (2008) Mechanisms of salinity tolerance. Annu. Rev. Plant Biol. 59, 651-681.

[2] Kim, J., Liu, Y., Zhang, X., Zhao, B. and Childs, K.L. (2016) Analysis of salt-induced physiological and proline changes in 46 switchgrass (Panicum virgatum) lines indicates multiple response modes. Plant Physiology and Biochemistry. 105, 203-212.

[3] Hernández, J.A., Corpas, F.J., Gomez, M., Río, L.A. and Sevilla, F. (1993) Salt-induced oxidative stress mediated by activated oxygen species in pea leaf mitochondria. Physiologia Plantarum. 89, 103-110.

[4] Møller, I.M., Jensen, P.E. and Hansson, A. (2007) Oxidative modifications to cellular components in plants. Annu. Rev. Plant Biol. 58, 459-481.

[5] Blumwald, E. (2000) Sodium transport and salt tolerance in plants. Current opinion in cell biology. 12, 431-434.

[6] Gupta, B., Huang, B. (2014) Mechanism of salinity tolerance in plants: physiological, biochemical, and molecular characterization. International journal of genomics. 2014, 1-18.

[7] Jungklang, J., Sunohara, Y. and Matsumoto, H. (2004) Antioxidative enzymes response to NaCl stress in salt-tolerant Sesbania rostrata. Weed Biology and Management. 4, 81-85.

[8] Nigussie, Z., Alemayehu, G. (2013) Sesbania sesban (L.) Merrill: Potential uses of an underutilized multipurpose tree in Ethiopia. African Journal of Plant Science. 7, 468-475.

[9] Gomase, P.V. (2012) Sesbania sesban Linn: a review on its ethnobotany, phytochemical and pharmacological profile. Asian journal of biomedical and pharmaceutical sciences. 2, 11.

[10] Oosting, S., Mekoya, A., Fernandez-Rivera, S. and Van der Zijpp, A. (2011) Sesbania sesban as a fodder tree in Ethiopian livestock farming systems: Feeding practices and farmers' perception of feeding effects on sheep performance. Livestock Science. 139, 135-141.

[11] Arnon, D.I. (1949) Copper enzymes in isolated chloroplasts. Polyphenoloxidase in Beta vulgaris. Plant physiology. 24, 1.

[12] Bates, L., Waldren, R. and Teare, I. (1973) Rapid determination of free proline for water-stress studies. Plant and soil. 39, 205-207.

[13] Jogeswar, G., Pallela, R., Jakka, N., Reddy, P., Rao, J.V., Sreenivasulu, N. and Kishor, P.K. (2006) Antioxidative response in different sorghum species under short-term salinity stress. Acta Physiologiae Plantarum. 28, 465-475.

[14] Claiborne, A. (1985) Catalase activity, In: Greenwald, R.A. (Ed.), Handbook of Methods for Oxygen Free Radical Research, CRC Press, Boca Raton, FL. 283 – 284.

[15] Gao, R., Yuan, Z., Zhao, Z. and Gao, X. (1998) Mechanism of pyrogallol autoxidation and determination of superoxide dismutase enzyme activity.Bioelectrochemistry and Bioenergetics. 45, 41-45.

[16] Marklund, S. Marklund, G. (1974) Involvement of the superoxide anion radical in the autoxidation of pyrogallol and a convenient assay for superoxide dismutase. European journal of biochemistry. 47, 469-474.

[17] Abd_Allah, E.F., Hashem, A., Alqarawi, A.A., Bahkali, A.H. and Alwhibi, M.S. (2015) Enhancing growth performance and systemic acquired resistance of medicinal plant Sesbania sesban (L.) Merr using arbuscular mycorrhizal fungi under salt stress. Saudi journal of biological sciences. 22, 274-283.

[18] Ashraf, M. Bashir, A. (2003) Salt stress induced changes in some organic metabolites and ionic relations in nodules and other plant parts of two crop legumes differing in salt tolerance. Flora-Morphology, Distribution, Functional Ecology of Plants. 198, 486-498.

[19] Patel, A.D., Bhensdadia, H. and Pandey, A.N. (2009) Effect of salinisation of soil on growth, water status and general nutrient accumulation in seedlings of Delonix regia (Fabaceae). Acta Ecologica Sinica. 29, 109-115.

[20] Mao, P., Zhang, Y., Cao, B., Guo, L., Shao, H., Cao, Z., Jiang, Q. and Wang, X. (2016) Effects of salt stress on eco-physiological characteristics in Robinia pseudoacacia based on salt-soil rhizosphere. Science of The Total Environment. 568, 118-123.

[21] Xu, X., Xu, H., Wang, Y., Wang, X., Qiu, Y. and Xu, B. (2008) The effect of salt stress on the chlorophyll level of the main sand-binding plants in the shelterbelt along the Tarim Desert Highway. Chinese Science Bulletin. 53, 109-111.

[22] Alam, M.A., Juraimi, A.S., Rafii, M. and Abdul Hamid, A. (2015) Effect of salinity on biomass yield and physiological and stem-root anatomical characteristics of purslane (Portulaca oleracea L.) accessions. BioMed research international. 2015, 1-15.

[23] Taïbi, K., Taïbi, F., Abderrahim, L.A., Ennajah, A., Belkhodja, M. and Mulet, J.M. (2016) Effect of salt stress on growth, chlorophyll content, lipid peroxidation and antioxidant defence systems in Phaseolus vulgaris L. South African Journal of Botany. 105, 306-312.

[24] Misra, N., Gupta, A.K. (2005) Effect of salt stress on proline metabolism in two high yielding genotypes of green gram. Plant Science. 169, 331-339.

[25] Akram, M.S., Ashraf, M. and Akram, N.A. (2009) Effectiveness of potassium sulfate in mitigating salt-induced adverse effects on different physio-biochemical attributes in sunflower (Helianthus annuus L.). Flora-Morphology, Distribution, Functional Ecology of Plants. 204, 471-483.

[26] Zouhaier, B., Najla, T., Abdallah, A., Wahbi, D., Wided, C., Chedly, A. and Abderrazak, S. (2015) Salt stress response in the halophyte Limoniastrum guyonianum Boiss. Flora-Morphology, Distribution, Functional Ecology of Plants. 217, 1-9.

[27] Hu, T., Li, H.-y., Zhang, X.-z., Luo, H.-j. and Fu, J.-m. (2011) Toxic effect of NaCl on ion metabolism, antioxidative enzymes and gene expression of perennial ryegrass. Ecotoxicology and environmental safety. 74, 2050-2056.

[28] Mei, D., Hang, L., Zhanbin, L. and Kangning, H. (2016) Effects of salinity on water status, ion contents, chlorophyll contents and gase exchange parameters in seedlings of *Atraphaxis bracteata* A. Los. Fresen. Environ. Bull. 25, 3311-3316.

[29] Yang, G., He, X., Zhao, C., Xue, L. and Chen, J. (2016) A saline water irrigation experimental investigation into salt-tolerant and suitable salt concentration of Haloxylon ammodendron from Gurbantunggut Desert, Northwestern China. Fresen. Environ. Bull. 25, 3408-3416.

[30] Rejeb, K.B., Abdelly, C. and Savouré, A. (2014) How reactive oxygen species and proline face stress together. Plant Physiology and Biochemistry. 80, 278-284.

[31] Ahmad, M.S.A., Ashraf, M. and Ali, Q. (2010) Soil salinity as a selection pressure is a key determinant for the evolution of salt tolerance in Blue Panicgrass (Panicum antidotale Retz.). Flora-Morphology, Distribution, Functional Ecology of Plants. 205, 37-45.

[32] Wu, G., Jiao, Q. and Shui, Q. (2015) Effect of salinity on seed germination, seedling growth, and inorganic and organic solutes accumulation in sunflower (Helianthus annuus L.). Plant Soil Environ. 61, 220-226.

[33] Rana, V., Ram, S., Sedhil, R., Nehra, K. and Sharma, I. (2015) Physiological, Biochemical and Morphological Study in Wheat (Triticum aestivum L.) RILs Population for Salinity Tolerance. Journal of Agricultural Science. 7, 119.

[34] Gill, S.S., Tuteja, N. (2010) Reactive oxygen species and antioxidant machinery in abiotic stress tolerance in crop plants. Plant Physiology and Biochemistry. 48, 909-930.

[35] Xu, R., Yamada, M. and Fujiyama, H. (2013) Lipid peroxidation and antioxidative enzymes of two turfgrass species under salinity stress. Pedosphere. 23, 213-222.

[36] Yadav, R.K., Tripathi, K., Ramteke, P.W., Varghese, E. and Abraham, G. (2016) Salinity induced physiological and biochemical changes in the freshly separated cyanobionts of Azolla microphylla and Azolla caroliniana. Plant Physiology and Biochemistry. 106, 39-45.

[37] Cavalcanti, F.R., Oliveira, J.T.A., Martins-Miranda, A.S., Viégas, R.A. and Silveira, J.A.G. (2004) Superoxide dismutase, catalase and peroxidase activities do not confer protection against oxidative damage in salt-stressed cowpea leaves. New Phytologist. 163, 563-571.

[38] Pan, Y., Wu, L.J. and Yu, Z.L. (2006) Effect of salt and drought stress on antioxidant enzymes activities and SOD isoenzymes of liquorice (Glycyrrhiza uralensis Fisch). Plant Growth Regulation. 49, 157-165.

[39] Chunthaburee, S., Dongsansuk, A., Sanitchon, J., Pattanagul, W. and Theerakulpisut, P. (2016) Physiological and biochemical parameters for evaluation and clustering of rice cultivars differing in salt tolerance at seedling stage. Saudi journal of biological sciences. 23, 467-477.

[40] Cha-um, S., Chuencharoen, S., Mongkolsiriwatana, C., Ashraf, M. and Kirdmanee, C. (2012) Screening sugarcane (Saccharum sp.) genotypes for salt tolerance using multivariate cluster analysis. Plant Cell, Tissue and Organ Culture (PCTOC). 110, 23-33.

[41] Al-Dakheel, A.J., Hussain, M.I. and Rahman, A.Q.M.A. (2015) Impact of irrigation water salinity on agronomical and quality attributes of Cenchrus ciliaris L. accessions. Agricultural Water Management. 159, 148-154.

Received: **05.04.2017**
Accepted: **20.09.2017**

CORRESPONDING AUTHOR

Mohamed Tarroum
Department of Botany and Microbiology
College of Science
King Saud University
Riyadh, 11451 – Saudi Arabia

e-mail: med_taroum@yahoo.fr

© by PSP Volume 26 – No. 12A/2017 pages 7789-7800 Fresenius Environmental Bulletin

EVALUATION OF FACTORS RELATED TO WELL-BEING EFFECTS OF URBAN GREEN SPACES ON USERS

Serap Yilmaz*, Tugba Duzenli, Deryanur Dincer

Department of Landscape Planning and Design Karadeniz Technical University, Turkey

ABSTRACT

The satisfaction of urban green areas depend on people's perceptions of environment, their preferences and the extent to which they fulfil the needs of environment. Within this context, the physical features of urban green spaces and the activities that they offer have a great role in its impact on users' mental-physical-social well-being. This study aimed to focus particularly on whether there is a correlation between satisfaction, well-being and how users describe social-mental and physical well-being and which values they use to describe them.

The questionnaire was conducted in two phases. In the first phase, the general evaluations of the users related to urban green areas have been examined. In the second phase, 20 statements have been prepared through making use of previous studies in order to describe the emotions related to mental-physical-social well-being that green areas caused for the users.

As a result, it has been determined that the satisfaction of the green spaces with the user, the usage frequency of the green spaces, the proximity to the green spaces and the well-being formed by the individuals are related to each other. The strongest correlations in urban green spaces are satisfaction and mental well-being; proximity to green spaces and social well-being.

KEYWORDS:
Urban green space, Well-being, Satisfaction, Frequency of use, Proximity

INTRODUCTION

Urbanisation affects environment negatively leading to air pollution, noise, waste products, the destruction of natural areas for urban development, the degeneration in quality of urban life, the decrease in urban landscape and reduced green space for recreation [1, 2]. However, for urban quality of life, urban green spaces are significant as they are important in cities because they enable people to have interaction with nature and one another [3]. They improve human health through generating ecosystem services including climate regulation, capture of pollutants or food regulation. Moreover, they also enable the interaction of neighbors and community integration, and provide a beneficial place for health, relaxation and nature contemplation [4-8]. Decreases in urban green spaces alienate people who live in urban areas from nature and destroy the positive relationship between the citizens and nature [9, 10]. Therefore, the alienation between natural world and the individual grows due to the impacts of urban culture. Consequently, people in cities feel less satisfied with the life [11].

Urban green spaces neutralize unfavorable impacts and enable to sustain the urban quality of life [2] since interaction with nature is a basic human need and availability of urban green area becomes significant in this context [12-14] and in the concept of the urban quality of life [15, 8].

Well-Being effect of Urban Green Space. Urban green spaces are described by Gupta et al. (2012) as a fundamental part of urban areas [16]. They are also considered as crucial in maintaining the environmental quality and sustainability by Gupta et al. (2012) [16]. There are different types of urban green areas including parks, gardens and recreation venues, informal green spaces such as river or sea fronts, green spaces surrounding historical sites, railway corridors, street trees, urban agriculture, citizenial lawns, and roof gardens [16, 17]. Urban citizens are provided with a great number of benefts by urban green areas. For instance, these areas act as lungs which represent clean air, water and soil for natural urban environment [16]. In consequence of these benefits, the cities are contributed ecologically to a great extent by urban green spaces. Nevertheless, citizens' use of these areas is linked to satisfaction the users have while using them, and therefore it becomes important to examine the term satisfaction. It was suggested by Bertram and Rehdanz (2015) that urban green space affects life satisfaction in a positive way [15]. Previous studies cited social integrative role of urban green spaces for individuals who live in arge and dense cities [18, 19]. Likewise, it was asserted that urban green areas unite different parts of the city, they encourage people to come together and build a sense community [20]. As indicated by Kaplan and Kaplan (1982), as well as building a sense of community, urban green areas also offer -

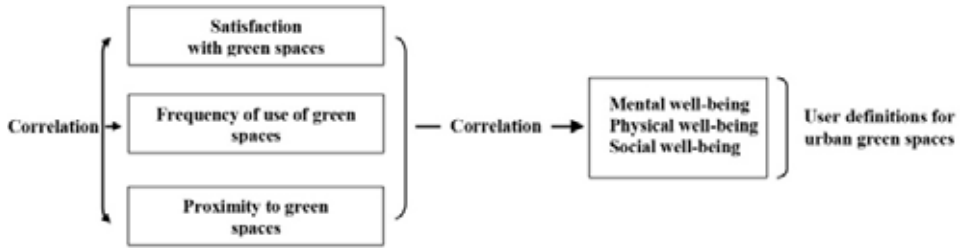


FIGURE 1
Research Framework

opportunities like mental well-being, obtaining a range of information, physical exercise, and comfort [21]. As long as the needs and expectations of a green space user are fulfilled thanks to the provided opportunities, the satisfaction rate rises and the quality of life enhances [22]. Citizens' perception of urban areas is related to functionality of urban green spaces. Citizens' perception of urban areas is connected to functionality of urban green spaces. Urban green spaces are supposed to provide opportunities for not only social but also physical activities and they should become areas that enable people to meet for a number of activities such as walking, relaxing, playing, meeting and observing surrounding environment [24].

Urban green spaces are of great importance for being social centres where users from different cultures and socio-economical classes come together and fulfil social needs such as meeting and sharing life and where citizens integrate and interact with nature [22, 25, 26] in addition to enhancing the degree of a city's liveability by offering different kinds of social, economical, and ecological opportunities [1, 2]. With the help of urban green spaces, individuals also recover from stress physically and mentally [27]. Therefore, urban green spaces are considered relaxing and satisfactory. According to Yılmaz et al. (2016), urban green areas are expected to meet the desires of users such as visual aesthetics, personal values, social interaction and identity, psychological and physical satisfaction so as to increase satisfaction. Urban green areas are studied from different perspectives with regard to user satisfaction [22]. Some studies investigated the physical and/or social aspects and some others explored their benefits to mental-physical health [12, 22, 23, 27-29] and the others studied their social benefits [4, 22, 24]. Furhermore, the recreational activities in urban greespaces are significant in that they could be related to people's physical health and psychological well- being [30, 31]. Within the past three decades, more and more studies have emphasized that urban green spaces are a resource in promoting public health. Green places have been thought to advance health through restoring mental fatigue [9], functioning as a resource for physical activities [32], and diminishing all-cause and cause-specific mortality [33]. Nonetheless, a majority of research have focused on the resources that decrease stress levels [28, 34, 35].

When compared to the studies on the effects of urban green areas on physical well-being and mental well-being, it has been seen that fewer studies have been conducted on the benefits of interacting with green areas on social well-being [36]. However, socializing also has a great role in people's well-being [36, 37] becasue the increases in social interaction [38-40]and physical activity [40, 41] are linked to the use of green spaces. Therefore, socializing has an important role in mental well-being [36, 42, 43] and physical well-being [36, 44]. In addition to these, it is merely possible to make use of urban green areas when these areas are used; if the individuals live closer to green areas, they have more social activities and use green areas more [45, 46]. The farther individuals live from green areas, the less they use those areas [35, 47].

Research Framework and Study Questions. The satisfaction of urban green areas depends on people's perceptions of environment, their preferences and the extent to which they fulfil the needs of environment. Within this context, the physical features of urban green spaces and the activities that they offer have great role in its impact on users' mental-physical-social well-being. However, it is also of great importance to know the way the satisfaction of green areas reflects into people's lives and the kind of emotions they arise. This study aimed to focus particularly on whether there is a correlation between satisfaction, well-being and use (the frequency of visiting green areas and living close to green areas), and how users describe social-mental and physical well-being and which values they use to describe them.

Research Framework has been formed to explain the correlation between the users' satisfaction of green areas, the frequency of using these areas, their perceptions of closeness to these areas and the correlation of these with well-being (Figure 1). Within this context, the study aims to reveal the factors that best describe the relationship between *"the*

well-being that the environment provides and satisfaction-the frequency of use-the perceived proximity of home to green areas". In accordance with these users' assessments of their satisfaction of green spaces, frequency of use and perception of distance were analyzed in three aspects: mental well-being, social well-being and physical well-being. The hypotheses of the study are: (a) user satisfaction in urban green areas is related to citizens' perceived proximity of home to green, the frequency of using green areas and the well-being that those areas provide to them; (b) Urban green areas could affect physical - mental - social well-being of society positively through creating positive emotions for the users.

METHOD

Study Area. The study area is Rize Municipality borders and the study has been conducted in Rize city centre. The green areas that exist in Rize city centre are used as the study materials. The population of Rize city centre is 145.739. Rize is chosen for study area because of the increase in the green areas in the city. While urbanization in our country is directly proportional with the increased number of buildings and decrease in green areas, an opposite development is seen in Rize.

In this study, urban green space is described as a range of parks which are positioned in different regions in Rize. These parks are described as places where users are not involved only visually but also in which they do a range of activities (Table 1).

The Questionnaire. The questionnaire was conducted on 450 users from study areas, and 150 visitors participated from each park. Regardless of their education level and age, the participants are selected in a random way. The participants are merely required to know Rize city center and use the green areas. The participants are chosen from those who have accepted to take part in the questionnaire. The questionnaire has been conducted using a 5-point Likert scale ranging from 1= "strongly agree" to 5= "strongly disagree".

The questionnaire was conducted in two phases. In the first phase, the general evaluations of the users related to urban green areas have been examined. In order to achieve this aim, the questions below were asked:

- Does the quantity of the green areas in the city satisfy you?
- Do you think that you have perceived proximity of home to green?
- Do you use green areas frequently?
- Does the time you spend in green areas affect your mental health positively?
- Does the time you spend in green areas affect your physical health positively?
- Does the time you spend in green areas affect your socialization positively?

TABLE 1
Description of the three cases studied

Urban Green Spaces	Description
Park I 	This urban place provides its users with opportunities of sitting, watching, eating-drinking and walking. However, it doesn't include enough opportunities for physical activities (such as sports field) Large trees generate an enclosed atmosphere and give people the chance to be in both sunny and shady places. This area is well-protected and it has the quality of being a botanical garden.
Park II 	This urban place has an historical and cultural quality; there are benches where people can sit and look at the cultural building. It provides opportunity for its users to sit, watch the view and eat-drink and it gives the chance to children to play games. However, it doesn't have enough opportunities for physical activities (such as sports field, walking routes etc.) It has various botanical elements (tall plants, bushes and seasonal flowers) and rich topographical shapes.
Park III 	This urban green area is bounded with seaside on one side and a roadway on the other side. Therefore, the effect of noise is decreased through coniferous treesused in road side and the topography. It provides its users with sitting, watching, walking and sport opportunities and children with playing opportunities.

TABLE 2
The correlation values between satisfaction of urban green areas and variables

	1	2	3	4	5	6
Satisfaction	-	,430**	,633**	,318**	,319**	,408**
Frequency of use		-	,657**	,906**	,811**	,413**
Proximity to green space			-	,602**	,522**	,653**
Mental well-being				-	,932**	,397**
Social well-being					-	,313**
Physical well-being						-

** The correlation is significant at the level of 0.01 (2-tailed)

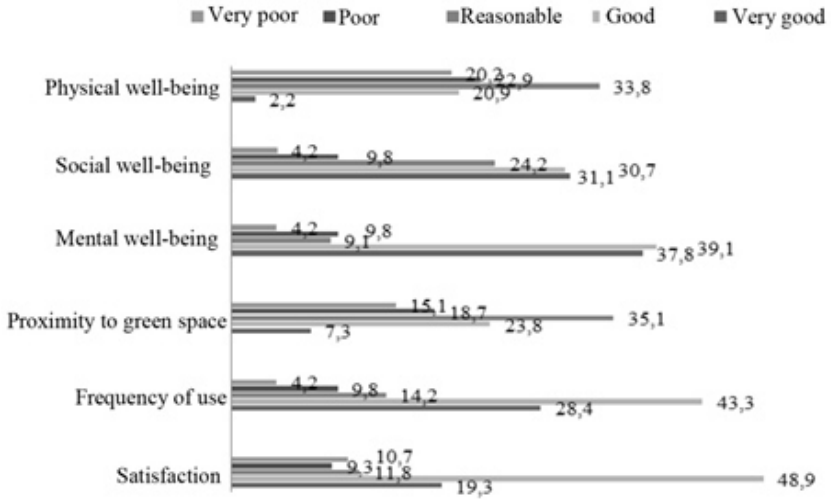


FIGURE 2
Arithmetic means related to urban green areas

In the second phase, 20 statements have been prepared through making use of previous studies in order to describe the emotions related to mental-physical-social well-being that green areas caused for the users [4, 22]. The users gave points to the statements between 1-5 (5-point Likert scale). These results were analyzed with factor and regression analysis and the following questions were tried to be answered:

- What is / are the factor / factors that best describe(s) urban green areas?
- Which correlation or correlations between the satisfaction green areas cause people to have, the frequency of use, perceived proximity of home to green and well-being (mental well-being, physical well-being, social well-being) are the strongest?

Data analysis. In the first stage and the second stage, $\chi 2$-tests were conducted by SPSS (v. 17.0) to determine if these responses are statistically significant. The results of the $\chi 2$-tests indicated that all the categories are statistically significant and correlation analysis was used to analyze the correlation between satisfaction and frequency of use, proximity to green areas and the well-being effect of green areas, and discrepancy is anlayzed through T-test.

Data in the second stage were assessed through factor analysis. In the second stage, the collected data were evaluated by factor analysis. In factor analysis, factors whose eigenvalues equal to 1 or are greater than 1 were considered as significant factors. Factors of which eigenvalues approximately equal to 1 were added to evaluation for the purpose of explaining total variance close to 65% values according to cumulative percentage values. Thus, variables that had factor concentration greater than 0, 65 on the factors that were subjected to rotation were determined as descriptive variables of green areas. The questions which defined the correlation between "satisfaction, the frequency of use and distance" are analyzed through "regression" analysis and model/models have been described.

RESULTS AND DISCUSSION

Results are explained in two stages. In the first stage, general evaluations have been done on urban green spaces in Rize. The second stage indicates the findings of the questionnaire survey such as the feelings that the green spaces arouse in users.

I. Stage: General evaluations of the users related to urban green areas: In order to test research hypothesis, the data related to "satisfaction, the frequency of use, proximity to green space and well-being" (Figure 2) and the correlations of these variables were evaluated in Table 2.

The results showed that,

- 48. 9% of the participants decribed their satisfaction in green areas as good ($\chi2$= 248.289, 4df, p< 0.01).
- 43.3 % the participants stated that they use green areas "frequently" ($\chi2$= 225.578, 4df, p < 0.01).
- 35. 1% the participants stated that they live close to green areas ($\chi2$= 96,467, 4df, p < 0.01).
- 39.1% the participants stated that green areas are good for mental well-being; 37.8% of them stated that green areas are very good for mental well-being ($\chi2$= 24.336, 1df, p < 0.01).
- 31.1% the participants stated that green areas are very good for social well-being; 30.7% of them stated that green areas are good for social well-being ($\chi2$= 136.911, 4df, p < 0.01).
- 33.8% the participants stated that green areas are reosanably good for physical well-being; 20.9% of them stated that green areas are good for social well-being ($\chi2$= 115.889, 4df, p < 0.01).

According to these results, green areas in the city of Rize provide its users with mental and social well-being at average levels, and they provide its users with physical well-being at a lower level. However, the environment plays a vital role in physical well-being, mental well-being and social well-being [34, 40, 47-49]. The activities that the environment has are important to form the effect of satifaction [12, 21, 40, 49]. Therefore, the reason why the physical well-being is at a lower level is that the green areas have fewer physical activities. Nevertheless, open space activities provide various affordances like socialization and create positive effects psychologically and socially [22]. According to Akpınar (2016), higher frequency of physical activity results in less stress and better mental health [50]. Moreover, previous studies show that physical activity in a green space leads to mental and health benefits [51, 52]. Within this context, the physical activity opportunities that green spaces have affect both social well-being and mental well-being. In addition to these evaluations, the frequency of use by the users is also an important finding because the use of green areas affects socialization [22, 38], physical activity [40] and mental well-being [53]. As a consequence, it increases the level of well-being that the society feels in urban green spaces.

In order to reveal the correlation between variables related to urban green areas, a correlation analysis has been done and the results have been evaluated (Table 2):

When urban green areas have been evaluated, it has been seen that the correlation between the variables and satisfaction is significant at the level of 0.01 and positive. Findings verify the statement, which is in the first hypothesis of the study, "User satisfaction in urban green areas has correlation with citities' proximity to green space, the frequency of using these areas and the well-being that they provide for the users." The satisfaction that the users have toward urban green areas and its correlation with the variables is quite important because satisfaction of green areas is related to perceptions of people on green areas and the extent to which those areas fulfill their needs. These findings indicate that green areas in the city of Rize fulfill its users' needs at an average level.

II. Stage: User evaluations on well-being. Determining the mean values for parks according to the points given to the questions related to urban green areas. In this stage, 20 statements which have been prepared based on previous studies [4, 22] and which define the well-being effect that green areas provide for its users have been evaluated as questionnaire questions: Firstly, the points that have been given by the users to each question in the questionnaire have been specified (Figure 3).

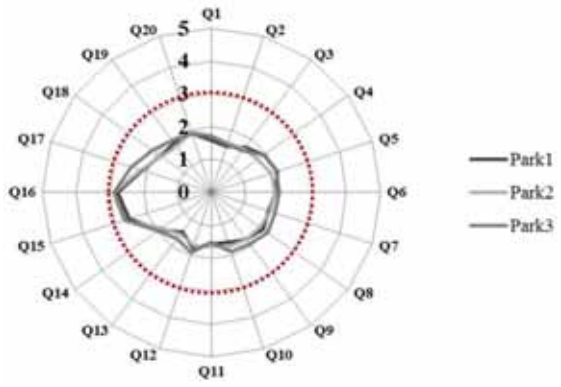


FIGURE 3
Mean values of the points given to the questions for parks (Attitude statements scored from 1 [strongly agree] to 5 [strongly disagree]).

Secondly, factor analysis has been done for the statements that describe the well-being effect of green areas and that have been evaluated by the users. The factor groups have been illustrated in Table 3. Finally, model / models has / have been formed through evaluating the correlations of the factors with satisfaction, the frequency of use and perceived proximity to green place (Table 4,5,6).

When the points given to the questions by the users have been evaluated, it has been seen that these three parks have similar points:

- According to user evaluations of Park 1; The questions that had the highest scores in describing the Park 1 are as follows: Q13 "*Contact with nature*" (1.47), Q2 "*I feel peace*" (1.46), Q11 "*I breath clean air*" (4.03). The Q16 "*Meet with others*" (2.77) had the lowest score.
- According to user evaluations of Park 2; The questions that had the highest scores in describing the Park 2 are as follows: Q2 "*I feel peace*" (1.58), Q13 "*Contact with nature*" (1.57), Q11 "*I*

breath clean air" (1.63) and Q3 "*I get relaxed*" (1.64). The Q16 "*Meet with others*" (2.88) had the lowest score.

- According to user evaluations of Park 3; The questions that had the highest scores in describing the Park 3 are as follows: Q11 "*I breath clean air*" (1.51), Q2 "*I feel peace*" (1.54), (1.57) and Q3 "*I get relaxed*" (1.57). The Q15 "*Being together with our beloved/ friends*" (2,67) and Q16 "*Meet with others*" (2.87) had the lowest score.

The points given to the questions by the users indicated that while green areas provide "green texture" for the city, they also provide mental, physical and social well-being opportunities because even the question that had the lowest point; "*Meet with others*" (2.87) has been answered as "agree" by the user. All of the 20 statements that express the feelings and sharings of the users in urban green space had positive results in Likert scale (strongly agree, agree). The results showed that green areas in Rize provide mental well-being, physical well-being and social well-being opportunities for the users. Green areas have mental well-being opportunities such as "peace, relaxing, happiness and seeing life positively", physical well-being opportnities such as "fresh air, contact with nature, sports activities and walking" and social opportunities such as "meeting and talking". The results of the study indicated that urban green spaces in cities positively affect well-being of users by keeping away those from the noise and stress of the city, and in consequence of this effect, feelings, which describe psychological recover such as happiness and tranquillity arouse. Through building opportunities for coming together with other citizens and conversation, urban green spaces create chances for socialization. The results are consistent with the previous studies that prove that natural areas have mental and physical well-being effect on individuals [4, 23, 40, 54-57] and social well-being [58].

The most important reason why urban green areas in Rize arouse well-being effect on people has been thought to be the effect of naturalness of those areas because according to the definitions in Table 1, it is seen that these areas are the places that have dense planting and natural view. Naturalness is recognized with its crucial role in quality of life which is described to be linked to experience of quietness and peacefulness to users [9, 23, 57]. According to Carrus et al. (2013), well-being enhances with the level of naturalness [59]. The evaluations in line with the findings verify the hypothesis which suggests that "urban green areas are likely to affect society's physical-mental-social well-being positively through leading to positive emotions for users".

Factor analysis evaluations related to the statements describing the well-being effect of urban green areas. The statements that describe the well-being effect of urban green areas in Rize and that have been evaluated by the users have been analyzed through factor analysis. Urban green spaces in Rize were explained with 3 factors (Table 3).

TABLE 3
Factor analysis of the questions

Question number		*Factor Loadings*			*Communality*
		1	2	3	
	FACTOR 1				
(Q2)	I feel peace	**,823**			,736
(Q1)	I feel happy	**,821**			,734
(Q3)	I get relaxed	**,809**			,703
(Q4)	Feel in a good mood	**,753**			,730
(Q11)	I breath clean air	**,635**			,688
(Q6)	The negative feelings that I have turn into positive ones	**,622**			,668
(Q10)	I feel healthy	**,614**			,678
(Q7)	I get rid of the daily life stress	**,597**			,668
(Q5)	Cheers me up/ I feel relaxed	**,585**			,705
(Q12)	I spend enjoyable time	**,544**			,587
	FACTOR 2				
(Q20)	Being alone with the nature		**,802**		,717
(Q19)	Cycling		**,779**		,700
(Q13)	Contact with nature (picking flower, observing-feeding, photographing plants and animals)		**,647**		,612
(Q9)	Walking		**,619**		,701
(Q14)	Sports activities		**,601**		,571
(Q8)	I keep away from the city noise		**,587**		,575
	FACTOR 3				
(Q16)	Meet with others			**,742**	,565
(Q17)	Share life with my friends and my family			**,692**	,639
(Q15)	Being together with our beloved/ friends			**,637**	,421
(Q18)	I am happy with spending some time and talking with my family			**,583**	,623
	% of variance	**49,549**	**8,920**	**6,639**	**65,107**

These factors symbolize 65% of variables which define urban green spaces, and when the contents of these statements were analyzed: Factor 1 was described as mental well-being; Factor 2 was described as physical well-being and Factor 3 was described as social well-being. According to the information about urban green spaces in Rize, the most effective definition was "*mental well-being*" (49,549% of variance). Besides, "*physical well-being*" (8,920% of variance) and "*social well-being*" (6,639% of variance) were secondary definitions.

The reason why urban green areas in Rize were described with "*mental well-being*" has been the naturallness that has been provided by the tall trees that they have, the bushes and the topography because the the effects such as peace, happiness, overcoming negative thoughts that are provided by naturallness have an effect on mental well-being. These findings have also been supported by the previous studies [4, 22, 23, 40, 55-57.]

The second factor that describes urban green areas is "*physical well-being*". However, this is not a high rate descriptor for the urban green areas in Rize because green areas do not have enough physical activity opportunities for their users as illustrated in Table 1 (sports fields, walking routes, etc.). This has been supported by the other studies in literature: If urban green areas provide physical activity opportunities for their users, they increase individuals' physical activity [60-62] and they positively affect physical well-being.

The third factor that describes urban green areas is "*social well-being*". This is a low level descriptor for the urban green areas in Rize. The reason of this is not the inadequency in socilization opportunities in green areas, it is the discrepancy that social and cultural structure creates: For example, individuals feel insecure while talking to the people they do not know.

TABLE 4
The correlations of factors with satisfaction and proximity to green space

	Factor 1	Factor 2	Factor 3
Satisfaction	,396**	,330**	,239**
Proximity to green space	,350**	,389**	,623**
Factor 1 (mental well-being)	-	,785**	,526**
Factor 2 (physical well-being)		-	,529**
Factor 3 (social well-being)			-

** The correlation is significant at the level of 0.01 (2-tailed)

Determining the correlations between the factors describing urban green areas and satisfaction-perceived proximity-frequency of use. The correlation between the factors describing urban green areas and satisfaction- proximity to green space-frequency of use was evaluated. As a result of these evaluations, it was revealed that factors have a statistical correlation with "*satisfaction and proximity to green space*"; however, they do not have a statistical correlation with "*frequency of use*". The correlation values are illustrated in Table 4.

Proximity to green space and satisfaction about urban green places has strong correlations with mental well-being, physical well-being and social well-being. These findings are supported by other studies as well [38, 40, 46, 63]. Urban green areas structure the society and provide spaces for them to share life together. Urban green areas encourage people to form a sincere society through meeting and cooperating. This affects individuals' physical, psychological and social well-being [22, 38, 46, 63]. Moreover, individuals who have proximity to urban green areas do more social activities, they visit green areas more, and they meet more people and develop a strong sense of belonging [38, 46, 53]. This also enables users to do more physical activities as well as affecting mental and social well-being positively [22, 29, 64] because physical activity opportunities in green areas positively affect physical well-being and mental well-being. Higher frequency of physical activity results in less stress and better mental well-being. Moreover, previous studies point out that physical activity in a green space provides mental well-being [62, 65, 66]. Urban green areas are extremely influencial on user satifaction due to these opportunities that they offer.

Determining the regression values of the factors describing urban green areas and satisfaction-perceived proximity-frequency of use. In this stage of the study, regression analysis is done in order to obtain information about the strenght of the correlations between variables revealed by the previously conducted correlation analysis. Within this context, it is aimed to determine the factors that describe the urban green areas in the strongest way based on the dependent variables "*satisfaction*" and "*proximity to green space*". In the multiple regression analysis which is implemented to determine the effects of the factors on user satisfaction, stepwise method has been used and the analysis has been completed in three steps. The values have indicated a gradual increase and in the 3rd and the last step the value of R^2 has been evaluated, and the results have been evaluated as follows:

TABLE 5
Regression analysis of satisfaction through factors

	Unstandardized efficients		Co-Standardized Coefficients		
Model	B	Std. Error	Beta	t	Sig.
(Constant)	1,190	,121		9,853	,000
FACTOR1	**,416**	**,086**	**,347**	**4,845**	**,000**
FACTOR2	,041	,077	,038	,532	,595
FACTOR3	,036	,051	,036	,695	,487

a. Dependent Variable: Satisfaction
R:,399 R^2:,159 Adj. R^2: ,153 $F_{(3\text{-}449)}$:28,11 P < 0,000

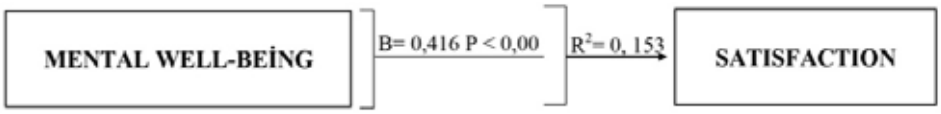


FIGURE 4
Factor values of the effect of mental well-being on satisfaction

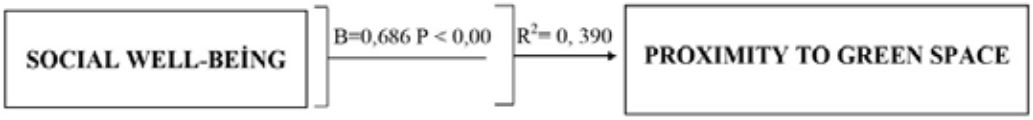


FIGURE 5
Factor values of the effect of socialwell-being on proximity to green space

Factor 1, factor 2 and factor 3 have been undergone regression analysis with satisfaction. It has been seen that only factor 1(mental well-being) has had a statistically significant effect on satisfaction. Factor 2 and Factor 3 have not been added to the model as they have not had a scientifically significant effect on satisfaction. Factor 1 has an effect on satisfaction which is 15,9% (Table 5). The multiple regression equation of the model is as follows: Satisfaction = 1,190 + 0,416 x Factor 1 (Figure 4).

Multiple regression analysis that has been done to determine the effects of factors on proximity to green space has been completed in three steps, and in the last step the value of R^2 has been evaluated, and the results have been evaluated as follows:

TABLE 6
Regression analysis on factor values with proximity to green space

Model	Unstandardized Coefficients		Co-Standardized Coefficients	t	Sig.
	B	Std. Error	Beta		
(Constant)	,915	,122		7,486	,000
FACTOR1	-,075	,087	-,053	-,870	,385
FACTOR2	,152	,078	,119	1,949	,052
FACTOR3	**,686**	**,052**	**,588**	**13,242**	**,000**

a. Dependent Variable: Proximity to green space R:,628 R^2:,394 Adj. R^2: ,390 $F_{(3-449)}$:96,821 P < 0,000

As a result of regression analysis, it is seen that only factor 3 (social well-being) has a statistically significant effect on proximity to green space. Factor 1 and Factor 2 have not been added to the model as they have not had a scientifically significant effect on proximity to green space. Factor 3 has an effect on proximity to green space which is 39, 4 % (Table 6). The multiple regression equation of the model is as follows: Proximity to green space= 0,915 + 0,686 x Factor 3 (Figure 5).

When the results of this study have been evaluated, it has been revealed that there is a correlation between satisfaction that green areas arouse in individuals, the frenquency of use of those areas, proximity to green space and well-being (mental well-being, physical well-being, social well-being). However, which one of the correlations is the strongest? The answer to this question has been searched for through the factor and regression analysis. According to the data obtained from the results;

- The factor that best describes urban green areas is "*mental well-being*".
- The most effective factor urban green areas have on user satisfaction is *"mental well-being"*.
- The most effective factor on perceived proximity to green space is: "social well-being".
- The frequency of using urban green areas does not have any correlations with any of the factors.

Urban green spaces remain in the forefront with "mental well-being" effect by users, and the most effective and the strongest factor on the sense of satisfaction is "mental well-being" because the fact that green areas arouse positive feelings for users positively affects their quality of life. By affecting the environmental quality, green areas help individuals reduce their stress, increase opportunities for them to have social interactions, help them recover from mental fatigue and they create spaces for physical activities. Previous studies also have similar findings [17, 22, 29, 39, 40].

The reason why the most effective factor on the perceived proximity to urban green areas is "social well-being" is that urban green areas create opportunities for individuals to gather their neighbors and to communicate with the ones who they are acquainted with but do not communicate. As a result of this, people have more social activities, visit green areas more, communicate more with more neighbors and they develop a strong sense of belonging. These findings have similarities with previous studies [38, 40, 46].

Social relations have a great role on individuals'

well-being [36, 37]; through contributing psychological development, social relations also positively affect mental well-being [42, 43, 53, 67].and strengthening social connections has an important effect on individuals' physical well-being as well [22, 38]. Proximity to green areas enables outer spaces to be used more frequently [40, 68, 69].Consequently, urban green spaces positively affect individuals' lives in terms of social, mental and physical well-being.

CONCLUSION

This study has focused on the presence of the correlation between satisfaction arousing from urban green areas, the frequency of use, the perceived proximity to green space and well-being. There had been no previous studies which focused on integrating the correlation between satisfaction of green areas, the use (the frequency of use, perceived proximity to green spaces) and well-being. In this study, the correlations among proximity to green spaces, satisfaction, use and well-being have been analyzed in a detailed way. The findings have answered the questions about the strongest correlation and the strongest factor that affects these correlations. The results indicated that:

- The satisfaction that green areas arouse in individuals, the frequency of use, perceived proximity to green spaces and well-being have correlations with one another.
- The strongest correlations in urban green spaces are between satisfaction and mental well-being; and between perceived proximity to green spaces and social well-being.

The most important factor to reach these findings is that in the green areas where this study has been conducted, there have been tall trees, topographic variety and the scene. These components have increased the effect of well-being by strengthening the naturalness of green areas because views of nature are related to increased social interaction, physical activity and mental healing.

In this study, unlike other studies, the frequency of the use of green areas has not been described as a strong factor that affects well-being. However, previous studies suggested that the frequency of use positively affects well-being [40, 64, 70].Further research should be conducted on the reasons of differences in these findings and they should be revealed. The answers to the questions such as whether the designing features of green spaces or being a small city affect these results should be studied.

REFERENCES

[1] Woolley, H. (2003) Urban Open Spaces. Spon Press, London.

[2] Kabisch, N., Haase, D. (2013) Green spaces of European cities revisited for 1990–2006. Landsc Urban Plan. 110, 113-122.

[3] James, P., Tzoulas, K., Adams, M.D., Barber, A., Box, J., Breuste, J., Elmqvist, T., Frith, M., Gordon, C., Greening, K.L., Handley, J., Haworth, S., Kazmierczak, A.E., Johnston, M., Korpela, K., Moretti, M., Niemela, J., Pauleit, S., Roe, M.H., Sadler, J., Ward Thompson, C. (2009) Towards an integrated understanding of green space in the European built environment. Urban For Urban Gree. 8, 65-75.

[4] Chiesura, A. (2004) The role of urban parks for the sustainable city. Landsc Urban Plan. 68(1), 129-138.

[5] Larondelle, N., Haase, D., Kabisch, N. (2014) Mapping the diversity of regulatingecosystem services in European cities. Global Environ. Change. 26, 119-129.

[6] Carrus, G., Scopelliti, M., Lafortezza, R., Colangelo, G., Ferrini, F., Salbitano, F., Agrimi, M., Portoghesi, L., Semenzato, P., Sanesi, G. (2015) Go greener, feel better? Thepositive effects of biodiversity on the well-being of individuals visiting urbanand peri-urban green areas. Landsc Urban Plan. 134, 221-228.

[7] Marselle, M.R., Irvine, K.N., Lorenzo-Arribas, A., Warber, S.L. (2015) Moving beyondgreen: exploring the relationship of environment type and indicators ofperceived environmental quality on emotional well-being following groupwalks. Int. J. Environ. Res. Public Health. 12(1), 106-130.

[8] Barrera, F.D.L, Reyes-Paecke, S., Banzhaf, E. (2016) Indicators for Green Spaces in Contrasting Urban Settings. Ecol Indic. 62, 212-219.

[9] Kaplan R. (1983) The Role of Nature in The Urban Context. In: Altman, I., Wohlwill, J. (Eds.) Behav Natural Environ, Plenum Press, New York.

[10] Kellert, R.S. (2005) Building for Life: Designing and Understanding The Human-Nature Connection. Island Press, USA.

[11] Kaplan, S. (1988) Perception and Landscape: Conceptions and Misconceptions. In J. L. Nasar (Ed.) Environmental Aesthetics: Theory, Research and Application. - Cambridge University Press, New York.

[12] Kaplan, R. and Kaplan, S. (1989) The Experience of Nature: A Psychological Perspective. Cambridge University Press, New York.

[13] Van den Berg, A.E., Ter Heijne, M. (2005) Fear Versus Fascination: An Exploration of Emotional Responses to Natural Threats. J Eng Psychol. 25(3), 261-272.

[14] Bonnes, M., Passafaro, P., Carrus, G. (2011) The Ambivalence of Attitudes Toward Urban Green Areas: Between Proenvironmental Worldviews and Daily Citizenial Experience. Environ Behav Environ Behav. 43(2), 207-232.
[15] Bertram, C., Rehdanz, K. (2015) The role of urban green space for human well-being. Ecol Econ. 120, 139-152.
[16] Gupta, K., Kumar, P., Pathan, S.K., Sharma, K.P. (2012) Urban Neighborhood Green Index – A measure of green spaces in urban areas. Landsc Urban Plan. 105(3), 325-335.
[17] Kabisch, N., Qureshi, S., Haase, D. (2015) Human-Environment Interactions in Urban Green Spaces - A Systematic Review of Contemporary Issues and Prospects for Future Research. Environ Impact Asses. 50, 25-34.
[18] Qin, J., Zhou, X., Sun, C., Lian, Z. (2013) Influence of green spaces on environmental satisfaction and physiological status of urban citizens. Urban For Urban Gree. 12(4), 490-497.
[19] Kamierczak, A. (2013) The contribution of Local Parks to Neighbourhood Social Ties. - Landsc Urban Plan. 109, 31-44.
[20] Stewart, W.P., Liebert, D., Larkin, K.W. (2004) Community identities as visions for landscape change. Landsc Urban Plan. 69, 315-334.
[21] Kaplan, S., Kaplan, R. (1982) Cognition and Environment: Functioning in An Uncertain World. Praeger, New York.
[22] Yılmaz, S., Düzenli, T., Mumcu, S. (2016) Assessing Urban Green Areas in Terms of User Satisfaction: Case Study of Trabzon City. Journal of Balkan Ecology. 19, 275-290.
[23] Wan, C., Shen, G.Q. (2015) Salient Attributes of Urban Green Spaces in High Density Cities: The Case of Hong Kong. Habıtat Int. 49, 92-99.
[24] Wright Wendel, H.E., Zarger, R.K., Mihelcic, J.R. (2012) Accessibility and Usability: Green Space Preferences, Perceptions, and Barriers in a Rapidly Urbanizing City in Latin America. Landsc Urban Plan. 107, 272-282.
[25] Ward Thompson, C. (2009) Towards an integrated understanding of green space in the European built environment. Urban For Urban Gree. 8, 65-75.
[26] Madureira, H., Nunes, F., Oliveira, J.V., Cormier, L., Madureira, T. (2015) Urban citizens' beliefs concerning green space benefits in four cities in France and Portugal. Urban For Urban Gree. 14: 56-64.
[27] Grahn, P., Stigsdotter, A.U.K. (2010) The relation between perceived sensory dimensions of urban green space and stress restoration. Landsc Urban Plan. 94(3-4), 264-275.
[28] Ulrich, R.S. (2006) Evidence-Based Health-Care Architecture. Lancet. 368, 38-39.
[29] Schipperijn, J., Stigsdotter, A.U.K., Randrup, T.B., Troelsen, J. (2010) Influences on The Use of Urban Green Space–A Case Study in Odense, Denmark. Urban For Urban Gree. 9, 25-32.
[30] Maas, J., van Dillen, S.M.E. (2009) Verheij RA and Groenewegen PP. Social contacts as a possible mechanism behind the relation between green space and health. Health & Place. 15, 586-595.
[31] Tzoulas, K., James, P. (2010) Peoples' Use of, and Concerns about, Green Space Networks: A Case Study of Birchwood, Warrington New Town, UK. Urban For Urban Gree. 9, 121-128.
[32] Bjork, J., Albin, M., Grahn, P., Jacobsson, H., Ardo, J., Wadbro, J., Ostergren, P.O., Skarback, E. (2008) Recreational values of the natural environment in relation to neighbourhood satisfaction, physical activity, obesity and well-being. Journal of Epidemiology & Community Health. 62(4), e2-e2.
[33] Mitchell, R., Popham, F. (2008) Effect of exposure to natural environment on health inequalities: an observational population study. Lancet. 372, 1655-1560.
[34] Kaplan, S. (2001) Meditation, restoration, and the management of mental fatigue. Environ Behav. 33, 480-506.
[35] Nielsen, T.S. Hansen, K.B. (2007) Do green areas affect health? Results from a Danish survey on the use of green areas and health indicators. Health and Place. 13, 839-850.
[36] Newton, J. (2017) Well-being and the natural environment: a brief overview of the evidence. 2007. Retrieved Febuary 28, 2017 from: /http://www.sustainable-development.gov.uk/what/documents/Well-beingAndTheNatural EnvironmentReport. docS.
[37] Diener, E., Seligman, M. (2002) Very happy people. Psychological Science. 13, 80-83.
[38] Sullivan, W.C., Kuo, F.E., DePooter, S.F. (2004) The fruit of urban nature: Vital neighborhood spaces. Environ Behav. 36, 678-700.
[39] Maas, J., van Dillen, S.M.E. (2009) Verheij RA and Groenewegen PP. Social contacts as a possible mechanism behind the relation between green space and health. Health Place. 15, 586-595.
[40] Hadavi, S. (2016) Direct and Indirect Effects of the Physical Aspects of the Environment on Mental Well-Being. Environ Behav. 1-34.
[41] Sugiyama, T., Leslie, E., Giles-Corti, B., Owen, N. (2008) Associations of neighbourhood greenness with physical and mental health: Do walking, social coherence and local social interaction explain the relationships? J Epidemiol Commun. 62(5), e9.
[42] Burns, G. (2006) "Naturally happy, naturally healthy: the role of the natural environment in well-being". The science of well-being. Oxford University Press, Oxford.

[43] Reis, H., Gable, S. (2003) Toward a positive psychology of relationships. In: Keyes & Haidt, J. (eds.) Flourishing: positive psychology and the life well-lived. American Psychological Association, Washington.
[44] Taylor, A.F., Wiley, A., Kuo, F.E., Sullivan, W.C. (1998) Growing up in the Inner City: Green Spaces As Places to Grow. Environ Behav. 30(1), 3-27.
[45] Sullivan, W. (2004) Forest, Savannah, City: Evolutionary landscapes and human functioning, in: Bartlett, P. (Ed.) Urban Place: reconnecting with the natural World. Academic Exchange, Atlanta.
[46] Brook, I. (2010) The Importance of Nature, Green Spaces, and Gardens in Human Well-Being. Ethics, Place & Environment. 13(3), 295-312.
[47] Peschardt, K.K., Stigsdotter, U.K. (2013) Associations Between Park Characteristics and Perceived Restorativeness of Small Public Urban Green Spaces. Landsc Urban Plan. 112, 26-39.
[48] Kweon, B.S., Ellis, C.D., Leiva, P.I., Rogers, G.O. (2010) Landscape components, land use, and neighborhood satisfaction. Environ Plann B. 37, 500-517.
[49] Lee, S.W., Ellis, C.D., Kweon, B.S., Hong, S.K. (2008) Relationship between landscape structure and neighborhood satisfaction in urbanized areas. Landsc Urban Plan. 85, 60-70.
[50] Akpınar, A. (2016) How is Quality of Urban Green Spaces Associated with Physical Activity and Health? Urban For Urban Gree. 16, 76-83.
[51] Mackay, G.J., Neill, J.T. (2010) The Effect of "Green Exercise" on State Anxiety and The Role of Exercise Duration, Intensity, and Greenness: a Quasi-Experimental Study. Psychology Sport Exercise. 11, 238-245.
[52] Barton, J., Prett, J. (2010) What is the best dose of nature and green exercise for improving mental health? A multi-study analysis. Environ Sci Technol. 44(10), 3947-55.
[53] Matsuoka, R.H., Kaplan, R. (2008) People needs in the urban landscape: Analysis of landscape and urban planning contributions. Landsc Urban Plan. 84, 7-19.
[54] Ulrich, R.S. (1991) Effects of Health Facility İnterior Design on Wellness: Theory and Scientific Research. Journal of Health Care Design. 3, 97-109. (Reprinted in Marberry, S.O. (Ed.) Innovations in Healthcare Design. Van Nostrand Reinhold, New York.
[55] Carrus, G., Lafortezza, R., Colangelo, G., Dentamaro, I., Scopelliti, M., Sanesi, G. (2013) Relations between naturalness and perceived restorativeness of different urban green spaces. Psyecology. 4(3), 227-244.
[56] MacKerron, G., Mourato, S. (2013) Happiness is greater in natural environments. Global Environ Chang. 23, 992-1000.
[57] Shan, X.Z. (2014) Socio-Demographic Variation in Motives for Visiting Urban Green Spaces in a Large Chinese City. Habitat Int. 41, 114-120.
[58] Farida, N. (2013) Effects of outdoor shared spaces on social interaction in a housing estate in Algeria. Frontiers of Architectural Research. 2(4), 457-467.
[59] Carrus, G.R. (2013) Lafortezza G, Colangelo Dentamaro I, Scopelliti M and Sanesi G. Relations between naturalness and perceived restorativeness of different urban green spaces. Psyecology. 4(3), 227-244.
[60] Paquet, C., Orschulok, T.P., Coffee, N., Howard, N.J., Hugo, G., Taylor, A.W., Adams, R.J., Daniel, M. (2006) Public parks and physical activity among adolescent girls. Pediatrics. 118, 1381-1389.
[61] Floyd, M.F., Spengler, J.O., Maddock, J.E., Gobster, P.H., Suau, L.J. (2008) Park-based physical activity in diverse communities of two U.S. cities: an observational study. Am J Prev Med. 34, 299-305.
[62] Akpınar, A. Cankurt M. (2016) How are characteristics of urban green space related to levels of physical activity: Examining the links. Indoor Built Environ. 0(0): 1-11.
[63] Kuo, F.E., Sullivan, W., Levine Coley, R., Brunson, L. (1998) Fertile ground for community: Inner-city neighbourhood common spaces. Am J Commun Psychol. 26(1), 823-851.
[64] Ward Thompson, C., Aspinall, P.A. (2011) Natural environments and their impact on activity, health, and quality of life. Applied Psychology: Health and Well-being. 3, 230-260.
[65] Barton, J., Pretty, J. (2010) What is the best dose of nature and green exercise for improving mental health? A multi-study analysis. Envir Sci Tech. 44(10). 3947-3955.
[66] Mackay, G.J., Neill, J.T. (2010) The Effect of "Green Exercise" on State Anxiety and The Role of Exercise Duration, Intensity, and Greenness: a Quasi-Experimental Study. Psychology Sport Exercise. 11, 238-245.
[67] Öztürk, S., Bozdoğan, E. (2014) Determination of the perceived quality of urban life in new and traditional housing textures. Fresen. Environ. Bull. 23(10), 2415-2421
[68] Shackleton, C.M., Blair, A. (2013) Perceptions and use of public green space is influenced by its relative abundance in two small towns in South Africa. Landsc Urban Plan. 113, 104-112.
[69] Hadavi, S., Kaplan, R. (2016) Neighborhood satisfaction and use patterns in urban public outdoor spaces: Multidimensionality and two-way relationships. Urban for Urban Gree. 19, 110-122.

[70] Ellis, C.D., Lee, S.W., Kweon, B.S. (2006) Retail land use, neighborhood satisfaction and the urban forest: An investigation into the moderating and mediating effects of trees and shrubs. Landsc Urban Plan. 74,70-78.

Received: **07.04.2017**
Accepted: **04.10.2017**

CORRESPONDING AUTHOR

Serap Yilmaz
Department of Landscape Planning and Design
Karadeniz Technical University, Turkey

e-mail: serapyilmaz@ktu.edu.tr

© by PSP Volume 26 – No. 12A/2017 pages 7801-7805 Fresenius Environmental Bulletin

CYANOBACTERIA BLOOM MITIGATION USING CALCIUM HYDROXIDE AND AN ILLITE COMPOSITE ALGICIDE

Hongqiang Wang[1], Anna Zhang[3], Lieyu Zhang[2,*]

[1]School of Environmental and Safety Engineering, University of South China, Hengyang 421001, China
[2]Chinese Research Academy of Environmental Sciences, Beijing 100012, China
[3]School of Environmental and Municipal Engineering, Tianjin Chengjian University, Tianjin 300384, China

ABSTRACT

A method was developed for cyanobacteria bloom (unicellular and colonial *Microcystis aeruginosa*) mitigation using calcium hydroxide and an illite composite algicide. The maximum cell removal efficiency was 84.72% when calcium hydroxide was used alone. When illite and calcium hydroxide were used together, the removal efficiency increased to 90.43% within 9 h. In addition, the results also showed that the composite algicide could remove total nitrogen (TN) and total phosphorus (TP) in eutrophic water. However, the removal efficiency of TP is more evident than that of TN under the same composite algicide doses. Thus, the method would provide an alternative composite algicide to mitigate cyanobacteria blooms using calcium hydroxide and illite in eutrophic water.

KEYWORDS:
Cyanobacteria blooms, calcium hydroxide, illite, unicellular *M. aeruginosa*, colonial *M. Aeruginosa*

INTRODUCTION

Cyanobacteria blooms in lakes are one of the most serious problems in the world[1]. *Microcystis aeruginosa*, a typical bloom-forming species, is of major concern because most strains can produce microcystins and anatoxin, which can hazardous to the health of aquatic life, livestock, and even people [2-5]. Therefore, the control of toxic *Microcystis* is an important issue in both ecology and public health[6].

There are numerous means of controlling cyanobacteria blooms. Ultimately, preventing these blooms by adding flocculants is considered one of the most effective means [7-10]. For example, Li and Pan [9] found that *M. aeruginosa* can be effectively flocculated by positively charged protein and chitosan-modified soil. The method greatly reduces the potential environmental impacts by using totally biodegradable modifiers in natural waters. However, the target algae used in these studies were unicellular *M. aeruginosa* strains, where as natural *Microcystis* blooms are typically composed of colonial forms of *M. aeruginosa* [11]; thus, little data have been published about environmental factors affecting colonial *Microcystis* [12].

In the current work, we investigated the flocculent potential of calcium hydroxide and an illite composite algicide on unicellular and colonial *M. aeruginosa*. In addition, we also studied the capacity of composite algicide on eutrophic water remediation.

MATERIALS AND METHODS

Cyanobacteria culture. Axenic unicellular *M. aeruginosa* was obtained from the Culture Collection of Algae at the Institute of Hydrobiology, Chinese Academy of Sciences. The cyanobacteria were cultured in sterilized BG11 medium (pH 7.4) at 25 ℃ and a light intensity of 2500 lux, with a 12:12 h light: dark cycle. The cyanobacteria were cultured for 4 days to the exponential phase at a density of 10^6cellsmL^{-1} and were then used to assay the flocculating property of calcium hydroxide and an illite composite algicide. The growth medium for all cultures was BG11 [13].

Sample collection and preparation. Illite was obtained from Pingdingshan in Henan Province, China. It was smashed and sieved using screens from 80-mesh to 160-mesh.The illite and $Ca(OH)_2$ were prepared as slurries by adding deionized water to obtain concentrations of 40.0 g L^{-1} and 10.0 g L^{-1}, respectively.

Removal of *M. aeruginosa*. The capacity of calcium hydroxide and an illite composite algicid to remove cyanobacteria was tested using unicellular and colonial *M. aeruginosa*at room temperature.

Unicellular *M. aeruginosa* was harvested by centrifugation (at 12000 rpm) and suspended in a 0.5% NaCl solution to keep the cells alive. Colonial *M. aeruginosa*was obtained from Dianchi Lake, China. In the experiments, the colonial *M. aeruginosa* was diluted with BG11medium. The initial cell concentration for all flocculation experiments was controlled at an optical density of 0.100 - 0.150 at a wavelength of 680 nm ($OD_{680\ nm}$) [14].

The composite algicide was added to 60 mL of cyanobacteria culture in a 100mL beaker, followed

by standing for 9 h. In the control groups, the composite algicide was not added. At the end of the settling period, a sample was collected from 2 cm below the surface for analysis. Each experiment was performed in triplicate.

Analysis methods for the concentration of chlorophyll-a. The concentration of chlorophyll-a was measured as an indicator of the change of the concentration of *M. aeruginosa* cells during the flocculation experiment. The chlorophyll-a concentration was determined using standard methods [15].

The clearance of cyanobacteria (r, %) in every sample based on the chlorophyll-a concentration was determined after an 9 h exposure by the following formula:

$$r = \frac{T_2 - T_1}{T_2} \times 100\% \quad (1)$$

where T_1 and T_2 are the chlorophyll-a concentration after flocculation and the control, respectively.

Water analysis. At the end of the settling period, water quality parameters, such as the total nitrogen (TN) and the total phosphorus (TP), were determined using standard methods [15].

Data analysis. Differences between the groups were evaluated using a one-way analysis of variance with the removal efficiency of cyanobacteria and membrane pore size as the factors. A probability level of 0.05 was used to establish significance ($P< 0.05$). All statistical analyses were performed using SPSS 19.0 and Origin 8.0 software.

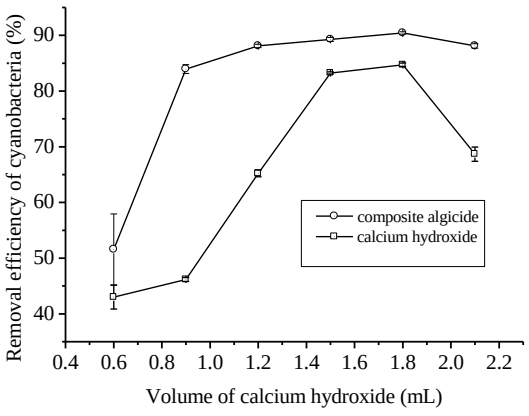


FIGURE 1
Cyanobacteria removal efficiencies for calcium hydroxide alone and the composite algicide

RESULTS AND DISCUSSION

Removal effect of $Ca(OH)_2$ and illite. As shown in Fig. 1, calcium hydroxide alone could remove the unicellular *M. aeruginosa* cells at all volumes tested. At the lowest volume (0.6 mL), calcium hydroxide alone removed 43.02% *M. aeruginosa* cells, whereas the maximum removal was found at a volume of 1.8 mL, with an 84.72% removal ratio. In addition, Fig. 1 also shows that the removal effect of calcium hydroxide was influenced by the presence of illite. After the addition of 1.5 mL stock solutions of illite, the removal efficiency was clearly higher than that when calcium hydroxide was used alone. The *M. aeruginosa* cell removal efficiency further increased with increasing calcium hydroxide volume, and the removal efficiency of 1.8 mL calcium hydroxide with 1.5 mL illite was over 90%. Compared to using calcium hydroxide alone and the composite algicide, the removal efficiency increased from 46.18% to 83.95%, especially when the dose of calcium hydroxide was 0.9 mL.

Vandamme et al. [16] also reported that magnesium hydroxide precipitates at a pH of 10-11 and can cause the flocculation of microalgae through charge neutralization and/or by a sweeping mechanism. Chen and Pan [17] also found marine harmful algal blooms (HABs) could be mitigated using clay, soil, or sand modified with xanthan and calcium hydroxide. The algal removal effect of xanthan was significantly enhanced when more $Ca(OH)_2$ was added.

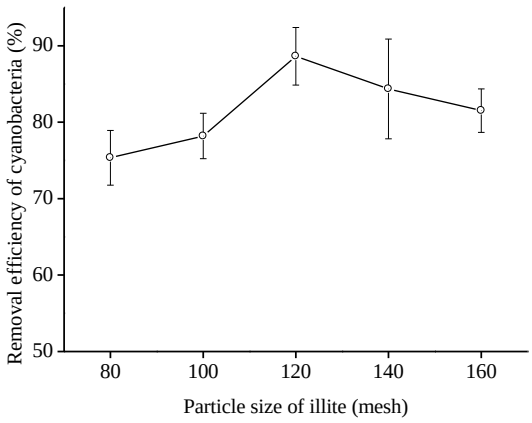


FIGURE 2
Effect of the particle size of illite on unicellular *M. aeruginosa* removal

Removal effect of the particle size of illite. Different particle sizes of illite showed different removal efficiencies of unicellular *M. aeruginosa* cells (Fig. 2). The removal efficiency of *M. aeruginosa* cells greatly increased in comparing an80 to 120 mesh particle size of illite. After that, the removal efficiency started to decrease. When the particle size was 120 mesh, the removal percentage of cyanobacteria was 88.62%. Hence, the optimum particle size of illite for this method is120 mesh.

Removal effect of the addition dosage of illite. The effect of the addition dosage of illite on unicellular *M. aeruginosa* removal is shown in Fig. 3. The cyanobacteria removal efficiency increased

sharply from 0.1 g to a critical value; when the addition dosage of illite was above the critical value, the removal efficiency decreased sharply. The highest cyanobacteria removal efficiency was 91.37%.

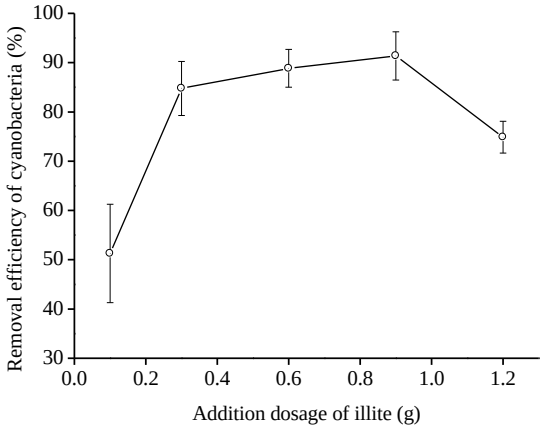


FIGURE 3
Effect of the addition dosage of illite on unicellular *M. aeruginosa* removal

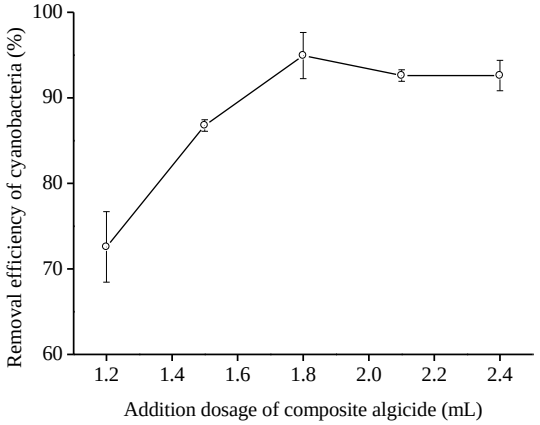


FIGURE 4
Effect of the addition of the composite algicide on unicellular *M. aeruginosa* removal

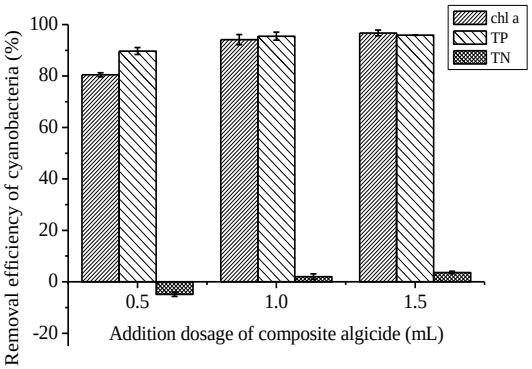


FIGURE 5
Effect of the composite algicide on chl a, TP and TN

Removal effect of the addition dosage of the composite algicide. The unicellular *M. aeruginosa* removal by composite algicide is illustrated in Fig. 4. The addition dosage of composite algicide significantly influenced the removal of *M. aeruginosa*. With increasing dose, cyanobacteria removal efficiency increased and then decreased. The optimum additive amount was 1.8 mL. At this dose, the removal efficiency of cyanobacteria was 94.94%. When the added dose was 2.1 mL, the removal efficiency declined.

Removal effect of the composite algicide on chl a, TP and TN. The target cyanobacteria used in many studies was unicellular *M. aeruginosa*, but natural *M. aeruginosa* often forms colonies, aggregating several tens and hundreds of cells in transparent mucilaginous sheath materials [18]. Zhang et al. [11] and Zhao et al. [19] also found that the cellular defense system of colonial *M. aeruginosa* was stronger than that of unicellular *M. aeruginosa*. Therefore, we collected *Microcystis* from Dianchi Lake and investigated the removal effects on colonial *M. aeruginosa* cells, TN and TP in artificial water using a composite algicide. The results are illustrated in Fig. 5. The removal efficiencies of chl a, TP and TN with different addition dosages of composite algicide were compared, which increased from 80.46%, 89.72%, and -4.85% to 96.74%, 95.90%, and 3.63% when the dose increased from 0.5 mL to 1.5 mL, respectively. In addition, it can also be concluded that the removal efficiency of chl a and TP are more evident than that of TN under the same composite algicide doses. Therefore, the pollutants of TN and TP in the water are also removed by the composite algicide when these pollutants participate in the cyanobacteria flocculation. These pollutants of water also decreased, mainly because of the coflocculation effect [20].

Harmful cyanobacteria blooms have increasingly occurred worldwide, and the effective removal or inhibition of these algal blooms has become critically important [8]. Especially during cyanobacteria blooms, *M. aeruginosa*, as one of the most dominant cyanobacterial species, can release intracellular metabolites, such as microcystins (MCs), taste- and odor-causing substances, and other organic matter, into water[1, 21], which will threaten the safety of drinking water and aquatic life [2, 5, 22]. Ingestion of cyanobacterial toxins through the food chain poses a high risk to human health [23-24].

A variety of technologies have been explored to remove harmful cyanobacteria blooms [25-27], but each technology has its own advantages and disadvantages. In general, conventional settling can be optimized by the introduction of flocculation, which can result in the formation of flocs [10]. In the current work, we found that calcium hydroxide could induce algal cell flocculation. A huge increase in efficiency was obtained when the volume of calcium

hydroxide was increased from 0.9 to 1.5 mL. Up to 1.8 mL, the most efficient algae removal was obtained. At volumes of calcium hydroxide exceeding 1.8 mL, the removal efficiencies decreased. Şirin et al. [28] also found that the flocculation efficiency of the microalgae *Phaeodactylum tricornutum* improved at pH=9.75 when alkalinity-induced flocculation was performed.

Illite is a 2:1 layer type clay: its structure consists of two tetrahedral sheets that sandwich an octahedral sheet [29]. Illite has attracted great attention in environmental pollution treatments, due to its numerous outstanding properties, such as a large surface area, excellent swelling ability, high sorption capacity, and low cost [30]. It has been reported that the sorption of Pb^{2+}, Co(II) and U(VI) on illite was drastic [29, 31-33]. In the current work, we found that the removal efficiency of cyanobacteria could be enhanced by adding illite and that the settling velocity could also be improved.

CONCLUSIONS

In this study, calcium hydroxide and an illite composite algicide were successfully applied to remove cyanobacteria blooms (unicellular and colonial *M. aeruginosa*), TN and TP. The removal efficiency of chl a, TP and TN were up to 96.74%, 95.90%, and 3.63% when the dose was 1.5 mL, respectively. The removal efficiencies of chl a and TP were more efficient than that of TN under the same composite algicide doses.

ACKNOWLEDGEMENTS

This work was kindly supported by the National Science-technology Support Plan Projects of China (2015BAL04B01), the National Natural Science Foundation of China (51108447; 51208485and 51678549), the China Postdoctoral Science Special Foundation(201104499), the Key Science and Technology Project of Henan Province of China (172102310720) and the Key Scientific Research Foundation of the Higher Education Institutions of Henan Province, China (16A610006).

REFERENCES

[1] Liu, Y., Xie, P. and Wu, X.P. (2009) Grazing on toxic and non-toxic *Microcystis aeruginosa* PCC7820 by *Unio douglasiae* and *Corbicula fluminea*. Limnology. 10(1), 1-5.

[2] Zimba, P.V., Khoo, L., Gaunt, P.S., Brittain, S. and Carmichael, W.W. (2001) Confirmation of catfish, *Ictalurus punctatus* (Rafinesque), mortality from *Microcystis* toxins. J. Fish Dis. 24(1), 41-47.

[3] Azevedo, S.M.F.O., Carmichael, W.W., Jochimsen, E.M., Rinehart, K.L., Lau, S., Shaw, G.R. and Eaglesham, G.K. (2002) Human intoxication by microcystins during renal dialysis treatment in Caruaru—Brazil. Toxicology. 181-182, 441-446.

[4] Katırcıoğlu, H., Akin, B.S. and Atici, T. (2004) Microalgal toxin (s): characteristics and importance. Afr. J. Biotechnol. 3(12), 667-674.

[5] Otten, T.G. and Pearl, H.W. (2015) Health effects of toxic cyanobacteria in the U.S. drinking and recreational waters: our current understanding and proposed direction. Current Environmental Health Reports. 2(1), 75-84.

[6] Park, M.H., Kim, K.H., Lee, H.H., Kim, J.S. and Hwang, S.J. (2010) Selective inhibitory potential of silver nanoparticles on the harmful cyanobacterium *Microcystis aeruginosa*. Biotechnol. Lett. 32(3), 423-428.

[7] Divakaran, R. and Pillai, V.S. (2002) Flocculation of algae using chitosan. J. Appl. Phycol, 14(5), 419-422.

[8] Wang, Z.Y., Wang, C., Wang, P.F., Qian J., Hou, J., Ao, Y.H. and Wu, B.H. (2015) The performance of chitosan/montmorillonite nanocomposite during the flocculation and floc storage processes of *Microcystis aeruginosa* cells. Environ. Sci. Pollut. R. 22(14), 11148-11161.

[9] Li, L. and Pan, G. (2016) Cyanobacterial bloom mitigation using proteins with high isoelectric point and chitosan-modified soil. J. Appl. Phycol. 28(1), 357-363.

[10] Li, J.H., Cao, X., Ge, Z.G., Yang, X.Y. and Zheng, Z. (2016) Flocculation of *Microcystis aeruginosa* by steel slag and its safety evaluation. J. Appl. Phycol. 28(1), 261-268.

[11] Zhang, S.H., Chang, J.J., Cao, J.Y. and Yang, C.L. (2015) Comparative Studies on Growth and Physiological Responses of Unicellular and Colonial *Microcystis aeruginosa* to *Acorus calamus*. B. Environ. Contam. Tox. 94(2), 225-231.

[12] Wang, Y.W., Zhao, J., Li, J.H., Li, S.S., Zhang, L.H. and Wu, M. (2011) Effects of calcium levels on colonial aggregation and buoyancy of *Microcystis aeruginosa*. Curr. Microbiol. 62(2), 679-683

[13] Rippka, R., Deruelles, J., Waterbury, J.B., Herdman, M. and Stanier, R.Y. (1979) Generic assignments, strain histories and properties of pure cultures of cyanobacteria. Journal of General Microbiology. 111(1), 1-61

[14] Clesceri, L.S., Greenberg, A.E., Eaton, A.D. (1999) Standard Methods for the Examination of Water and Wastewater. American Public Health Association.

[15] Chinese, E.P.A. (2012) Methods for Water and Wastewater Analysis, fourth ed. Environmental Science Publishing House of China, Beijing.

[16] Vandamme, D., Beuckels, A., Markou, G., Foubert, I. and Muylaert, K. (2015) Reversible flocculation of microalgae using magnesium hydroxide. Bioenerg. Res. 8(2), 716-725.
[17] Chen, J. and Pan, G. (2012) Harmful algal blooms mitigation using clay/soil/sand modified with xanthan and calcium hydroxide. J. Appl. Phycol. 24(5), 1183-1189.
[18] Yang, Z., Kong, F., Shi, X., Zhang, M., Xing, P. and Cao, H. (2008) Changes in the morphology and polysaccharide content of *Microcystis aeruginosa* (Cyanobacteria) during flagellate grazing. J. Phycol. 44(3), 716-720.
[19] Zhao, J., He, X.M., Sun, P.S. and Zhang, S.H. (2013) Different Sensitivities of Unicellular and Colonial Microcystis Strains (Cyanophyceae) to Six Emergent Macrophytes. Pol. J. Environ. Stud. 22(5), 1539-1546.
[20] Dai, G.F., Zhong, J.Y., Song, L.R., Guo, C.J., Gan, N.Q. and Wu, Z.B. (2015) Harmful algal bloom removal and eutrophic water remediation by commercial nontoxic polyamine-co-polymeric ferric sulfate-modified soils. Environ. Sci. Pollut. R. 22(14), 10636-10646.
[21] Zhou, S.Q., Shao, Y.S., Gao, N.Y., Deng, Y., Qiao J.L., Ou, H.S. and Deng, J. (2013) Effects of different algaecides on the photosynthetic capacity, cell integrity and microcystin-LR release of *Microcystis aeruginosa*. Sci. Total Environ. 463-464, 111-119.
[22] Ma, X.X., Wang, Y.N., Feng, S.Q. and Wang, S.B. (2015) Comparison of four flocculants for removing algae in Dianchi Lake. Environ. Earth Sci. 74(5), 3795-3804.
[23] Shen, P.P., Shi, Q., Hua, Z.C., Kong F.X., Wang, Z.G., Zhuang, S.X. and Chen, D.C. (2003) Analysis of microcystins in cyanobacteria blooms and surface water samples from Meiliang Bay, Taihu Lake China. Environ. Int. 29(5), 641-647.
[24] Shao, J.H., Li, R.H., Lepo, J.E. and Gu, J.D. (2013) Potential for control of harmful cyanobacterial blooms using biologically derived substances: Problems and prospects. J. Environ. Manage. 125, 149-155.
[25] Yan, R., Wu, Y.H., Yang, L.Z., Fang, Y.M. and Kerr, P.G. (2011) Scutellaria baicalensis georgi controls cyanobacterial blooms and benefits to aquatic ecosystem. Fresen. Environ. Bull. 20(1), 19-26.
[26] Zhang, H.W., Zhu, W., Gong, M. and Fan, Y.J. (2016) Influence of alkali catalysts on the supercritical water gasification of cyanobacteria. Fresen. Environ. Bull. 25(8), 2970-2976.
[27] Xiong, Y., Wang, H.Q., Zhang, L.Y., Wang, L. and Che, W. (2017) Preparation of Sodium Alginate/ Graphene Oxide /Gallic Acid Complex Gel Beads and their Algae Removal Performance. Fresen. Environ. Bull. 26(4), 2926-2930.
[28] Şirin, S., Trobajo, R., Ibanez, C. and Salvadó, J. (2012) Harvesting the microalgae Phaeodactylum tricornutum with polyaluminum chloride, aluminium sulphate, chitosan and alkalinity-induced flocculation. J. Appl. Phycol. 24(5), 1067-1080.
[29] Gao, Y., Shao, Z.Y. and Xiao, Z.H. (2015) U(VI) sorption on illite: effect of pH, ionic strength, humic acid and temperature. J. Radioanal. Nucl. Ch. 303(1), 867-876.
[30] Poinssot, C., Baeyens, B. and Bradbury, M.H. (1999) Experimental and modelling studies of caesium sorption on illite. Geochim Cos-mochim Acta. 63(19), 3217-3227.
[31] Bradbury, M.H. and Baeyens, B. (2009) Sorption modelling on illite. Part II: Actinide sorption and linear free energy relationships. Geochim. Cosmochim. Ac. 73(4), 1004-1013.
[32] Liu, X., Chen, Y.T., Chi, Y.L., Guo, Z.J. and Cai, L.S. (2012) Effect of pH, ionic strength, foreign ions, humic acid and temperature on sorption of radionuclide ^{60}Co (II) on illite. J. Radioanal. Nucl. Ch. 292(3), 1357-1366.
[33] Du, Y.F., Yin, Z.X., Wu, H.Y., Li, P., Qi, W. and Wu, W.S. (2015) Sorption of U (VI) on magnetic illite: effects of pH, ions, humic substances and temperature. J. Radioanal. Nucl. Ch. 304(2), 793-804.

Received: **09.04.2017**
Accepted: **20.08.2017**

CORRESPONDING AUTHOR

Lieyu Zhang
Chinese Research Academy of Environmental Sciences, Beijing 100012, China

e-mail: zhanglieyu@163.com

© by PSP Volume 26 – No. 12A/2017 pages 7806-7814 Fresenius Environmental Bulletin

LEVELS OF HEAVY METALS IN TWO FISH SPECIES *IAGO OMANENSIS* AND *AUXIS THAZAR* FROM THE GULF OF AQABA, RED SEA

Tariq Al-Najjar[1,*], Mwaffaq Al Khushman[2], Maroof Khalaf[1], Mohammad Wahsha[3], Khalid Abu Khadra[4]

[1]Department of Marine Biology, The University of Jordan, Aqaba Branch, Jordan
[2]Aqaba International Laboratories, Ben Hayyan, Aqaba Special Economic Zone Authority, Aqaba, Jordan
[3]Marine Science Station, The University of Jordan, Aqaba Branch, Jordan
[4]Department of Biological Sciences, Yarmouk University, Irbid, Jordan

ABSTRACT

Heavy metals concentration of Zn, Cr, Cd and Cu in liver, gills and muscles of the two fish species *Iago omanensis* and *Auxis thazar* were determined using flammable Atomic Absorption Spectrophotometer (AAS). Fish species were collected from the northern Gulf of Aqaba during the period from June 2015 – Jan 2016. Liver were found to be the major organ of bioaccumulation for Zn, Cr, Cd and Cu for *Auxis thazar*, while muscles were found to be the lowest organ of bioaccumulations. However, gills were found to be the site of bioaccumulation for Cu, Cr and Zn in *Iago omanensis* and the lowest concentrations were observed in muscles. The results showed that fish species had significant statistical differences for all the heavy metal concentrations studied, high concentrations of Cu was in *Iago omanensis*, whereas, the higher concentrations of Cr, Zn and Cd was in *Auxis thazar*. Fish length had a very weak relationship on most of the heavy metal concentrations for the two fish studied.

KEYWORDS:
Heavy metals, Fishes, Levels, Concentrations, Aqaba, Red Sea

INTRODUCTION

Contamination of aquatic systems by heavy metals has become a global health problem in the last decades. Heavy metals may enter aquatic systems from different natural and anthropogenic sources, including industrial or domestic wastewater, application of pesticides and inorganic fertilizers, storm runoff, leaching from landfills, shipping and harbour activities, geological weathering of the earth crust and atmospheric deposition [1].

Heavy metals constitute one of the most insidious and dangerous pollutants known to human. They are now considered to be among the most effective environmental contaminants, and their release into the environment is increasing since the last decades, threatening all creature and environment [2]. There were many reports about fish contamination by chemical in the marine environment [3]. Fish may concentrate large amounts of metals from water and they might be toxic for human consumption [4].

However, in recent years heavy metal concentrations were found to be raised in coastal ecosystems. As a result, aquatic organisms are exposed to elevated levels of heavy metals [5]. Heavy metals are now considered to be among the most effective environmental contaminants. The releasing of the heavy metals into the environment is increasing in the last decades, threatening invertebrates, fish, and humans [6]. Fish are relatively situated at the top of the aquatic food chain; therefore, they normally accumulate heavy metals from food, water and sediments [7]. Which they are not readily converted into harmless components, they are often accumulated in the tissues of organisms, which can't excrete those [2].

The susceptibility of the Gulf of Aqaba to heavy metals pollution was revealed and stated through several studies [8, 9, 10, 11, 12, 13, 14, 15, 16, 7, 17, 18]. The Gulf of Aqaba is surrounded mostly by dry desert lands giving a great chance to get polluted with metals carried by air winds [19]. In addition to that the development of Aqaba city after the declaration from the Jordanian authority that Aqaba city is special economic zone authority (ASEZA) in the year 2000 leading to huge increasing in human activities through large investment in the industrial, commercial and tourism which affecting the landscape and marine ecosystem. All these factors consequently will increase the level of heavy metals in the Gulf of Aqaba.

The main objective of this study is to analyse, assess and establish data base about the levels of heavy metals (Cu, Cd, Zn, and Cr) in a selected two fish species, *Iago omanensis* and *Auxis thazar*, lives in the deep water and consumed by the locals of the Gulf of Aqaba.



FIGURE 1
Study Area

MATERIALS AND METHODS

Study area. The Gulf of Aqaba is a semi-enclosed water body located in the southern part of Jordan and at the northern end of the Red Sea; a subtropical arid area between longitude 34° 25' to 35° 00' E and latitude 28°00' to29°33' N (Fig. 1). After the declaration of Aqaba as an economic free zone, the region became extremely attractive for tourism and a large number of hotels are located along the coasts of Jordan, Egypt, Palestine and Saudi Arabia; many new hotels and industries are currently constructed, especially along the Jordanian coast. Therefore, the Gulf water quality, in general, and heavy metal pollution, in particular is environmental threats for these countries.

Samples collection and preparation. Fish samples were bought from the Aqaba local fishermen, a total of 20 fish samples were bought to be utilized during this study, 10 fish samples from the species *Auxis thazar* and the other 10 samples from the species *Iago omanensis*. Samples were selected based on the length to insure that there is a variation in the fish length. All samples were placed in clean plastic bags once the fishermen brought them to the fishermen port, and taken directly to the lab of Marine Science Station. Each fish was washed with distilled water, to get rid of any contaminant of heavy metals on the fish. For each fish sample, morphometric data including weight and length were measured and recorded. Then fishes were dissected using a stainless steel knife. Samples from the liver, muscle and gills were taken and kept in glass Petri dishes. The samples of each organ were taken and placed in glass Petri dishes, before placed into an oven at 85 oC until dry. Dry samples were grinded using a mechanical homogenizer. The grinded dry samples were collected in plastic bags for storage at room temperature for further analysis.

Sample digestion and heavy metals analysis. About (0.3 gm) of dry weight from each tissue was taken into a crucible and dry ached using Carbolite muffle furnace at 550 °C for 6 hours. The ash was treated with 5ml hot concentrated nitric acid for digestion. The Teflon beakers containing the washed samples were heated on a hotplate under the fume hood until the solution started to boil. Samples solutions were filtered using a 0.45 µM Millipore membrane filter paper into Teflon beakers. Teflon beakers were then washed with small amounts of distilled water and the washed distilled water was filtered using the same filter paper and added to the samples. This process was repeated until washed samples volume reached 25 ml. Finally filtered solution were transferred to plastic bottles and stored at room temperature to be analysed for the heavy metals. Blanks were prepared using the same method except without a tissue (only heated 10 ml HNO3 on the hot plate until it starts to boil, then filtered using the same method). The final heavy metals concentrations were measured in (µg.g-1) for Cu, Cr, Cd and Zn using Analytikjena Flame Atomic Absorption Spectrophotometer Nov AA 400, available at the Marine Science Station.

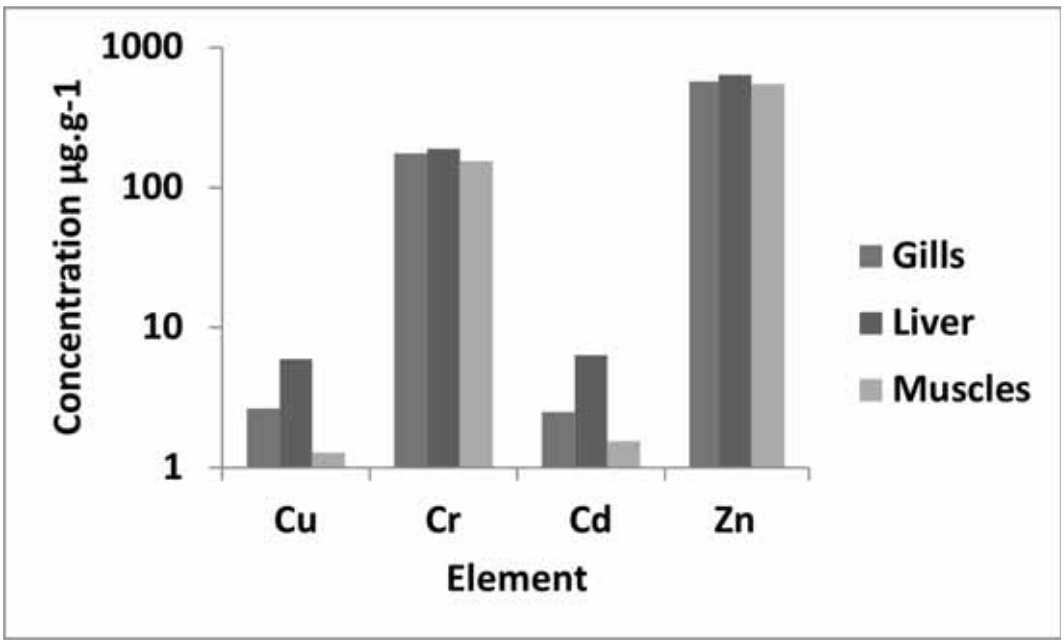


FIGURE 2
Mean concentrations of Cu, Cr, Cd and Zn (µg.g^{-1}) in liver, muscles and gills of *Auxis thazar*

Statistical analysis. Statistical analysis was carried out using Minitab v16.1.1 (developed by researchers from the Pennsylvania State University). Concentrations levels were compared for different organs and weights. Analysis of Variance (ANOVA) test was used to compare the means between different organs, while regression test was used to investigate any relationships between the length and the heavy metals concentrations in the organs exist.

RESULTS

Heavy metal concentrations among the different organs of *Auxis thazar*. The mean concentrations of Cu, Cr, Cd, and Zn in all sampled organs were determined (Figure 2). Significant difference have been observed between different organs for Cu (P Value = 0.026). Livers were found to be the major site of Cu bioaccumulation, with a mean of 5.97 µg.g^{-1}, followed by the Gills, with a mean concentration of 2.64 µg.g^{-1}. The lowest Cu concentrations were found in muscles with a mean of 1.28 µg.g^{-1}. Our study show no significant differences in the Cr concentrations between different organs (P Value = 0.58). However, the higher concentrations of Cr were found in livers followed by gills and muscles with mean concentrations of 189.3, 174.98 and 154.81 µg.g^{-1}, respectively.

Significant difference for the mean concentrations of Cd between all organs was obtained (P Value ≤ 0.0001). Livers were found to be the major site of Cd bioaccumulation, with a mean of 6.34 µg.g-1, followed by the Gills, with a mean concentration of 2.5µg.g-1.The lowest Cd concentrations were measured in muscles with a mean of 1.55 µg.g^{-1}. However, the mean concentrations of Zn between all sampled organs were not significant (P Value = 0.322). The higher concentrations of Zn were found in livers followed by gills and muscles with mean concentrations of 638.2, 570.6 and 549.4 µg.g^{-1}, respectively.

Heavy metal concentrations among the different organs of *Iago omanensis*. Figure 3 shows the mean concentrations of Cu, Cr, Cd and Zn in all sampled organs of *Iago omanensis*. Significant difference in Cu mean concentrations have been observed between different organs (P Value = 0.0049). Gills were found to be the major site of Cu bioaccumulation, with mean of 18.60 µg.g^{-1}, followed by the livers, with a mean concentration of 13.24 µg.g^{-1}.The lowest Cu concentrations were measured in muscles with a mean concentration of 9.14 µg.g^{-1}.

Significant difference in Cr mean concentrations have been obtained between different organs (P Value = 0.01). Gills were found to be the major site of Cr bioaccumulation, with a mean of 105.22 µg.g^{-1}, followed by the livers, with a mean concentration of 80.73 µg.g^{-1}.The lowest Cr concentrations were measured in muscles with means concentrations of 72.74 µg.g^{-1}. The mean concentrations of Cd in different organs were not significant (P Value = 0.0611). The higher concentrations of Cd were in livers followed by gills and muscles with mean concentrations of 2.83, 2.25 and 1.83 µg.g^{-1}, respectively.

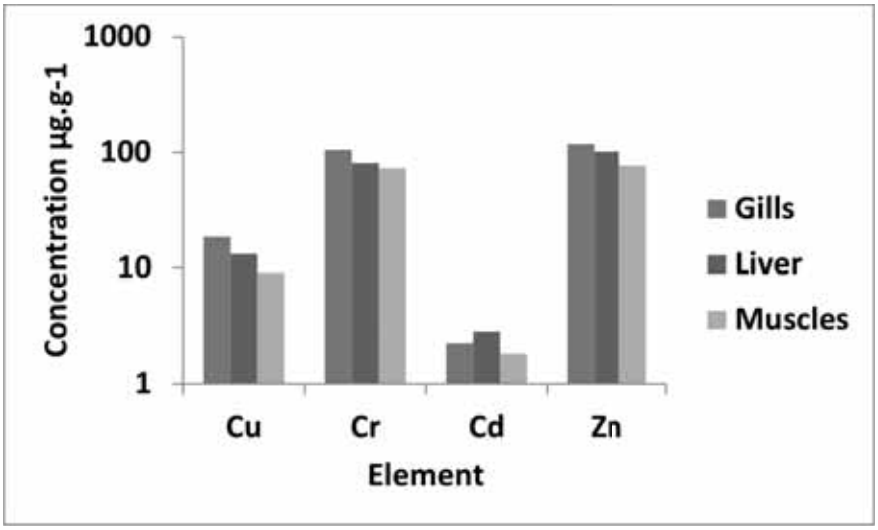


FIGURE 3
Mean concentrations of Cu, Cr, Cd and Zn (µg.g^{-1}) in liver, muscles and gills of *Iago omanensis*

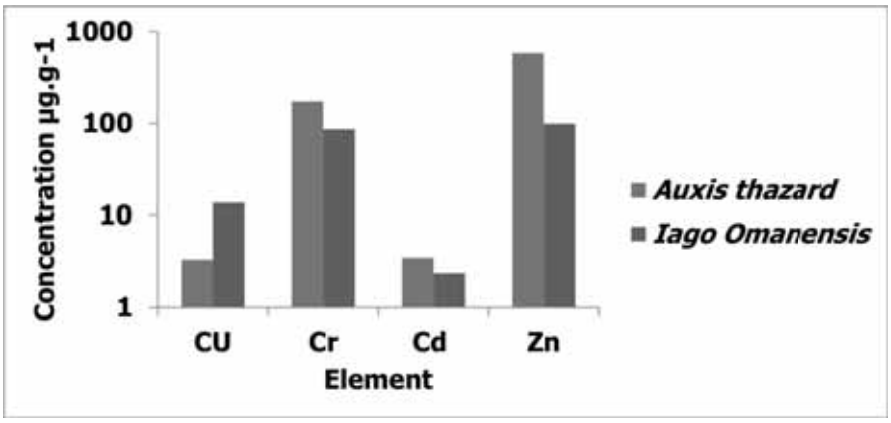


FIGURE 4
Mean Concentrations of Cu, Cr, Cd and Zn (µg.g^{-1}) in *Iago omanensis* and *Auxis thazar*

The mean concentrations of Zn in different organs were not significant (P Value = 0.268). The higher concentrations of Zn were in gills followed by liver and muscles with mean concentrations of 117.99, 101.66 and 76.72 µg.g^{-1}, respectively.

Heavy metal concentrations among the different fish species. Figure 4 shows the mean concentration of Cu, Cr, Cd and Zn for *Auxis thazar* and *Iago omanensis*. The difference in the mean concentrations were highly significant for Cu (P value<0.0001). The higher Cu means concentration was in *Iago omanensis* with mean concentration of 13.66 µg.g^{-1} and the lower concentrations of Cu was 3.3µg.g^{-1} in *Auxis thazar*. The difference in the mean concentrations of Cr were highly significant (P value<0.0001). The higher Cr concentrations were in *Auxis thazar* with a mean concentration of 173.01 µg.g^{-1} and the lower concentrations was 86.23µg.g^{-1} for *Iago omanensis*. The difference in the mean concentrations of Cd were significant (P value= 0.036). The high Cd concentrations were in *Auxis thazar* with a mean concentration of 3.46 µg.g-1 and the low concentrations was 2.36µg.g^{-1} for *Iago omanensis*. The difference in concentrations of Zn were highly significant (P value<0.0001). The higher Zn concentrations were in *Auxis thazar* with a mean concentration of 586.09 µg.g^{-1}and the lower concentrations was 98.79µg.g^{-1} for *Iago omanensis*.

Relationship between fish length and heavy metals concentrations. Tables 1 and 2 summarize the results of the correlation coefficient for heavy metals between fish length and final metal concentrations of *Auxis thazar* and *Iago omanensis*. The results showed that the fish length had no effect on most of the concentrations of both species. All concentrations that were affected by the length had positive relationships with it. R^2 were generally found to be low. The correlation between elements of *Auxis thazar* were very low except the correlation between

Cr and Zn R^2 =0.831. The correlations between elements of *Iago omanensis* generally were very low.

TABLE 1
The correlation coefficient between fish length of *Auxis thazar* and final metal concentrations; metal concentrations with each other's.

	Cu	Cr	Cd	Zn
Length	0.052	0.009	0.002	0.0034
Cu		0.054	0.323	0.063
Cr			0.11	0.831
Cd				0.183

TABLE 2
The correlation coefficient between fish length of *Iago omanensis* and final metal concentrations; metal concentrations with each other's.

	Cu	Cr	Cd	Zn
Length	0.023	0.293	0.0001	0.181
Cu		0.137	0.0009	0.0017
Cr			0.015	0.07
Cd				0.179

DISCUSSION

Heavy metals between different fish species. The results of this study revealed that, heavy metals concentrations were significantly different between the two fish species of this study; this could be due to the different feeding habitat and habits of the two species. The higher concentration of Cr, Cd and Zn were found in *Auxis thazar*, whereas, the higher concentrations of Cu was in *Iago omanensis*. The deep sea fish *Iago omanensis* occupying the deep sea water, the main food contents are cephalopods which comprise more than 50% of the stomach contents, the other 50% was small fish and about 10% was decapods [20]. The analysis of food contents of *Auxis thazar* by Kumaran [21] showed that the 42% of the stomach contents was crustaceans. Several studies showed that the feeding habits in addition to sex play important role in the final metal concentrations of different fish species. Wahbeh and Mahasneh [9], found significant differences in heavy metal concentrations in six coral reef fish species from the same area, they included species with different feeding habits, from piscivorous species such as the lizardfish (*Synodus variegates*) to those feeding on invertebrates, such as the goatfish (*Parupeneus barberinus*), or on algae, such as the Sergeant Major fish (*Abufefduf saxatilis*). In a study on three species, *Oreochromis mossambicus* an omnivore fish, *Ophiocephalus striatus* a piscivore fish and *Heteropneustes fossilis* a detritivore fish, it was found that the piscivore had the highest bioaccumulation for all metals that was measured because of the bio-magnification factor, except for Fe and Mn, were the highest in the detritivore species, which might be due to very high levels in the sediments [22]. Cephalopods were found to have the highest levels of Cu, Fe, Zn, Cr, Cd and Pb compared to other species, since they feed on crustaceous and small mollusks. Bivalves and fish species that consume algae and planktons as a part of their regular diet had the lowest metal bioaccumulation levels [23].

The result of this study indicate a significant high copper concentrations in cartilaginous fish *Iago omanensis* than bone fish *Auxis thazar* this could be due to the role of Cu as a cofactor for the key antioxidant enzyme copper, zinc superoxide dismutase (Cu, Zn-SOD) in lower vertebrates [24].

In this study the sex of the fish was not taken into consideration due to the limitation number of samples available. However, different studies showed that sex could be a major source of metal accumulation between different fish species.

Heavy metals between different organs. Our result indicated that, metals concentrations vary among different fish organs. It was found that the livers of *Auxis thazar* fish species had higher levels of Cu, Cr, Zn and Cd compared to muscle tissues and gills. At the same time Gills of *Iago omanensis* had higher levels of Cu, Cr and Zn, whereas livers had the higher levels of Cd.

The high accumulation of heavy metals in the liver of the two species has likewise been reported in several studies [25, 26, 15, 16]; these studies suggested that the liver plays an important role in the metabolic processes of heavy metals in fishes. According to Kotz et al. [27], muscles are primary part of metal intake, the liver is an organ that specializes in metal storage and detoxification, and the gills are directly exposed to the surrounding environment. The results of this investigation are in accordance with the study of Abu Hilal and Ismail [18], They reported that the muscles have the lowest concentration of metals in most of the nine species that were studied, while stomach and liver had the highest. Moreover, the findings of this study are in accordance with the study by Khalaf et al. [15], They obtained significant differences for most of the heavy metal elements among different organs of the same species, particularly the presence of low concentrations of Cu, Pb, Zn, Cd and Fe in the muscle of *D. macarelleus* and low concentrations of Ni, Pb, Zn and Fe in the muscle of *D. macrosoma*. Similarly, in *D. russelli* the lowest concentrations of Cu, Pb, Zn, Cd and Fe were found in muscle. In contrast, the highest concentrations of Cu, Pb, Cd and Fe were mainly concentrated in the liver and the kidney. Al-Najjar et al. [16], have found that there are no significant differences in the concentrations of metals between *Caesio varilineata* and *Caesio lunaris*, but it was found that different organs has concentrate dif

TABLE 3
Maximum permissible limit of heavy metals in fish muscle (µg/g dry. wt.) according to the international standards. Data are adopted from [17].

International standards	Heavy metals in fish muscles (µg/g dry. wt.)		
	Cu	Zn	Cd
FAO	100	100	0.17
FAO/WHO limit	100	133	1.67
WHO	100	333.3	3.33
European community	-	-	0.17
England	66.67	167	0.67
Auxis thazar	1.2	549.4	1.55
Iago omanensis	9.14	76.72	1.83

TABLE 4
Heavy metals in muscles (µg/g dry. wt.) of fish from the Red Sea and other regions. Data are adopted from [17].

Fish Species	Heavy metals in fish muscles (µg/g dry. wt.)				
	Site	Cu	Zn	Cr	Cd
Auxis thazar	Gulf of Aqaba	1.2	549.4	154.81	1.55
Iago omanensis	Gulf of Aqaba	9.14	76.72	72.74	1.83
Acanthopagurus bifaclatus	Red Sea	0.51	4.34	0.72	0.26
Ctenochaetus striatus	Gulf of Aqaba	0.87	21.38	1.36	0.83
Scomberomorus commerson	Yemen	1.30	8.00	0.90	0.39
Boops boops	Black Sea	3.08	6.81	0.22	0.10
Thunnus thynnus	Mediterranean Sea	1.01	16.54	0.74	0.05
Nemipterus japonicas	Hurghada, Red Sea	0.28	2.13	0.82	0.02
Caranxsex faciatus	Jeddah coast,	0.91	5.33	0.00	0.90

ferent metals. Agusa et al. [28], studied trace elements concentrations in the livers and muscles of *Euthynnus affinis* collected from Malaysia, and found that almost all elements have higher concentrations in the liver than those in the muscle, especially Zn, were they found that *E. affinis* had extremely high level of Zn in liver compared to the muscle of *E. affinis*.

The present results indicated that the lowest concentrations of the heavy metals were usually recorded in muscle of the two species rather than the gills and livers. Although fish muscle is the most important part to be used for human consumption, fish gills and liver may also be consumed to some extent. Target organs such as liver, kidney, gonads and gills, have a tendency to accumulate heavy metals in high values, as shown in many species of the fish in different areas [29, 30, 31, 32]. It is generally accepted that muscle is not an organ in which metals accumulate [33]. Similar results were reported from a number of fish species showing that muscle is not an active tissue in accumulating heavy metals [34]. This is agreed with the present study.

Our results indicate that gills of *Iago omaniasis* accumulate more heavy metals Cu, Cr and Zn than the muscles and the livers. The reason for the high heavy metal concentrations in the gills could be due to the metal complexion with the mucus that is impossible to be removed completely from the tissue before the analysis [35].

Correlations between different fish length and heavy metal bioaccumulation. No correlations were detected between the body length of the two fish species and the heavy metal concentrations, the correlations obtained for all heavy metals were very weak. Consistent with the results obtained by Nussey et al. [36] on heavy metals bioaccumulation in the fresh water fish *Labeo umbratus*, In contrast to our study the negative relationship with the fish size for Mn in gills and liver, for Pb in liver, skin and gills have been reported by Authman [37], Also he reported that bioaccumulation of copper, iron, lead, manganese and zinc increase with the increase in fish size, whereas aluminium, cadmium and mercury showed negative relationship with fish size. Recently, Al-Najjar et al. [18] reported week correlation between different element concentrations in *Cheilinus trilobatus* fish and length, at the same time the highest correlation was found between Ni and Co (R^2=0.71), Co and Fe (R^2=0.28), Ni and Mg (R^2=0.70) and between Co and Mg (R^2=0.72).

Comparison with other concentrations and WHO. The heavy metals concentrations of Cu and Cd in the examined fish species from the Gulf of Aqaba were below the permissible limits for human consumption (Table 3). The results in previous literatures were lower than our obtained data for other fish species. For example, Abdallah [38], determined the concentrations of Cd, Pb, Cu and Zn in muscles of *Sardinellaaurita, Sardinella. rivulatus* and *Synodussaurus* from two main harbors in Alexandria, Egypt, the reported heavy metals levels was much higher than those obtained in the two species of the current work. However, heavy metals levels in our study were generally higher than those found in the fish of the Red Sea recorded by [39, 40, 41, 42] (Table 4).

After all, fishes of this study were found to be safe for human consumption and do not cause any threat to the health of human consumers.

REFERENCES

[1] Wahsha, M., Al-Absi, E., Bini, C., Bani Yassen, A., Al-Zyoud, W. and Al-Jawasreh, R. (2016) Effects of toxic elements on leaf morphology of *Halophila stipulacea* grow in mine dump sediments in southeast Jordan. International Journal of Environmental Quality. 21, 33-40.

[2] Miguel, G. and Salvador, G. (2015) Handbook of Mineral Elements in Food. Wiley-Blackwell, 792 p.

[3] Hajeb, P., Jinap, S., Ismail, A., Fatimah, A.B., Jamilah, B. and Abdul Rahim, M. (2009) Assessment of Mercury Level in Commonly Consumed Marine Fishes in Malaysia. Food Control. 20, 79–84.

[4] Rasheed, R.O. (2012) Assessment of some Heavy Metals in Muscle Tissue of Silurus triostegus from Derbendikhan Reservoir, Kurdistan Region –Iraq. Raf. J. Sci. 23(1), 11-18.

[5] Kalay, M. and Canil, M. (1999) Heavy Metal Concentrations in Fish Tissues from the Northeast Mediterranean Sea. Bulletin of Environmental Contamination and Toxicology. 63, 673-681.

[6] Bini, C. and Wahsha, M. (2014) Potentially Harmful Elements and Human Health. Book Chapter In: Bini, C. and Bech, J. (eds.) Potentially harmful elements in the environment and the impact on human health. Springer. 401-463.

[7] Al-Najjar, T., Abu Khadra, K., Rawashdeh, O.Y., Khalaf, M. and Wahsha, M. (2015) Levels of Trace Metals in (Euthynnus affinis) Fish from the Gulf of Aqaba, Jordan. Fresen. Environ. Bull. 24(9), 2995-3000.

[8] Wahbeh, M.I. (1985) Levels of Zinc, Iron, Magnesium and Cadmium in the Tissue of Fish from Aqaba, Jordan. Dirasat. 12, 35-42.

[9] Wahbeh, M.I. and Mahasneh, D.M. (1987) Concentrations of Metals in the Tissues of Six Species of Fish from Aqaba, Jordan. Dirasat. (14), 119-129.

[10] Al-Sayed, M. (2008) Levels of Trace Metals in Some Carnivorous Fish of Gulf of Aqaba, Red Sea. Master Thesis. Hashemite University, Zarka.

[11] Al-Zgool, A. (2008) Levels of Trace Metals in Food Chain of Some Carnivores Fishes (Family: Carangidae) Collected from the Gulf of Aqaba, Red Sea. Master Thesis. Hashemite University, Zarka.

[12] Batayneh, M. (2010) Levels of Trace Metals in Some Herbivorous Fish of Gulf of Aqaba, Red Sea. Master Thesis. Hashemite University, Zarka.

[13] Ismail, N.S. and Abu-Hilal, A.H. (2008) Heavy Metals in Three Commonly Available Coral Reef Fish Species from the Jordan Gulf of Aqaba, Red Sea. Jordan Journal of Biological Sciences. 2, 61-66.

[14] Abu-Hilal, A.H. and Ismael, N.S. (2008) Heavy Metals in Eleven Common Species of Fish from the Gulf of Aqaba, Red Sea. Jordan Journal of Biological Sciences. 1, 13-18.

[15] Khalaf, M.A., Al-Najjar, T., Alawi, M. and Disi, A.M. (2012) Levels of Trace Metals in Three Fish Species *Decapterus macrellus*, *Decapterus macrosoms* and *Decapterus russelli* of the Family Carangidae from the Gulf of Aqaba, Red Sea, Jordan. Natural Science. 4, 362-367.

[16] Al-Najjar, T., Khalaf, N., Allawi, M. and Disi, A. (2012) Levels of Trace Metals in Two Fish Species *Caesio varilineata* and *Caesio lunaris* of the Family Caesionidae from the Gulf of Aqaba, Red Sea. Fresen. Environ. Bull. 21(5), 1152-1157.

[17] Gassaymeh, R. (2016) Levels of Heavy Metals in Mesopelagic Fish Species (*Polysteganus coeruleopunctatus*, *Argyrops Spinifer* and *Argyrops Filamentosus*) of the Family Sparidae from the Northern Gulf of Aqaba, Red Sea. Master Thesis. Jordan University, Aqaba.

[18] Al-Najjar, T., Al-Momani, R., Khalaf, M., Wahsha, M., Sbaihat, M., Khalaf, N., Abu Khadra, K. and Magames, H. (2016) Levels of Heavy Metals in Fishes (*Cheilinus trilobatus*) From the Gulf of Aqaba, Jordan. Natural Science. 8(06), 256.

[19] Chen, Y., Paytan, A., Chase Z., Measures C., Aaron, J., Sergio, B., San, A., Wilhelmy, U. and Anton F.P. (2008) Sources and Fluxes of Atmospheric Trace Elements to the Gulf of Aqaba, Red Sea. Journal of Geophysical Research. 1-13.

[20] Waller, G.N.H. and Baranes, A. (1994) Food of *Iago omanensis*, A Deep Water Shark from the Northern Red Sea. J. Fish Biol. 45, 37-45.

[21] Kumaran, M. (1964) Studies on the Food of *Euthynnus affinis* (Cantor), *Auxis thazard* (Lacepède), *Auxis thynnoides Bleeker* and *Sarda orientalis* (Temminck and Schlegel). Proc. Symp. Scombroid Fishes, Part II. Mar. Biol. Assoc. India, Symp. Ser. 1, 599-606.

[22] Wijesinghe, M., Jayatunga, Y. and Hewamanna, R. (1999) Bioaccumulation of Heavy Metals in Three Species of Fresh Water Fish from Weras Ganga: Evidence for Bio-Magnification. Vidyodaya Journal of Science. 8, 203-206.

[23] Ahdy, A., Abdallah, A. and Tayel, F. (2007) Assessment of Heavy Metals and Nonessential Content of Some Edible and Soft Tissues. Egyptian Journal of Aquatic Research. 33, 85-97.

[24] Nam, Y.K., Cho, Y.S., Kim, K.Y., Bang, I.C., Kim, K.H., Kim, S.K. and Kim, D.S. (2006) Characterization of Copper, Zinc, Superoxide Dismutase from a Cartilaginous Shark Species, *Scyliorhinus torazame* (*Carcharhiniformes*). Fish Physiol Biochem. 32, 305-315.

[25] Honda, K., Sahrul, M., Hidaka, H. and Tatsukawa, R. (1983) Organ and Tissue Distribution of Heavy Metals and their Growth-Related Changes in Antarctic Fish, *Pagothenia Borchgrevinki*. Agricultural and Biological Chemistry. 47, 2521–2532.

[26] Agusa, T., Kunito, T., Yasunaga, G., Iwata, H., Subramanian, A., Ismail, A. and Tanabe, S. (2005) Concentrations of Trace Elements in Marine Fish and its Risk Assessment in Malaysia. Marine Pollution Bulletin. 51, 896-911.

[27] Kotze, P.H., Preez, H.H. and Van Vuren, H.J. (1999) Bioaccumulation of Copper and Zinc in *Oreochromis mossambicus* and *Clarias garicpinus*, from the Olifants River, Mpumalanga, South Africa. Water SA. 25, 99–110.

[28] Agusa, T., Kunito, T., Kubota, R., Tanabe, R. and Iwata, H. (2012) Exposure, Metabolism, and Effects of Arsenic in Residents from Arsenic-Contaminated Groundwater Areas of Southeast Asia. Interdisciplinary Studies on Environmental Chemistry Environmental Pollution and Ecotoxicology. 125–132.

[29] Kargin, F. (1996) Seasonal Changes in Levels of Heavy Metals in Tissues of *Mullus barbatus* and *Sparus aurata* Collected from Iskanderun Gulf (Turkey). Water, Air Soil Pollut. 90, 557-562.

[30] Yilmaz, A.B. (2003) Levels of Heavy Metals (Fe, Cu, Ni, Cr, Pb and Zn) in Tissue of *Mugil Cephalus* and *Trachurus Mediteraneus* from Iskenderun Bay, Turkey. Environ. Res. 92, 277-281.

[31] Yilmaz, A.B. (2005) Comparison of Heavy Metal Levels of Grey Mullet (*Mugil cephalus L.*) and Sea Bream (*Sparus aurata L.)* Caught in Iskendrun Bay (Turkey). Turk. J. Vet. Anim. Sci. 29, 257-262.

[32] Abdel moniem, M., Khaled, A. and Iskander, M. (1994) A Study on Levels of Some Heavy Metals in El-Mex Bay, Alexandria, Egypt. In: Proceeding of the Fourth Conference on Environmental Protection Must, Alexandria, Egypt 155-174.

[33] Legorburu, I., Canton, L., Millan, E. and Casado, A. (1988) Trace metal levels in fish from Unda iver (Spain) *Anguillidae, Mugillidae* and *Salmonidae. Environ*. Technol. Lett. 9, 1373-1378.

[34] Karadede, H. and Unlu, E. (2000) Concentrations of Some Heavy Metals in Water, Sediment and Fish Species from the Ataturk Am Lake (Euphrates), Turkey. Chemosphere. 41, 1371-1376.

[35] Al-Weher, M.S. (2008) Levels of Heavy Metal Cd, Cu and Zn in Three Fish Species Collected from the Northern Jordan Valley, Jordan. Jordan Journal of Biological Sciences. 1(1), 41 - 46.

[36] Nussey, G., Vuren, V. and Preez, D. (2000) Bioaccumulation of Chromium, Manganese, Nickel and Lead in the Tissues of the Moggel, *Labeo umbratus* (Cyprinidae), from Witbank Dam, Mpumalanga. Water S.A. 26, 269-284.

[37] Authman, M. (2008) *Oreochromis niloticus* as A Biomonitor of Heavy Metal Pollution with Emphasis on Potential Risk and Relation to Some Biological Aspects. Global Veterinaria. 2, 104-109.

[38] Abdallah, M.A.M. (2008) Trace Element Levels in Some Commercially Valuable Fish Species from Coastal Waters of Mediterranean Sea, Egyption. Journal of Marine System. 73, 114-122.

[39] Hanna, R.G.M. (1989) Levels of Heavy Metals in Some Red Sea Fish before Hot Brine Pools' Mining. Marine Pollution Bulletin. 20, 631–635.

[40] Abdelmoneim, M.A. and El-Deek, M.S. (1992) Lethrinus Family: A Model of Edible Red Sea Fish with Low Heavy Metals Accumulation. In: Proceedings of the 2nd Alexandria Conference (Food Sci. Tech.). Egypt: Fac. Agri., Alexandria Univ. 439-448.

[41] Emara, H.I., El-Deek, M.S. and Ahmed, N.S. (1993) A Comparative Study on the Levels of Trace Metals in Some Mediterranean and Red Sea Fishes. Chem Ecol. 8, 119-127.

[42] Ali, A.A., Elazein, E.M. and Alian, M.A. (2011) Investigation of Heavy Metals Pollution in Water, Sediment and Fish at Red Sea- Jeddah Coast- KSA at Two Different Locations. Journal of Applied Environmental Biological Sciences. 1(12), 630-637.

Received: **09.04.2017**
Accepted: **05.10.2017**

CORRESPONDING AUTHOR

Tariq Al-Najjar
Department of Marine Biology,
The University of Jordan,
Aqaba Branch – Jordan

E-mail: t.najjar@ju.edu.jo

© by PSP Volume 26 – No. 12A/2017 pages 7815-7824 Fresenius Environmental Bulletin

A MODIFIED GIS-BASED WATER-SEDIMENT-ADSORBED PHOSPHORUS COUPLING MODEL AND ITS APPLICATION IN A TYPICAL WATERSHED OF SEMIARID REGIONS

Lei Wu[1,2,3,*], Shanshan Qiao[1,3], Xia Liu[4]

[1.]Key Laboratory of Agricultural Soil and Water Engineering in Arid and Semiarid Areas, Ministry of Education, Northwest A&F University, Yangling, Shaanxi 712100, P.R. China

[2.]State Key Laboratory of Soil Erosion and Dryland Farming on the Loess Plateau, Northwest A&F University, Yangling, Shaanxi 712100, P.R. China;

[3.]College of Water Resources and Architectural Engineering, Northwest A&F University, Yangling, Shaanxi 712100, P.R. China

[4.]Construction Department, Northwest A&F University, Yangling, Shaanxi 712100, P.R. China

ABSTRACT

Chinese Loess Plateau is considered as one of the serious soil erosion regions in the world. Nutrient loss through runoff and sediment in highly erodible areas not only decreases soil fertility, but also creates many environmental problems. In this study, an integrated modelling framework for the distributed coupling of hydrological process, soil erosion and adsorbed nonpoint source (NPS) pollution was established to investigate adsorbed NPS pollution in a typical watershed of Loess Plateau. Results indicate that: 1) the modified method is well validated and can be applied to the hilly and gully region, Loess Plateau; 2) the adsorbed total phosphorus (TP) load showed an overall decreasing trend from 1995 to 2012, the average TP pollution load from 2009 to 2012 reduced about 78% comparing with the early governance period (1995-1998), the high risk regions of TP load mainly occurred in the gentle sloping farmland which are located at the main river banks of the watershed. Results may provide data supporting for soil and water conservation planning in the hilly and gully region of Loess Plateau.

KEYWORDS:
Modified dynamic model, Water-sediment-adsorbed NPS pollution, Distributed coupling effects, Soil and water conservation, Loess Plateau

INTRODUCTION

The adsorbed nonpoint source (NPS) pollution can be interpreted as that eroded soil carries a great number of adsorbed pollutants into various water bodies and forms a kind of typical NPS pollution [1-2].Loess Plateau is considered as one of the most severe soil loss regions in China or even in the world [3]. Serious soil loss not only affects agricultural production, but also leads to diffuse pollution and threatens water quality [4-8]. NPS pollution output is affected by the comprehensive influence ofrainfall distribution, land use pattern, livestock and poultryfarming, human activities and other factors [9-10]. NPS pollution load takes onstrong regional distributions due to the difference of the local economic conditions, soil types and planting structure [11-12]. Phosphorus is an important component of NPS pollutants [13]. The loss process of phosphorus is very complex and the loss pathways include soil erosion, surface runoff and leaching leakage, where soil erosion is an important way of phosphorus loss [14-15]. In the loess hilly and gully region, NPS pollution loads are closely related to soil erosion especially for few transient rainstorms in flood season [16-17]. Therefore, this study focuses on a typical watershed to explorethe coupling mechanism of water-sediment-adsorbed NPS pollution.

The essence of adsorbed phosphorus pollution is soil erosion [18-19]. The study of soil erosion has expericened multiple stages including field experiments, modeling and the application of most advanced technology in the world [20-23]. Where models are the necessary means for the study of NPS pollution peocess at a river basin scale [24-25]. The USLE/RUSLE is commanly used in modelling pollutants adsorbed to sediment because of well solving the quantitative estimation of multi-year average soil erosion amount [26-27]. The modified RUSLE equation [28], the Chinese soil loss equation (CSLE) [29-30], AnnAGNPS model [31-32] and SWAT model [33-35] were also extensively applied to evaluate NPS pollution load. Many previous studies have applied models to analyze scenarios of agricultural impacts on nutrients loadings at catchment scale [36-37], and the corresponding scenario studies have been performed over a broad range of climatic conditions, with a large focus on measures targeting land cover/use and land management for reducing the source load of nitrogen and phosphorus in the landscape [38-40]. Besides, the research of NPS pollution with advanced technologies and algorithms such as GIS and RS, BP neural network, genetic algorithm and fruit fly algorithm also gets a rapid development [41-45].

The distributed models such as Basins, SHE, IHDM and EUROSEM [46], KINEROS [47-48] have an entensive application gradually due to requirements of high simulation efficiency and accuracy, the distributed research on NPS pollution has become a popular trend [49-50], and dynamic simulation has also become an important way to grasp time variations of sediment yield and NPS pollution [51-53]. However, the existing distributed dynamic model often paid more attention to event-based rainfall process, it less considers effects of the sediment delivery relationship on dynamic changes of adsorbed NPS pollution in the upper and lower reaches of a watershed.

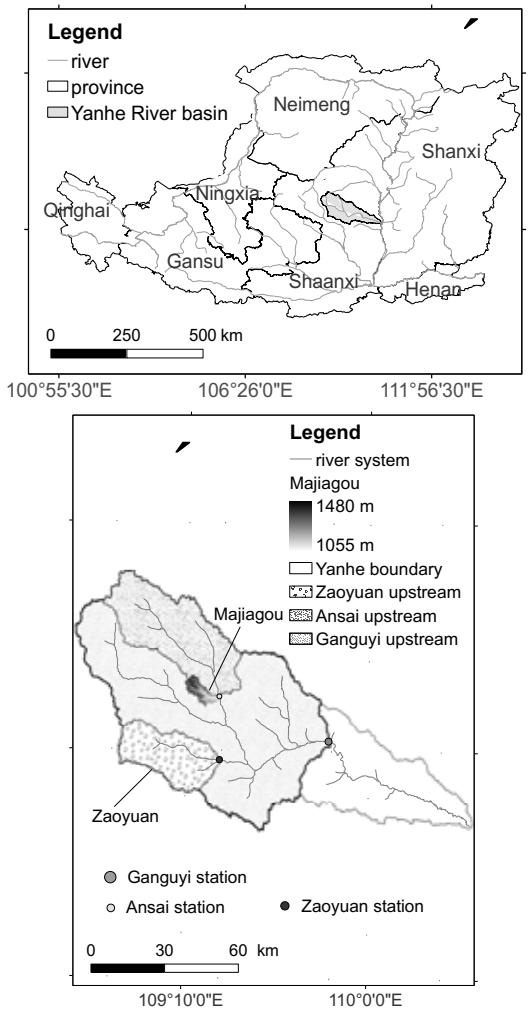


FIGURE 1
The study area: the relative location between the Yanhe River basin and the Chinese Loess Plateau under river system and provincial administrative divisions; the geographical location sketch of the Majiagou River watershed, Zaoyuan hydrological station, Ansai hydrological station and Ganguyi hydrological station in the river system of Yanhe River basin

Therefore, this study aims to 1) modify a GIS-based dynamic model of adsorbed NPS pollution load; 2) evaluate spatiotemporal evolutions of adsorbed TP NPS pollution before and after returning farmland in the Majiagou River watershed. Results may provide a scientific basis for NPS pollution control and watershed management in the hilly and gully region of Loess Plateau.

MATERIALS AND METHODS

Study area. Majiagou river, which is the protection area of drinking water source in Ansai County, is one of the first grade tributaries of the Yanhe River (Fig.1). The main channel is about 17.4 km in length, the average gully slope is about 6.5‰ [54]. The Majiagou River watershed (109°9′30″~109°18′59″E, 36°49′42″~36°56′42″N), with a total catchment area of 73.83 km^2, is one of the typical soil erosion regions in the Loess Plateau [55]. The watershed belongs to warm-temperature and semi-arid continental monsoon climate, the annual average temperature is 6-11°C, the evaporation is greater than 1000 mm, the annual precipitation is about 500 mm, the storm in 6-10 months accounts for about 80% of the total annual precipitation [56]. After the implementation of returning farmland to forestland/grassland in past ten years, the soil erosion of the watershed decreased from 8740 t/km^2 to 5700 t/km^2 in 2008 [57].

Environmental database. The parameters included in this study include digital elevation model (DEM), daily precipitation data, runoff, land use types, soil properties (Table 1). Where reclassified land use types of the Majiagou River watershed are consisted of farmland, grassland, forestland, settlements, water area and sand land. Soil types of the watershed are mainly composed of tillage erosive loessal soil and erosive loessal soil.

The modified dynamic nonpoint source pollution model. The dynamic-continuous modelling studies on sediment yield are very critical and necessary for accurately estimating temporal trends of adsorbed NPS pollution load [58]. However, the commonly used sediment yield model mainly reflects the multi-year average level, it is not a dynamic method and can not express the spatial transport process of pollutants. Rainfall runoff and human activity are two important factors affecting NPS pollution [59-61]. According to the related study results [62-64], the rainfall erosivity factor and the sediment delivery ratio (*SDR*) affected by rainfall runoff could be defined as the dynamic hydrological factor; the *BET* factor and the *SDR* factor affected by human activities might be designed as the dynamic

TABLE 1
Descriptions and sources of the environmental database in the Majiagou River watershed

Data name	Format	Description	Source
DEM	Raster	30 m spatial resolution DEM data of the Majiagou River watershed	Computer Network Information Center, Chinese Academy of Sciences (http://datamirror.csdb.cn/index.jsp)
Land use	Vector	Farmland, grassland, forest land, residential area, water area, sandy land	Data Center for Cold and Arid Region Sciences (http://westdc.westgis.ac.cn/)
Soil	Excel	Physical and chemical properties (organic matter, mechanical composition, coefficient of soil structure, etc.)	Loess Plateau Data Center, National Earth System Science Data Sharing Infrastructure, National Science & Technology Infrastructure of China (http://loess.geodata.cn/)
Runoff and sediment	Excel	Time series of annual observed values in Ganguyi hydrological station (1956-2012), Ansai and Zaoyuan hydrological stations (2006-2012)	
Precipitation	Txt	Daily values in Ansai, Yanan, Yanchang and other rain-gauge stations (1957-2013)	China Meteorological Data Sharing Service Network (http://data.cma.cn/data/)

land management factor, so the dynamic equation of adsorbed NPS pollution was put forward as follows:

$$L_{p,i} = C_p \times \eta_p \times A \times K \times LS \times \left(R_i \times \lambda_{q,i}\right) \times \left(B_i \times E_i \times T_i \times \lambda_{m,i}\right) \quad (1)$$

where L is the annual adsorbed NPS pollution load, (t); C_p is the background content of P in topsoil (g kg^{-1}); η_p is the enrichment ratio of P; A is the watershed area, (hm^2); R is the rainfall erosivity factor, (MJ·mm/hm^2·h·a); K is the soil erodibility factor, (t·hm^2·h/hm^2·MJ·mm); LS is the topographical factor; B is the biological measure factor; E is the engineering measure factor; T is the tillage measure factor; λ represents the average sediment delivery ratio (SDR), the subscript i represents the i-th year, and the λ_i may be approximately assumed to be divided into the product of $\lambda_{q,i}$ related only to hydrological conditions and $\lambda_{m,i}$ related only to land management measures.

Impacts of hydrological features on pollutants transport are mainly manifested in the moving action of sediment from erosion source to the river course by rainfall runoff [65]. $\lambda_{q,i}$ can be estimated by the formula of sloping runoff energy that is widely used in most parts of northern China [66]. According to the definition of $\lambda_{q,i}$, it can be supposed as follows,

$$\frac{\lambda_{q,i}}{\lambda_q} = \frac{E_i}{E} = \frac{\left(\frac{\rho g}{4} \cdot \sin 2\theta\right) \cdot P_{h,i}}{\left(\frac{\rho g}{4} \cdot \sin 2\theta\right) \cdot P_h} = \frac{\int_0^{t_i} \left(I_i - f_i\right) dt}{\int_0^t \left(I - f\right) dt} \quad (2)$$

where E is the average runoff power per unit area of slopes (J m^{-2});ρ is the liquid density (kg m^{-3}); g is the gravitational acceleration (m s^{-2}); θ is the slope gradient (°); P_h is the runoff depth (mm); I is the rainfall intensity; f is the infiltration rate; t is the rainfall duration (min). Letters of ρ, g and θ are all constants when there are no changes in sloping surface.

Impacts of human activities on pollutants transport are mainly demonstrated in subtractive effects of NPS pollution load by all kinds of soil conservation measures [67-68]. In general, the condition of underlying surface has an important effect on rainfall runoff and nutrient pollution output [69]. In order to dynamically study impacts of land management activities on the sediment transport process, the ratio of sediment during the governance period (1970-2012) and the base period (1956-1969) was defined as the dynamic influencing factor of land management activities [70-72]. Under the annual changes of $\lambda_{m,i}$, B, E and T, the dynamic land management factor (α) was introduced and defined as,

$$\alpha_i = \frac{B_i \times E_i \times T_i \times \lambda_{m,i}}{B \times E \times T \times \lambda_m} = \frac{0.449x_i - 5062.6}{0.4436x_i - 4559.9} \quad (3)$$

where x_i represents the runoff amount in the i-th year (10^4 m^3), n is the number of years.

In addition, considering the above dynamic model may not completely reflect spatiotemporal variations of the watershed underlying surface, especially can not embodies the physically-based complex sediment delivery relationship between the upper and lower reaches of the watershed under different land use conditions [73]. So the spatial influencing factor (β) considering upstream and downstream relationships of a watershed [74] was introduced as follows,

$$\beta_i = \frac{Q_{w,i}}{Q_i - Q_{b,i}} \quad (4)$$

where $Q_{w,i}$ is the annual saturated water when the saturated sediment transport is the observed sediment transport amount in a hydrological station, $Q_{b,i}$ is the annual base flow, Q is the observed annual runoff amount.

Stated thus, by substituting Eq. (2) _ Eq. (4) into Eq. (1), the integrated model of adsorbed NPS pollution load can be rewritten as follows,

$$L_{p,i} = \alpha_i \times \beta_i \times \frac{\int_0^{t_i} \left(I_i - f_i\right) dt}{\int_0^t \left(I - f\right) dt} \times R_i \times \lambda \times K \times LS \times B \times E \times T \times A \times C_p \times \eta_p \quad (5)$$

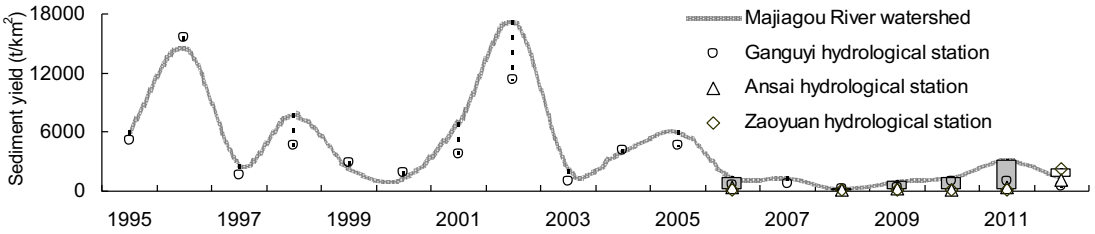


FIGURE 2

Comparison of sediment yield modulus between Ganguyi hydrological station, Ansai hydrological station, Zaoyuan hydrological station and Majiagou River watershed based on the modified model

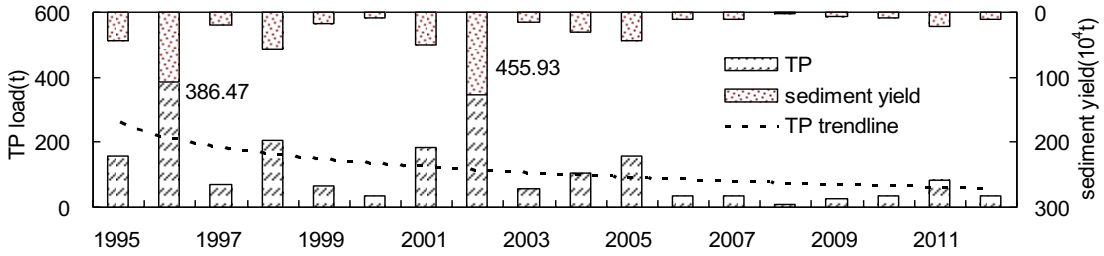


FIGURE 3

Temporal variations of sediment yield and TP load by the modified model in the Majiagou River watershed from 1995 to 2012

Description of model factors. In this study, a half-month simple algorithm of rainfall erosivity established by Zhang *et al.* (2003) was used to calculate the monthly and annual rainfall erosivity [75]. Soil erodibility is used to evaluate properties whether the soil is susceptible to erosion [76]. The modified method presented by Zhang et al. (2007) was applied to evaluate *K* values [26]. Based on soil properties of the study area, the average *K* value of soil erodibility in the watershed was calculated as 0.0542 $Mg.h.MJ^{-1}.mm^{-1}$. *LS* factor reflects the contribution degree of terrain factors to soil erosion, it can be divided into slope length factor (*L*) and slope gradient factor (*S*). According to the existing method of *LS* factor [77-78], the multi-year average *LS* value in the Majiagou River watershed was determined as 12.9. Based on the related research results of *B*, *E* and *T* factors in the Loess hilly region [79-81], the average *B*, *E* and *T* values of the watershed were in turn assigned to 0.1562, 0.497 and 0.712. The average annual *SDR* values of the Majiagou River watershed were determined by the research results of the Yanhe River basin by Zhu et al. (2007) [82].

RESULTS AND DISCUSSION

Validation of erosion and sediment yield. Soil erosion in the loess hilly and gully region is closely related to the soil nutrient loss. According to Li & Zheng (2012) simulation results of soil erosion in the Yanhe River watershed from 2001 to 2010 [83], the average annual erosion modulus of Yanhe River watershed is 5812.28 t/km^2, there are small relative error with the average simulated value of 6307.86 t/km^2 in the Majiagou River watershed from 1995 to 2012. The observed results of sediment yield in Ganguyi hydrological station from 1961 to 2008 [84] and the simulated values in this study both showed a decreasing trend although there were various fluctuations in individual years (Fig. 2), it indicates that the sediment yield reduction in the study area are consistent with the background of returning farmland project [85]. After model modification, the simulated value of the multi-year average sediment yield modulus in Majiagou River watershedhas changed from 5803.23 t/km^2 to 4510.66 t/km^2. Comparing with the Ganguyi hydrological station, the relative error of the modified model decreasedby 30%-40% [86]. For Ansai and Zaoyuan hydrological stations, the simulation accuracy also improved a lot (Fig. 2). The above results demonstrate that the modified dynamic model has scientific rationality and can be applied for NPS pollution load estimation in the loess hilly and gully region.

Temporal evolutions of adsorbed NPS pollution load. Fig.3 shows temporal variations of sediment yield and TP load in the Majiagou River watershed. Totally, the NPS pollution load in the watershed presents a decreasing trend, and the annual changing trends of TP load have similar fluctuations with the sediment yield. This result can be attributed to the soil and water conservation measures which may be effective in intercepting nutrient loss. In the late 1990s, the erosion-type NPS pollution problems are very prominent in the Majiagou River watershed.

With the continuous implementation of soil and water conservation measures, the benefits of water and sediment reduction are becoming more and more remarkable in the watershed, the average TP pollution load was44.72 t/a from 2009 to 2012, which decreased by about 78% comparing with the early governance period (1995-1998). On the whole, rainfall and human activity are two important factors affecting dynamic changes of adsorbed NPS pollution load. Rainfall is the motive power of soil and water loss, it can affect the formation and development of adsorbed NPS pollution by splash effects of raindrops and moving actions of runoffs. The positive human activities are the restraining factors of soil erosion, they can reduce NPS pollution load by increasing vegetation cover and weakening soil erosivity.

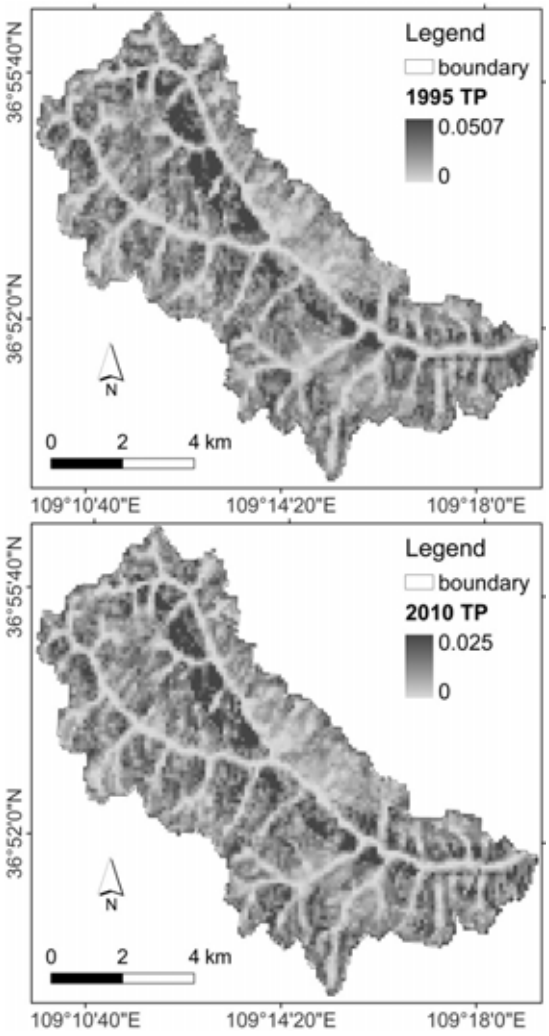


FIGURE 4
Spatial evolutions of adsorbed TP NPS load modulus (t/hm^2·a) in the Majiagou River watershed in 1995 and 2010

Spatial evolutions of adsorbed NPS pollution load. Fig.4 shows spatial distributions of adsorbed TP NPS pollution load in the Majiagou River watershed in 1995 and 2010. Spatial patterns of adsorbed TP NPS pollution load are similar to spatial distributions of sediment yield, the spatial difference of TP load in these two typical years mainly depends on the spatial distribution of land use types, and it is also closely related to spatial changes of topography and soil types. The main river banks from northwest to southeast in the Majiagou River watershed are the high risk regions of TP load. Therefore, sediment is not only a kind of NPS pollution, but also the pollutants carried by sediment may bring a potential pollution risk for water quality of receiving waters. The gentle sloping farmland located in both sides of the river was the most contributors for adsorbed NPS pollution load in the Majiagou River watershed, soil and water conservation measures should be simultaneously implemented in sloping farmland of the loess hilly and gully region.

Coupling relationship between land use changes and adsorbed NPS pollution. Fig.5a shows the area ratio of reclassified land use types of the Majiagou River watershed in 1995 and 2010. It can be seen that farmland and grassland area both account for more than 45% of the total watershed area in 1995 and 2010, they are the main NPS pollution source of the Majiagou River watershed. The existing survey results indicate that the sloping farmland in the watershed occupies 73.46% of the total farmland area, and the farmland is mainly distributed on both sides of the main river banks.

Fig. 5b shows trends of average and maximum adsorbed TP load in different land use types in 1995 and 2010. The average TP load in 1995 is listed as follows: farmland (0.0157 t/hm^2, 46.2%), villages and towns (0.0088 t/hm^2, 26%), grassland (0.0025 t/hm^2, 18.1%), and forestland (0.0033 t/hm^2, 9.7%); in 2010 the average TP load changed into villages and towns (0.0146 t/hm^2, 54.1%), forestland (0.0053 t/hm^2, 19.5%), farmland (0.0046 t/hm^2, 17.1%) and grassland (0.0025 t/hm^2, 9.4%). The changing trends of maximum TP load in 1995 are as follows: farmland (0.0772 t/hm^2, 57.1%), grassland (0.0284 t/hm^2, 21.1%), villages and towns (0.0167 t/hm^2, 12.4%), and forestland (0.0127 t/hm^2, 9.4%); in 2010 the maximum TP load changed into villages and towns (0.0307 t/hm^2, 39.4%), farmland (0.0198 t/hm^2, 25.4%), forestland (0.0155 t/hm^2, 19.9%), and grassland (0.0119 t/hm^2, 15.3%).

On the whole, the total average TP load modulus in 1995 and in 2010 are 0.034 t/hm^2 and 0.027 t/hm^2 respectively, and the total maximum TP load modulus in 1995 and in 2010 are 0.135 t/hm^2 and 0.078 t/hm^2 respectively. Statistical analysis shows that the highest contribution ratio of adsorbed NPS pollution load has changed from farmland in 1995 to villages and towns in 2010. Although the returning farmland project has been implemented since 1999,

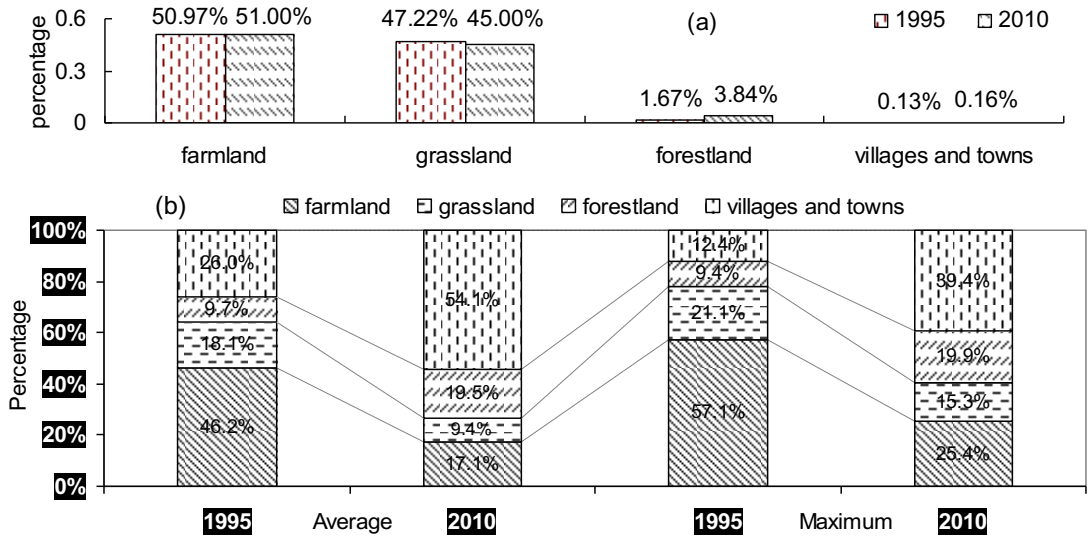


FIGURE 5

Coupling relationship between land use types and adsorbed TP NPS load (t/hm^2) in the Majiagou River watershed in 1995 and 2010: (a) area percentage of land use types (%), (b) percentage trends of average and maximum TP load (%).

farmland is still one of the main sources of nutrient loss, this is mainly because a large amount of farmland was transferred to orchard land and did not effectively develop conservation measures. Therefore, strengthening targeted management of critical sources is the key to control agricultural NPS pollution in the hilly and gully region, Loess Plateau.

CONCLUSIONS

1) A GIS-based distributed-dynamic modelling method was further modified and verified to investigate effects of returning farmland on adsorbed NPS pollution in the Majiagou River watershed from 1995 to 2012. Results show that the modified model has characteristics of simple algorithm, good application and easy expansion, it may provide a useful means for predicting adsorbed NPS pollution load in the hilly and gully region of Loess Plateau.

2) The overall adsorbed TP load tracked to a decreasing trend from 1995 to 2012. The average adsorbed TP load was 44.72(t/a) from 2009 to 2012, which decreased by about 78% comparing with the early governance period (1995-1998). The highest contribution ratio of adsorbed NPS pollution load has changed from farmland in 1995 to villages and towns in 2010. So the implementation of soil and water conservation measures plays a key role in the management and control of NPS pollution, it has a certain guiding significance for the planning of NPS pollution control strategies.

3) The spatial distribution patterns of adsorbed TP NPS pollution are basically consistent with sediment yield, high risk values of adsorbed TP NPS pollution load mainly occurs along the main river banks from northwest to southeast in the whole Majiagou River watershed. The returning sloping farmland projects have great benefits for NPS pollution load reduction. The results also potentially emphasize the necessity of making further efforts to soil and water conservation measures in highly erodible sloping farmland of Chinese Loess Plateau.

ACKNOWLEDGEMENTS

This study was supported by the National Natural Science Foundation of China (51679206, 51309194), Zhongying Youth Scholars of Northwest A&F University (Z111021720), Youth Science and Technology Nova Project in Shaanxi Province (2017KJXX-91), the Fundamental Research Funds for the Central Universities (2452016120), Special Research Foundation for Young teachers (2452015473), International Science and Technology Cooperation Funds (A213021603), the Doctoral Fund of Ministry of Education of China (20130204120034), the Initial Scientific Research Funds for PhD from Northwest A&F University (2012BSJJ004).

REFERENCES

[1] Shi, H. (1997) Non point source pollution of soil and water loss type. Bulletin of Soil and Water Conservation. 17(7), 99-101.

[2] Wu, L., Ma, X.Y., Liu, X. (2014) Assessment of Herbicide Transport and Distribution in Subsurface Environments of an Orange Field. Water Environment Research. 86(8), 729-740.

[3] Jiao, J.Y., Wang, W.Z., Hao, X.P. (1999) Precipitation and erosion characteristics of different types of rainfall in the Loess Plateau. Journal of Arid Land Resources and Environment. 13(1), 34-42.
[4] Pimentel, D., Harvey, C., Resosudarmo, P., Sinclair, K., Kurz, D., McNair, M., Crist, S., Shpritz, L., Fitton, L., Saffouri, R., Blair, R.(1995) Environmental and economic costs of soil erosion and conservation benefits. Science. 267(5201), 1117-1123.
[5] Zhang, S.G., Zhang, X.H., Wang, Y.L. (2004) Reflections on non point source pollution control problem in the Yellow River. Soil and Water Conservation in China. 8, 11-12.
[6] Elser, J., Bennett, E. (2011) Phosphorus cycle: a broken biogeochemical cycle. Nature. 478(7367), 29-31.
[7] Wu, L., Liu, X., Ma, X.Y. (2016) Spatio-temporal variation of erosion-type non-point source pollution in a small watershed of hilly and gully region, Chinese Loess Plateau. Environmental Science and Pollution Research. 23, 10957-10967.
[8] Wu, L., Qi, T., Li, D., Yang, H.J., Liu, G.Q., Ma, X.Y., Gao, J.E. (2015) Current status, problems and control strategies of water resources pollution in China. Water Policy. 17(3), 423-440.
[9] Wu, L., Gao, J.E., Ma, X.Y., Li, D. (2015) Application of modified export coefficient method on the load estimation of non-point source nitrogen and phosphorus pollution of soil and water loss in semiarid regions. Environmental Science and Pollution Research. 22(14), 10647-10660.
[10] Özkan, Ş., Vitali, A., Lacetera, N., Amon, B., Bannink, A., Bartley, D.J. (2016) Challenges and priorities for modelling livestock health and pathogens in the context of climate change.Environmental Research.151, 130-144.
[11] Liu, J., Chen, X.H., Xu,Z.C., Guo, Q.W., Wu, G.Y., Wang, Z.L. (2015) Simulation and Analysis of Temporal and Spatial Distribution of Non-point Source Pollution in the Dongjiang River Basin. Areal Research and Development. 34(2), 154-160.
[12] Zuo, D.P., Xu, Z.X., Yao, W.Y., Jin, S.Y., Xiao, P.Q., Ran, D.C.(2016) Assessing the effects of changes in land use and climate on runoff and sediment yields from a watershed in the Loess Plateau of China. Science of the Total Environment. 544, 238-250.
[13] Wu, L., Long, T.Y., Cooper, W.J. (2012) Temporal and Spatial Simulation of Adsorbed Nitrogen and Phosphorus Non-point Source Pollution load in Xiao Jiang Watershed of Three Gorges Reservoir Area, China. Environmental Engineering Science. 29(4), 238-247.
[14] Shan, B.Q., Yin, C.Q., Yu, J., Bai, Y. (2001) Study on phosphorus transport in the surface layer of soil with rainfall simulation method. Acta Scientiae Circumstantiae. 21(1), 7-12.
[15] Wu, L., Liu, X., Ma, X.Y. (2016) Tracking Soil Erosion Changes in an Easily-Eroded Watershed of the Chinese Loess Plateau. Polish Journal of Environmental Studies. 25(1), 332-344.
[16] Austin, A.T., Yahdjian, L., Stark, J.M., Belnap, J., Porporato, A., Norton, U., Ravetta, D.A., Schaeffer, S.M. (2004) Water pulses and biogeochemical cycles in arid and semiarid ecosystems. Oecologia. 141, 221-235.
[17] Teng, H., Xia, J.X., Ren, H.T. (2015) Study on GTGP effect of soil and water conservation function in Yan river basin in the loess plateau. Journal of Sediment Research. 4, 14-19.
[18] Yan, M.S., Gao, Y.F., Yang, S.T., Wang, X.L., Xaym, N. (2009) Research Progress and Prospect of Soil Erosion and Adsorbed Phosphorus Loss. Bulletin of Soil and Water Conservation. 29(5), 234-237.
[19] Wu, L., Liu, X., Ma, X.Y. (2017) Spatiotemporal variations of adsorbed nonpoint source nitrogen pollution in a highly erodible Loess Plateau watershed. Polish Journal of Environmental Studies. 26(3), 1343-1352.
[20] Chen, T.F., Cui, P.(2006) Prediction of soil erosion on the embankment slope of Xichang to Panzhihua highway, Sichuan, China. Journal of Chengdu University of Technology (Science & Technology Edition). 33(4), 371-375.
[21] Cui, S.F., Pan, Y.H., Wu, Q.Y., Zhang, Z.H., Zhang, B.X., Hao, C.H., Ren, S.G.(2013) Simulation and prediction of sediment under interval coverage on Lou soil slope. Journal of Soil and Water Conservation. 27(5), 7-11.
[22] Borrelli, P., Märker, M., Schütt, B. (2015) Modelling Post-Tree-Harvesting soil erosion and sediment deposition potential in the turano river basin (Italian central Apennine). Land Degradation and Development. 26(4), 356-366.
[23] Wu, L., Long, T.Y., Liu, X., Ma, X.Y. (2013) Modeling impacts of sediment delivery ratio and land management on adsorbed non-point source nitrogen and phosphorus load in a mountainous basin of the Three Gorges reservoir area, China. Environmental Earth Sciences. 70(3), 1405-1422.
[24] Wang, H.L., Li, X.Y., Xie, Y. (2011) Application prospects of multi-model approach for modelingnon-point source pollution. Advances in Water Science. 22(5), 727-732.
[25] Yao, W.Y., Xiao, P.Q. (2012) Research direction of the study of soil erosion in the Loess Plateau. Advances in Science and Technology of Water Resources. 32(2), 73-78.

[26] Zhang, K.L., Peng, W.Y., Yang, H.L. (2007) Soil erodibility and its estimation for agricultural soil in China. Acta Pedologica Sinica. 44(1), 7-13.
[27] Yu, J.X., Zheng, B.F., Liu, Y.F., Liu, C.L. (2011) Evaluation of soil loss and transportation load of adsorption N and P in Poyang Lake Watershed. Acta Ecologica Sinica. 31(14), 3980-3989.
[28] Wu, L., Long, T.Y., Liu, X., Mmereki, D. (2012) Simulation of Soil Loss Processes Based on Rainfall Runoff and the Time Factor of Governance in the Jialing River Watershed, China. Environ Monit Assess. 184(6), 3731-3748.
[29] Liu, B.Y., Xie, Y., Zhang, K.L. (2001) Soil erosion predicting model. Beijing: Chinese science and Technology Press.
[30] Cheng, L., Yang, Q.K., Xie, H.X., Wang, C.M., Guo, W.L. (2009) GIS and CSLE based quantitative assessment of soil erosion in Shaanxi, China. Journal of Soil and Water Conservation. 23(5), 61-66.
[31] Hong, H.S., Huang, J.L., Zhang, L.P., Du, P.F. (2005) Modelling pollutant loads and management alternatives in Jiulong River watershed with AnnAGNPS. Environmental Science. 26(4), 63-69.
[32] Zhang, Q.L., Chen, Y.X., Yu, Q.G., Deng, H., Tian, P. (2007) A review on nonpoint source pollution models. Chinese Journal of Applied Ecology. 18(8), 1886-1890.
[33] Huang, H.Q., Zhang, W.C. (2004) Improvement and application of GIS-based distributed SWAT hydrological modeling on high altitude, cold, semi-arid catchment of Heihe River basin, China. Journal of Nanjing Forestry University (Natural Sciences Edition). 28(2), 22-26.
[34] Qin, Y.M., Xu, Y.L., Li, H.E. (2009) SWAT model of nonpoint source pollution under different land use scenarios in the Heihe river basin. Acta Scientine Circumstantiae. 29(2), 440-448.
[35] Li, B.B., Zheng, F.L., Long, D.C., Jiang, Z.S. (2009) Spatial distribution of soil erosion intensity in Zhifanggou small watershed based on GIS. Scientia Geographica Sinica. 29(1), 105-110.
[36] Hashemi, F., Olesen, J.E., Dalgaard, T., Børgesen, C.D. (2016) Review of scenario analyses to reduce agricultural nitrogen and phosphorus loading to the aquatic environment. Science of the Total Environment. 573, 608-626.
[37] Wu, L,, Chang, H.Y., Ma, X.Y. (2017) Amodified method for pesticide transport and fate in subsurface environment of a winter wheat field of Yangling, China. Science of the Total Environment. 609, 385–395.
[38] Lin, C., Ma, R.H. (2016) Identification of phosphorus loss spatial features in typical land use patterns coupled with remote sense and soil analysis. Applied Engineering in Agriculture. 32(5), 521-530.
[39] Zang, Y.Z., Lin, C., Jin, Z.F., Fang, F., Zhou, S.L. (2016) Research on the dynamic change of adsorbed phosphorus load under land use change background in the coastal areas. Resources and Environment in the Yangtze Basin. 25(7), 1093-1102.
[40] Wu, L., Liu, X., Ma, X.Y. (2016) Impacts of Grain for Green project on spatiotemporal variations of soil erosion in a typical watershed of Chinese loess hilly and gully region. Fresen. Environ. Bull. 25(11), 4506-4516.
[41] Zhao, X.N., Wu, P.T., Feng, H., Wang, W.Z., Wu, F.Q.(2004) Research on slope soil erosion based on manpower neural network. Science of Soil and Water Conservation. 2(3), 32-35.
[42] Dai, H.L., Cao, S.L., Geng, X.Y.(2008) CFNN modification and its application in predicting soil erosion on slope land. Journal of Sichuan University (Engineering Science Edition). 40(5), 45-50.
[43] Caro, A., Legarda, F., Romero, L., Olondo, C. (2012) Map on predicted deposition of Cs-137 in Spanish soils from geostatistical analyses. Journal of Environmental Redioactivity. 115c (1), 53-59.
[44] Ochoa-Cueva, P., Fries, A., Montesinos, P., Rodríguez-Díaz, J.A, Boll, J.(2015) Spatial Estimation of Soil Erosion Risk by Land-cover Change in the Andes of Southern Ecuador. Land Degradation and Development. 26(6), 565-573.
[45] Brooks, E.S., Dobre, M., Elliot, W.J., Wu, J.Q., Boll, J. (2016) Watershed-scale evaluation of the Water Erosion Prediction Project (WEPP) model in the Lake Tahoe basin. Journal of Hydrology. 533, 389-402.
[46] Wang, H., Cai, Q.G., Zhu, Y.D. (2003) Evaluation of the EUROSEM model for predicting water erosion on steep slopeland in the Three Gorges Reservoir Area, China. Geographical Research. 22(5), 579-589.
[47] Singh, R., Panigrahy, N., Philip, G.(1999) Modified rainfall simulator infiltrometer for infiltration, runoff and erosion studies. Agricultural Water Management. 41(3), 167-175.
[48] Liao, Y.S., Zhuo, M.N., Li, D.Q., Cai, Q.G.(2012) A GIS-based distributed soil erosion and sediment yield model for typical watersheds in hilly loess areas: a case study in Shejiagou catchment. Journal of Sediment Research. (1), 7-13.
[49] Xia, J, Xue, J.F. (2010) A Distributed Soil Erosion and Sediment Transport Sub-model in Non-point Source Pollution and Its Application in Guishui Watershed. Journal of Resources and Ecology. 1(3), 231-237.

[50] Hu, H.X., MA, Y.H. (2008) Soil and Water Loss and Agricultural Non-point Source Pollution. Chinese Agricultural Science Bulletin. 24(6), 408-412.
[51] Yao, R.H., Wang, D., Zhao, Y., Zhang, J. (2012) Research Progress of Non-point Source Pollution Models in Water Environment. Journal of China Hydrology. 32(2), 11-15.
[52] Huang, J.J., Lin, X.J., Wang, J.H., Wang, H. (2015) The precipitation driven correlation based mapping method (PCM) for identifying the critical source areas of non-point source pollution. Journal of Hydrology, 524, 100-110.
[53] Long, T.Y., Wu, L., Li, J.C., He, C. (2012). Development of a dynamic adsorbed phosphorus pollution load model and its application to the jialing river basin, China. Fresen. Environ. Bull. 21(12), 3920-3929.
[54] Li, D.K. (2009) Vegetation change and its response to climate in the hill and ravine region of the Loess Plateau in Northern Shaanxi. Acta Botanica Boreali-Occidentalia Sinica. 29(5), 867-873.
[55] Fu, Y.L., Zhang, X.P., Chen, F.J., Wan, L., Wu, Y., Liu, G.B. (2010) Land Use/Cover Pattern Survey under the Background of Grain for Green Policy Implementation in the Loess Hilly-Gully Region-A Case Study of Majiagou Catchment, Ansai County. Research of Soil and Water Conservation. 17(6), 81-85.
[56] Jia, L.Z., Gao, J.E., Zhang, Y.X., Zhang, M.J., Wang, X.W., Li, X.H.(2014) Analysis of Rainstorm Erosion Disaster in Terrace Field in Loess Hilly and Gully Region. Research of Soil and Water Conservation. 21(4),7-11.
[57] Wu, Y., Zhang, X.P., Chen, F.J., Wan, L., Fu, Y.L., Liu, G.B. (2010) Preliminary investigation on soil erosion and spatial distribution after returning farmland in typical watershed of Northern Shaanxi Province. Research of Soil and Water Conservation. 17(4), 29-33.
[58] Gessesse, B., Bewket, W., Bräuning, A. (2015) Model-Based Characterization and Monitoring of Runoff and Soil Erosion in Response to Land Use/land Cover Changes in the Modjo Watershed, Ethiopia. Land Degradation and Development. 26(7), 711-724.
[59] Mu, X.M., Zhang, X.Q., Shao, H.B., Gao, P., Wang, F., Jiao, J.Y., Zhu, J.L. (2012) Dynamic Changes of Sediment Discharge and the Influencing Factors in the Yellow River, China, for the Recent 90 Years. Clean – Soil, Air, Water. 40(3), 303–309.
[60] Liu, X.Y., Yang, S.T., Dang, S.Z., Luo, Y., Li, X.Y., Zhou, X. (2014) Response of sediment yield to vegetation restoration at a large spatial scale in the Loess Plateau. SCIENCE CHINA: Technological Sciences. 57(8), 1482-1489.
[61] Lieskovský, J., Kenderessy, P.(2014) Modelling the effect of vegetation cover and different tillage practices on soil erosion in vineyards: A case study in vráble (Slovakia) using WATEM/SEDEM. Land Degradation and Development. 25(3), 288-296.
[62] Liu, L.M. (2009) Simulation study of nonpoint source pollution and its environmental effects on water in Jialing River watershed. Doctoral Dissertation of Chongqing University, 71-90.
[63] Long, T.Y., Li, J.C., Liu, L.M. (2008) Adsorbed nonpoint source pollution load of Jialing River basin. Environmental Science. 29(7), 1811-1817.
[64] Miao, C.Y., Yang, L., Chen, X.H., Gao, Y. (2012) The vegetation cover dynamics (1982–2006) in different erosion regions of the Yellow River basin, China. Land Degradation & Development. 23(1), 62–71.
[65] Wu, L., Long, T.Y., Liu, X., Guo, J.S. (2012) Impacts of climate and land-use changes on the migration of non-point source nitrogen and phosphorus during rainfall-runoff in the Jialing River Watershed, China. Journal of Hydrology. 475, 26-41.
[66] Cao, W.H., Zhang, X.M. (2014) Watershed sediment movement and its simulation. Beijing: Science Press. 56-59.
[67] Schilling, K.E., Isenhart, T.M., Palmer, J.A., Wolter, C.F., Spooner, J. (2011) Impacts of Land-Cover Change on Suspended Sediment Transport in Two Agricultural Watersheds. Journal of the American Water Resources Association (JAWRA). 47(4), 672-686.
[68] Sarma B., Sarma, A.K., Mahanta, C., Singh, V.P. (2015) Optimal Ecological Management Practices for Controlling Sediment Yield and Peak Discharge from Hilly Urban Areas. Journal of Hydrologic Engineering. 20(10), 04015005.
[69] Srivastava, P., Hamlett, J.M., Robillard, P.D., Day, R.L. (2002). Watershed optimization of best management practices using annagnps and a genetic algorithm. Water Resources Research. 38(3), 1-14.
[70] Gao, P., Zhang, X.C., Mu, X.M., Wang, F., Li, R., Zhang, X.P. (2010) Trend and change-point analyses of streamflow and sediment discharge in the Yellow River during 1950-2005. Hydrological Sciences Journal. 55(2), 275-285.
[71] Li, C.Z., Wang, H., Yu, F.L., Yang, A.M., Yan, D.H. (2011) Impacts of soil and water conservation on runoff and sediment in Yanhe River basin. Science of Soil and Water Conservation. 9(1), 1-8.
[72] Xu, X.X., Gao, Z.X., Zhao, J.N. (2012) Trends of runoff and sediment load of Yanhe River basin and their related driving forces during 1956-2009. Journal of Sediment Research. (2), 12-18.

[73] Xie, W.C., Li, T.H. (2012) Research Comment on Watershed Sediment Delivery Ratio. Acta Scientiarum Naturalium Universitatis Pekinensis. 48(4), 685-694.
[74] Xie, W.C. (2012) Research on watershed sediment delivery ratio in the hilly region of Loess Plateau: A case study in the Yanhe basin. Beijing: Master's degree thesis of Peking University.
[75] Zhang, W.B., Xie, Y., Liu, B.Y. (2003) Spatial variation of rainfall erosion in China. Journal of Mountain Science. 21(1), 33-40.
[76] Lu, J.Z., Chen, X.L., Li, H., Liu, H., Xiao, J.J., Yin, J.M. (2011) Soil erosion changes based on GIS/RS and USLE in Poyang lake basin. Transactions of the CSAE. 27(2), 337-344.
[77] Liu, B.Y,, Bi, X.G,, Fu, S.H. (2010) Beijing Soil Erosion Equation. Beijing: Science Press. 52-67.
[78] McCool, D., Brown, L.C., Foster, G.R., Mutchler, C.K., Meyer, L.D. (1987) Revised slope steepness factor for the Universal Soil Loss Equation. Transaction of the ASAE. 30(5), 1387-1396.
[79] Xie, Y., Lin, Y., Zhang, Y. (2003) The development and application of the Universal Soil Loess Equation. Progress in Geography. 22(3), 279-287.
[80] Zhang, Y., Liu, X.C., Li, Z.G., Zhu, Q.K. (2012) Surveying soil erosion condition in Loess Plateau using soil erosion model. Transactions of the Chinese Society of Agricultural Engineering. 28(10), 165-171.
[81] Qin, J.J. (2013) Study on the soil erosion prediction in the watershed of Three Gorge Region by CSLE: a case study in Kai County. Chongqing: Master dissertation of Southwest University. 1-96.
[82] Zhu, H.F., Kang, M.Y., Zhao, W.W., Guo, W.W. (2007) Effects of Soil and Water Conservation Measures on Erosion, Sediment Delivery and Deposition in Yanhe River Basin. Research of Soil and Water Conservation. 14(4), 1-4.
[83] Li, T.H., Zheng, L.N. (2012) Soil erosion changes in the Yanhe watershed from 2001 to 2010 based on RUSLE model. Journal of Natural Resources. 27(7), 1164-1175.
[84] Ren, Z.P., Zhang, G.H., Yang, Q.K. (2012) Characteristics of runoff and sediment variation in Yanhe River basin in last 50 years. Journal of China Hydrology. 32(5), 81-86.
[85] Zhao, G., Mu, X., Wen, Z., Wang, F., Gao, P. (2013) Soil erosion, conservation, and eco-environment changes in the Loess Plateau of China. Land Degradation & Development. 24, 499-510.
[86] Wu, L., Liu, X., Ma, X.Y. (2016) Application of a modified distributed-dynamic erosion and sediment yield model in a typical watershed of a hilly and gully region, Chinese Loess Plateau. Solid Earth. 7(6), 1577-1590.

Received: **10.04.2017**
Accepted: **30.09.2017**

CORRESPONDING AUTHOR

Lei Wu
Key Laboratory of Agricultural Soil and Water Engineering in Arid and Semiarid Areas, Ministry of Education, Northwest A&F University, Yangling, Shaanxi 712100, P.R. China

e-mail: lwu@nwsuaf.edu.cn

© by PSP Volume 26 – No. 12A/2017 pages 7825-7831 Fresenius Environmental Bulletin

FILTRATION RATE, OXYGEN CONSUMPTION, PHOSPHOROUS AND NITROGENOUS EXCRETION OF MYTILUS GALLOPROVINCIALLIS AND EFFECT IN AQUEOUS ENVIRONMENT

Kostas Katsoulis*

University of Thessaly School of Health Sciences, Faculty of Veterinary Science, 224 Trikalon Street, P.O. Box 199, Karditsa, 43100 Greece

ABSTRACT

Mussels are suspension feeders, producing faeces pellets and pseudo faeces as a waste product. Large-scale mussel farms are known to produce significant volumes of bio deposits, which can be settled beneath the farm, thereby altering sediment characteristics and the benthic community structure. The purpose of this study was to determine the influence of mussel Mytilus galloprovinciallis on soluble nutrient dynamic and its effect in aqueous environment by direct observations. Two experiments were carried out in water tanks. The first one was done using water with flow, while in the second one there was no flow. Two water tanks were used: one of them was a control tank, while in the other tank, 320 mussels were placed in four net bags. Dissolved oxygen and chlorophyll-a concentration were declined in the presence of Mytilus galloprovinciallis; marked increases that were observed especially in the concentrations of $N\text{-}NH_4$, $P\text{-}PO_4$, POC were a result of nutrient regeneration via excretion of Mytilus galloprovinciallis.

KEYWORDS:
Mytilus galloprovinciallis, filter feeder, mussel excretion, nutrient dynamic, mussel tank, aquatic ecosystem

INTRODUCTION

Mussels are enormously successful filter feeders. Their high filtering capacity allows them to remove particles from large volumes of water changing the dynamic of cycling nutrients. Their filtering activities have the potential to shift energy from the pelagic to the benthic region, resulting in changes in food web [1, 2 and 3]. Over the past 20 years, mussels of the genus *Mytilus* have been successfully used as indicators of contamination (heavy metals, municipal and urban effluents) in coastal areas providing a time-integrated indication of chemical contamination. In addition, mussels not only initiate the sedimentation of small particles, such as feces and pseudofaeces, but also increase the organic content of sediments, causing severe ecological impacts on aquatic ecosystem. The enriched organic sediment also increases microbial oxygen consumption, resulting in reduced oxygen concentrations [4, 5, 6, 7 and 8]. Little information exists regarding the role of Mytilus galloprovinciallis in nutrient regeneration. Thus, a laboratory experiment was designed to examine the influence of Mytilus galloprovinciallis on soluble nutrient dynamics.

MATERIALS AND METHODS

Two experiments were carried out under controlled conditions in water tanks in a coastal area in the region of Pieria, Greece. The first one was carried out using water with flow, while in the second one there was no flow. Two water tanks, 69 cm x 95 cm x 144 cm, were used; one of them was a control tank. Approximately 320 mussels with a mean shell length of 70 mm were placed in the other tank in four tight net bags - each net bag contained 80 mussels -. Mytilus galloprovinciallis were collected from Kitros, a site near the field station, and were placed in the water tank for an equilibration period of about two weeks prior to the initiation of the study. Fresh seawater was constantly circulated through the tank to maintain a food supply for the mussels during the equilibration period. Water was pumped externally from an outlet at 3m depth in the tank with a tubing pump at a rate of 1.3 m^3 / h. Four water samples were taken every 3 hours (0h, 3h, and 6h). Each experiment (water with flow and without flow) was repeated 4 times. The water sample bottles were immediately returned to the laboratory in insulated containers. These samples were filtered within 3h of collection through Whatman GF / C glass-fiber filters. Samples were kept frozen until analysis of chlorophyll-a, $N\text{-}NO_3$, $N\text{-}NH_3$, $P\text{-}PO_4$, POC, $N\text{-}NO_2$. Chlorophyll-a was determined by H.M.S.O method by filtration of the water sample using methanol as appropriate while chlorophyll-a concentration in the extract was determined spectrophotometrically. Dissolved oxygen concentration was measured using an automatic

TABLE 1
Changes of parameters in two experiments in relation with time

TREATMENT	Category	TIME	Chlorophyll-a (µg \ L)	N-NO_3 (µg/L)	N-NO_2 (µg\L)	N-NH_4 (µg \ L)	P-PO_4 (µg \ L)	POC (µg C \ L)	O_2 (mg O_2 \ L)	pH	Salinity (‰)	Temperature (^{0}C)
TANK WITH-OUT MUSSEL	WATER WITH OUT FLOW	0	0,57±0,039^a	242,2±22,55^a	8,7±0,84^a	6,45±0,66^a	25,09±0,67^a	669,4±224,2^a	5,77±0,109^a	8,15±0,03^a	36,5±0,22^a	14,87±0,10^a
		3	0,45±0,040^a	218,4±23,45^a	7,2±1,07^a	6,45±0,55^a	24,13±0,88^a	----------	5,82±0,105^a	8,17±0,03^a	35,6±0,10^a	14,62±0,10^a
		6	0,40±0,030^a	236,5±23,28^a	8,8±0,86^a	6,94±0,58^a	22,96±1,35^a	687,7±241,9^a	5,9±0,095^a	8,15±0,03^a	35,75±0,1^a	14,62±0,10^a
TANK WITH MUSSEL	WATER WITH OUT FLOW	0	0,67±0,037^a	211,8±20,06^a	8,7±0,81^a	7,21±0,85^a	24,59±0,47^a	697,3±244,1^a	5,95±0,112^a	8,18±0,02^a	36,37±0,2^a	14,87±0,10^a
		3	0,41±0,020^a	233,5±25,03^a	7,6±1,1^a	8,8 ± 0,74^b	26,3 ± 0,62^b	----------	5,7 ± 0,12^a	8,14±0,02^a	35,7±0,11^a	14,62±0,10^a
		6	0,23±0,028^b	244,5±23,90^a	9,1±0,82^a	10,1±1,01^b	27,01±0,47^b	877 ± 237,7^b	5,47±0,110^b	8,14±0,03^a	35,7±0,09^a	14,62±0,10^a
TANK WITH-OUT MUSSEL	WATER WITH FLOW	0	0,45±0,024^a	240,08±14,8^a	8,34±0,33^a	6,01±0,83^a	25,34±0,72^a	646,8±213,8^a	6,4 ± 0,11^a	8,15±0,03^a	36 ± 0,00^a	14,5±0,091^a
		3	0,33±0,025^a	229,90±10,6^a	8,32±0,65^a	5,85±1,01^a	26,28±0,48^a	----------	6,37±0,13^a	8,13±0,05^a	35,8±0,05^a	14,32±2,74^a
		6	0,24±0,008^a	227,25±11,9^a	7,96±0,55^a	7,11±0,84^a	24,75±0,38^a	707,6±204,9^a	6,4 ± 0,11^a	8,14±0,05^a	36 ± 0,00^a	14,37±0,05^a
TANK WITH MUSSEL	WATER WITH FLOW	0	0,52±0,014^a	241,5±14,87^a	8,39±0,33^a	5,35±0,82^a	24,83±0,42^a	799,2±252,4^a	6,5±0,13^a	8,15±0,05^a	35,8±0,08^a	14,5±0,091^a
		3	0,30±0,017^a	265,7±13,58^b	8,75±0,65^a	7,1±0,485^b	26,67±0,41^a	----------	6,17±0,16^a	8,13±0,04^a	35,8±0,05^a	14,37±0,05^a
		6	0,19±0,017^b	245,92±8,93^a	8,2±0,55^b	8,47±0,63^b	28,19±0,34^b	1141,1±255,1^b	5,97±0,12^b	8,12±0,04^a	35,62±0,1^a	14,5±0,091^a

Values are expressed as mean values ± standard error of the mean
a, b Mean scores in the same column and for the same category and time without a superscript in common, are significantly different ($P \leq 0.05$)

oxymeter model. Determination of P-PO_4 was based on the reaction of the ions with an acidified molybdate reagent to yield a phosphomolybdate complex, the extinction of which was measured [9]. Determination of N-NH_3 was based on the reaction of phenol and hypochlorite to form indophenols [10]. Determination of N-NO_3 and N-NO_2 was done using a scientifically approved method. The nitrate was reduced to nitrite when the water sample ran through a column containing amalgamated cadmium filings. The produced nitrite was determined by diazotizing with sulphanilamide and coupling with N-(1-naphthyl)-ethylenediamine to form a coloured azo dye, the extinction of which was measured. Determination of particulate organic carbon was done by wet ashing with a mixture of potassium dichromate and concentrated sulphuric acid [11].

RESULTS AND DISCUSSION

The mean values of chlorophyll-a, dissolved oxygen, particulate organic carbon, N-NO_3, N-NO_2, N-NH_3 and P-PO_4, are shown in table 1. In order to evaluate statistically the results of the biological experimentation, both the non-parameter methodology by Man-Whitney and the distribution control method were used. Statistical analyses were done using SPSS 8.0 with a significance level of p = 0.05.

In water tank 1, the water flowed (WF) while in water tank 2 there was no flow.

Chlorophyll-a

Tank 1: Chlorophyll-a concentrations in tank with mussels (MT) decreased by an average of

63,4% after 6h, while in control tank chlorophyll-a dropped by 46,6%. Significant differences were observed after 6h between control and mussel tank, while chlorophyll-a concentration reached a minimum value of 0,19 μg/l in the mussel tank after 6h.

Tank 2: Chlorophyll-a concentrations in tank with mussels decreased by an average of 66% after 6h, while in control tank chlorophyll-a dropped by 30%. Significant differences were observed after 6h between control and mussel tank, while chlorophyll-a concentration reached a minimum value of 0,23 μg / l in the mussel tank after 6h.

N-NO_3

Tank 1: N-NO_3 concentrations in tank with mussels increased by an average of 1,8 % after 6h, while in control tank they decreased by 5,3 %. Significant differences were observed in the 3h between control and mussel tank.

Tank 2: N-NO_3 concentrations in tank with mussels increased by an average of 15,4 % after 6h, while in control tank they were reduced by 2,3 %. Significant differences were not observed between control and mussel tank.

P-PO_4

Tank 1: P-PO_4 concentrations in tank with mussels increased by an average of 13,5 % after 6h, while in control tank they were reduced by 2,3 %. Significant differences were observed in the 6h between control and mussel tank, while P-PO_4 concentration reached a maximum value of 28,19 μg / l in the mussel tank after 6h.

Tank 2: P-PO_4 concentrations in tank with mussels increased by an average of 9,8 % after 6h, while in control tank they were reduced by 8,5 %. Significant differences were observed in the 3h and 6h between control and mussel tank, while P-PO_4 concentration reached a maximum value of 27,01 μg / l in the mussel tank after 6h.

N-NO_2

Tank 1: N-NO_2 concentrations in tank with mussels decreased by an average of 2,2% after 6h, while in control tank they were reduced by 4,5 % after 6h. Significant differences were observed in the 6h between control and mussel tank.

Tank 2: N-NO_2 concentrations in tank with mussels increased by an average of 4,5 % after 6h, while in control tank concentration was constant. Significant differences were not observed between control and mussel tank.

N-NH_4

Tank 1: N-NH_4 concentrations in tank with mussels increased by an average of 58 % after 6h, while in control tank they increased by an average of 18,3 %. Significant differences were observed in the 3h and 6h between control and mussel tank, while N-NH_4 concentration reached a maximum value of 8,47 μg / l in the mussel tank after 6h.

Tank 2: N-NH_4 concentrations in tank with mussels increased by an average of 40,4 % after 6h, while in control tank they increased by an average of 7,5 %. Significant differences were observed in the 3h and 6h between control and mussel tank, while N-NH_4 concentration reached a maximum value of 10,1 μg / l in the mussel tank after 6h.

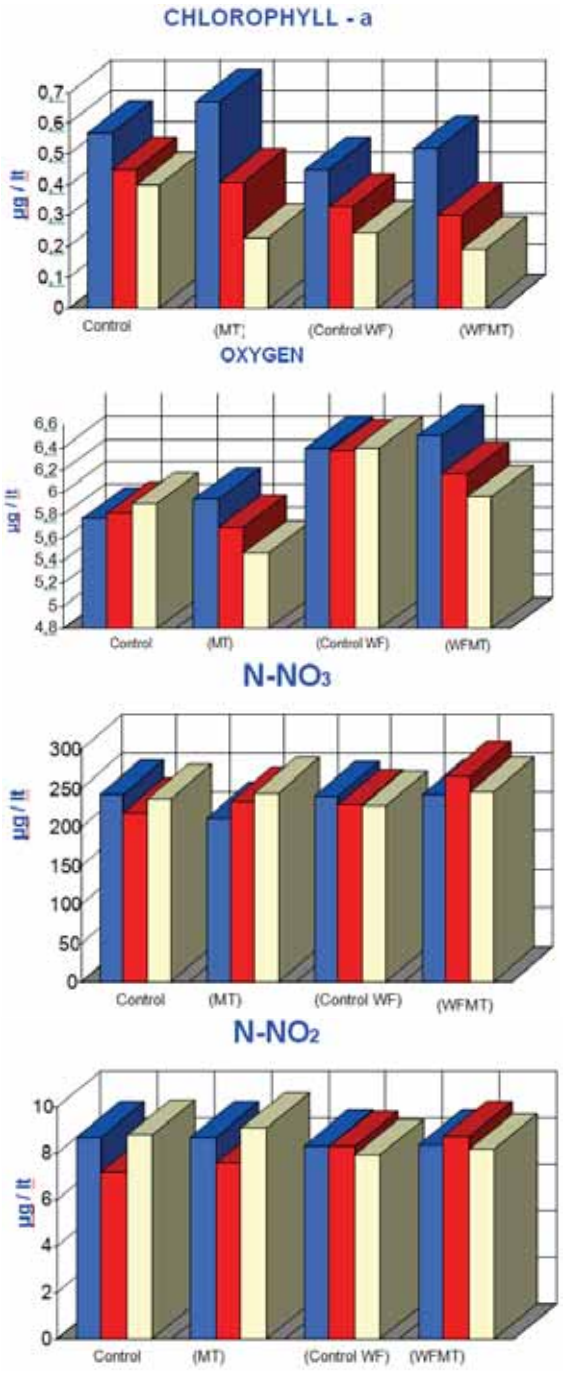


FIGURE 1
Mussel excretion (N-NO_3, N-NO_2), filtration, oxygen consumption for M. galloprovinciallis after temperature acclimation at 14 - 15 ^{0}C.

POC

Tank 1: POC concentrations in tank with mus-

sels increased by an average of 42,8 % after 6h, while in control tank they increased by an average of 9,4 %. Significant differences were observed between control and mussel tank after 3h.

Tank 2: POC concentrations in tank with mussels increased by an average of 25,8 % after 6h, while in control tank they increased by an average of 2,8 %. Significant differences were observed after 6h between control and mussel tank, while POC concentration reached a maximum value of 877 μg / in the mussel tank after 6h.

Dissolved oxygen

Tank 1: Dissolved oxygen concentration in tank with mussels decreased by an average of 8,1 % after 6h, while in control tank was constant. Significant differences were observed in the 6h between control and mussel tank.

Tank 2: Dissolved oxygen concentration in tank with mussels decreased by an average of 8 % after 6h, while in control tank it increased by an average of 2,2 %. Significant differences were observed in the 6h between control and mussel tank.

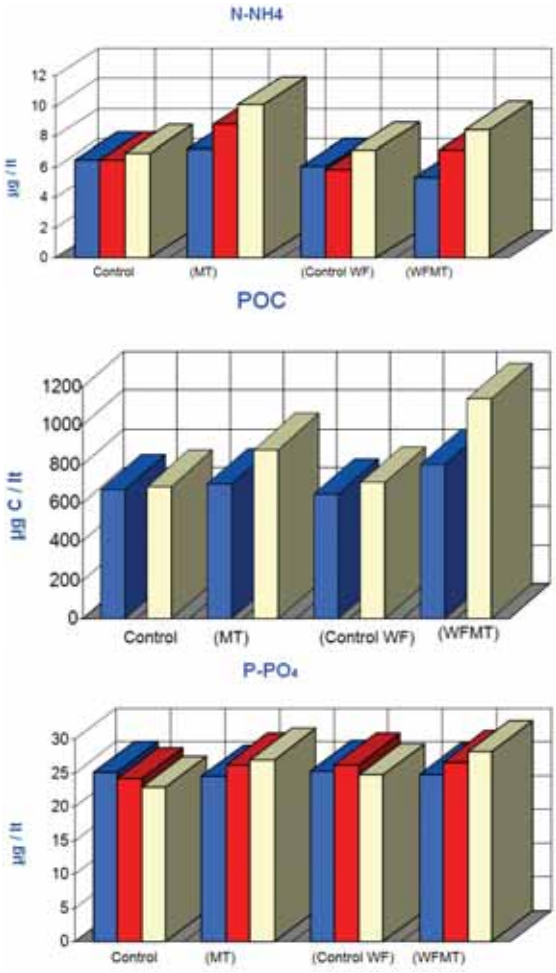


FIGURE 2
Mussel excretion (N-NH_4, P-PO4, POC) for Mytilus galloprovinciallis after temperature acclimation at 14 - 15 ^{0}C.

Our data demonstrate the potential role of mussels Mytilus galloprovinciallis in causing changes in water quality parameters. In the presence of mussels, chlorophyll concentrations rapidly decreased and reached 66 % of the initial value after 6h. This change reflects the efficient filter feeding of the mussel Mytilus galloprovinciallis. My results support the general findings of other researchers sustaining that other species of mussels can graze large portions of seston and chlorophyll. Marked reductions in chlorophyll have been reported in shallow water systems at high population densities of mussels [12, 13 and 14]. Chlorophyll-a concentration also were also reduced dramatically (60%) in the western and west central basins of Lake Erie between 1988 and 1991 and in Saginaw Bay (59%) subsequent to establishment of large Dreissena populations [15, 16 and 17].

The significant difference that was observed in concentrations of dissolved oxygen in both experiments was due to the respiration demands of Mytilus galloprovinciallis. Mussel respiration can be partitioned into two components: the standard minimum for maintenance (no feeding) and the active component, associated with feeding including the mechanical cost of water transport and the physiological cost of digestive processes. The increased organic input of sediment has been shown to increase sediment oxygen consumption [18]. The mineralization of sedimented organic matter consumes oxygen and releases nutrients into the water column.

Our results also indicate that mussels Mytilus galloprovinciallis can play an important role as a nutrient source by regenerating nutrients back into the water column in soluble forms. Marked increases in concentrations of N-NH_4, P-PO_4 and lower increases in concentrations of N-NO_2 and N-NO_3 may be attributed to nutrient regeneration via excretion of Mytilus galloprovinciallis, while the great rates of release in the end of 6h were all significant at the 95 % level. The influence of bivalve culture on denitrification rates have not yet been fully characterised [19] and previous studies on the impacts of mussel farms on denitrification rates have been inconsistent, showing both increase and decrease in farm-affected sediments [4]. According to [20], an increase was measured in natural denitrification but a decrease in potential denitrification under shellfish cultures was observed. This indicates the complex interactions of processes involved in sediment denitrification and their susceptibility to environmental parameters such as oxygen and nitrate availability and organic input [21]. In estuaries, nutrients that regenerated from the decomposition of organic matter in the sediments, play an important role and can supply up to 100% of the nutrient requirements of primary producers in the overlying water [19, 21-30]. Increases in soluble nitrogen and phosphorus forms were observed in the western basin of

Lake Erie since invasion by zebra mussels. These increases were attributed to nutrient regeneration via excretion [13]. Other researchers [31, 32] have showed that the primary excretory product of zebra mussels is ammonium nitrogen. They also presented the direct excretion of NH_4 and PO_4 by Mytilus edulis [33].

Marked increases in concentrations of POC may be attributed to nutrient regeneration via excretion of Mytilus galloprovinciallis, while the great rates of release in the end of 6h were all significant at the 95 % level. Our results support the general findings of other researchers asserting that mussel populations remove particulate material from the water column transforming some of this material into biomass and releasing some constituents in form of dissolved material or as excretion products formed as particles [1, 13, 14, 16, 29 and 34 - 37]. The effects of biodeposits from suspended mussel culture on the local benthic environment have been considered in a number of studies. Heavy sedimentation of faeces and pseudofaeces beneath mussel farms effectively lead to organic enrichment and thus alter macrofaunal communities [8, 20 and 38 - 45]. The establishment of high densities of the mussel has resulted in a substantial increase in the flux of particulate matter from the water column to the benthos resulting in an increase in sediment organic content.

CONCLUSION

The experiment showed that dissolved oxygen and chlorophyll-a concentration decreased in the presence of Mytilus galloprovinciallis. Substantial increases that were observed especially in the concentrations of $N\text{-}NH_4$, $P\text{-}PO_4$ and POC were a result of nutrient regeneration via excretion of Mytilus galloprovinciallis. Consequently the results support the general findings of other researchers that mussels can graze large portions of chlorophyll, and alter nutrient dynamics in aquatic systems. The increased transfer rate of organic particulates from the water column to the sediment may also lead to anoxic conditions due to microbial degradation.

REFERENCES

[1] Fanslow, D.L., Nalepa, T.F. and Lang, G.A. (1995) Filtration rates of the zebra mussel (Dreissena - polymorpha) on natural seston from Saginaw bay, lake Huron. Journal of great lakes research. 21(4), 489 - 500.

[2] Reeders, H.H. and Bji de Vaate, A. (1990) Zebra mussels, a new perspective for water quality management. Hydrobiologia. 200 – 201, 437 – 450.

[3] Sprung, M. and Rose, U. (1988) Influence of food size and food quality on the feeding of the mussels Dreissena polymorpha. Oecologia. 77, 526 – 532.

[4] Kautsky, N. and Evans, S. (1987) Role of biodeposition by Mytilus edulis in the circulation of matter and nutrients in a Baltic coastal ecosystem. Marine Ecology Progress Series. 38, 201–212.

[5] Kljaković – Gašpić, Z., Odžak, N., Ujević, I., Zvonarić, T. and Barić, A. (2006) Biomonitoring of trace metals (Cu, Cd, Cr, Hg, Pb, Zn) in the eastern Adriatic using the Mediterranean blue mussel (2001 – 2005). Fresen. Environ. Bull. 15 (9a), 1045 – 1052.

[6] Blaise, C., Gagné, F., Salazar, M., Salazar, S., Trottier, S. and Hansen, P.–D. (2003) Experimentally-induced feminisation of freshwater mussels after long-term exposure to a municipal effluent. Fresen. Environ. Bull. 12(8), 861 – 864.

[7] Arslan, O.C., Parlak, H., Boyacioglu, M., Karaslan, M. and Katalay, S. (2014) Changes in the glutathione-s transferase activity of the mussel *Mytilus galloprovincialis* during exposure to bisphenol-a.

[8] Solić, M., Jozić, S. and Krstulović N. (2010) Interactive effects of temperature and salinity on the rate of concentration of *escherichia coli* in mussels (*Mytilus galloprovincialis*) and oysters (*Ostrea edulis*). Fresen. Environ. Bull. 19 (8a), 1639 – 1644.

[9] Koroleff, F. (1972b) Determination of phosphorous. In: Methods of sea water analysis, edit. By K. Grasshoff. Verlag Chemie, Weinheim. 117 - 125.

[10] Koroleff, F. (1972a) Determination of ammonia. In: Methods of seawater analysis, edit. by K. Grasshoff. Verlag Chemie, Weinheim. 126 - 133.

[11] Strickland, J. and Parsons, R. (1968) A practical handbook of seawater analysis, Bull.Fish. Res. Board Canada. 167, 1 - 311.

[12] Effler, S.W., Brooks C.M., Whitehead, K., Wagner, B., Doerr, S.M., Perkins, M., Siegfried, C.A., Walrath, L., and Canale, R.P. (1996) Impact of zebra mussel invasion on river water - quality. Water environment research. 68(2), 205 – 214.

[13] Holland, R.E., Johengen, T.H. and Beeton, A.M. (1995) Trends in nutrient concentrations in Hatchery bay, western Lake Erie, before and after D. polymorpha. Canadian Journal of Fisheries and Aquatic Science. 52, 1202 – 1209.

[14] Mellina, E., Rasmussen, J.B. and Mills, E.L. (1995) Impacts of zebra mussel on phosphorus cycling and chlorophyll in lakes. Can. J. Fish. Aquat. Sci. 52, 2553 – 2573.

[15] Fahnenstiel, G.L., Lang, G.A., Nalepa, T.F. and Johengen, T.H. (1995) Effects of zebra mussel colonization on water quality parameters in Saginaw bay, Lake Huron. J. Great Lakes Res. 21(4), 435 - 448.
[16] Leach, J.H. (1993) Impacts of the zebra mussel on water quality and fish spawning reefs in western Lake Erie. In: Gossiaux, C, Landrum, P. and Fisher S. 1998. The assimilation of contaminants from suspended sediment and algae by the zebra mussel, Dreissena polymorpha. Chemosphere. 36(15), 3181 - 3197.
[17] MacIsaac, H.J., Sprules, W.G., Johannson, O.E. and Leach, J.H. (1992) Filtering impacts of larval and sessible zebra mussels in western Lake Erie. Oecologia. 92, 30 – 39.
[18] Schneider, D.W. (1992) A bioenergetics model of zebra mussel, Dreissena polymorpha, growth in the Great Lakes. Can. J. Fish. Aquat. Sci. 49, 1406 –1416.
[19] Newell, R.I.E. (2004) Ecosystem influences of natural and cultivated populations of suspension-feeding bivalve molluscs: a review. J. Shellfish Res. 23, 51–61.
[20] Gilbert, F., Souchu, P., Bianchi, M., and Bonin, P. (1997) Influence of shellfish farming activities on nitrification, nitrate reduction to ammonium and denitrification at the water–sediment interface of the Thau lagoon, France. Mar. Ecol., Prog. Ser. 151, 143–153.
[21] Herbert, R.A. (1999) Nitrogen cycling in coastal marine ecosystems. FEMS Microbiol. Rev. 23, 563–590.
[22] Arnott, D.L. and Vanni, M.J. (1996) Nitrogen and phosphorus recycling by the zebra mussel (Dreissena polymorpha) in the western basin of lake - Erie. Canadian Journal of Fisheries and Aquatic Science. 53(3), 646 - 659.
[23] Crawford, C.M., Macleod, C.K.A. and Mitchell, I.M. (2003) Effects of shellfish farming on the benthic environment. Aquaculture. 224, 117–140.
[24] Danovaro, R., Gambi, C., Luna, G.M. and Mirto, S. (2004) Sustainable impact of mussel farming in the Adriatic Sea (Mediterranean Sea): evidence from biochemical, microbial and meiofaunal indicators. Mar. Pollut. Bull. 49, 325–333.
[25] Gibbs, M., Funnell, G., Pickmere, S., Norkko, A. and Hewitt, J. (2005) Benthic nutrient fluxes along an estuarine gradient: influence of the pinnid bivalve Atrina zelandica in summer. Mar. Ecol., Prog. Ser. 288, 151–164.
[26] Hatcher, A., Grant, B. and Schofield, B. (1994) Effects of suspended mussel culture (Mytilus spp.) on sedimentation, benthic respiration and sediment nutrient dynamics in a coastal bay. Mar. Ecol., Prog. Ser. 115, 219–235.
[27] Howell, E.T., Marvin, C.H., Bilyea, R.W., Kauss, P.B. and Somers, K. (1996) Changes in environmental conditions during Dreissena colonization of a monitoring station in Eastern Lake Erie. J Great Lakes Res. 22, 744–56.
[28] James, W.F, Barko, J.W. and Eakin, H.L. (2001) Phosphorus recycling by zebra mussels in relation to density and food resource availability. Hydrobiologia. 455, 55–60.
[29] Johengen, T.H., Nalepa, T.F., Fahnenstiel, G.L. and Goudy, G. (1995) Nutrient changes in Saginaw bay, lake Huron, after the establishment of the zebra mussel. J. Great Lakes Res. 21, 449 – 464.
[30] Nixon, S.W. (1981) Remineralization and nutrient cycling in coastal marine ecosystems. In: Nielson, B.J. and Cronin, L.E. (Eds.), Estuaries and Nutrients. Humana Press, New Jersey, 111–138.
[31] Gardner, W.S., Cavaletto, J.F., Johengen, T.H., Johnson, J.R., Heath, R.T. and Cotner, J.B., (1995) Effects of the zebra mussel, Dreissena polymorpha on community nitrogen dynamics in Saginaw bay, Lake Huron. J. great lakes res. 21, 529 – 544.
[32] Heath, R.T, Fahnenstiel, G.L, Gardner, W.S, Cavaletto, J.F. and Hwang, S.J. (1995) Ecosystem-level effects of zebra mussels (Dreissena polymorpha): An enclosure experiment in Saginaw Bay, Lake Huron. J Great Lakes Res. 21, 501–516.
[33] Prins, T.C., Escaravage, V., Smaal, A.C. and Peeters, J.C.H. (1995) Nutrient cycling and phytoplankton dynamics in relation to mussel grazing in e mesocosm experiment. Ophelia. 41, 289 - 315.
[34] Dame, R. and Dankers, N. (1988) Uptake and release of materials by a Wadden Sea mussel bed. J. Exp. Mar. Biol. Ecol. 118, 207 - 216.
[35] Klerks, P., Fraleigh, P.C. and Lawniczak, J.E. (1996) Effects of zebra mussels on seston levels and sediment deposition in western Lake Erie. Can. J. Fish. Aquat. Sci. 53, 2284 - 2291.
[36] Madenjian, C.P. (1995) Removal of algae by the zebra mussel population in western Lake Erie: a bioenergetics approach. Can. J. Fish. Aquat. Sci. 52, 381 – 390.
[37] Nicholls, K.H. and Hopkins, G.J. (1993) Recent changes in lake Erie phytoplankton: cumulative impacts of phosphorous loading reductions and the zebra mussel introduction. J. Great Lakes Res. 637 - 647.
[38] Baudinet, D., Alliot, E., Berland, B., Grenz, C., Plante-Cuny, M.-R., Plante, R., and Salen-Picard, C. (1990) Incidence of mussel culture on biogeochemical fluxes at the sediment–water interface. Hydrobiologia. 207, 187–196.
[39] Dahlback, B. and Gunnarsson, L.A.H. (1981) Sedimentation and sulfate reduction under a mussel culture. Marine Biology. 63, 269 - 275.

[40] Grenz, C., Hermin, D., Baudinet, D., and Daumus, R. (1990) In situ biochemical and bacterial variation of sediments enriched with mussel biodeposits. Hydrobiologia. 207, 153–160.
[41] Hargrave, B.T. (ed.) (1994) Modelling benthic impacts of organic enrichment from marine aquaculture. Canadian Technical Report on Fisheries and Aquatic Sciences. 1949, xi+125 pp.
[42] Hartstein, N.D. and Rowden, A.A. (2004). Effect of biodeposits from mussel culture on macroinvertebrate assemblages at sites of different hydrodynamic regime. Mar Environ Res. 57(5), 339-357.
[43] Mattsson, J. and Linden, O. (1983) Benthic macrofauna succession under mussels, Mytilus edulis L. (Bivalvia), cultured on hanging long lines. Sarsia. 68, 97–102.
[44] Mirto, S., Rosa, R.L., Danovaro, R. and Mazzola, A. (2000) Microbial and meiofaunal response to intensive mussel-farm biodeposition in the coastal sediments of the Western Mediterranean. Marine Pollution Bulletin. 40(3), 244–252.
[45] Tenore, K.R., Corral, J. and Gonzalez, N. (1985) Effects of intense mussel culture on food chain patterns and production in coastal Galicia, NW Spain. ICES CM 1985/F: 62.

Received: **19.04.2017**
Accepted: **09.10.2017**

CORRESPONDING AUTHOR

Kostas Katsoulis
University of Thessaly School of Health Sciences, Faculty of Veterinary Science, 224 Trikalon Street, P.O. Box 199, Karditsa, 43100 Greece

e-mail: desiriskk@yahoo.gr

© by PSP Volume 26 – No. 12A/2017 pages 7832-7837 Fresenius Environmental Bulletin

GREEN SYNTHESIS OF COPPER OXIDE NANOPARTICLES USING *OCIMUM BASILICUM* EXTRACT AND THEIR ANTIBACTERIAL ACTIVITY

Melda Altikatoglu[1,*], Azade Attar[2], Fatih Erci[3], Corina Marilena Cristache[4], Ibrahim Isildak[2]

[1]Yildiz Technical University, Faculty of Arts and Sciences, Department of Chemistry, Davutpasa Campus, Esenler, Istanbul, Turkey
[2]Yildiz Technical University, Faculty of Chemical and Metallurgical Engineering, Department of Bioengineering, Davutpasa Campus, Esenler, Istanbul, Turkey
[3]Necmettin Erbakan University, Department of Biotechnology, Konya, Turkey
[4]Carol Davila University of Medicine and Pharmacy, Bucharest, Romania

ABSTRACT

The investigation aims the synthesis of copper oxide nanoparticles (CuO NPs) using Ocimum basilicum plant extract at room temperature. This method is completely a green method, free from toxic and harmful solvent. The CuO NPs were sytnhesized by mixing copper sulphate dehydrate ($CuSO4.5H_2O$) and aqueous Ocimum basilicum leaf extract. The biosynthesized copper oxide nano-particles were characterized by UV-vis spectro-scopy, Fourier-transform infrared spectroscopy (FT-IR) and scanning electron microscopy (SEM). The existence of the CuO NPs was revealed by UV-vis spectroscopy. The FTIR spectra of control (leaf extract) and synthesized CuO NPs identified the functional groups of the active components. SEM images brought out that the particles were spherical in shape, and the size was found to be ranging under 70 nm. Further, the synthesized CuO NPs were tested for antibacterial activity by standart disc diffusion method. The nanoparticles were found to have antibacterial activity against pathogenic bacterial strains *Escherichia coli* and *Staphylococcus aureus* by the observation of inhibition zones around each well.

KEYWORDS:
Copper nanoparticles, green method, antibacterial activity, *Ocimum basilicum* leaf extract.

INTRODUCTION

The field of nanotechnology is one of the most active areas of research in modern materials science. Metal nanoparticles found many applications in different fields because of their unique optical, electronic, mechanical, magnetic, and chemical properties [1-5]. Various methods have been used for synthesis of nanoparticles including, chemical, physical, electrochemical, photochemical and biological techniques [6-14]. Although most of the methods are successful in producing pure and well defined nanoparticles, they are quite expensive or potentially dangerous for the environment.

Synthesis of nanoparticles taking assistance of green methods has attained enormous attention in the recent years [15-20]. Plant systems widely distributed along the ecological boundaries, are easily available and safe to handle. Such studies could prove to have a huge effect in the immediate future, if plant tissue culture and downstream processing procedures are applied in order to synthesize metallic as well as oxide nanoparticles on industrial scale [2, 17]. As metal nanoparticles are widely used in the areas of human contact, the necessity to develop eco-friendly methods for nanoparticle synthesis that do not use toxic chemicals has been constantly growing. Green synthesis of copper nanoparticles is of great interest because of many advantages: copper is highly conductive and also cheaper than silver and gold [1]. Copper oxide (CuO) nanoparticles are important due to their applications as antimicrobials and in gas sensors, batteries, high temperature superconductors, solar energy conversion tools, and so on [21-24]. Human beings have been using copper (Cu) and copper complexes for various purposes for centuries, such as water purifiers, algaecides, fungicides, and as antibacterial and antifouling agents. Copper-based compounds are efficient biocidal properties, which are generally used in several health related application [25-27].

Biosynthesis of metal nanoparticles by plants is currently under development. The synthesis of metal nanoparticles using inactivated plant tissue, plant extracts, exudates, and other parts of living plants is a modern alternative for their production [28]. It is a very cost effective method and therefore a prospective commercial alternative for large-scale production [27]. Biosynthesis of copper oxide nanoparticles CuO NPs using microorganisms such as bacteria, fungi, yeast have been reported in the literature [29-31]. Plants attracted few researchers to use their extracts in green synthesis of copper oxide nanoparticles such as Carcia papaya leaf extract [32], Aloe vera leaf extract [33], and Centella asiatica leaf extract [34], Malva sylvestris leaf extract [35], Rosa

sahandina broth extract [17], Gloriosa superba L. plant extract [25].

The present study reports for the first time, the synthesis and characterization of copper oxide (abbreviated CuO NPs) using Ocimum basilicum leaves extract and copper sulphate. In context of nanoparticles, the particles synthesized so far utilizing Ocimum species are silver [36-39] gold [40], platinum [41] and zinc [42]. Also, the antibacterial characteristics of the synthesized nanoparticles were evaluated in this study.

MATERIALS AND METHODS

Materials. All the chemical reagents used in this experiment were of analytical grade. The Ocimum basilicum leaves were collected from a local source (Istanbul-Turkey). Ocimum basilicum leaves were washed several times with distilled water to remove dust particles and then sun dried to remove the residual moisture. 10 g of leaves were boiled in 100 ml of distilled water for 10 min. Then the mixture was cooled to room temperature and filtered with Whatman No. 1 filter paper and stored in refrigerator for further experiments.

Synthesis of Copper Oxide Nanoparticles. In a typical reaction mixture, 100 ml of aqueous 1mM copper sulphate dehydrate $CuSO_4.5H_2O$ was treated with 10 ml aqueous leaf extract of Ocimum basilicum and stirred magnetically at room temperature for about 4 hrs. The formation of the particles can be seen within 2 hrs. The solution was aged for 15 hrs. Nanoparticles prepared were centrifuged and washed with double distilled water twice. Nanoparticles was collected, dried at 60 ^oC in an oven.

Characterization of Copper Oxide Nanoparticles. Copper oxide nanoparticles synthesized by this green method were characterized by UV-Vis spectrophotometer (Shimadzu) and Fourier-transform ınfrared (FTIR-Shimadzu) spectrum in the range 4000-400 cm^{-1}. The shape and grain size were characterized by using scanning electron microscopy (SEM, Hitachi).

Antimicrobial tests. *E. coli* (ATCC25922) and *S. aureus* (ATCC25923) were used as reference strains for Gram-negative and Gram-positive bacteria, respectively. Strains were grown on nutrient agar.

The synthesized CuO NPs were tested for antibacterial activity by standart disc diffusion method. Nutrient agar plates were seeded with 24 h broth culture of *E. Coli*. Each strain was swabbed uniformly onto the individual plates using sterile cotton swaps. Wells of 10mm diameter were made on nutrient agar plates using gel puncture. 50-100 mikro l of CuO NPs solution was pipetted onto each well on all plates. Control discs are placed with $CuSO_4$ and distilled water to assess the effect of $CuSO_4$ on parhogens. Then the plates were incubated at 37 ^oC for 24 h, the zone incubation measured in millimeter (mm) of the every well and also the values were noted.

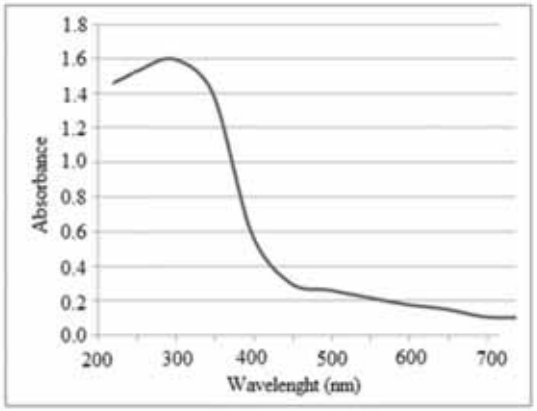


FIGURE 1
UV–vis spectra of CuO nanoparticles

RESULTS AND DISCUSSION

Identification and Characterization of the Synthesized CuO NPs. UV-vis spectroscopy is a very useful technique for analyzing nanoparticle formation and the stability of metal nanoparticles in aqueous solution [43]. The UV-visible absorption spectrum of CuO NPs prepared from copper sulphate is shown in Fig. 1. The copper nanoparticles prepared have displayed an absorption peak at between 280 and 300 nm which is assigned to the absorption of CuO NPs. This spectrum confirms the presence of CuO only, as there is no other measurable peak observed. The incidence of the surface plasmon absorption reflects the shape and size of the nanoparticles [32].

FTIR spectroscopy was used to identify the functional groups of the active components based on the peak value in the region of infrared radiation. The FTIR spectra of control leaf extract (before reaction without $CuSO_4$) and synthesized CuO NPs (after reaction without $CuSO_4$) are shown in Fig. 2. The broad and strong peak at around 3440 cm^{-1} can be attibuted the O-H groups of alcohols and phenols. This peak shifted to lower field at 3393 cm^{-1} in the synthesized CuO NPs. The band at 2850 cm^{-1} is assigned to C-H stretching. The peaks observed in the range of 680-1454 cm^{-1} have been assigned to alcohols and phenolic groups, C-N stretching vibtarions of amines. The major peak was observed to be 510 cm^{-1} should be a stretching of Cu-O. The bands at

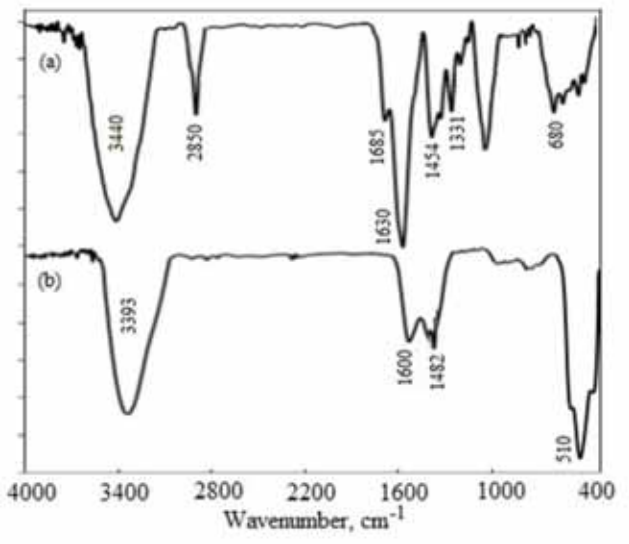


FIGURE 2
FTIR spectra for Ocimum basilicum leaf extract (a) and synthesized CuO NPs (b)

TABLE 1
Diameter zone of inhibition by CuO NPs and extract against pathogenic bacteria.

Pathogenic bacteria	Inhibition zone (mm)	
	CuO NPs	Extract
Staphylococcus aureus	7.2±0.3	3.5±0.3
Escherichia coli	9.8±0.3	4.3±0.2

Values are the mean ± SE of inhibition zone in mm. $P < 0.01$ as compared with the control

1630 cm^{-1} of the leaf extract shifted to lower field at 1600 cm^{-1}, in the product. The similar results has been reported in literature where CuO NPs was synthesized using different leaves extracts [17, 32, 35].

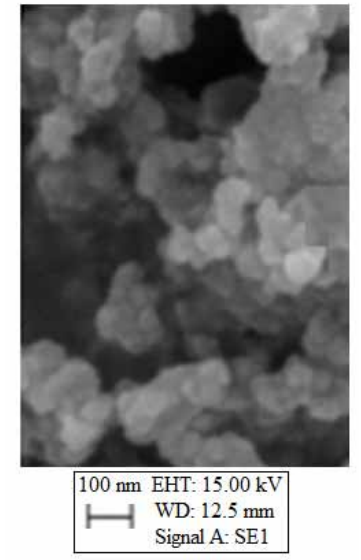


FIGURE 3
SEM image of the synthesized CuO nanoparticles

The SEM image for as prepared CuO NPs is shown in Fig.3. It clearly showed well dispersed, spherical shape distribution of CuO NPs prepared with Ocimum basilicum extract with particle sizes ranging under 70 nm.

Antibacterial activity. The antibacterial activity of the synthesized copper oxide nanoparticles using Ocimum basilicum leaf extract was examined against both Gram-negative (*E. coli*) and Gram-positive (*S. aureus*) bacteria by disc diffusion test. The diameter of the inhibition zones (mm) around each well with CuO NPs are represented in Table 1. The negative control (distilled water) was not shown any activity against the bacterial strains tested. On the contrary, antibacterial activity was observed against pathogens when CuO NPs used. Diameter of the zone of inhibition were measured as 7.2±0.3 and 3.5±0.3 mm for CuO NPs and leaf extract against pathogenic bacteria, respectively when *S. aureus* was used. Also 9.8±0.3 and 4.3±0.2 mm zone of inhibition was measured for *E. coli*. The antibacterial test results showed that *S. aureus* is less susceptible to CuO NPs when compared to *E. coli* which is in agreement with the results reported in literature [25].

Obtained experimental results have shown that synthesized CuO NPs have antibacterial activity on both gram pozitive and negative bacteria. Therefore

the antibacterial activity of the NPs could be explained by some mechanisms such as; copper ions released subsequently may bind to DNA molecules and lead to disordering of the helical structure by cross-linking within and between the nucleic acid strands. Copper ions inside bacterial cells also disrupt the biochemical process [25, 44]. Cu2+ and Ag+ ions were also studied well to disrupt the bacterial cell membranes and gain entry in order to disrupt enzyme function. Indirect effects through changes in the surrounding charge environment also have an impact on the effectiveness of nanoparticulate metals against microorganisms [25, 45]. Another proposed mechanism is, there will be copper ions released from the nanoparticles that may attach to the negatively charged bacterial cell wall and rupture it, thereby leading to protein denaturation and caused cell death [46-49].

CONCLUSIONS

In this paper, it was reported for the first time, the use of Ocimum basilicum extracts for the green synthesis of CuO nanoparticles. This method has many advantages such as economic viability, ease to scale up and less time consuming. The characteristics of the obtained CuO nanoparticles were studied using the UV-vis, FTIR and SEM techniques. The use of environmentally benign materials like plant extracts, for the synthesis of nanoparticles offers numerous benefits of ecofriendliness and compatibility. The synthesized CuO NPs are highly stable and have significant effect on both Gram-positive and Gram-negative bacteria. This could provide a faster synthesis rate comparable to those of chemical methods, and could potentially be used in areas such as food and medical applications.

ACKNOWLEDGEMENTS

This study was supported by grants from the 'General Directorate of Agricultural Research and Policies' research fund (TAGEM-14/AR-GE/06).

REFERENCES

[1] Suresh, Y., Annapurna, S., Singh, A.K., Bhikshamaiah, G. (2014) Green Synthesis and Characterization of Tea Decoction Stabilized Copper Nanoparticles. International Journal of Innovative Research in Science, Engineering and Technology. 3(4), 11265-11270.

[2] Ashokkumar, S., Ravi, S., Kathiravan, V., Velmurugan, S. (2015) Synthesis of silver nanoparticles using A.indium leaf extract and their antibacterial activity. Spectrochimica Acta Part A: Molecular and Biomolecular Spectros-copy. 134, 34-39.

[3] Bar, H., Bhui, D.K., Sahoo, G.P., Sarkar, P., De, S.P., Misra, A. (2009) Green synthesis of silver nanoparticles using latex of Jatropha curcas. Colloid Surf. A 339, 134-139.

[4] Tuutijarvi, T., Lu, J., Sillanpaa, M., Chen, G. (2009) As(V) adsorption on maghemite nanoparticles. J. Hazard. Mater. 166, 1415-1420.

[5] Tuutijarvi, T., Lu, J., Sillanpaa, M., Chen, G. (2010) Adsorption mechanism of arsenate on crystal gamma - Fe2O3 nanoparticles. J. Environ. Eng. 136, 897-905.

[6] Kathiravan, V., Ravi, S., Ashokkumar, S. (2014) Synthesis of silver nanoparticles from Melia dubia leaf extract and their in vitro anticancer activity. Spectrochimica Acta Part A: Molecular and Biomolecular Spectroscopy, 130, 116-121.

[7] Sun, Y., Yin, Y., Mayers, B.T., Herricks, T., Xia, Y. (2002) Uniform Silver Nanowires Synthesis by Reducing $AgNO_3$ with Ethylene Glycol in the Presence of Seeds and Poly(Vinyl Pyrrolidone). Chem. Mater. 14, 4736-4745.

[8] Yin, B., Ma, H., Wang, S., Chen, S. (2003) Electrochemical Synthesis of Silver Nanoparticles under Protection of Poly(N-vinylpyrrolidone). J. Phys. Chem. B, 107 8898-8904.

[9] Dimitrijevic, N.M., Bartels, D.M., Jonah, C.D., Takahashi, K., Rajh, T. (2001) Radiolytically Induced Formation and Optical Absorption Spectra of Colloidal Silver Nanoparticles in Supercritical Ethane. J. Phys. Chem. B, 105, 954-959.

[10] Callegari, A., Tonti, D., Chergui, M. (2003) Photochemically Grown Silver Nanoparticles with Wavelength-Controlled Size and Shape. Nano Lett. 3, 1565-1568.

[11] Zhang, L., Shen, Y.H., Xie, A.J., Li, S.K., Wang, C. (2008) One-step synthesis of silver nanoparticles in self-assembled multilayered films based on a Keggin structure compound. J. Mater. Chem. 18, 1196-1203.

[12] Swami, A., Selvakannan,P.R., Pasricha, R., Sastry, M. (2004) One-Step Synthesis of Ordered Two-Dimensional Assemblies of Silver Nanoparticles by the Spontaneous Reduction of Silver Ions by Pentadecylphenol Langmuir Monolayers. J. Phys. Chem. B 108, 19269-19275.

[13] Naik, R.R., Stringer, S.J., Agarwal, G., Jones, S., Stone, M.O. (2002) Peptide templates for nanoparticle synthesis derived from polymerase chain reaction-driven phage display. Adv. Funct. Mater. 14, 25-30.

[14] Devi, H.S. and Singh, T.D. (2014) Synthesis of Copper Oxide Nanoparticles by a Novel Method and its Application in the Degradation of Methyl Orange. Advance in Electronic and Electric Engineering. 4(1), 83-88.

[15] Vinod Kumar, V., Anbarasan, S., Christena, L.R., SaiSubramanian, N., Anthony, S.P. (2014) Bio-funtionalized silver nanoparticles for selective colorimetric sensing of toxic metal ions and antibacterial studies. Spectrochimica Acta Part A: Molecular and Biomolecular Spectroscopy. 129, 35-42.

[16] Chandran, S.P., Chaudhary, M., Pasricha, R., Ahmad, A., Sastry, M. (2006) Synthesis of gold nanotriangles and silver nanoparticles using Aloe Wera plant extract, Biotechnol. Prog. 22, 277-583.

[17] Jafarirad, S., Mehrabi, M. and Pur, E.R. (2014) Biological Synthesis of Zinc Oxide and Copper Oxide Nanoparticles. International Conference on Chemistry, Biomedical and Environment Engineering. 62-64.

[18] Raveendran, P., Fu, J., Wallen, S.L. (2003) Completely "green" synthesis and stabilization of metal nanoparticles", J. Am. Chem. Soc. 125, 13940–13941.

[19] Kalimuthu, K., Babu, R.S., Venkataraman, D., Mohd, B., Gurunathanm, S. (2008) "Biosynthesis of silver nanocrystals by Bacillus licheniformis", Colloids Surf. B 65, 150–153.

[20] Simakin, A.V., Voronov, V.V., Kirichenko, N.A., Shafeev, G.A. (2004) Nanoparticles produced by laser ablation of solids in liquid environment, Appl. Phys. A 79, 1127-1132.

[21] Premkumar, T., Geckeler, K.E. (2006) Nanosized CuO particles via a supramolecular strategy. Small. 2(5), 616–620.

[22] Ren, G., Hu, D., Cheng, E.W., Vargas-Reus, M.A., Reip, P., Allaker, R.P. (2009) Cha-racterisation of copper oxide nanoparticles for antimicrobial applications. Int J Antimicrob Agents. 33(6), 587–590.

[23] Hsieh, C.T., Chen, J.M., Lin, H.H., Shih, H.C. (2003) Synthesis of well-ordered CuO nanofibers by a self-catalytic growth mecha-nism. Appl Phys Lett. 82(19), 3316–3318.

[24] Zhang, X., Wang, G., Liu, X., Wu, J., Li, M., Gu, J., Liu, H., Fang, B. (2008) Different CuO nanostructures: synthesis, characterization, and applications for glucose sensors. J Phys Chem C Nanomater Interfaces. 112(43), 16845–16849.

[25] Raja Naika, H., Lingaraju, K., Manjunath, K., Kumar, D., Nagaraju, G., Suresh, D., Nagabhushana, H. (2015) Green synthesis of CuO nanoparticles using Gloriosa superba L. Extract and their antibacterial activity. Journal of Taibah University for Science. 9, 7-12.

[26] Borkow, G., Zatcoff, R.C., Gabbay, J. (2009) Reducing the risk of skin pathologies in diabetics by using copper impregnated socks. Med. Hypotheses 73, 883-886.

[27] Vellora, V., Padil T. and Cerník, M. (2013) Green synthesis of copper oxide nanoparticles using gum karaya as a biotemplate and their antibacterial application. Int J Nanomedicine. 8, 889–898.

[28] Huang, J., Li, Q., Sun, D., Lu, Y., Su, Y., Yang, X., Wang, H., Wang, Y., Shao, W., He, N. (2007) Biosynthesis of silver and gold nanoparticles by novel sundried Cinnamomum camphora leaf. Nanotechnology. 18(10), 105104-105115.

[29] A.V. Singh, R. Patil, A. Anand, P. Milani, W.N. Gade, Biological synthesis of copper oxide nano particles using Escherichia coli. Current Nanoscience. 6(2010), 365-369.

[30] Rahman, A., Ismail, A., Jumbianti, D., Magdalena, S., Sudrajat, H. (2009) Synthesis of copper oxide nanoparticles by using Phormidium cyanobacterium. Indo. J. Chem. 9, 355-360.

[31] Honary, S., Barabadi, H., Fathabad, E.G., Naghibi, F. (2012) Green synthesis of copper oxide nanoparticles using Penicilium aurantiogriseum, Penicilium citrinum and Penicilium waksmanii. Digest J. Nanomater. Biostruct. 7, 999-1005.

[32] Sankar, R., Manikandan, P., Malarizhi, V., Fathima, T., Shivashangari, K.S., Ravikumar, V. (2014) Green synthesis of colloidal copper oxide nanoparticles using Carcia papaya and its application in photocatalytic dye degradation. Spectrochimica Acta A: Molecular and Biomolecular Spectroscopy. 121, 746-750.

[33] Gunalan, S., Sivaraj, R., Venckatesh, R. (2012) Aloe barbadensis Miller mediated green synthesis of mono-disperse copper oxide nanoparticles: Optical properties. Spectrochimica Acta A: Molecular and Biomolecular Spectroscopy. 97, 1140-1144.

[34] Devi, H.S., Singh, T.D. (2014) Synthesis of copper oxide nanoparticles by a novel method and its application in the degradation of methyl orange. Advance in Electronic and Electric Engineering. 4, 83-88.

[35] Awwad, A.M., Albiss, B.A., Salem, N.M. (2015) Antibacterial Activity of synthesized Copper Oxide Nanoparticles using Malva sylvestris Leaf Extract. SMU Medical Journal, 2(1), 91-101.

[36] Garima, S., Riju, B., Kunal, K., Ashish, R.S., Rajendra, P.S. (2011) Biosynthesis of silver nanoparticles using Ocimum sanctum (Tulsi) leaf extract and screening its antimicrobial activity. J Nanopart Res. 13, 2981–2988.

[37] Naheed, A., Md, K.A., Singh, V.N., Salman, F.S., Seema, S. (2009) Ocimum mediated biosynthesis of silver nanoparticles. In: ICMENS '09 proceedings of the 2009 fifth international conference on MEMS, NANO, and smart systems, Dubai, 80–84.

[38] Kiruba Daniel, S.C.G., Kumar, R., Sathish, V. Sivakumar, M., Sunitha, S., Anitha, S.T. (2011) Green Synthesis (Ocimum tenuiflorum) of Silver Nanoparticles and Toxicity Studies in Zebra Fish (Danio rerio) Model. Int J NanoSci Nanotechnol. 2, 103–117.
[39] Mallikarjuna, K., Narasimha, G., Dillip, G.R. Praveen, B., Shreedhar, B., Sree Lakshmi, C., Reddy, B.V.S., Deva Prasad Raju, B. (2011) Green synthesis of silver nanoparticles using Ocimum leaf extract and their characterization. Dig J Nanomater Biostruc. 6, 181–186.
[40] Singhal, G., Riju, B., Ashish, R.S., Rajendra, P.S. (2012) Ecofriendly Biosynthesis of Gold Nanoparticles Using Medicianally Important Ocimum basilicum Leaf Extract. Adv Sci Eng Med. 4, 62–66.
[41] Soundarrajan, C., Sankari, A., Dhandapani, P., Maruthamuthu, S., Ravichandran, S., Sozhan, G., Palaniswamy, N. (2012) Rapid biological synthesis of platinum nanoparticles using Ocimum sanctum for water electrolysis applications. Bioprocess Biosyst Eng. 35, 827–833.
[42] Salam, H.A., Sivaraj, R., Venckatesh, R. (2014) Green synthesis and characterization of zinc oxide nanoparticles from Ocimum basilicum L. var. purpurascens Benth.-Lamiaceae leaf extract. Materials Letters. 131, 16–18.
[43] Muniyappan, N., Nagarajan, N.S. (2014) Green synthesis of silver nanoparticles with Dalbergia spinosa leaves and their applications in bio-logical and catalytic activities. Process Bio-chemistry. 49, 1054-1061.
[44] Kim, J., Cho, H., Ryu, S., Choi, M. (2000) Effects of Metal Ions on the Activity of Protein Tyrosine Phosphatase VHR: Highly Potent and Reversible Oxidative Inactivation by Cu^{2+} Ion. Arch. Biochem. Biophys. 382, 72-80.
[45] Stohs, S.J., Bagchi, D. (1995) Oxidative mechanisms in the toxicity of metal ions. Free Radic. Biol. Med. 18, 321-336.
[46] Sondi, I., Sondi, B.S. (2004) Silver nano-particles as antimicrobial agent: a case study on E. coli as a model for Gram-negative bacteria. J. Colloid Interface Sci. 275, 177-182.
[47] Azam, A., Ahmed, A.S., Oves, M., Khan, M.S., Memic, A. (2012) Size-dependent antimicrobial properties of CuO nanoparticles against Gram-positive and -negative bacterial strains. Int. J. Nanomed. 7, 3527-3535.
[48] Lin, Y.E., Vidic, R.D., Stout, J.E., Mccartney, C.A., Yu, V.L. (1998) Inactivation of Mycobacterium avium by copper and silver ions. Water Res. 32, 1997-2000.
[49] Nawaz, M., Han, M.Y., Kim,T., Manzoor, Amin, U. (2012) Silver disinfection of Pseudomonas aeruginosa and E. coli in rooftop harvested rainwater for potable purposes. Sci. Total Environ. 431, 20-25.

Received: **24.04.2017**
Accepted: **01.10.2017**

CORRESPONDING AUTHOR

Melda Altikatoglu
Yildiz Technical University, Faculty of Arts and Sciences, Department of Chemistry, Davutpasa Campus, Esenler, Istanbul – Turkey

e-mail: maltikatoglu@yahoo.com

© by PSP Volume 26 – No. 12A/2017 pages 7838-7848 Fresenius Environmental Bulletin

EVALUATION OF HEAVY METALS UPTAKE BY WHEAT GROWING IN SEWAGE IRRIGATED SOIL: RELATIONSHIP WITH HEAVY METAL IN SOIL AND WHEAT GRAINS

Zafar Iqbal Khan[1,*], Sana Iqbal[1], Fauzia Batool[1], Kafeel Ahmad[1], Mohamed Soliman Elshikh[2], Abdulaziz Al Sahli[2], Mohamed El-Zaidy[2], Humayun Bashir[1], Ijaz Rasool Noorka[3], Muhammad Sher[4],Ahmad Muneeb[1], Aima Iram Batool[5], Shahzadi Mahpara[6],Mumtaz Akhtar[5], Naunain Mehmood[5], Hazoor Ahmad Shad[4], Yunus Dogan[7], Hira Muqaddas[8], Muhammad Ayub[9]

[1]Department of Botany, University of Sargodha, Sargodha, Pakistan
[2]King Saud University, College of Science, Department of Botany and Microbiology
[3]Department of Plant Breeding and Genetics University College of Agriculture, University of Sargodha, Pakistan
[4]Department of Chemistry, University of Sargodha, Sargodha, Pakistan
[5]Department of Zoology, University of Sargodha, Sargodha, Pakistan
6Department of Plant Breeding & Genetics, Faculty of Agricultural Sciences, Ghazi University, Dera Ghazi Khan, Pakistan
[7]Buca Faculty of Education, Dokuz Eylul University, Izmir, Turkey
[8]Department of Zoology, the Women University, Multan, Pakistan
[9]Govt. College University Faisalabad, Pakistan

ABSTRACT

Experimentation was carried out in Sahiwal, Sargodha, Pakistan to evaluate the contamination level in wheat variety (Millat-2011), irrigated with different treatments of household waste water in a Completely Randomized Design with three repetitions. There were five treatments viz. T1 (100% ground water), T2 (25% wastewater, 75% groundwater), T3 (50% wastewater, 50% ground water), T4 (75% wastewater, 25% ground water), T5 (100% wastewater). Analyzed parameters were heavy metal concentration in wheat and soil, metal correlation between food crop and soil, pollution load index, bioconcentration factor, health risk index, daily-intake of metals, and enrichment factor. Current results showed that concentration of heavy metals and metalloids in soil and grains increased due to supply of waste water. Cr, Cd, Ni, Fe, Mn, Cu and Zn showed significantly positive correlation while Co showed positive but non-significant correlation in all treatment groups. Mn showed highest bio-concentration factor and enrichment factor values while Cd showed highest health risk index, daily metal intake and pollution load index values. Level of metal toxicity in humans could increase due to irrigation of food crops with untreated waste water. Hence application of waste water must be avoided or its proper treatment before application to agricultural fields must be done.

KEYWORDS:
Contamination, domestic sewagewater, heavy metals, wheat (Millat-2011)

INTRODUCTION

Wheat is the staple foodstuff for the populace of Pakistan; hence it is cultivated approximately in every part of the country. It contributes about 2.8% to GDP and around 13.1% to the farming. Wheat production is increasing over years but its per capita fulfillment is low [1].

Soil's physical and chemical characteristics are significantly affected by frequent wastewater irrigation. Persistent usage of waste water for crop cultivation might result in heavy metal buildup. Accumulation of metal level beyond tolerable range proves to be hazardous for human health. Soil becomes launching point of perilous materials due to increased anthropogenic activities involving noxious wastes[2].Soil contamination by heavy metals like copper, zinc, lead, mercury, chromium, copper and nickel occurs due to long-standing practice of using waste water for agronomical land [3, 4].

Heavy metals are significant ingredients for plants and humans in small quantities. But in high concentrations heavy metals (copper, chromium, fluorine, molybdenum, nickel, selenium and zinc) may be detrimental to plants animals and humans. Some elements like mercury, cadmium, lead and arsenic are lethal even in minute amount [5].

Aim of present study was to investigate the heavy metal levels in commonly consumed crop(wheat) treated with domestic waste water and their consequences on health of living organisms.

MATERIALS AND METHODS

Study area. Experimentation was done at Sahiwal, Sargodha, Punjab, Pakistan in 2016. Its coordinates are 31° 58' 23" North, 72° 19' 32" East.

TABLE 1
Physicochemical parameters of water

Physico-chemical parameters	E.C. (µS/cm)	$Ca^{2+}+Mg^{2+}$	Na^{+}	CO_3^{2-}	HCO_3^{1-}	Cl^{1-}	SAR	RSC
				(meq/L)				
T-I	1457	3.74	14	0.15	8.85	3.84	3.29	4.69
T-II	1563	5.20	9.10	0.21	7.83	5.49	5.75	2.19
T-III	1464	7.89	8.7	0.37	8.39	6.34	4.15	0.39
T-IV	1468	1.95	12.2	0.79	4.37	8.05	12.2	4.45
T-V	1619	1.99	13.7	1.78	7.37	6.11	14.7	5.33

TABLE 2
Analysis of variance for heavy metal concentrations in water

Source of variation	Degree of Freedom	Mean Squares							
		Cd	Ni	Fe	Mn	Cu	Cr	Zn	Co
Treatments	4	0.005^{***}	0.016^{***}	3.058^{ns}	0.10^{***}	0.029^{***}	0.018^{***}	16.12^{***}	0.010^{***}
Error	10	0.001	0.001	2.766	0.002	0.01	0.001	0.052	0.001

*** Significant at 0.001 probability levels; ns= non-significant

Plant cultivation and sample collection. Fifteen (15) pots were taken and about 2.5 kg soil was added in each pot. Seeds of wheat variety (Millat-2011) were cultivated in five different treatments (T-I were irrigated by 100% ground water, T-II were irrigated by 75% ground water and 25% waste water, T-III were irrigated by 50% ground water and 50% waste water, T-IV were irrigated by 25% ground water and 75% waste water and T-V were irrigated by 100% waste water). Plants were irrigated two times a week. Wheat was harvested in April 2016. Threshed, oven-dried, ground seed samples were digested by using wet digestion method [6]. Water samples were analyzed to determine their electrical conductivity, sodium, carbonate, bi-carbonate, chloride, sodium adsorption ratio, residual sodium carbonate, calcium and magnesium concentrations. Soil samples were analyzed to evaluate the soil pH, electrical conductivity (EC), available phosphorus, available potassium, saturation and organic matter content.

Sample analysis. Heavy metal content was evaluated in soil and wheat samples by atomic absorption spectrophotometer (AAS; GBC 932) and standard calibration curves were drawn for each metal and metalloid. Metal concentration transferred from soil to wheat grains was determined in terms of bio-concentration factor and health risk index by following Cui et al. [7]. Pollution load index was calculated by method described by Liu et al. [8]. Daily intake of metals was determined using methodology reported by Wang et al. [9]. Ravichandran et al. [10] was followed for calculation of enrichment factor.

RESULTS AND DISCUSSION

Physicochemical properties of water. Physicochemical properties of water taken from five treatment groups showed that multiple factors change the composition of waste water with passage of time (Table 1). Electrical conductivity of sampled water was higher than that of the values observed by WHO (400-600 µS/cm). Darvishi et al. [11] found higher concentrations of calcium, magnesium and bicarbonate while low sodium adsorption ratio (SAR) and sodium concentration was observed as compared to current study. Hassan et al. [13] reported high values of chloride in contrast to the present research work. Current RSC (Residual Sodium Carbonate) values were higher in comparison to the values found by Rattan et al. [14].

Mean concentrations of heavy metals in water. Statistical analysis of data showed significant effect (p<0.05) of different regimes on Co, Cu, Mn, Cd, Ni, Cr and Zn concentrations and non-significant effect (p>0.05) on Fe concentration (Table 2). Order of mean concentrations of heavy metals in water samples at treatment-I was Cd >Ni >Zn >Cr >Cu >Mn>Co >Fe, at treatment-II and IV was Zn >Cd > Ni >Cu >Cr >Mn>Co >Fe, at treatment-III was Zn >Cd > Ni >Cu >Cr>Mn>Fe >Co and at treatment V was Zn >Cd >Ni >Cu>Mn>Cr>Fe >Co (Table 3; Fig. 1).

Current Cd concentration was higher in water samples of all treatment groups as compared to Ayers and Westcot [15]. Ni concentration in current study exceeded greater the findings of Akhtar et al. [16] and the standard value (1.2 mg/L) for nickel set by Indian Standards [17] and FAO [18]. Gulfraz et al. [19] observed higher concentration of iron in comparison to current study. In plants, iron becomes

unavailable at high pH but is available at low pH [20]. Current value of manganese was higher than the value set by Indian Standards [17] and FAO [18]. Alloway [21] reported that high concentration of manganese can damage kidneys, brain, developing fetus and liver. Jakubus and Czekala [22] observed higher value of copper in comparison to the present study. Current value for Cu concentration was higher than the permissible values of copper (0.2 mg/L) set by Indian Standards [17] and FAO [18]. Current values of Cr were higher than the standard value (0.1 mg/L) described in Indian Standards [17] and FAO [18] and could be potentially dangerous for the health of animals and plants.

The current Zn concentration in all treatment groups above the permissible limit (2.0 mg/L) suggested by Indian Standards [17] and FAO [18]. Zn concentration in waste water was high due to the use of brass as cleaning agent, body care products, soaps and detergents. Jakubus and Czekala [22] observed higher concentration of Zn as compared to that of current work. Shad et al. [23] and Gulfraz et al. [19] observed high values of cobalt in contrast to the current observation. Cobalt blocks the biosynthetic pathway of the synthesis of chlorophyll pigments [24].

Physicochemical properties of soil. Soil pH observed in current study was comparable (Table 4) while available potassium and phosphorus concentration was higher than that of Nafees and Amin [26]. Yourtchi and Bayat [27] observed higher values of electrical conductivity and organic matter while low values for available potassium and phosphorus were observed in contrast to the present study. Electrical conductivity values increase due to the supply of sewage water [28].

TABLE 3
Mean concentration of heavy metals (mg/L) in water

Metals	T-I	T-II	T-III	T-IV	T-V	Permissible limit
Cd	2.285±0.18	2.298±0.17	2.331±0.16	2.375±0.14	2.382±0.15	0.01*
Ni	1.515±0.19	1.546±0.18	1.588±0.20	1.650±0.17	1.705±0.16	0.20*
Fe	0.563±0.21	0.629±0.20	0.993±0.19	0.868±0.22	1.029±0.18	5.0*
Mn	0.875±0.23	0.933±0.22	1.035±0.18	1.168±0.21	1.326±0.19	0.2**
Cu	1.025±0.25	1.106±0.21	1.155±0.23	1.195±0.22	1.286±0.24	0.2*
Cr	1.041±0.22	1.083±0.20	1.133±0.19	1.190±0.21	1.230±0.18	0.1**
Zn	1.245±0.26	5.143±0.24	5.176±0.23	6.545±0.25	7.233±0.22	2**
Co	0.799±0.17	0.826±0.15	0.857±0.18	0.912±0.16	0.937±0.17	0.05*

Source *:WWF [25]; Source **: FAO [18]

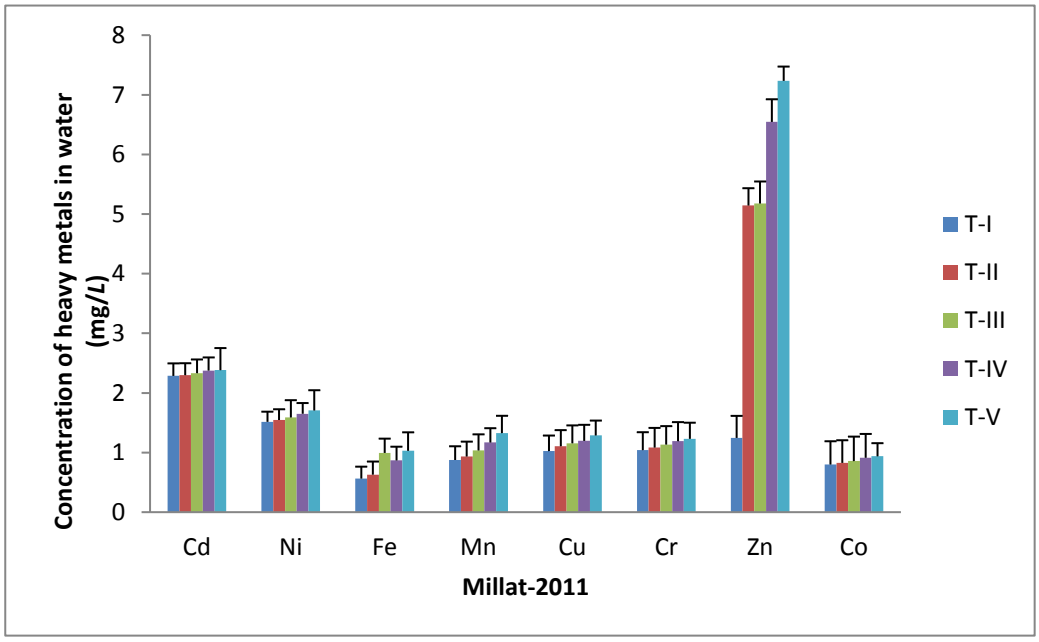


FIGURE 1
Variation of heavy metals in soil of wheat variety (Millat-2011)

TABLE 4
Physicochemical parameters of soil

Physico-chemical parameters	pH	E.C. (µS/cm)	Organic matter %	Available phosphorus (mg/kg)	Available potassium (mg/kg)	Saturation %	Textural class
T-I	7.05	5.40	0.69	7.0	327	33	Loamy
T-II	7.50	4.18	1.05	10.9	344	37	Loamy
T-III	7.59	2.92	0.87	10.3	332	39	Loamy
T-IV	7.63	2.56	1.07	11.2	370	40	Loamy
T-V	7.75	2.38	1.03	14.7	359	42	Loamy

TABLE 5
Analysis of variance for heavy metal concentrations in soil of wheat variety (Millat-2011)

Source of variation	Degree of freedom	Mean Squares							
		Cd	Ni	Fe	Mn	Cu	Cr	Zn	Co
Treatments	4	0.12^{***}	0.030^{***}	86.30^{***}	0.06^{***}	0.582^{***}	0.023^{***}	0.092^{***}	0.013^{***}
Error	10	0.001	0.001	0.161	0.001	0.011	0.001	0.001	0.01

*** Significant at 0.001 probability levels

TABLE 6
Mean concentration of heavy metals (mg/kg) in soil of wheat variety (Millat- 2011)

Met-als	T-I	T-II	T-III	T-IV	T-V	PML (mg/kg)
Cd	2.001±0.13	2.028±0.09	2.090±0.11	2.118±0.12	2.156±0.10	1.49[a]
Ni	1.356±0.15	1.416±0.13	1.466±0.11	1.528±0.12	1.613±0.14	9.06[a]
Fe	2.786±0.17	3.365±0.15	3.877±0.16	3.964±0.14	4.073±0.13	56.90[b]
Mn	0.645±0.19	0.680±0.16	0.700±0.15	0.725±0.18	0.766±0.17	46.75[a]
Cu	1.923±0.20	2.236±0.17	2.621±0.18	2.861±0.19	2.981±0.16	8.39[a]
Cr	2.048±0.23	2.143±0.20	2.178±0.22	2.211±0.21	2.285±0.19	9.07[a]
Zn	1.085±0.25	1.315±0.23	1.395±0.20	1.441±0.22	1.553±0.24	44.19[a]
Co	1.595±0.29	1.661±0.25	1.705±0.28	1.728±0.26	1.763±0.27	9.1[c]

Source [a]: Singh et al. [36]; Source [b]: Dosumuet al. [37]; Source [c]: Dutch Standards [38]

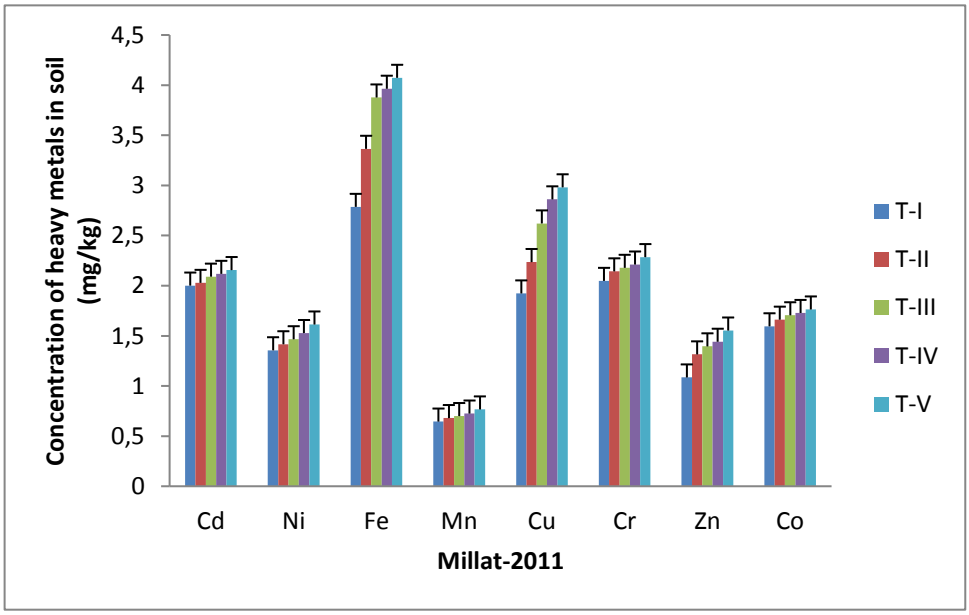


FIGURE 2
Variation of heavy metals in soil of wheat variety (Millat-2011)

TABLE 7
Analysis of variance for heavy metal concentrations in grains of wheat variety (Millat-2011)

Source of variation	Degree of freedom	Mean Squares							
		Cd	Ni	Fe	Mn	Cu	Cr	Zn	Co
Treatments	4	0.052***	0.029**	0.286***	0.266***	0.337**	0.026***	0.103**	0.401ns
Error	10	0.001	0.000	0.020	0.005	0.006	0.001	0.002	0.391

;**, *** significant at 0.01 and 0.001 probability levels; ns= non-significant

TABLE 8
Mean concentration of heavy metals in grains of wheat variety (Millat-2011)

Metals	T-I	T-II	T-III	T-IV	T-V	PML (mg/kg)
Cd	2.253±0.15	2.310±0.11	2.383±0.14	2.438±0.12	2.595±0.13	0.2
Ni	1.691±0.19	1.736±0.16	1.830±0.18	1.871±0.17	1.933±0.15	67
Fe	1.856±0.13	2.235±0.10	2.323±0.12	2.423±0.09	2.706±0.11	425.5
Mn	1.391±0.17	1.740±0.15	1.833±0.13	1.988±0.16	2.190±0.14	500
Cu	0.780±0.20	0.955±0.18	1.040±0.17	1.346±0.19	1.623±0.06	73.3
Cr	0.460±0.23	0.541±0.20	0.585±0.22	0.656±0.19	0.695±0.21	2.3
Zn	1.706±0.25	1.741±0.23	1.785±0.21	1.858±0.24	2.168±0.22	99.4
Co	0.125±0.09	0.195±0.06	0.135±0.08	0.303±0.07	0.335±0.05	50

Source: FAO/WHO [41]

Mean concentrations of heavy metals in soil. Statistical analysis of soil data demonstrated significant effect (p<0.05) on concentrations of Fe, Zn, Cu, Co, Cr, Mn, Ni and Cd in all treatment groups (Table 5). Order of mean concentrations of heavy metals and metalloids in the soil for growing wheat variety (Millat-2011) at treatment Iwas Fe >Cr >Cd >Cu >Co >Ni > Zn >Mn and at treatment-II, III, IV and V was Fe >Cu >Cr >Cd >Co >Ni >Zn >Mn (Table 6; Fig.2).

Song et al. [29] found higher Cd concentration as compared to present findings. Adriano [30] observed higher Ni and Cr concentrations as compared to the current values. Value of Fe in soil samples was lower than study carried out by Rattan et al. [14] while higher as compared to Mojiri and Aziz [31]. Gupta et al.[32] observed higher Mn concentration as compared to current study. Asdeo [33] showed greater value of copper (24.732 mg/kg) in contrast to the present value. Singh and Kansal [34] found higher Zn concentration in comparison to current finding. Allaway [35] found cobalt concentration to be in the range of 1-40 mg/kg in uncontaminated soil.

Mean concentrations of heavy metals in grains. Statistically significant (p<0.05) results for Cr, Ni, Fe, Cd, Zn, Mn and Cr concentration were obtained for ANOVA with respect to different treatments (Table 7). Order of mean concentrations of heavy metals in wheat grains at treatment I was Cd >Fe >Zn >Ni >Mn>Cu >Cr >Co, at treatment-II was Cd >Fe >Zn >Mn>Ni >Cu >Cr >Co, at treatment-III was Cd >Fe >Ni >Zn >Mn>Cu >Cr >Co, at treatment-IV was Cd >Fe >Mn>Ni >Zn >Cu >Co >Cr and at T-V was Fe >Cd >Mn>Zn >Ni >Cu >Cr >Co (Table 8; Fig.3).

Adriano [30] observed lower Cd and Cr concentration in wheat grains as compared to the present values. Gulfraz et al. [19] reported higher concentration of nickel and cobalt as compared to the current study. Rattan et al. [14] showed higher concentration of iron than present study. Mn concentration in observed wheat grains samples was lower than value observed by Rattan et al. [14] while higher as compared to that of Gulfraz et al. [19]. Bao et al. [39] reported higher concentration of copper in wheat grains in comparison to current samples. Ekmekyaparet al. [40] observed higher zinc concentration as compared to current findings.

Correlation. Cd, Ni, Fe, Mn, Cu, Cr and Zn showed positive and significant correlation while Co showed positive non-significant correlation for wheat variety (Millat-2011; Table 9). High correlation coefficient indicated good association between plants and soil [42]. Current results were comparable to that of Ahmad et al.[43] and Rattan et al. [14] who observed positive and significant correlation between plants and soil.

Bio-concentration Factor (BCF). Order of mean bio-concentration factor at treatment I, II and IV was Mn>Zn >Ni >Cd > Fe >Cu >Cr >Co, at treatment III was Mn>Zn >Ni >Cd >Co >Fe > Cu > Cr and at treatment V was Mn>Zn >Cd >Ni >Fe >Cu >Cr >Co.BCF for wheat variety (Millat-2011) was

highest for manganese while lowest for cobalt in all treatments except for treatment III (Table 10). Present BCF values for iron, copper, chromium and cobalt were less than 1 while for cadmium, nickel, manganese and zinc, values were greater than 1. Iqbal et al.[44] observed BCF>1 for cadmium and chromium while BCF<1 for nickel. Current BCF values were higher than the values investigated by Machelett et al. [45] and Puschenreiter et al. [46]. Present value of cadmium was greater than that of Wang et al. [47]. Ran et al. [48] reported low BCF value for zinc, cadmium, copper and nickel in contrast to the present work.

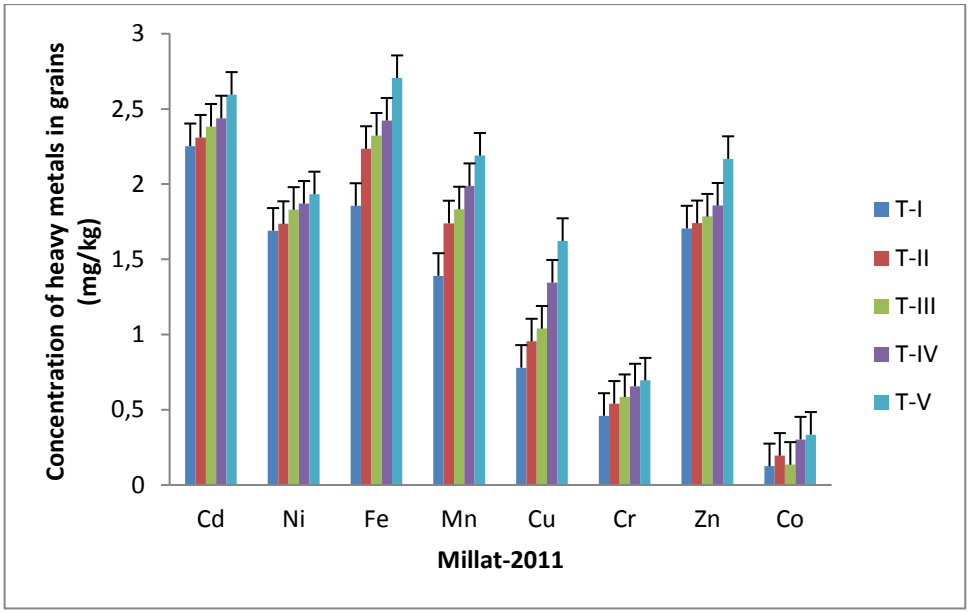


FIGURE 3
Variation of heavy metals in grains of wheat variety (Millat-2011)

TABLE 9
Metal correlation between soil and grains of wheat variety (Millat-2011)

Correlation	
Metals	**Soil-Grain**
Cd	0.935**
Ni	0.949**
Fe	0.873**
Mn	0.907**
Cu	0.909**
Cr	0.913**
Zn	0.790**
Co	0.174ns

**. Correlation is significant at the 0.01 level

TABLE 10
Bio-concentration factor for wheat variety (Millat-2011)

Treatments	Heavy metals							
	Cd	Ni	Fe	Mn	Cu	Cr	Zn	Co
T-I	1.1259	1.2470	0.6661	2.1565	0.4056	0.2246	1.5723	0.0783
T-II	1.1390	1.2259	0.6641	2.5588	0.4271	0.2524	1.3239	0.1173
T-III	1.1401	1.2482	0.5991	2.6185	0.3967	0.2685	1.2795	0.6070
T-IV	1.1510	1.2244	0.6112	2.7420	0.4704	0.2966	1.2893	0.1753
T-V	1.2036	1.1983	0.6643	2.8590	0.5444	0.3041	1.3960	0.1900

TABLE 11
Pollution Load Index for wheat variety (Millat-2011)

Treatments	Heavy metals							
	Cd	Ni	Fe	Mn	Cu	Cr	Zn	Co
T-I	1.3429	0.1496	0.0489	0.0137	0.2292	0.2257	0.0245	0.1752
T-II	1.3610	0.1562	0.0591	0.0145	0.2665	0.2362	0.0297	0.1825
T-III	1.4026	0.1618	0.0681	0.0149	0.3123	0.2401	0.0315	0.1873
T-IV	1.4214	0.1686	0.0696	0.0155	0.3410	0.2437	0.0326	0.1898
T-V	1.4469	0.1780	0.0715	0.0163	0.3553	0.2519	0.0351	0.1937

TABLE 12
Daily Intake of Metal for wheat variety (Millat-2011)

Treatments	Heavy metals							
	Cd	Ni	Fe	Mn	Cu	Cr	Zn	Co
T-I	0.0119	0.0089	0.0098	0.0073	0.0041	0.0024	0.0090	0.0006
T-II	0.0122	0.0092	0.0118	0.0092	0.0050	0.0028	0.0092	0.0010
T-III	0.0126	0.0096	0.0123	0.0097	0.0055	0.0031	0.0094	0.0054
T-IV	0.0129	0.0099	0.0128	0.0105	0.0071	0.0034	0.0098	0.0016
T-V	0.0137	0.0102	0.0143	0.0116	0.0086	0.0036	0.0114	0.0017

TABLE 13
Health Risk Index for wheat variety (Millat-2011)

Treatments	Heavy metals							
	Cd	Ni	Fe	Mn	Cu	Cr	Zn	Co
T-I	11.9409	0.4481	0.0140	0.1798	0.1033	0.0016	3.0139	0.0154
T-II	12.243	0.4600	0.0169	0.2249	0.1265	0.0019	3.0756	0.0240
T-III	12.6299	0.4849	0.1758	0.2369	0.1378	0.0020	3.1535	0.1275
T-IV	12.9214	0.4958	0.0183	0.2569	0.1783	0.0023	3.2824	0.0373
T-V	13.7535	0.5122	0.0204	0.2830	0.2150	0.0024	3.8301	0.0412

TABLE 14
Enrichment factor for wheat variety (Millat-2011)

Treatments	Heavy metals							
	Cd	Ni	Fe	Mn	Cu	Cr	Zn	Co
T-I	0.1511	9.2221	4.9817	23.0651	3.5437	0.0569	3.5368	0.4306
T-II	0.1528	9.0663	4.9668	27.3671	3.7314	0.0640	2.9780	0.6450
T-III	0.1530	9.2313	4.4806	28.0061	3.4666	0.0681	2.8782	3.3353
T-IV	0.1545	9.0551	4.5709	29.3269	4.1102	0.0752	2.9003	0.9634
T-V	0.1615	8.8622	4.9682	30.5776	4.7566	0.0771	3.1401	1.0440

Pollution Load Index (PLI). Severity of pollution was evaluated by using pollution load index. PLI is reflection of sample quality and an effective tool to compare extent of contamination at different places [48]. PLI above or equal to 1 indicates increased contamination level and decline in quality [49]. The pollution load index was in decreasing order of Cd >Cu >Cr >Co >Ni >Fe >Zn >Mn in all treatment groups (Table 11). Results indicated high PLI values for cadmium and low for manganese in soil. The results were comparable to Ahmad et al.[43] where PLI was low for all metals but Cd. Likuku et al. [50] found higher PLI value for cadmium (1.63) in comparison to the present value. Similarly, Khan et al.[51] observed higher pollution load index values for nickel, cadmium, chromium, copper and zinc when compared to current findings.

Daily Intake of Metal (DIM). Toxicity level of metals in humans depends upon daily consumption. Daily intake of contaminated food effects human health badly. Order of daily intake of metals at treatment I and II was Cd >Fe >Zn >Ni >Mn>Cu >Cr >Co; at treatment III was Cd >Fe >Mn>Ni >Zn >Cu >Co >Cr; at treatment IV was Cd >Fe >Mn>Ni >Zn

>Cu >Cr >Co. while at treatment V was Fe >Cd >Mn>Zn >Ni >Cu >Cr >Co. Daily intake of metals was highest for Cd while lowest for Co and Cr in all treatment groups (Table 12). Sajjad et al. [52] reported that population of a country is at greater risk with DIM≥1. Current values of DIM were less than 1 for all metals.

Health Risk Index (HRI). Health risk index was calculated to take into account the risks associated with consuming heavy metal contaminated wheat grains (Millat-2011).Order of health risk index at treatment I was Cd >Zn >Ni >Mn>Cu >Fe >Co >Cr, at treatment II, IV and V was Cd >Zn >Ni >Mn>Cu >Co >Fe >Cr and at treatment III was Cd >Zn >Ni >Mn>Fe >Cu >Co >Cr (Table 13). Health risk index value was highest for cadmium and lowest for chromium (Table 13). Current HRI values were higher for Zn and lower for Ni as compared to values reported by Singh et al.[36] whereby HRI values for Zn, Ni and Cu were 0.01, 0.003 and 0.39 mg/day, respectively. Khan et al.[53] reported lower HRI values for metals cadmium, chromium, copper, manganese, zinc and nickel in contrast to the present study. HRI for Mn was comparable while for Zn was higher as compared to that of Kamal et al. [54].

Enrichment Factor (EF). Heavy metal uptake increases in plants while acquiring water from soil to maintain its essential functions [55]. EF was worked out to estimate the metal pollution of soil. Order of enrichment factor at treatment I, II and V was Mn>Ni >Fe >Cu >Zn >Co >Cd >Cr, at treatment III was Mn>Ni >Fe >Cu >Co >Zn >Cd >Cr and at treatment IV was Mn>Ni >Fe >Cu >Zn >Co >Cd >Cr (Table 14).

Enrichment factor for soil grown with wheat variety (Millat-2011) was highest for manganese in all treatments (Table 14). Value of EF was used to investigate the elements present in soil [8, 56]. Present EF values of Zn, Cr and Cd were lower while higher for Ni and Cu as compared to the work of Abuduwaili et al. [57]. Highest enrichment factor for heavy metals in vegetables was reported by Chary et al. [58]. Present value was lower for Cr, Cu, higher for Ni and for Zn the value was similar to the observations of Gupta et al. [59]. Current Ni values were lower for chromium, cobalt, copper and zinc; higher for manganese and comparable for Ni to the reported values of Taha et al. [60].

CONCLUSION

Usage of waste water for irrigation purpose is a common practice these days due to shortage of canal water in Pakistan. Soil and crops persistently irrigated with waste water have elevated levels of heavy metals. In current investigation, increased concentration of iron was observed in soil and grains (Millat-2011) treated with diverse doses of domestic waste water. Cadmium could be considered potentially dangerous as it exceeded WHO limits and its HRI value was >1. This could be due to the application of untreated waste water. Waste water should be avoided or it should be treated properly before it is given to crops to avoid the detrimental effects of heavy metals.

ACKNOWLEDGEMENTS

The Higher Education Commission, Pakistan is acknowledged for providing the financial support through the research project # 20-3546/NRPU/R&D/14/536 to the fourth author. The author thanks all the supporters of this project and the referees for their constructive comments.

REFERENCES

[1] Anonymous (2009) Agriculture: Economic survey of Pakistan 2008-09. Finance Ministry of Pakistan, Finance Division Economic Advisor's Wing, Islamabad.

[2] Kho, F.W.L., Law, P.L., Ibrahim, S.H., and Sentian, J. (2007) Carbon Monoxide Levels along Roadway.Int J Environ SciTechnol. 4, 27-34.

[3] Dougherty, T.C. and Hall, A.W. (1995) Environmental Impact Assessment of Irrigation and Drainage Projects. FAO Irrigation and Drainage, 53.

[4] Rattan, R.K., Datta, S.P., Chandra, S. and Saharan, N. (2002) Heavy Metals and Environmental Quality: Indian Scenario.Fertilizer News. 47, 21-40.

[5] Divrikli, U., Horzum, N., Soylak, M. and Elci, L. (2006) Trace Heavy Metal Contents of some Spices and Herbal Plants from Western Anatolia, Turkey. Int J Food SciTechnol. 41, 712-716.

[6] Ang, H. and Lee, K. (2005) Analysis of Mercury in Malaysian Herbal Preparations: A Peer-Review. J Biomed Sci. 4, 6-31.

[7] Cui, Y.G., Zhu, Y.G., Zhai, R.H., Chen, D.Y., Huang, Y.Z., Qui, Y. and Liang, J.Z. (2004) Transfer of Metals from Near a Smelter in Nanning, China. Environ Int. 30, 785-791.

[8] Liu, D.H., Wang, F.Y., Zhou, W.L. and Yang, Y.J. (2012) Heavy Metal Pollution in Street Dusts from Different Functional Zones of Luoyang City and its Potential Ecological Risk. Chinese J Environ Sci. 33, 253-259.

[9] Wang, Z.W. Nan, Z.R, Wang, S.L. and Zhao, Z.J. (2011) Accumulation and Distribution of Cadmium and Lead in Wheat (*Triticumaestivum* L.) Grown in Contaminated Soils from the Oasis, North-West China. J Sci Food Agri. 91, 377-84.

[10] Ravichandran, M., Baskaran, M., Santschi, P.H. and Bianchi, T. (1995) History of Trace Metal Pollution in Sabine-Neches Estuary, Beaumont, Texas. Environ SciTechnol. 29, 1495-1503.
[11] Darvishi, H.H., Manshouri, M. and Farahani, H.A. (2010) The Effect of Irrigation by Domestic Waste Water on Soil Properties. J Soil Sci Environ Manag. 1, 30-33.
[12] Hassan, N.U., Mahmood, Q., Waseem, A.,Irshad, M., Faridullah, and Parvez, A. (2013) Assessment of Heavy Metals in Wheat Plants Irrigated with Contaminated Wastewater. Pol J Environ Stud. 22, 115-123.
[13] Rattan, R.K., Datta, S.P., Chhonkar, P.K., Suribabu, K. and Singh, A.K. (2005) Long Term Impact of Irrigation with Sewage Effluents on Heavy Metal Content in Soils, Crops and Groundwater- A Case Study. Agri Ecosyst Environ. 109, 310-322.
[14] Ayers, R.S. and Westcot, D.W. (1994) Water Quality for Agriculture. FAO Irrigation and Drainage Paper. 29, 1-130.
[15] Akhtar, N., Inam, A. and Khan N.A. (2012) Effects of City Wastewater on the Characteristics of Wheat with Varying Doses of Nitrogen, Phosphorus and Potassium. Recent Res SciTech. 4, 18-29.
[16] Indian Standards (IS) (1982) Tolerance Limits for Inland Surface Water Subject to Pollution, Indian Standards IS, 2296.
[17] FAO (1985) Water Quality for Agriculture (Ed.) Irrigation and Drainage paper. Rome. 29, 1-174.
[18] Gulfraz, M., Mussaddeq, Y., Khanum, R. and Ahmad, T. (2003) Metal Contamination in Wheat Crops (*Triticumaestivum* L.) Irrigated with Industrial Effluents. Online J Bio Sci. 3, 335-339.
[19] Morrissey, J. and Guerinot, M.L. (2009) Iron Uptake and Transport in Plants: The Good, the Bad, and the Ionone. Chem Rev. 109, 4553-4567.
[20] Alloway, B.J. (Ed.) (1990) Heavy Metals in Soils. Blackie and Son Ltd., Glasgow.
[21] Jakubus, M. and Czekała, J. (2001) Heavy Metal Speciation in Sewage Sludge. Pol J Environ Stud.10, 245-250.
[22] Shad, H.A., Khan, Z.I., Ahmad, K., Rizwan, Y. and Tahir, H.M. (2014) Human Health Hazards Caused by Heavy Metals Accumulation in Wheat Variety "*Sehar-2006"* Irrigated with Domestic Sewage Water. Biologia (Pakistan). 60, 99-102.
[23] Kurdziel, B.M., Prasad, M.N.V. and Strzalka, K. (2004) Photosynthesis in Metal Stressed Plants. In: Prasad, M.N.V. (Ed.) Heavy Metal Stress in Plants: From Bimolecular to Ecosystems, Springer Verlag, Berlin, 146-181.
[24] WWF (2007) Report on National Surface Water Classification Criteria. Irrigation Water Quality Guidelines for Pakistan. February, 2007. Waste Water Forum Pakistan.
[25] Nafees, M. and Amin, A. (2014) Evaluation of Heavy Metals Accumulation in Different Parts of Wheat Plant Grown on Soil Amended with Sediment Collected from Kabul River Canal. J Agri Res. 52, 383-394.
[26] Yourtchi, M.S. and Bayat, H.R. (2013) Effect of Cadmium Toxicity on Growth, Cadmium Accumulation and Macronutrient Content of Durum Wheat (Dena CV.). Intl J Agri Crop Sci. 6, 1099-1103.
[27] Narwal, R.P., Gupta, A.P., Singh A. and Karwasra, S.P.S. (1993) Composition of Some City Waste Waters and Their Effect on Soil Characteristics. Annals Bio. 9, 239-245.
[28] Song, D., Zhuang, D., Jiang, D., Fu, J. and Wang, Q. (2015) Integrated Health Risk Assessment of Heavy Metals in Suxian County, South China. Int J Environ Res Publ Health. 12, 7100-7117.
[29] Adriano, D.C. (1986) Trace Elements in the Terrestrial Environment.Springer-Verlag, New York.
[30] Mojiri, A. and Aziz, H.A. (2011) Effects of Municipal Wastewater on Accumulation of Heavy Metals in Soil and Wheat (*Triticumaestivum*L.) with Two Irrigation Methods. Roman Agric Res. 28, 217-222.
[31] Gupta, A.P., Antil, R.S and Singh, A. (1986) Proceedings of National Seminar on Environmental, Sewer Waters Composition and Their Effect on Soil Properties. Biores Technol. 65, 171-173.
[32] Asdeo, A. (2014) Toxic Metal Contamination of Staple Crops (Wheat and Millet) in Peri-Urban Area of Western Rajasthan. Int Refereed J Engr Sci. 3,8-18.
[33] Singh, J. and Kansal, B.D. (1985) Effect of Long Term Application of Municipal Waste Water on some Chemical Properties of Soil. J Res Punjab Agri Univ. 22, 235-242.
[34] Allaway, W.H. (1968) Agronomic Control over the Environmental Cycling of Trace Elements. Adv Agron. 20, 235-274.
[35] Singh, A., Sharma, R.K., Agrawal, M. and Marshall, F.M. (2010) Health Risk Assessment of Heavy Metals via Dietary Intake of Foodstuffs from the Wastewater Irrigated Site of a Dry Tropical Area of India. Food Chem Toxicol. 48, 611-619.
[36] Dosumu, O.O., Abdus-salam, N., Oguntoye, S. and Afdekale, F.A. (2005) Trace Metals Bioaccumulation by Some Nigerian Vegetables. Centrepoint. 13, 23-32.
[37] Dutch Standards (2000) Circular on Target Values and Intervention Values for Soil Remediation.

[38] Bao, Z., Wu, W., Liu, H., Chen, H., and Yin, S. (2014) Impact of Long-Term Irrigation with Sewage on Heavy Metals in Soils, Crops, and Groundwater a Case Study in Beijing.Pol J Environ Stud. 23, 309-318.

[39] Ekmekyapar, F., Şabudak, T. and Şeren, G. (2012) Assessment of Heavy Metal Contamination in Soil and Wheat (*Triticum aestivum* L.) Plant around the Corlu–Cerkezkoy Highway in Thrace Region. Global NEST J. 14, 496-504.

[40] FAO/WHO (2001) Report on the 32nd Session of the Codex Committee on Food Additives and Contaminants ALINORM 01/12, Beijing. China.20-24 March 2000. Joint FAO/WHO Food Standard Programme. Codex Alimentarius Commission. 24th Session. 2-7 July. Geneva Switzerland.

[41] Pentecost, A. (1999) Analyzing Environmental Data. Testing if a Relationship Occurs Between Two VariablesUsing Correlation. Pearson Education Limited, England, 102-106.

[42] Ahmad, K., Khan, Z.I., Yasmin, S., Ashraf, M. and Ishfaq, A. (2014) Accumulation of Metals and Metalloids in Turnip (*Brassica rapa* L.) Irrigated with Domestic Wastewater in the Peri-Urban Areas of Khushab City, Pakistan. Pak J Bot. 42, 511-514.

[43] Iqbal, H.H., Taseer, R., Anwar, S., Mumtaz, M. and Shahid, N. (2016) Human Health Risk Assessment: Heavy Metal Contamination of Vegetables in Bahawalpur, Pakistan. Bull Environ Stud. 1, 10-17.

[44] Machelett, B., Metz, R. and Bergmann, H. (1993) Schwer Metal Transfer Untersuchungenan Landwirtscha Lichen and Gartnerischen-NutzpflanzenUnterGleichen Anbaubedingungen. VDLUFA-Schrienreihe. 37, 579-582.

[45] Puschenreiter, M., Horak, O., Friesl, W. and Hartl, W. (2005) Low-Cost Agricultural Measures to Reduce Heavy Metal Transfer into the Food Chain – A Review. Plant Soil Environ.51, 1-11.

[46] Wang, Z.W., Nan, Z.R., Wang, S.L. andZhao, Z.J. (2011) Accumulation and Distribution of Cadmium and Lead in Wheat (*Triticumaestivum* L.) Grown in Contaminated Soils from the Oasis, North-West China. J Sci Food Agric. 91, 377-84.

[47] Ran, J., Wang, D., Wang, C. and Zhang, H. (2016) Heavy Metal Contents, Distribution and Prediction in a Regional Soil–Wheat System. Sci Total Environ. 544, 422-431.

[48] Tomlinson, D.L., Wilson, J.G., Harris, C.R. and Jeorey, D.W. (1980) Problems in the Assessments of Heavy Metal Levels in Estuaries and Formation of a Pollution Index. Helgoland Marine Research. 33, 566-575.

[49] Likuku, A.S., Mmolawa, K.B. and Gaboutloeloe, G.K. (2013) Assessment of Heavy Metal Enrichment and Degree of Contamination around the Copper-Nickel Mine in the Selebi Phikwe Region, Eastern Botswana. Environ Eco Res. 1, 32-40.

[50] Khan, S., Cao, Q., Zheng, Y.M., Huang, Y.Z. and Zhu, Y.G. (2008) Health Risks of Heavy Metals in Contaminated Soils and Food Crops Irrigated with Wastewater in Beijing, China. Environ Poll. 152, 686-692.

[51] Sajjad, K., Farooq, R., Shahbaz, S., Khan, M.A. and Sadique, M. (2009) Health Risk Assessment of Heavy Metals for Population via Consumption of Vegetables. World Appl Sci J. 6, 1602-1606.

[52] Khan, M., Malik, U.R.N. and Muhammad, S. (2013) Human Health Risk from Heavy Metal via Food Crops Consumption with Wastewater Irrigation Practices in Pakistan. Chemosphere. 93, 2230-2238.

[53] Kamal, A.K.I., Islam, M.D.R., Hassan, M., Ahmed, F., Mirza, A.T.M., Rahman, T. and Moniruzzaman, M. (2016) Bioaccumulation of Trace Metals in Selected Plants within Amin Bazar Landfill Site, Dhaka, Bangladesh. Environ Proc. 3, 179-194.

[54] Tani, F.H. and Barrington, S. (2005) Zinc and Copper Uptake by Plants under Two Transpiration Part I. Wheat (*Triticumaestivum* L.). Environ Poll. 138, 538-547.

[55] Huang, S.S., Hua, M., Jin, Y., Wu, X.M., Liao, Q.L. and Zhu, B.W. (2008) Concentrations and Sources of Heavy Metal in Atmospheric Dust Fall in the Nanjing City, East China. Earth Sci Frot. 15, 161-166.

[56] Abuduwaili, J., Zhang, Z.Y. and Jiang, F.O (2015) Assessment of the Distribution, Sources and Potential Ecological Risk of Heavy Metals in the Dry Surface Sediment of Aibi Lake in Northwest China. PLoS One. 10, e0120001.

[57] Chary, S., Kamala, N., Samuel, C.T. and Suman, R.D. (2008) Assessing Risk of Heavy Metals from Consuming Food Grown on Sewage Irrigated Soils and Food Chain Transfer. Ecotoxicol Environ Saf. 69, 513-524.

[58] Gupta, S., Jena, V., Jena, S., Davic, N., Matic, N., Radojevic, D. and Solanki, J.S. (2013) Assessment of Heavy Metal Contents of Green Leafy Vegetables. Croat J Food Sci Technol. 5, 53-60.

[59] Taha, K.K., Shmou, M., Osman, M.H. and Shayoub, M.H. (2013) Soil-Plant Transfer and Accumulation Factors for Trace Elements at the Blue and White Niles. J Appl Ind Sci. 1, 97-102.

Received: **25.04.2017**
Accepted: **07.09.2017**

CORRESPONDING AUTHOR

Zafar Iqbal Khan
Department of Botany,
University of Sargodha,
Sargodha – Pakistan

E-mail: zikhan11@gmail.com

© by PSP Volume 26 – No. 12A/2017 pages 7849-7859 Fresenius Environmental Bulletin

ECOSYSTEM SERVICE EVALUATION OF STREAMS FOR NUTRIENT AND BACTERIA PURIFICATION IN A GRAZED WATERSHED

Theodoros Chalazas*, Ourania Tzoraki, David Cooper, Maria Adamantia Efstratiou, Vasileios Bakopoulos

[1]University of the Aegean, Department of Marine Sciences, University Hill 81131 Mytilene, Lesvos Island, Greece.
[2]Centre for Ecology and Hydrology, ECW Building, Deiniol Rd, Bangor, Gwynedd, LL57 2UW, UK.

ABSTRACT

The importance of sustainable development of river systems based on ecological and socio-economic criteria is widely recognized. The "Integrated Valuation of Ecosystem Services and Tradeoffs" (InVEST) model, an ecosystem based model which couples biophysical and economic models, is used to examine the nutrient and bacteria mitigation processes in the ungauged grazed area draining to the Gulf of Kalloni, a semi-enclosed bay in Lesvos, Greece. Point sources and grazing land loads are neglected by the InVEST model, leading to poor estimation of nutrient loads at this site. We include additional terms to account for these sources. We also apply climate change scenarios to assess their likely impact on nutrient export and hydrology over the drainage area. We show that the nutrient mitigation capacity is currently exceeded in four sub-basins with a compensation cost of up to 20 million dollars over a 20 year period.

KEYWORDS:
Streams, Nutrients, Bacteria, Farming loads, Water Purification

INTRODUCTION

The importance of the sustainable development of river systems based on ecological and socioeconomic criteria is widely recognized. The concept of river basin management based on ecosystem services follows a holistic approach that recognizes the cultural, provisioning and regulating role of these services [1]. Cultural services are indicative of the aesthetic quality of terrestrial and aquatic environments, provide a living laboratory for science and education and support cultural and recreational activities. Food, energy, raw material, medicinal and biotechnology production are key provisioning roles. Finally, the regulating role covers a wide range of hazard reduction, waste treatment, climate regulation and biological interactions [2]. The regulating services are essential for maintaining river basins in a healthy state and their significance may be expressed in monetary terms so as to ensure that values can be compared across ecosystem services [3].

Many well-known studies describe detail of only a few regulating services and benefits per service [4, 5, 6, 7, 8, 9, 10] or use complex monitoring and modeling systems to inform decision makers [11, 12]. In an effort to introduce greater simplicity, the Natural Capital Project [13] developed the "Integrated Valuation of Ecosystem Services and Tradeoffs" (InVEST) model, as an open-source modelling toolbox that allows users to assess the current and future responses of ecosystem services by coupling biophysical and economic models.

The "Water Purification: Nutrient Retention" sub-model of InVEST evaluates the capacity of vegetation and soil to mitigate nutrient losses from surface runoff. In an example study using this sub-model, a reduction of over 55% in nutrient retention capacity was observed in the Miyun reservoir watershed, China [14] due to residential expansion (280%) in the past 20 years. The water purification service was used by Wang et al. (2014) to assess in combination with the other provisioning ecosystem services the spatial patterns of relationships between ecosystem services and the well-being of residents. A consistent tendency and a spatially coupled pattern was observed emphasizing the need to regulate ecosystem services in line with human well-being [15].

In Greece much of the land surface is classified as short vegetation, which is generally managed as grazed land. While used for livestock grazing, this land is not generally considered a significant non-point sources of pollution (nutrient loads and bacteria) by environmental models. In this study, we include grazed land in an application of the InVEST model in Greece, to estimate the influence of its management on ecosystem services. The aim is to propose a general framework of ecosystem services assessment and corresponding benefits of limiting nutrients and fecal material in the river basins with limited data and in areas where agriculture is the main land use. Nutrient and fecal contamination mitigation is an essential ecosystem service reducing eutrophication, groundwater nitrification and water infection. Fecal contamination is often a serious

problem in water health, originating from fresh fecal material produced by livestock and wild animals or by farm wastes (manure, slurry) [16]. Flash floods or irrigation practices mobilize nutrients and fecal material which through hydrological pathways can reach major water bodies or the sea.

MATERIALS AND METHODS

Study site. Our study site is the area draining to the semi-enclosed Gulf of Kalloni, Lesvos, Greece. The area of the river basins that drain into the Gulf of Kalloni (Figure 1) is estimated at approximately 406 km^2, a quarter (24.5%) of the island's total area of 1633.6 km^2). The most important rivers are the Tsiknias (84.6 km^2) and the Mylopotamos (50 km^2) draining to the northern part of the bay, the Potamia (48.6 km^2) to the west and the Vouvaris (24.3 km^2) to the east. The Tsiknias river basin covers most of the northern and central parts of the island, having a maximum elevation of 968m (Lepetymnos mountain). The geological formations of the watershed are mostly volcanic (dacites, latites and latitic andesites), while towards the coastline there are fluvio-torrential Pleistocene deposits, comprising a coastal aquifer (area 31.42 km^2) (Figure 1). Within the drainage area are small and sparsely scattered villages where the main occupations are focused on the primary sector, the main land uses being grazing, olive groves, forests and annual crops.

The rivers of the drainage area have eutrophic episodes due to both natural and anthropogenic causes. Human influences on ecosystem services include livestock farming, urbanization and tourism. Rivers carry organic matter, nutrients and other pollutants from these sources to the Gulf of Kalloni, particularly during intense flood events.

Water balance measurement. To provide initial estimates of the freshwater volume entering the bay, stream flow was measured in spring, winter and early summer of 2013-14 at 13 locations along the coast (Figure 1). Two meteorological stations operate in the basin (a) Stipsi (396m altitude) with annual mean rainfall of 870mm and (b) Agia Paraskevi (95m altitude) with an annual mean rainfall of 664mm. Since 2014, a telemetry station (Prini) has operated on the main channel of the Tsiknias river providing water level data at 15min intervals. Monthly flow measurements are used to estimate the rating curve relating water level to flow for this river.

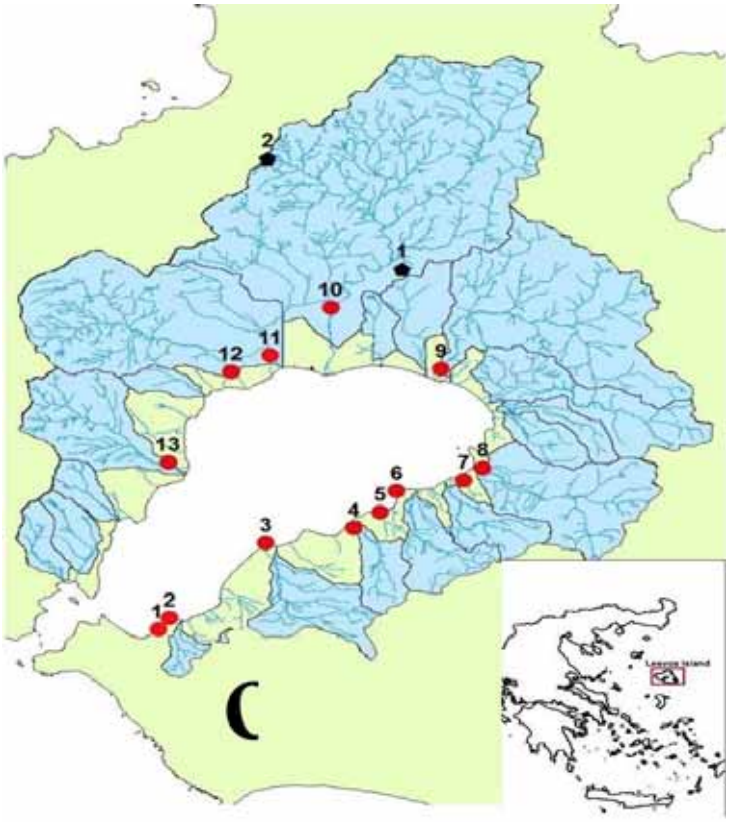


FIGURE 1
Drainage network and monitoring points of water flow. Monitoring points of water flow (red). Meteorological stations (black).

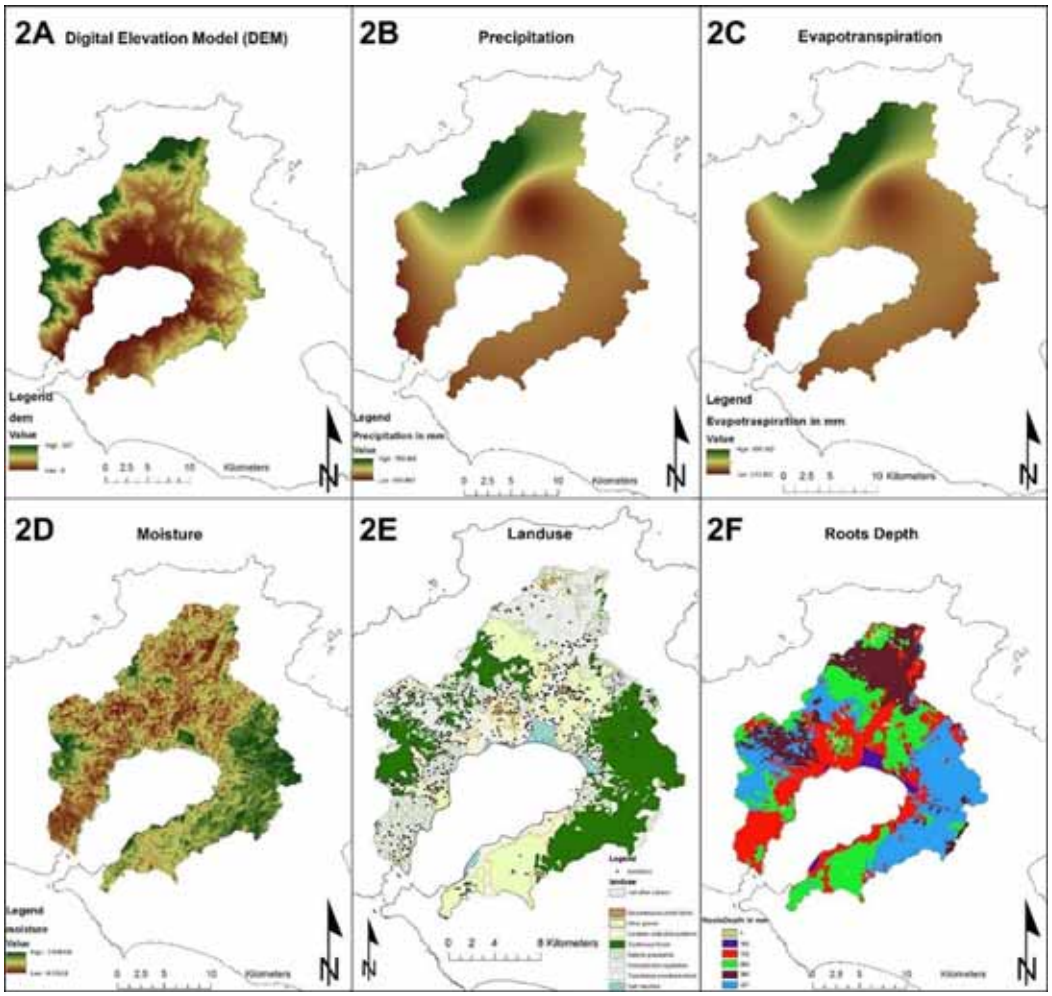


FIGURE 2
GIS maps of the required data

Microbial measurement. To estimate the fecal bacterial load entering the Gulf of Kalloni the *Escherichia coli* (*E. coli*) concentrations in stream water were measured, *E.coli* being an indicator of fecal contamination used in applicable legislation. Water samples were collected aseptically from the streams and transported under refrigeration to the microbiology laboratory of the Department of Marine Sciences at the University of the Aegean. The air and water temperatures were within normal limits for the time of year. In the laboratory, the concentration of *E. coli* in the samples was measured in accordance with ISO 9308-1: 2000. Appropriate quantities of water were filtered through nitrocellulose filters with pore diameter 0.45 μm. Each filter was placed on an appropriate nutrient substrate and was incubated as set out in the standard.

InVEST model. The "Water Purification: Nutrient Retention Model" of InVEST calculates the amount of nutrient retained in the land area associated with each pixel and aggregates export and retention of nutrients per basin. The model is defined on a gridded map with each pixel (grid square) having its own characteristics. Calculations at pixel level can represent the heterogeneity in runoff due to soil type, precipitation and vegetation cover. The valuation part of the model uses water treatment costs and a discount rate to determine the value contributed by the natural water purification function. The model also calculates the economic value provided by the retention of nutrients, avoiding any further nutrient processing costs. The model incorporates data on the amount of runoff, the pollutant load, the ability of different types of vegetation to transmit pollutants, water treatment costs for pollutants of interest and the feasibility of meeting water quality standards.

The data needs of the model are as follows:

- **Digital elevation model (DEM).** A GIS raster dataset, with an elevation value for each pixel. (Figure 2A) The ASTER GDEM with a one arc second (30m) grid of elevations of Lesvos Island was used.

- **Root restricting layer depth.** A GIS raster dataset with an average root restricting layer depth value for each cell. (Figure 2F) A detailed review of root zone depth of existing plants was carried out.

- **Precipitation.** A GIS raster dataset with a non-zero value for average annual precipitation for each cell (Figure 2B) The annual precipitation data were derived from the gauges at Sigri, Agia Paraskevi, Akrasi and University Hill for the period 2003-2013.

- **Plant Available Water Content.** A GIS raster dataset with a plant available water content value for each cell. (Figure 2D). The NDVI (normalized difference vegetation index) was used to extract the soil water content.

- **Average Annual Potential Evapotranspiration.** A GIS raster dataset, with an annual average potential evapotranspiration (PET) value for each cell (Figure 2C). Turc's equation was used to derive the PET of the study area [17].

- **Land use/land cover.** A GIS raster dataset, with an integer LULC code for each cell. (Figure 2E) Satellite images (Landsat 4-5 TM 1990; 2008) are used to classify land uses/covers of Lesvos Island.

- **Watersheds.** A shapefile of polygons. This is a layer of watersheds such that each watershed contributes to a point of interest where water quality is measured. (Figure 1) The ArcSWAT delineation tool was used to delineate the drainage area.

- **Biophysical Table.** A .csv table of land use/land cover (LULC) classes, containing defaults values of water quality export coefficients for each class.

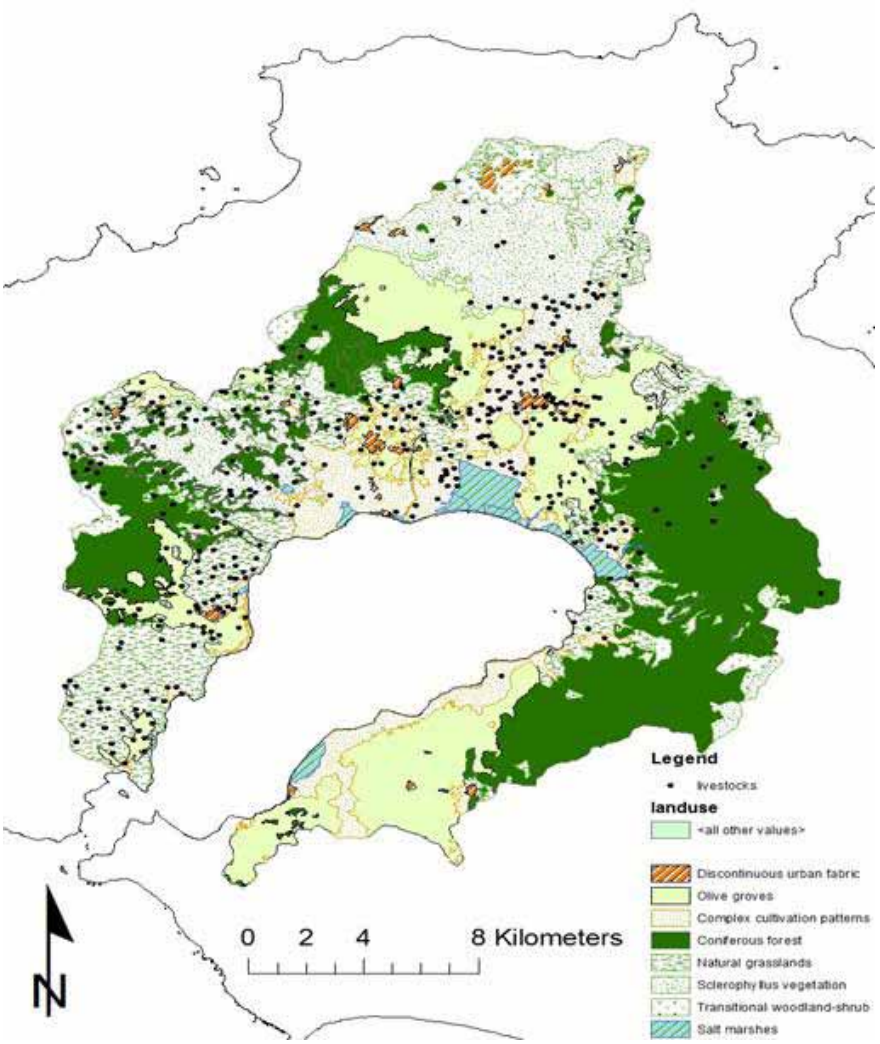


FIGURE 3
Livestock (dots) in the Kalloni drainage area showing land use distribution. This figure is used to correct the calibration of the model.

TABLE 1
Stream flow at the 13 locations in the Kalloni drainage area

id	Name	Flow, L/sec				Average value (Mean)	Flow, hm^3/year (Sum)
		1/12/2013	6/4/2014	7/6/2014	4/3/2015		
1	Nyfida beach - a	0	0	0	0	0	-
2	Nyfida beach - b	0	0	0	0	0	-
3	Glaros	31.3	59.8	Stagnant water	770	287	9.1
4	Loutsas	43.4	68.9	0	197	77	2.4
5	Saint Paulos	54	60.8	Stagnant water	102	72	2.3
5α	Fishing port	28.5	Stagnant water	Stagnant water	Stagnant water	29	0.9
6	Makris	182	303.6	13.3	323	205	6.5
7	Achladeri	59.4	147.1	7.14	24	59	1.9
8	Vouvaris	981	266.6	49.8	1427	681	21.5
9	Mylopotamos	142.7	294	26.6	714	294	9.3 (14.6*)
10	Tsiknias	76.1	0	188.3	2450	679	21.4 (23.9*)
11	Christou	0	0	Stagnant water	Stagnant water	0	0.0 (11.9*)
12	Potamia	43.9	400.7	0.5	2273	680	21.4 (12.5*)
13	Parakoila	125.6	40.1	32.9	372	143	4.5
							101.1

(*water volumes a reported in the "River basin management plan of Aegean islands district-GR14")

RESULTS

Water flow estimation. The total annual volume of freshwater that flows into the Gulf of Kalloni is estimated using the instantaneous flow measurements shown in Table 1. The average value of only four flow measurements typically leads to significant errors in annual flow estimation. For example, in the Tsiknias river (sampling point 10) the four measurements provide an overall annual flow equal to 21.4hm^3 which is slightly larger than the simulated mean annual runoff of the past twenty years 18.6 hm^3 and approximately equal to the value of 20.75 hm^3 found by processing 15-minute level measurement values for the period 11 September 2014 to 3 September 2015. The hydrological year 2014-2015 was one of the wettest years of the last four decades, so the increased runoff estimates are not unexpected. The measured annual outflow of the Mylopotamos, Tsiknias, Christou and Potamia rivers was also compared to that of the "River Basin Management of the Water District Aegean Islands GR14» as shown in Table 1 (asterisked in the final column). Total inflow of fresh water was estimated as 101.1hm^3. It should be noted that the conversion of L/sec to hm^3 was made under the assumption that there is flow for 365 days a year, which does not apply to all streams entering the gulf.

Nutrient estimation. During the period December 2014 to February 2015 low surface water concentrations of nitrate and phosphate nutrients were measured in the Tsiknias river (NO_3^--N, 0.8 mgL^{-1}; NO_2^--N, 21 μgL^{-1}; PO_4^{-3}-P, 497 μgL^{-1}) as shown to figure 4 [18], values similar to those measured by Polatidou et al. (2013) (NO_3^--N, 0.2 mgL^{-1}; NO_2^--N, 1.5 μgL^{-1}; PO_4^{-3}-P, 82 μgL^{-1}). Similar low concentrations of nutrients were measured in the aquifer water (NO_3^--N, 0.9 mgL^{-1}, NO_2^--N, 7 μgL^{-1}, PO_4^{-3}-P, 214 μgL^{-1}), all within the permissible limit for drinking water.

Since the mean flow of the Tsiknias for the study period (December 2014-February 2015) is 1.65 m^3s^{-1}, the annual loads of nitrogen and phosphorus flowing into the Gulf of Kalloni from the Tsiknias are approximately 23 t N and 8.5 t P.

To estimate nutrient losses using InVEST, we first applied the model using the default values of the biophysical table giving nutrient loads by land use. For the Kalloni drainage area, simulation based on default values, recommended by previous studies [18], does not provide adequate results. The nutrient loads exported to the Gulf are estimated to be much lower than the measured values (approximately 10 t N and 4 t P from the whole basin and 4.5 t N and 2 t P from the sub-basin of Tsiknias). This is largely because the model does not adequately account for nutrient losses from grazed land in the drainage area. We have therefore recorded the number of sheep and goat farms for each land use (Figure 3) as a means of correcting the calibration. A density-dependent pollution coefficient was calculated for grazed land. This coefficient was calculated based on the number of farms in each land use divided by the corresponding land use area (ha) and ranged from 0.0014 to 0.242 for all land uses with livestock farming. This

extended the existing eight (8) land uses in the biophysical table to 71 new land uses each with a different export coefficient based on both LULC and the livestock density. Nutrient export estimates from the new land uses were optimized based on their pollution coefficient until the result of the model simulations approached the measured values.

Optimizing the biophysical table of 71 different land uses with farms based on livestock density in the Tsiknias sub-basin provides a relatively accurate picture of the total load of nutrients entering the gulf, assuming other basins behave in a similar manner in terms of the connection between grazed land and the nutrient load. The total nutrient export of all basins to the gulf is calculated as 60 t N and 22 t P (Figures 5 and 6).

Microbial estimation. The measured microbial load in streams flowing into the Gulf of Kalloni during the two years of sampling is shown in Figure 7. Concentrations of *E. coli*, were low with higher values observed during periods of high flow. Low and zero concentrations were measured in spring (April 2014 sampling) after heavy rains. This was expected, because at the end of the winter rain period the soils of the basin of each river are normally flushed from the preceding rain and no fecal origin material is exported to the system. The source of high bacterial load in the Parakoila River (position 13) is believed to be the sewer system of Parakoila village, which continuously discharges fecal material of human origin to the river.

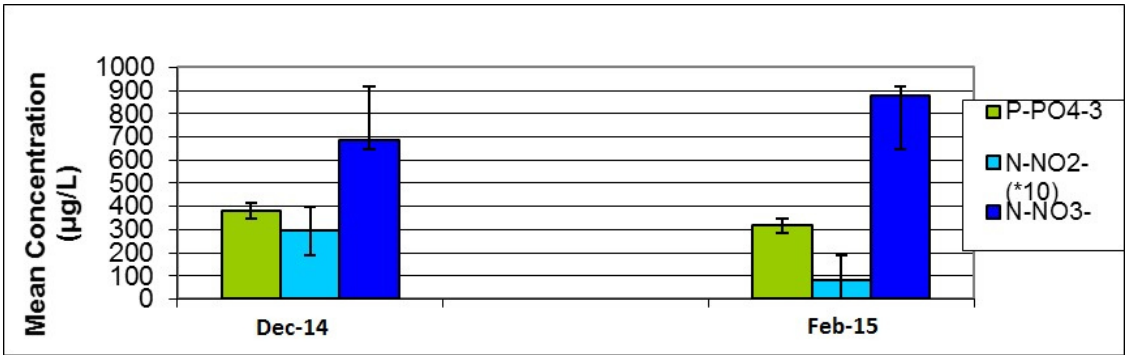


FIGURE 4
Phosphate-P, Nitrite-N and Nitrate-N concentration in surface and groundwater

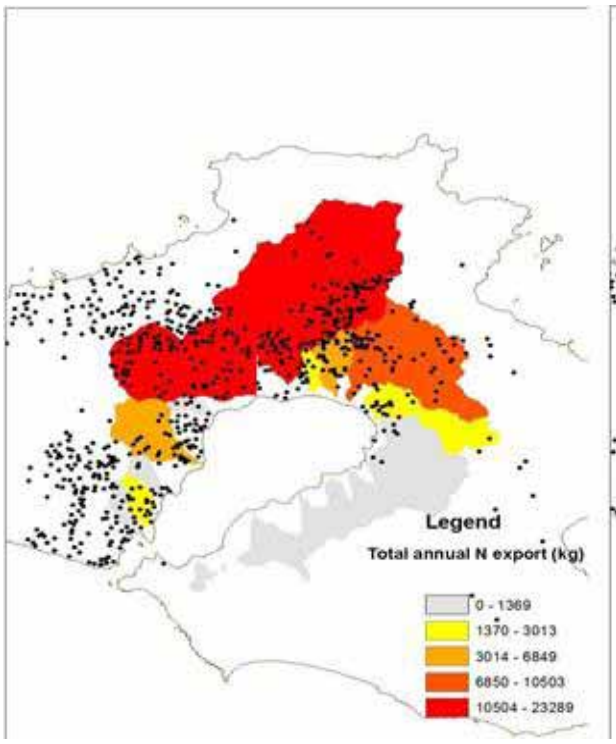


FIGURE 5
Total N export

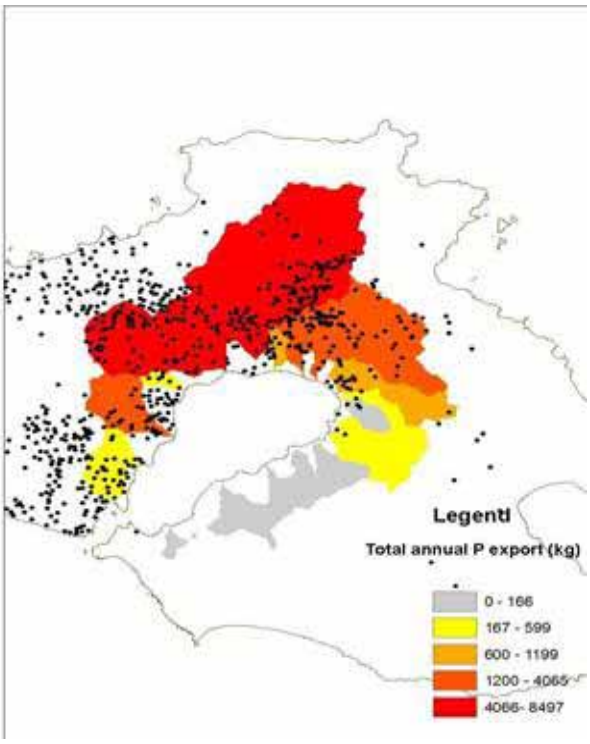


FIGURE 6
Total P export

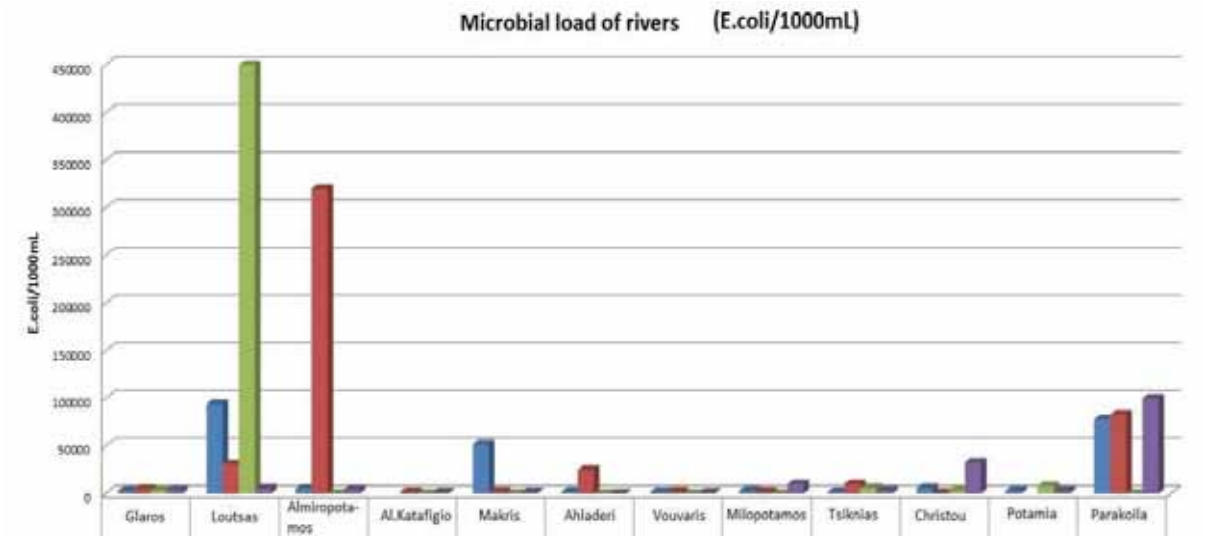


FIGURE 7
Microbial load of rivers in the Kalloni drainage area (E. coli/1000ml)

TABLE 2
Microbial load of rivers in the Kalloni drainage area *(E. coli/1000ml)*

	6/4/2013	1/12/2013	12/4/2014	20/2/2015
Glaros	2900	4800	3000	3700
Loutsas	94000	31000	450000	5500
Almiropotamos	5100	320000	0	4500
Al.Katafigio		1800	0	1600
Makris	52000	2300	0	1800
Ahladeri	2200	25000	0	270
Vouvaris	1900	2200	0	1200
Milopotamos	3100	2100	0	10000
Tsiknias	2000	10000	6000	3400
Christou	5900	900	3000	33000
Potamia	3000		8000	3100
Parakoila	78000	83000	0	100000

Higher concentrations of *E. coli* were found in the Loutsas and Almyropotamos streams, both of which flow into an area of intensive shellfish harvesting which is a significant local source of income. Increased concentrations of microorganisms of fecal origin, detected during routine examination of shellfish harvested for human consumption, have led in the past to interruption of harvesting. The high concentration of fecal origin bacterial load in the Loutsas stream, is believed to be due to untreated municipal waste water discharge from the village of Vassilika. High coliform concentration in the watercourse which flows into the Ag. Pavlos was not systematic, and can be attributed to the occasional presence of fecal material on the day of sampling.

The 'water purification' model of InVEST includes a component to simulate bacteria mitigation. We modified the biophysical table to include an *E.coli* export coefficient, with the bacteria calibration procedure accounting for urban areas and land uses with livestock farms to estimate the source distribution of bacteria of fecal origin in the drainage area, and to find any direct link between bacteria and grazed land. Having calculated an annual average of *E. coli* export to the bay (12880 * 10^11 *E.coli*), contributions from grazed land were calibrated several times until the result of the model approached the measured data (figure 8).

Climate change. The InVEST model was applied to a climate change scenario for the year 2100. Large scale predictions over the Mediterranean suggest up to 35% rainfall reduction and 3-5 °C warming by 2071-2100 [19]. Scenario changes in precipitation and average annual potential evapotranspiration were calculated from current precipitation and mean temperature. The precipitation was reduced by 200 mm and the average annual potential evapotranspiration was calculated based on the new precipitation and a 3°C warming using Turc's equation [17].

Changing these two driving variables and re-running the model suggests a very slight increase in annual nutrient export (less than 1 t in each of N and P) and a decrease in the mean runoff in each sub-basin.

Estimation of remedial measures. The economy of the area draining to the Gulf of Kalloni is strongly dependent on its olive farming and unrestricted grazing, while the gulf itself has great historical, tourist, recreational and social value and hundreds of people are occupied in sardine fishing and shellfish harvesting. Both the tourist and fishing industries are affected by severe eutrophication events in the bay, particularly after heavy rain, when microbiological pollution frequently results in an interruption to fishing activities. Local authorities and the local community need appropriate guidelines to handle these environmental issues and a user-friendly model to support mitigation measures. The InVEST model using GIS identifies the sub-basins and streams contributing the greatest terrestrial fluxes to the sea and enables remediation actions under scenarios to be considered.

To find the acceptable N and P limits in each sub-basin for good hydrological status, we used the river classification system at the country level in geographic zone two (2). This gives an upper limit for good ecological status of 0.942 mgL^{-1} for N as nitrate and 0.117 mgL^{-1} for P as phosphate (Greek River Nutrient Classification System GR-NCS) [20]. Table 2 shows for the most important rivers of the Kalloni drainage area the total nutrient load exported to the bay, the permitted export load limits for each nutrient, and the load that needs to be removed to achieve "good" hydrological status (table 3).

Applying the InVEST model suggests that inputs to the bay should be reduced by some 3 t of N and 10 t of P annually. To achieve the required reduction the construction of enhanced wetland treatment systems for the retention of nutrients is suggested. These systems can remove contaminants such as nutrients by diverting the river, using natural processes provided by vegetation, soil and organisms. The annual retention capacity of such a system is approximately 2 t P and 1.3 t N, with construction and maintenance costs of $ 2 million and $ 75,000 per year respectively [21]. A management proposal for the breakdown of nutrients would be to provide three facilities in the Tsiknias sub-basin and one for each of the Potamia, Parakila and Mylopotamos sub-basins. The total indicative cost of construction is $ 12 million with an annual maintenance cost of $ 450,000. Also untreated wastewater disposal from coastal settlements seems to contribute significantly to the high microbial load in the bay. To deal with this wastewater aspect, we propose the construction of chlorine contact tanks with reflectors to remove microorganisms of fecal origin in the river Loutsas. The cost of construction of each tank would be approximately $200,000, with an annual operating cost of $5.300 [22, 23].

DISCUSSION

The main contributing rivers, the Tsiknias and the Potamia, drain a large area of grazing land. The density of farms used for grazing has been found to be directly associated with high loads of nutrients and bacteria entering the bay via surface runoff. This is consistent with the findings of other studies which have found that animal farming activities export microbial load to surface water in combination with other activities such as manure application and contributions from wildlife [24]. In the Kalloni drainage area manure application is not managed in a controlled way, but is spread directly by grazing animals and released to surface runoff during rain events.

While the InVEST model estimates of lumped annual fluxes are consistent with measured values, **t**he model does not provide temporal variability in simulating of the pollutants of interest. The very high monitoring and analysis cost of bacterial load estimation is the main reason for the lack of high frequency data to test model performance. Nevertheless, our application of the InVEST model to simulate bacteria fluxes gave satisfactorily results and may be used as a guide for basin managers to eliminate fecal pollution.

The InVEST model simulations shows a small relative flux increase under climate change scenarios and fluxes generally do not appear to be very sensitive to precipitation, temperature and evapotranspiration changes, even though extreme scenarios were considered. Generally, the structure of the InVEST model does not include complex hydrological modules, nor are irrigation and cessation of flow accommodated. Climate models predict a regional change in precipitation intensity and peak flow volume rather than a change in the total precipitation amounts, but the InVEST model has no means of accounting for rainfall intensity or the effect of individual flash flood events.

The model also lacks the ability to incorporate significant components of the nutrient mass balance such as the contribution of precipitation and the nutrients attached to the eroded material, a key factor in mountain areas, but also in intensively farmed areas.

Finally the model does not account for soil and in-stream processes in the nutrient cycle. It is suggested that the empirical export coefficient equations of well-known models such as the MONERIS and LOICZ be included in InVEST. In this way InVEST model would be more accurate without losing the simplicity and ease of understanding for users and basin managers.

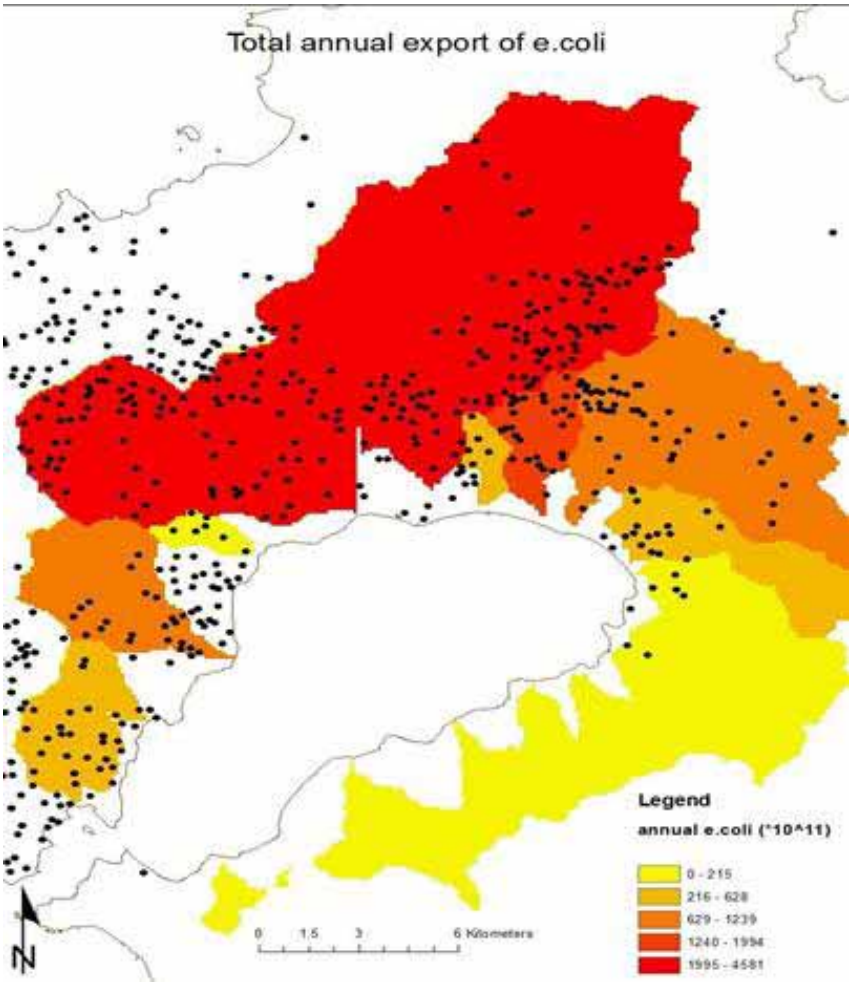


FIGURE 8
Total load of E coli exported from each sub-basin to the bay

TABLE 3
Total nutrient load exported to the bay, permitted export load limits for each and the nutrient removal needed to achieve acceptable status

	Tsiknias	Potamia	Parakoila	Milopotamos	Vouvaris	Ahladeri	Makris	Loutsas	Glaros
Flow (hm^3/yr)	21.4	21.4	4.5	9.3	21.5	1.9	6.5	2.4	9.1
Total export N(kg/yr)	23289	10519	3098	6917	1244	323	410.2	456	995
Total export P(kg/yr)	8500	4000	1200	2500	283	57	64	53	122
Permitted limit N(kg/yr)	20508	20508	4239	8761	20253	1790	6123	2261	8572
Permitted limit P(kg/yr)	2504	2504	526.5	1088	2515	222.3	760.5	280.8	1064.7
Total N(kg/yr) for removal	2781	0	0	0	0	0	0	0	0
Total P(kg/yr) for removal	5996	1496	673.5	1412	0	0	0	0	0

While InVEST can provide estimates of nutrient and *E. coli* loads to the Gulf of Kalloni, the use of indicators for the assessment of marine ecological status would provide a better view of the permissible limit of nutrient export to the bay. With the nutrient values calculated in this study, and data on chlorophyll and dissolved oxygen, a more reliable analysis of the ecological status of the entire bay could be calculated. The cost of a range of nutrient and bacterial removal options could be computed, with advantages and disadvantages of each, as an aid to water resources planning.

CONCLUSION

Application of the InVEST ecosystem services model to estimate nutrient loads to the Gulf of Kalloni using default export coefficients leads to underestimation of loads. We attribute this to underestimation of loads from grazing land, and provide new export coefficients based in the density of livestock farms. The "Water Purification: Nutrient Retention" sub model of InVEST in combination with calibration including the influence of livestock farms is judged to be effective in estimating loads and in providing user friendly output for use in developing management scenarios. The model is also successfully used for estimation of bacterial loads. On the basis of the results we recommend and provide costs for nutrient and bacterial mitigation measures.

Simulations of the effect of scenario changes in climate on nutrients and run-off suggests no major change, although because the model generates annual load estimates the effect of changes in the within-year distribution of rainfall or pollutant sources may not be adequately captured by InVEST.

ACKNOWLEDGEMENTS

Theodoros Chalazas is funded by ERASMUS+ for his research visit to Hangzhou Dianzi University, China. We extend special thanks to Hangzhou Dianzi University (HDU), School of Management, the International Office and Dr. Zhang Ning for making the visit possible. We thank students and staff of the Marine Science Department Provatas S., Provatas N., Spartalidou O.-M., Vagi M. Kostopoulou M. for their help in field work and laboratory analysis. Also Prof. Kalabokidis Kostas (Geography department) who provided us with the meteorological data. Prof. Tzoraki is grateful to the Coastal Zone Management MSc for providing partial support with the necessary software. This work was partly funded by the North Aegean Region, as a part of the project "Environmental Health research of Kallonis gulf, National project".

REFERENCES

[1] UNEP-MAP (2010) Chapter 2 Ecosystem and their services In: Ecosystems and Human Well-being: A Framework for Assessment, 49-70, Island Press, Washington, DC.

[2] Kelble, C.R., Loomis, D.K., Lovelace, S., Nuttle, W.K., Ortner, P.B., Fletcher, P., Cook, G.S., Lorens, J.J., Boyer, J.N. (2013) The EBM-DPSER Conceptual Model: Integrating Ecosystem Services into the DPSIR Framework. PLoS ONE. 8(8), e70766.

[3] Boithias, L., Terrado, M., Corominas, M., Ziv, G., Kumar, V., Marques, M., Schuhmacher, M., Acuna, V. (2016) Analysis of the uncertainty in the monetary valuation of ecosystem services — A case study at the river basin scale. Science of the Total Environment. 543(Part A), 683-690.

[4] Cross, W.F., Baxter, C.V., Donner, K.C., Rosi-Marshall, E.J., Kennedy, T.A., Hall, R.O. Jr, Kelly, H.A., Rogers, R.S. (2011) Ecosystem ecology meets adaptive management: Food web response to a controlled flood on the Colorado River, Glen Canyon. Ecological Applications. 21(6), 2016-2033.

[5] Eskew, E.A., Price, S.J. and Dorcas, M.E. (2012) Effects of River-Flow Regulation on Anuran Occupancy and Abundance in Riparian Zones. Conservation Biology. 26(3), 504-512.

[6] Webb, J.A., Nicol, S.J., Norris, R.H., Stewardson, M.J., Wealands, S.R., Lea, P. (2012) Ecological Responses to Flow Alteration: Assessing Causal Relationships with Eco Evidence. Wetlands. 32(2), 203-213.

[7] Gido, K.B., Propst, D.L., Olden, J.D., Bestgen, K.R. (2013) Multidecadal responses of native and introduced fishes to natural and altered flow regimes in the American Southwest. Canadian Journal of Fisheries and Aquatic Sciences. 70(4), 554-564.

[8] Bea, S.A., Wainwright, H., Spycher, N., Faybishenko, B., Hubbard, S.S., Denham, M.E. (2013) Identifying key controls on the behavior of an acidic-U(VI) plume in the Savannah River Site using reactive transport modeling. Journal of Contaminant Hydrology. 151, 34-54.

[9] Laflen, J.M., Foster, G.R. and Onstad, C.A. (1985) Simulation of individual- storm soil loss for modeling the impact of soil erosion on crop productivity. Soil erosion and conservation. Soil conservation Society of America, Ankeny, Iowa, 285-295.

[10] Bernal, S., von Schiller, D., Sabater, F., Martí, E. (2013) Hydrological extremes modulate nutrient dynamics in Mediterranean climate streams across different spatial scales. Hydrobiologia. 719(1), 31-42.

[11] McCorquodale, J.A. (2007) Storm-water jets and plumes in rivers and estuaries. Canadian Journal of Civil Engineering. 34(6), 691-702.

[12] Tzoraki, O., Nikolaidis, N.P., Cooper, D., Kassotaki, E. (2014) Nutrient mitigation in a temporary river basin. Environmental Monitoring and Assessment. 186(4), 2243-2257.

[13] Natural Capital Project. (2006–2017) Natural Capital Project [Internet]. Available from: http://www. naturalcapitalproject.org.

[14] Li, Y., Luo, Y., Liu, G. (2013) Effects of land use change on ecosystem services: A case study in Miyun reservoir watershed. Shengtai Xuebao/ Acta Ecologica Sinica. 33(3), 726-736.

[15] Wang, D.S., Zheng, H., Ouyang, Z.Y. (2014) Ecosystem services' spatial characteristics and their relationships with residents' well-being in Miyun Reservoir watershed. Shengtai Xuebao/ Acta Ecologica Sinica. 34(1), 70-81.
[16] Cho, K.H., Patchepsky, Y.A., Oliver, D.M., Muirhead, R.W., Park, Y., Quilliam, R.S., Shelton, D.R. (2016) Modeling fate and transport of fecally-derived microorganisms at the watershed scale: State of the science and future opportunities. Water Research. 100, 38-56.
[17] Turc, L. (1961) Estimation of irrigation water requirements, potential evapotranspiration: a simple climatic formula evolved up to date. Annals of Agronomy. 12, 13-49.
[18] Provatas, S., Tzoraki, O., Spartalidou, O.-M., Kostopoulou, M., Kyriakidis, F. (2015) Spatiotemporal analysis of river water quality of insular basins: The case of Tsiknias, Lesvos. 11th Hellenic Symposium of Oceanography and Fishery, 13-17 May 2015, Mytilene, Lesvos, Greece.
[19] Alpert, P., Krichak, S.O., Osetinsky, I., Dayan, M., Haim, D., Shafir, H. (2008) Climatic trends to extremes employing regional modeling and statistical interpretation over the E. Mediterranean. Global Plan. Change. 63, 163–170.
[20] Laschou S. (2010) Identifying Reference Conditions and Classification System Development of Nutrient for Assessment of Chemical-physico- chemical state of the Greek rivers. Master Thesis, University of Athens-HCMR, Athens.
[21] Herr J., Brown and Caldwell (2016) Selecting the most cost effective bmps for the removal of specific no point source pollutants. NEWEA (New England Water Environment Association) annual conference.
[22] US EPA (1986) Design Manual. U.S. Environment Protection Agency, EPA/625/1-86/021, Cincinnati, OH.
[23] White, G.C. (2010) Handbook of Chlorination and Alternative Disinfectants, 5th ed, Wiley Interscience Publication, N.Y.
[24] Cho, K.H., Patchepsky, Y.A., Kim, M., Pyo, J., Park, M., Kim, Y.M., Kim, J.W., Kim, J.H. (2016) Modeling seasonal variability of fecal coliform in natural surface waters using the modified SWAT. Journal of Hydrology. 535, 377-385.

Received: **28.04.2017**
Accepted: **26.09.2017**

CORRESPONDING AUTHOR

Theodoros Chalazas
Department of marine sciences
University of the Aegean
Mytilini– Greece

e-mail: chalazasthodoros@gmail.com

© by PSP Volume 26 – No. 12A/2017 pages 7860-7873 Fresenius Environmental Bulletin

AN EVALUATION OF SEDIMENT YIELD EVOLUTIONS FOR DIFFERENT SUB-CATCHMENTS AND LAND USE TYPES IN THE YANHE RIVER WATERSHED, LOESS PLATEAU

Lei Wu[1,2,3,*], Mengling Peng[1,2], Xia Liu[4]

[1]College of Water Resources and Architectural Engineering, Northwest A&F University, Yangling, Shaanxi 712100, P.R. China
[2]Key Laboratory of Agricultural Soil and Water Engineering in Arid and Semiarid Areas, Ministry of Education, Northwest A&F University, Yangling, Shaanxi 712100, P.R. China
[3]State Key Laboratory of Soil Erosion and Dryland Farming on the Loess Plateau, Northwest A&F University, Yangling, Shaanxi 712100, P.R. China
[4]Construction Department, Northwest A&F University, Yangling, Shaanxi 712100, P.R. China

ABSTRACT

A GIS-based dynamic sediment yield model based on the USLE equation was established to investigate sediment yield evolutions in an easily-eroded watershed of the Loess Plateau from 1995 to 2012. Results indicate that: 1) the dynamic model considering annual changes of precipitation and land management can be used as an effective tool to evaluate sediment yield levels of the Loess Plateau; 2) The annual sediment yield in the Yanhe River watershed has an overall decreasing trend, the average sediment yield modulus from 2009 to 2012 was 1013.3 t/km^2.a, it decreased by about 80.7% compared with the early governance period (1995-1998). The river banks are the main spatial source areas of sediment peak value in the whole Yanhe River watershed, effects of soil and water reduction were significant in the Yanhe River upstream basin and the Xingzi River basin; 3) The sediment yield intensity in 2010 presented an overall increasing trend compared with 1995, the intensity of sediment yield modulus is still increasing for the high intensity of rainfall erosivity. The contribution rate of sediment yield (239-452 t/hm^2) in water area dramatically increased to 80.8% in 2010. Results may provide scientific reference for the ecological environment planning of the Loess Plateau.

KEYWORDS:
Sediment yield, Dynamic model, Sub-catchment, Land use change, Yanhe River watershed

INTRODUCTION

The Loess Plateau is one of the serious soil erosion regions in China or even in the world [1]. Serious soil erosion not only exacerbates deterioration of ecological environment, but also leads to a large number of sediment flowing into the Yellow River [2]. Factors affecting soil erosion were divided into two categories: natural factors and anthropogenic factors [3]. Natural factors in this region mainly include the concentrated precipitation, the loose soil, the fragmentized topography and the degraded vegetation ecosystem, etc. [4]; and anthropogenic factors include destruction of vegetation (such as reclamation, deforestation, overgrazing) and slope land reclamation (such as land reclamation on steep slopes, slope tillage, overgrazing), or lack of preventive measures for mining and road repairing, etc. [5]. The natural factor (or called the potential factor) is the prerequisite to the occurrence and development of soil erosion, the anthropogenic factor is the main reason for the aggravation of soil erosion [6]. Yanhe River is the first grade tributary of the Yellow River, the soil in the watershed is mainly the loessial soil, its erosion wear resistance is poor, the watershed is one of the most typical erosion regions of the Loess Plateau [7]. After the implementation of returning farmland project in the late 1990s, the land use patterns and soil erosion status both have undergone great changes in this watershed [8-9]. Therefore, the modeling assessment of sediment load under returning farmland conditions in the Yanhe River watershed has important significance for revealing characteristics of sediment yield in this region, enhancing soil and water conservation effectiveness, preventing soil degradation and reducing sediment into the Yellow River.

Because of lacking enough measured data, it is very difficult, even impossible to apply conceptual and physical models in evaluating erosion and sediment yield for many large watersheds [10-11]. Therefore, empirical models are widely used in sediment yield modeling, particularly when only limited data are available [12]. In all empirical models of soil loss, the Universal Soil Loss Equation (USLE) [13] is one of the typical models in the study of sheet, rill and slope erosion at field and catchment scales [14-16]. Due to its convenience in application and compatibility with geographical information system (GIS), the USLE or its revised form (RUSLE) [17] has been dominantly used in GIS-based soil erosion assessments in different countries [18-20]. GIS-based models have been increasingly used to identify critical zones of high or low sediment yield and then to prioritize sites for restoration or implementation of best practices [21]. The application effects of these models have been validated in many recent studies [22], and this erosion module has been applied in some physical-based nonpoint source (NPS) models to assess soil erosion amount [23-25]. The spatially distributed NPS models like GWLF, SWAT, SEDEM and AGNPS models are all based on USLE or its revised form [26]. Besides, various regression models and intelligent algorithms have been developed so far to identify the relation between discharge and sediment load [27].

However, many studies have demonstrated that the application of the USLE/RUSLE model needs proper corrections based on watershed characteristics and research purposes [28]. For instance, based on the current situation of China's soil and water conservation, Liu et al. (2001) proposed simple Chinese soil loss equation (CSLE) based on USLE/RUSLE [29], it has been used in the quantitative study of soil erosion in many regions by Chinese scholars [30-31]. Santos et al. (2017) combined the USLE and the SDR to investigate the processes of sediment propagation in a semi-arid region and the identification of areas susceptible to water erosion [32].

Land use change can accelerate or reduce soil erosion by changing vegetation types and coverage, soil properties, terrain, slope, slope length and other factors [33]. Land use change has direct or indirect impact on ecological environment factors [34], it has been widely applied to studies of surface runoff, soil erosion and nonpoint source pollution [35]. Therefore, the objectives of this study are to: 1) establish and verify a dynamic sediment yield model suitable for the hilly and gully region of the Loess Plateau; 2) simulate the spatiotemporal distribution of sediment yield by the combined use of dynamic model, remote sensing and GIS techniques; and 3) evaluate impacts of sub-catchment and land use change on sediment yield of the Yanhe River watershed. Results may also provide methodological reference for the study of watershed sediment yield and data support for the comprehensive management of the hilly and gully region, Loess Plateau.

MATERIALS AND METHODS

Study area. The Yanhe River, which originates from the Baiyu Mountain of Jingbian County, is the first grade tributary between Hekou town and Longmen in the middle reaches of the Yellow River (Fig.1a). The full-length of Yanhe River mainstream is 286.9 km, it flows through five counties (districts) including Jing-bian, Zhi-dan, An-sai, Baota and Yangchang in Shaanxi province from northwest to southeast, and finally it empties into the Yellow River in Nanhe ditch, Yan-chang county (Fig. 1b). The Yanhe River watershed (108°38′~110°29′E and 36°21′~37°19′N) (Fig. 1c) has criss-cross ravines and gullies, broken terrain, and low vegetation coverage. The total watershed area is 7725 km^2, where the area of soil erosion is 7127 km^2, which accounts for 92.3% of the total area. The governance area is 2533.8 km^2 , and the governance rate is 35.6% [36]. The average annual precipitation is about 495.6 mm and almost 60% of the precipitation occurs in 7-9 months. The average annual runoff amount is about 293 million m^3 [37]. Soils in this watershed mainly consist of loessal soil, alluvial soil, clay soil and Heilu soil etc., where the most widely distributed soil is loessal soil.

Environmental database. The environmental data in the study include digital elevation (DEM), land use, soil, meteorological data, runoff, and sediment (Table 1).

Dynamic sediment yield model. In general, the shallow gully erosion is one of the main ways of soil erosion in the middle and lower part of the sloping land, especially it has an important role in the slope soil erosion of Chinese loess plateau [38], in addition, not all eroded soil is actually delivered to the basin outlet, so the shallow gully erosion was introduced to estimate sediment yield of the Yanhe River watershed based on the RUSLE model,

$$Q_s = \lambda \cdot R \cdot K \cdot L \cdot S \cdot G \cdot C \cdot P \quad (1)$$

where Q_s is the average annual sediment yield (t/(ha• a)); λ is the sediment delivery ratio; R is the rainfall erosivity factor, MJ • mm/(ha • h • a); K is the soil erodibility factor, t • ha • h/(ha • MJ • mm); LS is the slope length and slope gradient factor; G is the shallow gully erosion factor; C is the vegetation cover and management factor; P is the soil and wa-

ter conservation factor; λ represents the average sediment delivery ratio.

As far as the whole basin is concerned, its topography and soil characteristics are basically invariant for a relatively short time [39]. Dynamic variations of soil erosion and sediment yield arise predominately from those of hydrology conditions including rainfall amount and rainfall intensity, and human activities including land use management measures, soil and water conservation measures etc. [40-41]. Therefore, based on previous studies [42-44], factors of K, L, and S in Eq. (1) can be assumed to be constant because they reflect topography and soil characteristics, but the other factors will change year by year with hydrological conditions and human activities. Thus, Eq. (1) will change into the continuous model of annual sediment yield as:

$$Q_{s\,i} = K \cdot L \cdot S \cdot G \cdot R_i \cdot C_i \cdot P_i \cdot \lambda_i \quad (2)$$

where subscript i represents the i -th year and no subscript for the average year.

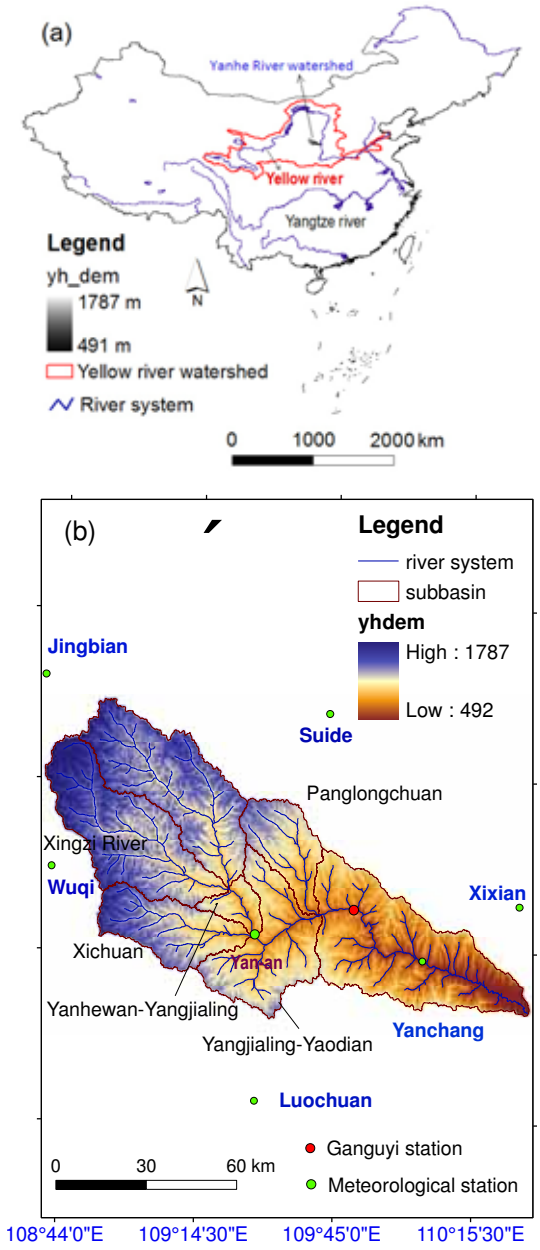


FIGURE 1

(a) the relative location of the study area; (b) geographical location of meteorological stations, longitude and latitude coordinates, digital elevation model (DEM), and the delineation of sub-catchment and river systems of the Yanhe River watershed

TABLE 1
Descriptions and sources of the environmental database in the Yanhe River watershed

Data layer	Format	Description	Source
DEM	Raster	30 m spatial resolution DEM data of the Yanhe River watershed	Computer Network Information Center, Chinese Academy of Sciences http://www.gscloud.cn/
Land use	Raster	100 m spatial resolution reclassified land use types: farmland, grassland, forest land, rural settlements, water area, sandy land	Data Center for Cold and Arid Region Sciences http://westdc.westgis.ac.cn/
Meteorological data	DBF	Daily meteorological data from 8 rain gauges (1957-2012)	China Meteorological Data Sharing Service Network http://www.cdc.sciencedata.cn/
Soil	DBF	Physical properties: soil textures (clay, silt, sand, rock percentages), organic matter content	Loess Plateau Data Center, National Earth System Science Data Sharing Infrastructure, National Science & Technology Infrastructure of China (http://loess.geodata.cn/)
Runoff and sediment	Excel	Daily observed values of runoff and sediment in Ganguyi hydrological stations (1956-2011)	

The variations of R_i in Eq. (2) depend only on hydrological conditions while C_i and P_i only on human activities, but λ_i not only on hydrological conditions but also on human activities. Supposing that the factor λ_i can be divided approximately into the product of $\lambda_{r,i}$ related only to hydrological conditions and $\lambda_{m,i}$ related only to human activities, Eq. (2) will be written as:

$$Q_{s\,i} = K \cdot L \cdot S \cdot G \cdot R_i \cdot C_i \cdot P_i \cdot \lambda_{r,i} \cdot \lambda_{m,I} \quad (3)$$

$\lambda_{r,i}$ can be estimated by the sediment transport capacity that is widely used in hillslope and fluvial geomorphology [45]. The widely used equation is:

$$\frac{\lambda_{r,i}}{\lambda_r} = \frac{TC_i}{TC} = \left(\frac{q_i}{q}\right)^{1.4} \quad (4)$$

where TC is the average sediment transport capacity per unit width of slope (kg m^{-3}); q is the average runoff amount per unit width (m^3); λ_r is the average sediment delivery ratio related only to hydrological conditions.

$\lambda_{m,i}$ can be determined by definition of the land management factor η_i which is only related to human activities:

$$\eta_i = \frac{\lambda_{m,i} \cdot C_i \cdot P_i}{\lambda_m \cdot C \cdot P} \quad (5)$$

The Chinese government has been carried out various soil and water conservation measures in the Yanhe River watershed since the late 1960s [46-47]. Generally, the time range from 1956 to 1969 is determined as the base period, the time ranges of 1970-1996 and 1997-2012 are regarded as two different governance periods [48]. The land management factor can be supposed to be equal to the ratio of the regression relationship between runoff and sediment of Ganguyi hydrological station in different periods [49].

$$\eta_{i1} = \frac{0.4507\,Q_i - 0.5053}{0.4448\,Q_i - 0.4494} \quad (1956\text{-}1996) \quad (6)$$

$$\eta_{i2} = \frac{0.4037\,Q_i - 0.4266}{0.4448\,Q_i - 0.4494} \quad (1997\text{-}2012) \quad (7)$$

where η_{i1} and η_{i2} are the land management factor during 1956-1996 and 1997-2012 period, respectively; Q_i is the annual runoff amount of the basin in the i-th year ($10^8 m^3$).

Therefore, Eq. (3) can be rewritten as:

$$E_{s,i} = \eta_i \cdot \left(\frac{q_i}{q}\right)^{1.4} \cdot R_i \cdot \lambda \cdot K \cdot L \cdot S \cdot G \cdot C \cdot P \quad (8)$$

Determination of model factors. Rainfall erosivity was estimated by a half-month simple algorithm of rainfall erosivity established by Zhang et al. (2003) in this study [50]; Soil erodibility in this study was determined by the existing empirical equation [51], the K factor are calculated by the modified method of soil erodibility [52]; the slope length and slope gradient factor was determined by the previous results [53]; the shallow gully erosion factor is mainly affected by precipitation, the intensity of convergent flow, and soil property. Its value can be estimated by the existing research results [54]; the values of the C factor in the Yanhe River

watershed was obtained according to the relevant literatures and statistical data [55-56]; based on land use types, the *P* values in this study are determined by the related literature [57-58]. The average and annual values of the related factors in the Yanhe River watershed are shown in Table 2 and Figure 2.

RESULTS

Validation of sediment yield model. The previous results of the Yanhe River watershed can be used to verify the established sediment yield model. The previous research results of sediment variations in Ganguyi hydrological station from 1961 to 2008 and the simulation results of sediment yield in this study were comparatively analyzed that the sediment yield both showed a decreasing trend although there were slight fluctuations in individual years, it indicates that the overall changing trends of sediment yield in the study area are consistent with the background of returning farmland.

In addition, according to Li and Zheng (2012) dynamic simulation results of soil erosion in the Yanhe River watershed from 2001 to 2010 [59], the annual average erosion modulus of Yanhe River watershed is 5812.28 t/(km^2.a), it has little difference with the average simulated value of 5051.68 t/(km^2.a) in this study from 1995 to 2012, the relative error is 13.09%; these results demonstrate that the established dynamic sediment yield model has scientific rationality and good reliability.

Temporal variations of sediment yield. The inter-annual rainfall variability will be the key driver of variations in annual sediment yield, but Fig.3 shows that the sediment yield amount in the study area has an overall decreasing trend from 1995 to 2012, power algorithm fitting a curve through sediment yield over time can prove that soil and water conservation measures have a significant effect on sediment export from the watershed. The average sediment transport modulus in recent years (2009-2012) is 1013.3 t/km^2, it has decreased by about 80.7% compared with the early governance (1995-1998). For the occurrence of non extreme heavy rainfall in the watershed, the main reason for the decreasing sediment mainly can be attributed to soil and water conservation measures. Since the late 1990s, a lot of targeted soil and water conservation measures were implemented in the Yanhe River watershed, the intensity of soil and water conservation measures was gradually increased in the middle reaches of the Yellow River, underlying surface conditions were continuously improved and soil erosion risks reduced a lot. Especially after 2003, the sediment transport in the study area not only has an overall decrease trend, but also the inter-annual fluctuation is small and the whole sediment transport level is low. It also fully shows that the continuous improvement of the underlying surface conditions and the effective implementation of soil and water conservation measures in recent years have significant reduction benefits of water and sediment.

Spatial variations of sediment yield. Fig.4 shows spatial distribution of the sediment yield modulus in the Yanhe River watershed in 1995 and 2010. Due to more sloping farmland, peak values of the sediment transport modulus mainly occur along the main river banks from northeast to southeast. Spatial variations of sediment transport in the whole watershed are largely related to spatial distribution of land use types. The large spatial variations of sediment transport are also closely related to spatial characteristics of rainfall, topography and soil types.

TABLE 2
The average value of each factor for the dynamic erosion and sediment yield model

Factor	*K* (t•hm^2•h/hm^2•MJ•mm)	*LS*	*G*	*C*	*P*
Value	0.01765	12.9	1.5	0.3359	0.2135

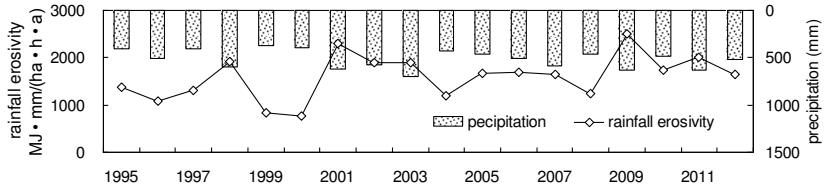


FIGURE 2
Annual precipitation (mm) and rainfall erosivity (MJ•mm/hm^2•h•a) in the Yanhe River watershed

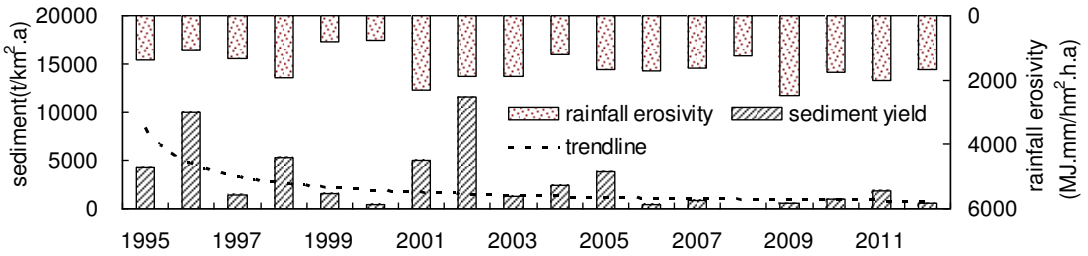


FIGURE 3
Comparison of the rainfall erosivity and the sediment transport modulus from 1995 to 2012 in the Yanhe River watershed

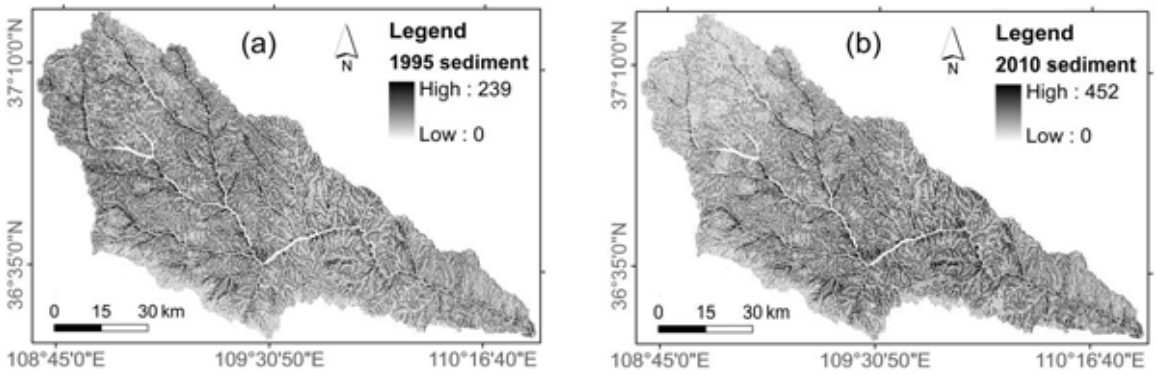


FIGURE 4
Spatial distribution of sediment yield modulus in the Yanhe River watershed (a) 1995, (b) 2010 (t/hm^2)

Table 3 shows that percentage of different sediment yield modulus in 1995 and 2010 may both decrease with the increase of sediment yield gradations. Although the soil and water conservation measures were implemented in this area since 1997, the sediment yield modulus in 2010 did not decrease as we deduced. The main reason may be attributed to the large rainfall erosivity in 2010.

DISCUSSION

Sediment yield in each sub-catchment. Fig.5 shows (a) percentage of different sediment yield modulus in different sub basins and (b) contribution ratio of each sub basin for different sediment yield modulus in the Yanhe River watershed in 1995. It can be seen from Figure 5a that in 1995 the sediment yield modulus of 0-30 t/hm^2 held a dominant position in each sub basin of the Yanhe River watershed, it accounted for more than 70% of each sub basin; secondly, the sediment yield modulus of 30-40 t/hm^2 and 40-70 t/hm^2 accounted for about 20% of each sub basin, the modulus of 70-239 t/hm^2 accounted for the smallest proportion, the average proportion was less than 1%; the sediment yield modulus of 20-30 t/hm^2 in Yanhe River upstream basin, Xingzi River basin and Yanhewan to Yangjialing section were all more than 20%, and the sediment yield modulus of 10-20 t/hm^2 in Yanhe River upstream basin and Xingzi River basin exceeded the proportion of 0-10 t/hm^2. So the sediment yield modulus of 0-30 t/hm^2 is the primary occurrence form of sediment Yield in the Yanhe River watershed. It can be seen from Figure 5b that the contribution ratio of the Yanhe River downstream is highest in all sediment yield modulus, it is more than 25%. Secondly, the contribution ratios of each sediment yield modulus in Xingzi River basin and Yanhe River upstream basin were all more than 15%. Therefore, Yanhe River downstream basin, Yanhe River upstream basin and Xingzi River basin are the key regions for the implementation of soil and water conservation measures.

TABLE 3
Percentage of different sediment yield gradations in the Yanhe River watershed in 1995 and 2010

Year	Different sediment yield gradations (t/hm^2)						
	0~10	10~20	20~30	30~40	40~70	70~239	239~452
1995	31.29%	26.92%	20.61%	12.61%	7.77%	0.81%	0.0%
2010	27.07%	24.79%	18.13%	12.77%	14.57%	2.66%	0.003%

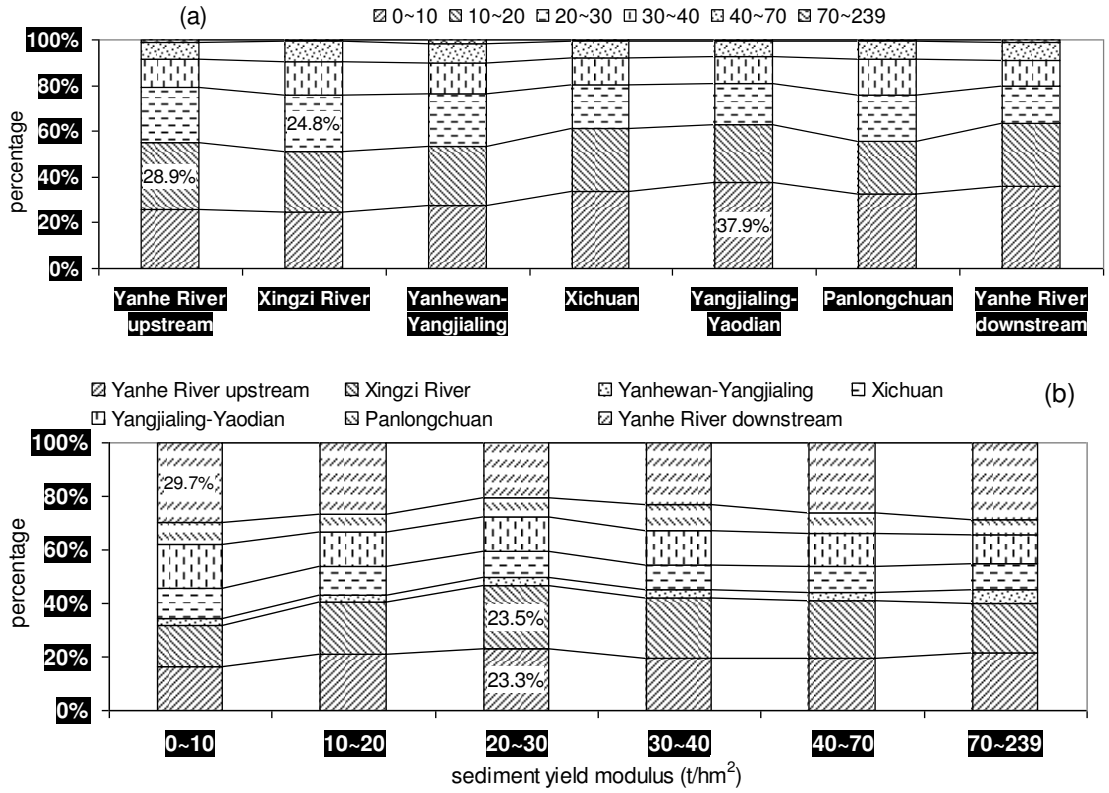


FIGURE 5
(a) Percentage of different sediment transport modulus in different sub basins of the Yanhe River watershed in 1995; (b) Contribution ratio of each sub basin for different sediment transport modulus in the Yanhe River watershed in 1995

Fig.6 shows (a) percentage of different sediment yield modulus in different sub basins and (b) contribution ratio of each sub basin for different sediment yield modulus in the Yanhe River watershed in 2010. It can be seen from Fig. 6a that in 2010 the sediment transport modulus of 0-30 t/hm^2 still occupied a dominant position in each sub basin of the Yanhe River watershed, it accounted for more than 70% of each sub basin, where the proportions of Yanhe upstream basin and Xingzi River basin accounted for more than 75%; secondly, the percentage of sediment yield modulus with a specific value of 30-239 t/hm^2·had an increase trend in other five basins, this is particularly evident in Yanhe River downstream basin, the main reason may be attributed to the implementation of the returning farmland policy since 1997. It can be seen from Fig. 6b that the contribution ratio of the Yanhe River downstream is still the highest percentage in all sediment transport modulus, the sediment yield intensity shows a rising trend compared with 1995, the contribution ratio of Yanhe River downstream significantly increased with the increase of sediment yield modulus, it increased from 21.5% to 76.9%. Therefore, effects of reducing soil and water were significant in the Yanhe River upstream basin and the Xingzi River basin, the Yanhe River downstream basin should further strengthen soil and water conservation measures under the condition of rapid regional economic development.

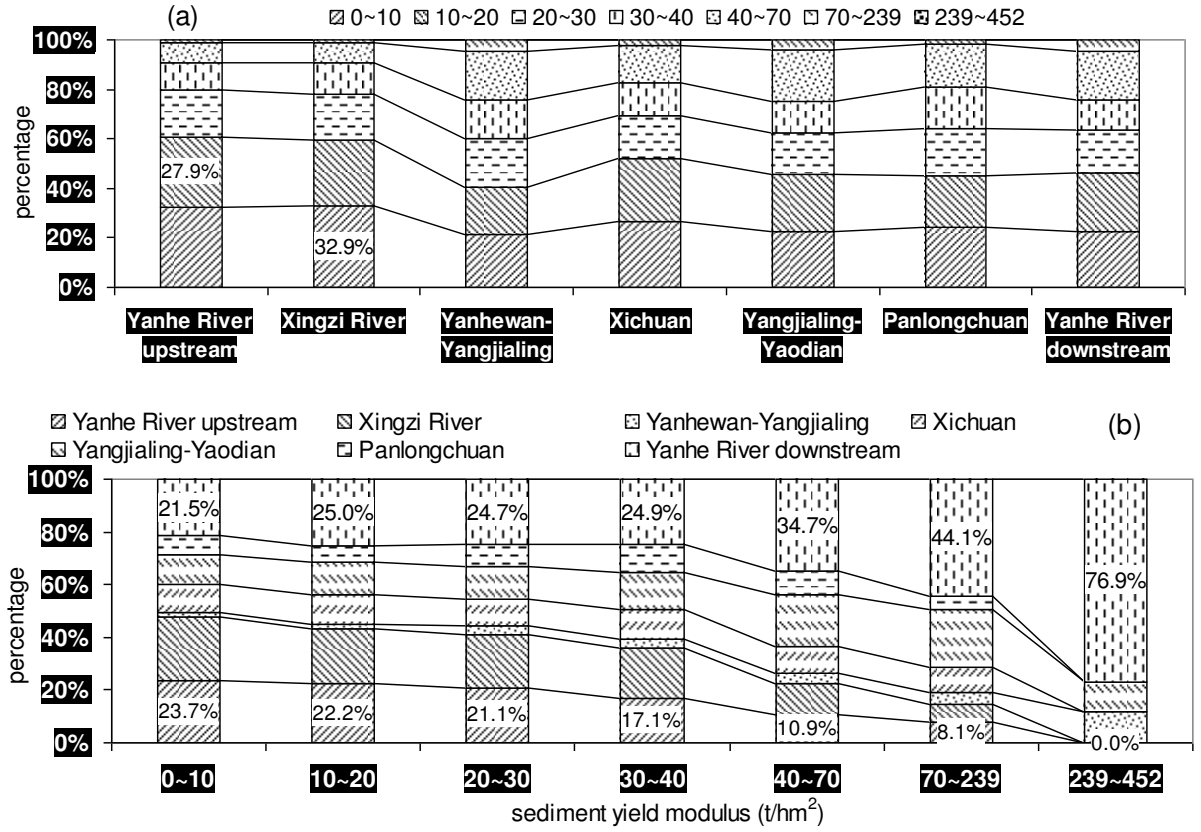


FIGURE 6

(a) Percentage of different sediment transport modulus in different sub basins of the Yanhe River watershed in 2010; (b) Contribution ratio of each sub basin for different sediment transport modulus in the Yanhe River watershed in 2010

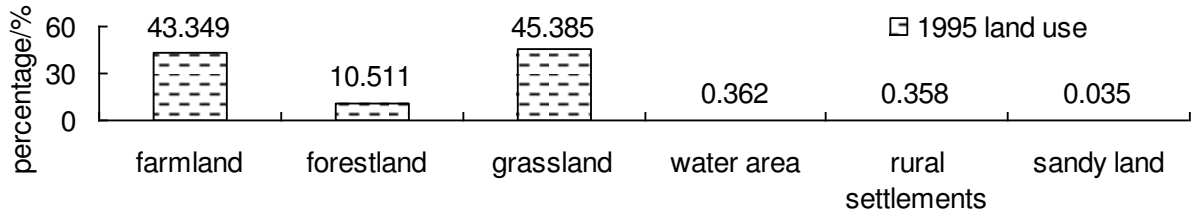


FIGURE 7

Percentage of reclassified land use types in the Yanhe River watershed in 1995

Sediment yield of different land use types in 1995. Fig. 7 shows percentage of reclassified land use types in the Yanhe River watershed in 1995. Farmland and grassland are the two main land use types in the watershed and account for 43.349% and 45.385% respectively.

Fig. 8 shows contribution ratios of each land use type for different sediment transport modulus in the Yanhe River watershed in 1995. It can be seen that the contribution ratio of the grassland has the biggest percentage of 64.1% for the sediment transport modulus of 0-10 t/hm^2, it is followed by the forestland and farmland. The contribution ratio of grassland has a decreasing trend with the increase of sediment yield modulus. However, the contribution ratio of farmland has a significant increasing trend with the increase of sediment yield modulus. The farmland contribution ratio for the sediment yield modulus of 0-30 t/hm^2 has a sharp increase speed, and it is gradually stabilized when the sediment yield modulus is greater than the value of 30 t/hm^2 and also occupies a leading position for the contribution ratio of sediment yield in different land use types. In addition, with the increase of sediment yield modulus, the contribution ratio of

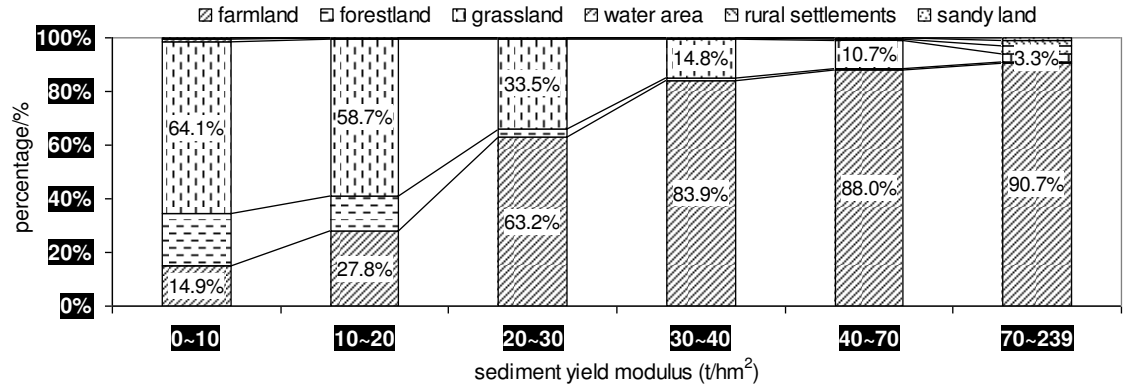


FIGURE 8
Contribution ratios of each land use type for different sediment transport modulus in the Yanhe River watershed in 1995

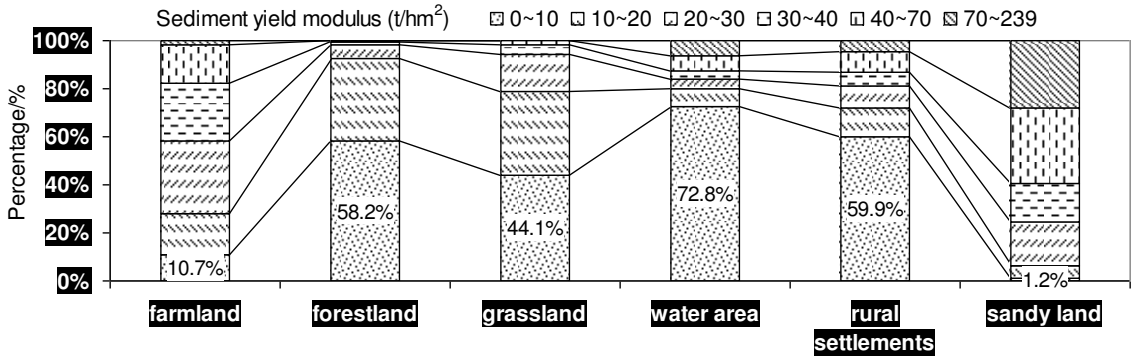


FIGURE 9
Percentage of each sediment transport modulus under different land use types in the Yanhe River watershed in 1995

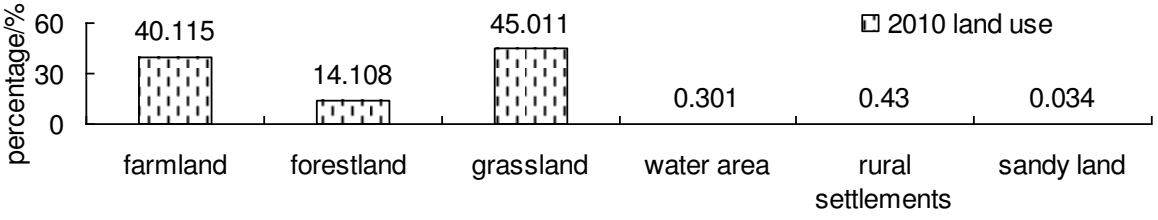


FIGURE 10
Percentage of reclassified land use types in the Yanhe River watershed in 2010

farmland increased significantly, the contribution ratio of forestland also has a gradual decreasing trend, the contribution ratios of rural settlements and sandy land has a slight increasing trend.

Fig. 9 shows percentage of each sediment transport modulus under different land use types in the Yanhe River watershed in 1995. The sediment transport modulus of 20-30 t/hm^2·in farmland accounted for the largest percentage of 30.08%, it was followed by the sediment yield modulus of 30-40 t/hm^2. For forestland, grassland, water area and rural settlements, the sediment yield modulus of 0-10 t/hm^2 accounted for a large proportion, they were 58.2%, 44.1%, 72.8% and 59.9% respectively; for the sandy land, proportion of the sediment yield modulus of 40-239 t/hm^2 increased significantly, they were increased to 31.66% and 27.8% respectively. Therefore, the high intensity of erosion and sediment yield mainly comes from the sandy land and farmland, and it is quite necessary to take reasonable tillage and soil conservation measures to reduce soil erosion.

Sediment yield of different land use types in 2010. Fig. 10 shows percentage of reclassified land use types in the Yanhe River watershed in 2010. Farmland and grassland are the two main land use types in the watershed and account for 40.115% and 45.011% respectively. Compared with 1995, the farmland area decreased but the forestland area increased in 2010. Fig. 11 shows the contribution ratio of each land use type for different sediment transport modulus in the Yanhe River watershed in 2010. For the sediment transport modulus of 0-239 t/hm^2, the contribution ratio of grassland has a decreasing trend with the increase of sediment yield modulus. However, the contribution ratio of farmland has a significant increasing trend with the increase of sediment yield modulus. Compared with 1995, the contribution ratio of the grassland for the sediment transport modulus of 0-10 t/hm^2 has the maximum percentage of 65.11%, it is followed by the forestland and farmland; for the sediment transport modulus of 10-20 t/hm^2, although the contribution ratio of the grassland decreased to 58.02%, it is still the maximum value, it is followed by farmland; for the sediment transport modulus of 20-239 t/hm^2, the contribution rate of farmland increased significantly, it took the dominant position in all land use types. Besides, with the increase of sediment modulus, the contribution rates of forest land also decreased gradually, however, the contribution ratio of farmland in the sediment yield modulus of 239-452 t/hm^2 fell sharply, and the contribution rate of water area and rural settlements increased dramatically to 80.8% and 11.5%.

Fig. 12 shows percentage of each sediment yield modulus for different land use types in the Yanhe River watershed in 2010. Compared with 1995, the sediment yield modulus of 40-70 t/hm^2·in farmland accounted for the largest proportion of 30.97%, it was followed by the sediment yield modulus of 30-40 t/hm^2, and the sediment yield intensity had an increasing trend. For forestland, grassland, water area and rural settlements, the sediment yield transport modulus of 0-10 t/hm^2 still accounted for a large proportion, they were 37.1%, 39.3%, 64.2% and 58.1% respectively. Compared with other land use types, the percentage of the sandy land sediment yield modulus of 40-239 t/hm^2 significantly increased to 29.6% and 53.3% respectively. Therefore, although returning farmland measures show good benefits of water and sediment reduction, the intensity of sediment yield modulus is still increasing for the high intensity of rainfall erosivity, which indicates that soil and water conservation measures need to be strengthened in the Yanhe River watershed in order to resist the increase of erosion and sediment yield intensity.

CONCLUSIONS

1) Based on watershed characteristics of the study area, a distributed, dynamic sediment yield model based on the USLE equation was established to investigate impacts of returning farmland measures on sediment yield in the Yanhe River watershed from 1995 to 2012. Validation results indicate that the established model coupling with GIS has characteristics of simple algorithm and highly practical value, it can be used as an effective method to evaluate erosion and sediment yield of the hilly and gully region, Loess Plateau.

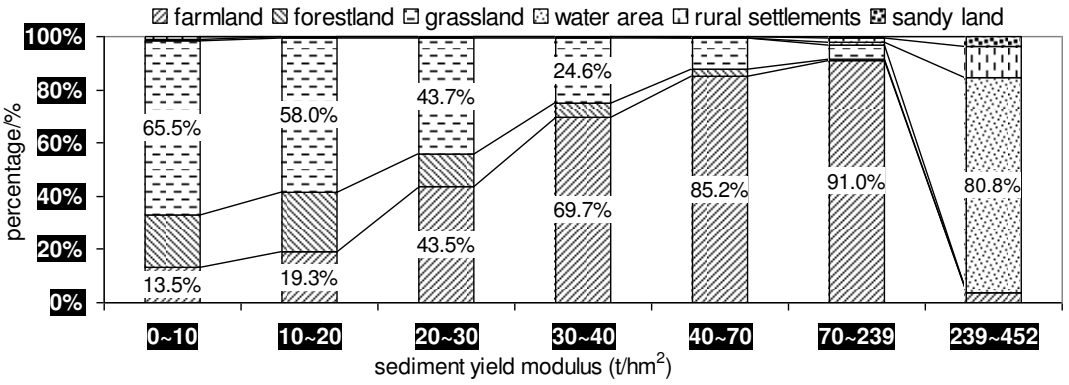


FIGURE 11
Contribution ratios of each land use type for different sediment transport modulus in the Yanhe River watershed in 2010

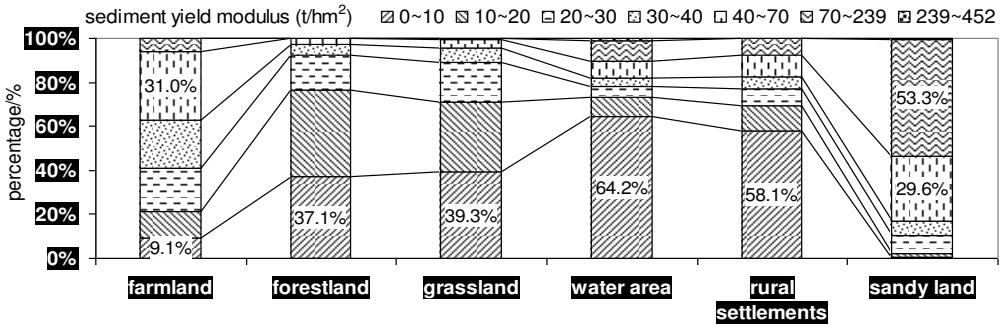


FIGURE 12
Percentage of each sediment transport modulus under different land use types in the Yanhe River watershed in 2010

2) The sediment transport amount in the study area has an overall decreasing trend from 1995 to 2012, the average sediment transport modulus from 2009 to 2012 was 1013.3 t/km^2, it decreased by about 80.7% compared with the early governance from 1995 to 1998 (5239.8 t/km^2). Spatial variations of sediment yield in the whole watershed were largely related to spatial distribution of land use types, peak values of the sediment yield modulus mainly occurred along the main river banks from northeast to southeast through the whole Yanhe River watershed. Effects of reducing soil and water were significant in the Yanhe River upstream basin and the Xingzi River basin, the Yanhe River downstream basin should further strengthen soil and water conservation measures.

3) The sediment yield modulus of 0-30 t/hm^2 held a dominant position in each sub basin of the Yanhe River watershed, it accounted for more than 70% of the total sediment yield modulus in each sub basin in 1995 and 2010. Compared with 1995, the whole sediment yield intensity for the farmland had a rising trend, the contribution ratio of farmland increased significantly with the increase of sediment yield modulus both in 1995 and 2010, but in 2010 the contribution ratio of water area for the sediment yield modulus of 239-452 t/hm^2 increased dramatically to 80.8%.

ACKNOWLEDGEMENTS

Thanks for the data support from "Loess Plateau Data Center, National Earth System Science Data Sharing Infrastructure, National Science & Technology Infrastructure of China (http://loess.geodata.cn)". This study was supported by the National Natural Science Foundation of China (51679206, 51309194), Zhongying Youth Scholars of Northwest A&F University (Z111021720), Youth Science and Technology Nova Project in Shaanxi Province (2017KJXX-91), Arid meteorological science research-the process and mechanism of drought disaster in northern China (201506001), Youth Science and Technology Nova Project in Shaanxi Province (2017KJXX-91), Zhongying Youth Scholars of Northwest A&F University (Z111021720), the Fundamental Research Funds for the Central Universities (2452016120), Special Research Foundation for Young teachers (2452015374), International Science and Technology Cooperation Funds (A213021603).

REFERENCES

[1] Fu, B.J., Zhao, W.W., Zhang, Q.J., Liu, Y. (2014) The Loess Plateau landscape pattern change and soil erosion. Beijing: Science Press.

[2] Wu, L., Liu, X., Ma, X.Y. (2016) Impacts of Grain for Green project on spatiotemporal variations of soil erosion in a typical watershed of Chinese loess hilly and gully region. Fresen. Environ. Bull. 25(11), 4506-4516.

[3] Li, X.X., Ni, J.R. (2009) Spatial similarity between soil erosion and its influencing factors based on information entropy theory. Progress in Geography. 28(2), 161-166.

[4] Jia, Z.W., Jiang, Z.S. (1991) Analysis of soil erosion affected by human activities in the middle part of the Loess Plateau. Bulletin of Soil and Water Conservation. 11(1), 28-33.

[5] Wang, H.B., Xu, J.X., Yan, M. (2011) Effect of Socio-economic Factors on Soil Erosion: A Literature Review. Progress in Geography. 30(3), 268-274.

[6] Wu, W.B., Ji, C.C., Li, X.S., Lu, S.L., Ma, C. (2010) Environmental Factors Affect Water Erosion of Soil. Soil and Water Conservation in China. (5), 36-38.

[7] Zhao, D.B., Liang, W., Yang, Q.K., Liu, A.L. (2008) Analysis of dynamic land use changes of past 30 years in the hilly area of Loess Plateau. Bulletin of Soil and Water Conservation. 28(2), 22-26.

[8] Wu, L., Liu, X., Ma, X.Y. (2016) Impacts of Grain for Green project on spatiotemporal variations of soil erosion in a typical watershed of Chinese loess hilly and gully region. Fresen. Environ. Bull. 25(11), 4506-4516.

[9] Wu, L., Liu, X., Ma, X.Y. (2016) Tracking Soil Erosion Changes in an Easily-Eroded Watershed of the Chinese Loess Plateau. Polish Journal of Environmental Studies, 25(1), 332-344.

[10] Tang, Z.H., Cai, Q.G. (2002) Review on the studies of Chinese main soil erosion and sediment yield models. Journal of Mountain Science, 20(4), 466-475.

[11] Jasrotia, A.S., Singh, R. (2006) Modeling runoff and soil erosion in a catchment area, using the GIS, in the Himalayan region, India. Environ Geol. 51, 29–37.

[12] Merritt, W.S., Letcher, R.A., Jakeman, A.J. (2003) A review of erosion and sediment transport models. Environmental Modelling & Software. 18, 761-799.

[13] Wischmeier, W.H., Smith, D.D. (1978) Predicting rainfall erosion losses: a guide to conservation planning. Agriculture Handbook, vol. 537. US Department of Agriculture, Washington, DC., 58 pp.

[14] Terranova, O., Antronico, L., Coscarelli, R., Iaquinta, P. (2009) Soil erosion risk scenarios in the Mediterranean environment using RUSLE and GIS: an application model for Calabria (southern Italy). Geomorphology. 112, 228-245.

[15] Kinnell, P.I.A. (2010) Event soil loss, runoff and the universal soil loss equation family of models: a review. J Hydrol. 385, 384-397.

[16] Gao, G.Y., Fu, B.J., Lu, Y.H., Liu, Y., Wang, S., Zhou, J. (2012) Coupling the modified SCS-CN and RUSLE models to simulate hydrological effects of restoring vegetation in the Loess Plateau of China. Hydrol Earth Syst Sci. 16, 2347–2364.

[17] Renard, K.G., Foster, G.R., Weesies, G.A., McCool, D.K., Yoder, D.C. (1997) Predicting Soil Erosion by Water: A Guide to Conservation Planning with the Revised Universal Soil Loss Equation (RUSLE). USDA Agriculture Handbook 703, 384pp.

[18] Cohen, M.J., Shepherd, K.D., Walsh, M.G. (2005) Empirical reformation of the universal soil loss equation for erosion risk assessment in a tropical watershed. Geoderma. 124, 235–252.

[19] Krishna Bahadur, K.C. (2009) Mapping soil erosion susceptibility using remote sensing and GIS: a case of the Upper Nam Wa Watershed, Nan Province, Thailand. Environ Geol. 57, 695-705.

[20] Prasannakumar, V., Shiny, R., Geetha, N., Vijith, H. (2011) Spatial prediction of soil erosion risk by remote sensing, GIS and RUSLE approach: a case study of Siruvani river watershed in Attapady valley, Kerala, India. Environ Earth Sci. 64, 965–972

[21] Hamel, P., Falinski, K., Sharp, R., Auerbach, D.A., Sanchez-Canales, M., James Dennedy-Frank, P. (2017) Sediment delivery modeling in practice: Comparing the effects of watershed characteristics and data resolution across hydroclimatic regions. Science of the Total Environment. 580(2017), 1381–1388.

[22] Nigel, R., Rughooputh, S. (2010) Mapping of monthly soil erosion risk of mainland Mauritius and its aggregation with delineated basins. Geomorphology. 114, 101–114.

[23] Polyakov, V., Fares, A., Kubo, D., Jacobi, J., Smith, C. (2007) Evaluation of a non-point source pollution model, AnnAGNPS, in a tropical watershed. Environ Model Soft. 22, 1617–1627.

[24] Gronsten, H.A., Lundekvam, H. (2006) Prediction of surface runoff and soil loss in southeastern Norway using the WEPP Hillslope model. Soil Till Res. 85, 186-199.

[25] Singh, R.K., Panda, R.K., Satapathy, K.K., Ngachan, S.V. (2012) Runoff and sediment yield modelling for a treated hilly watershed in Eastern Himalaya using the water erosion prediction project model. Water Resour Manage. 26, 643–665.

[26] Vente, J.D., Poesen, J., Verstraeten, G., Govers, G., Vanmaercke, M., Rompaey, A.V., Arabkhedri, M., Boix-Fayos, C. (2013) Predicting soil erosion and sediment yield at regional scales: where do we stand? Earth-science Reviews. 127(2), 16-29.

[27] Altunkaynak A. (2009) Sediment load prediction by genetic algorithms, Advances in Engineering Software. 40(2009), 928–934.

[28] Wu, L., Long, T.Y., Liu, X., Ma, X.Y. (2013) Modeling impacts of sediment delivery ratio and land management on adsorbed non-point source nitrogen and phosphorus load in a mountainous basin of the Three Gorges reservoir area, China. Environmental Earth Sciences. 70(3), 1405-1422.

[29] Liu, B.Y., Xie, Y., Zhang, K.L. (2001) Soil erosion predicting model. Beijing: Chinese science and Technology Press.

[30] Cheng, L., Yang, Q.K., Xie, H.X., Wang, C.M., Guo, W.L. (2009) GIS and CSLE based quantitative assessment of soil erosion in Shaanxi, China. Journal of Soil and Water Conservation. 23(5), 61-66.

[31] Song, W.L., Zhang, R.H., Gao, Y.F., Lu, J.X., Yang, S.T., Qu, W., Zhao, D.J. (2014) Study on soil erosion intensity classification based on field survey, remote sensing data and CLSE model. South-to-North Water Transfers and Water Science & Technology. 12(5), 170-174.

[32] Santos, J.C.N.D., Andrade, E.M.D., Medeiros, P.H.A., Palacio, H.A.D.Q., Neto, J.R.D.A. (2017) Sediment delivery ratio in a small semi-arid watershed under conditions of low connectivity, Artigo Científico. 48(1), 49-58.

[33] Chen, L.D., Lv, C.H. (2012) Study on the scale effect of soil loss and land use in Loess Hilly Region. Beijing: Science Press.

[34] Wijesekara, G.N., Gupta, A., Valeo, C., Hasbani, J.G., Qiao, Y., Delaney, P., Marceau, D.J. (2012) Assessing the impact of future land-use changes on hydrological processes in the Elbow River watershed in southern Alberta, Canada. Journal of Hydrology. 412(1), 220-232.

[35] Simonneaux, V., Cheggour, A., Deschamps, C., Mouillot, F., Cerdan, O. Le Bissonnais, Y. (2015) Land use and climate change effects on soil erosion in a semi-arid mountainous watershed (High Atlas, Morocco). Journal of Arid Environments. 122, 64-75.

[36] Wu, Z. (2007) A regional soil erosion model design and development based on GIS. Xi'an: Master's degree thesis of Northwestern University.

[37] Ren, Z.P., Zhang, G.H., Yang, Q.K. (2012) Characteristics of runoff and sediment variation in Yanhe River basin in last 50 years. Journal of China Hydrology. 32(5), 81-86.

[38] Li, B.B., Zheng, F.L., Long, D.C., Jiang, Z.S. (2009) Spatial distribution of soil erosion intensity in Zhifanggou small watershed based on GIS. Scientia Geographica Sinica. 29(1), 105-110.

[39] Wu, L., Liu, X., Ma, X.Y. (2016) Spatio-temporal variation of erosion-type non-point source pollution in a small watershed of hilly and gully region, Chinese Loess Plateau. Environmental Science and Pollution Research. 23, 10957-10967.

[40] Molla, T., Sisheber, B. (2017) Estimating soil erosion risk and evaluating erosion control measures for soil conservation planning at Koga watershed in the highlands of Ethiopia. Solid Earth. 8, 13-25.

[41] Wu, L., Long, T.Y., Liu, X., Mmereki, D. (2012) Simulation of Soil Loss Processes Based on Rainfall Runoff, and the Time Factor of Governance in the Jialing River Watershed, China. Environmental Monitoring and Assessment. 184(6), 3731-3748.

[42] Wu, L., Long, T.Y., Cooper, W.J. (2012) Temporal and Spatial Simulation of Adsorbed Nitrogen and Phosphorus Non-point Source Pollution load in Xiao Jiang Watershed of Three Gorges Reservoir Area, China. Environmental Engineering Science. 29(4), 238-247.

[43] Long, T.Y., Wu, L., Li, J.C., He, C. (2012) Development of an adsorbed phosphorus pollution load model and application to the Jialing River basin, China. Fresen. Environ. Bull. 21(12b), 3920-3929.

[44] Wu, L., Liu, X., and Ma, X. (2016) Application of a modified distributed-dynamic erosion and sediment yield model in a typical watershed of a hilly and gully region, Chinese Loess Plateau, Solid Earth. 7, 1577-1590.

[45] Prosser, I.P., Rustomji, P. (2000) Sediment transport capacity relations for overland flow. Progress in Physical Geography. 24, 179-193.

[46] Yao, W.Y., Xu, J.H., Ran, D.C. (2011) Analysis and evaluation of water and sediment change situation in the Yellow River Basin. Zhengzhou: Yellow River Conservancy Press.

[47] Qiu, L.J., Zheng, F.L., Yin, R.S., Yu, F.Y. (2011) Quantification of Impacts of Precipitation Change and Human Activities on Streamflow in the Yanhe River Basin. Advances in Climate Change Research. 7(5), 357-362.

[48] Xu, X.X., Gao, Z.X., Zhao, J.N. (2014) Trends of runoff and sediment load of Yanhe River Basin and their related driving forces during 1956-2009. Journal of Sediment Research. 2012(2), 12-18.

[49] Ran, D.C., Yao, W.Y., Wu, Y.H., Li, X.M., Lv, X.Z. (2014) Effect of forest-grass vegetation on reducing flood and sediment from 1997 to 2006 in Yanhe basin. Science of Soil and Water Conservation. 12(1), 1-9.

[50] Zhang, W.B., Xie, Y., Liu, B.Y. (2003) Spatial variation of rainfall erosion in China. Journal of Mountain Science. 21(1), 33-40.

[51] Liu, B.Y., Bi, X.G., Fu, S.H. (2010) Beijing Soil Erosion Equation. Beijing: Science Press, 52-67.

[52] Zhang, K.L., Peng, W.Y., Yang, H.L. (2007) Soil erosion and its estimation for agricultural soil in China. Acta Pedologica Sinica. 44(1), 7-13.

[53] Wang, X.Y., Wang, X.F., Wang, Q.P., Wang, Z.G., Cai, X.G. (2004) Loss of nonpoint source pollutants from Shixia small watershed, Miyun Reservoir, Beijing. Scientia Geographica Sinica. 24(2), 227-231.
[54] Jiang, Z.S., Zheng, F.L., Wu, M. (2008) China Water Erosion Prediction Model. Beijing: Science Press, 200-202.
[55] Wu, L., Liu, X., Ma, X.Y. (2017) Effects of elevation on sediment yield in a highly erodible watershed of Chinese Loess Plateau. Fresen. Environ. Bull. 26(5), 3300-3308.
[56] Wu, L., Qi, T., Zhang, J. (2017) Spatiotemporal Variations of Adsorbed Nonpoint Source Nitrogen Pollution in a Highly Erodible Loess Plateau Watershed. Polish Journal of Environmental Studies. 26(3), 1343-1352.
[57] Cheng, J.M., Song, T., Li, Y. (2012) Estimation of nitrogen and phosphorus loading of agricultural nonpoint sources along Nanxi Lake based on GIS. Research of Soil and Water Conservation. 19(3), 284-288.
[58] Xie, H.X. (2008) Study on the spatio-temporal change of soil loss and on the assessment of impacts on Environment of soil and water conservation in Yanhe basin. Xi'an: Doctoral Dissertation of Shaanxi Normal University, 47-59.
[59] Li, T.H., Zheng, L.N. (2012) Soil erosion changes in the Yanhe watershed from 2001 to 2010 based on RUSLE model. Journal of Natural Resources. 27(7), 1164-1175.

Received: **08.05.2017**
Accepted: **09.08.2017**

CORRESPONDING AUTHOR

Lei Wu
College of Water Resources and
Architectural Engineering,
Northwest A&F University,
No. 23 Weihui Road, Yangling District,
Shaanxi, 712100 – P.R. China

e-mail: lwu@nwsuaf.edu.cn

© by PSP Volume 26 – No. 12A/2017 pages 7874-7884 Fresenius Environmental Bulletin

PROBABILITY WEIGHTED MOMENTS AND THEIR EFFECTS ON THE RAINFALL DEPTH–DURATION–FREQUENCY CURVES

Omer Levend Asikoglu[1,*], Ertugrul Benzeden[2]

[1]Ege University, Department of Civil Engineering, Bornova, Izmir, Turkey
[2]Dokuz Eylul University, Department of Civil Engineering, Buca, Izmir, Turkey

ABSTRACT

The generalized depth–duration–frequency (DDF) relationships that define rainfall depth as the function of rainfall duration (*d*) and frequency or recurrence interval (*T*) are extensively used for design purposes in hydrological applications. To generalize the DDF relationships at a site, the parameters of the selected parent distribution must provide several divergence criteria (i.e., quantile functions of different durations must not intersect each other).

The divergence criteria established on the parameters of a parent frequency distribution, such as the generalized extreme value (GEV), must be satisfied by the parameters of the exponential functions that are fitted to the observed probability weighted moments.

This study presents examples of the GEV-based generalized DDF curves for the annual maximum rainfalls with durations from 1 h to 24 h and recorded at the Izmir, Marmaris, and Zonguldak gauges. In addition, the current research discusses a few problems related to generalizing and using the DDF curves, as well as several reasonable solutions for these problems.

KEYWORDS:
Probability Weighted Moments (PWM), Generalized Extreme Value (GEV) Distribution, Generalized Depth–Duration–Frequency (DDF) relationships

INTRODUCTION

The annual maxima of rainfall for a standard duration is the largest cumulative rainfall depth ($X(d)$) in a moving time window of a d length (d = 5, 10, 15, 30 min.; 1, 2,…, 24 h) of the pluviograph records of a gauging station [1, 2]. Therefore, d is not precisely a random variable but a parametric property of the random variable $X(d)$. The probabilistic character of the random variable $X(d)$ is defined by an appropriate frequency distribution function $F[X(d)]$ fitted to the observations and by the quantile function $\hat{X}(d,T)$, which is the inverse of the frequency distribution function [3].

$$\hat{X}(d,T) = F^{-1}_{X(d)}(1-1/T), \quad (1)$$

where T is the return period (or recurrence interval) and $\hat{X}(d,T)$ is the estimation of the annual maximum rainfall depth with a standard duration of d for the underlying probability of $F_T = 1-1/T$.

When certain conditions are met for the rainfall durations of $d_1 \le d \le d_m$, the quantile functions defined by Eq. (1) generate a divergent (i.e., non-intersecting at large values of T) group of curves. These depth–duration–frequency (DDF) curves are used in many hydrological designs to obtain the project rainfall depth of certain duration (d) and return period (T) [3, 4, 5]. The DDF relationship developed for a particular station enables the estimation of the extreme rainfall depths of a return period (T) for the durations other than the standard ones.

The DDF curves can be obtained either by fitting the parametric or semi-parametric functions to the estimated quantile values from an appropriate parent frequency distribution model through the regression methods [1, 2, 6] or by generalizing the quantile function of the parent frequency distribution model (i.e., if the conditions of divergence are realized) [7, 8].

The parameters in the frequency distribution model adapted to the random hydrological observations can be estimated by such methods as moments, L-moments, and maximum likelihood method [9, 10, 11, 12]. The L-moments or probability weighted moments (PWMs) [11, 13] used in the current study often have finite values, their moment ratios are limited, and they are not significantly affected by outlier observations. Apart from these advantages, PWMs can provide considerably efficient and unbiased estimates, particularly for short observation series [10, 11, 12, 14, 15, 16, 17].

The current study investigates the effect of the relationship between the sample PWM estimations and the duration d of the maximum rainfall series on the descriptive statistics (L-coefficient of variation, *LCv*; L-coefficient of skewness, *LCs*; and L-coefficient of kurtosis, *LCk*), on the parameters of the considered frequency distribution model of the generalized DDF curves and on the divergence criteria of the

generalized DDF curves [7, 18]. For the İzmir, Marmaris, and Zonguldak stations, the issues to be considered and problems that may be encountered in generalizing the DDF curves are addressed. Solutions are likewise suggested.

PWM METHOD

PWMs. PWM of the ordered annual maximum rainfall series $X_i(d)$ is expressed in Eq. (2) as follows [10, 13]:

$$b_r(d) = \frac{1}{N}\sum_{i=1}^{N}\frac{\binom{i-1}{r}}{\binom{N-1}{r}}X_i(d) = \frac{1}{N}\sum_{i=1}^{N}P_i^r X_i(d) \quad , \quad (2)$$

where N is the record length, d is the rainfall duration, and r is the order of the moments.

A significant exponential relationship exists between PWMs and the duration d of the maximum rainfall for $d_1 \le d \le d_m$ [1, 7, 18].

$$\hat{\beta}_r(d) = a_r \cdot d^{s_r}\ ;\ r = 0,1,2,3,..., \quad (3)$$

where a_r and s_r are the coefficients of the exponential relationship between the smoothed function of the rth order PWM, $\hat{\beta}_r(d)$, and rainfall duration d.

An important physical feature of an extreme rainfall is that its values are constantly positive and the total amount of rainfall $X(d)$ increases with rainfall duration d. Therefore, the parameters a_r and s_r in Eq. (3) are positive for each r order ($a_r>0$, $s_r>0$). Eq. (2) shows that the condition $b_r(d) < b_{r-1}(d) < b_{r-2}(d) < ... < b_0(d)$ is provided for PWMs for a certain duration d because the weights P_i^r gradually decrease as r orders increase.

Therefore, the a_r coefficients in Eq. (3) decrease as r orders increase ($a_r < a_{r-1} < a_{r-2} < ... < a_0$). Regardless of the parent frequency distribution model that the $X_i(d)$ sub-series came from, the basic characteristics of the PWM sample statistics do not change. That is, these properties are independent of the main frequency distribution model.

By contrast, the s_r exponents in Eq. (3) may vary systematically with the r order or may be nearly constant. In the case that the exponents s_r are sufficiently close to each other to be regarded as constant ($s_r \cong \tilde{s},\ r = 0,1,2,3,...$), Eq. (3) is reduced to Eq. (4).

$$\hat{\beta}_r(d) \cong a_r \cdot d^{\tilde{s}}\ ;\ r = 0,1,2,3,... \quad (4)$$

This process is called "simple scaling process" if the sample PWM estimations are defined as in Eq. (4) [1, 5]. For an extreme rainfall process with a simple scaling character, the dimensionless descriptive statistics, such as the L-coefficient of variation ($\tilde{\tau} = LCv$), L-coefficient of skewness ($\tilde{\tau}_3 = LCs$), and L-coefficient of kurtosis ($\tilde{\tau}_4 = LCk$), reduce to constant values depend on the a_r coefficients.

L-moments and L-moment Ratios. When the generalized DDF relationships based on an appropriate frequency distribution model are described by PWMs (or L-moments) [3], the following first four L-moments and L-moment ratios related to the rainfall duration d should be defined:

$$l_1(d) = b_0(d) \quad (5)$$

$$l_2(d) = 2b_1(d) - b_0(d) \quad (6)$$

$$l_3(d) = 6\left[b_2(d) - b_1(d)\right] + b_0(d) \quad (7)$$

$$l_4(d) = 20b_3(d) - 30b_2(d) + 12b_1(d) - b_0(d) \quad (8)$$

$$t(d) = l_2(d)/l_1(d);\quad 0 < t(d) < 1 \quad (9)$$

$$t_3(d) = l_3(d)/l_2(d);\quad -1 < t_3(d) < 1 \quad (10)$$

$$t_4(d) = l_4(d)/l_2(d);\quad -1 < t_4(d) < 1. \quad (11)$$

When the exponential functions adapted to PWMs (Eq. 3) are used instead of the PWM sample estimates in the preceding equations, the L-moments and L-moment ratios are obtained in a smoothed form as follows:

$$\hat{\lambda}_1(d) = \hat{\beta}_0(d) \quad (12)$$

$$\hat{\lambda}_2(d) = 2\hat{\beta}_1(d) - \hat{\beta}_0(d) \quad (13)$$

$$\hat{\lambda}_3(d) = 6\left[\hat{\beta}_2(d) - \hat{\beta}_1(d)\right] + \hat{\beta}_0(d) \quad (14)$$

$$\hat{\lambda}_4(d) = 20\hat{\beta}_3(d) - 30\hat{\beta}_2(d) + 12\hat{\beta}_1(d) - \hat{\beta}_0(d) \quad (15)$$

$$\hat{\tau}(d) = \hat{\lambda}_2(d)/\hat{\lambda}_1(d) = 2\frac{\hat{\beta}_1(d)}{\hat{\beta}_0(d)} - 1 \quad (16)$$

$$\hat{\tau}_3(d) = \hat{\lambda}_3(d)/\hat{\lambda}_2(d) = \left\{6\left[\frac{\hat{\beta}_2(d)}{\hat{\beta}_0(d)} - \frac{\hat{\beta}_1(d)}{\hat{\beta}_0(d)}\right] + 1\right\} \Big/ \hat{\tau}(d) \quad (17)$$

$$\hat{\tau}_4(d) = \hat{\lambda}_4(d)/\hat{\lambda}_2(d) = \left\{20\frac{\hat{\beta}_3(d)}{\hat{\beta}_0(d)} - 30\frac{\hat{\beta}_2(d)}{\hat{\beta}_0(d)} + 12\frac{\hat{\beta}_1(d)}{\hat{\beta}_0(d)} - 1\right\} \Big/ \hat{\tau}(d) \quad (18)$$

The preceding statistics provide important information about the location (λ_1), scale (or spread) (τ), skewness (τ_3), and kurtosis (τ_4) of the distribution. Hosking [3] showed that for $X \ge 0$, the absolute values of the L-coefficient of skewness and L-coefficient of kurtosis are below 1 ($|\tau_3|<1$, $|\tau_4|<1$). The L-coefficient of variation is in the range of $0<\tau<1$.

In the generalization studies of the DDF curves of extreme rainfall over a suitable range of rainfall duration $d_1 \le d \le d_m$, two different approaches can be applied to describe the relationship between the dimensionless descriptive statistics and rainfall duration d.

The first approach is to adapt empirical functions, such as exponential and semi-logarithmic, to define the relationship between the statistics, such as $t(d)$, $t_3(d)$, and $t_4(d)$, computed directly from the observed PWMs and the rainfall duration d. The second approach is to use the smoothed (indirectly computed) statistics, such as $\hat{\tau}(d), \hat{\tau}_3(d)$, and $\hat{\tau}_4(d)$, obtained by placing the exponential functions $\hat{\beta}_r(d)$ adapted to the $b_r(d)$ values. This study discussed the

application of the second approach.

Testing the equality hypothesis of the s_r coefficients in the exponential PWM relationships. The smoothed statistics, which was indirectly computed via exponential functions, are considerably sensitive to the sample estimates of the a_r and s_r coefficients of the exponential functions in Eq. (3). The descriptive statistics (i.e., $\hat{\tau}(d), \hat{\tau}_3(d), \hat{\tau}_4(d)$) are reduced to constant values that are independent of the rainfall duration (depending only on the ratios of a'_r / a'_0) if the s_r values approximate each other or if they vary randomly (the s_r values approach a constant value, such as $\tilde{s}$).

$$\tilde{\tau} = 2\frac{a'_1}{a'_0} - 1 \quad (19)$$

$$\tilde{\tau}_3 = \left\{6\left[\frac{a'_2}{a'_0} - \frac{a'_1}{a'_0}\right] + 1\right\} / \tilde{\tau} \quad (20)$$

$$\tilde{\tau}_4 = \left\{20\frac{a'_3}{a'_0} - 30\frac{a'_2}{a'_0} + 12\frac{a'_1}{a'_0} - 1\right\} / \tilde{\tau}. \quad (21)$$

In the preceding equations, the $a'_0, a'_1, a'_2 \ldots$ values are the updated values of the $a_0, a_1, a_2 \ldots$ coefficients based on the *principle of parallelism*. The processes with such constant descriptive statistics are called *the simple scaling processes*. In these processes, only the mean of the process ($\hat{\mu}(d) = \hat{\beta}_0(d) = \hat{\lambda}_1(d)$) varies with the rainfall duration. Thus, all rainfall series (of durations $d_1, d_2, \ldots, d_m$) scaled with the smoothed means ($\hat{\beta}_0(d) \cong a_r d^s = \hat{\mu}(d)$) can be identified by an identical frequency distribution model [1, 2, 5, 6, 19].

The s_r coefficients are obtained by solving the linear regressions between the logarithm of the sample PWMs ($Y_{rj} = \ell n\left|b_r(d_j)\right|$) and the rainfall durations ($Z_j = \ell n(d_j)$. The equality hypothesis of the expected values of the s_r coefficients can be tested by applying the "unified parallelism test" ($H_0 : E\{s_0\} = E\{s_1\} = \ldots = E\{s_L\}$). The error variances $\hat{S}^2_{er}$ of the log–linear relationships are obtained by using data pairs (Z_j, Y_{rj}) for every duration *d* and order *r*. If the expected values of the error variances are the same, then the mutual slope becomes the arithmetic mean of the s_r values ($\tilde{s} = \bar{s}$) because the independent variable Z_j is the same in all regressions [20].

$$\bar{s} = \frac{1}{L+1}\sum_{r=0}^{L} s_r. \quad (22)$$

The mean error variance of the (L+1) number of the log–linear relationships is equal to the average of the error variances of the log–linear equations.

$$S_I^2 = \frac{1}{L+1}\sum_{r=0}^{L} \hat{S}^2_{er}. \quad (23)$$

The variance of s_r coefficients around the mean value is calculated as follows:

$$S_{II}^2 = \frac{1}{L}\left[\sum_{j=1}^{m}(Z_j - \bar{Z})^2\right] \cdot \sum_{r=0}^{L}(s_r - \bar{s})^2, \quad (24)$$

where $\bar{Z}$ is the logarithmic mean of the rainfall durations and S_{II}^2 and S_I^2 are the X^2 (chi-square) variables with degrees of freedom $\nu_{II} = L$ and $\nu_I = (L+1)(m-2)$, respectively. The equality hypothesis of the expected values of the s_r coefficients can be tested with the ratio of the variances S_{II}^2 and S_I^2 [20].

$$f = S_{II}^2 / S_I^2. \quad (25)$$

If the *f*-statistic calculated from this equation is below the critical value $f_p(\nu_{II}; \nu_I)$ that corresponds to the *p*-significance level, then the H_0 hypothesis is accepted ($E\{s_0\} = E\{s_1\} = \ldots = E\{s_L\}$). In this case, the a_r coefficients in the exponential relationship should be corrected as follows:

$$a'_r = \exp(\bar{y}_r - \bar{s}\,\bar{Z}),\ r = 0,1,2,\ldots,L. \quad (26)$$

After this correction, the fixed statistics $\tilde{\tau}$, $\tilde{\tau}_3$, and $\tilde{\tau}_3$ should be recalculated based on the corrected a'_r coefficients.

If the equality hypothesis of the s_r coefficients is rejected, then these coefficients should be evaluated if they vary uniformly with the *r*-orders of PWMs. The fact that the s_r coefficients do not change uniformly with the *r*-order indicates significant sampling errors or outliers in the observation sequences. In this case, if the s_r coefficients are equal to the value of $\bar{s}$ computed using Eq. (22), then constructing the DDF curves with the simple scaling character may be feasible.

Examining the a_r coefficients in exponential PWM functions. The smoothed descriptive statistics $\hat{\tau}(d)$, $\hat{\tau}_3(d)$, and $\hat{\tau}_3(d)$, which depend on the nondimensional proportions $\hat{\phi}_r(d) = \hat{\beta}_r(d) / \hat{\beta}_0(d)$ of the exponential functions fitted to the observed PWM values, must satisfy the following inequalities in the interval $d_1 \le d \le d_m$:

$$0 < \hat{\tau}(d) = 2 \cdot \hat{\phi}_1(d) - 1 < 1 \quad (27)$$

$$-1 < \hat{\tau}_3(d) = \left\{6\left|\hat{\phi}_2(d) - \hat{\phi}_1(d)\right| + 1\right\} / \hat{\tau}(d) < 1. \quad (28)$$

The moment ratio must be in the range of $0.5 < \hat{\phi}_1(d) < 1$ or the coefficient of a_1 must provide the inequality in Eq. (29).

$$a_0 / 2 < a_1 < a_0. \quad (29)$$

Therefore, the condition of $\hat{\lambda}_2(d) > 0$ and the inequality in Eq. (27) can be realized. Moreover,

$\hat{\tau}(d)$ is an increasing function of the rainfall duration d for $s_1>s_0$; and a decreasing function of d for $s_1<s_0$.

Eq. (28) indicates that the condition in Eq. (29) should be provided. In addition, $\hat{\phi}_2(d)$ should be in the range of $2\hat{\phi}_1(d) < \hat{\phi}_2(d) < \left|4\hat{\phi}_1(d)-1\right|/3$ or the a_2 coefficient should provide the following inequality:

$$2a_1/3 < a_2 < (4a_1 - a_0)/3. \quad (30)$$

The smoothed function of $\hat{\tau}_3(d)$ is an increasing function of the rainfall duration d for $s_2 > s_1 \geq s_0$ and a decreasing function of d for $s_2 < s_1 \leq s_0$. The functions ($\hat{\beta}_r(d)$) that do not fulfill the constraints in Eqs. (29) and (30) cause incompatible and inconsistent DDF curves to be produced.

GENERALIZED DDF CURVES BASED ON GEV DISTRIBUTION

Specifications and Parameter Estimations of the GEV Distribution. Generalized extreme value (GEV) is a considerably flexible three-parameter distribution model that is often used in practice to define the frequency distribution of extreme-type hydrometeorological events [12, 21, 22].

The cumulative distribution function of the GEV distribution is expressed as follows:

$$F[X(d)] = \exp\left\{-\left[1-\frac{k(d)}{\alpha(d)}\{X(d)-\xi(d)\}^{1/k(d)}\right]\right\}; k(d)\neq 0, \quad (31)$$

where $X(d)$ is the rainfall depth; and $\xi(d)$, $\alpha(d)$, and $k(d)$ are the location, scale, and shape parameters of the distribution, respectively. The quantile function of GEV is expressed in Eq. (32) [12, 23].

$$X(d,u) = \xi(d) + \frac{\alpha(d)}{k(d)}\left(1-e^{-k(d)u}\right); \; k(d)\neq 0, \quad (32)$$

where u is the Gumbel reduced variate that corresponds to the probability of $F = 1-1/T$ [24].

$$u = -\ln\left[-\ln(F)\right] = -\ln\left[-\ln(1-1/T)\right]. \quad (33)$$

The indirect (smoothed) L-moment estimates of the GEV distribution parameters can be calculated using the following equations for the d rainfall duration [11, 12, 22, 23]:

$$\hat{C}(d) = \frac{2}{3+\tau_3(d)} - \frac{\ln 2}{\ln 3} = \frac{2\hat{\beta}_1(d)-\hat{\beta}_0(d)}{3\hat{\beta}_2(d)-\hat{\beta}_0(d)} - \frac{\ln 2}{\ln 3} \quad (34)$$

$$\hat{k}(d) = 7.859\cdot\hat{C}(d) + 2.9554\cdot\hat{C}^2(d) \quad (35)$$

$$\hat{\alpha}(d) = \frac{\hat{k}(d)\cdot\hat{\lambda}_2(d)}{\left[1-2^{-\hat{k}(d)}\right]\Gamma\left[1+\hat{k}(d)\right]} \quad (36)$$

$$\hat{\xi}(d) = \hat{\lambda}_1(d) + \frac{\hat{\alpha}(d)}{\hat{k}(d)}\left\{\Gamma\left[1+\hat{k}(d)\right]-1\right\}. \quad (37)$$

In these equations, $\hat{\beta}_0, \hat{\beta}_1$, and $\hat{\beta}_2$ are the smoothed PWMs; $\hat{\lambda}_1(d), \hat{\lambda}_2(d)$, and $\hat{\lambda}_3(d)$ are the first three L-moments; and $\Gamma[\cdot]$ is the incomplete gamma function [19].

If the shape parameter is $k(d)=0$, then the GEV distribution becomes the Gumbel (EV1) distribution with L-moment ratios of $\tau_3 = 0.1699, \tau_4 = 0.1504$ [9, 20]. For the negative values of the shape parameter ($k(d)<0$), the GEV distribution is the lower bounded extreme value type II (EV2) distribution in the range of $\xi(d)+\alpha(d)/k(d) < X < +\infty$. For the negative shape parameter ($k(d)>0$), the GEV distribution is the upper bounded extreme value type III (EV3) distribution in the range of $-\infty < X < \xi(d)+\alpha(d)/k(d)$ [12].

Divergence criteria of the generalized DDF curves. In the second and higher order statistical moments of the annual maximum rainfall, the uncertainties are generally high due to sampling errors. Therefore, the uncertainties of parametric functions, which are adapted to the high order statistical moments or distribution parameters based on these statistics, are also high. In particular, if the parametric functions adapted to the scale and shape parameters cannot provide the divergence criteria, then the DDF curves for the different rainfall durations intersect with each other over large recurrence intervals. These curves also produce estimates that do not fit the nature of the rainfall phenomenon.

To ensure that the DDF curves of the two rainfall durations (e.g., d_1 and $d_2>d_1$) do not intersect in large recurrence intervals, the criteria that quantile estimates must satisfy are as follows [7, 18]:

$$\hat{X}(d_2,T) > \hat{X}(d_1,T) \quad (38)$$

$$\frac{\partial\hat{X}(d_2,T)}{\partial T} \geq \frac{\partial\hat{X}(d_1,T)}{\partial T}. \quad (39)$$

The first criterion is based on the principle that "for the same frequency, the rainfall depth of a longer duration is higher than the rainfall depth of a shorter duration," which is also inherent in the rainfall phenomenon. The second criterion is a mathematical principle, in which the slopes of the DDF curves (or quantile functions) of the durations d_1 and d_2 must be satisfied for the first criterion to be realized.

These criteria, which apply to any parent frequency distribution, can also be expressed in terms of the u Gumbel reduced variate instead of T [7]:

$$\hat{X}(d_2,u) > \hat{X}(d_1,u) \quad (40)$$

$$\frac{\partial\hat{X}(d_2,u)}{\partial u} \geq \frac{\partial\hat{X}(d_1,u)}{\partial u}. \quad (41)$$

To satisfy the preceding criteria, the parameters

$\hat{\xi}(d)$ and $\hat{\alpha}(d)$ of the GEV distribution must increase with the duration of d and the parameter $\hat{k}(d)$ must be constant or decreasing [7].

$$\xi(d_2) > \xi(d_1) \quad (42)$$

$$\alpha(d_2) > \alpha(d_1) \quad (43)$$

$$k(d_2) \le k(d_1) \quad (44)$$

When the information on PWMs and L-moments is combined with the preceding criteria, the divergence criteria of the generalized DDF curves can be written in terms of the smoothed L-moments and descriptive statistics as follows:

$$\hat{\lambda}_1(d_2) > \hat{\lambda}_1(d_1) \quad (45)$$

$$\hat{\lambda}_2(d_2) > \hat{\lambda}_2(d_1) \quad (46)$$

$$\hat{\tau}_3(d_2) \ge \hat{\tau}_3(d_1). \quad (47)$$

Maximum rainfall observations constantly provide the first two of these criteria. The third criterion shows that the L-skewness of the process must increase monotonically or remain constant with the rainfall duration d. The exponential functions $\hat{\beta}_r(d)$ must not intersect to satisfy the divergence criterion of Eq. (47). The reason is that $\hat{\lambda}_3(d)$ is the linear combination of the exponential functions of $\hat{\beta}_r(d)$. That is, the s_r coefficients must be of increasing character with the r-order of moments ($s_0 \le s_1 \le s_2 \ldots \le s_r$) or must remain constant.

The extreme rainfalls of long duration (d >1–2 h) measured in the Turkish stations do not generally provide this criterion, although short-term ($d \le 1$–2 h) extreme rainfalls do.

Furthermore, estimates made from generalizing the DDF curves provide divergence criteria and reflect the physical facts of moderate magnitude. That is, these estimates are in a reasonable range.

If the shape parameter $\hat{k}(d)$ in a generalized GEV-based DDF model approximates the critical value (i.e., −1/3), then the DDF curves can yield overestimated rainfalls for long rainfall durations and for recurrence intervals, such as $T > N$.

APPLICATION AND RESULTS

This section uses the maximum rainfall observations with durations ranging from $1 \le d \le 24$ h at the meteorological stations of Izmir (N = 57 years), Marmaris (N = 36 years), and Zonguldak (N = 57 years) as examples to construct the generalized DDF curves and analyze the problems encountered in the application.

Table 1 provides the coefficients of the $\hat{\beta}_r(d)$ exponential functions adapted to the sample PWMs and the determination coefficients. For the three stations, Figures 1, 2, 3, and 4 illustrate the $b_r(d)$ sample PWMs and $\hat{\beta}_r(d)$ exponential functions adapted to

TABLE 1

Coefficients of the $\hat{\beta}_r(d)$ exponential functions

Moment Order r	Izmir			Marmaris			Zonguldak		
	a_r	s_r	R^2	a_r	s_r	R^2	a_r	s_r	R^2
0	23.946	0.3021	0.9931	45.230	0.3528	0.9980	33.601	0.3211	0.9983
1	14.846	0.2818	0.9950	27.424	0.3698	0.9981	20.915	0.3221	0.9979
2	11.181	0.2670	0.9948	20.340	0.3808	0.9948	15.625	0.3267	0.9977
3	9.144	0.2554	0.9938	16.453	0.3877	0.9938	12.637	0.3317	0.9973

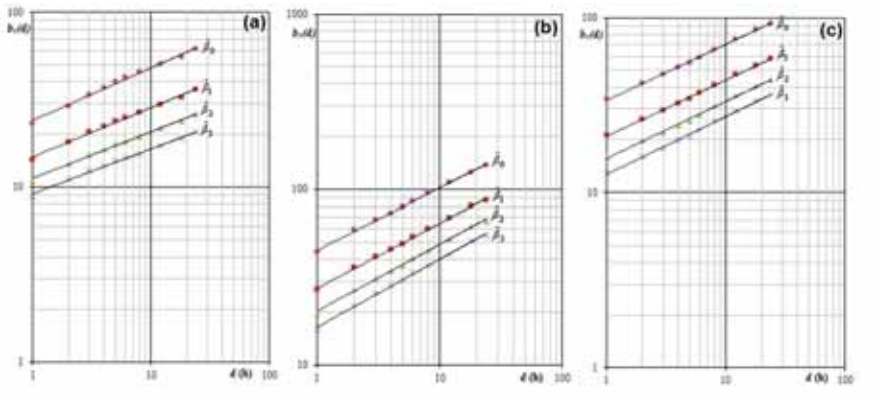


FIGURE 1

Sample PWMs and adapted $\hat{\beta}_r(d)$ exponential functions of the (a) Izmir, (b) Marmaris, and (c) Zonguldak stations

these values, $t(d)$ and $t_3(d)$ descriptive statistics calculated from the sample PWMs and $\hat{\tau}(d)$ and $\hat{\tau}_3(d)$ continuous functions based on the smoothed PWMs, sample estimates of the shape parameters $k(d)$ of the GEV distribution, and $\hat{k}(d)$ continuous functions obtained based on the indirect $\hat{\tau}_3(d)$ functions, respectively.

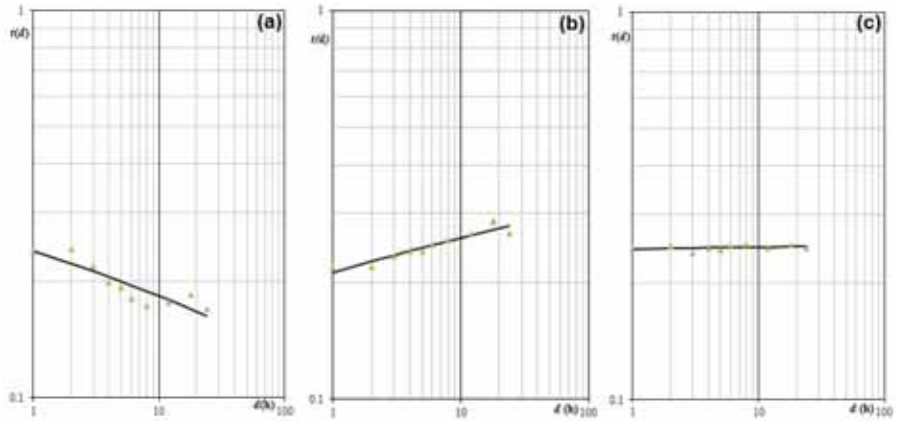


FIGURE 2

Sample $t(d)$ statistics and $\hat{\tau}(d)$ indirect functions of the (a) Izmir, (b) Marmaris, and (c) Zonguldak stations

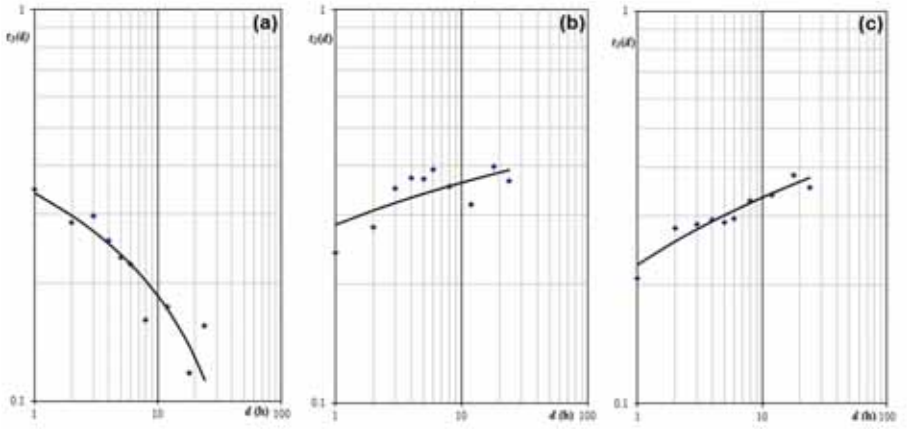


FIGURE 3

Sample $t_3(d)$ statistics and $\hat{\tau}_3(d)$ indirect functions of the (a) Izmir, (b) Marmaris, and (c) Zonguldak stations

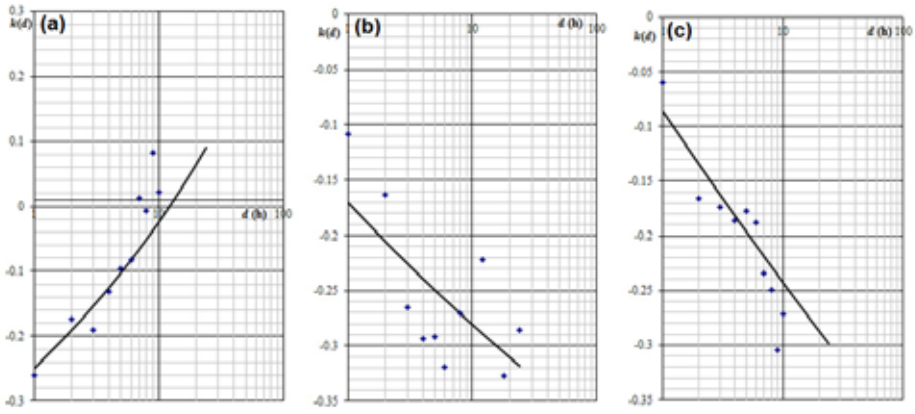


FIGURE 4

Sample $k(d)$ statistics and $\hat{k}(d)$ indirect functions of the (a) Izmir, (b) Marmaris, and (c) Zonguldak stations

TABLE 2
Results of the equality hypothesis test of the s_r coefficients (Critical *f* statistic at the significance level of $p = 0.05$ is $f_{0.05}(3;32) = 2.9$)

Stations	$\bar{s}$	$\sum_{r=0}^{3} S_{er}^2$	$\sum_{r=0}^{3} (s_r - \bar{s})^2$	S_{II}^2	S_I^2	$f = S_{II}^2 - S_I^2$
Izmir	0.2766	0.00198	122.10^{-5}	0.00355	0.00050	7.17
Marmaris	0.3728	0.00128	70.10^{-5}	0.00202	0.00032	6.33
Zonguldak	0.3254	0.00102	7.10^{-5}	0.00021	0.00026	0.81

Relationship between PWMs and rainfall duration. For the three stations, strong exponential relationships between the sample PWMs and rainfall durations are significant and the determination coefficients (R^2) of the log–linear regressions are nearly the same for all the moment orders (r = 0, 1, 2, 3). The a_r coefficients of the exponential functions provide the criteria in Eqs. (29) and (30). The s_r coefficients (or exponents) of the exponential functions decrease with the r moment order, that is, (1) regularly in İzmir, (2) faster in Marmaris, and (3) slower in Zonguldak. The tests of variance ratios indicate that the hypothesis that the s_r coefficients (slopes) are not different from the mean value ($\tilde{s} = \bar{s}$) is accepted for the Zonguldak station and rejected in the İzmir and Marmaris stations at the significance level of p = 0.05 (see Table 2).

Relationship between the L-moment statistics and rainfall duration. When the variation of the L-coefficient of variation ($t(d)$ and $\hat{\tau}(d)$) and skewness ($t_3(d)$ and $\hat{\tau}_3(d)$) is evaluated with rainfall duration, both statistics are decreasing in the Izmir station and increasing in the Marmaris station. In the Zonguldak station, the L-coefficients of variation remain nearly constant, whereas the L-coefficients of skewness significantly increase with rainfall duration (see Figures 2, and 3). These findings show that the distribution characteristics of extreme rainfall in the Marmaris and Zonguldak stations are comparatively similar. By contrast, the distribution characteristics of extreme rainfall in the Izmir station are different from those in the two stations.

The L-coefficients of variation indicate that the standard deviations of extreme rainfall in the Izmir station are increasing more gradually than the means. However, the standard deviations in the Marmaris and Zonguldak stations increase more rapidly than the means. In the $\hat{\tau}_3(d)$ curves, the generalized DDF curves for any three parameter probability distribution model will not be divergent in the Izmir station but divergent in the Marmaris and Zonguldak stations. Accordingly, the geographical and meteorological factors that are responsible for this contradictory situation should be investigated.

Variation of the *k*(*d*) shape parameter with rainfall duration. The Marmaris and Zonguldak stations have no theoretical situation in terms of the divergence constraints to be provided in the GEV-based DDF curves. The frequency distribution of extreme rainfall in both stations can be generalized using the EV2-type distribution model, in which the $\hat{k}(d)$ shape parameter uniformly decreases with rainfall duration. By contrast, the shape parameter in the Izmir station is increasing steadily in the range of $-0.25 < \hat{k}(d) < 0.091$. Consequently, maximum rainfall with durations of $1 \le d \le 8$ h, d = 12 h, and $d \ge 18$ h should be presented with three types of GEV distributions, such as EV2, EV1 (Gumbel), and EV3, respectively.

If the L-coefficient of skewness ($t_3(d)$ or $\hat{\tau}_3(d)$) has a decreasing character with the rainfall duration, then the divergence criterion $k(d_2) \ge k(d_1)$ for the shape parameter is not provided. In this case, the generalized DDF curves for short durations, such as 1 h and 2 h; and long durations, such as 18 h and 24 h, can produce extreme rainfall estimates that are inconsistent with observations. However, the constant acceptance ($\tilde{k}$) of the shape parameter may be a solution.

GEV-based generalized DDF curves. The GEV-based DDF curves for the three rainfall durations (d_1 = 1, d_2 = 6, and d_3 = 24 h) in the İzmir, Marmaris, and Zonguldak stations are plotted based on the Gringorten formula and are illustrated in Figures 4, 5, and 6, respectively, with extreme rainfall observations. These curves are constructed using the distribution parameters ($\hat{\xi}(d), \hat{\alpha}(d)$, and $\hat{k}(d)$), which are indirectly calculated from the exponential functions $\hat{\beta}(d)$ regardless of whether the divergence criteria are satisfied.

When these curves are evaluated based on the stations, the distribution type changes and the DDF curves for the Izmir station intersect with each other (see Figure 4) in a recurrence interval of $T^* \cong 1000$ years ($u \cong 6.9$). The reason is the increase of the

$\hat{k}(d)$ values with the increase of *d* in the interval of $-0.25 < \hat{k}(d) < 0.091$. Therefore, the GEV-based generalized DDF curves for the Izmir station does not satisfy the divergence criteria. However, these curves can be used in practice because they provide fairly reasonable estimates for the recurrence interval of $T \leq 100$ years ($u \leq 4.6$).

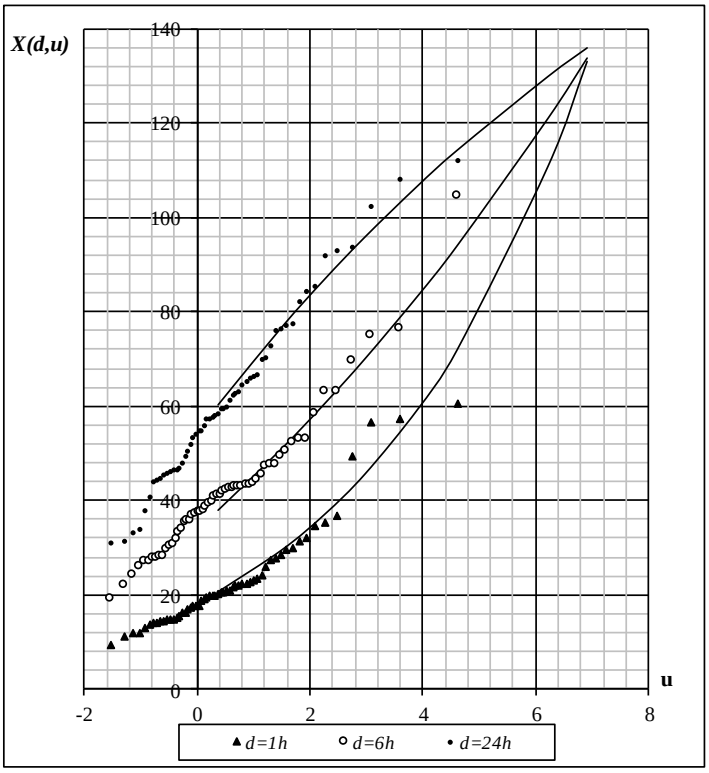


FIGURE 4
DDF curves in the Izmir station (for *T* = 2–1000 years)

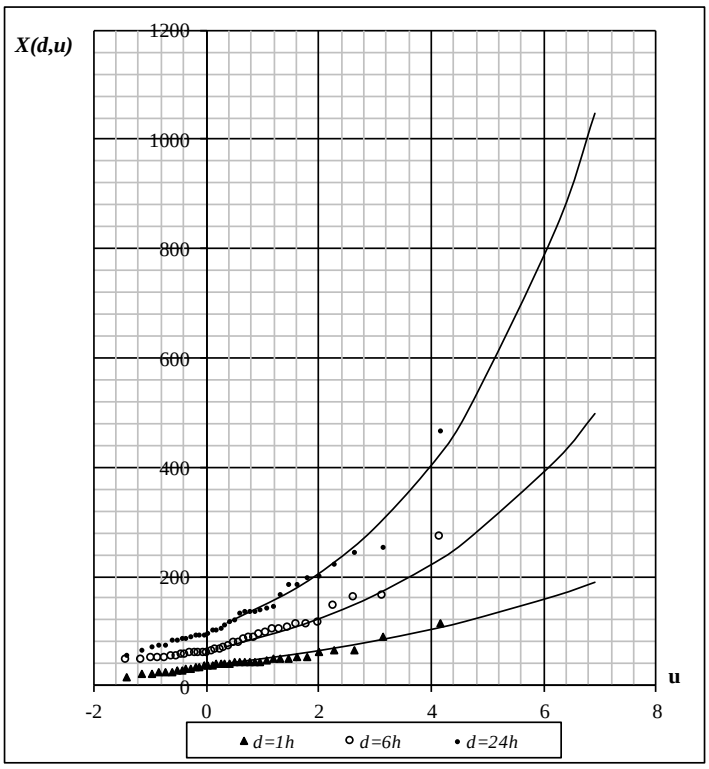


FIGURE 5
DDF curves in the Marmaris station (for *T* = 2–1000 years)

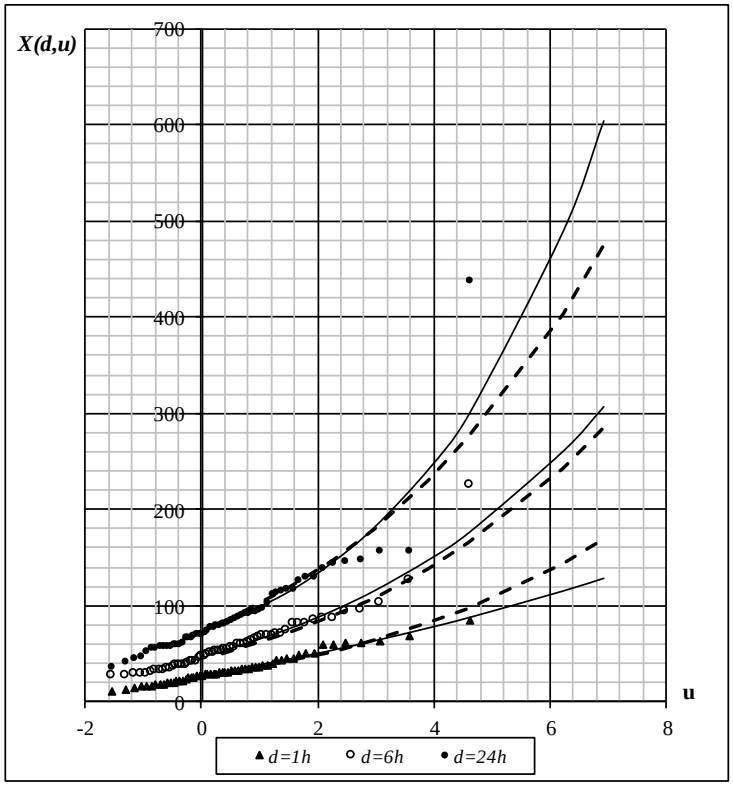


FIGURE 6
DDF curves in the Zonguldak station (for T = 2–1000 years)

The GEV-based generalized DDF curves can be used for theoretical estimation purposes (see Figure 5) because the divergence criteria are provided in the Marmaris station. However, the estimates of extreme rainfalls with extended durations (d > 8 h) for large return periods (T > 100 years) are unreasonably high.

The generalized DDF curves obtained for the Zonguldak station (see Figure 6), where the L-coefficient of variation is nearly constant ($\tilde{\tau} \cong 0.248$), are similar to those in the Marmaris station. In the Zonguldak station, the generalized DDF curves provide high estimates for the large values of the recurrence interval ($T \geq 500$ years) because the shape parameter $\hat{k}(d)$ approaches −1/3 for long rainfall durations ($d \geq 18$ h). Although the L-coefficient of variation is nearly constant in this case, the steady increase of the L-coefficient of skewness with the rainfall duration is due to the a_2 and s_2 coefficients of the exponential function $\hat{\beta}_2(d)$, which is adapted to the $b_2(d)$ values. Table 1 shows that the equality (parallelism) hypothesis of the coefficients s_0, s_1, s_2, s_3 in the Zonguldak station is accepted. Therefore, an EV2-based generalized DDF curve generated with constant parameters ($\bar{s} = 0.3254$) is also a feasible solution for the Zonguldak station. Figure 6 illustrates the generalized DDF curves of this solution with the dashed lines.

CONCLUSIONS AND RECOMMENDATIONS

The variation of PWMs of extreme rainfall with the duration d can be defined as nearly ideal with the exponential functions when the range of the duration ($d_1 \leq d \leq d_m$) is selected appropriately. The studies conducted in other geographical regions [6, 19, 25, 26] indicate that the statistical characteristics of short-, medium-, and long-duration rainfalls can be different. Although the distribution characteristics, such as the variation and skewness of short-term rainfall in Turkey increases with the rainfall duration d, the characteristics of medium- and long-term rainfall can significantly decrease with the rainfall duration. Therefore, dividing the observations into two or three appropriate ranges of durations (stepwise solutions) would be beneficial in generalizing DDF curves.

In many stations in Turkey, the statistical characteristics and probability behaviors of the annual maximum rainfall of duration d = 24 h are generally inconsistent with the characteristics and behavior of rainfall in short durations.

In general, the statistical and probabilistic behavior of extreme rainfall of the durations between

$2 \le d \le 12$ h is substantially compatible. In addition, the variability and skewness characteristics of the different and even the same geographical regions change in the opposite direction because of the rainfall duration. Possible physical, climatic, and measurement reasons are a matter of interest. Although the conventional moments and PWMs of the maximum rainfall are uniformly increasing functions of the rainfall duration, this regularity inadequately reflects the descriptive statistics, such as variability, skewness, and sharpness. One of the main reasons for this result is that the descriptive statistics are sensitive to the a_r and s_r parameters of the exponential functions that are adapted to the sample statistical moments. Minimal changes in these parameters can cause significant changes in the descriptive statistics.

One of the major practical problems encountered is that the divergence criteria of the DDF quantile functions are often not achieved. Although the divergence criteria are provided theoretically, the estimations made, particularly for long durations and large recurrence intervals of the DDF curves, are unreasonably high. Therefore, the use of the two-parameter probability distributions instead of the three-parameter probability distribution models, which has added parameters and is considerably flexible, are often convenient. The selection of a simple scaling-type generalized DDF relationship with constant variation and skewness statistics would also be appropriate.

REFERENCES

[1] Burlando, P. and Rosso, R. (1996) Scaling and multiscaling models of depth–duration–frequency curves for storm precipitation. J. Hydrology. 187, 45-64.

[2] Koutsoyiannis, D., Kozonis, D. and Manetas, A. (1998) A Mathematical Framework for Studying Rainfall Intensity-Duration-Frequency Relationships. J. Hydrology. 206, 118-135.

[3] Wenzel, H.G. (1982) Rainfall for Urban Stormwater Design. Chap. 2: Urban Stormwater Hydrology, Water Resources Monograph, 7, AGV, Washington D.F.

[4] Stedinger, J.R., Vogel, R.M., Fofoula-Georgiou, E. (1993) Frequency Analysis of Extreme Events. In: Maidment, D.R., Handbook of Hydrology, Chapter 18, McGraw-Hill, NY.

[5] Gupta, V.K. and Waymire, E. (1990) Multiscaling properties of spatial rainfall and river flow distributions. J. Geophys. Res. 95(D3), 1999–2009.

[6] Bougadis, J. and Adamowski, K. (2006) Scaling model of a rainfall intensity – duration – frequency relationship. Hydrol. Process. 20, 3747–3757.

[7] Haktanir, T. (2003) Divergence criteria in extreme rainfall series frequency analyses. Hydrological Sciences–Journal. 48(6), 917-937.

[8] Overeem, A., Buishand, A., Holleman, I. (2008) Rainfall depth-duration-frequency curves and their uncertainties. J. Hydrology. 348, 124– 134.

[9] Kite, G.W. (1977) Frequency and Risk Analysis in Hydrology. Water Resources Publications. Fort Collins, CO.

[10] Hosking, J.R.M. (1986) The Theory of Probability Weighted Moments. Research Report RC12210, IBM Research Division, Yorktown Heights, N.Y.

[11] Hosking, J.R.M. (1990) L-moments: analysis and estimation of distributions using linear combinations of order statistics. J. Royal Stat. Soc., Series B. 52,105–124.

[12] Rao, A.R. and Hamed, H.H. (2000) Flood Frequency Analysis. CRC Press, USA.

[13] Greenwood, J.A. Landwehr, J.M. Matalas, N.C. and Wallis, J.R. (1979) Probability-weighted moments: definition and relation to parameters of several distributions expressable in inverse form. Water Resour. Res. 15, 1049–1054.

[14] Bayazit, M., Onoz, B., (2008) Flood and Drought Hydrology. Nobel Publishing, Istanbul.

[15] Saf, B., Dikbas, F. and Yasar, M. (2007) Determination of regional frequency distributions of floods in West Mediterranean River Basins in Turkey. Fresen. Environ. Bull. 16(10),1300–1308

[16] Anli, A.S. (2015) Regional and point precipitation estimation for 1975-2010 period over semi-arid Central Anatolia Region of Turkey. Fresen. Environ. Bull. 24(2a), 427-433

[17] Seckin, N., Yurtal, R., Haktanir, T. and Topaloglu, F. (2010) Regional flood frequency analysis of Ceyhan River Basin in Turkey using L-moments method. Fresen. Environ. Bull. 19 (11a), 2616-2624.

[18] Haktanir, T., Cobaner, M. and Kisi, O. (2010) Frequency analyses of annual extreme rainfall series from 5 min to 24 h. Hydrol. Process. 24, 3574–3588.

[19] Nhat L.M., Tachikawa Y., Sayama T. and Takara K. (2007) Regional rainfall intensity-duration-frequency relationships for ungauged catchments based on scaling properties. Annuals of Disas. Prev. Res. Inst., Kyoto Univ. 50, 33–43.

[20] Hald, A. (1952) Statistical Theory with Engineering Applications, Wiley-Toppan.

[21] NERC (1975) Hydrological Studies, Flood Studies Report Vol. I, Natural Environment Research Council, London, UK.

[22] Hosking, J.R.M., Wallis, J.R. and Wood, E.F. (1985) Estimation of the generalized extreme-value distribution by the method of probability-weighted moments. Technometrics. 27, 251–261.

[23] Haan, C.T. (2002) Statistical Methods in Hydrology, 2nd edition, Iowa State Press.
[24] Gumbel, E.J. (1958) Statistics of Extremes, Columbia University Press, N.Y.
[25] Aronica, G.T. and Freni, G. (2005) Estimation of sub-hourly DDF curves using scaling properties of hourly and sub-hourly data at partially gauged site. Atmospheric Research. 77, 114–123.
[26] Bengtsson, L. and Milloti, S. (2010) Extreme storms in Malmö, Sweden. Hydrol. Process. 24, 3462–3475.

Received: **11.05.2017**
Accepted: **21.08.2017**

CORRESPONDING AUTHOR

Omer Levend Asikoglu
Ege University,
Department of Civil Engineering,
Bornova, Izmir, Turkey

e-mail: omerasikoglu@ege.edu.tr

© by PSP Volume 26 – No. 12A/2017 pages 7885-7892 Fresenius Environmental Bulletin

IMPROVEMENT OF WATER USE PRODUCTIVITY THROUGH THE SRFR MODEL IN BORDER STRIP IRRIGATION OF WHEAT ACROSS HAMIDIYEH FARMS (KHUZESTAN, IRAN)

Arash Tafteh*, Mohammad Reza Emdad

Department of Irrigation and Soil Physics, Soil and Water Research Institute, Agricultural Research Education and Extension Organization (AREEO), Karaj, Iran

ABSTRACT

Scarcity of water resources makes their management one of the most important challenges faced in arid and semiarid regions. Water use management and increased water use productivity are among the most significant management options for conserving water resources, especially in the agriculture sector. This study focused on water use productivity of three fields in Hamidiyeh in Khuzestan Province, Iran. Information on the existing irrigation situation was collected and the SRFR model was then calibrated during the first year of the study. Following that, the model was used to simulate the design for the dimensions of the border strips, irrigation duration, and inflow rate, while selecting the most suitable options. Since the root zone was 40 centimeters deep and the net irrigation water was 50 millimeters deep, it was found that the most appropriate inflow rate, irrigation duration and strip length and width for achieving the maximum water use efficiency of 50% were 18 l/s, 3-3.5 hours, and 180 and 10 meters, respectively. In the second year of the study, the findings obtained from the model were applied in the farms and the results were evaluated. It was observed that the model suitably estimated water use efficiency in border strip irrigation and could be used in this irrigation practice in farms. Moreover, management of border strip irrigation by the model increased water use productivity from 0.61 in the first year to 0.89 in the second year. Therefore, this model was suggested to be used for increasing water use productivity and water use management in Khuzestan Province.

KEYWORDS:
Water use productivity, border strip irrigation, SRFR model

INTRODUCTION

Since the agriculture sector is the major consumer of water in Iran, water use management in agriculture is a critical issue. There are two determining factors involved in water use management and improved water use productivity: 1) fertilization and yield increase, which impose great costs on the farmers who avoid using them, 2) improvement in water use efficiency, which can be easily controlled in the region. Extensive research has been conducted on determining water use efficiency and water management, which will be referred to in this article. Surface irrigation is one of the oldest irrigation practices widely used in most regions of the world. Since plants use only the water stored in the root zone, water that gets out of this zone through runoff or percolation is considered lost water. Water use efficiency is defined as the ratio of water that infiltrates into the root zone to the total depth of water entering the farm. In this respect, Raine and McClymont [16] reported that the ability of the irrigation system to uniformly distribute and apply water was an economically important factor in conserving the water resources. Moreover, the suitable design and management of irrigation could ensure water. Also climate warming increase water requirement and limited surface water resources [4]. Water shortage was reduced yield of plants, and plant sensitive is variable in each period growth. Reducing yield reduces water productivity, so management of water in sensitive stage of plant growth is very important [21]. The main problem with surface irrigation practices is their low efficiency, mainly resulting from poor irrigation management [8]. However, if correct irrigation management is applied and temporal and spatial changes are made in soil characteristics, we can expect to achieve high efficiency in surface irrigation [5]. The irrigation researchers have developed various models to determine the effects of plot or strip dimensions, and also of inflow rate and slope changes, on water use efficiency and on other related components. SIRMOD and SRFR are among the common and recent practical models used to study the effects of strip dimensions (strip length and

width), inflow rate, slope and other parameters related to water use efficiency in farms. This serves to introduce suitable irrigation management practices and upgrade water use efficiency [25, 1, 22]. Using these models, extensive research has been conducted on optimizing the dimensions in surface irrigation to increase water use efficiency [26, 3, 10]. Kanoni et al. [7] reported that water use efficiency in corn fields ranged from a minimum of 12 to a maximum of 70%, while water use efficiency in sugar beet fields varied from about 30 to 80%. Mokari Gahroodi et al. [11] used the SRFR 4.1.3 model to simulate furrow irrigation noticing how it was able to simulate volumetric water balance components with good accuracy, yielding acceptable results for short to relatively long furrows.

The maximum error in the model was about six% for surface runoff and minimum three% for the inflow volume. Moridnejad et al. [13] carried out a study to increase water use efficiency in sugar cane fields using the SRFR 4.1.3 model. They employed 10 different inflow rates into the furrows. The results indicated that the inflow rate of approximately 1.5 l/s was required for achieving use efficiency higher than 70%. Taghizadeh et al. [23] evaluated the SRFR 4.1.3 model based on zero inertia and kinematic wave, using field information. The results revealed that the model exhibited maximum variations in relation to inflow rate, irrigation duration, and infiltration equation parameters. In a study on optimization of inflow rate and calibration of infiltration parameters, Valipour and Montazar [24] showed that the SFRF 4.1.3 model was highly capable in optimizing and simulating the actual conditions, and could be used satisfactorily in simulating surface irrigation. In 2001, Montesionos et al. [12] used a genetic algorithm to optimize inflow rate and irrigation duration, indicating that the two parameters were very important from the technical and economic points of view. Chen et al. [2] used the SRFR 4.1.3 model to optimize the dimensions of strips in border strip irrigation. They reported that soil water storage of about 49 millimeters exhibited the best performance and irrigation duration of 120 minutes was required for 200-meter long strips in soils with semi heavy-textured soils. They proposed strips with length of less than 120 meters and width of 3-5 meters, which improved water use efficiency by up to 26%. In their research in 2014, Nie et al. [15] found that the SRFR 4.1.3 model performed a good simulation of field data and could be used successfully for water management in surface irrigation. Studies on strip dimensions, inflow rate, and irrigation duration, and of their effects on water use efficiency, play an important role in water use management. Irrigation management is supposed to save water and also prevent agricultural soils from being washed away and damaged. The low efficiency of surface irrigation often results from poor strip design and poor irrigation management and planning. Multivariable analysis has been recommended for surface irrigation management because it yields much better results [19-9]. Therefore, it is necessary to study the contributing factors and recommend the most suitable scenario for irrigation in order to raise water use efficiency [27].

Review of previous research indicated that strip length and width, inflow rate, and irrigation duration were among the most important factors contributing to water use efficiency [6-14]. Therefore, we studied the effects of changing strip dimensions, irrigation duration, and inflow rate on water use efficiency and on water use productivity in wheat fields of Hamidiyeh (Khuzestan Province). Moreover, we suggested the most appropriate strip dimensions, inflow rate, and irrigation duration for achieving higher water use productivity and water use efficiency.

MATERIALS AND METHODS

In 2014 and 2015, three experimental fields were selected in Hamidiyeh (Ramseh) in Khuzestan Province to study the current conditions concerning water use efficiency. The three selected pilots were located in the Karkheh Watershed 25 kilometers west of Ahvaz with the longitude of 47˚41´ to 50˚39´ E and latitude of 29˚58´ to 33˚4´ N. Figure 1 displays the map of the selected fields.

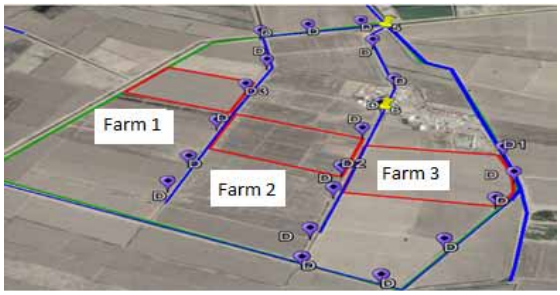


FIGURE 1
Map of the selected fields

Soil samples were taken from each pilot to measure the physical properties of the soils. Table 1 lists the means of a few physical and chemical properties of the soils in the pilots. Field studies in the region showed that surface irrigation using strips 8 meters wide and 200 meters long was the common irrigation practice. The slope of the lands in the region was 2 meters per thousand meters. Given the transverse slope of the region and the leveling that had been carried out, the slope was not a limiting factor for plant growth. Land preparation was carried out by plowing and disking.

TABLE 1
Some soil properties in selected farms

Depth cm	Soil texture	Volumetric Field capacity %	Volumetric Permanent wilting point %	pb gr/cm3	KS m/d	EC ds/m	pH
0-25	Clay Loam	31.9	19	1.48	0.045	4.5	7.2
25-45	Clay Loam	36.4	23	1.53	0.045	5	7.5
45-60	Clay Loam	36.2	22	1.53	0.045	5.4	7.7

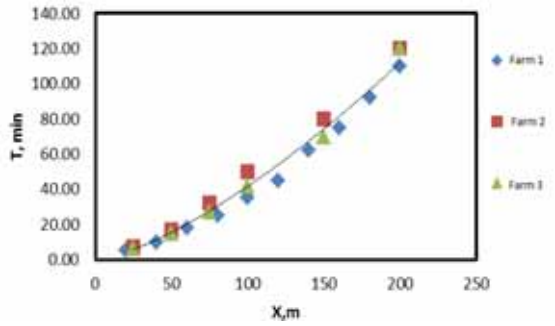


FIGURE 2
Rate of water advancement in the studied farms

The seeds were sown using a centrifugal broadcaster. The Chamran wheat cultivar was planted from 6 to 11 November, 2014 and 2015. The root zone at the end of seed formation stage (mid-March) was about 40 centimeters deep [22]. Taking into consideration the root zone depth and physical properties of the soil in the region, the net water depth each irrigation was determined using Equation 1:

$$dn = \sum_{i=1}^{n} \left(\frac{FC_i - PWP_i}{100}\right) \times D_i \quad (1)$$

In the above equation, d_n is the net irrigation need (mm), FC is the field capacity of each layer in the soil (%), PWP is the permanent wilting point for each layer (%), D is the depth of each layer (mm), and index *i* is the layer number. The soil permeability in the three selected pilots was measured through three replications (nine permeability measurements) using double-ring. Considering the mean values of the measurements made in the three pilots, the soil permeability equation (the mean of the three selected pilots) indicated that the average permeability equation follows Equation 2:

$$Z = kt^a + f_0 t \quad (2)$$

Where, Z represents the cumulative infiltration (mm), t is the contact time between water and soil (h), the empirical parameters of the equation are represented by *a* and *k*, and f_0 stands for the final infiltration rate of the soil (mm/h). The infiltration conditions for the SRFR model can be acceptably defined using this equation. As recommended by Strelkoff and Clemmens [20], the modified Kostiakov-Lewis method was employed for this purpose. The average final infiltration rate in the pilots was 4 mm/h, while the empirical parameters of the equation were determined to be 0.15 for a, and 14.04 for k. The heavy texture of the soils and the high soil bulk density (1.51 g/cm^3) reduced soil infiltration rate while decreasing cumulative infiltration. The average changes in the rate of water advancement through the soil in the studied pilots have been displayed in Figure 2.

The results indicated that the irrigation water was of suitable quality with respect to salinity (its average salinity was 1.9 dS/m) and, therefore, it was not a limiting factor for plant growth. Information related to irrigation management in the pilots included the number, the dates, and durations of irrigations. Water use efficiency was determined for each of the three irrigations in every pilot. After studying and gaining a complete understanding of the pilots, the SRFR model was calibrated for the current conditions. Then, the important design parameters including strip length and width and inflow rates for the strips in the region were the studied. At the next stage, the most suitable, practical and applicable scenario was recommended with respect to strip length and width, inflow rate, and irrigation duration needed for increasing water use efficiency. The scenario was finally implemented in the second year and the results were evaluated.

At the end of each crop year, the wheat in each strip was harvested and the yield and volume of water used for each strip were used to determine water use productivity through Equation 3:

$$WP = \frac{Yd}{Vg} \quad (3)$$

In the above equation, WP is water use productivity (kg/m^3), Y_d is wheat grain yield (kg), and V_g is the volume of irrigation water flowing into the field (m^3).

RESULTS AND DISCUSSION

Considering the changes in inflow rate and irrigation depth, Table 2 displays the range of changes in water use efficiency in the selected pilots. As shown in this figure, water use efficiency in the selected pilots varied from 27 to 32% in the first year, suggesting that most of the applied water discharged from the root zone (40 cm deep) through percolation.

TABLE 2
The range of changes in water use efficiency in the selected pilots in first year.

	Replication	Flow (l/s)	Depth of water (mm)	Net depth of water (mm)	Measured applied Water efficiency (%)	Simulated applied Water efficiency (%)	Error (%)	Water productivity (Kg/m3)
	1	19	161	50	31	28	6.9	0.60
Farm 1	2	17	185	50	27	25	7.4	0.56
	3	20	172	50	29	26	10.3	0.58
	1	18	156	50	32	30	6.2	0.71
Farm 2	2	17	160	50	31	28	9.6	0.68
	3	19	188	50	26	24	7.6	0.57
	1	18	180	50	28	25	10.7	0.59
Farm 3	2	19	165	50	30	27	10.0	0.63
	3	19	160	50	31	28	9.6	0.66

TABLE 3
Applied water efficiency for the slope of 0.2%, strip width of 8 meters

Dimension		Net depth of water	Flow l/s							
			15		18		20		22	
length m	widths m	d_n mm	Cut-off time h	Applied Water efficiency **(%)**	Cut-off time h	Applied Water efficiency **(%)**	Cut-off time h	Applied Water efficiency **(%)**	Cut-off time h	Applied Water efficiency **(%)**
			2.5	39	2	39	2	36	2	34
150	8	50	3	34	2.5	34	2.5	31	2.5	29
			3.5	30	3	30	3	27	3	25
			2.5	43	2.5	38	2.5	36	2.5	33
180	8	50	3	38	3	33	3	31	3	28
			3.5	34	3.5	30	3.5	28	3.5	25
			3.5	37	3	35	3	32	3	30
200	8	50	4	34	3.5	32	3.5	29	3.5	27
			4.5	31	4	29	4	26	4	24
			4	36	3.5	34	3.5	31	3.5	29
220	8	50	4.5	33	4	31	4	28	4	26
			5	31	4.5	29	4.5	26	4.5	24
			5	34	4.5	31	4.5	28	4.5	26
250	8	50	5.5	32	5	29	5	26	5	24
			6	30	5.5	27	5.5	24	5.5	22

Calibration revealed that the model yielded a suitable estimate of efficiency under the current conditions (with an error of 7-11%, 9% on average). It could be used to simulate water use efficiency by taking into account changes in strip dimensions and inflow rate. The initial information including strip dimensions, inflow rate into the strips, irrigation duration, slope, and information related to infiltration, which are the most important parameters in surface irrigation [6], was used to implement the SFRF 4.1.3 model for various conditions. These parameters matched the existing conditions in the region and could be used in the farms. Strips 150-250 meters long and 8-12 meters wide, inflow rates of 15-22 l/s, and various irrigation durations were tested in the SRFR4.1.3 model to determine the effects of changes in these parameters on water use efficiency. The multivariate analysis is recommended for managing surface irrigation and for determining water use efficiency because its results will be far more desirable [9]. Table 3 lists the results obtained for the slope of 0.2%. Moreover, strip width of 8 meters was selected (which is the minimum width allowing combines to enter the strip).

TABLE 4
Applied water efficiency for the slope of 0.2%, strip width of 10 meters

Dimension		Net depth of water	Flow l/s							
			22		18	20			22	
Cut-off time h	Applied Water efficiency **(%)**	Applied Water efficiency **(%)**	Cut-off time h	Applied Water efficiency **(%)**	Applied Water efficiency **(%)**	Cut-off time h	Applied Water efficiency **(%)**	Applied Water efficiency **(%)**	Cut-off time h	Applied Water efficiency **(%)**
			3	41	2.5	40	2.5	38	2.5	35
150	10	50	3.5	36	3	35	3	33	3	30
			4	33	3.5	32	3.5	30	3.5	27
			3	46	2.5	45	2.5	41	2.5	39
180	10	50	3.5	41	3	40	3	36	3	34
			4	38	3.5	37	3.5	33	3.5	31
			4	41	3.5	39	3.5	36	3.5	33
200	10	50	4.5	37	4	35	4	32	4	29
			5	35	4.5	33	4.5	30	4.5	27
			4.5	40	4	37	4	34	4	32
220	10	50	5	37	4.5	34	4.5	31	4.5	29
			5.5	35	5	32	5	29	5	27
			5.5	39	5	35	5	32	5	29
250	10	50	6	37	5.5	33	5.5	30	5.5	27
			6.5	35	6	31	6	28	6	25

TABLE 5
Applied water efficiency for the slope of 0.2%, strip width of 10 meters

Dimension		Net depth of water	Flow l/s							
			22		18	20			22	
Cut-off time **h**	Applied Water efficiency **(%)**	Applied Water efficiency **(%)**	Cut-off time h	Applied Water efficiency **(%)**	Applied Water efficiency **(%)**	Cut-off time h	Applied Water efficiency **(%)**	Applied Water efficiency **(%)**	Cut-off time h	Applied Water efficiency **(%)**
			3.5	42	3	40	3	37	3	35
150	12	50	4	38	3.5	36	3.5	33	3.5	31
			4.5	35	4	32	4	29	4	27
			4	44	3.5	42	3.5	38	3.5	36
180	12	50	4.5	40	4	38	4	34	4	32
			5	37	4.5	35	4.5	31	4.5	29
			5	41	4.5	38	4.5	34	4.5	32
200	12	50	5.5	38	5	35	5	31	5	29
			6	36	5.5	33	5.5	29	5.5	27
			5.5	41	5	37	5	35	5	31
220	12	50	6	39	5.5	35	5.5	33	5.5	29
			6.5	37	6	33	6	31	6	27
			6.5	41	6	37	6	33	6	31
250	12	50	7	39	6.5	35	6.5	31	6.5	29
			7.5	37	7	33	7	29	7	27

The inflow rate into the strips was defined within the 15-22 l/s range. The results indicated that strip length of 180-200 meters exhibited higher use efficiency than other ranges. Moreover, water use efficiency in strips 180 meters long (and 8 meters wide) at inflow rate of 15-18 l/s, slope of 0.2%, and mean irrigation duration of 3-3.5 hours varied from 34 to 38%. Furthermore, in strips 200 meters long and the same width, the mean water use efficiency was about 43% if inflow rate of 15-18 l/s was applied. Table 4 evaluates and compares various strip lengths (150-250 meters) with constant width of 10 meters and inflow rate of 15-22 l/s (at slope of 0.2% and net irrigation depth of 50 mm). The results of implementing the SRFR 4.1.3 model showed that the mean water use efficiency was about 43% at strip length and width of 180 and 10 meters if inflow rates of 15-18 l/s were applied, respectively.

Under these conditions, the most suitable water use efficiency in the field (about 46%) was obtained with strips 180 meters long and 10 meters wide at inflow rate of 15-18 l/s and irrigation duration of about 3-3.5 hours. It should be noted that if, under the mentioned conditions, strip length of 200 meters was used, the mean water use efficiency at inflow rate of 15-18 l/s would be about 41%. In other words, water use efficiency declined as strip length increased. Moreover, this paper explored various strip

lengths of 150 to 250 meters at the constant strip width of 8 meters and inflow rate of 15-22 l/s, slope of 0.2%, and net irrigation depth of 50 mm (Table 5).

The results of implementing the SRFR 4.1.3 model indicated that water use rate in the field (44%) was achieved at strip length and width of 180 and 12 meters, respectively, at inflow rate of 15-18 l/s. If strip length increased to 200 meters (at strip width of 12 meters), the mean use efficiency at inflow rate of 15-18 l/s decreased to 41% as irrigation duration extended.

As can be seen, the average water use efficiency in strips 180 meters long and 8 meter wide at inflow rate of 15-18 l/s, irrigation duration of 3.5-4 hours, and net irrigation depth of 70 mm was about 46% in the two studied slopes. These results were consistent with those obtained by Raghuwanshi [17] who adopted the SRFR 4.1.3 model, reporting a border strip irrigation efficiency of up to 50%. The results of the present research indicated that the highest use efficiency was obtained at strip length of 180 meters. This revealed the mean changes in use efficiency at that length and at three different strip widths (Figure 3).

It was found that 10 meters was the best strip width and inflow rate of 15-18 l/s did not lead to any remarkable reduction in water use efficiency when there were strips 10 and 12 meters long. However, at strip width of 8 meters, the slope of decline in water use was steeper than changes in inflow rate, and the inflow rate of 15 l/s was recommended for this strip width. Moreover, there were severe reductions in efficiency at all three strip widths and inflow rates higher than 19 l/s. Therefore, inflow rate of higher than 19 l/s into each strip was not recommended.

The results obtained from the three experimental fields during the first year were used in the second year, based on recommendations of the SFRF 4.1.3 model, on strips 180 meters long and 10 meters wide. All the measured parameters in the second year were also studied (Table 6).

The results of evaluation indicated that the new model was able to make good estimates of border strip irrigation conditions with an error margin of 6-15%. The water use productivity improved from 0.6 to 0.9 kg/ha on average through applying the proposed management model (Table 7).

Since fertilization conditions were the same in both years, the results of statistical analysis showed that there were no significant differences between the yields of the two years. Therefore, the only factor increasing water use productivity, as was shown by using the SRFR model, was the modification in strip dimensions and inflow rate.

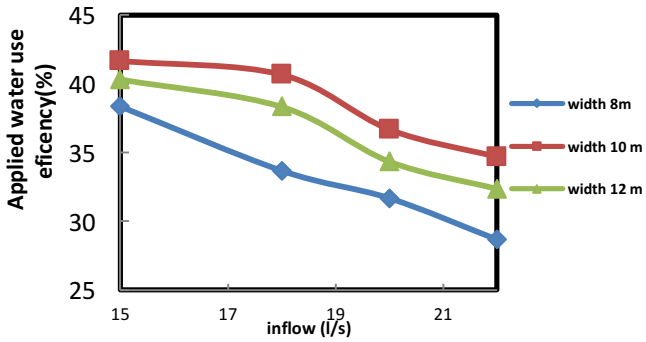


FIGURE 3
Changes in applied water use efficiency at three different strip widths

TABLE 6
The range of changes in water use efficiency in the selected pilots in second year.

	Replication	Flow (l/s)	Depth of water (mm)	Net depth of water (mm)	Measured applied Water efficiency (%)	Simulated applied Water efficiency (%)	Error (%)	Water productivity (Kg/m3)
Farm 1	1	18	110	50	45	40	0.11	0.97
	2	20	115	50	43	37	0.14	0.81
	3	22	120	50	41	35	0.15	0.97
Farm 2	1	18	114	50	44	40	0.09	1.01
	2	20	142	50	35	37	0.06	0.8
	3	22	152	50	33	35	0.06	0.75
Farm 3	1	18	108	50	46	40	0.13	0.98
	2	20	125	50	40	37	0.08	0.89
	3	22	132	50	38	35	0.08	0.83

TABLE 7
Statistical analysis of seed yield of wheat in two years

Farm	First year yield		Second year yield	
	2900		3200	
1	2800	**2900b**	2830	**3240a**
	3000		3480	
	3300		3440	
2	3250	**3250a**	3420	**3420a**
	3200		3400	
	3200		3170	
3	3100	**3150a**	3342	**3263a**
	3150		3277	
Mean	3281**A**		3100**A**	

CONCLUSIONS

Considering the excessive financial costs of using plant nutrient packages, the best way for farmers to manage water in fields is to reduce the application of plant nutrient in surface irrigation. The present research showed that reducing strip length from 200 to 180 meters the water use efficiency from 22 to 45% (more than two-fold). Therefore, it is recommended that strips 180 meters long and 10 meters wide, inflow rate of 15-18 l/s, and irrigation duration of 3-3.5 hours be used in border strip irrigation to improve water use efficiency to about 45%. Moreover, the SRFR proved to be a highly desirable model for managing water use in agricultural lands, capable of simulating water management in the fields. As a significant achievement in farm water management, water use productivity improved by 50% through applying water use management in surface irrigation.

REFERENCES

[1] Bautista, E., Schlegel, J.L. and Strelkoff, T.S. (2012) WinSRFR 4.1 - User Manual. USDA-ARS Arid Land Agricultural Research Center. 21881 N. Cardon Lane, Maricopa, AZ, USA.

[2] Chen, B., Zhu, O. and Zhigang, S., Lanfang W. and Fadong, L. (2012) Evaluation on the potential of improving border irrigation performance through border dimensions optimization: a case study on the irrigation districts along the lower Yellow River. Irrig Sci. 31, 715–728.

[3] Eldeiry, A., Garcia, L., Ei-Zaher, A.S.A. and El-Sherbini Kiwan, M. (2005) Furrow Irrigation System Design for Clay Soils in Arid Regions. Appl. Eng. Agric. 21(3), 411- 420.

[4] Fu, A., Chen, Y., Li, W., Zhang, S., Wang, R. and Li, D. (2017) Effects of climate warming on surface water availability and water demand for oases in arid regions of northwest China. Fresen. Environ. Bull. 26(5), 3268-3279.

[5] Gatta, G., Giuliani, M.M., Monteleone, M., Nardella, E. and De Caro A. (2007) Deficit irrigation scheduling in processing tomato. Water saving in Mediterranean agriculture and future research needs. 1, 277-289.

[6] Gillies, M.H., Smith, R.J. and Raine, S.R. (2008) Measurement and Management of Furrow Irrigation at the Field Scale. Irrigation Australia 2008-Share the Water, Share the Benefits: Irrigation Australia National Conference and Exhibition, Melbourne, Australia.

[7] Kanoni, A., Karimi, M., Esmaeli, V., and Taghinejad, J. (2005) Evaluation of furrow Irrigation efficiency under different management in region of Moghan. Final report of the Institute of Technical and Engineering Research. 53p. (In Persian with English Abstract).

[8] Khatri, K.L. and Smith, R.J. (2006) Real-time prediction of soil infiltration characteristics for management of furrow irrigation. Irrigation Science. 25(1), 33-43.

[9] Ma, J.J., Sun, X.H., Guo, X.H. and Li, Y.F. (2010) Multi-objective Fuzzy Optimization Model for Border Irrigation Technical Parameters. J. Drain. Irrig. Mach. Eng. 28(2), 160-178.

[10] Mailhol, J.C., Ruelle, P. and Popova, Z. (2005) Simulation of furrow irrigation practices _SOFIP_: A field-scale modelling of water management and crop yield for furrow irrigation. Interfaces. 241, 37-48.

[11] Mokari Gahroodi, E., Liaghat, A.M. and Nahvinia, M.J. (2013) Application of WinSRFR3.1 Model in Furrow Irrigation Simulation. Iranian Journal of Irrigation and Drainage. 1(7), 59-67 (In Persian with English Abstract).

[12] Montesionos, P., Camacho, E. and Alvarez, S. (2001) Seasonal furrow irrigation model with genetic algorithms (OPTIMEC). Agriculture Water Management. 52, 1–16.

[13] Moridnejad, A., Kavei Deylami, R. and Sadi, A. (2010) Optimization of furrow irrigation under implemented conditions in Salman Farsi Agro-Industry by using of SRFR model. Collected paper of third National Conference on Irrigation and Drainage Network Management. Shahid Chamran University. Ahvaz. Department of Water Sciences, 8 pages. https://www.civilica.com/Paper-IDNC03-IDNC03_618.html.(In Persian with English Abstract).
[14] Navabian, M., Liaghat, A.M., Smith, RJ. and Abbasi, F. (2009) Empirical Functions for Dependent Variables in Cutback Furrow Irrigation. Irrig. Sci. 27(3), 215-222.
[15] Nie, W.B., Fei1, L.J. and Ma, X.Y. (2014) Applied Closed-end Furrow Irrigation Optimized Design Based on Field and Simulated Advance Data. J. Agr. Sci. Tech. 16, 395-408.
[16] Raine, R. and Mcclymont, J. (1997) The development of guidelines for surface irrigation in areas with variable infiltration. Proceeding of Australian Society of Sugarcane Technologists. 293-301.
[17] Raghuwanshi, N.S., Saha, R, Mailapalli, D.R., and Upadhyaya, S.K.J. (2011) Infiltration Evaluation Strategy for Border Irrigation Management. Journal of Irrigation and Drainage Engineering. 137(9), 602-609.
[18] Saha, R. (2010) An investigation of surface and subsurface flow characteristics during an alfalfa irrigation event. Ph.D. Thesis, Univ. of California, Davis, CA.
[19] Sanchez, C.A., Zerihun, D. and Farrell-Poe K.L. (2009) Management Guidelines for Efficient Irrigation of Vegetables Using Closed-end Level Furrows. Agric. Water Manage. 96(1), 43-52.
[20] Strelkoff, T.S., and Clemmens, A.J. (2006) Hydraulics of surface systems. Design and operation of on-farm irrigation systems, 2nd Ed. Chap. 13. Hoffman, G.J., Evans, R.G., Jensen, M.E., Martin, D.L. and Elliott, R.L. (eds.) ASABE Special Monograph, American Society of Agricultural and Biological Engineers, St. Joseph, MI.
[21] Tafteh, A., Babazadeh, H., EbrahimiPak, N.A., and Kaveh F. (2013) Evaluation and improvement of crop production functions for simulation winter wheat yields with two types of yield response factors. Journal of Agricultural Science. 5(3), 111-122.
[22] Tafteh, A., Emdad, M.R. and Ghalebi, S. (2017) Investigation of effective factors on water use efficiency of border irrigation at actual and extensible root zone depth of wheat in Hamidieh (Khuzestan). Water and Soil resources Conservation. 6(4), 75-90 (In Persian with English Abstract).
[23] Taghizadeh, Z., Verdinejad, V.R., Ebrahimian H. and Khanmohammadi, N. (2012) Field Evaluation and Analysis of Surface Irrigation System with WinSRFR (Case Study Furrow Irrigation). Journal of Water and Soil. 26(6), 1450-1459.
[24] Valipour, M. and Montazar, A.A. (2012) An Evaluation of SWDC and WinSRFR Models to Optimize of Infiltration Parameters in Furrow Irrigation. Am. J. Sci. Res. 69, 128- 142.
[25] Walker, W. (1989) Guideline for designing and evaluating surface irrigation systems. FAO Irrigation and Drainage Paper, No. 45, Rome, 1-137.
[26] Zerihun, D., Sanchez, C.A. and Farrell-Poe, K.L. (2005) Analysis and design of border irrigation systems. Trans. ASAE. 48(5), 1751–1764.
[27] Zou, W., Lu, X. and Han X. (2017) Effect of irrigation regime on soybean biomass, yield, water use efficiency in a semi-arid and semi-humid region in northeast China. Fresen. Environ. Bull. 26(3), 1865-1875.

Received: **11.05.2017**
Accepted: **30.08.2017**

CORRESPONDING AUTHOR

Arash Tafteh
Department of Irrigation and Soil Physics
Soil and Water Research Institute
Agricultural Research Education and Extension Organization (AREEO)
Karaj – Iran

e-mail: arash_tafteh@yahoo.com

© by PSP Volume 26 – No. 12A/2017 pages 7893-7899 Fresenius Environmental Bulletin

PROTECTIVE CHARACTERISTICS OF CAFFEIC ACID PHENETHYL ESTER(CAPE) ON NEURODEGENERATIVE EFFECTS OF ORGANOPHOSPHATE INSECTICIDE IN RATS

Lacine Aksoy[1,*], Omer Hazman[1], Ahmet Buyukben[2]

[1]Department of Chemistry, Biochemistry Division, Faculty of Science and Arts, Afyon Kocatepe University, 03200 Afyonkarahisar, Turkey
[2]Cay Vocational School, Afyon Kocatepe University, 03200 Afyonkarahisar, Turkey

ABSTRACT

This study was designed to examine the potential oxidative stress of malathion, an insecticide with organophosphate, on the brain and relevant effects of CAPE. The control group was not subject to any administration. Sham group was administered a dissolvent, DMSO. MAL group was injected 0.8 g/kg malathion. CAPE group rats were administered 10 μM/kg CAPE dissolved in DMSO. CAPE + MAL group was first administered 10 μM/kg CAPE dissolved in DMSO, and one hour later they were administered 0.8 g/kg malathion. MAL + CAPE group rats were first administered 0.8 g/kg malathion, and one hour later they were administered 10 μM/kg CAPE dissolved in DMSO. MDA, NO, GSH, CAT levels were measured in blood and brain tissue and acetylcholinesterase and erythrocyte SOD and GPx levels were measured in serum. The obtained results indicated that malathion was a neurotoxic agent, produced lipid peroxidation in erythrocytes, hence did not cause any damage other than lipid peroxidation on the brain. In addition to lipid peroxidation, free radical formation could be mentioned as well. It is considered that CAPE has a supportive effect on the antioxidant system against the damage caused by malathion, and has a protective effect on neurotoxicity.

KEYWORDS:
Malathion, CAPE, Lipid peroxidation, Oxidant, Antioxidant

INTRODUCTION

Organic phosphate (OP) compounds are insecticides containing one or more phosphorus atoms in their structure. The interaction of these compounds occurs via digestion and respiration. Various poisoning cases occur due to the unconscious use. They are used in controlling the effects of pests in agriculture and in households. Although there exists accidental poisoning due to exposure or inhalation, severe poisoning usually occurs due to suicidal intake. OP compounds were used for many years with respect to their low photo toxicity and fast dissolution rate, and their low toxicity effects in mammals. Organophosphates cause acetylcholine accumulation through the inhibition of acetylcholinesterase in target tissues [1]. Thus, they cause irreversible acute or chronic intoxication along with the damage on nerve functions [2]. Insecticides with organophosphate are absorbed through the respiratory tract and gastrointestinal mucosa. Insecticides are quickly absorbed through the skin lipophilic character of organophosphate. They accumulate on fatty tissue, liver, kidney and salivary glands after being absorbed dermally or inhalation [3, 4].

Insecticides with OP are organically composed of phosphoric or phosphoric acid linked ester or amides. Malathion is one of the most important components of this category. Malathion or O,O-dimethyl-S- (1,2-Dicarbethoxyethyl) phosphorothioate is often used to expel insects in fruits and vegetables [5, 6]. Compared to other insecticides with organophosphate as parathion or mevinphos, malathion has lower toxicity in mammals. This largely depends on the presence of enzymes that are capable of hydrolyzing the carboxyl group in order to obtain mono and dicarboxylic acid analogs of malathion. Empirical research and occupational exposure proved that malathion is slightly toxic. It exhibits the poisoning symptoms that insecticide with organophosphate exhibit. Fatality occurs due to inhibition of cholinesterase, accumulation of acetylcholine, and deterioration of the nervous system [7]. The malathion taken into the body is transformed into maloxon with a metabolite, and when hydrolyzed other toxic analogs of malathion, monocarboxylic and dicarboxylic acids occur. Other hydrolysis products in the urine are dimethylthio phosphoric acid and dimethylthio phosphoric acid [8].

Propolis is a substance collected by the bees from saps to cover the holes and cracks in the hive and to provide hygiene via preventing the entrance of foreign substances and microorganisms. Caffeic acid phenethyl ester (CAPE) is the most important active component of propolis. CAPE, structurally similar to flavonoids, has two annular structures. Two functional "–OH" groups of the molecule are in one of these annular structures. Hydroxyl groups ex-

hibit oxidant and reductant characteristic due to actively exchanging electrons. They are also lipophilic in nature, since they carry long carbon groups in aromatic and aliphatic structure. Thus the molecule easily passes the cell membrane structure and reaches the region of influence. When administered intraperitoneally, CAPE reaches a sufficient blood concentration. In 10 mmol/kg concentration, CAPE blockades the xanthine-xanthine oxidase system and the formation of reactive free oxygen radicals. This situation is confirmed in various studies through the significant decrease of malondialdehyde level formed secondarily to the oxidation of the polyunsaturated fatty acids. CAPE was proven to repress the protein tyrosine kinases, cyclooxygenase and lipoxygenase activity and thus to inhibit lipid peroxidation [9, 10].

There are various studies that indicate the antimutagenic, antiviral, antifungal, antioxidative effects of propolis [11, 12]. In this study, CAPE is administered to rats that are exposed to organophosphate toxication. It was aimed to investigate the neuroprotective effects of CAPE on the oxidative stress induced by malathion.

MATERIALS AND METHODS

Animals and Experimental Design.42 male Wistar Albino rats, which are 3 months old and weigh 180-240 grams, are used. Animal experimentation ethics committee approval (date 14.06.2012 and reference number 180) was obtained for the study. The study was conducted in accordance with the Guide for the Care and Use of Laboratory. Ras were distributed into 6 groups, each containing 7 rats, according to their weights. The control group (Group 1) was not subject to any substance administration. Sham group (Group 2) rats were administered dimethyl sulfoxide (DMSO).MAL group (Group 3) rats were intraperitoneally injected with a dose of 0.8 g/kg malathion. CAPE group (Group 4) rats were administered 10 µM/kg CAPE dissolved in DMSO, via intraperitoneal injection. CAPE+MAL group (Group 5) rats were administered 10 µM/kg CAPE dissolved in DMSO via intraperitoneal injection an hour before the injection of 0.8 g/kg dose of malathion. MAL+CAPE group (Group 6) rats were administered 10 µM/kg CAPE dissolved in DMSO via intraperitoneal injection an hour after the injection of 0.8 g/kg dose of malathion. 24 hours after the administrations necessary blood and brain tissue samples were taken from all animals due to the application of ketamine HCl 50 mg/kg/im (Alfamin, Egevet, Istanbul, Turkey) ve xylazine HCl 7 mg/kg/im (Rampun, Bayer AG, Germany).

Biochemical analysis in plasma, erythrocyte and brain tissue. Blood samples were separated into plasma and erythrocytes. For malondialdehyde (MDA) measurement in erythrocyte sample for the measurement of Jain et al.'s [13] method was used and to determine the levels of MDA in brain tissue samples Ohkawa et al.'s [14] method was applied. These methods are founded on the reaction of thiobarbituric acid (TBA) with MDA. NO determination in plasma samples and brain tissue homogenates was conducted according to the method explained in Miranda et al. [15]. In this method, nitrate is converted to nitrite via Vanadium (III) chloride (VCl_3). The absorbance of the complex formed by the reaction of nitrite and sulfanilamide with N-(1-Naphthyl) ethylene diamine dihydrochloride (NEDD) in acidic media was measured. GPx (RANSEL) and SOD (RANSOD) activities were determined using the commercial kits (Randox Labs, Crumlin, United Kingdom). GSH concentration in erythrocyte samples and brain tissue homogenates were measured by the method defined by Beutler et al. [16]. Catalase (CAT) is an enzyme, which is known to break H_2O_2 into water and oxygen. Measurement of the activity of this enzyme was performed using H_2O_2 as a substrate [17].

Total protein concentrations in tissue homogenates were measured via the commercial kits (Fluka 51254) [18]. In all biochemical measurements, ELISA (Biotek ELx800) was used.

Statistical Analysis. Data obtained in the study is presented as mean ± standard deviation. Data were evaluated by one-way variance analysis (One Way ANOVA) and Duncan Posttest. Statistical evaluations were performed using SPSS 15.0 software package.

RESULTS

Oxidative Stress Markers and Acetylcholinesterase Activity in Blood and Sample Tissues.MDA concentrations in plasma and brain tissue were measured in this study. According to Table 1, plasma MDA concentration in malathion administered group was found to be statistically significant ($p<0.05$) in comparison to sham and control groups. MDA concentration values of MAL+CAPE group and CAPE+MAL group was observed to statistically significantly ($p<0.05$) increase in comparison to sham group values. MDA concentration of solely CAPE group significantly ($p<0.05$) decreased in comparison to MALgroup. Significant ($p<0.05$) difference was observed in the MDA concentration values of the brain tissue MALgroup in comparison to the sham and control group values. CAPE group's MDA concentration values were observed to have significant ($p<0.05$) difference when compared to the MAL group values. MDA concentrations of the preventive and therapeutic groups exhibited a significant ($p <0.05$) increase in comparison to the MDA concentrations of MAL group. MDA concentrations

of the preventive and therapeutic groups preventive and therapeutic group of MDA concentration values appeared to have a significant ($p < 0.05$) increase only in comparison to the MDA concentration values for the CAPE group. A significant ($p < 0.05$) decrease was observed in the concentration values of the CAPE group when compared to the control group MDA concentrations.

As the NO concentrations presented in Table 1 are scrutinized, it is possible to observe that plasma NO concentrations of the MAL group are statistically significantly ($p<0.05$) different than the NO concentrations of the CAPE+MAL group, determined as the preventative group. NO concentrations of the Sham group are as well found to be statistically significantly ($p<0.05$) different than the NO concentrations of the CAPE+MAL group, determined as the preventative group. Brain tissue CAPE group's NO concentrations were found to be statistically significantly ($p<0.05$) different from all other groups. NO concentrations of the control group were also found to be statistically significantly ($p<0.05$) different from all other groups. NO concentrations of the MAL group were determined as statistically significantly ($p<0.05$) higher than the MAL+CAPE and CAPE+MAL groups.

In Table 1, it is observed that malathion administered group's acetylcholinesterase concentration is statistically significantly ($p<0.05$) different than all other groups. In the acetylcholinesterase concentration of the CAPE administered group statistically significantly ($p<0.05$) difference was observed when compared to the MAL and MAL+CAPE groups. The control group's acetylcholinesterase concentration exhibited significant ($p<0.05$) difference in comparison to CAPE and CAPE+MAL groups.

TABLE 1
Blood and Brain Tissue Oxidative Stress Markers and Acetylcholinesterase Activity

	Control	Sham	MAL	CAPE	CAPE+ MAL	MAL+CAPE
MDA(Erytrocyte) **nmol/gHb**	31.29±0.7^{a}	29.83±0.95^{a}	48.38±1.79^{d}	35.86±1.98^{b}	35.52±0.99^{b}	39.33±2.55^{c}
MDA(Brain) **nmol/g protein**	122.90±6.99^{a}	96.38±8.46^{d}	48.58±4.13^{b}	73.49±8.98^{c}	67.11±5.52^{c}	71.78±6.19^{c}
NO (Plasma) **µmol/L $(NO)_{\chi}$**	110.88±9.73^{ab}	115.64±5.32^{a}	114.57±6.05^{a}	108.36±2.27^{ab}	103.89±8.53^{b}	107.23±4.83^{ab}
NO (Brain) **µmol $(NO)_{\chi}$/mg protein**	326.98±5.71^{d}	358.79±20.05^{a}	353.91±8.02^{a}	225.93±7.80^{b}	250.37±8.1^{c}	248.70±9.47^{c}
Asetilkolinesteraz (Serum) **IU/L**	171.69±21.16^{c}	155.39±33.86^{bc}	95.25±5.94^{a}	135.16±25.52^{b}	135.96±10.86^{b}	178.20±19.20^{c}

a, b, c, d, : Differences between the groups that are coded with different letters in the same line are significant ($p<0.05$). MAL represents the group administered with malathion; CAPE represents the group solely administered with caffeic acid phenethyl ester; CAPE+MAL represents the group administered 10 µM/kg CAPE, after one hour, 0.8 g/kg malathion was injected; MAL+CAPE represents the group administered 0.8 g/kg malathion, after an hour, 10 µM/kg CAPE was administered.

TABLE 2
Erytrocyte and Brain Tissue Antioxidant Enzyme Activities

	Control	Sham	MAL	CAPE	CAPE+MAL	MAL+CAPE
GSH (Erytrocyte**)** **nmol/gHb**	5.28±0.24^{b}	6.49±0.63^{c}	6.27±0.41^{c}	7.12±0.34^{a}	6.73±0.23^{ac}	6.60±0.36^{ac}
GSH (Brain) **µmol/g protein**	731.76±18.65^{a}	428.82±20.99^{b}	737.28±33.43^{a}	728.62±6.46^{a}	433.91±7.01^{b}	690.48±6.55^{c}
CAT (Erytrocyte) **k/g Hb**	2.95±0.10^{ae}	2.12±0.05^{c}	1.34±0.08^{b}	3.01±0.07^{a}	2.68±0.03^{d}	2.86±0.05^{e}
CAT (Brain) **k/g protein**	3.51±0.06^{b}	2.28±0.07^{c}	1.48±0.14^{d}	2.10±0.07^{a}	2.47±0.06^{e}	2.07±0.09^{a}
SOD (Erytrocyte) **U/g Hb**	1007.17±84.51^{b}	1046.52±236.49^{b}	622.04±181.37^{a}	1176.04±219.78^{b}	1058.46±271.29^{b}	921.19±65.10^{b}
GPx (Erytrocyte) **U/g Hb**	56.38±13.30^{b}	61.67±16.12^{b}	39.77±7.05^{a}	54.50±3.02^{ab}	96.86±16.58^{c}	104.98±7.05^{c}

a, b, c, d, e: Differences between the groups that are coded with different letters in the same line are significant ($p<0.05$). MAL represents the group administered with malathion; CAPE represents the group solely administered with caffeic acid phenethyl ester; CAPE+MAL represents the group administered 10 µM/kg CAPE, after one hour, 0.8 g/kg malathion was injected; MAL+CAPE represents the group administered 0.8 g/kg malathion, after an hour, 10 µM/kg CAPE was administered.

Antioxidant Enzime Activities in Erythrocytes and Brain Tissue.GSH concentrations in erythrocytes and brain tissue were measured in the study. As seen in Table 2, in erythrocytes, GSH concentrations of the MAL group were significantly ($p<0.05$) different than the GSH concentrations of the CAPE and the control group. GSH concentrations of the preventive and therapeutic groups were observed to have a significant ($p<0.05$) increase when compared to the GSH concentrations of the control group. In the brain, GSH concentrations of the MAL group presented a significant ($p<0.05$) increase when compared to GSH concentrations of the preventive and therapeutic groups. GSH concentrations of the CAPE group were observed to significantly ($p<0.05$) increase in comparison to the GSH concentrations of the preventive and therapeutic groups. MAL+CAPE administered group's and CAPE+MAL administered group's GSH concentrations exhibited significant ($p<0.05$) difference when compared to the malathion group.

CAT concentrations in erythrocyte and brain were measured in the study. According to Table 2, erythrocyte CAT concentrations of the MALgroup were found to significantly ($p<0.05$) decrease in comparison to the sham and control groups. CAPE group's CAT concentration values were found to be significantly ($p<0.05$) increasing in comparison to the sham and MAL groups' values. CAT concentration of the CAPE group was observed to have a significant ($p<0.05$) difference when compared to the CAT concentrations of the preventive and therapeutic groups. As the bran CAT concentration values are scrutinized (Table 2), all groups' CAT concentrations exhibit statistically significant ($p<0.05$) difference from each other, while the CAT concentrations of the CAPE group exhibited no significant difference than the MAL+CAPE group.

Erythrocyte SOD concentrations are as well measured in this study. As Table 2 is scrutinized, it is observed that erythrocyte SOD concentrations of the MAL group is statistically significantly ($p<0.05$) different than all other groups. When erythrocyte GPx concentrations are scrutinized, GPx concentration of the MAL group is found to be significantly ($p<0.05$) different than all other groups, except the GPx concentrations of the CAPE group. GPx concentrations of the control and sham groups were observed to have significant ($p<0.05$) difference when compared to the CAPE+ MAL and MAL+CAPE groups.

DISCUSSION AND CONCLUSION

Pesticides are chemo-toxins, which are capable of stimulating the formation of reactive oxygen species (ROS). Different types of pesticides were found to increase the production of ROS species such as hydrogen peroxide, superoxide anion and hydroxyl radical. It is known that, ROS formation causes oxidative stress, and this oxidative stress causes an imbalance between the free radical production and the antioxidant activity, thus the situation results in cellular damage. ROS increase in the cell increases the lipid peroxidation as well. The increase of ROS could cause the deterioration of the antioxidant defense and the deficiency in repairing the oxidative impairment leads to damage [19, 20].

Biomembranes and intracellular organelles are susceptible to the attacks of oxidants due to the unsaturated fatty acids in membrane phospholipids. Malondialdehyde (MDA), which is one of the most important products of the lipid peroxidation, causes the crosslinking of the compounds in the cell membrane and the adverse effects such as change of enzyme activity and ion permeability, via affecting the ion exchange through the cell membranes. MDA occurs as the final product of the lipid peroxidation and is an important indicator in oxidative damage. Pesticides were reported to increase the MDA level in tissues. Several in vivo and in vitro studies proved increase in MDA levels due to the administration of chlorpyrifos and diazinon[21, 22]. In this study, in erythtocytes, MDA levels in the MALgroup were found to be higher than the control group levels and it was concluded that lipid peroxidation occurred.

However, several studies reported that OP administration caused no change in MDA levels. In a study conducted by Alp et al. [23], effects of CAPE and ellagic acid against OP toxication were investigated and it was reported that no difference of MDA levels in the kidney and lung tissues for the MAL group were observed in comparison to the MDA levels of the control group. This study as well revealed similar findings. MDA levels of the MAL is not higher than the values of the control group.

Nitric oxide is a molecule, which has antioxidant and pro-oxidant properties. NO yields a reaction with superoxide to form a more toxic oxidant, peroxynitrite (ONOO), through a radical termination reaction at a high and constant speed. It is difficult to detect NO, since it is capable to transform into other molecules in a short time. Nitrite and nitrate, which are the stable oxidation end-products of NO, could be traced in biological fluids and are results of in vitro and in vivo production of NO [24]. In this study, no change of plasma NO values were observed. Hence, the higher levels of NO in the brain in MAL group in comparison to the control group is an indication of the increase in free radical formation.

Organophosphate insecticides cause excessive stimulation in the cholinergic synapse due to the inhibition of AChE and cholinesterase enzymes. Measurement of serum cholinesterase is a commonly used marker. Organophosphates cause acetylcholine accumulation in tissues by irreversibly binding to the acetylcholinesterase enzyme in the central and autonomic nervous system, neuromuscular end

plate and erythrocytes. Due to the accumulation of acetylcholine, increased cholinergic effects occur as a result of the excessive stimulation of the muscarinic and nicotinic receptors. Through the neurotoxic effect created in such a way, they cause acute or chronic poisoning [25]. Various studies indicated that organophosphate pesticide applications inhibit acetyl cholinesterase. Similarly, present study indicates that acetylcholine esterase levels in the MAL were lower that the control group. It is possible to acknowledge the neurotoxic effects caused by CAPE and the positive effects of CAPE when employed as treatment.

The inactivation of the reactive oxygen species and their removal from the environment are strongly related to the anti-oxidative defense mechanism. Antioxidants prevent the lipid peroxidation and cell damage via preventing peroxidation chain reactions or consolidating the free radicals. Main antioxidants are glutathione, superoxide dismutase, GPx, and CAT [26]. SOD is an endogenic antioxidant enzyme, which plays an important role against the damage caused by the free oxygen radicals in our body. SOD enzyme transforms the superoxide radical into the less reactive hydrogen peroxide. As the superoxide radical is not removed from the environment, it reacts with nitric oxide and transforms into a strong oxidant agent, peroxynitrite. Consequently, SOD enzyme protects the cells against the superoxide radical and peroxynitrite exposure [27, 28]. In this study it was observed that SOD enzyme activity for MAL group was lower than all other groups. It is possible that the SOD enzyme could be used in erythrocytes, since it is capable of transforming superoxide radicals that are increased due to the oxidative stress caused by malathion into H_2O_2.

CAT and GPx, which are endogenic antioxidant enzymes, reduce the hydrogen peroxide in the environment into water, rendering it into a harmless substance. CAT and GPx enzyme activities in the erythrocytes od the malathion administered group could appear to be low, since they might be used to reduce the hydrogen peroxide and the oxidative stress caused by it. Use of CAPE as preventive and curative in erythrocytes as well provides positive effects on the CAT and GPx enzyme activities. CAT activity in the brain could be interpreted similar to the phenomenon in the erythrocytes.

Glutathione (GSH) is a non-protein tripeptide that has a variety of cellular functions such as providing the detoxification of electrophilic xenobiotics and removal of ROS from the cells [29, 30]. The brain is an organ, which is particularly susceptible to oxidative damage. It has high levels of ROS production, highly oxidative metabolism and includes intensive levels of PUFA in the cell membranes. GSH is prominent among several ROS removal agents. This system does not only serve as the peroxide remover, but also regulates the redox state of the cells. ROS play a significant role in the formation of damage in the neurodegenerative processes. Some of the neural cells are more resistant to oxidative stress. It is acknowledged that high GSH content is a significant contribution to such resistance. Lipoproteins in the central nervous system are extremely important in supporting several brain functions. High PUFA content in the brain membranes, which has a considerably low defense, makes this tissue especially important against oxidative damage [31, 32]. In the present study, the GSH concentrations of neither the MAL group, nor the CAPE group exhibited a difference when compared to the control group. In the erythrocytes, the GSH concentrations of both the MAL group and the CAPE group were found to be higher than the control group.

Consequently, as the acetyl cholinesterase levels demonstrate, malathion has neurotoxic effects. Malathion also leads to lipid peroxidation in the erythrocytes and does not cause any other damage in the brain other than lipid peroxidation damage, similar to the findings of other studies. This suggests that the damage occurring in the brain could be protein-based. When the nitric oxide levels were scrutinized, it was observed that malathion increased the free radical formation. Besides, it is possible to observe CAPE's lipid peroxidation reducing effects and inhibitory effects on the formation of free radicals. Due to the high GSH, CAT, SOD and GPx levels in brain and/or erythrocytes, it is possible to assert that CAPE is an agent, which supports the antioxidant system and protects the brain tissue against the malathion induced damage.

REFERENCES

[1] Jeyaratnam, J. and Maroni M. (1994) Organophosphorous compounds. Toxicology. 91, 15–27.

[2] Abu-Qare, A.W. and Abou-Donia, M.B. (2001) Simultaneous determination of malathion, permethrin, DEET (N,N-diethyl-m-toluamide), and their metabolites in rat plasma and urine using high performance liquid chromatography. Journal of Pharmaceutical and Biomedical Analysis. 26, 291-299.

[3] Karalliedde, L. and Senanayake, N. (1989) Organophosphorus insecticide poisoning. British Journal of Anaesthesia. 63, 736-750.

[4] Zendzian, R.P. (2003) Pesticide residue on/in the washed skin and its potential contribution to dermal toxicity. Journal of Applied Toxicology. 23, 121-136.

[5] Namera, A., Yashiki, M., Nagasawa, N., Iwasaki, Y. and Kojima, T. (1997) Rapid analysis of malathion in blood using head space-solid phase microextraction and selected ion monitoring. Forensic Science International. 88, 125-131.

[6] Yoshii, K., Tsumura, Y., Ishimitsu, S., Tonogai,Y. and Nakamuro K. (2000) Degradation of malathion and phenthoate by glutathione reductase in wheat germ. Journal of Agricultural and Food Chemistry. 48, 2502-2505.
[7] Thompson, T.S., Treble, R.G, Magliocco, A., Roettger, J.R. and Eichhorst J.C. (1998) Case study: fatal poisoning by malathion. Forensic Science International. 20. 89-98.
[8] Zhao, X. and Hwang, H.M. (2009) A study of the degradation of organophosphorus pesticides in river waters and the identification of their degradation products by chromatography coupled with mass spectrometry. Archives of Environmental Contamination and Toxicology. 56, 646-653.
[9] Tsai, C.F., Kuo, Y.H., Yeh, W.L., Wu, C.Y., Lin, H.Y., Lai, S.W., Liu, Y.S., Wu, L.H., Lu, J.K. and Lu, D.Y. (2015) Regulatory effects of caffeic acid phenethyl ester on neuroinflammation in microglial cells. International Journal of Molecular Sciences. 16, 5572-5589.
[10] Tolba, M.F., Omar, H.A., Azab, S.S., Khalifa, A.E., Abdel-Naim, A.B. and Abdel-Rahman, S.Z. (2014) Caffeic acid phenethyl ester: A review of its antioxidant activity, protective effects against ischemia-reperfusion injury and drug adverse reactions. Critical Reviews in Food Science and Nutrition. 56, 2183-2190.
[11] Murtaza, G., Karim, S., Akram, M.R., Khan, S.A., Azhar, S., Mumtaz, A. and Bin Asad, M.H. (2014) Caffeic acid phenethyl ester and therapeutic potentials. BioMed Research International. 2014, 145342.
[12] Akyol, S., Ugurcu, V., Altuntas, A., Hasgul, R., Cakmak, O. and Akyol, O. (2014) Caffeic acid phenethyl ester as a protective agent against nephrotoxicity and/or oxidative kidney damage: a detailed systematic review. Scientific World Journal. 2014, 561971.
[13] Jain, S.K., McVie, R., Duett, J. and Herbst, J.J. (1989) Erythrocyte membrane lipid peroxidation and glycolylated hemoglobin in diabetes. Diabetes. 38, 1539-1543.
[14] Ohkawa, H., Ohishi, N. and Yagi, K. (1979) Assay for lipid peroxides in animals and tissues by thiobarbituric acid reaction. Analytical Biochemistry. 95, 351-358.
[15] Miranda, K.M., Espey, M.G. and Wink, D.A. (2001) A rapid, simple spectrophotometric method for simultaneous detection of nitrate and nitrite. Nitric Oxide. 5, 62-71.
[16] Beutler, E., Dubon, O. and Kelly, B.M. (1963) Improved method for the determination of blood glutathione. Journal of Laboratory and Clinical Medicine. 61, 882-888.
[17] Aebi, H. (1974) Methods of Enzymatic Analysis, Catalase. Academic Press Inc. New York and London. 673-677.
[18] Bradford, M.M. (1976) A rapid and sensitive method for the quantitation of microgram quantities of protein utilizing the principle of protein-dye binding. Analytical Biochemistry. 7, 248-254.
[19] Glusczak, L., Loro, V.L., Pretto, A., Moraes, B.S., Raabe, A., Duarte, M.F., Fonseca, M. B, Menezes, C. C. and Sousa Valladao, D.M., 2011. Acute Exposure to Glyphosate Herbicide Affects Oxidative Parameters in Piava (Leporinus obtusidens), Archives of Environmental Contamination and Toxicology. 61, 624-630.
[20] García-Díaz, E.C., Gómez-Quiroz, L.E.,Arenas-Ríos, E., Aragón-Martínez, A., Ibarra-Arias, J.A. and Retana-Márquez, M.D. (2015) Oxidative status in testis and epididymal sperm parameters after acute and chronic stress by cold-water immersion in the adult rat. Systems Biology in Reproductive Medicine. 2, 1-11.
[21] Altuntas, I., Kilinc, I., Orhan, H., Demirel, R., Koylu, H. and Delibas, N. (2004) The effects of diazinon on lipid peroxidation and antioxidant enzymes in erythrocytes in vitro. Human & Experimental Toxicology. 23, 9-13.
[22] Sutcu, R., Altuntas, I., Buyukvanli, B., Akturka, O., Ozturk, O., Koylu, H. and Delibas, N. (2007) The effects of diazinon on lipid peroxidation and antioxidant enzymes in rat erythrocytes: role of vitamins E and C. Toxicology and Industrial Health. 23, 13-17.
[23] Alp, H., Aytekin, İ., Atakişi, O. and Ogün, M. (2011) The Effects of Caffeic Acid Phenethyl Ester and Ellagic Acid on Oxidative Stress Created by Acute Malathion Toxicity in Rat. Ataturk University Journal of Veterinary Sciences. 6, 117-124.
[24] Cemek, M., Büyükokuroğlu, M. E., Yürümez, Y., Yavuz, Y., Aslan A., Büyükben, A. and Aymelek, F. (2010) Tissue trace and major element levels in organophosphate insecticide fenthion (Lebaycid) toxicity in rats: prophylactic and therapeutic effect of exogenous melatonin. Ecotoxicology and Environmental Safety. 73, 206-212.
[25] Hazarika, A., Sarkar, S.N., Hajare, S., Kataria, M. and Malik, J.K. (2003) Influence of malathion pretreatment on the toxicity of anilofos in male rats: a biochemical interaction study. Toxicology. 185, 1-8.
[26] Ertekin, A, Karaca, M., Akkan, H.A., Cemek, M. and Ormancı, N. (2003) Investigation of the lipid peroxidation, antioxidant substances, antioxidant vitamins and some hematologic-biochemical parameter levels in Gentamycine induced nephrotoxicosis in dog. Turkish Journal of Veterinary and Animal Sciences. 27, 535-540.

[27] Matsubara K., Higaki T., Matsubara Y. and Nawa A. (2015) Nitric oxide and reactive oxygen species in the pathogenesis of preeclampsia. International Journal of Molecular Sciences. 16, 4600-4614.
[28] McCord, J.M. and Fridovich, I. (1969) Superoxide dismutase. An enzymic function for erythrocuprein (hemocuprein). Journal of Biological Chemistry. 244, 6049–6055.
[29] Meister, A. and Anderson, M.E. (1983) Glutathione. Annual Review of Biochemistry. 52, 711-760.
[30] Paglia, D.E. and Valentine, W.N. (1967) Studies on the quantitative and qualitative characterization of erythrocyte glutathione peroxidase. Journal of Laboratory and Clinical Medicine. 70, 158–169.
[31] Dringen, R. (2000) Glutathione metabolism and oxidative stress in neurodegeneration. European Journal of Biochemistry. 267, 4903.
[32] Griffith, O.W. (1999) Biologic and pharmacologic regulation of mammalian glutathione synthesis. Free Radical Biology and Medicine. 27, 922-935.

Received: **16.05.2017**
Accepted: **28.09.2017**

CORRESPONDING AUTHOR

Lacine Aksoy
Afyon Kocatepe University
Science and Arts Faculty
Chemistry Department,
Biochemistry Division,
03200, Afyonkarahisar – Turkey

e-mail: lacinetur@aku.edu.tr
lacinetur@gmail.com

© by PSP Volume 26 – No. 12A/2017 pages 7900-7905 Fresenius Environmental Bulletin

PERFORMANCE ANALYSIS OF A BETA TYPE STIRLING ENGINE WITH REGENERATIVE DISPLACER

Yasar Onder Ozgoren*

Afyon Kocatepe University, Technology Faculty, Automotive Engineering Department Afyonkarahisar, Turkey

ABSTRACT

In this study, a beta-type Stirling engine was manufactured and tested. Two displacer configurations were used and compared. As a novel approach in the first configuration, regenerator material was placed inside the displacer to increase the engine performance by minimizing heat, pressure, and dead volume losses. In the second configuration, non-regenerative displacer was used. The engine performance was determined by using of displacers of regenerative and non-regenerative. A thin copper wire mesh was used as regenerator material. The engine performance experiments were conducted at 573 ±5 K hot end temperature and 300 ±5 K cold end temperature. Tests were performed within the range of 1-5 bar charge pressure with helium as the working fluid. The maximum engine torque and maximum engine power were obtained at 5 bar charge pressure with regenerative displacer. Maximum engine torque and maximum engine power were measured as 1.92 Nm at 626 rpm and 142.53 W at 810 rpm, respectively.

KEYWORDS:
Stirling engine, regenerative displacer, low temperature difference, beta type, regeneration

INTRODUCTION

Energy is an important requirement for both developed and developing countries. The renewable energy sources have become important due to decreasing fossil energy reserves, increasing of energy demands and negative effects on the ecological life of fossil energy sources. Renewable energy sources consist of solar, wind, geothermal, biomass, solid waste, and tidal energy [1].

A Stirling engine is a machine operating in closed regenerative thermodynamic cycles, which are based on compression and expansion of the working fluids at different temperature levels [2, 3]. The ideal Stirling cycle consists of two isochoric and two isothermal thermodynamic process [4]. Stirling engines operated with external combustion principle can be used with any kind of energy sources such as solar energy, geothermal energy, radioisotope, waste energy, etc. [5, 6].

Stirling engine is classified at two groups as kinematic and free-piston. In free piston Stirling engines, the piston and the displacer are connected to the engine block by means of springs. The cycle is formed by the synchronization between the piston and the displacer that is provided by the spring force and the pressure force [7]. In kinematic Stirling engines the synchronization between the piston and the displacer is provided with a drive mechanism such as crank, rhombic, ross yoke, lever, etc. [7, 8].

Kinematic Stirling engines can be designed in three different mechanical configurations: alpha, beta and gamma. The alpha type Stirling engine consists of two pistons working in separated cylinders placed with a phase angle of 90°. In the gamma type Stirling engines, a power piston and a displacer are worked at separated cylinders. Displacer provided with reciprocating motion of the working fluid between the hot volume and the cold volume. In beta-type engines, the displacer and the piston are coaxially located inside the same cylinder [9-11].

Stirling engines are consist of three volumes: hot, cold and regenerator. The engine performance is mostly depends on the properties of these volumes. An increase in the difference of the hot volume temperature and the cold volume temperature increases the engine performance. However, the temperature difference between cold and hot volumes is limited due to material properties. Dead volume is also another parameter on engine performance. Higher dead volume causes a power loss in Stirling engines.

The regenerator is located between the hot and the cold volumes. The working material transfers its thermal energy to the regenerator while it moves from the hot volume to the cold volume. While it moves from the cold volume to the hot volume, it regains the thermal energy that it has left in the previous process. The heat recovery are obtained owing to the heat exchange of the working material inside the regenerator. Surface and geometric characteristics of the regenerator region affect the regeneration process in Stirling engines [2].

Kongtragool and Wongwises were developed in an isothermal model for investigation in the effects

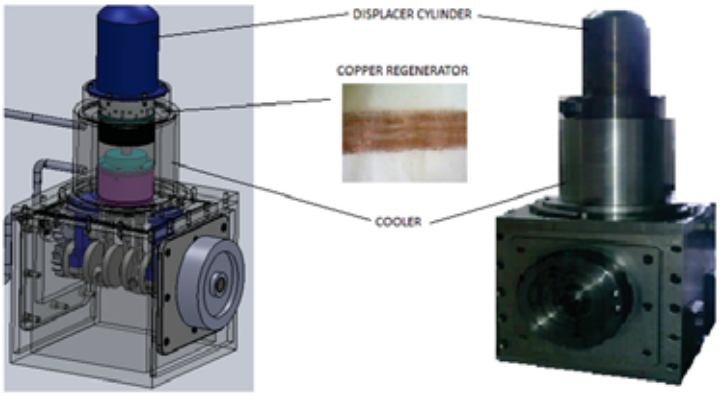


FIGURE 1
The test engine

on engine performance of the regenerator effectiveness and dead volumes. In this analysis, it was obtained that the engine efficiency increases with increasing dead volume and decreasing regenerator effectiveness [12]. Timoumi et al. was developed a numerical simulation model taking into account the thermal losses in order to increase engine performance and analyze their operations. The experimental data obtained from the General Motor GPU-3 Stirling engine compared to a numerical simulation model. The analysis results and experimental results were very close to each other [13]. A thermodynamic model based on isothermal analysis developed by Puech and Tishkova to determine the net cyclic work and the heat stored in the regenerator at an engine cycle. An analytical formula was also proposed to determine the effects of dead volume and imperfect regeneration [14]. Eid investigated the effects of stainless steel regenerator materials having various mesh sizes on the surface of the displacer on the engine performance using a model which bases on the Schmitt analysis. It was determined that the engine power and engine efficiency increased by using regenerative displacer with respect to the GPU-3 engine [15].

In this study, a beta type crank drive Stirling engine with a regenerative displacer was designed and manufactured. Copper wire regenerator material was used in the regenerator. Helium was used as a working fluid. Engine performance experiments were performed by using regenerative and non-regenerative displacers. Engine torque and power of the regenerative and non-regenerative engine were compared at different charge pressures.

TEST ENGINE AND EXPERIMENTAL SETUP

Test engine. The manufactured beta-type Stirling engine consists of an engine block, a crankshaft, a power piston, a power cylinder, a displacer, a displacer cylinder, a water jacket, and a flywheel. A photograph and a transparent solid drawing of the test engine are shown in Figure 1.

The regenerator is placed inside the displacer of the beta-type Stirling engine. Displacer consists of two parts, which are the upper and the lower parts. The end of upper part of the displacer was built in the form of a dome to facilitate the flow of working fluid. The upper and the lower parts of the displacer are connected to each other with a screw. The displacers of the engine were manufactured in two configurations of non-regenerative and regenerative. The flow of the working fluid between the cold and the hot volumes in the non-regenerative displacer is provided by the space between the displacer and its cylinder. The lower part of the regenerative displacer compose of the regenerator volume. A teflon ring is placed on the displacer piston to provide the working fluid passes through the regenerator volume. A 0.35 mm thick thin copper wire was placed in the regenerator volume with a fill factor of 20%. The regenerative and non-regenerative displacers are given in Figure 2.



FIGURE 2
Regenerative and non-regenerative displacers

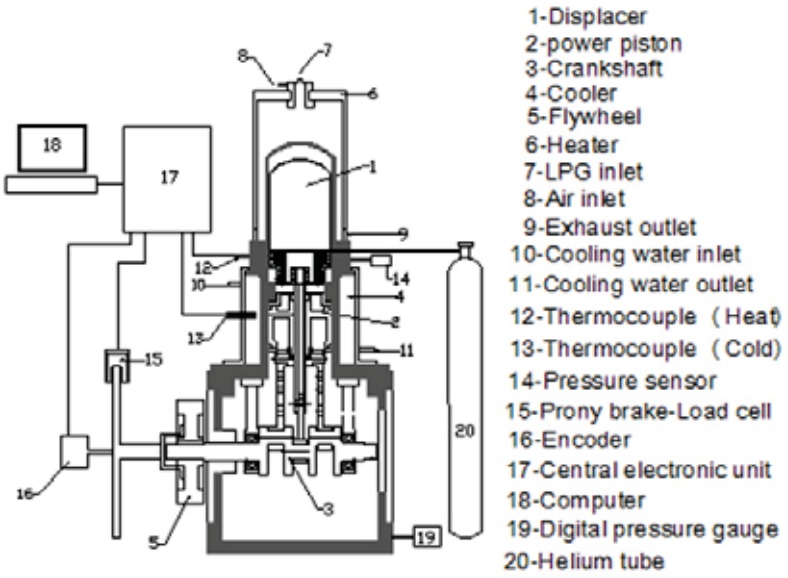


FIGURE 3
The experimental setup

TABLE 1
Technical specifications of the test engine

Engine			
Engine type	Beta	Power piston diameter	94 mm
Compression ratio (ε)	1.583	Displacer diameter	94 mm
Power piston swept volume (V_2)	270.54 cc	Power piston stroke	40 mm
Displacer swept volume (V_1)	277.59 cc	Displacer stroke	40 mm
Swept volume ratio ($K= V_2/ V_1$)	0.97	Total dead volume	171.91 cc
Regenerator			
Regenerator material	Copper wire mesh		
Wire diameter	0.35 mm		
Wrapping number (10 mm x 10mm)	12		
Regenerator fullness ratio	20 %		

Experimental setup. The experimental setup consists of the test engine, a prony-type dynamometer, a pressure sensor, a load cell, an infrared thermometer, an encoder and the associated software. A schematic illustration of the experimental setup are shown in Figure 3.

The Prony-type dynamometer is consisted of a shaft with a braking disk on top, a hydraulic braking system that provide loading by compressing the brake disk, an ESIT BB20 branded load cell, and a torque lever that transmits the braking force to the load cell. The accuracy of the Prony type dynamometer is 0.003 Nm. A Lika branded encoder with 5000 pulses was used to measure the engine speed. The data coming from the load cell, encoder and pressure sensor was simultaneously transferred in the computer with the interface program. The surface temperatures measured by a DT-8863 branded infrared thermometer with ±1 °C accuracy and −50 to 800 °C measurement range.

The test engine is run at the different working conditions before engine performance experiments. After solving mechanical and thermal problems, tests are performed at various engine speeds and different charge pressures. Helium is used as the working fluid and the charge pressure is applied in the engine block. The charge pressure was measured with a digital manometer between 0-10 bar at ±0.01 accuracy. Charge pressures were changed between 1.0 bar and 5.0 bar with 1 bar intervals. The tests were carried out at 573 ±5 K hot end and 300 ±5 K cold end temperatures. The heat energy was provided to the engine using an LPG fueled heater. Technical specifications of the engine are given in Table 1.

RESULTS AND DISCUSSION

In the Figure 4, the variations of the engine power and engine torque depending on the engine speed for non-regenerative and regenerative displacers are given for 3, 4 and 5 bar charge pressure. The maximum engine torques with the non-regenerative and regenerative displacers were obtained as 1.01 Nm and 1.92 Nm, respectively. While engine torque was higher at low engine speeds, it decreased with increasing of the engine speed due to insufficient

heat transfer, mechanical and viscous frictions, flow losses, pressure losses etc. The maximum engine power with the non-regenerative and regenerative displacers were obtained as 42.9 W and 142.53 W, respectively. Engine power depends on engine speed and engine torque. Engine power increases to a certain level with increasing engine speed and then decreases again. Because of inadequate the heat transfer rate and increasing of the friction losses, a decline in engine power is observed after a certain engine speed.

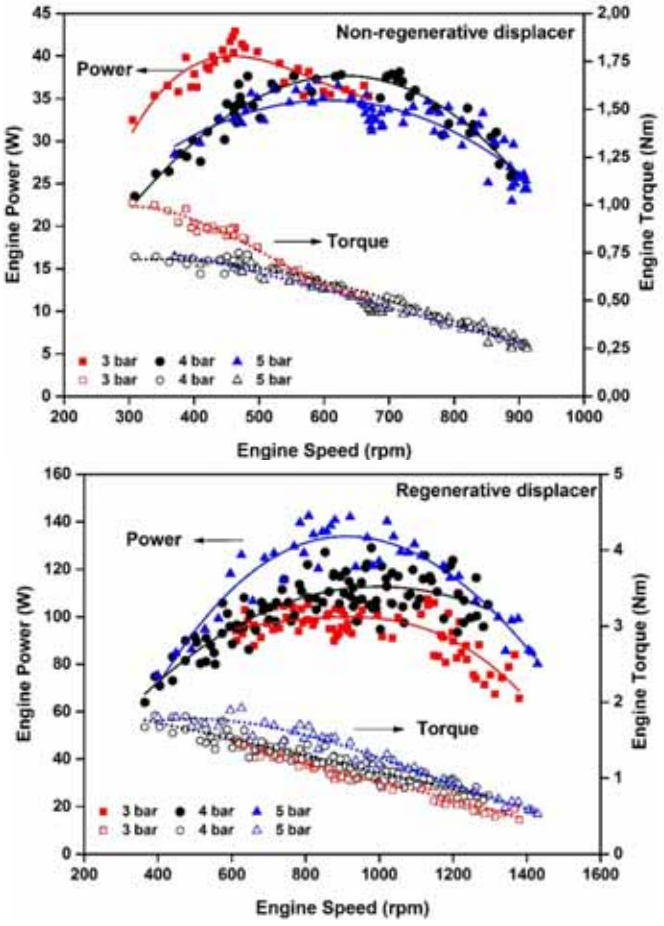


FIGURE 4

The variations of the engine power and engine torque depending on the engine speed for non-regenerative and regenerative displacers

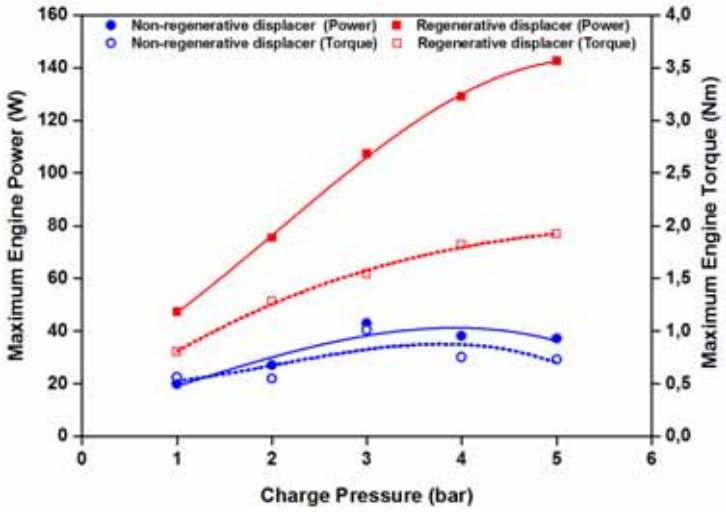


FIGURE 5

The variations of maximum engine power and engine torque depending on the charge pressure

The variations of the maximum engine power and maximum engine torque depending on the charge pressure for non-regenerative and regenerative displacers are shown in Figure 5. While the maximum engine power and engine torque with non-regenerative displacer were obtained at 3 bar charge pressure, they were obtained at 5 bar charge pressure with regenerative displacer. When the results of regenerative and non-regenerative displacers at 3 bar charging pressure were compared, it was found that the maximum engine power and engine torque with regenerative displacer increased by 150% and 52%, respectively. Heat-exchange between regenerator and working fluid result in the increasing of the in-cylinder pressure and working fluid mass. Thereby, the engine power was prominently increased in despite of increasing of the dead volume. The heat recovery was increased with the use of regenerative displacer and higher torque values were obtained at low and high speeds of the engine. In addition, it was observed that the range of the engine torque and engine power depending on the charge pressure was increased.

CONCLUSIONS

In this study, a beta-type Stirling engine was tested with non-regenerative and regenerative displacers at different charge pressures. Tests were performed at 573 ±5 K hot end temperature and 300 ±5 K cold end temperature. The best engine performance with non-regenerative and regenerative displacers were obtained at 3 bar and 5 bar charge pressure, respectively. The maximum engine power and torque was measured as 142.53 W at 810 rpm and 92 Nm at 626 rpm respectively with regenerative displacer. The maximum engine torque and engine power values were obtained 1.5 and 2.5 times higher than non-regenerative displacer. In despite of increasing of the dead volume, the engine performance increased with use of the regenerative displacer.

ACKNOWLEDGEMENTS

This study was supported by The Scientific and Technological Research Council of Turkey (TUBITAK) in frame of the project code of 109M172. As researcher, I thank The Scientific and Technological Research Council of Turkey.

REFERENCES

[1] Cinar, C., Aksoy, F., Okur, M. (2013) Design, manufacturing and performance tests of a Stirling engine with rhombic drive mechanism. Journal of the Faculty of Engineering and Architecture of Gazi University. 28(4), 795-801.

[2] Walker, G. (1980) Stirling engines. United States: Oxford University Press.

[3] Ahmadi, M.H., Ahmadi M.A., Pourfayaz F., Bidi M., Hosseinzade H., Feidt M. (2016) Optimization of powered Stirling heat engine with finite speed thermodynamics. Energy Conversion and Management. 108, 96–105.

[4] Mabrouk, M.T., Kheiri, A., Feidt, M. (2015) Effect of leakage losses on the performance of a β type Stirling engine. Energy. 88, 111–117.

[5] Yang, H.-S., Cheng, C.-H. (2017) Development of a beta-type Stirling engine with rhombic-drive mechanism using a modified non-ideal adiabatic model. Applied Energy. 200, 62–72.

[6] Aksoy F., Cinar C. (2013) Thermodynamic analysis of a beta-type Stirling engine with rhombic drive mechanism. Energy Conversion and Management. 75, 319–324.

[7] Karabulut, H., Solmaz, H., Okur, M., Şahin, F. (2013) Dynamic and thermodynamic analysis of gamma type free pıston Stirling engine, Journal of the Faculty of Engineering and Architecture of Gazi University. 28(2), 265-273.

[8] Wang, K., Sanders, S.R., Dubey, S., Choo, F.H., Duan, F. (2016) Stirling cycle engines for recovering low and moderate temperature heat: A review. Renewable and Sustainable Energy Reviews. 62, 89–108.

[9] Alfarawi, S., Al-Dadah, R., Mahmoud, S. (2016) Enhanced thermodynamic modelling of a gamma-type Stirling engine. Applied Thermal Engineering. 106, 1380–1390.

[10] Ahmadi, M.H., Ahmadi, M.A., Pourfayaz, F. (2017) Thermal models for analysis of performance of Stirling engine: A review. Renewable and Sustainable Energy Reviews. 68, 168–184.

[11] Alfarawi, S., Mahmoud, S., AL-Dadah, R. (2017) Modelling and parametric study of an efficient Alpha type Stirling engine performance based on 3D CFD analysis. Energy Conversion and Management. 145, 93–106.

[12] Kongtragool, B., Wongwises, S. (2006) Thermodynamic analysis of a Stirling engine including dead volumes of hot space, cold space and regenerator. Renewable Energy. 31, 345–359.

[13] Timoumi, Y., Tlili, I., Nasrallah, S.B. (2008) Performance optimization of Stirling engines. Renewable Energy. 33(9), 2134-2144.

[14] Puech, P., Tishkova, V. (2011) Thermodynamic analysis of a Stirling engine including regenerator dead volume. Renewable Energy. 36(2), 872-878.

[15] Eid, E. (2009) Performance of a beta-configuration heat engine having a regenerative displacer. Renewable Energy. 34(11), 2404-2413.

Received: **16.05.2017**
Accepted: **02.10.2017**

CORRESPONDING AUTHOR

Yasar Onder Ozgoren
Afyon Kocatepe University,
Technology Faculty,
Automotive Engineering Department
Afyonkarahisar - Turkey

e-mail: yasarozgoren@aku.edu.tr

© by PSP Volume 26 – No. 12A/2017 pages 7906-7913 Fresenius Environmental Bulletin

PREDICTING POLLUTANT EMISSIONS OF A 300MW CFBB USING BIDIRECTIONAL LEARNING MACHINE

Guo-Qiang Li[1,2,*], Lu Zhang[1], Keith C C Chan[2], Jun-Nan Zou[1], Li-Zhuang Xu[1]

[1]Key Lab of Industrial Computer Control Engineering of Hebei Province, Yanshan University, Qinhuangdao 066004, China
[2]Department of Computing, Hong Kong Polytechnic University, Hung Hom 999077, Hong Kong

ABSTRACT

With the rapid development of economy in these years, the condition has become more and more severe that human being have polluted environment. In order to implement and reduce pollutant emissions for a power plant, an accurate model is required. This study proposed an improved Extreme Learning Machine (ELM) called Bidirectional learning machine (BLM) to establish precise and rapid models of pollutant emissions involving NOx emissions and Dust content in flue gas for a 300MW Circulating fluidized bed boiler (CFBB). Experimental results show, compared with two recently published state-of-the-art algorithms Extreme Learning Machine (ELM) and Least Square Fast Learning Network (LSFLN), BLM with less running time could achieve better generalization performance and more highly repeatability and reproducibility for predicting pollutant emissions.

KEYWORDS:
Circulating fluidized bed boiler (CFBB), NOx emissions, Dust content in flue gas, Extreme Learning Machine

INTRODUCTION

With the development of the economy, environmental pollution becomes more and more serious and attracts more and more people's attentions. As one of the main source of pollutant emissions, coal-fired boilers in power plants has attracted many attentions. In order to protect our living environment, pollutant emissions involving NOx, SO2, Dust content in flue gas, et al, allowed from coal-fired boilers are strictly limited in more and more countries. In China, a very stringent pollutant emission standard was addressed to thermal power plants by Ministry of Environmental Protection on July 1, 2014. Take NOx emissions for example, the maximum NOx emissions is limited to 100mg/Nm3.

For power plants, combustion optimization technology is an effective and economic method to reduce pollutant emissions from coal-fired boilers [1, 2]. The reduction of pollutant emissions such as NOx and Dust content in flue gas could be achieved by optimizing the operational parameters, such as Primary air, Secondary air, and Coal feed quantity, et al. [3, 4]. However, the optimization of operational parameters has heavily relied on the correlation between pollutant emissions and operational parameters [5, 6]. Therefore, precise and rapid prediction models of pollutant emissions are required for reducing pollutant emissions by combustion optimization technology [7].

However, the combustion process of a coal-fired boiler in power plants is a multi-variables strong coupling nonlinear system, and it's very difficult to establish an accurate mathematical model by Mechanism modeling methods. Because there are abundant real-time operational information easily collected from supervisory information systems (SIS) in power plants. Therefore, many researchers have been committed to modeling pollutant emissions from coal-fired boilers by machine learning methods, which could achieve very good performance in predicting pollutant emissions. Zhang, et al. adopted a generalized regression neural network to establish the model between the NOx emissions and operational parameters, which could achieve very good prediction performance because its R-square achieves 0.9267 [8]. Zhou, et al. built an efficient NOx emissions model of a coal-fired utility boiler using optimized support vector regression(SVR) by ant colony optimization(ACO), whose correlation coefficient(R) achieve 0.9360 [9]. Li, et al. employed teaching-learning-based optimization (TLBO) method to adjust the hyper-parameters of least squares support vector machine (LS-SVM) to build an effective NOx emission model of a 330MW coal-fired boiler[10]. However, the above two models needs a long time to optimize the parameters of SVR or LS-SVM. R.C. Booth and W.B. Roland apply an online real-time neural network to several commercially operating coal-fired boilers, and reduce NOx emissions up to 60% and unburned carbon in ash 30% and meanwhile improve heat rate up to 2% overall [11]. Madhavan, et al. adopts a general regression neural network to predict NOx emissions based on 10 dominant features, and obtains a better performance [12]. Elshafei, et al. investigates a multi-step-ahead prediction of NOx emissions from simple linear to state-of-the-art nonlinear approaches for a coal-fired boiler [13]. In addition, there are many published research studies to predict pollutant emissions [14-18].

For this study, to establish the correlation between NOx emissions, Dust content in flue gas and operational parameters, a large amount of real-time data is collected from the supervisory information systems of a 300 MW Circulating fluidized bed boiler in a power plant. In the present paper, bidirectional learning machine (BLM) which could be thought of an improved Extreme learning machine is presented to set up the prediction models of NOx emissions and Dust content in flue gas based on the collected operational parameters. A model comparison study including extreme learning machine (ELM)[19] and least square fast learning network (LSFLN)[20] modelling approaches is presented. Results of the model comparison study reveal that for the analyzed Circulating fluidized bed boiler, the model based on BLM could better predict NOx emissions and Dust content in flue gas than the other two methods.

The rest of this study is organized as follows: a simply review of Extreme Learning Machine is given in Section 2. Bidirectional Learning Machine is proposed in Section 3. Modeling pollutant emissions and experimental comparison is given in Section 4. Finally, Section 5 summarizes the conclusions of this paper.

FUNDAMENT OF ELM

Extreme learning machine (ELM) is a single hidden layer forward neural network, which overcomes disadvantages of traditional artificial neural networks, such as lower learning speed, time consuming for training process, and local optimum, et al. Due to the outstanding performance, ELM has been applied varies of areas, such as handwritten digit classification[21,22], fault diagnosis[23,24], and electroencephalograph (EEG)[25], et al. In addition, in order to further improve the performance of ELM, many researchers have developed many ELM variants such as regularized extreme learning machine (RELM)[26], Optimally Pruned Extreme Learning Machine(OP-ELM)[27], evolutionary extreme learning machine (E-ELM) [28], online sequential extreme learning machine (OS-ELM)[29], and so on.

The core work of ELM analytically determines the output weights by least square method. We simply review the learning process of ELM, whose structure is the same as Figure 1.

Suppose N distinct samples $\{X, Y\}$, in which $x_i = [x_{i1}, x_{i2}, \cdots, x_{in}]^T \in R^n$ is the n-dimensional feather vector of the i^{th} sample, and $y_i = [y_{i1}, y_{i2}, \cdots, y_{il}]^T \in R^l$ is the corresponding l-dimension output vector. Then the output G of hidden layer could be calculated by the follows formula:

$$G = \begin{bmatrix} g(b_1 + W_1 x_1) & \cdots & g(b_1 + W_1 x_N) \\ \vdots & \ddots & \vdots \\ g(b_m + W_m x_1) & \cdots & g(b_m + W_m x_N) \end{bmatrix} \quad (1)$$

where $g(\cdot)$ is the activation function of hidden neurons, b_i is the bias of i^{th} hidden neuron and the W_i is the input weight connecting the i^{th} hidden neuron and all input neurons.

Then the output of the ELM could be calculated as follows:

$$\mathrm{Y} = \mathrm{G}\beta \quad (2)$$

where β is the output weights connecting output neurons and hidden neurons

According to least square method, the output weight matrix β could be estimated analytically:

$$\|\tilde{\beta}\mathrm{G} - \mathrm{Y}\| = \min_{\beta} \|\beta G - Y\| \quad (3)$$

$$\tilde{\beta} = YG^+ \quad (4)$$

where $G^+$is the Moore-Penrose generalized inverse of G.

The training process of ELM is given as follows:

1: Randomly generated the input weights β and hidden biases$b$;

2: Calculate hidden layer output matrix G by Eq.(1);

3: Analytically determine output weight matrix β by Eq.(4)

Then the final output of ELM could be calculate by Eq.(2).

BIDIRECTIONAL LEARNING MACHINE

An improved Extreme Learning Machine is proposed in this section. Because the input weights(containing hidden biases) and output weights are analytically determined from two directions, we called the improved Extreme Learning Machine as Bidirectional Learning Machine, which is a single layer feedforward neural network. The BLM's structure is given in Fig.1. The learning process of the BLM is described in detail as follows.

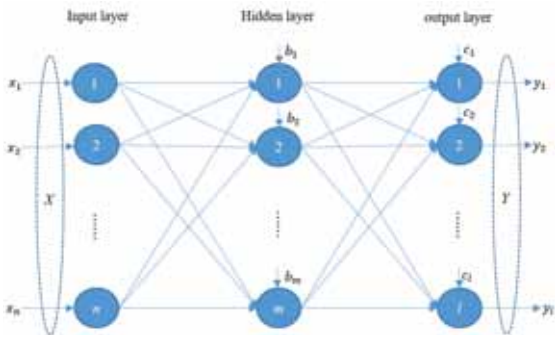


FIGURE 1
Structure of the Bidirectional Learning machine

Approximation problem. Suppose, there are N distinct samples $\{X, Y\}$, in which $x_i = [x_{i1}, x_{i2}, \cdots, x_{in}]^T \in R^n$ is the n-dimensional feather vector of the i^{th} sample, and $y_i = [y_{i1}, y_{i2}, \cdots, y_{il}]^T \in R^l$ is the corresponding l-dimension output vector. In BLM, there are m hidden neurons. W is a $m \times n$ weight matrix which consists of the weight values of the connection between input neurons and hidden nerons, $b = [b_1, b_2, \cdots, b_m]$ is the hidden bias vector,

β is a $l \times m$ matrix which consists of the weight values of the connection between hidden neurons and output neurons, and the vector $c = [c_1, c_2, \cdots, c_l]^T$ is the biases of output neurons. $g(\cdot)$ and $f(\cdot)$are the activation functions of hidden neurons and output neurons respectively.

Then the BLM's mathematical model could be described as:

$$\begin{cases} y_{j1} = f\left(c_1 + \sum_{k=1}^{m} \beta_{1k} g\left(b_k + \sum_{i=1}^{n} W_{ki}\, x_{ji}\right)\right) \\ y_{j2} = f\left(c_2 + \sum_{k=1}^{m} \beta_{2k} g\left(b_k + \sum_{i=1}^{n} W_{ki}\, x_{ji}\right)\right), j = 1,2,\cdots,N \\ \vdots \\ y_{jl} = f\left(c_l + \sum_{k=1}^{m} \beta_{lk} g\left(b_k + \sum_{i=1}^{n} W_{ki}\, x_{ji}\right)\right) \end{cases} \quad (5)$$

where β_{lk} is the weight value connecting the l^{th} output neuron and the k^{th} hidden neuron, W_{ki} is the weight value connecting the k^{th} hidden neuron and the i^{th} input neuron

The Eq.(5) could be transformed into the following form:

$$y_j = f\left(c + \sum_{k=1}^{m} \beta_k\, g\left(b_k + W_k x_j\right)\right) \quad (6)$$

$$Y = f(cI + \beta G) = f\left([\beta \quad c]\begin{bmatrix} G \\ I \end{bmatrix}\right) \quad (7)$$

$$G = \begin{bmatrix} g(b_1 + W_1 x_1) & \cdots & g(b_1 + W_1 x_N) \\ \vdots & \ddots & \vdots \\ g(b_m + W_m x_1) & \cdots & g(b_m + W_m x_N) \end{bmatrix} = g\left(\begin{bmatrix} b_1 + W_1 x_1 & \cdots & b_1 + W_1 x_N \\ \vdots & \ddots & \vdots \\ b_m + W_m x_1 & \cdots & b_m + W_m x_N \end{bmatrix}\right) = g\left(\widehat{W}\hat{X}\right) \quad (8)$$

$$\widehat{W} = \begin{bmatrix} W_1 & W_2 & \cdots & W_m \\ b_1 & b_2 & \cdots & b_m \end{bmatrix} and \hat{X} = \begin{bmatrix} x_1 & x_2 & \cdots & x_N \\ 1 & 1 & \cdots & 1 \end{bmatrix} \quad (9)$$

where β_k is the weight vector connecting the all output neurons and the k^{th} hidden neuron, W_k is the weight vector connecting the k^{th} hidden neuron and all input neuron, G is called hidden output matrix, and $I = [1,1,\cdots,1]_{1\times N}$.

Determination of input weight and hidden biases. For an invertible activation function $f(\cdot)$, the Eq.(7) could be rewritten as

$$\beta G = f^{-1}(Y) - cI \quad (10)$$

Suppose, the output weight β and the bias c are known, then the hidden layer output matrix G could be obtained by:

$$\left\|\beta\tilde{G} - [f^{-1}(Y) - cI]\right\| = \left\|\beta\tilde{G} - f^{-1}(Y) + cI\right\| = \min_{G}\|\beta G - f^{-1}(Y) + cI\| \quad (11)$$

According to the Moore-Penrose (M-P) Generalized Inverse, the Minimum Norm Least-Squares Solution of the linear system could be written as:

$$\tilde{G} = \beta^{+}(f^{-1}(Y) - cI) = g\left(\widehat{W}\hat{X}\right) \quad (12)$$

For an invertible activation function $g(\cdot)$, the Eq.(12) could be rewritten as:

$$\widehat{W}\hat{X} = g^{-1}\left(\tilde{G}\right) = g^{-1}\left(\beta^{+}(f^{-1}(Y) - cI)\right) \quad (13)$$

where $g^{-1}(\cdot)$ is the invertible function of $g(\cdot)$.

Then the Minimum Norm Least-Squares Solution of Eq(13) could be written as:

$$\left\|\widetilde{\widehat{W}}\hat{X} - g^{-1}(G)\right\| = \left\|\widetilde{\widehat{W}}\hat{X} - g^{-1}\left(\beta^{+}(f^{-1}(Y) - cI)\right)\right\| = \min_{\widehat{W}}\left\|\widehat{W}\hat{X} - g^{-1}\left(\beta^{+}(f^{-1}(Y) - cI)\right)\right\| \quad (14)$$

Then the Eq.(14)could become as

$$\widetilde{\widehat{W}} = g^{-1}\left(\beta^{+}(f^{-1}(Y) - cI)\right)\hat{X}^{+} \quad (15)$$

However, the output weight β and the bias c are unknown at the beginning of learning process. So we can randomly assign values for the output weight β and the bias c under two conditions. The two conditions are given as follows: (1) the range of random assigned values is between 0 and 1; (2) the rank of β is the value of the $min\{m, n\}$. When there are negative values before the computation of the invertible function $f^{-1}(\cdot)$ and $g^{-1}(\cdot)$, their absolute values would be taken the place of these negative values in order to keep the presence of invertible computation. This cannot effect the performance of BLM because we will recalculate the output weight β and the bias c in the following section, which would take place of the randomly assigned β and c.

Determination of output weight and output biases. After determining the input weights and biases, the BLM could be thought of a linear system, and the output weights β and output biases c could be analytically determined by the following form:

$$\left\|f\left(\tilde{\gamma}\begin{bmatrix} G \\ I \end{bmatrix}\right) - Y\right\| = \min_{\gamma}\left\|f\left(\gamma\begin{bmatrix} G \\ I \end{bmatrix}\right) - Y\right\| \quad (16)$$

where $\gamma = [\beta \quad c]$.

For an invertible activation function $f(\cdot)$, the combination matrix γ could be analytically determined by Eq.(17)

$$\left\|\tilde{\gamma}\begin{bmatrix} G \\ I \end{bmatrix} - f^{-1}(Y)\right\| = \min_{\gamma}\left\|\gamma\begin{bmatrix} G \\ I \end{bmatrix} - f^{-1}(Y)\right\| \quad (17)$$

According to the Moore-Penrose Generalized Inverse, the Minimum Norm Least Squares Solution of the linear system could be written as:

$$\tilde{\gamma} = f^{-1}(Y)\begin{bmatrix} G \\ I \end{bmatrix}^{+} = f^{-1}(Y)H^{+} \quad (18)$$

where $H = [G^T \quad I^T]^T$.

Then the output weight and output biases could be calculated by the following formula:

$$\begin{cases} \beta = \tilde{\gamma}(1{:}\,l, 1{:}\,m) \\ c = \tilde{\gamma}(l+1, 1{:}\,m) \end{cases} \quad (19)$$

Training process of BLM. The training process of BLM is as described as Algorithm 1.

Algorithm 1. BLM

Input: N samples $X_i = [x_{i1}, x_{i2}, \cdots, x_{in}]^T \in R^n, Y_i = [y_{i1}, y_{i2}, \cdots, y_{il}]^T \in R^l$, $i = 1,2,\cdots,N$, and m hidden neurons.

1: Randomly generated the output weight matrix β and output biases c;

2: Analytically calculate hidden layer output matrix G by Eq.(12);

3: Analytically calculate the input weight W and hidden biases b by Eq.(13) and Eq.(9);

4: Recalculate the hidden output G by Eq.(8);

5: Analytically determine output weight matrix β and output biases c by Eq.(18) and Eq.(19);

Output: The final output of BLM could be calculate by Eq.(7).

MODELING POLLUTANT EMISSIONS

Brief description of Circulating fluidized bed boiler (CFBB). In CFBB, the fuels in the coal yard would be translated into the coal powder storehouse by grab machines and belt conveyors, and be crushed into fine particles of nearly uniform size by coal-breakers. Then the fine particles would be put into the furnace together with lots of desulfurizers (Calcium carbonate). In order to full complete the desulfurization reactor, the furnace temperature should keep in around 850℃. A lot of flue gas would be generated and flied into the cyclone separator from the furnace outlet. Many fine particles would be divided from flue gas by the cyclone separator and resent into the furnace by an external heat exchanger, and the flue gas would pass many equipment containing the flue gas duct, super-heaters, economizers, air preheaters and the dust catcher, et al, and finally discharge into the atmosphere.

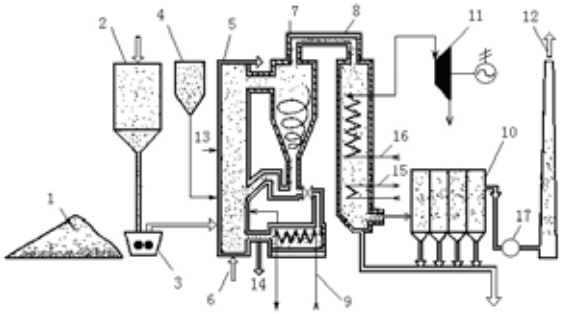


FIGURE 2
Composition of a Circulating fluidized bed boiler: 1 Fuels, 2 Fuel bunker, 3 Coal-breaker, 4 Limestone bin, 5 Water-cooled wall, 6 Air-distributor, 7 Segregator, 8 Flue gas duct, 9 External heat exchanger, 10 Dust Catcher, 11 Steam turbine-generating unit, 12 Exhaust chimney, 13 Inlet of secondary air, 14 Sullage pipe,15 Economizers, 16 Super-heaters, 17 Binduced-draft fan

The mainly contribution of the flue gas is to preheat the water in pump, and the preheated water would be sent into the water-cooled wall to further heat the water. Once achieving a certain temperature, the heated water would translated into steam which would fly to the steam turbine and make the turbine rotor rotate in order to make thermal energy translate into mechanical energy and then translate into electrical energy. The steam would be cooled down and translate into water which would resend into the water-cooled wall by the external heat exchanger in turn. The system of a Circulating fluidized bed boiler is given in Figure 2.

Data preparation. In this section, we adopt the data collected from a 300MW CFBB under operational conditions of an actual power plant. Below gives a brief description of the data set. Due to the limits of the field equipment & structure and sampling techniques, 2880 samples with 120 attribute parameters are collected, which contains Load (MW); Coal feed quantity (t, A,B,C,D and Average); Primary air (volumes(KNm3/h, one left and two right), pressure setting value (Pa), fan current (AMP, A, B), fan inlet temperature (℃, A, B)); Boiler feed water flow(t/h, A, B, C, D); oxygen concentration in the flue gas (%) and its bias (%); NOx emissions (mg/Nm3) ; Dust content in flue gas (mg/Nm3), et al. During the sample period, these samples are collected under the same kind of coal, so the impact of the coal properties was neglected.

Here the focus is to set up correlations between the operational parameters and NOx emissions, as well as Dust content in flue gas by BLM. The 118 operational parameters are taken as the input parameters for BLM, and the other two pollutant emission parameters (NOx emissions and Dust content in flue gas) as output parameters.

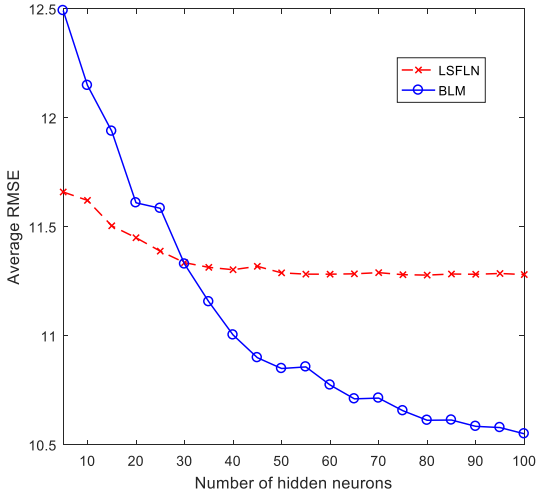


FIGURE 3
Performance varies with number of hidden neurons for NOx emissions

Results and Comparation. All evaluations are carried out by means of the Matlab2016b computational environment running on a computer with windows 10(64 bit), 3.16 GHz CPU and 4GB RAM.

In this paper, in order to evaluate the performance of the models built by BLM, the NOx emissions and Dust content in flue gas modeling results obtained by ELM and LSFLN are compared. It should be noted that, before modeling, all samples are divided into two parts: 1440 samples are taken as training samples and the other 1440 samples as test samples, in addition, the 'Sig' function is taken as the activation function of hidden neurons for ELM, LSFLN and BLM, and the 'Linear' function as the activation function of output neurons. In order to keep a watchful eye to the generalization performance of an algorithm, each algorithm adopted in the experiments is uniformly assigned a number of hidden neurons which varies from 5 to 100 by the step

of 5. Moreover, 30 trials are carried out for each algorithm with a given number of hidden neurons. The performance evaluation criteria selected for the comparative study is the Maximum, Minimum, Mean, and Standard Deviation (S.D.) of the accuracy quantified in terms of the Root Mean Square Error (RMSE) and the R-square, for the problems.

According to the experiments and Figure 3, for the NOx emissions, the average RMSE of each algorithms would reduce with the increasing of the number of hidden neurons. When the neurons achieves 100, results of the three algorithms listed in Table 1 show better performance than that of them with less hidden neurons. Because the average RMSE obtained by ELM is very large, even when the number achieves 100, the average RMSE obtained by ELM only achieves 28.0692 and its average R-square 0.4439. We can conclude that ELM is not suitable for use in the prediction of NOx emissions. In order to keep high readability of Figure 3 and state the superiority of BLM, we didn't plot the varying cure of ELM with the number of hidden neurons in Figure 3. Both LSFLN and BLM achieve good performance. When the number is set as less than 30, the LSFLN shows better performance because it owns more complex network structure than BLM. However, when the number of hidden is set as more than 30, the BLM shows better performance, and more and more significant with the increase of the number, the superiority of complex network structure of LSFLN would disappear. The Figure 4 gives the predictions of test samples of BLM and Table 1 gives the performance evaluations for three algorithms with 100 hidden neurons. When the hidden neurons achieve 100, the average RMSE and R-square of BLM respectively achieve 10.5500 and 0.9418, however those of LSFLN respectively achieve 11.2804 and 0.9333.

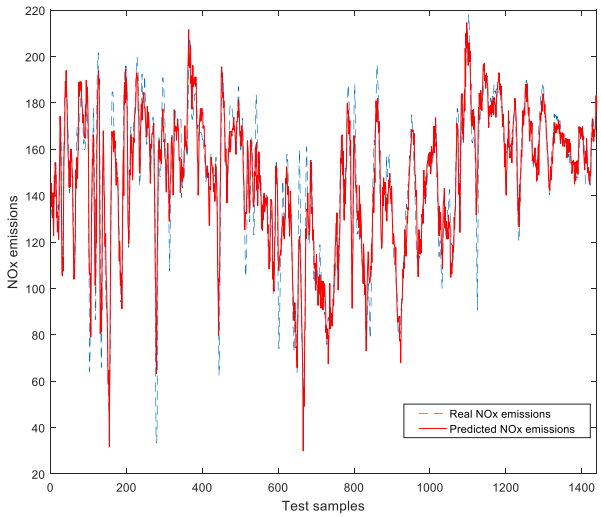


FIGURE 4
The predicted values by BLM for NOx emissions

TABLE 1
Performance comparison for NOx emissions and Dust content in flue gas

Output	Performance index		ELM	LSFLN	BLM
NOx emissions	RMSE	Min	26.7417	11.2626	10.2038
		Max	29.5238	11.3111	10.9366
		Mean	28.0692	11.2804	10.5500
		S.D.	0.6821	0.0163	0.1887
	R-square	Min	0.3381	0.9328	0.9373
		Max	0.5228	0.9333	0.9456
		Mean	0.4439	0.9331	0.9418
		S.D.	0.0440	1.9821×10^{-4}	2.1557×10^{-3}
	Training time(s)	Mean	0.0714	0.2776	0.1734
Dust content in flue gas	RMSE	Min	0.5144	0.4168	0.3806
		Max	0.5559	0.4177	0.3929
		Mean	0.5331	0.4176	0.3865
		S.D.	0.0109	1.6059×10^{-4}	2.9373×10^{-3}
	R-square	Min	0.2398	0.6870	0.7291
		Max	0.4390	0.6872	0.7490
		Mean	0.3608	0.6870	0.7398
		S.D.	0.0511	4.9829×10^{-5}	4.4802×10^{-3}
	Training time(s)	Mean	0.0688	0.2599	0.1516

As seen from the running time and S.D., ELM needs the least time but its repeatability is the worst, the repeatability of LSFLN is the best but needs the most time. Although the repeatability of BLM is not better than LSFLN, even when the obtained worst RMSE and R-square (the maximum of RMSE and the minimum of R-square) by BLM are better than the obtained best RMSE and R-square by LSFLN. Therefore, we conclude that the BLM with less running time could better performance in prediction of NOx emissions.

According to the experiments and Figure 5, for the dust content in flue gas, the obtained average RMSEs by the above three methods would reduce with the increasing of the number of hidden neurons. When the hidden neurons achieve 100, obtained results by the three algorithms still listed in Table 1 show better performance than those of them with less hidden neurons. We still didn't plot the varying cure of ELM with the number of hidden neurons in Figure 5 because of the similar reasons. For LSFLN, when the number is set as less than 10, it shows better performance than BLM. However, when the number of hidden neurons more than 10, the BLM could achieve better average RMSE, and better and better with the increasing of the number of hidden neurons. In addition, the average RMSE of LSFLN varies very little from 10 hidden neurons to 100 ones, the superiority of whose complex network structure did not present. The Figure 6 gives the predictions of test samples of BLM with 100 hidden neurons. When the hidden neurons achieve 100, the average RMSE and R-square of BLM respectively achieve 0.3865 and 0.7398, but those of LSFLN only achieve 0.4176 and 0.6870 respectively. For the running speed and repeatability, the conclusions of predicting dust content in flue gas are the same as those of predicting NOx emissions. Therefore, we conclude that the BLM with less running time could not only predict NOx emissions very well, but also predicting dust content in flue gas very well. BLM could be thought of an effective machine-learning tool for the prediction of pollutant emissions.

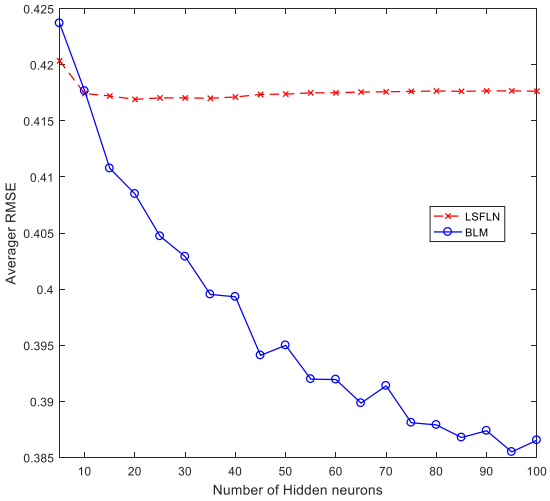


FIGURE 5
Performance varies with the number of hidden neurons for Dust content in flue gas

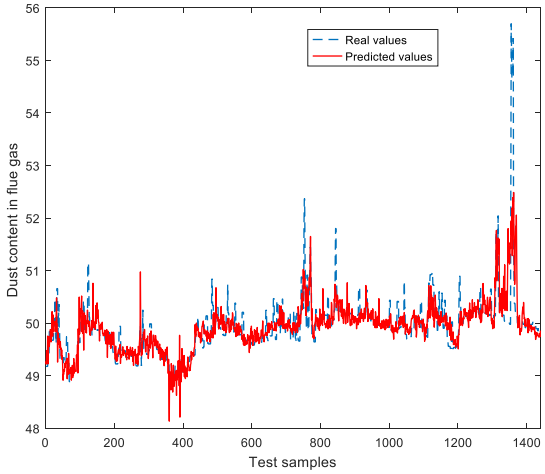


FIGURE 6
The predicted values by BLM for Dust content in flue gas

CONCLUSION

In this study, a novel NOx emissions model and a dust content in flue gas model for a 300MW CFBB were established by the proposed neural network-Bi-directional Learning Machine(BLM). To train and test the proposed BLM model, a large amount of real-data were collected from the SIS of a 300MW coal-fired power plant, in which 118 operational parameters are employed as the inputs of the model, and NOx emissions and dust content in flue gas as outputs. The experimental results reveal that the proposed BLM model with very fast learning speed and highly repeatability could achieve a high predictive accuracy and good generalization performance. Compared with other two state-of-the-art methods (ELM and LSFLN), BLM could outperform in terms of the performance evaluation criteria (RMSE and R-Square). Therefore, the BLM model could be an alternative learning machine tool for predicting NOx emissions and dust content in flue gas, and be the basis of combustion optimization of a coal-fired boiler in power plants in order to reduce NOx emission and dust content in flue gas.

ACKNOWLEDGEMENTS

Project supported by the National Natural Science Foundation of China (Grant No. 61403331), Program for the Top Young Talents of Higher Learning Institutions of Hebei (Grant No. BJ2017033), Natural Science Foundation of Hebei Province (Grant No. F2016203427), China Postdoctoral Science Foundation (Grant No. 2015M571280), Doctorial Foundation of Yanshan Univerity (Grant No.B847).

REFERENCES

[1] Belosevic, S., Tomanovic, I., Crnomarkovic, N. Milicevic, A., Tucakovic, D. (2015) Modeling and optimization of processes for clean and efficient pulverized coal combustion in utility boilers. Thermal Science. 20(5), 223-223.

[2] Ilamathi, P., Selladurai, V., Balamurugan, K. (2013) A novel approach for modelling of NOx emission reduction in a tangentially fired coal boiler. International Journal of Oil Gas & Coal Technology. 6(4), 449-461.

[3] Zhou, H., Cen, K., Fan, J. (2004) Modeling and optimization of the NOx emission characteristics of a tangentially fired boiler with artificial neural networks. Energy. 29(1), 167-183.

[4] Luo, Z., Wang, F., Zhou, H. Liu R., Li W., Chang G. (2011) Principles of optimization of combustion by radiant energy signal and its application in a 660 MWe down- and coal-fired boiler. Korean Journal of Chemical Engineering. 28(12), 2336-2343.

[5] Secco, S.D, Juan, O., Louis-Louisy, M. Lucas J.Y., Plion, P., Porcheron, L. (2015) Using a genetic algorithm and CFD to identify low NOx configurations in an industrial boiler. Fuel. 158, 672-683.

[6] Belosevic, S., Tomanovic, I., Crnomarkovic, N. Milicevic A. (2016) Modeling of pulverized coal combustion for in-furnace NOx reduction and flame control. Thermal Science. 186-186.

[7] Tan, P., Zhang, C., Xia, J. Fang, Q., Chen, G. (2016) NOx Emission Model for Coal-Fired Boilers Using Principle Component Analysis and Support Vector Regression. Journal of Chemical Engineering of Japan. 49(2), 211-216.

[8] Zheng, L., Yu, M., Yu, M. (2008) Monitoring NOx Emissions from Coal Fired Boilers Using Generalized Regression Neural Network. International Conference on Bioinformatics and Biomedical Engineering. IEEE:1916-1919.

[9] Zhou, H., Zhao P., J., Zheng L., Wang, C., Cen, K. (2012) Modeling NOx emissions from coal-fired utility boilers using support vector regression with ant colony optimization. Engineering Applications of Artificial Intelligence. 25(1), 147-158.

[10] Li, G., Niu, P., Zhang, W., Liu, Y. (2013) Model NOx emissions by least squares support vector machine with tuning based on ameliorated teaching–learning-based optimization. Chemometrics & Intelligent Laboratory Systems. 126(8), 11-20.

[11] Booth, R.C, Roland, W.B.J. (1998) Neural network-based combustion optimization reduces NOx emissions while improving performance. IEEE Industry Applications, Dynamic Modeling Control Applications for Industry Workshop. 1–6

[12] Madhavan, K.S., Reddy, T.K., Krishnaiah, J. Dhanuskodi, R., Sowmiya, S. (2012) Development of Artificial Neural Network (ANN) based Prediction Model for NOx Emissions from Utility Boilers. International Conference on Advanced Research in Mechanical Engineering.

[13] Smrekar, J., Potočnik, P., Senegačnik, A. (2013) Multi-step-ahead prediction of NOx emissions for a coal-based boiler. Applied Energy. 106(11), 89-99.

[14] Lv, Y., Yang, T., Liu, J. (2015) An adaptive least squares support vector machine model with a novel update for NOx emission prediction. Chemometrics & Intelligent Laboratory Systems. 145, 103-113.

[15] Lughofer, E., Macián, V., Guardiola C., Klemen E.P. (2011) Identifying static and dynamic prediction models for NOx emissions with evolving fuzzy systems. Applied Soft Computing Journal. 11(2), 2487-2500.
[16] Baek, S.H., Park, H.Y., Ko, S.H. (2014) The effect of the coal blending method in a coal fired boiler on carbon in ash and NOx emission. Fuel. 128(14), 62-70.
[17] Tan, P., Xia, J., Zhang, C. Fang, Q., Chen,G. (2014) Modeling and Optimization of NOx Emission in a Coal-fired Power Plant using Advanced Machine Learning Methods. Energy Procedia. 61, 377-380.
[18] Liukkonen, M., Hälikkä, E., Hiltunen, T., Hitunen, Y. (2012) Dynamic soft sensors for NOx, emissions in a circulating fluidized bed boiler. Applied Energy. 97(3), 483-490.
[19] Huang, G.B., Zhu, Q.Y., Siew, C.K. (2006) Extreme learning machine: theory and applications, Neurocomputing. 70, 489–501.
[20] Li, G., Niu, P., Wang, H., Liu, Y. (2014) Least Square Fast Learning Network for Modeling the Combustion Efficiency of a 300WM Coal-Fired Boiler. Neural Networks. 5157-66
[21] Pang, S., Yang, X. (2016) Deep Convolutional Extreme Learning Machine and Its Application in Handwritten Digit Classification. Computational Intelligence & Neuroscience. 2016(3), 1-10.
[22] Mcdonnell, M.D, Tissera, M.D, Vladusich, T., Van, S.A, Tapson, J. (2015) Fast, Simple and Accurate Handwritten Digit Classification by Training Shallow Neural Network Classifiers with the 'Extreme Learning Machine' Algorithm. Plos One. 10(8), e0134254.
[23] You, C.X., Huang, J.Q., Lu, F. (2016) Recursive reduced kernel based extreme learning machine for aero-engine fault pattern recognition. Neurocomputing. 214, 1038-1045.
[24] Yang, X., Pang, S., Shen, W. Lin, X., Jiang, K., Wang, Y. (2016) Aero Engine Fault Diagnosis Using an Optimized Extreme Learning Machine. International Journal of Aerospace Engineering. 2016, 1-10.
[25] Peng, Y., Lu, B.L. (2016) Discriminative manifold extreme learning machine and applications to image and EEG signal classification. Neurocomputing. 174(PA), 265-277.
[26] Deng, W., Zheng, Q., Chen, L. (2009) Regularized extreme learning machine, In: Proceedings of the IEEE Symposium on Computational Intelligence and Data Mining, CIDM'09. pp. 389–395.
[27] Miche, Y., Sorjamaa, A., Bas, P. Jutten, C., Lendasse, A. (2010) OP-ELM: Optimally Pruned Extreme Learning Machine. IEEE Transactions on Neural Networks. 21(1), 158-162.
[28] Zhu, Q-Y, Qin, A.K, Suganthan, P.N, Huang, G-B. (2005) Evolutionary extreme learning machine, Pattern Recognition. 38, 1759 -1763.
[29] Liang, N.Y, Huang, G.B, Saratchandran, P. Sundararajan, N. (2006) A fast and accurate online sequential learning algorithm for feedforward networks, IEEE Trans. Neural Network. 17(6) 1411–1423.

Received: **16.05.2017**
Accepted: **22.09.2017**

CORRESPONDING AUTHOR

Guo-Qiang Li
Key Lab of Industrial Computer Control Engineering of Hebei Province,
Yanshan University,
Qinhuangdao 066004 – China

e-mail: zhihuiyuang@163.com

© by PSP Volume 26 – No. 12A/2017 pages 7914-7924 Fresenius Environmental Bulletin

DETERMINATION OF HEAVY METAL BIOAVAILABILITY IN ATMOSPHERIC DUST COLLECTED FROM COAL MINING AREAS AND HEALTH RISK ASSESSMENT

Yafen Han[1], Xiaoxing Wei[2], Qi Li[1,3,*], Jieyun Liu[1], Na Liu[1]

[1]School of Environment and Surveying Engineering, Suzhou University, Suzhou 234000, China
[2]Beijing Institute of Aerospace Control Devices, Beijing 100142, China
[3]State Engineering & Technological Research Center for Coal Mine Water Disaster Prevention, Suzhou University, Suzhou 234000, China

ABSTRACT

This study aimed at investigating the concentrations, chemical fractions, bioavailabilities and health risks of Cu, Pb, Cr, Ni and Cd in atmospheric dust generated in Suzhou coal mining area. 45 dust samples were collected and then analyzed using BCR sequential extraction scheme and the *in vitro* gastrointestinal test. The results showed that noticeable enrichments of Cu, Pb, Ni and Cd were found in the coal mining areas. Analysis of chemical fractions indicated that Cd was mainly found in the acid soluble fraction, Pb and Cu were mainly found in the reducible fraction, Ni and Cr were mainly found in the residual fraction. The bioavailabilities of the five trace metals were in the following order: Cd>Pb>Cu>Ni>Cr in the gastric phase and Cu>Pb>Cd>Ni>Cr in the intestinal phase. Significant correlation and regression relationships were found between the gastrointestinal phase and reducible fraction for almost all the studied elements, which suggested that most metal ions extracted from the gastrointestinal phase were mainly supplied from the reducible fraction. Finally, the results of the health risk assessment model were assessed and found to be far below 1.0, which indicated that these metals did not pose a significant risk to the local residents.

KEYWORDS:
Coal mining area, Atmospheric dust, Heavy metals, Bioavailability, Health risk assessment

INTRODUCTION

Atmospheric dust is a type of particulate matter, which can be raised by surface wind and naturally settle to the ground owing to gravity. As a carrier and transporter, atmospheric dust can easily attract many pollutants, such as heavy metal ions with high concentrations [1, 2]. Heavy metals accumulated in atmospheric dust are mainly derived from various anthropogenic activities, such as agricultural practices, industrial activities, solid waste disposal and exploitation of minerals [3]. Due to their high toxicity and non-degradability, heavy metals can cause serious damage to the environment, and even have potentially harmful effects to human health, because they can enter the body through unintentional ingestion and be actively bioavailable [4-7].

The environmental behavior of heavy metals is complex and strongly depends on their chemical fractions and bioavailability [8, 9]. The total content of a certain metal element can be divided into a number of chemical fractions according to their mobility, and each fraction can be obtained by the sequential extraction procedure (SEP). Generally, the SEP considers the amounts of a trace element released from an analyte under different physicochemical environmental conditions as the basis for estimating the relative bonding strength of this metal in various chemical fractions [10]. In recent years, several SEP methods, such as that of the European Communities Bureau of References (BCR), have been well developed and extensively applied to different environmental media, such as soil, dust, and sediments, to characterize the chemical phase associations of metals [8, 11-14]. Another procedure focusing on the assessment of the bioavailability of metals, known as the physiologically based extraction test (PBET), is usually comprised of two simulated *in vitro* digestion steps: gastric and intestinal steps [15, 16]. The PBET is a simple process with a short experimental period and low cost. Moreover, the results of this procedure can be correlated to bioavailability determined using *in vivo* or animal tests [17, 18]. Currently, SEP and PBET have become the most functional tools for predicting the environmental behavior of metals in contaminated solid materials. However, quantitative analyses that investigate the relation between the two procedures are rarely reported in the literature.

Coal mining involves a series of activities, such as excavating, stacking, jigging, coal washing and transporting. These processes can produce large quantities of coal wastes that contain dangerously high levels of heavy metals, e.g., Cd, Pb, Ni, Mn, and As [19]. The coal waste can be gradually weathered and decomposed into fine particles by

meteorological factors, resulting in the release of large amounts of atmospheric dust. In addition, mining activities are usually associated with ground subsidence and soil erosion, which may further intensify the risk of air pollution in the mining area. Therefore, the production and dispersion of atmospheric particles in coal mining areas have become a great concern in recent years. Suzhou coal mining area is an important part of the Huaibei coalfield in China. Some previous studies, which investigated the chemical composition of soils, sediments, and plants in Suzhou coal mining area, have found a significant accumulation of heavy metals in these media [20, 21]. However, limited studies have been conducted on the atmospheric dust in this area. The main objectives of this work were: (a) to determine the total contents, chemical fractions, and bioavailability of Cu, Pb, Cr, Ni, and Cd in the atmospheric dust generated in Suzhou coal mining area; (b) to identify the relationship between the chemical fractions of the above trace elements obtained by BCR procedure and the bioavailable metal amounts extracted by *in vitro* test; (c) to assess the possible health risks of heavy metals exposure to the local residents.

MATERIALS AND METHODS

Study site and sampling. Suzhou city is located in the northern part of the Anhui Province, China (116°09'E to 118°10'E and 33°18'N to 34°38'N). The city has a total area of 9785 km^2, and is situated in the Huanghe-Huaihe plain. It experiences a typical continental monsoon climate of a warm temperate zone, and it is characterized by four clearly distinct seasons and a wide variation in temperature ranging from 32℃ in summer to -2℃ in winter. The annual average precipitation is 880 mm, and the predominant wind direction is northeast. Suzhou city is affluent in coal resources, and hence, the intensive exploiting activities in this area have been running for nearly 30 years. The amounts of dusts and contaminant that produced from activities of mining industries and transportation have been increasing with the rapid growth in the coal production in recent years, thus causing serious atmospheric environmental pollution.

Atmospheric dust samples were collected from villages and settlements in five coal mining areas and one reference area (Fig. 1). The five coal mining areas were Taoyuan (TY), Qinan (QN), Qidong (QD), Luling (LL), and Zhuxianzhuang (ZXZ), which are located in the southeast of Suzhou. The reference area was chosen in the Xieji village (XJ), which is an unpolluted area with a low level of industrial activities located in the northeast of Suzhou and upwind of the five coal mining areas. In each sampling area, 5–8 dust samples were collected in early March 2015 from the surfaces of wooden doors and glass windows using a rabbit hair brush and a plastic spade, and then stored in clean sample bags. Each sample was weighing about 50 g. Before the analysis, all samples were air-dried for 3 days at room temperature, passed through a 0.149-mm mesh nylon sieve and stored in sealed plastic bags.

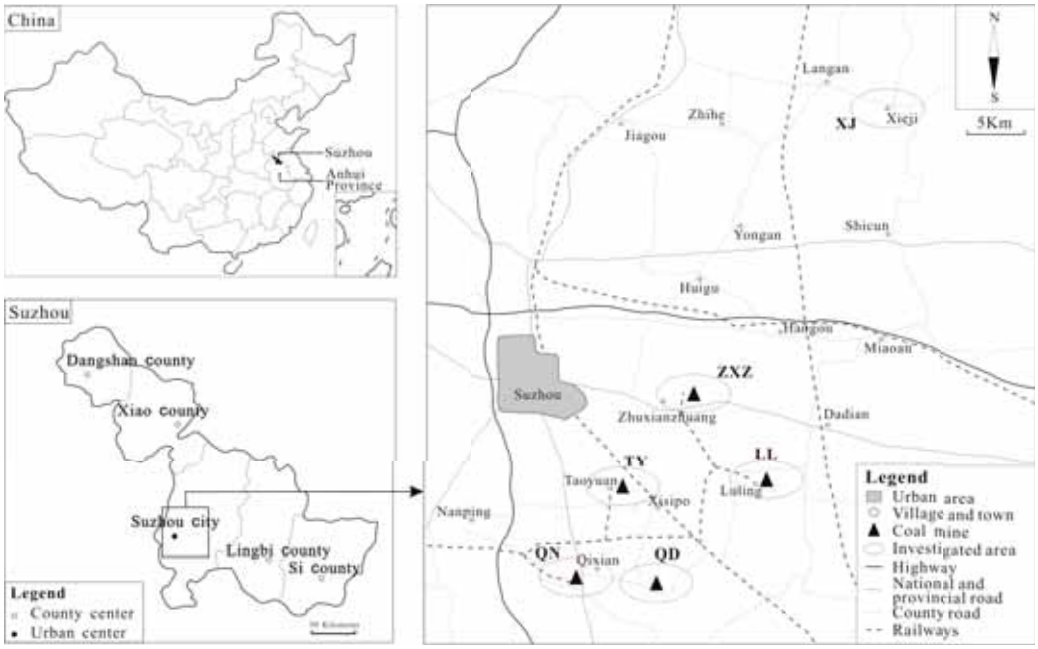


FIGURE 1
Map of the sampling area

TABLE 1
Extractants, extraction conditions, and separation methods used in the modified BCR procedure

Step	Extracted fraction	Extractants (1.0 g of dust sample)	Condition	Separation of the extracts
1	Acid soluble (F1)	40 ml of 0.11 M acetic acid	Room temperature and continuous shaking at 180 rpm for 16 h	After each step, the extracted liquid was filtered through 0.45 μm filter membrane to 50 ml volumetric flask for analysis. Then, 20 ml of MilliQ water was added to the solid residue by continuous shaking for 15 min and centrifugation was performed for 20 min. The supernatant was decanted and discharged carefully to avoid losing the solid residues.
2	Reducible (F2)	40 ml of 0.5 M hydroxylamine hydrochloride (pH 1.5)		
3	Oxidizable (F3)	(a) 10 ml of 8.8 M hydrogen peroxide (pH 2–3) ; (b) 10 ml of 8.8 M hydrogen peroxide (pH 2–3) ; (c) 50 ml of 1.0 M ammonium acetate (pH 2).	(a) Room temperature, occasional manual shaking for 1 h; (b) Water-bath at 85±1℃until the volume is reduced to 2–3 ml (c) Room temperature, continuous shaking at 180 rpm for 16 h	

Sample pretreatment. (1) Sample digestion procedure. Before analyzing the total concentrations of heavy metals, the atmospheric dust samples were wet digested by a concentrated acid mixture (HNO_3, HCl, $HClO_4$, and HF). The digestion process was as follows: Firstly, 0.15 g of each sieved sample was weighed and transferred into a Teflon digestion tank. Secondly, 6 ml of HNO_3 and 2 ml of HCl were added. The tank was then heated at 110 ℃ for 2 h on a hot plate (SH230N, Hanon Instruments Co., LTD, China) and allowed to cool at room temperature. Then, 2 ml of $HClO_4$ and 3 ml of HF were slowly added and the mixture was heated again at approximately 200 ℃ for thermal decomposition until the digestion solution was near dryness. Finally, the remaining digest was transferred to a 50 ml volumetric flask after cooling to room temperature, and MilliQ water was subsequently added to fill the remaining volume of the flask.

(2) Sequential extraction procedure. A modified BCR sequential extraction procedure was used to analyze the chemical fractions of trace metals in the atmospheric dust samples. Fractions of metals, defined by the extraction method, include acid soluble (F1), reducible (F2, bound to Fe/Mn oxides), oxidizable (F3, bound to organic matter and sulfides) and residual (F4, bound to primary and secondary minerals). F1, F2, and F3, shown in Table 1 along with their extractants, extraction conditions, and separation methods, are generally considered to be eco-toxicological relevant "extractable fractions". The residual fraction (F4) of the trace elements in atmospheric dust was calculated by the difference between the total concentration and the sum of the above three fractions.

(3) In vitro digestion procedure. The PBET method was applied to dust samples to determine the bioavailability of heavy metals. In this test, 40 ml of synthetic gastric solution at pH 2.5 was added to 0.4 g of dust samples in a polyethylene centrifuge tube. The simulated gastric solution was prepared by dissolving 0.5 g citric acid, 0.5 g malic acid, 1.25 g pepsin, 420 μl of lactic acid, and 500 μl of acetic acid in 1 L MilliQ water. After 1 h of extraction at a body temperature of 37℃and a shaking speed of 100 rpm, the mixture was centrifuged for 15 min at 4000 rpm, and then 5 ml of supernatant was suctioned out by using a disposable syringe. The obtained supernatant was filtered through a 0.45 μm membrane filter and preserved at 4℃as an analyte of the gastric phase. For simulating the digestive conditions in the small intestine, another 5 ml of the prepared gastric solution was supplied into the centrifuge tube at pH 7.0 (adjusted by saturated $NaHCO_3$ solution), and then 70 mg of bile salts and 20 mg pancreatin were added. A four-hour extraction was performed at a body temperature of 37℃and a shaking speed of 100 rpm, and the pH of the mixture was maintained at 7.0 adjusted by adding 12 M HCl or a saturated $NaHCO_3$ solution every 15 min. After centrifugation, the supernatant was collected, filtered and preserved as an analyte of the intestinal phase using the same treatment procedure described for the gastric phase.

Analysis method and quality control. All of the digested and extracted analytes were analyzed for Cu, Pb, Cr, Ni, and Cd. The concentrations of Cu, Cr, and Ni in the analytes were determined using a flame-atomic absorption spectrophotometer (F-AAS, Model TAS-990FG, Purkinje General Instrument, Beijing, China), while the concentrations of Pb and Cd were determined using a graphite furnace-atomic absorption spectrophotometer (GF-AAS, similar to the above model and manufacturer).

Quality control measures were adopted to improve the accuracy of the results during pretreatment and analysis of the samples. To avoid sample contamination, all the glassware and centrifuge tubes were treated with dilute nitric acid for 24 h and rinsed thoroughly with MilliQ water before use. In addition, MilliQ water was also used for the dilution of samples and the preparation of standard solutions. Moreover, reagent blanks and duplicate samples were also performed in the digestion and extraction procedure. In order to eliminate analytical bias, the data was obtained from the difference between the measured values and blank values, and the relative standard deviations of replicates were

kept within 10%.

Data statistics. Statistical analyses of the data in this work were carried out by Excel 2003 and SPSS 13.0 software packages for windows, and the figures were drawn by CorelDraw 12.0. Correlation analysis and multiple-stage linear regression analysis were conducted to identify the relationships between the metal concentrations in the gastrointestinal phases and in the BCR phases.

(1) Calculations of heavy metal bioavailability. In this study, the bioavailability of each metal was calculated as the ratio between the content of metal ions measured in the *in vitro* gastric phase or intestinal phase and the total concentration in the atmospheric dust sample, as described by the following formula:

$$BA(\%) = \frac{C_{extracted} \times V}{C_{total} \times M} \times 100\% \qquad (1)$$

Where BA (%) is the bioavailability of a specific metal in the atmospheric dust, and $C_{extracted}$ ($\mu g \cdot mL^{-1}$) is the concentration of the metal ion in the analyte obtained by gastric phase or intestinal phase treatments. C_{total} ($\mu g \cdot g^{-1}$) is the total concentration of a specific metal in the atmospheric dust. M (g) is the weight of the dust involved in the *in vitro* digestion (0.4 g in this study); V (mL) is the volume of the digestive solution in the centrifuge tube (40 mL in this study).

(2) Risk assessment model. The dissolved metal content in gastrointestinal system, which represents the maximum amount that can be absorbed by human body, provides an accurate and reliable index for health risk evaluation. This value can revise the conservative result of traditionally assessment using the total concentration value. Modeled risk assessment in this work was conducted by comparing the ingested metal amount of local resident through incidental ingestion exposure pathway with the maximum allowable daily intake (ADI), and the calculating formula was given as follows:

$$W_{int} = \frac{C_{total} \times BA \times Ing}{BM} \qquad (2)$$

$$Risk = \frac{W_{int}}{ADI} \times 100\% \qquad (3)$$

Where W_{int} ($\mu g \cdot kg^{-1} \cdot day^{-1}$) is the daily ingested metal amount per unit body weight for each receptor, and it is calculated from the values obtained by the *in vitro* bioavailability results; C_{total} ($\mu g \cdot g^{-1}$) is the total concentration of a specific heavy metal in the atmospheric dust; Ing ($g \cdot day^{-1}$) is the incidental ingestion rate of atmospheric dust particles (assumed to be 0.2 $g \cdot d^{-1}$ for children and 0.1 $g \cdot d^{-1}$ for adults in this study); BW (kg) is the average body weight (assumed to be 15.4 kg for children and 56 kg for adults in this study); ADI ($\mu g \cdot kg^{-1} \cdot day^{-1}$) is the maximum allowable dose level of a specific heavy metal recommended by the U.S. Environmental Protection Agency(USEPA) [22]. In addition, the bioavailability of the metals tested in the intestinal phase, with respect to the human digestive characteristics, was the value chosen to represent the BA (%) index.

RESULTS AND DISCUSSION

Heavy metal concentration in atmospheric dust. The total concentrations of heavy metals in the atmospheric dust samples collected from the investigated areas were listed in Table 2. Considering that currently there are no unified guidelines or regulations for the maximum allowable limits of heavy metals in dust, the soil background values of Anhui province (BVA) and the National Secondary Environmental Quality Standards for Soil (EQSS, GB15618-1995) were also listed in Table 2 and used for comparison. As shown in Table 2, the metal concentrations in the five mining areas were 47.65–68.52 $\mu g \cdot g^{-1}$ of Cu, 35.62–44.51 $\mu g \cdot g^{-1}$ of Pb, 37.70–72.67 $\mu g \cdot g^{-1}$ of Cr, 40.55–50.60 $\mu g \cdot g^{-1}$ of Ni, and 0.67–0.79 $\mu g \cdot g^{-1}$ of Cd. The average concentrations of Cu, Pb, Ni and Cd in the atmospheric dust samples collected from the mining areas are significantly higher than both those of BVA and the analytical results of dusts collected from the reference area, which indicated that the atmospheric environmental quality in the investigated areas were

TABLE 2
Descriptive statistical results of heavy metal concentrations ($\mu g \cdot g^{-1}$) in the atmospheric dust samples

Area	Sampling Sites	Index	Cu	Pb	Cr	Ni	Cd
Mining Area	TY	Mean	59.08	40.60	72.67	41.78	0.75
	(n=8)	SD	13.92	4.44	19.80	5.18	0.10
	QN	Mean	68.52	42.26	37.70	49.30	0.67
	(n=8)	SD	20.61	6.72	7.04	7.39	0.12
	QD	Mean	49.48	44.51	42.71	40.55	0.73
	(n=8)	SD	9.32	7.87	9.79	5.15	0.10
	LL	Mean	47.65	35.62	45.47	44.48	0.79
	(n=8)	SD	14.84	8.72	12.28	10.08	0.18
	ZXZ	Mean	54.55	38.63	58.92	50.60	0.79
	(n=8)	SD	11.74	4.80	14.66	7.91	0.07
Reference Area	XJ	Mean	19.14	21.25	40.53	26.41	0.28
	(n=5)	SD	1.82	4.49	7.20	3.07	0.07
BVA	-		20.4	26.6	67.5	29.8	0.097
EQSS	-		50	250	150	40	0.3

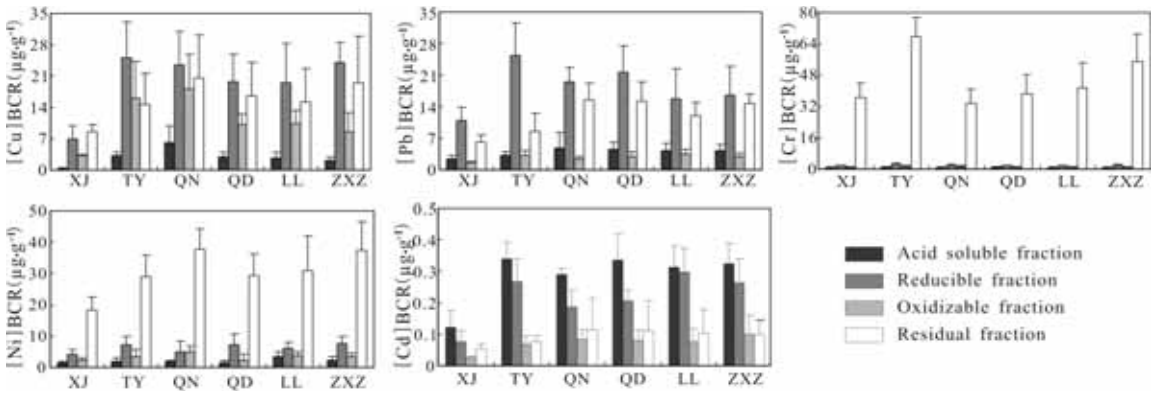


FIGURE 2
Chemical fractions of Cu, Pb, Cr, Ni and Cd in atmospheric dust

extremely affected by the coal mining activities, such as mineral exploitation, coal processing and transportation. However, compared to the EQSS values, almost none of the metal elements showed significant pollution except for Cd, whose concentration is nearly 2–3 times higher than the national standard limits.

Chemical fractions of heavy metals in atmospheric dust. The chemical fractions of Cu, Pb, Cr, Ni and Cd in the atmospheric dust samples were quantitatively tested and summarized in Fig. 2. The solubility and consequently the availability of metals were mainly dependent on their specific chemical fraction distributions. In four chemical fractions defined by the BCR method, F1, F2, and F3 had greater potential to mobilize from dust and to become bioavailable to the local residents [12]. Fig. 2 showed that the percentages of the total extractable fractions (F1+F2+F3) of the tested heavy metals were ordered as follows: Cd>Pb>Cu>Ni>Cr. In addition, more than 60% of the total concentrations of Cu, Pb and Cd were present within the extractable fractions. In fact, the extractable percentages of Cd ranged from 81.42% to 89.71% in the investigated areas, which implied that Cd was the most mobile metal among the tested heavy metals, and it had high potential toxicity. However, less than 30% of the total concentrations of Ni and Cr existed in the extractable fractions.

Metals extracted in the acid soluble fraction are generally precipitated or co-precipitated with carbonate, and can be easily released if the conditions become more acidic, thus it could have dangerous effects on the environment [23]. The percentages of the tested metals in this fraction in the atmospheric dust samples were 39.66%–45.76%, 7.92%–11.96%, 3.71%–7.66%, 1.99%–8.86%, and 1.41%–2.33% of the total metal contents for Cd, Pb, Ni, Cu, and Cr, respectively. The highest percentage associated with the acid soluble fraction was observed for Cd, which indicated that the Cd availability is susceptible to the pH or the ionic changes in the environment.

On the other hand, Pb was the highest toxic heavy metal present in the reducible fraction. About 10.92–25.47 $\mu g \cdot g^{-1}$ of Pb (accounts for 42.92%–62.74% of the total Pb concentration) was found in the reducible fraction, implied that Pb sorption on Fe-Mn oxides was probably the most important mechanism that controlled the behavior of this element in the atmospheric dust, because Pb could precipitate with metal oxides or could be adsorbed at the surface of metal oxide [24]. Additionally, a considerable amount of Cu and Cd (accounted for 34.56%–44.05% and 27.43%–37.45% of the total metal concentrations, respectively) were also extracted in this fraction.

Metals associated with the oxidizable fraction are ordinarily bound to organic matter and sulfides [25]. They are assumed to remain in the soil and dust for long times, and not considered very mobile and bioavailable under anaerobic conditions. However, under oxidizing or aerobic conditions, the degradation of organic matter can accelerate the release of the toxic metals. In this study, the extractability order of the five metals in the oxidizable fraction followed this order: Cu (15.88%–27.08%) > Cd (8.92%–12.42%) > Ni (5.88%–9.85%) ≈ Pb (5.89%–9.60%) > Cr (1.97%–3.72%), suggested that Cu availability was strongly influenced by the organic contents in the atmospheric dust.

Furthermore, the results showed that more than 90% of Cr and more than 70% of Ni were retained in the residual fraction (F4), which indicated that Cr and Ni were the most non-mobile and inactive elements, and that they were mainly controlled by the crystalline structure of the minerals present in the dust. The other toxic metals (Cu, Pb, and Cd) were present in this fraction at the following levels: 24.87%–44.63%, 21.27%–38.02%, and 10.29%–18.58%, respectively, of the total metal content.

Metal bioavailability in atmospheric dust evaluated by PBET. The extracted contents of Cu, Pb, Cr, Ni, and Cd in the gastric and intestinal phases for the investigated dust samples in the five

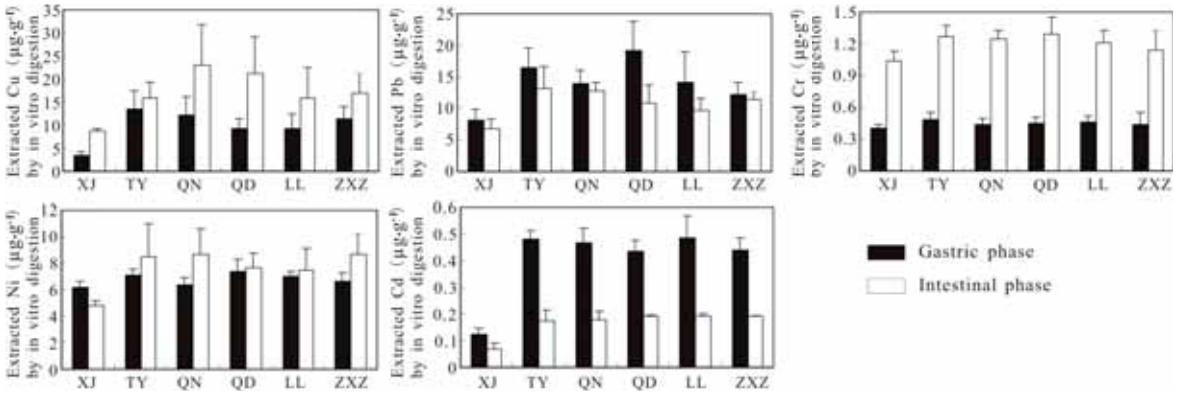


FIGURE 3
Extracted contents of Cu, Pb, Cr, Ni and Cd in the gastric and intestinal phases by the *in vitro* digestion test

TABLE 3
Bioavailability (%) of metals in the atmospheric dust samples obtained by the *in vitro* digestion test

Sampling	Gastric					Intestinal				
Sites	Cu	Pb	Cr	Ni	Cd	Cu	Pb	Cr	Ni	Cd
TY	22.59±2.57	40.72±6.19	0.72±0.31	17.36±3.05	65.33±11.3	27.56±5.01	32.10±5.88	1.94±0.59	20.10±3.97	22.81±4.65
QN	18.89±6.52	33.00±2.63	1.15±0.20	13.24±2.40	72.17±17.01	35.5±14.49	30.81±4.98	3.43±0.79	17.66±3.37	26.38±3.44
QD	19.17±3.58	42.86±8.78	1.11±0.28	18.65±3.81	60.38±8.47	42.72±13.27	25.11±7.13	3.30±1.00	19.10±2.42	26.66±3.31
LL	20.19±6.67	39.24±6.19	1.11±0.35	16.58±3.88	61.79±7.11	33.60±7.33	28.22±8.14	2.78±0.73	16.79±1.15	25.36±4.49
ZXZ	21.72±6.25	31.42±1.55	0.81±0.28	13.52±2.69	56.36±10.14	31.68±8.27	29.75±4.07	2.08±0.68	17.12±2.07	24.47±2.71
CM	18.03±3.34	38.53±3.45	1.03±0.24	23.77±3.03	47.09±16.18	46.10±3.07	34.09±14.55	2.62±0.49	18.27±1.84	25.11±8.19
Avg	20.24±5.17	37.57±6.72	0.99±0.32	16.75±4.42	61.41±13.34	35.53±11.08	29.74±7.59	2.70±0.91	18.17±2.81	25.14±4.39

mining areas and the reference area were shown in Fig. 3. In Fig. 3, obvious variations among different sampling areas could be observed, showing that the extracted metal contents in both the gastric and intestinal phases from atmospheric dust samples of the mining areas were generally higher than those of the reference area.

The bioavailability is an important index for assessing the potential adverse effects of heavy metals in atmospheric dust, and in this study, it was calculated based on the results of the *in vitro* digestion test. Table 3 listed the bioavailability values of Cu, Pb, Cr, Ni, and Cd in the gastric and intestinal phases for the areas investigated in this study. In the gastric phase, Cd presented the highest bioavailability (47.09%–72.17%), followed by Pb (31.42%–42.86%), Cu (18.03%–22.59%), and Ni (13.24%–23.77%); while only 0.72%–1.15% of Cr was dissolved in the simulated gastric solution, which indicated that it was weakly active and rarely absorbed in the body's digestive system. On the other hand, the order of metal bioavailability in the intestinal phase was Cu (27.56%–46.10%) > Pb (25.11%–34.09%) > Cd (22.81%–26.66%) > Ni (16.79%–20.10%) > Cr (1.94%–3.43%), which was slightly different from that of the previous phase.

Moreover, the results showed that the average bioavailability values of Pb and Cd in the gastric phase were higher than those in the intestinal phase. In contrast, the bioavailability of Cu, Ni, and Cr in the intestinal phase was higher than that in the gastric phase. Similar findings observed in 13 sediment samples from Lake Taihu [26] and in 14 mildly acidic and alkali soil samples [27] have been reported. pH is considered as an important factor that affects the solubility of Pb and Cd in digestive juice. When dust passes from the acidic gastric phase into the neutral intestinal phase, the dissolved metals may precipitate again by complexation, because of the higher pH value, which causes the relative decline in the bioavailability values of Pb and Cd in the intestinal phase. However, the strong complexation ability of Cu, Ni, and Cr with the digestive enzymes (e.g., pepsin, bile salt, pancreatin) enables them to exhibit higher solubility in the intestinal phase rather than in the gastric phase, especially for Cu, which is the most active element in the intestinal phase. Therefore, the toxicity of Cu to organisms should be more carefully monitored, because the absorption process of the human body mainly occurs in the epithelium of the intestine.

The relationship between gastro-intestinal phase and chemical fractions. In order to further cognize the quantitative relationship between the extracted metal contents in gastrointestinal phase and those in the four fractions of BCR, correlation and multiple-stage linear regression analyses were conducted and the results were shown in Table 4 and 5. Table 4 showed that both gastric and intestinal phases of almost all metals had the highest correlation with F2. This suggested that the extracted

TABLE 4
Coefficients of correlation between the extracted concentrations in the gastrointestinal phase and those in the BCR fractions for Cu, Pb, Cr, Ni, and Cd (n=45)

Cu	Gastric	Intestinal	Pb	Gastric	Intestinal	Cr	Gastric	Intestinal
F1	0.204	0.154	**F1**	0.339*	0.072	**F1**	0.321*	0.169
F2	0.850**	0.560**	**F2**	0.794**	0.635**	**F2**	0.465**	0.127
F3	0.706**	0.458**	**F3**	0.476**	0.172	**F3**	0.039	0.199
F4	0.027	0.187	**F4**	0.176	0.031	**F4**	0.013	0.020
Ni	**Gastric**	**Intestinal**	**Cd**	**Gastric**	**Intestinal**			
F1	0.013	-0.282	**F1**	0.778**	0.547**			
F2	0.402**	0.325*	**F2**	0.602**	0.735**			
F3	-0.230	0.120	**F3**	0.272	0.479**			
F4	-0.181	0.722**	**F4**	0.185	0.263			

TABLE 5
Relationships between the extracted metal concentrations in the gastrointestinal phase and those in the BCR fractions using stepwise multiple linear regression analysis

Elements	Regression equation	Correlation coefficients
Cu	G=0.326F2+0.216F3+1.03	0.902
	I=0.484F2+7.489	0.560
Pb	G=0.471F2+0.563F1+1.102F3+0.077	0.878
	I=0.266F2+6.042	0.636
Cr	G=0.053F2+0.349	0.465
	I not significant	-
Ni	G=0.099F2+6.218	0.402
	I=0.390F2+0.181F4-0.330	0.886
Cd	G=0.883F1+0.429F2+0.063	0.829
	I=0.133F1+0.271F2+0.292F3+0.049	0.816

metals in the gastrointestinal phase were mainly associated with the reducible fraction, which was coinciding with the results of the previous research conducted by investigating metal bioavailability in nine contaminated soils from Balikesir region in Turkey using the PBET and BCR methods [28]. In addition, strong positive correlations were also observed between the gastrointestinal phase and the other chemical fractions. For example, the significant correlations between the gastric phase and acid soluble fraction were described as follows: Pb: 0.339, $P<0.05$; Cr: 0.327, $P<0.05$; Cd: 0.778, $P<0.01$. While the following results were obtained between the gastric phase and the oxidizable fraction: Cd: 0.547, $P<0.01$. Further, the results for the relation between the intestinal phase and the acid soluble fraction were as follows: Cu: 0.706, $P<0.01$; Pb: 0.476, $P<0.01$. While the results for the relation between the intestinal phase and the oxidizable fraction were as follows: Cu: 0.458, $P<0.01$; Cd: 0.479, $P<0.01$. This meant that the two fractions (F1 and F3) will also influence the metal bioavailability in the gastric and intestinal phases. However, metal concentrations extracted by the PBET method had very low correlations with the residual fraction (F4), with the exception of Ni in the intestinal phase (0.722, $P<0.01$), showing that metals in the residual fraction were stable and hard to release in the digestive juice.

Equations that describe the relationship between the gastrointestinal phase and the different fractions of BCR were obtained for each element according to the results of the multiple-stage linear regression analysis (Table 5). As shown in Table 5, there were significant differences among the regression equations of the five metals, which could provide a reasonable basis for identifying the source of the gastric or intestinal bioavailable metal concentrations and comprehending the extracting behavior of each metal in the body's digestive system. The Cu concentration mainly depended on F2 and F3 in the gastric phase and only depended on F2 in the intestinal phase. The concentration of Pb in the gastric solution was dependent on F1, F2, and F3, while the Pb found in the intestinal solution was dependent on F2. However, for Cr, there was no significant linear relationship between the intestinal phase and any BCR fraction, while its gastric concentration was found to be dependent on the F2 fraction. Further, the Ni concentration in the gastric extracts was only dependent on the F2 fraction, while on both F4 and F2 in the intestinal extracts. On the other hand, the concentration of Cd in the gastric solution was dependent on F1 and F2, while that in the intestinal solution was dependent on both F1, F2, and F3.

Health risk assessment. The daily ingested metal amounts through the incidental ingestion pathway were calculated for both adults and children according to the results obtained on the bioavailability of the five trace elements in the atmospheric dust from the investigated areas, and their corresponding health risks were also evaluated by

TABLE 6
Daily metal intakes through the incidental ingestion pathway and their corresponding health risks on the local adults and children in the investigated areas

Index	Area	Receptor	Sampling site	Cu	Pb	Cr	Ni	Cd
W_{int} ($\mu g \cdot kg^{-1} \cdot d^{-1}$)	Reference area	Adults	CM	1.57×10^{-2}	1.20×10^{-2}	1.85×10^{-3}	8.56×10^{-3}	1.20×10^{-4}
		Children	CM	1.14×10^{-1}	8.76×10^{-2}	1.35×10^{-2}	6.22×10^{-2}	8.70×10^{-4}
	Coal mining area	Adults	TY	2.85×10^{-2}	2.35×10^{-2}	2.27×10^{-3}	1.52×10^{-2}	3.08×10^{-4}
			QN	4.11×10^{-2}	2.28×10^{-2}	2.23×10^{-3}	1.56×10^{-2}	3.16×10^{-4}
			QD	3.79×10^{-2}	1.95×10^{-2}	2.32×10^{-3}	1.38×10^{-2}	3.43×10^{-4}
			LL	2.83×10^{-2}	1.73×10^{-2}	2.16×10^{-3}	1.33×10^{-2}	3.47×10^{-4}
			ZXZ	3.01×10^{-2}	2.03×10^{-2}	2.04×10^{-3}	1.54×10^{-2}	3.41×10^{-4}
			Average	3.32×10^{-2}	2.07×10^{-2}	2.20×10^{-3}	1.46×10^{-2}	3.31×10^{-4}
		Children	TY	2.07×10^{-1}	1.71×10^{-1}	1.65×10^{-2}	1.10×10^{-1}	2.24×10^{-3}
			QN	2.99×10^{-1}	1.66×10^{-1}	1.62×10^{-2}	1.13×10^{-1}	2.30×10^{-3}
			QD	2.76×10^{-1}	1.42×10^{-1}	1.68×10^{-2}	1.00×10^{-1}	2.50×10^{-3}
			LL	2.06×10^{-1}	1.26×10^{-1}	1.57×10^{-2}	9.69×10^{-2}	2.52×10^{-3}
			ZXZ	2.19×10^{-1}	1.48×10^{-1}	1.48×10^{-2}	1.12×10^{-1}	2.48×10^{-3}
			Average	2.41×10^{-1}	1.50×10^{-1}	1.60×10^{-2}	1.07×10^{-1}	2.41×10^{-3}
ADI ($\mu g/kg \cdot d^{-1}$)				40	3.5	3	20	1
Risk (%)	Reference area	Adults	CM	0.039	0.344	0.062	0.043	0.012
		Children	CM	0.285	2.503	0.450	0.311	0.087
	Coal mining area	Adults	TY	0.071	0.672	0.076	0.076	0.031
			QN	0.103	0.652	0.074	0.078	0.032
			QD	0.095	0.558	0.077	0.069	0.034
			LL	0.071	0.494	0.072	0.067	0.035
			ZXZ	0.075	0.581	0.068	0.077	0.034
			Average	0.083	0.591	0.073	0.073	0.033
		Children	TY	0.517	4.886	0.550	0.551	0.224
			QN	0.748	4.743	0.541	0.566	0.230
			QD	0.689	4.057	0.562	0.500	0.250
			LL	0.515	3.590	0.523	0.484	0.252
			ZXZ	0.547	4.224	0.494	0.561	0.248
			Average	0.603	4.300	0.534	0.533	0.241

comparing the results with the allowable daily intake (ADI) recommended by US EPA (Table 6). As shown in Table 6, the highest ingested amounts of Cu and Ni were in the QN area with W_{int} values of 4.11×10^{-2} and 1.56×10^{-2} $\mu g \cdot kg^{-1} \cdot d^{-1}$ for adults, and of 2.99×10^{-1} and 1.13×10^{-1} $\mu g \cdot kg^{-1} \cdot d^{-1}$ for children, respectively. On the other hand, the largest ingested amount of Pb was in the TY area (2.35×10^{-2} $\mu g \cdot kg^{-1} \cdot d^{-1}$ for adults and 1.71×10^{-1} $\mu g \cdot kg^{-1} \cdot d^{-1}$ for children), and Cr reached its highest level in the QD area (2.32×10^{-3} $\mu g \cdot kg^{-1} \cdot d^{-1}$ for adults and 1.68×10^{-2} $\mu g \cdot kg^{-1} \cdot d^{-1}$ for children), while the largest ingested amount of Cd was in the LL area (3.47×10^{-4} $\mu g \cdot kg^{-1} \cdot d^{-1}$ for adults and 2.52×10^{-3} $\mu g \cdot kg^{-1} \cdot d^{-1}$ for children). The daily ingested amounts for all the investigated metals, by both adults and children, were clearly higher in the coal mining areas than those in the reference area. For example, all the average W_{int} values of Cu, Pb, Cr, Ni, and Cd for children in the coal mining areas all exceed the W_{int} values in the reference area by 111.5%, 71.8%, 18.8%, 71.2%, and 176.9%, respectively. Among different groups of receptors, children are exposed to a significantly higher daily level of toxic metals than adults, because of the difference in their body weight as well as the typical behavior of children, such as the repetitive sucking on hands/fingers and the chewing of non-food objects, which can increase the dust intake [3,29]. Therefore, compared to adults, children are more prone to get contact with dust in larger doses and more likely sensitive to it.

In comparison with the ADI limits recommended by US EPA, risk values of the five trace elements in the coal mining areas followed the order of Pb>Cu>Cr≈Ni>Cd, and range from 0.033% to 0.591% for adults and from 0.241% to 4.300% for children. Although these values were higher than the risk values in the reference area (0.012%–0.344% for adults and 0.087%–2.503% for children), they did not exceed 1.0, which indicated that the incidental ingestion of atmospheric dust in these mining areas might not have significant harmful effects on the local residents. However, this could not ensure the safety of the area, because there are many other exposure routes to heavy metals, such as soil, food, and water, which may increase their intakes. In fact, several similar studies on risk assessment of heavy metals in dust defined a potential health risk limit of 0.1 [30]. In this study, the risk values in the investigated areas of the five metals were all below 0.1. However, it should be noted that the highest risk value of Pb ingestion for children in the coal mining area has reached 4.886%, which could readily increase to the potential risk limit if the incidental ingestion rate increased due to the ingrained unsanitary habits. Therefore, it is recommended that measures, such as spraying water regularly in the streets and increasing the awareness on the hygienic habits in

schools and communities, should be implemented by the local government as quickly as possible to improve the level of hygiene in the coal mining areas in order to minimize the dust intake and avoid the potential risk to children.

CONCLUSIONS

Because of the strong anthropogenic inputs caused by mining activities, atmospheric dust samples collected from Suzhou coal mining area had higher average concentrations of Cu, Pb, Ni, and Cd than both BVA and the samples collected from the reference area, showing significant enrichment of trace metals in the region. Sequential extraction results showed that Cd was the most mobile element with the highest percentage (81.42%–89.71%) of the extractable fractions (F1+F2+F3) in the total Cd content. Pb and Cu were mainly associated with the reducible fraction (F2), while a considerable amount of Cu was also extracted in the oxidizable fraction (F3). More than 90% of Cr contents and 70% of Ni contents were retained in the residual fraction (F4), indicating the high stability of these two metals in the atmospheric dust. The differences in bioavailability between the investigated metals were obtained by *in vitro* digestion procedure, the results of which were in the following order: Cd>Pb>Cu>Ni>Cr in the gastric phase, and Cu>Pb>Cd>Ni>Cr in the intestinal phase. pH and complexation with a digestive enzyme were considered important factors that influenced the dissolution and activation of the trace metals in the simulated digestive solution.

Correlation and multiple-stage linear regression analyses suggested that the reducible fraction (F2) was the dominant source of the metal quantities extracted in the gastrointestinal phase, followed by the acid soluble fraction (F1) and the oxidizable fraction (F3), confirmed that the metals existed in these three fractions are more likely to be bioavailable. There was scarcely any significant correlation between the residual fraction (F4) and the gastrointestinal bioavailability of the five metals, except for Ni in the intestinal phase. Moreover, metal intakes through incidental dust ingestion, by adults and children, were far below the ADI values recommended by the US EPA, which indicated that they did not pose significant health risks to the local residents. However, the Pb intakes for children could still possibly cause potential harm risk if the dust ingestion rate increased. To avoid the potential risk, measures related to improvement of hygiene level should be conducted in the coal mining areas.

ACKNOWLEDGEMENTS

This work was financially supported by the Key Natural Science Project of Suzhou University (Project No. 2016yzd07) and the Leading Talent Special Project of Anhui Province (Project No. 2014lj01).

REFERENCES

[1] Al-Khashman, O.A. (2004) Heavy metal distribution in dust, street dust and soils from the work place in Karak Industrial Estate, Jordan, Atmospheric Environment. 38(39), 6803-6812.

[2] Wang, S.M., Yu, H., Song, L., Xie, Y.C. and Zhu, Q.H. (2015) Air quality in a mountainous city: a case study in Chongqing, China. Fresen. Environ.Bull. 24(9), 2699-2706.

[3] Rout, T.K., Masto, R.E., Ram, L.C., George, J. and Padhy, P.K. (2013) Assessment of human health risks from heavy metals in outdoor dust samples in a coal mining area. Environmental Geochemistry and Health. 35(3), 347-356.

[4] Shi, G., Chen, Z., Bi, C., Wang, L., Teng, J., Li, Y. and Xu, S. (2011) A comparative study of health risk of potentially toxic metals in urban and suburban road dust in the most populated city of China. Atmospheric Environment. 45(3), 764-771.

[5] Unsal, Y.E., Tuzen, M. and Soylak, M. (2014) Evaluation of metal concentrations of soil samples from Yahyali-Kayseri, Turkey. Fresen. Environ. Bull. 23(10), 2488-2491.

[6] Kwasowski, W., Kozanecka, T., Gorska, E.B., Gozdowski, D. and Kowalczyk, P. (2016) Application of heavy metals in street dust in the monitoring of changes in environment. Fresen. Environ. Bull. 25(1), 103-112.

[7] Yang, Q., Chen, H.G. and Li, B.Z. (2015) Source identification and health risk assessment of metals in indoor dust in vicinity of phosphorus mining, Guizhou Province, China. Archives of Environmental Contamination and Toxicology. 68(1), 20-30.

[8] Bakircioglu, D., Kurtulus, Y.B. and Ibar, H. (2011) Investigation of trace elements in agricultural soils by BCR sequential extraction method and its transfer to wheat plants. Environmental Monitoring and Assessment. 175(1-4), 303-314.

[9] Dousis, P., Anastopoulos, I., Gasparatos, D., Ehaliotis, C. and Massas, I. (2013) Effect of time and glucose-C on the fractionation of Zn and Cu in a slightly acid soil. Communications in Soil Science and Plant Analysis. 44(1-4), 722-732.

[10] Alomary, A.A. and Belhadj, S. (2007) Determination of heavy metals (Cd, Cr, Cu, Fe, Ni, Pb, Zn) by ICP-OES and their speciation in Algerian Mediterranean Sea sediments after a five-stage sequential extraction procedure. Environmental Monitoring and Assessment. 135(1-3), 265-280.
[11] Mei, F.M., Xu, C.Y. and Zhou, L. (2011) Chemical species and bioavailability of Cu, Pb, Zn, Ni and Cd of dustfall from Xi'an park in China. Environmental Chemistry. 30(7), 1284-1290. (In Chinese)
[12] Sungur, A., Soylak, M., Yilmaz, S. and Özcan, H. (2014) Determination of heavy metals in sediments of the Ergene River by BCR sequential extraction method. Environmental Earth Sciences. 72(9), 3293-3305.
[13] Soylak, M., Uzek, U., Narin, I., Tuzen, M., Turkoglu, O. and Elci, L. (2004) Application of the sequential extraction procedure for dust samples from Kayseri-Turkey. Fresen. Environ. Bull. 13(5), 454-457.
[14] Zhu, X.D., Yang, F. and Wei, C.Y. (2015) Factors influencing the heavy metal bioaccessibility in soils were site dependent from different geographical locations. Environmental Science and Pollution Research. 22(18), 13939-13949.
[15] Ruby, M.V., Davis, A., Schoof, R., Eberle, S. and Sellstone, C.M. (1996) Estimation of lead and arsenic bioavailability using a physiologically based extraction test. Environmental Science& Technology. 30(2), 422-430.
[16] Oomen, A.G., Hack, A., Minekus, M., Zeijdner, E., Cornels, C., Schoeters, G., Verstraete, W., Van, D.W.T., Wragg, J., Rompelberg, C.J.M., Sipps, A.J.A.M. and Van, W.J. (2002) Comparison of five in-vitro digestion models to study the bioaccessibility of soil contaminants. Environmental Science & Technology. 36(15), 3326-3334.
[17] Ruby, M.V., Davis, A., Link, T.E., Schoof, R., Chancy, R.L., Freeman, G.B. and Bergstrom, P. (1993) Development of an in-vitro screening-test to evaluate the in-vivo bioaccessibility of ingested mine-waste lead. Environmental Science & Technology. 27(13), 2870-2877.
[18] Karadaş, C. and Kara, D. (2011) In-vitro gastro-intestinal method for the assessment of metal bioavailability in contaminated soils. Environmental Science and Pollution Research. 18(4), 620–628.
[19] Chen, M., Zhu, L.J., Wu, Y.G., Fu, T.L. and Ran, Y. (2014) Enrichment of heavy metals in coal gangue by puff balls and mechanism research. Chinese Journal of Geochemistry. 33(4), 419–424.
[20] Li, Z.C., Gui, H.R., Sun, L.H. and Gong, W. (2013) Pollution and migration ability assessment of heavy metals in sediments from Luling mine subsidence area section of Tuohe River. Environmental Science and Technology. 36(7), 13-17. (In Chinese)
[21] Li, Q., Han, Y.F., Xu, D.S. and Gao, Y. (2014) Enrichment Characteristics and Pollution Assessment of Three Food Crops around Gangue Dump. Journal of Safety and Environment. 14(5), 321-326. (In Chinese)
[22] US EPA. (2010) United States Environmental Protection Agency. US EPA Regional Screening Level table, Available at http://epa.gov/reg3hwmd /risk/human/.
[23] Kazi, T.G., Jamali, M.K., Kazi, G.H., Arain, M.B., Afridi, H.I. and Siddiqui, A. (2005) Evaluating the mobility of toxic metals in untreated industrial wastewater sludge using a BCR sequential extraction procedure and a leaching test. Analytical and Bioanalytical Chemistry. 383(2), 297-304.
[24] Businelli, M., Casciari, F., Businelli, D. and Gigliotti, G. (2003) Mechanisms of Pb(II) sorption and desorption at some clays and goethite-water interfaces. Agronomie. 23(23), 210-225.
[25] Peng, J.F., Song, Y.H., Yuan, P., Cui, X.Y. and Qiu, G.L. (2009) The remediation of heavy metals contaminated sediment. Journal of Hazardous Materials. 161(2), 633–640.
[26] Ren, J.H., Williams, P.N., Luo, J., Ma, H.R. and Wang, X.R. (2015) Sediment metal bioavailability in Lake Taihu, China: evaluation of sequential extraction, DGT, and PBET techniques. Environmental Science and Pollution Research. 22(17), 12919-12928.
[27] Li, Y. and Zhang, M.K. (2013) A comparison of physiologically based extraction test(PBET) and single-extraction methods for release of Cu, Zn and Pb from mildly acidic and alkali soils. Environmental Science and Pollution Research International. 20(5), 3140-3148.
[28] Karadaş, C. and Kara, D. (2012) Chemometric evaluation for the relation of BCR sequential extraction method and in vitro gastro-intestinal method for the assessment of metal bioavailability in contaminated soils in Turkey. Environmental Science and Pollution Research. 19(4), 1280-1295.
[29] Abuduwailil, J., Zhang, Z.Y. and Jiang, F.Q. (2015) Evaluation of the pollution and human health risks posed by heavy metals in the atmospheric dust in Ebinur Basin in Northwest China. Environmental Science and Pollution Research. 22(18), 14018-14031.

[30] Ferreira-Baptista, L. and De Miguel, E. (2005) Geochemistry and risk assessment of street dust in Luanda, Angola: A tropical Urban environment, Atmospheric Environment. 39(25), 4501-4512.

Received: **20.05.2017**
Accepted: **03.10.2017**

CORRESPONDING AUTHOR

Qi Li
School of Environment and Surveying Engineering,
Suzhou University,
Suzhou 234000 - China

e-mail: liqi821113@163.com

© by PSP Volume 26 – No. 12A/2017 pages 7925-7930 Fresenius Environmental Bulletin

LATEWOOD PROPORTION INSIDE GROWTH RINGS BY BALD CYPRESS STEMS IN SERBIA

Dusan Jokanovic*, Dragica Vilotic, Vesna Nikolic, Marina Nonic, Jovana Devetakovic, Dragica Stankovic

Faculty of Forestry, University of Belgrade, Kneza Višeslava 1, Belgrade

ABSTRACT

In the paper, there was analyzed participation of the latewood zone inside growth rings of bald cypress from two different locations in Serbia. Its proportion has been monitored depending on three factors – growth rings width, age and stem height. Between growth rings width and latewood zone proportion was established negative correlation. For that reason, stems on Bačka Palanka, whose growth rings are narrower, have greater latewood zone proportion compared to stems from Veliko ratno ostrvo, that have faster radial increment. Greater latewood proportion contributes to better mechanical and technical properties of the stems from Bačka Palanka. As for relations between latewood proportion, from one side, and age and stem height, from the other side, there is also established negative correlation. Bearing on mind that bald cypress belongs to soft conifers, its latewood proportion almost never exceeds more than 1/3 of the whole growth rings width.

KEYWORDS:
Bald cypress, latewood proportion, stem height, growth rings, age

INTRODUCTION

Juvenile wood is produced by the young cambium in the live active crown and forms a cylinder of wood surrounding the pith that extends the length of the tree [1]. Juvenile wood is low in stiffness and strength, and thus wood from fast-growing young trees is less desirable for solid wood products [2]. This wood has a high proportion of early-wood-type tracheid and thus lower specific gravity, thinner cell walls, wider micro-fibril angle, and less latewood than mature wood [3]. Because of its tracheid characteristics, juvenile wood has significantly lower strength and stiffness, more longitudinal shrinkage, and less radial and tangential shrinkage than mature wood [4, 5, 6].

Many studies have been devoted to determining cambial age of growth rings in which juvenile wood formation stops and mature wood formation begins. There is no abrupt shift from juvenile to mature wood within 1 year. Instead, the change takes several years and gradually grades from one into the other [7]. Nearly all wood properties are highly variable from ring to ring within the juvenile zone and relatively constant within the mature zone [8].

Various methods have been used to determine the age of transition from juvenile to mature wood. The simplest method is the so-called threshold or graphic method where a value is selected from graphs to define when a property has reached that of mature wood [9, 10, 11, 12]. A second method is to use linear segmented regression models [13, 14, 15] or nonlinear regression models [16, 17] to estimate the age of demarcation.

Depending on changeable light conditions, there is physiological and anatomic adaptability by changed values of analyzed stomata characteristics by *Paulownia* [18]. Based on [19], it can be deduced that Douglas-fir is a tree with relatively high radial and height increment in Serbian environmental conditions and could be used for plantations and cultures establishing.

MATERIALS AND METHODS

Study area. There are just two seed stands with bald cypress in Serbia. They are situated near Belgrade (Veliko ratno ostrvo) and in the northern part of Serbia (Novi Sad). Stems present there satisfy a few significant criteria for performing anatomical analysis: generative origin; good physiological and health condition; absence of any technical deformation.

After suitable stems have been chosen and fallen (overall 6), wood cross-sections were taken. It was performed from two heights – from the base (0.3 m) and from the breast height (1.3 m). Cross-sections were about 2 cm thick. The final step before making permanent anatomical preparations was cutting the cross-sections through diameter in order to do all necessary measurements.

The aim of the paper was, first of all, to determine transition zone between early- and latewood as precisely as possible, and to follow participation of these zones from the pith (in the region of juvenile wood) to the bark (zone of mature wood).

Laboratory work. Wood samples for analysis originated from bald cypress trees located in Veliko

ratno ostrvo and Backa Palanka area. Parts of the wood were transported into the Laboratory of the Faculty of Forestry, where all macroscopic and microscopic analysis, including all phases for making permanent anatomical preparations, have been performed. Samples of wood parts were prepared with a width of about 8 mm. These parts were taken in a north-south and east-west direction, respectively. Prepared material was fixed in formaldehyde-acetic:acid:ethyl alcohol in ration 1:1:18. Before making transversal, tangential and radial wood sections, there was no need for cooking the samples in the water on a high temperature in order to soften it, because bald cypress does not have so hard wood. The next step was to make blocks of samples with a length of 18 mm and they were made in a radial direction. Each block was numbered from 1 to n, going from the pith to the bark. Sections of samples in all directions (transversal, tangential and radial) were made using a Reichert sliding-microtome. Thickness of all sections was about 17-18 μm. Samples were colored with a combination of safranin and aniline for about 5 min, and then transferred through alcohol solutions of different concentrations (50 %, 70 %, 96 % and 100 %). The samples treated with different concentrations of alcohol solutions were conserved with Canada balsam. The last step was drying of the samples at a temperature of 60° C [20, 21, 22].

Measurements. Each growth ring was measured at its transversal cut, from the pith to the bark. After that, it was necessary to define transition zone between early- and late-wood. It was not so simple, because growth rings and boundary between each other by bald cypress are not so visible. Therefore was applied Mork's formula [23] that marks latewood zone as a part of the growth ring whose radial cell wall thickness is equal or greater than radial diameter of any cell lumen. Performing this implied observing of all growth ring parts at a very high magnification under microscope (100 and 400 times) in order to separate carefully early- and latewood zone. It was also necessary to find minimal difference in the color between these zones (early zone does physiological function and therefore is brighter, while late zone is responsible for mechanical function and has a dark color). After both above mentioned patterns have been satisfied, determining of latewood zone proportion inside growth rings started.

RESULTS AND DISCUSSION

Based on obtained results shown in the figures 1-4, it is obvious a greater latewood zone proportion in Backa Palanka than on Veliko ratno ostrvo. That can be related to the whole growth rings width. Stems from Backa Palanka grow slower, and therefore they form narrower growth rings then the others from Veliko ratno ostrvo. These two variables characterize inverse tendencies – wider growth rings have smaller proportion of the latewood zone and reverse, narrower growth rings means a greater latewood zone proportion.

Maximal values for latewood zone proportion inside the growth rings on both locations are not more than 1/3 from the whole growth rings width. This is completely compatible with results obtained for Serbian spruce in the National Park Tara [24], [25], where earlywood zone includes 2/3 or even ¾ from the whole growth rings width. As for wood structure of fir from Veliki Jastrebac mountain [26], it was also established much greater proportion of early- than latewood zone on the whole cross-section.

There was found decreasing of latewood percentage proportion with the stem height on both locations (figures 1-4). One research [27] found that, at both good and medium sites, ring width was found to increase towards the top of the stems while latewood proportion and dry density showed a negative relation with stem height. This completely coincides with obtained results for bald cypress.

Decreasing of latewood proportion with age has also been noticeable for both locations (figures 1-4). This can be explained with the fact that close to the bark mechanical wood properties gradually become poorer. Group of authors [28] established a clear relation between mechanical and physiological elements in oak pedunculate wood – percentage proportion of mechanical elements falls in the latewood zone away from the pith, while proportion of vessels (physiological elements) rises. Some researchers such as [29, 30] claimed that changing of growth rings width by oaks affects much more changing of latewood than of earlywood zone width. Contrary, for bald cypress from both locations, increasing of the whole growth rings width means simultaneously increasing of earlywood zone proportion with no significant effect on the latewood zone proportion.

Two authors [31] made a relation between wood density and growth speed establishing linear dependence form up to the maximum. As for some fast-growing species [32] wood density goes down with further growth rings width increasing.

It should be emphasized the existence of negative relation between growth rings width and latewood zone proportion by bald cypress, and it is valid on both levels – site and individuals inside population.

Obtained results of the paper [33] show a bit different relation between growth rings width and proportion of latewood zone. This research was performed on various black locust clones and established that all fast-growing clones, apart from one,

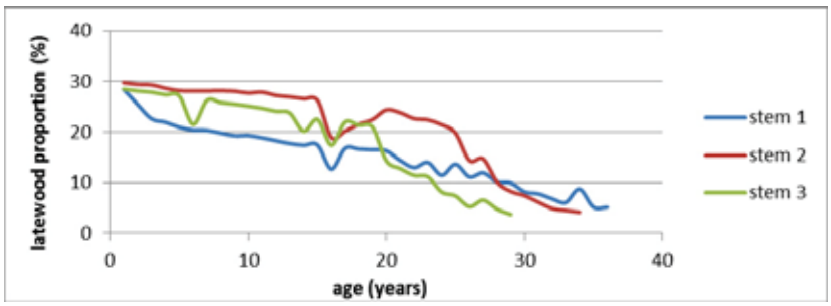


FIGURE 1
Location-Veliko ratno ostrvo, 0.3m

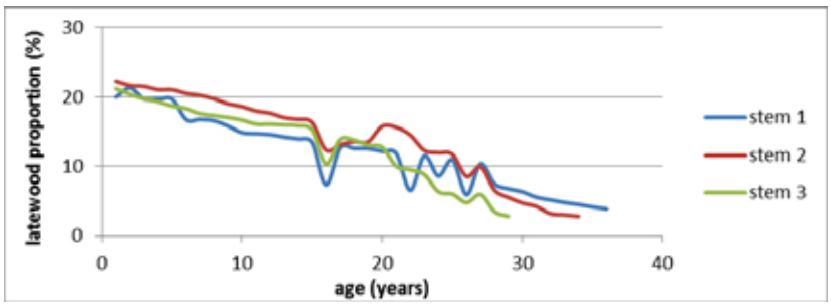


FIGURE 2
Location-Veliko ratno ostrvo, 1.3m

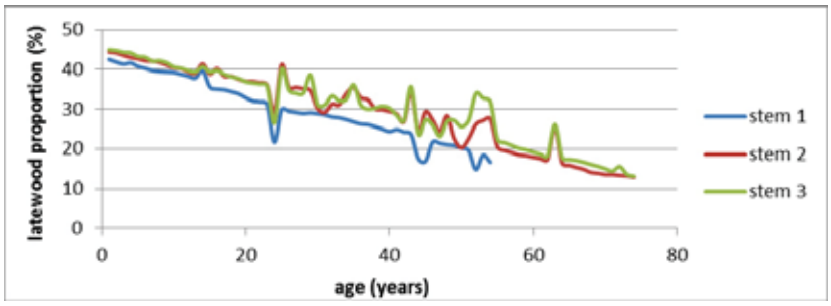


FIGURE 3
Location-Bačka Palanka, 0.3m

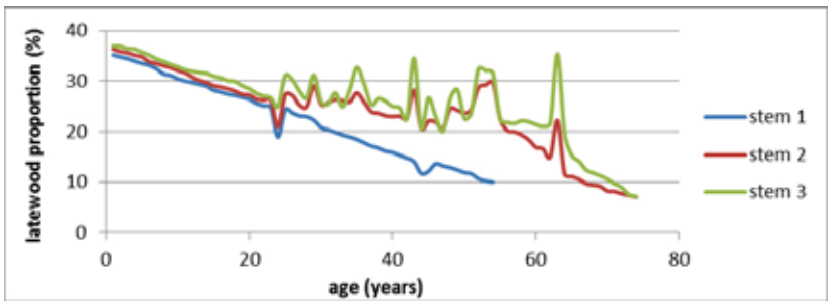


FIGURE 4
Location-Bačka Palanka, 1.3m

have greater proportion of latewood zone with increasing of growth rings width. The only clone that did not confirm this claim grew on better site conditions than all the others. It means that higher site quality causes smaller proportion of latewood zone.

Most studies indicate that high wood density in ring-porous hardwoods is associated with fast growth [34, 35, 36, 37, 38, 39, 40]. According to [41], this is because the width of early-wood remains fairly constant from year to year while the dense latewood with fewer vessels increases as ring width increases. However, there are some exceptions to this generalization. The first rings near the pith (juvenile wood) do not necessarily follow the above pattern and the proportion of different types of cells might also have a substantial influence on wood density [42, 43, 44].

As for participation of some elements related to

microscopic wood structure in early- and latewood zone, dimensions of vessels of *Quercus* sp have been observed [45]. It was concluded that latewood vessels made up the majority of vessels less than 4 cm long. In current-year shoots, there was no clear difference between early- and latewood vessels. The first-formed vessels nearest the pith were as small as the latewood vessels; vessels near the middle of the wood ring were largest. In all other rings, early- and latewood vessels were clearly distinguishable.

In another study conducted by [46] the length and diameter (width) of vessels in black locust early- and latewood were measured. Obtained results show significant differences in vessels width between two zones (47 μm in early- and 24 μm in latewood zone, respectively).

By other ring-porous species, in a radial direction, the vessel member diameter of early-wood increased in the first growth rings near the pith and then remained stable towards the bark [47]. The other research [48] found a similar radial trend in early-wood vessel diameter by some other ring-porous species such as oak.

By bald cypress from both researched sites, [21] followed behavior and values of some elements of microscopic wood structure inside different wood zones. Woody rays height is bigger in the early- than in the latewood zone, unlike its number per mm^2. As for tracheid width, its values go up from the pith to the bark in the early-wood in Veliko ratno ostrvo, and the same occurs in the latewood zone in Backa Palanka. The same trend is valid for the number of tracheid per mm^2 – increasing with age in the earlywood zone in Veliko ratno ostrvo, and in the latewood zone in Backa Palanka, as well. Tracheid lengths are much bigger in Veliko ratno ostrvo, and this difference is particularly significant in the earlywood zone.

CONCLUSIONS

Based on obtained results, it can be deduced:

- proportion of the latewood zone is bigger by stems from Backa Palanka than from Veliko ratno ostrvo – it can be related to growth rings width
- maximal values of the latewood proportion do not reach 1/3 from the whole growth rings width
- there is clear negative relation between latewood zone proportion and stem height – it is valid for both researched sites
- from the pith to the bark decreases participation of the latewood zone by both researched sites
- greater latewood zone proportion in Backa Palanka shows better mechanical and technical properties of stems from that area

ACKNOWLEDGEMENTS

This paper has been supported from the project "Forest plantations in function of forest cover increasing in Serbia", number 31041 that was financed from Ministry of science and technological development.

REFERENCES

[1] Clark, A., Daniels, R.F. and Jordan, L. (2006) Juvenile/mature wood transition in loblolly pine as defined by annual ring specific gravity, proportion of latewood, and microfibril angle. Wood and Fiber Science. 38(2), 292-299.

[2] Senft, J.F., Bendtsen, B.A. and Galligan, W.L. (1985) Weak wood: Fast-grown trees make problem lumber. J. Forestry. 83(8), 477-484.

[3] Thomas, R.J. (1984) The characteristics of juvenile wood. In: Kellison, R.C. (ed.) Proc. Symposium on Utilization of the Changing Wood Resources in the Southern United States. North Carolina State University, Raleigh, NC, 40-52.

[4] Pearson, R.G. and Gilmore, R.C. (1971) Characterization of the strength of juvenile wood of loblolly pine. Forest Prod. J. 21(1), 23-31.

[5] Bendtsen, B.A. (1978) Properties of wood from improved and intensively managed trees. Forest Prod. J. 28(10), 61-72.

[6] Bendtsen, B.A. and Senft, J.F. (1986) Mechanical and anatomical properties in individual growth rings of plantation-grown eastern cottonwood and loblolly pine. Wood and Fiber Science. 18(1), 23-28.

[7] Zobel, B.J. (1980) Inherent differences affecting wood quality in fast-grown plantations. In Proc IUFRO Conference Division 5, Oxford, UK, 169-188.

[8] Saranpää, P. (2003) Wood density and growth. In R Barnett and G Jeronimidis, eds. Wood quality and its biological basis, Blackwell Publishing & CRC Press, Biological Sciences Series, Oxford, UK. 87-117.

[9] Clark, A. and Saucier, J.R. (1989) Influence of initial planting density, geographic location, and species on juvenile wood formation in southern pine. Forest Prod. J. 39(7/8), 42-48.

[10] Jozsa, L.A. (1998) Basic wood properties of second-growth western hemlock. Special Publication No. SP-38, Forintek Canada Corporation, Vancouver, BC, 51.

[11] Clark, A. and Edwards, M.B. (1999) Effect of six site-preparation treatments on Piedmont loblolly pine wood properties at age 15. In J.D. Haywood, ed. Proc. Tenth Biennial Southern Silvicultural Research Conference, Shreveport, L.A., USDA Forest Service, Southern Research Station. 316-320.

[12] Clark, A., Daniels, R.F. and Miller, J.H. (2006) Effect of controlling herbaceous and woody competing vegetation on wood quality of planted loblolly pine. Forest Prod. J. 56(2), 40-46.
[13] Loo, J.A., Tauer, C.G. and McNew, R.W. (1985) Genetic variation in the time of transition from juvenile to mature wood in loblolly pine (*Pinus taeda* L.). Silvae Genet. 34(1), 14-19.
[14] Szymanski, M.B. and Tauer, C.G. (1991) Loblolly pine provenance variation in age of transition from juvenile to mature wood specific gravity. Forest Sci. 37(1), 160-174.
[15] Sauter, U.H.R., Mutz and Munro, B.D. (1999) Determining juvenile-mature wood transition in Scots pine using latewood density. Wood Fiber Sci. 31(4), 416-425.
[16] Hodge, G.R. and Purnell, R.C. (1993) Genetic parameter estimates for wood density, transition age, and radial growth in slash pine. Can. J. For. Res. 23, 1881-1891.
[17] Tasissa, G. and Burkhart, H.E. (1998) Juvenile-mature wood demarcation in loblolly pine trees. Wood Fiber Sci. 30(2), 119-127.
[18] Mitrovic, S., Jokanovic, D., Vilotic, D., Miljkovic, D., Veselinovic, M., and Stankovic, D. (2017) Stomata characteristics of two Paulownia species under different conditions of light. Fresen. Environ. Bull. 26(3), 1876-1882.
[19] Veselinovic, M., Vilotic, D., Mitrovic, S., Cule, N., Stankovic, D., Jokanovic, D., Madzgalj, J. (2017) Air pollutant effects on chlorenchyma cell and chloroplasts of Douglas-Fir (Pseudotsuga Menziesii (Mire.) Franco) needles. Fresen. Environ. Bull. 26(3), 1974-1979.
[20] Vilotić, D. (1992) Anatomska građa stabla virgiliskog hrasta (Quercus virgiliana /Ten/ Ten.) na različitim staništima Deliblatske peščare. Doctoral dissertation, University of Belgrade – Faculty of Forestry.
[21] Jokanović, D. (2016) Anatomske osobine stabala *Taxodium distichum* (L.) Rich. na aluvijalnim staništima u Srbiji. Doctoral dissertation, University of Belgrade – Faculty of Forestry.
[22] Jokanović, D., Vilotić, D., Mitrović, S., Miljković, D., Rebić, M., Stanković, D. and Nikolić, V. (2015) Correlations between the anatomical traits of *Gymnocladus canadensis* Lam. in heartwood and sapwood of early-and latewood zones of growth rings. Arch. Biol. Sci. 67(4), 1399-1404.
[23] Denne, M.P. (1989) Definition of latewood according to Mork (1928). IAWA Bulletin. 10, 59-62.
[24] Vilotić, D. (1994) Anatomska građa stabla omorike (Pančić) Purkyne sa područja Nacionalnog parka Tara in the Monograph: Omorika – *Picea omorika* (Pančić) Purkyne na području Nacionalnog parka Tara. Bajina Bašta. 33-39.
[25] Matijević, B. (1988) Anatomska građa drveta *Picea omorika* (Pančić) Purkyne sa lokaliteta Crvene stene – Tara in the Monograph: Flora Nacionalnog parka Tara. Bajina Bašta. 557-561.
[26] Vilotić, D. (1992) Anatomska građa debla jele (*Abies alba* Mill.) in the Monograph: Flora severnog dela Velikog Jastrepca. Kruševac. 350-351.
[27] Adamopoulos, S., Milios, E., Doganos, D. and Bistinas, I. (2009) Ring width, latewood proportion and dry density in stems of *Pinus brutia* Ten. Eur. J. Wood Prod. 67, 471-477.
[28] Rao, R.V., Aebischer, D.P. and Denne, M.P. (1997) Latewood density in relation to wood fiber diameter, wall thickness, and fiber and vessel percentages in *Quercus robur* L. IAWA Journal. 18(2), 127-138.
[29] Gasson, P. (1987) Some implications of anatomical variations in the wood of pedunculated oak (*Quercus robur* L.) including comparisons with common beach (*Fagus sylvatica* L.). IAWA Bulletin. 8, 149-166.
[30] Lei, H., Milota, M.R. and Gartner, B.L. (1996) Between-and-within-tree variation in the anatomy and specific gravity of wood in Oregon white oak (*Quercus garryana* Dougl.). IAWA Journal. 17, 445-461.
[31] Zhang, S.Y. and Zhong, Y. (1991) Effect of growth rate on specific gravity of East-Liaoning oak (*Quercus liaotungensis*) wood. Can. J. For. Res. 21, 255-260.
[32] Nepveu, G. (1993) The possible status of wood quality in oak breeding programs (*Quercus petraea* Liebl and *Quercus robur* L.). Ann. Sci. For., 50(Suppl.1), 388-394.
[33] Adamopoulos, S., Passialis, C. and Voulgaridis, E. (2010) Ring width, latewood proportion and density relationships in black locust wood of different origins and clones. IAWA Journal. 31(2), 169-178.
[34] Guiher, J.K. (1965) Effect of rings-per-inch on specific gravity of red oak. For. Prod. J. 15, 409-411.
[35] Panshin, A.J. and de Zeeuw, C. (1980) Textbook of wood technology. Ed. 4, McGraw-Hill, New York.
[36] Baas, P. (1982) New perspectives in wood anatomy. W. Jung Publishers, The Hague, The Netherlands.
[37] Zobel, B.J. and Van Buijtenen, J.P. (1989) Wood variation – its causes and control. Springer Verlag, New York.
[38] Tsoumis, G. (1991) Science and technology of wood: structure, properties, utilization. Van Nostrand Reinhold, New York.
[39] Guyette, R.P. and Stambaugh, M. (2003) The age and density of ancient and modern oak wood in streams and sediments. IAWA Journal. 24, 345-353.

[40] Saranpää, P. (2003) Wood density and growth. In: Barnett, J.R. and Jeronimidis, G. (eds.) Wood quality and its biological basis. 87-117.
[41] Wheeler, E.A. (1987) Anatomical and biological properties of juvenile wood in conifers and hardwoods. 41st Annual Meeting, FPRS Louisville, Kentucky.
[42] Knigge, W. and Koltzenburg, C. (1965) The influence of timber qualities and ecological conditions on the cell sizes and on the proportions of types of cell in hardwoods in the temperate zones. IUFRO Section 41 Comm. Fiber Char., Melbourne, Australia, 2, 51.
[43] Zhang, S.Y. and Zhong, Y. (1992) Structure-property relationship of wood in East-Liaoning oak. Wood Sci. Technol. 26, 139-149.
[44] Tsuchiya, R. and Furukawa, I. (2009) Radial variation in the size of axial elements in relation to stem increment in *Quercus seratta*. IAWA Journal. 30, 15-26.
[45] Cochard, H. and Tyree, M.T. (1990) Xylem dysfunction in *Quercus*: vessel sizes, tyloses, cavitation and seasonal changes in embolism. Tree Physiology. 6, 393-407.
[46] Adamopoulos, S. and Voulgaridis, E. (2002) Within-tree variation in growth rate and cell dimensions in the wood of black locust (*Robinia pseudoacacia*). IAWA Journal. 23, 191-199.
[47] Frey-Wyssling, A. and Bosshard, H.H. (1959) Cytology of the ray cells in Sapwood and Heartwood. Holzforschung. 13, 129-137.
[48] Helinska Raczkowska, L. (1994) Variation of vessel lumen diameter in radial direction as an indication of juvenile wood growth in oak (*Quercus petraea* Liebl.). Ann. Sci. For. 51, 283-290.

Received: **23.05.2017**
Accepted: **23. 09.2017**

CORRESPONDING AUTHOR

Dusan Jokanovic
Faculty of Forestry
University of Belgrade,
Kneza Višeslava 1 – Belgrade

e-mail: dusan.jokanovic@sfb.bg.ac.rs

© by PSP Volume 26 – No. 12A/2017 pages 7931-7940 Fresenius Environmental Bulletin

ASSESSMENT OF THE IMPACTS OF INDUSTRIAL EFFLUENT DISCHARGES ON THE EPILITHIC DIATOMS COMMUNITY AND WATER QUALITY OF SAHNAHAN STREAM, MALATYA, TURKEY

Betul Celik*, Vesile Yildirim

Firat University, Biology Department, Elazig, Turkey

ABSTRACT

In this study, the effect of an industrial effluent discharges on the water quality and epilithic algae of Şahnahan Stream (Malatya-Turkey). Şahnahan stream's epilithic algae and water quality were examined between May 2012-April 2013 which identified 3 station taken the samples of monthly periods. During the study, a total of 141 taxa were identified, most of which belonged Bacillariophyta (123), other taxonomic groups present were Chlorophyta (9), Cyanophyta (5), Charophyta (3) and Dinophyta (1). Temperature, pH, total hardness dissolved oxygen, organic matter, nitrit, nitrat sulfate, total phosphore, orthophosphate were measured and analysed. Water quality and epilithic algal community differed significantly between sites upstream and downstream of the discharge. At the same time, changes in the dominant algae groups were observed.

KEYWORDS:
Water quality, Stream, Epilithic algae, Pollution, Biothic indices

INTRODUCTION

Water, which is the basic element needed directly or indirectly at every stage of life, has been under intense press as a result of various human activities especially in recent years. Nowadays, one of the most important problems to threaten the aquatic ecosystems is pollution. Changing the natural structure and stream beds affects negatively the flora and fauna living in these environments and can lead to decrease in numbers of some species over time and even to extinction of some species [1]. It is necessary to determine the benthic algae communities spreading in streams and to significantly take advantage of them. Diatoms are commonly used as indicators of various environmental parameters, such as salinity, pH, and nutrient. Diatoms are also known to be sensitive to toxic substances and organic contaminants. The effects of contaminants on the species composition and diversity of algae including diatoms were demonstrated in field studies of rivers in Spain and Northern Canada [2]. In our country and around the world, the studies on algae have increased as time progresses.

Gürbüz and Kıvrak determined water quality of Karasu Stream by using some diatom indexes in their study. According to the data of SI and TDI, they reported that downstream of the river basin was polluted dramatically and was exposed to eutrophication. Besides, they also reported that all the indexes used in their study, except GDI, showed strong correlations with the dissolved O_2 and nutrient levels [3].

Solak examined epilithic diatom samples in order to determine the water quality of upper Porsuk River. As a result of the study, total 57 species of diatom were detected and the water quality of Porsuk River was detected by using SLA, EPI-D, TDI, DESCY indexes in terms of these species. According the index values, it was observed that there were certain differences between three stations, and there were also significant correlations among the indexes [4].

Serdar and Verep tried to determine the water quality of İyidere and Çiftekavak brooks by using physicochemical parameters and saprobic system. As a result of the evaluation of physicochemical data and biological findings obtained in this study, it was seen that the data of physicochemical and biological water quality showed parallelism [5]. Kıvrak, Uygun and Kalyoncu used diatom indexes to evaluate the water quality of Akarçay (Afyonkarahisar). In the initial part of the river, some taxa such as *Cocconeis placentula, Cyclotella meneghiana, Ulnari ulna, Gomphonema parvulum* become the dominant diatom species in benthic diatom community. In the lower part of the river, *Nitzschia palea* becomes dominant in benthic diatom community. Diatom indexes and physicochemical analysis results have shown that the initial parts of the river are moderately polluted and the end parts of the river are excessively polluted [6].

Szulc did a research on the benthic diatoms of 50 years ago and today's benthic diatoms of Pilica River. This study appeared by comparing a study done in 2005 with the results of previous studies

done by Kadlubowska in 1957. Szulc detected 181 taxa from samples collected for analysis by concentrating on 2 stations in the town Spala of Poland. Water quality classes were determined by carrying out biological analyses by using OMNIDIA software [7].

The general objectives of this research were to study the diatom flora and communities along an rural and urban gradient of Şahnahan river, to evaluate the ecological status and water quality of river using diatoms and to determine in the trophic level of Şahnahan river. The main aims of the present paper were to identify the most important environmental variables regulating patterns in the species composition of epilithic diatoms and to evaluate the use of these algal communities both for monitoring of direct and diffuse human impacts.

MATERIALS AND METHODS

I. Station: This station constituting the clean part of the stream flows within a deep valley and has a high current velocity. Around it, there are a lot of high plants. Especially, poplar trees prevent the stream from receiving lights partly.

II. Station: Since the waste water from the treatment facility of Malatya 2. Organized Industrial Zone is discharged into this station; this station constitutes the dirty part of the stream. The fact that there are a large number of high trees in the II. station prevents the stream from receiving the light; the soil structure consists of partly rocks. Şahnahan Stream, whose color changes due to dirty water and blackens, affects the environment negatively by the odour it gives off.

III. Station: It is established on the entrance of the district Yazıhan. In the II. station, the stream flows in a wide area and has an extremely high current velocity. While around the station there are partly high plants, there are only plains in some regions. It is observed that the color of water is yellowish or brown all the year round due to the effect of dirty water from II. Station (Figure 1).

The water temperature, pH, dissolved oxygen of stream water were measured directly by means of a thermometer and a pH-meter (YSI 63 /cond/temp), respectively. Dissolved oxygen, Ca^{++} Mg^{++} were determined through titration analysis. Spectrophotometric method was employed for the analysis of NH_4, NO_3, NO_2, SO_4 [8].

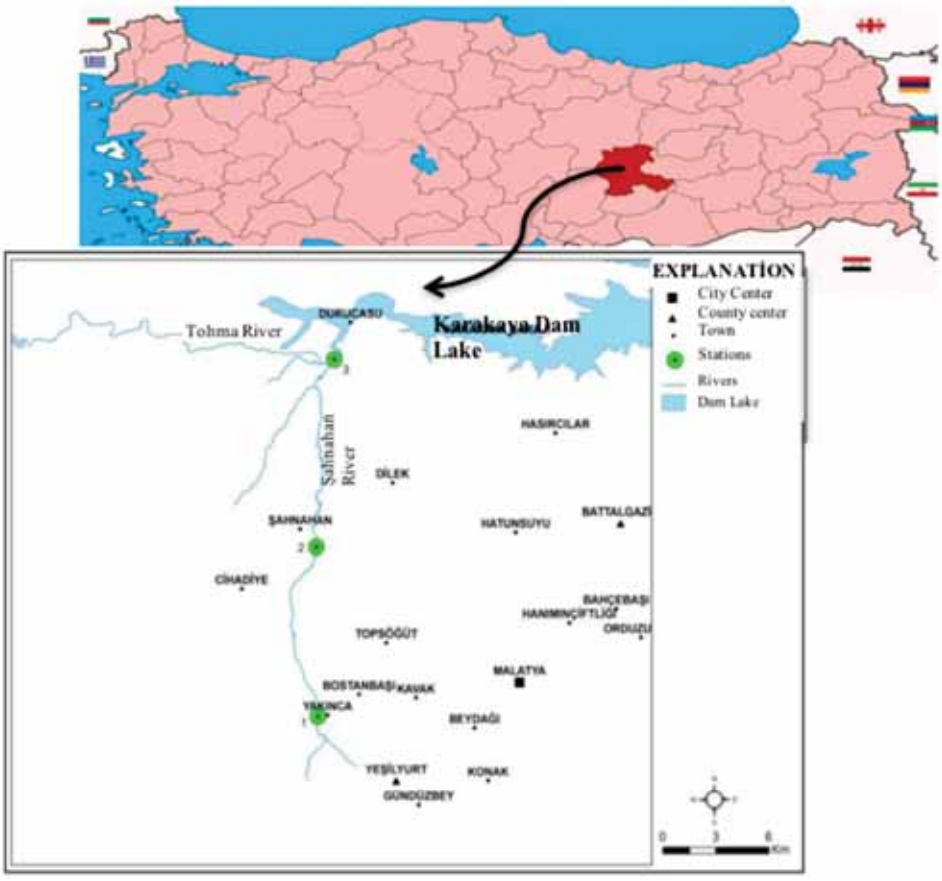


FIGURE 1
The map of Şahnahan Stream and location of sampling stations

TABLE 1
Variations in concentrations of some physical and chemical parameters in Şahnahan Stream

Parameters	Stations		
	I.Station	II.Station	III.Station
Water temperature°C	17,05	17,49	15,12
pH	8,95	8,41	7,83
Dissolved O_2 mg/l	8,3	8,54	8,68
NH_4-N mg/l	5,72	7,65	17,37
NO_3-N mg/l	1,84	15,53	0,69
NO_2-N mg/l	0,02	0,05	0,18
Cl^- mg/l	4,9	531,1	34,12
SO_4 mg/l	20,22	93,5	171
Ca^{++} mg/l	70,35	59,42	79,19
Mg^{++} mg/l	8,44	9,82	12,78

Epilithic algae were sampled on monthly basis in three stations between May 2012 and April 2013. Algae were collected into plastic containers monthly as pooling upper-surface by scraping from several rocks. At least three water-mounted slides were examined for algae and living diatoms from every station to obtain an estimate of algal relative abundance [9, 10].

To prepare permanent diatom slides, organic material of subsamples was digested with nitric/ solphuric acid. Neutralized samples were dried on coverslip, which were mounted on slides with balsam. Two hundred frustule per samples were identified and counted at 1000 X magnification in order to obtain the estimated frequencies of different species of epilithic diatoms. Species were identified according to Kramer and Lange Bertolat [11-14]. Frequency, similarity, relative density, evenness, Shannon Weaver indexes of the epilithic algae and all the biotic indexes (EPI-D, TID, SID, IDP, DI-CH), by using OMNIDIA software, were calculated [15, 16].

RESULTS AND DISCUSSION

As a result of the works done around Şahnahan Stream, the water temperature values showed parallelism with the seasonal temperatures. While the highest water temperature value (26.9°C) was determined in II. station, the lowest water temperature value (7°C) was determined in III. station. The III. station has lower water temperature values due to the fact that it is established over Tohma river, has high flow rate and is supplied with cold sources. However, the water temperature changes in 3 stations are relatively close to each other. While the temperature of the streams is low in coastal regions, the difference in the physical properties of the streams depends on the climatic conditions of the region through which they pass [17]. The dissolved oxygen values showed parallelism with the water temperature values; while highest oxygen value was determined in II. station (10.3 mg/L), the lowest oxygen value was also detected in II. station (7.5 mg/L). pH values differed between the values 7.2 and 9.7 throughout the stream. On the source extensions of the streams, there is high value of dissolved oxygen due to the turbulence and low temperature [18]. While the lowest average pH value was determined in III. station, the values close to 9 were detected in I. station, the average value was determined 8.41 in II. station. These two stations show more basic characteristics than III. station. The most suitable pH range for aquatic organisms is between the values 6.5–8.5 [19]. The nitrate nitrogen values of Şahnahan stream differed between the values 0.03 mg/L and 87.78 mg/L. While the maximum value was determined in II. station in April, the pollution mixture is considered to become high in that month. This thought is supported by the increases in the amount of ammonium nitrogen and chloride in the same month. The rate of nitrate nitrogen increases as a result of organic pollution and mixing of surface water in the streams [18, 20, 21]. The nitrite nitrogen values differed between ALA and 0.27 mg/L. While the lowest value appeared in I. station, the highest value was observed in III. station. The highest average value was determined in III. station (0.18mg/L). While the nitrite is scarce in clean water, it can be in high concentrations in the water in which the organic pollution is present [22-24]. While ammonium nitrogen values differed between ALA and 21.62 mg/L, the maximum value was determined in II. station in April. However, they differed between 16.38 mg/L–18.36 mg/L in III. station and were at extremely high levels. While ammonium nitrogen varies based on pH and temperature, very little ammonium prevails in the oxygen-rich spring water and the water evaluated to be clean in terms of pollution factor [18, 25]. This high level of ammonium nitrogen is extremely high when evaluating in terms of drinking water. It has been reported by some researchers that the fact that ammonium is higher than 0.2-1.5 mg/L in drinking water sources is very harmful to human health. Besides this, the tolerance to ammonium limit was

detected 0.10 mg/L in terms of the fish, and how important a change in this value is to the aquatic environment has been reported by the studies [24, 26, 27, 28]. The chloride values in Şahnahan Stream differed between 2.66 mg/L-1160.22 mg/L. Like high increase in nitrate and ammonium nitrogen, the maximum value was reached in II. station in April and it showed a substantial increase. Entrance of a big pollution into this station in April is in question. The waste water from the organized industry mixes in this station. The change in the color of water in April became at noticeable level. When the stream is under the influence of external factors (rock structure, agricultural pesticides, industrial wastes, etc.) periodically, the chloride amount of the stream becomes extremely high in the affected regions. It has been observed in a study done in Köprüçay River that the fact that the mouth of the river is close to the sea puts the river under the influence of the sea, and increases the amount of chloride [29]. The amount of chloride differs between 30mg/L-300 mg/L in dirty water [30]. The amount of sulphate throughout Şahnahan Stream showed an increase, and the values obtained differed between 18.15 mg/L-654.60 mg/L. The sulphate, in natural water, is effective in cases such as the growing of plants, the biological productivity, the protein metabolism. Therefore, the lack of it both prevents the algae development and inhibits the growing of plants [29]. In dirty polluted water, the sulphate value differs approximately between 100 mg/L-200 mg/L [19]. Similarly, the calcium values differ between 41.58 mg/L-193.73 mg/L. The calcium is an alkali mineral which is very abundant in the seas and freshwater and is biologically the most important element since it forms the skeleton basis of most living creatures [31]. The magnesium values of Şahnahan stream differ between 0.71 mg/L–19.02 mg/L. Magnesium is also crucial since it is an important component of chlorophyl molecule [31]. These two alkali soil minerals are the most abundant elements in freshwater. The chemical functions of both elements resemble each other much in the formation of carbonate salts. Ca^{++} is more abundant in natural water than those two ions (Table 1) [31].

While genus *Navicula* sp. has the most taxon numbers in I. and II. stations within the Bacillariophyta group of the epilithic algae flora, they are *Navicula* sp. and *Nitzschia* sp. in III. station. The dominant organisms are *Cocconeis placentula* var. *lineata* in I. station, *Gomphonema parvulum* in II. station and *Gomphonema olivaceum* in III. station. The most abundant species in I. station are *Ulnari ulna, Gomphonema minitum, Cocconeis placentula* var. *lineata* and *Navicula tripunctata*. The most abundant taxa in II. station are *Cymbella affinis, Ulnaria ulna, Cocconeis placentula* var. *lineata, Gomphonema minitum, Achnanthes lanceolata, Cocconeis placentula* var. *placentula, Cymbella sinuata, Gomphonema parvulum* var. *parvulum, Navicula tripunctata*. The most abundant taxa in III. station are *Ulnaria ulna, Nitzschia amphibia, Cocconeis placentula* var. *lineata, Cymbella affinis, Gomphonema minutum, Diatoma vulgaris, Gomphonema olivaceum* var. *olivaceum, Nitzschia constricta* (Table 4). While *Cymbella affinis* is littoral and is seen in the epilithic or epiphytic fluent and still/standing water, it is commonly found in generally alkali and calcareous environments [32, 33]. This type was encountered frequently in the epilithic flora of II. and III. stations throughout the study. Meanwhile, II. station shows alkali properties due to waste matters coming from outside. The environment and water ground of III. station consist of mostly rocks. This is in harmony with the environmental conditions under which *Cymbella affinis* develops characteristically. *Gomphonema minutum* is common in eutrophic water, is not present in environments weaker than mesosaprobic since it is sensitive to pollution [34]. However, it was detected in this study that it exists in the eupolytrophic stations as well as in eutrophic water. In addition to this, it was also detected in the stations having the characteristics of betamesosaprob and beta alpha mesosaprob in terms of saprobic value. *Gomphonema olivaceum* is a common type and prevalent in oligotrophic water and eutrophic rivers [34]. While Şahnahan Stream varies between eupolytrophic and eutrophic in terms of trophic diatom index, this type was encountered in all the stations even if just a bit. This taxon also spread in the betamesosaprob region in terms of the saprobic index. Kalyoncu stated that when this taxon spread in the alpha beta mesosaprob region and the pollution decreased, it showed an increase in the numbers of cells [35, 36]. The differences were recorded in the numbers of cells of this type encountered in all the stations all the year round. This type was encountered intensively especially in the epilithic algae flora of III. station. *Nitzschia amphibia* has a wide spread area/range. Hassal expressed that this type has a wide spread area from the water containing weak electrolytic (but not dysotroph) to the water containing very strong electrolytic [37]. This type is common in almost every station. This type was encountered frequently especially in the epilithic algae flora of III. station, which is betamesosaprob in terms of saprobic and is eutrophic in terms of trophic diatom index. *Diatoma vulgaris*, which is a common type in littoral regions, is also common in the regions in which the current velocity is low [37]. This type was encountered in all the stations all the year round even if just a bit. Based on the seasonal temperatures, the differences were recorded in the algae types. The temperature increase starting in the spring led to a significant increase in the number of algae types except Bacillariophyta until the end of the summer. Some researchers reported that in spring and summer months, this temperature change affected the development of the algae positively and there was a significant increase in their numbers [33].

When the epilithic types are compared in the stations in terms of diversity, the values close to each other among the stations attract the attention. Shannon Wiener diversity (H′) values were recorded 0.13 in I. station; 0,12 in II. station; 0,09 in III. station. Evenness diversity values were determined 0,6 in I. station; 0,68 in II. station; 0,73 in III. station. Increases and decreases are observed in diversity values, based on the changes in water quality. Nevertheless, however good the water quality is, the stream load affects this diversity. The algae flora may deteriorate or vary against the factors such as current velocity, duration of receiving light, natural disasters, altitude difference. The process of adaptation starts over time and compatible types form the algae flora of the stream [29].

In the determination of water quality carried out based on the average values of physicochemical variables measured during the study; according to Klee, while the stream is included in II.-III. quality class in terms of the value of nitrite nitrogen, it is included in IV. quality class in terms of the values of ammonium nitrogen. The other parameters refer to different quality classes; however, the classification is done in terms of ammonium nitrogen by the Water Quality Control Regulation (WQCR) [38]. Therefore, the water quality level is at IV. quality class level in all the stations. That is, excessive pollution is present. The results obtained from the epilithic flora according to EPI-D refer to I.-II. quality class in I. station, that is to say, to very little polluted part of the stream. According to Klee, based on the average value calculation made, I. station is included in I.-II. quality class and is in harmony with EPI-D epilithic diatom results. IDP referred to III. quality class in the epilithic flora. SID referred to II. quality class in the epilithic flora, that is, to moderately polluted part of the stream. TID index refers to IV. quality class in the whole diatom flora, that is, I. station is eupolytrophic. This is in direct harmony with the WQCR. According to Klee, II. station is III. quality class, that is, alpha mesosaprob in the average value calculation done. According to the WQCR, it is IV. quality class, that is, excessively polluted. EPI-D index, based on the epilithic diatoms, refers to II. quality class and showed deviation on a large scale. DI-CH, based on the epilithic diatoms, refers to III. quality class. IDP index, based on the epilithic diatoms, refers to III. quality class. SID index is beta alpha mesosaprob, based on the epilithic diatoms. TID index, based on the epilithic diatoms, refers to eupolytrophic. According to Klee, III. station is included in II.-III. quality class. According to the WQCR, it is included in IV. quality class. EPI-D index is II. quality class, based on the epilithic diatoms. DI-CH, based on the epilithic diatoms, referred to II. quality class. IDP index referred to III. quality class in all, and showed a half-step deviation towards bad side, according to the classification of Klee. SID index, based on the epilithic diatoms, refers to beta mesosaprob quality class. Based on the epilithic diatoms, the stream is in III.-IV. quality class in TID index (Table 2, Table 3).

TABLE 2
Monthly index values average in terms of the epilithic algae.

MONTHLY INDEX VALUES AVERAGE			
	1 EPL	**2 EPL**	**3 EPL**
EPI-D	1,35	1,46	1,69
DI-CH	4,45	4,24	4,10
SID	2,17	2,23	2,00
TID	2,70	2,80	2,79

TABLE 3
With physicochemical data, the water quality classes of the stations according to KLEE and WQCR

	NO_2-N	**NO_3-N**	**NH_4-N**	**Cl^-**	**DO**
1. STATION	**0,02**	**1,84**	**5,72**	**4,9**	**8,3**
KLEE quality class	**II-III**	**I-II**	**IV**	**I**	**I-II**
WQCR quality class	**III**	**I**	**IV**	**I**	**I**
2. STATION	**0,05**	**15,53**	**7,65**	**531,1**	**8,54**
KLEE quality class	**II-III**	**III-IV**	**IV**	**IV**	**I-II**
WQCR quality class	**III**	**III**	**IV**	**IV**	**I**
3. STATION	**0,18**	**0,69**	**17,37**	**34,12**	**8,68**
KLEE quality class	**III**	**I**	**IV**	**III**	**I-II**
WQCR quality class	**IV**	**I**	**IV**	**I**	**I**

TABLE 4
List of epilithic taxa in Şahnahan stream and monthly relative abundance avarages (%)

EPILITHIC TAXA	Mean relative abundance (%)		
	I. Station	II. Station	III. Station
BACILLARIOPHYTA			
Centrales			
Cyclotella iris Brun & Heribaud Joseph	**37,74**	**0,42**	**7,76**
Cyclotella sp. (Kuetzing) Brebisson	**1,37**	**-**	**1,94**
C. menenghiniana Kuetzing	**-**	**0,29**	**2,23**
Melosira lineata (Dillwyn) C. Agardh	**-**	**-**	**0,40**
Pennales			
Amphora ovalis (Kützing) Kützing	**-**	**0,17**	**0,82**
A. lybica Ehrenberg	**1,37**	**3,90**	**5,21**
A. inariensis Krammer	**2,34**	**-**	**1,59**
A. holsatica Hustedt	**0,22**	**-**	**-**
Achnanthes lanceolata (Brebisson) Grunow	**0,67**	**3,48**	**2,42**
A. minutissima Kuetzing	**1,92**	**-**	**0,66**
A. lanceolata var. viridula	**-**	**2,38**	**-**
Achnanthes sp. Bory De Saint-Vincent	**-**	**2,64**	**-**
Anomoeoneis sphaerophora E. Pfitzer	**-**	**-**	**15,63**
Anomoeoneis sp. E. Pfitzer	**-**	**-**	**0,38**
Aulacoseira rotula	**-**	**-**	**0,10**
Cocconeis placentula var. *lineata (*Ehrenberg) Van Heurck	**25,43**	**7,24**	**6,39**
C. placentula var. *placentula* Ehrenberg	**13,95**	**4,37**	**1,28**
C. placentula var. *euglypta* (Ehrenberg) Grunow	**1,37**	**-**	**0,07**
C. pediculus Ehrenberg	**4,31**	**5,99**	**0,85**
Cymbella affinis Kuetzing	**5,14**	**3,02**	**7,14**
C. sinuata Gregory	**0,97**	**2,43**	**2,81**
C. silesiaca Bleisch	**2,05**	**3,47**	**0,66**
C. minuta Hılse	**5,26**	**15,63**	**2,26**
C. helvetica Kuetzing	**-**	**-**	**1,32**
C. cistula (Ehrenberg) Kırchner	**-**	**-**	**1,49**
*C. caespitosa (*Kuetzing) Brun	**-**	**0,50**	**0,56**
C. amphicephala Naegeli	**-**	**-**	**0,25**
C. amphicephala var. *hercynica* A. Schmidt	**-**	**-**	**0,33**
Caloneis sp. Cleve	**-**	**-**	**0,11**
C. bacillum (Grunow) Cleve	**0,22**	**-**	**0,57**
Caloneis sphaerophora A. Cleve	**-**	**-**	**0,48**
Cymathopleura solea (Brebisson) W. Smith	**-**	**-**	**0,37**
Diatoma vulgaris Bory De Saint Vincent	**2,37**	**0,33**	**8,87**
D. monofiliformis Kuetzing	**5,89**	**-**	**0,83**
Diploneis elliptica (Kuetzing) Cleve	**0,46**	**-**	**0,57**
Ellerbeckia arenaria R. M. Crawford	**-**	**-**	**0,57**
Fragilaria capuccina var. *vaucheria* (Kuetzing) Lange-Bertalot	**-**	**1,22**	**0,56**
F. ulna var. *acus* (Kuetzing) Lange-Bertalot	**0,67**	**-**	**0,92**
F. parasitica var. *parasitica* (W. Smith) Grunow	**-**	**-**	**0,10**
F. tenera (W. Smith) Lange-Bertalot	**-**	**-**	**0,66**
F. pulchella (Ralfs) Lange-Bertalot	**-**	**-**	**1,14**
F. fasciculata (J.G. Agardh) Lange-Bertalot	**-**	**-**	**1,70**
F. crotonensis Kitton	**-**	**-**	**0,4**
F. capuccina var. *rumpens* (Kuetzing) Lange-Bertalot	**-**	**1,52**	**0,07**
F. capuccina var. *capuccina* Desmazieres	**-**	**-**	**0,17**
Frustulia vulgaris (Thwaites) De Toni	**0,22**	**0,17**	**-**
Gomphonema minutum (J.G. Agardh) J.G. Agardh	**6,77**	**24,60**	**4,37**
G. truncatum Ehrenberg	**1,92**	**2,35**	**1,18**
G. parvulum var. *parvulum* (Kuetzing) Kuetzing	**1,32**	**12,02**	**1,47**
G. olivaceum var. *olivaceum* (Hornemann) Brebisson	**0,57**	**16,13**	**8,17**
G. olivaceum var. *salinarum* Pantocsek	**-**	**-**	**3,70**

EPILITHIC TAXA	Mean relative abundance (%)		
	I. Station	II. Station	III. Station
BACILLARIOPHYTA			
Pennales			
G. insigne Gregory	-	-	**3,25**
G. gracile Ehrenberg	-	**2,48**	**1,16**
G. clavatum Ehrenberg	**0,44**	**0,17**	**1,43**
G. angustatum (Kuetzing) Robenhorst	**1,92**	**5,88**	**1,91**
G. affine Kuetzing	-	**0,17**	**11,11**
G. acuminatum Ehrenberg	-	**0,17**	**0,58**
G. tergestinum Fricke	-	**1,61**	-
G. augur Ehrenberg	-	**0,11**	-
G. amoneum Lange- Bertalot	**4**	**0,17**	-
G. angustum J.G. Agardh	**0,46**	-	-
Gyrosigma nodiferum (Grunow) Reimer	**0,34**	-	**1,91**
G. attenuatum (Kuetzing) Robenhorst	-	-	**1,33**
G. acuminatum (Kuetzing) Robenhorst	-	-	**0,17**
Hanitzschia amphyoxus (Ehrenberg) Grunow	**0,68**	**1,61**	**4,68**
Meridon circulare var. *circulare* (Greville) C. Agardh	**4**	**0,33**	**0,57**
Navicula cincta (Ehrenberg) Ralfs	-	-	**0,21**
N. viridula (Kuetzing) Ehrenberg	-	-	**0,70**
N. tuscula (Ehrenberg) Grunow	**2,74**	**0,77**	**11,71**
N. trivialis Lange-Bertalot	**0,22**	**2,96**	**1,15**
N. radiosa Kuetzing	**12,82**	**0,67**	**1,68**
N. pygmaea Kuetzing	-	-	**0,76**
N. pupula Kuetzing	**2,34**	**0,32**	**2,10**
N. porifera Hustedt	-	-	**0,07**
N. phyllepta Kuetzing	**0,68**	-	**0,67**
N. menisculus Schumann	-	-	**0,07**
N. kotschyi Grunow	-	-	**0,29**
N. heimansii Van Damm & Kooyman	-	-	**5,05**
N. exigua Gregory	-	-	**0,07**
N. cuspidata (Kuetzing) Kuetzing	-	**0,11**	**1,02**
N. crytocephala Kuetzing	-	**1,61**	**1,83**
N. similis Krasske	-	-	**0,51**
N. schoenfeldii Hustedt	-	-	**0,25**
N. tripunctata (O. F. Müller) Bory de Saint-Vincent	**19,74**	**10,55**	**1,51**
N. cryptotenella Lange-Bertalot	**0,44**	**0,85**	**0,61**
N. coconeiformis Gregory	-	-	**0,50**
N. clementioides Hustedt	-	-	**0,14**
N. capitatoradiata Germain	-	-	**0,48**
N. angusta Grunow	-	**2,80**	**13,42**
N. veneta Kuetzing	**0,68**	**1,61**	-
N. jaagi Meister	-	**1,85**	-
N. halophila (Grunow) Cleve	-	**9,68**	-
N. decussis Oestrup	-	**1,85**	-
Nitzschia linearis (J.G. Agardh) W. Smith	**4,44**	**5,56**	**1,11**
N. subacicularis Hustedt	-	-	**1,27**
N. scalpelliformis Grunow	-	-	**0,51**
N. commutata Grunow	-	-	**0,51**
N. hungarica Grunow	**0,22**	**0,22**	**3,05**
N. tryblionella Hanitzsch	-	-	**1,94**
N. solita Hustedt	-	-	**0,22**
N. sigma (Kuetzing) W. Smith	-	-	**4,07**
N. recta Hanitzsch	**4,11**	**1,04**	**8,38**
N. palea (Kuetzing) W. Smith	**10,04**	**8,5**	**4,46**
N. nana Grunow	-	-	**6,29**
N. intermedia Hanitzsch	-	**0,42**	**0,35**
N. hanitzschiana Robenhorst	-	-	**0,38**

EPILITHIC TAXA	Mean relative abundance (%)		
	I. Station	II. Station	III. Station
BACILLARIOPHYTA			
Pennales			
N. frustulum (Kuetzing) Grunow	-	-	**0,57**
N. dissipata (Kuetzing) Grunow	**0,68**	**0,17**	**0,96**
N. constricta (Kuetzing) Ralfs	**1,37**	**0,11**	**3,93**
N. capitellata Hustedt	-	**0,32**	**1,96**
N. calida Grunow	-	-	**0,07**
N. amphibioides Hustedt	-	-	**0,10**
N. amphibia Grunow	**0,89**	**2**	**7,83**
N. pellucida Grunow	**0,22**	-	-
Pinnularia microstauron (Ehernberg) Cleve	-	-	**0,57**
Pinnularia gibba Ehrenberg	-	**0,17**	-
P. superdivergentissima Chaumont & Germain	-	-	**0,10**
Surirella minuta Brebisson	**0,22**	-	**0,57**
S. brebissoni Krammer et Lange-Bertalot	-	-	**7,15**
S. angusta Kuetzing	-	**0,11**	**0,21**
Stephanodiscus neoastrea Hakansson & Hickel	-	-	**0,21**
Stephanodiscus agassizensis Hak&Kling	**0,68**	-	-
Ulnaria ulna (Nitzsch) P. Compere	**33,52**	**22,23**	**12,51**

When the indexes are evaluated in terms of our country, it has been recorded by the researchers that the reliability of DI-CH index is higher than the other indexes studies. This subject was researched in a study done in Isparta and Darıören river, and it was detected that DI-CH index showed high reliability for this region [39]. By determining 6 stations in a study done in Ağlasun and Isparta streams, it was tried to detect the water quality based on Klee and Belgian Biotic index. According to the study, while some stations formed organically very little polluted or never polluted part of the stream, some stations formed moderately dirty part of the stream and some of them formed excessively polluted part of the stream, based on the average values of physicochemical parameters [40]. EPI-D, SID, TDI and IDP indexes were used to evaluate the water quality of Akarçay. TDI index values indicated that the stream was polluted by organic matters rich in phosphate. It was repeated that EPI-D index was sensitive to the stream eutrophication and organic pollution. Similarly, according to Rott, the reaction of the types to organic pollution was determined by calculating Saprobic Index (SID). By revealing the effects of eutrophication and organic pollution of the stream using Pampean diatom index (IDP), it was tried to separate these two cases from each other [41]. In this study, by calculating EPI-D, SID, TID, DI-CH and IDP indexes, to what extent the stream was polluted, the eutrophication effects, organic pollution and the reaction of the types to organic pollution were determined (Table 2, Table 3).

In this study, by concentrating on the ecology of the algae, their seasonal changes were examined and the water quality measurements were made. Today, the studies done on the algae has not been limited to the matters such as the algae systematics, the heavy metal pollution, but has been on many features of the algae. Under the influence of global warming emerging to a large extent by the hand of human, our water resources are decreasing day by day. The decrease of water also means the extinction of the algae which are our basic source of oxygen. Therefore, the studies are being done around the world now on the biological monitoring methods and on how to apply those methods. When the studies done on the algae are examined, it attracts the attention that the members of the Bacillariophyta group are more dominant than the other groups in terms of both the number and the diversity. This situation directs the researchers studying the biological monitoring to many fields such as being able to obtain better results while determining the water quality and to inspect the compatibility of the water quality indexes with our country (Turkey) water quality results.

REFERENCES

[1] Dirican, S., Barlas, M. (2005) The Epylithic Diatoms of Dipsiz-Çine (Muğla-Aydın) Streams. Ecology. 14(54), 25-30.

[2] Potapova, M., Desianti, N., Enache, M. (2016) Potential Effects of Sediment Contaminants on Diatom Assemblages in Coastal Lagoons of New Jersey and New York States. Marine Pollution Bulletin. 107(2),453-458 pp.

[3] Gürbüz, H. and Kıvrak, E. (2002) Use of epilithic diyatomes to evaluate water quality in the Karasu River of Turkey. Journal Environmental Biology. 23(3), 239-246.

[4] Solak, C.N. (2011) The Application of Diyatome Indices in theUpper Porsuk River Kütahya –Turkey. Turkish Journal of Fisheries and Aquatic Sciences. 11, 31-36.
[5] Serdar O., Verep B. (2012) İyidere and Çiftekavak Stream of Water Quality Determination of Using Benthic Macroinvertebrates. Annual Conference of the German Limnological Society, Koblenz, Germany.
[6] Kıvrak, E., Uygun, A., Kalyoncu, H. (2012) Application of Diatom Indices to Assess Water Quality of The Akarçay Stream (Afyonkarahisar, Turkey). Afyon Kocatepe University Journal of Science. 12 (2012) 021003, 27-38.
[7] Szulc, B. (2007) Benthic diyatomes of Pilica River 50 years ago and today. Oceanological and Hydrobiological studies. XXXVI (Suplement 1), 221-226.
[8] American Public Association (APHA 1985) Standart Methods for Examination of Water, 16th. edition, Washington, 1268p.
[9] Round, F.E. (1953) An investigation of two benthic algal communities in Malharm Tarn, Yorkshire. Journal Ecology. 41, 97-174.
[10] Sladeckova, A. (1962) Limnological methods for the periphyton (Aufwuchs) comunity. Bot. Rev. 28(2), 286-350.
[11] Krammer, K., Lange-Bertalot, H. (1986) Bacillariophyceae. 1. Teil: Naviculaceae. In: Ettl, H., Gerloff, J., Heynig, H. and Mollenhauer, D. (eds.) Süsswasser flora von Mitteleuropa. Band 2/1. Gustav Fischer Verlag: Stuttgart, New York. 876 pp.
[12] Krammer, K., Lange-Bertalot, H. (1988) Bacillariophyceae. 2. Teil: Bacillariaceae, Epithemiaceae, Surirellaceae. Süsswasserflora von Mitteleuropa, Band 2/2. VEB Gustav Fischer Verlag: Stuttgart, 596 pp.
[13] Krammer, K., Lange-Bertalot, H. (1991) Bacillariophyceae. 3. Teil: Centrales, Fragilariaceae, Eunotiaceae. Süsswasserflora von Mitteleuropa, Band 2/3. Gustav Fischer Verlag: Stuttgart, New York, 576 pp.
[14] Krammer, K., Lange-Bertalot, H. (1991) Bacillariophyceae. 4. Teil: Achnanthaceae, Süsswasserflora von Mitteleuropa. Band 2/4. Gustav Fischer Verlag: Stuttgart, New York, 437 pp.
[15] Lecointe, C., Coste, M. and Prygiel, J. (2003) Omnidia 3.2. Diatom index software including diatom database with taxonomic names, references and codes of 11645 diatom taxa.
[16] Bere, T. (2016) Are diatom-based biotic indices developed in eutrophic, organically enriched waters reliable monitoring metrics in clean waters? Ecol. Indic. 62, 312-316.
[17] Schmitz, W. (1954) Grunlangen der Untersuchung der Temperaturverhaltnisse in den Flie Bgewassern. – Ber. Limnol. Flusstn. Freudenthal. 6, 51-56.
[18] Tanyolaç, J. (2009) Limnology. Hatipoğlu Press, Ankara, 294p.
[19] Höll, K. (1979) Wasser (Untersuchung, Beurteilung, Aufbereitung, Chemie, Bakteriologie, Virologie, Biologie). 6. Auflage, de Gruyter, Berlin.
[20] Karpuzcu, M. (1994) Environmental Pollution and Control. Kubbealtı Neşriyat, 4. Press, İstanbul, 37-39.
[21] Solak, C.N. (2003) Investigation of Physcochemical and epilithic algae in Akçay River (Muğla-Denizli) (Master Thesis). Muğla Üniversity Science Institue, Muğla, Turkey.
[22] Girgin, S., Kazancı, N. (1994) Ankara Çayı'nda Su Kalitesini Belirlemek İçin Taban Büyük Omurgasızların Fiziko-Kimyasal Parametrelerle Birlikte Kullanılması. XII. National Biology Congess Proceeding, Edirne, 235-239.
[23] Egemen, Ö. (2006) Water Quality. Ege University Faculty of Fisheries. Vol:14, 150 pp, Bornova, İzmir.
[24] Taş, B. (2011) Investigation of Water Quality of Lake Gaga. The Black Sea Journal Science. 1(3), 43-46.
[25] Egemen, Ö., Sunlu, U. (1996) Water Quality. Ege University Faculty of Fisheries Vol:14, İzmir.
[26] Ünlü, A., Çoban, F., Tunç, M.S. (2008) Investigation of Lake Hazar Water Quality Accorging to Physical and Inorganic Chemical Parameters. Gazi University Journal of Engineering and Architect. 23(1), 119-127.
[27] Altuner, Z. (1988) A study of the diyatome flora of Aras River, Turkey. Nova Hedwigia. 46, 225-263.
[28] Yıldız, K., Atıcı T. (1996) Ankara River' Diyatomes, Gazi University Journal of Science. 6, 59-87.
[29] Çiçek, L., Ertan, Ö.O. (2012) The Relationship with Some Physicochemical Parameters of Köprüçay River Epilithic Algae Diversity. Journal of Eğirdir Aquaculturel Faculty. 8(1), 22- 41.
[30] Hütter, A.L. (1984) Laborbucher Chemie, Wasser und Wasseruntersuchung. 2., neu bearbeitete und erweiterte Auflage, Berlin, Munchen.
[31] Tanyolaç, J. (2000) Limnology. Hatipoğlu Press, Ankara, 263p.
[32] Adrian, S. (2011) Study of the epilithic diyatome communities from the Cerna River (PhD Thesis), Cluj-Napoca, Romania.
[33] Round, F.E. (1984) The Ecology of Algae, Cambridge University Press Cambridge.
[34] Cox, E.J. (1996) Identification of Freswater Diyatomes from Live Material. Chapman&Hall. First Edition, 158p.
[35] Kalyoncu, H. (2002) Physical, Chemical and Biological Investigation of Aksu River (PhD Thesis). Süleyman Demirel Üniversity, Science Institute, Isparta.

[36] Kalyoncu, H. (1996) A Research on Isparta Stream' Algae (Master Thesis). Süleyman Demirel Üniversity, Science Institute, Isparta. 109p.
[37] Türe, E., Kılçık, F. (2002) Ecological Features of Some Diyatomes in Waters. Education Seminar. 1-50 pp.
[38] Water Quality Control Regulation, (Changed table 1:RG-13/2/2008-26786) 1-50 pp. 56, 9-15.
[39] Kalyoncu, H., Çiçek, N.L., Akköz, C., Yorulmaz, B. (2009) Comparative performance of diyatome indices in aquatic pollution assessment. African Journal of Agricultural Research, 4(10), 1032-1040.
[40] Kalyoncu, H., Zeybek, M. (2008) Benthic Fauna of Ağlasun and Isparta Streams and Determination of Water Quality According to Physicochemical Parameters and Belgium Biotic Index. Biyoloji Bilimleri Araştırma Dergisi. 2(1), 41-48.
[41] Serdar, O., Verep, B. (2012) İyidere and Çiftekavak Stream of Water Quality Determination of Using Benthic Macroinvertebrates. Annual Conference of the German Limnological Society, Koblenz, Germany.

Received: **23.05.2017**
Accepted: **03.10.2017**

CORRESPONDING AUTHOR

Betul Celik
Firat University
Biology Department
Elazig – Turkey

e-mail: betulduzleme@gmail.com

© by PSP Volume 26 – No. 12A/2017 pages 7941-7950 Fresenius Environmental Bulletin

THE ASSESSMENT OF LANDSCAPE FRAGMENTATION IN AN AGRICULTURAL ENVIRONMENT: DEGRADATION OR CONTRIBUTION TO ECOSYSTEM SERVICES?

Derya Gulcin[1,*], K Tuluhan Yilmaz[2]

[1]Department of Landscape Architecture, Faculty of Agriculture, University of Adnan Menderes, 09970, Aydin, Turkey
[2]Department of Landscape Architecture, Faculty of Agriculture, University of Cukurova, 01330, Adana, Turkey

ABSTRACT

Large number of studies on "landscape fragmentation", were conducted in the literature. Most of them focused on habitat loss (species loss), open space loss, and changes in land use/ cover (LULC), and landscape mosaic (landscape pattern/metrics etc.). Fragmentation was one of the most widely used concept amongst these topics that attracts attention due to high urbanization and dramatic changes of the cities. It was emphasized in various articles that fragmentation has adverse impacts on landscape however, it differs in various ways including, quantity of elements, naturalness and ecological values of landscape mosaic. To support this hypothesis, we applied a reference method for measuring fragmentation. In this context, Hedge Network (HN) approach was adopted and applied in lower plain of the ancient Meander River in Aydin Province, Turkey due to its agricultural character. Spontaneous vegetation cover in ditches of irrigated fields are permanent due to the water supply from irrigation system and precipitation in the study area. In this context, hedgerow types along permanent fields were recorded from 15 sampling plots. Thus, this study enabled an enhanced interpretation and biotope/biodiversity based understanding of landscape fragmentation.

KEYWORDS:
Fragmentation, agricultural landscape, hedge network, landscape metrics, ecosystem services

INTRODUCTION

Landscape changes as a result of human impacts (urbanization, agricultural expansion etc.) and natural processes (volcanic eruptions, climatic change, wildfire etc.) affected the spatial pattern of landscapes that need to be analyzed through quantitative methods to identify changes in their ecological functions [1, 2]. Analyzing and assessing these changes were also emphasized within the European Landscape Convention (ELC) to promote the protection, management and planning of European landscapes [3]. Landscape fragmentation is the results of landscape changes. It is used as a leading factor that breaks up a continuous habitat, land use type, biota or ecosystem causing the loss of biodiversity [4, 5, 6]. Fragmentation become a major focus of most habitat and nature conservation studies [7, 8]. Human activities, such as the development of agricultural or urban areas in places once supporting forests or wetlands resulted division of contiguous ecosystems into smaller areas called "patches" in landscape ecology [4, 9, 10, 11]. The main criteria to determine fragmentation of a landscape including number of patches, mean patch size and the total amount of edge was highlighted by Forman and Rutledge [4, 9] . Many research conducted in distinct types of landscapes with a large number of ways depending on the field of interest. The causes and effects of fragmentation change according to the quantity of elements in landscape mosaic, their naturalness and ecological values. For instance, fragmentation of forests due to logging, agricultural activities, road construction or urban sprawl can be harmful to plant species composition and wildlife. In this case, habitat loss which means broad-scale removal of native vegetation or other plant or animal habitats [12] can be seen as a critical threat [13, 14, 15]. Conversely, this fragmentation can improve forest access and park visits [16, 17, 18, 19, 20]. Another example can be given from European cultural landscapes such as, hedgerows cause fragmentation in agricultural land by separating fields and surrounding them. They constitute boundaries, meanwhile contributes to open space network of the territory [21, 22]. Therefore, fragmentation has not only negative effects, but it can also be beneficial in terms of different aspects (ecological, visual, historical, cultural and social). Taylor [23] stated that the rural planner can measure it on the basis of agricultural efficiency, while the bio-scientists measure fragmentation's immediate impact upon local populations of flora and fauna. Land planners determine the cost of reuniting fragmented acreage so that it can be converted to build space, or to other rural activities.

To measure fragmentation, many landscape indices have been presented for different purposes, diversity, contagion, and fractal dimension [24, 25, 26, 27]. Landscape indices are categorized as non-spa-

tial and spatial [28, 9]. When non-spatial indices describe landscape composition incorporating measurements of the number of patch classes or proportions of total area, spatial indices describe patch attributes and include information relevant for measuring fragmentation [9]. Two main purposes of these indices are; (i) provide a tool at a regional level utilizing knowledge of ecosystem processes, (ii) allow us to analyze a wide variety of ecosystem processes regarding management and valuation [29]. These purposes have encouraged the improvement of several landscape indices, analysis and software programs, such as Fragstats, spatial analysis of landscape patches (Patch Analyst), or Landscape Fragmentation Tool (LFT) for ArcGIS which are able to calculate specific parameters in an accessible format [30, 31, 32, 33, 34, 15]. Some of the landscape indices [35, 30, 36, 26, 37, 38, 9, 39, 15, 40, 41], and their major value criteria for the measurement and interpretations are presented as below (Table 1).

Fragmentation in Agricultural Landscapes and Contribution to Ecosystem Services. Agricultural landscapes have a large potential for ecological functions via supporting urban green infrastructure and creating valuable habitats for animal species besides providing food. Additionally, they provide recreational and aesthetic values in terms of ecosystem services [42, 43]. From an ecological-based approach, ecosystem services describe interactions of organisms and the environment at different scales. Understanding of these services are associated with identifying their functions in ecology that can be often characterized by species or populations, habitat types and their functional roles. The determination of landscape structure, assessment of environmental factors and measurement of ecosystem service providers within an appropriate scale are the steps for managing ecosystem services. Additionally, it is important to monitor environmental changes particularly impacts of urbanization on rural landscape as well as arable lands [44, 45].

It is emphasized that the sustainable development of rural landscapes requires a multi-dimensional management approach covering both socio-economic development, and environmental protection. Preventing agricultural landscape degradation needs to maintain heterogeneity of spatial structure, habitat and biological diversity with particular reference to plant diversity. Agricultural landscapes, in most cases, contain a network of ecological corridors, including field boundaries and margins, hedgerows and woodlots as crucial habitats [46].

Many agricultural landscapes are a mixed of existent vegetation patches that are references to elaborate fragmentation studies [47, 27, 34]. Although some studies claim that fragmentation of agricultural land affects both the capacity of agricultural production its visual quality [48] in some cases spontaneous vegetation occurred along hedgerows, surrounding crop fields, may contribute to plant species diversity and habitats for animal species.

Jaskulski and Jaskulska, [46] presented a detailed review on plant diversity in agricultural landscapes. It was reported that diverse flora and fauna in arable fields are closely related to habitat diversity incorporating hedgerows which are a key ecological element in Western Europe [49]. It is also stated that linear woodlots, mostly made up by woody vegetation, are present in England, Central and Eastern Europe, North America as well as on other continents [50, 51, 52, 53, 54, 55]. Planted and natural woody species showed higher diversity and richness along the hedgerows in Canada. In spontaneously occurred hedgerows 31 woody, and 94 herbaceous plant species were identified while in Poland, 77 woody plant species were found in woodlots [49, 49, 56]. Czarnecka [57] identified 67 plant species along 4 field boundaries within a total length of 1000 m [43].

TABLE 1
Major value criteria for landscape fragmentation, their interpretation and sample indices

Major value criteria	Interpretation examples	Examples of indices
Composition	Habitat change degree Farmland heterogeneity Landscape transition/change Potential for ecological restoration	Landscape fragmentation indices (Number of patches, percentage of landscape, largest patch index), Edge density, Patch Density (PD), Mean Patch Size (MPS), Splitting index (S), Degree of landscape division (D), Effective mesh size (m), Core area index (CAI)
Shape	Landscape scenarios, LULC change, transboundary movements, Plant establishment and growth	Shape index (SI), Shape complexity index, Fractal dimension, Square pixel
Configuration	Isolation degree Connectivity level	Proximity index, Buffer index, Connectivity
Diversity	Species richness Potentials for nature restoration	Shannon diversity index, Shape diversity, Simpson's diversity index (D)

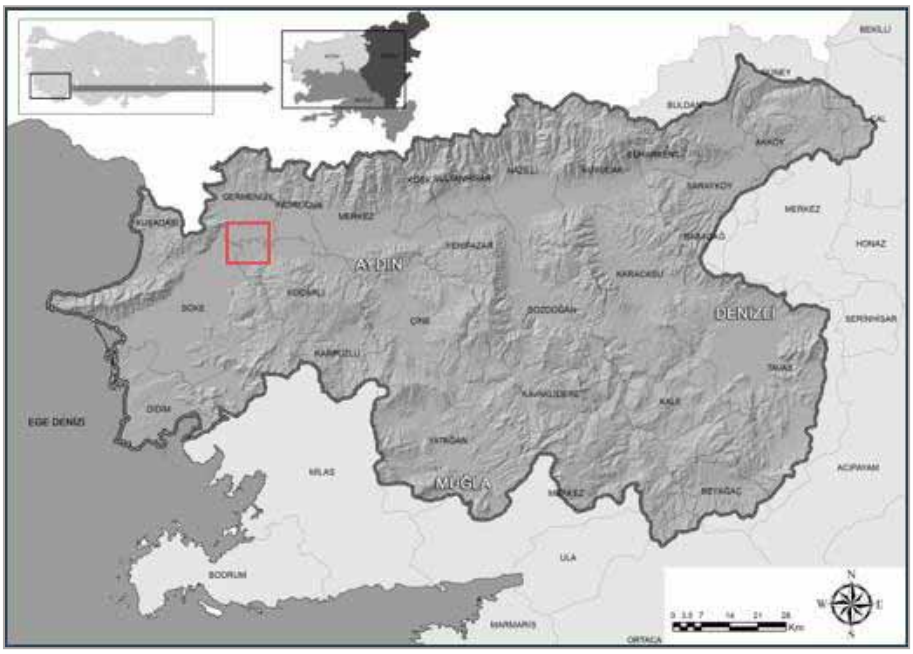


FIGURE 1
Geographical location of the study area

Agricultural practices such as tillage, grazing, irrigation systems, manuring, mulching etc. have a strong impact on weed density and distribution [58]. Wild flora in cultivated fields in which intensive agricultural practices are carried out, is poor in species richness as a result of periodic herbicide treatments and ploughing. In organic agriculture, use of ecological production systems by green fertilization, biological control, organic waste, rotation and mineral additives supports weed colonization in crop fields [59]. Aytok et al. [60] reported that use of manure in dune fields for watermelon cropping, encourages weed colonization through transport of weed seeds. However, repeated use of chemical fertilizers prevents possible weed colonization that would be triggered by introduction of manure into the soil. It is a fact that species richness of weed flora increases in abandoned fields during post-cultivation succession. Celik et al. [61] determined weed species composition within the derelict land in Cukurova Plain located in southern Turkey. The results showed important changes on species richness of weed communities in a succession of over a decade. Within a ten year period between 1998 and 2008 number of weed species reached 34 while only 14 species were recorded in the initial survey in the abandoned field. One of the main drivers of rapid colonization of weed flora in abandoned fields is seed transport from species-rich communities maintained by hedgerows, located along field margins. Lind et al. [62] stated that organically managed orchards present a rich combination of habitats such as hedges which enhancing the ecological balance by means of providing a refuge for rare species, as well as for natural enemies of pests, and pollinators.

Study Area. The study area is located in Aydin Province, the southwestern part of Turkey. The central and western parts of the province are fertile plains irrigated by the largest river (Great Meander) in the Aegean region, and surrounded by the Aydın Mountains to the north and the Menteşe Mountains to the south (Figure 1). The western end of the province is the Aegean coast with extensive salt marshes located around the river estuary, and the Lake Bafa a major feature of the Menderes delta area.

Approximately 363,200 hectares out of 800.700 hectares (total cover of the province) arable land are cultivated in the plain of Aydin while main crops are maize, cotton, wheat, chestnut, olive and fig**.** Agriculture become more significant recently as a result of increasing trend of exported products. According to the Environmental Status Report of the province, fig, olive and chestnut hold the first place in the country's fruit production. Cotton, is ranked as the second mostly cultivated crop among all cities in Turkey.

Eşbah et al. [63] stated that agricultural landscapes are discreet mosaic of different types of patches and corridors, therefore to achieve and maintain connectivity it is necessary to evaluate the composition and configuration of these elements. In this composition, hedges created by spontaneous vegetation has an important role on landscape ecology that needs to be assessed to determine landscape frag-

mentation. Within this context, we selected ten sample quadrats that have different size and number of patches respectively in Aydin Province.

MATERIALS AND METHODS

High quality digital maps with a resolution of 0.5 m x 0.5 m were obtained as a mosaic data set from GIS office of the Republic of Turkey Ministry of Environment and Urbanization. There is still a gap exists when relevant literature is reviewed about fragmentation approaches. To clarify this, we focused on the species richness of spontaneous vegetation in the scope of bio-diversity and biotope context, and to describe the fragmentation pattern, a reference method by Gulinck and Wagendorp [27] was applied.

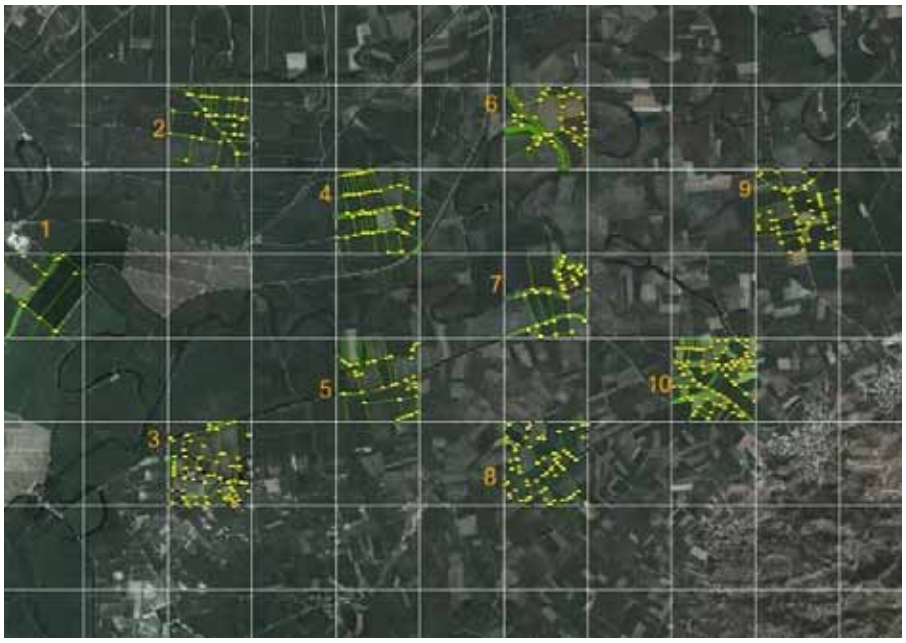


FIGURE 2
Ten sample quadrats located on Great Meander Plain

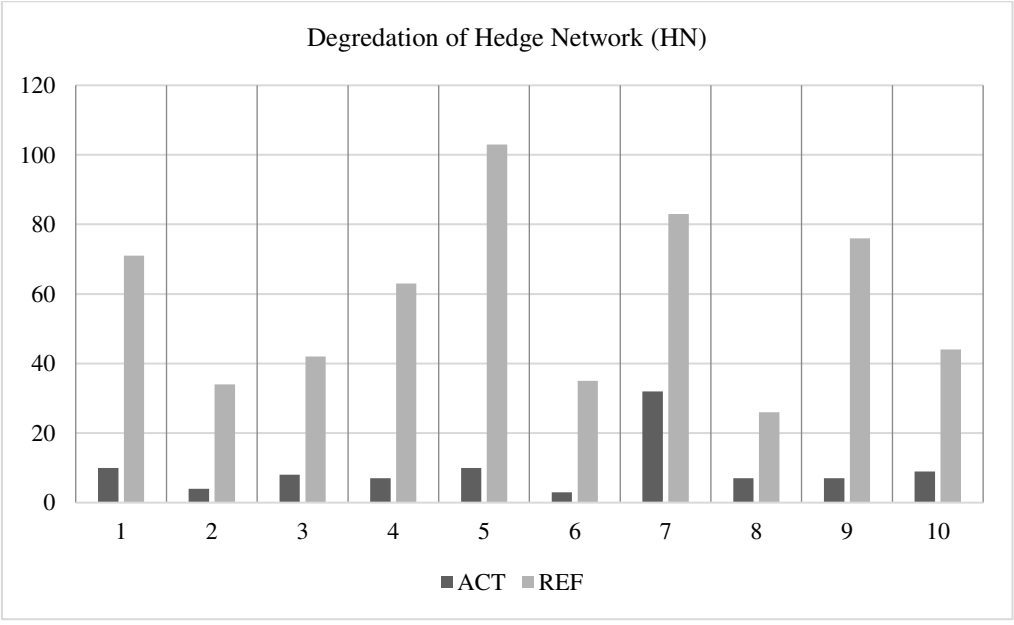


FIGURE 3
The values of ACT and REF representing degradation of HN

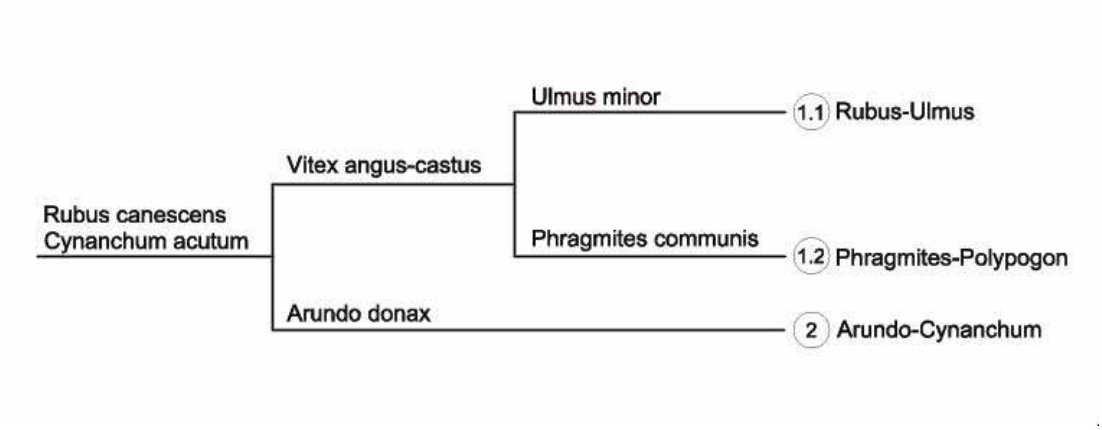


FIGURE 4
Twinspan groups of three distinct plant communities with their dominant and characteristic species

TABLE 2
The fragmentation metrics of ten sample quadrats

Sample Number (1km x1 km)	Number of patches	Actual number of nodes	Reference number of nodes	Minimum patch size (ha)	Maximum patch size (ha)	Total actual patch size (ha)	Total length of hedgerows (km)
1	38	10	71	0,026	10,63	2,55	5,2
2	28	4	34	0,075	14,58	7,31	9,0
3	28	8	42	0,132	14,66	11,23	8,8
4	34	7	63	0,067	24,19	1,62	4,4
5	68	10	103	0,021	13,83	3,37	10,2
6	29	3	35	0,959	11,20	2,60	7,9
7	52	32	83	0,007	12,83	4,23	13,7
8	21	7	26	0,104	18,63	1,66	3,9
9	55	7	76	0,015	7,12	2,03	4,0
10	32	9	44	0,055	10,14	5,50	5,4

In Figure 3, ten sample agricultural fields located on the plain (1 km x 1 km) are presented (Figure 2) using ArcMap 10.3. The approximate number of patches, actual (ACT)/reference (REF) number of nodes, minimum/maximum/actual patch sizes and the total length of hedgerows were calculated. Comparing ACT and REF values provides the degradation level of HN (Figure 4).

RESULTS AND DISCUSSION

Data Evaluations on Landscape Metrics. The table illustrates the fragmentation metrics of ten sample quadrats in the plain. The number of patches differ between 21 and 68. Sample 5 has the highest number of the patch among all sample quadrats. Although Sample 8 has the lowest number of patch, its actual number of node reached the peak. Overall, sample 3 has the largest actual patch size with approximately 11, 2 hectares. Total length of hedgerows change between 3, 9 and 13, 7 kilometers (Table 2).

The bar chart compares the values of ACT and REF representing degradation of HN for ten different sample quadrats (1km x 1km) located on Great Meander Plain (Figure 3). It is noticeable that ACT values are below number 11 except the seventh quadrat which has the highest number of ACT value. As for the REF value, the fifth quadrat has the highest number while the eighth quadrat has the lowest number.

Data Evaluations on Plant Cover of Hedgerow Network. A total of 26 vascular plant taxa were recorded from 15 sampling plots representing unique hedgerow types, during the field surveys. Those comprise 11 woody perennials and 15 herbaceous taxa. During the surveys only tall weeds were taken into consideration while ground covering annuals that are characteristic species of roadside communities were neglected. List of recorded taxa and their presence/abundance/coverage values were shown on the Table 3. Figure 4 shows Twinspan groups of three distinct plant communities with their dominant and characteristic species.

TABLE 3
List of recorded taxa and their presence/abundance/coverage values

Quadrat number	1	2	3	4	5	6	7	8	9	10	11	12	13	14	15
Number of Plant taxa	20	13	16	13	6	1	3	2	10	11	4	6	6	6	6
Olea europaea var. sylvestris	1		1												
Ulmus minor	3	3	3	3	3										
Prunus cf divaricata	2		2		2										
Punica granatum	R														
Ficus carica	R														
Pistacia terebinthus	R				R										
Asparagus acutifolius	R		R		R										
Glycyrrhiza glabra	+	+	+	+	+										
Sonchus asper	+	+	+	+	+										
Malva sylvestris	+	+	+	+	+										
Silybum marianum	+	+	+	+	+	+	+	+	+	+					
Rumex pulcher	+	+	+	+	+	+	1	+	1	+					
Foeniculum vulgare	+	+	+	+	+	+	+	+	+	+		+	+	+	+
Conyza canadensis	1	1	1	1	1	+	+	+	+	+	+				
Cynanchum acutum	1	1	1	1	1	1	+	+	+	+	+	3	3	2	3
Piptatherum miliaceum	2	2	2	2	2		+	+							
Daucus carota	1	1	1	1	1	+	+	+	+	+		+	+	+	+
Rubus canescens	4	4	4	4	4	+	+	+	+	+	+	+	+	+	+
Vitex agnus-castus	2	2	2	2	2		+	+		+					
Phragmites communis	+					4	4	4	4	4					
Polypogon monspeliensis						+	+	+	+	+					
Verbascum sp.						1	1	1	1	1					
Morus alba						1									
Salix alba							1								
Arundo donax											4	4	4	4	4
Rumex conglomeratus												+	+	+	+

R: Rare / **+**: Abundant / **Coverage 1**: <25 / **2**: 25-50 / **3**: 51-75 / 4: 75<

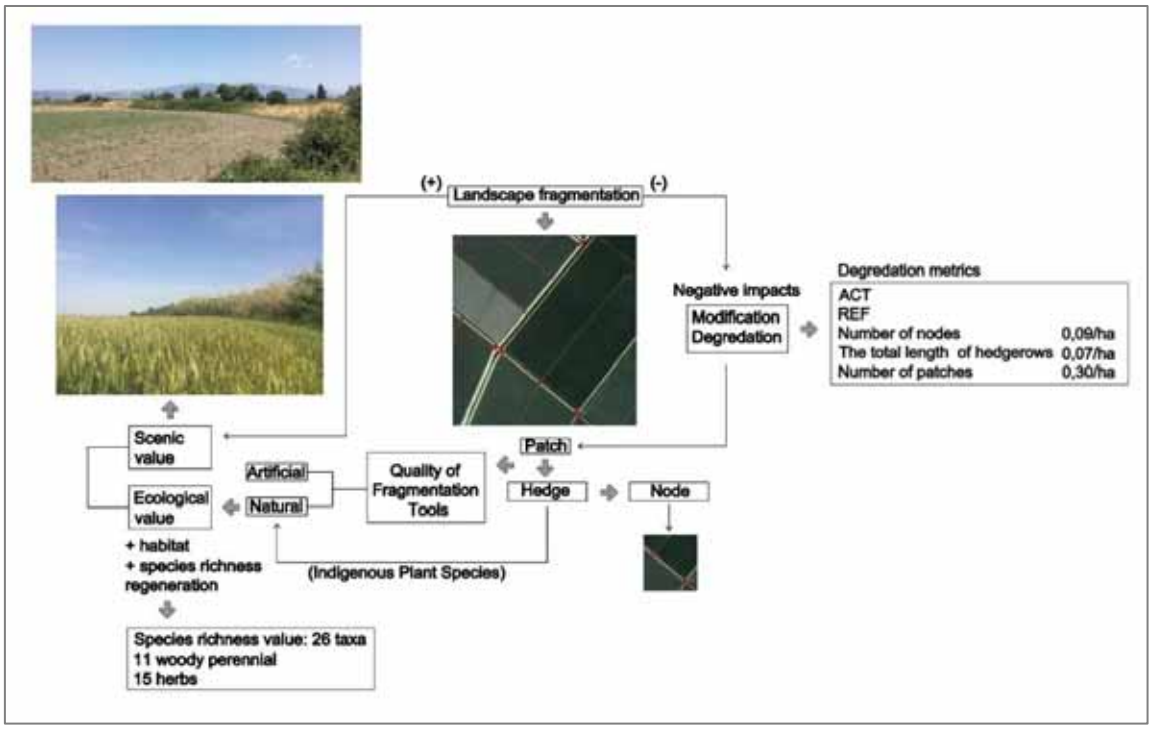


FIGURE 5
Characterization of fragmentation pattern of hedgerow network and assessment of its contribution to ecosystem services in the study area

CONCLUSIONS

Landscape fragmentation has both positive and negative impacts on agricultural fields. As for the negative impacts, it may cause modification and degradation by dividing the fields. On the other hand, this division comprises patches and surrounded by usually rows of trees, shrubs or spontaneous vegetation cover defined as hedgerow. In the intersection of hedgerows, there are nodes. Hedgerows serve suitable habitats for indigenous plant species as a contribution of fragmentation elements to the agro-ecosystem. Figure 5 shows characterization of fragmentation pattern of hedgerow network and assessment of its contribution to ecosystem services in the study area. Degradation of HN is represented by the degradation metrics. The number of nodes, hedgerows and patches per hectare was calculated to show the level of degradation. Degradation indicator of other facts are ACT and REF. Overall, there is a striking difference between their values.

The function of hedgerows differs according to the quality of fragmentation elements as artificial and natural. Burel [22] indicated that hedgerow networks provide high degree of connection, ameliorate or interrupt many fluctuations in the landscape due to their rectilinear shape. They have a role in corridor of movement and being scattered for many forest species, such as small mammals, carabids, and plants [22]. As negative impacts, the modification and degradation builds up patches, however this kind of fragmentation is one of the basic character of crop fields.

The Great Meander River basin as one of the 26 basins of Turkey is remarkably important in terms of water resources and ecological, historical and geographical/physical characteristics. This pilot study, combining two methods (landscape metrics and vegetation analysis) can be used as reference guideline for landscape fragmentation studies in agricultural environment. Applying presented methodology, agricultural landscapes can be ranked according to their capacity to support a certain range of bio-diversity, and to create wildlife habitats as a unique ecosystem service. For this aim landscape metrics such as number and size of patches, hedgerows, and biological indicators as species richness and diversity of vascular plants can be incorporated into the assessment of landscape fragmentation. Additionally, planners who interested in landscape ecology may gain insights into landscape fragmentation in a holistic manner. Regarding landscape fragmentation, there are various approaches taken into consideration. Therefore, planners and managers are usually confronted with the complexity of these approaches and methods that applied. Leitão et al. [64] stated that when significant relationships between structural landscape features and ecological functions are established, landscape metrics-based approaches can constitute useful tools for planning. Incorporating our ecological approach into the landscape-metrics based approaches contributes to a better understanding and evaluation of green infrastructure formed by crop fields in agricultural environment.

REFERENCES

[1] Turner, M.G. (1989) Landscape ecology: the effect of pattern on process. Ann Rev Ecol Syst. 20, 171–197.
[2] Lindenmayer, D.B., Fischer, J. (2006) Habitat fragmentation and landscape change: an ecological and conservation synthesis. Island Press.
[3] Council of Europe (2000) European Landscape Convention. Florence.
[4] Forman, R. (1995) Land mosaics, The Ecology of Landscapes and Regions. Cambridge University Press, Cambridge, p. 632.
[5] Fahrig, L. (2003) Effects of habitat fragmentation on biodiversity. Ann. Rev. Ecol. Evol. Syst. 34, 487–515.
[6] Carvalho, F.M.V., De Marco P. Jr., Ferreira, L.G. (2009) The Cerrado into-pieces: habitat fragmentation as a function of landscape use in the savannas of central Brazil. Biological Conservation. 142, 1392–1403.
[7] McGarigal, K. and Cushman, S.A. (2002) Comparative evaluation of experimental approaches to the study of fragmentation studies. Ecological Applications. 12, 335–345
[8] Hobbs, R.J., Yates, C.J. (2003) Turner Review No. 7. Impacts of ecosystem fragmentation on plant populations: generalising the idiosyncratic. Australian Journal of Botany. 51(5), 471-488.
[9] Rutledge, D.T. (2003) Landscape indices as measures of the effects of fragmentation: can pattern reflect process? Wellington: Department of Conservation.
[10] La Greca, P., La Rosa, D., Martinico, F., Privitera, R. (2011) Agricultural and green infrastructures: The role of non-urbanised areas for eco-sustainable planning in a metropolitan region. Environmental Pollution. 159(8), 2193-2202.
[11] Mhlanga, L., Nyikahadzoi, K., Haller, T. (Eds.) (2013) Fragmentation of Natural Resources Management: Experiences from Lake Kariba (Vol. 2). LIT Verlag Münster.
[12] Sivertsen, D.P. (1995) Habitat loss – its nature and effects (including case studies from New South Wales). In: Bradstock R.A., Auld T.D., Keith D.A., Kingsford R.T., Lunney D. and Sivertsen D.P. (eds.) Conserving Biodiversity: Threats and Solutions. Surrey Beatty & Sons, Chipping Norton, 29–42.

[13] Plieninger, T. (2006) Habitat loss, Fragmentation, and Alteration–Quantifying the Impact of Land-use Changes on a Spanish Dehesa Landscape by Use of Aerial Photography and GIS. Landscape Ecology. 21(1), 91-105.
[14] Mendoza, E., Fay, J., Dirzo, R. (2005) A quantitative analysis of forest fragmentation in Los Tuxtlas, southeast Mexico: patterns and implications for conservation. Revista Chilena de Historia Natural. 78, 451-467.
[15] Liu, S., Dong, Y., Deng, L., Liu, Q., Zhao, H., Dong, S. (2014) Forest fragmentation and landscape connectivity change associated with road network extension and city expansion: a case study in the Lancang River Valley. Ecological Indicators. 36, 160-168.
[16] Trombulak, S.C., Frissell, C.A. (2000) Review of ecological effects of roads on terrestrial and aquatic communities. Conserv. Biol. 14, 18–30
[17] Fu, W., Liu, S., Degloria, S.D., Dong, S., Beazley, R. (2010) Characterizing the "fragmentation-barrier" effect of road networks on landscape connectivity: a case study in Xishuangbanna, Southwest China. Landscape and Urban Planning. 95, 122–129.
[18] Edwards, D.P., Tobias, J.A., Sheil, D., Meijaard, E., Laurance, W.F. (2014) Maintaining ecosystem function and services in logged tropical forests. Trends in ecology & evolution. 29(9), 511-520.
[19] Pütz, S., Groeneveld, J., Henle, K., Knogge, C., Martensen, A.C., Metz, M., Metzger, J.P.W., Riberio, M.C., Paula, M.D., Huth, A. (2014) Long-term carbon loss in fragmented Neotropical forests. Nature Communications, 5, 5037.
[20] Mitchell, M.G., Suarez-Castro, A.F., Martinez-Harms, M., Maron, M., McAlpine, C., Gaston, K.J., Johansen, K. Rhodes, J.R. (2015) Reframing landscape fragmentation's effects on ecosystem services. Trends in Ecology & Evolution. 30, 190–198.
[21] Forman, R.T., Baudry, J. (1984) Hedgerows and hedgerow networks in landscape ecology. Environmental management. 8(6), 495-510.
[22] Burel, F. (1996) Hedgerows and their role in agricultural landscapes. Critical reviews in plant sciences, 15(2), 169-190.
[23] Taylor, P.D. (2002) Fragmentation and cultural landscapes: tightening the relationship between human beings and the environment. Landscape and Urban Planning. 58(2), 93-99.
[24] Turner, M.G. (1989) Landscape ecology: the effect of pattern on process. Annual review of ecology and systematics. 20(1), 171-197.
[25] Hulshoff, R.M. (1995) Landscape indices describing a Dutch landscape. Landscape ecology. 10(2), 101-111.
[26] Jaeger, J.A. (2000) Landscape division, splitting index, and effective mesh size: new measures of landscape fragmentation. Landscape ecology. 15(2), 115-130.
[27] Gulinck, H., Wagendorp, T. (2002) References for fragmentation analysis of the rural matrix in cultural landscapes. Landscape and Urban Planning. 58(2–4), 137–146.
[28] Gustafson, E.J. (1998) Quantifying landscape spatial pattern: what is the state of the art? Ecosystems. 1(2), 143-156.
[29] Geoghegan, J., Wainger, L.A., Bockstael, N.E. (1997) Spatial landscape indices in a hedonic framework: an ecological economics analysis using GIS. Ecological economics. 23(3), 251-264.
[30] McGarigal, K., Marks, B.J. (1995) Spatial pattern analysis program for quantifying landscape structure. Gen. Tech. Rep. PNW-GTR-351. US Department of Agriculture, Forest Service, Pacific Northwest Research Station.
[31] Elkie, P., Rempel, R., Carr, A. (1999) Patch analyst user's manual. Ont. Min. Natur. Resour. Northwest Sci. & Technol. Thunder Bay, Ont. TM–002, 16.
[32] Vogt, P., Riitters, K.H., Estreguil, C., Kozak, J., Wade, T.G., Wickham, J.D. (2007) Mapping spatial patterns with morphological image processing. Landscape ecology, 22(2), 171-177.
[33] Riiters, K.H., Wickham, J.D., Wade, T.G. (2009) An indicator of forest dynamics using a shifting landscape mosaic. Ecol. Indicators. 9, 107–117.
[34] Llausàs, A., Nogué, J. (2012) Indicators of landscape fragmentation: the case for combining ecological indices and the perceptive approach. Ecological Indicators. 15(1), 85-91.
[35] Krummel, J.R., Gardner, R.H., Sugihara, G., O'neill, R.V., Coleman, P.R. (1987) Landscape patterns in a disturbed environment. Oikos. 48(3), 321-324.
[36] Frohn, R.C. (1998) Remote sensing for landscape ecology: new metric indicators for monitoring, modeling, and assessment of ecosystems. Lewis Publishers, Boca Raton, Florida. 99p.
[37] Gulinck, H., Múgica, M., de Lucio, J.V., Atauri, J.A. (2001) A framework for comparative landscape analysis and evaluation based on land cover data, with an application in the Madrid region (Spain). Landscape and urban planning. 55(4), 257-270.
[38] Leitão, A.B., Ahern, J. (2002) Applying landscape ecological concepts and metrics in sustainable landscape planning. Landscape and urban planning. 59(2), 65-93.

[39] Shoyama, K., Braimoh, A.K. (2011) Analyzing about sixty years of land-cover change and associated landscape fragmentation in Shiretoko Peninsula, Northern Japan. Landscape and Urban Planning. 101(1), 22–29.
[40] Weissteiner, C.J., García-Feced, C., Paracchini, M.L. (2016) A new view on EU agricultural landscapes: Quantifying patchiness to assess farmland heterogeneity. Ecological Indicators. 61, 317-327.
[41] Wei, W., Shi, P., Zhou, J., Li, C., Xie, B. (2017) Analysis of Urban Expansion and Landscape Patterns in Arid Inland: A Case Study of Liangzhou District in Northwest China. Fresen. Environ. Bull. 26(6), 3880-3885.
[42] Dramstad, W.E., Fry, G., Fjellstad, W.J., Skar, B., Helliksen, W., Sollund, M.L.B., Tveit, M.S., Geelmuyden, A.K., Framstad, E. (2001) Integrating landscape based values- Norwegian monitoring of agricultural landscapes. Landscape and Urban Planning. 57(3), 257–268.
[43] Junge, X., Schüpbach, B., Walter, T., Schmid, B., Lindemann-Matthies, P. (2015) Aesthetic quality of agricultural landscape elements in different seasonal stages in Switzerland. Landscape and Urban Planning. 133, 67-77.
[44] Gokyer, E. (2014) Monitoring landscape change and urban growth of Bartin, Turkey, and its environmental effects. Fresen. Environ. Bull. 23(10), 2407-2414.
[45] Say, N., Ozyurt Okten, S., Aysu, A., Yalcinkaya, N.M. (2017) Transformation of Land Use /Land cover (LULC) Under Rapid Urbanization in Adana, Turkey. Fresen. Environ. Bull. 26(5), 3479-3485.
[46] Jaskulski D., Jaskulska I. (2012) Plant diversity in agroecosystems and agricultural landscapes. Gbolagade A.L. (ed.). Environmental Sciences. Biodiversity Conservation and Utilization in a Diverse World. Chapter 1, ISBN 978-953-51-0719-4, 10.5772/47729.
[47] Meeus, J.H.A., Wijermans, M.P., Vroom, M.J. (1990) Agricultural landscapes in Europe and their transformation. Landsc. Urban Plan. 18, 289–352.
[48] Brabec, E., Smith, C. (2002) Agricultural land fragmentation: the spatial effects of three land protection strategies in the eastern United States. Landscape and Urban Planning. 58(2), 255-268.
[49] Boutin, C., Jobin, B., Bélanger, L. (2003) Importance of riparian habitats to flora conservation in farming landscapes of southern Québec, Canada. Agriculture, ecosystems & environment. 94(1), 73-87.
[50] Baudry, J., Bunce, R.G.H., Burel, F. (2000) Hedgerows: an international perspective on their origin, function and management. Journal of environmental management. 60(1), 7-22.
[51] Ryszkowski, L., Karg, J., Bernacki, Z. (2003) Biocenotic function of the mid-field woodlots in West Poland: study area and research assumptions. Polish Journal of Ecology. 51(3), 269-281.
[52] Lazarev, M.M. (2006) Transformation of the annual water budget of soils under shelterbelts. Eurasian Soil Science. 39(12), 1318-1322.
[53] Brandle J.R., Hodges L., Zhou X.H. (2004) Windbreaks in North American agricultural systems. In: Nair P.K.R., Rao M.R., Buck L.E. (eds.) New Vistas in Agroforestry. Advances in Agroforestry, vol 1. Springer, Dordrecht. ISBN 978-90-481-6673-2, 65-78.
[54] Onyewotu, L.O.Z., Stigter, C.J., Oladipo, E.O., Owonubi, J.J. (2004) Air movement and its consequences around a multiple shelterbelt system under advective conditions in semi-arid northern Nigeria. Theoretical and applied climatology. 79(3-4), 255-262.
[55] Tsitsilas, A., Stuckey, S., Hoffmann, A.A., Weeks, A.R., Thomson, L.J. (2006) Shelterbelts in agricultural landscapes suppress invertebrate pests. Animal Production Science. 46(10), 1379-1388.
[56] Orłowski, G., Nowak, L. (2005) Species composition of woody vegetation of three types of mid-field woodlots in intensively managed farmland (Wrocław Plain, south-western Poland). Pol. J. Ecol. 53(1), 25-36.
[57] Czarnecka J. (2011) Baulks of Western Wolhynia as the habitats of rare calciphilous plant species. Water-Environment-Rural Area 11, 2(34), 43–52. (in Polish)
[58] Karkanis, A., Bilalis, D., Efthimiadou, A., Efthimiadis, P. (2010) Effects of cultural practices on weed flora in Virginia (flue-cured) organic tobacco (Nicotiana tabacum L.): green manure and irrigation systems. Turkish Journal of Agriculture and Forestry. 34(6), 487-496.
[59] Bulut, S., Öztürk, A., Karaoğlu, M.M., Yildiz, N. (2013) Effects of organic manures and non-chemical weed control on wheat. II. Grain quality. Turkish Journal of Agriculture and Forestry. 37(3), 271-280.
[60] Aytok, O., Yilmaz, K.T., Ortaş, I., Cakan, H. (2013) Changes in mycorrhizal spore and root colonization of coastal dune vegetation of the Seyhan Delta in the postcultivation phase. Turkish Journal of Agriculture and Forestry. 37(1), 52-61.
[61] Celik, I., Yilmaz, K.T., Eswaran, H., Mermut, A., Dingil, M., Kaya, Z., Demirbaş, A., Aksit, I., Ortaş, I., Gök, M., Akpınar, C., Nagano, T., Ae, N., Koca, Y.K., Kapur, S. (2010) Reconstructing the Past by Regenerating Biodiversity: A Treatise on Weed Contribution to Soil Quality at a Post-cultivation Succession. In Sustainable Land Management. Springer Berlin Heidelberg, 363-378.

[62] Lind K., Lafer, G., Schloffer, K., Innerhofer, G and Meister, H. (2003) Organic Fruit Growing. Lind, K. (Ed.) CAB international, CABI Publishing, ISBN: 0 85199 640X, Chapter 2, p.31.
[63] Esbah, H., Cook, E.A., Hepcan, S., Kara, B., Deniz, B. (2012) Ecological networks: potential of agricultural landscapes. Proceedings of the 1st GreenNet Conference, 31st of January 2012, Erfurt, 80-86.
[64] Leitão, A.B., Miller, J., Ahern, J., McGarigal, K. (2012) Measuring landscapes: A planner's handbook. Island Press. Washington DC.

Received: **26.05.2017**
Accepted: **13.10.2017**

CORRESPONDING AUTHOR

Derya Gulcin
Department of Landscape Architecture,
Faculty of Agriculture,
University of Adnan Menderes,
09970, Aydin – Turkey

e-mail: derya.yazgi@adu.edu.tr

© by PSP Volume 26 – No. 12A/2017 pages 7951-7956 Fresenius Environmental Bulletin

APPROXIMATION MODEL FOR CARBON DIOXIDE INCREASING LEVEL AND IMPACT OF VENTILATION SYSTEM IN A UNIVERSITY CLASSROOM

Wannawit Taemthong*

King Mongkut's University of Technology North Bangkok, Faculty of Engineering, Bangkok, Thailand

ABSTRACT

One aspect of indoor air quality in green buildings concerns carbon dioxide levels. This paper presents different situations connected to estimating carbon dioxide levels based on experimental research. The research project was undertaken in a university classroom of 64 square meters. Three situations were analyzed, involving 7, 15, and 25 students being present in the room. In a two-hour experiment, carbon dioxide levels reached 750, 1700, and 2450 ppm for 7, 15, and 25 students, respectively. The carbon dioxide levels increased approximately at a rate of 4.21, 11.43, and 18.68 ppm per minute across the three experiments. The input of fresh air could alleviate the carbon dioxide level problem. This paper presents data on conditions both before and after a fresh air intake fan is in operation. Operating such fresh air intake fans impacts on electricity costs since Thailand has a hot and humid climate. Power consumption when using air conditioning increases by approximately 45%. Therefore, minimizing the usage of fresh air intake fans could optimize energy usage while providing good indoor air quality.

KEYWORDS:
Indoor air quality, Carbon dioxide, Classroom, Model, and Ventilation.

INTRODUCTION

Green building initiatives are concerned about indoor air quality. Living in green buildings conventionally promises good health and lower electricity bills. It provides a better indoor environment, yet reduces energy demands. While the low ventilation rates consume less energy, they may result in poor indoor air quality, potentially causing health issues for occupants in the long run [1]. Sufficient ventilation following green building guidelines, such as those espoused by the Leadership in Energy and Environmental Design (LEED), could culminate in better indoor environmental quality conditions within buildings. LEED certification ensures healthier, more productive places, generating reduced stress on the environment by encouraging energy and resource-efficient buildings. Moreover, they potentially lead to savings from increased building value, higher lease rates and decreased utility costs [2]. A study of one LEED platinum campus building revealed levels of CO_2 concentration at less than 600 ppm, within the ASHRAE standard 62.1-2010 [3]. Ventilation supplying fresh air in an air-conditioned office consumes a considerable amount of energy [4]. Poor ventilation could cause excessive humidity and the accumulation of gaseous and/or chemical exposure [5]. Higher indoor air quality initiates a non-linear increasing trend in annual thermal energy consumption [6].

Green building projects encompass many aspects, such as location and transportation, sustainable sites, water efficiency, energy and atmosphere, materials and resources and indoor environmental quality. Indoor environmental quality is generally concerned with several factors, including ventilation rates, carbon dioxide levels, volatile organic compound levels, the concentration of dust, air speed, temperature, and humidity. Occupants of green buildings have been shown to be more satisfied with their indoor environmental quality than occupants of conventional buildings [7].

Indoor environmental in buildings is crucial from occupant's health. Most Europeans spend more than 90% of their time indoors, overall indoor air pollution exposures attribute to their health [8]. Researcher in this area should inform the public on their innovative solutions for healthier indoor climate [9]. Indoor air quality could be impacted by urban daily air quality index [10]. Since, strong emission sources and location of the house could affect indoor environment in buildings [11, 12].

In school buildings, poor indoor air quality can cause a reduction in students' performance as assessed by short-term, computer-based tests; whereas good air quality in classrooms can enhance children's concentration and teacher productivity [13]. High levels of CO_2 has been shown to have a negative influence on pupils' learning ability [14]. One study revealed that levels of carbon dioxide increased to 4800 ppm during the first two lessons in a not well-ventilated classroom of 25 students [15]. However, research has also shown that a mechanical

ventilation system was able to ensure the highest outdoor air supply rates in a classroom, independent of the season [16]. Not only does increase ventilation result in less dilution, but high ventilation rates can have a huge impact on energy costs and comfort [17].

In order to design appropriate ventilation systems, the effects of increasing rates of CO_2 need to be studied. It is useful to understand the properties of ventilation rates and carbon dioxide generation rates in order to evaluate indoor air quality and ventilation efficiency in mechanically ventilated buildings [18]. Several methods are used to estimate and model CO_2. Lawrence and Braun [19] suggested a methodology for estimating CO_2 using field measurements and developed a CO_2 schedule to manage demand-controlled ventilation in small commercial buildings. Lu et al [18] introduced a method of estimating occupant CO_2 generation rates from measurements in mechanically ventilated buildings, while Jiang et al. [20] used real-time CO_2 measurements as estimator tools for assessing CO_2 levels. In addition, Weekly et al. [21] developed partial and ordinary differential equations for modeling and estimating CO_2 in a conference room setting. However, none of the studies mentioned examined increasing rates of CO_2 levels in the classroom environment. Therefore, the objective of this research is to determine a model for estimating and predicting CO_2 levels in classrooms in order to help in designing ventilation systems suitable for use in schools.

METHODOLOGY

In developing models for estimating and predicting CO_2 levels in the classroom, the following data collection were considered. There were two stages of data collections in this research. First, increasing rates of CO_2 in a classroom setting were studied without the operation of any ventilation system. Secondly, the impact of operating a ventilation system on CO_2 concentrations was studied through examining cases wherein CO_2 concentrations were higher than the accepted threshold. With respect to carbon dioxide levels, the Occupational Safety and Health Administration (OSHA) specifies the limit of carbon dioxide level in the general industry workplace as being 5,000 ppm for a time weighted average [22]. A generally satisfactory rate for indoor CO_2 concentration lies between 1,000-1,200 ppm [23]. Therefore, the level of CO_2 used as a threshold in this research.is 1,000 ppm.

Data Collection. One classroom with a size of 64 square meters was selected for this experimental study as shown in Figure 1. It has a ceiling height of 3.5 meters. The experiment was conducted involving three cases of 7, 15 and 25 students. In each case, the level of CO_2 concentration was recorded every two hours and at 20 minutes intervals, as shown in Figure 2. The classroom was equipped with two air conditioning units. A fresh air supply fan with capacity of 362 cfm. or 616 m^3/hr is located at 2.5 m. from floor level at the back of the room. The fan was operated in the second stage of the experiment and the results are explained in the analysis section of this paper.

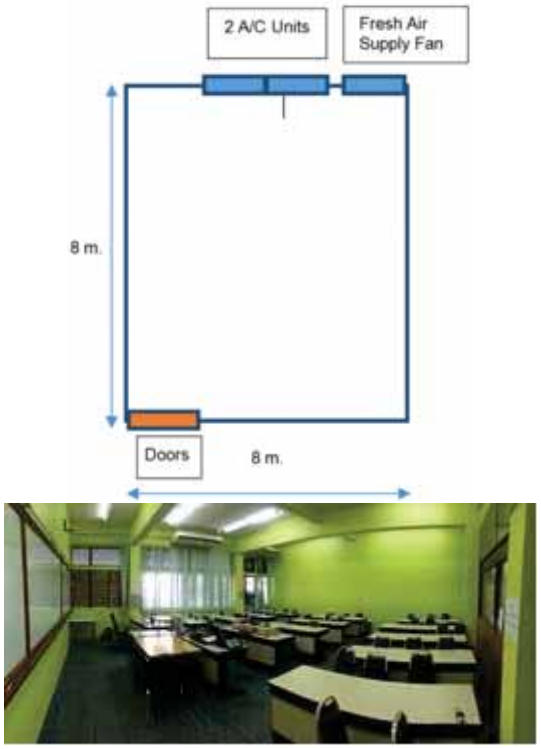


FIGURE 1
Experimental study room at Faculty of Engineering

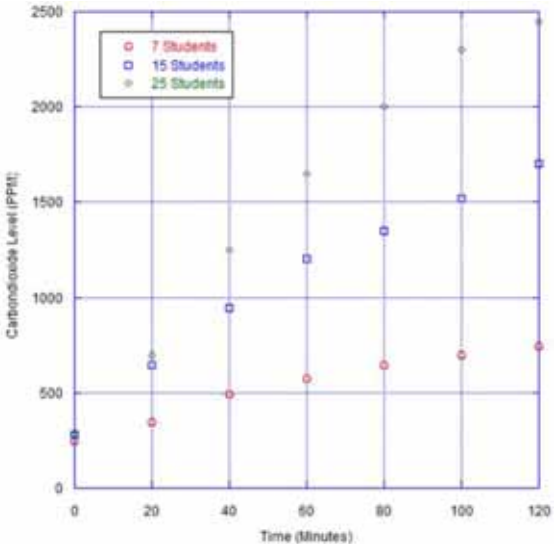


FIGURE 2
Carbon dioxide level at 20 minute intervals for 7, 15, and 25 students

Curve Fitting. Curve fitting was achieved by employing the linear regression method. This is a

statistical technique for modeling the relationship between variables [24]. In our experiments, two variables were found. Carbon dioxide level in a classroom is a function of the time that students are present in a room. Two models were chosen for curve fitting. They are straight line and second degree polynomial models. These were chosen since their patterns are similar in the form of the collected data in Figure 2. Their general forms are shown in equations 1 and 2.

$$y = ax + b \quad (1)$$

where y = carbon dioxide concentration in PPM; x = time in minute; a = slope of a straight line; and b = y-interception.

$$y = a + bx + cx^2 \quad (2)$$

where y = carbon dioxide concentration in PPM; x = time in minute; a, b, c = constant values.

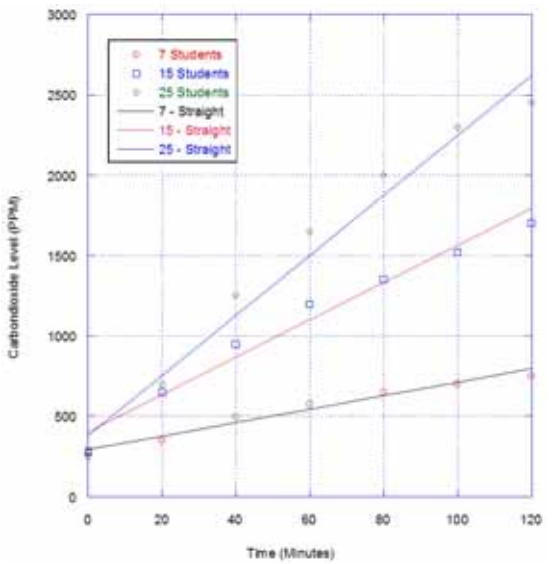


FIGURE 3
Straight line models for 7, 15 and 25 students

ANALYSIS

By using linear regression analysis methods with the collected data and models selected, a straight line function and second degree polynomial of 7, 15 and 25 students can be determined and summarized in Table 1. Their plots are compared with the collected data and shown in Figures 3 and 4 for the straight line models and second degree polynomial models, respectively. The coefficients of determination, R^2 are shown in Table 2. Second degree polynomial functions can fit the behavior of CO_2 increasing rates better than the straight line function. This is due to the fact that the average R^2 of the polynomial function, which is 0.999, is higher than the straight line function, which is 0.985.

TABLE 1
Results from curve fitting using linear regression methods on raw data in two forms of function

Number of Students	Straight Line Functions	2nd Degree Polynomial Functions
7	$y = 286.2 + 4.21x$	$y = 242.5 + 6.83x - 0.02x^2$
15	$y = 407.1 + 11.43x$	$y = 299.9 + 17.86x - 0.05x^2$
25	$y = 397.8 + 18.68x$	$y = 236.9 + 28.33x - 0.08x^2$

TABLE 2
Coefficient of determination, R^2 of fitted functions

Function	Number of Students	R^2	Average R^2
Straight Line	7	0.982	0.985
	15	0.986	
	25	0.988	
2nd Degree Polynomial	7	0.998	0.999
	15	0.999	
	25	0.999	

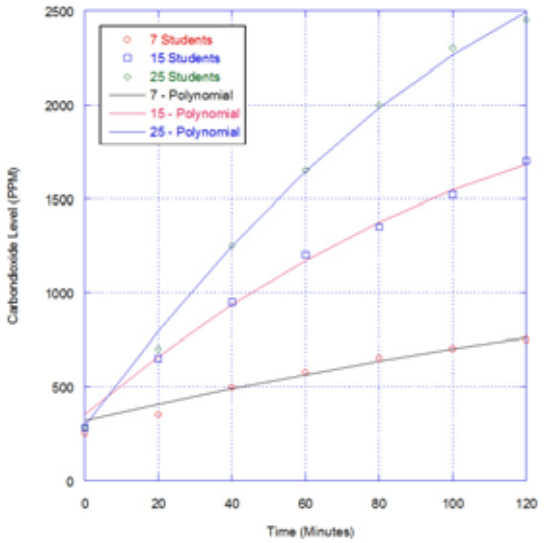


FIGURE 4
Second degree polynomial models for 7, 15 and 25 students

The impact of employing ventilation fans is then studied. Bringing fresh air into the room can reduce CO_2 concentration, as shown in Figure 5. It was found from Figure 4 that CO_2 concentrations exceed the threshold at approximately the 45th and 30th minute time scales in the 15 and 25 student experiments, respectively. For the seven student experiment, the CO_2 concentration was well below 1000 ppm throughout the two-hour experiment. This can roughly indicate that a 9.1 square meter space is required for one person in a two-hour session. If the space ratio per student is less than this number, a mechanical ventilation system is required to maintain acceptable indoor air quality based on the CO_2 aspect. Figure 5 illustrates the data gained in the two experiments where ventilation fans were operated. The fans were operated manually when CO_2 inside

room exceeded 1000 ppm. The ventilation fans supply fresh air at a rate of 362 cfm, or 616 m^3/hr. The fresh air supply fan can reduce the CO_2 to be under 1,000 ppm in the case of the 15 student experiment. However, the ventilation fans cannot bring the CO_2 concentration below 1,000 ppm in the 25 student case scenario. Test durations in Figure 5 are less than 120 minutes due to classes adjourning before time. The actual ventilation rate for the 15 student case, which offers good indoor air quality, was 24.13 cfm/person. This number is higher than the 15 cfm/person recommended by the Thai standards. The minimum ventilation rate required for a classroom in Thailand stands at 15 cfm/person [25].

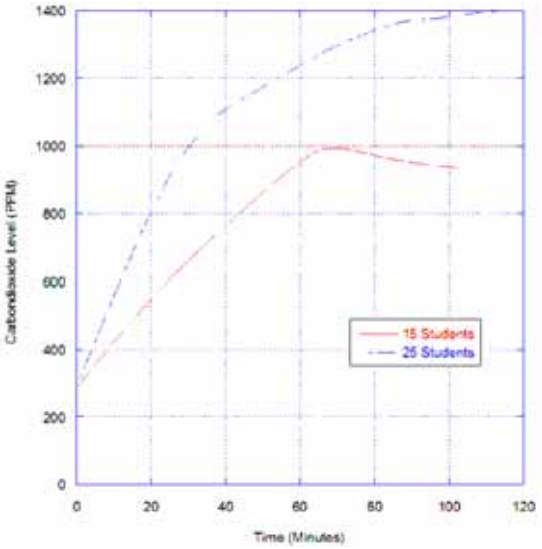


FIGURE 5
Impacts of ventilation fans on 15 and 25 student experiments

TABLE 3
CO_2 emission rates of students in the classroom

Number of students	Slope of straight line functions, ppm/minute	Average, ppm/student/minute
7	4.21	0.60
15	11.43	0.76
25	18.68	0.75
	Average	0.70

However, ventilation fans serve to bring hot and humid air into rooms since Thailand is subject to a typically hot and humid climate. Electricity consumption increases since air conditioning units work harder and consume more electricity, as shown in Figure 6. The 15 student experiment consumed an increased rate of electricity of 49%, in order to take the CO_2 concentration level down from approximately 1750 ppm to 935 ppm indicating that lower CO_2 concentration is harder to reduce and consumes more electricity. Meanwhile, in the 25 student experiment an additional 45% of electricity was consumed in order to reduce the CO_2 concentration from approximately 2450 ppm to 1400 ppm, indicating that higher CO_2 levels can be reduced more easily with less electricity consumption.

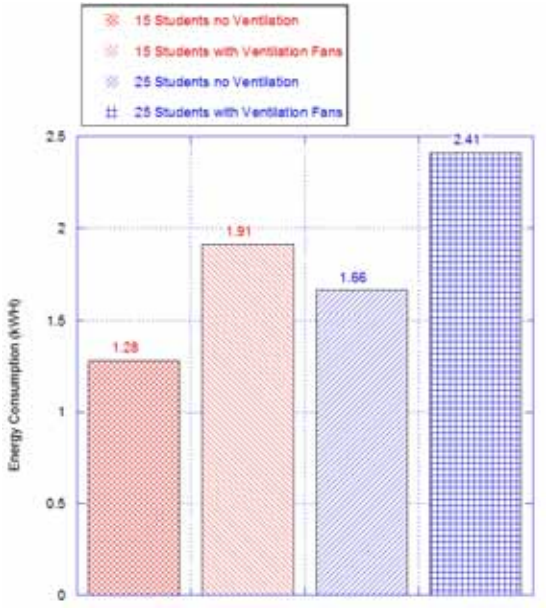


FIGURE 6
Electricity consumption in kilo Watts Hour for 15 and 25 student experiments

From the three straight line functions observed in Table 1, CO_2 increasing rates can be roughly estimated as 4.21, 11.43 and 18.68 ppm per minute for 7, 15 and 25 students, respectively. An average CO_2 increasing rate per student per minute can be calculated and shown in Table 3, standing at 0.70 ppm/student/minute. This number can be used roughly in estimating CO_2 concentration in classrooms. Students tended to slowly emit carbon dioxide as time passed during experiments. This can be observed in the fact that the initial slope is steeper than it is in latter stages, as can be seen from Figure 4.

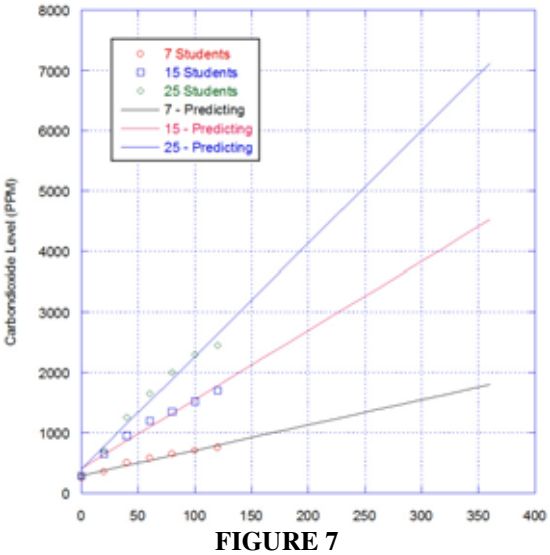


FIGURE 7
A straight line model in predicting future values

Although the polynomial function is better fitted to actual CO_2 values than the straight line function, in predicting accuracy the polynomial function should not be used when predicting future values. The straight line function can be employed to roughly estimate CO_2 concentration in classrooms with acceptable accuracy. Figures 7 and 8 show the results connected to predicting values for both functions. In the first 120 minutes the polynomial functions show better accuracy. Meanwhile, they least able to predict accuracy in the last 240 minutes compared with the straight line function. Thus, this research recommends using the straight line model in estimating CO_2 concentration in a classroom which is occupied for more than two hours.

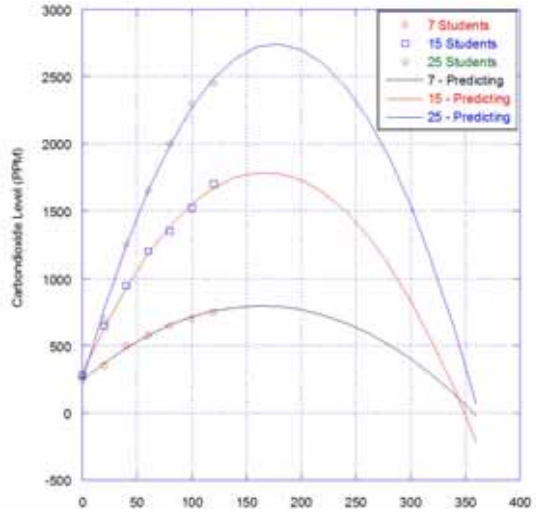


FIGURE 8
A polynomial model should not be used for predicting future values

CONCLUSIONS

This research proposes the second degree polynomial function for estimating purposes since it can best describe the increasing rate of CO_2 concentration in classrooms. The model can be used as a guideline for estimating CO_2 in the first two-hour period. However, the straight line model should be used to estimate CO_2 concentration beyond that, as shown in Figure 7. This is due to the fact that the polynomial model emerged as the worst predictor function, as shown in Figure 8. Thai standards recommend the ventilation rate of fans as being 15 cfm/person. However, this research recommends ensuring a ventilation rate at greater than 24 cfm/person for a two-hour class and four square meter area per student. Higher CO_2 levels can be brought down easily with less electricity consumption, whereas with lower CO_2 concentration levels it is harder to reduce and the process consumes more electricity. The results from this research are parallel with Wong et al. [26] who stated that 56% more energy would be consumed in order to decrease the CO_2 level from 1000 ppm to 800 ppm in order to achieve excellent indoor air quality. Building designers need to understand that good indoor air quality consumes more electricity. As a result, fresh air intake fans in the context of a densely occupied room over a long session consume more electricity. Designing an appropriate supply fan in terms of the capacity of students in class is a challenging task in the context of saving energy usage in buildings. Variable speed supply fans which are able to alleviate CO_2 concentration according to the number of students present in a classroom can potentially minimize the energy usage from air conditioning units.

ACKNOWLEDGEMENTS

This research was supported by the royal Thai government funding of fiscal year 2014 through the King Mongkut's University of Technology North Bangkok (KMUTNB). The author wishes to thank him gratefully.

REFERENCES

[1] Wang, H., Xie, L., Liu S. and Xu J. (2016) A model based control of CO_2 concentration in multi zone ACB air conditioning systems. Proceeding of the 12th IEEE International conference on control and automation. 467-472.
[2] Leadership in Energy & Environmental Design (LEED) (2017) Why LEED? Available from: http://leed.usgbc.org/leed.html. [April 27, 2017].
[3] Hua, Y., Gocer, O. and Gocer K. (2014) Spatial mapping of occupant satisfaction and indoor environment quality in a LEED platinum campus building. Building and Environment. 79, 124-137.
[4] Wong, L.T. and Mui, K.W. (2008) A transient ventilation demand model for air-conditioned offices. Applied Energy. 85, 545-554.
[5] Bernstein, J.A., Alexis, N., Bacchus, H., Bernstein, L., Fritz, P., Horner, E., Li, N., Nel, A., Oullette, J., Reijula, K., Reponen, T., Seltzer, J., Smith, A. and Tarlo, S.M. (2008) The health effects of nonindustrial indoor air pollution. Journal of Allergy and Clinical Immunology. 121, 585-591.
[6] Wong, L.T. and Mui, K.W. (2009) An energy performance assessment of indoor air quality acceptance for air-conditioned offices. Energy Conversion and Management. 50, 1362-1367.
[7] Liang, H., Chen, C., Hwang, R., Shih, W. and Lo, S. (2014) Satisfaction of occupants toward indoor environment quality of certified green office buildings in Taiwan. Building and Environment. 72, 232-242.

[8] Arvanitis, A., Kotzias, D., Kephalopoulos, S., Carrer, P., Cavallo, D., Cesaroni, G., Brouwere, K.D., Oliveira-Fernandes, E. de O., Forastiere, F., Fossati, S., Fromme, H., Haverinen-Shaughnessy, U., Jantunen, M., Katsouyanni, K., Kettrup, A., Madureira, J., Mandin, C., Molhave, L., Nevalainen, A., Ruggeri, L., Schneider, T., Samoli, E. and Silva, G. (2010) The index-pm project: Health risks from exposure to indoor particulate matter. Fresen. Environ. Bull. 26, 323-326.

[9] Kotzias, D. and Pilidis, G. (2017) Building design and indoor air quality experience and prospects. Fresen. Environ. Bull. 26, 323-326.

[10] Luo, X., Zhao, Z., Chen, Y., Ge, X., Huang, Y., Sue, C., Sun, X., and Zhang, D. (2017) Effects of emission control and meteorological parameters on urban air quality showed by the 2014 youth Olympic games in China. Fresen. Environ. Bull. 26, 4798-4807.

[11] Sakellaris, I.A., Tolis, E.I., Sarage, D.E. and Bartzis, J.G. (2017) Vocs, Pahs and Ions measurements in an office environment in the vicinity of a small industry. Fresen. Environ. Bull. 26, 292-300.

[12] Sabaziotis, V., Galinos, K., Missia, D., Kalimeri, K.K., Tolis, E.I. and Bartzis, J.G. (2017) Indoor air quality in residences at the city of Kozani, Greece: Effects of the house location. Fresen. Environ. Bull. 26, 255-262.

[13] Clements-Croome, D.J, Awbi, H.B., Bako´-Biro´, Zs, Kochhar, N. and Williams, M. (2008) Ventilation rates in schools. Building and Environment. 43, 362–367.

[14] Griffiths, M. and Eftekhari, M. (2008) Control of CO_2 in a naturally ventilated classroom. Energy and Buildings. 40, 556-560.

[15] Heudorf, U., Neitzert, V. and Spark, J. (2009) Particulate matter and carbon dioxide in classrooms – The impact of cleaning and ventilation. Int. J. Hyg. Environ. Health. 212, 45–55.

[16] Gao, J, Wargocki, P. and Wang, Y. (2014) Ventilation system type, classroom environmental quality and pupils' perceptions and symptoms. Building and Environment. 75, 46-57.

[17] Prill, R. (2000) Why Measure Carbon Dioxide Inside Buildings? Washington State University Extension Energy Program, Available from: http://www.energy.wsu.edu/Documents/CO2inbuildings.pdf. [April 27, 2017]. 9.

[18] Lu, T., Knuutila, A., Viljanen, M. and Lu, X. (2010) A novel methodology for estimating space air change rates and occupant CO2 generation rates from measurements in mechanically ventilated buildings. Building and Environment. 45, 1161-1172.

[19] Lawrence, T.M. and Braun, J.E. (2007) A methodology for estimating occupant CO_2 source generation rates from measurements in small commercial buildings. Building and Environment. 42, 623-639.

[20] Jiang, C., Masood, M.K., Soh, Y.C. and Li, H. (2016) Indoor occupancy estimation from carbon dioxide concentration. Energy and Buildings. 131, 132-141.

[21] Weekly, K., Bekiaris-Liberis, N., Jin, M. and Bayen, A.M. (2015) Modeling and estimation of the humans' effect on the CO_2 dynamics inside a conference room. IEEE Transactions on Control Systems Technology. 23, 1770-1781.

[22] OSHA (2017) Carbon Dioxide, Available from: https://www.osha.gov/dts/chemical sampling/data/CH_225400.html. [May 1, 2017].

[23] ASHRAE (2014) ASHRAE Technical FAQ: What is the allowable level of carbon dioxide in an occupied space? Available from: https://www.ashrae.org/File%20Library/docLib/Technology/FAQs2014/TC-04-03-FAQ-35.pdf. [May 1, 2017].

[24] Montgomery, D.C., Peck, E.A. and Vining, G.G. (2012) Introduction to linear regression analysis 5th Edition: 1.

[25] Engineering Institute of Thailand (EIT) (2005) Standards for acceptable indoor air quality. EIT Standard Number 3010, Thailand.

[26] Wong, L.T., Mui, K.W, Shi, K.L. and Hui, P.S. (2008) An energy impact assessment of indoor air quality acceptance for air-conditioned offices. Energy Conversion and Management. 49, 2815-2819.

Received: **26.05.2017**
Accepted: **29.08.2017**

CORRESPONDING AUTHOR

Wannawit Taemthong
King Mongkut's University of
Technology North Bangkok,
Faculty of Engineering,
Bangkok – Thailand

e-mail: wannawit@gmail.com

© by PSP Volume 26 – No. 12A/2017 pages 7957-7966 Fresenius Environmental Bulletin

ANTI-BIOFILM ACTIVITY OF BENZYL SUBSTITUTED HEXAHYDROIMIDAZO [1,5-*a*] PYRIDINIUM BROMIDE SALTS AGAINST SOME PATHOGENIC MICROORGANISMS

Nur Ceyhan-Guvensen[1,*], Hayati Turkmen[2]

[1]Mugla Sitki Kocman University, Faculty of Sciences, Department of Biology, 48170 Mugla, Turkey
[2]Ege University, Faculty of Sciences, Department of Chemistry, 35100 Izmir, Turkey

ABSTRACT

The principle aim of this study was to evaluate the anti-biofilm activity of newly synthesized hexahydroimidazo [1,5-*a*] pyridinium bromides with varying benzyl substituents to test as biofilm eradication agents against 10 opportunistic pathogens. To our knowledge this important aspect of their anti-biofilm and antioxidant activity has not yet been discussed in the literature. Anti-biofilm activity of benzyl substituted hexahydroimidazo[1,5-*a*]pyridinium bromide salts (B1-B9) was tested accoriding to microtitre plate method. Additionally, the best biofilm production of *E.coli* ATCC 8739 was monitoring with SEM (Scanning Electron Microscopy). The antioxidant activity of these salts were studied by the method of ABTS (2,2 azinobis(3-ethylbenzothiazoline-6-sulfonic acid)) radical cation. In this study we have shown that these compounds possess excellent, broad spectrum anti-biofilm activity against opportunistic microorganisms: the bacteria *Staphylococcus aureus, Staphylococcus epidermidis, Bacillus cereus, Micrococcus luteus, Proteus vulgaris, Escherichia coli, Salmonella typhimurium, Klebsiella pneumoniae* and the yeasts *Candida albicans, Candida krusei.* All of these compounds inhibited bacterial and fungal biofilm formation at concentrations ranging from 0.78 to 400 µg/mL, 3.12 to 50 µg/mL, respectively (biofilm inhibitory concentration=BIC). Additionally, these compounds have been found to possess antioxidant potential with the highest inhibitory percentage of 92.4% using ABTS radical cation assay. The obtained results revealed that all the salts displayed anti-biofilm and antioxidant activity against the tested microorganisms, indicating that these salts could use in the design of new therapeutics and more effective antimicrobials for the control and prevention of biofilm infections caused by the spread of pathogenic microorganisms to the environment.

KEYWORDS:
Hexahydroimidazo [1,5-a] pyridinium bromides, imidazolinium salts, anti-biofilm activities, antioxidant activities, pathogenic microorganisms

INTRODUCTION

Opportunistic microorganisms are rapidly emerging as problematic pathogens in healthcare settings. Biofilm formation is an important reason for bacterial resistance to antimicrobials. A biofilm is a structured consortium of bacteria embedded in a self-produced polymer matrix consisting of polysaccharide, protein and extracellular DNA [1]. The microorganisms can attach to diverse abiotic such as foreign body materials, oil pipelines, industrial hot tubs or biotic systems such as heart valves, teeth, mucosa and grow in highly stable communities [2-5]. Biofilm-associated microorganisms behave differently from planktonic (freely suspended) organisms with respect to growth rates and ability to resist antimicrobial treatments and therefore pose a public health problem [3].

Clinically, microbial biofilms are extremely problematic, and are implicated in implantable medical device-associated infections as well as many non-implant related chronic infections in humans [6-7], many of which are recalcitrant to standard antimicrobial regimens. Microbial biofilms, with their community defenses, are a ubiquitous feature of bacteria in nature and in many bacterial infections. Native valve endocarditis, cystic fibrosis bronchopneumonia, periodontitis, bladder infections, otitis media, musculoskeletal infections, necrotizing fasciitis, biliary tract infection, osteomyelitis, bacterial prostatitis, meloidosis, chronic tonsillitis, rhinosinusitis, infectious kidney stones, chronic wounds, dental caries, and infections associated with foreign body material (contact lenses, urinary and venous catheters, mechanical heart valves, arteriovenous shunts, vascular grafts, peritoneal dialysis peritonitis, endotracheal tubes, stents, orthopedic devices, intrauterine device, other prostheses, etc.) are all examples of biofilm-related diseases [1, 7-10]. All these chronic infections are characterized by persisting inflammation and tissue damage [3, 11]. Biofilm formation has been proposed to be a key to the survival of pathogens in the context of infections [12, 13]. Chronic infections are infections that 1) persist in spite of antibiotic therapy, the innate and adaptive immune system

and inflammatory response of the host, and 2) in contrast to colonization, are characterized by immune response and persisting pathology [14]. Industrially, microbial biofilms are responsible for billions of dollars in lost productivity every year, occurring in almost every water-based process causing pipe blockage corrosion and contamination [15, 16].

The resident bacterial community in a biofilm has added defenses and multiple mechanisms for survival, such as defenses against phagocytosis, UV radiation, viral attack, shear stress, and dehydration, as well as against biocides, antibiotics, and host immunity. Biofilms have demonstrated the ability to persist in 100 to 1000 times the concentrations of antibiotics and biocides that can inhibit planktonic cells [17-20]. Antibiotic treatment is often unsuccessful when bacteria are organized in biofilms, because the latter give bacteria potent increased antibiotic resistance [7, 21]. These biofilm characteristics are the root of many persistent bacterial infections [15]. The biofilm allow adaptation to overcome multiple stresses and to survive most sequential therapies [10, 22, 23].

Current disinfection practices rely on convensional disinfectants that are typically biocidal or toxic to bacteria, but as noted above, these biocides are typically ineffective at controlling biofouling [7, 24, 25]. In this case, control of biofilm formation or maintenance must be synthesized new anti-biofilm compounds that have anti-biofilm activities [16, 24, 26, 27]. Imidazole derivatives has attracted more attention during recent years due to their biological activities. These compounds have been shown to possess antihelmintic, antifungal, antibacterial and anticancer activities [28]. Besides their biological actions, diazol(in)ium salts find wide applications in the preparation of N-heterocyclic carbenes (NHCs) and their metal complexes [29-31], some of which have attracted important attention as potential pharmaceuticals [31]. In addition, diazol(in)ium salts, as potential antiseptics/disinfectants, have been researched by some investigators [32-35].

The imidazolinium, benzimidazolium and tetrahydropyrimidinium salts and their metal complexes previously designed by Türkmen et al. (Fig. 1.) (1-9) had been shown to possess low toxicity. According to the data, LD_{50} values of all these compounds after oral application in mice in 24 h showed low toxicity according to EPA and WHO [39]. In this regard, the present study was carried out to examine theirs efficacy against biofilm formation, and ability to eradicate preformed biofilms. The tested bacteria and fungi in the work are important opportunistic human pathogens that causes several chronic organ infections especially in immuno-compromised patients and in elders [22, 36-38]. Much effort is now being invested to understand the anti-biofilm activity of these salts, with a view toward designing and/or improving new therapeutics and more effective antimicrobial agents against persistent biofilm infections by pathogens.

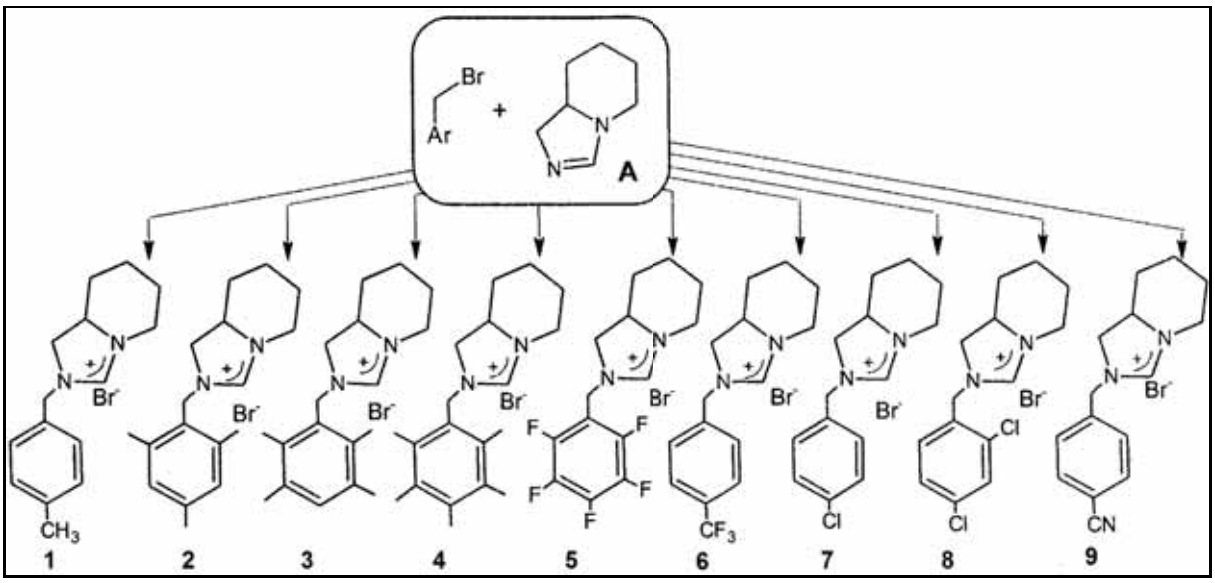


FIGURE 1
Synthesis and formula of the salts used for anti-biofilm activity. The purity of the salts was checked by TLC with Merck Kieselgel GF 254 Plates, elemental analyses and 1H and 13C NMR (Varian Mercury AS 400).

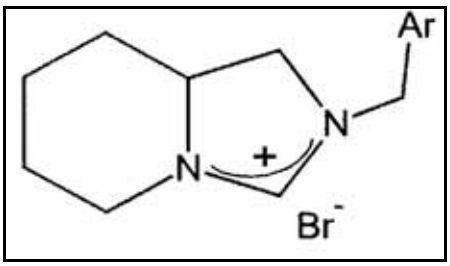


FIGURE 2
Structure of hexahydroimidazo [1,5-*a*] pyridinium bromide.

MATERIALS AND METHODS

Microbial Strains and Growth Media. In vitro antimicrobial studies were carried out against 10 test microorganisms (four Gram-positive bacteria: *S. aureus* (6538/P), *S. epidermidis* (ATCC 12228), *B. cereus* (CCM 99) and *M. luteus* (ATCC 9341), four Gram-negative bacteria: *P. vulgaris* (ATCC 6897), *E. coli* (ATCC 8739), *S. typhimurium* (CCM 5445) and *K. pneumoniae* (CCM 2318), and two yeasts: *C. albicans* (ATCC 10231) and *C. krusei* (ATCC 6258), which were obtained from the Microbiology Department Culture Collection of Ege University, Faculty of Science. Stock cultures of bacteria were maintained on nutrient agar (NA) (Merck) and yeasts were potato dextrose agar (PDA) (Merck) at 4 ºC.

Benzyl Substituted Hexahydroimidazo [1, 5-a] Pyridinium Bromide Salts. In our study the salts used for anti-biofilm activity had been previously synthesized by Türkmen et al. [39]. In their work, the salts had been obtained by quaternization of 1, 5, 6, 7, 8, 8a- hexahydroimidazo [1, 5- *a*] pyridine, by variously substituted benzyl bromides. 2- (2, 4, 6- tetramethylbenzyl)- 1, 5, 6, 7, 8, 8a- hexahydroimidazo [1,5- *a*] pyridin- 2-ium bromide (2), 2- (2, 3, 5, 6- tetramethylbenzyl)- 1, 5, 6, 7, 8,8ahexahydroimidazo[1, 5- *a*]pyridin- 2- ium bromide (3), 2-(pentamethylbenzyl)-1,5,6,7,8,8a-hexahydroimidazo[1,5-*a*]pyridin- 2 - ium bromide (4) are known in the literature [40, 41]. The other salts (1, 5-9) had been prepared according to the published procedure. The purity of the salts had been checked by TLC with Merck Kieselgel GF 254 Plates, elemental analyses and 1H and 13C NMR (Varian Mercury AS 400). Formula of the salts (1-9) were shown in Figure 1 and structure of hexahydroimidazo [1,5-*a*] pyridinium bromide was shown in Figure 2.

Anti-biofilm Activity Tests. Anti-biofilm activity of benzyl substituted hexahydroimidazo[1,5-*a*]pyridinium bromide salts (1-9) was tested in 96-well microtitre with glass pieces (1x1cm) [42-44]. Dilution series using sterile distilled water were prepared at the required quantities of 1600, 800, 400, 200, 100, 50, 25, 12.5, 6.25, 3.12, 1.56, 0.78 µg/ml concentrations in wells and were added in TSB containing the bacterial suspension at 10^6 CFU/ml. The plates were incubated in the bacterial cultures for 24 h at 37 °C and in the fungal cultures for 72 h at 20 °C under stationary conditions and total growth was measured at 570 nm (Perkin Elmer-Lambda 25). Biofilm was measured by discarding the medium, rinsing the wells with 200 mL of water (three times) and staining the bound cells with crystal violet (0.4%, w/v) for 15 min, followed by washing with water (200 mL) to remove unbound stain. The dye was solubilized in 200 mL of 33% (v/v) acetic acid, and absorbance at 570 nm was determined using a microtitre plate reader (Thermo Scientific-Multiskan FC). Six replicates were used for each sample and each experiment was performed three times. The percentage of biofilm inhibition was calculated by the formula:
Percentage of inhibition = ([Control OD_{570nm} - Test OD_{570nm}]/Control OD_{570nm}) x 100

The biofilm inhibitory concentration (BIC) was determined as the lowest concentration that produced visible disruption of biofilm formation and a significant reduction in the readings when compared with the control wells at OD_{570nm} [45, 46]. The wells containing TSB and with the solutions of 1-9 were used as blanks.

SEM Analysis. The biofilm samples for SEM monitoring were prepared as described by Lembke et al. [47] and Thenmozhi et al. [43]. The biofilms on glass pieces (1x1cm) were fixed for 1 h in a solution containing 2.5% glutaraldehyde. The glass pieces were washed in 0.1M sodium acetate buffer (pH 7.3). Samples were dehydrated through a graded series of ethanol, critical-point dried, gold sputtered and examined with a JEOL, JSM-7600F SEM (USA).

Assay of Antioxidant Activities for 1-9 by In-vitro Method. The antioxidant activity was determined using ABTS (2,2 azino-bis(3-ethylbenzothiazoline-6-sulfonic acid)) radical cation method [48] with some modifications described by Rossini et al. [49] and Pieniz et al. [50]. ABTS radical cation was dissolved inwater (7 mM). ABTS radical cation was produced by reacting ABTS radical cation stock solution with 2.45 mM potassium persulfate (final concentration) and allowing the mixture to stand in dark at room temperature for 16 h before use. The stock solution was used for a maximum of 3 days. Before use, ABTS radical cation solution was diluted with ethanol, to an absorbance of 0.700 ± 0.020 at 734 nm. Samples were diluted with ethanol to obtain inhibition between 20 and 95% of the blank absorbance. Ascorbic acid was used as the standard in the range 0-9 µg/ml. After addition of 10 ml of sample (or standards) in

1.0 ml of ABTS radical cation solution, the absorbance was read at 30 s interval for 5 min. Likewise, a same proportion (10 ml) of culture medium or ultrapure water were used as controls. All determinations were carried out at least three times. The percentage inhibition of absorbance at 734 nm was calculated using ascorbic acid standard curve.

Statistical Analysis of Data. The data from all experiments were analysed using the SPSS software (version 16.0). Values were expressed as mean±SE. Standard errors (SE) between replicate samples for all experiments were calculated and an unpaired two-tailed t-test was performed to determine whether there was a statistically significant difference between growth as biofilms of microorganisms. All tests were considered significant at the level $p<0.05$. Error bar plots in figures are shown as one SE. The values for each experiment are the mean values of results from three experiments unless otherwise stated.

RESULTS AND DISCUSSION

The opportunistic pathogens are the leading cause of morbidity and mortality in enfected patients. Infections can be difficult to eradicate due to their propensity to form biofilms and their inherent resistance to antibiotics. Treatment regimens generally involve a rigorous and aggressive antibiotic assault to minimize the detrimental cycle of infection, inflammation, and subsequent scar tissue formation [37, 46]. Biofilm-embedded bacteria and yeast are tenacious and 100–1000 times more resistant to antimicrobial treatment [51]. Thus, inhibition of biofilm formation and/or dispersal of preformed biofilms may make biofilm-embedded bacteria and yeast more susceptible to antimicrobial agents. Hence, we have investigated the effects of variously substituted benzyl bromides (1-9) against on eight bacterial and two fungal opportunistic pathogens. To determine the BICs of the 1-9 on these microorganisms, the compounds with concentrations at 0.78 to 1600 µg/ml was assessed and the BICs were found as 0.78-400 µg/mL (Table 1).

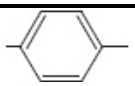
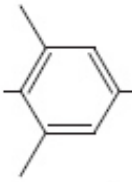
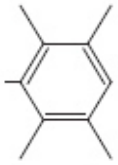
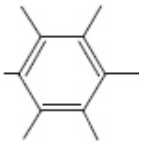
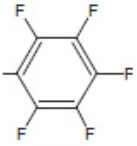
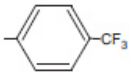
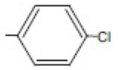
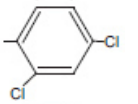
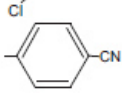
In the study, it was detected that was a poor correlation between lipophilicity of microbial cell walls and BIC values of multi methylated benzyl substituted salts, such as 1-4. The reasons of this might be high Clog*P* values (logarithms of 1-octanol/water partition coefficient parameter) [39] and lower anti-biofilm properties of 1-4. Also, steric and electronic interactions by influent. In addition to these, it was shown that anti-biofilm activity of electron-poor benzyls were higher than electron-rich ones in this work. Because most bacteria are negatively charged but still contain hydrophobic surface components, they prefer positive cations to bind in the biofilm [52, 53].

Moreover, the compounds tested here generally showed poor anti-biofilm activities against Gram-negative bacteria (Fig. 3.). The anti-biofilm activities against Gram-positive bacteria and fungus may depend on the differences between the cell structures of these microorganisms. Strong, tough, and elastic the Gram-negative cell wall is a remarkable structure which protects the contents of the cell. The cell walls of Gram-negative bacteria follow a more general structural format than that of gram-positive bacteria, which is strictly adhered to; Gram-negative bacteria have an outer membrane situated above a thin peptidoglycan layer. Sandwiched between the outer membrane and the plasma membrane, a concentrated gel-like matrix is found in the periplasmic space. Whereas, fungal cell wall has been shown to be primarily composed of chitin, glucans, mannans and glycoproteins [54].

The lowest BICs of antibiotics tested in the work were detected to be 12. 5 µg/mL against Gram-positive bacteria, Gram-negative and fungi (Table 1). Whereas, the BICs of the most active derivatives (6, 7, 8 and 9) were shown to be as low as 0.78 mg/mL. Interestingly, all these four derivates inhibited biofilm formation against two different yeast species at the same concentration 3.12 µg/ml (BIC). Additionally, they showed pronounced effect on the inhibition of Gram-positive and Gram-negative biofilm formation at very low concentrations (0.78-50 µg/mL). In Gram-negative bacteria, the outer membrane contains substautial amounts of protein and phospholipid and in addition, most or all of the lipopolysaccharide of the cell envelope. One of Gram-negative bacteria *K.pneumoniae* contains a discrete detectable layer of polysaccharides outside of the cell wall polymer named as capsule. Therefore, susceptibility of *K. pneumoniae* (CCM 2318) biofilm against the compounds might be lower than the other bacteria in the study (Fig. 3b).

The inhibition of biofilm formation was calculated for all tested microorganisms and their BICs were found to be 0.78-400 µg/mL which showed a significant reduction ($P< 0.05$) in biofilm formation by spectrophotometric quantification. In addition, visible reductions in biofilms of all tested microorganisms on the treated slides were observed by SEM monitoring. All data was not given in the study and *E. coli* was selected as a representating microorganism. Eventually, SEM analysis of the biofilms formed in the presence and absence of benzyl substituted hexahydroimidazo [1,5-a] pyridinium bromide salts confirmed the inhibition of *E.coli* biofilm formation by 1, 2, 3, 4, 6 and 7 (Fig. 4.). Combination of these active compounds with traditional antibiotics will help design more effective antimicrobials and therapeutic approaches for biofilm-treatments.

TABLE 1
Anti-biofilm and antioxidant activity of hexahydroimidazo [1,5-a] pyridinium bromides against tested pathogenic microorganisms.

Salts	Ar	Antioxidant activity (%)*	BIC (µg/ml)									
			Gram positive bacteria				Gram negative bacteria				Yeasts	
			SA	SE	BC	ML	PV	EC	ST	KP	CA	CK
1		75.5±0.09	25	25	100	50	50	25	50	25	12.5	12.5
2		12.5±1.00	100	50	400	50	200	400	200	400	50	25
3		15.8±2.06	100	25	400	50	25	100	100	400	50	12.5
4		56.2±0.71	50	25	200	25	50	50	50	50	50	6.25
5		60.8±0.47	25	25	200	50	100	100	100	50	50	3.12
6		92.4±1.82	12.5	3.12	6.25	3.12	12.5	3.12	3.12	50	3.12	3.12
7		90.5±2.00	12.5	3.12	6.25	3.12	25	12.5	6.25	50	3.12	3.12
8		89.6±0.15	3.12	3.12	25	6.25	12.5	12.5	3.12	25	3.12	3.12
9		87.5±0.20	12.5	12.5	25	6.25	25	12.5	0.78	50	3.12	3.12
Standard antibiotics	Ampicillin		50	12.5	100	6.25	25	25	12.5	50	-	-
	Nystatin		-	-	-	-	-	-	-	-	12.5	12.5

*: Values represent the mean±SE of three independent experiments; -: Not tested; BIC: Biofilm inhibitory concentration; SA: *Staphylococcus aureus;* SE: *Staphylococcus epidermidis;* BC: *Bacillus cereus;* ML: *Micrococcus luteus;* PV: *Proteus vulgaris;* EC: *Escherichia coli;* ST*: Salmonella typhimurium;* KP: *Klebsiella pneumoniae;* CA: *Candida albicans; and* CK: *Candida krusei.*

The antioxidant activity was evaluated by ABTS radical cation method (Table 1). 1-9 exhibited high ability to scavenge the radical ABTS, with inhibitory percentages ranging from 12.5 to 92.4% (Table 1). From the results of antioxidant activity, it was recognized clearly that 6 and 7 could produce the highest amount of antioxidant activity, 92.4% and 90.5%, respectively. Conversely, 2 and 3 showed weak antioxidant activity, with an inhibitory percentage of 12.5% and 15.8%, respectively. As a general result, there were noticeable antioxidant activities of these derivates. Considering their potency as potential antioxidants especially 6 and 7 can find wide application in functional pharmaceutical formulations.

CONCLUSION

A biofilm focus also provides new strategies for treatment of chronic infections. Biofilm-based treatments might block initial bacterial attachment to a surface, block or destroy EPS formation, inter-

fere with cell-cell signaling pathways, and use bacteriostatic or bactericidal agents at the same time. Microbial biofilms, which characterized by their resistance to the traditional antimicrobials, are considered as a renewable source of contamination by pathogens.

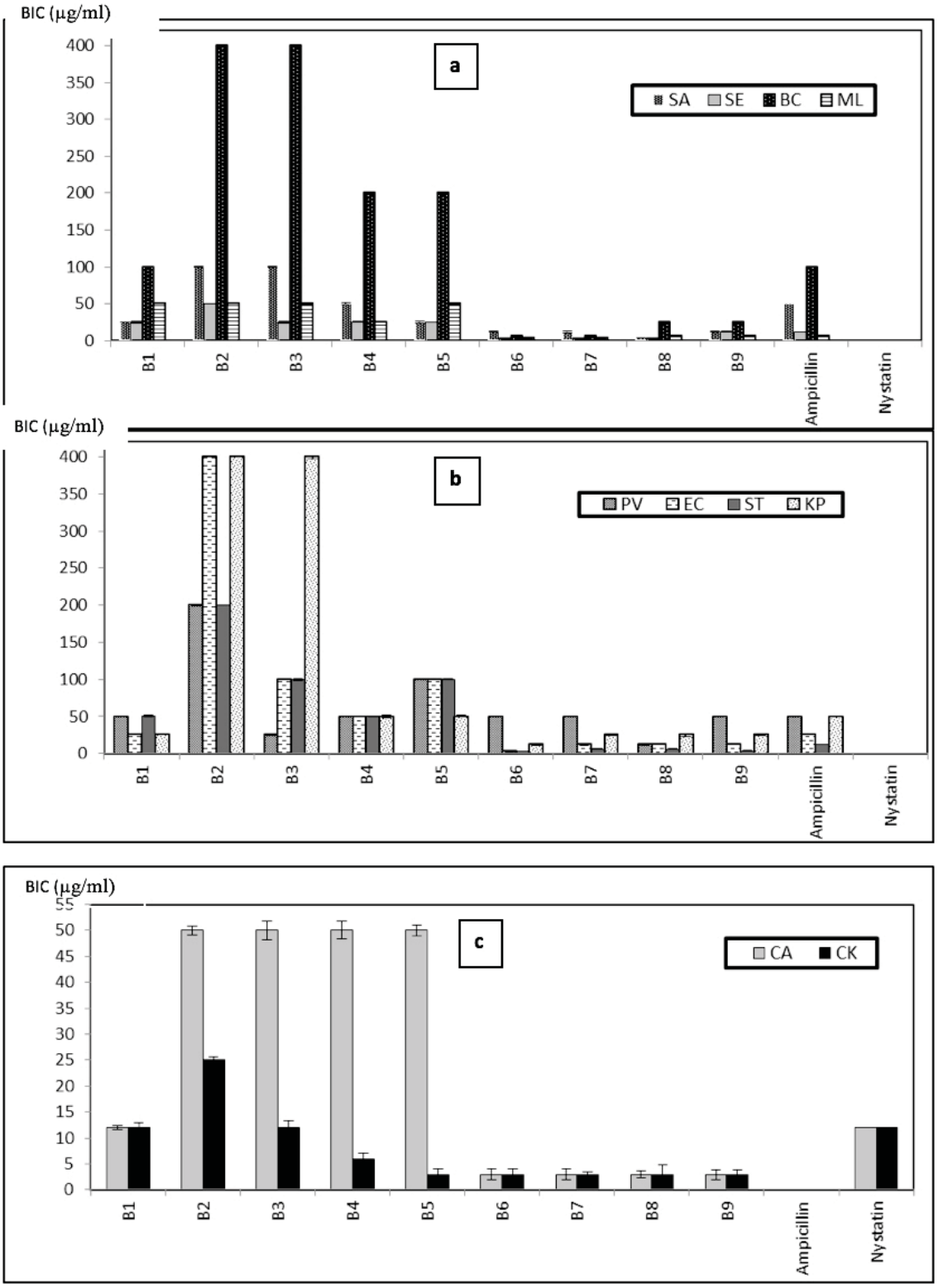


FIGURE 3
Inhibition effect of hexahydroimidazo[1,5-a]pyridinium bromides (1-9) and standard antibiotics (a) on Gram-positive bacteria, (b) on Gram-negative bacteria and (c) on yeasts.

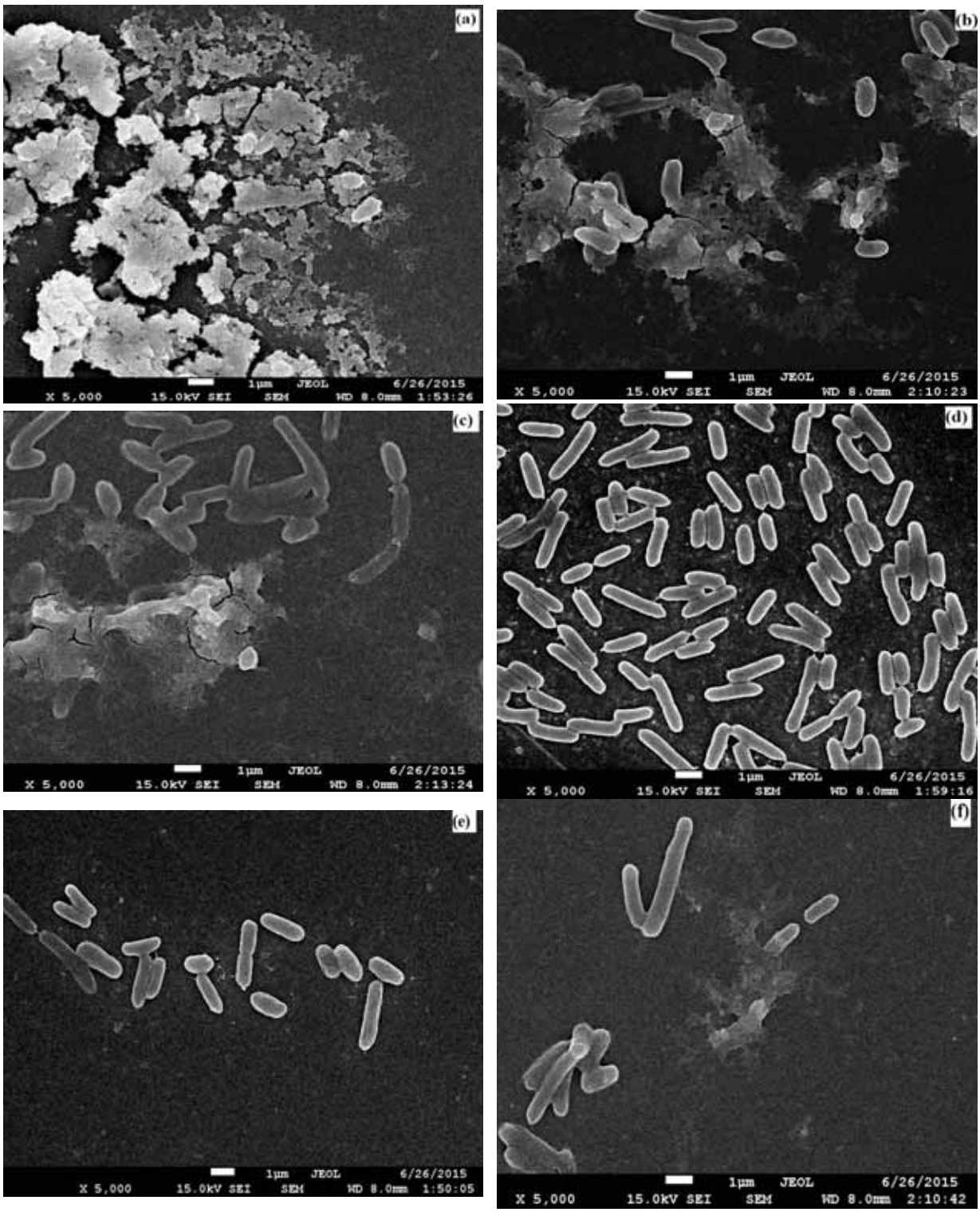


FIGURE 4
SEM images of effect of some hexahydroimidazo [1,5-a] pyridinium bromides on *E.coli* (ATCC 8739) biofilm. (a) biofilm formation by *E.coli* (derivate-free control), (b) biofilm treated with 2, (c) biofilm treated with 3, (d) biofilm sample treated with 4, (e) biofilm treated with 6, (f) biofilm treated with 7; scale bar:1 µm

Anti-biofilm activity-based theraphies that not only attempt to eradicate bacteria but also affect the biofilm's community structure and communications may prove more effective than a single or sequential strategy such as antibiotic therapy. Furthermore, the employment of anti-biofilm agents may help

address the significant patient cost (in terms of morbidity and mortality) and financial burden imposed by infections caused by persistent biofilm-microorganisms.

For these reasons, our research focus has been on anti-biofilm activity of benzyl substituted hexahydroimidazo[1,5-a] pyridinium bromides. The results show that tested microorganisms was susceptible in biofilm forms. They indicate that the imidazolinium, benzimidazolium and tetrahydropyrimidinium salts (1-9) and their metal complexes possess remarkable anti-biofilm activity and are effective against biofilm populations (sessile) of tested microorganisms. In this work, 1-9 shows superior characters as anti-biofilm effect and antioxidant property. Therefore, these groups may be new sources of anti-biofilm agents and antioxidants with potential value for therapeutics. They should be explored further as a means to control biofilm-associated infections caused by pathogens.

ACKNOWLEDGEMENTS

The authors declare no conflict of interest.

REFERENCES

[1] Høiby, N., Ciofu, O., Johansen, H.K., Song, Z., Moser, C., Jensen, P.O., Molin, S., Givskov, M., Tolker-Nielsen, T., Bjarnsholt, T. (2011) The clinical impact of bacterial biofilms. Int J Oral Sci. 3, 55-65.

[2] Brooun, A., Liu, S.H., Lewis, K. (2000) A dose-response study of antibiotic resistance in *Pseudomonas aeruginosa* biofilms. Antimicrob Agents. 44, 640-646.

[3] Donlan, R.M. (2001) Biofilms and device-associated infections. Emerg Inf Dis. 7, 45-55.

[4] Augustin, M., Ali-Vehmas, T., Atroshi, F. (2004) Assessment of enzymatic cleaning agents and disinfectants against bacterial biofilms. J Pharm Pharmaceut Sci. 7(1), 55-65.

[5] Grant, D.M., Bott, T.R. (2005) Biocide dosing strategies for biofilm control. Heat Transfer Eng. 26(1), 44-50.

[6] Gorman, S.P., Jones, D.S. (1991) Biofilm complications of urinary tract devices, In: Wilson, M., Devine, D. (eds.): Medical Implications of Biofilms. Cambridge University Press, Cambridge, 136-170.

[7] Taylor, P.K., Yeung, A.T.Y., Hancock, R.E.W. (2014) Antibiotic resistance in *Pseudomonas aeruginosa* biofilms: Towards the development of novel anti-biofilm therapies. J Biotechnol. 191, 121-130.

[8] Costerton, W., Veeh, R., Shirtliff, M., Pasmore, M., Post, C., Ehrlich, G. (2003) The application of biofilm science to the study and control of chronic bacterial infections. J Clin Invest. 112, 1466–1477.

[9] Behlau, I., Michael, S. (2008) Gilmore microbial biofilms in ophthalmology and infectious disease. Arch Ophthalmol. 126(11), 1572-1581.

[10] Wolcott, R.D., Ehrlich, G.D. (2008) Biofilms and chronic infections. JAMA. 299(22), 2682-2684.

[11] Bjarnsholt, T., Jensen, P.Ø., Fiandaca, M.J., Pedersen, J., Hansen, C.R., Andersen, C.B., Pressler, T., Givskov, M., Høiby, N. (2009) *Pseudomonas aeruginosa* biofilms in the respiratory tract of cystic fibrosis patients. Pediatr Pulmonol. 44, 547-558.

[12] Singh, P.K., Schaefer, A.L., Parsek, M.R., Moninger, T.O., Welsh, M.J., Greenberg, E.P. (2000) Quorum-sensing signals indicate that cystic fibrosis lungs are infected with bacterial biofilms. Nature. 407, 762-764.

[13] Furlani, R.E., Yeagley, A.A., Melander, C. (2013) A flexible approach to 1,4-di-substituted 2-aminoimidazoles that inhibit and disperse biofilms and potentiate the effects of b-lactams against multi-drug resistant bacteria. Eur J Med Chem. 62, 59-70.

[14] Høiby, N., Bjarnsholt, T., Givskov, M., Molin, S., Ciofu, O. (2010) Antibiotic resistance of bacterial biofilms. Int J Antimicrob Agents. 35, 322-332.

[15] Fux, C.A., Stoodley, P., Hall-Stoodley, L., Costerton, J.W. (2003) Bacterial biofilms: a diagnostic and therapeutic challenge. Expert Rev Anti Infect Ther. 1(4), 667-83.

[16] Mohini, Y., Prasad, R.B.N., Karuna, M.S.L., Poornachandra, Y., Kumar, C.G. (2014) Synthesis, antimicrobial and anti-biofilm activities of novel Schiff base analogues derived from methyl-12-aminooctadec-9-enoate. Bioorg Med Chem Lett. 24, 5224-5227.

[17] El-Azizi, M., Rao, S., Kanchanapoom, T., Khardori, N. (2005) In vitro activity of vancomycin, quinupristin/dalfopristin, and linezolid against intact and disrupted biofilms of staphylococci. Ann Clin Microbiol Antimicrob. 7(4), 2.

[18] Flemming, H.C., Neu, T.R., Wozniak, D.J. (2007) The EPS matrix: the "house of biofilm cells". J Bacteriol. 189(22), 7945-7947.

[19] Tamura, A., Ara, T., Imamura, Y., Fujii, T., Wang, P.L. (2008) The effects of antibiotics on in vitro biofilm model of periodontal disease. Eur J Med Res. 13, 439-445.

[20] Ozdemir, G., Ceyhan, N. (2010) Efficacy of various biocides against biofilm bacteria isolated from cooling waters of a petrochemical industry. Asian J Chem. 22, 7393.

[21] Marcano, A., Ousmane, B., Thebault, P., Crétois, R., Marais, S., Duncan, A.C. (2015) Elucidation of innovative anti-biofilm materials Aracelys. Colloid Surface B. 136, 56-63.

[22] Balaban, N., Gov, Y., Bitler, A., Boelaert, J.R. (2003) Prevention of *Staphylococcus aureus* biofilm on dialysis catheters and adherence to human cells. Kidney Int. 63, 340-345.

[23] Balaban, N., Cirioni, O., Giacomett, A., Ghiselli, R., Braunstein, J.B., Silvestri, C., Mocchegiani, F., Saba, V., Scalise, G. (2007) Treatment of *Staphylococcus aureus* Biofilm Infection by the Quorum-Sensing Inhibitor RIP. Antimicrob Agents Ch. 51, 2226-2229.

[24] Beeton, M.L., Aldrich-Wright, J.R., Bolhuis, A. (2014) The antimicrobial and anti-biofilm activities of copper (II) complexes. J Inorg Biochem. 140, 167–172.

[25] Siddiqui, M.F., Rzechowicz, M., Oh, H.S., Saeidi, N., Hui, L.J., Winters, H., Fane, A.G., Chong, T.H. (2015) The efficacy of tannic acid in controlling biofouling by *Pseudomonas aeruginosa* is dependent on nutrient conditions and bacterial density. Int Biodeter Biodegr. 104, 74-82.

[26] Pan, B., Huang, R., Zheng, L., Chen, C., Han, S., Qu, D., Zhu, M., Wei, P. (2011) Thiazolidinone derivatives as novel anti-biofilm agents: Design, synthesis, biological evaluation, and structureeactivity relationships. Eur J Med Chem. 46, 819-824.

[27] Ye, Y., Fang, F., Li, Y. (2015) Synthesis and anti-biofilm activities of dihydro-pyrrol-2-one derivatives on *Pseudomonas aeruginosa.* Bioorg Med Chem Lett. 25, 597-601.

[28] De Luca, L. (2006) Naturally occurring and synthetic imidazoles: their chemistry and their biological activities, Curr Med Chem. 13, 1-23.

[29] Ozdemir, I., Denizci, A., Ozturk, H.T., Çetinkaya, B. (2004) Synthetic and antimicrobial studies on new gold(I) complexes of imidazolidin-2-ylidenes., mAppl. Organometal. Chem. 18, 318-322.

[30] Díez-González, S., Marion, N., Nolan, S.P. (2009) N-Heterocyclic carbenes in late transition metals catalysis. Chem. Rev. 109, 3612-3676.

[31] Hindi, K.M., Siciliano, T.J., Durmus, S., Panzner, M.J., Medvetz, D.A., Reddy, D.V., Hogue, L.A., Hovis, C.E., Hilliard, J.K., Mallet, R.J., Tessier, C.A., Cannon, C.L., Youngs, W.L. (2008) Synthesis, stability, and antimicrobial studies of electronically tuned silver acetate N-heterocyclic carbenes. J. Med. Chem. 51, 1577-1583.

[32] Hindi, K.M., Panzner, M.J., Tessier, C.A., Cannon, C.L., Youngs, W.J. (2009) The medicinal applications of imidazolium carbene-metal complexes. Chem. Rev. 109, 3859-3884.

[33] Latala, A., Nedzi, M., Stepnowski, P. (2009) Toxicity of imidazolium and pyridinium based ionic liquids towards algae. *Chlorella vulgaris, Oocystis submarina* (green algae) and *Cyclotella meneghiniana, Skeletonema marinoi* (diatoms). Green Chem. 11, 1371-1376.

[34] Petkovic, M., Ferguson, J., Bohn, A., Trindade, J., Martins, I., Carvalho, M.B., Leitao, M.C., Rodrigues, C., Garcia, H., Ferreira, R., Seddon, K.R., Rebeloa, L.P.N., Pereira, C.S. (2009) Exploring fungal activity in the presence of ionic liquids. Green Chem. 11, 889.

[35] Garg, G., Chauhan, G.S., Gupta, R., Ahn. JH. (2010) Anion effects on anti-microbial activity of poly[1-vinyl-3-(2-sulfoethyl imidazolium betaine)]. J. Colloid Interf. Sci. 344, 90-96.

[36] Smith, K., Hunter, I.S. (2008) Efficacy of common hospital biocides with biofilms of multi-drug resistant clinical isolates. J Med Microbiol. 57, 966-973.

[37] Bandara, H.M.,Yau, J.Y., Watt, R.M., Jin, L.J., Samaranayake, L.P. (2009) *Escherichia coli* and its lipopolysaccharide modulate in vitro *Candida* biofilm formation. J Med Microbiol. 58, 1623-1631.

[38] Hou, S., Zhou, C., Liu, Z., Young, A.W., Shi Z., Ren, D., Kallenbach, N.R. (2009) Antimicrobial dendrimer active against *Escherichia coli* biofilms. Bioorg Med Chem Lett. 19(18), 5478-5481.

[39] Türkmen, H., Ceyhan, N., Yavaşoğlu, N.Ü.K., Özdemir, G., Çetinkaya, B. (2011) Synthesis and antimicrobial activities of hexahydroimidazo [1,5-a] pyridinium bromides with varying benzyl substituents. Eur J Med Chem. 46, 2895-2900.

[40] Türkmen, H., Pape, T., Hahn, F.E., Çetinkaya, B. (2008) Annulated N-heterocyclic carbene ligands derived from 2-methylaminopiperidine: Their complexes and catalytic applications. Organometallics. 27(4), 571-575.

[41] Türkmen, H., Can, R., Çetinkaya, B. (2009) Mono-, bis- and tris-piperidine fused imidazolinium salts: their *in situ* catalytic applications for C-C bond formation in aqueous solutions. Appl. Organometal. Chem. 23, 365-369.

[42] Limsuwan, S., Voravuthikunchai, S.P. (2008) Boesenbergia pandurata (Roxb.) schltr., *Eleutherine americana* merr. and *Rhodomyrtus tomentosa* (Aiton) Hassk. as antibiofilm producing and antiquorum sensing in *Streptococcus pyogenes.* FEMS Immunol Med Microbiol. 5, 429-436.

[43] Thenmozhi, R., Nithyanand, P., Rathna, J., Pandian, S.K. (2009) Antibiofilm activity of coral-associated bacteria against different clinical M serotypes of *Streptococcus pyogenes*. FEMS Immunol Med Microbiol. 57, 284-294.

[44] Nithyanand, P., Thenmozhi, R., Rathna, J., Pandian, S.K. (2010) Inhibition of *Streptococcus pyogenes* Biofilm Formation by Coral-Associated Actinomycetes. Curr Microbiol. 60. 454-460.
[45] Baldassarri, L., Creti, R., Recchia, S., Imperi, M., Facinelli, B., Giovanetti, E., Pataracchia, M., Alfarone, G., Orefic, G. (2006) Therapeutic failures of antibiotics used to treat macrolide-susceptible *Streptococcus pyogenes* infections may be due to biofilm formation. J Clin Microbiol. 44, 2721-2727.
[46] Bakkiyaraj, D., Pandian, S.K. (2010) In vitro and in vivo antibiofilm activity of a coral associated actinomycete against drug resistant *Staphylococcus aureus* biofilms. Biofouling. 26(6), 711-777.
[47] Lembke, C., Podbielski, A., Hidalgo-Grass, C., Jonas, L., Hanski, E., Kreikemeyer, B. (2006) Characterization of biofilm formation by clinically relevant serotypes of group A Streptococci. Appl Microbiol Biotechnol. 72, 2864-2875.
[48] Re, R., Pellegrini, N., Proteggente, A., Pannala, A., Yang, M., Rice-Evans, C. (1990) Antioxidant activity applying an improved ABTS radical cation decolorization assay. Free Radic Biol Med. 26, 1231-1237.
[49] Rossini, K., Noreña, C.P.Z., Olivera, F.C., Brandelli, A. (2009) Casein peptides with inhibitory activity on lipid oxidation in beef homogenates and mechanically deboned poultry meat. LWT Food Sci Tech. 42, 862-867.
[50] Pieniz, S., Andreazza, R., Anghinoni, T., Camargo, F., Brandelli, A. (2014) Probiotic potential, antimicrobial and antioxidant activities of *Enterococcus durans* strain LA18s. Food Control. 37, 251-256.
[51] Presterl, E., Grisold, A.J., Reichmann, S., Hirschl, A.M., Georgopoulos, A., Graninger, W. (2005) Viridans streptococci in endocarditis and neutropenic sepsis: biofilm formation and effects of antibiotics. J Antimicrob Chemother. 55, 45–50.
[52] Rosenberg, M., Kjelleberg, S. (1986) Hydrophobic interactions in bacterial adhesion. Adv Microb Ecol. 9, 353–393.
[53] Donlan, R.M. (2002) Biofilms: Microbial Life on Surfaces. Emerg Inf Dis. 8(9), 230-242.
[54] Beveridge, T.J. (1999) Structures of gram-negative cell walls and their derived membrane vesicles. J. Bacteriol. 181(16), 4725-4733.

Received: **31.05.2017**
Accepted: **28.09.2017**

CORRESPONDING AUTHOR

Nur Ceyhan-Guvensen
Mugla Sitki Kocman University
Faculty of Sciences
Department of Biology
48170, Mugla – Turkey

e-mail: nurceyhan@msn.com

© by PSP Volume 26 – No. 12A/2017 pages 7967-7973 Fresenius Environmental Bulletin

COMPRESSIVE PROPERTIES ANALYSIS FOR CONCRETE MATERIALS UNDER ACID-FREEZING RAIN ACTION

Yinlei Sun[1,2], Liansheng Tang [1,2,*]

[1]School of Earth Sciences and Engineering, Sun Yat-sen University, Guangzhou 510275, China
[2]Guangdong Provincial Key Laboratory of Mineral Resources and Geological Processes, Guangzhou 510275, China

ABSTRACT

Acid-Freezing rain is one of the most calamity weather phenomenon in Northeast China, it often occurs in early winter or late winter and early spring. In this paper, to investigate the mechanics property after the acid-freezing rain acting, different concrete grades with C15, C25 and C35 were prepared. The acid-freezing rain acting on the concrete was simulated in the laboratory conditions for 7d, 14d and 21d. With the triaxial rock mechanics testing machine, the compressive properties were investigated. The results showed that the surficial layers of the concretes were damaged under the acid-freezing rain and the compressive strength awfully decrease due to the intergranular suction losing.

KEYWORDS:
Acid-freezing rain, concrete, compressive property, intergranular suction

INTRODUCTION

Acid-freezing rain is one of the most calamity weather phenomenon in Northeast China, it often occurs in early winter or late winter and early spring [1]. Freezing rain is composited with super-cooled water droplets which are caused with the rain crashing the objects less than 0 °C [2]. In Northeast China, the waste gases from heating and industries are rich in sulfur dioxide and nitrogen oxides, which result in the pH value of the freezing rain less than 5.6. Concrete [3], as a common building material, is constituted with cement, granular aggregates, water and mineral admixtures [4]. Durability of concrete under acid-freezing rain action is of great importance to hydraulic structures in cold areas. The ice formation process in concrete pores was applied to evaluate the damages in concrete caused by freeze-thaw cycle [5]. The effect of sodium chloride solution, freeze–thaw cycling and externally applied load on the performance of concrete was experimentally investigated [6]. The behaviors of strength and deformation of plain concrete under triaxial compressions after 0, 25, 50 and 75 cycles of freeze-thaw were experimentally studied with the static and dynamic triaxial experimental machine [7]. A series of tests designed to determine the specific role coarse aggregate had on the freeze-thaw durability of pervious concrete using the ASTM C666A procedure [8]. The effect of coupled deterioration by freeze–thaw, carbonation and chlorides on concrete service life was studied [9]. Overall, the literatures on the concrete in the cold region focus on the freeze–thaw cycle. As an important calamity weather, acid-freezing rain effecting on the concrete is payed less attention.

In this paper, different concrete grades with C15, C25 and C35 were prepared. The acid-freezing rain (pH=5.5) acting on the concrete was simulated in the laboratory conditions for 7d, 14d and 21d. With the triaxial rock mechanics testing machine, the compressive properties were investigated. Combined with SEM tests, the micro-structures were observed to reveal the failure mechanism.

MATERIALS AND METHOD

Materials. Portland cement (PC) produced in Set cement factory was used in this study. The chemical compositions of the PC are summarized in Table 1. Two groups of crushed stone aggregates with the size of 0-4 mm and 4-16 mm were used for concrete production. Maximum aggregate size was 16 mm. The specific gravities of the fine and coarse aggregates were 2.47 and 2.66, respectively. The absorption values of the fine and coarse aggregates were 2.6% and 0.56%, respectively. The mixing water was tap water. The admixture was silicate concrete enhancer. Three groups of cubic concrete specimens, with C15, C25, C35 grade, were prepared respectively. The mixing proportion of concrete were summarized in Table 2. After an appropriate casting procedure, the concretes were placed in a room at 20℃ for primary curing for 28d. To guarantee accuracy of the compressive tests, the length error of the pressure-bearing surface was less than 1mm, the angle error between the proximal surfaces was less than 0.5 °. To observe the compressive tests conveniently, three lines were labelled on the surface of concrete.

TABLE 1
Chemical compositions of the PC

Component (%)	CaO	SiO_2	Al_2O_3	Fe_2O_3	MgO	SO_3	K_2O	Na_2O	LOI	Insoluble residue
PC	60.55	21.42	3.61	5.32	4.76	2.28	0.59	0.32	0.64	0.51

TABLE 2
Mixing proportion of concrete

Strength grade	Cement (kg/m^3)	Fly-ash (kg/m^3)	Sand (kg/m^3)	Crushed stone (kg/m^3)	Water (kg/m^3)	Admixture (kg/m^3)
C15	200	100	838	1026	195	6.3
C25	275	80	790	1047	180	8.17
C35	335	90	725	1045	175	10.63

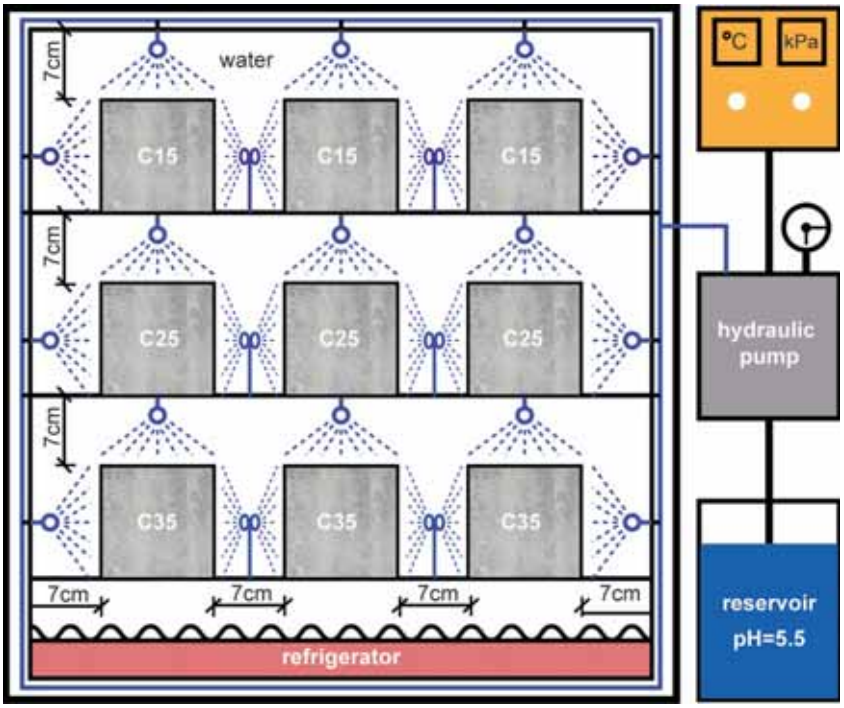


FIGURE 1
Acid-freezing rain simulated in the concrete rapid freezing and thawing chamber.

Method. The concrete rapid freezing and thawing chamber (DR-2B) was used for simulating the acid-freezing rain action. The minimum simulated temperature of the chamber was -40℃. The compressive tests were executed with the triaxial rock mechanics testing machine (RMT-150). The detailed experimental methods were shown as follows:

(1) The concretes were placed in a room at 20℃ for primary curing for 28d [10]. To guarantee accuracy of the compressive tests, the length error of the pressure-bearing surface was less than 1mm, the angle error between the proximal surfaces was less than 0.5°. To observe the compressive tests conveniently, three lines were labelled on the surface of concrete.

(2) The concrete samples were gently cleaned with dry cloth and rechecked for the sizes and flatness, then different groups of concretes were respectively moved into the freezing and thawing chamber. The space between the sample was 70mm and the distance from the inner surface of the chamber to the sample surface was 70mm. The temperature of the inner chamber was -20℃.

(3) The acid-freezing rain, with the pH 5.5, was deployed with the distilled water and sulfuric acid solution. To sure each face suffered the acid-freezing rain sufficiently, the sprinklers were used to simulate the rainfall (shown in Figure 1). The interval of the rainfall was two hours. Due to the cold experiment environment, the sprinklers were easily plugged by the ice. To pretest this phenomenon occurring, once the rainfall was simulated, the chamber was cut off.

And the rainfall was finished, the gas was continuously input to prevent none residual water. Finally, 15mm frozen layer covering the concrete surfaces (according to China Meteorological Administration issued in 2015, the thickness of the freezing rain was 10 ~ 20mm) was formed by acid-freezing rain. The freezing time were respectively designed with 0d, 7d, 14d and 21d.

(4) Due to the thickness of the ice was far less than concrete, the ability of ice under the compression was neglected. Before compressive test, the concretes were immersed in the water (18 ~ 20℃) for ten minutes to thaw the surficial ice to ensure the surface smooth. Then the samples were cleaned with the dry cloth, and rechecked the aspects. Once the precisions of the concretes were not reaching the standard (the length error of the pressure-bearing surface was less than 1mm, the angle error between the proximal surfaces was less than 0.5 °), the concretes must be discarded. Then the butter was smear on the compressive surface to decrease the friction.

(5) The PVC plastic, cohered on the compressive surface of concrete with butter, was used for decreasing the friction. The pretesting speed was set as 0.2kN/s with the preload 5kN. Then the compression increased with the loading speed 0.03mn /s. Once the concrete was destroyed, the machine was turned off. During the compressive procedure, the data were collected with computer. The compressive tests were performed with the triaxial rock mechanics testing machine shown in Figure 2. And the typical samples for X-ray scanning were collected with drilling apparatus and scanned at Shanghai Synchrotron Radiation Facility (SSRF) in China [11, 12].

RESULTS AND DISCUSSIONS

Loss Ratio of The Mass. The loss ratio of the mass before and after acid-freezing rain action were contrastively analyzed in Figure 3. For the action time less than 14d, the loss ratio of the C15 ~ C35 were escalating trend. Once the action time more than 14d, the loss ratio of C15 concrete presented moderating trend but escalating trend for C25 and C35. For the action time 7d, the loss ratio of the mass, almost same for C15 and C35, was larger than C25. When the action time was not less than 7d, the loss ratio of C35 concrete was less than C15, but larger than C25. And the water-cement ratio of C35 was less than C25. The free water was decreasing with the hydration reacting, which resulted in the plasticity of cement losing. Due to the hydration products increasing, the pores between particles were gradually filled and the gel was mixed with the crystal of the hydration products, which impelled the cement with certain strength into hardening stage.

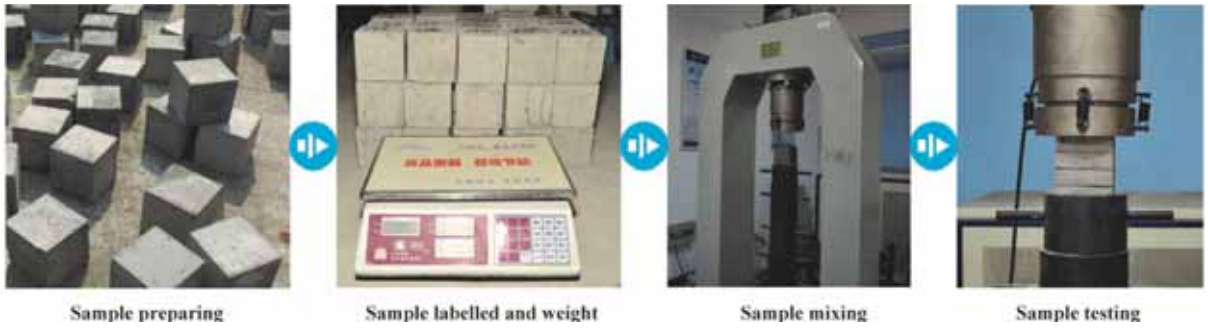


FIGURE 2
Compressive test procedure.

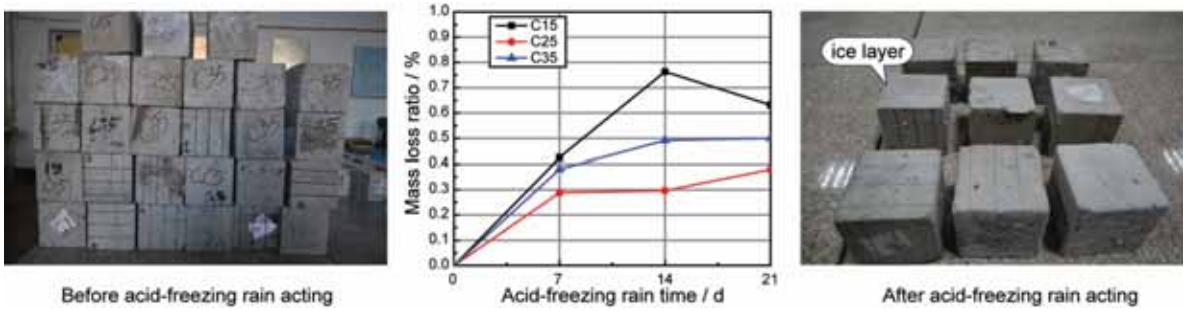


FIGURE 3
The relationship between mass loss rate and acid-freezing rain action time.

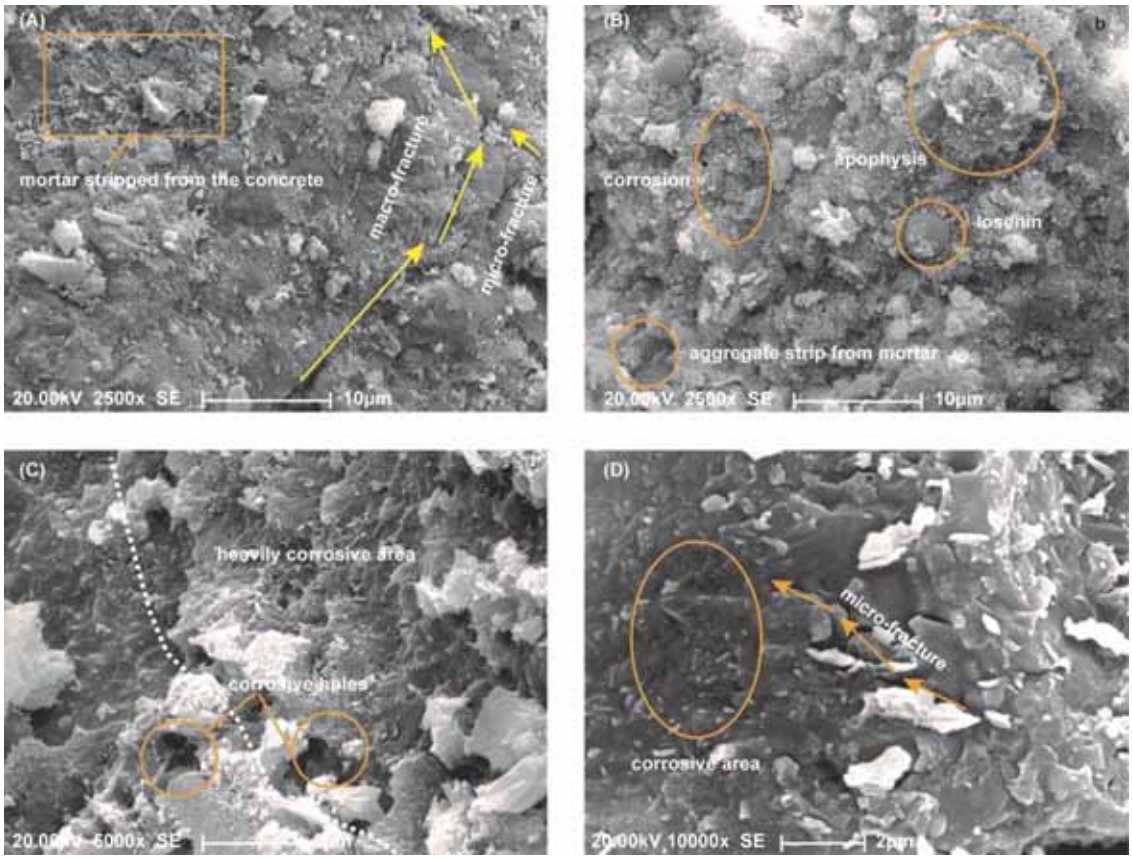


FIGURE 4
SEM tests for the typical samples.

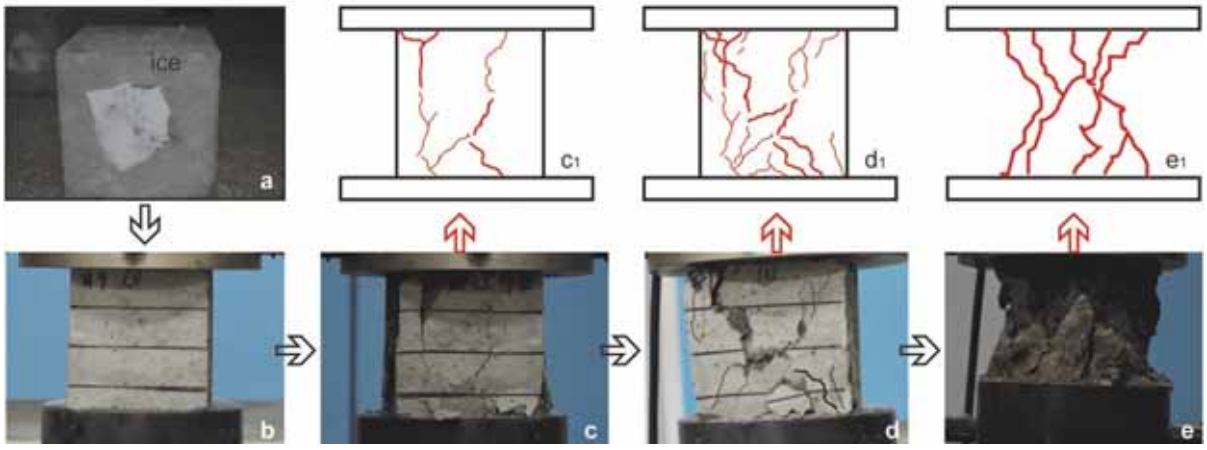


FIGURE 5
The failure process under the compressive test and the binary images of the fractures.

Test Phenomenon. After the action of freezing rain, an ice layer was formed and four obvious macro-changes including erosion, layered damage, aggregate and mortar separating, micro-fracture were observed on the concrete surfaces. In other words, the surface layer was damaged and the aggregates peeled off the concrete under the acid-freezing action. Lots of alveolate micro-holes were observed on the surfaces of the concretes, which were corroded by the sulfuric acid solution. The loosening phenomenon of aggregates appeared in the surficial layer. With the effect time increasing, the flake phenomenon aggravated gradually. For 7d freezing rain action, a few mortar on the surface stripped from the C15 concrete. Once the effect time reached to 14d, the aggregates distinctly stripped from the mortar.

As the time increasing continuously, the micro-fractures appeared in the coupling places between mortar and aggregates (near the macro-fractures), which were mainly caused by the critical water and ice. Once the surficial water frozen into ice, the expanding volume impelled the critical water transferring. The fatigue stress generated with the hydrostatic pressure and seepage pressure jointly effecting. When the fatigue stress was larger than the maximum adhesion stress of the coupling place, the micro-pores and -fractures were increasing and extending, which resulted in the aggregates separating from the mortar and the mortar stripping phenomenon. With the SEM test of surficial concrete, the micro- and macro-fractures, aggregates stripping from mortar phenomenon were observed in Figure 4.

During the compressive test, new fractures appeared near the block corners observed from the side view with the internal stress increasing shown in Figure 5. And the fractures, appeared in the middle block of the vertical direction, developed from the middle to the upper and lower corners of the concrete block. The core concrete, under the triaxial compression state, could suffer certain pressures in the incipient stage. But the ability disappeared as soon as the cross section and the horizontal constraining force of the concrete decreasing. With the compressive stress increasing, more fractures developed towards the inner. And lots of apophysis of the side surfaces and stripping phenomenon were observed obviously. Finally, an infundibular shape formed with two forward and reverse centrums shown in Figure 5. The adhesive failure modes were mainly observed between the coarse aggregates and cements. With the concrete grade increasing to C35, a small part of split course aggregate were observed.

Morphology Analysis. The typical concrete samples were analyzed with X-ray computed tomography method, which was performed with X-ray imaging and biomedical application beam line (BL13W1) at Shanghai Synchrotron Radiation Facility (SSRF) in China. And Six 10-cm diameter specimens of cylindrical concrete were investigated with the spatial resolution of 6.25μm. To obviously observe the morphology of concrete, six typical crossing sections were analyzed. The images shown the internal structures composed of aggregates (dark blue), cement (red) and gas (white), shown in Figure 6. The images before compressive tests indicated that some tiny holes existed in the volume and the aggregates were more large. The aggregates present rounded shapes. But the images after compressive tests indicated that more holes and fragments existed in the volumes. With the concrete strength increasing, the porosity of the bulk decreased and the aggregates were more and more large (more integrated). For the C15 concrete, the pores existed near the aggregates and the shapes of the aggregates were angular, which indicated that the compressive destruction often crossed through the aggregates. But for the C35 concrete, the pores often existed in the cement, which indicated that the cracks often be along the aggregates.

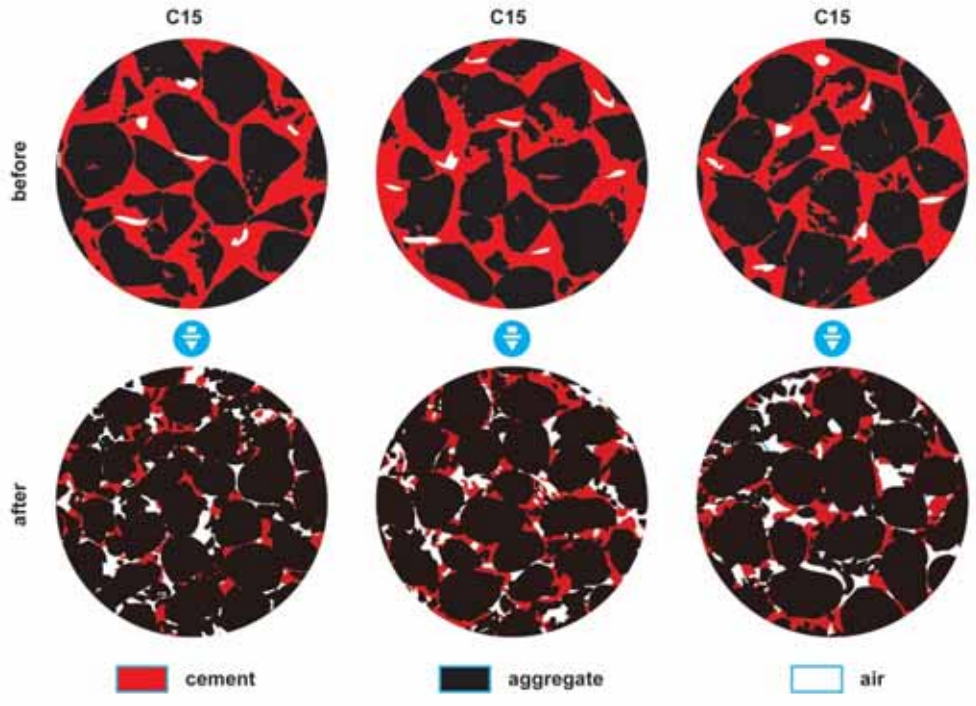


FIGURE 6
The crossing images for the concrete samples before and after compressive tests.

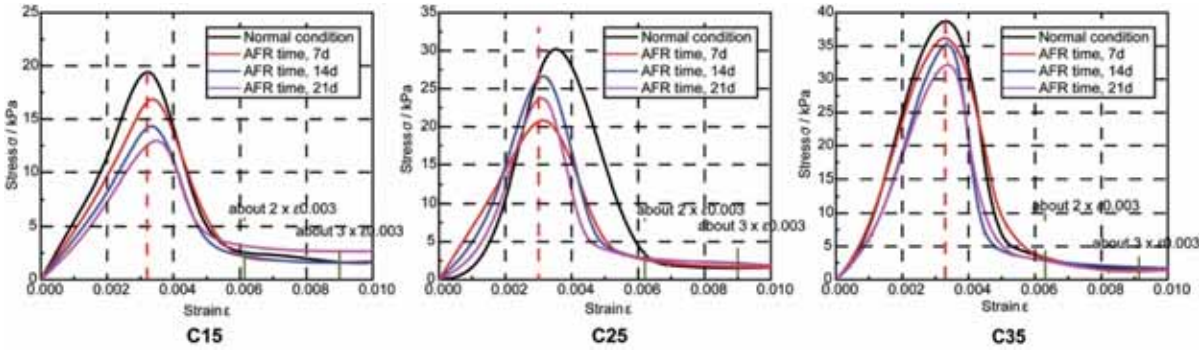


FIGURE 7
Stress-strain in different acid-freezing acting time, acid-freezing rain is abbreviated to AFR.

Compressive Strength. Figure 7 shows that the stress-strain relations in different acid-freezing acting time. For the 7d freezing rain action, the compressive strength of the C15, C25 and C35 concretes were decreasing respectively with 10%, 9% and 7% compared with the concrete without suffered freezing rain action. With the action time increasing, the decreasing ranges of the compressive strength were accordingly increasing, i.e. for 14d with 16%, 14%, 12% and for 21d with 26%, 22%, 16%. The different decreasing degrees shown that the compressive strength after acid-freezing rain action were related to the concrete grade and the action time. With the concrete grade increasing, the action under the freezing rain was weakening. And the loss of the compressive strength was increasing with the action time increasing. For the same grade concrete, the attenuation rate of the compressive strength was gradually decreasing with the action time increasing. But for the same action time of the acid-freezing rain, the attenuation rate of the compressive strength was gradually decreasing with the concrete grade increasing.

Shown in Figure 7, the increasing ratios of stress for normal condition and action time 7d were larger than 14d and 21d. The main reason was that the strength of the concrete was enhanced for long action time of freezing rain. The stress reached the maximum when the strain was about 0.003. The peak stress of C15 concretes acted for 0, 7, 14 and 21d were respectively 19MPa, 17MPa, 16MPa and 14MPa. In other words, the peak stress present decline trend. For the 21d action time, the decrease of peak stress was 25% of the normal condition. With the concrete grade increasing, the decreasing percentage of the peak stresses became gradually lower, i.e. the decreasing percentages were respectively 25%, 20%, 15% for the action time 21d. With the test proceeding, the compressive strength present moderating trend. If the strain was twice of the peak stress, the residual stress tend to be minimum. Figure 7 showed that the residual stress of the concrete acted freezing rain for 21d was equal to 7d and normal condition but larger than 14d. With the strain increasing, the residual stress of 21d was larger than other conditions. But for C25 and C35 concretes, the residual stresses for different conditions were almost same.

The whole variation tendency indicated that the compressive strength under the acid-freezing rain was far less than that in normal condition. In this study, the fly-ash and others small particle materials was mixed into the concrete to improve the pore structures and decrease the proportion of the macro-pores. Meanwhile, the micro-pores of the cement paste increased awfully. And the pores between the hydration products were filled with the small particle materials. With the hydration reaction continuing, the internals spaces originally occupied by the water were eventually formed into the interconnected pores. As the concrete grade increasing, the hardening rate was accordingly increasing. The water in the concrete was frozen into ice, which resulted in the intergranular suction between particles decreasing [13, 14]. As the main component of intergranular suction, the structure suctions, developed by the cementing force, were damaged by the frost heave and acid erosion. And due to the interfanular suction decreasing, the appearances of holes and fractures naturally resulted in the stress paths breaking. Under the external load, the concrete block was more easily damaged than that in the normal condition. And the phenomenon was more obvious with the acid-freezing rain continuing.

CONCLUSIONS

For the action time of acid-freezing rain less than 14d, the loss ratio of the C15 ~ C35 were escalating trend. Once the action time more than 14d, the loss ratio of C15 concrete presented moderating trend but escalating trend for C25 and C35. Four obvious macro-changes including erosion, layered damage, aggregate and mortar separating, micro-fracture were observed on the concrete surfaces.

The fractures, appeared in the middle block of the vertical direction, developed from the middle to the upper and lower corners of the concrete block. The core concrete, under the triaxial compression state, could suffer certain pressures in the incipient stage. But the ability disappeared as soon as the cross section and the horizontal constraining force of the concrete decreasing. Lots of apophysis of the side surfaces and stripping phenomenon were observed obviously. An infundibular shape was finally formed with two forward and reverse centrums.

Due to the intergranular suction decreasing, the appearances of holes and fractures naturally result in the stress paths breaking. Under the external load, the concrete block was easier damaged than that in the normal condition. And the phenomenon was more obvious with the acid-freezing rain continuing.

ACKNOWLEDGEMENTS

The work presented in this paper is supported by the National Natural Science Foundation of China (41572277), the Natural Science Foundation of Guangdong Province, China (2015A030313118) and Science and Technology Program of Guangzhou, China (201607010023).

REFERENCES

[1] Fang, C. (2010) Analysis of formation of freezing rain on February 24, 2010 in Shenyang, Liaoning province. Journal of Meteorology and Environment, 26(6), 43-46.
[2] Bernstein, B.C. (2010) Regional and Local Influences on Freezing Drizzle, Freezing Rain, and Ice Pellet Events. Weather & Forecasting, 15(5), 485-508.
[3] Larssen, T., Lydersen, E., Tang, D., He, Y., Gao, J., Liu, H., Duan, L., Seip, H.M., Vogt, R.D., Mulder, J. (2006) Acid rain in China. Environ Sci Technol. 40(2), 418.
[4] Evangelista, L., Brito, J.D. (2016) Durability performance of concrete made with fine recycled concrete aggregates. Cement Concrete Comp. 32(1), 9-14.
[5] Cai, H., Liu, X. (1998) Freeze-thaw durability of concrete: ice formation process in pores. Cement & Concrete Research. 28(9), 1281-1287.
[6] Sun, W., Mu, R., Luo, X., Miao, C., Sun, W., Mu, R., Luo, X., Miao, C. (2002) Effect of chloride salt, freeze–thaw cycling and externally applied load on the performance of the concrete. Cement & Concrete Research, 32(12), 1859-1864.
[7] Shang, H.S., Song, Y.P., Qin, L.K. (2008) Experimental study on strength and deformation of plain concrete under triaxial compression after freeze-thaw cycles. Building & Environment, 43(7), 1197-1204.
[8] Kevern, J.T., Wang, K., Schaefer, V.R. (2010) Effect of Coarse Aggregate on the Freeze-Thaw Durability of Pervious Concrete. J Mater Civil Eng. 22(5), 469-475.
[9] Kuosa, H., Ferreira, R.M., Holt, E., Leivo, M., Vesikari, E. (2014) Effect of coupled deterioration by freeze–thaw, carbonation and chlorides on concrete service life. Cement Concrete Comp. 47(47), 32-40.
[10] Urquhart, L.C., O'Rourke, C.E., Winter, G. (2015) Design of concrete structures. McGraw-Hill.
[11] Chen, R.C., Dreossi, D., Mancini, L., Menk, R., Rigon, L., Xiao, T.Q., Longo, R. (2012) PITRE: software for phase-sensitive X-ray image processing and tomography reconstruction. J Synchrotron Radiat. 19(Pt 5), 836-845.
[12] Liu, J., Pereira, G.G., Regenauer-Lieb, K. (2014) From characterisation of pore-structures to simulations of pore-scale fluid flow and the upscaling of permeability using microtomography: A case study of heterogeneous carbonates. J Geochem Explor. 144(5), 84-96.
[13] Tang, L., Sang, H., Deng, X. (2014) Experimental study on cementation strength of unsaturated granite residual soil. Paper presented at the 4th International Conference on Green Building, Materials and Civil Engineering, Hong Kong.
[14] Tang, L. (2001) New suggestion on shear strength in unsaturated soil based on suction between grains. Chinese Journal of Geotechnical Engineering. 23(4), 412-417.

Received: **01.06.2017**
Accepted: **17.10.2017**

CORRESPONDING AUTHOR

Liansheng Tang
School of Earth Sciences and Engineering,
Sun Yat-sen University,
No. 135 Xingang Xi Road,
Guangzhou 510275 – P.R. China

e-mail: eestls@mail.sysu.edu.cn

© by PSP Volume 26 – No. 12A/2017 pages 7974-7980 Fresenius Environmental Bulletin

EFFECT OF DIFFERENT WAVELENGTHS OF LIGHT ON GROWTH, PIGMENT CONTENT AND PROTEIN AMOUNT OF *CHLORELLA VULGARIS*

Gokce Kendirlioglu, A Kadri Cetin*

Department of Biology, Faculty of Science, Firat University, 23119 Elazig, Turkey

ABSTRACT

Algae constitute the main source of materials that can be used as raw materials for many high-value bioproducts, the most prominent ones of which are vitamins, lipids, chlorophyll and carotenoids. The key to economic production of biomass and bioproducts from microalgae is to optimize their growth conditions. Microalgae require optimal lighting conditions for efficient photosynthesis. Photoperiod, light intensity and wavelength of light are some of the important factors affecting the rate of photosynthesis. Light conditions directly affect the growth, pigment content and protein amount in microalgae. The aim of this study is to show the effects of light wavelength on growth, pigment content and protein amount in *Chlorella vulgaris*. Different wavelengths of light (blue, green, red and white light) were used to test their effects on growth, pigment content and protein amount in *Chlorella vulgaris*. The results show that the highest growth and amount of protein in *Chlorella vulgaris* were in cultures illuminated with red light. The amounts of chlorophyll and astaxanthin reached their highest values under different lights. The highest amounts of chlorophyll a and chlorophyll b were observed in cultures illuminated with green light while the highest amount of astaxanthin was observed in cultures illuminated with blue light.

KEYWORDS:
Chlorella vulgaris, wavelength, chlorophylls, astaxanthin, protein

INTRODUCTION

Algae are important organisms in that they are the basic producers of photosynthetic and organic materials which can be primitive, single cell or multicellular. They convert light energy into chemical energy during photosynthesis. Algae store energy in the form of starch and carbohydrate (complex sugar) as a result of photosynthesis [1]. Today, microalgae have become a focal point of attention in biotechnological studies aimed at using them as a renewable source of energy to overcome environmental problems caused by fossil fuels. Many algae biotechnologists have begun to investigate the mechanisms of photosynthesis of algal cells and to study the unique bioactive substances they produce such as various pigments, proteins, fatty acids and vitamins. Furthermore, microalgae are rich in oil content and their photosynthetic efficiency is much greater than that of terrestrial plants. Today, more than 40.000 microalgae have been identified by molecular and microscopic methods, and a significant portion of them have been found to have high lipid content. Oil content in microalgae generally ranges from 20 to 50% and makes up about 80% by weight of dry biomass in some species. Consequently, the biotechnological use of microalgae biomass for biofuel production has been increasing in recent years [2-6]. Microalgae undergo morphological and biochemical changes as a survival strategy under extraordinary conditions such as nutrient deficiency, high light intensity or high salt concentration. High levels of lipid accumulation have been found in microalgae grown under stress conditions, while significant biomass increases have been achieved with high growth rates [7]. Several studies have investigated how to achieve an increase in growth rate in various algae species [1, 8-10].

As with all plants, microalgae produce their own food by photosynthesis and form the basic nutrients of organisms that feed on them. It is known that microalgae are traditionally used in aquaculture as the main source of food for fish, some crustacean larvae and juvenile bivalves. Being of widespread occurrence, algae are affected by various external and internal factors. Light is the most important factor affecting autotrophic growth and photosynthetic activity of algae [1]. Since light is the source of energy that directs photosynthesis, intensity and wavelength of light and photoperiod play an important role in increasing biomass efficiency of microalgae. Natural light or fluorescent light bulbs are used as sources of light in microalgae cultures. However, high intensity of light leads to photo-inhibition and photooxidation, while low intensity of light is a major growth-limiting factor. For this reason, intensity and wavelength of light, at which microalgae growth becomes saturated in cultures, are important factors in determining the efficiency of use of light [11].

It is known that different growth media and different wavelengths of light are required for the growth of different algal species. Generally, microalgae use wavelengths ranging from 400 to 700 nm for photosynthesis. The wavelength of light absorbed by microalgae differs among species [12]. The determination of the optimum wavelength of light for the growth of microalgae is one of the basic parameters to be investigated. The use of sunlight has an excellent effect on algal growth. However, changes in weather conditions adversely affect the growth of microalgae. Artificial sources of light are widely used in microalgae cultures to increase efficiency and to meet energy needs under controlled conditions. Intensity and wavelength of light are two of the most important parameters in microalgal growth. Microalgae require optimal lighting conditions to reach the maximum rate of photosynthesis [13].

The green alga, *Chlorella vulgaris*, is an important member of the food chain in aquatic habitats, and its role in aquaculture is increasing day by day. Becoming an alternative source of protein, *C. vulgaris* is also an important natural resource for the production of vitamins, lipids, chlorophyll and carotenoids. Like other microalgae, the nutritive quality, protein, fatty acid, and pigment of *C. vulgaris* are affected by light [14].

Many studies have shown that the biochemical compositions of microalgae can be altered by some interventions in the growing environment. Light is one of the most important factors that affect the growth of microalgae. Effects of photoperiod, intensity and wavelength both on the growth and bioactive compounds of microalgae are investigated. This study investigated the effects of different wavelengths of light on the biomass, pigment content and protein content of *Chlorella vulgaris*.

MATERIALS AND METHODS

Microalgae cultures. *Chlorella vulgaris* was cultivated in Jaworski's medium which was composed of distilled water and such chemical ingredients as $Ca(NO_3)_2.4H_2O$, KH_2PO_4, $MgSO_4.7H_2O$, $NaHCO_3$, EDTA FeNa, EDTA Na_2, H_3BO_3, $MnCl_2.4H_2O$, $(NH_4)6Mo_7O_2H_2O$, $NaNO_3$, Na_2HPO_4., cyanocobalamin, thiamine and biotin. The culture medium was sterilized at 121 °C and an atmospheric pressure of 1 for 15 min.

Chlorella vulgaris was inoculated into 250-mL Erlenmeyer flasks containing 100 mL of liquid nutrient medium. The Erlenmeyer flasks were incubated in a climate cabinet at 23 ±1 °C under a 16h light/8h dark regime. Having been taken from the cultures that reached a certain density, 10-mL samples were inoculated into Erlenmeyer flasks illuminated with white (380-730 nm) (control), red (625-740 nm), green (500-565 nm) and blue light (440-485 nm), and left to grow at 23 ±1 °C under a 16h light/8h dark regime for 10 days.

Determination of Cell Number. The number of algal cells was calculated by measuring the optical density at 680 nm using a visible density spectrophotometer. A standard curve relating to optical density was produced, which was subsequently used to calculate the number of individuals based on their optical density. The calculated number (as the average of three experiments) was used to construct growth curves. The relationship curve between OD 680 and cell number was plotted, and the cell number was obtained by regression.

Determination of Protein Amount. Lowry (1951) method was used for total protein analysis. Based on this method, 0.1-mL DOC solution was added in a 1-mL sample and the sample was kept at room temperature for 10 min. Afterwards, 0.1-mL TCA was added in the sample which was, then, centrifuged at 7500 rpm for 10 min. Following the removal of the supernatant, 1-mL Lowry solution was added in the precipitate and the precipitate was kept at room temperature for 20 min. Later on, 1-mL folin reagent was added in the sample, which was, then, kept for 30 min. Lastly, a standard curve was made by plotting absorbance at 750 nm and the results were evaluated based on the standard curve [15].

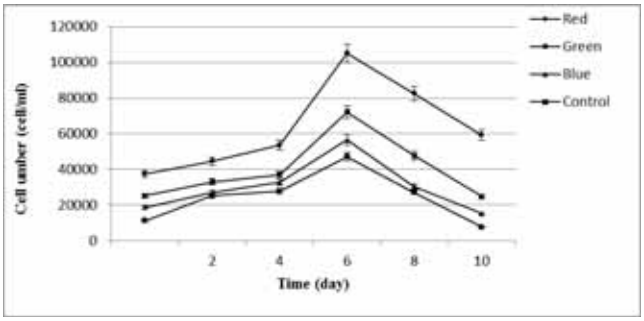


FIGURE 1
Effect of different wavelengths of light on cell number of *Chlorella vulgaris*

Determination of Pigment Content. The amount of chlorophyll was measured using the method of Strickland and Parsons [16]. A 5-mL culture was filtered through GF/C filter paper to determine the concentrations of pigment. Each filter paper was placed in 90% acetone at +4 °C, kept in the dark for 24 h, centrifuged at 3500 rpm for 5 min and analyzed for chlorophyll a and chlorophyll b by measuring the absorbances at 630, 645, 665 and 750 nm using a spectrophotometer.

The amount of astaxanthin was calculated using the method of Boussiba and Vonshak [17]. A 5-mL sample was taken from the culture media, centrifuged at 4000 rpm for 10 min to remove the supernatant, 30% methanol and 5% KOH were added in the precipitate and kept at 65 °C for 15 min to remove the chlorophyll. The supernatant in the tubes was decanted and the tubes were washed three times with distilled water. Then, 5-mL DMSO was added onto the precipitate and sonicated for 10 min (3.0 kHz). The samples were analyzed by calculating the amount of astaxanthin at 490 nm using a spectrophotometer [18].

RESULT AND DISCUSSION

Effect of different wavelengths of light on growth of *Chlorella vulgaris.* This study selected *Chlorella vulgaris*, a single-celled green algae, to investigate the effect of different wavelengths of light on growth of microalgae and investigated their growth characteristics in liquid cultures illuminated with different wavelengths of light; blue (450 nm), green (550 nm), red (660 nm) and white (400-700 nm). The results show that algal growth varies in cultures illuminated with different wavelengths of light. The growth of *Chlorella vulgaris* in liquid cultures was analyzed over a period of ten days and the results were presented in Figure 1. The results indicate that the number of cells, which was 11.000 cell/mL on the first day of inoculation, increased regularly until the sixth day. The maximum numbers of cells on day six were 105,122 cells/mL, 76.106 cell/mL, 54.472 cell/mL and 47.207 cell/mL in liquid cultures illuminated with red, white, blue and green light, respectively.

Subsequent measurements show that the number of cells decreased in all liquid cultures. Figure 1 demonstrates that the growth rate in cultures illuminated with red light was high while the growth rate in cultures illuminated with green light was low. It is stated that the number of cells largely depends on the wavelength of light and that the highest cell growth rate in *Chlorella vulgaris* is observed under red light while the lowest cell growth rate is observed under blue light. Furthermore, Kim et al. reported that the cell density of *C. vulgaris* grown under red light was 1.5 fold higher than under blue light following the first day of inoculation [19]. Wang et al. analyzed the growth rate of *Spirulina platensis* under red, blue, yellow and white light, and found that the highest growth rate occurred under red light, which is known to lead to an increase in the synthesis of organic matter and in the amount of chlorophyll and accelerate growth [20]. In this study, it has also been determined that the growth of *Chlorella vulgaris* under red light is significantly higher than in cultures illuminated with white, green and blue light. It is evident that illumination of *Chlorella* cultures with red light is one of the most effective ways to achieve maximum biomass.

Effect of different wavelengths of light on protein amount of *Chlorella vulgaris.* In photoautotrophic cultures, photons are one of the main sources of energy used by microalgae for the growth of cells, which is why the quality, intensity and wavelength of light are critical to the growth of microalgae. Photosynthesis, and consequently protein synthesis, in microalgae is controlled by light [20-22]. Proteins are the basic building blocks of living organisms. The composition of microalgae cells varies depending on the species, but mainly consists of protein, carbohydrate and lipid. To sustain cell growth, single-cell microalgae synthesize much more protein than carbohydrates and lipids under optimal growth conditions [23]. About 50% of the dry weight *of C. vulgaris* is composed of proteins. Figure 2 shows the changes in the protein content of *C. vulgaris* grown under different wavelengths of light. The amount of protein, which was 30 µg/mLon the first day of inoculation, increased in all cultures from day one and reached the maximum level on day six. The amounts of protein on day six were 266.04 µg/mL, 182.34 µg/mL, 124 µg/mL and 104.72 µg/mL in cultures illuminated with red, white (control), blue and green light, respectively (Fig. 2). Mohsenpour et al. state that the highest increase in protein in *Chlorella vulgaris* occurs under red light in the first five days and that light is one of the most important factors controlling the increase in protein [22].

Effect of different wavelengths of light on chlorophyll a and chlorophyll b and astaxanthin amounts of *C. vulgaris.* Figure 3 presents the variations in the amount of chlorophyll a of *C. vulgaris* illuminated with different wavelengths of light. The maximum values of chlorophyll a in cultures illuminated with white (control), green, blue and red light were obtained on day six. The maximum amount of chlorophyll a was measured as 0.241 mg/mL in cultures illuminated with green light. Chlorophyll a values in white, blue and red light on day six were 0.164 mg/mL, 0.118 mg/mL and 0.092 mg/mL, respectively. Having reached their highest values on day six at all wavelengths, the amounts of chlorophyll a decreased after day six. Figure 3 shows that the variations in the amounts of chlorophyll a were similar

in *C. vulgaris* illuminated with white, blue, green and red light and that the values of chlorophyll a showed an increase in the first six days followed by a decrease. However, it was also observed that the amount of chlorophyll a was always higher in *C. vulgaris* illuminated with green light than in those illuminated with other wavelengths.

Figure 4 demonstrates the variations in the amount of chlorophyll b of *C. vulgaris* cultures. The amounts of chlorophyll b in cultures illuminated with white, blue, green and red light increased and reached their maximum values from the first day of inoculation until the sixth day. The maximum value of chlorophyll b in cultures illuminated with green was the highest (0.187 mg/mL). The variations in the amounts of chlorophyll b were similar in cultures illuminated with four different lights and the lowest growth rate was observed in cultures illuminated with red (Fig. 4). The variations in the amounts of chlorophyll a and chlorophyll b were largely similar. Both photosynthetic pigments regularly increased from the first day of inoculation to the sixth day and reached their maximum values under different wavelengths of light. The amounts of chlorophyll a and chlorophyll b were always higher in cultures illuminated with green light than in those illuminated with white, blue and red light.

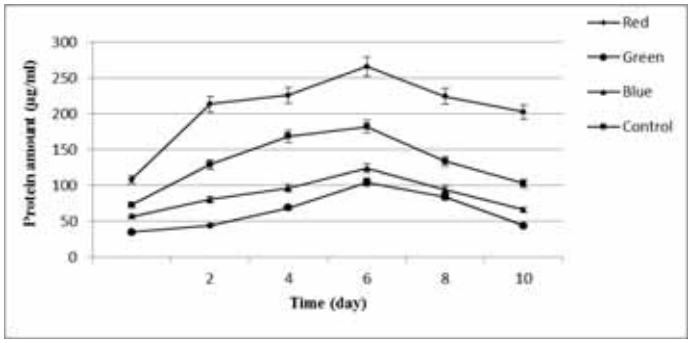


FIGURE 2
Effect of different wavelengths of light on protein amount of *Chlorella vulgaris*

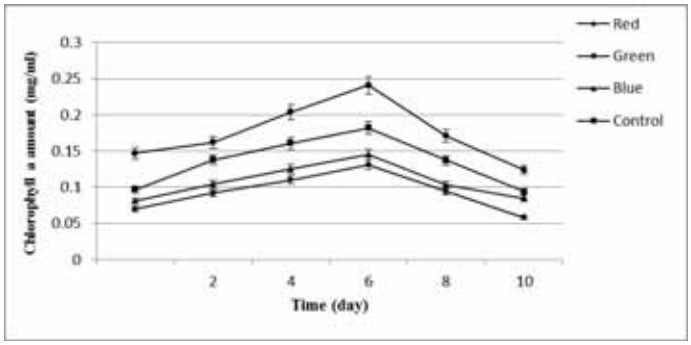


FIGURE 3
Effect of different wavelengths of light on chlorophyll a amount of *Chlorella vulgaris*

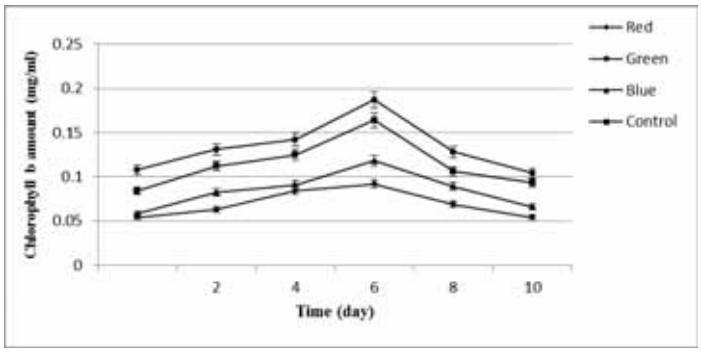


FIGURE 4
Effect of different wavelengths of light on chlorophyll b amount of *Chlorella vulgaris*

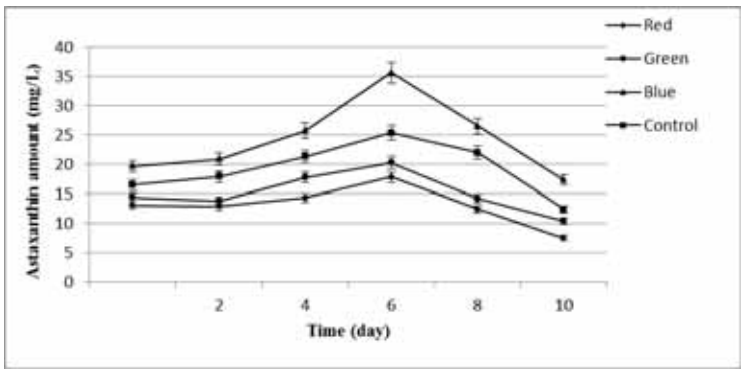


FIGURE 5
Effect of different wavelengths of light on astaxanthin amount of *Chlorella vulgaris*

Microalgae have a wide potential for valuable pharmaceuticals, pigments and other fine chemicals. Microalgae are important sources of pigments. One of the most important one is astaxanthin (3,3-dihydroxy-β,β-carotene-4,4′-dione), a red colored ketocarotenoid pigment, which is in growing demand in food and nutrition industry and cosmetics sector. Astaxanthin is a powerful coloring agent and an antioxidant. As with many biochemicals, there are some factors that affect the accumulation of pigments in the cell. These factors have been investigated by many studies [25-27]. Light is considered to be one of the most important factors playing a role in the accumulation of astaxanthin [26]. The quality, wavelength and emission spectra of light affect astaxanthin production as well as algal cultivation. For this reason, the amount of astaxanthin was found to be different in *Chlorella vulgaris* cultures illuminated with different wavelengths (Fig. 5). The amount of astaxanthin in *Chlorella vulgaris* cultures illuminated with different wavelengths of light increased until day six. However, the amount of astaxanthin was higher in cultures illuminated with blue light than in those illuminated with white, green and red (Fig. 5). The (maximum) amounts of astaxanthin at all wavelengths on day six were 35.65 mg/L under blue, 25.35 mg/L under white, 20.30 mg/L under green and 17.85 mg/L under red light. Previous works have shown that blue light stimulates astaxanthin accumulation [27, 28].

In conclusion, this study has shown that the optimal growth of *Chlorella vulgaris* occurred under red light. *Chlorella vulgaris* reached its maximum growth on day six and the growth rate was better under red light than under white (control), blue and green light. The highest numbers of cells on day six were 105,122 cells/mL under red, 76.106 cell/mL under white, 54.472 cell/mL under blue and 47.207 cell/mL under green light. The amount of protein was also higher in red light-illuminated cultures than in other cultures. The amounts of chlorophyll a and chlorophyll b were higher under green light than under others and maximal values were reached on day six. Unlike chlorophyll, astaxanthin showed maximum increase under blue light. It was concluded that wavelength of light has different effects on cell growth and protein amount, and that the increase in biomass and protein is better under red light; the increase in astaxanthin is better under blue light; and the increase in chlorophyll a and chlorophyll b pigment is better under green light.

CONCLUSION

Microalgae can produce a wide variety of valuable chemicals under photoautotrophic cultivation conditions. Light is the main source of energy under photoautotrophic cultivation conditions and inorganic carbon (such as CO_2) is used as a source of carbon. Photons are absorbed as nutrients by microalgae, which is why wavelength is very important for cell growth. The growth and protein, chlorophyll a, chlorophyll b and astaxanthin amounts of *Chlorella vulgaris* can be regulated by different wavelengths of light. The best light for cell growth and protein amount is red; for chlorophyll a and chlorophyll b green; and for astaxanthin amount blue. This study is important in terms of the selection of light at the appropriate wavelength to increase the amount of metabolite desired to be obtained in commercially produced cultures.

REFERENCES

[1] Singh, S.P. and Singh, P. (2015) Effect of temperature and light on the growth of algae species: A review. Renewable and Sustainable Energy Rewievs. 50, 431-444.
[2] Chisti, Y. (2007) Biodisel form microalgae, Biotechnol Adv.25, 294-306.
[3] Hu, Q., Sommerfeld, M., Jarvis, E., Ghirardi, M., Posewitz M., Seibert M. and Darzins, A. (2008) Microalgal triacylglycerols as feedstocks for biofuel production: perspectives and advances, Plant J. 54, 621-639.

[4] Meng, X., Yang, J., Xu, X., Zhang, L., Nie, Q. and Xian, M. (2009) Biodisel production from oleaginous microorganisms. Renew Energ. 34, 1-5.
[5] Bohola, V., Desikan, R., Santhos, S.K., Subburamu, K., Sanniyasi, E. and Bux, F. (2011) Effects of parameters affecting yield and thermal behaviour of *Chlorella vulgaris*. Journal of Biosicience and Biongineering. 111, 3, 377-382.
[6] Agirman, N. and Cetin, A.K. (2015) Effects of Nitrogen Starvations on Cell Growth, Protein and Lipid Amount of *Chlorella vulgaris*. Fresen. Environ. Bull. 24, 11, 3643-3648.
[7] Wu, H. and Miao, X. (2014) Biodisel quality and biochemical changes of microalgae Chlorella pyrenoidosa and *Scenedesmus obliquus* in response to nitrate levels. Bioresorce Technology. 170, 421-427.
[8] Chiu, S.Y., Kao, C.Y., Chen, C.H., Kuan, T.C., Ong, S.C. and Lin, C.S. (2008) Reduction of CO2 by high-density culture of Chlorella sp. In a semicontinuous photobioreactor. Biosource Technology. 99, 3389-3396.
[9] Liu, Z.Y., Wang, G.C. and Zhou, B.C. (2008) Effect of Iron on Growth and Lipid Accumulation in *Chlorella vulgaris*, Bioresource Technology. 99, 4717-4722.
[10] Yadavalli, R., Ramogapol, R.S. and Rao, C.S. (2012) Lipid Accumilation Studies in *Chlorella pyreniodosa* Using Customized Photobioreactor-Effect of Nitrogen Source, Light Intensity and Mode of Operatio. Int J Eng Research and Appl. 3, 2446-2453.
[11] Gammanpila, A.M., Rupasinghe, C.P. and Subasinghe, S. (2015) Light Intensity and Photo Period Effect on Growth and Lipid Accumilation of Microalgae Chlorella vulgaris and Nannochloropsis sp. for Biodisel Production. Proceedings of 12 th ISERD Tokyo Japan 26th.
[12] Blair, M.F., Kokabian, B. and Gude, V.G. (2014) Light and growth medium effect on Chlorella vulgaris biomass production. Journal of Environmental Chemical Engineering. 2, 665-674.
[13] Zhao, Y., Wang, J., Zhang, H., Yan, C. and Zhang, Y. (2013) Effects of various LED light wavelengths and intensities on microalgae-based simuitaneous biogas upgrading and digestate nutrient reduction process. Bioresource Technology. 136, 461-468.
[14] Seyfabadi, J., Ramezanpour, Z. and Khoeyi, Z.A. (2011) Protein, fatty acid, and pigment content of Chlorella vulgaris under different light regimes. J Apply Phycol. 23, 721-726.
[15] Lowry, O.H., Rosebrough, N.J., Farr, A.L. and Randall, R.J. (1951) Protein measurement with the folin phenol regent. J Biol Chem. 193, 265-75.
[16] Strickland, J.D.H. and Parsons, T.R. (1972) A practical handbook of seawater analysis, Fishery Research Board, Canada. 310p.
[17] Boussiba, S. and Vonshak, A. (1991) Astaxanthin accumulation in the green alga *Haematococcus pluvialis*. Plant Cell Physiol. 32, 1077–1082.
[18] Davies, B.H. (1976) Analysis of carotenoid pigments. In: Chemistry and Biochemistry of Plant pigments. Godwin, T.W. (ed.) Academic Pres, New York. Vol 2, 38-165.
[19] Kim, D.G., Lee, C., Park, S.M. and Choi, Y.E. (2014) Manuplation of light wavelength at appropriate growth stage to enhance biomass productivity and fatty acid methyl ester yield using *Chlorella vulgaris*. Bioresource Technology. 159, 240-248.
[20] Wang, C.Y., Fu, C.C. and Liu, Y.C. (2007) Effects of using light-emitting diyotes on the cultivation of *Spirulina platensis*. Biochemical Engineering Journal. 37, 21-25.
[21] Matthijs, H.C.P., Balke, H., Van Hes, U.M., Kron, B.M.A., Mur, L.R. and Binot, R.A. (1996) Application of Light-Emitting diyotes in Bioreactors: Flashing Light Effects and Energy Economy in Algal Culture (*Chlorella pyrenoidosa*), Biotechnology and Bioengineer-ing. 50, 98-107.
[22] Carvalho, A.P., Silva, S.O., Baptista, J.M. and Malcata, F.X. (2011) Light requirements in photobioreactors: an overview of biophotonic aspects. Appl Microbiol Biotechnol. 89,1275-1288.
[23] Mohsenpour, S.F., Richards, B. and Willoughby, N. (2012) Spectral conversion of light for enhanced microalgae growth rates and photosynthetic pigment production. Bioresource Technology. 125, 75-81.
[24] Das, P., Aziz, S.S. and Obbard, J.P. (2011) Two phase microalgae growth in the open system for enhanced lipid productivity. Renewable Energy. 36, 2524-2528.
[25] Mohsenpour, S.F. and Willoughby, N. (2013) Luminescent photobioreactor design for improved algal growth and photosynthetic pigment production through spectral conversion of light. Biosource Technology. 142, 147-153.
[26] Kim, Z.H., Kim, S.H., Lee, H.S. and Lee, C.G. (2006) Enhanced Production of Astaxanthin by flashing light using Haematococcus pluvialis. Enzyme and Microbial Technology. 39, 414-419.
[27] Katsuda, T., Lababpour, A., Shimahara, K. and Katoh, S. (2004) Astaxanthin production by *Haematococcus pluvialis* under illumination with LEDs. Enzyme and Microbial Technology. 35, 81-86.

[28] Lababpour, A., Hada, K., Shimahara, K., Katsuda, T. and Katoh, S. (2004) Effects of Nutrient Supply Methods and Illumination with Blue Light Emitting diyotes (LEDs) on Astaxanthin Production by *Haematococcus pluvialis*. Journal of Bioscience and Bioengineering. 6, 452-456.

Received: **05.06.2017**
Accepted: **21.09.2017**

CORRESPONDING AUTHOR

A Kadri Cetin
Department of Biology,
Faculty of Science,
Firat University,
23119 Elazig - Turkey

e-mail: akadricetin@gmail.com

© by PSP Volume 26 – No. 12A/2017 pages 7981-7991 Fresenius Environmental Bulletin

STUDY ON OLS CORRELATION ESTIMATION OF FARMERS' ENTHUSIASM FOR GRAIN PRODUCTION AND GRAIN PRODUCTION CIRCULATION UNDER THE BACKGROUND OF URBANIZATION CONSTRUCTION IN OLS

Bangxi Li*, Jingdong Luan

School of Economics and Management, Anhui Agricultural University

ABSTRACT

The issue of food security is an important economic issue in our country, and its stability is closely related to farmers' production enthusiasm. China is a populous country, and the population is growing rapidly, and the demand for food and food production needs more urgent. The country (or region) to achieve modernization is the only way for economic and social development in the inevitable phenomenon. Therefore, in the process of industrialization and urbanization, it will inevitably accompany by changes which is resulting in a series of economic and social problems. Under the background of urbanization in China, it is very important to improve the enthusiasm of farmers to ensure food security. This paper takes 1991~2015 years of China's grain production and production inputs data as the background which is based on the wide investigation, it also combined with the mathematical method of evaluation by using MATLAB to analyse of OLS correlation on the stage farmers' enthusiasm for growing grain and grain circulation. We point out the existing problems of food security problems and the corresponding solutions.

KEYWORDS:
Food safety, Enthusiasm of farmers, MATLAB, OLS correlation

INTRODUCTION

The key characteristics of China's agriculture and rural areas, that is, China's agriculture is the main livelihood of agriculture as the core of agriculture. Agriculture takes on a large number of social functions, which determines the characteristics of China's agricultural support as the characteristics of livelihood, compensation and non trade distortions [1- 3]. China's financial support for agriculture policy covers a very wide range, the "three rural" support policy is equivalent to the WTO agricultural support policy, which will overestimate China's agricultural domestic support level. With the rapid development of economy, Chinese for the "three rural" financial expenditure growth, but compared to the number of agricultural population, Chinese income level has multi functions of agriculture and social contribution which eliminates the need for two structures, the China level of support to the "three agriculture" is still low [4- 6]. Constantly strengthening and improving domestic agricultural support is not only important to ensure the healthy development of China's agriculture under the open conditions, but also to ensure the world's food security is very important. China's food policy has two basic objectives: China's food can get adequate supply and grain farmers to normalize their income. It is necessary to discuss what kind of food policy should be developed to achieve these two objectives. To enable farmers to produce adequate food, first of all we must study the conditions of efficient food production. These conditions are the basis for the development of food policy [7]. According to the modern agricultural technology and the practice of grain farming in developed countries, efficient food production should have the following characteristics: large-scale production, the use of modern agricultural science and technology, family farm business meets the land for long-term investment needs, the land can be relatively smooth to achieve the merger in order to achieve the scale of production, the remaining farmers can be more smoothly achieved with the separation of land and thus transferred to other industries, and therefore we can ensure that farmers get similar income with other occupations.

After the reform and opening up, China turns to focus on the grain production and circulation of the market transition. Until today, food production circulation also contains many elements of the planned economy, which includes state-owned grain enterprises in the circulation, and the companies still occupy the main channel status rather than all the flow of participants equal competition [8], the minimum grain purchase price and various subsidies rather than let market returns farmers, "rice bags" governor responsibility system rather than the

market mechanism to ensure food supply, the urban and rural separation of the household registration system used to farmers long-term rather than the farmers themselves choose [9- 11]. To sum up these institutional arrangements and policies, it is necessary to ensure that the area of cultivated land and grain acreage is enough to encourage farmers to plant grain. However, the previous analysis shows that all of these institutional arrangements with the colour of the planned economy will result in loss of efficiency [12]. The result is that there are still a large number of farmers who carry out inefficient grain farming on the small and shredded land, the low capital and human capital inputs for food production. The gap between the incomes of the long-term low-income urban residents is getting bigger and bigger, the relatively high quality talent in the countryside is lost, and the efficiency of grain production is much lower than that of the developed countries, so that it is increasingly difficult to participate in the international competition of grain. Theory and practice continue to remind us that we should change our thinking about China's food problems [13]. A noteworthy choice is used to take the road to market. The market-oriented road organized food production and circulation that we can guide the grain production and circulation of participants in an effective way to produce food and distributed to consumers. Whether marketability is feasible, it depends on the price signal which has the function of resource allocation, whether the market is effective which depends on the externalities of food production. If the grain production is not external market which is effective, there is no market failure.

In this paper, we will use econometric methods to study the above model. We use econometric methods to analyse the factors that affect the total grain output, as well as the relationship between farmer grain enthusiasm and grain production and circulation [14]. Grain production is a variable, and its increase and decrease and the number of sown areas have a lot of relevance. The use of fertilizers to increase the yield per unit area of crops, it is equivalent to the expansion of arable land area. China's rural population accounts for seventy percent of the total population of China, a very large number. It is a feature of China's agriculture which is labour-intensive in China's agricultural production [15, 16]. Now, the impact of agricultural labour on grain production can not be ignored. With the development of economy, the conditions of agricultural production improved significantly, the growth of agricultural machinery has been increasing rapidly, and the level of agricultural mechanization has been continuously improved. At this stage, agricultural production by the agricultural machinery to bear the work has accounted for more than forty percent of the impact on grain production which can not be underestimated [17]. In addition, floods and droughts are the main natural disasters of agriculture. For agriculture, irresistible natural forces have a great impact on grain production. Based on the data of fertilizer application, grain crop area and affected area in China from 1991 to 2015, this paper uses the econometric model to track the study, expecting to describe more accurately the influence of the three on the total agricultural grain in China, we can find out the extent influence of China 's total grain.

EXPERIMENTAL AND METHODS

The present situation of grain production in China. Prices and other interests of the signal significantly affect the enthusiasm of farmers to grow grain and agricultural production, at the same time there are positive and negative externalities, negative externalities are likely to exceed positive externalities. Agriculture is not generally considered to be weak, and the grain market is the market that is closest to the perfectly competitive model in the real world, and it is the one that does not require government intervention. Food production and circulation, including China's grain production and circulation, can be mainly through the market to organize and coordinate. How can China's grain production and circulation become market-oriented According to certain steps, the need for a set of institutional reforms can see results, which requires a market-oriented road map to determine the content of these policies and the implementation of the steps [18]. In order to abolish the urban and rural separation of the household registration system, the establishment of personal income tax declaration system helps to prepare for the reform. The abolition of urban and rural separation of the household registration system can also help to encourage farmers to migrant workers, and constantly reduce the farmers settled in the city to become ordinary citizens of the conditions. If the farmers have the conditions to settle in a city and apply for settlement, then within a certain range they have to sell its contract as a prerequisite [19, 20]. After the city has become an ordinary citizen, enjoy the social welfare of ordinary citizens. The implementation of income which is called “the minimum purchase price of grain policy” subsidies to farmers, in order to stabilize the income of farmers, so that food prices issued the correct signal. The reform of the grain circulation system allows all kinds of capital to enter, state-owned grain enterprises and other entered the capital equal competition, and we can also reduce the cost of circulation and improve the efficiency of circulation. If the state-owned grain enterprises can not survive and develop in the market competition, the restructuring is over. Promote the domestic food market and the international food market convergence which makes full use of the

international food market [21-23]. The international food prices may be a long time in the case of high, the use of market-oriented way helps to improve the income of farmers, and thus reduce the resistance to reform.

After the reform, China's grain production and the whole rural areas will show a new look, more and more farmers will be completely separated from the land, the process of urbanization will be greatly accelerated; with the increasing number of large farmers, the family farm began to scale With the expansion of the scale of the family farms, the agricultural production technology has been continuously improved, the farmers' agricultural human capital investment will get the normal return, the agronomy education and training will be fully developed, the quality of the farmers will be continuously improved, thus becoming a new professional Farmers, farmers will have a more substantial increase in income [24]. At this point, China's agriculture will have the embryonic form of modern agriculture.

It is unrealistic to try to keep the peasants' long-term stability in rural areas through the small peasant economy in order to maintain domestic political stability. China's agriculture, including food production, must take the road of marketization, although there are all kinds of problems and difficulties in adjustment, but we have no choice. China's agricultural accumulation of the problem is too much, already no way feasible, we can only face bravely [25-27]. At present, China's grain production and circulation problems are mainly concentrated in the following areas.

(1) Less arable land

The basic condition is inadequate arable land. Agricultural food science and technology did not make a fundamental breakthrough. Food acreage is still a decisive factor in the ever-increasing total grain output. With the rapid development of urbanization and industrialization, arable land occupation will continue to intensify. Can not be ignored is the land desertification, soil degradation, "three three waste" pollution and other issues. In recent years there is still a few million kilometres to reduce the number of cultivated land, and it is an important factor in China's grain production which is an important constraint.

(2) Water shortage and drought threat

China is a serious shortage of water in the world, the annual agricultural production of more than 20 billion cubic meters of water, and the distribution is very uneven, water and soil resources do not match. At the same time, drought in northern China is serious which causes desertification of arable land, a continuous reduction of arable land, and a shortage of water resources. In addition, in recent years, China's natural disasters are serious, adverse weather factors are more, the northern part of the precipitation duration is too small, and the drought trend is serious. Water shortage and drought have become the limiting factor in the production and production of major grain producing areas.

(3) Water pollution

Environmental and water pollution reduces the quality of food and agricultural products in China, pollution increases the shortage of water resources, leading to ecological fragility, drought and floods, but also it is affecting food production growth and reducing the effective supply of food.

(4) Poor and unemployed

In accordance with the concept of food security, we can ensure that everyone has food to eat, and this is easy to ensure that food security must pay attention to solve the problem.

(5) Frequent natural disasters

Especially in the western region of China, the ecological environment is poor, land ridge, drought, ice disaster, snowstorm, earthquake and flood occurred. The frequent occurrence of natural disasters, objectively irresistible reasons, exposed China's weak agricultural base. The problems of insufficient agricultural inputs are the factors that affect food security.

(6) Low efficiency of grain

In recent years, due to fertilizer, pesticides, agricultural diesel and other agricultural means of production costs, farmers have a substantial increase in the cost of grain farming, agricultural comparative benefits decline. With the rapid development of urbanization and industrialization in China, the number of migrant workers in rural areas increased, especially the young and middle - aged workers working in more than half of the main producing areas, the agricultural labour force showed structural shortage and the grain production appeared "sideline" trend [28]. Some local advocates "one county and one industry", "one village one product", vigorously adjust the agricultural industry structure, planting turmeric, flue-cured tobacco, *konjac*, oil, cotton, Chinese herbal medicine, mulberry, fruit trees and other cash crops. Compared with the cash crops, the benefits of grain production are obviously low, leading to the enthusiasm of farmers to grow grain is not high, to promote the steady development of grain production more difficult.

Sources of date. Food security is essential to national production, and food security issues are more important for food production and circulation. Food production depends on food production capacity, and food security is ultimately a matter of integrated food production capacity. The problem of comprehensive grain production capacity can be understood as economic growth. Economic growth factors can be divided into land, capital, technology, labour, system five categories [29]. According to food production $yield = acreage \times mu$, the

TABLE 1
Statistics of Total Grain Output and Production Factors (1991 - 2015)

Dates	Food production (Ten thousand tons)	Amount of agricultural fertilizer application (Million kilograms)	Grain sown area (Thousand hectares)	Disaster area (Ha)	General power of agricultural machinery (Million kilowatts)	Agricultural labor force (Million people)
1991	38728	1660	114047	16209	18022	31151
1992	40731	1740	112884	15264	19497	30868
1993	37911	1776	108845	22705	20913	31130
1994	39151	1931	110933	23656	22950	31254
1985	40208	1999	111268	20393	24836	31663
1996	39408	2142	110123	23945	26575	32249
1997	40755	2357	112205	24449	28067	33225
1998	44624	2590	113466	17819	28708	38914
1999	43529	2806	112314	27814	29389	39098
2000	44264	2930	110560	25895	30308	38699
2001	45649	3152	110509	23133	31817	37680
2002	44510	3318	109544	31383	33802	36628
2003	46662	3594	110060	22267	36118	35530
2004	50454	3828	112548	21233	38547	34820
2005	49417	3981	112912	30309	42016	34840
2006	51230	4084	113787	25181	45208	35177
2007	50839	4124	113161	26731	48996	35768
2008	46218	4146	108463	34374	52574	36043
2009	45264	4254	106080	31793	55172	36513
2004	45706	4339	103891	27319	57930	36870
2010	43070	4412	99410	32516	60387	36546
2011	46947	4637	101606	16297	64028	35269
2012	48402	4766	104278	19966	68398	33970
2013	49804	4928	104958	24632	72522	32561
2014	50160	5108	105638	25064	76590	31444
2015	50427	5224	106349	25512	79967	32318

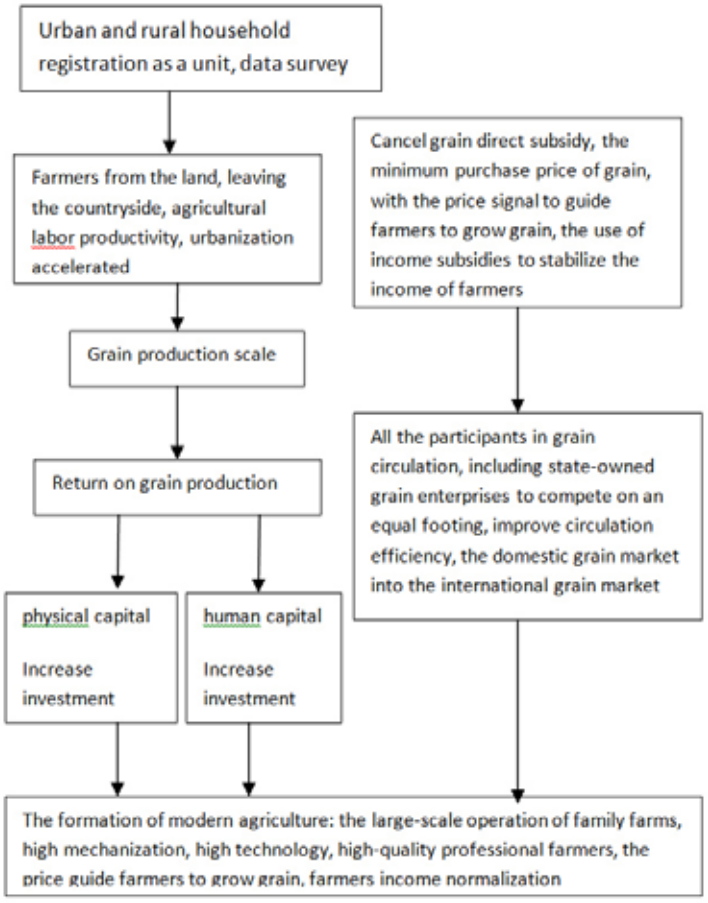


FIGURE 1
China's grain production and circulation market roadmap.

total grain production depends on the acreage and mu yield, excluding climate effects and other uncontrollable factors. The potential for food production is ultimately determined by land, capital, technology, labour and institutions [30, 31]. And the production of five other factors, namely total grain production and grain sown area, that is, total grain output and grain sown area, total sown area, the use of fertilizer, the number of workers, affected area has a great relationship. Table 1 is China's 1991 ~ 2015 total grain output and the production of statistical data.

The model set. This article selects the OLS model which is the abbreviation of ordinary least square, and it means ordinary least squares. Ordinary least squares estimation is used to find parameters $\beta 1$、$\beta 2\ldots\ldots$ The estimated value of the sum is the square of the sum of squares and Q. The weight of each square item in the formula is the same as that of the ordinary least squares regression parameter estimation method. Under the condition, the error is equal or not, the ordinary least squares estimator is a linear unbiased estimation of the minimum variance regression parameters [32]. This method can be used to calculate the parameters of the econometric model, which is the most basic and the most used method in econometrics.

The assumptions of the model are as follows.

1. Zero mean is given.

$$E(u_i) = 0 \quad i = 1,2,3,\cdots,n \tag{1}$$

2. Co variance without autocorrelation presents here.

$$COV(u_i, u_k) = E[(u_i - Eu_i)(u_k - Eu_k)]$$
$$= E(u_i, u_k) = \begin{cases} \sigma^2, & i = k \\ 0, & i \neq k \end{cases} \tag{2}$$

3. The random disturbance term is not related to the explanatory variables.

$$Cov(X_{ji}, u_i) = 0 \quad j = 2,3,\cdots,k \tag{3}$$

4. There is no multi co linearity.

5. We can get the normality of residuals.

$$\mu_i \sim N(0, \sigma^2) \tag{4}$$

Production efficiency refers to the ratio between the actual output of the process and the maximum output under fixed input which reflects the extent to the maximum output. The intended target or the best operational service is achieved. It also measures the performance of economic individuals in terms of output, cost, income, or profit [33]. The efficiency of production has a large impact on the increase in production. The model was developed using the stochastic frontier production model *Battese and Coelli (1995).* This model proposes a method to estimate the random production and technical efficiency function at the same time, which can guarantee the influence of technical efficiency loss under the condition of unbiased and effective. The theoretical model is here.

$$Y_i = f(X_i; \beta)\exp(\varepsilon \equiv V_i - U_i) \tag{5}$$

$$\ln Y_i = \ln f(X_i; \beta) + V_i - U_i \tag{6}$$

The model (6) is the logarithmic form of the model (5), Y represents the actual output, $f(\bullet)$ represents the deterministic output on the production possibility boundary, which represents the best output under the existing technical conditions. X_i represents the input element (including Land, capital, labour, and other input factors) and β represents unknown parameters. ε is the synthetic error term, V_i is the factor that can not be controlled in the production of the sample unit. It is used to judge the effect of measurement error and random interference, such as statistical error, climate, natural disaster $V_i \square N(0, \sigma_V^2)$ and the distance between the sample output and the production possibility boundary, U_i is the inefficient part of the production technology of the sample unit" i ", U_i is subject to the truncated normal distribution [34].

$$U_i \geq 0, \quad U_i \square N(m_i, \sigma_u^2) \tag{7}$$

The technical efficiency function of the sample unit can be expressed.

$$m_i = \delta_0 + \sum_{K=1}^{n} \delta_K z_{Ki} + \omega_i \tag{8}$$

In (8) ω_i must obey the extreme value of the random variable, Z_K determines the efficiency of the production of farmers out of the first variable k, δ_0 and δ_K are the parameters to be estimated. Z_K reflects the effect of variables on farmers' technical efficiency. Negative values indicate that the variables have a positive effect on technical efficiency. Positive values indicate negative effects. Although the stochastic frontier production function has the parameter linearity, the error term of the regression equation does not satisfy the classical hypothesis of the least squares method, it also contains two unobservable variables of the technical efficiency factor and the random disturbance factor [35]. Therefore, the *OLS* method can not be used to estimate the parameters The According to Battese & Corra proposed the maximum likelihood estimation of the basic idea, with two parameters $\sigma^2 = \sigma_v^2 + \sigma_u^2$ and $\gamma = \sigma_u^2 / (\sigma_v^2 + \sigma_u^2)$ alternative observation error variance and technical efficiency variance σ_u^2 thus have $\gamma \in (0,1)$.

Here is the model.

$$\mathrm{Yield} = \alpha_0 + \alpha_1 \mathrm{Fertilizer} + \alpha_2 \mathrm{Area} + \alpha_3 \mathrm{Disaster} + \alpha_4 \mathrm{Power} + \alpha_5 \mathrm{Labor} + \varepsilon \tag{9}$$

Among them, α_0 、 α_1 、 α_2 、 α_3 、 α_4 、 α_5 、 ε is undetermined parameters, *Yield* is the total grain yield, Fertilizer, Area, Disaster, Power and Labour respectively represent the use of chemical fertilizer, grain sown area, disaster area, total power of agricultural machinery and agricultural labour force. Statistical analysis results are presented in table 2.

TABLE 2
Statistical analysis data

Variable	Mean	Standard deviation	MAX.	MIN.
Yield	44945.64	4150.73	51230	37911
Fertilizer	3384.08	1116.05	5108	1660
Area	109339.60	4055.78	114047	99410
Disaster	24413.88	5194.93	34374	15264
Power	41334.80	17725.77	76590	18022
Labour	34716.40	2632.49	39098	30868

Figure 2 gives the relationship between fertilizer use and grain yield.

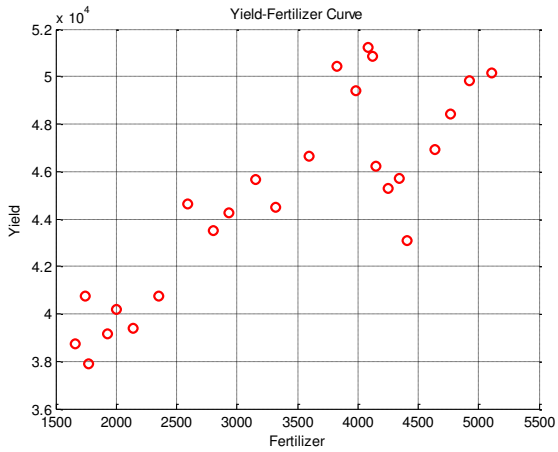


FIGURE 2
The relationship between fertilizer use and grain yield

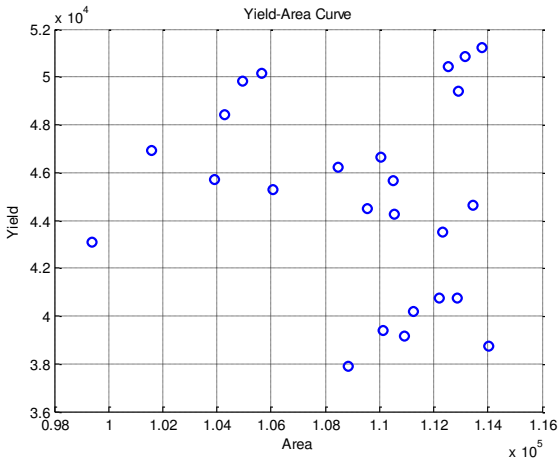


FIGURE 3
Relationship between grain sown area and grain yield

Figure 3 shows Relationship between grain sown area and grain yield.

Figure 4 presents relationship between disaster area and grain yield.

Figure 5 tells us the relationship between total power of agricultural machinery and total grain output.

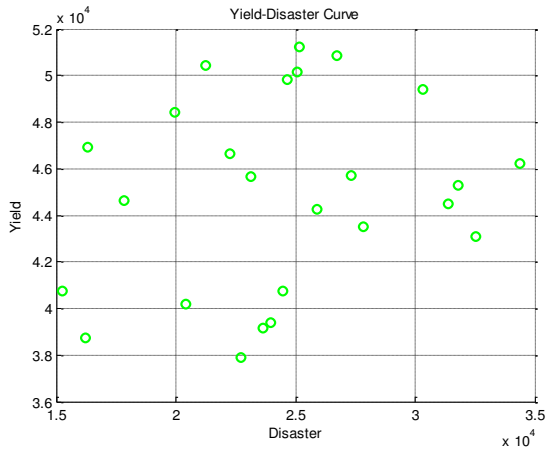


FIGURE 4
Relationship between disaster area and grain yield

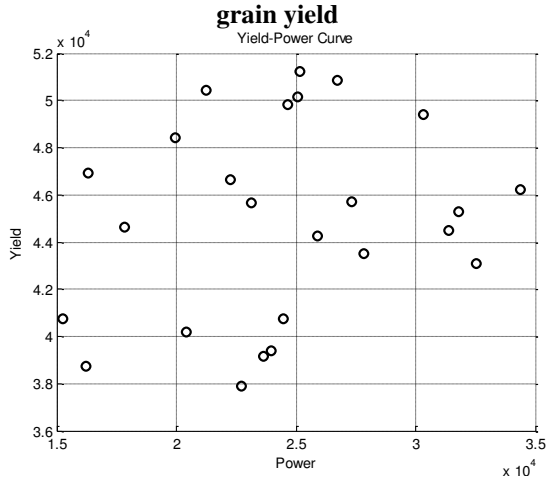


FIGURE 5
Relationship between total power of agricultural machinery and total grain output

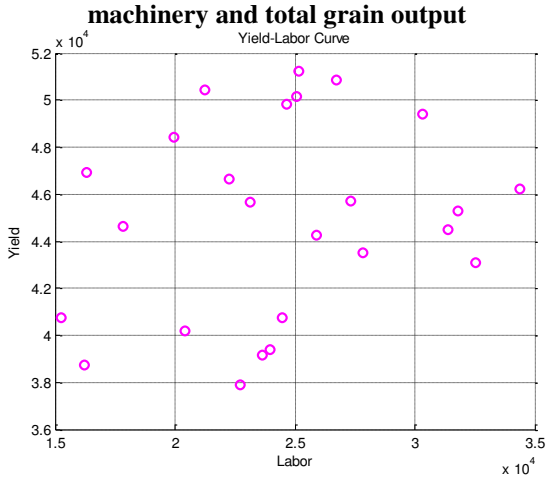


FIGURE 6
The relationship between labor input and grain output

Figure 6 gives the relationship between labour input and grain output.

(1) OLS estimation results

Based on the above data and OSL linear regression model:

Variable	Coefficient	Std. Error	t-Statistic	Prob.
Yield	-26695.08	7507.527	-3.555775	0.0021
Fertilizer	5.994511	0.609713	9.831685	0.0000
Area	0.536701	0.057858	9.276245	0.0000
Disaster	-0.135873	0.029720	-4.571732	0.0002
Power	0.090822	0.042053	-2.159696	0.0438
Labor	-0.007390	0.070511	-0.104814	0.9176

R-squared	0.980829	Mean dependent var	44945.64
Adjusted R-squared	0.975783	S.D. dependent var	4150.729
S.E. of regression	645.9230	Akaike info criterion	15.98480
Sum squared resid	7927113.	Schwarz criterion	16.27733
Log likelihood	-193.8100	F-statistic	194.4114
Durbin-Watson stat	1.715679	Prob(F-statistic)	0.000000

$$Y = -26695.08 + 5.994511 Fertilizer + 0.536701 Area \pm 0.135873 Disaster + 0.090822 Power \pm 0.007390 Labor$$

(7507.527) (0.609713) (0.057858) (0.029720) (0.042053) (0.070511)

T = （-3.555775） (9.831685) (9.276245) (-4.571732) (-2.159696) (-0.104814)

R-Squared = 0.980829 df=19

From the above results, we can see that the coefficient of determination is R-Squared=0. 980829, and which shows that the model is very good.

(2) Test and correction of Multi co linearity

Fertilizer, Area, Disaster, Power, Labour multiple co linearity test, get the correlation between the variables, as shown in table 3.

As can be seen from table 3, Fertilizer, Area, Disaster, Power, Labour, there is a high degree of linear correlation between the need to be amended.

(3) Stepwise regression method

Stepwise regression method was used to correct. The results of regression are shown in table 4.

Among them, the largest r^2 to join Fertilizer, is based on Fertilizer, in addition to other variables stepwise regression [36]. The results are shown in table 5.

Among them, the largest r^2 join Area, Fertilizer, Area which is based on the gradual addition of other variables stepwise regression. The results are shown in table 6.

TABLE 3
Estimation results of OSL linear regression model

Variable	Coefficient	Std. Error	t-Statistic	Prob.
Yield	-26695.08	7507.527	-3.555775	0.0021
Fertilizer	5.994511	0.609713	9.831685	0.0000
Area	0.536701	0.057858	9.276245	0.0000
Disaster	-0.135873	0.029720	-4.571732	0.0002
Power	0.090822	0.042053	-2.159696	0.0438
Labor	-0.007390	0.070511	-0.104814	0.9176

(a)

R-squared	0.980829	Mean dependent var	44945.64
Adjusted R-squared	0.975783	S.D. dependent var	4150.729
S.E. of regression	645.9230	Akaike info criterion	15.98480
Sum squared resid	7927113.	Schwarz criterion	16.27733
Log likelihood	-193.8100	F-statistic	194.4114
Durbin-Watson stat	1.715679	Prob(F-statistic)	0.000000

(b)

TABLE 4
Statistics of Total Grain Output and Production Factors (1991 - 2015)

	Fertilizer	Area	Disaster	Power	Labor
Fertilizer	1.000000	-0.616566	0.400644	0.952746	0.314885
Area	-0.616566	1.000000	-0.238039	-0.741538	-0.060970
Disaster	0.400644	-0.238039	1.000000	0.310096	0.409704
Power	0.952746	-0.741538	0.310096	1.000000	0.128834
Labors	0.314885	-0.060970	0.409704	0.128834	1.000000

TABLE 5
Regression estimation results

Variable	Fertilizer	Area	Disaster	Power	Labor
Parameter estimation	3.158761	-0.14429	0.182715	0.165219	0.553797
t-VALUE	7.716525	-0.68297	1.126564	4.775066	1.799071
r^2	0.721363	0.019877	0.052295	0.165219	0.123364

TABLE 6
Regression results for adding new variables (1)

adding variable	Area	Disaster	Power	Labor
Parameter estimation	0.631835	-0.10622	-0.26297	0.146656
t-VALUE	11.07516	-1.11232	-3.97217	0.79565
r^2	0.957624	0.736199	0.837737	0.729157

Among them, the largest r^2 has to join Disaster, Fertilizer, Area, Disaster, which is based on the gradual addition of other variables stepwise regression, the results are shown in table 7.

TABLE 7
Regression results for adding new variables (2)

adding variable	Disaster	Power	Labor
Parameter estimation	-0.11151	-0.03681	0.002836
t-VALUE	-3.63213	-0.82605	0.037402
r^2	0.973974	0.958958	0.957627

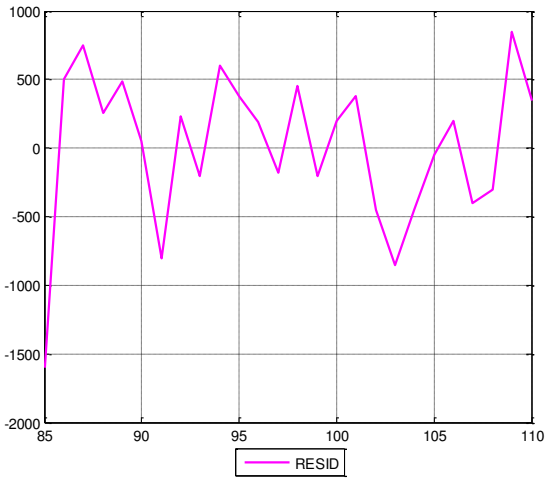


FIGURE 7
Model residuals

It is obvious that when the labour is added, the test value of the parameter is not significant, which is mainly because the labour causes multi-co linearity.

The results of multiple linear regressions are shown as follows.

Y = -27110.39+ 5.954533 Fertilizer + 0.538519 Area +-0.136393 Disaster +0.088210 Power

(6217.065) (0.463769) (0.053816) (0.028570) (0.033023)

T = （-4.360641） (12.83943) (10.00673) (-4.571732) (-2.671134)

R-Squared=0.980817 Adjusted R-squared= 0.976981 F-statistic=255.6537

(4) Residual estimation The OLS method has a high requirement for the residuals, and it is necessary to estimate the residual of the model. The residuals of the model are shown in figure 7.

TABLE 8
Regression results for adding new variables (3)

adding variable	Power	Labor
Parameter estimation	-0.08821	0.082863
t-VALUE	-2.67113	1.34134
r^2	0.980817	0.082863

TABLE 9
The results of multiple linear regressions

Variable	Coefficient	Std. Error	t-Statistic	Prob.
C	-27110.39	6217.065	-4.360641	0.0003
ssX1	5.954533	0.463769	12.83943	0.0000
X2	0.538519	0.053816	10.00673	0.0000
X3	-0.136393	0.028570	-4.773986	0.0001
X4	0.088210	0.033023	-2.671134	0.0147

(a)

R-squared	0.980817	Mean dependent var	44945.64
Adjusted R-squared	0.976981	S.D. dependent var	4150.729
S.E. of regression	629.7498	Akaike info criterion	15.90538
Sum squared resid	7931696.	Schwarz criterion	16.14915
Log likelihood	-193.8172	F-statistic	255.6537
Durbin-Watson stat	1.706044	Prob(F-statistic)	0.000000

(b)

(5) Determination model after a series of model checking and setting, it can be considered that the modified model has no multi-co linearity.

Finally, the model can be set as follows.

Y = -27110.39 + 5.954533 Fertilizer +0.538519 Area +0.136393 Disaster +0.088210 Power

(6217.065) (0.463769) (0.053816) (0.028570) (0.033023)

T = （-4.360641） (12.83943) (10.00673) (-4.571732) (-2.671134)

R-Squared=0.980817 Adjusted R-squared= 0.976981 F-statistic=255.6537

6）Model analysis

- Food production.

As the explanatory variable, from the table we can see that it is volatile, but the overall trend is still growing.

2) Planting area.

With the reduction of planted area, food production will be corresponding reduction; the two are positively related relationship.

- 3) Fertilizer use.

With the increase in the use of chemical fertilizers, food production is also a corresponding increase, the two are positively related.

- 4) Disaster area.

The increase in the area of disaster will reduce food production, and they are negatively correlated. Total power of agricultural machinery is including farming machinery, irrigation and drainage machinery, harvesting machinery, agricultural transport machinery, plant protection machinery,

animal husbandry machinery, forestry machinery, fishing machinery and other agricultural machinery. Its increase will also increase food production.

RESULTS AND DISCUSSION

Results. The model shows that the grain yield and agricultural fertilizer, grain planting area, total power of agricultural machinery is proportional. Therefore, it should be the level of scientific research in fertilizer research on the investment, and helps us to achieve a greater degree of grain income. The sown area of grain can be protected by all kinds of measures to help keep the soil and water, so as to keep the effective planting ability of the soil. The total power of agricultural machinery is no doubt that science and technology has become the first productive force in modern society, how to better realize the mechanization of agricultural production, it is also the focus of our consideration. The agricultural labour force is excluded from the model, which is contrary to what we had previously thought, which makes it necessary for us to consider the significance of the transfer of rural labour force. The main way to increase the income of farmers is likely to be moving out of rural areas, that is to say, the transfer of rural labour is the main way to increase the income of farmers now or in the future. That is, the transfer of agricultural labour force in the process of urbanization has no significant effect on the total grain production.

Discussion. In the short term in order to ease the tight supply of food, should improve the enthusiasm of farmers to grow grain, which is the only way to expand the sown area. The enthusiasm of farmers mainly depends on the income and expectation of grain, and the difference between income and cost. Therefore, one should adopt a pronged approach to improve and stabilize grain prices, on the other hand we also should control the excessive increase of the agricultural goods prices, and the latter is often neglected, which must bring special attention. The positive effect can not let prices growth which is offset by the negative effect of the latter, otherwise high grain yield has become an empty word. The Chinese government in the implementation of strict price controls on agricultural supplies control the cost of grain.

According to the law, every one of us must protect arable land, and we can curb the trend of grain farming area decline. To take effective measures to increase protection efforts, the government can strict control of illegal occupation of land, so as to ensure the total dynamic balance. At the same time, it is necessary to take measures in the process of urbanization to deal with the erosion of cultivated land and limit the conversion of existing land property rights. Strengthening agricultural infrastructure and ecological environment construction, we improve the comprehensive agricultural development capacity and sustainable development capacity. In order to accelerate agricultural scientific and technological progress, engineers strive to improve yields (37). Actively we can introduce foreign advanced scientific research, make use, digestion, absorption or innovation. Therefore, we can establish and improve the agricultural technology promotion system, cultivate a wide range of agricultural technology extension service agencies by increasing new varieties, new technologies. The relationship between agriculture and natural weather is closely related to drought and floods and other natural disasters are vulnerable to fragile agriculture losses, the need to improve the market economy system of agricultural insurance for farmers helps us to share the pressure. At the same time, according to the situation of grain production, we should gradually establish the system of monitoring and early warning of grain production, demand, reserve, market dynamics, and the tracking of unexpected events.

CONCLUSION

In the process of industrialization and urbanization, China faces the situation of large proportion of agricultural population and surplus labour. On the one hand, farmers need to solve the ways of improving their living through work. On the other hand, China's non-agricultural economy Development also needs this strong army of labour as a power force of support. In the context of economic construction and urbanization, the farmers' enthusiasm for grain production needs more attention. This paper mainly focuses on the cultivation of farmers' inputs, such as fertilizers, mechanization. And then, we analyse the OLS correlation between planting enthusiasm and production circulation which includes the China's total grain output, grain sown area and the use of fertilizer. The total power of agricultural machinery is positively related to the proportion of disaster area which has a negative correlation. Therefore, we must fundamentally solve the problem to ensure that China's food security. It is not only useful to the government policy guidance, but it is helpful to promote the optimization of China's grain structure and encourage farming, hence, the government in the law of strong restrictions ensure arable land safety and the food safety.

Based on the above analysis, exogenous factors affect the production of the positive policies, little changes in a certain period of time, helps to improve the yield from water, fertilizer, medicine, science and technology investment in four aspects. Water is used to resist the adverse natural factors and the loss itself does not increase food to improve

the yield, grain yield which should start from improving the fertilizer effects. First, we must ensure that the fertilizer three elements are relatively ideal. Second, we must improve the fertility of land and fertilizer. Third, we must do a scientific and rational structure. Fourth, the government increases investment in science and technology to improve the circulation of agricultural products and farmers' enthusiasm

REFERENCES

[1] Chapagain, S. (2014) Study On Wheat Farmer's Perception And Adaptation Measures Under Climate Change And Vulnerability Context Of Bardiya District.

[2] Johnson, M. (2016). The Taiwan" economic miracle" found its way into the heart of Western scholarship not simply because of the rapid increase in the number of objects manufactured; there was always a second and social point to be made. History under the Nationalist state. Taiwan: Beyond the Economic Miracle: Beyond the Economic Miracle.

[3] Chowdhury, A. (2014). Factors Affecting Productivity And Efficiency Of Rice Production In Haor Area In Bangladesh: Likely Impact On Food Security (Doctoral dissertation).

[4] Johnson, M. (2016) The Taiwan" economic miracle" found its way into the heart of Western scholarship not simply because of the rapid increase in the number of objects manufactured; there was always a second and social point to be made. History under the Nationalist state. Taiwan: Beyond the Economic Miracle: Beyond the Economic Miracle.

[5] Kohl, T., Sapei, E., Rocha, I.M., Galvao, T.L., Ribeiro da Silva, M.D., Ribeiro da Silva, M.A. (2015). Modeling of fast pyrolysis of wood for prediction of bio-oil composition. In Asia Pacific Confederation of Chemical Engineering Congress 2015: APCChE 2015, incorporating CHEMECA 2015. (p. 2410). Engineers Australia.

[6] Kanika, M., Ramaswami, B. (2015). Caste, Female Labor Supply and the Gender Wage Gap in India: Boserup Revisited. In 2015 Conference, August 9-14, 2015, Milan, Italy (No. 212218). International Association of Agricultural Economists.

[7] Cunguara, B., Mather, D., Walker, T., Mouzinho, B., Massingue, J., Uaiene, R. (2016). Exploiting the potential for expanding cropped area using animal traction in the smallholder sector in Mozambique (No. 249697). Michigan State University, Department of Agricultural, Food, and Resource Economics.

[8] Borlu, Y. (2014). Following the Maize: Regulation and Production in the Agricultural Landscape in Turkey in the 2000s (Doctoral dissertation, The Pennsylvania State University).

[9] Wohlfart, C., Liu, G., Huang, C., Kuenzer, C. (2016). A River Basin over the course of Time: Multi-temporal analyses of Land surface dynamics in the Yellow River basin (China) based on medium resolution remote sensing data. Remote Sensing. 8(3), 186.

[10] Saldaña-Zorrilla, S.O. (2015) Spatial model of incomes and migration[M]//Natural Disasters, Foreign Trade and Agriculture in Mexico. Springer International Publishing, 69-88.

[11] Cunguara, B., Mather, D., Walker, T., Mouzinho, B, Massingue, J., and Uaiene, R.,. (2016) Exploiting the potential for expanding cropped area using animal traction in the smallholder sector in Mozambique[R]. Michigan State University, Department of Agricultural, Food, and Resource Economics.

[12] Kanika, M. and Ramaswami, B. (2015) "Caste, Female Labor Supply and the Gender Wage Gap in India: Boserup Revisited." 2015 Conference, August 9-14, 2015, Milan, Italy. No. 212218. International Association of Agricultural Economists.

[13] Xie, Hualin, Lingjuan Cheng, and Tiangui Lv. "Factors Influencing Farmer Willingness to Fallow Winter Wheat and Ecological Compensation Standards in a Groundwater Funnel Area in Hengshui, Hebei Province, China." *Sustainability* 9.5 (2017): 839.

[14] Zhou, Yunbo, and Yan Qin. "Income Inequality of China's Total Resident and the Factors Which Impact It." Empirical Analysis on Income Inequality of Chinese Residents. Springer Berlin Heidelberg, 2012. 125-149.

[15] Wohlfart, C., Liu, G., Huang, C., Kuenzer, C. (2016). A River Basin over the course of Time: Multi-temporal analyses of Land surface dynamics in the Yellow River basin (China) based on medium resolution remote sensing data. Remote Sensing. 8(3), 186.

[16] Nelson, R. (2013). Determinants of producer resiliency: Investigating the probability that agricultural producers exit the industry in the face of drought (Doctoral dissertation, Colorado State University).

[17] Marden, S. (2015). Agriculture, development and structural change in reform-era China (Doctoral dissertation, The London School of Economics and Political Science (LSE)).

[18] Mburu, G.N. (2016). Factors Affecting Production Of Dairy Products In Kenya: A Case Of Co-Operative Societies In Kiambu County (Doctoral Dissertation, Kca University).

[19] Ahmed, Y.A., Rostam, B.N., Mohammed, B.A. (2015). Sharing the agriculture and industrial sectors in the economic growth of Iraq: an Ordinary Least Squares (OLS) application. Journal of Emerging Trends in Economics and Management Sciences. 6(5), 340-353.
[20] Daniel, Z. (2015). The Impact Of Irrigation Schemes On Farmers'income And Livelihoods In The Upper East Region Of Ghana (Doctoral Dissertation, Kwame Nkrumah University Of Science And Technology).
[21] Hailu, A.D.D.I.S.U. (2016). Value chain analysis of vegetables: The case of Ejere District, West Shoa Zone, Oromia National Regional State of Ethiopia (Doctoral dissertation, Haramaya University).
[22] Sequeira, S., Nunn, N., Qian, N. (2017) Migrants and the Making of America: The Short- and Long-Run Effects of Immigration during the Age of Mass Migration. No. w23289. National Bureau of Economic Research.
[23] Bodenhorn, H. and Cuberes, D. (2015) Finance and urbanization in early nineteenth-century New York. Clemson University working paper.
[24] Su, C.W., Liu, T.Y., Chang, H.L., Jiang, X.Z. (2015). Is urbanization narrowing the urban-rural income gap? A cross-regional study of China.Habitat International. 48, 79-86.
[25] Marshall, J. (2016) "The Taiwan" economic miracle" found its way into the heart of Western scholarship not simply because of the rapid increase in the number of objects manufactured; there was always a second and social point to be made. History under the Nationalist state." Taiwan: Beyond the Economic Miracle: Beyond the Economic Miracle.
[26] Zhihong, S.H.E.N., Kusano, E., Chien, H., Koyama, O. (2014). Predictive analysis of nitrogen balances resulting from the production and consumption of livestock products in the Huang-Huai-Hai Region, China.Japan Agricultural Research Quarterly. JARQ, 48(3), 331-342.
[27] Uebele, M. and Gallardo-Albarrán, D. (2015) "Paving the way to modernity: Prussian roads and grain market integration in Westphalia, 1821–1855."Scandinavian Economic History Review. 63.1,69-92.
[28] Nunn, N., Qian, N. and Sequeira, S. (2017) "Migrants and the Making of America: The Short and Long Run Effects of Immigration during the Age of Mass Migration."
[29] Stoeckl, N., Chaiechi, T., Farr, M., Jarvis, D., Álvarez-Romero, J.G., Kennard, M.J., Pressey, R.L. (2015). Co-benefits and trade-offs between agriculture and conservation: A case study in Northern Australia.Biological Conservation. 191, 478-494.
[30] Wainaina, P. (2016). Tradeoffs, Complementarities and Synergies between Different Agricultural Technologies: Insights from Maize Farmers in Kenya(Doctoral dissertation, Dissertation, Göttingen, Georg-August Universität, 2016).
[31] Ahmed, Y.A., Rostam, B.N. and Mohammed, B.A. (2015) "Sharing the agriculture and industrial sectors in the economic growth of Iraq: an Ordinary Least Squares (OLS) application." Journal of Emerging Trends in Economics and Management Sciences. 6.5, 340-353.
[32] Boone, C. and Wilse-Samson, L. (2014). "Modernization, Rural Migration, and Market Withdrawal: Evidence from the Great Depression."
[33] Adil Ahmed Ali, I. (2015). Economic Efficiency and International Competitiveness of Wheat and Faba Bean in Northern and River Nile States-Sudan (Doctoral dissertation, UOFK).
[34] Kulkarni, K. (2016).Indian Agriculture–Productivity, Climate Change and Institutions An essay in Agricultural Economics. BS thesis. Università Ca'Foscari Venezia.
[35] Ogolla, M. (2016). Factors Influencing Poultry Production Among Poultry Farmers in Eldoret Town, Uasin Gishu County, Kenya (Doctoral dissertation, University Of Nairobi).
[36] Usman, S. (2016). Analysis of wheat value chain: The case of Sinana District, Bale Zone, Oromia Region, Ethiopia (Doctoral dissertation, Haramaya University).
[37] Chapagain, S. (2014). Study On Wheat Farmer's Perception And Adaptation Measures Under Climate Change And Vulnerability Context Of Bardiya District.

Received: **09.06.2017**
Accepted: **30.09.2017**

CORRESPONDING AUTHOR

Bangxi Li
School of Economics and Management, Anhui Agricultural University

e-mail: libangxi1983@126.com

© by PSP Volume 26 – No. 12A/2017 pages 7992-8000 Fresenius Environmental Bulletin

RESPONSE OF MICROBIAL ACTIVITY TO ADDITION OF *NERIUM OLEANDER* L. LEAVES IN SOIL UNDER DIFFERENT MOISTURE CONDITIONS

Sahin Cenkseven[1], Burak Kocak[2,*], Secil Berna Kuzu[2], Hatice Korkmaz-Guvenmez[2], Cengiz Darici[2]

[1]Cukurova University, Faculty of Agriculture, Department of Soil Science and Plant Nutrition, Adana-01330, Turkey
[2]Cukurova University, Faculty of Science and Letters, Department of Biology, Adana-01330, Turkey

ABSTRACT

Nerium oleander L. (Common oleander, Apocynaceae), is a widespread toxic plant of Mediterranean region and was reported that this plant have both herbicidal and insecticidal activities. Therefore, it's essential to monitor the effects of leaves on soil microbial activity before using it commercially in agricultural fields. In this study, oleander leaves were mixed with soils at doses of half (L0.5), same (L1) and double (L2) of soil organic carbon level and carbon mineralization (Cmin) was measured for 30 days at 28°C under 80% and 60% of field capacity (FC) of control soils. Soil cellulase and xylanase activities with counts of aerobic bacteria and fungi were determined on 15th and 30th days of Cmin. Highest cumulative carbon mineralizations were also observed at L2 dose. Control soil was significantly different with L1 and L2 ($P < 0.05$) under 80% FC but there were no differences under 60% FC at the end of incubation period. Carbon mineralization was generally, significantly and positively correlated with microbial populations and enzyme activities under 80% FC ($P < 0.05$). Highest bacteria counts were obtained in L1 on 15th day and in L0.5 on 30th day while fungi counts were highest in L1 on 15th day and in L2 on 30th days under both moistures. Soil enzyme activities generally were enhanced all treatments and highest at L2 dose. Our results showed that addition of oleander leaves to the soils under different field capacities generally stimulated both activities and populations of soil microorganisms.

KEYWORDS:
Soil microbial activity, Cellulase, Xylanase *Nerium oleander* L., Total aerobic bacteria and fungi counts

INTRODUCTION

Soil is home to plant, animal and microorganisms on earth's surface. Microscopic life (bacteria, fungi, algae, protozoa and viruses) and macroscopic life (earthworms, nematodes, mites, insects and root systems of plants) sustain in soil. Many environmental factors like amount and type of nutrients, available moisture, aeration, pH, temperature etc. affect the numbers and kinds of microorganisms in soil ecosystems. Soil bacteria and fungi are main driving factors in biogeochemical cycles and recycling of organic matter. Furthermore, contributions to plant nutrition and health, soil structure and fertility were made by soil microorganisms through affecting aboveground. One of the main habitats for microorganisms on earth is soil by developing around soil particles. Populations of microorganisms including bacteria and fungi are generally much higher than those in fresh water or marine habitats [1].

In decomposition of polymeric compounds like cellulose, xylan etc. enzymes produced by microorganisms play a key role in soil systems that are catalyzing many significant reactions required for sustaining life processes of microorganisms in soil, decomposition of organic residues, organic matter formation and nutrient cycling [2]. These enzymes are rapidly being synthesized, released and/or decomposed in soil ecosystems and thus, they are very important in nutrient cycling. Also, relationship between soil organic matter (SOM) quality with its turnover and extracellular enzymes within the soil matrix has attracted much attention [3]. Soil enzymes are best indicators in changes of biochemical structure of SOM or carbon content [4]. Changes in SOM are noticeable in enzyme activity that is measurable. Plant cell walls are consisted of large amounts of cellulose and hemicellulose and soil microorganisms must synthesize both cellulose and hemicellulose degrading enzymes to access these substrates and use them as an energy source [3].

One of most important factors that affecting carbon cycling in soils is moisture [5]. There have been many research articles about effects of moisture on carbon and nitrogen mineralizations in mineral soils conducted in laboratory experiments. These researches showed that activities in SOM were based on increase or decrease in soil moisture. Effects of moisture on carbon mineralization in mineral soils were widespread still being investigated under controlled conditions in laboratories [5]. However, there weren't any researches about soil microbial activity under the effects of addition of leaves of *Nerium oleander* L. in the literature.

Nerium oleander L. (Common oleander, Apocynaceae) is an evergreen shrub and a native plant of Mediterranean regions of Europe and cultivated as ornamental shrubs throughout the tropical and subtropical parts of the world. All organs of oleander are toxic, and contain mostly neriifolin, thevetin A, thevetin B, and oleandrin which are cardiac glycosides. Ingestion of oleander leaves causes nausea, vomiting, abdominal pain, diarrhea, and hyperkalemia and treatment for this poisoning is administration of activated charcoal and supportive care [6]. There are some reports of herbicidal and insecticidal activity of oleander leaves and if it will be sold commercial in future, effects of leaves on soil microbial activity should be determined before it's sold commercially in the world. It's essential that leaves or their extracts should be mixed with soils in order to monitor their effects on soil microorganisms and determine their decomposition in soil [7, 8, 9, 10].

This is the first research to demonstrate and give an insight about effects of oleander leaves on some soil biological parameters under controlled conditions. Therefore, the objective of this investigation was to determine how oleander leaves influence on soil organic carbon mineralization under two different field capacities (80 and 60%), counts of bacteria and fungi, cellulase and xylanase activities in the mineralization process by measuring them on 15th and 30th days. We hypothesized that addition leaves of oleander would decrease carbon mineralization, soil microbial populations and enzyme activities.

MATERIALS AND METHODS

Study sites, preparation and analysis of plant and soil samples. Soils and leaves of oleander (*Nerium oleander* L.) have been taken from three plants from Cukurova University Campus, Adana (37°3'26" N, 35°21'19" E), Turkey, in February 2014. Semi-arid Mediterranean climate conditions have been characterized in Adana (mean annual precipitation: 659 mm; mean annual temperature: 19.1 °C for 35 yr). Both soils and leaves were air-dried. Soils were sieved through a 2-mm mesh sieve and leaves have been powdered and then homogenized before analysis. Soil texture was determined by Bouyoucos hydrometer [11], field capacity (%) by 1/3 atmospheric pressure with a vacuum pump [12], pH by a 1:2.5 soil-water suspension with pH-meter (inoLab pH/Cond 720, WTW GmbH, Weilheim, Germany), $CaCO_3$ content (%) by a Scheibler calcimeter. Organic carbon (C) and total nitrogen (N) contents of soils and leaves (%) were determined by modified Walkley and Black method and Kjeldahl method, respectively [13].

Soil organic carbon mineralization. Soil samples (100 g) were placed in 750 mL incubation vessels and the final moisture contents of both soils were adjusted to 80% and 60% of their own field capacity before incubation at 28°C over 30 days [14]. Powdered leaves of oleander were separately mixed with 100 g soils at the half (L0.5), same (L1) and double (L2) doses of soil organic carbon level (1.81%) to observe its effects on soil microbial activity for 30 days of incubation. Calculation of doses were based on as following: if 100 g of leaves have 41.17 g C, it's required to mix 2.20 g of leaves with 100 g soils which is equal to soil organic carbon level (1.81 %). 2.20 g (L0.5), 4.40 g (L1) and 8.80 g (L2) powdered leaves were mixed with soils for these treatments while soils contain no leaves were used as control. The CO_2 produced from microbial activity was absorbed periodically in 40 mL saturated $Ba(OH)_2$ solution in small beakers, which were placed on the top of the soil in incubation vessels. Every 3 days CO_2 produced by microbial respiration was measured by titration with oxalic acid in these closed vessels [15]. Three replicates were used for each treatments and control Cumulative C mineralization (mg CO_2-C 100 g^{-1} soil) was calculated by summing up all 3 days CO_2 until end of incubation period while their rates on 15th and 30th days were calculated by dividing cumulative mineralized C by its soil organic C of control and all treatments. Cumulative C mineralization of control soils were taken as 100% to find and compare increase and decrease percentage of all treatments [16].

Counts of soil bacteria and fungi. Heterotrophic culturable total aerobic bacteria and fungi were determined by soil-dilution plate method. 0.1 g soil was taken from each incubation vessels on 15th and 30th days and were placed in Eppendorf tubes containing 0.9 mL of 0.9% sterile sodium chloride and homogenized. After homogenization, Serial tenfold dilutions of soil suspensions (10^{-5}) were plated in triplicate on plate count agar (PCA, Merck, Germany) for total aerobic bacteria count and on potato dextrose agar (PDA, Merck). 200 μg mL^{-1} Ampicillin (Sigma, Germany) was added to PDA medium to inhibit bacterial growth. The inoculated PCA and PDA plates were respectively incubated at 37°C for 1 day and at 28°C for 14 days, before the colonies were counted [17].

Cellulase (EC 3.2.1.4) and xylanase (EC 1.11.14) assay. 1 g soil from each incubation vessel on 15th and 30th days were taken and incubated with 0.5 mL toluene and 20 mL of Na-P buffered (pH 6) with 2% CMC (carboxymethyl cellulose) and 2% xylan at 30°C for 24 h [18, 19]. Cellulase activity was measured using 2% (w/v) soluble CMC dissolved in sodium-phosphate buffer (pH 6.0) as the substrate. Reaction mixtures were incubated for 24 h at 30°C. After incubation, the suspensions were mixed well and centrifuged ad 12000 g for 20 min.

and the reducing sugars released were measured using the DNS assay with glucose as the standard sugar. Xylanase activity was assayed by measuring the reducing sugars released from 2% (w/v) xylan (from oat spelts, Sigma) suspended in sodium phosphate (pH 6.0) when incubated with supernatant at 30°C for 24h. The amounts of reducing sugars released were determined using the DNS as [20] with glucose as the standard sugar [21].

Statistical analysis. Tukey honestly significant difference (HSD) test in one-way ANOVA was performed to determine the differences in C mineralization over incubation time among the treatments. Two-way ANOVA was conducted for determining interactions of doses and moistures on carbon mineralization, soil microbial populations and their cellulase and xylanase activities. Also, a Pearson's correlation analysis was used to analyze the correlation between biological parameters. Results are given in table and figures as mean values ± standard errors of three replicates. Differences between the data were declared as significant at the $P < 0.05$. All statistical analysis was carried out using SPSS v.22 (IBM, Armonk, New York, USA).

RESULTS AND DISCUSSION

Some physical and chemical properties and carbon and nitrogen contents of leaves of oleander were given in Table 1. Soils were sandy loam and slightly alkaline. Carbon and nitrogen contents were 1.81% and 0.28% in soils and 41.17 and 1.06% in leaves, respectively. C/N ratio of soil was found 6.79 (Table 1).

Cumulative carbon mineralization of controls of both field capacities were taken and considered as 100% for following comparisons of increases made by treatments: Under 80% FC, L0.5, L1 and L2 doses enhanced carbon mineralization for 10.0%, 22.6% and 33.6% on 15th day, 4.8%, 18.3% and 19.0% on 30th day compared to its control, respectively (Table 2). On the other hand, under 60% FC, cumulative CO_2 respired by all treatments under 60% FC was for 10.6%, 12.2% and 18.8% on 15th day and 3.1, 6.7 and 6.6% compared to its control, respectively (Table 2). Generally, CO_2-C evolution was higher at 80% FC than 60% FC. Highest cumulative carbon mineralizations were measured at L2 dose under both field capacities on both days (Figure 1). Under 80% FC, significant ($p< 0.05$) differences were found between control and all treatments on 15th day and all treatments except L0.5 dose on 30th day. Under 60% FC, there was only significant difference between control and L2 ($p< 0.05$) on 15th day while no significant differences were found between control and treatments on 30th day (Figure 1).

TABLE 1
Some physical and chemical properties of *Nerium oleander* L. soils and carbon and nitrogen contents of its leaves (mean ± S.E.; n = 3)

Samples	Characteristics	
Soil	Clay (%)	15.69 ± 2.15
	Silt (%)	13.72 ± 2.20
	Sand (%)	70.59 ± 1.90
	Texture Type	Sandy Loam (SL)
	pH	8.05 ± 0.01
	$CaCO_3$ (%)	5.06 ± 0.03
	Field Capacity (%)	30.28 ± 0.06
	C (%)	1.81 ± 0.05
	N (%)	0.28 ± 0.04
	C/N ratio	6.79 ± 0.75
Leaves	C (%)	41.17 ± 0.41
	N (%)	1.06 ± 0.04
	C/N ratio	39.03 ± 1.76

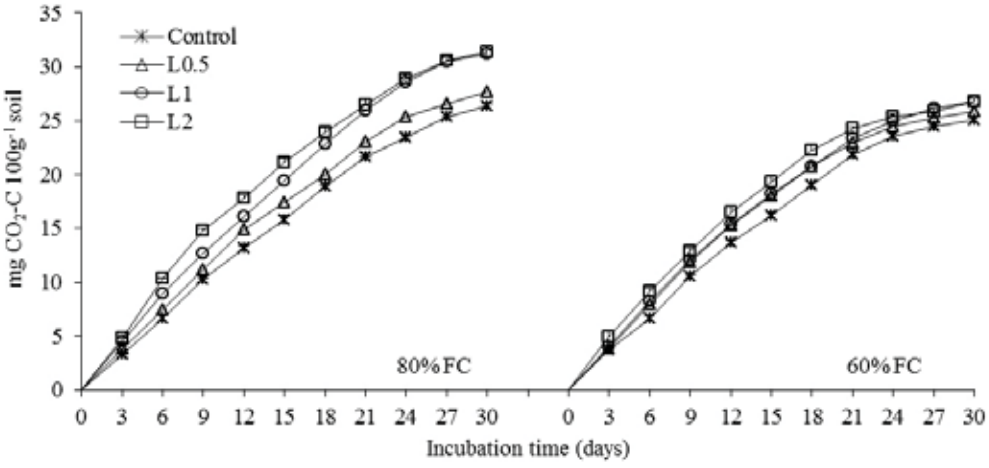


FIGURE 1
Cumulative carbon mineralized (mean ± SE, n = 3) at 80 and 60% FC of soils with addition of oleander leaves at L0.5, L1 and L2 doses over 30 days at 28 °C.

TABLE 2
Carbon mineralization and its rate in the soils at L0.5, L1 and L2 of oleander leaves at 80% and 60% of field capacities during 30 days at 28 °C.

		Cmin (mg CO_2-C 100 g^{-1} soil)		Cmin rate (%)	
		15th day	30th day	15th day	30th day
80% FC	Control	15.85 ± 0.35^{d}	26.41 ± 0.12^{b}	0.88 ± 0.03^{a}	1.46 ± 0.01^{a}
	L0.5	17.44 ± 0.34^{c}	27.68 ± 0.49^{b}	0.64 ± 0.02^{b}	1.02 ± 0.03^{b}
	L1	19.44 ± 0.27^{b}	31.24 ± 0.50^{a}	0.54 ± 0.01^{b}	0.86 ± 0.02^{b}
	L2	21.17 ± 0.40^{a}	31.43 ± 0.44^{a}	0.39 ± 0.01^{c}	0.58 ± 0.01^{c}
60% FC	Control	16.26 ± 0.27^{b}	25.12 ± 0.14^{a}	0.90 ± 0.03^{a}	1.39 ± 0.01^{a}
	L0.5	17.98 ± 0.61^{ab}	25.90 ± 0.62^{a}	0.66 ± 0.04^{b}	0.95 ± 0.04^{b}
	L1	18.25 ± 0.87^{ab}	26.79 ± 0.39^{a}	0.50 ± 0.04^{c}	0.74 ± 0.02^{c}
	L2	19.32 ± 0.53^{a}	26.78 ± 0.28^{a}	0.36 ± 0.02^{d}	0.49 ± 0.01^{d}

Different letters denote significant differences among different doses of oleander leaves for each field capacity. Cmin: Carbon mineralization, Cmin rate: Ratio of carbon mineralization, (mean ± SE, n = 3).

Carbon mineralization (Cmin) rates were obtained highest in controls and they were significantly different with all treatments ($P < 0.05$) under both field capacities on 15th and 30th days Increasing doses of leaves added to the soils lowered Cmin rates (Table 2).

In general, addition of oleander leaves has increased soil carbon mineralization, counts of total aerobic bacteria and fungi and their enzyme activities in soils. Increasing doses of oleander leaves have increased carbon mineralization under 80% FC that significantly differed with control but no significant difference was found between control and all treatments under 60% FC at the end of incubation period. 20% increase in moisture may possibly stimulated carbon mineralization and therefore, soil respiration (Figure 1). On the other hand, same doses under 80% FC have increased Cmin from beginning of incubation period. Highest cumulative carbon mineralization was measured at L2 dose under both field capacities while it was higher under 80% FC than 60% FC on 30th day. It's reported that main factor affecting soil biological activity in the Mediterranean area was moisture that is similar with our study that our results of carbon mineralization were affected by different moistures [22]. In another study, addition of *Laurus nobilis* L. (bay leaf) leaves at different soil organic carbon levels have increased soil carbon mineralization for 54 days under 80% FC at 28°C [16]. In addition to that it was reported that addition of *Eucalyptus camuldulensis* leaves to soils stimulated carbon mineralization at 28°C for 30 days and claimed that leaves were significant carbon resources for soil microorganisms [23]. Teklay et al. [2] also found that leaves of some agroforestry species have increased carbon mineralization at 20°C for 40 days and indicated that decomposition of leaves had a strong relationship with its quality. Mafongoya et al. [25], indicated that addition of *Acacia karro* Hayne, *Acacia nilotica* Delile and *Gliricidia sepium* (Jacq.) Kunth ex Walp. leaves to soils have increased carbon mineralization than their control at 28°C for 56 days. These studies contribute our results of carbon mineralization that addition of leaves of *Nerium oleander* generally has produced more CO_2 than their controls under both 80 and 60% field capacities and on 15th and 30th days. Cmin rates were decreased as increasing doses of leaves that is based on higher carbon input into soil in all treatments than their control.

Nutrient availability, especially nitrogen limits the activity and growth of soil microorganisms in the decomposition process. Litter decomposition rate was controlled by C to element ratio that is important parameter determining whether the specific element is mineralized or immobilized during decay [26]. It was reported that critical C/N rate of broad leaves should be around 20 – 30; below this value, a net nitrogen release generally exists [27]. C/N rate of oleander leaves in this study was 39.03% and it was opposite compared to previous studies which higher C/N ratio didn't affect negatively the decomposition of leaves.

Generally, populations of bacteria and fungi on 15th day were higher than 30th day in all treatments under 80% and 60% FC. Highest bacteria counts were observed at L1 dose on 15th day and 0.5L dose on 30th day (Table 3). All doses of oleander leaves increased bacteria population compared to their controls in both days with exception of L0.5 dose under 80% FC on 30th day. There were found significant differences between control and all treatments under both field capacities on 30th day ($P < 0.05$). On the other hand, effects of oleander leaves on counts of bacteria were variable on 15th day but they were decreased as doses of leaves increased on 30th day. There were only significant differences among control and L1 ($p< 0.05$) under 60% FC and control and all treatments except L0.5 ($p< 0.05$) under 80% FC on 15th day.

Counts of total aerobic bacteria on 15th day were variable and in the range of $16.2 – 50.2 \times 10^5$ cfu/g soil under 80% FC and $6.9 – 53.7 \times 10^5$ cfu/g soil under 60% FC while oleander leaves have decreased bacteria population at increasing doses on 30th day. This was similar for counts of fungi on 15th day but increasing doses of leaves have increased fungi population on 30th day under both field capacities. Ogunmwonyi et al. [1] found that

TABLE 3
Aerobic bacteria-fungi populations and their rates in the soils mixed with oleander leaves under at L0.5, L1 and L2 doses under 80 and 60 % field capacities at 15th and 30th day of incubation.

		Bacteria Count ($\times 10^5$ cfu/ g soil)		Fungi Count ($\times 10^5$ cfu/ g soil)		Ratio of fungi to bacteria (F/B)	
		15th day	30th day	15th day	30th day	15th day	30th day
80% FC	Control	18.6^{c}	15.9^{c}	2.7^{b}	1.0^{b}	0.14^{b}	0.06^{bc}
	L0.5	36.2^{c}	42.4^{a}	18.0^{ab}	1.3^{b}	1.10^{a}	0.03^{c}
	L1	50.2^{a}	30.6^{b}	44.7^{a}	14.0^{a}	0.90^{a}	0.47^{ab}
	L2	38.6^{a}	27.2^{b}	35.3^{a}	22.0^{a}	0.90^{a}	0.80^{a}
60% FC	Control	6.9^{b}	5.7^{b}	3.7^{b}	1.0^{b}	0.53^{a}	0.20^{bc}
	L0.5	35.6^{ab}	35.2^{a}	13.3^{ab}	6.7^{ab}	0.38^{a}	0.19^{c}
	L1	53.7^{a}	29.0^{a}	28.0^{a}	8.0^{ab}	0.65^{a}	0.28^{ab}
	L2	31.3^{ab}	28.3^{a}	23.0^{ab}	13.7^{a}	0.74^{a}	0.48^{a}

Values are means. Different letters denote significant differences among different doses of oleander leaves for each field capacities. cfu: count forming unit.

TABLE 4
Soil Cellulase and Xylanase activity in the soils mixed with oleander leaves at L0.5, L1 and L2 doses under 80 and 60% field capacities at 15th and 30th day of incubation

		Cellulase Activity (U/g)		Xylanase Activity (U/g)	
		15th day	30th day	15th day	30th day
80% FC	Control	0.112^{c}	0.118^{c}	0.445^{b}	0.483^{b}
	L0.5	0.128^{bc}	0.119^{c}	0.468^{b}	0.499^{b}
	L1	0.136^{ab}	0.135^{b}	0.485^{b}	0.534^{ab}
	L2	0.155^{a}	0.156^{a}	0.630^{a}	0.581^{a}
60% FC	Control	0.124^{a}	0.113^{c}	0.451^{b}	0.490^{c}
	L0.5	0.122^{a}	0.124^{ab}	0.453^{b}	0.526^{b}
	L1	0.123^{a}	0.141^{a}	0.541^{a}	0.598^{a}
	L2	0.142^{a}	0.131^{ab}	0.561^{a}	0.608^{a}

Values are means. Different letters denote significant differences among different doses of oleander leaves for each field capacities.

bacterial counts were in the order of $10^5 – 10^7$ cfu/g of soil, while fungal counts were in the order of $10^3 – 10^5$ cfu/g of soil in Obafemi Awolowo University, Nigeria. L1 dose have caused highest microorganism populations on 15th day while soil bacteria and fungi counts were respectively highest at L0.5 and L2 dose on 30th day under both field capacities. Reaction of doses of leaves to bacteria and fungi population were similar on 15th day but it was opposite on 30th day under field capacities. Some reports showed that leaves of oleander have both antimicrobial effects [28]. Therefore, it's possible to say that decomposition of leaves after 15th day caused occurrence of seconder metabolites in leaves or new compounds that soil bacteria and fungi used it as an energy source. Liu et al. [29] reported that culturable bacteria, fungal counts were only significantly affected by leaf litter species on 90th day.

The ratio of bacterial to fungal count (F/B) were in the range of 0.03 – 1.10 in all treatments and was highest (1.10) on 15th day and lowest (0.03) on 30th day dose at L0.5 under 80% FC. F/B of all treatments including control at the end of incubation period were lower than on 15th day. F/B ratio of doses of leaves were similar only on 15th day under 80% FC. On the other hand, L1 and L2 treatments were significantly different and higher than control (Table 3). Significant differences were found between control and all treatments under 80% FC ($p< 0.05$), between control and L2 on 30th day under both field capacities ($p<0.05$) and there were no significant differences between control and all treatments on 15th day under 60% FC.

Ratio of fungi to bacteria were definitely increased by L1 and L2 compared to control under both field capacities on both days but L0.5 only increased it on 15th day under 80% FC. Malik et al. [30] indicated that addition of litters to the soils caused abundance in fungi population and claimed that fungi to bacteria ratio are linked with carbon potential of soils. Lange et al. [31] reported that fungal-to-bacterial ratio was positively affected by plant diversity and indicated that soil bacteria population were more closely linked with abiotic differences caused by plants while fungi were more affected by organic matter inputs from plants.

Soil cellulase activity was generally increased by addition of leaves compared to control under both field capacities except 15th day of 60% FC and there were found no significant differences between control and all treatments in the same day under 60% FC (Table 4). There was only significant difference between control and L1 ($p< 0.05$) on both days under

60% FC. No significant differences were found between control and L0.5 but there were found with L1 and L2 on both days under 80% FC ($p< 0.05$). Highest cellulase activity was observed in L2 except 30th day under 60% FC. Soil xylanase activity was clearly increased as increasing doses of leaves. Significant differences were found among control and L2 on 15th day ($p< 0.05$) and 30th day ($p< 0.05$) under 80% FC. There were also found between control and both L1 and L2 on both days under 60% FC ($p< 0.05$). Highest xylanase activity was observed in L2 in all treatments.

Correlations in all parameters (counts of bacteria and fungi, cellulase and xylanase activities and carbon mineralizations) were present in Table 5. Under 80% FC, positive and significant correlations between carbon mineralization and all parameters were generally found on both days ($p< 0.05$). Also, xylanase activity under 80% FC significantly correlated with cellulase activity ($p< 0.05$) on both days. On the other hand, cumulative carbon mineralization under 60% FC was only positively and significantly correlated with only fungi population, xylanase activity and its rate on 15th day while only xylanase activity and its rate on 30th day ($p< 0.05$; Table 5). On both days, fungi populations were significantly and positively correlated with xylanase activity in carbon mineralization under 60% FC ($p< 0.05$).

Interactions of doses × field capacities were significant in aerobic bacteria population on 15th day, fungi population, cellulase activities and cumulative carbon mineralization on 30th day ($p< 0.05$).

Cellulase is one of the most important enzymes in soils which use cellulose as a polymer substrate, are mostly exist in the form of wood. However, plant cell walls consist of cellulose as a polysaccharide and assume the role of main input to soils. Cellulase, produced by microorganisms, hydrolyses cellulose into glucose. Activity of this enzyme by microorganisms can be affected by many parameters like pH, temperature and substrate concentration [32]. Kong and Dommergues [33] reported that carboxymethyl cellulose as a substrate were used as an indicator of cellulase activity. However, Joshi et al. [34] indicated that soil fungal and bacterial populations were significantly correlated with cellulase activity.

In this study, soil cellulase activity was generally increased by addition of leaves compared to their controls except L0.5 and L1 doses on 15th day under 60% FC and no change in L0.5 dose on 30th day under 60% FC (Table 4). Cellulase activity at L0.5 dose was similar in all treatments while L1 and L2 were low in 60% FC than 80% FC on both days. Maximum cellulase activity was observed at L2 dose on 15th day under 80% FC with an increase of 38% compared to control in this study. Nagaraju et al. [31] clearly indicated that effluents from sugar industry has altered both soil physical and chemical properties, affected the microorganisms and improved the soil cellulase activity, but it was decreased with the time. Moreover, same authors also indicated that the enzyme activity was improved up to 50% by increasing the amounts of effluents and then decreased. Also, it was reported that increase of soil organic matter by addition of maize straw to a loam soil has increased soil cellulase activity significantly after 45 days incubation and then decreased within time and its incubation for 90 days showed that cellulase was bonded strongly and immobilized more on its substrate [35]. Li et al. [36] mixed maize shoot and root residues into soil and then incubated them at 20°C for 150 days at 40% and 70% field capacities and reported that high soil water content treatment significantly increased the cumulative respiration and cellulase activity compared to the low soil water content treatment. Cellulase activity was more stable under 80% FC than under 60% FC as increasing doses of leaves increased enzyme activity compared to control under 80% FC while it was variable under 60% FC in this study.

Xylanase activity was reported to be a sensitive indicator for detecting changes in organic matter inputs and outputs and is reported for being responsible in the turnover of slowly decomposable material. Determining enzyme activities in soil and litter will enhance our understanding of studies dealing with effects of organic amendments like litter, compost etc., microbial community structure or abiotic and biotic variables on microbial processes [2].

TABLE 5
Correlation coefficients relating counts of bacteria and fungi, cellulase and xylanase activities in soils and the cumulative amount of CO_2 evolved under 80 and 60% FC on 15th and 30th days.

		15th day				30th day			
		BC	FC	Cel	Xyl	BC	FC	Cel	Xyl
80% FC	FC	0.816**				-0.03			
	Cel	0.577*	0,552			-0.118	0.874**		
	Xyl	0.371	0,221	0.870**		0,077	0.851**	0.773**	
	Cmin	0.736**	0.742**	0.915**	0.757**	0.21	0.871**	0.807**	0.823**
60% FC	FC	0.50				0.654*			
	Cel	-0.361	0.451			0.590*	0.451		
	Xyl	0.453	0.745**	0,354		0.534	0.786**	0.638*	
	Cmin	0.495	0.610*	0.016	0.626*	0.371	0.448	0.524	0.723**

BC: Bacteria count, FC: Fungi count, Cel: Cellulase, Xyl: Xylanase, Cmin: Carbon mineralization *: P < 0.05, ** : P < 0.01

Soil xylanase activities were also increased by all treatments. However, soil xylanase activities were increased as increasing doses of leaves and also, they were lower on 15th day than 30th day except L2 dose under 80% FC. In contrast, there were found only significant and positive correlation between fungi counts and xylanase activity on 15th day under 60% FC ($P < 0.01$) and correlations between all parameters on 30th day under 60% FC were variable (Table 5). No significant correlation among counts of total aerobic bacteria and xylanase activity was found in all treatments. Amin et al. [37] compared the effects of maize leaves and roots on soil Cmin for 43 days at 15°C and on soil cellulase and xylanase activities and claimed that Cmin of leaves was higher than roots and they found that microorganisms grew rapidly in the beginning of decomposition of high quality litter and produced non-efficient enzymes in degrading recalcitrant cell walls while, in the presence of the more recalcitrant maize roots, microorganisms grew slowly but produced high efficient enzymes. This study contributes our xylanase results that all treatments have increased enzyme activity as increasing doses of leaves on both days under both field capacities (Table 4).

CONCLUSIONS

In conclusion, all treatments have increased soil microbial counts while only L1 and L2 doses have affected significantly their enzyme activities under both field capacities. It's possible to conclude that aerobic bacteria and fungi can use oleander leaves as an energy source in this study and therefore, both their cellulase and xylanase activities were enhanced by addition of leaves. All doses of oleander leaves enhanced carbon mineralization under both capacities. While there were significant differences between control and all treatments under 80% FC, there were found no differences among same factors under 60% FC. It's possible to say that moisture is main driving factor in decomposition of oleander leaves through carbon mineralization in this study. Carbon mineralization was generally significantly correlated with soil microbial counts and enzyme activities under 80% FC. It was observed that all doses of oleander leaves generally didn't have any negative effect on soil carbon mineralization, microbial populations and their enzyme activities under both 80% and 60% of field capacities.

ACKNOWLEDGEMENTS

Authors thank Scientific Research Projects Coordination Unit of Cukurova University for funding this research under Project No.: FEF2013BAP27.

REFERENCES

[1] Ogunmwonyi, I.N., Igbinosa, O.E., Aiyegoro, O.A. and Odjadjare, E.E. (2008) Microbial analysis of different top soil samples of selected site in Obafemi Awolowo University, Nigeria. Scientific Research and Essays. 3, 120-124.

[2] Sinsabaugh, R.L., Antibus, R.K. and Linkins, A.E. (1991) An enzymatic approach to the analysis of microbial activity during plant litter decomposition. Agriculture, Ecosystems and Environment. 34, 43-54.

[3] Stemmer, M., Gerzabek, M.H. and Kandeler, E. (1998) Invertase and xylanase activity of bulk soil and particle-size fractions during maize straw decomposition. Soil Biology and Biochemistry. 31, 9-18.

[4] Yan, J., Pan, G., Li, L. and Quan, G. (2009) Cellulase Activity in Physically Isolated Fractions of a Paddy Soil. 2009 International Conference on Environmental Science and Information Application Technology, Wuhan. 613-616.

[5] Moyano, F.E., Vasilyeva, N., Bouckaert, L., Cook, F., Craine, J., Curiel Yuste, J., Don, A., Epron, D., Formanek, P., Franzluebbers, A., Ilstedt, U., Kätterer, T., Orchard, V., Reichstein, M., Rey, A., Ruamps, L., Subke, J.-A., Thomsen, I.K. and Chenu, C. (2012) The moisture response of soil heterotrophic respiration: interaction with soil properties. Biogeosciences. 9, 1173-1182.

[6] Bandara, V., Weinstein, S.A., White, J. and Eddleston, M. (2010) A review of the natural history, toxinology, diagnosis and clinical management of Nerium oleander (common oleander) and Thevetia peruviana (yellow oleander) poisoning. Toxicon. 56, 273-281.

[7] Boulogne, I., Germosen-Robineau, L., Ozier-Lafontaine, H., Jacoby-Koaly, C., Aurela, L. and Loranger-Merciris, G. (2012). Acromyrmex octospinosus (Hymenoptera: Formicidae) management. Part 1: Effects of TRAMIL's insecticidal plant extracts. Pest Management Science. 68(2), 313-320.

[8] Dheeba, B., Sampathkumar, P., Kannan, K., Kannan, M. and Tamizharasi, T. (2014) Comparison of Herbicidal Activity of Datura metal and Nerium oleander on the Weed, Parthenium hysterophorus in Green Gram Crop. National Academy Science Letters-India. 37(3), 269-274.

[9] El-Sayed, S.H. and El-Bassiony, G.M. (2016) Larvicidal, Biological and Genotoxic Effects and Temperature-Toxicity Relationship of Some Leaf Extracts of Nerium oleander (Apocynaceae) on Culex pipiens (Diptera: Culicidae). Journal of Arthropod-Borne Diseases. 10(1), 1-11.

[10] Khanh, T.D., Hong, N.H., Xuan, T.D. and Chung, I.M. (2005) Paddy weed control by medicinal and leguminous plants from Southeast Asia. Crop Protection. 24(5), 421-431.
[11] Bouyoucos, G.J. (1951) A recalibration of the hydrometer method for making mechanical analysis. Agronomy Journal. 43, 434-438.
[12] Demiralay, I. (1993) Toprak Fiziksel Analizleri. Erzurum, Turkey: Atatürk Üniversitesi Ziraat Fakültesi (in Turkish).
[13] Duchaufour, P. (1970) Precis de Pedologie. Paris, France: Masson et C1e (in French).
[14] Schaefer, R. (1967) Characteres et evolution des activites microbiennes dans une chaine de sols hydromorphes mesotrophiques de la plaine d'Alsace. Revue d'Ecologie et de Biologie du Sol. 4, 567–592.
[15] Benlot, C. (1977) Recherches sur les activites biochimiques dans les successions de sols derives de cendres volcaniques sous climat tropical humide (Zaire-Indonesie). Paris, France: ENS Lab de Zoologie (in French).
[16] Koçak, B. and Darici, C. (2016) Priming effects of leaves of Laurus nobilis L. and 1,8-cineole on carbon mineralization. Chilean Journal of Agricultural Research. 76, 100-104.
[17] Atlas, M.R. (2005) Handbook of media for environmental microbiology. 2nd. Ed. Boca Raton, FL, USA: CRC Press.
[18] Criquet, S. (2002). Measurement and characterization of cellulase activity in sclerophyllous forest litter. Journal of Microbiological Methods. 50, 165-173.
[19] Khalili, B., Nourbakhsh, F., Nili, N., Khademi, H. and Sharifnabi, B. (2011) Diversity of soil cellulase isoenzymes is associated with soil cellulase kinetic and thermodynamic parameters. Soil Biology and Biochemistry. 43, 1639-1648.
[20] Miller, G.L. (1959) Use of dinitrosalicylic acid reagent for determination of reducing sugar. Analytical Chemistry. 31, 426-428.
[21] Wood, T.M. and Bhat, K.M. (1988) Methods for measuring cellulase activities. Methods of Enzymology. 160, 87-112.
[22] Fioretto, A., Papa, S., Pellegrino, A. and Fuggi, A. (2007) Decomposition dynamics of Myrtus communis and Quercus ilex leaf litter: Mass loss, microbial activity and quality change. Applied Soil Ecology. 36, 32-40.
[23] Boga, T., Sagliker, H.A. and Cenkseven, S. (2017) The first effect of Eucalyptus camaldulensis leaves and eucalyptol additions on soil carbon mineralization. Fresen. Environ. Bull. 26, 1052-1060.
[24] Teklay, T., Nordgren, A., Nyberg, G. and Malmer, A. (2007) Carbon mineralization of leaves from four Ethiopian agroforestry species under laboratory and field conditions. Applied Soil Ecology. 35, 193-202.
[25] Mafongoya, P.L., Barak, P. and Reed, J.D. (2000) Carbon, nitrogen and phosphorus mineralization of tree leaves and manure. Biology and Fertility of Soils. 30, 298-305.
[26] Berg, B. and Staaf, H. (1981) Leaching, accumulation and release of nitrogen in decomposing forest litter. In Editors F.E. Clark and T. Rosswall, Terrestrial Nitrogen Cycles, Stockholm. 33, 163-178.
[27] Torreta, N.K. and Takeda, H. (1999) Carbon and nitrogen dynamics of decomposing leaf litter in a tropical hill evergreen forest. European Journal of Soil Biology. 35, 57-63.
[28] Malik, R., Bokhari, T.Z., Siddiqui, M.F., Younis, U., Hussain, M.I. and Khan, I.A. (2015) Antimicrobial activity of Nerium oleander L. and Nicotiana tabacum L.: A Comparative Study. Pakistan Journal of Botany. 47, 1587-1592.
[29] Liu, Y.X., Wang, S.L., Wang, Q.K. and Zhang, J.A. (2010) Effects of mixed-species leaf litter on litter decomposition and soil microbial communities in experimental subtropical plantation forest. Journal of Food, Agriculture and Environment. 8, 1102-1107.
[30] Malik, A.A., Chowdhury, S., Schlager, V., Oliver, A., Puissant, J., Vazquez, P.G.M., Jehmlich, N., von Bergen, M., Griffiths, R.I. and Gleixner, G. (2016) Soil Fungal:Bacterial Ratios Are Linked to Altered Carbon Cycling. Frontiers in Microbiology. 7,1247.
[31] Lange, M., Habekost, M., Eisenhauer, N., Roscher, C., Bessler, H., Engels, C., Oelmann, Y., Scheu, S., Wilcke, W., Schulze, E.D. and Gleixner, G. (2014) Biotic and Abiotic Properties Mediating Plant Diversity Effects on Soil Microbial Communities in Experimental Grassland. PLoS ONE. 9(5), e96182.
[32] Nagaraju, M., Narasimha, G. and Rangaswamy, V. (2009) Impact of sugar industry effluents on soil cellulase activity. International Biodeterioration and Biodegradation. 63, 1088-1092.
[33] Kong, K.T. and Dommergues, Y. (1972) Limitation of cellulolysis in organic soils. II. Study of soil enzymes. Revue d'Ecologie et de Biologie du Sol. 9, 629-640.
[34] Joshi, S.R., Sharma, G.D. and Mishra, R.R. (1993) Microbial enzyme activities related to litter decomposition near a highway in a subtropical forest of North East India. Soil Biology and Biochemistry. 25, 1763-1770.
[35] Sinegani, A.A.S. and Sinegani, M.S. (2013) Adsorption, immobilization and activity of cellulase in soil: the impacts of maize straw and its humification. Brazilian Archives of Biology and Technology. 56, 885-894.

[36] Li, Z.Q., Zhao, B.Z. and Zhang, J.B. (2016) Effects of maize residue quality and soil water content on soil labile organic carbon fractions and microbial properties. Pedosphere. 26, 829-838.
[37] Amin, B.A.Z., Chabbert, B., Moorhead, D. and Bertrand, I. (2014) Impact of fine litter chemistry on lignocellulolytic enzyme efficiency during decomposition of maize leaf and root in soil. Biogeochemistry. 117, 169-183.

Received: **10.06.2017**
Accepted: **03.10.2017**

CORRESPONDING AUTHOR

Burak Kocak
Department of Biology
Cukurova University
Adana – Turkey

e-mail: burakkocak@gmx.com

© by PSP Volume 26 – No. 12A/2017 pages 8001-8007 Fresenius Environmental Bulletin

RAINFALL-TRIGGERED LIMITED DATA-BASED ANALYSIS OF LANDSLIDES IN TRABZON PROVINCE, TURKEY

Ebru Eris*

Department of Civil Engineering, Ege University, Bornova, Izmir, Turkey

ABSTRACT

Rainfall is one of the most important triggering factors of landslides. Researchers carry out various scientific studies on identification of the rainfall amount that trigger landslides. The Eastern Black Sea region is a landslide-prone area in Turkey. The population of the region is affected by the landslides because of high rainfall and the steep topography of the region. The aim of this study is to investigate the relationship between rainfall and landslide for the Trabzon province the most vulnerable city to landslides in the region. For this purpose, rainfall and rainfall-induced landslides data are used. The relation between rainfall and landslide events is analyzed considering meteorological records of rain-gauge stations.

KEYWORDS:
Landslide, rainfall threshold, Trabzon

INTRODUCTION

Landslides can be seen as a primary cause of soil erosion, which is a serious geo-environmental issue causing land degradation, and has posed a serious threat to the security of ecology and environment, and socio-economic sustainable developments [1-4]. Although there can be many different causes of landslides such as earthquakes, clear cutting, mining; rainfall is the most common landslide-triggering factor in many regions across the world. Rainfall induced landslides have been investigated by many researchers who have mostly attempted to determine the amount of rainfall that can trigger soil erosion. Rainfall thresholds are derived by the analysis of historical rainfall and landslide data. Rainfall intensity-duration thresholds for triggering landslides have been widely identified in many different climates and geological settings [5-13].

In Turkey, landslides are one of the most important natural hazards. During the period of 1959-1994, landslides damaged 76995 buildings throughout Turkey [14] in addition to causing deaths of people, destroying agricultural lands and roads etc. For this reason, regional landslide susceptibility assessments have crucial importance for the landslide-prone areas of Turkey [15].

Various-scale landslides occur almost every year in the Trabzon Province in the Eastern Black Sea Region of Turkey. More than 178 events triggered by rainfall were identified by historical records from 2005 to 2008 in the province [16]. In Trabzon, rainfall-induced landslides lead to considerable damage, even causing human losses.

This study aims to analyze and summarize landslides in Trabzon and to determine empirical rainfall intensity–duration thresholds for landslides in the Trabzon province using limited data. The method employed in establishing rainfall thresholds is compared to available thresholds developed for other regions in the world.

MATERIALS AND METHODS

Study Area and Data. Trabzon is located between 39º15' - 40º15' East-longitudes and 41º08' - 40º30' North-latitudes in the middle of the Eastern Black Sea Region of Turkey (Figure 1). Elevation increases from sea level to reach up to 3000 m. Generally, mountains, hills and high plateaus take part in inner lands of the region.

Trabzon has a mild and humid climate with heavy uniform rainfall and relatively warm temperatures all year round. Rainfall is heaviest in autumn and spring. The temperature difference between the day and night is not very high. During the winter, the lowest average minimum temperature is seen in January around 5 °C. Summers are warm and humid with the average maximum temperature around 28 °C in July and August. Generally, annual rainfall in Trabzon (approximately 900 mm) is higher than the long-term average annual rainfall (approximately 646 mm) for Turkey.

Although there are 12 rainfall gauging stations located in Trabzon province, only daily rainfalls and hourly durations recorded by 7 stations are used in this study. Daily rainfall data between the years 1995 and 2016 and rainfall duration of each station located in Trabzon are given in Table 1, from which it can

be seen that the rainfall data are discontinuous and there are some gaps in the recording periods.

Relationship between Landslides and Rainfall. Landslide is affected by geological and morphological factors as well as external triggering factors such as earthquakes, human activities and extreme climatic events, heavy rainfall, and hydrology [17]. Heavy rainfall among these factors occurs frequently in the Eastern Black Sea Region. Climate in the Eastern Black Sea Region is very humid. Comparison of climate and landslide density maps of Turkey (Figure 2a and 2b) shows the similarity between the two events. This demonstrates that landslide is affected by the variation in the climate of the region.

Factors affecting the occurrence of landslides in Trabzon are the morphology of the province, geological structure, weathering of rocks, meteorological characteristics, settlement types, and various types of excavation works. Heavy rainfall, sloping topography, and the removal of forests for agricultural purposes increase the landslide risk [18, 19]. Trabzon is one of the leading provinces where landslide risk is high in Turkey, with 662 landslides causing 245 dead people since 1950 [20].

Potential landslide risk map for Trabzon is given in Figure 2c [21, 22]. According to this map, about 64% of Trabzon province land is at risk against landslide. This is because most of the settlement areas within this 64% of the province are in river basins and on sloping terrain [20].

In 1998, 50 people were killed and 100 residences were damaged. Between the years 2004 and 2009, various landslides occurred and caused damage. Daily and cumulative rainfall is shown in Figure 3 together with a field photograph of landslide event occurred in 2009, for Uzungol gauging station. It can be noticed that landslide on 21 November 2009 in Uzungol were triggered by approximately 75 mm of rainfall which killed 2 people.

Landslide records in Trabzon province are very rare from between 1900 to 1950 however; more data are available from 1950 to 1987. Recording of this period is only related to deep landslides. However, a clear relationship was not able to be found between deep landslides and precipitation. In addition, deep landslides represent only 3% of the landslides in Trabzon [23].

Since 1995, important landslide events were considered in the study area when all available landslide data, obtained through local and national administrations, technical and scientific articles, thesis and internet news, are all taken into account. Although Disaster and Emergency Management Presidency (AFAD with Turkish acronym) has a database of landslide events, the factors that cause landslides are not clearly present for each event. The most important 24 rainfall-triggered landslides between 1995 and 2016 are carried out using available rainfall data in the rainfall threshold analyses explained below.

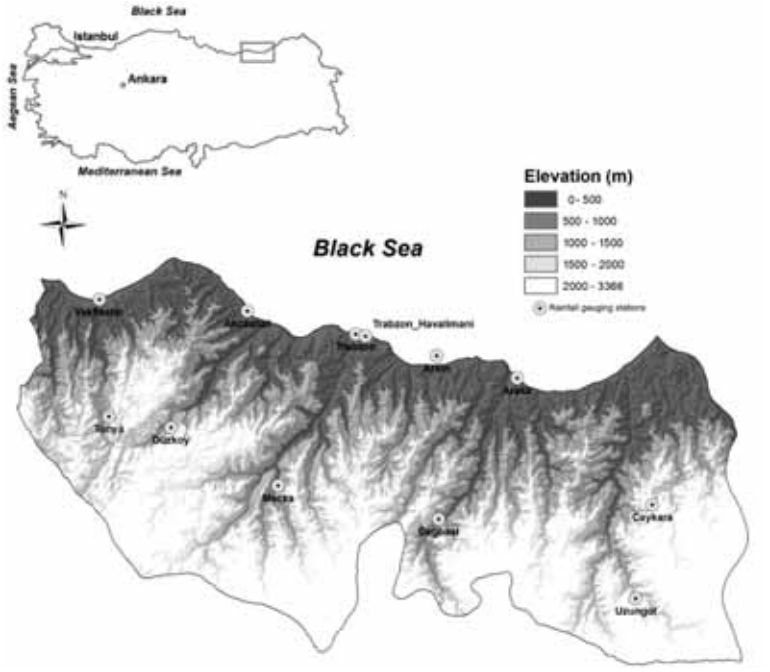


FIGURE 1
Study area and rainfall gauging stations

TABLE 1
Rainfall data and rainfall duration of gauging stations

Station No	Station		Years																			
			1995	1996	1997	1998	1999	2000	2001	2002	2003	2004	2005	2006	2007	2008	2009	2010	2011	2012	2013	2014	2015	2016
1302	Vakfıkebir	Rainfall																						
		Duration																						
1471	Arsin	Rainfall																						
		Duration																						
1472	Araklı	Rainfall																						
		Duration																						
1962	Uzungol	Rainfall																						
		Duration																						
1623	Tonya	Rainfall																						
		Duration																						
1624	Duzkoy	Rainfall																						
		Duration																						
1626	Macka	Rainfall																						
		Duration																						
1787	Dagbasi	Rainfall																						
		Duration																						
1801	Caykara	Rainfall																						
		Duration																						
17037	Trabzon	Rainfall																						
		Duration																						
17038	Trabzon Havalimani	Rainfall																						
		Duration																						
17626	Akacaabat	Rainfall																						
		Duration																						

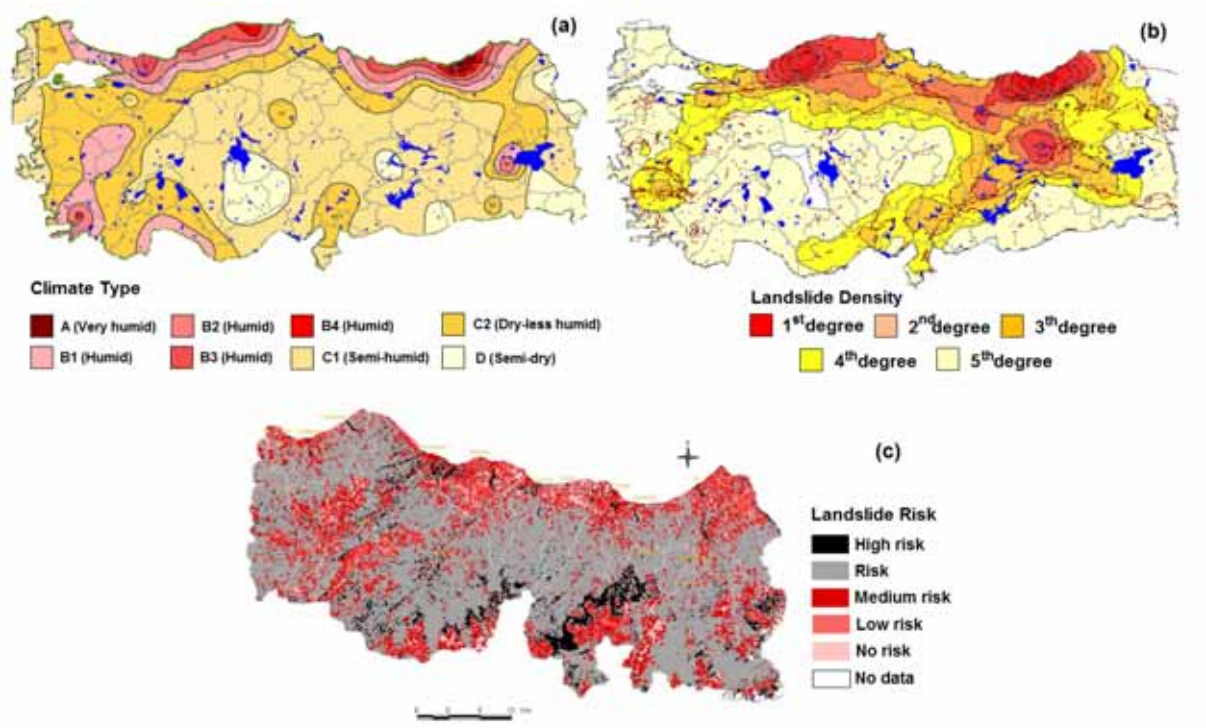


FIGURE 2
(a) Climate classification of Turkey, (b) Landslide density map of the settlements (1950-2010) and (c) Potential landslide hazard map for Trabzon

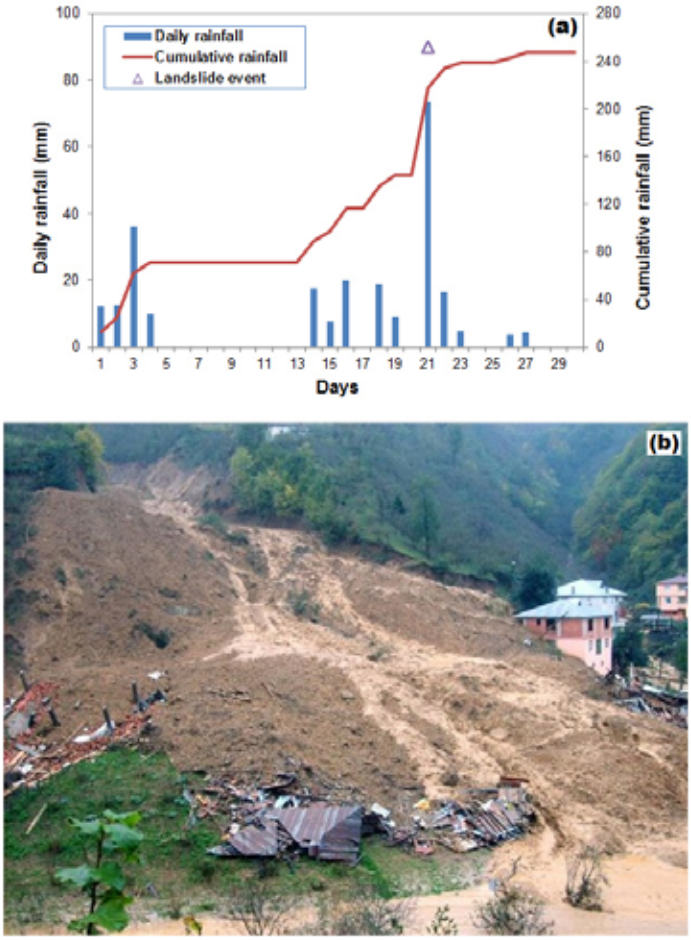


FIGURE 3
(a) Daily and cumulative rainfall and landslide events for Uzungol gauging station in 2009, (b) field photograph of landslide event (Source: http://www.ntv.com.tr/)

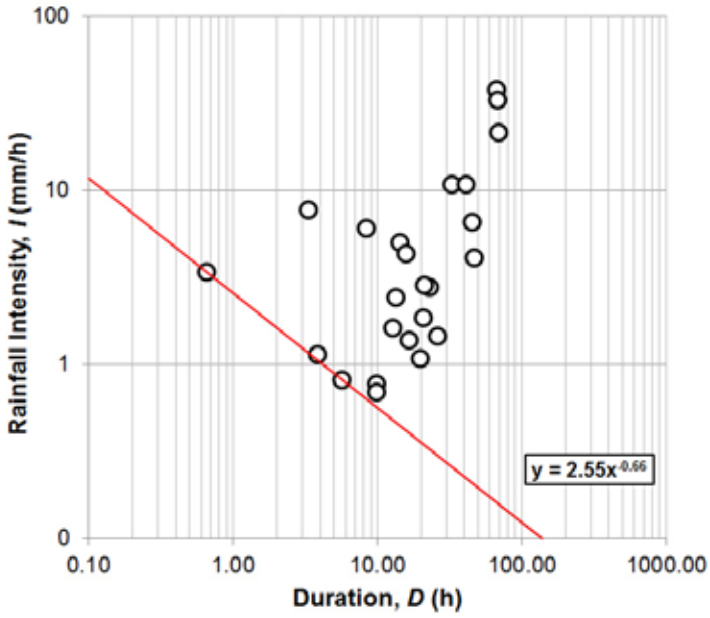


FIGURE 4
Rainfall intensity-duration threshold curve for landsliding in Trabzon

TABLE 2
Some rainfall intensity-duration threshold equations

Study by	Case Study	Equation
Caine (1980)	Over the world	$I = 14.82\ D^{-0.39}$
Cancelli and Nova (1985)	Northern Italy	$I = 44.67\ D^{0.78}$
Wieczorek (1987)	California	$I = 1.7+9\ D^{-1}$
Crosta and Frattini (2001)	Over the world	$I = 0.48+7.2\ D^{-1}$
Aleotti (2004)	Italy	$I = 19\ D^{-050}$
Guzetti et al. (2007)	Mid-latitude climate for D<300h	$I = 18.6\ D^{-0.81}$
Guzetti et al. (2007)	Mid-latitude climate for D>300h	$I = 0.82\ D^{-0.19}$
Dahal and Hasegawa (2008)	Himalaya, Nepal	$I = 73.9\ D^{-0.79}$
Rosi et al. (2016)	Slovenia	$I = 37.7\ D^{-0.68}$
Baltaci (2010)	Trabzon	$I = 8.641\ D^{-0.4591}$
Akcali (2011)	Trabzon	$I = 0.69\ D^{-0.99}$
Akcali and Arman (2013)	Trabzon for D<6h	$I = 57.73\ D^{-2.33}$
Akcali and Arman (2013)	Trabzon for D>6h	$I = 2.75\ D^{-0.63}$
This study (2017)	Trabzon	$I = 2.55\ D^{-0.66}$

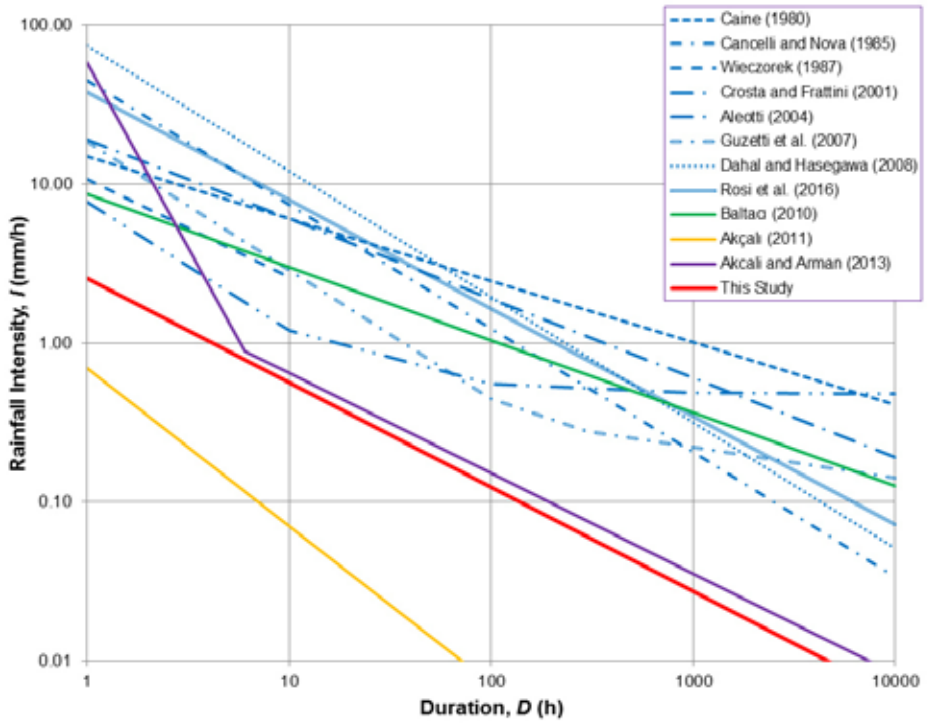


FIGURE 5
Rainfall intensity-duration thresholds compiled from various studies

RESULTS

Threshold Analysis. Determination of rainfall thresholds for the initiation of landslides can be important as a decision-making tool in risk management. For this purpose, two approaches have been proposed. The first approach is based on physical, process-based models whereas the second one is based on the definition of empirical thresholds [6, 7, 9, 12, 13, 24-26]. The thresholds are usually obtained by drawing lower-bound lines to the rainfall conditions resulted in landslides plotted in linear, semi-logarithmic, or logarithmic coordinates. Most commonly, the thresholds are drawn visually.

The threshold for Trabzon, as defined by the lower boundary envelope of the points representing landslide-triggering rainfall events, is expressed as:

$$I = 2.55\ D^{-0.66} \quad (1)$$

where I is hourly rainfall intensity in mm/h and D is rainfall duration in hours (Figure 4). Among the 24 landslide data, the proposed curve optimally defines the rainfall events with durations $0.65\text{h} \leq D \leq 70\text{h}$. In the threshold analysis, the nearest gauging stations

to be the landslide locations are selected. When rainfall data and/or rainfall duration are not available at the nearest gauging station to the landslide event, the data of the next station is used. The total rainfall observations of the current and previous days are considered as rainfall events causing the corresponding landslide event.

Different rainfall intensity threshold values are available for different climatic regions over the world. Fifty two previous works of intensity-duration thresholds for the initiation of landslides at global, regional and local contexts were summarized by [12]. Some of these relations together with previous works for Trabzon are given in Table 2 and Figure 5.

In the threshold analysis made by [27], 21 landslide events between the years 1990 and 2009 were used. The threshold line proposed by [28] seems to be different from the other lines in Figure 5. This study modified by [23] and classified thresholds depending on the duration of rainfall, whether it is shorter or longer than 6 hours. The landslide data used by [23] is up to the year 2010. On the other hand, the landslide data used in this study is for the period up to 2016 and the threshold line is between the lines obtained by [23] and [27].

According to [12], the threshold lines generally depend on the climatic environment of the region. It is stated that the thresholds defined by various researchers for mid-latitude climates are steeper (the power value of D is between -0.70 and -0.81) than the thresholds obtained for mountainous regions (the power value of D in between -0.48 and -0.64). This is a result that almost matches the threshold for landslides in Trabzon.

CONCLUSIONS

In this study, relations between rainfall and landslide events in Trabzon province, Turkey, is analyzed. An empirical rainfall intensity-duration threshold for landslides in Trabzon is proposed. The main problem here is that the data of gauging stations in Trabzon are not continuous and they generally have missing data.

For the risk mitigation studies, landslide early warning systems can be implemented by using rainfall-landslide thresholds as proposed in this study. Although early warning systems have been frequently proposed for Trabzon, there is no system currently in operation.

The proposed empirical relation takes rainfall only into account; it does not consider other factors causing landslide such as slope, land use, vegetation, etc. The proposed threshold equation seems to be a reasonable approximation when it is compared to previous equations developed from data of landslides in Trabzon.

There are only a few intensity-duration threshold studies on landslides at local scale in Turkey. At present, such a general threshold relation is not available for the whole country. This can be considered an important gap in terms of both research and practice. Therefore further studies should be carried out to obtain local-scale rainfall thresholds triggering rainfall-induced landslides. This particularly emerges for landslide-prone regions.

REFERENCES

[1] Myrodinis, D., Ioannou, K., Sapountzis, M. and Fotakis, D. (2010) Development of a sustainable plan to combat erosion for an island of the Mediterranean region. Fresen. Environ. Bull. 19(8b), 1694-1702.

[2] Stathis, D., Sapountzis, M. and Myronidis, D. (2010) Assessment of land-use change effect on a design storm hydrograph using the SCS curve number method. Fresen. Environ. Bull. 19(9a), 1928-1934.

[3] Yonter, G. and Uysal, H. (2017) The effects of unmixed and mixed applied tobacco waste on runoff, soil loss, drainage, pH and EC. Fresen. Environ. Bull. 26(3), 2126-2132.

[4] Yonter, G. and Uysal, H. (2017) The effects of unmixed and mixed applied olive mill waste on runoff, soil loss, drainage, pH and EC. Fresen. Environ. Bull. 26(3), 2237-2244.

[5] Campbell, R.H. (1975) Soil slips, debris flows, and rainstorms in the Santa Monica Mountains and vicinity, Southern California. Professional Paper 851, US Govt. Print. Off., Washington, D.C.

[6] Caine, N. (1980) The rainfall intensity: duration control of shallow landslides and debris flows. Geografiska Annaler. Series A, Physical Geography. 62, 23–27.

[7] Cancelli, A. and Nova, R. (1985) Landslides in soil debris cover triggered by rainstorms in Valtellina (Central Alps – Italy). Proceedings of the 4th International Conference on Landslides, Tokyo, Jpn. Geol. Soc., Tokyo, 267–272.

[8] Cannon, S.H. and Ellen, S.D. (1985) Rainfall conditions for abundant debris avalanches in the San Francisco Bay Region, California. California Geology. 38, 267–272.

[9] Aleotti, P.A. (2004) Warning system for rainfall-induced shallow failures. Engineering Geology. 73, 247–265.

[10] Wieczorek, G.F. and Guzzetti, F. (1999) A review of rainfall thresholds for triggering landslides. Proceedings of the EGS Plinius Conference, Maratea, Italy, 407–414.

[11] Wieczorek, G.F., Morgan, B.A. and Campbell, R.H. (2000) Debris-flow hazards in the Blue Ridge of central Virginia. Environmental and Engineering Geosciences. 6, 3–23.

[12] Guzzetti, F., Peruccacci, S., Rossi, M. and Stark, C.P. (2007) Rainfall thresholds for the initiation of landslides in central and southern Europe. Meteorology and Atmospheric Physics. 98, 239–267.
[13] Rosi, A., Peternel, T., Jemec-Auflic, M., Komac, M., Segoni, S. and Casagli, N. (2016) Rainfall thresholds for rainfall-induced landslides in Slovenia. Landslides. 13, 1571-1577.
[14] Ildir, B. (1995) Distribution of landslides and applications related to disaster legislations in Turkey. Proceedings of 2nd National Landslide Symposium of Turkey, Sakarya University, 1–9 (in Turkish).
[15] Duman, T.Y., Can, T., Gokceoglu, C. and Nefeslioglu, H.A. (2005) Landslide susceptibility mapping of Cekmece area (Istanbul, Turkey) by conditional probability. Hydrology and Earth System Sciences Discussions. 2(1), 155-208.
[16] Bayrak, T. and Ulukavak, M. (2009) A view of Trabzon landslides. International Symposium on Modern Technologies, Education and Professional Practice in Geodesy and Related Fields, Sofia, 109-113.
[17] Karsli, F., Atasoy, M., Yalcin, A., Reis, S., Demir, O. and Gokceoglu, C. (2009) Effects of land-use changes on landslides in a landslide-prone area (Ardesen, Rize, NE Turkey). Environmental Monitoring and Assessment. 156, 241–255.
[18] Ozdemir, A. (2008) Preventing natural hazard risks through sustainable site design. Polish Journal of Environmental Studies. 17(4), 457-462.
[19] Reis, S. and Yomralioglu, T. (2005) In Trabzon Province, Turkey, Potential Landslide Areas Are Detected with GIS. ESRI ArcNews, 27 (2), Redlands, CA, USA.
[20] Reis, S., Nisanci, R. and Yomralioglu, T. (2009) Designing and developing a province-based spatial database for the analysis of potential environmental issues in Trabzon, Turkey. Environmental Engineering Science. 26(1), 123-130.
[21] Reis, S. (2003) Design and application of Geographic Information System (GIS) for enviromental planning database purpose: a model of Trabzon information system, Karadeniz Technical University, Trabzon (in Turkish).
[22] Trabzon AFAD. Available online: http://www.trabzonafad.gov.tr/index.asp?id=haritalar (Accessed on 02.06.2014).
[23] Akcali, E. and Arman, H. (2013) Landslide early warning system suggestion based on landslide-rainfall threshold: Trabzon Province. IMO Technical Bulletin. 396, 6307-6332 (in Turkish).
[24] Wieczorek, G.F. (1987) Effect of rainfall intensity and duration on debris flows in central Santa Cruz Mountains, California. In: Debris flows/avalanches: processes, recognition and mitigation. Reviews in Engineering Geology No: 7, Crosta, G., Wieczorek, G.F. (Eds.) Geological Society of America, Boulder, CO, 93–104.
[25] Crosta, G. and Frattini, P. (2001) Rainfall thresholds for triggering soil slips and debris flow. Proceedings of EGS 2nd Plinius Conference 2000, Mediterranean Storms. Siena, 463–488.
[26] Dahal, R.K. and Hasegawa, S. (2008) Representative rainfall thresholds for landslides in the Nepal Himalaya. Geomorphology, 100(3), 429-443.
[27] Baltaci, H. (2010) Investigating of the relationship between landslide and precipitation and the assessment of minimum threshold values for Eastern Black Sea Region (Rize, Trabzon, Giresun), Istanbul Technical University, Eurasia Institute of Earth Sciences, Istanbul (in Turkish).
[28] Akcali, E. (2011) Modelling and analysis of landslide-rainfall relationship in Trabzon province, Sakarya University, Institute of Natural Sciences, Sakarya (in Turkish).

Received: **11.06.2017**
Accepted: **06.10.2017**

CORRESPONDING AUTHOR

Ebru Eris
Ege University
Department of Civil Engineering
Bornova, 35100, Izmir – Turkey

e-mail: ebru.eris@ege.edu.tr

© by PSP Volume 26 – No. 12A/2017 pages 8008-8022 Fresenius Environmental Bulletin

THE TURKISH SURVEYING PRIVATE SECTOR

Okan Yildiz, Yakup Emre Coruhlu*

Karadeniz Technical University, Faculty of Engineering, Department of Geomatics Engineering, 61080, Trabzon, Turkey

ABSTRACT

The increasing importance of the private sector in the execution of surveying/geomatics engineering services needed for works ranging from cadastre to various engineering activities throughout the world and in Turkey has drawn increased attention. Turkey has taken its position in the world, with more than 2600 private engineering offices and approximately 200 Licensed Surveying Engineering Offices. The surveying private sector is utilized in the execution of almost all surveying activities in our country today, especially in cadastre services. In addition, considering the increase in the number of technical personnel (Geomatics Engineer/Technician) each year, the importance of the sector in terms of employment stands out. Despite the rapid development of the sector in recent years, traditional issues and domestic and foreign developments have had both positive and negative impacts on the sector. It is important to engage in strategic planning, amplifying the weak aspects and making use of the strong aspects of the sector under these impacts. For this purpose, sector representatives were contacted directly through the survey method in this study. SWOT (Strength, Weakness, Opportunities, and Threats) analysis of the sector was conducted with the obtained data. Accordingly, it was determined that the sector consists of micro enterprises known on the local level of the sector.

KEYWORDS:
Surveying private sector, surveying activities, licensed surveying engineering office, SWOT Analysis

INTRODUCTION

Considering national and international developments, the Surveying Private Sector (SPS) now plays significant roles in basic mapping activities and various engineering projects. The SPS in Turkey is represented by corporate bodies (enterprises) known as Private Surveying Engineering Offices (PSEOs) and Licensed Surveying Engineering Offices (LSEOs) [1]. The aforementioned enterprises are affiliated with the Union of Chambers of Turkish Engineers and Architects (UCTEA)/Chamber of Survey and Cadastre Engineer (CSCE). The active role of the SPS in mapping activities in Turkey dates back to the 1950s. Whereas there were 7 enterprises countrywide during those periods, that number reached 240 in the decade after the publication of regulations on maps and plans based on registration [2, 3]. The mentioned enterprises maintained their activities (land subdivision, parcelling, expropriation, renunciation for roads, etc.) in business items created by change operations post cadastre. The service purchasing method from the private sector was applied for cadastre work for the first time in Turkey in 1988. However, based on pilot regions, it was determined that the method could not be popularized countrywide. During this period, in the report published by the State Planning Organization (SPO), it was determined that the SPS should be restructured. In the same report, the services not made or not popularized by the SPS, including responsibility for plan applications, basic cadastre work, renovations and other change operations, the establishment of information systems, infrastructure mapping, the popularization of land readjustment [4], mining operation maps, project applications in structuring services, and consultancy and controlling services, are listed [5]. The most active period of the SPS was after the purchase of the Production Numerical Cadastral Base from the private sector after 2005. The private sector had a voice in basic cadastre work with the regulations on Cadastre Law [6]. The cadastre work was accelerated by using both internal sources (General Directorate of Land Registry and Cadastre GDLRC Floating Capital) and external credits (World Bank sources) intensely [1]. A threefold performance increase has occurred as the private sector has taken on an active role in basic cadastre work (Figure 1).

Basic mapping activities (application, land use conversion etc.), the result of work conducted under the body of GDLRC, and change operations on demand have been transferred to LSEOs. Despite there being 2029 LSEOs planned for the country initially, a total of 196 LSEOs operate today [7, 8]. In contrast, the number of PSEOs exceeds 2600 (Figure 2). The number approaches 3000 when adding the enterprises not registered in 2016, despite being officially established [9].

Considering the developments in this area around the world, the private sector now plays a significant role in the increase of productivity in production concerning engineering activities. Parallel to this development, the share of the private sector in surveying work is increasing gradually. Hence, some

international organizations, such as the International Federation of Surveyors (FIG), United Nations (UN), European Union (EU) and World Bank (WB), have published various notifications, reports and declarations to increase the effectiveness of land administration systems, which are important to sustainable development [10- 15]. The mentioned notifications have noted that the private sector should benefit more in the development of Land Administration Systems [16]. As a similar development, in a worldwide study by FIG in 1994, the developments in the next 20 years in the area of cadastre, one of the basic mapping activities, have been summarized in a report known as Cadastre 2014. The report mentioned the *"Increase of contribution of the private sector"* as one of the possible reform movements in cadastral systems in the future [17]. In other evaluations, specific to cadastre, *"affordable, fast and safe cadastre"* services are mentioned worldwide. It is stated that the solution is for the private sector and the public sector to act jointly [18, 7, 19].

Considering basic mapping engineering activities transferred to the SPS in the most recent period in Turkey, it is observed that almost all activities in this area are being conducted by the private sector. Although the exact numbers are unknown, it is estimated that the sector creates significant employment. The projects realized by GDLRC, such as the Completion Project of Turkey Cadastre and the Land Registry and Cadastre Modernization Project, including renovation work [20], contributed significantly to the process [21] stated that the collaboration with the World Bank and projects realized in the area of land and cadastre services have increased the business capacity of the SPS in international standards, with the World Cadastre Summit organizing broad participation in Turkey in 2015. As a result, Turkey has made efforts to share its knowledge about mapping with the world through the private and public sectors. According to [22], cadastre projects of USD 2.9 billion were funded by the World Bank throughout the world in 2015. It has been observed that project studies have been initiated under the title of the *"Exportation of the Turkish Cadastre System"* in this area of the Turkish Cooperation and Coordination Agency (TCCA, in Turkish TIKA).

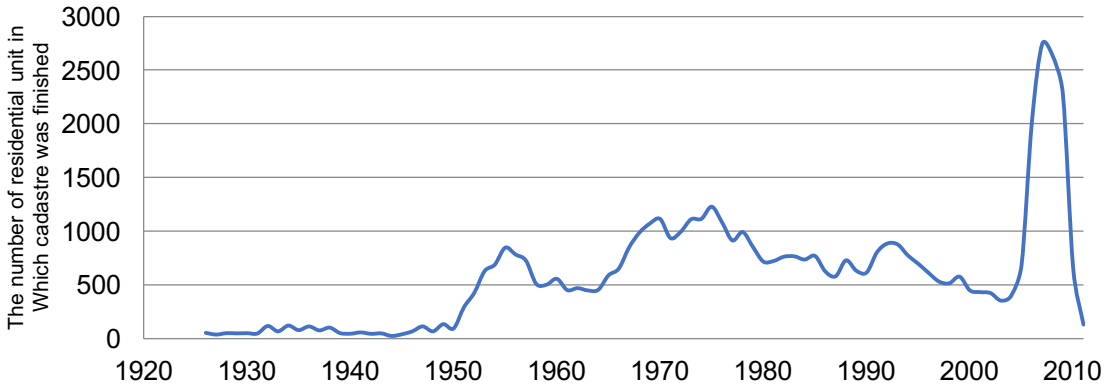


FIGURE 1
Distribution of cadastre works in Turkey by years [7].

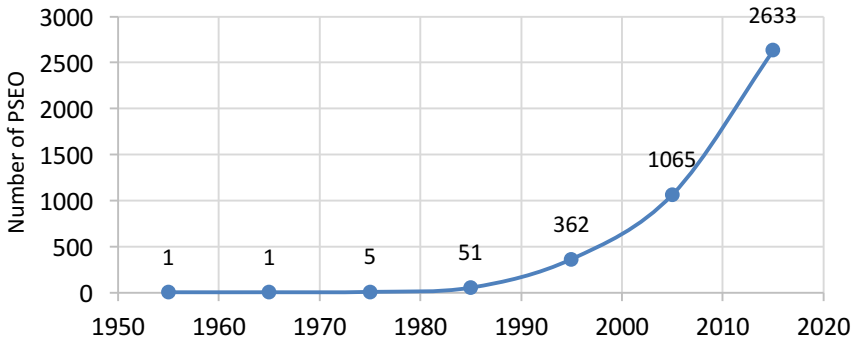


FIGURE 2
Number of PSEO [7]

Despite the increasing importance of the SPS, it is observed that the sector faces problems based on various factors in Turkey. One of them is the rapidly increasing number of graduates with Geomatics Engineering degrees. According to the Measuring, Selection and Placement Center, MSPC (in Turkish OSYM), 1600 students have been placed in 20 Geomatics Engineering Departments in Turkey [23]. Although a Department of Geomatics Engineering exists in 12 universities, the placement of students cannot be realized due to the lack of infrastructure. Accordingly, it is thought that incremental growth in the number of graduates will occur in the future. A 300% increase in PSEOs in the last decade in Turkey is the most significant reflection of the issue, according to the Chamber of Survey and Cadastre Engineers, CSCE (in Turkish HKMO) [9]. In addition, the other issues are as follows: non-registration of activities conducted based on the contract in terms of administration and finance, failure to provide minimum price audits, and failure to provide corporate and technical standards amongst PSEOs [7].

The fundamental motivations of the study are as follows: Will the sector be adequate in creating employment? Does the increase of the labour force create threats or opportunities for the sector? What are the current conditions of the sector? What new business areas are needed? The existing problems should be determined, and the solution recommendations should be developed.

MATERIALS AND METHODS

The recognition of opportunities and threats in addition to strong and weak aspects has great importance strategically for increasing the effectiveness of the SPS in Turkey. Primarily, research on understanding the sector is needed. The most important factor sustaining the SPS as a part of service sector is certainly the personnel structure. The software, equipment and market conditions are the other factors.

The sector is analysed based on research under the following categories:

- Administrative and technical infrastructure of the enterprises forming the SPS,
- External shareholders with which to conduct projects,
- The situation of the sector in terms of economic growth,
- Recognition on national and international levels,
- Other unofficial activities operated in the sector, and
- External threats and opportunities for the sector.

The data shall be collected with the classification of the sector in terms of economics through research of its potential, alternative operational areas and scientific analysis regarding the corporate structure. Thus, understanding how to respond to opportunities and threats or remove the weaknesses shall be determined by revealing the strong and weak aspects of the sector. SWOT analysis shall be used as a method.

SWOT is an abbreviation of the first letters of Strengths, Weaknesses, Opportunities and Threats. An analysis concerning both quantitative and qualitative features can be realized through this method, which analyses these four parameters belonging to existing structures in detail. A strategical view of an existing program can be formed with an investigation of the SWOT matrix created as a result of the analysis. Whereas the strong and weak aspects are determined through an internal evaluation in the organization, the opportunities and threats are revealed through external evaluations. The factors of organization, personnel, opportunities, products, etc., are subjected to internal evaluations, whereas political, economic, and social developments are taken into consideration in external evaluations. Thus, it aims to develop plans and strategies to take advantage of the existing strong aspects and opportunities at the top level and minimize the impact of threats and weaknesses [24, 25]. The results obtained directly through the survey method shall be discussed. The surveys are the data collection method used to reach more people and collect information in a short time [26, 27]. The surveys are comprised of a list of written questions and include information collection about the investigated issues by asking people for information directly about the research. It is possible to reveal the situation by reaching many people in a short time through this form of data collection [27]. The survey data were collected in 5 ways: e-mail, telephone, face-to-face conversation, karma and the internet [28].

The study was conducted by directly reaching the offices and companies forming the SPS through the internet. CSCE, which archives the registers of offices and companies, was utilized. Lecturers (3 people) and experts (3 people) were utilized to create the survey forms and question options. Better results were obtained in the application phase of the survey questions after checking the content integrity and expediency. In addition, the confidentiality of the survey was provided [29]. A total of 131 sector representatives from various cities of Turkey contributed to the surveys. The distribution of these representatives countrywide is shown in Figure 3. The sector is represented by approximately 2600 Geomatics Engineers as of 2016.

RESULTS

Questions were asked to PSEOs and LSEOs forming the SPS to identify their organizational structures. The obtained results are shown in Figure

4, which is comprised of two graphics. Figure 4 (a) reflects the corporate structures of organizations that took part in the survey, whereas Figure 4/b reflects the distribution of their establishment dates. Accordingly, 74% of the enterprises were established after 2000. A considerable increase (300%) stands out in the number of enterprises established after 2000. According to another result, limited companies have gained importance, rather than the offices established traditionally.

One of the most significant indicators reflecting the situation of the enterprises forming the SPS is their hardware. The quality of software and hardware used in mapping adds qualification to the services in terms of cost-speed-quality. In addition, adequate and qualified hardware is one of the most significant criteria requested for the commitments realized in national and international areas. Thus, questions were asked to observe the hardware profile of the enterprises, and the number of average hardware per enterprise was determined (Figure 5). The enterprises own significant sources in terms of hardware, with GNSS devices with CORS-tr and two Total Stations for each, as well as seven laptops and desktop computers and one plotter on average.

Another strategic issue that reveals the SPS's strength is the number and quality of the used hardware. Thus, the hardware used in enterprises was evaluated for the sample groups. A monopoly of a single hardware was determined according to the obtained results (Figure 6).

The most strategical point in the service sector the SPS is the number and quality of the personnel. Accordingly, the average number of personnel per enterprise was determined for all enterprises. On average, 2 geomatics engineers, 2 surveying technicians, 1 topographer and 1 other technical personnel correspond to each enterprise.



FIGURE 3
Country wide distribution of sample group answering the survey (red provinces)



(a) **(b)**

FIGURE 4
Corporate classification of sample group on yearly basis

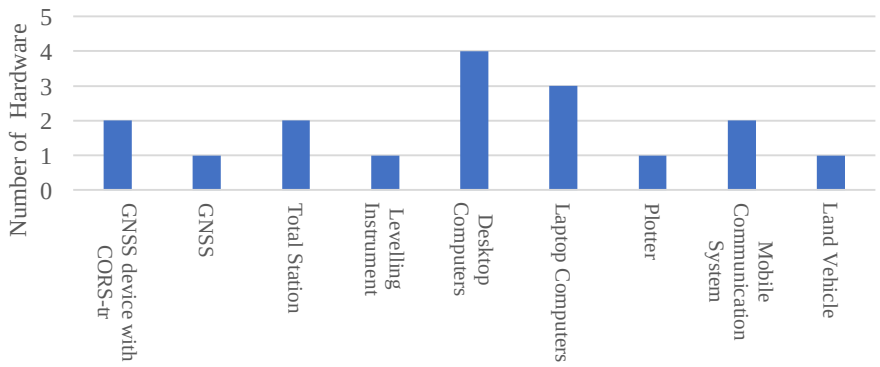


FIGURE 5
Number of Average Hardware per Enterprise

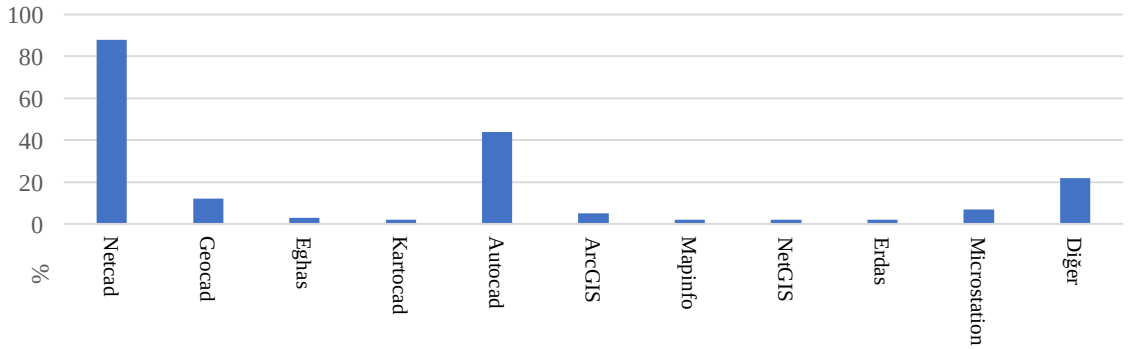


FIGURE 6
Type of Hardware Used in Enterprises

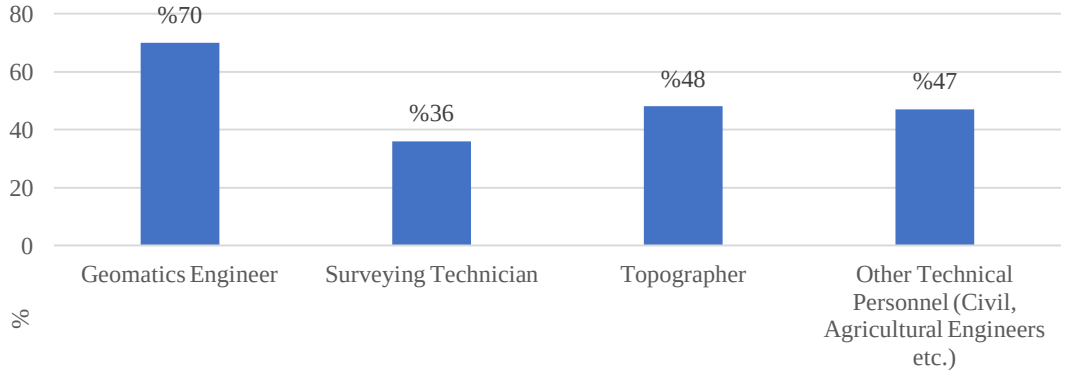


FIGURE 7
Number of Personnel Working for the Enterprises for Five Years and More

The number of personnel working for five years or more was assessed to reflect the quality of the enterprise in terms of corporation, therefore the sample group was asked about the number of personnel working for five years and over. Although the results are stable regarding the employment of Geomatics Engineers when calculating for the total number of personnel, the number of personnel working for five years or more is under 50% regarding the employment of intermediate staff (Surveying Technicians, Topographer, etc.) (Figure 7).

The sample group was asked about the size and property of the places in the SPS; the proportion of accreditations by the ISO, Turkish Standards Institution (TSE); whether they had received consultancy

services from universities; and the major contribution of qualified services in production. It was determined that 43% of the employers own the property of their business, 64% of them operate in working places smaller than 100 m^2, 80% of them have not been accredited, and 89% of them do not receive any consultancy services (Figure 8).

The sample group was asked to determine the profile of external shareholders, which was turned into the graphics shown in Figure 9. The applications made toward real persons are apparent. This result, no doubt, is accepted as a reflection of the formation of the sector from PSEOs, in other words, office types defined as micro enterprises to a large extent. Secondary, it is found that the existence of municipalities arises from public work activities tendered highly by those organizations and realized ex officio. The third rank of GDLRC arises from the opening policy to the private sector executed after 2005. Finally, it stands out that 60% of sector business is conducted in construction companies with surveying companies as a subcontractor.

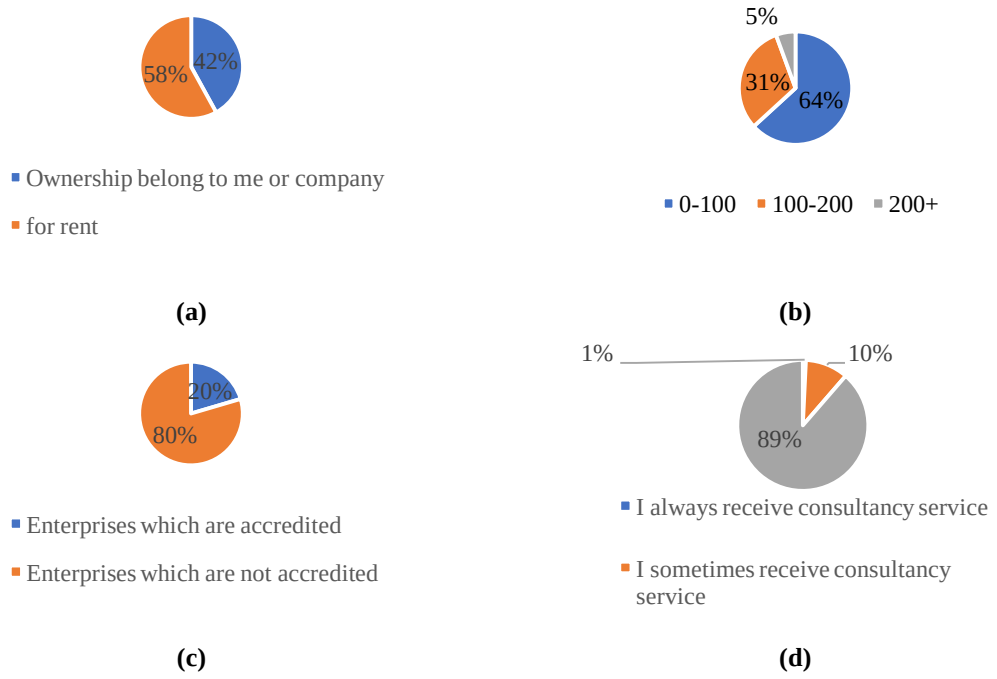


FIGURE 8
Property (a), Area (b), Accredit (c) and Consultancy Service (d) Graphics of Premises of Enterprises

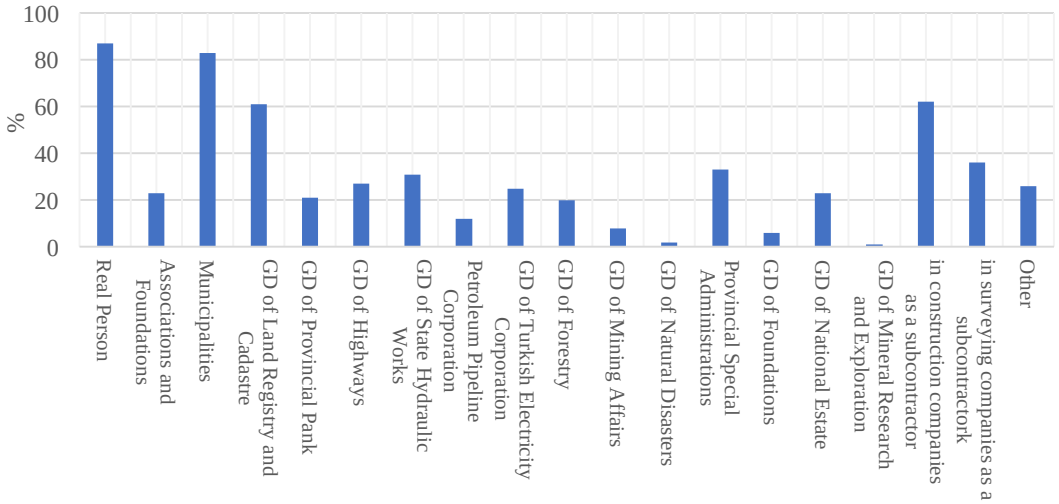


FIGURE 9
Distribution of Person/Organization that Enterprises Conduct Joint Work

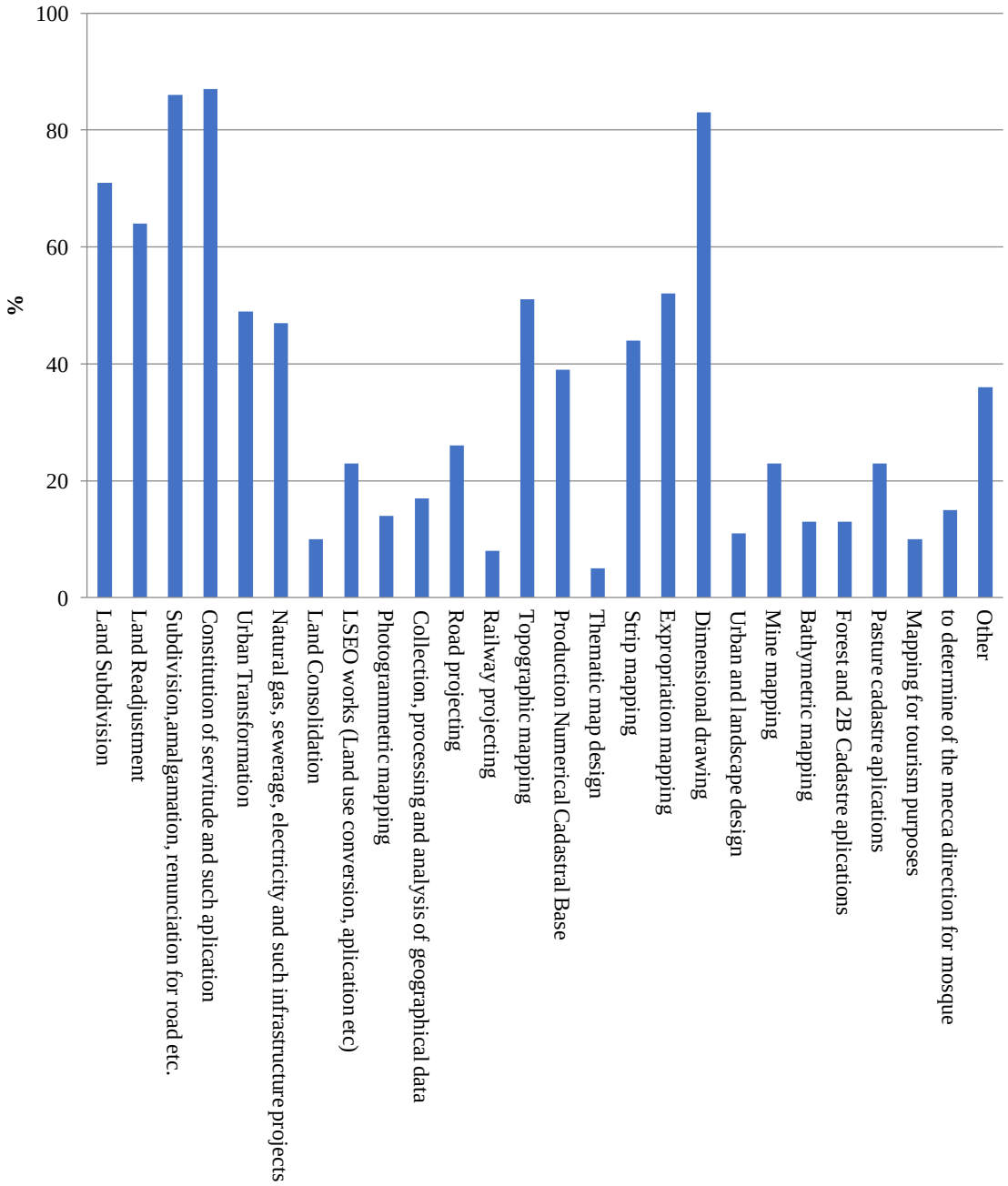


FIGURE 10
Distribution Graphic of the Projects Conducted by the Companies

TABLE 1
Work outside of business items published by the CSCE

• **Land Valuation**	• Numerical Land Model Production
• **3-dimension modelling**	• Treasure hunting application map
• **Deformation surveying**	• Fathometer
• 3D building facade modelling	• Construction/construction business, archaeology, architecture
• Cubage	• Tus applications
• **Navigation maps**	• **Lecturing in university**
• **Industrial surveying**	• **Conciliation transactions and real estate business**
• **Consultancy services,**	

The sample group was asked to determine the transaction variety conducted in the SPS and the size of those activities. Engineering service wage scales and transaction types in other unit wage scales published on the website [23] of CSCE were utilized. The traditional transaction types (parcelling, amalgamation, renunciation for road, land subdivision, and dimensional drawing work) belonging to the sector according to the data presented in Figure 10 still form the main sources of the sector.

It is understood that the enterprises have made progress in urban transformation applications, coming to the fore in the last few years. Similarly, LSEO activities are assessed as one of the most important expansions providing growth to the sector and increasing the transaction variety. According to the results of the survey, the sector is not at the requested level in the treatment of geographic data and analysis activities. One of the other outstanding results is that land consolidation work has not been popularized in our country, which has large amounts of agricultural land. The negative reflection of the situation in the sector is seen in the survey results.

Presented in Figure 10, it was asked whether there were any activities other than transactions and, if so, what they were. This question was aimed at researching whether there are surveying or other activities not recorded by the CSCE. The results are presented in Table 1.

Revising these data, it was understood that a large part of the answers remain within the scope of the transactions, as presented in Figure 10. However, as seen in the answers, titles such as *"land valuation"*, *"3D Modelling"*, *"deformation surveying"*, *"navigation map production"*, and *"industrial surveying"* have not been priced by the CSCE. Similarly, when activities such as *"lecturing in university"* and *"conciliation transactions"* are considered under the title of "*consultancy and expertise*", CSCE does not take place in the unit price scale.

The offices and companies not operating for a certain time can be encountered due to the establishment of enterprises in the SPS and market or private conditions. The number of enterprises not realizing any projects by years was determined for the sample group regarding the last five years to establish an opinion about the dimension of the weakness. The answers are presented in Figure 11. Accordingly, the number of enterprises not realizing any projects shows a considerable declining tendency in the last five years.

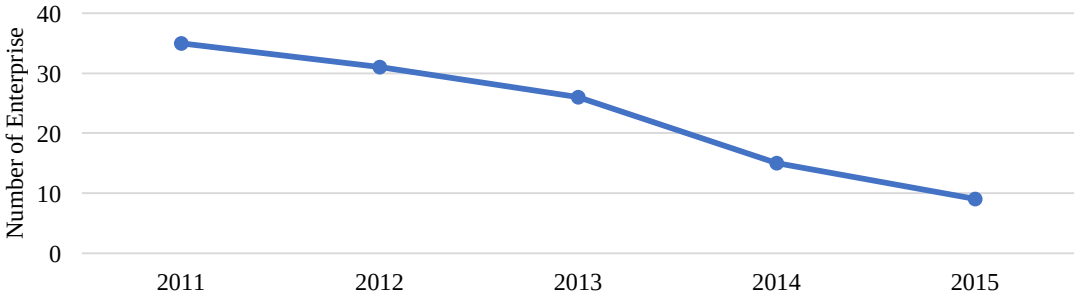


FIGURE 11
Number of enterprises not realized any project by years

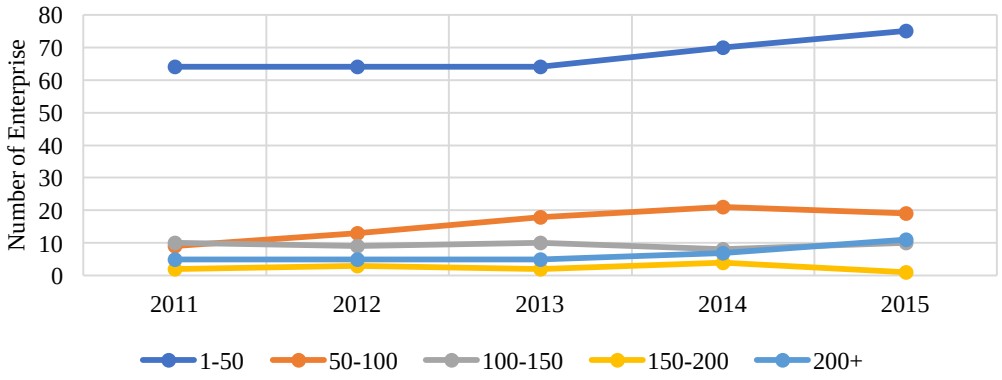


FIGURE 12
Number of projects realized by years

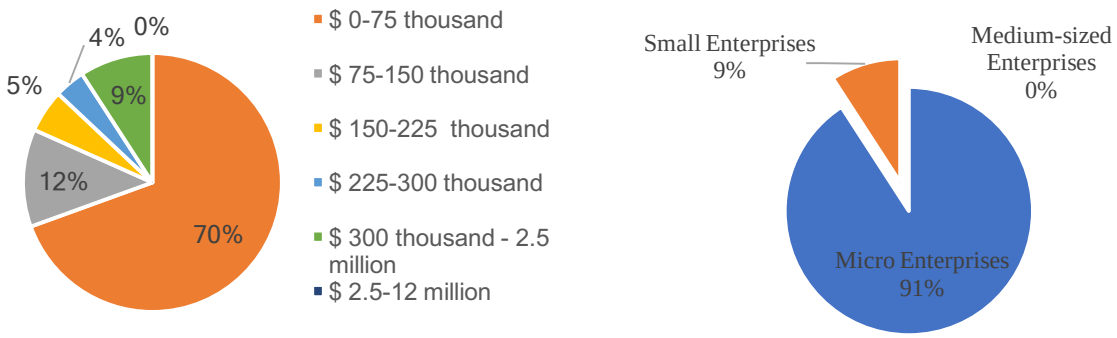


FIGURE 13
Classification of SPS according to 2015 approximate financial statements

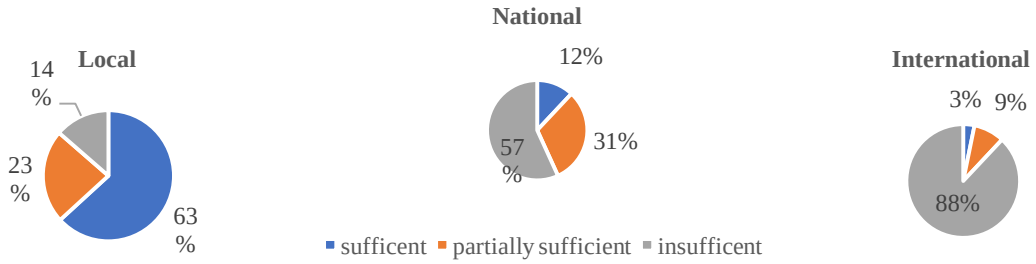
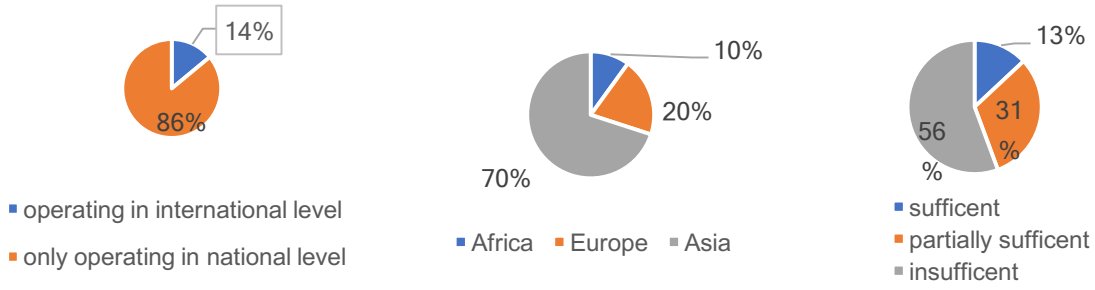


FIGURE 14
Recognition of SPS



(a) **(b)** **(c)**

FIGURE 15
Activity rate, scope and competition force of enterprises in international level

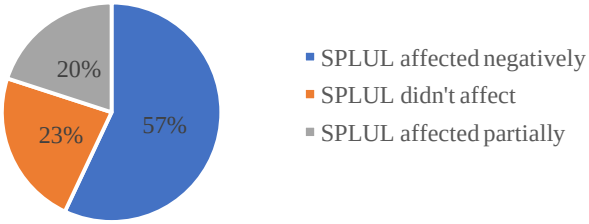


FIGURE 16
Affect of SPLUL on project activities

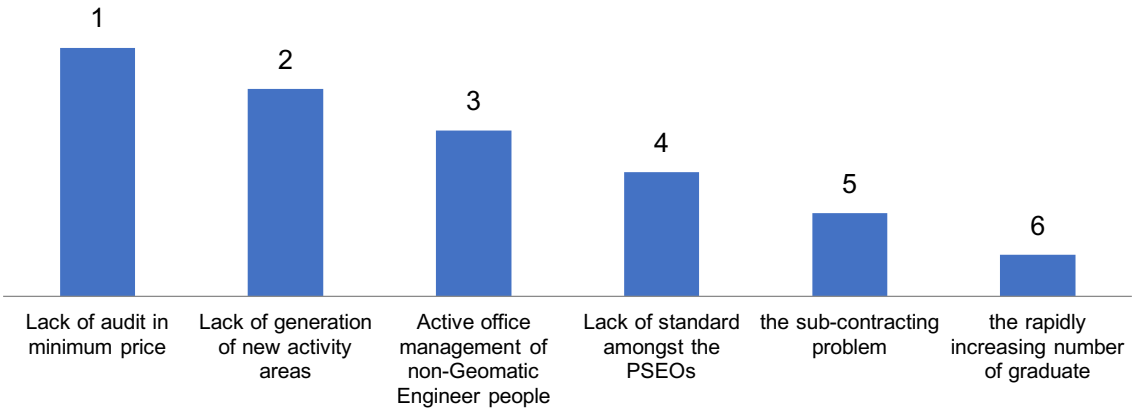


FIGURE 17
Arrangement graphic of problems of SPS according to the order of importance

Within the scope, the number of projects realized by year was determined via another answer to have an idea about the economic size of the enterprises. The average number of projects that an enterprise can produce in a year was primarily estimated through CSCE registers. The number of projects was grouped as (1-50), (50-100), (100-150), (150-200) and (200+), and the question was designed. Revising the obtained data, the number of enterprises producing (1-50) band forms almost half of the total number joining in the survey (Figure 12).

The income groups were formed regarding the classifications foreseen by the Regulation of the Definition, Qualifications and Classification of the Enterprises of Small and Medium Sizes [30] for the classification of the SPS in terms of economic size. According to the mentioned regulation, enterprises with a financial statement below $ 300 thousand on a yearly basis are considered as micro enterprises, enterprises with financial statement between $ 300 thousand - 2.5 million are considered as small enterprises, and enterprises with financial statements between $ 2.5-12 million are considered as medium-sized enterprises. According to the survey results, a large part of the enterprises (70%) were found to have an annual financial statement in the $0-75 thousand category (Figure 13). When organizing a classification according to related regulation, it was concluded that 91% of the enterprises in the survey had a financial statement below $300 thousand; thus, they were considered as micro enterprises. In contrast, 9% of them are small enterprises. Medium-sized enterprises are not part of the survey results (Figure 13).

The sample group was asked questions to make determinations about the recognition level of the enterprises, which is one of the major components in private sector activities. The adequacy of enterprises in terms of local, national and international recognition was determined, and the obtained data are presented in Figure 14 with graphics. Accordingly, it was concluded that only the local-level recognition of the enterprises is in question.

The enterprises were asked whether they operate on an international level and, if so, what kind of activities they conduct in what regions over the world and their adequacy in terms of international competition. The results are presented in Figure 15. Only 14% of the enterprises taking part in the survey worked on an international level (Figure 15/a). It was also determined that those enterprises operated substantially in the Asia Continent (70%) (Figure 15b). They were found inadequate in terms of international competition (Figure 15c). As an answer to the activities conducted on an international level, the transaction types were listed as follows: *topographic services, triangulation and levelling network, infrastructure projects, base map, photogrammetric mapping, airport map, NATO projects,* and *dam works*.

Soil Protection and Land Use Law, SPLUL (in Turkish TKAKK), which entered into force in 2005 to prevent the deterioration and protection of agricultural lands in Turkey, restricted the division of agricultural land [31]. Thus, questions were asked to the sample group to determine the level of impact of the regulation on the sector. A large part of the sample group (77%) was affected negatively by the legal regulation partially or directly, according to the obtained data (Figure 16).

A question was designed to determine the impact of the current issues on employers, and the answers are presented in Figure 17. According to the obtained results, the failure of providing a minimum price audit ranks first. Because this issue brings up the rear in importance ranking despite the rapid increase of graduates in our country, the data stand out as one of the most attention-grabbing results of the survey.

DISCUSSION

Revising the data obtained by the survey results as a whole, the enterprises forming the SPS are legally private (I), economically service producing (II), a liberal profession in terms of functionality (III), and micro-, small- and medium-sized businesses in terms of size (IV). The vast majority of the enterprises (84%) are formed by micro enterprises with annual financial statements below TL 1 million. In addition, the annual financial statements of 63% are below TL 250 thousand. In this respect, the formation of the sector from local and micro enterprises to a large extent may be considered as the weak side of the sector.

There are approximately 15000 registered members according to CSCE data; 41% of these members are under the age of 35. In addition, 1600 new enterprises (60% of total enterprise number) have been established in the last decade (Table 2) [23].

On the other hand, 1593 people have been placed in 20 Departments of Map/Geomatics/Geodesy and Photogrammetry Engineering in various universities providing education in Turkey in 2015 [23]. In addition, 12 departments continue their studies to place students. Considering the rapidly increasing number of graduates, it is seen that the sector has major functionality in creating employment. With the rapidly increasing number of graduates, with the increase reaching up to 300% in the last decade, the number of PSEOs might be perceived as an internal threat in terms of employers at first appearance. However, the rapidly increasing number of graduates brings up the rear in the perception of the threat due to the results of the survey (Figure 17). On the other hand, whereas the number of enterprises not realizing any projects in the last five years has plummeted (Figure 11), the number of projects realized by years increased at the same level (Figure 12). These results show that the rapid increase in the number of graduates has not created a threat for the sector for now. In other words, these results show that the market created by surveying services, for now, is adequate despite the increasing number of graduates.

Although this issue is noted by the employers, it is understood by the survey results that the new activity areas should be created (Figure 17). Revising Figure 10 reflecting the activity areas of the sector, *urban transformation applications, LIHKAB activities, treatment of geographic data, thematic map design,* and *3B cadastre* vs. new areas are included in the sector in the last years. Activities such as *land valuation*, which does not take place in the unit price scale of the CSCE, *industrial surveying, and expertise and consultancy services* are understood to be actively realized by the sector. The results presented in Figure 17 indicate that land consolidation has not been popularized. At this point, it can be considered that the inadequacy of land consolidation work, which is a major factor of rural area regulation, is one of the weak aspects of the sector in Turkey, which owns large amounts of agricultural land. This issue, arising from the public, can be perceived as an external threat as well.

When evaluating the sector in terms of international competition, it is understood that the sector remains incapable in this field, and it conducts activities mostly in the Asian market through the construction sector. It is observed that these activities consist of topographic services, triangulation and levelling networks, infrastructure projects, base maps, photogrammetric mapping work, airport maps, NATO projects, and dam work. Regarding the mentioned activities, the important part is that they are realized as subcontractors in construction projects. According to [32], the construction sector ranks among the sectors leading the world's economy. The construction sector incorporates many sub-sectors and gathers many different expertise fields under the same umbrella. Both employment opportunities and high budget construction projects indicate the importance of the construction sector in terms of the global economy and development. Thus, many factors affecting the construction sector directly also affect the world economy. The size of the construction sector in the world economy is estimated to be approximately USD 3.5 trillion, and this figure forms approximately 8% of total GNP of the world [33]. Hence, the construction sector functions as a locomotive in terms of the SPS in international competition. Regarding the sector in terms of international competition, the constraint of the market, the low level of recognition, constraint in the product range in activities and cadastre are considered as the weak aspects of the sector because they cannot obtain shares from large markets throughout the world.

TABLE 2
CSCE Member Statistics [9]

CSCE Number of Total Members	Number of Registered Members in the Last Decade	Number of PSEO Opened in the Last Decade	Number of Total PSEO
15000	7000	1600	2633

TABLE 3
Surveying private sector SWOT matrix

	POSITIVE	NEGATIVE
	Strengths	**Weaknesses**
INTERNAL FACTORS	• It is based on an approximately 70-year experience. • Most of the business items in the surveying sector are conducted by the private sector in Turkey. • Almost 3000 businesses (PSEO and LSEO) • Wide range of business activities • Rate of recruitment • Sufficiency in terms of staff and equipment	• The sector is made up substantially of micro-businesses that address the local market. • Lack of corporate, technical, etc., standards amongst the PSEOs. • Insufficiency in physical conditions • Low awareness on national and international levels • Insufficient amount of activities on an international level • Lack of audit at minimum price • Lack of accreditation of businesses • Lack of cooperation with universities • Activities not recorded by the CSCE • Instability in the recruitment of long-term staff • Not being active in the areas related to information technologies, such as GIS
	Opportunities	**Threats**
EXTERAL FACTORS	• Increase in the turnover with the recent developments in the construction sector • Increase of the importance of surveying private sector due to developments in international arena • Institutions that serve in the surveying sector, especially GDLRC, purchasing services from the sector frequently • New business items that came up with the urban transformation • 2B cadastre applications • Developments in terms of 3D cadastre around the world	• Volatility in the construction sector • Limitations in the conditions to share the premises of EPLUS • Working with construction and surveying companies as a sub-contractor • Lack of generation of new activity areas • Monopolization of the software • Not extending the landscaping of rural area, such as land consolidation by the state

It should be taken into consideration that 90% of the sample group consists of small businesses when evaluating the survey results in terms of software, hardware and personnel. From this point, the number of personnel and hardware can be considered capable. However, a monopoly stands out in single software regarding the distribution of the software used by the enterprises. This situation may cause negative results in reaching qualified and affordable software to the enterprises. In addition, this situation can be deemed as an external threat within the scope of SWOT analysis.

According to the results obtained from the survey results, less than 10% of the use of GIS software between the enterprises shows that the SPS does not take up enough space in GIS-based projects. This result may also be considered as weak aspects of the sector. GIS-based applications in Turkey have been used effectively by local governments since the 1990s. However, there are many technical, institutional and legal problems in these applications at present [34]. For example, the Turkish Spatial Addressing Registration System (SARS) project, which is planned to be completed by the end of 2018 in Turkey, has been tendered for $100 million. This project is one of the most important GIS projects to be realized in Turkey within the municipalities. Within this project, GIS-based Numerating Maps and Allocation Maps based on Cadastral Parcels should be produced and used as a base for SARS. Although these applications should be done and included in the system included by geomatics engineers, it is seen that they have been carried out by inexperienced and non-geomatics engineer personnel [35]. These and similar situations lead to the fact that the SPS is not as powerful in GIS-based applications.

From the data collected through the survey results, it is found that the number of businesses that did not have any project activities within the past five years declined significantly (Figure 11). In line with this, the number of projects increased (Figure 12). These results match up with each other. Considering that the sample group is made up mostly of businesses established recently (Figure 4), it is evident that these newly established businesses easily adapt to the market conditions. Nevertheless, we can

come to a conclusion that the projects are undervalued because the financial balance sheets of most of these businesses are below TRY 1-250 thousand despite the increase in the number of projects (Figure 13). This problem is incurred from unreliable audits of minimum prices in the sector.

The results obtained from the study and the evaluations of the project team are presented in Table 3 in the form of a SWOT matrix.

CONCLUSIONS AND RECOMMENDATIONS

Considering the period starting from the 1950s, when the Surveying Private Sector activities commenced in Turkey, until today, it is observed that a substantial part of the surveying services, executed by the state, especially by GDLRC, has been handed over to the private sector. According to the report published by the State Planning Organization (SPO) in 2001, it is seen that all the business items that cannot be realized and extended by Surveying Private Sector are being completed by the sector now. This finding is reverberated onto the quotation of prices per unit published by the CSCE as well as the results of the survey. It is obvious that the sector is an important source of income and recruitment for the economy of the country, with experience of over 65 years, more than 3000 PSEOs and approximately 200 LSEOs. However, despite the pace of developments in the sector within recent years, traditional problems and domestic and international problems affect the sector both negatively and positively. It is important to make use of the strengths and fortify the weaknesses as well as plan strategically towards this goal while considering these impacts.

When examining international developments, the incentives of many institutions, especially FIG, are relevant in terms of the transfer of surveying services to the private sector, particularly during the past 20 years. During this period, in line with these developments in the world, Turkey has assigned important roles to its Surveying Private Sector for the development of the sector and the realization of the surveying services in a fast and quality way. However, despite these developments, the sector appears to be obliged greatly to the micro-businesses, which are only known locally, whereas the activities in the international arena seem to be mostly in the Asian market with the construction sector. Thus, the sector must play a part directly in the international markets in the field of surveying, particularly in cadastre. At this point, the World Cadastre Summit held by the Ministry of Environment and Urban Planning in 2015 along with the initiative of TCCA to export the Turkish Cadastre System via the private sector needs to be assessed as a move of the sector to exist in the international arena.

Despite the number of businesses and projects, the increasing number of graduates in the sector as well as the businesses, which are stuck with a balance sheet between Turkish Liras 1-250 thousand and remain at a micro level, point to an important issue. This issue is, in fact, the "*lack of audit at minimum prices"*, which is placed in the first position by the sample group of the survey. In other words, the projects are undervalued. The point in the question can be only surpassed with the strict audits of CSCE and finance corps. It is believed that the projects being realized over their real value will increase employee satisfaction and affect the sector positively.

Another result of the study shows that due to new business items, such as the urban transformation applications and tenders for production numerical cadastral base, the sector turns this increase into an opportunity for now. Nevertheless, it is obvious that new business items and new markets will be required considering that the number of Departments of Geomatics Engineering exceeds 32 and that almost 1600 students are placed every year in these departments. Otherwise, a possible recruitment issue is predicted to affect the Department of Geomatics Engineering adversely.

Another issue that the sector experiences a lack of standards. It is observed that the businesses cannot sustain the minimal conditions in terms of staff, equipment, software and space. This results in dissatisfaction in customers. This can be overcome only by accreditation of the businesses in the sector by independent institutions.

Considering the business items in the quotation of prices per unit as well as the areas of activity listed in the CSCE Private Surveying Engineering Office Registration Regulations, it is observed that these are not enough to represent the state of this profession. As is understood from the results of the study, areas such as "valuation of premises, industrial measurements, and consultancy services" are required to officially be areas of interest of this profession. Therefore, a substantial amount of the activities realized by the sector can be registered. However, the contradiction in terms used for the definition of the business areas of the sector should be clarified, and these business items should be defined and classified clearly. In addition to these recommendations, to reveal the exact financial size of the sector, the CSCE needs to extend the audit at minimum prices and collect statistical data regarding the sector.

ACKNOWLEDGEMENTS

This study was supported by the Research Fund of Karadeniz Technical University, Project number: FBB-2016-5469.

REFERENCES

[1] Demir, O., Uzun, B., Coruhlu, Y.E., (2015) Progress of cost recovery on cadastre based on land management implementation in Turkey. Survey Review. 47(340), 36-48.

[2] Official Gazette (1973) Regulation on maps and plans subject to registration, Published Date: 06.08.1973, Gazette Number: 14617.

[3] Ipek, M. (2008) To Constitute the Infrastructure of the Spatial Information System in Turkey for Digital Cadastre Production on Private Sector Approach, CSCE 2. Cadastre Summit Congress, Proceedings, 21-24 May, Ankara, Turkey, 133-140. (in Turkish).

[4] Uzun, B. (2009) Using Land Readjustment Method as an Effective Urban Land Development Tool in Turkey. Survey Review. 41(311), 57-70.

[5] SPO (2001) The Eighth Five-year Development Plan: Map Land Registry Cadastre, Geographical Information and Remote Sensing Systems (Land and Land Policies, Land Consolidation, Land Use) Specialization Commission Report, Ankara, Turkey (in Turkish).

[6] Official Gazette (2005a) Law on the Amendment of Cadastre Law, Law Numbered: 5304, Published Date: 22.05.2005, Gazette Number: 25744.

[7] Yildiz, O., Coruhlu, Y.E., Demir, O., Murat, M.O. (2015) Private Sector Role and Effect in Turkish Cadastral System, WCS-CE - The World Cadastre Summit, Congress & Exhibition Istanbul, Turkey. See; http://wcadastre.org/page/52-en-proceedings, (Access: 07.02.2017).

[8] Yomralioglu, T. and Cete, M. (2015) Cadastre or land administration: A case study of Turkey. WCS-CE—The World Cadastre Summit, congress & exhibition. Istanbul, Turkey. See http://wcadastre.org/page/52-en-proceedings, (Access: 07.02.2017).

[9] URL-1 (2016) Chamber of Survey and Cadastre Engineers, http://www.hkmo.org.tr/

[10] FIG (1995) FIG Statement on Cadastre, FIG Publication No: 11 http://www.fig.net/resources/publications/figpub/pub11/figpub11.asp

[11] UN (1996) the Bogor Declaration, United Nations Interregional Meeting of Experts on the Cadastre, Bogor, Indonesia. http://www.fig.net/resources/publications/figpub/pub13a/fig_pub13A.pdf

[12] UNECE (1996) Land Administration Guidelines, United Nations Publication, ISBN 92–1–116644–6, New York and Geneva. http://www.unece.org/fileadmin/DAM/hlm/documents/Publications/land.administration.guidelines.e

[13] UN and FIG (1999) Report of the Workshop on Land Tenure and Cadastral Infrastructures for Sustainable Development, Final Edition, Bathurst, Australia. http://www.un.org/esa/sustdev/csd/ecn172000-bp3.pdf

[14] PCCEU (2003) Permanent Committee on Cadastre in the European Union, Common Principles on Cadastre in the European Union. http://www.eurocadastre.org/pdf/principios_i.pdf

[15] EU (2004) European Union Land Policy Guidelines, Guidelines for Support to Land Policy Design and Land Policy Reform Processes in Developing Countries, EU Task Force on Land Tenure, https://ec.europa.eu/europeaid/sites/devco/files/methodology-eu-land-policy-guidelines-200411_en_2.pdf

[16] Çete, M., Yomralioglu, T. (2011) New land administration system for Turkey: ATLAS, Chamber of Survey and Cadastre Engineers, 13. Turkey Map Scientific and Technical Assembly, April 18 – 22, Ankara, Turkey (in Turkish).

[17] Kaufmann, J. Steudler, D. (1998) Cadastre 2014 – a Vision for a Future Cadastral System. http://www.eurocadastre.org/pdf/cadastre_2014.pdf

[18] Zeuw, K. (2015) The Need for Fast, Cheap and Good Land Administration, WCS-CE - The World Cadastre Summit, Congress & Exhibition, Istanbul, Turkey. http://wcadastre.org/files/handouts/176.pdf

[19] Konbul, Y., Çete, M. (2015) Role of Private Surveyors in Cadastre: The Turkish Case, WCS-CE - The World Cadastre Summit, Congress & Exhibition Istanbul, Turkey. http://wcadastre.org/page/52-en-proceedings

[20] Yildiz, O., Coruhlu, Y.E., Demir, O. (2015) A Visional Overview to Renovation Concept on Cadastral Works in Turkey. Sigma Journal of Engineering and Natural Sciences-Sigma Muhendislik ve Fen Bilimleri Dergisi. 33(4), 503-519.

[21] Gulluce, I. (2015) TR Minister of Environment and Urbanism Mr. Idris Güllüce, World Cadastre Summit opening speech, WCS-CE - The World Cadastre Summit, Congress & Exhibition, Istanbul, Turkey. http://wcadastre.org/page/52-en-proceedings

[22] Altun, A. (2015) Export of Turkish Cadastral System (Türk Kadastral Sisteminin İhracı in Turkish), WCS-CE - The World Cadastre Summit, Congress & Exhibition, Istanbul, Turkey. http://wcadastre.org/files/fulltexts/fulltext151.pdf

[23] URL-2 (2016) Official Web page of Measurement, Selection and Placement Center Presidency, http://www.osym.gov.tr/

[24] Karadeniz, E., Kandır, S.Y., Önal, Y.B. (2007) A Pilot Study of Selected Partners' Evaluating Turkish Tourism Investments by SWOT Analysis, Anatolia. Turizm Araştırmaları Dergisi. 18, 195-205
[25] Dyson, R.G. (2004) Strategic Development and SWOT Analysis at the University of Warwick. European Journal of Operational Research. 152(3), 631–640.
[26] Cohen, L. and Manion, L. (1994) Research Methods in Education (Fourth Edition), Rutledge, New York.
[27] Cepni, S. (2010) Introduction to Research and Projects. Fifth Edition, Trabzon, ISBN: 9789754170009, 416s (in Turkish).
[28] URL-3 (2012) http://www.egitim.aku.edu.tr/anket.ppt. 15.04.2012
[29] Coruhlu, Y.E., Demir, O. (2015) Institutional and occupational development of foundations (GDF) and its experts on land market: A case study in Turkey. Fresen. Environ. Bull. 24(2A), 695-706.
[30] Official Gazette (2005b) Regulation of the definition of small and medium-sized enterprises, Qualifications and Classification. Gazette Number: 25997.
[31] Official Gazette (2005c) Soil Protection and Land Use Law. Law numbered 5403 Gazette Number: 25880.
[32] Ozorhon, B. (2012) Construction Sector in Turkey and Its Place in the World, Istanbul Trade Chamber Publication. Publication No: 2012-31, İstanbul, Turkey, (in Turkish).
[33] Ozdemir, E. and Kılıç, S. (2011) 2008 Global Economic Crisis and Construction Sector: A Field Survey in terms of Marketing. Anadolu University Journal of Social Science. 11(2), 43-68, (in Turkish).
[34] Cete, M., Durduran, S., Geymen, A. (2008) Urban Information Systems in Turkey. Proceedings of the Institution of Civil Engineers-Municipal Engineer. 162(2), 103-109.
[35] Yildirim, V. (2012) Turkish street addressing system and geocoding challenges. Proceedings of the institution of civil engineers-municipal engineer. 167(2), 99-107.

Received: **13.06.2017**
Accepted: **20.10.2017**

CORRESPONDING AUTHOR

Yakup Emre Coruhlu
Karadeniz Technical University,
Faculty of Engineering,
Department of Geomatics Engineering,
61080, Trabzon – Turkey

e-mail: yecoruhlu@ktu.edu.tr

© by PSP Volume 26 – No. 12A/2017 pages 8023-8029 Fresenius Environmental Bulletin

IN VITRO EFFECTS OF SOME PESTICIDES ON GLUTATHIONE-S TRANSFERASE ACTIVITY

Mehmet Emin Diken[1], Serap Dogan[2], Mehmet Dogan[3,*], Yasemin Turhan[3]

[1]Balikesir University Science and Technology Application and Research Center, 10145 Altieylul-Balikesir, Turkey
[2]Balikesir University Faculty of Science and Literature Department of Molecular Biology and Genetics, 10145 Altieylul-Balikesir, Turkey
[3]Balikesir University Faculty of Science and Literature Department of Chemistry, 10145 Altieylul-Balikesir, Turkey

ABSTRACT

Human populations have been constantly exposed to pesticides due to their extensive use and presence in food and drinking water. Therefore, the aim of this study is to compare the inhibitory effect of three commonly used pesticides such as glyphosate (herbicide) and lambda-cyhalothrin and deltamethrin (insecticides) on glutathione S-transferase (GST) activity *in vitro* in human blood. GST enzyme activity was spectrophotometrically determined with observation of the formation of 1-chloro-2,4-dinitrobenzene-glutathione (CDNB-GSH) conjugate. GST activities were suppressed by all the pesticides tested; the deltamethrin was the most potent inhibitor, reducing GST activity *in vitro* in a dosage-dependent manner. The inhibition mechanism of pesticides on GST was different from each other. The inhibition types of glyphosate, lambda-cyhalothrin and deltamethrin pesticides were uncompetitive, mixed and competitive, respectively.

KEYWORDS:
Glutathione S-transferase, pesticides, environmental toxicity, inhibition.

INTRODUCTION

Today, conscious societies are aware of the importance of plant-derived foods in healthy nutrition. Besides, the increase of herbal nutritional needing due to the rapid increase of the world population, the development of greenhouse due to the intense demand for fresh fruits and vegetables in every season, climate change due to global warming and other ecological changes are provided suitable environments for the growth and diversification of some diseases and harmfulness in polyculture agriculture. This problem can be solved by taking measures that are not cost-effective, most importantly not causing environmental pollution, by producing high-quality products and yielding unit area [1]. In the world, pesticides are being used extensively in order to eliminate the harmful effects of agriculture areas and to obtain quality products. Pesticides used in agricultural struggle cause the product increase destructing of target organisms as well as damage to non-target organisms. However, these pesticides remain in the water, soil, fruits and vegetables for a long time without deterioration and cause environmental pollution and thus cause various damages that can reach human beings through the food chain [2-5]. Moreover, it is also stated that pesticides constitute a "risk factor" for breast cancer because of their lipophilic character, high bioaccumulation and estrogenic activity [2].

People meet pesticides in various forms. A large community, including producers, marketers, practitioners and finally consumers of pesticide agricultural products are exposed to pesticides acutely or chronically at different degrees. Pesticides entering the organism in various ways have negative effects on systems such as nervous system, endocrine system, immunity protection system, liver, heart and muscle [2]. An important system within the affected systems is the human defense system, i.e. the antioxidant system.

The most important feature of the antioxidant defense system is that all components of the system function in such a way as to create a synergy against reactive oxygen species [6]. For this reason, antioxidant enzymes have a vital important for regulating cell balance and their inductions are a consequence of the response to contaminants [7]. Antioxidant enzymes are the key components induced by oxidative stress and form endogenous enzymes (superoxide dismutase, glutathione peroxidase, glutathione-S transferases (GST), catalase, mitochondrial calcium chromoxidase system, hydroperoxidase) and exogenous enzymes (Vitamin E and C, some drugs) [8].

GST, an endogenous antioxidant enzyme, is an important group of enzymes involved in xenobiotic metabolism and detoxification of endogenous and exogenous substances. This enzyme protects cell membranes, DNA and proteins against reactive oxygen species that are triggered by environmental stress factors. GST is responsible for neutralizing mutagens, carcinogens and other toxic substances. It is known that GST is found in plants, insects, yeasts, bacteria and especially the liver, and plays a key role in detoxification [2].

Different pesticides have been reported to induce oxidative stress due to generation of free radicals and alteration in antioxidant defense mecha-

nism. For example, Souza et al. investigated biomarkers such as acetylcholinesterase, GST and catalase of pesticide exposure in placenta samples from pregnant women living in an area of agricultural exploitation with intensive pesticide application [9]; Ojha et al. the effect of commonly used organophosphate pesticides on lipid peroxidation and antioxidant enzymes in rat tissues [2]; Medina-Diaz et al. the effect of chlorpyrifos and methyl parathion on GST levels in HepG2 cells [10]; Gomez-Martin et al. the contribution of genetic polymorphisms of the pesticide-metabolizing enzymes paraoxonase-1 (PON1) and GST on N7-MedG levels [4]; Matic et al. the role of GST A1, M1, P1 and T1 gene polymorphisms and potential effect modification by occupational exposure to different chemicals in Serbian bladder cancer male patients [11]; Song et al. the effects of different pesticides on superoxide dismutase and GST activities [3]; Ezemonye and Tongo the effects of the organochlorine pesticide, endosulfan and the organophosphate pesticide, diazinon on the activity of GST of different tissues in the African common toad, Bufo regularis [12]; Kaya and Yiğit the changes in glutathione S-transferase, glutathione reductase and total glutathione in Vicia sativa L. "Selcuk-99" under flurochloridone stress [13]; Arslan et al. the suitability of using GST of *M. galloprovincialis* as potential biomarker of BPA in the environment [14]; and Kolarova et al. the primary cause of reproductive disturbances in salmonids from the Ticha Orlice river [15]. As can be seen from the above studies, no studies showing the effects of pesticides such as glyphosate (herbicide) and lambda-cyhalothrin and deltamethrin (insecticides) on GST activity have been found. Therefore, the aim of this study is to examine the effects of glyphosate (herbicide) and lambda-cyhalothrin and deltamethrin (insecticides) which cause environmental pollution and which can be passed into human body in different ways, *in vitro* on GST activity, which is an endogenous antioxidant enzyme. For this purpose, the inhibitory effects of pesticides such as glyphosate (herbicide) and lambda-cyhalothrin and deltamethrin (insecticides) on GST activity isolated from human blood were firstly investigated and then the inhibitory effects of pesticides were compared with previous studies in the literature.

MATERIALS AND METHODS

Materials. Blood samples used in this study were taken EDTA (ethylenediamine tetraacetic acid) tubes from healthy humans before each experiment. Chemicals, such as potassium dihydrogen phosphate, reducing glutathione (GSH), 1-chloro-2,4-dinitrobenzene (CDNB) were purchased from Merck and Sigma. Enzyme activity was determined using a PerkinElmer Lambda 35 UV-Visible spectrophotometer.

Preparation of Hemolysate. Approximately 2 mL of venous blood was drawn by sterile vacuum injectors from healthy young humans for erythrocyte antioxidant enzyme activity measurements. Blood was transferred to eppendorf tubes and centrifuged at 2500 rpm for 15 min at +4 °C. The plasma remaining in the upper part was discarded, red blood cells were washed three times with 0.16 M KCl in +4 ^{o}C for 5 min at 2500 rpm, then diluted 1/5 with cold distilled water, centrifuged at 10000 rpm for 30 min at +4 °C and the erythrocytes were disintegrated [16].

Measurement of GST enzyme activity. GST catalyzes the reaction between 1-chloro-2,4-dinitrobenzene (CDNB) and the glutathione-SH group. GST activity was measured using the artificial CDNB and GSH. Kinetic analysis was made in assays containing various concentrations of GSH at fixed CDNB concentration. One unit of GST activity was defined as the amount of enzyme producing 1 µmol of GS-DNB conjugate/min at 340 nm and 37 °C [17].

Kinetic study of GST inhibition. GST inhibitions were determined kinetically in assays containing various concentrations of GSH at a fixed concentration of each pesticide. The results were then summarized in double-reciprocal Lineweaver–Burk plots and the inhibitory constant, Ki, was determined based on the reciprocal velocity versus reciprocal concentration [18].

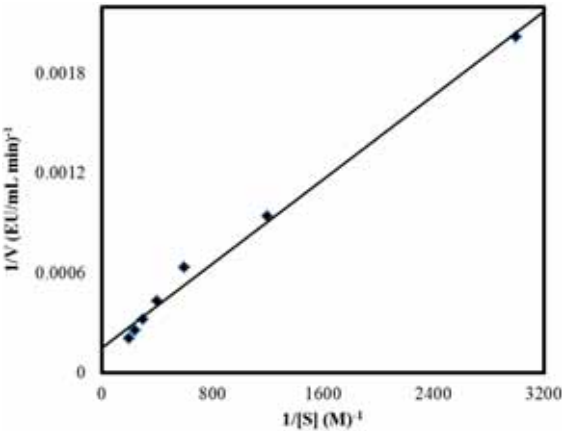


FIGURE 1
Lineweaver-Burk graph for human blood GST

RESULTS AND DISCUSSIONS

Kinetic analysis of GST activity. The kinetic parameters, V_{max} and K_m for various GSH concentrations at fixed CDNB concentration were determined using Lineweaver-Burk graphs (Figure 1). K_m and V_{max} values were calculated as $6x10^{-3}$M and 10.000 EU/mL min, respectively.

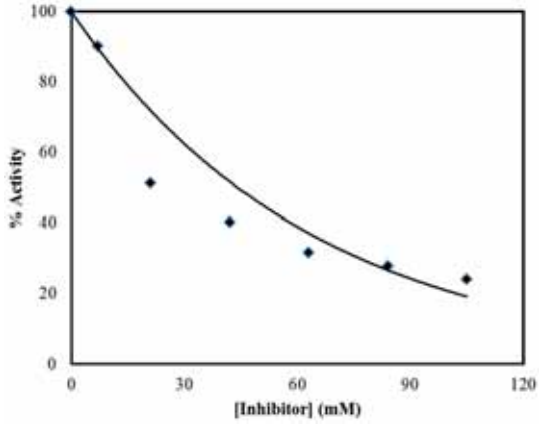


FIGURE 2
The graph of percent activity against glyphosate concentrations

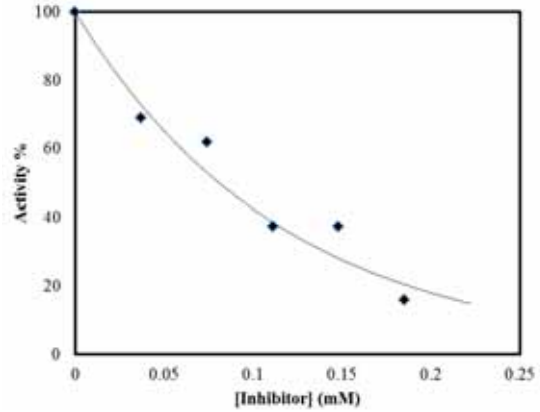


FIGURE 3
The graph of percent activity against lambda-cyhalothrin concentrations

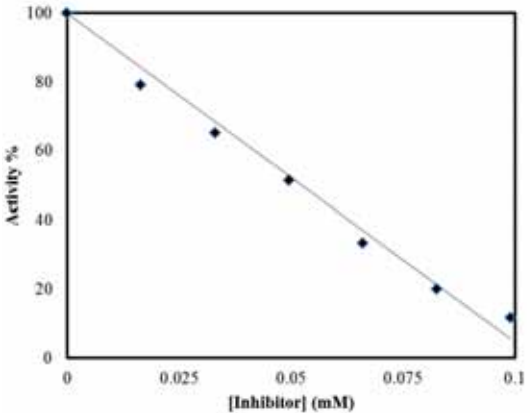


FIGURE 4
The graph of percent activity against deltamethrin concentrations

The effect of pesticides on GST activity. Many medicinal drugs and many pesticides have biologically important functions as a direct result of their effects on enzymes. Enzymes are large proteins (polymers of a-amino acids) which enable specific chemical reactions to occur at reasonable rates at moderate temperatures and at near neutral pH [19,20]. The reactions catalyzed by enzymes are responsible for such important biochemical processes. Consequently, the growth and replication of every living organism depends on the proper and coordinated functioning of a large number of enzymes [21]. It was found in literature that the effects of organic and/or inorganic compounds on different biochemical reactions were different. In some cases, a substance that is an activator for a reaction can act as an inhibitor for another reaction [22]. GST is a soluble protein with low molecular weight in various cells and tissues. GSTs are a family of detoxification enzymes that catalyze the conjugation of glutathione (GSH) with electrophilic compounds, thus preventing toxicity. Some GST isoenzymes have antioxidantase activity to defense against oxidative damage and peroxidative products of DNA and lipids [23, 24]. The toxicity of many exogenous compounds can be modulated by induction of GSTs. So they might be playing an important role in detoxifcation metabolism [3]. As can be seen from the results in Figures 2, 3 and 4, three pesticides have shown inhibitory effect on GST enzyme. As the concentration of the pesticides increased, the percentages of inhibition increased and the enzyme showed less activity. It was also found that the variation of GST activity was different from pesticide to pesticide. From the experimental results, the inhibition percentages at 7, 21, 42, 63, 84 and 105 mM concentrations for glyphosate were found as 10, 49, 60, 69, 73 and 76; those at 37, 74, 111, 148 and 185 μM concentrations for lambda-cyhalothrin as 31, 39, 63, 64 and 84; and those at 17, 33, 50, 66, 83 and 100 μM concentrations for deltamethrin as 21, 35, 49, 67, 80 and 88, respectively. When the experimental results were examined, it can be said that that deltamethrin inhibited enzyme activity more at low concentrations and the strongest inhibitor among the used pesticides was deltamethrin, followed by lambda-cyhalothrin and glyphosate pesticides, respectively. Again, the concentrations of inhibitor required to decrease the enzyme activity by 50% were calculated separately for each pesticide from the equations of the curves in Figures 2-4. These values may vary depending on the enzyme and its inhibitors. The IC_{50} values for the glyphosate, lambda-cyhalothrin and deltamethrin pesticides were determined as 43300, 58 and 51 μM, respectively. Among the tested pesticides, deltamethrin showed the highest inhibitory activity against human blood GST enzyme, whereas glyphosate exhibited the lowest activity. These results show that pesticides trigger oxidative stress in living cells and that GST enzyme activity decreases. Some researchers showed that the expression of GST was a crucial factor in determining the sensitivity of cells and organs in response to a variety of toxins in the aquatic organism, and dose-effect relationship [25,26]. It was also demonstrated that there was significant dose-effect relationship between the concentration of pesticides and GST activity [3]. The calculated IC_{50} values for the inhibitor-affecting substances on

TABLE 1
IC_{50} values of some chemicals and pesticides for glutathione S-transferase activity

Inhibitors	Substrates	IC_{50} (µM)	Enzyme sources	References
Tannic acid	CDNB	13,50	*M. troglodyte*	[27]
Quercetin	CDNB	13,55	*M. troglodyte*	[27]
Tannic acid	CDNB	8,19	*C. anachoreta*	[27]
Quercetin	CDNB	5,68	*C. anachoreta*	[27]
Glyphosate	GSH	43300	Human blood	In this study
Lambda-cyhalothrin	GSH	58	Human blood	In this study
Deltamethrin	GSH	51	Human blood	In this study

TABLE 2
Inhibition types and inhibition constants of some GST enzymes

Inhibitors	Substrates	[Inh] [M]	K_i [M]	K_i' [M]	Inhibition types	Enzyme sources	References
Quercetin	CDNB	-----	$5{,}93\times10^{-6}$	-----	Competitive	*M. troglodyta*	[27]
Quercetin	CDNB	-----	$3{,}60\times10^{-6}$	-----	Noncompetitive	*C. anachoreta*	[27]
Quercetin	GSH	-----	$6{,}70\times10^{-7}$	-----	Competitive	*C. anachoreta*	[27]
Tannic acid	CDNB	-----	$7{,}93\times10^{-6}$	-----	Competitive	*M. troglodyta*	[27]
Tannic acid	GSH	-----	$6{,}58\times10^{-6}$	-----	Competitive	*M. troglodyta*	[27]
6,7-dihydroxy-3-(3',4'-dihydroxyphenyl)coumarin	CDNB	-----	$13{,}62\times10^{-6}$	-----	Noncompetitive	Human placental	[31]
6,7-dihydroxy-3-(3',4'-dihydroxyphenyl)coumarin	GSH	-----	$7{,}54\times10^{-6}$	-----	Mixed	Human placental	[31]
Ag^{+}	GSH	-----	$0{,}1\times10^{-6}$	-----	Noncompetitive	turkey liver	[33]
Hg^{2+}	GSH	-----	68×10^{-6}	-----	Noncompetitive	turkey liver	[33]
Hypericin	GSH	-----	248×10^{-6}	-----	Uncompetitive	Rat	[30]
Hypericin	CDNB	-----	150×10^{-6}	-----	Noncompetitive	Rat	[30]
Deltamethrin	GSH	$1{,}7\times10^{-5}$	81×10^{-6}	-----	Competitive	Human blood	In this study
Deltamethrin	GSH	$2{,}1\times10^{-5}$	$5{,}1\times10^{-6}$	-----	Competitive	Human blood	In this study
Lambda-cyhalothrin	GSH	$7{,}4\times10^{-5}$	$1{,}3\times10^{-5}$	$7{,}4\times10^{-5}$	Mixed	Human blood	In this study
Lambda-cyhalothrin	GSH	$1{,}11\times10^{-5}$	$1{,}1\times10^{-5}$	$11{,}1\times10^{-5}$	Mixed	Human blood	In this study
Glyphosate	GSH	$3{,}5\times10^{-2}$	$3{,}8\times10^{-3}$	-----	Uncompetitive	Human blood	In this study
Glyphosate	GSH	$5{,}3\times10^{-2}$	$1{,}8\times10^{-3}$	-----	Uncompetitive	Human blood	In this study

GST activity were given in Table 1 [27]. According to these results, the most effective inhibitor of GST was quercetin.

Inhibition Types. Oxidative stress is involved in pathophysiology of several toxins and diseases. The balance between the production of free radicals and antioxidant defenses in the body has important health implications. Reduction in the activities of antioxidant enzymes changes the redox status of the cells. *In vitro* inhibition is known to provide a useful tool for studying both the metabolism of xenobiotics catalyzed by GSTs and the involvement of GST in resistance. Reduction of the activity of the enzyme by a specific inhibitor may involve a single mechanism or may be a consequence of two or more inhibitor mechanisms. The enzyme binding of a specific inhibitor is very important in the interpretation of the obtained data [28]. In this study, kinetic inhibition parameters and types of inhibition of pesticides were determined with respect to GSH as a substrate.

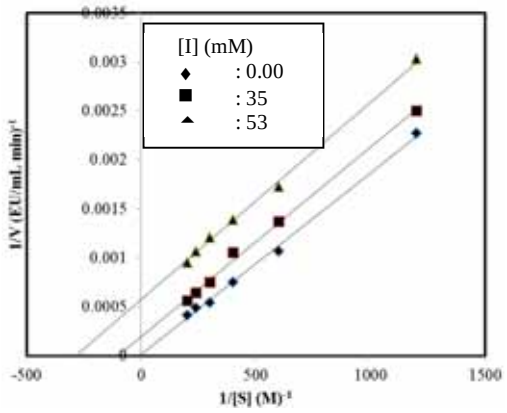


FIGURE 5
Lineweaver-Burk double reciprocal plots showing uncompetitive inhibition of human blood GST by glyphosate pesticide using CDNB as a substrate

Figure 5 showed that the inhibition type for glyphosate pesticide using GSH as a substrate was uncompetitive inhibition. Series of parallel lines in Lineweaver-Burk plot indicates uncompetitive inhibition. Uncompetitive inhibition requires that the inhibitor affects the catalytic function of the enzyme but not its substrate binding. In uncompetitive inhibition, inhibitor binds exclusively to the enzyme-substrate complex [29]. The dependencies obtained justified for this type inhibition. As seen from Table 2, Tuna et al. found that inhibition type for rat GST was uncompetitive for hypericin inhibitor when [CDNB] was used as the fixed and [GSH] was used as the varied substrate [30].

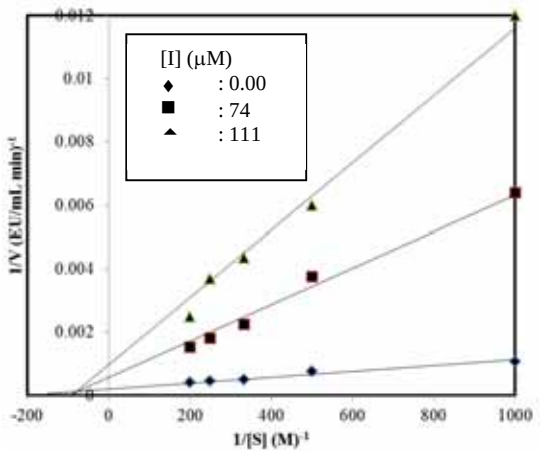


FIGURE 6
Lineweaver-Burk double reciprocal plots showing uncompetitive inhibition of human blood GST by lambda-cyhalothrin pesticide using CDNB as a substrate

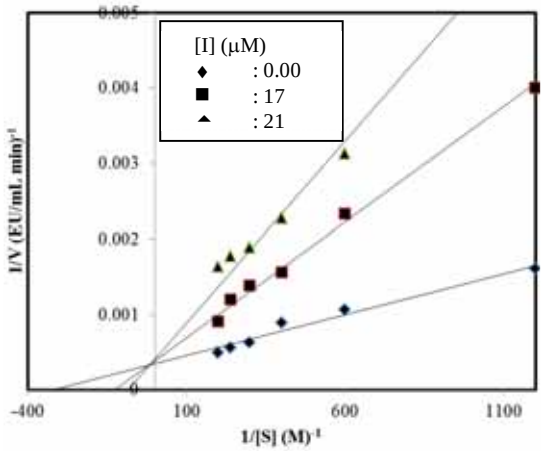


FIGURE 7
Lineweaver-Burk double reciprocal plots showing uncompetitive inhibition of human blood GST by deltamethrin pesticide using CDNB as a substrate

The type of inhibition may vary depending on the inhibitors and substrates used to decrease the activity of the enzyme. Lineweaver-Burk plot obtained for GST enzyme was shown in Figure 6 when GSH as substrate and lambda-cyhalothrin as inhibitor were used. When Figure 6 was examined, the curves intersect above the x-axis to the left of the y-axis. This suggested that the inhibition type was mixed-type inhibition. In this type of inhibition, inhibitor decreases the enzyme activity to bind both enzyme and the enzyme-substrate complex, and obtains two inhibition constants [22]. The inhibition constants obtained were given in Table 2. Similar result was found by Alparslan and Danış for human placental GST using GSH as substrate and 6,7-dihydroxy-3-(3', 4'-dihydroxyphenyl) coumarin as inhibitor [31].

Figure 7 shows the effect of deltamethrin pesticide on GST enzyme activity when GSH is used as the substrate. As seen from Figure 7, at certain inhibitor concentrations, the curves intersect on the y-axis. This indicates that the inhibition type is competitive type inhibition. In inhibition of this type, the enzyme competes with the substrate to bind to the active center of the enzyme. The substrate or the inhibitor binds to the active site of the enzyme. It is not possible to bind them together. The structure of inhibitor is similar to the substrate, so that binding of the substrate to the active site is prevented. In the competitive inhibition, inhibitor acts to reduce the concentration of free enzyme present for binding of the substrate. If the substrate concentration is increased, the effect of inhibitor can be eliminated [32]. Similar results were found by different researchers (Table 2) [33]. For *M. troglodyta* GST, Tang et al. found that inhibition type was competitive for quercetin and tannic acid pesticides when [GSH] was used as the fixed and [CDNB] was used as the varied substrate; and again, for *C. anachoreta* GST they found that inhibition type was competitive for quercetin acid pesticide when [CDNB] was used as the fixed and [GSH] was used as the varied substrate [27]. Results of the present study clearly showed a dose-dependent decrease in GST activities.

CONCLUSIONS

- Effects of three pesticides on GST activity were significant and different.
- GST activity were induced at low concentration and inhibited at high concentrations.
- Deltamethrin had the highest inhibition power on GST activity.
- The values obtained showed to be very strong inhibitors of pesticides when compared to the IC_{50} values obtained in the literature.
- The inhibition mechanism of pesticides on GST activity was different from each other.
- The inhibition types of glyphosate, lambda-cyhalothrin and deltamethrin pesticides on GST activity were uncompetitive, mixed and competitive, respectively.

REFERENCES

[1] Palüzar, H. (2013) Pestisitlerin vücut savunma sistemi enzimleri üzerine etkilerinin in vitro incelenmesi. Trakya Üniversitesi Fen Bilimleri Enstitüsü. Doktora Tezi. Edirne

[2] Ojha, A., Yaduvanshi, S.K., Srivastava, N. (2011) Effect of combined exposure of commonly used organophosphate pesticides on lipid peroxidation and antioxidant enzymes in rat tissues. Pesticide Biochemistry and Physiology. 99, 148–156.

[3] Song, Y., Chen, M., Zhou, J. (2017) Effects of three pesticides on superoxide dismutase and glutathione-S-transferase activities and reproduction of Daphnia magna. Archives of Environmental Protection. 43(1), 80–86.

[4] Gomez-Martin, A., Altakroni, B., Lozano-Paniagua, D., Margison, G.P., Vocht F., Povey, A.C., Hernandez, A.F. (2015) Increased N7-methyldeoxyguanosine DNA adducts after occupational exposure to pesticides and influence of genetic polymorphisms of paraoxonase-1 and glutathione s-transferase M1 and T1. Environmental and Molecular Mutagenesis. 56, 437-445.

[5] Anwar, W.A. (1997) Biomarkers of human exposure to pesticides. Environmental Health Perspectives. 105(4), 801-806.

[6] Chaudiere, J., Ferrari-Iliou, R. (1999) Intracellular antioxidants: from chemical to biochemical mechanisms. Food Chem. Toxicol. 37, 949–962.

[7] Doyotte, A., Cossu, C., Jacquin, M-C., Babutb, M., Vaseral, P. (1997). Antioxidant enzymes, glutathione and lipid peroxidation as relevant biomarkers of experimental or field exposure in the gills and the digestive gland of the freshwater bivalve unio tumidus. Aquatic Toxicology. 39, 93-11.

[8] Oruç, E.Ö., Sevgiler, Y., Uner, N. (2004) Tissue-specific oxidative stress responses in fish exposed to 2,4-D and azinphosmethyl. Comparative Biochemistry and Physiology Part C. 137, 43–51.

[9] Souza, M.S., Magnarelli, G.G., Rovedatti, M.G., Santa Cruz, S., Pechen De D'Angelo A.M. (2005) prenatal exposure to pesticides: analysis of human placental acetylcholinesterase, glutathione s-transferase and catalase as biomarkers of effect. Biomarkers. 10(5), 376-389.

[10] Medina-Diaz, I.M., Rubio-Ortiz, M., Martinez-Guzman, M.C., Davalos-Ibarra, R.L., Rojas-Garcia, A.E., Robledo-Marenco, M.L.,. Barron-Vivanco, B.S., Giron-Perez, M.I., Elizondo, G. (2011) Organophosphate pesticides increase the expression of alpha glutathione S-transferase in HepG2 cells. Toxicology in vitro. 25, 2074–2079.

[11] Matic, M.G., Coric, V.S., Savic-Radojevic, A.R., Bulat, P.V., Pljesa-Ercegovac, M.S., Dragicevic, D.P., Djukic, T.I., Simic, T.P., Pekmezovic, T.D. (2014) Does occupational exposure to solvents and pesticides in association with glutathione s-transferase A1, M1, P1, and T1 polymorphisms increase the risk of bladder cancer? The Belgrade Case-Control Study, Plos ONE. 9(6), e99448.

[12] Ezemonye, L., Tongo, I. (2010) Sublethal effects of endosulfan and diazinon pesticides on glutathione-S-transferase (GST) in various tissues of adult amphibians (Bufo regularis). Chemosphere. 81(2), 214-217.

[13] Kaya, A., Yigit, E. (2012) Interactions among glutathione S-transferase, glutathione reductase activity and glutathione contents in leaves of Vicia faba L. subjected to flurochloridone. Fresen. Environ. Bull. 21(6b), 1635-1640.

[14] Arslan, Ö.Ç., Parlak, H., Boyacioglu, M., Karaslan, M.A., Katalay, S. (2014) Changes in the glutathione-s transferase activity of the mussel Mytilus galloprovincialis during exposure to bisphenol-A. Fresen. Environ. Bull. 23(10a), 2525-2530.

[15] Kolarova, J., Svobodova, Z., Zlabek, V., Randak, T., Hajslova, J., Suchan, P. (2005) Organochlorine and pahs in brown trout (Salmo trutta fario) population from Ticha Orlice river due to chemical plant with possible effects to vitellogenin expression. Fresen. Environ. Bull. 14(12a), 1091-1096.

[16] Doğan, S. (2006) The in vitro effects of some pesticides on carbonic anhydrase activity of Oncorhynchus mykiss and Cyprinus carpio carpio fish. Journal of Hazardous Materials. A132, 171–176.

[17] Habig, W., Pabst, M.J., Jakoby, W.B. (1974) Glutathione S-tTransferases. The first enzymatic step in mercapturic acid formation, The Journal of Biological Chemistry. 249(22), 7130-7139.

[18] Doğan, S., Diken, M.E., Alan, Ü., Yılmaz, B., Alkan, M., Doğan, M. (2016) Some kinetic and inhibition properties of deepwater pink shrimp from Aegean Sea: pH, temperature, kinetic and inhibition. Advances in Food Sciences. 38(4), 155-164.

[19] Splittgerber. A.G. (1983) Simplified treatment of two-substrate enzyme kinetics. Journal of Chemical Education. 60(8), 651-655.

[20] Hammes, G.G. Enzyme Catalysis and Regulations. Academic: New York, 1982.

[21] Cromartie, T.H. (1986) The Inhibition of Enzymes by Drugs and Pesticides. Journal of Chemical Education. 63(9), 765-768.

[22] Doğan, S., Turan, P., Doğan, M., Alkan, M. and Arslan, O. (2007) Inhibition kinetic of Ocimum basilicum L. polyphenol oxidase. International Journal of Chemical Reactor Engineering. 5(A46), 1-15).
[23] Gadagbui, B.K.M., James, M.O. (2000) The influence of diet on the regional distribution of glutathione S-transferase activity in channel catfish intestine. Journal of Biochemical and Molecular Toxicology. 14, 148–154.
[24] Chen, R., Liu, H., Li, D.X., Chen, Y. (2006) A review of glutathione S-transferase in aquatic animal. Journal of Xiamen University (Natural Science). 45, 176–184.
[25] Van der Oost, R., Beyer, J., Vermeulen, N.P.E. (2003) Fish bioaccumulation and biomarkers in environmental risk assessment: a review. Environmental Toxicology and Pharmacology. 13, 57–149.
[26] Xu, Y.G., Zhang, J.L., Li, X.F., Liu, L. (2013) Study on chronic toxicity of Difenoconazle to Daphnia magna and its effect on GST enzymatic activity. Hubei Agricultural Sciences. 52, 79–83.
[27] Tang, F., Zhang, X., Liu, Y., Gao X., Liu N. (2014) In vitro inhibition of glutathione s-transferases by several insecticides and allelochemicals in two moth species. International Journal of Pest Management. 60(1), 33-38.
[28] Lee, C.Y., Whitaker, J.R. (1995) Enzymatic browing and its prevention. American Chemical Society, Washington, DC.
[29] Voet, D., Voet, J.G. (2004) Biochemistry. John Wiley & Sons, Inc., Hoboken, NJ, USA. 485-486.
[30] Tuna, G., Erkmen, G.K., Dalmizrak, O., Dogan, A., Ogus, I.H., Ozer, N. (2010) Inhibition characteristics of hypericin on rat small intestine glutathione-S-transferases, Chemico-Biological Interactions. 188, 59-65.
[31] Alparslan, M.M., Danış, Ö. (2015) In vitro ınhibition of human placental glutathione s-transferase by 3-arylcoumarin derivatives. Arch. Pharm. Chem. Life Sci. 348, 635-642.
[32] Doğan, S., Doğan, M., Arslan, O. (2009) Prevention of enzymatic browning and its inhibition. Food Processing: Methods, Techniques and Trends. Novapublishers, NY.
[33] Akkemik, E., Taser, P., Bayindir, A., Budak, H., Ciftci, M. (2012) Purification and characterization of glutathione s-transferase from turkey liver and inhibition effects of some metal ions on enzyme activity. Environmental Toxicology and Pharmacology. 34, 888-894.

Received: **15.06.2017**
Accepted: **18.08.2017**

CORRESPONDING AUTHOR

Mehmet Dogan
Balıkesir University
Faculty of Science and Literature
Department of Chemistry,
10145 Altıeylül, Balikesir – Turkey

e-mail: mdogan@balikesir.edu.tr

© by PSP Volume 26 – No. 12A/2017 pages 8030-8040 Fresenius Environmental Bulletin

RESEARCH ON THE METHOD OF NEW GENERATION OF MULTI-SENSOR INFORMATION FUSION TECHNOLOGY TO PROMOTE THE DEVELOPMENT OF WISDOM AGRICULTURE IN 'INTERNET +' MODE

Zhen Zhang*, Xueping Xiong

College of Economics & Management, Huazhong Agricultural University, Wuhan, 430070, HuBei, China

ABSTRACT

After entering in the 21st century, the development of science and technology has led to the revolution in agricultural technology. The Internet has deeply affected all lifestyles in China. Agricultural production and modern network marriage, the agriculture and the Internet technology linked together innovative production methods, but also it gave birth to the modern wisdom agriculture. In this paper, *ZigBee* wireless sensor network node is used as the research object combined with Internet technology, the characteristics of the terminal node, wireless sensor network general terminal node design requirements. The hardware focuses on the WSN node design of wisdom agriculture. Secondly, this paper uses the 3G node as the base station and the sink node, the node obtains the environment information acquisition and control of the greenhouse by the Zigbee node. Therefore, we can develop the greenhouse environment monitoring system, which based on the wireless network, and carry on the multi-sensor data fusion to the wireless sensor network, Data measurement accuracy and performance. Aiming at the dynamic change of the sensing nodes in the Zigbee self-organizing network, the algorithm has optimized to realize the intelligent control of the water valve and the sunshine curtain. The system of mobile resource management based on mobile Agent is established.

KEYWORDS:
Zigbee, Wisdom agriculture, Self-organizing network, Agent

INTRODUCTION

With the development of human civilization, agricultural production has made a huge leap. From the production tools, production methods continue to update, our crop production continues to improve, and people's living standards have been greatly improved [1]. As China's rapid development of sensor technology, IT and wireless communication technology, sensors with data acquisition, computing storage and WSN are widely used in agriculture. The wireless sensor network is a self-organizing system, which is composed of a large number of stationary or micro sensor nodes to detect information by wireless communication. The nodes and nodes communicate the heat, infrared and sonar of the surrounding environment through a variety of sensors. A wide range of physical phenomena include temperature, humidity, light intensity and transmit information via wireless communication. This information has sent to the network owner to achieve the purpose of collecting and processing information at any time. Therefore, the design of sensor nodes has become the wireless sensor network research. At the beginning in 2017, intelligent agriculture and normalization will be at the cusp [2, 3]. The operation mode of traditional agriculture cannot meet the needs of sustainable development of agriculture [4, 5]. The emergence of intelligent agriculture for the development of modern agriculture provides a bright road, wisdom agriculture, while the traditional agriculture does not have the high-tech and reasonable management in exchange for the optimal resource use [6]. It is comprehensive and strong system engineering, so that China's agriculture can achieve low energy consumption, high efficiency and environmental protection, which is the world's new trend of agricultural development.

Wisdom agriculture is a new type of agriculture that has been developed in recent years in the western countries to combine high-tech and agricultural production [7, 8]. It is characterized by "wisdom", which uses satellite global positioning system, wisdom fertilization and high production. Porter is a Minnesota farmer who drives a tractor to work in the fields, and on the surface, it is no different from any other farmer. However, his tractor installed 600 computers, and the screen can be seen on an area of 760 hectares, the computer will tell him where the need for fertilization. If you install a satellite signal reception device, you can receive the global satellite positioning system issued by remote sensing telemetry information and the information, which can be intelligent soil survey, reasonable fertilization and agricultural environmental moni-

toring. Soil survey and reasonable fertilization can reduce the amount of fertilizer, reduce waste, and reduce investment. Soil surveys should first be taken for soil samples. If the farmer drives a terrain-like vehicle on the land before sowing, the soil sample data has collected and entered into the computer [9, 10]. At the same time, the GPS system records the location of the sample collection site [11]. In addition, the fertilization software stored in the computer, which can be, based on different types of fertilizers and different crop fertilization standards. Crop yield cannot only accurately monitor the output, but also it can draw the output distribution map [12]. At the same time, the satellite global positioning system records the geography of the harvester, so you can draw the output map and calculate the output of each land, and the distribution of production can also determine where the lack of fertilizer. Wisdom agriculture can target the soil structure. The United States Department of Agriculture Productions in Iowa developed a "Satellite-Directed Agricultural Production Joint Program" that was tested on 450 hectares of farmland grown with soybeans, corn, oats and alfalfa. Tractors can carry out under the joint plan [13, 14]. Domestic research on intelligent agriculture has also carried out in many research institutes and universities. In 1995, Hu Jiandong, Xiao Jianjun and their partners used the principle of fuzzy control to design a multi-span greenhouse control system, which combined the fuzzy control technology to make the greenhouse environment to achieve the best growth. Based on the greenhouse automation technology and production practice, this paper summarizes and collects the expert system of knowledge, which has based on ZigBee. In 1998, Jiangsu Polytechnic University, Li Pingping developed industrial control greenhouse automatic control system, which can use various sensors to measure greenhouse temperature, humidity, light intensity and other environmental factors. Comparison of the status quo at home and abroad, it is difficult to find the wisdom of the development model of wisdom on the ills. The most embarrassing is the domestic more demonstration projects, just stay in the test and demonstration stage [15]. In summary, intelligent wisdom, agriculture to replace traditional agriculture is the inevitable development of agriculture, it is in line with China's national conditions, intelligent wisdom agriculture can promote the transformation of agricultural development mode, which can achieve efficient use of various agricultural resources and improve the environment sustainable development goals. High-tech can promote the transformation of agricultural development mode, intelligent management can achieve the efficient use of various agricultural resources, but also it can achieve the goal of improving the sustainable environment. We cannot only maximize the rural real estate productivity, but also we can achieve high quality, low energy consumption and sustainable development of agriculture.

This paper attempts to use the Internet technology for modern agriculture, which has called "wisdom agriculture" of high-tech agricultural engineering. We can use the satellite; remote sensing, computer and automatic control of high-tech agricultural production improve our production. The international advanced farmland farming technology will extend to the country to solve the agricultural development bottlenecks, reduce pollution and take the road of sustainable agricultural development. At present, the node design needs to consider the expectation of the network protocol in the wireless sensor network. It is a simple protocol stack to support the effective operation of the wireless sensor network. The access is flexible and convenient, and it uses the broadcast information to avoid the interactive response. Concise signalling patterns based on the requirements of the wireless sensor network protocol such as Zigbee protocol, which is suitable for wireless communication protocol of sensor network to maximize the savings in network energy and wood, and Zigbee can access a large number of nodes at any time [16, 17]. In this paper, ZigBee node as the research object has combined with Internet technology, the hardware focuses on the wireless sensor hardware design of universal terminal node. Secondly, this paper completes the software design scheme of the terminal node by realizing the data acquisition, energy detection, wireless communication operation and debugging of the software part. The design of the network system has the characteristics of low cost and small size. The test results show that the network supports the network topology, which used in the field of environmental inspection.

EXPERIMENTAL

The prepared equipment and location. The prepared equipment. The SHT10 is a highly integrated temperature and humidity sensor chip that provides fully calibrated digital outputs [18]. It includes a capacitive polymer hygrometer, a thermometer, which is made of energy gap material and serial interface circuit to achieve seamless connection. HA2003 use advanced photoelectric conversion module, the light intensity value has high-precision light intensity measurement, and it can choose the voltage or current output, the current output in the long cable transmission, which has no signal attenuation.

Carbon dioxide sensor TGS4160 is from the Shenzhen New World Technology, which sells one of the gas sensors, on the carbon dioxide sensor TGS4160 principle and application information, you can view the site of carbon dioxide sensor TGS4160 PDF products. TGS4160 is a kind of sol-

id-state electrochemical carbon dioxide sensor (CO2 sensor) produced by FIGARO in Japan. The device has the advantages of small volume, long life, good selectivity and good stability, which can be widely used in automatic ventilation system or CO2 gas long-term monitoring and other applications [19]. The following will explain to you the internal structure of the sensor and the working principle in Table 1.

Device function. (1) Greenhouse environmental information sensor nodes. The parameters of greenhouse environment temperature, humidity, light intensity, CO2 concentration, soil moisture and temperature have obtained. The temperature of the greenhouse was higher than that of the greenhouse. We can strengthen CO2 concentration, wind speed, rainfall and other information.

(2) Information collection and transmission of the convergence node. The Zigbee network technology and 3G-network technology are used to realize the information collection and transmission of the node. By setting the wireless frequency and the Zigbee ID, the network and identification in different greenhouses have realized. The 3G network realizes the data transmission between the greenhouse information and the server.

(3) Field control node. Based on the Zigbee/3G network, the control signals are sent to the field control nodes, and the implementing agencies of the greenhouse are controlled by the relay to realize the remote real-time regulation of the greenhouse environment.

Device development and configuration. The developed sensor nodes are consisting of a wireless acquisition device, a sensor and a power supply module, where the temperature and humidity nodes are equipped with a radiation shield [20]. The Zigbee wireless acquisition equipment developed by Shanghai Shun Zhou Electronic Technology which can be used to realize the centre node, routing node and terminal node arbitrarily set [21, 22].

(1) Aggregation nodes. The convergence node adopts the intelligent gateway of Zhenjiang DaKeMao Information System Co., Ltd. Intelligent gateway system using ARM1176JZF-S core as a smart gateway microprocessor, and integrated Zigbee, 3G and other modules, software integration BOA server, SQLite3 database. The ARM controller connects to the Zigbee coordinator node via the serial port to obtain the environmental parameters collected by the Zigbee wireless sensor network.

(2) Greenhouse Environment Control Nodes. The node system of greenhouse environment control includes intelligent gateway system through the 3G network, and the control signal has sent by the server. The convergence node through the Zigbee coordination node will control the signal transmission to the control node, through the 485 bus to the signal conversion module; the signal conversion model will control the signal, which has converted to 16 relay control signals for actuator control.

Location Test sites and installations. The experiment has carried out in two Venlo type glass greenhouses in the agricultural demonstration park. The greenhouse was 9.6 m, the distance was 4 m, the shoulder height was 4 m, and the span was 9, covering an area of 1382.4 nf. Greenhouse is equipped with skylights, side windows, shade, outside shade, wet curtain fan and other control equipment, planting crops mainly lettuce, cucumber and other vegetable crops.

Monitoring method. Fruits and vegetables on the growth environment have strict requirements, so the modern agriculture has to build a greenhouse to control the growth of plants. It can be seen that the environment plays an important role in the greenhouse [23]. Intelligent greenhouse system can be real-time monitoring and remote control of the greenhouse different electrical equipment, such as rolling machine, irrigation and so on. The technical staff in the office will be able to monitor the environment of multiple greenhouses to control, so that plants can get the best growth environment.

TABLE 1
Sensor technical parameters

NO.	Sensor type	Model	Signal type	technical parameter
1	temperature and humidity sensor	SH10	D	supply voltage is 2.4 ~ 5.5V Operating temperature and humidity: -20 ℃ ~ 60 ℃, 0 ~ 70% RH
2	Light sensor	HA2003	A	Range: 0 ~ 20 million lx Error: ± 5% Operating voltage: DC5 ~ 24V Output signal: 0 ~ 2V, 0 ~ 5V, 0 ~ 10V, 0 ~ 20mA, 4 ~ 20mA
3	CO2 sensor	TGS4160	A	Measuring range: 0 ~ 5000ppm; Heater voltage: 5.0 ± 0.2VDC; Heater current: 250mA; Operating temperature: - 10 ~ +50 ℃

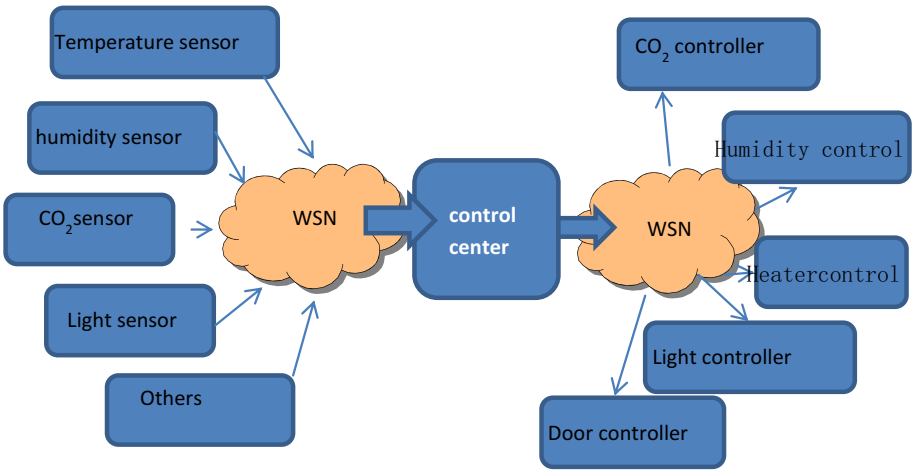


FIGURE 1
Schematic diagram of Intelligent Greenhouse

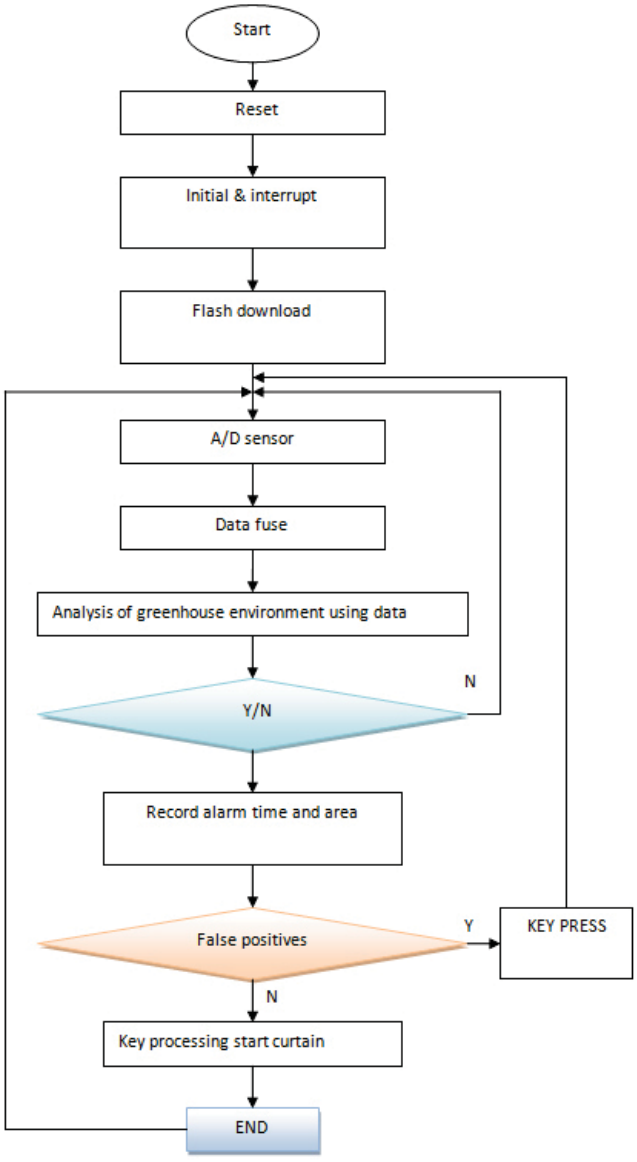


FIGURE 2
Work process of intelligent gateway

Greenhouse information environment collection. In the greenhouse environment, a single greenhouse can be a wireless sensor network for measurement control area, the use of different sensor nodes and a simple actuator with the node, which constitute a wireless network with the soil moisture, soil composition, pH value, precipitation, temperature, air humidity, light intensity and CO2 concentration. The nodes have used to obtain the optimum conditions for crop growth. At the same time, the method of biological information acquisition has applied to the wireless sensor node. We can see the schematic diagram of Intelligent Greenhouse in Figure 1.

Intelligent gateway work process. Greenhouse environment intelligent gateway work process is shown in figure 2. First, the server initiates the 3G network service program. After the service function is successful, the intelligent gateway terminal performs the network connection and starts to listen to the interrupt signal from the user and the information acquisition node [24]. The system has interrupted for the serial data of the information collection, environmental information, and real-time environmental information, which reported to the server. When the data is from the server's query and control instructions, the system has the relevant instructions to answer. When the server instruction is used for the data query instructions, the query needs to feedback the corresponding data. When the instructions has environmental control, the system sent to the server control instructions analysis, and the control command sent through the 485 port to achieve the greenhouse environment control.

Experimental system and measurement process. Construction of intelligent agricultural greenhouses networking information system can achieve agriculture from production to quality control and transport network management. Intelligent agriculture greenhouses networking information system mainly research temperature, chemistry and other sensors on the whole process of monitoring and data management of agricultural products which combined with Zigbee in the cultivation, production. Figure 3 shows the architecture of Intelligent Agriculture.

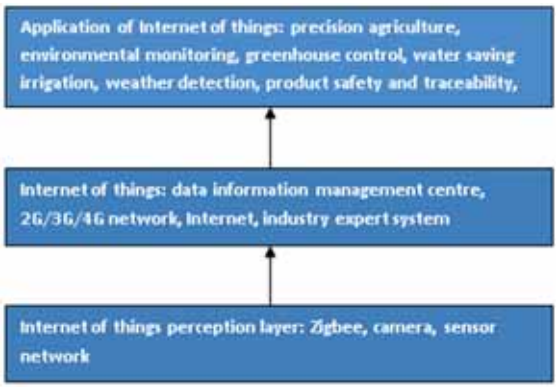


FIGURE 3
The architecture of Intelligent Agriculture

At present, wireless technology is widely used in agriculture, but most of them have the application of basic station star topology. The general application of agriculture helps farmers find problems in a timely manner, and accurately determine the location of the problem, so that agriculture may be gradually from the human as the centre, which dependents on mechanical production mode to information and software-centric production model. Figure 4 shows the network architecture of control system by our design. The main control system for the embedded system by using ARM9 processor and Linux operating system can control the equipment management. The embedded gateway has connected to the internal and external information transmission channels, which are wireless way, the external network to IP-based network technology, by providing general packet wireless business, based on GPRS communication network [25, 26]. The internal network adopts short distance and low power ZigBee wireless communication technology. The system combines the data of special series of agricultural fields to collect and transmit the data such as temperature and humidity, PH value, light and soil nutrient in agricultural environment.

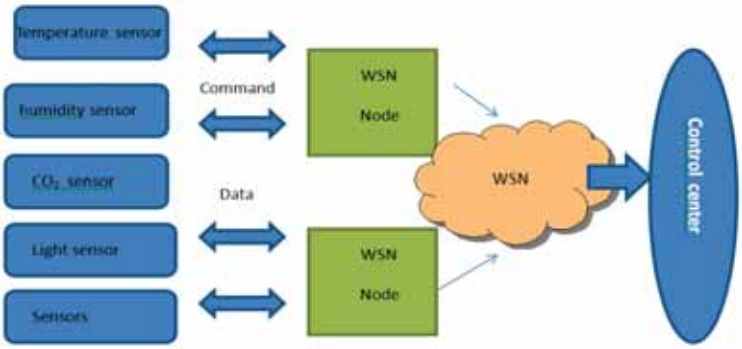


FIGURE 4
The architecture of Intelligent Agriculture in this paper

Multi-sensor information fusion model. Device Modelling. As the greenhouse environment control is the main object of temperature and humidity, and the temperature and humidity in different areas of the greenhouse are different, so the sensor nodes arranged for the greenhouse diagonal position set two temperature and humidity. For light and CO2, Direct regulation, a basis for regulation of temperature and humidity is the middle of the greenhouse in the middle of a light set and CO2 environmental information collection node. Conventional multi-sensor data fusion takes into account the spatial fusion of data belonging to different spatial sensors at the same time or time integration of data at different times for the same sensor. However, in the greenhouse environment monitoring and control multi-sensor system, wireless network data acquisition and transmission process interference will cause some of the sensor data loss or error [27, 28]. If the temperature positively correlated with the light, it negatively correlated with the humidity. Therefore, the multi-sensor data fusion should consider the interaction between the parameters to achieve the data fusion between heterogeneous sensors.

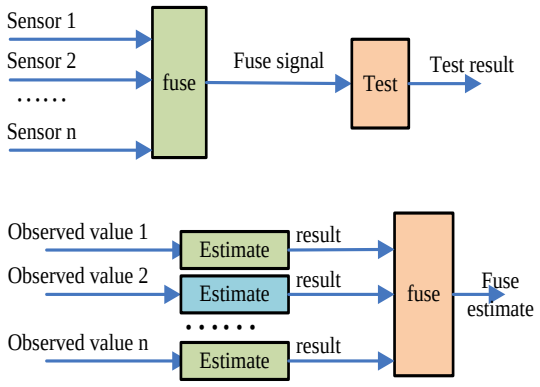


FIGURE 5
The process of two level fusion by environmental wireless measurement and control network

According to the three-layer structure system of greenhouse environment monitoring, the fusion process is shown in Figure 5. The node is at the same time the sensor observations of the node layer fusion, and then the convergence layer of the node fusion results is using weighted least squares fusion algorithm for heterogeneous sensor fusion by improving data accuracy.

Kalman tracking filter. Dr. Kalman designs Kalman filter, and it is the application of a wide range of filters, which can make the minimum MSE. In the XY coordinates, the state equation of object has expressed as follows.

$$x_p(k+1) = x_s(k) + V_s(k)T \qquad (1)$$

The formula (1) for the simplest tracking filter is the α-β filter.

$$\boldsymbol{X}(t+1) = \boldsymbol{\phi}(t)\boldsymbol{X}(t) + \boldsymbol{\Gamma}(t)\boldsymbol{A}(t) \qquad (2)$$

$$\boldsymbol{X}(t) = \begin{vmatrix} x(t) \\ \dot{x}(t) \\ y(t) \\ \dot{y}(t) \end{vmatrix} \quad \boldsymbol{\phi}(t) = \begin{vmatrix} 1 & T & 0 & 0 \\ 0 & 1 & 0 & 0 \\ 0 & 0 & 1 & T \\ 0 & 0 & 0 & 1 \end{vmatrix} \qquad (3)$$

$$\boldsymbol{\Gamma}(t) = \begin{vmatrix} T^2/2 & 0 \\ T & 0 \\ 0 & T^2/2 \\ 0 & T \end{vmatrix} \text{ 及 } \boldsymbol{A}(t) = \begin{vmatrix} a_x(t) \\ a_y(t) \end{vmatrix} \qquad (4)$$

X (T) is the state vector of the t moment, which includes the position and velocity components $\dot{x}(t), x(t), \dot{y}(t), y(t)$, t+1 is the next observation time; T is the interval of the two observation. $a_x(t)$ and $a_y(t)$ is the random acceleration with covariance matrix $\boldsymbol{Q}(t)$ [29-32]. Observation equation is as (5).

$$\boldsymbol{Y}(t) = \boldsymbol{M}(t)\boldsymbol{X}(t) + \boldsymbol{V}(t) \qquad (5)$$

and

$$\boldsymbol{Y}(t) = \begin{vmatrix} x_m(t) \\ y_m(t) \end{vmatrix} \boldsymbol{M}(t) = \begin{vmatrix} 1 & 0 & 0 & 1 \\ 0 & 0 & 0 & 0 \end{vmatrix} \boldsymbol{V}(t) = \begin{vmatrix} v_x(t) \\ v_y(t) \end{vmatrix} \qquad (6)$$

$\boldsymbol{Y}(t)$ is a measure of t moments, which includes the position parameter $x_m(t)$ and $y_m(t)$,$\boldsymbol{V}(t)$ is a zero mean noise, and its covariance matrix is $\boldsymbol{R}(t)$.

First, we assume that the solution of the t moments can express by the recursive form of (t-1) moments. Here, assuming t-1 time as optimal detection $\hat{\boldsymbol{X}}(t-1|t-1)$, and its error covariance matrix $\boldsymbol{P}(t\text{-}1|t\text{-}1)$ which is known, the signs $\hat{\boldsymbol{X}}(t|s)$ in the expression "∧" is a kind of estimate, the expression means to $\boldsymbol{Y}(s)$ of the observation of estimation $\boldsymbol{X}(t)$. There are six steps in the recursive algorithm [33].

Here is the prediction and covariance matrix.

$$\hat{\boldsymbol{X}}(t|t-1) = \boldsymbol{\phi}(t-1)\hat{\boldsymbol{X}}(t-1|t-1) \qquad (7)$$

$$\boldsymbol{P}(t|t-1) = \boldsymbol{\phi}(t-1)\boldsymbol{P}(t-1|t-1)\boldsymbol{\phi}^{\mathrm{T}}(t-1) + \boldsymbol{\Gamma}(t-1)\boldsymbol{Q}(t-1)\boldsymbol{\Gamma}^{\mathrm{T}}(t-1) \qquad (8)$$

Calculate the predicted values and calculate the filter gain matrix

$$\hat{\boldsymbol{Y}}(t|t-1) = \boldsymbol{M}(t)\hat{\boldsymbol{X}}(t|t-1) \qquad (9)$$

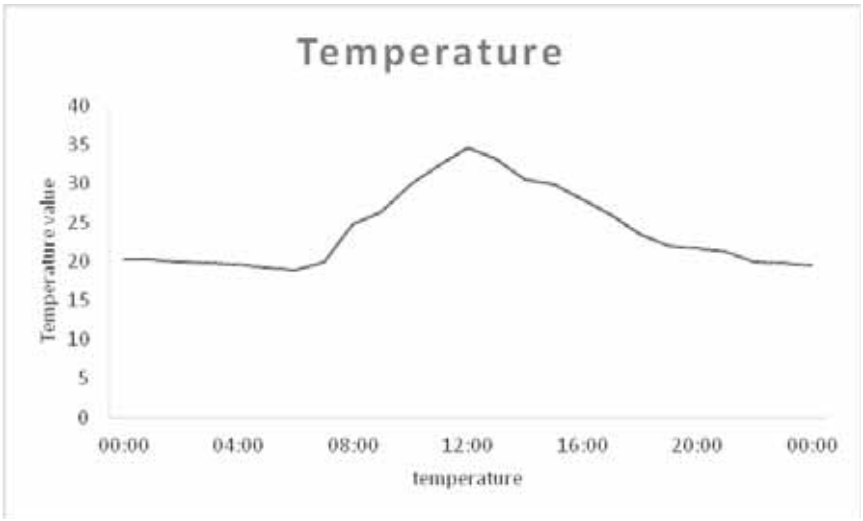
$$\boldsymbol{\Delta}(t) = \boldsymbol{P}(t|t-1)\boldsymbol{M}^{\mathrm{T}}(t)[\boldsymbol{M}(t)\boldsymbol{P}(t|t-1)\boldsymbol{M}^{\mathrm{T}}(t) + \boldsymbol{R}(t)]^{-1} \qquad (10)$$

Calculate new smoothed estimates:

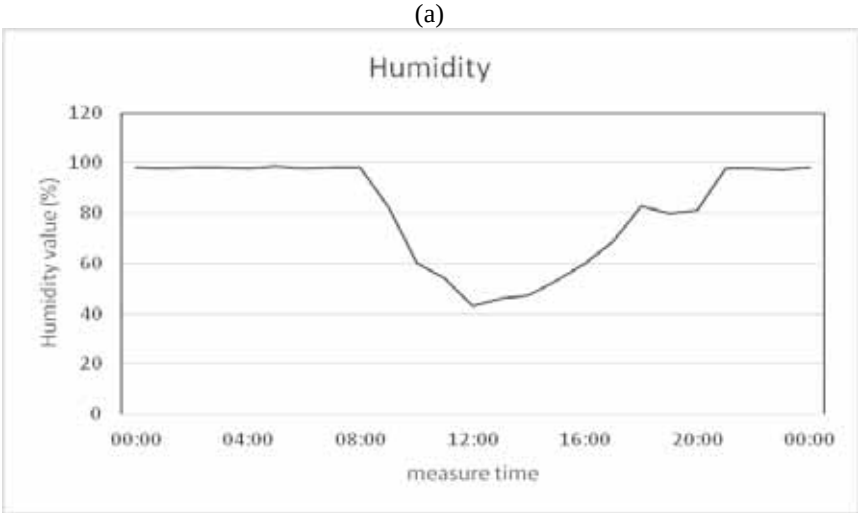
$$\hat{\boldsymbol{X}}(t|t) = \hat{\boldsymbol{X}}(t|t-1) + \boldsymbol{\Delta}(t)[\boldsymbol{Y}(t) - \hat{\boldsymbol{Y}}(t|t-1)] \qquad (11)$$

Calculate new covariance matrix:

$$\boldsymbol{P}(t|t) = [\boldsymbol{I} - \boldsymbol{\Delta}(t)\boldsymbol{M}(t)]\boldsymbol{P}(t|t-1) \qquad (12)$$



(a)



(b)

FIGURE 6
The Kalman filtering results

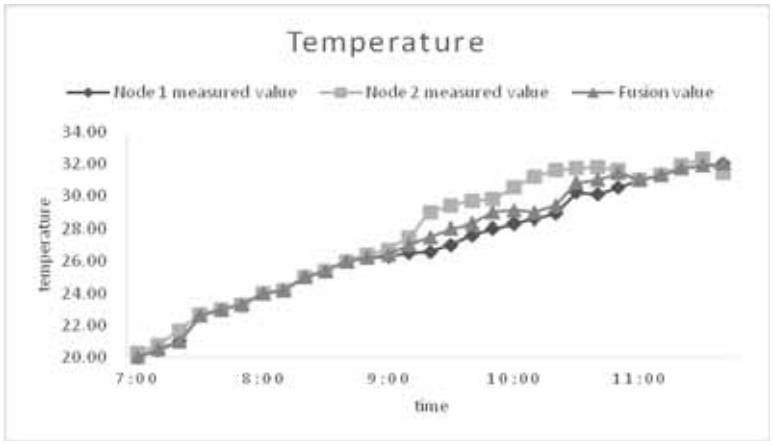
In short, the recursive algorithm from an estimated value $\hat{\boldsymbol{X}}(t-1|t-1)$ and its covariance matrix $\boldsymbol{P}(t-1|t-1)$ helps to obtain a new observation $\boldsymbol{Y}(t)$ and in the recursive algorithm in the six volumes, you can get a new estimate $\hat{\boldsymbol{X}}(t|t)$ and its covariance matrix $\boldsymbol{P}(t|t)$.

RESULTS AND DISCUSSION

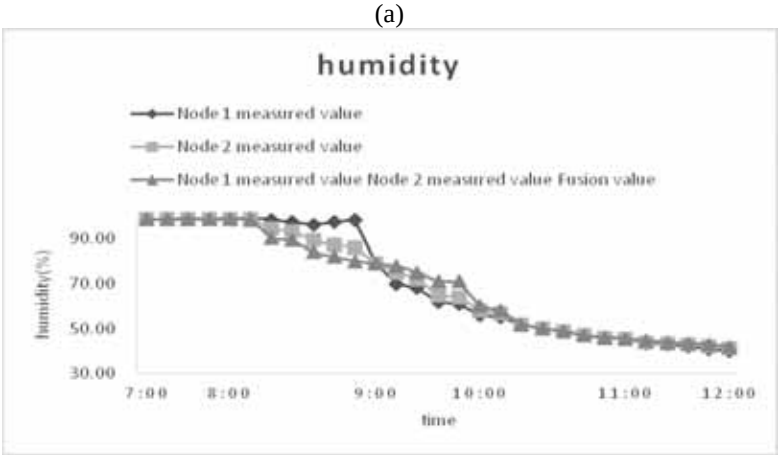
Result of Kalman filter. In order to test the fusion effect of the sensor nodes, the environmental information of the temperature, humidity and light intensity in the greenhouse was collected by three nodes, and the collection time was from 10:00 to 22:00, The points were collected at intervals of 10 min, and 144 data were collected. Figure 6 shows the temperature and humidity filtering results of node 1 and node 2 respectively. It can be seen from the filtering result that the measured values of the temperature parameters of the two nodes are not fluctuating and the results of the filtering are smaller than those of the measured values [34]. For the humidity filter results, the night greenhouse is in a closed state, due to crop respiration, making the greenhouse humidity close to 100%, while the humidity sensor in more than 98% humidity will be data fluctuations, through Kalman filter, which can achieve data smooth [35, 36].

The filtering result of the light intensity of node 3 is shown in Fig. 6. At noon, the light intensity of the greenhouse has abruptly changed due to the short time change of the outside illumination. The data filtering can be realized by Kalman filter.

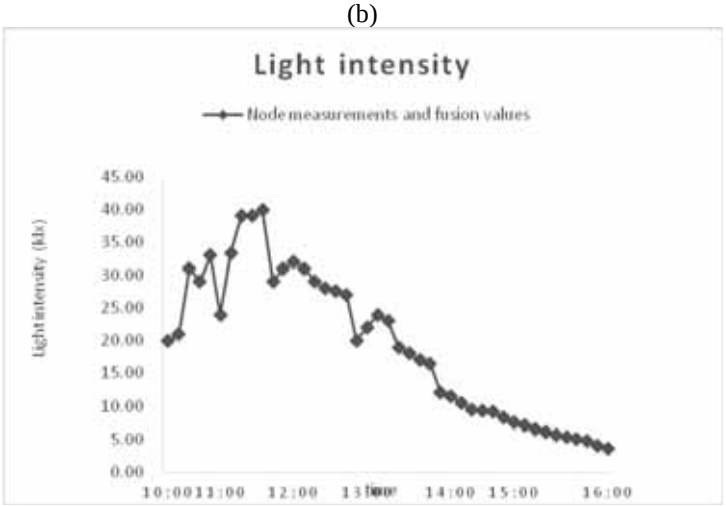
Convergence layer node fusion results. In order to test the fusion effect of convergence level, the fusion effect test has selected from 7:00 to 12:00 in the range of temperature and humidity change. Figure 7 shows the fusion values for temperature, humidity, and light intensity in the greenhouse using the weighted least squares algorithm.



(a)



(b)



(c)

FIGURE 7
The test results after data fusion

Since only one light sensor is set up in this study, the fusion value of the illumination is the measured value of the light according to the least squares fusion algorithm in the fusion process. Prior to 10:00 am, the temperature and humidity fusion values were averaged [37]. Greenhouse at 9:00 am opened the side windows ventilation, mountain in the experimental greenhouse is on the east side of the open space. The west side of another greenhouse is the natural ventilation mainly by the east side of the window to achieve indoor temperature hot and humid, which located in the greenhouse on the east side of the temperature and humidity node values. The nodes have located in the greenhouse on the west side of the temperature and humidity behind 1 hour after the change, through the weighted least squares fusion, temperature and humidity fusion values closer to the node 2, which better reflect the greenhouse temperature and humidity changes. 10:00 after the greenhouse and

outdoor dynamic wet and heat balance, the temperature and humidity fusion value is the average.

CONCLUSION

Internet of Things is an important part of a new generation, which extends and expands on an Internet-based basis, but it extends new areas in the client and extends between anything and things for information exchange and communication. This article applies the Internet of Things to agriculture, and helps the peasants from the traditional farming methods to the modern agriculture, and the high-tech improves the efficiency of agricultural production. We study the intelligent agricultural and further establish a wireless network monitoring platform. The use of wireless network measurement helps to obtain the best conditions for the growth of various crops, which can provide a scientific basis for accurate greenhouse regulation to improve the crop growth environment in order to achieve increased production, improve quality, adjust the growth cycle, and improve the purpose of economic income. On the other hand, the system developed a greenhouse system based on wireless network environment measurement, short-distance transmission and long-distance transmission combined with Zigbee network that based on the node of greenhouse environment collection. At the same time, the two-layer information fusion method has adopted, and the sensor node fusion has carried out by using the *Kalman* filter method. The weighted least squares method has used to fuse the nodes to realize the information of the heterogeneous that can improve the accuracy of the sensor data acquisition.

ACKNOWLEDGEMENTS

The authors acknowledge the National Natural Science Foundation of China (Grant: 51578109), the National Natural Science Foundation of China (Grant: 51121005).

REFERENCES

[1] Tang, D., Huang, D., Yang, Z., Ji, Q. (2017) Developmental trend of microfluidic chip and biosensor technologies and the integration mode with machine learning model and wearable device. International Journal of Biomedical Engineering and Technology. 23(2-4), 281-302.

[2] Vermesan, O., Friess, P. (Eds.) (2014) Internet of things-from research and innovation to market deployment. Aalborg: River Publishers, 74-75.

[3] Friess, P. (2013) Internet of things: converging technologies for smart environments and integrated ecosystems. River Publishers.

[4] Vermesan, O., Friess, P., Guillemin, P., Sundmaeker, H., Eisenhauer, M., Moessner, K., Cousin, P. (2013) Internet of things strategic research and innovation agenda. River Publishers Series In Communications. 7.

[5] Guo, X. (2017) Using airborne lidar to map habitat structure and connectivity across Alberta's managed forest for biodiversity conservation (Doctoral dissertation, University of British Columbia).

[6] Rashvand, H.F. and Hsiao, K.-F. (2014) Robotic Platforms and Their Applications. Journal Of Platform Technology. 2(4), 3-33.

[7] Kranz, M. (2016) Building the Internet of Things: Implement New Business Models, Disrupt Competitors, Transform Your Industry. John Wiley & Sons.

[8] Yamamoto, S. (ed.) (2016) Human Interface and the Management of Information: Information, Design and Interaction: 18th International Conference, HCI International 2016 Toronto, Canada, July 17-22, 2016, Proceedings. Vol. 9734. Springer.

[9] Aki, L. and Jennifer Y. (2016) New professionals: Looking ahead. Public Sector. 39(3), 22.

[10] Shirakata, K., Yonemoto, K., Yamasaki, H., Ura, Y., Minote, H., Shiihara, A., Mugitani, T. (2015) Development of hardware-in-the-loop simulator for experimental Winged Rocket. In Asia-Pacific International Symposium on Aerospace Technology. (APISAT 2015) (p. 114). Engineers Australia.

[11] Aiello, G., Giovino, I., Vallone, M., Catania, P., Argento, A. (2017) A decision support system based on multisensor data fusion for sustainable greenhouse management. Journal of Cleaner Production.

[12] Maneta, M., Kimball, J., He, M., Payton Gardner, W. (2017, April). A satellite-driven, client-server hydro-economic model prototype for agricultural water management. In: EGU General Assembly Conference Abstracts. 19, 10743.

[13] Huang, Zhiquan, Yu Fu, and Fuchu Dai. (2017) Study for Multi-Resources Spatial Data Fusion Methods in Big Data Environment. Intelligent Automation & Soft Computing (2017), 1-6.

[14] Hribljan, J.A., Suarez, E., Bourgeau-Chavez, L., Endres, S., Lilleskov, E.A., Chimbolema, S., ... & Chimner, R.A. (2017). Multi-date, multi-sensor remote sensing reveals high density of carbon-rich mountain peatlands in the páramo of Ecuador.Global Change Biology.

[15] Mangalraj, P., and Anupam Agrawal (2017) Novel approach on fusion of multisensor images based on neutrosophic domain in consideration of regional relevance. Multimedia Tools and Applications (2017), 1-18.
[16] Burgess, A., Roberts, C., Black, K., Mellis, C. (2015) Student ability and learning experience in assessing peers alongside supervisors in the long case. Focus on health professional education: a multi-disciplinary journal. 16(2), 27.
[17] Hammoodi, A.S., Celebi, F. and Yildrim, R. (2017) Wireless Sensor Networks Nodes Distributed in Shapes of Polygons for Promote Distance, Time Delay and Optimization Energy Consumption via Bluetooth. J Comput Eng Inf Technol. 6(3).
[18] Herron, A., Cresswell, R., Barnett, B. (2015) Integrated surface-ground water interaction approaches that can account for water quantity and quality transport[C]//36th Hydrology and Water Resources Symposium: The art and science of water. Engineers Australia. 1325.
[19] Torbick, N., Chowdhury, D., Salas, W. (2017) Monitoring Rice Agriculture across Myanmar Using Time Series Sentinel-1 Assisted by Landsat-8 and PALSAR-2[J]. Remote Sensing. 9(2), 119.
[20] Morris, A. and Campbell, D.E. (2015) The Script Concordance Test for clinical reasoning in paediatric medicine: Medical student performance and expert panel reliability. Focus on Health Professional Education: A Multi-disciplinary Journal. 16(2), 4.
[21] Burns, R.G.H. (2015) Bernard Herrmann's relationship with jazz: The final years of his life and career (1968 to 1975) [C]//Into The Mix People, Places, Processes: Proceedings of the 2014 IASPM-ANZ Conference. International Association for the Study of Popular Music. 11.
[22] Fang, S., Zhu, Y., Xu, L., Zhang, J., Zhou, P., Luo, K., Yang, J. (2017) An integrated system for land resources supervision based on the IoT and cloud computing. Enterprise Information Systems, 11(1), 105-121.
[23] Kinsella, E.A, Bossers, A., Jenkins, K., et al. (2015) Interprofessional preceptor and preceptee educational programing: An interdisciplinary needs assessment. Focus on Health Professional Education: A Multi-disciplinary Journal. 16(2), 70.
[24] Kelly, J., Wiseman, J., Mazzone, S., Miller, D., Newham, J., Ryan, B., Martinez, L. (2015). Managing Two Worlds Together: Stage 3: Improving Aboriginal Patient Journeys-Rural and Remote Sites Case Studies. Managing Two Worlds Together: Stage 3: Improving Aboriginal Patient Journeys-Rural and Remote Sites Case Studies, vi.
[25] Kohl, T., Sapei, E., Rocha, I. M., et al. (2015) Modeling of fast pyrolysis of wood for prediction of bio-oil composition[C]//Asia Pacific Confederation of Chemical Engineering Congress 2015: APCChE 2015, incorporating CHEMECA 2015. Engineers Australia. 2410.
[26] Andiappan, V., Tan, R.R., Aviso, K.B., Ng, D.K. (2015) Systematic approach for the design of trigeneration systems based on reliability aspects. In: Asia Pacific Confederation of Chemical Engineering Congress 2015: APCChE 2015, incorporating CHEMECA. 2015 (p. 147). Engineers Australia
[27] O'Neill, A., Gooding, K., Wright, A., Hoban, A. (2015) Water sensitive urban design on the line. 9th International Water Sensitive Urban Design (WSUD 2015), 383.
[28] Lowe, J.., Nichols, L.A. (2013) Utilisation of a Native American nursing conceptual framework: implications for practice and research. Australian Journal of Advanced Nursing, The 31(2), 13.
[29] Singley, B. (2016) Warrior: A legendary leader's dramatic life and violent death on the colonial frontier Libby Connors 2015 [Book Review]. Australian Aboriginal Studies. 1, 95.
[30] Friess, P. (2013) Internet of things: converging technologies for smart environments and integrated ecosystems. River Publishers.
[31] McDonald, D. (2015) Ecosystem services from soil. 9th International Water Sensitive Urban Design (WSUD 2015). 351.
[32] Black, R. (2015) The social and economic impacts of an ecotourism joint venture on local communities: A Rwandan case study. CAUTHE 2015: Rising Tides and Sea Changes: Adaptation and Innovation in Tourism and Hospitality). 390.
[33] Lausch, A., Erasmi, S., King, D.J., Magdon, P., Heurich, M. (2017) Understanding Forest Health with Remote Sensing-Part II—A Review of Approaches and Data Models. Remote Sensing, 9(2), 129.
[34] Caldicott, R.W. and Harris. A. (2015) Freedom camping: Is it changing the face of caravanning in Australia. CAUTHE 2015: Rising Tides and Sea Changes: Adaptation and Innovation in Tourism and Hospitality. 409.
[35] Hoye, E., and Johnson, P.C. (2016) Capturing the hunter valley feeling in wedding tourism photography. CAUTHE 2016: The Changing Landscape of Tourism and Hospitality: The Impact of Emerging Markets and Emerging Destinations. 810.

[36] Nakagawa, N., Ishitobi, H., Takeuchi, T. (2015) Adsorption and desorption properties of the PtRu nanoparticle catalysts deposited on the different supports. Asia Pacific Confederation of Chemical Engineering Congress 2015: APCChE 2015, incorporating CHEMECA 2015. Engineers Australia.

[37] Aziz, M.A., Imteaz, M., Rasel, H.M., Hasan, M.M. (2015) Perfomance testing of'comb separator'-a novel sewerage overflow screening device. In3rd ASEAN Australian Engineering Congress (AAEC 2015): Australian Engineering Congress on Innovative Technologies for Sustainable Development and Renewable Energy (p. 7). Engineers Australia.

Received: **16.06.2017**
Accepted: **24.09.2017**

CORRESPONDING AUTHOR

Zhen Zhang
College of Economics & Management,
Huazhong Agricultural University,
Wuhan, 430070, HuBei – China

e-mail: zhangzhen_hau@163.com

© by PSP Volume 26 – No. 12A/2017 pages 8041-8046 Fresenius Environmental Bulletin

THE LONG-TERM CHANGES OF MAIN SURFACE-DWELLING ARTHROPOD GROUPS WITH TIME SINCE FIRE IN *PINUS BRUTIA* FORESTS OF SOUTHWESTERN ANATOLIA

Burcin Yenisey Kaynas*

Mehmet Akif Ersoy University, Faculty of Science and Arts, Department of Biology, Burdur, Turkey

ABSTRACT

Fire is one of the most important ecological factors in Mediterranean ecosystems. The effects of fire on animal communities are generally considered in terms of short- and long-term. This paper examined the long-term changes of certain surface-active arthropod groups with successional gradient after fire in *Pinus brutia* Ten. forests of southwestern Anatolia. Five sites burned in different years and a control site unburned for at least 50 years were selected. Sampling for arthropod groups was conducted in four pit-fall traps in four transects in three replication plots at every successional site and in two plots at the control site. Microhabitat variables regarding structures of vegetation and litter layer were recorded and associated with abundances of groups. As a result, it was found that abundances of common arthropod groups, spiders, springtails and cockroaches, displayed significant changes with successional gradient after fire. While abundances of spiders and springtails had non-linear changes with time since fire, cockroaches tended to increase towards the late successional stages. The abundance of spiders was found positively correlated cover of subshrub and leaf and negatively correlated with cover of shrub. Branch cover was the only microhabitat variable that affected communities of springtail. Cockroaches was positively correlated microhabitat attributes increased with successional gradient. These results show that the characteristics of vegetation and litter layer in the successional process had decisive role in the community structure of these groups.

KEYWORDS:
Forest fires, Brutia pine, Mediterranean ecosystems, Araneae, Collembola, Blattodea.

INTRODUCTION

Fire has been one of the most crucial ecological factors for many ecosystem types in the world. Mediterranean ecosystems, including *Pinus brutia* Ten. forests, are recognized as resilient to fire as consequence of the high recovering ability of plant communities after fire. In the process termed the autosuccession, re-establishment of pre-fire species composition occurs very rapid [11, 18]. Recovery of plant communities attracted much attention but relatively few studies have examined post-fire responses of higher order species [19].

The resilience of arthropod communities in relation to fire depends upon many factors such as regularity of disturbance, habitat preferences of arthropod groups [22]. In fire-induced ecosystems, arthropod communities adapted to certain fire regime and developed high resiliency capability to fire [5, 7, 26]. It was revealed that changes in community structure of arthropod groups caused by fire are minimal and short-term [1, 16]. In the absence of fire or under late fire conditions, reductions in abundance of these groups were determined [4]. In Boreal ecosystems, it was revealed that fire-adapted insects are threatened depend upon decreasing fire [32]. Long-term response of arthropods to fire was associated substantially changes on habitat structure [8, 27]. For Mediterranean ecosystems, to draw a general model concerning response to fire at population or community scale is very difficult, but on a regional scale, two resiliency components, elasticity and inertia, along with the mosaic pattern of the fires and the possibilities of local emigration and emigration result in relative stability of the animal communities [28]. At the functional scale, greater stability is achieved by replacement of functionally similar species that dominate under different environmental conditions in the heterogeneous parts of the region [21].

Surface-dwelling arthropods are frequently used to evaluating short- and long-term effects of fire [e.g. 3, 9, 12]. In this study, it was aimed to study changes of certain surface-active arthropod groups with successional gradient after fire in *Pinus brutia* forests and microhabitat variables that affected to these arthropod groups in this process.

MATERIALS AND METHODS

The study was conducted in several *P. brutia* forests located in the Marmaris region (36°50′ N, 28°17′ E) and its surrounding areas, which is situated on the Mediterranean coast of southwestern Turkey.

The successional gradient consisted of five areas burned 3, 6, 9, 16, and 26 years previously and an area unburned for at least 50 years. The samplings were performed at three replication sites for every successional site and at two for the unburned forests.

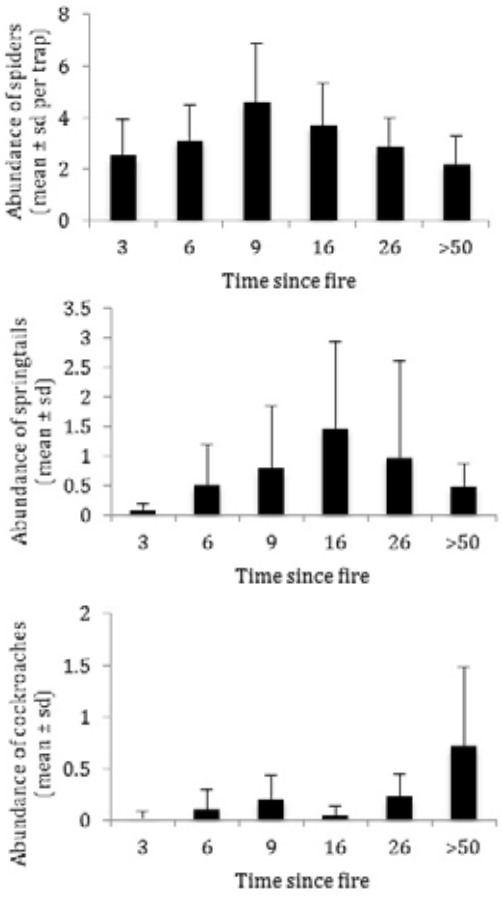


FIGURE 1
Changes in abundances of spiders, springtails and cockroaches with time since fire.

In every successional sites, arthropods were sampled with four pit-fall traps that were placed along a transect at 10-m intervals. Four transects were used at every replication site. Sampling was carried out from March to October of 2006. At the end of each sampling period insects caught in the pit-fall traps were removed and brought to the laboratory for preparation.

Microhabitat structure of the sites was analyzed with the point quadrat technique [31]. Plant species were identified, the height of plant at this point was measured, and the surface characteristics were recorded.

Habitat variables measured for each site were height and total cover of vegetation, plant species richness, cover of plant functional types (tree, shrub and subshrub) and cover of biotic and abiotic surface components (soil, stone, and rock). Features of sampling area and details of sampling procedure were described in [15].

To test the statistical significance of any changes in abundances of arthropod groups among successional sites, analysis of variance (ANOVA) was applied. Total counts during sampling were used. In the ANOVA, abundances were expressed as mean number of individuals per four traps in a transect. Logarithmic transformations were used when the parametric test assumptions were not met in the data. Totally six successional stages were compared using means of abundances from transects at the replication sites. Linear and quadratic regression was used to test change in abundance with successional gradient. Correlation analysis was used to examine interactions between microhabitat variables and arthropod groups.

TABLE 1
The arthropod groups displayed changes depend upon time since fire

	Model	R^2	F	p
Spiders	Quadratic	0.141	5.321	0.007
Cock-roaches	Linear	0.177	14.221	<0.0001
Spring-tails	Quadratic	0.113	4.127	0.021

RESULTS

A total 1145 individuals from 7 surface-dwelling arthropod orders were evaluated in this study. Among these groups, spiders (Araneae) (33.9%) was found very abundant in compare with earwigs (Dermaptera), diplurans (Diplura), woodlices (Isopoda) and scorpions (Scorpionidae) were represented very few individuals in total.

In the study, it was found that evaluated all common surface-dwelling groups, spiders, springtails (Collembola) and cockroaches (Blattodea), displayed significant changes depend on successional gradient. Spiders and springtails were the orders had non-linear changes with time since fire (Figure 1). Both orders were abundant in middle successional stages. Spiders was represented 876 individuals in all sampling site. Its abundance was significantly higher 9 years after fire than earliest and oldest stages ($F= 3.466$; $df= 5$; $p= 0.008$) and had decreasing trend toward early and late successional stages (Table 1). Its abundance positively correlated cover of subshrub and leaf and negatively correlated with cover of shrub (Table 2). Springtails were represented 199 individuals in all sites. Its abundance was the highest 16 years after fire and similar to spiders decreased towards early and late stages. Branch cover was the only microhabitat variable that correlated with the abundance of springtail negatively (Table 2).

In total 55 individuals were caught belong to cockroaches during sampling period. Its abundance displayed raising trend with successional gradient

TABLE 2
Spearman rank correlation coefficients between arthropod groups and microhabitat variables

	Spiders	Cockroaches	Springtails
Vegatation characteristics			
Height		0.452***	
Cover		0.342**	
Stratification		0.389**	
Richness		0.463***	
Plant growth type			
Tree		0.421***	
Shrub	-0.244*	0.248*	
Subshrub	0.251*		
Surface components			
Biotic			
Leaf	0.262*		
Branch			-0.313**
Needle		0.531***	
Abiotic			
Soil		-0.332**	
Stone		-0.291**	
Rock			

* p<0.05, ** p<0.01, ***p< 0.0001

TABLE 3
Abundances of non-target groups in successional stages (mean of replication sites).

	Time since fire					
	3	*6*	9	16	26	>50
Diptera	35	63	44	54	41.7	64.5
Hemiptera	2.7	0.7	1.3	0.7	1.0	7.5
Homoptera	3.3	1.7	1.7	2.7	1.3	1.0
Non-formicine Hymenoptera	25.0	16.7	19.0	9.3	10.3	8.5

(Table 1, Figure 1) and it was caught in remarkable high numbers in unburned site in comparison younger successional sites (p<0.0001). As an expected result the abundance of this group was positively correlated microhabitat attributes increased with successional gradient (Table 2).

Addition the surface-dwelling arthropod taxa, the findings on non-target insect taxa such as Diptera, Hemiptera, Homoptera and non-formicine Hymenoptera were revealed in Table 3.

DISCUSSION

In many ecosystems of the world, invertebrate species have adapted to past disturbance regimes created by fire. Fire has led to strong selective processes not only among plants but also invertebrates [22]. High resilience capability with regards to arthropod communities was reported in many studies carried out in fire-induced ecosystems [1, 4]. A few studies performed in Mediterranean basin to determine direct effects of fire on arthropod communities noted similar results about rapid recovery process [e.g. 16].

In Mediterranean basin, post-fire age of stands is known one of the most important factors that affect the arthropod fauna [15, 30]. The results obtained from this study are in agreement with this statement that surface-active arthropod communities exhibited changes depend upon successional gradient after fire. To increase of number of individuals and species of certain arthropod groups such as wood-borers, species developing under bark of damaged trees, species associated with fungi and certain soil and litter-dwelling groups and predators was reported in many studies [25]. Post-fire habitat conditions and increasing feeding resources were attracted many arthropod groups to burned area.

In contrast increasing trend, most arthropod groups involved in this study such as spiders and springtails, display non-linear changes with successional gradient. Non-linear fire effects in habitat structure significantly affect some insect communities [19]. York stated that abundances of many arthropod groups including spiders, springtails decreased due to frequent fires and this decrease was attributed to a reduction in the amount of litter and associated moisture levels, and a simplification of habitat structure [33].

Spiders has been known resilient to burning and has rapid recovery capability [1, 4, 23, 24]. However, responses of spiders to fire and habitat changes after fire varied with habitat type and disturbance history [e.g. 12, 20]. In a study performed in *P. brutia* forests right after fire, spiders was found one of the few ar-

thropod groups affected negatively by fire [16]. Despite abundances of spiders was lowest in earliest stage of succession and mature forest, site burned 9 years after fire supported more number of individuals. Cover of shrubs and subshrubs significantly affected its abundances. Subshrubs composed of seeder species, *Cistus salviifolius* and *Cistus creticus* which were re-colonized intensely after fire had high cover 3, 6 and 9 years after fire and decreased towards later stages [17]. Jiménez-Valverde and Lobo revealed that the herbaceous and subshrub cover were significant variables for spider communities in Mediterranean ecosystems [14].

Similar to spiders, springtails were found in high numbers in middle stages of the succession. Though known as a fire tolerant group [10, 29], it was represented in low numbers in earlier stages. Their abundances was found negatively correlated woody component of litter layer. Structure and quality of litter significantly affect the communities of microarthropods including springtails [2]. Litter contains different components; e.g. leaves, twigs and other wood which will be inhabited by different species of springtails as an effect of different composition rates [13].

Cockroaches was the only group that displayed increase with successional gradient. Its abundance was found very high in unburned mature pine forests by comparison with other successional stages. These findings in accordance with the study performed by Kaynaş [16] in *P. brutia* forests right after fire. In that study it was stated that cockroaches completely disappeared from the burned sites despite being caught in unburned forests. Thus, it can be stated that it takes a long time for recovery of cockroaches after disappearance due to fire in *P. brutia* forests. Contrary to this, Abbott et al. indicated that changes in community structure of cockroaches caused by fire are minimal and short-term [1]. Arnold et al. similarly stated that distance from burn did not affect the species richness and abundance of cockroaches but both richness and abundance increased with bark and litter cover and decreased at lower temperatures [6]. Dry habitat conditions and lack of litter cover after fire in Mediterranean ecosystems may cause the cockroaches to be unable to re-colonize in post-fire areas.

CONCLUSIONS

In conclusion, long-term changes of arthropod groups in successional gradient substantially depend on habitat characteristics especially structure of vegetation and litter layer and habitat preferences of the taxa. Arthropod groups increase at the stage where their habitat requirements overlap with the habitat structure. Representing of different successional stages in the landscape is very important to diversity of arthropods.

ACKNOWLEDGEMENTS

Many thanks to Çağatay Tavşanoğlu, Anıl Soyumert, Oksal Macar, Filiz Yeni, Yasin İlemin, Okan Ürker, Hüseyin Yılmaz, Sinan Kaynaş and many undergraduate students for their help during the fieldwork, Atilla Küçükala, the Director of Marmaris National Park for his logical support, and Forest Management Directorate of Marmaris, Directorate of Marmaris National Park, and Aksaz Military Marine Base Command for allowing to conduct this study in the areas under their responsibility. The study was financially supported by Hacettepe University Scientific Research Unit (Project no: 02.02.601.004).

REFERENCES

[1] Abbott, I., Burbidge, T., Strehlow, K., Mellican, A. and Wills, A. (2003) Logging and burning impacts on cockroaches, crickets and grasshoppers, and spiders in Jarrah forest, Western Australia. Forest Ecology and Management. 174, 383-399.

[2] Abbott, D.T. and Crossley, D.A. (1982) Woody litter Decomposition following clear-cutting. Ecology. 63, 35–42.

[3] Andersen, A.N. (1991) Responses of ground-foraging ant communities to three experimental fire regimes in a savanna forest of tropical Australia. Biotropica. 23(4b), 575–85.

[4] Andersen, A.N. and Müller, W.J. (2000) Arthropod responses to experimental fire regimes in an Australian tropical savannah: ordinal-level analysis. Austral Ecology. 25, 199-209.

[5] Arnan, X., Rodrigo, A. and Retana, J. (2006) Post-fire recovery of Mediterranean ground ant communities follows vegetation and dryness gradients. Journal of Biogeography. 33(7), 1246–58.

[6] Arnold, K.T., Murphy, N.P. and Heloise, G. (2017) Post-fire recovery of litter detritivores is limited by distance from burn edge. Austral Ecology. 42, 94–102.

[7] Fernández Fernández, M.M. and Salgado Costas, J.M. (2004) Recolonization of a burnt pine forest (*Pinus Pinaster*) by Carabidae (Coleoptera). European Journal of Soil Biology. 40(1), 47–53.

[8] Gardner, S.M, Cabido, M.R., Valladares, G.R. and Díaz, S. (1995) The influence of habitat structure on arthropod diversity in Argentine semi-arid Chaco forest. Journal of Vegetation Science. 6, 349–56.

[9] Gongalsky, K.B. and Persson, T. (2013) Recovery of soil macrofauna after wildfires in Boreal forests. Soil Biology and Biochemistry. 57, 182–91.

[10] Gongalsky, K.B., Malmström, A., Zaitsev, A.S., Shakhab, S.V., Bengtsson, J. and Persson, T. (2012) Do burned areas recover from inside? An experiment with soil fauna in a heterogeneous landscape. Applied Soil Ecology. 59, 73–86.

[11] Hanes, T.L. (1971) Succession after fire in the chaparral of southern California. Ecological Monographs. 41, 27–52.

[12] Hanula, J.L. and Wade, D.D. (2003) Influence of long-term dormant-season burning and fire exclusion on ground-dwelling arthropod populations in longleaf pine flatwoods ecosystems. Forest Ecology and Management 175(1–3), 163–84.

[13] Irmler, U. (2006) Climatic and litter fall effects on Collembolan and Oribatid mite species and communities in a beech wood based on a 7 years investigation. European Journal of Soil Biology. 42(1), 51–62.

[14] Jiménez-Valverde, A. and Lobo, J.M. (2007) Determinants of local spider (*Araneidae* and *Thomisidae*) species richness on a regional scale: climate and altitude vs. habitat structure. Ecological Entomology. 32, 113–122.

[15] Kaynaş, B.Y. (2017) Long-term changes in surface-active beetle communities in a post-fire successional gradient in *Pinus brutia* forests. iForest. 10, 376-382.

[16] Kaynaş, B.Y. (2016) The effects of fire on surface-dwelling arthropod communities in *Pinus brutia* forests of southwestern Anatolia. Iğdır University Journal of the Institute of Science and Technology. 6(2), 33-39.

[17] Kaynaş, B.Y. (2008) Studies on long-term effects of fire on small mammal community and changes of community structure after fire in *Pinus brutia* forest ecosystems, PhD Thesis, Hacettepe University, Institute of Natural Sciences, Ankara, Turkey (in Turkish with English abstract).

[18] Keeley, J.E. (1986) Resilience of Mediterranean shrub communities to fire. In: Dell, B., Hopkins, A.J.M., Lamont, B.B. (Eds.) Resilience in Mediterranean Type Ecosystems. Tasks for vegetation science, vol. 16, Springer, Dordrecht.

[19] Kim, T.N. and Holt, R.D. (2012) The direct and indirect effects of fire on the assembly of insect herbivore communities: examples from the Florida scrub habitat. Oecologia. 168, 997-1012.

[20] Koponen, S. (2005) Early succession of a boreal spider community after forest fire. Journal of Arachnology. 33(2), 230-235.

[21] Moretti, M., de Bello, F., Roberts, S.P.M. and Potts, S.G. (2009) Taxonomical vs. functional responses of bee communities to fire in two contrasting climatic regions. Journal of Animal Ecology. 78, 98-108.

[22] Moretti, M., Duelli, P. and Obrist, M.K. (2006) Biodiversity and resilience of arthropod communities after fire disturbance in temperate forests. Oecologia. 149(2), 312–27.

[23] Moretti, M., Obrist, M.K., and Duelli, P. (2004) Arthropod biodiversity after forest fires: winners and losers in the winter fire regime of the southern Alps. Ecography 27(2), 173–86.

[24] Moretti, M., Conedera, M., Duelli, P., and Edwards, P. (2002) The effects of wildfire on ground-active spiders in deciduous forests on the Swiss southern slope of the Alps. Journal of Applied Ecology. 39(2), 321-336.

[25] Muona, J., and Rutanen, I. (1994) The short-term impact of fire on beetle fauna in boreal coniferous forest. Annales Zooligici Fennici. 31, 109-121.

[26] Orgeas, J. and Andersen, A.N. (2001) Fire and biodiversity: responses of grass-layer beetles to experimental fire regimes in an Australian tropical savanna. Journal of Applied Ecology. 38(1), 49-62.

[27] Parr, C.L., Robertson, H.G., Biggs, H.C. and Chown, S.L. (2004) Response of African savanna ants to long-term fire regimes. Journal of Applied Ecology. 41, 630-642.

[28] Prodon, R., Fons, R., Athias-Binche, F. (1987) The impact of fire on animal communities in Mediterranean area. In: Trabaud, L. (ed) The Role of Fire in Ecological Systems, SPA Academic Publishing, The Hague. 121-157.

[29] Puga, J.R.L., Abrantes, N.J.C., de Oliveira, M.J.S., Vieira, D.C.S., Faria, S.R., Gonçalves, F., and Keizer, J.J. (2017) Long-term impacts of post-fire mulching on ground-dwelling arthropod communities in a eucalypt plantation. Land Degradation and Development. 28(3), 1156-1162.

[30] Radea, C. and Arianoutsou, M. (2000) Cellulose decomposition rates and soil arthropod community in a *Pinus halepensis* Mill. forest of Greece after wildfire. European Journal of Soil Biology. 36, 57-64.

[31] Sutherland, W.J. (2006) Ecological Census Techniques, a handbook, 2nd edition. Cambridge University Press, UK, pp. 446.

[32] Wikars, L-O. (1992) Skogsbränder och insekter. Entomologisk Tidskrift. 113(4), 1-11.

[33] York, A., (1999) Long-term effects of frequent low-intensity burning on the abundance of litter-dwelling invertebrates in coastal blackbutt forests of southeastern Australia. Journal of Insect Conversation. 3, 191-199.

Received: **17.06.2017**
Accepted: **15.10.2017**

CORRESPONDING AUTHOR

Burcin Yenisey-Kaynas
Mehmet Akif Ersoy University,
Faculty of Science and Arts,
Department of Biology,
İstiklal Campus, Burdur – Turkey

e-mail: bykaynas@mehmetakif.edu.tr

© by PSP Volume 26 – No. 12A/2017 pages 8047-8061 Fresenius Environmental Bulletin

ASSESSMENT OF HEAVY METAL CONTAMINATION AND ACCUMULATION PATTERNS IN THE COASTAL AND DEEP SEDIMENTS OF LAKE SALDA, TURKEY

Huseyin Caldirak[1], Bedri Kurtulus[1], Mustafa Can Canoglu[2,*], Evren Tunca[3]

[1]Mugla Sitki Koçman University, Faculty of Engineering, Geological Engineering Department, 48000, Mentese, Mugla, Turkey
[2]Sinop University, Faculty of Engineering and Architecture, Environmental Engineering Department, 57000, Sinop, Turkey
[3]Ordu University, Fatsa Marine Science Faculty, Marine Science and Technology Engineering Department, 52400, Ordu, Turkey

ABSTRACT

In this study, contamination levels were found for 8 different metals (Cu, Pb, Zn, Ni, Mn, Fe, Cd, Cr) and metalloids (As) in sediment samples, coming from 9 different stations, through statistical analysis and sediment assessment at Lake Salda (Turkey). The correlation, cluster, factor and Mann Whitney-U analysis were used for evaluation of the results, and the values of all metals were compared with the limit values of PEL (probable effect level), ERM (effect range median), TEL (threshold effect level), and ERL (effect range low). According to the correlation, PCA and cluster analysis, highest correlation was determined as being between Cu-Mn, Cu-Zn, Fe-Ni, Cr-Ni and Fe-Cr. The weakest relationships with other metals were identified as Pb and As. Additionally, deep and shallow stations were compared and station-based anthropogenic effects were demonstrated. The status of the sediments was considered separately for the studied elements. According to the results, contamination factor, enrichment factor, geoaccumulation index, potential ecological risk factor and quotient toxic unit showed up the highest values for Ni. However, Pb results seemed quite serious at several stations according to the results of the research. The pollution load index was used to find out the baseline and ideal levels throughout the lake.

KEYWORDS:
Heavy metals, metalloid, pollution, sediment assessment methods, Lake Salda

INTRODUCTION

Several of the metals (like Cu, Fe, and Zn) are needed for the continuation of life, although a number of the metals (such as Pb, Cd and Hb) exhibit toxic effects, even in low concentrations. Whether they are essential or nonessential, all metals have a toxic effect on every living thing over a certain threshold. Accumulation of heavy metals in aquatic environments has constituted one of the most serious environmental problems for a long period of time due to intensive industrialization. Large quantities of toxic heavy metals like Cd, Pb, Cr, and Hg are released into ecosystems as contaminants after anthropogenic activities [1]. Whether the source is lithogenic or anthropogenic metals are persistent environmental contaminants [2]. The accumulation of metals has become a serious cause for concern which needs urgent consideration [3]. Heavy metal contamination has been studied by numerous researchers [4-11].

Determination of the metal content in sediment is important for aquatic ecosystems, because sediment can provide extremely important information about the environmental and geochemical pollution status [12, 13]. The data obtained from the sediment quantiles provided strong evidence of the spatio-temporal anthropogenic effect [14]. As a result, research of heavy metal accumulation in sediment has been studied at both sea and fresh water sites [15, 16]. In addition, the sediment should be thought of not only as an environment where the accumulation of metals by deposition, but also a secondary pollutant source from where the metals enter the water or food chain again. This leads changes in environmental conditions [17, 18]. This situation is a key factor in the increased impact of heavy metal accumulation in the sediment. Besides, the existence of very different creatures living in the sediment at the bottom of the food chain, must not be forgotten. A large number of these living beings store intense heavy metal in their bodies once exposed to them. Consumption of these living beings, by creatures higher up the food chain, enables these intense metals to be easily passed up the food chain until they are eventually consumed by humans.

Lake Salda is known to be one of the deepest lakes in Turkey, with a maximum depth of 184 m. Due to its location, it was determined as an area for natural protection in 1989, and a tourism centre in 2004 by the Culture and Tourism Ministries of Turkey. The lake water is rich in magnesium and is one of two important high alkaline lakes, along with Lake Van, also in Turkey. The magnesite deposits located on the west side of the lake, were related to

"White Rock" which has been discovered on Mars [19].

The aim of this study is to determine the current metal situation, anthropogenic sourced metal amount, toxic effect, and rate of potential risk posed to the ecosystem of the current location. This will be done using different statistical and sediment research methods in Lake Salda, which an extremely important lake, not just in Turkey, but in the world. This study will hopefully be the starting point for continued research in the field.

MATERIALS AND METHODS

Study Area. Lake Salda is located in the Burdur sub-basin, in Yesilova district (Figure 1). It is known to be one of the deepest lakes in Turkey, with a maximum depth of 184 m. The lake water is highly alkaline with pH values ranging between 8.90 to 9.05. The lake water is also rich in magnesium, and is one of two important high alkaline lakes, as mentioned, along with Lake Van. The lake is 1139 meters above sea level and covers an area of almost 45 km^2. The surrounding mountains, bedded ultramafic and carbonate rocks, of Lake Salda, form a drainage basin approximately 148 km^2. The lake is fed by four main streams, Zehra from the north, Karakova from the west, Köpek from the south-west, and Kuruçay stream from the southern side of the lake. Also, there are many agricultural activities on the northeast of the catchment area.

The geology of the area is mostly dominated by ultramafic rocks and alluvial deposits. Quaternary Alluvial Unit and Cretaceous Marmaris Peridotite are dominant around the area of the lake. (Figure 2). Marmaris Peridotite occurs as serpentinised ultramafic rocks in some parts but, harzburgite sections are more widespread than any other rock type [20]. Besides, Late Triassic/Lias aged Dutdere Limestone has appeared due to tectonic impact, this is another important lithological unit of the study area. It is located in the south-eastern part of the lake. Dutdere Limestone occurred as medium-thick bedded, locally massif, consisting of recrystallized limestone algae in several areas, and was deposited in a shallow carbonate shelf environment [21].

Sediment assessment methods. Background content, or pre-industrial reference values, which are necessary for most of the sediment assessment methods, have been obtained from the literature. The data chosen for this study was by Turekian and Wedepol [22]. These are some of the most preferred for pre-industrial reference values [17, 23, 24].

Contamination factor (C_f^i) is one of the most important sediment assessment methods. It is extremely simple and effective. It is also the starting point for many further evaluations including the contamination for every metal to be done separately. It was first used by [25]. The formula is as follows.

$$C_f^i = C^i / C_n^i \quad (1)$$

C^i = Metal concentration in the sample

C_n^i = Pre-civilization reference value

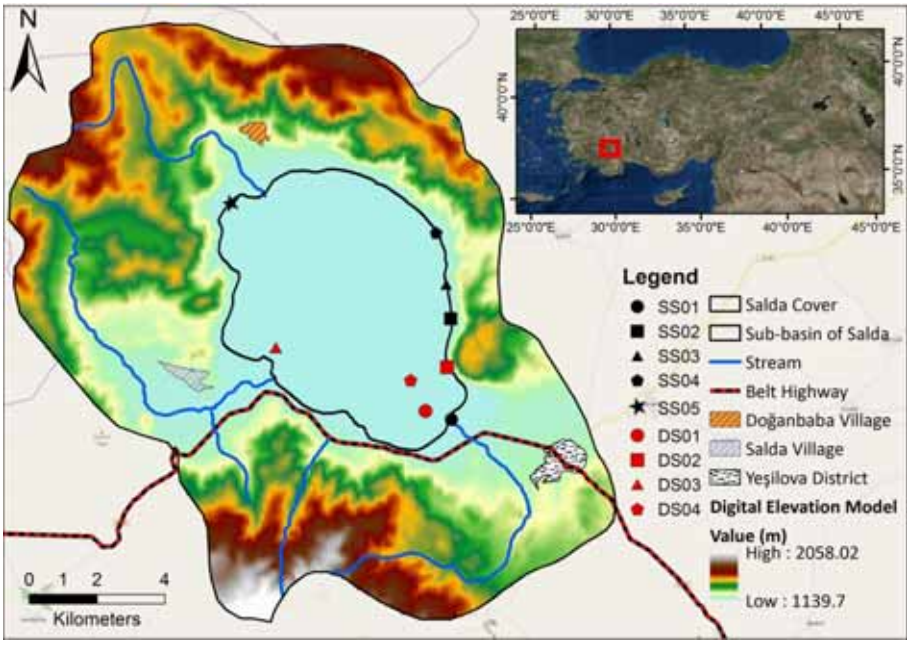


FIGURE 1
Location Map with Sample Locations

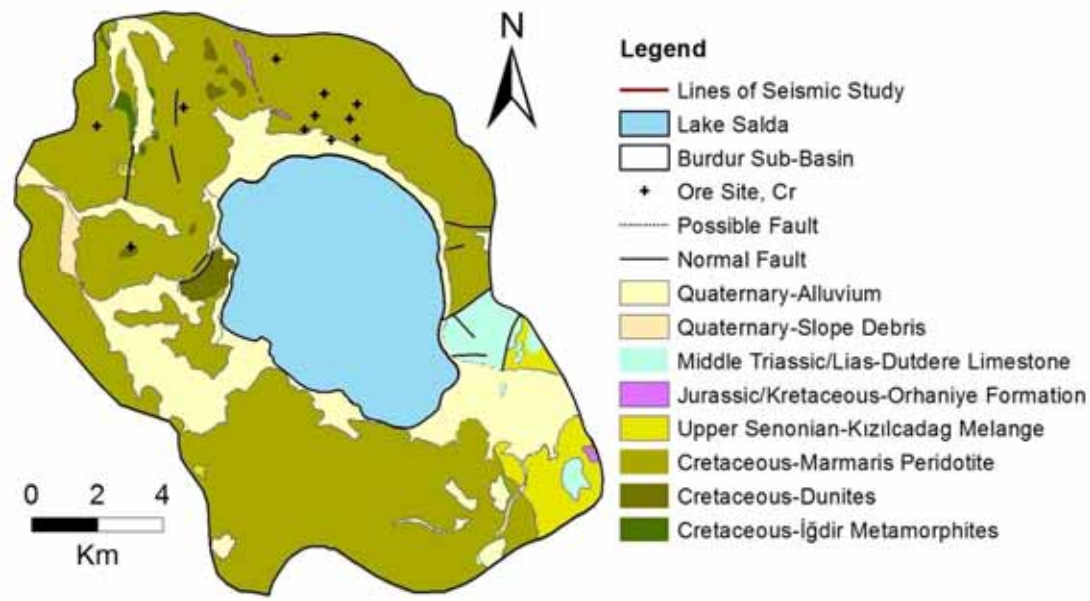


FIGURE 2
Geology Map of the Study Area

Degree of contamination (C_d) method determines the total of the contamination factors for metals [25]. The formula is as follows.

$$C_d = \sum_{i=1}^{n} C_f^i \quad (2)$$

C_f^i= Contamination factor

However, the degree of contamination is a difficult method to study, because it is not possible for all metals to be studied in every situation. This issue has been eliminated with the development of a formula by Abrahim and Parker [26]. The difference between mCd from Cd is mCd, used to give an average value. The formula of modified degree of contamination (mC_d) is as follows;

$$mC_d = \frac{\sum_{i=1}^{n} C_f^i}{n} \quad (3)$$

C_f^i= Contamination factor

n= Total number of metals

The Pollution load index (PLI) method provides easy comparison of different locations in the same or different studies, and was developed by Tomlinson et al. [27]. The formula is as follows.

$$PLI = (C_{f1} \times C_{f2} \times C_{f3} \ldots \times C_{fn})^{1/n} \quad (4)$$

C_{f1}= Contamination Factor

n= Total number of metals

Enrichment factor (EF) is another extremely important method which helps in determining the anthropogenic sourced metal pollution [28]. The formula is as follow;

$$EF = \frac{C_n / C_{ref}}{B_n / B_{ref}} \quad (5)$$

C_n= Metal concentration in sample

C_{ref}= Metal concentration in reference environment (Earth's crust)

B_n= Reference element (Fe) concentration in sample

B_{ref}= Reference element concentration in reference environment

One element of high concentration on earth's crust is used as a reference element. The high concentrated elements are effected less from anthropogenic additive relatively for this reason, Fe was chosen as the reference element in this study. There are many studies in which Fe has been used as the reference element [29, 30].

One of the methods that is used for determining levels of anthropogenic contamination, is the Geoaccumulation index (I_{geo}). The calculation is done as follows [31].

$$I_{geo} = log_2 \frac{C_n}{1.5 \times B_n} \quad (6)$$

C_n= Metal concentration in the sediment

B_n= Background content of the metal

1.5= Constant for natural fluctuation

Potential Ecological Risk Factor ($\boldsymbol{E_r^i}$) is another method used to look at levels of contamination caused by metals and the risk for the aquatic environment. It was first introduced by Hakanson [25]. The formula is as follow;

$$E_r^i = T_r^i X \frac{Ci}{Co} \quad (7)$$

T_r^i= Toxic response factor

C_i= Metal concentration in sample

C_o= Pre-civilization reference value

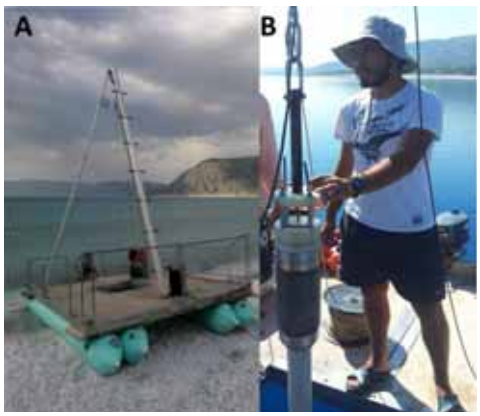


FIGURE 3
Floating Platform (A) and Core Sampler on Field (B)

The sum of the toxic units (Σ TU s) is the sum of the values obtained by proportioning metal amounts determined using samples, and the PEL (Probable Effect Level) value belongs to those metals [32, 33]. Quotient toxic unit is the percentage type of the ratio the toxic unit value of every metal to Σ TU value. They are frequently used [34, 35].

Statistical methods. The Mann Whitney-U test has been used in order to keep sample numbers to the number to a minimum, regardless of normality of distribution. The test has a 95% level of significance. For the same reason, the Spearman Correlation Analysis was preferred in correlation analysis. The correlation tests have a 95% and 99% level of significance respectively. The extraction method for Principle Component Analysis was carried out according to the Varimax, with Kaiser Normalization. Cluster analysis was done using the Ward's method, on Euclidean distance intervals and the Z-score correction [36]. All statistics were collated using SPSS v21.

Sampling and Element Analysis. Using a floating platform (Figure 3a), sediment samples were collected at shallow and deep points of the lake. This was done using the gravity method (Figure 3b), which is used for core logging on lakes. Samples were taken at the deepest points. The deepest measurement was DS02 with a depth of 96 meters, and was chosen for the possible extension of the main fault that was located on the south-western side of the lake.

The gravity corer is a general-purpose tool that relies on its weight for penetration into the seabed. In this study, a 20 kg weight was used for the core sampler. The sediment that was in the first cm of the core, was used for analysis. Surface sampling was also done on the coastal sides of the lake, which was almost 50 cm in depth, by hand from the aquatic environment (Table 1).

TABLE 1
Basic Information for Sample Locations

Locations	X	Y	Depth (m)
SS01	740164	4155772	<0.5
SS02	740144	4158764	<0.5
SS03	740009	4159788	<0.5
SS04	739714	4161318	<0.5
SS05	733647	4162215	<0.5
DS01	739392	4156021	36
DS02	740038	4157335	96
DS03	734975	4157915	22
DS04	738961	4156947	48

TABLE 2
Reference Material for Sediment Samples

Name	mg/kg	Calculate ppb	Measure ppb	mg/kg	Recovery
Cu	30	240	214.63	26.8	89.4
Pb	37.7	301.6	300.8	37.6	99.7
As	27.6	220.8	300.2	37.5	136.0
Ni	44.9	359.2	400.8	50.1	111.6
Cr	104	832	772.2	96.5	92.8
Cd	0.26	2.08	2.668	0.3	128.3
Mn	34600	276800	177100	22137.5	64.0
Fe	67400	539200	512400	64050.0	95.0
V	170	1360	1037	129.6	76.3
Co	19.8	158.4	201.4	25.2	127.1
Zn	223	1784	2800	350.0	157.0

TABLE 3
Heavy Metal Concentrations of Sediment Samples and Limit Values

Locations	Cu (ppm)	Pb (ppm)	Zn (ppm)	Ni (ppm)	Mn (ppm)	Fe (ppm)	As (ppm)	Cd (ppm)	Cr (ppm)
SS01	**8.73**	6.57	19.78	**1691.54**	**550.25**	**44682.84**	1.02	0.09	**160.07**
SS02	1.42	6.07	3.12	221.32	73.32	5692.02	1.48	0.05	36.16
SS03	1.64	2.17	5.72	454.22	173.58	12690.75	0.70	0.05	77.72
SS04	***0.88***	***1.72***	***2.37***	***47.00***	***9.00***	***2579.96***	1.24	***0.03***	***10.48***
SS05	3.21	5.36	18.11	548.33	304.70	19761.49	***0.65***	0.05	107.02
DS01	3.95	13.14	20.50	477.25	321.50	17568.75	1.61	0.10	84.53
DS02	2.81	**383.11**	11.48	234.91	202.59	11445.86	0.87	0.07	55.76
DS03	3.03	19.29	16.06	361.68	205.18	12618.28	**2.30**	0.12	58.95
DS04	5.81	196.92	**31.06**	442.61	413.67	19167.91	1.38	**0.18**	85.18
Max.	8.73	383.11	31.06	1691.54	550.25	44682.84	2.30	0.18	160.07
Min.	0.88	1.72	2.37	47.00	9.00	2579.96	0.65	0.03	10.48
Median	3.03	6.57	16.06	442.61	205.18	12690.75	1.24	0.07	77.72
PEL	197	91.3	315	36			17	3.53	90
ERM	390	110	270	50			85	9	145
TEL	35.7	35	123	18			5.90	0.6	37.3
ERL	70	35	120	30			33	5	80
Reference	45	20	95	68	850	47200	13	0.3	90
Tox.	5	5	1	5	1		10	30	2

SS: Shallow Sediment DS: Deep Sediment
Bolt Character: Refers Maximum Value Italic Character: Refer Minimum Value
PEL: Probable effect level [37]
ERM: Effect range median [38]
TEL: Threshold effect level [37]
ERL: Effect range low [38]
Reference: Distribution of the elements in the earth's crust (shales) [22]
Tox: Toxic response factor [25, 39].

The samples were analysed at the Research and Application Centre for Environmental and Earth Sciences, Istanbul University. The 3051a microwave extraction method (microwave assisted acid digestion of sediments, sludge, soils, and oils) was used for microwave heating. Porcelain crucibles were weighed, both empty and with sediment samples, on precision scales with a sensitivity of 4 digits. Then, the sediments in the porcelain crucibles were heated with digit heat model drying and a sterilization oven for 1.5 hours. After heating, they were weighed again, and the dry unit weight was calculated. Dry sediments were grinded using an agate mortar, 0.2 g was weighed for each sample. The samples were put into microwave tubes and mixed with 1.5 ml (1 unit) nitric acid (HNO3) and 4.5 ml (3 unit) hydrochloric acid (HCl). They were put into the Marsxpress model microwave. The samples were dissolved with acid in 3 different sets in the microwave system. The sets were 300, 600, and 1200 watts, and 120, 150, and 180 C with 100% performance and 15 minutes for each, respectively. After 45 minutes, the samples were taken out and put into the refrigerator to reduce temperature. The tubes were opened carefully in the fume cupboard in order to let the gas resulting from the reaction out. Lastly, the samples were integrated with water, up to 25 ml in sterilized tubes, to prepare for samples analysis. Two devices were chosen to complete analysis based on the reference material (Table 2). The Perkin Elmer Atomic Absorption Spectroscopy (Perkin Elmer F-AAS 400) was used for the level 1ppm (mg/l) and the elements Iron (Fe), Manganese (Mn) and Zink (Zn). The Perkin Elmer Graphite Atomic Absorption Spectroscopy (Perkin Elmer GF-AAS 600) was used for the level 1ppb (µg/l) and the elements Copper (Cu), Lead (Pb), Nickel (Ni), Cadmium (Cd), Chromium (Cr), Arsenic (As) and Vanadium (V). Repeatability standard deviation value has been presented below as 5%. The decomposition process of sediments has been done using the same procedure, as standard sediment. Background corrections, which were sourced by decomposition acid, have also been done.

RESULTS AND DISCUSSIONS

Amounts for each element. All the results obtained for the studied elements have been given in Table 3 as totals for Lake Salda. Table 3 also provides various limit values for the studied metal and metalloid. Although Pb and Cr values have high concentrations at some stations, Ni amounts have been

determined as over the limit values for all of the stations. Ni is the most common element, while evaluating the elements according to the limit values, Fe is the most common and Cd is the least common element by amount. The other elements are under the limit values except Pb, Cr and Ni.

PEL: "Represents the concentration above which adverse effects are expected to occur frequently", TEL: "Represents the concentration below which adverse effects are expected to occur only rarely" [37], ERM: "Represents the chemical concentration above which adverse effects would frequently occur", ERL: "Represents the chemical concentration below where adverse effects would be rarely observed" [38] are meaningful for the limit values [40]. When Cr value was analysed on the basis of station, the highest value was observed in SS01 station. 160.07 mg/kg value is above all limit values for this station (Table 3). However, the lowest amount determined for Cr, which is 36.16 mg / kg (SS02), remained below all of the values in Table 3.

The highest values of Pb were observed in DS02 and DS04 stations which are located in the inner part of the lake. Also, the amount of Pb found in the other interior stations of the lake, was more than in the shore sections. Mann Whitney-U analysis also supports this data, in which a comparison was made between inner and coastal areas. According to the results, the Pb amount in the inner part of the lake is more than in the coastal part ($p<0.05$). So, this supports the hypothesis about Pb entering the lake via anthropogenic sources and also being deposited into the lake. The other result that supports this case is Cluster Analysis. According to the distance matrix of the analysis (Proximity Matrix), Pb is the farthest element in all studied elements, which also means having a lesser relationship with the other elements (Table 4). This situation can be clearly seen in the analysis of the dendrogram (Figure 4). It can also be seen in the Principle Component Analysis (Figure 5). Pb can be observed as the farthest element from the others, together with the Component and Rotated Component Matrix results (Table 5). Including correlation analysis results Pb (Table 6), Cd can be seen as the most related element to Pb for all analysis. Also, as is related with Pb in factor analysis results, the amount of As is far below the limit. However, Pb-Cd relation is also an important result. Because, like Pb, Cd is also one of the elements accumulated as a result of anthropogenic activities, Cd amount is more in the inner parts, like Pb, than the coastal parts of the lake ($p<0.05$). In addition to these results, there was not observed to be any element which has a significant difference between inner parts and coastal parts of the lake among the studied elements, except for Cd and Pb ($p>0.05$).

Nickel forms several minerals and is strongly enriched in ultramafic and mafic lithologies. Cr is also enriched in ultramafic rocks up to as much as 1000–3000 mg/kg, along with elements such as Ni. A large proportion of the Ni in stream sediment is held in detrital silicate and oxide minerals that are resistant to weathering. The range of Ni values in soil vary from 0.2 to 450 mg/kg according to rock type [41]. On the other hand, anthropogenic sources of nickel could come from fertilisers, steel works, metal plating and coinage, fuel combustion and detergents [42]. In the presence of some organic complexing agents, Ni is capable of forming neutral or negatively charged complexes, making the metal highly mobile in relation to other trace elements. Consequently, Ni concentrations may be high in stream water contaminated by sewage and leachate from waste tips [43].

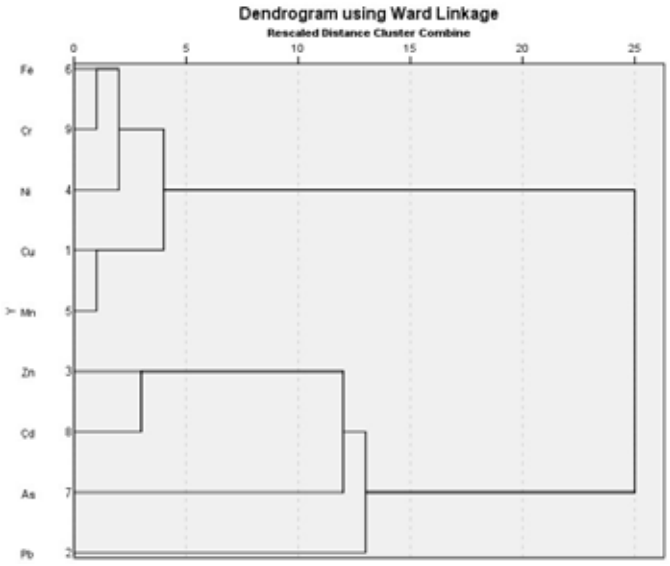


FIGURE 4
Dendrogram of Cluster Analysis

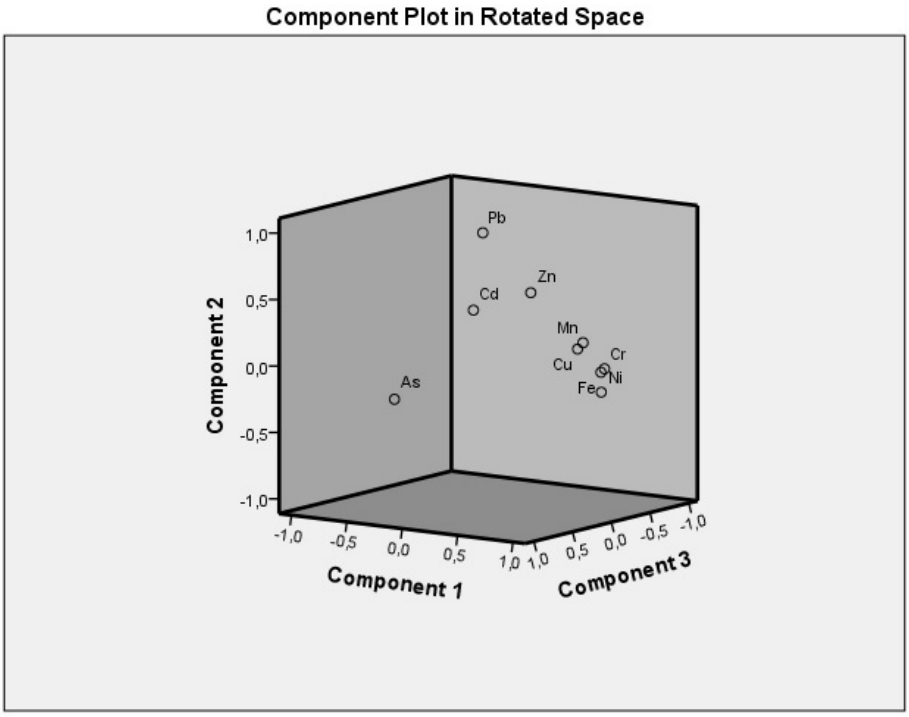


FIGURE 5
Component Plot of Factor Analysis

TABLE 4
Cluster Analysis

	Cu	Pb	Zn	Ni	Mn	Fe	As	Cd	Cr
Cu	.000	4.178	2.119	1.503	1.064	1.139	4.365	2.675	1.580
Pb	4.178	.000	3.877	4.804	4.207	4.580	4.728	3.620	4.590
Zn	2.119	3.877	.000	3.227	1.603	2.599	4.011	1.652	2.498
Ni	1.503	4.804	3.227	.000	1.844	.853	4.755	3.785	1.293
Mn	1.064	4.207	1.603	1.844	.000	1.111	4.562	2.644	1.126
Fe	1.139	4.580	2.599	.853	1.111	.000	4.761	3.421	.848
As	4.365	4.728	4.011	4.755	4.562	4.761	.000	3.142	4.910
Cd	2.675	3.620	1.652	3.785	2.644	3.421	3.142	.000	3.436
Cr	1.580	4.590	2.498	1.293	1.126	.848	4.910	3.436	.000

TABLE 5
Component and Rotated Component Matrix Results

	Component (Component Matrix[a])			Component (Rotated Component Matrix[b])		
	1	2	3	1	2	3
Cu	.976			.939	.202	.190
Pb		.544	-.766	-.135	.923	-.121
Zn	.724	.475	-.201	.585	.604	.288
Ni	.891	-.378	.130	.959	-.161	
Mn	.985			.947	.242	.130
Fe	.961	-.244		.992		
As	-.124	.598	.752	-.195	-.184	.932
Cd	.556	.786	.150	.380	.517	.734
Cr	.937	-.284		.973		-.109

a: 3 components extracted.
b: Rotation converged in 5 iterations.

TABLE 6
Correlation Analysis

	Cu	Pb	Zn	Ni	Mn	Fe	As	Cd	Cr
Cu	1.000								
Pb	.606*	1.000							
Zn	.970**	.655*	1.000						
Ni	.834**	.255	.764**	1.000					
Mn	.989**	.600	.945**	.827**	1.000				
Fe	.897**	.355	.827**	.936**	.927**	1.000			
As	.178	.336	.245	-.173	.118	-.145	1.000		
Cd	.811**	.855**	.851**	.469	.782**	.552	.533	1.000	
Cr	.916**	.364	.864**	.945**	.909**	.945**	-.109	.593	1.000

*. Correlation is significant at the 0.05 level (2-tailed).
**. Correlation is significant at the 0.01 level (2-tailed).

Relationships between the elements. Cu and Mn elements show the highest correlation (Cu-Mn: r=0.989) on the correlation analysis and component matrix (Tables 5 and 6). There are other studies where strong correlations between these elements have been noted, but there are situations where the correlation cannot be observed due to changes tin location [44]. The correlation between Cu and Zn follows this correlation (Cu-Zn: r=0.970). The same case is also valid for the correlation between Cu and Zn. While strong correlations are apparent between these two elements [45], there are some cases where the correlation couldn't be observed [28]. Both Cu and Zn can correlate with all studied elements, except As. These elements also have the strongest correlations, Mn with other elements, according to the strongest relationship distance matrix. The elements having the closest distances are Fe-Ni (0.853 euclidean distance) and Fe-Cr (0.848 euclidean distance) (Table 4, Figures 4 and 5) and also, they have parallel results on the cluster analysis. The Elements As and Pb have the weakest relationships with other elements for two analysis. As did not correlate with any element in the correlation analysis. There is not another element which correlated with any other element except As. Pb has its strongest correlation with Cd which is not essential for maintaining life (Pb-Cd: r=0.855). The other elements correlated with Pb are Zn and Cu. However, the correlation between these two elements is relatively weak (Pb-Zn: r=0.655, Pb-Cu: r= 0.606). Fe-Ni and Fe-Cr relationships are extremely strong as shown by the cluster analysis (Fe-Ni: r=0.936, Fe-Cr: r=0.945). There are some cases where such correlations have been observed, or different impacts on sediment from these elements [46, 47, 48].

Evaluation of the sediment. On the basis of the sediment assessment methods, the central point is to determine the amount of metal as injected to the porous medium by anthropogenic effects. This basis can be by comparing the metal amount of the existing sediment with the average of the pre-industrial era, or earth's crust that belong to that era. In the next step, the risk posed by ecologic and toxic effects are tried to be determined by the elements injected to the porous medium artificially. Many ways are used in the evaluation of sediment. Some methods reveal the current status for each element, and some are aimed at understanding the total effect of all studied elements.

Contamination Factor (C_f^i), Degree of contamination (C_d) and Modified degree of contamination (mC_d) and Pollution Load Index (PLI). Both C_f^i, and C_d, as well as mC_d are frequently used methods used for showing the status of existing ecosystems [13, 28, 49]. These methods, which are simple and very effective, can provide us with detailed information about the status of available sediment.

C_f^i values are, in general, under 1 for the study carried out (Table 7). This result means relatively low contamination, according to the 4-way scale created by Hakanson [28]. However, especially Ni, reveals the profile as being highly contaminated for many sites, unlike the general situation. The lowest C_f^i value was obtained for Ni, at station SS04. Ni is on the lowest level of the scale at this station. Pb has reached the highest level on the scale, as Ni, at the DS02 and DS04 stations. This is not a risky case, except for these 2 stations. Cr shows moderate contamination according to the scale at stations SS01 and SS06. Other stations are clean in terms of Cr.

C_d is actually the total of C_f^i values of all the studied elements. This doesn't reveal the current situation one by one, unlike the contamination factor. Instead, it reveals the total current status of all the elements for only one value. The values obtained by Hakanson are evaluated on the 4-way scale [28]. Accordingly, if Lake Salda is evaluated on the basis of station, the highest values are obtained for SS01 and DS02. Considerable contamination was recorded at these stations, which is the third step of the 4-way scale. SS04 is the station where the lowest Cd value has been recorded and low contamination found, measuring only at the bottom step of the scale (Table 8).

TABLE 7
Contamination Factors of the Sediment Samples

	Contamination Factor								
	Cu	**Pb**	**Zn**	**Ni**	**Mn**	**Fe**	**As**	**Cd**	**Cr**
SS01	0.19	0.33	0.21	24.88	0.65	0.95	0.08	0.30	1.78
SS02	0.03	0.30	0.03	3.25	0.09	0.12	0.11	0.16	0.40
SS03	0.04	0.11	0.06	6.68	0.20	0.27	0.05	0.17	0.86
SS04	0.02	0.09	0.02	0.69	0.01	0.05	0.10	0.09	0.12
SS05	0.07	0.27	0.19	8.06	0.36	0.42	0.05	0.16	1.19
DS01	0.09	0.66	0.22	7.02	0.38	0.37	0.12	0.34	0.94
DS02	0.06	19.16	0.12	3.45	0.24	0.24	0.07	0.24	0.62
DS03	0.07	0.96	0.17	5.32	0.24	0.27	0.18	0.41	0.66
DS04	0.13	9.85	0.33	6.51	0.49	0.41	0.11	0.61	0.95
C_f^i<1		1≤C_f^i<3			3≤C_f^i>6		C_f^i≥6		
respectively to low		moderate			considerable		very high		

TABLE 8
Sediment Methods, Reveal the Current Status through Total Metal Amount

SS01	**SS02**	**SS03**	**SS04**	**SS05**	**DS01**	**DS02**	**DS03**	**DS04**
Degree of contamination (C_d)								
23.36	4.5	8.44	1.19	10.77	10.13	24.2	8.27	19.37
C_d≤8		8≤C_d≤16		16≤C_d≤32			C_d≥32	
low		moderate		considerable			very high	
Modified degree of contamination (mC_d)								
3.26	0.50	0.94	0.13	1.20	1.12	2.69	0.92	2.15
mC_d < 1.5	1.5 ≤ mC_d < 2	2 ≤ mC_d < 4	4 ≤ mC_d < 8		8 ≤ mC_d < 16	16 ≤ mC_d < 32		mC_d ≥ 32
nil to very low	low	moderate	high		very high	extremely high		ultra-high
Pollution Load Index (PLI)								
0.59	0.16	0.21	0.06	0.33	0.43	0.40	0.38	0.68
0			1			>1		
perfection			baseline			deterioration		

mC_d gives only one value for total current status of all elements as C_d. However, it relates the current situation to the number of elements, unlike Cd. This method was developed by Abrahim and Parker, designed as a 7-way scale [26]. Accordingly, 9 stations were studied at Lake Salda switches between two scales, the bottom, nil, to very low contamination and the 3rd step is moderate contamination (Table 8).

PLI is a method starting from C_f^i that reveals the current situation based on all the general elements, and evaluates with a 3-way scale, it was developed by Tomlinson et al. [27]. However, there are more detailed scales available [50]. Both scales, according to the recent literature, have been used in former studies [28, 46]. The results for all stations were determined on the first and second level, which are ideal level and baseline on the study carried out. Level 3 deterioration was not observed at any of the stations (Table 8). SS04 was identified as the cleanest station according to the PLI. Stations SS01 and DS04 were found to have relatively higher levels of contamination compared with other stations.

Enrichment Factor (EF) and Geoaccumulation Index (I_{geo}). Both EF and I_{geo} are methods used to identify the level of contamination in the environment separately from the base metal. EF is a method which reveals the geochemical profile of different areas and allows comparison of the profiles in these areas [51]. For this reason, it has been used in many studies that demonstrate the accumulation of sediment profiles [44, 52]. However, when assessing the EF profile it has been seen that scales comprising a different number of digits have been used for various studies according to the literature [51, 52, 53]. The highest value obtained for Pb was in DS02 station during this study (Table 9). Pb almost doubled the highest value, which took it almost to the level of extremely high on the scale. Pb has also been determined as being at a very high level for station DS04. No problem can be seen for Pb, except for at these two stations. Pb levels on the other stations are observed at the bottom of the scale. Another important element is Ni for the EF profile. Ni has been not shown up to be high at all stations, different from Pb. Ni is at level 3 or 4 for all stations according to the

5-way scale. Cr is one other element which attracts attention. Cr has been determined as moderate at all stations (determined very close to the border of moderate but minimal only in station SS01). Other elements have been determined as minimal for all stations except these elements. EF also shows a table similar to the I_{geo} (Table 10). The stations DS02 and DS04, are located on the 5. and 4. places on the 7-way scale for Pb, respectively, and these values are the highest for Pb. The lowest level on the scales has been determined for Pb at other stations. Unlike the EF, I_{geo} has determined the situation of Ni at SS01 as being at level 6, which was determined as the highest for all the studied metals. 1, 2 and 4. levels have been identified for the other stations in the scale. Any condition that would cause problems for other metals, wasn't detected by I_{geo}. Although Ef and I_{geo} give parallel results in this study, the situation of EF is more concerning according to I_{geo}.

Potential Ecological Risk Factor (E^i_r), Sum of the toxic units (Σ TU s) and Quotient Toxic Unit. In this study, Potential Ecological Risk Factor (E^i_r) was used to determine the effect on living beings and the ecosystem separately for all metals, not anthropogenic sourced metal accumulation, which was different to the other methods. It is one of the methods used for sediment studies [45, 54]. Hakanson [25] determined a 5-step scale for evaluating the results. The method used for assessing the total toxic effect formed by high risk metals, is the potential ecological risk index. This index shows the total for the metals; Hg, Cd, As, Pb, Cu, Cr, Zn. However, the assessment of potential ecological risk index was not done because Hg content was not to be included in this study. According to the results, Ni and Pb are the what need to be focused on (Table 11). Ni was found to be at step 3., a considerable amount, at station SS01 and step 2., a moderate level, at station SS05. On the other hand, Pb was determined as considerable at station DS02, and as moderate at station DS04. There wasn't observed to be an urgent situation in terms of other metals, and all metals were determined as low for all situations.

TABLE 9
Enrichment Factor Values of Studied Heavy Metals

Enrichment factor (EF)									
	Cu	**Pb**	**Zn**	**Ni**	**Mn**	**Fe**	**As**	**Cd**	**Cr**
SS01	0.20	0.35	0.22	26.28	0.68		0.08	0.32	1.88
SS02	0.26	2.52	0.27	26.99	0.72		0.95	1.29	3.33
SS03	0.14	0.40	0.22	24.84	0.76		0.20	0.62	3.21
SS04	0.36	1.57	0.46	12.65	0.19	Reference element	1.75	1.64	2.13
SS05	0.17	0.64	0.46	19.26	0.86		0.12	0.37	2.84
DS01	0.24	1.76	0.58	18.86	1.02		0.33	0.92	2.52
DS02	0.26	78.99	0.50	14.25	0.98		0.28	0.98	2.56
DS03	0.25	3.61	0.63	19.90	0.90		0.66	1.52	2.45
DS04	0.32	24.25	0.81	16.03	1.20		0.26	1.50	2.33
EF<2 minimal		2≤EF<5 moderate		5≤EF<20 significant		20≤EF<40 very high		EF≥40 extremely high	

TABLE 10
Geoacummulation Values (I_{geo}) of Studied Heavy Metals

Geoaccumulation Index (I_{geo})									
	Cu	**Pb**	**Zn**	**Ni**	**Mn**	**Fe**	**As**	**Cd**	**Cr**
SS01	-2.95	-2.19	-2.85	4.05	-1.21	-0.66	-4.25	-2.32	0.25
SS02	-5.57	-2.30	-5.51	1.12	-4.12	-3.64	-3.72	-3.27	-1.90
SS03	-5.37	-3.79	-4.64	2.15	-2.88	-2.48	-4.81	-3.16	-0.80
SS04	-6.25	-4.13	-5.91	-1.12	-7.15	-4.78	-3.97	-4.07	-3.69
SS05	-4.39	-2.49	-2.98	2.43	-2.07	-1.84	-4.90	-3.26	-0.34
DS01	-4.10	-1.19	-2.80	2.23	-1.99	-2.01	-3.60	-2.13	-0.68
DS02	-4.59	3.67	-3.63	1.20	-2.65	-2.63	-4.49	-2.66	-1.28
DS03	-4.48	-0.64	-3.15	1.83	-2.64	-2.49	-3.08	-1.88	-1.20
DS04	-3.54	2.71	-2.20	2.12	-1.62	-1.89	-3.82	-1.30	-0.66
Igeo≤0 practically uncontaminated	0<*Igeo*<1 uncontaminated to moderately		1<*Igeo*<2 moderately	2<*Igeo*<3 moderately to strongly		3<*Igeo*<4 strongly	4<*Igeo*<5 strong to extremely		*Igeo*≥5 extremely

TABLE 11
Table of Potential Ecological Risk Factor (E^i_r) Values

Potential Ecological Risk Factor (E^i_{rf})									
	Cu	**Pb**	**Zn**	**Ni**	**Mn**	**Fe**	**As**	**Cd**	**Cr**
Samples	0.97	1.64	0.21	124.38	0.65		0.79	9.04	3.56
SS01	0.36	1.85	0.19	33.73	0.39		0.77	7.43	1.86
SS02	0.18	0.54	0.06	33.40	0.20		0.54	5.03	1.73
SS03	0.10	0.43	0.02	3.46	0.01		0.96	2.69	0.23
SS04	0.36	1.34	0.19	40.32	0.36		0.50	4.70	2.38
SS05	0.10	0.51	0.00	5.62	0.02		0.71	2.41	0.51
DS01	0.31	95.78	0.12	17.27	0.24		0.67	7.14	1.24
DS02	0.34	4.82	0.17	26.59	0.24		1.77	12.20	1.31
DS03	0.65	49.23	0.33	32.55	0.49		1.06	18.31	1.89
DS04	0.97	1.64	0.21	124.38	0.65		0.79	9.04	3.56
Er^i <40 Low		40≤Er^i<80 moderate		80≤Er^i<160 considerable		160≤Er^i<320 high		320≥Er^i very high	

TABLE 12
Proportional Toxic Unit Values of the Elements

Quotient Toxic Unit										
	Cu	**Pb**	**Zn**	**Ni**	**Mn**	**Fe**	**As**	**Cd**	**Cr**	**ΣTU**
SS01	0.09%	0.15%	0.13%	95.83%			0.12%	0.05%	3.63%	49.03
SS02	0.11%	0.99%	0.15%	91.30%			1.30%	0.20%	5.97%	6.73
SS03	0.06%	0.17%	0.13%	92.87%			0.30%	0.10%	6.36%	13.59
SS04	0.29%	1.23%	0.49%	85.13%			4.77%	0.50%	7.59%	1.53
SS05	0.10%	0.35%	0.35%	91.73%			0.23%	0.08%	7.16%	16.60
DS01	0.14%	0.99%	0.45%	91.12%			0.65%	0.20%	6.46%	14.55
DS02	0.12%	36.61%	0.32%	56.92%			0.45%	0.18%	5.41%	11.46
DS03	0.14%	1.89%	0.46%	90.11%			1.21%	0.31%	5.88%	11.15
DS04	0.19%	13.77%	0.63%	78.51%			0.52%	0.33%	6.04%	15.66

Σ TUs, has been used for evaluating the general reliability of the stations, and toxic effects originating from metals have been shown using this method (Table 12). According to the results, the highest value for total level of toxic effects was found at station SS01. SS05, DS04, DS01 stations follow, respectively. In the study benefited from the Quotient Toksik Unit, determining the ratios of total toxic effects of metals one by one. The results show the highest rate was shown to be Ni. The impact of Ni on toxic effect changes between from 95.8% and 56.92% (Table 12). Cr is another important element in relation to the toxic effect. The ratio of Cr ranges from 10.34% and 3.63%. Pb reaches higher ratios of between 36.61% and 13.77% at stations DS02 and DS04, respectively.

CONCLUSIONS

The study carried out aimed to determine the anthropogenic sourced metal accumulation in the environment and to understand the toxic effect of the amounts of metal on the aquatic ecosystem by investigating metal quantities in the sediment of Lake Salda. Also, it reveals the relationship between metal deposition and environmental pollution. The metal accumulation was mostly found to be Pb and Ni elements at stations DS02, DS04 and SS01. DS02 and DS04 seemed to be an extension of a fault, and SS01 is along the main stream that recharges the lake. Ni amounts could come from the ultramafic rocks. However, the high amounts of Pb are likely to be due to the anthropogenic effects, although the lake is an area of natural protection. There is strong evidence to suggest Pb has accumulated in the lake through movement. Ni has been determined as having the highest risk for the lake. Along with the variation of Ni amounts, it measures on the higher parts of the scales used for all the studied stations: the metals were studied using sediment assessment methods. Lake Salda is an area of natural protection, and has been for a long time. However, Ni is a common metal for industrial use. Ni comes probably from the dissolved antigorite minerals which are observed in the study area and its near environ. Pb results are also extremely important, these were taken in the deeper parts of the lake with Ni at two stations. Cr is also an element that should be evaluated based on the risk range for the lake, and Cr is enriched by ultramafic rocks, along with elements such as Ni, but there is an ore site for Cr on the northern side of the lake, Cr is

again another element that occurs in significant quantities in rocks. That is out of question for any risky situation for the other elements. The lake was evaluated as both element and station base. So, the results of 2 stations (SS01 and DS04) were concluded to be more critical than the others. SS01 is one of the main streams that recharges the lake, and is on the Yeşilova site. DS04 is the deepest sediment that was collected (96 m depth) and is on the extension of the main fault.

To conclude, Lake Salda, nowadays, is regularly discussed throughout Turkey, because there are plans to build a dam on the Düden brook, which merges with Karakova stream in the western part and is one of the main recharging surface waters for the lake. So, there are several campaigns being introduced so people can understand the importance of the lake. Although Lake Salda is one of the most important lakes in Turkey, and even the world, there are few studies about it. As the study is new it will be of importance for current works. Finally, it seems that the lake, which is of great importance, could be at risk of anthropogenic pollution from Pb and Ni elements, as shown in all of the results. The reasons could be natural for other elements including Ni, though Ni can be anthropogenic as revealed in the results. However, industrial and agricultural activities in surrounding villages, also the belt highway, which is located on the southern part of the lake, could be reasons for the pollution, especially Pb.

ACKNOWLEDGEMENTS

The authors give thanks to The Scientific and Technological Research Council of Turkey (TUBITAK) “113Y408”, “2210/C-2015”, and Muğla Sıtkı Koçman University “BAP 15/048” projects for their financial support.

REFERENCES

[1] Sany, S.B.T., Salleh, A., Sulaiman, A.H., Sasekumar, A., Rezayi, M. and Tehrani, G.M. (2013) Heavy Metal Contamination in Water And Sediment Of The Port Klang Coastal Area, Selangor, Malaysia. Environmental Earth Sciences. 69, 2013-2025.

[2] Shafie, N.A., Aris, A.Z., Zakaria, M.P., Haris, H., Lim, W.Y. and Isa, N.M. (2013) Application Of Geoaccumulation Index And Enrichment Factors On The Assessment Of Heavy Metal Pollution In The Sediments. Journal Of Environmental Science And Health Part A-Toxic/Hazardous Substances & Environmental Engineering. 48, 182-190.

[3] Hahladakis, J., Smaragdaki, E., Vasilaki, G. and Gidarakos, E. (2013) Use of Sediment Quality Guidelines and Pollution Indicators for The Assessment of Heavy Metal and Pah Contamination in Greek Surficial Sea and Lake Sediments. Environmental Monitoring and Assessment. 185, 2843-2853.

[4] Qi, Y., Ma, J. and Fan, G. (2015) Assessment of heavy metals contamination in Fen River channels. Fresen. Environ. Bull. 24, 1990-1995.

[5] Yorulmaz, B., Yılmaz, F. and Genç, T.O. (2015) Heavy metal concentrations in European eel (Anguilla amguilla L., 1758) from Köyceğiz-Dalyan lagoon system. Fresen. Environ. Bull. 24, 1607-1613.

[6] Çağlar, M. (2015) Heavy metal accumulation in the sediments of the littoral zone of a deep alkaline lake. Fresen. Environ. Bull. 24, 4622-4627.

[7] Peng, S., Lei, T., Zhou, R., Zhang, J. and Wang, X. (2016) Long-term heavy metal pollution and health risk assessment in the Haine River, China. Fresen. Environ. Bull. 25, 3837-3846.

[8] Koca, F.D., Kızıldağ, N, Darici, C. and Duman, F. (2016) Determination of heavy metal accumulation in water, sediment and smartweed (Polygonum Amphibium) from Sarımsaklı Dam lake (Kayseri – Turkey). Fresen. Environ. Bull. 25, 1373-1382.

[9] Ahmad, K., Khan, Z.I., Ashfaq, A., Akram, N.A., Ashraf, M., Yasmeen, S., Turafelli, V., Laudadio, V., Fracchiolla, M. and Cazzato, E. (2016) Contamination and accumulation of heavy metals in brinjal (Solanum Melongena L.) grown in a long-term wastewater-irrigated agricultural land of Sargodha, Pakistan. Fresen. Environ. Bull. 25, 2404-2410.

[10] Markovic, M., Miloradov, M.V., Ignjatovic, L., Obrovski, B., Cavic, A. and Mihajlovic, I. (2017) Ecological status of artificial accumulation Lake Vrutci, case study, Serbia. Fresen. Environ. Bull. 26, 5184-5189.

[11] Yang, T., Li, X., Xu, Y., Chen, Q., Zhao, X. and Zhou, S. (2017) Potential ecological risk and contamination of heavy metals in Feng River, China.

[12] Uluturhan, E., Kontas, A. and Can, E. (2011) Sediment Concentrations of Heavy Metals in The Homa Lagoon (Eastern Aegean Sea): Assessment of Contamination and Ecological Risks. Marine Pollution Bulletin. 62, 1989-1997.

[13] Rahman, M.S., Saha, N. and Molla, A.H. (2014) Potential Ecological Risk Assessment of Heavy Metal Contamination in Sediment and Water Body Around Dhaka Export Processing Zone, Bangladesh. Environmental Earth Sciences. 71, 2293-2308.

[14] Wang, C., Liu, S., Zhao, Q., Deng, L. and Dong, S. (2012) Spatial Variation and Contamination Assessment of Heavy Metals in Sediments in The Manwan Reservoir, Lancang River. Ecotoxicol Environ Saf. 82, 32-39.
[15] Alkan, N., Alkan, A., Akbas, U. and Fisher, A, (2015) Metal Pollution Assessment in Sediments of The Southeastern Black Sea Coast of Turkey. Soil & Sediment Contamination. 24, 290-305.
[16] Liu, Y., Peng, Y., Yue, D., Yin, Q., Xiao, L., (2015) Assessment of Heavy Metal Enrichment, Bioavailability, And Controlling Factors in Sediments of Taihu Lake, China. Soil & Sediment Contamination. 24, 262-275.
[17] Sutherland, R.A. (2000) Bed Sediment-Associated Trace Metals in An Urban Stream, Oahu, Hawaii. Environmental Geology. 39, 611-627.
[18] Wang, Z.M., Chen, L.D., Zhang, H.P. and Sun, R.H. (2014) Multivariate Statistical Analysis and Risk Assessment of Heavy Metals Monitored in Surface Sediment of The Luan River and Its Tributaries, China. Human and Ecological Risk Assessment. 20, 1521-1537.
[19] Russell, M.J., Ingham, J.K., Zedef, V., Maktav, D., Sunar, F., Hall, A.J. and Fallick, A.E. (1999) Search for Signs of Ancient Life on Mars: Expectations from Hydromagnesite Microbialites, Salda Lake, Turkey. Geological Society of London Journal. 156, 869–888.
[20] Sarp, H. (1976) Petrographic and Geological Survey From Ophiolitic Cortege Of The Region Located On North-West Yeşilova (Burdur-Turkey). Ph.D. Thesis in University of Geneve, Geneve, Switzerland.
[21] Ersoy, Ş. (1989) Geology Of The Güney Mountain And Kelebek Mountain Located Between Fethiye (Muğla)-Gölhisar (Burdur) Area. Ph.D Thesis in İstanbul University Institute of Graduate Studies In Science, İstanbul.
[22] Turekian, K.K. and Wedepohl, K.H. (1961) Distribution Of The Elements In Some Major Units Of The Earth's Crust. Geological Society of America Bulletin. 72, 175-192.
[23] Ghrefat, H.A., Abu-Rukah,Y. and Rosen, M.A. (2011) Application Of Geoaccumulation Index And Enrichment Factor For Assessing Metal Contamination In The Sediments Of Kafrain Dam, Jordan. Environmental Monitoring And Assessment. 178, 95-109.
[24] Zamani Hargalani, F., Karbassi, A., Monavari, S.M. and Abroomand Azar, P. (2014) A Novel Pollution Index Based On The Bioavailability Of Elements: A Study On Anzali Wetland Bed Sediments. Environmental Monitoring And Assessment. 186, 2329-2348.
[25] Hakanson, L. (1980) An Ecological Risk Index For Aquatic Pollution Control A Sedimentological Approach. Water Research. 14, 975-1001.
[26] Abrahim, G.M.S. and Parker, R.J. (2008) Assessment of Heavy Metal Enrichment Factors And The Degree Of Contamination In Marine Sediments From Tamaki Estuary, Auckland, New Zealand. Environmental Monitoring and Assessment. 136, 227-238.
[27] Tomlinson, D.L., Wilson, J.G., Harris, C.R. and Jeffrey, D.W. (1980) Problems In The Assessment Of Heavy-Metal Levels In Estuaries And The Formation Of A Pollution Index. Helgolander Meeresuntersuchungen. 33, 566-575.
[28] El-Said, G.F., Draz, S.E., El-Sadaawy, M.M. and Moneer, A.A. (2014) Sedimentology, Geochemistry, Pollution Status And Ecological Risk Assessment Of Some Heavy Metals In Surficial Sediments Of An Egyptian Lagoon Connecting To The Mediterranean Sea. J Environ Sci Health A Tox Hazard Subst Environ Eng. 49, 1029-44.
[29] Manasreh, W., Hailat, I. and El-Hasan, T.M. (2010) Heavy Metal And Anionic Contamination In The Water And Sediments In Al-Mujib Reservoir, Central Jordan. Environmental Earth Sciences. 60, 613-621.
[30] Esen, E., Kucuksezgin, F. and Uluturhan, E. (2010) Assessment Of Trace Metal Pollution In Surface Sediments Of Nemrut Bay, Aegean Sea. Environmental Monitoring and Assessment. 160, 257-266.
[31] Müller, G. (1969) Index Of Geoaccumulation In Sediments of the Rhine River. Geojournal. 2, 108-118.
[32] Pedersen, F., Bjørnestad, E., Andersen, H.V., Kjølholt, J. and Poll, C. (1998) Characterization Of Sediments From Copenhagen Harbour By Use Of Biotests. Water Science And Technology. 37, 233-240.
[33] Zheng, N., Wang, Q., Liang, Z. and Zheng, D. (2008) Characterization of Heavy Metal Concentrations in the Sediments of Three Freshwater Rivers in Huludao City, Northeast China. Environmental Pollution. 154, 135-142.
[34] Bakan, G. and Özkoç, H.B. (2007) An Ecological Risk Assessment Of The Impact Of Heavy Metals In Surface Sediments On Biota From The Mid-Black Sea Coast Of Turkey. International Journal Of Environmental Studies. 64, 45-57.
[35] Hu, B., Li, J., Zhao, J., Yang, J., Bai, F. and Dou, Y. (2013) Heavy Metal In Surface Sediments Of The Liaodong Bay, Bohai Sea: Distribution, Contamination, And Sources. Environmental Monitoring And Assessment. 185, 5071-5083.

[36] Tunca, E., Ucuncu, E., Kurtulus, B., Ozkan, A. D. and Atasagun, S. (2013) Accumulation Trends Of Metals And A Metalloid In The Freshwater Crayfish Astacus Leptodactylus From Lake Yenicaga (Turkey). Chemistry And Ecology. 29, 754-769.

[37] Smith, S.L., Macdonald, D.D., Keenleyside, K.A., Ingersoll, C.G. and Field, L.J. (1996) A Preliminary Evaluation Of Sediment Quality Assessment Values For Freshwater Ecosystems. Journal Of Great Lakes Research. 22, 624-638.

[38] Long, E.R., Morgan, L.G. (1991) The Potential For Biological Effects Of Sediment-Sorbed Contaminants Tested In The National Status And Trends Program, Noaa Technical Memorandum Nos Oma 52. National Oceanic And Atmospheric Administration, Seattle, Washington, 175.

[39] Xu, Z.Q., Ni, S.J. and Tuo, X.G. (2008) Calculation Of Heavy Metals Toxicity Coefficient In The Evaluation Of Potential Ecological Risk Index. Environmental Science And Technology. 31, 112-115.

[40] Macdonald, D.D., Ingersoll, C.G. and Berger, T.A. (2000) Development And Evaluation Of Consensus-Based Sediment Quality Guidelines For Freshwater Ecosystems. Arch Environ Contam Toxicol. 39, 20-31.

[41] Mielke, J.E. (1979) Composition of the Earth's crust and distribution of the elements, In: Siegel, F.R. (Edt.), Review of Research on Modern Problems in Geochemistry, International Association of Geochemistry and Cosmochemistry, UNESCO, Paris, 13–37.

[42] Reimann, C. and de Caritat, P. (1998) Chemical Elements in the Environment—Factsheets for the Geochemist and Environmental Scientist, Berlin, Germany.

[43] Wuana, R.A. and Okieimen, F.E. (2011) HeavyMetals in Contaminated Soils: A Review of Sources, Chemistry, Risks and Best Available Strategies for Remediation. International Scholarly Research Network. 2011, 1-20.

[44] Ghrefat, H.A., Abu-Rukah, Y. and Rosen, M.A. (2011) Application Of Geoaccumulation Index And Enrichment Factor For Assessing Metal Contamination In The Sediments Of Kafrain Dam, Jordan. Environmental Monitoring and Assessment. 178, 95-109.

[45] Yuan, Z., Taoran, S., Yan, Z. and Tao, Y. (2014) Spatial Distribution And Risk Assessment Of Heavy Metals In Sediments From A Hypertrophic Plateau Lake Dianchi, China. Environmental Monitoring And Assessment. 186, 1219-1234.

[46] Kukrer, S., Seker, S., Abaci, Z.T. and Kutlu, B. (2014) Ecological Risk Assessment Of Heavy Metals In Surface Sediments Of Northern Littoral Zone Of Lake Cildir, Ardahan, Turkey. Environmental Monitoring And Assessment. 186, 3847-3857.

[47] Sener, S., Davraz, A. and Karaguzel, R. (2014) Assessment Of Trace Metal Contents In Water And Bottom Sediments From Egirdir Lake, Turkey. Environmental Earth Sciences. 71, 2807-2819.

[48] Veerasingam, S., Venkatachalapathy, R. and Ramkumar, T. (2014) Historical Environmental Pollution Trend And Ecological Risk Assessment Of Trace Metals In Marine Sediments Off Adyar Estuary, Bay Of Bengal, India. Environmental Earth Sciences. 71, 3963-3975.

[49] Okbah, M.A., Nasr, S.M., Soliman, N.F. and Khairy, M.A. (2014) Distribution and Contamination Status Of Trace Metals In The Mediterranean Coastal Sediments, Egypt. Soil And Sediment Contamination: An International Journal. 23, 656-676.

[50] Singh, A.K., Hasnain, S.I. and Banerjee, D.K. (1999) Grain Size And Geochemical Partitioning Of Heavy Metals In Sediments Of The Damodar River - A Tributary Of The Lower Ganga, India. Environmental Geology. 39, 90-98.

[51] Hasan, A.B., Kabir, S., Reza, A.H.M.S., Zaman, M.N., Ahsan, A. and Rashid, M. (2013) Enrichment Factor And Geo-Accumulation Index Of Trace Metals in Sediments of the Ship Breaking Area Of Sitakund Upazilla (Bhatiary-Kumira), Chittagong, Bangladesh. Journal Of Geochemical Exploration. 125, 130-137.

[52] Haris, H. and Aris, A.Z. (2012) The Geoaccumulation Index And Enrichment Factor Of Mercury In Mangrove Sediment Of Port Klang, Selangor, Malaysia. Arabian Journal Of Geosciences. 6, 4119-4128.

[53] Zhang, J. and Liu, C.L. (2002) Riverine Composition And Estuarine Geochemistry Of Particulate Metals In China - Weathering Features, Anthropogenic Impact And Chemical Fluxes. Estuarine Coastal And Shelf Science. 54, 1051-1070.

[54] Yan, X., Gao, D., Zhang, F., Zeng, C., Xiang, W. and Zhang, M. (2013) Relationships Between Heavy Metal Concentrations In Roadside Topsoil And Distance To Road Edge Based On Field Observations In The Qinghai-Tibet Plateau, China. Int J Environ Res Public Health. 10, 762-75.

Received: **21.06.2017**
Accepted: **15.10.2017**

CORRESPONDING AUTHOR

Mustafa Can Canoglu
Sinop University,
Faculty of Engineering and Architecture,
Environmental Engineering Department,
57000 Sinop – Turkey

E-mail: mccanoglu@sinop.edu.tr

© by PSP Volume 26 – No. 12A/2017 pages 8062-8068 Fresenius Environmental Bulletin

EFFECT OF FLOCCULANT ON THE SETTLEMENT OF IRON TAILINGS

Hongzheng Zhu[1,2], Jinbo Zhu[1,*], Alejandro Lopez Valdivieso[2], Hainan Wang[1], Zhengyan Zhou[1]

[1]School of Materials Science and Engineering, Anhui University of Science and Technology, Huainan, China
[2]Instituto de Metalurgia, Universidad Autonoma de San Luis Potosi, San Luis Potosi, Mexico

ABSTRACT

Quick settlement of iron tailings is necessary for the prevention of environmental pollution, meanwhile high concentration is required for the utilization of the sediment. The effect of the flocculant on the settlement of iron tailings with whole size, ＞45 μm and ≤45 μm were respectively researched in the terms of settle velocity and sediment concentration. The comparison on the settle efficiencies of different size fraction at the dose of 0.3 and 0.5 ml explained that the flocculant reflects more influence on bridge than viscosity and more influence on ultrafine particles than coarse particles. Different settlement schemes were calculated and compared, the results indicated that pre-classification of the iron tailings is effective for saving flocculant and enhancing the settle efficiency.

KEYWORDS:
Iron tailing, flocculant, dose, settle velocity, sediment concentration

INTRODUCTION

Large amounts of iron tailings is generated from iron ore concentrating mills in China [1, 2], which is usually concentrated in tailing ponds for long-time settlement [3, 4]. These processes may cause environmental pollution and hidden troubles, therefore the plan that backfill the goaf with the iron tailings is proposed [5–7]. However, the iron tailings are difficult to settle rapidly [8, 9], many investigations were carried out in the past to select the appropriate flocculants. Panda et al. [10] used wheat starch as a flocculant for the selective flocculation of ultrafine synthetic mixtures of hematite and kaolinite; Huang et al. [11] researched the disposal of Bayer red mud based on selective flocculation desliming process by using humics as the flocculant; Nan et al. [12] studied the selection of flocculating agent in tailings backfill engineering project. But the method that pre-classification and then respectively settle was scarcely explored. Lots of researches were carried out to search prominent factors of the settlement of iron tailings. Chen et al. [13] researched the removal of copper and turbidity from simulated micro-etch copper waste by different magnetic seeds, coagulants dosages and flocculant dosages; Qiu et al. [14] studied the preparation and application of PAM/MMT W/W emulsion under different particle sizes, reagent dosages, gelatin concentrations, PH values and viscosities; Jia et al. [15] explored the effect of PH, flocculant dosages and initial contaminant concentrations on the removal of Cu (Ⅱ) and tetracycline from water. However, these achievements are difficultly commercialized in the plants because of the low controllability and high complexity. In present work, an attempt was made to study the settlement of different size fraction of iron tailings in terms of settle velocity and sediment concentration.

EXPERIMENT

Sample preparation. The iron tailings used in this study was sampled from an iron ore concentrating mill of China. The size distribution of the iron tailings mixed with water in the original sample was analyzed as shown in Fig.1 by the Wet sieving apparatus (SFS-Ⅰ, Landsky Science and technology Co., Ltd, China) and the Laser particle size analyzer (SALD-7101, Shimadzu corp., Japan).

An initial observation of Fig.1 shows that the particle sizes distribute as a similar parabola with high yield at the middle sizes. The section of ≤45 μm is deemed to settle difficultly, and its yield of this sample is near to 25.55 %. Numerous research on the classification of minerals shows that the slurry is realizable to be classified at 45 μm [16, 17], therefore comparative settlements of the slurry with whole size and pre-classified at 45 μm were explored.

The slurry was stirred continuously and uniformly for a sample with the volume of 1000 ml, and the sample was dried to weigh the solids. The result shows the weight of the solid in 1000 ml of slurry is about 135.42 g, that is, the concentration is 135.42 g/l. This concentration is known as the ratio of the mass of solids to volume of slurry (q) [18].

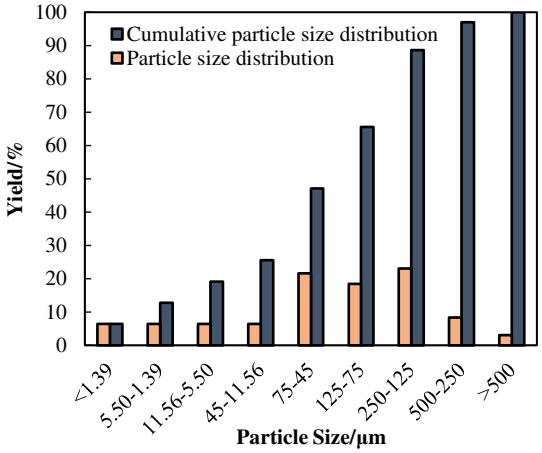


FIGURE 1
Particle size distribution of the iron tailings

Reagent and vessel. Measuring glass cylinders with volume of 500 ml and height of 230 mm were chose for the experiments, and a paper ruler of 230 mm was pasted on the cylinder for clear measurement of the settlement.

Polyacrylamide with the molecular weight of one million was selected as the flocculating reagent for present study. The industrial water from the iron ore concentrating mill is sampled for the experiments, and a flocculant was prepared by adding 1 g of polyacrylamide into 999 ml of industrial water [19]. The concentration of the flocculant is constant of 0.1 %.

Method. During all the experiments, a pre-solution consist of a certain weight of the iron tailings solids and a certain volume of the industrial water was stirred uniformly in a glass beaker of 100 ml, then it was added into the measuring glass cylinder with 400 ml industrial water in it to prepare the desired solid concentration of slurry. Calculate from the slurry concentration and the size distribution, the weight of whole size, ≤45 μm and ＞45 μm respectively were 67.71 g, 17.30 g and 50.41 g in the slurry of 500 ml.

Determination of the flocculant dose was done on the basic of some previous work, and free settlements were selectively done to observe the settle velocity and clarity. The flocculant with a certain dose was added into the slurry, and then the cylinder was waggled drastically for ensuring the mixing uniformity. The position of the obvious interface of the water and solids was recorded with time variation, and the settle velocity (v) can be calculated as:

$$v = \frac{L}{t} \quad (1)$$

where L is the distance from the free surface to the interface and t is the least time for the distance.

The velocities with different flocculant dose and different size range were compared for analyzing the optimal settlement scheme, meanwhile the optimal flocculant dose were determined. According to the settle velocity, a corresponding particle diameter (D_a) can be evaluated by the equation of Stokes.

$$D_a = \sqrt{\frac{v\mu}{54.5\chi(1-\lambda)^n(\delta-\rho)}} \quad (2)$$

where μ is the dynamic viscosity of the industrial water at 20 ℃, n is the concentration interference index (n=5-0.7Re), χ is the shape index of iron tailings, δ is the particle density, ρ is the industrial water density and λ is the ratio of the volume of solids to volume of liquid, it can be obtained from [20]:

$$\lambda = \frac{q}{\delta} \quad (3)$$

The values of D_a with different flocculant dose and different size range were analyzed for measuring the properties of agglomeration.

RESULTS AND DISCUSSION

Settlement of iron tailings of whole size. The flocculant dose was set as 0.3, 0.5, 1.0, 1.5, 2.0, 3.0 and 5.0 ml in per 500 ml of slurry, meanwhile the free settlement was carried out. The results were shown in Fig.2 and Fig.3.

Fig.2 shows the effect of flocculant dose on the settle velocity and time. In Fig.2, it is observed that with an initial increase of flocculant dose, the settle velocity increases up to 2.66 m/h and the settle time decreases down to 263.9 s. With a further increase of flocculant dose, the settle velocity starts to decrease and the settle time starts to increase. The settle velocity of the free settlement is about 0.57 m/h, and the settle time is about 1011.6 s.

From Fig.3, without the effect of flocculant, the concentration and volume of the sediment respectively are 1218 g/l and 55.0 ml. Under the effect of flocculant, with the dose increase the sediment concentration trends to increase and the maximum value is 964 g/l, meanwhile the sediment volume trends to

decrease and the minimum value is 70 ml. The minimum sediment concentration is 888 g/l and the maximum sediment volume is 76 ml, when the flocculant dose is 1.0 ml.

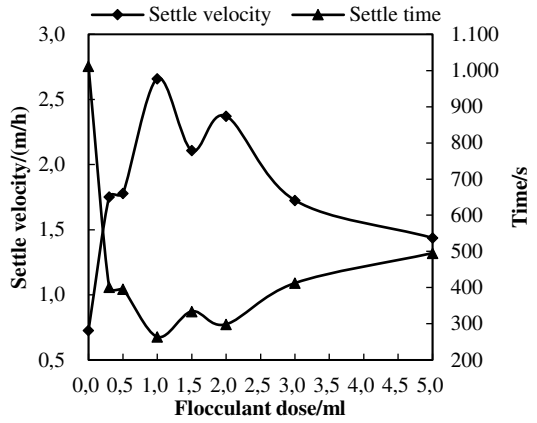


FIGURE 2
Relationship between flocculant with v and t

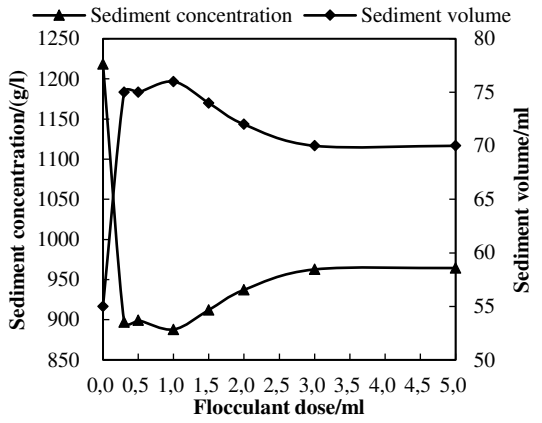


FIGURE 3
Effect of flocculant dose on concentration and volume of sediment

It can be obtained from the analysis of Fig.2 and Fig.3 that with the flocculant dose of 1.0 ml, the settle velocity is the maximum, but the sediment concentration is the minimum. Regardless of the dose increase or decrease from 1.0 ml, the variation trend of settle velocity and sediment concentration is the same. Therefore the dose of smaller values than 1.0 are selected for the further research on the size fraction of ＞45 μm and ≤45μm, and an optimal settle scheme is expected. The results also indicate that under the effect of the flocculant the bridge between particles appears, and the floc was formed with a large diameter which leads to larger settle velocity but also low sediment concentration. When the flocculant dose is larger than the critical value of 1.0, more particles are bridged that the sediment concentration higher, but the viscosity of the slurry becomes higher that the resistance of the floc motion higher which results in settle velocity decrease (22).

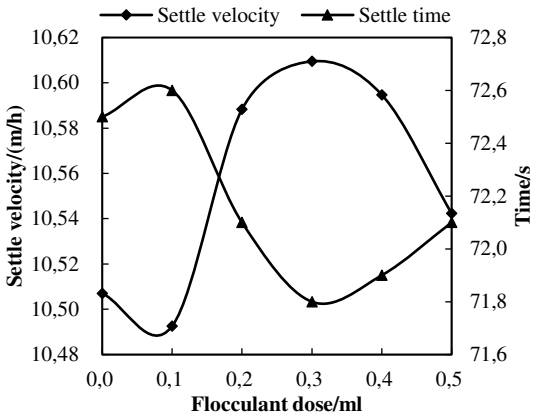


FIGURE 4
Curves of flocculant dose with v and t

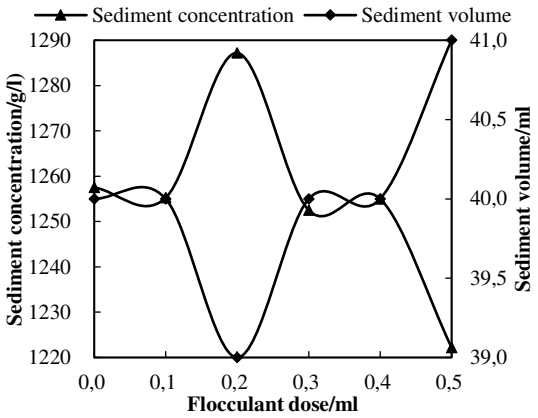


FIGURE 5
Curves of flocculant dose with sediment concentration and volume

Settlement of iron tailings of ＞45 μm. The flocculant dose of 0.1, 0.2, 0.3, 0.4 and 0.5 was taken for the settlement of ＞45 μm, meanwhile the free settlement was carried out. The results are shown in Fig.4 and Fig.5.

Analysis of the free settlement results shown in Fig.4 and Fig.5 showed that the settle velocity is 10.51 m/h about 13.43 times larger than the value of the whole size, and the sediment concentration is 1257 g/l that 1.03 times the number for the whole size.

From Fig.4, with the initial increase of the flocculant dose from 0.1 to 0.3, the settle velocity decreases and the settle time increase distinctly. With the further increase of the dose, the settle velocity slightly increases and the settle time decreases. The maximum settle velocity is about 10.61 m/h meanwhile the minimum settle time of 71.8 s with the dose of 0.3 ml. The variations about the concentration and volume of the sediment are complex as shown in Fig.5, and the extrema severally appear at the dose of 0.2 ml and 0.5 ml. With the dose of 0.2

ml, the sediment concentration is about 1287 g/l and the volume is about 39 ml. With the dose of 0.5 ml, the sediment concentration is about 1222 g/l and the volume is about 41 ml.

Based on the analysis of the settle velocity, the critical flocculant dose is 0.3 ml, whereas the critical dose is 0.2 ml from the analysis of sediment concentration. The reason about the difference of the critical dose may be that the viscosity caused by the extra 0.1 ml flocculant plays an unimportant role in the floc motion, In other words, the actual critical dose must be between 2.0 and 3.0 ml.

Settlement of iron tailings of ≤45μm. From the elementary knowledge of the minerals properties, it is undisputed that without flocculant the settlement of ≤45μm is so difficult. Thus the flocculant dose was set as 0.1, 0.2, 0.3, 0.4 and 0.5 for the settlement of ≤45 μm. The results are shown in Fig.6 and Fig.7.

An observation of Fig.6 shows that with the increase of the dose from 0.1 ml to 0.3 ml, the bridging action of the flocculant plays a crucial role in the increase of the settle velocity that from 23.43 m/h to 31.71 m/h. With the further dose increase, the viscosity increases which leads to a slight decrease of the settle velocity.

Fig.7 shows the variation of the sediment concentration and sediment volume influenced by the flocculant dose. The general trend of the sediment concentration is decreasing with the increase of the dose except the dose of 0.3 ml, and the reverse trend of the sediment volume. The extrema of the sediment concentration are 651 g/l and 589 g/l, and ones of the sediment volume are 26 ml and 29 ml.

The analysis on the settlement of ≤45μm shows that from dose of 0.2 ml to 0.3 ml the sediment concentration slightly increases and the sediment volume is almost constant, it may be due to more ultrafine particles are bridged and flocculated. The weight of the sediment is increased by the ultrafine particles, but the volume is influenced scarcely. So there is no doubt that the critical dose of the sediment concentration is 0.3 ml.

Comparison on the settle efficiency of different size fraction with the same flocculant dose. D_a considers the properties of the particles and the fluid is used for estimating the settle efficiency, moreover, the experiment results of flocculant dose of 0.3 ml and 0.5 ml are selected for comparison, because the dose both were designed for the three groups experiment. The calculation results are shown in Fig.8.

As shown in Fig.8, with the more 0.2 ml flocculant the D_a of 0.5 ml is larger than ones of 0.3 ml, it means that the flocculant reflects more influence on bridge than viscosity. Moreover, the D_a of each size fraction is smaller than the actual size, it may be due to the effect of the viscosity. According to the decline of the difference between that two dose, the size fraction can be sorted as ≤45 mm, ＞45 mm and whole size, it indicates that the flocculant reflects more influence on ultrafine particles than coarse particles.

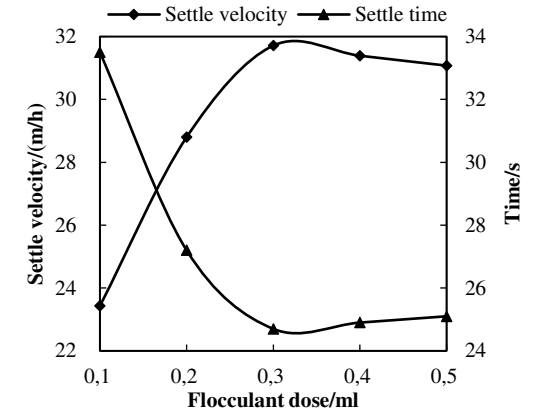


FIGURE 6
Curves of flocculant dose with v and t

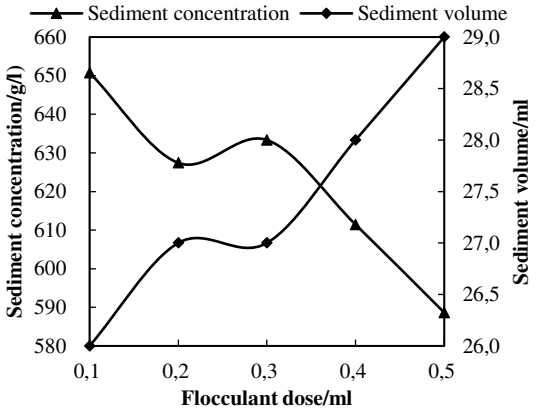


FIGURE 7
Curves of flocculant dose with sediment concentration and volume

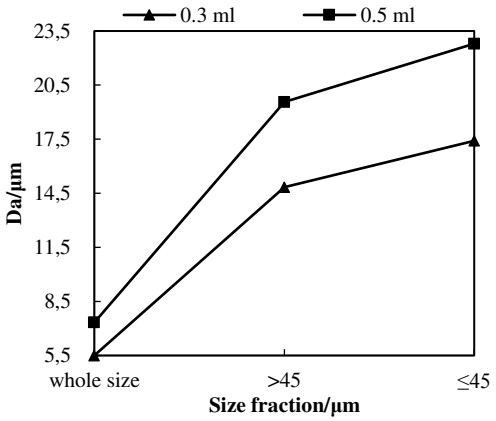


FIGURE 8
D_a of different size fraction with different flocculant dose

Comparison on different settle schemes. The average settle velocities of the schemes are calculated and shown in Fig.9, and the average sediment concentrations are shown in Fig.10. The legend in the two figures represents the dose of ≤45 μm fraction, and the unit is ml.

An observation of Fig.9 shows that five curves are almost straight and parallel, it demonstrates that the effect on the average settle velocity from the dose of ≤45 μm is larger than one of ＞45 μm. Arrange the dose of ≤45 μm in accordance with the decreasing sequence of the average settle velocity as 0.3, 0.4, 0.5, 0.2 and 0.1, and more remarkable that the velocities of the dose of 0.3, 0.4 and 0.5 are close.

The curves in Fig.10 are also parallel but not straight, it indicates that both ≤45 μm and ＞45 μm influence the average sediment concentration of the schemes, but the laws on the variation of the average sediment concentration influenced by the dose of ≤45 μm of every dose of ＞45 μm are the same. The decreasing sequence of the average sediment concentration can be sorted with the dose of ≤45 μm that 0.1, 0.3, 0.2, 0.4 and 0.5.

Based on the analysis, these two sequences are different. But only when the dose of ≤45 μm is 0.3 ml, both large average settle velocity and sediment concentration can simultaneously be obtained, and when the dose of ＞45 μm is 0.2 ml at the same time the average sediment concentration is the largest. Thus two schemes, the ≤45 μm dose is 0.3 ml and the ＞45 μm dose respectively are 0.0 and 0.2 ml, are proposed to compare with the settlement of the whole size as shown in Fig.11. The scheme that 0.3 ml flocculant in ≤45 μm and no flocculant in ＞45 μm is called whole size (0.3), and one that 0.3 ml flocculant in ≤45 μm and 0.2 ml flocculant in ＞45 μm is called whole size (0.5).

It can be obviously observed that both the scheme (0.3) and scheme (0.5) are superior to the whole size. Compared with the whole size (0.3), the settle velocity and sediment concentration of scheme (0.3) respectively increase by 9.26 times and 5.39 %. Moreover, compared with the whole size (0.5), the settle velocity and sediment concentration of scheme (0.5) respectively increase by 9.12 times and 6.79 %. The comparison on the scheme (0.3) and scheme (0.5) shows that their velocities are almost equal, but the concentration of the scheme (0.5) is larger than that of the scheme (0.3) with the extra 0.2 ml flocculant in ＞45 μm. More importantly, pre-classification of the iron tailings is effective for saving flocculant and enhancing the settle efficiency.

CONCLUSION

Research on the settlements of different size fraction with pre-classification of the iron tailings was carried out. Based on these investigations, we come to the following conclusions:

(1) The study of the effect of flocculant dose on the settlement of the iron tailings with whole size indicates that the largest settle velocity and sediment concentration respectively are 2.66 m/h and 964 g/l

(2) Respective settlements of different size fraction were researched. Here, the results of settle velocity show that the critical doses of ＞45 μm and ≤45 μm are 0.3 ml, and the largest settle velocity respectively are 10.61 and 31.71 m/h. The results of

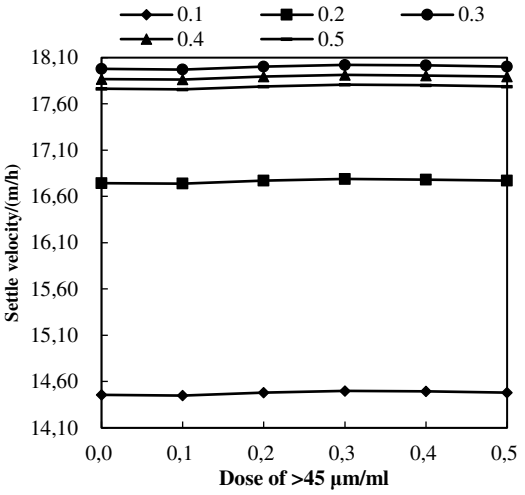


FIGURE 9
Average settle velocity

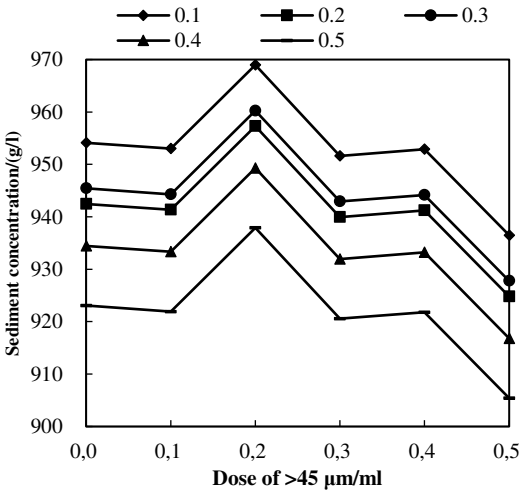


FIGURE 10
Average sediment concentration

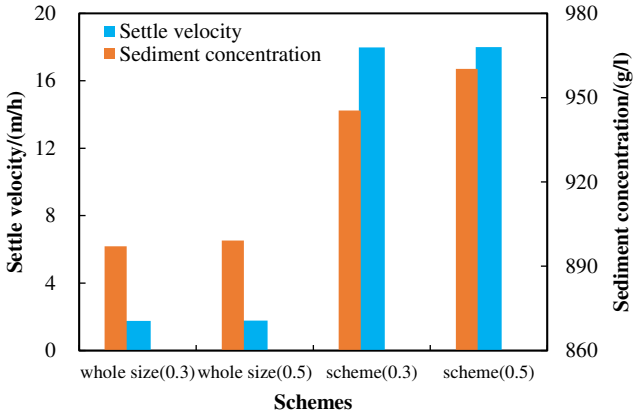


FIGURE 11
Comparison on different schemes

sediment concentration indicate that the critical doses of ＞45 μm and ≤45 μm respectively are 0.2 and 0.3 ml, and the maximum sediment concentration respectively are 1287 and 633 g/l.

(3) The comparison of different settle schemes demonstrates pre-classification of the iron tailings is effective for saving flocculant and enhancing the settle efficiency.

ACKNOWLEDGEMENTS

The authors would like to gracefully acknowledge the funding given by Anhui Provincial Education Department, China, through project KJ2016A188 for carrying out this work.

REFERENCES

[1] Li, C., Sun, H., Bai, J., Li, L. (2010) Innovative methodology for comprehensive utilization of iron ore tailings: Part 1. The recovery of iron from iron ore tailings using magnetic separation after magnetizing roasting. J Hazard Mater. 174, 71–77.

[2] Zhang, S., Xue, X., Liu, X., Duan, P., Yang, H., Jiang, T., Wang, D., Liu, R. (2006) Current situation and comprehensive utilization of iron ore tailing resources. J Min Sci. 42, 403–408.

[3] Ramos-Padrón, E., Bordenave, S., Lin, S., Bhaskar, I.M., Dong, X., Sensen, C.W., Fournier, J., Voordouw, G., Gieg, L.M. (2010) Carbon and sulfur cycling by microbial communities in a gypsum-treated oil sands tailings pond. Environ Sci Technol. 45, 439–446.

[4] Yong, R. N. (1983) U.S. Patent No. 4,399,039. Washington, DC: U.S. Patent and Trademark Office.

[5] Qiao, D., Zhang, X. (2011) Modern Mining Concept And Filling Technique. Nonferrous Met Sci Eng. 2, 3-11.

[6] Li, D.Q., Yang, C.X., Shi, S.H. (2009) Research of the application of total tailing high density backfilling technology in deep underground mine. Metal Mine, 7, 006.

[7] Kaiwei, X. (2000) Study on consolidated fill with tailing in the downward drift slicing and backfilling. GOLD. 2, 4-9.

[8] Nguyen, Q.D., Boger, D.V (1998) Application of rheology to solving tailings disposal problems. Int J Miner Process. 54, 217–233.

[9] Walters, L.J. (1992) Field settlement locations on subtidal marine hard substrata: Is active larval exploration involved, Limnol Oceanogr. 37, 1101–1107.

[10] Panda, L., Banerjee, P.K., Biswal, S.K., Venugopal, R., Mandre, N.R. (2013) Performance evaluation for selectivity of the flocculant on hematite in selective flocculation. Int J Miner Metall Mater. 20, 1123–1129.

[11] Huang, Y., Han, G., Liu, J., Wang, W. (2016) A facile disposal of Bayer red mud based on selective flocculation desliming with organic humics. J Hazard Mater. 301, 46–55.

[12] Nan, S., Zhang, Q., Guo, X. (2013) Application of flocculant in whole tailings cement filling of an iron mine. Disaster Adv. 6, 1–8.

[13] Chen, Y., Luo, M., Cai, W. (2016) Influence of operating parameters on the performance of magnetic seeding flocculation. Environ Sci Pollut Res. 23, 2873–2881.

[14] Qiu, J., Wang, H., Dong, S., Wang, H., Cheng, X., Du, Z. (2016) Study on the preparation of PAM/MMT W/W emulsion and its application as a flocculant. RSC Adv. 6, 7908–7913.

[15] Jia, S., Yang, Z., Yang, W., Zhang, T., Zhang, S., Yang, X., Dong, Y., Wu, J., Wang, Y. (2016) Removal of Cu (II) and tetracycline using an aromatic rings-functionalized chitosan-based flocculant: Enhanced interaction between the flocculant and the antibiotic. Chem Eng J. 283, 495–503.

[16] Abdullah, M.H., Mokhtar, M., Musta, B., Aris, A.Z. (2008) Hydrochemical analyses of a disturbed aquifer of a small island in Malaysia. Fresen. Environ. Bull. 17, 2043–2051.
[17] Papatheodorou, G., Hotos, G., Geraga, M., Avramidou, D., Vorinakis, T. (2002) Heavy metal concentrations in sediments of Klisova Lagoon (southeast Mesolonghi-Aetolikon Lagoon Complex), W. Greece. Fresen. Environ. Bull. 11, 951–956.
[18] Grote, M., Vockel, A., Schwarze, D., Mehlich, A., Freitag, M. (2004) Fate of antibiotics in food chain and environment originating from pigfattening (Part 1). Fresen. Environ. Bull. 13, 1216–1224.
[19] Afify, A.M.R., El-Beltagi, H.S. (2011) Effect of the insecticide cyanophos on liver function in adult male rats. Fresen. Environ. Bull. 20, 1084–1088.
[20] Edward, J.T. (1970) Molecular volumes and the Stokes-Einstein equation. J Chem Educ. 47, 261-269.

Received: **24.06.2017**
Accepted: **04.10.2017**

CORRESPONDING AUTHOR

Jinbo Zhu
School of Materials Science and Engineering,
Anhui University of Science and Technology,
Huainan 232001, Anhui – China

e-mail: zhujinbo1000@gmail.com

© by PSP Volume 26 – No. 12A/2017 pages 8069-8077 Fresenius Environmental Bulletin

STUDY ON THE INFLUENCE OF COPPER AND NICKEL IONS ON THE HYDROLYSIS-MBR PROCESS

Guangzhi Wang[1,*], Likun Huang[2], Zhi Xia[2]

[1]School of Environment, Harbin Institute of Technology, Harbin 150090, China
[2]School of Food Engineering, Harbin University of Commerce, Harbin 150076, China

ABSTRACT

In this study, the hydrolysis- membrane bioreactor process (the HMBR process) was employed to treat electroplating wastewater, and the influence of the heavy metal impact represented by Cu^{2+} and Ni^{2+} with different concentrations on treatment efficiency of the HMBR process and the variation of DOM and microbial activity in water were mainly studied. The results showed: under the impact of Cu^{2+} and Ni^{2+} with concentrations of 5 to 20 mg/L, the removal efficiencies of COD and NH_4^+-N in the HMBR process were above 75% and 45%, respectively; nitrifying bacteria had poor impact resistance to heavy metals; the HMBR process could endure 20 mg/L Cu^{2+} and Ni^{2+}, but the maximum tolerance of the MBR process was only 10 mg/L; the hydrolysis reactor could transform most of HPI in the sewage into HPO-A, thus improving the biodegradability of refractory organics, and the content of aromatic compounds decreased significantly; along with the increase of the concentration of Cu^{2+} and Ni^{2+}, the SOUR value in the MBR was declining, but the decrease of the SOUR value in the HMBR process was much less than the one in the MBR process, and the inhibition rate of SOUR in the HMBR process was nearly 5% lower than the one in the MBR process; because the hydrolysis could reduce the toxicity of heavy metal, the HMBR process had better microbial activity, less EPS content, and lower effluent concentration than the MBR process; the HMBR process could prevent the formation of colloid substances and DOM on the membrane surface efficiently, and had less cake layer and slower membrane fouling rate.

KEYWORDS:
Electroplating Wastewater, Hydrolysis, MBR, Heavy Metal

INTRODUCTION

Electroplating industry is one of the worst polluting industries in the world, and electroplating wastewater has complicated composition, multiplicate toxicities, high concentrated pollution, and feeble biochemistry character, in which the main contaminants are heavy metals (such as Cu, Ni, Cr, Zn, and Cd), cyanides, and organics [1]. There are different treatments to the different contaminants in the electroplating wastewater, for example, heavy metals, cyanides, and acid or alkali ions are treated mainly by physicochemical process [2-7], and COD and nitrogen pollutants are treated mainly by biochemical process [8-9]. However, many heavy metals in the electroplating wastewater has high biological toxicity, which would cause serious impact to biological treatment unit and make the follow-up biochemical processing frequently collapse. Thus, there are few studies to treat electroplating wastewater by biochemical process. Lai RiKun used micro-electrolysis as the pretreatment to treat electroplating wastewater, and after the A/O process the COD removal of the wastewater reached 75.08% [10]. Lu DaoFeng used the treatment combined hydrolytic acidification with improved A/O process for electroplating wastewater, in which process the mixture of electroplating wastewater and domestic sewage with 1:3 ratio was treated in the biological treatment unit in order to reduce the impact of toxic and hazardous substances in the electroplating wastewater to the biological treatment system, and the removal rates of COD and NH_4^+-N reached 83% and 98%, respectively [11].

Along with the implementation of the new Chinese national "Plating emission standards" (GB 21900-2008), the emission limits of biochemical Index in electroplating wastewater, such as COD, NH_4^+-N, and TN, had been significantly improved[12], and it should be the main urgent problem how to achieve standard discharge of electroplating wastewater in the presence of heavy metals. Recently, membrane bioreactor (MBR) has been widely applied to various types of wastewater treatment in order to meet higher emission requirements [13-17], which has a lot of advantages such as small occupation of land, high volume load, low sludge production, and high quality effluent. However, denitrification is inhibited in most MBR, which would influence the denitrification efficiency of the system. In this study, as to the specific water quality characteristics of electroplating wastewater, hydrolytic acidification was used as pretreatment means of MBR; the anoxic zone was set in MBR to reflux nitrification in aerobic zone [18-19]; the influence of different concentrations of heavy metals represented by Cu^{2+} and

TABLE 1
Water quality characteristics

Name	COD(mg/L)	NH^{4+}-N(mg/L)	TP(mg/L)	PH	Temperature(℃)
Value	250~440	30~40	3.5~6.0	6.4~7.6	10~18

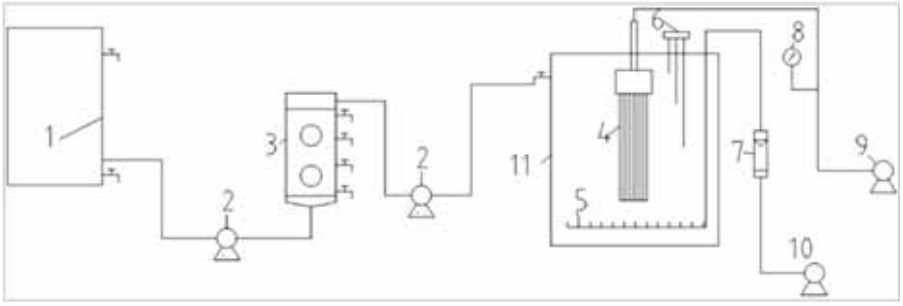


FIGURE 1
Schematic diagram of the lab-scale hydrolysis acidification-MBR reactor
1.Water tank; 2. Intake pump; 3. Hydrolysis reactor; 4. Hollow fiber membrane module; 5. Perforated pipes; 6. Three-needle gauge; 7. Gas flowmeter; 8. Vacuum gauge; 9. Vacuum pump; 10. Aeration pump; 11.MBR

Ni^{2+} on electroplating wastewater treatment efficiency of hydrolysis-MBR process was studied; and changes of DOM and microbial activity in water were studied too, in order to provide technical support for the application of this combined process in electroplating wastewater treatment.

MATERIALS AND METHODS

Experimental Water. During the start-up of the reactor, domestic sewage from the 2nd campus of Harbin Institute of Technology was used for domestication and cultivation of microorganisms, whose water quality characteristics were shown in Table 1. Considering toxicity of heavy metals and "Plating emission standards", electroplating wastewater was simulated by adding heavy metals (Cu^{2+} and Ni^{2+}), surfactant commonly used in electroplating (sodium dodecyl sulfonate), brightener (saccharin sodium), and stabilizer (polyethylene glycol) into the domestic sewage. The concentrations of sodium dodecyl sulfonate, saccharin sodium, and polyethylene glycol in water were 2.5 mg/L, 1 mg/L, and 3.5 mg/L, respectively. The heavy metal impact experiment was divided into 3 periods, and in different period the concentrations of Cu^{2+} and Ni^{2+} were 5 mg/L, 10mg/L, and 20 mg/L, respectively.

Experimental Device. The hydrolysis-MBR reactor (denoted by HMBR process) was composed of a hydrolysis reactor and an MBR, which was shown in Fig.1. Effective volumes of the hydrolysis reactor and the MBR were 11.8 L and 20 L, respectively. Both reactors were made by PMMA: the diameter, the effective height, and the effective volume of the hydrolysis reactor were 150 mm, 670 mm, and 11.8 L, respectively; `the size of the MBR was L×B×H=400×200×250 mm, of which effective volume was 20 L. HRT of the hydrolysis reactor and the MBR were 5 h and 9 h, respectively.

The mode of continuous water inlet and outlet was employed in the hydrolysis reactor, and the residence time was controlled by an intake pump. The mode of continuous water inflow and intermittent water outlet was employed in the MBR, and the effluent was controlled by a three-needle gauge, which kept influent flow rate less than effluent flow rate. A hollow fiber membrane was directly immersed in the wastewater of the reactor with an aperture of 0.2 μm and a membrane area of 0.2 m^2, which was made of polyvinylidene fluoride (PVDF). Trans-membrane pressure (TMP) was detected by a pressure sensor, and when TMP reached 0.2 MPa, the membrane module should be removed and cleaned. The hypoxia zone with an effective volume of 4 L was added in the improved MBR. Micro-porous aeration tubes were set up in the aerobic zone of MBR, in which an aeration pump was applied for continuous aeration, and aeration rate was controlled to 14 mL/min by a rotor flowmeter. Nitrification reflux was achieved by a peristaltic pump, and the reflux ratio was 150%.

The reference reactor was a single MBR, which was denoted by MBR process. The reactor influent of MBR process was the same as the influent of HMBR process, and other operating parameters remained. The experimental period was 6 days, and after an experimental period domestic sewage was used for pure culture to restore the microbial activity of the system. When COD removal rate reached 85% for two consecutive days, the restoring period ended, and the next experimental period began.

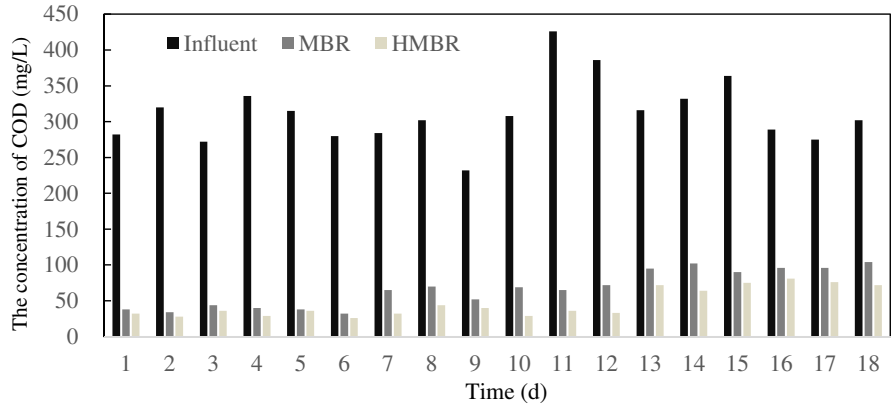


FIGURE 2
The concentrations of COD in influent, HMBR and MBR during different stages

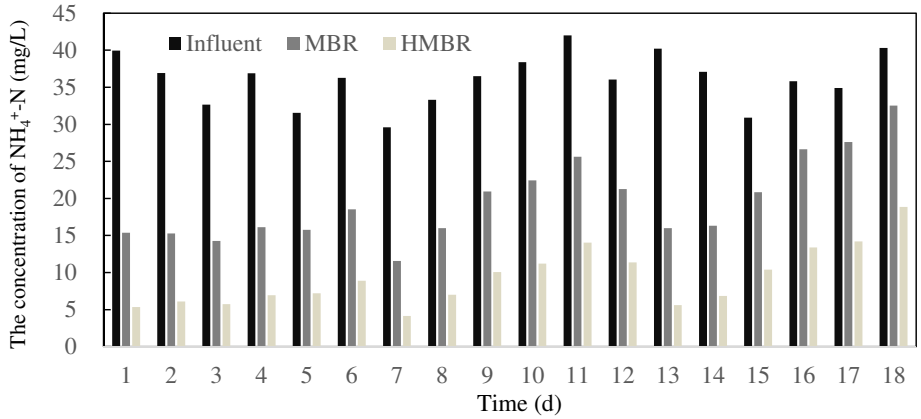


FIGURE 3
The concentrations of NH_4^+-N in influent, HMBR and MBR during different stages

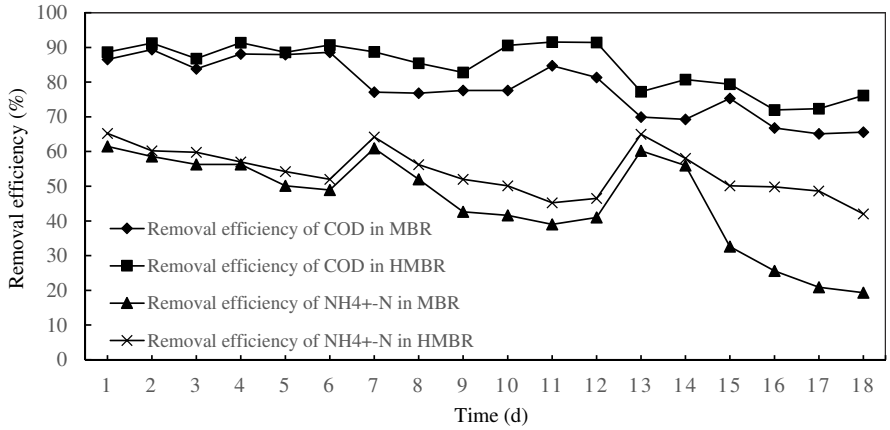


FIGURE 4
The COD and NH_4^+-N removal efficiency of HMBR and MBR processes in different stages

Seed Sludge. Seed sludges of the MBR and the hydrolysis reactor were from the Aerobic Stage in A/O Process and the sludge digestion workshop of a wastewater treatment plant in Harbin, respectively. At the start-up, the reactor run intermittently and COD was monitored, and then after the stable running of the system continuous water inflow was employed. At last, sludge concentrations in the hydrolysis reactor and MBR was kept around 8000 mg/L and 4500 mg/L, respectively.

Analysis Method. COD and NH_4^+-N were detected by using Chinese national standard method; MLSS and MLVSS were measured with gravimetric method; by using resin fractionation experiment, DOM was divided into 5 components, that were HPI, HPO-A, TPI-A, HPO-N, and TPI-N, which would be determined by a organic carbon analyzer (TOC-VCPN, Shimadzu, Japan); UV_{254} was measured with ultraviolet spectrophotometer (T6, Beijing Purkinje General Instrument Co., Ltd.) under the wavelength

of 254 nm; EPS, polysaccharide, and protein of aerobic sludge were detected by means of ammonia extraction, sulfuric anthrone reaction, and Lowry method, respectively; the microbial metabolism activity were determined by measuring the specific oxygen uptake rate (SOUR) (Oxi-3205SET1, TWT, Germany); membrane module was observed by using scanning electron microscope (SEM) (Quanta 200, FEI, USA)

RESULTS AND DISCUSSION

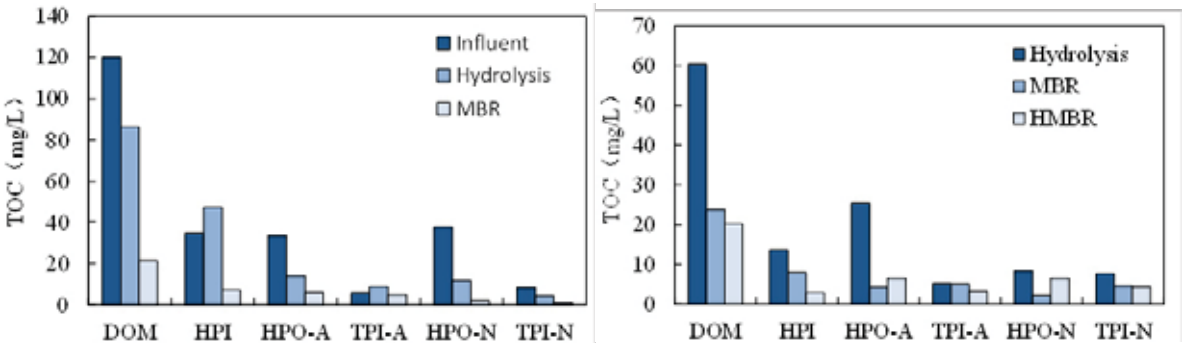
The impact of heavy metal could depress the microbial activity, and the ability of different microbe to tolerate heavy metal was different, which could be affected by the heavy metal impact in different ways. The influence of Cu^{2+} and Ni^{2+} on the HMBR process was investigated through pollutant removal rate, microbial activity, organic matter conversion, and membrane fouling. The main experimental results are as follows.

Effect of the impact load of heavy metals on treatment efficiency of COD and NH_4^+-N. Under different impact load of Cu^{2+} and Ni^{2+}, the removal efficiency of COD and NH_4^+-N in both HMBR and MBR process was shown in Fig.2, Fig.3 and Fig.4. In Fig.2, the influent COD was fluctuating between 260 mg/L and 426 mg/L, and average values of influent COD in three experimental periods were 301.0 mg/L, 323.0 mg/L, and 313.0 mg/L, respectively. Under the same condition, in the MBR process average values of effluent COD were 37.7 mg/L, 65.5 mg/L, and 97.2 mg/L, and average COD removal efficiencies were 87.7%, 79.2%, and 68.9%; in the HMBR process average values of effluent COD were 31.2 mg/L, 35.6 mg/L, and 73.3 mg/L, and average COD removal efficiencies were 89.6%, 88.4%, and 76.3%. According to the comparison between those results, in the first experimental period (the concentration of Cu^{2+} and Ni^{2+} was 5 mg/L) the difference of COD removal efficiency between two processes was little, because lower concentration of heavy metals had little effect on the microorganism, which would be quickly adsorbed by the microorganism. In the second experimental period (the concentration of Cu^{2+} and Ni^{2+} was 10 mg/L), the COD removal efficiency of the MBR process decreased rapidly, but the decrease amplitude of the COD removal efficiency of the HMBR process was relatively small. In the third experimental period (the concentration of Cu^{2+} and Ni^{2+} was 20 mg/L), the decrease amplitude of the COD removal efficiency of the MBR process further increased, and the difference of COD removal efficiency between two processes was enlarged. With the increase of the concentration of Cu^{2+} and Ni^{2+}, the COD removal efficiency in the HMBR process was above 75%, but the COD removal efficiency in the MBR process decreased to below 70%.

In Fig.3, the influent NH_4^+-N was fluctuating between 29.6 mg/L and 42 mg/L, and average values of influent NH_4^+-N in three experimental periods were 35.7 mg/L, 35.9 mg/L, and 36.5 mg/L, respectively. Under the same condition, in the MBR process average values of effluent NH_4^+-N were 15.9 mg/L, 19.6 mg/L, and 23.3 mg/L, and average NH_4^+-N removal efficiencies were 55.3%, 46.2%, and 35.8%; in the HMBR process average values of effluent NH_4^+-N were 6.7 mg/L, 9.6 mg/L, and 11.5 mg/L, and average NH_4^+-N removal efficiencies were 58.1%, 52.4%, and 52.3%. According to the comparison between those results, along with the prolonged operation and the increased heavy metal impact, the NH_4^+-N removal ability of both processes declined, which indicated that the longer the contact time between nitrifying bacteria and heavy metal ions was, the greater the inhibitory effect was, and nitrifying bacteria didn't have enough ability to resist heavy metal impact. In the second experimental period (the concentration of Cu^{2+} and Ni^{2+} was 10 mg/L), the effluent quality deteriorated rapidly: the NH_4^+-N removal efficiency of the HMBR and the MBR process was 50% and 40%, respectively. In the third experimental period (the concentration of Cu^{2+} and Ni^{2+} was 20 mg/L), when the concentration of heavy metals approached 20 mg/L, the NH_4^+-N removal efficiency of the MBR process was less than 20%, in which the system was going to break down, but the HMBR process was still with the NH_4^+-N removal efficiency of 45%. It's indicated that the buffer action of the hydrolysis reactor in the HMBR process could weaken the influence of heavy metal on the microbe in the aerobic zone, which kept better NH_4^+-N removal efficiency.

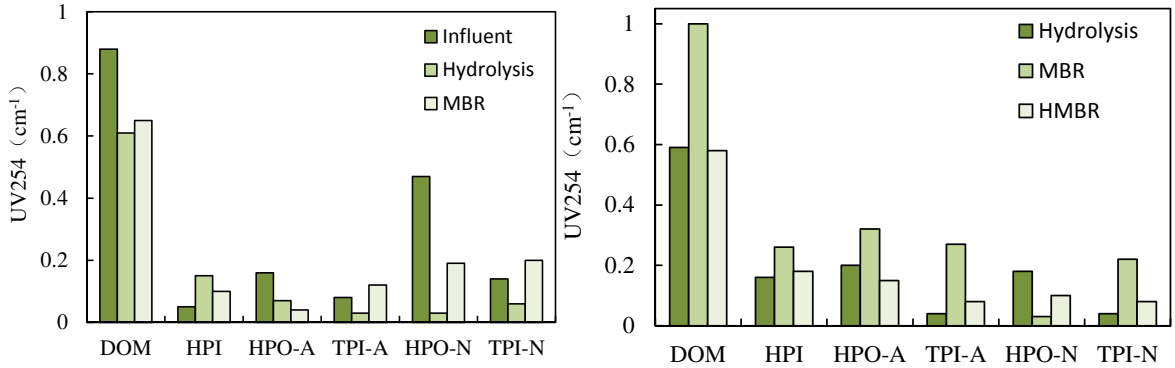
Effect of the impact load of heavy metals on dissolved organic matter in the system. Dissolved organic matter (DOM) comprises the following main components: humic substances, fulvic acids, hydrophilic organic acids, and some trace substance, such as carbohydrate and amino acids.

Recently, a lot of researchers holds that DOM could flocculate or adsorb heavy metals by bonding electrons, so DOM would play an important role in the biological treatment process of heavy metal wastewater. The change of DOM concentration in the effluent of both HMBR and MBR process at the beginning and end of the experiment was shown in Fig.5. It's shown in Fig.5 (a) that TOC removal efficiencies in the hydrolysis reactor and the MBR were 27.9% and 82.3%, respectively, which were coincident with COD removal efficiencies. The main components of TOC in the influent were HPI (29.0%), HPO-A (28.1%), and HPO-N (31.2%), which added up to 88.1%. Before the heavy metal impact (the concentration of Cu^{2+} and Ni^{2+} was 0 mg/L), the concentration of HPI in the hydrolysis reactor effluent



(a) Beginning（$Cu^{2+}$and Ni^{2+} were 0mg/L） (b) End（Cu^{2+} and Ni^{2+}were 20mg/L）

FIGURE 5
DOM in the effluent of HMBR and MBR processes



（a）Beginning（$Cu^{2+}$and Ni^{2+} were 0mg/L） （b）End（Cu^{2+} and Ni^{2+}were 20mg/L）

FIGURE 6
UV_{254} in the effluent of HMBR and MBR processes

further increased, but concentrations of HPO-A and HPO-N significantly reduced, both of which decreased by 50.6%. It's demonstrated that HPO-A (η=57.7%) and HPO-N (η=68.5%) were preferentially degraded in the hydrolysis, because HPO-A and HPO-N were hydrophobic and high molecular weight, which could be easily used by hydrolytic bacteria and were changed into hydrophilic small molecule organic acids (such as acetic acid) by the hydrolysis. The main component of DOM in the MBR effluent was HPI (84.6%). After the heavy metal impact (the concentration of Cu^{2+} and Ni^{2+} was 20 mg/L), the main component of DOM in the hydrolysis reactor was HPO-A (42.1%), and the HPI content significantly decreased, which removal efficiency was 32%. It's indicated that most of HPI in the water was converted into HPO-A after the heavy metal impact. Before the impact, the main components of MBR effluent were HPI, HPO-A, and TPI-A, and the concentrations of HPO-N and TPI-N were extremely low, which indicated that the biodegradation could effectively remove HPO-N and TPI-N. The effluent TOC of the HMBR process was lower the one of the MBR process, which was similar to the COD removal; and the main component of the MBR effluent was HPI (33.4%), but the main components of the HMBR effluent were HPO-A (32.4%) and HPO-N (32.4%). There was mainly hydrophobic substance in the HMBR effluent, but there was mainly hydrophilic substance in the MBR effluent. Considering that surfactant, fixative and brightener were all hydrophilic substances, the HMBR process should be more suitable for the treatment of wastewater containing more hydrophilic substances.

The change of UV_{254} in the effluent of both HMBR and MBR process at the beginning and end of the experiment was shown in Fig.6. It's shown in Fig.6(a) that the main component of UV_{254} in the influent was HPO-N (53.4%), which indicated that aromatic organics in the influent were mainly from HPO-N. 36.1% of UV_{254} in the influent was removed in the hydrolysis reactor, which indicated that a part of aromatic substances could be removed by the hydrolysis; but UV_{254} in the MBR effluent was 6.6% higher than in the hydrolysis effluent, which indicated that aromatic substances could accumulate in the MBR, and the degradation of UV_{254} in the HMBR process was mainly in the hydrolysis reactor. The main component of UV_{254} in the hydrolysis effluent was HPI (24.5%), and the hydrolysis process had the best treatment effect on HPO-N, the removal efficiency of which was 93.61%. The effluent situation after the heavy metal impact (the concentration of Cu^{2+} and Ni^{2+} was 20 mg/L) was shown in Fig.6 (b). It's discovered that the aromatic content in the

hydrolysis effluent after the impact significantly decreased, which could be due to the increase of microbial activity by the stimulation of heavy metals. The main components of UV_{254} in the MBR effluent were TPI-A, HPO-N, and TPI-N, whose content obvious increased comparing with the hydrolysis reactor because of the transformation of HPI and TPI-A. It should be recognized that the TPI-A content in the MBR effluent was higher than the one in the influent, which indicated that TPI-A had poor biodegradability and easily accumulated in the biological treatment unit. It's was shown in Fig.5 (b) that after the heavy metal impact the content of aromatic substances in the MBR effluent was almost twice as much as that in the HMBR effluent, and the content of aromatic substances in the HMBR effluent was slightly lower than in the hydrolysis effluent, which indicated that the aerobic treatment unit had poor degradability of aromatic substances.

Effect of the impact load of heavy metals on the activity of aerobic sludge in the system. The specific oxygen uptake rate (SOUR) was an important index to evaluate the microbial metabolism activity of sludge, and change of system influent characteristics and sludge characters would be judged by observing the change of SOUR at different time. The change of SOUR under the heavy metal impact with different concentrations in both HMBR and MBR process was shown in Fig.7.

It's shown in Fig.7 that during three experimental periods, SOUR values in the MBR process were 18.62 $mgO_2/(gVSS·h)$, 16.02 $mgO_2/(gVSS·h)$, and 12.58 $mgO_2/(gVSS·h)$ with the inhibitory rate of 5.1%, 15.4%, and 35.22%, respectively; but SOUR values in the HMBR process were 19.10 $mgO_2/(gVSS·h)$, 17.28 $mgO_2/(gVSS·h)$, and 14.01 $mgO_2/(gVSS·h)$ with the inhibitory rate of 4.4%, 11.9%, and 27.18%, respectively. It's indicated that the SOUR value of activated sludge in the MBR was declining along with the increase of heavy metal concentration. As the impact load of heavy metals increased, the decreased value of SOUR in the HMBR process was far less than that in the MBR process, and all the inhibitory rates of the HMBR process in the three experimental periods were almost 5% less than that of the MBR process; and the SOUR value of the HMBR process in the third experimental period (the concentration of Cu^{2+} and Ni^{2+} was 20 mg/L) was close to the SOUR value of the MBR process in the second experimental period (the concentration of Cu^{2+} and Ni^{2+} was 10 mg/L), which indicated that the HMBR process had a greater capability for resistance to impact loads. It's principally because the microbe in the hydrolysis reactor could adsorb some heavy metal ions, or be stimulated by heavy metals and secrete a lot of EPS to chelate heavy metals, which would decrease the concentration of heavy metal, relieve toxic effects of heavy metals, and protect the microbe in the subsequent aerobic unit as much as possible.

Effect of the impact load of heavy metals on the EPS of aerobic sludge in the system. The extracellular polymer substances (EPS) was formed by bacterial secretion, main components of which were protein and polysaccharide. In many studies, it's suggested that heavy metal could stimulate the aerobic microorganisms to secrete more EPS in order to reduce the toxicity of heavy metal [20,21], and EPS was the key factor influencing the membrane fouling in the MBR process. Polysaccharide was one of the main components of sludge EPS, which would affect the membrane fouling in the MBR process greatly. Variation of the polysaccharide in the effluent before and after the heavy metal impact was shown in Fig.8.

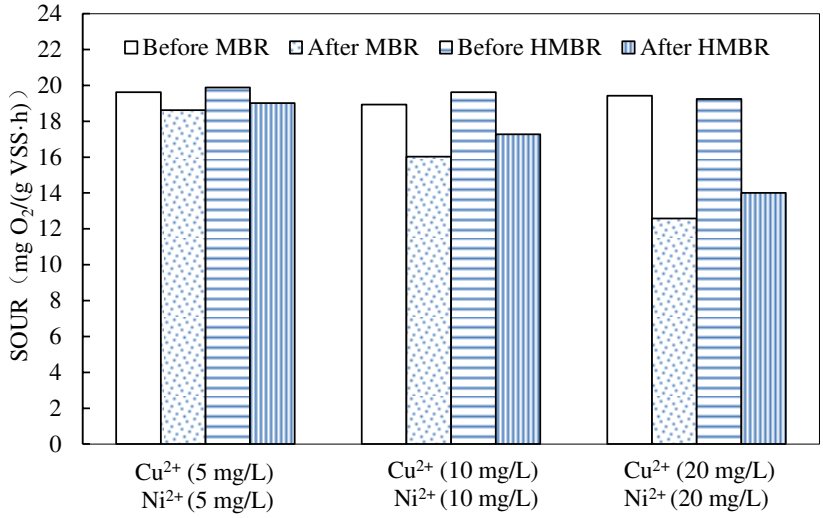
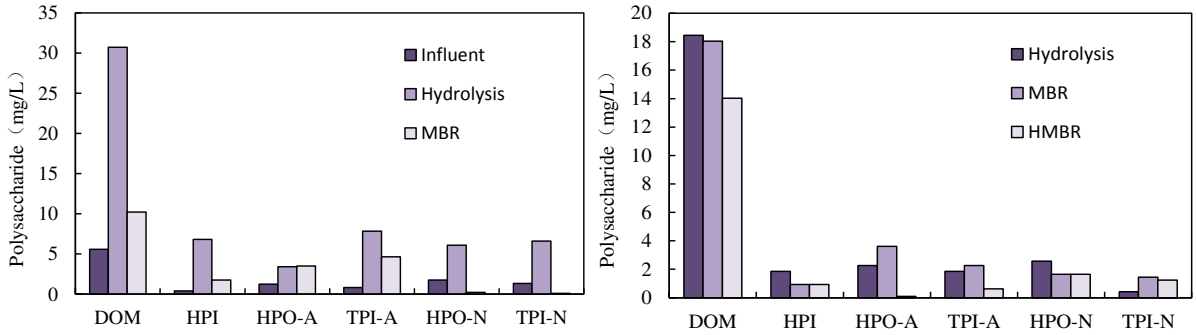
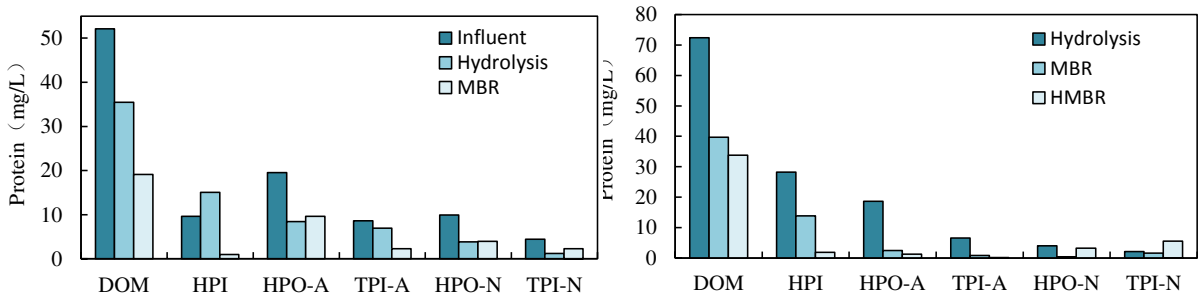


FIGURE 7
Effect of heavy metals on activated sludge SOUR



（a）Beginning（$Cu^{2+}$and Ni^{2+} were 0mg/L） （b）End （Cu^{2+} and Ni^{2+}were 20mg/L）

FIGURE 8
Polysaccharide in the effluent of HMBR and MBR processes



（a）Beginning（$Cu^{2+}$and Ni^{2+} were 0mg/L） （b）End（Cu^{2+} and Ni^{2+}were 20mg/L）

FIGURE 9
Soluble protein in the effluent of HMBR and MBR processes

It's shown in Fig.8 that polysaccharide mainly distributed in HPO-A (22.2%), HPO-N (31.5%), and TPI-N (24.1%). The concentration of polysaccharide in the hydrolysis effluent achieved 30.72 mg/L, which was nearly 6 times as much as that in the influent (the concentration of polysaccharide in the influent was 6.21 mg/L), since organic particles suspended in water were dissolved by the hydrolysis, which caused the significant increase to the concentration of polysaccharide. After the heavy metal impact, the concentration of polysaccharide in the hydrolysis reactor was only 18.21 mg/L, because the toxicity of heavy metal made the microbial activity in the hydrolysis reactor decrease substantially, thereby reducing the hydrolysis efficiency, and thus the dissolution rate of polysaccharide slowed down. Before the heavy metal impact, MBR had the high removal effect on dissolved polysaccharide, and the removal efficiency achieved 66.7%, but the concentration of polysaccharide in the MBR was 1.83 times that in the influent. Because particles was transformed into a number of polysaccharides by the hydrolysis, which made the concentration of polysaccharide increase in the hydrolysis effluent. In the MBR process, the content of polysaccharide from high to low ranked as follows: TPI-A (45.5%) > HPO-A and HPI > HPO-N and TPI-N, which indicated that MBR had better removal effect on neutral organic compound. After the heavy metal impact (the concentration of Cu^{2+} and Ni^{2+} was 20 mg/L) comparing with the concentration of polysaccharide in the MBR effluent, that in the HMBR effluent was lower, because the heavy metal impact made the sludge EPS in the MBR secrete more substances, and in the HMBR process under the protection of the hydrolysis reactor the microorganism had higher activity and better removal capacity, which could remove most of polysaccharides. In the MBR effluent HPO-A and TPI-A were the main ingredients, but in the HMBR effluent HPO-N and TPI-N were the main ingredients, which indicated that the HMBR process had a fine removal effect on both hydrophilic and over-hydrophilic organics.

Protein was one of the main components of EPS, too. The microbial activity in the sludge could to some extent be determined by measuring the concentration of protein dissolved in water. Variation of the protein in the effluent before and after the heavy metal impact was shown in Fig.9.

It's shown in Fig.9 that dissolved protein in the influent distributed uniformly; HPO-A was the most abundant (37.5%), TPI-N was the least (8.5%), and other three components had similar contents (about 18%). After the influent went through the hydrolysis reactor, the concentration of dissolved protein decreased 16.6 mg/L, because HPO-A, HPO-N, and TPI-N were substantially dissolved, which indicated that the hydrophobic protein was removed before the hydrophilic protein in the hydrolysis reactor. After the heavy metal impact (the concentration of Cu^{2+} and Ni^{2+} was 20 mg/L), the concentration of protein in the hydrolysis effluent significantly increased to

72.62 mg/L, which was 1.4 times that before the impact, because microorganisms secreted amounts of protein to combine with heavy metal ions, which reduced the bio-toxicity of heavy metal. After the heavy metal impact, HPI and HPO-A were the main components in the hydrolysis reactor, and other three components were with very low concentrations, which indicated that after the impact neutral substances were removed first. Before the impact, HPI had an extremely low concentration in the MBR, most of which was degraded, but the concentration of HPO was even higher than that in the hydrolysis effluent. After the impact, the treatment efficiency of the HMBR process was far higher than that of the MBR process, because the hydrolysis didn't only increase small molecule protein in water and the concentration of organic substrates, but also reduced the toxicity of heavy metals, which kept microbial activity much higher in the HMBR process. Furthermore, the protein in the HMBR process was mostly found in HPO-N and TPI-N, but in the MBR process was mostly found in HPI, which indicated that hydrophilic organic acids were preferentially degraded in the HMBR process.

CONCLUSIONS

Under the impact of Cu^{2+} and Ni^{2+}, the HMBR process had much better removal effect on COD and NH_4^+-N than the MBR process, in which the removal efficiency of COD and NH_4^+-N were above 75% and 45%, respectively. The increase of heavy metal concentration caused the big difference of removal efficiency between two processes, and nitrifying bacteria had poor impact resistance to heavy metals, so the NH_4^+-N removal efficiency was affected more by heavy metals. The HMBR process could endure 20 mg/L Cu^{2+} and Ni^{2+}, but the maximum tolerance of the MBR process was only 10 mg/L.

The HMBR process was suitable for treating wastewater containing more hydrophilic substances. After the heavy metal impact, the hydrolysis reactor could transform most of HPI in the sewage into HPO-A, thus improving the biodegradability of refractory organics, and the content of aromatic compounds decreased significantly. The HMBR effluent was mainly made up of hydrophobic substance, but the main component of the MBR effluent was hydrophilic substance, in which the content of aromatic compounds was almost twice that in the HMBR effluent.

Along with the increase of the concentration of Cu^{2+} and Ni^{2+}, the SOUR value in the MBR was declining, but the decrease of the SOUR value in the HMBR process was much less than the one in the MBR process, and the inhibition rate of SOUR in the HMBR process was nearly 5% lower than the one in the MBR process. Microorganisms in the hydrolysis reactor could adsorb some of heavy metal ions, or secrete a lot of EPS to chelate heavy metals, which reduced the heavy metal content and the bio-toxicity of heavy metal, protected microbes in the following aerobic unit, and demonstrated that the HMBR process displayed better resistance to impact load.

After the heavy metal impact, the hydrolysis reactor reduced the bio-toxicity of heavy metal because microorganisms secreted amounts of protein to combine with heavy metal ions, which caused that the protein concentration of the hydrolysis effluent increased significantly, and the dissolution rate of polysaccharide was slowed down by the decrease of microbial activity. Because the hydrolysis could reduce the toxicity of heavy metal, the HMBR process had better microbial activity, less EPS content, and lower effluent concentration than the MBR process.

Comparing with the MBR process, the HMBR process could prevent the formation of colloid substances and DOM on the membrane surface efficiently by buffer action of the hydrolysis reactor, which could slow the formation of sludge cake layer down. The HMBR process had less cake layer and slower membrane fouling rate than the MBR process, which could effectively extend the lifecycles of the membrane module.

ACKNOWLEDGEMENTS

This study was supported by the Postdoctoral Research Foundation of Heilongjiang Province (No.LBH-Q16132) and the Major Science and Technology Program for Water Pollution Control and Treatment (No.2013ZX07201-007). The authors would like to express their sincere thanks for the financial support in the process of accomplishing this study.

REFERENCES

[1] Feng, B., Fang, Z., Hou, J. (2013) Effects of heavy metal wastewater on the anoxic/aerobic-membrane bioreactor bioprocess and membrane fouling. Bioresource Technology. 142, 32-38.

[2] Labanowski, J., Feuillade, G. (2009) Combination of biodegradable organic matter quantification and XAD-fractionation as effective working parameter for the study of biodegradability in environmental and anthropic samples. Chemosphere. 74(4), 605-611.

[3] Shi, T., Wang, Z., Liu, Y. (2009) Removal of hexavalent chromium from aqueous solutions by D301, D314 and D354 anion-exchange resins. Journal of Hazardous Materials. 161(2-3), 900-906.

[4] Rajagopal, R., Beline, F. (2011) Anaerobic hydrolysis and acidification of organic substrates: Determination of anaerobic hydrolytic potential. Bioresource Technology. 102(10), 5653-5658.

[5] Orozco, A.F., Contreras, E.M., Zaritzky, N.E. (2010) Cr (VI) reduction capacity of activated sludge as affected by nitrogen and carbon sources, microbial acclimation and cell multiplication. Journal of hazardous materials. 176(1), 657-665.
[6] Saha, B., Orvig, C. (2010) Biosorbents for hexavalent chromium elimination from industrial and municipal effluents. Coordination Chemistry Reviews. 254(23-24), 2959-2972.
[7] Mehmood, C.T., Batool, A., Qazi, I.A. (2013) Combined Biological and Advanced Oxidation Treatment Processes for COD and Color Removal of Sewage Water. International Journal of Environmental Science and Development. 4(2), 88-93.
[8] Gao, D., Li, X.X., An, R., Fu, Y. and Ren, N.Q. (2010) Relationships between microbial community structure and the performance of MBR under different dissolved oxygen. China Environmental Science 31(2), 209-215.
[9] Liu, X.C., Liang, J., Xia, S.Q. (2017) Large full-scale application of membrane technology for water reclamation in Wuxi, China-case study. Fresen. Environ. Bull. 26(2A), 1791-1799.
[10] Lai, R. (2009) Study on treatment of the organic contamination in plating wastewater. South China University of Technology. 60.
[11] Lu, D.F., Xu, L.Z., Guo, Y.F. (2014) Treatment of actual electroplating tail water with hydrolytic acidification and innovated A/O process. Technology of Water Treatment. 40(9), 89-92.
[12] Li, E.C., Jin, X.W., Wu, S. (2016) An anoxic/oxic mebrane bioreactor for the treatment of concentrated cold-rolling wastewater from reverse osmosis process. Fresen. Environ. Bull. 25(1), 67-77.
[13] Yang, Y.F., Xia, S.Q., Hermanowicz, S.W. (2015) Full-scale engineering application of mbr system in municipal wastewater treatment plants around china's tai lake basin. Fresen. Environ. Bull. 24(11), 3616-3626.
[14] Amin, M.M., Bina, B., Hajizadeh, Y., Ebrahimi, A., Ghanbari, R. (2015) Feasibility of lab-scale vacuum-driven submerged hollow fiber anaerobic membrane bioreactor (SAnMBR) for the treatment of synthetic acidified wastewater. Fresen. Environ. Bull. 24(6A), 2220-2231.
[15] Huang, T.S., Jia, R.Y., Xia, S.Q. (2014) Effect of various parameters on microbial communities in membrane bioreactors treating municipal wastewater. Fresen. Environ. Bull. 23(4), 976-985.
[16] Zhang, J., Wang, P., Huang, F. (2014) Preparation and characterization of polyacrylonitrile/bentonite blend membrane for wastewater treatment. Fresen. Environ. Bull. 23(2), 455-462.
[17] Semerci, N., Cecen, F. (2007) Importance of cadmium speciation in nitrification inhibition. Journal Of Hazardous Materials. 147(1-2), 503-512.
[18] You, S., Tsai, Y., Huang, R. (2009) Effects of Heavy Metals on the Specific Ammonia and Nitrate Uptake Rates in Activated Sludge. Environmental Engineering Science. 2009, 26(7), 1207-1215.
[19] Labanowski, J., Feuillade G. (2009) Combination of biodegradable organic matter quantification and XAD-fractionation as effective working parameter for the study of biodegradability in environmental and anthropic samples. Chemosphere. 74(4), 605-611.
[20] Chen, W., Sun, F.Y., Wang, X.M. (2010) A membrane bioreactor for an innovative biological nitrogen removal process. Water Science and Technology. 61(3), 671-676.
[21] Fu, Z.M., Yang, F.L., Zhou, F.F. (2009) Control of COD/N ratio for nutrient removal in a modified membrane bioreactor (MBR) treating high strength wastewater. Bioresource Technology. 100(1), 136-141.

Received: **30.06.2017**
Accepted: **01.10.2017**

CORRESPONDING AUTHOR

Guangzhi Wang
School of Environment
Harbin Institute of Technology
Harbin 150090 – P. R. China

E-mail: hlk1980@163.com

© by PSP Volume 26 – No. 12A/2017 pages 8078-8083 Fresenius Environmental Bulletin

COMPARISON OF DAMAGE MECHANISM FOR TC4 BLADE OF STEEL BALL AND SAND SHOCK

Zhu Guanfang[1,*], Zhang Zhongping[1], Gao Pengpeng[2], Li Chunwang[1], Kang Yifan[1,3], Liu Jing[1]

[1]Institute of Science, Air Force Engineering University, Xi'an, 710051, China
[2]ESP Research Centre, Xi'an Shiyou University, Xi'an, 710075, China
[3]Institute of photonics and photon-technology, Northwest University, Xi'an, 710069, China

ABSTRACT

In this paper, the damage of common objects such as steel ball and sand on the aeroengine blader is studied. One level rotor-blade is considered as a research object on the basis of the Kinematic hardening plastic constitutive model, using the ANSYS / LS- DYNA software to simulate the shock from each one of ten balls and sands of different sizes and speed respectively. The impact of the relative kinetic energy, size of steel ball and sand shock on the size and shape of shock gap are analyzed carefully. A detailed comparison on the impact of the gap is made to or ball and its rough size that may be initially determined by characteristic of shock gap. The gap can be used to determine whether the external material is steel or gravel and the approximate size range.

KEYWORDS:
Steel ball, sand shock, the aeroengine blader damage, Kinematic hardening plastic constitutive model

INTRODUCTION

It is often subjected to high-speed air into the engine with outside objects (such as gravel, metal blocks, etc.) damage when aero engine blades work, this foreign object impact damage (Foreign object damage) referred to as FOD, which is easy to produce environmental pollution waste, causing pollution to the environment, and the aircraft releases many high concentrations of pollutants, such as nitrogen oxides, less than 0.1 microns in diameter fine particles, etc., constitute a harm to human health. The exhaust gas from the aircraft is cooled and solidified to form fine particles that can be sucked into the lungs of the human body and can even enter the blood circulation, form oxidative stress in the blood vessels, induce inflammation, cause atherosclerosis or obstruction of artery. There are heart and lung disease, asthma, the crowd, it will lead to other physical deterioration of their health [1-3]. FOD produced by the stress concentration, residual stress, microstructure damage weaken the blade of the high cycle fatigue resistance, which makes frequent high-frequency vibration of the leaves in the engine design life or inspection cycle facing the risk of premature failure.

When the airplane takes off, landed or low altitude, the outside object is easily sucked into the airflow through the powerful attraction of the engine intake airflow, impinging on the fan / compressor blades or other parts at the front of the engine, bringing the adverse effects on performance or structure of the engine, or even very serious consequences. The study of damage to the engine at home and abroad is mainly focused on the transient response during the impact process, and the residual stress of the blade after the impact and the effect on the fatigue life [4, 5]. In addition, it is necessary to the study identification of the damage to the leaves of foreign objects in order to reduce serious failure or accident caused by the FOD, preventing outside object damage and airport maintenance.

Hamilton [6], Chen [7], Weeks et al. [8], Oakley [9], Tranter et al. [10] and Duó [11] used commercial dynamics analysis software (MSC / DYTRAN or LS- The finite element numerical simulation is carried out to verify the feasibility of this problem based on ANSYS / LS - DY NA nonlinear finite element analysis method. The Johnson-Cook model [9] (including constitutive models and failure models) used by Oakley is an empirical material model; the modified Zerilli-Armstrong constitutive model used by Tranter et al. [10]; the Bammann model used by Duó et al. [11] Is a viscoplastic coupling damage material model; Oakley, Tranter and Duó and other research results that the respective use of the material model can be a good simulation of FOD damage. Liu Xiyang [12] compared the Johnson-Cook material model and the follow-up plastic material model, and found that the follow-up plastic material model can better describe the dynamic tensile behavior of titanium alloy. Chen Min [13] compares the follow-up plastic constitutive model with the modified Zerilli-Armstrong constitutive model and the Johnson-Cook model, indicating that the follow-up plastic constitutive model can better describe the dynamic mechanical

properties of TC4 materials at room temperature.

Therefore, this paper takes the rotor of a certain type of aeroengine titanium alloy as the research object, uses the large nonlinear ANSYS / LS - DY NA finite element program, and uses the plastic material model of the titanium alloy to compare the different radius and different speed Damage Law and Characteristics of Ball and Sand and Gravel on Blade's Air Intake.

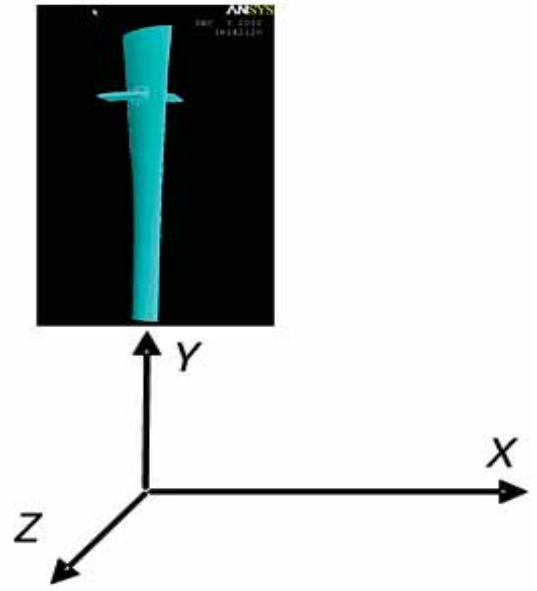


FIGURE 1
Leaf reference system and coordinate system

MATERIALS AND METHODS

The plasticized hardening constitutive equation [14] is:

$$\sigma_y = \left[1+\left(\frac{\dot{\varepsilon}}{C}\right)^{\frac{1}{P}}\right]\left(\sigma_0 + \beta E_p \varepsilon_p^{eff}\right) \quad (1)$$

$\varepsilon_p^{eff} = \int_0^t (\frac{2}{3}\dot{\varepsilon}_{ij}^p \dot{\varepsilon}_{ij}^p)^{\frac{1}{2}} dt$, $\dot{\varepsilon}_{ij}^p = \dot{\varepsilon}_{ij} - \dot{\varepsilon}_{ij}^e$, $E_p = \frac{EE_t}{E-E_t}$ and ε_p^{eff} are equivalent plastic strain; $\dot{\varepsilon}$ is strain rate; E_p is hardened plasticity modulus. The plasticity hardening model consists of two parts. The first half describes the effect of the strain rate on the dynamic yield stress. The latter part describes the effect of the plastic hardening process on the dynamic flow stress. The model determines the failure of the material by defining the failure plastic strain ε_f if the equivalent plastic strain is greater than the failure plastic strain, is $\varepsilon_p^{eff} > \varepsilon_f$ so the material will fail. β $(0 \le \beta \le 1)$ is hardening parameters, used to reflect the material isotropic hardening, with the hardening and mixing hardening, when $\beta = 0$ or $\beta = 1$, which expresses hardening and isotropic hardening, respectively.

In general, the hard objects that hit the blades are the gravel on the pavement of the airport or the ball that falls on the runway. The impact process takes place during the take-off and landing of the airplane. Therefore, the state of the study is determined as the state of the engine when the aircraft took off and landing, namely, the maximum acceleration state of the engine, when the blade rotation angle of 1036rad / s, and the state corresponds to the largest air flow, the engine speed maximum, the relative speed of foreign objects and leaves the largest, the same size, material, The greatest damage. Therefore, the maximum afterburner state of the engine is selected as the research state, and the process of impinging the ball and sandstone into the air inlet is simulated. The damage caused by the same position and velocity of the different radius and velocity is compared. The model is shown in Fig. 1, the length of the blade is 264.15 mm, the leaf distance is 182.5 mm from the central axis, and the angular velocity of the blade is 1036rad / s. The impact point is 210.35 mm from the root of the blade, 392.85 mm from the center point, the relative velocity v_z of the tangential direction is multiplied by the distance between the impact point and the central axis by 407 m / s, and the velocity of the blade along the x-axis with the plane is 77.8 m / s. The ball and sand are along x Axis forward speed v_1.

According to $v_0 = \sqrt{\frac{9800HS}{m}}$, $4.3 = \frac{m}{193S}\left[v_0 - v_1 + 180\ln\frac{180-v_0}{180-v_1}\right]$ calculated [15], so the sand relative to the aircraft in the x direction of the speed is $V_x = V_1 + 77.8$ m/s. And the axial velocity of the impacted blade is consistent with the velocity of the airflow. The relative velocity of the relative leaf is relative to the leaf is $v_r = \sqrt{v_x^{\ 2} + v_z^{\ 2}}$.

As the engine blades in the work, with a high rotational speed, at this time suffered the impact of foreign objects, due to rotation caused by the centrifugal stress on the impact of the damage process may have an impact. Therefore, the implicit-explicit sequence is used to obtain the initial stress (preload) of the model using the implicit solver, and then the initial stress is added to the structure before the explicit dynamic analysis. The initial stress affects the dynamic response of the analyzed structure will be included in the explicit analysis.

In the simulation process, a symmetrical penalty function contact algorithm is used between the blade and the steel ball, or between the sand and the sand, to define the point-to-surface contact, and the contact stiffness factor is set to 0.7. Using SOLID164 unit on the leaves, the titanium alloy leaves and steel ball model grid. Leaf grid edge

length 0.9mm, divided a total of 659187 units, the ball and sand and the size of the grid and the number of units according to the radius of slightly different. From the radius of 0.5mm on the 1st ball and sand, according to the radius of 0.5mm in order to increase the ten kinds of steel balls and sand as the object, the calculation of the respective different relative axial speed.

Table 1 is calculated parameters and material parameters. Data listed in the table, $E(10^9)$, $\sigma_0(10^9)$, ε_f and ν are from the literature [5]. Considering that the mass density of alloy steels in China is about 7800kg m^{-3}[6], the sixth data tangent moduli are derived from the literature [7], and the seventh data hardening parameters and the strain rate parameters of titanium alloys C and P are derived from the literature [2].

In Table 2, 3 separately the different radius and velocity of the ball and hit the sand leaves the gap created by the depth and width of the table for the v_x and v_z for the axial velocity, tangential velocity, the relative velocity is v_r, 1-4 respectively for steel ball and sand impacting blades, positive side gap morphology and morphology.

TABLE 1
Calculates parameters and material parameters

Parameter	$E(10^9)$	$\sigma_0(10^9)$	ρ	ν	ε_f	$E_t(10^9)$	β	C	P
Ti alloy	112.5	0.95	4500	0.33	0.18	1.125	0	153589	4.73
Steel ball	210.0	1.62	7800	0.30	0.06	$20e^9$	0	40	5
Sand	40	4	2800	0.20	0.0135	4	0	0	0

TABLE 2
Damage to the blades of steel balls with different radii and velocities

Number	Radius (10^{-3}m)	Axial relative speed v_x (m/s)	Tangential speed v_z (m/s)	Relative speed v_r (m/s)	Depth D (mm)	Width W (mm)	Thickness h (mm)	The speed of the ball after impact v_g (m/s)
1	0.5	225.1	407	465.1	0	0	0.7	359
2	1.0	198.7	407	452.9	2.2	2.0	0.8	191
3	1.5	183.1	407	446.3	4.7	3.7	0.9	228
4	2.0	172.5	407	442.0	6.9	4.1	1.1	292
5	2.5	164.7	407	439.1	6.4	5.8	1.0	377
6	3.0	158.6	407	436.8	6.9	6.4	1.1	390
7	3.5	153.7	407	435.1	9.0	6.6	1.4	386
8	4.0	149.6	407	433.6	10.7	7.0	1.5	385
9	4.5	146.2	407	432.5	12.4	7.9	1.7	390
10	5.0	143.2	407	431.5	13.4	8.9	1.8	395

TABLE 3
Damage to the leaves of sand at different radii and speeds

Number	Radius (10^{-3}m)	Axial relative speed v_x (m/s)	Tangential speed v_z (m/s)	Relative speed v_r (m/s)	Depth D (mm)	Width W (mm)	Thickness h (mm)	The speed of the ball after impact v_g (m/s)
1	0.5	252.8	407	479.1	0	0	0.7	477
2	1.0	237.5	407	471.2	0	0	0.7	465
3	1.5	224.1	407	464.6	0	0	0.7	457
4	2.0	213.4	407	459.6	0	0	0.7	451
5	2.5	204.7	407	455.6	2.1	4.4	0.8	449
6	3.0	197.6	407	452.4	3.2	5.6	1.0	444
7	3.5	191.6	407	449.8	6.3	7.2	1.2	430
8	4.0	186.5	407	447.7	8.1	8.8	1.4	424
9	4.5	182.1	407	445.9	8.6	9.9	1.4	427
10	5.0	178.1	407	444.3	10.0	10.5	1.5	424

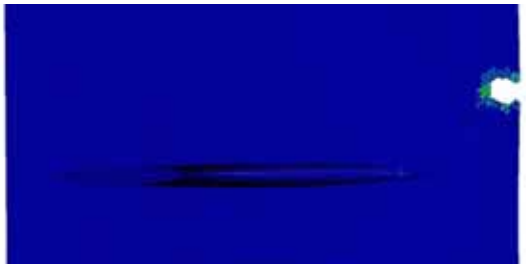


FIGURE 2
No. 3 steel ball impact side effect map

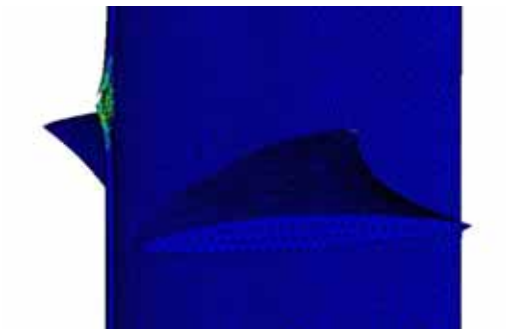


FIGURE 3
No. 3 steel ball impact side effect map



FIGURE 4
No. 5 sand impact side effect map



FIGURE 5
No. 5 Impact of gravel impingement

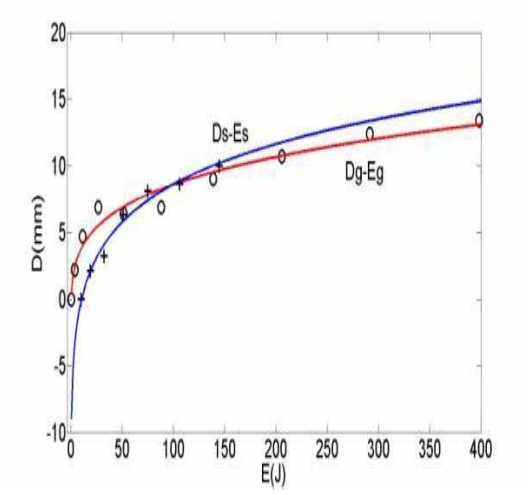


FIGURE 6
Relative energy and impact depth of ball and sand and gravel D-E curve

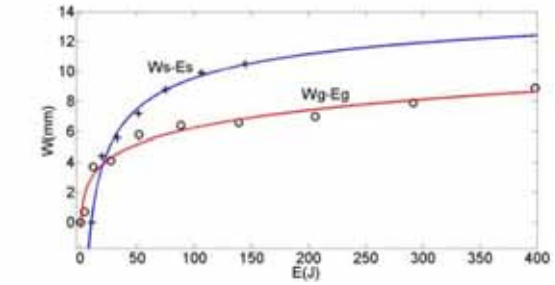


FIGURE 7
Relative energy and impact width of steel ball and gravel W-E curve

TABLE 4
Ratio of depth and width of ball and sand impact craters

Number	1	2	3	4	5	6	7	8	9	10
Steel ball (D/W)	-	3.14	1.27	1.34	1.1	1.08	1.36	1.53	1.57	1.51
Gravel (D/W)	-	-	-	-	0.47	0.57	0.875	0.92	0.89	0.95

TABLE 5
Ratio of ball and sand crater width and outer radius

Number	1	2	3	4	5	6	7	8	9	10
Steel ball (D/W)	-	2	2.47	2.2	2.32	2.13	1.89	1.75	1.76	1.78
Gravel (D/W)	-	-	-	-	1.76	1.87	2.06	2.2	2.2	2.1

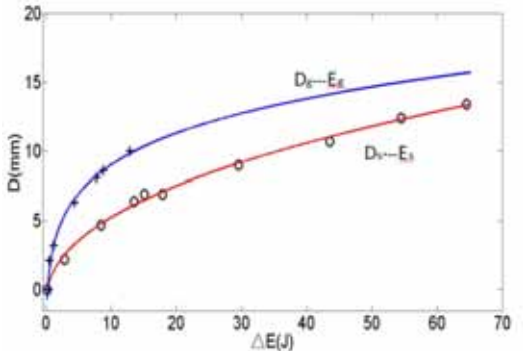


FIGURE 8
The relative energy difference between ball and sand and gravel and the depth of impact D-ΔE curve

RESULTS AND DISCUSSION

Table 2 and 3 show the size of the foreign matter, the speed of impact damage have an impact. Therefore, using the concept of relative kinetic energy [16, 17], the blade is used as the reference frame, the velocity of the impactor relative to the blade Vr, the kinetic energy of the impactor relative to the blade $E_r = \frac{1}{2} m V_r^2$

$D_g=3.648E_g^{0.2437}-2.618$ (2)
$W_g=8.989E_g^{0.1085}-8.557$ (3)
$D_s=29.75E_s^{0.09263}-36.97$ (4)
$W_s=-37.69E_s^{-0.3574}+16.83$ (5)
$D_g=2.324\triangle E_g^{0.4393}-1.176$ (6)
$W_g=3.211\triangle E_g^{0.2977}-2.335$ (7)
$D_s=17.67\triangle E_s^{0.1317-}14.92$ (8)
$W_s=-6.342\triangle E_s^{-0.5067}+11.49$ (9)

The data from Tables 4 and 5 and (2) - (9) and Figures 6, 7 and 8 show the following:

1. Formulas (2)-(5) show the relative kinetic energy of different materials, the impact of the depth of the impact of the gap and the width of the leaves,and we can see that whether it is steel or sand, the damage degree of the leaves increases exponentially with the increase of relative kinetic energy.

2. From Table 4, when the radius is in the range of 0.5 mm< r ≤5 mm, the relationship D >W is always present for all the steel balls, but the relationship D <W is always present for all the sands with the sharp shape of the crater. For the radius of less than 5mm of steel balls and sand, according to the depth of the two craters and the width of the ratio can be roughly determine the material outside the material. This shows the impact of foreign material on the shape of the pit.

3. It can be seen from Table 5 that the width of the striking blade gap of the ball and the gravel is greater than the radius of the foreign object itself, and their ratio () and radius are related to the relative energy. For the ball, when the radius is less than or equal to 3mm (or energy less than 82.7J), greater than or equal to 2; radius greater than 3mm (or energy greater than 82.7J), the ratio is less than 2. For gravel, when the radius is less than 3mm (energy less than 32.3J), less than 2; damage.

CONCLUSIONS

In this paper, the effects of ball and sand at different speeds and radii on the damage of leaves were studied by simulating the impact of foreign objects on the damage of the leaves. The relationship between the kinetic energy and the depth and width of the opposed beads was compared and compared. They hit the characteristics of the gap.

The simulation results provide a reference for the study of the damage law of the titanium alloy blade impacted by foreign objects. It is suitable for the field maintenance of the engine maintenance and the external field to reduce the damage and reduce the damage of the blade.

ACKNOWLEDGEMENTS

This work was supported by the National Natural Science Foundation of China (Grant No. 51575524) and National Natural Science Foundation of Shaanxi Province (Grant No. 2015JM5240).

REFERENCES

[1] Goudarzi, G., Alavi, N., Idani, E., Babaei, A.A., Salmanzadeh, S. and Mohammadi, M.J. (2017) Association of particulate maters attributed to outdoor air in Ahvaz, Iran during cold-warm season of 2017. Fresen. Environ. Bull. 26, 5428-5433.

[2] Tsakalidis, A. and Exarchou, E. (2017) The impact of the urban road networks' functional and traffic characteristics on air pollution: the case of thessaloniki, Greece. Fresen. Environ. Bull. 26, 5608-5615.

[3] Dagiliute, R., Kersiene, K. and Zaltauskaite, J. (2017) Minimum environmental criteria for the reduction of air pollution deriving from private transport: potential of a car fleet renewal. Fresen. Environ. Bull. 26, 5635-5641.

[4] Nowell, D., Duó, P. and Stewart, I.F. (2003) Prediction of fatigue performance in gas turbine raping after foreign object damage. Int. J. Fatigue. 25, 963-969.

[5] Boyce, B.L., Chen, X., Peters, J.O., Hutchinson, J.W. and Ritchie, R.O. (2003) Mechanical relaxation of localized residual stresses associated with foreign object damage. Mater. Sci. Eng. 349, 48-58.

[6] Hamrick, J.L. (1999) Effects of foreign object damage from small hard particles on the high-cycle fatigue life of Ti-6Al-4V. Air Force Institute of Technology, Dayton.

[7] Chen, X. (2001) Foreign object damage and fatigue cracking. Harvard University, Cambridge.

[8] Weeks, C., Bastnagel, P., Cook, T., Daiuto, R. and Delp, J. (2001). FOD Analytical Modeling - FOD Event Modeling. Improved High Cycle Fatigue Life Prediction, Appendix 5E, AFRL-ML-WP-TR-2001-4159, Wright-Patterson AFB.

[9] Oakley, S.Y. (2004) On the High- and Low-Cycle Fatigue of Aero-engine Compressor Blades Following Foreign Object Damage. University of Oxford, Oxford.

[10] Tranter, P.H., Gould, P.J. and Harrison, G.F. (2003) Laboratory Simulation and Finite Element Modulation of Aerofoil Impact Damage. Proceedings of the 8th National Turbine Fatigue High Cycle Fatigue Conference, Monterey, CA, USA.

[11] Duó, P., Liu, J., Dini, D., Golshan, M. and Korsunsky, A.M. (2007) Evaluation and analysis offorated due for foreign object damage. Mech. Mater. 39, 199-211.

[12] Liu, X.Y. (2010) TC4 titanium alloy dynamic constitutive relationship. Nanjing University of Aeronautics and Astronautics, Nanjing.

[13] Chen, M. (2012) TC4 titanium alloy mechanical properties test and dynamic material model. Nanjing University of Aeronautics and Astronautics, Nanjing.

[14] Hallquist, J.O. (2006) LS-DYNA theory manual. Livermore: Livermore Software Technology Corporation.

[15] Zhang, Z.P., Zhang, J., Chai, Q., Li, C.W. and Wu, X.L. (2015) Velocity Estimation for the Impact of Foreign Object against the Aero-engine Blade. Journal of Air Force Engineering University (Natural Science Edition). 16, 7-10.

[16] Thompson, S.R., Ruschau, J.J. and Nicholas, T. (2001) Influence of residual stresses on high cycle fatigue strength of Ti–6Al–4V subjected to foreign object damage. International Journal of Fatigue 23, 405-412.

[17] Yin, D.M., Qian, L.F., Li, B.M. and Xu, Y.D. (2012) Analysis for Effects of Foreign Object Shape on The Residual Stress Field of Engine Blade. Journal of Mechanical Strength. 34, 355-360.

Received: **03.07.2017**
Accepted: **03.10.2017**

CORRESPONDING AUTHOR

Zhu Guanfang
Institute of Science
Air Force Engineering University
Xi'an 710051 – China

e-mail: Zhugf2006@163.com

© by PSP Volume 26 – No. 12A/2017 pages 8084-8092 Fresenius Environmental Bulletin

RESEARCH ON THE REVERSE LOGISTICS MANAGEMENT OF MEDICAL WASTE BASED ON THE RFID TECHNOLOGY

Hao Liu, Zhong Yao*

School of Economics and Management, Beihang University, No. 37 Xueyuan Road, Haidian District, Beijing, 100191, P. R. China

ABSTRACT

To deal with the traditional problems of medical waste in recycling, this paper, using the theory of reverse logistics and RFID technology, designs a medical waste management system model considering hospital receiving, logistics transportation, and disposal plant receiving. Meanwhile, the economic and social value of the model is evaluated from the perspectives of hospital, disposal plant, regulators, and the public; and the deficiencies of the current study are also analyzed. The designed system model provides a novel way to solve the current medical waste management problems, and is able to improve the management performance, to reduce the environmental pollution, then realize the effective and safe medical waste management.

KEYWORDS:
RFID, Medical waste, Reverse logistics, Safety management

INTRODUCTION

Medical waste is a kind of waste produced by medical organizations in medical treatment, prevention, health care, and other related activities. These waste is usually directly or indirectly infectious, toxic and hazardous [1]. Because of its toxicity, harm, and infection, the medical waste has more influence on society and environment compared with other waste [1].

For the medical waste which may cause the spread of disease and environmental pollution, its recycling procedures and requirements are strict. The traditional recycling mode of medical waste exists some problems like unclear classification, difficulties in data collection, poor supervision, insufficient consciousness of reusing the waste, profiteering purpose of medical waste, etc., which makes serious impact on the development of national medical and health system and threats the natural environment and people's health.

To solve the traditional medical waste recycling problems, this study proposes a management model using the reverse logistics based on RFID technology. Meanwhile, the novelty of the application of RFID technology on the medical waste recycling and processing is analyzed based on the theory of reverse logistics. This technology provides an alternative way to effectively solve the problems existing in current situation.

MATERIALS

At present, a number of scholars are studying the reverse logistics management of waste. Kinobe et.al. analyzed the supply chain network of waste reverse logistics in the KITeezi dump in South African in detail combining the collection, processing and distribution. In view of the low proportion of recycling and utilizing waste, they put forward the favorable development strategy for reverse logistics [2]. Kilic et.al. analyzed the collection rates of the reverse logistics system of electronic waste in Turkey via a mixed integer linear programming model in ten different scenes [3]. He et.al. proposed the solution for the current problems of reverse logistics by analyzing the collection network and flow of medical waste recycled by the third party disposal company in China[4]. Rolewicz-Kalińska took Poland as an example to analyze the effects on the medical waste which some infects play on like legal requirements, organizational factors and economic aspects, etc.. Finally, they concluded that the effective logistics is the key for the quality and safety of medical waste [5]. Based on artificial neural networks and fuzzy logic, Efendigil et.al. applied the two-phase model to helping that decision makers choose the “most appropriate” third-party reverse logistics provider [6].Abdulrahman et.al. put forward the reverse logistics realization model and the method to recognize the reverse logistics obstacle with respect to management, financial, policy and infrastructure in the Chinese manufacturing industries [7]. Based on Analytical Hierarchy Process (AHP) and Technique for Order Preference by Similarity to Ideal Solution (TOPSIS), Senthil et.al. proposed the method of selection and evaluation of reverse logistics under fuzzy environment [8]. Xia et.al. analyzed the remanufacturing logistics process based on closed-loop supply chain management and proposed the corresponding solution for the related questions [9]. Based on the case study of a medical product manu-

facturer, Lee and Lam investigated how manufacturers identify the problem of reverse logistics and then they designed the business process to enhance the efficiency of operations and market competencies which can add their customers' value [10].

The information technology, especially the RFID technology and sensor technology, whose development has brought great revolution for the logistics supply chain management. By building model and simulation, Nativi and Lee have confirmed that the RFID technology brings higher environmental and economic benefits in the real-time inventory monitoring and information sharing [11]. In order to minimize the total reverse logistics cost and improve the utilization rate of collection points, based on the RFID technology, Lee and Chan used a genetic algorithm to design the framework of reverse logistics and optimize the collection points of waste [12]. Asif used the RFID technology to reduce uncertainties in Reverse logistic supply chain (RLSC) [13].Jayaraman et.al. have found that in the study of reverse logistics supply-chain channels, the key a company faces is to deal with the identification problem. By the RFID technology, we can reduce the overall distribution costs for the organization [14]. Through the fuzzy cognitive maps and genetic algorithms, as well as the hybrid qualitative and quantitative approach, Trappey et.al. modeled and evaluated the performance of RFID-enabled reverse logistic operations [15]. Sarac et.al. analyzed the benefits the RFID technology brings in the supply chain management by modeling, simulation, experiment, case study, etc. [16]. Based on the RFID technology, Poon et.al. developed the logistics resource management system (R-LRMS) and improved the management level of collection and sharing of data [17]. Alumur et.al. used a mixed-integer linear programming formulation to design a profit maximization modeling framework for reverse logistics network[18]. Ustundag and Tanyas built the simulation model to calculate the expected benefits that an integrated supply chain system brings based on the RFID technology through performance improvement in efficiency, accuracy, visibility, and security level [19].

The reverse logistics. In 1992, the Stock pointed out in the report that the reverse Logistics is usually used in the waste recycling management and hazardous substances in CLM (the Council of Logistics Management). From a general perspective, the reverse logistics includes the reduction of waste source, recycling, material substitution, material reuse and all aspects of waste disposal related to logistics activity [20]. In European, RevLog from reverse logistics research group (The European Group On Reverse Log is tics) thinks that Reverse logistics is a process that collect the raw materials, semi-finished products and finished goods from manufacturers, distributors or consumers to recycle locations or proper treatment plants and then plan, implement and control them[21]. The logistics term of Chinese national standard divided reverse logistics into two major categories, namely, returned logistics and waste material logistics. For reverse logistics, the processed objects mainly include the unqualified goods and packaging container for turnover use; for waste material logistics, it focuses on the items that have lost their original use value in economic activity [22].

The RFID technology. The radio frequency identification (RFID) technology is a kind of non-contact technology with automatic identification whose basic principle is to use the radio frequency signal and its spatial coupling and transmission characteristics to implement the automatic machine identification for the stationary or moving items, it does the identification work without manual intervention, so it can work in all kinds of bad environment [23]. The RFID system is mainly composed of RFID electronic tag, RFID read-write device and antenna these three parts.

The RFID electronic tag has the technology characteristics like fast reading and writing, better data safety, easy to use, all kinds of packaging forms, etc.. It can not only adapt to various working environment and conditions, especially in the bad environment with oil, dust, radioactive and others, but can also embed or attach to different types of products easily in different situation. The RFID electronic label has extensive application prospect in the field of recycling and handling medical waste because of its technology characteristics.

In the current academic circles, the researches on the two aspects, namely, the waste reverse logistics management and the application of RFID technology in the reverse logistics management, have laid the foundation of theory and practice for the innovation research of RFID technology in the medical waste reverse logistics.

METHODS

Based on the RFID technology, this article constructs the system model from the hospital recycling, logistics transportation and disposal plant receiving these three aspects combining with the basic reverse logistics theory. Then the business modules of system model are analyzed and evaluated in detail from technical and economic perspectives to verify the validity of the model. By reforming the traditional business process of medical waste and combining the RFID technology to optimize it, we can effectively solve the problems existing in the recycling process of traditional medical waste.

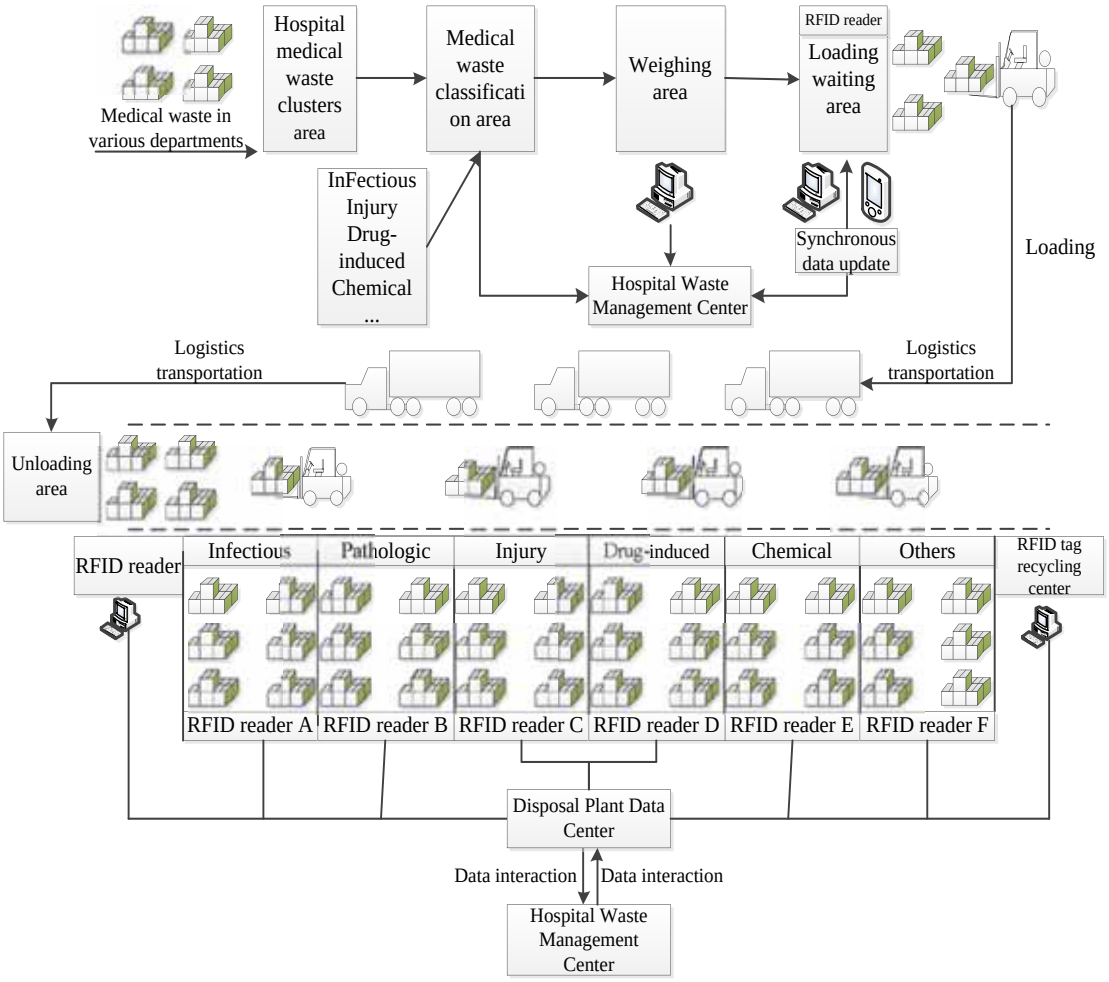


FIGURE 1
The overall system model

RESULTS

The system model is mainly composed of hospital recycling, logistics transportation and disposal plant receiving these three main links. Medical waste management system based on RFID technology can achieve the whole process of supervision from the hospital to plant, then effectively guarantee that the recycling and disposal of medical waste shall be carried out in accordance with the corresponding standard. At the same time, it can not only reduce the spread of disease, environmental pollution and other bad cases caused by poor regulation, but also enhance the oversight level of the industry. Without doubt, it will bring new changes in the technology and management mode.

(1) The overall design for the system model. As shown in Figure 1, the RFID technology is applied to the recycling system, it is mainly divided into hospital recycling, logistics transportation and disposal plant receiving these three parts. Hospital recovery is mainly to solve the waste problems like concentration, classification, weighing and loading. Logistics is mainly to solve the regulation of medical waste in the process of transportation. Through the application of RFID technology, it can implement the whole process of medical waste from loading and transport to the unloading at disposal plant as well as the monitoring and management which can ensure the transportation safety of the medical waste. The treatment is mainly for the goods shipped from the hospital medical waste storage according to the classification categories to the classification process in the disposal plant.

The hospital receiving. In hospital, the waste management center will collect the medical waste from various departments on a regular basis, and then which shall be classified and packaged in accordance with the classification standards. After pasting the RFID electronic tag and weighing, the RFID read-write device installed in the waste disposal area in hospital will automatically write the information into the RFID electronic tag on the package like the waste category, source, weight, etc.. At

the same time, the data will be synchronously updated to the hospital waste management center. After the check, the medical waste is loaded and transported.

Logistics transportation. After loading, the medical waste from different hospitals will be transported to waste treatment plants in accordance with the scheduled program. Every transport vehicle is equipped with RFID electronic tag which records the specific information like category of the vehicle, the unit, the lines, license, plate number, the driver, contact information, date, etc.. The detailed data is synchronized with waste management center and plant to ensure its consistency. During the transporting, through the global satellite positioning system (GPS), the trajectories of vehicle can be real-timely tracked to ensure the vehicle driving according to the predetermined route.

The disposal plant receiving. When the truck arrived at the disposal plant, the RFID reader laid in the factory will automatically read the electronic tag information of vehicle, and then match data to the waste management system. Next, the truck is allowed into the factory to unload once it is confirmed. Due to the disposal schedule, the disposal plant does not ensure that the waste is processed immediately, so it needs to be stored temporarily in accordance with the category.

The RFID reader laid in the temporary storage area will automatically read the information of RFID electronic tag on the waste packaging and check the data with the waste management system. After the check, waste is allowed into the corresponding storage area and the data is automatically updated.

(2) The hospital recycling model. As shown in Figure 2, the main recovery model in hospital is divided into centralized classification, weighing and writing data these three parts. Every day in the hospital each department produces different medical waste and the cleaners will collect them to the waste area, then complete the classification, packing and weighing. The waste treatment plant regularly arrange vehicles to recycle waste after the business processes such as writing the data of RFID electronic tag and so on.

The centralized classification. Hospital staffs will regularly collect medical waste from each department into the concentration area, then classify and package them according to the property like infectious, pathological injury, drugs and chemical. After the classification and packaging, the medical waste needs to be marked and pasted to the RFID electronic tag. In addition, to ensure the transportation safety, the outer packing is designed into one-time destruction and unrecoverable.

Weighing. The waste will be weighed by the weighing system after a series of process like classification, packaging and pasting RFID electronic label, etc.. When the packaged waste goes through the pressure sensor, the measured data will be sent to the weight house system and the weight of the waste is calculated, through the corresponding control procedures, the RFID read-write device decorated in the area of weight house would automatically write the weight data to the RFID electronic tag on the outer packing. Thus, the weighing process is completed.

Writing data. After weighing, the related information of the waste needs to be recorded before loading. With the RFID read-write device, the information will be written in the RFID electronic tag of outer packing like city, region, hospitals, departments, types of waste, etc.. Then the data is uploaded to the waste management center in hospital and the synchronous update is completed automatically.

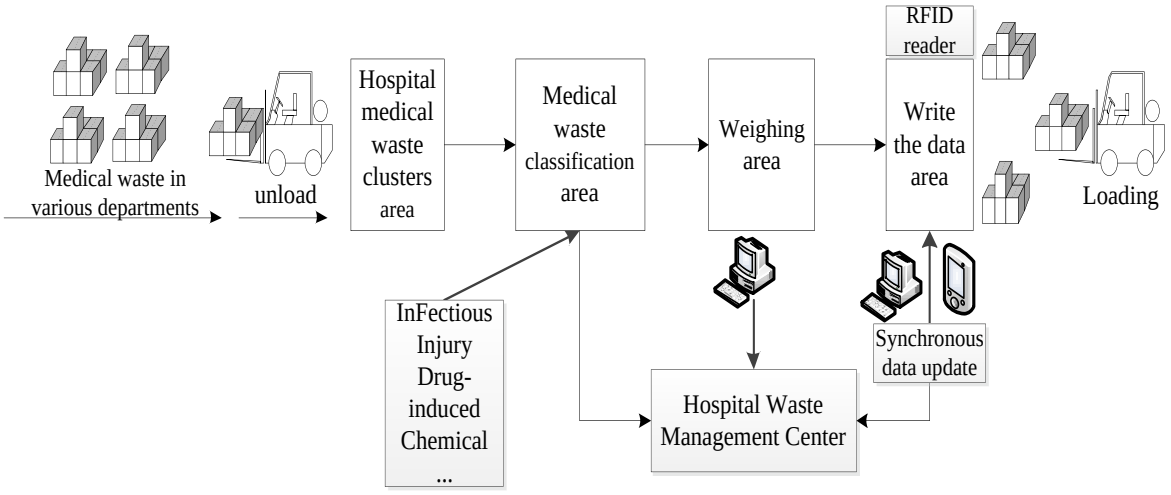


FIGURE 2
The hospital recycling model

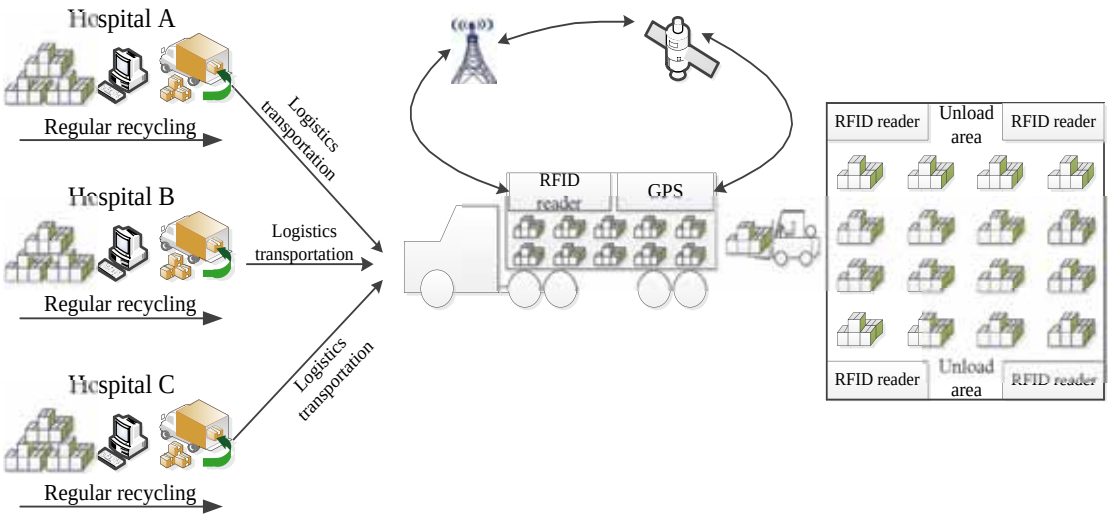


FIGURE 3
The model of logistics and transportation

(3) The model of logistics and transportation. As shown in Figure 3, the essence of logistics and transportation is that manage the medical waste from the hospital to plant. The transport link is segmented into three main parts including loading, transport and unloading. Through the Global Positioning System (GPS) and RFID technology, the medical waste data can be collected and controlled easily.

Loading. According to the agreement of hospital and waste disposal plants, the plant arranges vehicles to recycle hospital waste regularly. After completing weighing and writing data, the waste waits for loading. Before loading, according to the number and type of waste, the waste management center assign vehicles for waste, and write the vehicle information into the RFID electronic tag on waste packaging. When loading, check the information again, if there are no mistakes the loading is allowed. The RFID read-write device decorated in the loading area will automatically write the loading time to the RFID electronic tag on the outer packing of waste, and the data will be synchronously updated with the waste management center.

Transport. Every transport vehicle is equipped with RFID electronic tag, which records the information like the vehicle category, license plate number, the receiving head, the driver, contact information, docking of the hospital, the route, etc.. The information will be written by the RFID read-write device of loading area and at the same time, the database will be synchronously updated with that between the hospital and treatment plant.

The RFID read-write device and the Global Positioning System (GPS) are equipped inside the truck. The RFID read-write device will automatically read the information of RFID electronic tag on the waste packaging and interact the data with the waste management center of hospital in the form of wireless communication to ensure that the information of waste inside the car is consistent with the outbound data of waste management center in hospital like the waste types, quantity, weight, etc.. The Global Positioning System (GPS) can real-timely track and replay the vehicle trajectory. Once there is an emergency, the GPS can communicate with the hospital and treatment plants to ensure the transportation safety of the waste.

Unloading. When the transportation vehicle arrives at plant area, the specially-assigned persons are responsible for unloading. The RFID read-write device will automatically read the information of electronic tag on vehicle and check it with the database of waste management center in hospital and the plant. After the check, the waste is allowed to enter the unloading process. In the unloading process, the waste packaging is inspected to confirm that no unpacking happens and the theft or replacement is prevented during the transportation.

(4) The receiving model in disposal plant. As shown in Figure 4, as a result of the business process in the disposal plant, it does not ensure that all waste is processed immediately, for which can't be immediately processed, it is temporarily stored according to the category. The receiving model of treatment mainly includes receiving, weighing, classified storage these three parts.

Receive goods. After unloading, the plant personnel place the waste in the corresponding area according to the categories. The RFID read-write device decorated in the unloading zone will automatically read the electronic tag information on waste

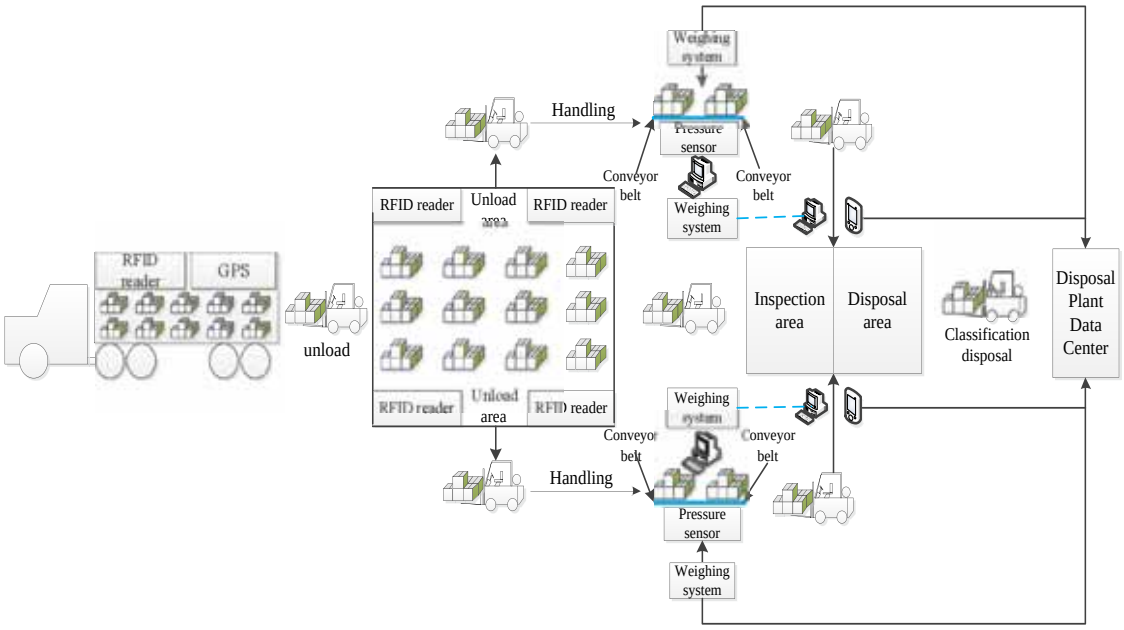


FIGURE 4
The receiving model in disposal plant

packing and check with the database of waste management center in hospital and the plant. After the check, the process of unloading and receiving is done.

Weighing. The disposal plant arranges the processing schedule according to their own processing capacity and the time into the factory. The forklift carries the waste to the conveyor belt of weighing system in turn to determine the weight through weighing. At the same time, the weight result will be compared with the data center of plant and the weight of RFID electronic tag on the outer packing. Within the permitted error, the weighing is completed after the conformation.

The classification of storage. After the procedures of weighing and testing, the forklift handles waste to the corresponding storage area according to its type. The RFID read-write device decorated in the waste storage area will automatically read the information of RFID electronic tag on the packaging of waste and check it with the data of plant center. After the confirmation, it is admitted into the storage area, and automatically the data is updated. According to the treatment schedule, the plant handles medical waste from the storage area in accordance with the corresponding processing method.

DISCUSSION

As shown in Figure 5, the system model with the support of RFID technology constructs the recycling process of medical waste from three aspects, namely, the hospital, the logistics transportation and the disposal plant. Among them, the hospital mainly includes these links like the collection, classification, packing, weighing, etc.. The disposal plant mainly includes receiving, weighing, storage, classification of processing, etc., and it can realize the reverse circulation from hospitals to plant through the logistics transportation. The article evaluates the system model from the four angles of hospital, disposal plant, regulators and the public.

The hospital. The application of RFID technology can realize the automatic and intelligent management of these four links including the collection of medical waste, classification, packaging and weighing to real-timely read, write and query the related information of medical waste like source, type, quantity, quality, etc.. The intelligent weighing system can realize the automatic and intelligent management of weighing and data entry to avoid the problems caused by artificial operation like low efficiency, inaccurate data, poor regulatory, etc.. The accurate and effective medical waste information reduces the economic loss caused by the wrong data. If the information supervision is strong, problems can be timely found out and then the related responsibility can be traced.

The disposal plant. The RFID read-write device decorated in the plant will automatically read the information of RFID electronic tag on the packaging of waste and complete the business process of medical waste quickly such as receiving, storing and so on. The intelligent weighing system can weigh the

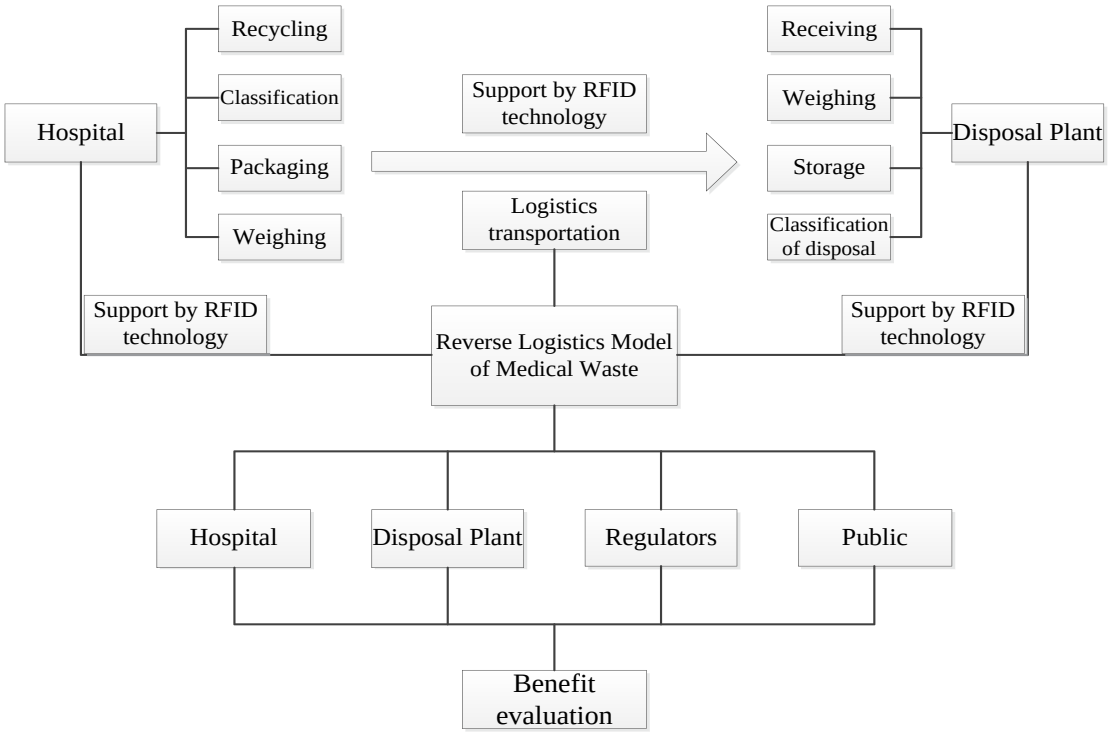


FIGURE 5
The evaluation model of reverse logistics

medical waste and check data to ensure the data consistency. The RFID technology can effectively solve the problems caused by the manual operation like receiving, weighing, storage, inventory, sorting, etc.. Each link is processed automatically and intelligently in strict accordance with the corresponding process to reduce the cost for enterprise. Meanwhile, to a great extent, the accurate and effective data improves the work efficiency and economic benefits of the enterprise.

The regulators. The management system of medical waste based on RFID technology effectively connects the hospital, logistics transportation and waste disposal plants. Through the system, the government regulators can real-timely monitor the key links of medical waste like collection, classification, transportation, storage, processing, etc., which changes the past poor situation caused by the poor sharing of information and the shortage of monitoring data, and effectively avoid the environmental pollution, the spread of disease and so on. Once something wrong is found out, the source of problem will be traced in a timely manner and the person with the corresponding responsibility will take charge to solve the problem from the source.

The public. The public are the indirect beneficiaries of the medical waste management system. The application of RFID technology can monitor the information of medical waste like the collection, classification, transportation, storage, processing, etc., which ensures the transport safety of the medical waste from hospitals to plants, avoid the theft of medical waste and eliminate the circulation of reprocessed medical waste in the market. At the same time, the construction of the system helps the medical waste to be dealt with in accordance with the corresponding processing standards and reduce the harm to people's health caused by the improper handling such as environmental pollution, the spread of disease and so on.

CONCLUSION

The management model of reverse logistics for medical waste using the RFID technology connects hospitals and waste disposal plants through the logistics transportation, which changes the recycling and process mode of hospital and plant and realizes the automatic and intelligent management of medical waste from production to handling. Through RFID technology, the data of medical waste can be collected and monitored real-timely to ensure it processed in strict accordance with the relevant standards and procedures, which reduces the environmental pollution and the spread of disease caused by wrong process and other problems. The application of RFID technology will bring great change for recycling medical waste on the technology and management, which has the vital significance to improve

the recycling management efficiency of medical waste and enhance the management level of industry.

The disadvantages of this article mainly embody in the following three aspects: 1) The research is limited to designing the system model and lack corresponding simulation experiments to verify and analyze the system model. 2) The data support is poor to analyze the system model quantitatively. 3) The system model is limited to the design stage and the application effect can't be evaluated from the practical perspective.

The current deficiencies of this article are the focus of future research. In the future research process, these three problems should be solved to realize the better research and management of reverse logistics for the medical wastes.

ACKNOWLEDGEMENTS

This work has been supported by the Natural Science Foundation of China (Project No. 71671011, No. 71332003).

REFERENCES

[1] Decree of the State Council of the People's Republic of China No. 380, Medical waste management regulations, (2003) Available at: http://www.nhfpc.gov.cn/mohzcfgs/pfg/200804/18302.shtml

[2] Kinobe, J.R., Gebresenbet, G., Niwagaba, C.B. and Vinnerås, B. (2015) Reverse logistics system and recycling potential at a landfill: A case study from Kampala City. Waste Management. 42, 82-92.

[3] Kilic, H.S., Cebeci, U. and Ayhan, M.B. (2015) Reverse logistics system design for the waste of electrical and electronic equipment (WEEE) in Turkey. Resources, Conservation and Recycling. 95, 120-132.

[4] He, Z.G., Li, Q. and Fang, J. (2016) The Solutions and Recommendations for Logistics Problems in the Collection of Medical Waste in China. Procedia Environmental Sciences. 31, 447-456.

[5] Rolewicz-Kalińska, A. (2016) Logistic Constraints as a Part of a Sustainable Medical Waste Management System. Transportation Research Procedia. 16, 473-482.

[6] Efendigil, T., Önüt, S. and Kongar, E. (2008) A holistic approach for selecting a third-party reverse logistics provider in the presence of vagueness. Computers & Industrial Engineering. 54(2), 269-287.

[7] Abdulrahman, M.D., Gunasekaran, A. and Subramanian, N. (2014) Critical barriers in implementing reverse logistics in the Chinese manufacturing sectors. International Journal of Production Economics. 147, 460-471.

[8] Senthil, S., Srirangacharyulu, B. and Ramesh, A. (2012) A decision making methodology for the selection of reverse logistics operating channels. Procedia Engineering. 38, 418-428.

[9] Xia, W.H., Jia D.Y. and He Y.Y. (2011) The remanufacturing reverse logistics management based on Closed-loop supply chain management processes. Procedia Environmental Sciences. 11, 351-354

[10] Lee, C.K.M. and Lam, J.S.L. (2012) Managing reverse logistics to enhance sustainability of industrial marketing. Industrial Marketing Management. 41(4), 589-598.

[11] Nativi, J.J. and Lee, S. (2012) Impact of RFID information-sharing strategies on a decentralized supply chain with reverse logistics operations. International Journal of Production Economics. 136(2), 366-377.

[12] Lee, C.K.M. and Chan, T.M. (2009) Development of RFID-based reverse logistics system. Expert Systems with Applications. 36(5), 9299-9307.

[13] Asif, R. (2011) Reverse Logistics: RFID the key to optimality. Journal of Industrial Engineering and Management. 4(2), 281-300.

[14] Jayaraman, V., Ross, A.D. and Agarwal, A. (2008) Role of information technology and collaboration in reverse logistics supply chains. International Journal of Logistics: Research and Applications. 11(6), 409-425.

[15] Trappey, A.J., Trappey, C.V. and Wu, C.R. (2010) Genetic algorithm dynamic performance evaluation for RFID reverse logistic management. Expert Systems with Applications. 37(11), 7329-7335.

[16] Sarac, A., Absi, N. and Dauzère-Pérès, S. (2010) A literature review on the impact of RFID technologies on supply chain management. International Journal of Production Economics. 128(1), 77-95.

[17] Poon, T.C., Choy, K.L., Chow, H.K., Lau, H.C., Chan, F.T. and Ho, K.C. (2009) A RFID case-based logistics resource management system for managing order-picking operations in warehouses. Expert Systems with Applications. 36(4), 8277-8301.

[18] Alumur, S.A., Nickel, S., Saldanha-da-Gama, F. and Verter, V. (2012) Multi-period reverse logistics network design. European Journal of Operational Research. 220(1), 67-78.

[19] Ustundag, A. and Tanyas, M. (2009) The impacts of radio frequency identification (RFID) technology on supply chain costs. Transportation Research Part E: Logistics and Transportation Review. 45(1), 29-38.

[20] Stock, J.R. (1992) Reverse Logistics, Oak Brook, IL: Council of Logistics Management.
[21] Revlog. The European working group on reverse logistics. (1998) Available at: http: //www.fbk. eur. nl /OZ/REVLOG/.
[22] He, M.K., Wu, Y., Mu, W.Z., He, T.F., Wang, Y.Q., Wu, R.T., Zhang, M., Liu, Z.X., Li, J.D. and Liu, J.X. China's national standard "Logistics term"(2001) Standards Press of China, General Administration of Quality Supervision, Inspection and Quarantine of the People's Republic of China (AQSIQ).
[23] Finkenzeller, K., (2010) [RFID Handbuch. English]: Fundamentals and Applications in Contactless Smart Cards, Radio Frequency Identification and Near-Field Communication, Third Edition, ISBN 978-0-470-69506-7.

Received: **05.07.2017**
Accepted: **29.09.2017**

CORRESPONDING AUTHOR

Zhong Yao
School of Economics and Management,
Beihang University, No. 37 Xueyuan Road,
Haidian District, Beijing, 100191, P. R. China

e-mail: iszhyao@buaa.edu.cn

© by PSP Volume 26 – No. 12A/2017 pages 8093-8099 Fresenius Environmental Bulletin

PUBLIC PERCEPTION OF ENVIRONMENTAL RISK IN TURKEY

Ayla Bilgin[1,*], Selim Latif Sanin[2]

[1]Artvin Coruh University, Engineering Faculty, Department of Environmental Engineering, Artvin, Turkey
[2]Hacettepe University, Engineering Faculty, Department of Environmental Engineering, Ankara, Turkey

ABSTRACT

Knowledge towards the understanding of environmental conscious and risks in Turkey is limited. In this study the answers from 635 people from different cities are evaluated who are asked to fill forms containing questions about environmental and social topics between years 2006-2012. With these results modern life concept and environmental risk perception of Turkish people are evaluated. First of all what Turkish people consider as risk and their ranks in their daily life is questioned. According to the findings in twenty-first century social factors have the priority for Turkish people. Environmental priorities are guided by the press. Turkish people would like to see professionals in the management of environmental topics. According to the results only %22 of the respondents were trained on civil defense topics. Nuclear energy is not accepted by the majority of the population. Results indicate the need for a systemic and extended education program towards the development of an environmental consciousness.

KEYWORDS:
Environmental Risk, Environmental Consciousness, Social Risk, Modern Life.

INTRODUCTION

Environmental consciousness is a measure of a person's ability to understand the nature of environmental processes and problems [1]. In recent years, comprehension of the importance of environmental consciousness in the world, as well as the understanding about the environment, have increased in a very short time as a result of tremendous developments in technologies in every field. As a result, the number and the effectiveness of the non-governmental organizations in the environmental arena have grown gradually [2]. As a result of rapid industrialization, the loss of a significant amount of soil and natural resources, destruction of ecosystems, the production of various amounts of toxic chemicals, and global warming have become important social problems. Not only natural resources, but also the social responses of the people living in the urban areas have seriously affected from these developments [3].

Environmental risk can be defined as the probability of changes that will take place in the ecosystem to influence life. The understanding of what the environmental risks, on the social scale, are among the top factors that determine our way of life. Knowing the importance for people and the ecosystem, general environmental quality description must be taken as the basics of life. Since the beginning of 1960s there is an awareness for the dependent long term effect of development and ecosystem protection. We see an increasing demand for the presence of environmental factors in the decision mechanisms of organizations in both developed and developing countries [4]. Parallel to these progresses many organizations are working on developing their own environmental risk evaluation methodologies [5].

Environmental risk and the perception of environmental risk are perceived differently in different societies [6].

Although there is no common scientific or social understanding about the perception of risk, all ideas about risk have a common element: the difference between the real and the probable. If the difference between reality and probability is approved, then the concept of "risk" is the probability of occurrence of a phenomenon, that is mostly undesirable (negative impacts), as a result of the natural events or human activities. The perceptions of risk differ significantly among social and cultural groups [7]. The perception of risk in the general sense is the analysis of individuals' decisions and reactions that are the result of their evaluation of modern technologies and all types of activities with their own interpretation upon the questions directed to them [8].

It has been proven that incidences and personal experiences are important factors in the perception of risk [9-11]. It is reported that personal character has an effect on the perception of risk and women have a higher capability of risk perception then men do [12, 13]. The media has an important role in risk perception of humans. While the media manipulates the general risk perception, personal judgements resist against the change coming from sources. Personal experiences have an important role in the perception of risk, as well [14].

In Turkey, earlier studies about the perception of risk have been conducted on students [15-18]. The

purpose of this study, is to understand and explain what is known about environmental risks and their sources in Turkey. The similar surveys have also been done to understand how people consider environmental risks in other countries [19]. A concept that an individual considers as a risk and the knowledge accumulation about environmental topics have been investigated by means of a questionnaire. This study is a guide to the society for better understanding of environmental sensitivities and to determine the necessary methods to mitigate the environmental risks that may be faced in the future.

METHOD

The questions were devised into ten groups in the questionnaire bearing the title "The Evaluation of Environmental Risk in Turkey". The data collection methodology was based on individual contact and questionnaire filling over internet. The survey was carried out between 2006-2012 years. The questionnaire was applied to a total of 635 individuals. The findings of the questionnaire were assessed in the social sciences statistics program (SPSS 19). The correlations between answers were determined through the application of Crosstab methods. The age distribution and educational levels of the subjects are given in Table 1.

TABLE 1
Ages and education levels of survey participants.

Age Level		
	Frequency	Percent
18-25	238	37.5
26-35	234	36.9
36-45	99	15.6
46-55	44	6.9
>55	20	3
Education		
	Frequency	Percent
İlliterate	6	0.9
Primary School	39	6.1
Middle School	31	4.1
High School	129	20.3
University	325	51.2
Master's degree	64	10.1
Doctorate	41	6.5
Total	635	100

RESULTS AND DISCUSSION

Priority Between Environmental and Social Risks. To see if there exists a discrimination between social and environmental risk perception and evaluation, subjects were asked to rank different risks. The results showed that; terrorism 33,8%, unemployment 15,8%, poverty and inflation 13% alcohol-drug-cigarette usage %10,2, were among the top concerns. Environmental risks; destruction of natural environment 8,8%, nuclear risk 5,2 % and risks from chemical compounds 1,8 % (Fig. 1). Relying on these results we can say that; although the environmental risks do not have a priority in the daily lives of Turkish people there is a clear anxiety for the environmental destruction.

Categorization of the Risks. When the risks are grouped for the natural disasters, changes in industries and technology or modern life, it's observed that risks from technological changes form a higher concern (Fig. 2). An accident similar to Chernobyl accident happened on April 26 1986 is also defined as one of the high risk (at the rate of % 68,8) concerns. Nuclear wastes are thought to form higher risk than nuclear power plants. Our reliance on energy is increasing in Turkey and in the world parallel to the progress in technology. Alternative solutions are produced in accordance with this situation. In the field study, the planned nuclear plant construction in Sinop province has been asked to the participant too. 36% of the population accepts the presence of a nuclear power plant in Turkey. Majority of the population expects a serious accident (%72) at some point, during economical life time of the reactor. On the other hand, terrorism (%73) and *drug usage* (%69,7) are predicted to form high risks as well for the society, compared to environmental risks. Among the attendants of questionnaire, environmental risks such as *lake, river, sea or air pollution and chemicals* are forming important risk groups for community. The lack of information on particular topics has been the outcome of this study. The subjects did not answer the question about radon gas (30 % unanswered), probably they don't have knowledge about "*radon"*. In addition, the question about genetic applications is also unanswered in the rate of %24.

The Developing Technologies and Risk Perception Depending on The Access. Risk perceptions of the people change depending on the activities and technologic improvements in the world. Although there isn't a nuclear waste activity in Turkey, the subjects have a great anxiety on the subject of storage. Public have information and knowledge about activities such as railway and airway transport and water dams in Turkey and in the world for a long time. In the same way, they have an experience and knowledge about their effects and risk degrees. But ambiguousness on new technologies and unknown processes make people anxious.

Ship transportation through straits*, petroleum refineries, traffic accidents, natural gas distribution lines, and biologic research laboratory* create similar concern (%30), although the frequency of traffic accidents is really high in Turkey (Fig. 3).

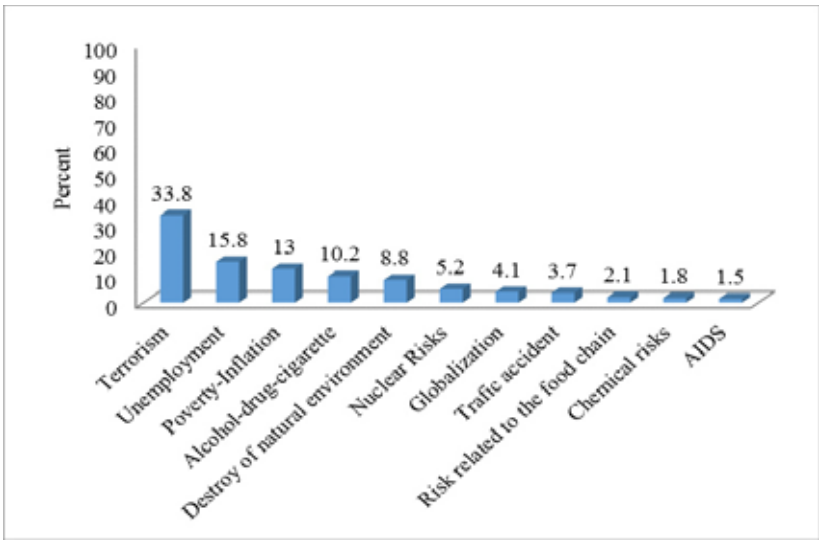


FIGURE 1

The question; "Please make a priority list for the current questions asked to you in regard of anxiety levels you feel?"

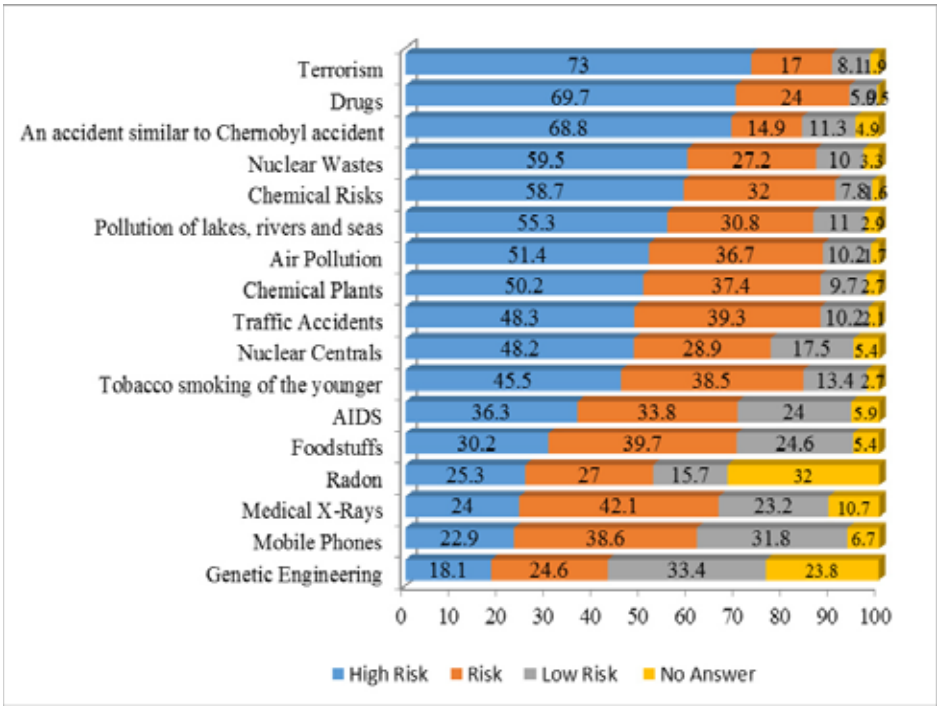


FIGURE 2

The question; "Evaluate the problems giving on the list according to the decrease of risk that are appropriate for you?"

How Should The Technology be Managed. According to the survey about the current management methods of the technologies and the future methods that should be applied for the management of these technologies which are thought to have risk against human and environment; participants think that the management should be in the hands of the government while significant amount of the participants say that they don't have any idea about the subject (Fig. 4). These results also show that people in Turkey prefer to see the professionals as the management authority (Fig. 5) for technology.

It can be concluded that the society is under informed about environmental events, mostly insufficient and incorrect, leads to anxiety against innovations and new technologies. There is a clear statement about industrial and nuclear power management strategies that the authorities must create a trust in the society and clear communication mechanisms must be established.

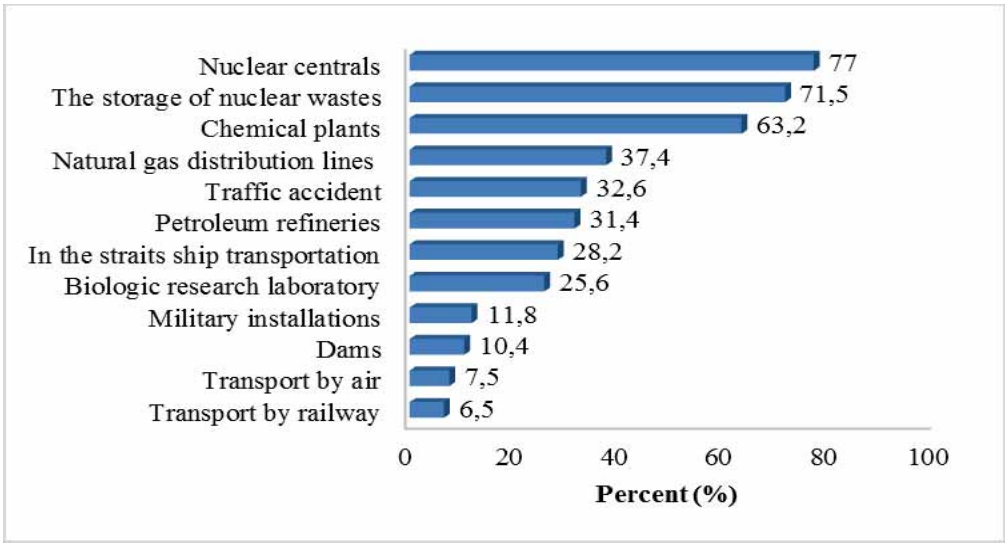


FIGURE 3
The question; "In your opinion which industrial factors or technologies may lead to a serious accident?"

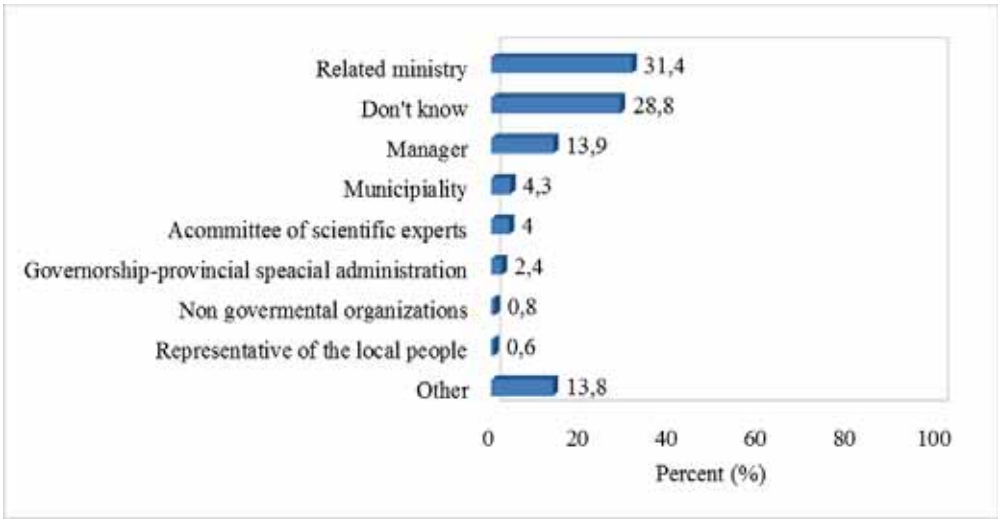


FIGURE 4
The question; "Who is governing organizations that are harmful to do environment?"

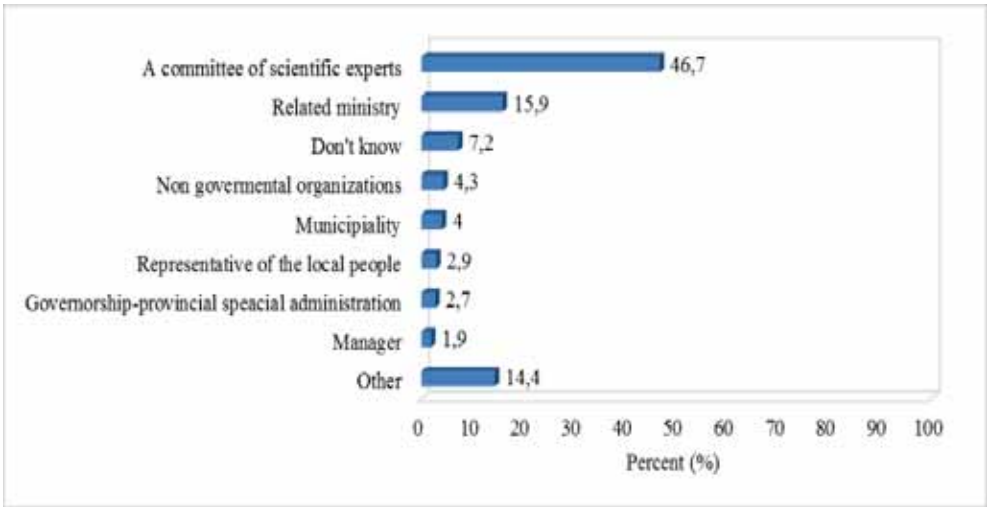


FIGURE 5
The question; "In your opinion who should govern the organizations that are harmful to do environment*?"*

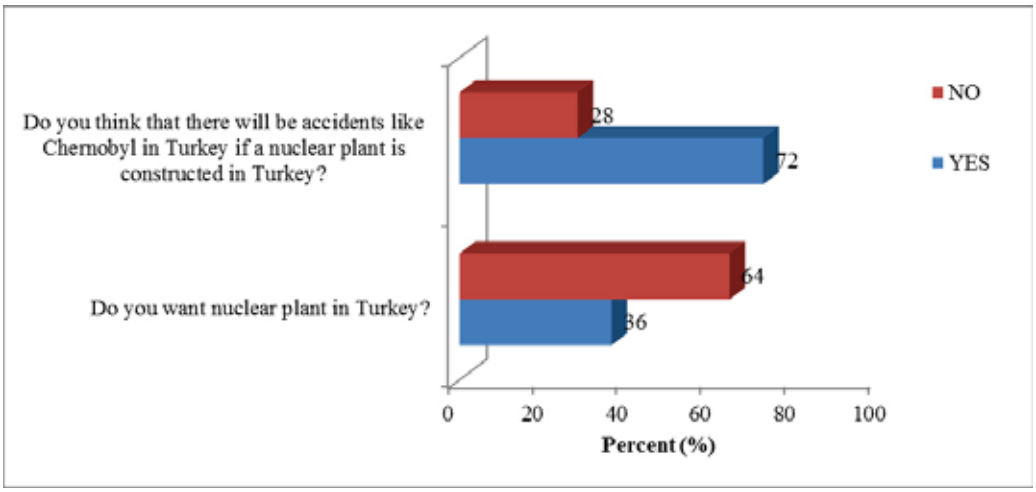


FIGURE 6
The questions in the questionnaire have "Yes" and "No" answers

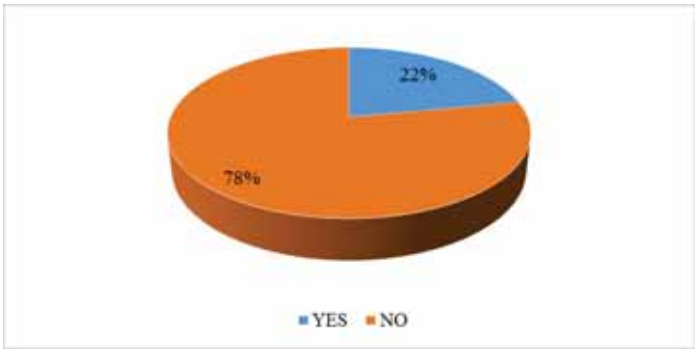


FIGURE 7
The question in the questionnaire is "Have you participated civil defense operation?"

Another important result of the survey is that only 22% of the subjects have taken *civil protection training* (Fig. 7*)*. This result may the foundation of responses to this questionnaire. There is general need to increase environmental health and safety training of professionals and public in Turkey.

Environmental risk and the perception of environmental risk are perceived differently in different societies [20]. A study conducted in Belgium and France in 2004 indicated that while terrorism is considered as a risk (22%) for the French people, in Belgium, 34% of the society perceives terrorism as a risk. Unemployment is a risk for 27% of the French population, while it is perceived as a risk by 14% of the population in Belgium. Destruction of the natural environment has been perceived as a risk by 21% of the population in France, while it is 30% for the population of Belgium [19]. When these conclusions are compared to Turkey following percentages are found: terrorism: 33.8%; unemployment: 15.8%; and environmental risk and destruction of the natural environment: 8.8%.

The results of the current study indicate that people have high risk concerns about nuclear power plants and the storage of nuclear waste. When the results of this study are compared to other studies, similar results have also been found [22-24].

A survey conducted in China, which analyzed the success of the government in relation to informing society during environmental accidents, indicates that 7% of the population finds the government successful while 54% of the population found the government unsuccessful [20]. The current study indicates that as is the case in China, the relevant authorities failed to provide the population with accurate information about environmental issues. This shows that as the population increases diffusion of information into the society slows down, which may be related to the number of people as well as the change in the education level.

Due to the shortages in "Environment Education" the close social circle is educating and informing the individual and shaping his environment consciousness. For the people, the social risks and social incidents are much more worrying than environmental risks. People do not have any agenda for the things that they see none of their business and thinking that *"some people are taking care of these situations"* they focus on their daily sustainable lives.

67% of the participants are university graduators. The existing anxieties of university graduators show that there are shortages in information and environment education.

Considering the power of press in the information of the public, it will have an important place to accommodate more education programs in the shaping of social environment consciousness.

CONCLUSION

The current study demonstrates the perspective of the Turkish society about the environmental and social risks.

The survey study indicates that the respondents of the survey consider social risks more important than environmental risks.

Lack of knowledge on a specific topic is the major risk enhancing issue.

Negative experience is also a significant barrier to overcome for the risk perception.

REFERENCES

[1] Yeung, S.P. (1998) Environmental Consciousness among students in senior secondary schools: the case of Hong Kong. Environmental Education Research. 4(3), 251-268.

[2] Uzun, N., Sağlam, N. (2005) Sosyo-ekonomik durumun çevre bilinci ve çevre başarısı üzerindeki etkisi. Hacettepe Üniversitesi Eğitim Fakültesi Dergisi. 29, 194-202.

[3] Asilsoy, B. (2012) A survey study on environmental consciousness in Famagusta Procedia - Social and Behavioral Sciences. 35, 675 – 681.

[4] Kwiatkowski, R.E. (1998) The role of risk assessment and risk management in environmental assessment. Environmetrics. 9, 587-598.

[5] Lasinio, G.J., Divino, F., Biggeri, A. (2007) Environmental risk assessment in the Tuscany region: a proposal. Environmetrics. 18, 315–332.

[6] Zhang, L., He, G., Arthur, P.J., Yong-long, L. (2013) Public perceptions of environmental risk in China. Journal of Risk Research. 16(2), 195-209.

[7] Renn, O. (1998). Three decades of risk research: accomplishments and new challenges. Journal of Risk Research. 1(1), 49–71.

[8] Sloviç, P. (1987) Perception of Risk. Science. 236, 280-285.

[9] Barnett, J., Breakwell, G.M. (2001) Risk perception and experience: hazard personality profiles of ındividual differences. Risk Analysis. 21(1), 171–178.

[10] Kasapoglu, A., Mehmet, E. (2004) Compa-rative behavioral response to future earth-quakes: the cases of Turkey and USA. Social Behavior and Personality. 32(4), 373–382.

[11] Siegrist, M., Gutscher, H. (2006) Flooding Risks: A Comparison of Lay People's Perceptions and Expert's Assessments in Switzerland. Risk Analysis. 26(4), 971–979.

[12] Andersson, H. (2011) Perception of Own Death Risk: An Assessment of Road-traffic Mortality. Risk Analysis. 31(7), 1069-82.

[13] Kellens, W., Zaalberg, R., Neutens, T., Vanneuville, W., Maeyer, P.D. (2011) An Analysis of the Public Perception of Flood Risk on the Belgian Coast. Risk Analysis. 31(7), 1055–1068.

[14] Wahlberg, A.F., Sjoberg, L. (2000) Risk perception and the media. Journal of Risk Research. 3, 31-50.

[15] Çelen, Ü., Yıldız, A., Atak, N., Tabak, R.H., Arısoy, M. (2002) Ankara üniversitesi sağlık eğitim fakültesi öğrencilerinin çevre duyarlılığı ve ilişkili faktörler. 8. Ulusal Halk Sağlığı Kongresi, Diyarbakır. Kongre Kitabı. 421.

[16] Özdemir, O., Yıldız, A., Ocaktan, E., Sarışen, Ö. (2004) Tıp fakültesi öğrencilerinin çevre sorunları konusundaki farkındalık ve duyarlılıkları. Ankara Üniversitesi Tıp Fakültesi Mecmuası. 57(3), 117-127.

[17] Talay, İ., Gündüz, S.N., Akpınar, N. (2004) On the status of environmental education and awareness of undergraduate students at Ankara University Turkey. International journal of Environment and Pollution. 21(3), 293-308.

[18] Yücel, M., Uslu, C., Altunkasa, F., Güçray, S.S., Say, N. (2008) Adana'da halkın çevre duyarlılığının saptanması ve bu duyarlılığı arttırabilecek önlemlerin geliştirilmesi. Adana Kent Sorunları Sempozyumu, TMMOB Yayını. 363-432.

[19] Carle, B., Charron, S., Milochevitch, A., Hardeman, F. (2004) An inquiry of options of the French and Belgian populations as regards risk. Journal of Hazardous Materials. 111(1-3), 21-27.

[20] Zhang, L., He, G., Mol, A.P.J., Yong-long, L. (2013) Public perceptions of environmental risk in China. Journal of Risk Research. 16(2), 195-209.

[21] Ho, J.C., Lee, C.T., Kao, S.F., Chen, R.Y., Ieong, M.C., Chang, H.L., Hsieh, W.H., Tzeng, C.C., Lu, C.F., Lin, S.L., Chang, P.W. (2014) Perceived environmental and health risks of nuclear energy in Taiwan after Fukushima nuclear disaster. Environment International. 73, 295–303.

[22] Hinman, G.W., Rosa, E.A., Kleinhesselink, R.R., Lowinger, T.C. (1993) Perceptions of nuclear and other risks in Japan and the United States. Risk Anal. 13, 449–455.

[23] Kanda, R., Tsuji, S., Yonehara, H. (2012) Perceived risk of nuclear power and other risks during the last 25 years in Japan. Health Phys. 102, 384–90.

Received: **08.07.2017**
Accepted: **28.09.2017**

CORRESPONDING AUTHOR

Ayla Bilgin
Artvin Çoruh University,
Engineering Faculty,
Department of Environmental Engineering,
Artvin – Turkey

e-mail: ayla.bilgin@gmail.com

© by PSP Volume 26 – No. 12A/2017 pages 8100-8108 Fresenius Environmental Bulletin

STUDY ON CONTROL MECHANISM OF LOOSE COAL WORKING FACE SURROUNDING ROCK AND APPLICATION UNDER HIGH GAS COAL SEAMS

Jia-zhuo Li[1,2,*], An-ying Yuan[1], Chuan-qi Zhu[1]

[1]Anhui Province Key Laboratory of Mining Response and Disaster Prevention and Control in Deep Coal Mine, Anhui University of Science and Technology, Huainan, Anhui 232001, China
[2]School Energy Resources and Safety, Anhui University of Science and Technology, Huainan, Anhui 232001, China

ABSTRACT

Most of coal mines in east China are high gas coal seams, so they are forced to adopt artillery mining. Taking the Xin zhuangzi coal mine as the engineering background, and using synthetical study methods, the fully-mechanized mining method was studied. The 66207 working face was arranged in the low stress zone for the mining of the above 66208 working face, by internal misaligned arrangement since mining design, thus, stress concentration caused by subsection coal pillar was avoided. Above the 7 coal seam 13m, it's like two meters thick, was cut by the technology of deep-hole presplit ting blasting using water gel explosive. The long-range and high tensile dynamic pressure impact was avoided for preventing the state transiting of key stratum. New hydraulic support and mining technology were designed, coal cutting and coal wall totally-enclosed in face guard with high pressure state. Based on the test result of 66207 working face, injecting water technique combination between long hole in the haulage roadway and tailgate in advance and shallow hole in the coal wall in advance was proposed. The working face was mining successfully with good safety and efficiency, realize the technological breakthrough of the three soft coal seam.

KEYWORDS:
Coal mines, working face, technological breakthrough, efficiency

INTRODUCTION

Coal is the main energy in China. The coal in the eastern region plays a key supporting role for the development of regional economy. The coal resource amount of Huainan coalfield is in rich reserves and accounts for 50% of the total in East China. With the continuous expansion of coal mining scale, coal mining difficulty gradually increases and results in a series of problems. The outstanding one is the surrounding rock (coal) stability control under the mining condition of coal seam groups. The coupling effect between the support and surrounding rocks by treating the two as an organic whole is investigated to solve this problem [1]. The petro physical parameters of the coal-bearing strata in Huainan coalfield using crossplot technique and statistical analysis method are researched [2]. He et al. thought that deep mining was reflected as the harsh environment of "three highs-disturbance", 5 mechanical properties change characteristics, 4 aspects of mine transformation, and 6 disaster forms [3]. On the basis of a large amount of field investigation, the theory of that there was the stress shell composed of "high-stress beam" in the surrounding rock space of stope was put forward [4]. Ning pointed out that coal wall was the mechanical model of stressed rod with simply supported upper end and solidly supported lower end and considered that the stopping position of 0.35 times above the coal wall develops fracture firstly, followed by the rib spalling of the whole coal wall [5]. Fang thought that there was arc "sliding surface" in coal wall and the key for controlling the wall stability was to control the "sliding surface" [6]. Wang proved that advancing acceleration was an effective measure for avoiding the coal wall caving [7]. Researchers around the world have conducted studies on this topic and got a series of achievements [8-13]. However, existing researches mainly concern about the medium-thick and medium-hard single coal seam using single technological means and have no mature experiences to learn from. Therefore, in accordance with the engineering conditions of 66207 working face in Xinzhuangzi Coal Mine, the surrounding rock stability of the fully mechanized coal face of three-soft coal seam was regarded as a systematic project under coal seam group mining conditions. Moreover, based on the overall concurrent coordination control needs of the surrounding rocks in the stope, a time-space-method 3D control technology for the surrounding rocks in the stope with large dip angle was put forward under the engineering background of the 66207 working face in Xinzhuangzi Coal Mine. The emphasis of this technology lies on the coordination and integration of vertical control technology.

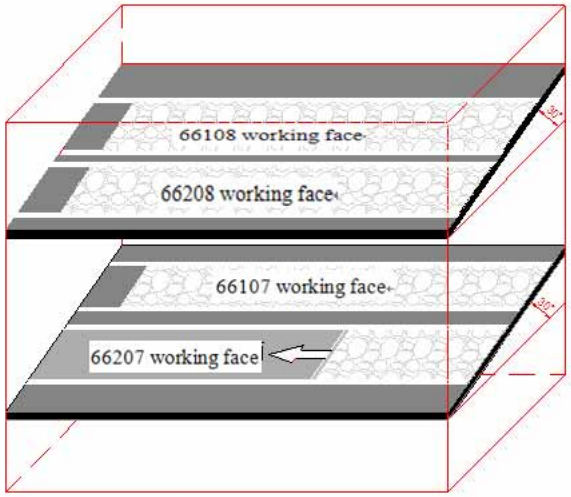


FIGURE 1
Position in space of four working faces

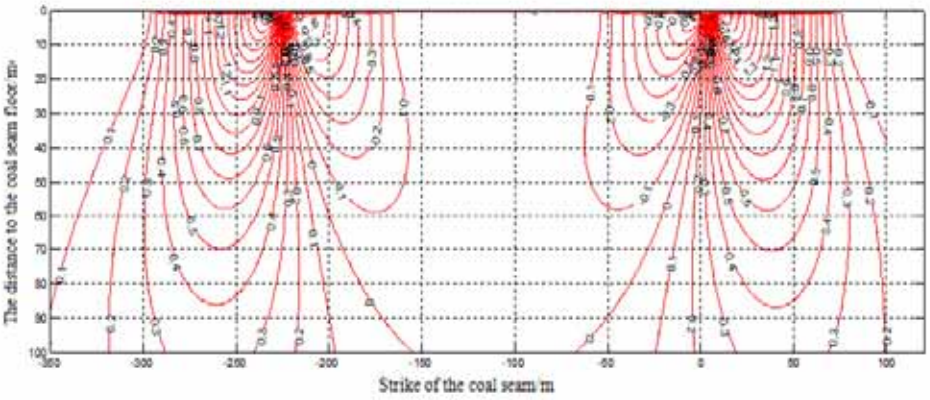


FIGURE 2
Propagation rule of additional vertical stress coefficient on floor direction

MATERIALS AND METHODS

The engineering and geological conditions. The 66207 working face has an elevation of -721m ~ -793 m, average thickness of coal 3.0 m, and a dip angle of 27°-34°(30° on average). The coal in this working face has an average coal point load strength index of 0.19 MPa and moisture content of 2.46%. Except the underlying B6 coal, the 66107 working face and overlying B8 and B10 coals have been mined on this working face. The spatial positions of the four working faces are shown in Figure 1. Figure 2 presents the comprehensive columnar section.

Main Technological Problems. The mining on coal seam group induces the superposition of the com plex stress field and displacement field between the mined coal seam and the adjacent coal seams. In case of coal pressure, these coal seams are in complex temporal and spatial relationships. The 66107 working face, which is neighbored with 66207 working face, has an elevation of -595 m~-693 m, strike length of 350 m, inclination length of 215 m, average thickness of 3.8 m, and average coal seam dip angle of 23°. During the stopping process, this working face saw violent rib spalling and roof caving, which greatly affected the safe and efficient production of working face. Comparing with the 66107 working face, the mining on 66207 working face required more complicated mining technology. Meanwhile, natural false roof was formed on 66207 working face due to the overall continuity damage during the stopping on 66208 working face. Moreover, the coal seam on this working face was mainly composed of

soft coal. The soft coal was provided with extremely low compressive strength, shearing strength, and cohesion and thus intensifies the wall caving degree of 66207 working face. The main technological problems encountered in the stopping of this working face are indicated as follows:

(1) The pressure relief effect and protection scope during mining the multiple protective layers of coal seam group, and the reasonable temporal and spatial distribution of the underlying coal seam stope.

(2) The determination on the large-dip-angle three-soft coal seam support, support strength, and reasonable working resistance, especially the way to realize the whole time-space high-strength support to coal wall and the whole-section control on natural false roof.

(3) Water injection on coal seam is a main technique mean for preventing the rib spalling of coal seam. However, the water penetration in coal is resulted from the coupling effect of internal and external factors and is subjected to the influences of artificially-controlled water injection process. Thus the problems arises as how to reasonably determine the water injection pressure, water flow, injection time, and the allocation way of drill hole (length, space, sealing way of drill hole etc.) .

(4) The implementation of the pressure relief technology on the tight roof of highly gassy mine, as well as the determination on the action mechanism, explosive development, drill hole layout, and blasting parameters of deep-hole pre-splitting blasting.

RESULTS AND DISCUSSION

Time-Space-Method 3D Controlling Technology for Surrounding Rock. On the basis of the technical conditions and mining geological conditions of coal seam, the location and layout of the stope are determined reasonably. Moreover, the geometrical parameters of working face, such as the layout, working face length, and mining height etc., are optimized to propose a new design plan.

Traditional plan. The airway of 66208 working face is externally alternated with that of 66207 working face. It is located in the gob of 66108 working face and is 10 m away from the crossheading of 66108 working face horizontally. The cut hole is 10 m in earlier phase and is increased to 170 m after stoping of 130 m along the strike.

In accordance with elastic-plastic mechanics theory, minor transverse stress load (being perpendicular to the spatial semi-infinite plane) applying on homogeneous isotropic spatial semi-infinite plane is defined as $q_1 d\xi$. On arbitrary point $M\ x, y$ in the floor strata, the stress induced by this load is expressed as:

$$\left.\begin{aligned} d\sigma_x &= \frac{2q_1 d\xi}{\pi} \frac{(x-\xi)^2 y}{\left[(x-\xi)^2 + y^2\right]^2} \\ d\sigma_y &= \frac{2q_1 d\xi}{\pi} \frac{y^3}{\left[(x-\xi)^2 + y^2\right]^2} \\ d\tau_{xy} &= \frac{2q_1 d\xi}{\pi} \frac{(x-\xi)y^2}{\left[(x-\xi)^2 + y^2\right]^2} \end{aligned}\right\} \quad (1)$$

Figure 3 shows the propagation law of additional vertical stress along the floor direction caused by the mining by integration of Eq.(1) using Matlab mathematics software. It is found that, the compressive stress on the floor ahead of coal wall presents a "bulbs"-shaped propagation. Bordered by the original rock stress contour of floor, stress is concentrated in the floor strata under the coal on both sides of the working face, while pressure is relived in the strata in the floor of the gob. Moreover, the original rock stress contour refers to the curve deeply penetrating into coal and obliquely extending along the strata in the floor of working face. Additional vertical stress decreases with the increase of buried depth and its the peak attenuates by negative exponential law. The stress concentration peaks in the range of 26 m away from the coal seam floor and rapidly diffuses beyond this range.

Figure 3-4 illustrate the simulation results of maximum principal stress field and failure zone on the dip section that is 10 m away from the back of coal wall using the nonlinear 3D numerical calculation software FLAC3D, as the 66208 working face is excavated for 200 m.

Being consistent with the theoretical calculation result, the working face layout in the plan proposed would result in the stress concentration on the upper part of 66207 working face and the rib spalling, roof leakage, fly waste accident subsequently. At the same time, the large dip angle, high mining height, and soft coal of the 66207 working face also intensify the spalling degree of coal wall of 66207 working face.

New plan. The airway of 66207 working face is designed in the low-stress region under the protection of floor stress shell of 66208 working face by an internal displacement of 10 m (see Figure 4). This design to avoid the stress concentration zone formed by the coal pillars in 8-groove section; the working face length is controlled at about 150 m.

The roof of B8 coal, which is 12 m above the B7 coal, are composed of the sandy mudstone of 7.3 m thick, B9 coal of 0.8 m thick, fine sandstone of 3m thick, and the medium sandstone of 11.0 m thick with favorable integrity and high strength. The sandy mudstone, 9 coal, and fine sandstone above the B8 coal are prone to be broken into loose structure and show slight influences on the mining on 66207 working face. However, since the overall continuous key strata medium of medium sandstone before the excavating on working face 66208 is transformed into

a quasi-continuous one, the mining disturbance of 66207 working face would change the quasi-continuous state into non continuous state. Such medium state conversion would result in a large area of dynamic pressure impact on the coal on front of 66207 working face and the support in the stope, which develops as the hidden dangers of 66207 working face. To realize the advance pre-splitting blasting of key sandstone strata during the roof caving process, deep-hole pre-splitting blasting is necessary.

Therefore, during the stoping process of 66208 working face, the highly gassy mine-orientated high-energy water-binder grain pre-splitting blasting technology was utilized in the transportation roadway by

explosive height of 23.0 m. Each group was drilled with three holes by space of 2 m(calculated by Eq.(2)). Group space was smaller than the periodic weighting layout. Meanwhile, to minimize the work amount, the group space was set as 30 m finally. Figure 5~6 show the allocation of drill holes.

$$E = Kr_b f^{\frac{1}{3}} \quad (2)$$

Where, K is adjustment coefficient and is set as 10~15 generally; r_b is the radius of drill hole; f refers to the strata harness.

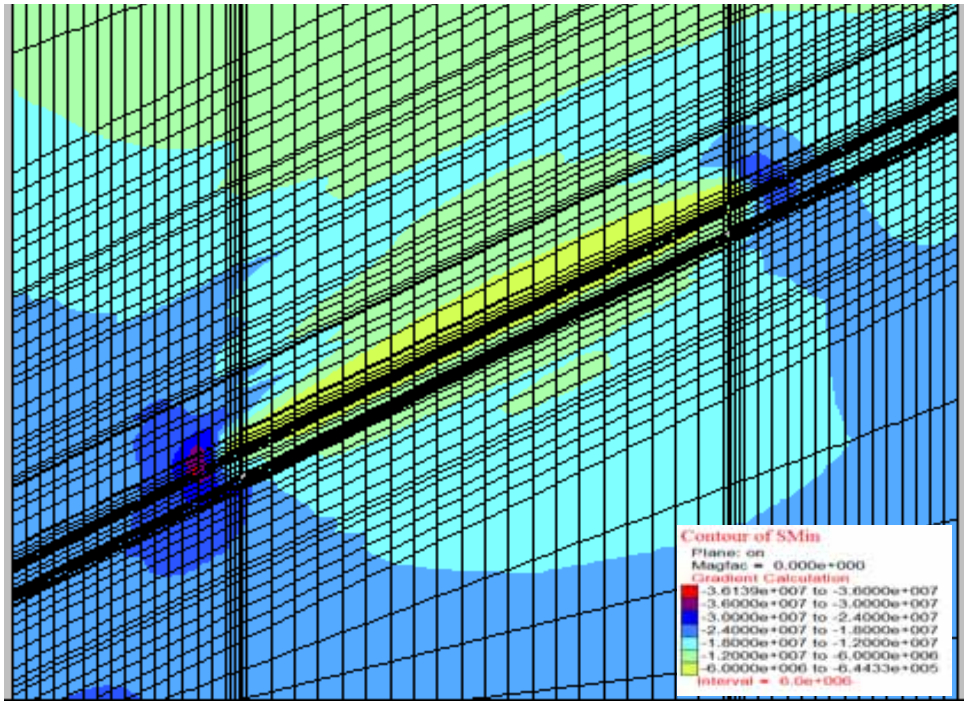


FIGURE 3
Cloud maps of principal stresses on dip section

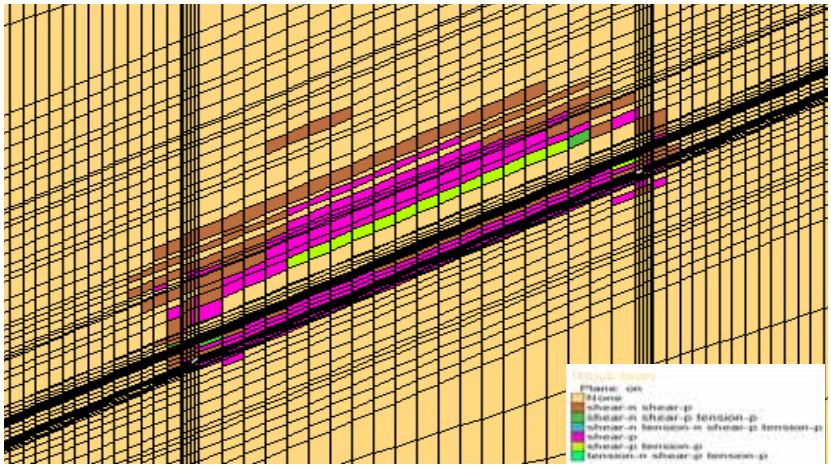


FIGURE 4
Failure zone on dip section

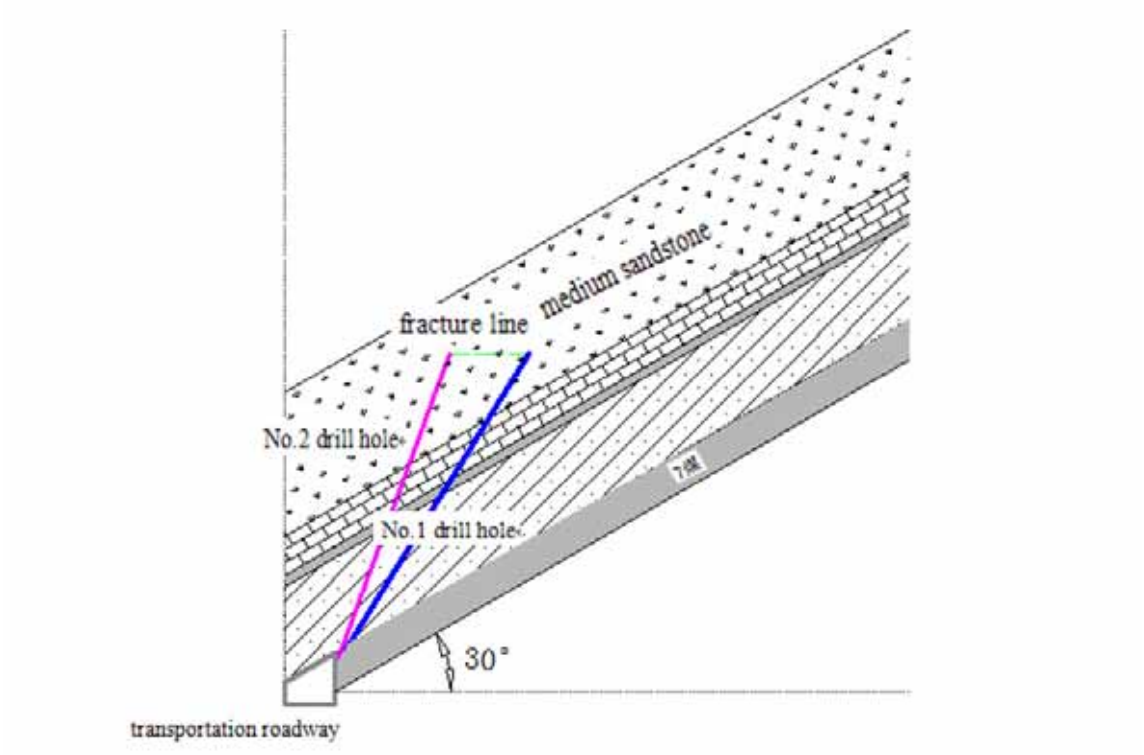


FIGURE 5
Layout of drill hole section

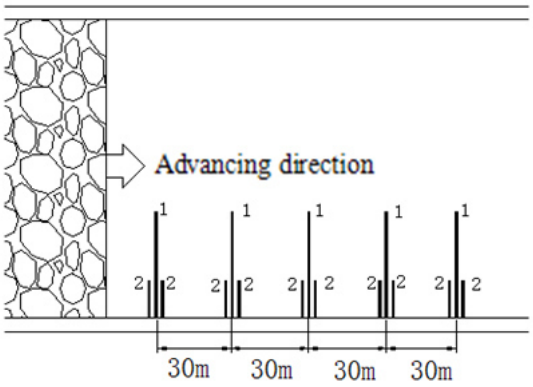


FIGURE 6
Layout of drill hole vertical view

According to horizon relationship of the strata in field, the drill hole parameter, explosive charge, and hole-sealing length were calculated, as shown in Table 1. The drill hole is sealed using yellow mud and pneumatic sealing machine. The drill hold depth is calculated according to the formula below:

$$S_b = \sqrt{(\frac{s-d}{\sin\alpha})^2 + [\tan\beta(s-b)]^2} \quad (3)$$

Where, S is the length of the working face; d is the horizontal distance between drill hole bottom with roadway; α is the angle between the drill hole and the roadway; β is the angle between the drill hole and the working face.

The physical properties improvement of coal was studied according the experimental study in laboratory. The test is repeated for 68 times in total (17 × 4). The experiment used the intelligent controlling direct shear apparatus at shear velocity of 0.1mm/min. Figure 7 shows the experiment process. Figure 8 displays the shear strength and axial load experimental results of coal and water under different preparation ratio conditions.

TABLE 1
Layout parameter of drill hole

position	No.	length/ m	Eleva- tionangle/°	Radius / mm	Explosive length/m	Explosive charge/kg	Sealing length/m
Crossheading	1	80	47	75	68	224.4	12
	2	36	70	75	26	85.8	10



FIGURE 7
Intelligent controlling direct shear apparatus

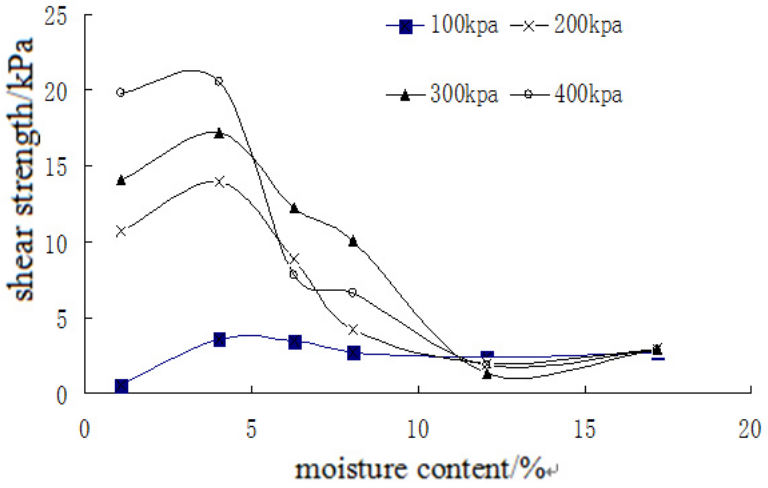


FIGURE 8
Moisture content- shear strength curve

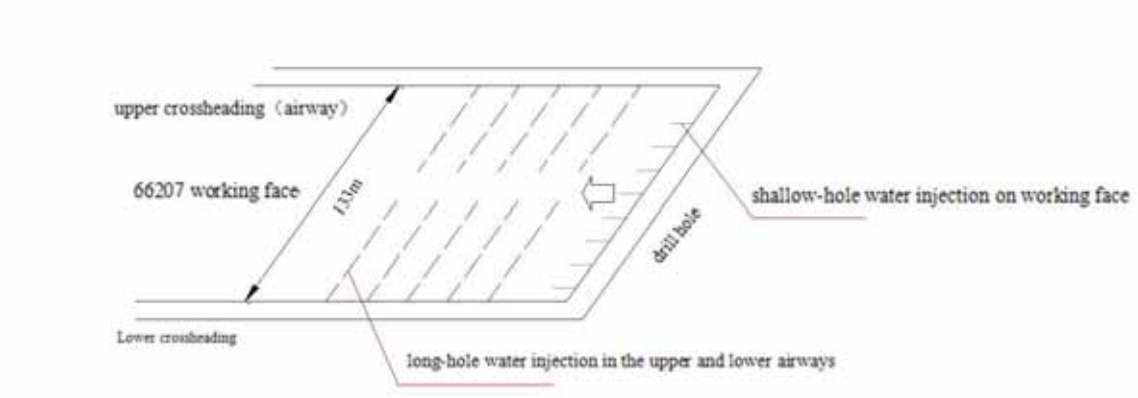


FIGURE 9
Water injection on 66207 working face

Laboratory test results show that: 66207 working face has extremely low natural moisture content and is easy to lose water due to the weak water-holding capacity. The shear strength increases with the increase of the moisture content in range of 0 ~ 4.03%, while sharply reduces with the increase of moisture content in a range of 4.03% ~ 12.7%. In the range of 1.07% ~17.07%, the sensitivity of cohesion to water is far higher than that of internal friction angle to moisture content.

According to the physical property variation law of coal before and after water injection obtained from the experiment, this study proposed an improved water injection technology, namely, injecting water to the upper and lower roadways 5 m ahead of coal wall through far and deep–drill holes under static pressure and injecting water into coal wall through shallow hole under dynamic pressure (Figure 9). Drilling parameters: the shallow drill holes for the water injection on the working face are 8 m in depth, 70 mm in diameter, and spaced by 4 ~5 m. The water injection on the upper and lower roadways was through the inclined crossheading drill holes in space of 10 m abandoned in the exploration position (or pumping area);injection time: the shallow drill hole water injection on the working face was conducted in the maintenance time. Single-hole water injection time should controlled in 45 min, or, the water injection is terminated in the case of water flowing out from the coal wall or adjacent drill holes; water injection pressure was set as 1~3 MPa on the coal wall of working face, while 3～5 MPa on the drill holes in upper and lower roadways.

The design of the hydraulic support with large dip angle and mining height lies in satisfying the coal seam occurrence conditions and optimizing the structure to ensure parameter reasonability, reduce the influences of adverse factors, and effectively improve the stability of hydraulic support. To achieve this purpose, a new hydraulic support was designed. The key parameters and structure were optimized as follows: the working resistance was increased into 8,800 KN and the pillars were changed into solid structure; the middle part of the support employed an overall top beam with internal retractable beam; the two-grade face guard structure under hydraulic control was applied. The first-grade face guard was 1100 mm long and the second-grade one was 700 mm. The side guard plate of top beam was 650 mm on the rear end; the jack of retractable beam had a stroke of 1,000 mm.

The coal cutter contains a roller with cutting depth of 800 mm and a retractable beam jack with stroke of 1,000 mm. It realizes the coal cutting of roller under the support of the working resistance of 1-grade face guard. Meanwhile, 10# metal mesh (3.4 mm in diameter) was placed on the roof to strengthen the roof management using capstan. During the placing, the retractable beams of corresponding support were all knocked out (or reach to the coal wall). Meanwhile, the face guard was retracted so that the placed rhombic metal mesh can hang down to facilitate mesh connection; after the metal mesh placement, the face guards were knocked out after workers retreated to the safe position between the front and rear pillars of the lateral support in the gob. The overall whole-time support of the internal roof plate-coal wall in the stope and the intrinsically personnel safe production were realized. Figure 11 is the scene of 66207 working face.

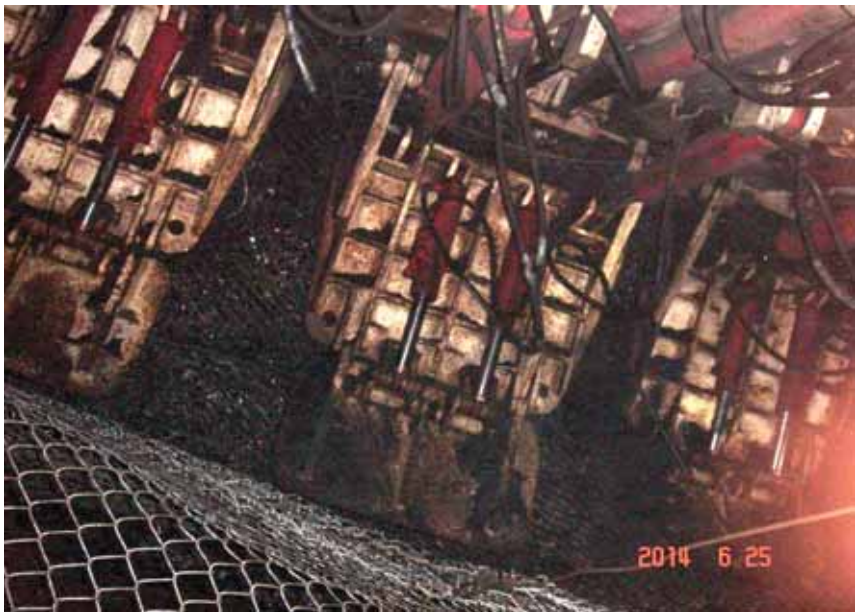


FIGURE 10
Graphics for the scene of 66207 working face

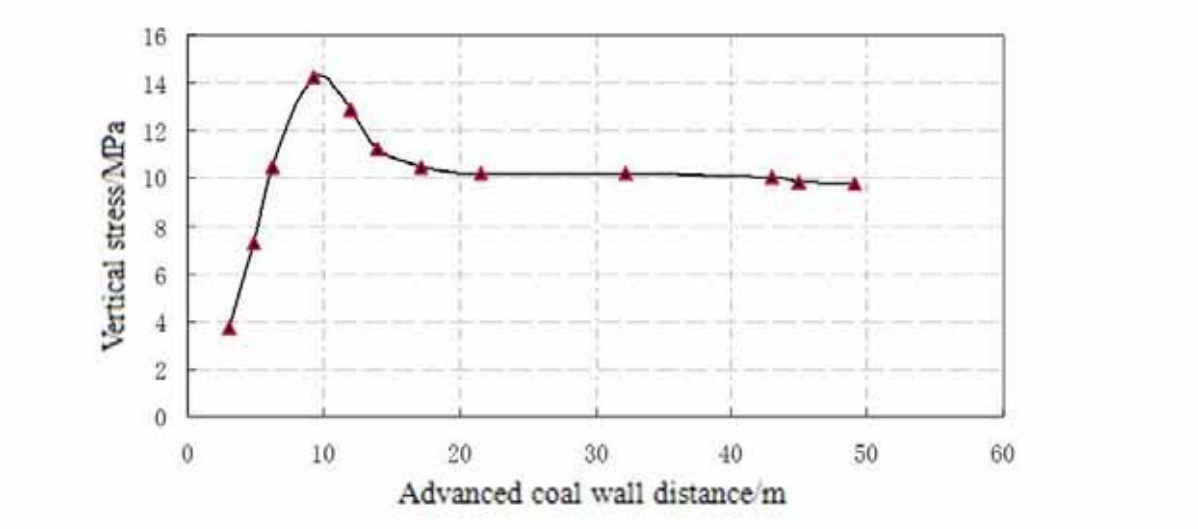


FIGURE 11
Stress Distribution on the strike

The advanced abutment pressure and the working resistance of hydraulic support on the working face were observed in field to validate the application effect of the key time-space-method 3D surrounding rock control technology. Figure 10 shows the observation results of advanced abutment pressure. Figure 11 shows the working resistance observation results on the hydraulic support in the middle part of the stope as the mining advances to a range of 90 m in March 3rd to March 18th. As shown, after the comprehensive time-space-method 3D technical measures were used to mine the 66207 working face, the key overlying strata was transformed from the quasi-continuous and periodic state into the non-continuous state. Subsequently, they filled the gob together with the underlying caved loose rock in time without large area dynamic load impact on the support of the working face. Instead, the support was applied with a smooth pressure and did not show the first weighting or periodic weighting phenomena. After water injection, some hydrophilic and soluble minerals in coal were dissolved. Meanwhile, a small amount of hydrophilic minerals swelled by absorbing water and presented enhanced anti-deformation capacity. Outwardly, the coal was softened and the abutment pressure influence range was greatly reduced to 21 m only. The peak value of abutment pressure was observed on the 9.6 m in front of the coal wall with a bearing pressure coefficient of 1.5.

CONCLUSIONS

(1) The surrounding rock stability of the fully mechanized coal face of three-soft coal seam was treated as system engineering under coal seam group mining conditions. According to the overall coordination needs of the control on surrounding rocks in the stope, this study proposed a key time-space-method 3D technology for controlling the surrounding rock in the stope, with the emphasis on the coordination and integration of vertical control technology.

(2) The design plan was indicated as follows: the low-stress area under the protection of 66208 floor stress shell distributing in the airway by a displacement of 10 m was put forward from the design origin of the mining area; then the key strata of the overlying strata of the 66207 working face was pre-split and blasted using water-binder grain. Moreover, targeted stope support and mining technology were designed. Finally, combining with the experimental result on the physical properties of 66207 working face, a mining technology was put forward, namely, near-field short-time shallow-hole water injection on the working face under dynamic pressure and long-hole pre-water injection on the two advanced roadways under static pressure.

(3) New breakthrough was achieved on stopping technology for three-soft coal seam with large dip angle. The technology has significant economic benefits by accelerating the advancing speed on 66207 working face by 6 times without the use of chemical filling materials. It provides a new study idea for the surrounding rock stability control in the three-soft coal seam stope with coal seam groups.

ACKNOWLEDGEMENTS

This research was supported by State Key Research Development Program of China (2017YFC 0804202), and the Nature Science Research Project of Anhui province (1408085MKL41).

REFERENCES

[1] Zhang, Y., Zhang, Y., Yu, T. and Hu, C.M. (2012) Characterization of degradation of dom from taihu lake under different conditions using multiple analytical techniques. Fresen. Environ. Bull. 21,1118-1126.

[2] Zhu, M., Bazail, N.A., Li, X.L., Huang, M.N., Mohammad, T., Lei, M. and Wang, H. (2017) Research on wetland ecological restoration of coal mining subsidence area in Suzhou, China. Fresen. Environ. Bull. 26, 5177-5183.

[3] Mao, D.H., Wang, Z.M., Wu, C.S., Zhang, C.H. and Ren, C.Y. (2014) Topsoil carbon stock dynamics in the Songnen Plain of Northeast China from 1980 to 2010. Fresen. Environ. Bull. 23,531-539.

[4] Xie, G.X. and Chang, J.C. (2009) Investigations into stress shell characteristics of surrounding rock in fully mechanized top-coal caving face. International journal of rock mechanics & mining science. 36, 172-181.

[5] Yu, N. (2009) Mechanism and control technique of the rib spalling in fully mechanized mining face with great mining height. Journal of China Coal Society. 34, 50-52.

[6] Fang, X.Q., He, J. and Li, H.C. (2009) A study of the rib fall mechanism in soft coal and its control at a fully mechanized top coal caving face. Journal of China University of Mining & Technology. 38, 640-644.

[7] Wang, J.C. and Chen, G. (2005) A study on the mine pressure law on the dead soft blast layer working face. China Mining Magazine. 14, 56-59.

[8] Yuan, Y., Tu, S.H., Wu, Q., Ma, X.T., Tu, H.S. and Sun, L.L. (2011) Mechanics of rib spalling of high coal walls under fully mechanized mining. Mining Science and Technology. 21, 129-133.

[9] Liu, C.Y., Huang, B.X., Chang, X.M., Wang, J.and Wei, M.T. (2008) Study on tip to face coal and rock stability control of fully mechanized stepped large cutting height mining in extremely soft thick seam. Journal of China University of Mining &Technology. 37, 734-739.

[10] Tu, S.H., Yuan, Y., Yang, Z., Ma, X.T. and Qi, W. (2009) Research situation and prospect of fully mechanized mining technology in thick coal seams in China. Procedia Earth and Planetary Science. 1, 35-40.

[11] Yin, X.W., Yan, S.H. and An, Y. (2008) Characters of the rib spalling in fully mechanized caving face with great mining height. Journal of Mining & Safety Engineering. 25, 222-225.

[12] Yan, S.H. and Yin, X.W. (2008) Discussing about the main theoretical problems of long wall with top coal caving. Journal of China Coal Society. 33, 481-484.

[13] Gong, P.L. and Jin, Z.M. (2004) Study on the structure characteristics and movement laws of overlying strata with large mining height. Journal of China Coal Society. 29, 7-11.

Received: **12.07.2017**
Accepted: **03.10.2017**

CORRESPONDING AUTHOR

Jia- zhuo Li
Anhui Province Key Laboratory of Mining Response and Disaster Prevention and Control in Deep Coal Mine, School Energy Resources and Safety, Anhui University of Science and Technology, Huainan, Anhui 232001 – China

e-mail: jiazhuo312@126.com

© by PSP Volume 26 – No. 12A/2017 pages 8109-8118 Fresenius Environmental Bulletin

GHOST FISHING EFFECTS OF LOST BOTTOM TRAMMEL NETS IN A STORM: A SIMULATION

Caner Enver Ozyurt[1,*], Ferhat Buyukdeveci[2], Volkan Baris Kiyaga[1]

[1]Cukurova University, Faculty of Fisheries, Balcali Campus, Sarıçam, Adana, 01330, Turkey
[2]Sinop University, Faculty of Fisheries, Akliman Abali Koyu, Sinop, 57000 Turkey

ABSTRACT

The ghost fishing effects of bottom trammel nets, which drift on rocks in the bad weather conditions were investigated in regards of mortality of commercially important and endangered species in this study. Underwater experiments were performed in Yumurtalik, Iskenderun Bay between June 2013 and October 2013. Two panel experimental nets were used and data were gathered by underwater observation. During the study, 26 different species, belonging to 17 families, were caught in experimental nets. Teleost and crustaceans formed 98% of the captured individuals. The 24-hour catch rate of the experimental nets showed a rapid decline in the first few weeks and, by the 60th day, the decline was 80%. Afterwards, the decline slowly continued. No individual was caught in experimental nets after the 105th day. For this reason, the fishing life of the lost nets was assumed to be day 105. In the region, the mortality numbers of teleosts and crustaceans caused by bottom trammel nets lost by the entire fishing fleet were identified as 1291 (100 kg) and 6102 (990 kg) individuals, respectively. This mortality rate (0.55% for fish) can be considered to be insignificant in all fisheries, but the mortality rates of threatened species, such as *Epinephelus marginatus* and *Chelonia mydas*, were found to be noteworthy.

KEYWORDS:
Lost net, ghost fishing, Iskenderun Bay, *Epinephelus marginatus*, *Chelonia mydas*

INTRODUCTION

Lost or abandoned fishing gear may continue to function in water and contribute to the mortality of marine organisms. This phenomenon is defined as "ghost fishing" [1]. All types of fishing gear may be lost during fishing activity, but not all have ghost fishing effects. Active fishing gear, such as trawls and seines, lose their fishing function after they are lost. However, passive fishing gear, such as gillnets, trammel nets and pots, may continue to be used in fishing. Therefore, these types of fishing gear are the main concern of ghost fishing.

Studies on ghost fishing do not have a long history. Early studies on ghost fishing were conducted on cage traps in the 1970s. [2-5]. The work related to set nets, especially drift nets and pelagic gillnets, was performed in the 1980s [6-8]. Recently, studies have focused on the effective fishing time of lost gill and trammel nets as well as the mortality rates they cause based on underwater observations. The experiments were performed under different fishery conditions, such as different areas, depths, and bottom types. For example, Kaiser et al. [9] studied the ghost fishing effect of gill and trammel nets in Wales, England, and Erzini et al. [10] studied the effect in Algarve, Portugal. Santos et al. [11] tried to determine the ghost fishing effect of a monofilament set net in Algarve, Portuguese. Sancho et al. [12] investigated the ghost fishing effect of tangle nets used in monkfish catching in northern Spain. Ayaz et al. [13] compared the ghost fishing effects of monofilament set nets with those of the multifilament nets in İzmir Bay, Turkey. Baeta et al. [14] compared the ghost fishing effect of trammel nets for a rocky bottom versus a sandy bottom. In all studies, it has been reported that an effective fishing time and mortality rate may change according to the area, depth, bottom type, species composition and abundance, as well as environmental factors, such as currents, waves, and so on.

Fishing gear may be lost for a variety of reasons, such as bad weather conditions, conflicts with other fishing gear, and vandalism [1]. The cause of their loss may change according to the fishing type and environmental conditions. For instance, long line and pot fishing areas overlap in Iskenderun Bay. Fishermen whose longline is attached in pots cut their buoyant ropes or consider different locations. This increases the pots losses [15], leading to increasing pot losses in this area. Trammel nets in sole fishing and trawl fishing are used in the same area in Iskenderun bay between October and November. This condition commonly causes conflict between the two types of fishing gear. Hence, sole trammel net losses are observed in this area.

Iskenderun bay has richer fishery sources than the other areas in the eastern Mediterranean [16]. For this reason, there are 11 fishing ports in which each type of fishery method, trawl, seine, set net, pot, and longline, is used in this bay. Yumurtalik is a small

but important fishery port. Ceyhan, which is an important river in Turkey, pours into this area, and there are many lagoons that have a slowly increasing depth. Sandy and muddy bottom structures are common in this area. However, there are some rocky fields in these areas. This region is also important for some threated species. For example, it is crucial for breeding and nesting of *Chlonia mydas* [17, 18]. In addition, *Epinephelus marginatus* is common on rocky habitat. These two species classified as endangered in the Red List of Threatened Species.

Fishery activity is performed around rocky fields which local fishermen call “Pistas, Abdulkerim, Orman kayası vs”. More than 40 fishing boats, which are smaller than 10 m, catch using a set net around them. Usually, trammel nets that are used to catch species belonging to sparids and serranids are set around and among these rocks. However, trammel nets set near rocks may be lost by drifting and tangling with rocks due to bad weather conditions [19]. Fishermen usually try to find lost nets and retrieve them. However, they are not always successful. It has been observed that the number of lost nets may increase by up to 40% after severe and unexpected storms, indicating that there is a risk of ghost fishing in the area.

In this study, the loss of trammel nets, which were set around rocks, was simulated; then, the ghost fishing effect was investigated by direct observation. Additionally, commercial fishing was simulated with control nets, which have the same characteristics as the lost nets. Hence, lost nets were compared to control nets in terms of different parameters, such as the species composition and catch ratio.

MATERIALS AND METHODS

Surveys were performed in Yumurtalik, Iskenderun Bay (Figure 1). Seven panel trammel nets were used in this study. The technical features of these trammel nets are similar to those used by fishermen. These nets were constructed of monofilament nylon; the inner mesh size was 64 mm, and outer mesh size was 240 mm. Each panel was approximately 100 m long and 2.4 m high.

The cause of loss is generally bad weather in the region. Nets drifting in the storm are attached rocks. To imitate this, two panel nets were drifted for two minutes by boat and attached to the rocks. These rocks were at a depth between 9 and 11 meters. After this operation, two lost nets covered one side of two rock masses with approximately 25 m of sandy bottom between them. After 24 hours of deployment of

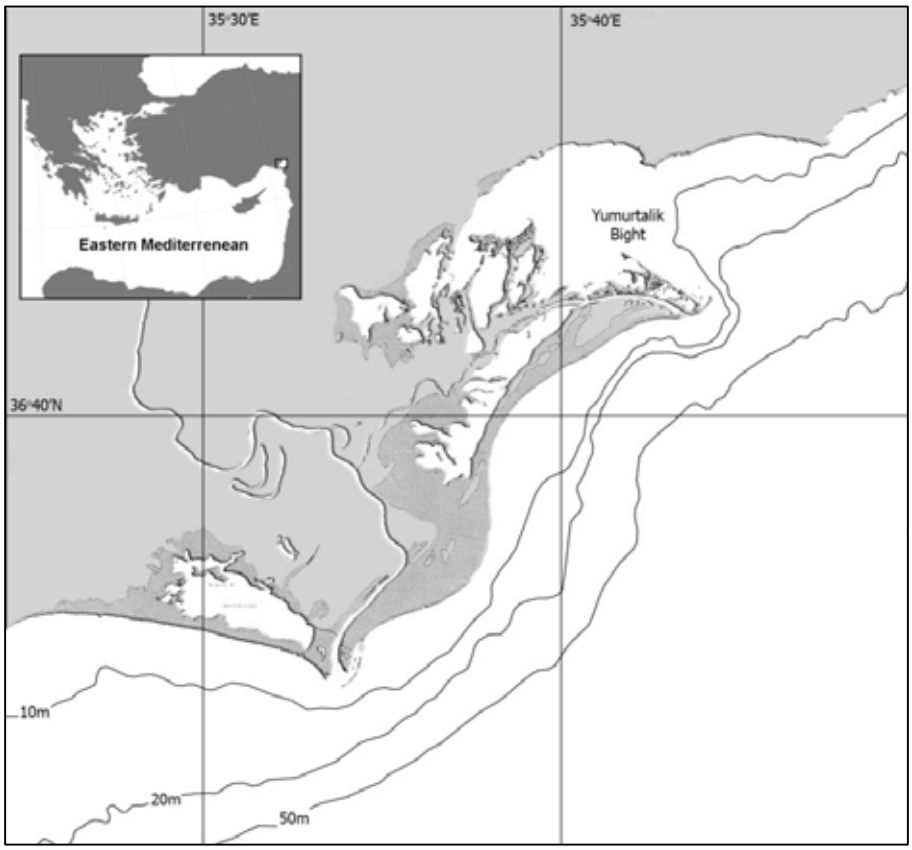


FIGURE 1
Study area



FIGURE 2
Measurement and marking of marine organisms in the underwater observation

the lost net, the first underwater observation was performed on 20.06.2012 and last was on 17.10.2012 (120 days after deployment). During this period, 25 underwater observations were conducted.

To determine the 24-h catch rate, the nets were monitored at 15-day intervals. Three underwater observations were performed for every fifteen-day period. Marine organisms that were entangled during the 15-day period were tagged with plastic tags one day before the first observation. After 24 hours, two scientific divers examined the two lost nets from beginning to end. Organisms entangled during this 24-hour period were recorded, and their lengths were measured and tagged by the diver (Figure 2). Entangled organisms were not removed from the nets. The 24-h catch rate of one panel net was determined by using the following formula:

$$C_r = \frac{\sum_{i=1}^{s} \sum_{j=1}^{p} \sum_{k=1}^{p} N_{ijk}}{O \times P}$$

In this equation:

C_r = 24 h catch rate of experimental nets,

S =Number of species observed in each period,

O = Number of underwater observations in each period,

P = Number of panel,

Nijk : number of individuals belonging to species i, observed on the panel k. during the sampling period j.

The weight of organisms entangled in the lost nets was calculated via length-weight relationship ($W = aL^b$). The length-weight relationships of many species were calculated from individuals that were caught in control nets; because few of the same species were caught, the length-weight relationships were taken from the literature.

In order to model the rate of decay of catch quantity and estimate the total catch in the lifetime of the gear exponential decay models were fitted to the pooled daily catch data in numbers ($N_t = N_0 e^{-rt}$) and in weight ($B_t = B_o e^{-rt}$). Where "N_t" and "B_t" were the 24 h catches in numbers and weight (g) respectively at the day t after deployment. "N_o" and "B_o" were the intercepts, "r" was the rate of decrease.

To evaluate the catching efficiency, five control nets with the same characteristics as the experimental nets were set near the experimental nets on same day as the underwater observation. The efficiency of the experimental nets was calculated by the formula:

Efficiency= Experimental nets catches/Control nets catches

The effective lost net number was calculated by the formula $T_{Ln} = (M_{Ln} x\ B_{Ln})\ x\ \alpha$. In this equation, T_{Ln} is the number of total effective lost nets; M_{Ln} is the mean of lost nets for one fishing boat; and B_{Ln} is the number of fishing boats that lost a net during the season in which this study performed. It was accepted that half of the total lost nets continued to be used in fishing (α=0.5). The number of fishing boats that lost nets was determined by talking to the fishery cooperative. Changes in the physical condition of the lost net were visually monitored and recorded with underwater photography.

RESULTS

During the surveys, two panels of experimental nets and five panels of control nets caught a total 26 species belonging to 17 families and 4 groups. Two-hundred-forty individuals were caught in the experimental nets, consisting of 53 teleosts, 183 crustaceans, 1 batoidae and 3 reptilia, and 1220 individuals were caught in the control nets, consisting of 127 teleosts, 1062 crustaceans, 30 batoidae and 1 reptilia. Approximately 98% of the total catch in both the experimental and control nets consisted of teleosts and crustaceans. The number and weight of the individuals caught in one experimental and control net panel are given Table 1. The length-weight relationship used to calculate the weight of the captured experimental nets is given in Table 2.

TABLE 1
Mean number and weight (g) of individuals caught in one panel (100 m) net

		Experimental Net		Control Net	
		n	w	n	W
Teleost		26.5	3575.969	25.4	2659.91
Clupeidae		1.5	10.685	1.2	33.636
	Sardinella maderensis	1.5	10.685	0.8	23.662
	Clupeidae sp.			0.4	9.974
Engraulidae		2.5	10.28	3.8	23.144
	Engraulis encrasicolus	2.5	10.28	3.8	23.144
Holocentridae				0.8	65.268
	Sargocentrum rubrum			0.8	65.268
Labridae		2.5	366.139		
	Sympodus tinca	2.5	366.139		
Mugilidae		0.5	356	0.8	287.82
	Liza aurata			0.2	91.456
	Mugilidae sp	0.5	356	0.6	196.364
Sciaenidae		1.5	1522.82	2.2	667.224
	Umbrina cirrosa	1.5	1522.82	2.2	667.224
Scombridae				0.2	5.022
	Scomber japonicus			0.2	5.022
Serraniidae		11	930.97	3.6	337.08
	Epinephelus marginatus	7	689.475	3	316.458
	Mycteroperca rubra	1	141.49		
	Serranus scriba	3	100.005	0.4	12.768
	Serraniidae sp.			0.2	7.854
Siganidae		0.5	10.63	3.2	340.026
	Siganus rivulatus	0.5	10.63	3.2	340.026
Sparidae		6.5	368.445	9.6	900.69
	Diplodus annularis	0.5	9.325		
	Diplodus sargus	1.5	104.185	2.2	142.902
	Diplodus vulgaris	1.5	34.25	1	52.412
	Lithognathus mormyrus			0.8	74.418
	Oblada melanura	0.5	14.135		
	Sparus aurata	2.5	206.55	5.6	630.958
Crustacea		91.5	6640.18	212.4	24900.456
Portunidae		71.5	4617.84	195.6	23334.72
	Callinectes sapidus	27	1812.22	126.6	17986.804
	Carcinus mediterraneus	44.5	2805.62	61.2	3850.768
	Portunus pelagicus			7.8	1497.148
Xanthidae		20	2022.34	10.2	1450.956
	Atergatis roseus	20	2022.34	10.2	1450.956
Squillidae				6.6	114.78
	Erugosquilla massavensis			6.6	114.78
Batoidea		0.5	180.63	6	1749.016
Dasyatidae		0.5	180.63	5.2	1515.81
	Dasyatis pastinaca	0.5	180.63	5.2	1515.81
Rajidae				0.4	202.076
	Rostroraja alba			0.4	202.076
Torpedinidae				0.4	31.13
	Torpedo torpedo			0.4	31.13
Reptilia		1.5		0.2	
Cheloniidae		1.5		0.2	
	Chelonia mydas	1.5		0.2	
Total		120	10396.779	244	29309.382

TABLE 2
Length-weight relationship of species caught in experimental nets (*: calculated from the data obtained from our different studies in the same area; **: Karakulak et al. [20]; and ***Özvarol and Gökoğlu [21])

Groups/Family	Species	Length Range			Length–weight relationship parameters			
		n	Min.	Max.	*a*	*b*	SE (*b*)	r^2
Teleost								
Clupeidae	*Sardinella maderensis**	119	10.80	30.70	0.007	3.022	0.033	0.987
Engraulidae	*Engraulis encrasicolus**	169	6.00	11.50	0.012	2.677	0.053	0.939
Labridae	*Sympodus tinca***	248	10.00	26.80	0.011	3.046	0.032	0.974
Sciaenidae	*Umbrina cirrosa**	76	13.50	50.00	0.014	2.894	0.038	0.998
Serraniidae	*Epinephelus marginatus*	16	11.00	24.30	0.023	2.837	0.102	0.983
	*Mycteroperca rubra****	74	30.20	78.00	0.008	3.142	0.029	0.989
	*Serranus scriba***	311	10.20	21.3	0.007	3.244	0.035	0.965
Siganidae	*Siganus rivulatus**	127	7.00	17.00	0.014	2.882	0.071	0.930
Sparidae	*Diplodus annularis**	113	6.40	21.60	0.013	3.098	0.041	0.981
	*Diplodus sargus**	42	11.20	25.90	0.009	3.223	0.053	0.989
	*Diplodus vulgaris**	26	10.50	19.10	0.017	2.930	0.095	0.979
	*Oblada melanura**	10	17.50	23.40	0.004	3.420	0.294	0.944
	*Sparus aurata**	131	8.90	23.60	0.012	3.034	0.025	0.991
Crustacea								
Portunidae	*Callinectes sapidus*	490	4.30	8.30	0.710	2.875	0.042	0.905
	Carcinus mediterraneus	237	2.10	5.70	0.430	3.175	0,063	0.914
Xanthidae								
	Atergatis roseus	48	4.20	7.20	0.890	2.816	0.124	0.918
Batoidea								
Dasyatidae	*Dasyatis pastinaca**	23	24.50	59.50	0.003	3.129	0.141	0.959

The decrease in the 24-h catch rate of the experimental nets for teleosts was very rapid during the first 45 days, with a slow decline between the 45th and 105th days. The changes in the control net were irregular for the first 60 days and then rapidly increased (Figure 3a). The 24-h catch rate of the experimental nets for crustaceans decreased by approximately 40% in the first 30 days, but there was a mild rise at the 45th day; the decline continued after this day. The changes in the 24-h catch rate for the control net were similar to those in the experimental nets (Figure 3b). When all groups were considered together, the 24-h catch rate of the experimental nets rapidly decreased in the first 60 days (80%) and then gradually decreased (Figure 3c). After the 105th day, no individuals were caught in the experimental nets. Therefore, the fishing life of the experimental nets was accepted as 105 days. The change in the 24-h catch rate of the lost nets as a number and weight were fitted via exponential functions ($N_t = 12.439e^{-0,038t}, r^2 = 0.91$, $B_t = 2784.2e^{-5.05t}, r^2 = 0.92$). According to this function, the number and weight of entangled individuals in the one panel experimental net were estimated to be 309.22 (teleost: 57.88, crustacean: 251.34) and 48968.22 g (teleost:4519.59, crustacean: 44448.63), respectively.

With all groups considered together, the catch rate of the control nets was higher than the experimental nets during the surveys. However, the initial catch rate of these nets was very similar (Figure 3c). Therefore, the first day catch efficiency of the experimental nets was 92%. However, the catch rate gap of these nets increased with time. The catching efficiencies on the 30th, 60th and 90th days were observed to be 52%, 31% and 5%, respectively. The catching efficiency of the experimental nets for teleosts was different from that for all groups. The catch rate of the experimental nets on the 1st, 15th, 45th and 60th days were higher than in the control nets. Hence, the catching efficiency of these days was higher (100%). However, the catch rates of the control nets on the 75th, 90th and 105th days were dramatically higher than the experimental nets, and the catching efficiencies on these days were determined to be 46%, 9% and 0% (no individuals were observed on the 105th day in experimental nets), respectively. The catching efficiency of the experimental nets for crustaceans was similar for all groups (1st: 90%; 15th: 65%; 45th: 60%; 60th: 57%, 75th: 20%, 90th: 9% and 105th: 0%).

During the surveys, four species were only found in the experimental nets (*Sympodus tinca*, *Mycteroperca rubra*, *Diplodus annularis*, and *Oblada melanura*), eight species were only found in the control nets (*Sargocentrum rubrum*, *Liza aurata*, *Scomber japonicus*, *Lithognathus mormyrus*, *Portunus pelagicus*, *Rostroraja alba*) and another 14 species were caught in both the experimental and control nets. The % values of teleosts and crustaceans caught in the experimental and control nets are given in Figure 4. According to this figure, while some teleost families, such as Serraniidae (experimental:

41.51%; control: 14.29%) and Labridae (experimental: 9.43%; control: 0%), were caught more in the experimental nets, some families, such as Sparidae (experimental: 24.53%; control: 38.10%) and Siganidae (experimental: 1.89%; control: 12.70%), were observed more often the control nets (Figure 4a.). A similar situation was observed for the crustaceans. While *Atergatis roseus* was caught more often in the experimental nets (experimental: 21.86%; control: 4.80%), *Callinectes sapidus* was caught more often in the control nets (experimental: 29.51%; control: 59.60%). *Portunus pelagicus* and *Erugosquilla massavensis* were only found in the control nets.

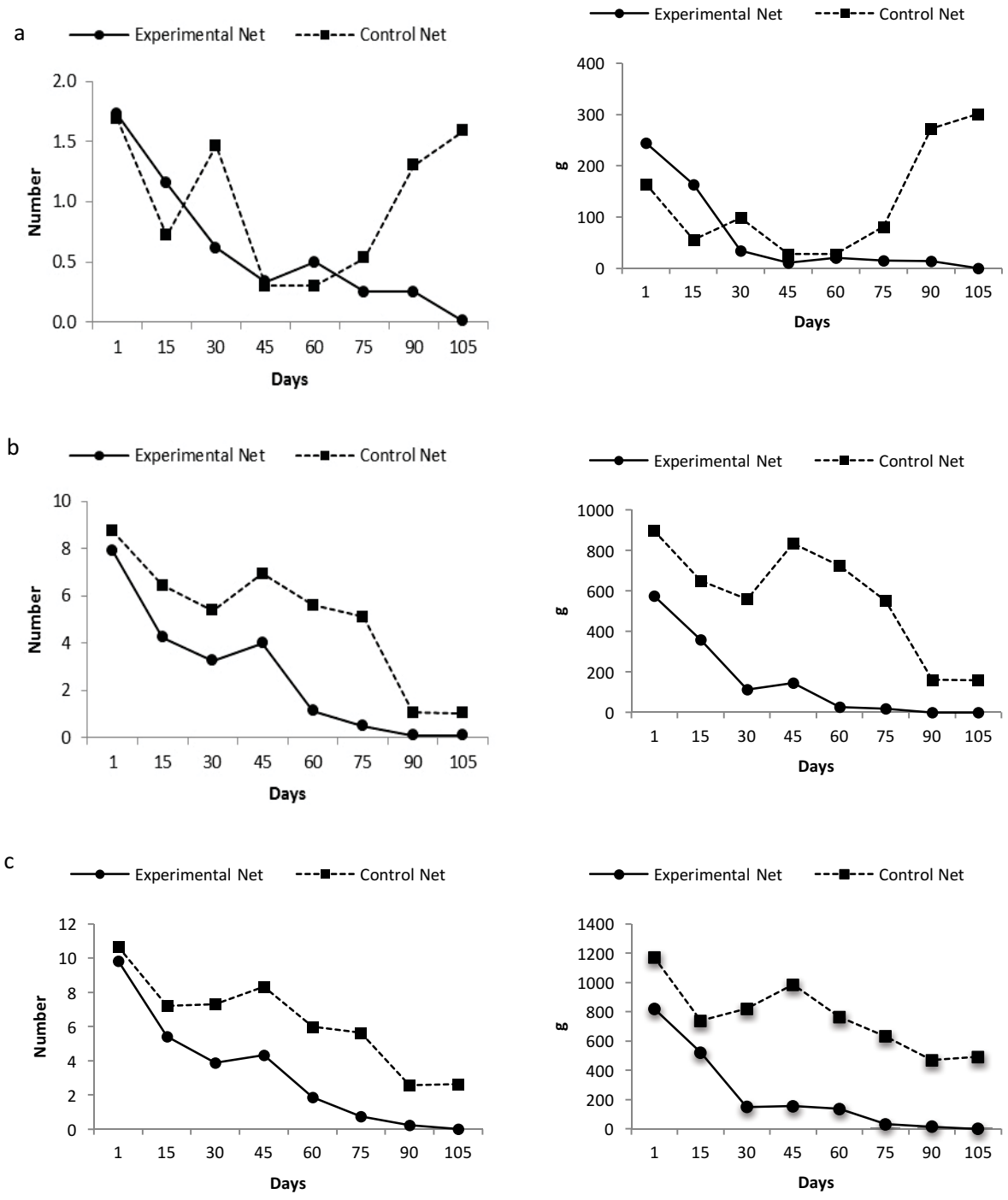


FIGURE 3
The changes in the 24-h catch rate of the experimental and control nets for teleosts (a), crustaceans (b) and all groups (c)

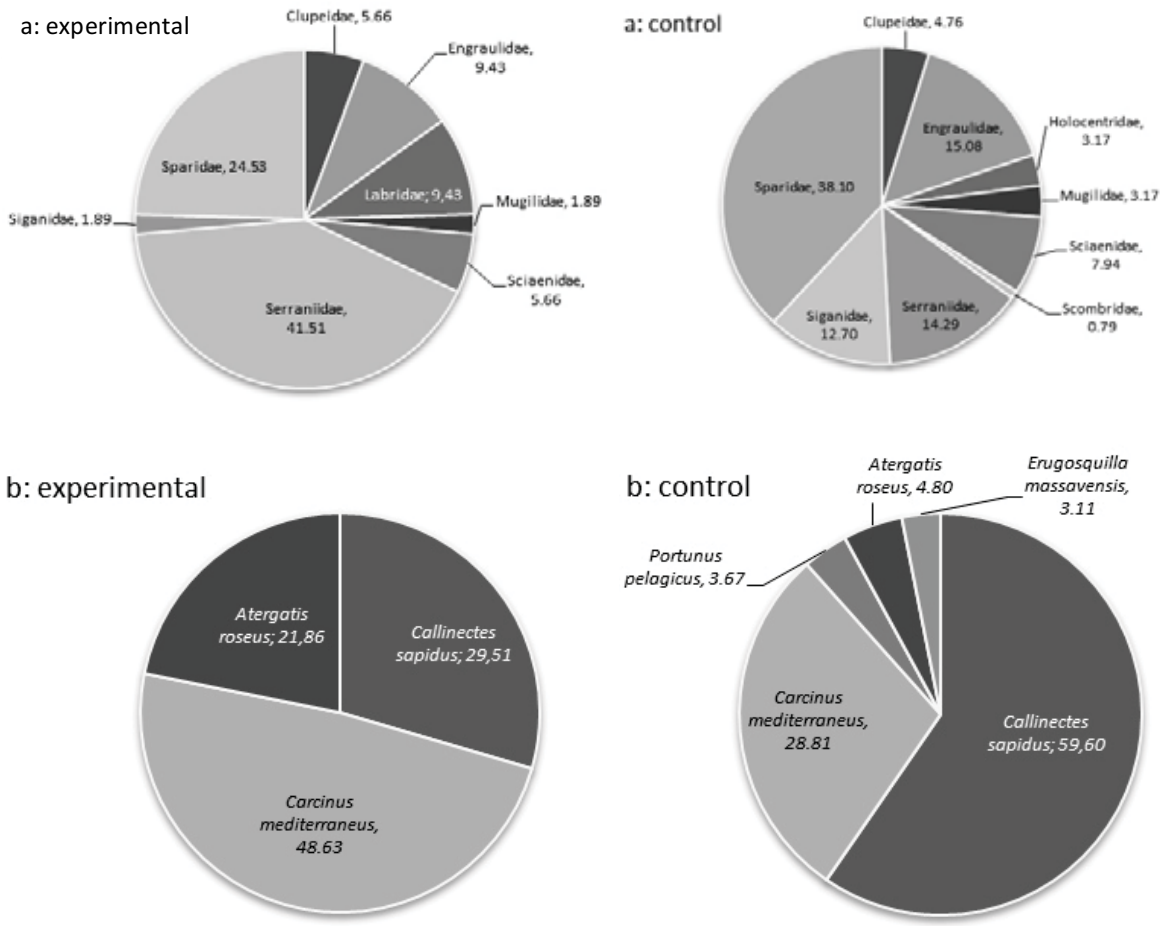


FIGURE 4
Percent of teleosts (a) and crustaceans (b) in the control and experimental nets

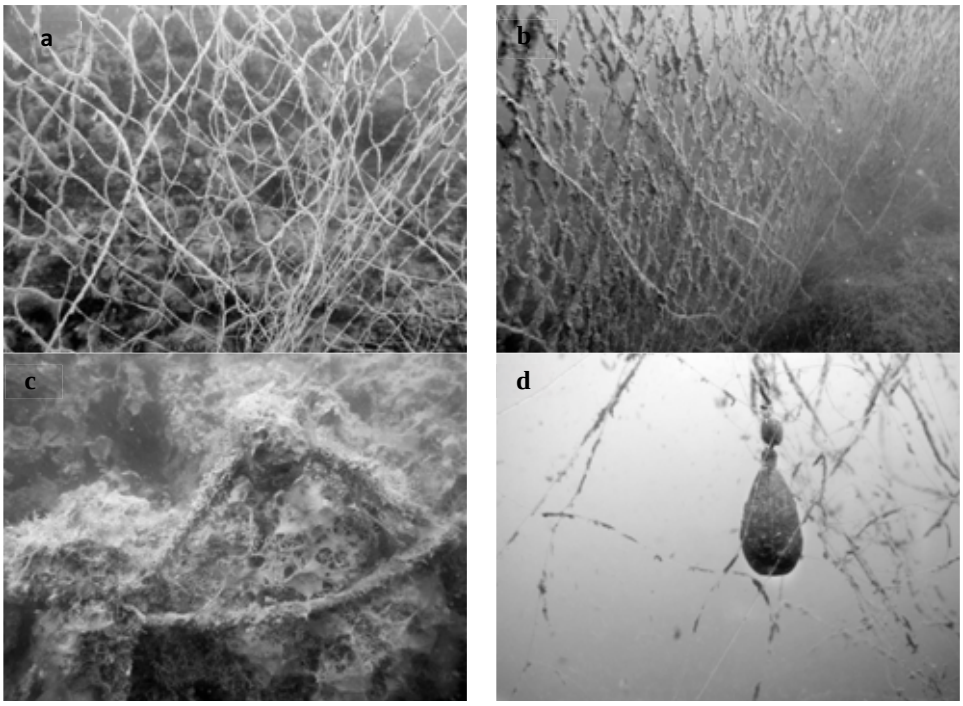


FIGURE 5
Time-dependent changes in the physical evolution of nets. a: 15th day after deployment; b: 30th day after deployment; c: rendered with the background; d: other fishing gear attached to the experimental net.

Particulate matter and detritus very rapidly accumulated on the experimental nets after deployment, which quickly increased the visibility of the nets. Figures 5a and 5b show the status of the experimental nets on the 15th and 30th days after deployment, respectively. Over time, the parts of the net that contacted the rocks and captured the marine organisms (especially crabs) formed large holes and tears. Additionally, nets that came into contact with the rock blended into the background (Figure 5c), and different fishing gear parts, such as the line, lead, and net, were attached to the experimental nets (Figure 5d).

In the fishery season in which this study was performed, 8 fishing boats were lost their trammel nets in the region. In an earlier study, the mean number of lost nets for one fishing boat was 5.58±0.86 panels [19]. Therefore, the number of total effective lost nets was determined as 22 panels in the noted area.

DISCUSSION AND CONCLUSION

The effect of lost fishing gear on marine organisms depends on the following three parameters: how much fishing gear was lost, how much time they could be used for fishing after their loss and the diversity and abundance of species in the region where the fishing gear was lost. There is no precise knowledge about how much fishing gear is lost worldwide. For this reason, it is difficult to predict the effect of lost nets on marine organisms worldwide. However, some studies have been performed in specific areas [22, 23] and one study was performed in Yumurtalik [19].

The amount of time that fishing gear is lost, especially bottom gill and trammel nets, affects fishing and is considered to be associated with the depth at which it was lost. In general, bottom gill and trammel nets are lost at greater depths have an increased fishing time compared to those lost at a shallow depth [1,24]. In the studies performed on bottom gill and trammel nets at a shallow depth, the physical evolution of these nets over time was similar [9-11,14]. Researchers have reported that particulate matter and detritus very rapidly accumulate on lost nets as well as that the visibility of the nets increases and net height steeply decreases with the load of accumulated matter and weight of marine organisms caught. This physical evolution of lost nets was revealed by light penetration and consequent biofouling and weather conditions, and bottom currents have a stronger influence at relatively shallow depths. It was mentioned that the 24-h catch rate and catching efficiency of lost nets steeply decreased in earlier weeks; then, they gradually declined. In light of these results, some researchers have mentioned that the rate of mortality caused by lost nets at a shallow depth is negligible in the setting of commercial fisheries [11, 25] The results obtained in this study are in agreement with those of previous studies. Considerable particulate matter and detritus very rapidly accumulated on the experimental nets, and damage was observed over time. The 24-h catch rates decreased by 80% in the first 8 weeks. The catching efficiency of the experimental nets was 92% on the first day, 31% on the sixtieth day, and decreased to 5% on the ninetieth day.

The total mortality of teleosts and crustaceans were determined to be 1291 (100 kg) individuals and 6102 individuals (990 kg), respectively, for all fishing fleets. According to the this result, mortality rate of fish was 0.55% caused by lost trammel nets. These mortality rate are not significant in respect of the total fishery landing of area (records of the fisheries cooperative: fish landing was 18t.). However, the mortality rates of *Epinephelus marginatus* and *Chelonia mydas* were remarkable. According to our calculations, approximately 350 *Epinephelus marginatus* individuals (26% of the total teleost mortality in lost nets) and 35 *Chelonia mydas* died due to lost nets in one fishery season. These species are classified as endangered in the Red List of Threatened Species (IUCN) and catching them is prohibited by Turkish fishery legislation. These data show that a lost net could pose a risk to threatened species in this area.

The difference in the species diversity and catch rate for lost nets that tangle in rocks compared to control nets is expected. Baeta et al. [14] reported that all species caught in sole trammel nets that were lost on the rocky bottom could be considered to be by-catch. Our results show that the experimental nets were more effective on Serraniidae (experimental: 41.51%; control: 14.29%), Labridae (experimental: 9.43%; control: 0%), and *Atergatis roseus* (experimental: 21.86%; control: 4.80%) and were distributed in the rocky area more than control nets.

The catch rate of the Sparidae family in the experimental nets was below that of the control nets (experimental: 24.53%; control: 38.10%). The species belonging to this family are generally reef-associated. For this reason, the catch rate of this family in the experimental nets that tangled in the rocks was expected to be higher. In underwater observations, it was observed that the species belonging to this family comfortably wandered around the lost net because they could easily pass through the holes and tears in the net.

In previous studies, it was reported that the teleost and crustacean catch rates in lost nets differed over time [9,10,14]. It was mentioned that in lost nets, initially the catch rate of teleosts was higher than that of crustaceans. However the catch rate of crustaceans was higher than that of teleosts with time. This change was explained by two reasons. First, decomposed individuals caught in the nets attract scavenger crustaceans and trap them in the nets. Second, the height of the nets (effective fishing area)

decreased over time. It was reported that while this case decreased the possibility of teleosts being caught, it did not affect the catching of crustaceans because they were caught near the lead line. However, our findings show that the catch rate of crustaceans is higher than that of teleosts during our surveys. This observation could be due to the species composition, abundance and season. Our individual observations demonstrated that the abundance of crustaceans is very high, even if there are no quantitative data in this area. Additionally, the water temperature was higher in the period in which this study was performed and the crustaceans were active. Therefore, these factors may have increased the catch rate of crustaceans in lost nets.

Similar trends were generally observed in various parameters, such as the physical evolution of lost nets, 24-hour catch rate and catching efficiency, in studies conducted in shallow water. The results obtained in this study are also in parallel with those of previous studies with respect to these parameters. However, the risks of lost nets should be evaluated by considering the characteristics of the area, such as the species composition and abundance. As in this study, lost nets can affect endangered species, even if the number of lost nets and fishing life of lost nets are limited. Hence, marine life may be affected more than expected.

ACKNOWLEDGEMENTS

This study was supported by the Cukurova University Research Foundation (Project No: FBA-2016-6247).

REFERENCES

[1] Breen, P. A. (1990) A review of ghost fishing by traps and gillnets. Proceeding of the Second International Conference on Marine Debris, Honolulu, Hawaii. 2–7 April 1989, 571-599.

[2] High, W. L. (1976) Escape of Dungeness crabs from pots. Marine Fisheries Review. 38, 19-23.

[3] Pecci, K. (1978) Ghost fishing of vented and unvented lobster, *Homarus americanus*, traps. Marine Fisheries Review. 40, 9-43.

[4] Sheldon, W.W. and Dow, R.L. (1975) Trap contribution of losses in the American lobster fishery. Fishery Bulletin. 73, 449-451.

[5] Smolowitz, R. (1978) Trap design and ghost fishing: an overview. Marine Fisheries Review. 40, 2-8.

[6] Barney, W. (1984) Lost gillnet retrieval project 1983–1984. Fisheries and Oceans, Fisheries Development Branch, Newfoundland Region. FDB-1983-84-26. Newfoundland, Canada.

[7] Carr, H. and Cooper, R. (1987) Manned submersible and ROV assessment of ghost gillnets in the Gulf of Maine. IEEE. 622-624.

[8] Carr, H.A., Amaral, E.H., Hulbert, A.W. and Cooper, R. (1985) Underwater survey of simulated lost demersal and lost commercial gill nets off New England. In: Proceedings of the Workshop on the Fate and Impact of Merine Debris, 27-29 November 1984, Honolulu, Hawaii (Shomura, R.S. and Yoshida, H.O. eds.). 439-447.

[9] Kaiser, M., Bullimore, B., Newman, P., Lock, K. and Gilbert, S. (1996) Catches in'ghost fishing'set nets. Marine Ecology Progress Series. 145, 11-16.

[10] Erzini, K., Monteiro, C., Ribeiro, J. Santos, M. Gaspar, M. Monteiro, P. and Borges, T.C. (1997) An experimental study of gill net and trammel net'ghost fishing'off the Algarve (southern Portugal). Marine Ecology Progress Series. 158, 257-265.

[11] Santos, M.N. Saldanha, H.J. Gaspar, M.B. and Monteiro, C.C. (2003) Hake (*Merluccius merluccius* L., 1758) ghost fishing by gill nets off the Algarve (southern Portugal). Fisheries Research. 64, 119-128.

[12] Sancho, G. Puente, E., Bilbao, A. Gomez, E. and Arregi, L. (2003) Catch rates of monkfish (Lophius spp.) by lost tangle nets in the Cantabrian Sea (northern Spain). Fisheries Research. 64, 129-139.

[13] Ayaz, A., Acarli, D., Altinagac, U., Ozekinci, U., Kara, A. and Ozen, O. (2006) Ghost fishing by monofilament and multifilament gillnets in Izmir Bay, Turkey. Fisheries Research. 79, 267-271.

[14] Baeta, F., Costa, M.J. and Cabral, H. (2009) Trammel nets' ghost fishing off the Portuguese central coast. Fisheries Research. 98, 33-39.

[15] Ozyurt, C.E. Akamca, E. Kiyaga, V.B. and Taşlıel, A.S. (2008) İskenderun Körfezi'nde Bir Balıkçılık Sezonunda Kaybolan Sepet Tuzak Oranı ve Kayıp Nedenleri. EÜ Su Ürünleri Dergisi. 25, 147-151.

[16] Kosswig, C. (1953) Some features of fisheries in Turkey. Hidrobiyoloji Mecmuası. 1, 145-153.

[17] Bjorndal, K.A. (1995) Biology and conservation of sea turtles: Smithsonian Institution Press Washington.

[18] Özdilek, H.G., Yalçin-Özdilek, S., Ozaner, F.S. and Sönmez, B. (2006) Impact of accumulated beach litter on *Chelonia mydas* L. 1758(Green turtle) hatchlings of the Samandag Coast, Hatay, Turkey. Fresen. Environ. Bull. 15, 95-103.

[19] Ozyurt, C.E., Mavruk, S. and Kiyaga, V.B. (2012) The rate and causes of the loss of gill and trammel nets in Iskenderun Bay (north-eastern Mediterranean). Journal of Applied Ichthyology. 28, 612-616.

[20] Karakulak, F., Erk, H. and Bilgin, B. (2006) Length–weight relationships for 47 coastal fish species from the northern Aegean Sea, Turkey. Journal of Applied Ichthyology. 22, 274-278.
[21] Özvarol, Y. and Gökoğlu, M. (2015) Length–weight relationship of *Hyporthodus haifensis* and *Mycteroperca rubra* (Pisces; Serranidae) from the North-Eastern Mediterranean Sea, Turkey. Journal of Applied Ichthyology. 31, 1165-1167.
[22] Santos, M.N., Saldanha, H., Gaspar, M.B. and Monteiro, C.C. (2003) Causes and rates of net loss off the Algarve (southern Portugal). Fisheries Research. 64, 115-118.
[23] Yildiz, T. and Karakulak, F.S. (2016) Types and extent of fishing gear losses and their causes in the artisanal fisheries of Istanbul, Turkey. Journal of Applied Ichthyology. 32, 432-438.
[24] Humborstad, O.B., Løkkeborg, S., Hareide, N. R. and Furevik, D.M. (2003) Catches of Greenland halibut (*Reinhardtius hippoglossoides*) in deepwater ghost-fishing gillnets on the Norwegian continental slope. Fisheries Research. 64, 163-170.
[25] Revill, A.S. and Dunlin, G. (2003) The fishing capacity of gillnets lost on wrecks and on open ground in UK coastal waters. Fisheries Research. 64, 107-113.

Received: **19.07.2017**
Accepted: **03.10.2017**

CORRESPONDING AUTHOR

Caner Enver Ozyurt
Çukurova University,
Faculty of Fisheries,
Balcalı Campus,
Sarıçam/Adana, 01330 – Turkey

e-mail: cozyurt@cu.edu.tr

© by PSP Volume 26 – No. 12A/2017 pages 8119-8124 Fresenius Environmental Bulletin

ISOLATION AND UTILIZATION OF A TRICLOPYR DEGRADING BACTERIUM, *BACILLUS CEREUS* TR-13

Jiangwei Zhu[1], Kun Xie[2,*], Yan Zhao[3]

[1]Collaborative Innovation Center of Sustainable Forestry in Southern China of Jiangsu Province, (Nanjing Forestry University), Nanjing 210037, China
[2]Key Laboratory of Crops with High Quality and Efficient Cultivation and Security Control, Yunnan Higher Education Institutions; College of Life Science and Technology, HongHe University, Mengzi 661100, China
[3]Shanghai Institute of Quality Inspection and Technical Research, Shanghai 200233, China

ABSTRACT

A strain TR-13 capable of highly degrading triclopyr was isolated from soil. The strain TR-13 was identified as *Bacillus cereus* based on 16S rRNA and analysis of morphology, physiological and biochemical characters. The optimal pH value and temperature were 7.0-7.5 and 30-35℃. The 7d degradation rate of 100 mg/L triclopyr by strain TR-13 could reach about 98.5% in inorganic salt medium. The strain TR-13 could hydrolyze triclopyr to 3,5,6-trichloro-2-pyridinol(TCP) ,but could not degrade TCP as the sole carbon source for its growth. The combined applications of the strain TR-13 and the strain CM-Z6 was considered an effective means for degrading triclopyr, because the strain CM-Z6 could degrade TCP. The degradation rate of triclopyr (100mg/L) by the strain TR-13 and the strain CM-Z6 could reach about 99% in 6d. In addition, the strain TR-13 could tolerate 800 mg/L of triclopyr and showed a high tolerance to triclopyr.

KEYWORDS:
Triclopyr, Biodegradation, *Bacillus cereus*

INTRODUCTION

Triclopyr (3,5,6-trichloro-2-pyridyloxyacetic acid) was a selective systemic herbicide used for control of woody and broadleaf plants along rights-of-way, in forests, on industrial lands and on grasslands [1,2]. The triclopyr residue in soil or water might bring some trouble to sensitive crops, soil microbes, aquatic systems and public health [3-5]. Therefore, triclopyr degradation and environmental fate were paid close attention. Photolysis and microbial degradation were considered the most important way of triclopyr degradation, especially microbial degradation [6-8]. The most common degradation pathway of triclopyr involves formation of 3,5,6-trichloro-2-pyridinol (TCP), TCP was a primary metabolite of triclopyr[9]. Particularly, TCP was a charged molecule at neutral pH and more leachable into groundwater and surface water than the parent compound[10,11]. It was moderately mobile due to its greater water solubility, which could cause the widespread contamination in soil and aquatic environment[12]. Therefore, in the process of microbial degradation of organic pollutants, not only need to focus on the number of parent pollutants, but also must pay attention to intermediate metabolites.

At present, a lot of attention has been given to the residue and pollution of triclopyr. However, there are only a very few studies on the degradation of triclopyr by microorganism. No reports on isolation of the triclopyr degrading bacterium have been published[13]. In this study, *Bacillus cereus* TR-13, a strain that could degrade triclopyr was isolated, its degradation potential and the application for environment protection were studied. The strain TR-13 could hydrolyze triclopyr to TCP, but could not degrade TCP as the sole carbon source for its growth. Some TCP degrading bacteria had been isolated previously. Li et al. isolated a highly efficient TCP degrading bacterium *Ralstonia* sp. T6 [14]. Lu et al. isolated *Cupriavidus* sp. DT-1, which could hydrolyze TCP utterly[15]. Therefore, the combined applications of the strain TR-13 and TCP degrading bacteria was considered an effective means for degrading triclopyr.

MATERIALS AND METHODS

Chemicals and Media. Chemicals: triclopyr (99.8%) was purchased from Dow Chemical Company. All other chemicals used were of analytical grade and commercially available.

Culture media. (1). Inorganic salt medium: $(NH_4)_2SO_4$ 0.1 g, $MgSO_4 \cdot 7H_2O$ 0.2 g, K_2HPO_4 0.1g, $CaSO_4$ 0.05 g, $FeSO_4 \cdot 7H_2O$ 0.01 g, water 1 L, pH 7.0. (2). Isolation medium: inorganic salt medium containing triclopyr (100 mg/L) was used to isolate triclopyr degrading bacteria. (3). Enrichment medium: peptone10 g, yeast extract powder 5 g, beef extract powder 3 g, sodium chloride 5 g, water 1 L, pH7.0.

Isolation and identification of triclopyr degrading bacteria. The soil sample was collected from forest in Jurong City, China, in which triclopyr and triclopyr-butoxyethyl ester have been used for more than 5 years. 5.0 g soil sample was placed in 100ml isolation medium for shaking culture at 30℃ (120 rpm). The concentration of the residual triclopyr was determined every 24h [16,17]. 5ml culture solution with 3d degradation rate >70% was transferred to enrichment medium containing same concentration of triclopyr, and continuously transferred for more than 5 times. After the degradation effect was verified again, the above enrichment medium was coated on inorganic salt culture plate containing triclopyr for inverted culture at 30℃. The eugonic bacterial colonies were selected and repeatedly streaked on the culture plate to obtain the pure culture. The new isolates were identified by using 16SrRNA sequence analysis. At the same time, the optimum pH and temperature of the strain TR-13 were tested.

Degradation of triclopyr by strain TR-13. Inoculums of triclopyr degrading bacteria were prepared in advance [18]. 5% strain TR-13 inoculum was inoculated in inorganic salt culture medium containing 100mg/L triclopyr, and then place it in the shaker (120rpm, 30 ℃). The concentration of triclopyr and TCP were determined every 24h [19,20].

Degradation of TCP by strain TR-13. The inorganic salt culture medium containing 20mg/L TCP was inoculated with 5% strain TR-13 inoculum, and then place it in the shaker (120rpm, 30℃). The concentration of TCP was determined regularly.

Degradation of triclopyr by combining strain TR-13 and strain CM-Z6. The strain CM-Z6 was a chlorpyrifos-methyl degrading bacterium deposited in our laboratory. It was identified as *Pseudomonas syringae* according to 16S analytical method (GenBank accession number KY038875). The strain CM-Z6 could effectively degrade TCP, and could degrade chlorpyrifos-methyl into CO_2 and H_2O completely. Because the strain TR-13 could not degrade TCP, the combined applications of the strain TR-13 and the strain CM-Z6 was considered an effective means for degrading triclopyr.

3% strain TR-13 inoculum and 5% strain CM-Z6 inoculum were inoculated simultaneously in inorganic salt culture medium containing 100mg/L triclopyr, and then place it in the shaker (120rpm, 30 ℃). The concentration of triclopyr and TCP were determined every 24h

Degradation of triclopyr by strain CM-Z6. In order to find out whether both strains have played a role in the combined degradation process, the ability of the strain CM-Z6 to degrade triclopyr was tested. 5% strain CM-Z6 inoculum was inoculated in inorganic salt culture medium containing 100mg/L triclopyr, and then place it in the shaker (120rpm, 30 ℃). The concentration of triclopyr was determined regularly.

Tolerance of the strain TR-13 on triclopyr. The concentration of triclopyr in the inorganic salt medium was adjusted respectively to 50mg/L, 100mg/L, 200mg/L, 400 mg/L and 800 mg/L. Then the strain TR-13 was inoculated respectively for shaking cultivation at 30℃. OD_{600} was determined regularly, so as to evaluate the tolerance of strain TR-13 on triclopyr.

RESULTS AND DISCUSSION

Identification and characterization of triclopyr degrading bacteria. A bacterium capable of utilizing triclopyr as the sole carbon source was isolated from the forest soil, named TR-13. The strain TR-13 was gram-positive, facultative aerobes, spore-forming, rod-shaped, 0.8-1.0×3.0-3.5 um in size. It formed white, smooth, non-pigmented colonies on the nutrient agar plate. The thallus could move. The optimum growth was at 30-35℃ and pH 7.0-7.5. It was positive for catalase, starch hydrolysis and VP test, but negative for gelatin liquefaction and indole test (Kaynar et al.2008; Ersoy et al.2008). Blastn of 16S rRNA sequence indicated that strain TR-13 showed nearly 99% similarity with 16S rRNA sequence of *Bacillus cereus* (The strain TR-13: GenBank accession number KY649624). The identification result was consistent with that of Biolog™ microorganisms identification system.

Degradation of triclopyr and TCP by the strain TR-13. The results in Fig. 1 showed that the triclopyr could be rapidly degraded by the strain TR-13. The degradation rate of triclopyr (100mg/L) by the strain TR-13 could reach about 98.5% in 7d. The degradation law of triclopyr under the experimental conditions accorded with the first order kinetic model ($C=C_0 \cdot e^{-kt}$), "t" was the degradation time, "k" was the degradation rate constant, "C_0" was initial concentration. $C=100e^{-0.4152t}$, $R^2=0.9984$, half life=1.83d. At the same time, it was found that TCP concentration continued to increase in the degradation process of triclopyr. In addition, TCP could not be degraded by the strain TR-13(Fig. 2). These results suggested that the strain TR-13 could not completely degrade triclopyr into CO_2 and H_2O. If the strain TR-13 was used for the degradation of triclopyr, it was necessary to consider degradation of TCP. It was believed that the combination of the strain TR-13 and a TCP degrading bacterium may be an effective means.

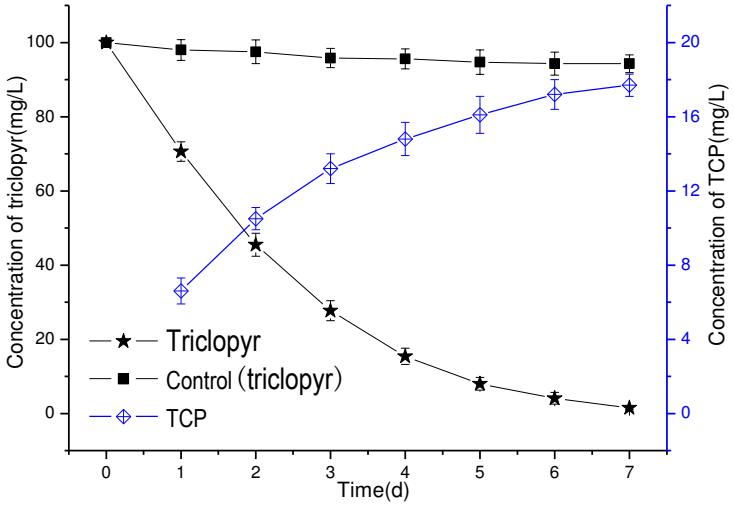


FIGURE 1
The curve on degradation of triclopyr by the strain TR-13 and the concentration of TCP

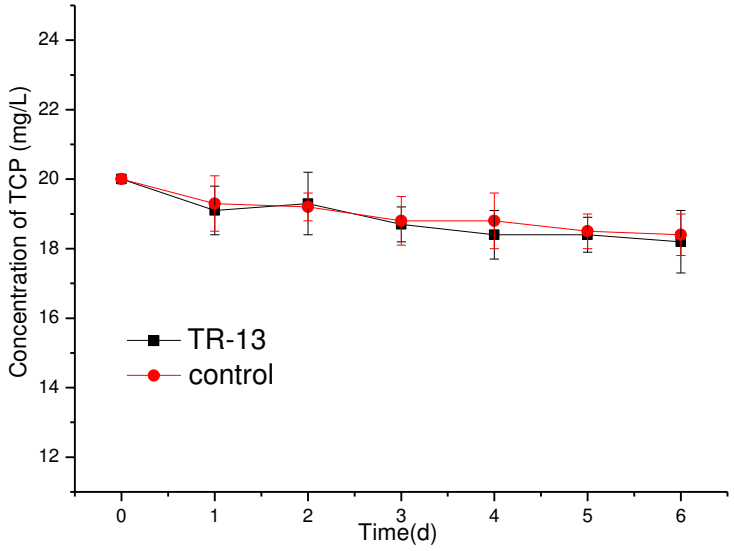


FIGURE 2
The curve on degradation of TCP by the strain TR-13

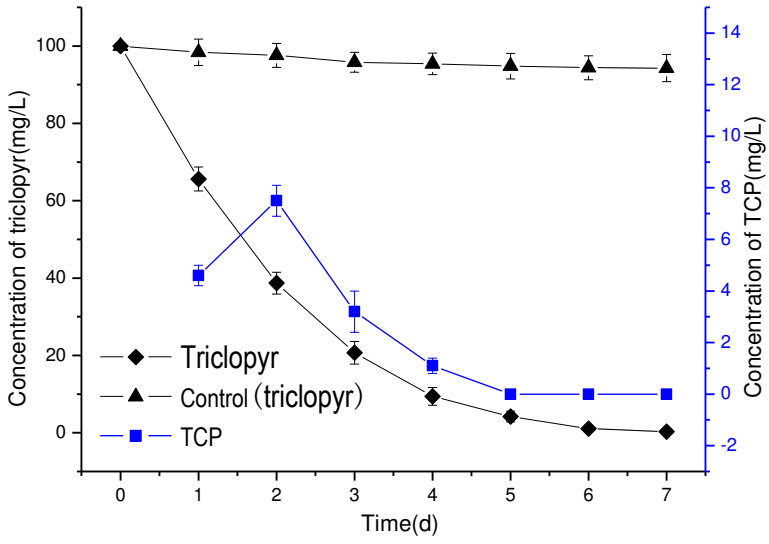


FIGURE 3
The curve on degradation of triclopyr by combining strain TR-13 and strain CM-Z6

Degradation of triclopyr by combining strain TR-13 and strain CM-Z6. Because the strain TR-13 could not degrade TCP, the combined applications of the strain TR-13 and TCP degrading bacteria was considered an effective means for degrading triclopyr. The results in Fig. 3 showed that the triclopyr could be rapidly degraded by the strain TR-13 and the strain CM-Z6 (the strain CM-Z6 could degrade TCP). The degradation rate of triclopyr (100mg/L) by the strain TR-13 and the strain CM-Z6 could reach about 99% in 6d. The fitted equation was $C=100e^{-0.4911t}$, $R^2=0.9926$, half life=1.62d. These data indicated that the degradation rate was faster when combined with the strain TR-13 and the strain CM-Z6. Because the results in Fig. 4 showed that the strain CM-Z6 could not degrade triclopyr alone, the increase in degradation rate was considered to be the result of the combined action of the two strains. So it was speculated that the strain TR-13 first degrades triclopyr into TCP, then TCP was degraded by strain CM-Z6. Degradation of TCP could help to reduce feedback suppression, and promote degradation of triclopyr.

Tolerance of the strain TR-13 on triclopyr. OD_{600} did not change significantly ($P>0.05$) when the concentration of triclopyr was increased from 50mg/L to 200mg/L. But OD_{600} would decrease gradually if triclopyr concentration increased to 400mg/L or 800mg/L (Fig.5). The results showed that the growth of the strain TR-13 had been inhibited by 400mg/L triclopyr (or more), but it was still growing. Therefore, it was preliminarily considered that the strain TR-13 could tolerate at least 800mg/L triclopyr under the experimental conditions. Although the strain TR-13 would be significantly inhibited by 800mg/L triclopyr, it still could effectively degrade triclopyr (because the triclopyr was used as the sole carbon source in the study.).

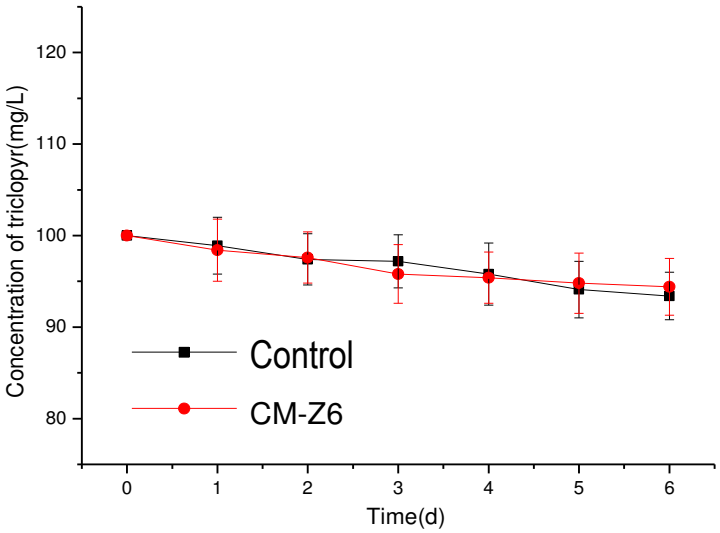


FIGURE 4
The curve on degradation of triclopyr by the strain CM-Z6

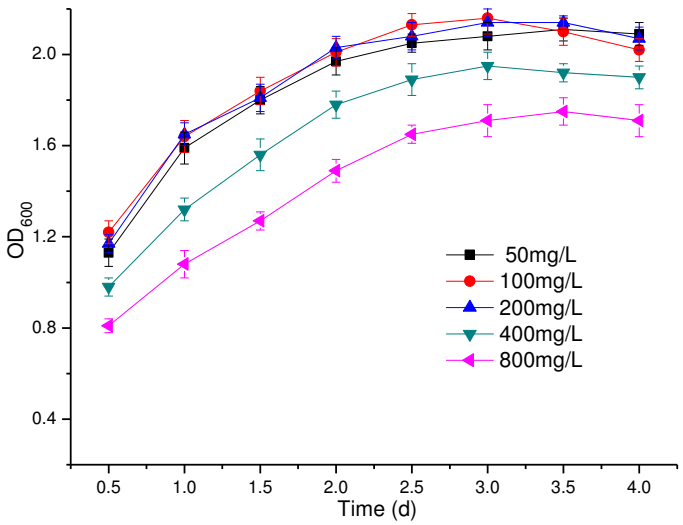


FIGURE 5
Effect of concentration of triclopyr on the growth of strain TR-13

According to the existing results, it was inferred that: ①The strain TR-13 had good tolerance on triclopyr. ②High concentration of triclopyr would inhibit the growth of the strain TR-13. ③The strain TR-13 had a strong degradation ability to triclopyr, which could be used in a wider range of triclopyr concentrations. ④It was possible that the strain TR-13 was used in the bioremediation of triclopyr pollution. The degradation ability of the strain TR-13 might be closely related with the long-term use of triclopyr in forest soil. Generally, soil microorganism that continuously encounter the artificially synthesized compound might induce the ability to degrade the compound [23, 24].

CONCLUSION

In this study, *Bacillus cereus TR-13* was isolated from soil, which could degrade triclopyr. The optimal pH value and temperature of strain TR-13 were 7.0-7.5 and 30-35℃. The strain TR-13 also had high tolerance to triclopyr. It could tolerate at least 800mg/L triclopyr under the experimental conditions. The degradation rate of triclopyr (100mg/L) by the strain TR-13 could reach about 98.5% in 7d, but TCP could not be degraded by the strain TR-13.The strain TR-13 could not completely degrade triclopyr into CO_2 and H_2O. Because the strain CM-Z6 could degrade TCP, the combined applications of the strain TR-13 and the strain CM-Z6 was considered an effective means for degrading triclopyr. The degradation rate of triclopyr (100mg/L) by the strain TR-13 and the strain CM-Z6 could reach about 99% in 6d. So it was speculated that the strain TR-13 first degrades triclopyr into TCP, then TCP was degraded by strain CM-Z6. Degradation of TCP could promote degradation of triclopyr.

ACKNOWLEDGEMENTS

This study was funded by the China Postdoctoral Science Foundation (No.2017M611827) and Applied Science Research Project of Honghe University (No.XJY15Z07 to K.X.), and partially by the Priority Academic Program Development of Jiangsu Higher Education Institutions and Ph.D Specific Research Project of Honghe University (No.XJ15B13 to K.X.).

REFERENCES

[1] Getsinger, K.D., Petty, D.G., Madsen, J.D. and Skogerboe, J.G. (2000) Aquatic dissipation of the herbicide triclopyr in Lake Minnetonka, Minnesota. Pest Management Science. 56(5), 388-400.

[2] Baglieri, A., Nègre, M., Trotta, F. (2013) Organo-clays and nanosponges for acquifer bioremediation: adsorption and degradation of triclopyr. Journal of Environmental Science & Health Part B Pesticides Food Contaminants & Agricultural Wastes. 48(9), 784-792.

[3] Mcmullin, R.T., Bell, F.W., Newmaster, S.G. (2012) The effects of triclopyr and glyphosate on lichens. Forest Ecology & Management. 264(1), 90-97.

[4] Qamar, M., Muneer, M., Bahnemann, D. (2006) Heterogeneous photocatalysed degradation of two selected pesticide derivatives, triclopyr and daminozid in aqueous suspensions of titanium dioxide. Journal of environmental managemen. 80(2), 99-106.

[5] Newton, M., Cole, E.C., Tinsley, I.J. (2008) Dissipation of four forest-use herbicides at high latitudes. Environmental Science and Pollution Research. 15(7), 573-83.

[6] Mccall, P.J., Gavit, P.D. (1986) Aqueous photolysis of triclopyr and its butoxyethyl ester and calculated environmental photodecomposition rates. Environmental Toxicology & Chemistry. 5(10), 879-885.

[7] Massiha, A., Issazadeh, K. (2011) Microbial degradation of pesticides in surface soil using native strain in Iran. International Conference on Biotechnology and Environment Management.

[8] Vassios, J.D., Nissen, S.J., Koschnick, T.J. (2014) Triclopyr Absorption and Translocation by Eurasian Watermilfoil (Myriophyllum spicatum) Following Liquid and Granular Applications. Weed Science. 62(1), 22-28.

[9] Fox, A.M., Haller, W.T., Getsinger, K.D. and Petty, D.G. (2002) Dissipation of triclopyr herbicide applied in Lake Minnetonka, MN concurrently with Rhodamine WT dye. Pest Management Science. 58(7), 677-686.

[10] Manclu´s, J.J., Montoya, A. (1995) Development of immunoassays for the analysis of chlorpyrifos and its major metabolite 3,5,6-trichloro-2-pyridinol in the aquatic environment. Anal. Chim. Acta. 311, 341-348.

[11] Suvarchala, G., Philip, G.H. (2016) Toxicity of 3,5,6-trichloro-2-pyridinol tested at multiple stages of zebrafish (Danio rerio) development. Environmental Science and Pollution Research. 23(15), 15515-15523.

[12] Yang, L., Zhao, Y. and Zhang, B. (2005) Isolation and characterization of a chlorpyrifos and 3,5,6-trichloro-2-pyridinol degrading bacterium. FEMS Microbiol. Lett. 251, 67-73.

[13] Petty, D.G, Getsinger, K.D, Woodburn, K.B.A (2003) Review of the Aquatic Environmental Fate of Triclopyr and its Major Metabolites. Journal of Aquatic Plant Management. 41(2), 69-75.

[14] Li, J., Liu, J., Shen, W. (2010) Isolation and characterization of 3,5,6-trichloro-2-pyridinol-degrading Ralstonia sp. strain T6. Bioresource Technology. 101(19), 7479-83.
[15] Lu, P., Li, Q., Liu, H. and Feng, Z. (2013) Biodegradation of chlorpyrifos and 3,5,6-trichloro-2-pyridinol by Cupriavidus sp. DT-1. Bioresource Technology. 127(1), 337-342.
[16] Ivanova, B., Spiteller, M. (2015) Solid-state UV-MALDI mass spectrometric quantitation of fluroxypyr and triclopyr in soil. Environmental Geochemistry and Health. 37(3), 557-574.
[17] Ebadi, A.G. (2008) Determination of residues of triclopyr in fishes of Caspian sea (Iran). Asian Journal of Chemistry. 20(5), 3497-3501.
[18] Zhu, J.W., Wu, L., Yang, N. (2016) Study on utilization of a nicosulfuron degrading bacterium, Bacillus pumilus ZHU-11. Fresen. Environ. Bull. 25(9), 3796-3801.
[19] Koch, H.M., Angerer, J. (2001) Analysis of 3,5,6-trichloro-2-pyridinol in urine samples from the general population using gas chromatography-mass spectrometry after steam distillation and solid-phase extraction. Journal of Chromatography B Biomedical Sciences & Applications. 759(1), 43-9.
[20] Anwar, S., Liaquat, F. and Khan, Q.M. (2009) Biodegradation of chlorpyrifos and its hydrolysis product 3,5,6-trichloro-2-pyridinol by bacillus pumilus strain C2A1. Journal of Hazardous Materials.168(1), 400-405.
[21] Kaynar, P. and Beyatli, Y. (2008) Protein profiles and biochemical characterizations of Bacillus spp. strains isolated from fishes. Fresen. Environ. Bull. 17, 1316-1321.
[22] Ersoy Omeroglu, E., Karaboz, I., Sukatar, A., Uzel, A., Sayan, M. and Sanlidag, T. (2008) Phenotypic and molecular characterization of luminous bacteria isolated from Izmir Gulf in Turkey: Vibrio harveyi TEM O5 and TEM S1 strains. Fresen. Environ. Bull. 17, 506-510.
[23] Petric, I., Karpouzas, D.G., Bru, D. (2016) Nicosulfuron application in agricultural soils drives the selection towards NS-tolerant microorganisms harboring various levels of sensitivity to nicosulfuron. Environmental Science and Pollution Research. 23(5), 1-14.
[24] Felsot, A., Maddox, J.V. and Bruce, W. (1989) Enhanced microbial degradation of carbofuran in soils with histories of carbofuran use. Bull. Environ. Contam. Toxicol. 26,781-788.

Received: **21.07.2017**
Accepted: **13.10.2017**

CORRESPONDING AUTHOR

Kun Xie
Key Laboratory of Crops with High Quality and Efficient Cultivation and Security Control,
Yunnan Higher Education Institutions;
College of Life Science and Technology,
HongHe University,
Mengzi 661100 – China

e-mail: xk_017@hotmail.com

© by PSP Volume 26 – No. 12A/2017 pages 8125-8130 Fresenius Environmental Bulletin

ANALYSIS OF WELLBORE STABILITY OF SHALE GAS RESERVOIR DRILLING

Ni Weijun[1,2,*], Li Qi[1,2], Song Xiaomei[3]

[1]Key Laboratory of MOE for Petroleum Engineering, China University of Petroleum (Beijing); Beijing, China.
[2]College of Petroleum Engineering, Xi'an Shiyou University, Xi'an Shaanxi, China.
[3]Changqing Branch, Research Institute of Drilling & Production Engineering Technology, Chuanqing Drilling Engineering Company, CNPC, Xi'an, Shaanxi, China.

ABSTRACT

Aiming at Posidonia shale well wall stability analysis problem in certain domestic oil filed, the Paper carries out test analysis by utilizing stress distribution and it is shown by experiment that: (1) when composite surface surfactant coordinates with water-based drilling fluid, it can effectively impede and postpone transmission of shale pore pressure and reduce shale permeability to increase shale well wall stability; (2) mechanical analysis model of horizontal well wall stability with bedding surface shale gas reservoirs has been established based on well wall stability pore elastic mechanics and single-structure surface strength theory and the model has considered the influence of shale layer bedding surface occurrence (direction and dip angle) and influence of weakening of bedding surface strength based on classic pore elasticity well wall stability model and the model can effectively guide optical design of horizontal well borehole drilling direction and drilling fluid density; (3) well wall structure type is an important factor to influence well wall stability and advantageous shale structure is a main factor to influence single well wall stability in practical drilling. Foresaid experiment result has certain guidance meaning for practical drilling process.

KEYWORDS:
Stress distribution, Posidonia shale, well wall stability

INTRODUCTION

Instability of well wall is worldwide technical difficult problem in drilling work and also is one of core problems for safe and efficient drilling. After borehole is formed after stratum is drilled, drilling fluid column pressure has replaced support provided by drilled stratum and original stress balance has been destroyed, which will lead to redistribution of stress in rock around borehole. If stress that is redistributed exceeds maximal load that rock can bear to the maximum (no matter tensile strength or compressive strength), it will lead to borehole instability [1]. At the same time, when drilling fluid invades stratum, it will lead to increase of stratum pore pressure and reduction of rock strength, which will further increase instability of well wall [2].

In development of shale gas, if horizontal-section horizontal well is drilled by taking instable bedding-formation shale as target layer, its own specificity exists and stress distributed secondarily around horizontal well has great difference from vertical well; in addition, because stress environment of shale reservoir stratum is complex and bedding/crack is well developed, it intensifies risk of collapse and instability of well wall. For example, for the first horizontal well of shale in China (W201-H1 Well), although oil-based anti-collapse drilling fluid system is adopted and drilling fluid density is increased gradually, collapse of the main shale-section well wall is still very serious. In order to solve the instability problem of bedding formation stratum, a large amount of researches have been carried out at home and abroad and fruitful achievements have been got [3]. Foreign Chenevert et al. has researched influence of bedding on well wall stability by adopting single weak-surface strength and anisotropy theory and domestic Chen Mian et al. has researched relationship between wellbore stability and bedding based on single weak strength theory and linear elasticity well wall stability model and Lu et al. has researched the influence of bedding surface occurrence on strength weakening of bedding surface [4]. However, aiming at well wall stability problem of bedding-formation horizontal shale well borehole, systematic and profound research is not carried out, because stress condition and borehole track, etc. in horizontal well and regular well has relatively special characteristics with influence of factors, such as shale stratum bedding formation occurrence and bedding formation strength weakening, etc., well wall collapse and instability of bedding-formation shale-gas horizontal well are more complex, while confirmation for borehole direction cannot be guided effectively

because understanding on mechanism of collapse and instability of horizontal well wall under influence of bedding is not sufficient [5-14].

Therefore, the author researches the influence of crustal stress direction, borehole track and shale bedding formation occurrence on stability of well wall and analyzes the influence of reduction of bedding-formation strength for invading of drilling fluid on well wall collapse simultaneously, analyzes living examples and verifies correction of methods in this paper to guide drilling direction of shale-gas horizontal well borehole and optimal design of drilling fluid density by taking bedding-formation horizontal shale well as research object.

Stress distribution model of shale-gas horizontal well wall. Fig. 1 is coordinate relationship of horizontal well wall stress of bedding formation shale. In the figure, (N, E, Z) is ground rectangular coordinate system; σ_H is maximal horizontal stress, MPa; σ_h is minimal horizontal stress, MPa; σ_v is vertical stress, MPa; ψ is axial direction of borehole (included angle of borehole axis and maximal horizontal stress direction, (°)).

For any shale-gas horizontal well section, it is supposed that hole deviation angle is 90°, so borehole track is mainly influenced by borehole direction. Therefore, surrounding rock stress condition of well wall is mainly controlled by azimuth angles relevant to angles, such as crustal stress direction, borehole direction, bedding surface occurrence (direction and dip angle), etc.; because azimuth angles herein include crustal stress direction, borehole direction, bedding surface direction and their logical relationship is not favorable for later analysis, especially extremely complex analysis on drilling direction description of well along crustal stress, borehole direction is defined simply as included angle (relative azimuth angle) of azimuth angle ψ_H of borehole under ground coordinate system and azimuth angle of maximal horizontal crustal stress; therefore, azimuth angle of crustal stress is not involved when analyzing surrounding rock stress of horizontal well wall, which can simplifies calculation procedure. Then, distribution model of surrounding rock stress of horizontal well wall:

$$\begin{cases} \sigma_r = p_m - \delta\phi\left[p_m - p(r,t)\right] \\ \sigma_\theta = \left[1+2\cos(2\theta)\cos^2\psi\right]\sigma_H + \left[1+2\cos(2\theta)\sin^2\psi\right]\sigma_H \\ \quad + \left(1-2\cos(2\theta)\right)\sigma_v + (\xi-1)\,p_m - \xi p(r,t) \\ \sigma_z = \left(\sin^2\psi + 2v\cos(2\theta)\cos^2\psi\right)\sigma_h + \left(\cos^2\psi + 2v\cos(2\theta)\sin^2\psi\right)\sigma_H \\ \quad -2v\cos(2\theta)\sigma_v + \xi\left[p_m - p(r,t)\right] \\ \tau_{\theta_z} = \sin(2\psi)\cos\theta\left(\sigma_H - \sigma_h\right) \end{cases} \quad (1)$$

Where, σ_r, σ_θ, σ_z and τ_{θ_z} are respectively well wall stress component under circular cylindrical coordinates of borehole, MPa; (r,θ,z) is borehole cylindrical coordinate system; p_m is fluid column pressure of drilling liquid, MPa; $p(r,t)$ is stratum pore pressure, MPa; δ is permeability coefficient; when well wall does not permeate, δ=0; when well wall permeates, δ=1; θ is well perigon (°); v is Poisson's ratio; a is effective stress coefficient; ϕ is stratum pore degree, %; ξ is vadose effect coefficient, which can be represented as:

$$\xi = \delta\left[\frac{a(1-2v)}{1-v} - \phi\right] \quad (2)$$

According to stress condition analysis, 3 main stresses in well wall can be obtained as:

$$\begin{cases} \sigma_i = \sigma_r = p_m - \delta\phi\left[p_m - p(r,t)\right] \\ \sigma_{j,k} = \dfrac{(\sigma_\theta + \sigma_z)}{2} \pm \dfrac{1}{2}\sqrt{(\sigma_\theta - \sigma_z)^2 + 4\tau_{\theta_z}^2} \end{cases} \quad (3)$$

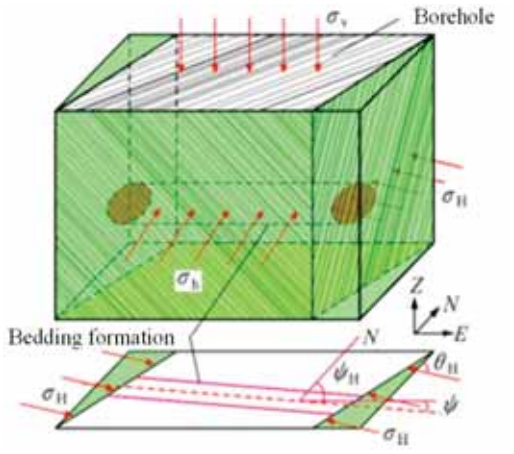


FIGURE 1
Coordinate Relationship of Horizontal Well Wall Stress of Bedding Surface Shale

Where: σ_i, σ_j and σ_k are respectively 3 main stresses on well wall, MPa. After ranking for the 3 main stresses, main stresses under three-direction stress condition are obtained as σ_1, σ_2 and σ_3. In formula (3), after ranking of 3 main stresses, calculation model of maximal and minimal main stress of shale-gas horizontal well wall can be obtained and collapse pressure can be obtained by combining with bedding-formation weak-surface stratum strength judgment principle. Included angle γ of maximal main stress and hole axis is:

$$\gamma = \frac{1}{2}\arctan\frac{2\tau_{\theta_z}}{\sigma_\theta - \sigma_z} \quad (4)$$

MATERIALS AND METHODS

Experiment test. Test material. Test sample is collected from Posidonia shale core sample products in certain domestic oil field. The sample is located in Jurassic Period shale bedding and is 1800m underground and is lifted to the ground by crustal movement. After searching 41~51m shale core depth, the position is located in carbonate rock stratum and has mature oil shale 0.88 % vitrinite reflectance Ro. Porosity measured by mercury intrusion method is about 1%. Samples from dark grey to black display that it has superior bedding and gray band with maximal thickness 1mm is embedded parallel melnikovite slice.

TABLE 1
Test for Physical Parameters of Posidonia Shale Reservoir

Maturity	0.88
Porosity (%)	1.1 ± 0.3
Average porosity radius (nm)	<4.1
Calcite content (wt%)	47.3 ± 0.5
Clay content (wt%)	27.8 ± 1.6
Quartz content (wt%)	17.2 ± 0.4
Iron pyrite (wt%)	5.3 ± 0.2
Total organic carbon (wt%)	5.8 ± 0.3
Water content (wt%)	~1

TABLE 2
Uniaxial Compressive Strength (UCS) and Elastic Property

E_{xy}^a	17.3 GPa	E_z^a	10.4 GPa
v_{xy}	0.18	v_{zy}	0.30
G_{xy}	8.9 GPa	G_z	5.5 GPa
UCS_{xy}	75 ± 7 MPa	UCS_z	115 ± 7 MPa
UCS_{45}	60 ± 10 MPa	v_{yz}	0.17
n	1.66		

Compressive strength parallel to bedding (UCS) is about 35%, which is lower than compressive strength of vertical bedding (z axis direction) and is significantly lower than compressive strength of diagonal bedding (45°direction), about 48%. At the same time, Young modulus also has anisotropy, $E_{xy}/E_z = n \approx 1.7$. Poisson's ratio is $v_{zy} = n \cdot v_{yz}$, where, v_{yz} is Poisson's ratio in adverse load direction and is precondition of horizontal isotropic elasticity. It is estimated that shear modulus of normal bedding of oil shale is: $G_z = E_{xy}/\left(1+n+2nv_{zy}\right)$. Along shear modulus, namely, symmetry plane, it can be calculated as: $G_{xy} = E_{xy}/\left(2+2v_{xy}\right)$. Physical and mechanical parameters are respectively provided in Table 1 and Table 2.

Sample preparation. Under drying condition, cylindrical sample is drilled along plane direction of core material bedding ($\alpha = 90^o - \beta$), $\alpha \in \left[30^o, 86^o\right]$, as shown in Fig. 1. Diameter of sample is 40mm and length is 80mm, which is parallel to end face and precision is $< 20\mu m$. In the end, drill hole with 8mm diameter is drilled in sample by solid carbon drill. In preparation process of hollow cylinder on wall, dust and drilling cuttings are cleared with large-power vacuum cleaner. Specific dimension is provided in Table 3.

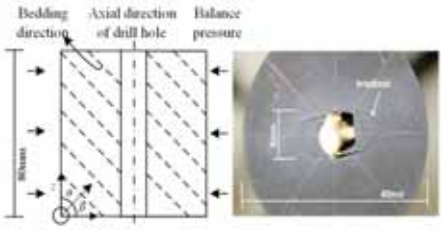


FIGURE 2
Sample Products

RESULTS AND DISCUSSION

Expansibility. Mixing bentonite and quartz sand by 1: 2 on site and weighing15g in total and pressed under 8MPa pressure for 30min, collected shale sample is utilized (diameter 25mm and length 16mm). In ZNP-1 swelling amount tester, water-based drilling fluid and water-based drilling fluid with composite surfactant contact respectively with shale sample and swelling amount data are read, as shown in Fig. 3.

TABLE 3
Estimation for Well Wall Collapse by Sample Dimension, Loading Rate and Critical Balance Pressure

Sample names	b (mm)	l(mm)	a (mm)	$\alpha(^o)$	Rate (MPa/min)	$P_{AE}\,(MPa)$	$P_{amp}\,(MPa)$	$P_{vp}\,(MPa)$	$P_E\,(MPa)$	$P^*\,(MPa)$
PN1	40	80	6	0	1	138	170	160	159	157± 10
PN2	50	80	10	0	0.5	130	-	144	144	140 ± 4
PN3	50	80	8	0	-	-	-	-	-	151 ± 5
PN4	40	80	8	86.4 ± 0.4	0.5	49	53	54	52	52 ± 2
PN5	40	80	8	78.4 ± 0.9	2	-	62	61	59	61 ± 2
PN6	40	80	8	73.3 ± 2.8	1	-	62	62	53	59 ± 8
PN7	40	80	8	63.0 ± 0.5	1	-	82	79	76	79 ± 3
PN8	40	80	8	53.6 ± 1.1	1	-	88	88	86	87 ± 5

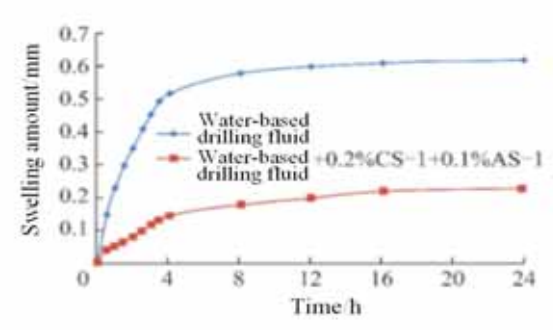


FIGURE 3
Influence of Composite Surfactant on Shale Swelling Amount after Contact with Water-based Drilling Fluid

Shale pressure transmission experiment. Pressure transmission experiment can be used to evaluate interaction between drilling fluid and shale. For the same shale, under the same experiment condition, the slower the upstream pressure transmits to downstream pressure, the stronger the suppression capability of drilling liquid to shale and shale tends to be stable. Because shale sample amount is relatively large, Posidonia shale core is adopted here.

It is shown from X diffraction analysis results that it contains 70% quartz, 15% feldspar, 5% chlorite, 5% illite and 5% calcite, with relatively fragile lithological characters. Pressure transmission experiment is carried out by utilizing HKY－3 shale pressure transmission experiment device by using different fluids and shale cores to evaluate influence of composite surfactant on shale well wall stability.

Experiment conditions are as follows: confining pressure is 3.5MPa, upstream pressure is controlled in 2.3MPa and return pressure is 2.6 MPa and data are recorded every 1 min and shale core length is 2cm and diameter is 2.5cm and pressure transmission experiment curve and calculated shale permeability result are shown in Fig.4.

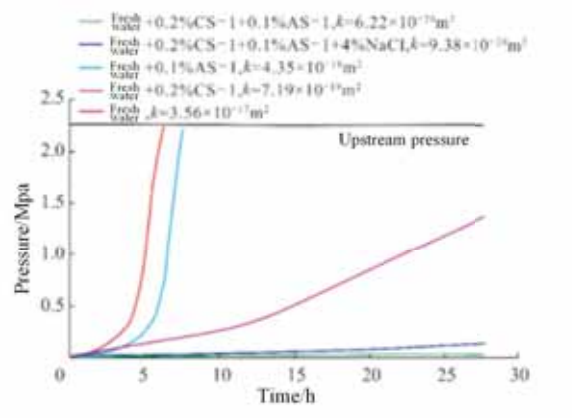


FIGURE 4
Pressure Transmission Experiment Result for Different Fluids Contacting with Shale

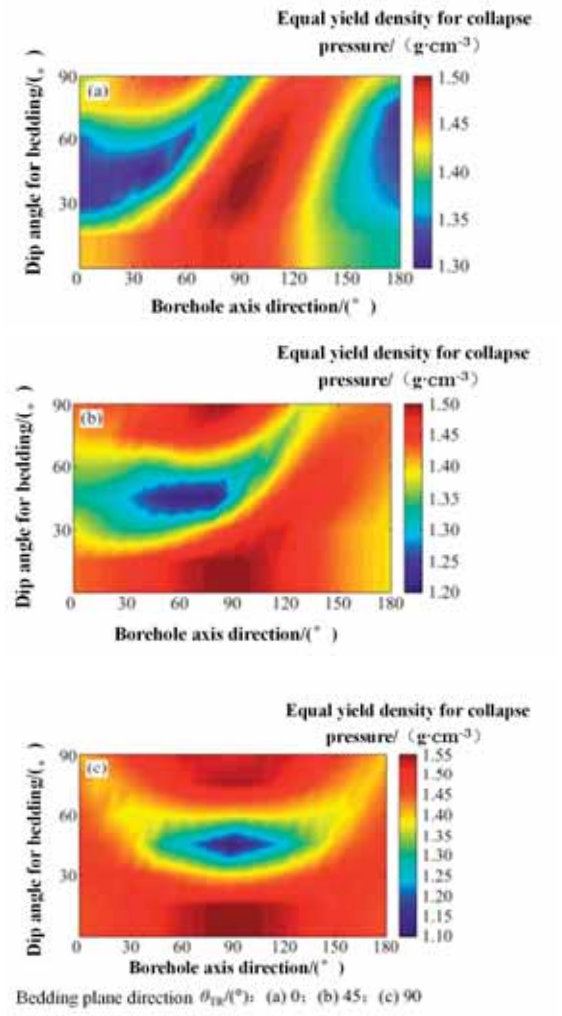


FIGURE 5
Influence of Bedding Surface Occurrence on Collapse Instability Principle

Influence of bedding surface occurrence. Fig.5 shows influence principle of borehole track and bedding surface under 3 kinds of conditions: 0°, 45° and 90°bedding surface direction. Stability area with minimal equal yield density (collapse density in brief) of collapse pressure is the best; stability in area with maximal collapse density is the worst. It can be seen from Fig.5 that: well wall collapse pressure is closely related to borehole axis direction, bedding surface direction, dip angle of bedding surface and well wall collapse density can reach 0.45 g/cm^3 under different conditions; collapse pressure distributes relatively gently when bedding surface direction is 0° and collapse density difference is 0.25 g/cm^3 in different drilling directions and dip angles of bedding surface; collapse pressure distribution degree increases when bedding surface direction is 45° and collapse density difference is 0.39 g/cm^3 in different drilling directions and dip angles of bedding surface; collapse pressure distribution difference is maximal when bedding surface

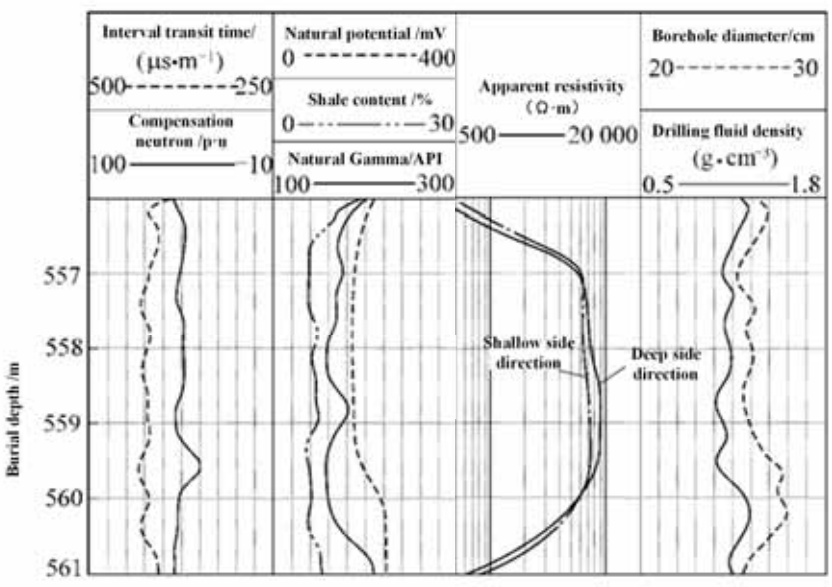


FIGURE 6
Relationship between Collapse Pressure and Hole Diameter by Log Presentation Forecast

direction is 90° and collapse density difference is 0.45 g/cm^3 in different drilling directions and dip angles of bedding surface; for different borehole axis direction and tip angle of bedding surface, with change of bedding surface direction, risk of well wall collapse and instability presents increase trend on the whole; at the same time, collapse instability risk difference increases gradually; stability for drilling in borehole along minimal horizontal main stress direction when tip angle of bedding surface is 45° and bedding surface direction is 90°.

Influence of bedding surface occurrence. In practical work, it is more general that there is no coring photo; at that time, it is very effective to obtain GSI quantitative characterization value of shale structure by utilizing log presentation and then to obtain collapse pressure and realize well wall stability evaluation. Taking Posidonia for example, drill with diameter of 215.9 mm is used for the well during the second section in fresh water with drilling density of 1.02 g/cm^3. GSI value is obtained by utilizing log presentation (foresaid formula is adopted for GSI by log presentation) and collapse pressure is calculated and relationship between collapse pressure and dimension of borehole diameter is shown in Fig.6. Collapse pressure by utilizing log presentation and borehole change trend are relatively identical and percent of contact area reaches 75%, which demonstrates that the method is effective. It can be known from equal yield density of collapse pressure drilling fluid and borehole that the well is normal or it has slight hole enlargement and well wall stability is favorable.

CONCLUSIONS

This paper researches influence of crustal stress direction, borehole track and shale bedding surface on well wall stability; at the same time, analyzes influence of bedding surface strength reduction by invasion of drilling fluid on well wall collapse; analyzes living example and verifies correction of methods in this paper to guide optical design of drilling direction of shale-gas horizontal borehole and drilling fluid density by taking test samples (collected from certain domestic oil field Posidonia shale core sample product) as research object and by taking horizontal well of bedding-surface shale as research object.

ACKNOWLEDGEMENTS

National Science Foundation of China (51574194), Project of Special Science Study of Shaanxi Education Department (16JK1613, 15JK1567), Project of science and technology industry of Shaanxi Province (2014K05-02), Youth Science and Technology Innovation Funded by Xi' an Shiyou University (2010QN011, 2016BS09).

REFERENCES

[1] Suarez-Rivera, R., Deenadayalu, C. and Yang, Y.K. (2009) SS: Unlocking the Unconventional Oil and Gas Reservoirs: The Effect of Laminated Heterogeneity in Wellbore Stability and Completion of Tight Gas Shale Reservoirs. Houston, Texas.

[2] Liang, C., Chen, M., Jin, Y. and Lu, Y.H. (2014) Wellbore stability model for shale gas reservoir considering the coupling of multi-weakness planes and porous flow. Journal of Natural Gas Science & Engineering. 21, 364–378.

[3] Yuan, J.L., Deng, J.G., Yu, B.H., Tan, Q. and Fan, B.T. (2012) Wellbore stability of horizontal wells in shale gas reservoirs. Natural Gas Industry. 32, 66-70.

[4] Liu, H.B., Meng, Y.F., Wan, S.X., Li, G., Jiang, Z.J. and Lü, B. (2010) Analysis of wellbore stability during gas drilling through high-pressure gas formations. Natural Gas Industry. 30, 59-62.

[5] Ma, T. and Chen, P. (2015) Wellbore stability analysis of inclined wells in the AY field. Electronic Journal of Geotechnical Engineering. 20, 1313-1329.

[6] Qiu, K., Gerryo, Y., Tan, C. and Marsden, J.R. (2008) Underbalanced Drilling of a Horizontal Well in Depleted Reservoir: A Wellbore Stability Perspective. Spe Drilling & Completion. 23, 159-167.

[7] Ma, T. and Chen, P. (2015) Wellbore stability analysis of inclined wells in the AY field. Electronic Journal of Geotechnical Engineering. 20, 1313-1329.

[8] Manshad, A.K., Jalalifar, H. and Aslannejad, M. (2014) Analysis of vertical, horizontal and deviated wellbores stability by analytical and numerical methods. Journal of Petroleum Exploration & Production Technology. 4, 359-369.

[9] Alves, J.L., Coehlo, L., Baud, P. and Junior, N.G. (2009) Wellbore stability analysis during the production of a carbonate reservoir. Egu General Assembly. 11, 5753-5759.

[10] Yan, G.R., Karpfinger, F., Prioul, R., Tang, H.Y., Jiang, Y.M. and Liu, C. (2014) Anisotropic Wellbore Stability Model and Its Application for Drilling through Challenging Shale Gas Wells. International Petroleum Technology Conference, Kuala Lumpur, Malaysia.

[11] Fan, L., Yang, X., Wang, H. and Sun, M.J. (2012). Application of Cationic Emulsion Polymer Drilling Fluid in Shale Gas Well. Petroleum Drilling Techniques. 4, 38-42.

[12] Salehi, S., Hareland, G. and Nygaard, R. (2010) Numerical simulation of wellbore stability in under-balanced-drilling wells. J Petrol Sci Eng. Journal of Petroleum Science & Engineering. 72, 229-235.

[13] He, S., Liang L.X., Zeng, Y.J., Ding, Y., Lin, Y.X. and Liu, X.J. (2016) The Influence of water-based drilling fluid on mechanical property of shale and the wellbore stability. Petroleum, 2, 61-66.

[14] Sun, Q.H., Deng, J.G., Chen, Z., Xu, Y.M., Yang, H.L. and Liu, H.L. (2014) Analysis of the Formation Mechanism of Crack Network in Shale by CT. Applied Mechanics & Materials, 2014. 568-570, 12-18.

Received: **21.07.2017**
Accepted: **13.10.2017**

CORRESPONDING AUTHOR

Ni Weijun
Key Laboratory of MOE for Petroleum Engineering, China University of Petroleum (Beijing);
Beijing – China

e-mail: 2069180899@qq.com

© by PSP Volume 26 – No. 12A/2017 pages 8131-8134 Fresenius Environmental Bulletin

EXPERIMENTAL STUDY OF PETROCHEMICAL OILY WASTEWATER TREATMENT FOR REUSE

Hai-Xiang Zhang[1], Yang Li[2], Zhan-Dong Li[1,3,*], Gui-tong Dong[4], Peng Wang[4], Wei Li[1]

[1]College of Petroleum Engineering Institute, Northeast Petroleum University, 163318 Daqing, Heilongjiang, China
[2] Daqing Vocational College, Daqing Heilongjiang, 163255, China
[3] Research Center of Natural Gas Hydrate, Northeast Petroleum University, Daqing Heilongjiang, 163318, China
[4]College of Earth Sciences Institute, Northeast Petroleum University, Daqing Heilongjiang, 163318, China

ABSTRACT

Through experimental research methods, analysis of microelectrolysis and Fenton oxidation method of combining the depth of the petrochemical oily wastewater treatment effect, summarised in the microelectrolysis and Fenton oxidation combined mode processing optimum parameters petrochemical and oily wastewater indicators, with a view to achieve water reuse standards.

KEYWORDS:
petrochemical oily wastewater, depth treatment, reuse.

INTRODUCTION

With industrial development, increasing the amount of oil used, but due to various technical and management development lags behind other reasons are not perfect makes a lot of oil into the water, forming pollution. Oily wastewater sources are very broad; the oil in the oil industry, oil refining, oil storage, transportation and petrochemical industries in the production process will generate a lot of oily wastewaters [1-5]. Oily wastewater pollution is mainly manifested in the following aspects: (1) affecting drinking water and groundwater resources, endangering aquatic resources; (2) endangering human health; (3) atmospheric pollution; (4) affecting crop production; (5) destructing the natural landscape, and even probably because of coalescence of the oil burner safety issues arising. Given oily wastewater pollution China provides the maximum allowable emission of oily wastewater concentration of 10 mg/l. Therefore, oily wastewater treatment is urgently needed in today's field of environmental engineering problems [6-10].

Such conventional wastewater treatment methods for large oil to coagulation, adsorption-based, but in varying degrees on the presence of complex structure, poor treatment effect problems [11-15]. In this study, that is, attempts to apply the micro electrolysis and Fenton oxidation method of combining the petrochemical depth treatment of oily wastewater, in order to improve the rate of oil, petrochemical achieve oily wastewater treatment reaches back to the standard.

EXPERIMENTAL

Test water samples and materials. Water samples were collected from the Daqing Petrochemical Plant oil refining process and the untreated wastewater before oil content was measured at 20 ~ 30.0 mg/l range, pH range of 6.8 to 7.9, water temperature range is 18.0 ~ 20.0oC. Experimental material comprising: a particle size of 1.0 mm ~ 3.0 mm scrap cast iron, activated carbon (specific surface area of 1400 m2/g, a pore volume of 90%) particle size 3.0 ~ 5.0 mm, 1.0 ~ 2.0 mm diameter copper shavings (Purchased from USA), a concentration of 30.0% hydrogen peroxide, the concentration of the standard sodium hydroxide solution.

Laboratory equipment and instruments. Laboratory equipment and instrument configuration include: microelectrolysis reaction column, Fenton reagent, a homemade laboratory sedimentation tanks, UV-vis. spectrophotometer (UV-2700, Shimadzu, Japan), pH detection meter (HACH, USA), electric mixer (Qingdao, China).

Experimental methods. Microelectrolysis test methods are: activated carbon, copper scrap and scrap iron pretreatment, according to a certain proportion of concentrated mass loaded microelectrolysis plexiglass column, and detection precision pH meter (PHS-3C) pH in water samples changes in the value of strict control, adjust the pH value of the parameter with dilute hydrochloric acid. After a certain time the reaction water samples taken adequate amount of oil, and oil removal rate effect is calculated.

Fenton oxidation process for the experiment: After the micro-electrolysis reaction effluent is transferred to Fenton reagent reactor, according to a certain proportion of hydrogen peroxide is added, after 200 rev/min conditions of constant agitation, sodium hydroxide solution was adjusted to pH 9.0, after sufficient precipitation amount of oily supernatant was measured.

RESULTS AND DISCUSSION

Iron - copper - carbon microelectrolysis experiments ternary 40.0 g of the total mass are fixed, pH is 4.0, the reaction time is 1 h, impact of iron copper - carbon at different mass ratio scheme on petrochemical oily wastewater treatment via univariate analysis mode is studied. Specific results are shown in Table 1.

TABLE 1
Impact of iron - copper - carbon at different mass ratio on petrochemical oily wastewater treatment

Mass ratio	2:1:0	2:0:1	2:1:1	2:2:1	2:3:1
Oil removal (%)	32.50	40.50	56.50	48.50	43.50

From Table 1, it is seen that the different iron - copper - carbon mass ratio has a significant impact on the petrochemical wastewater treatment. Oil removal significantly increased after adding a certain proportion of copper. Meanwhile, optimum value of treatment efficiency reached to 56.50% under a variety of experimental mass ratio of programs, then the corresponding iron - copper - carbon mass ratio is 2: 1: 1. Therefore, subsequent experiments used iron - copper - carbon mass ratio 2: 1: 1.

TABLE 2
Iron - copper - carbon microelectrolysis ternary orthogonal reaction results

pH	Liquid-solid ratio	Residence time (min)	Oil removal (%)
2.0	5:1	15.0	74.00
2.0	4:1	30.0	70.00
2.0	3:1	45.0	71.50
2.0	2:1	60.0	74.00
2.0	1:1	75.0	74.50
3.0	5:1	15.0	77.50
3.0	4:1	30.0	79.50
3.0	3:1	45.0	81.50
3.0	2:1	60.0	86.00
3.0	1:1	75.0	77.50
4.0	5:1	15.0	80.50
4.0	4:1	30.0	80.90
4.0	3:1	45.0	79.20
4.0	2:1	60.0	74.30
4.0	1:1	75.0	75.00
5.0	5:1	15.0	83.50
5.0	4:1	30.0	82.50
5.0	3:1	45.0	76.10
5.0	2:1	60.0	79.30
5.0	1:1	75.0	80.80
6.0	5:1	15.0	79.50
6.0	4:1	30.0	72.50
6.0	3:1	45.0	73.80
6.0	2:1	60.0	83.50
6.0	1:1	75.0	81.50
K1	72.81	79.02	74.81
K2	80.29	76.95	75.12
K3	77.93	76.40	79.05
K4	80.39	79.30	80.20
K5	78.09	77.80	80.35

Iron - copper - carbon microelectrolysis ternary orthogonal reaction. The acid-base reaction is fixed as factor A, liquid to solid ratio - B, and residence time - C in orthogonal experiments. The experimental results are shown in Table 2.

From Table 2, it is seen that in the ternary microelectrolysis orthogonal reaction, A is greater than C, C is greater than the factor B, in other words, the relevant factors orthogonal reaction of iron - copper - carbon microelectrolysis treatment effect ternary is ranked as follows: petrochemical oily wastewater liquid to solid ratio <reaction time <pH. From K point of view, in order to achieve the best experimental conditions, optimum solution for pH (4), residence time (5), of liquid to solid ratio (4), that is, treatment of wastewater in the oil and petrochemical to ensure that after the depth of treated wastewater reuse standards reached, water pH should be 5.0, liquid-solid ratio should be 2: 1, reaction time consuming should be 75 min, the best process parameters is fixed.

Fenton oxidation results. The results of the effect of the added amount of hydrogen peroxide on oil removal are shown in Table 3.

TABLE 3
Effect of the added amount of hydrogen peroxide on the oil removal

Hydrogen peroxide added (ml/l)	0.4	0.6	0.8	1.0	1.2	1.4
Oil removal (%)	70.00	78.00	81.00	89.00	73.00	32.00

The data in Table 3 show that when hydrogen peroxide is added at a concentration < 1.0 ml/l will increases oil removal by Fenton oxidation treatment. When hydrogen peroxide is added as 1.0 ml/l, the oil removal reaches the highest value, i. e. 89.00% after Fenton oxidation. When hydrogen peroxide is added in an amount > 1.0 ml/l, the hydrogen peroxide is added in an amount would rise by Fenton oxidation efficiency of wastewater treatment Petrochemical Oil declined. The impact mechanism comprising: at Fenton oxidation treatment of petrochemical wastewater, when hydrogen peroxide is too low in volume, increasing the amount of hydrogen peroxide can be added to make the number of OH radical Petrochemical oily wastewater systems continues to increase, improve oxidative degradation response effect, in order to promote the petrochemical oily wastewater residual small molecules dissolved and emulsified oil cost oil is oxidized, thereby enabling the waste oil is increased. However, when hydrogen peroxide is added in an amount up to 1.0 ml/l or more, Petrochemical Oil Wastewater hydrogen peroxide in excess of the state, leading to water and oxygen automatically decompose and can cause Petrochemical Oil Wastewater Fe2+ oxidation reaction and the formation of Fe3+ resulting OH radical production is suppressed, reducing the efficiency of the

petrochemical oily wastewater. Thus, according to the data in Table 3 Fenton Oxidation optimum amount of hydrogen peroxide determined to 1.0 ml / L.

Effect of pH on oil removal. The optimum amount of hydrogen peroxide was added over a link identified in 1.0 ml/l as the standard response time consuming constant 40 min, adjusted by means of dilute hydrochloric acid ternary microelectrolysis effluent pH optimum conditions were 2.0, 3.0, 4.0, 5.0, 6.0, and effect of different pH on petrochemical oily wastewater treatment is shown in Table 4.

TABLE 4
Effect of different pH on petrochemical oily wastewater treatment

pH	2.0	3.0	4.0	5.0	6.0
Oil removal (%)	30.00	52.00	85.00	89.50	63.00

In Table 4, for pH < 5.0, increasing pH increased processing efficiency, but when pH > 5.0, the oil removal efficiency significantly decreased. It is shown that optimum pH should be 5.0 in Fenton oxidation reaction.

CONCLUSIONS

This study was conducted study experimentally the petrochemical oily wastewater treatment and reuse of the relevant circumstances, study data showed that: (1) by micro-electrolysis technology applications can significantly reduce petrochemical oily wastewater oil content, this reaction Fe - copper - carbon micro electrolysis reaction ternary optimum mass ratio of 2: 1: 1, based on orthogonal experiment results obtained: In order to ensure that after the depth of treated wastewater reuse standards reached, water pH should be 5.0, liquid-solid ratio should be 2: 1, the reaction should be consuming 75 min, the best process parameters required; (2) after the oil and petrochemical waste water ternary micro electrolysis, Fenton oxidation method should be applied for further processing. Univariate results show: during Fenton oxidation, hydrogen peroxide optimum amount of 1.0 ml / L, pH optimum of 5.0, at a reaction time of 40 min conditions can be achieved in line with the standard processing requirements back.

ACKNOWLEDGEMENTS

The authors are grateful for the financial support by Petro China Innovation Foundation (2016D-5007-0212), the University Sci-tech Innovation teams in Heilongjiang Province (2009td08) and Natural Science Foundation of China (51490650)

REFERENCES

[1] Zhang, Y.R., Zhang, L.J., Zhao, T.T. (2015) Supercritical Water Gasification of Oily Wastewater. Oxid Commun. 38(2), 803.
[2] Wang, Y.B., Li, Q. (2015) Treatment of Petrochemical Wastewater via Supercritical Water Oxidation with Nano-Fe2O3. Oxid Commun. 38(3), 1373.
[3] Ma, L., Chen, X., Zhao, M. (2015) Study on Supercritical Water Oxidation of Petrochemical Wastewater. Oxid Commun. 38(3), 1378.
[4] Xie, R.C., Yao, Y., Gu, Z.Y., Yang, Z.B., Liu, Y. (2015) Oily Wastewater Treatment via an Effective Process. Oxid Commun. 38(4), 1830.
[5] Zuo, J.J., Han, R. (2015) Oily Wastewater Treatment Using Wet Peroxide Oxidation and Catalytic Wet Oxidation. Oxid Commun. 38(4), 1875.
[6] Chen, G.H., He, G.H. (2003) Separation of water and oil from waterin-oil emulsion by freeze/thaw method. Sep Purif. Technol. 31(1), 83–89.
[7] Abbasi, M., Salahi, A., Mohammadi, T. (2010) Dimensional analysis of permeation flux for microfiltration of oily wastewaters using mullite ceramic membranes, Desalination. 252, 113–119.
[8] Chakrabarty, B., Ghoshal, K., Purkait, M.K. (2008) Ultrafiltration of stable oil-in-water emulsion by polysulfone membrane, J. Membr. Sci. 325, 427–437.
[9] Peng, H., Tremblay, A.Y. (2008) Membrane regeneration and filtration modeling in treating oily wastewaters, J. Membr. Sci. 324, 59–662.
[10] Salahi, A., Abbasi, M., Mohammadi, T. (2010) Permeate flux decline during UF of oily wastewater: experimental and modeling, Desalination. 251, 153–160.
[11] Amirilargani, M., Mohammadi, T. (2009) Preparation and characterization of asymmetric polyethersulfone (PES) membranes, Polym. Adv. Technol. 20, 993–998.
[12] Marchese, J., Ocheoa, N.A., Pagliero, C., Almandoz, C. (2000) Pilot-scale ultrafiltration of an emulsified oilwastewater, Environ. Sci. Technol. 34, 2990–2996.
[13] Cheryan, M., Rajagopalan, N. (1998) Membrane processing of oily streams. Wastewater treatment and waste reduction, J. Membr. Sci. 151, 13–28.
[14] Shokrkar, H., Salahi, A., Mohammadi, T. (2012) Prediction of permeation flux decline during MF of oilywastewater using genetic programming, Chem. Eng. Res. Des. 90, 846–853.
[15] Salahi, A., Mohammadi, T. (2010) Experimental investigation of oily wastewater treatment using combined membrane systems, Water Sci. Technol. 62, 245–255.

Received: **22.07.2017**
Accepted: **17.09.2017**

CORRESPONDING AUTHOR

Zhan-dong Li
College of Petroleum Engineering Institute,
Northeast Petroleum University,
163318 Daqing, Heilongjiang – China

e-mail: lzd@nepu.edu.cn

© by PSP Volume 26 – No. 12A/2017 pages 8135-8145 Fresenius Environmental Bulletin

EVALUATION THE EFFECT OF GREEN SPACE ON AIR POLLUTION DISPERSION USING SATELLITE IMAGES AND LANDSCAPE METRICS: A CASE STUDY OF ISFAHAN CITY

Zahra Bagheri[1], Mozhgan Ahmadi Nadoushan[1,2,*], Maryam Foroughi Abari[1]

[1]Department of Environmental science, Isfahan (Khorasgan) Branch, Islamic Azad University, Isfahan, Iran
[2]Waste and wastewater research center of Islamic Azad University, Isfahan (Khorasgan) Branch, Isfahan, Iran

ABSTRACT

Rapid expansion of cities and mega-cities often affects the surrounding environment, reducing environmental sustainability and leading to other negative effects. To achieve a sustainable urban environment, it is critical that green spaces expand in harmony with urban expansion in a rational manner, compensating for losses in the environment due to urban growth. In this study, land use maps including 6 classes of green space, urban areas, roads, river, agriculture lands, and barren land were produced using maximum likelihood algorithm for 2010 and 2016 and the landscape metrics were analyzed using FRAGSTATS software. Then, a partial least square (PLS) model was applied to assess the effects of changes in the pattern of green space on air pollution. The model results indicate that reduction in the area of large green space patches promote air pollution, suggesting that there is a direct relation between increases in the area of large green space patches and air pollution reduction.

KEYWORDS:
Urban expansion, air pollution, landscape metrics, Landsat TM images

INTRODUCTION

Air quality has become a major challenge for mega-cities worldwide during recent decades and is a major issue concerning authorities in large cities and mega-cities, requiring serious amelioration measures [1-2]. Increase in industry and urbanization decreases the quality of air and is threatening human health in many ways. Air pollution has been estimated to be the cause of approximately two million premature deaths worldwide per year [3].

Air pollution often exceeds acceptable limits and is especially problematic in industrial mega-cities, where pollution is tied directly to the economy and the environment [4]. Major pollutants emitted by transportation and industry include CO_2, CO, NO_2, and SO_2, which can contaminate the air we breathe and contribute to high health-risk levels [5-6]. Particulate Matter (PM) of natural and anthropogenic origin dominates the health effects of air pollution in addition to its effects on the energy balance of the Earth- atmosphere system [3]. There are two separate standards exist for particulate matter, namely PM10, which refers to particles with aerodynamic diameter < 10 μm, and PM2.5, which refers to particles with aerodynamic diameter < 2.5 μm [7]

Population growth leads to urban area expansion, which in turn reduces per-capita Green Space (GS) area, initiating a number of environmental and ecosystem issues. The most simple and efficient approach with which to balance these deleterious effects on the environment is GS development. Urban green spaces are artificial versions of GS land use types, with critical contributions to urban sustainability [8-9]. Expansion and planning of such spaces can contribute to formulation of simultaneous adaptation and mitigation strategies [10]. Adaptation strategy consists of regulating urban land use, water management, public health, and social education to construct sustainable policies at a socio-economic level, while mitigation strategy controls pollutant emissions from industrial, residential, commercial, and transportation activities. These problem-solving strategies are especially efficient together: adaptation and mitigation can be combined in specific cases like tree planting and GS management [1, 11]. In general, air pollution mitigation is one of the most valuable advantages of urban GS, which are also referred to as the 'lungs' of urban areas [12-13]. The advantages of these areas include air and noise pollution reduction, water and soil protection, air temperature balance, and promotion of sustainable ecosystem for animal species, all of which justify creation of balanced social and environmental systems in urban areas. Appropriate planning and expansion with respect to adaptation and mitigation strategies is necessary if sustainable urban development is sought [14-15].

Several studies were done by some researchers on air pollution and land use changes which are challenging issues these days. Seker et al. (2008) used

Landsat satellite images analyze the coastal changes occurred in Kilyos - Karaburun region, Turkey as a result of open mining activities. Surface and spatial profiles achieved through multi-temporal remotely sensed data belonging to 1984, 1992 and 2001 [16]. Sakellaris et al. (2017) used air quality measurements in two buildings, an office building and a small plastic craft industry, both located in a semi-industrial area of Athens. The monitoring campaign lasted for three days during September 2014 and included Volatile Organic Compounds (VOC) and PM10 measurements [17]. Sarigiannis et al. (2017) developed an efficient method for the determination and quantification of 19 PAH compounds in the atmosphere of the Thessaloniki region in Greece. Air samples were collected in two sampling sites in the area of Thessaloniki between January and mid-April of 2013, an urban background site and a traffic site. Results showed that the concentrations in samples from the two monitoring stations showed variations both in PM fractions and PAH compounds. PAHs concentrations were higher in the urban background station, due to the increase in biomass combustion [18].

An attempt is made in this study to prepare land use maps of the study area during a 6-year period and assess land use changes, analyzing the changes in GS through spatial changes and landscape metrics and identifying the effect of urban GS on air pollutant mitigation using the partial least squares (PLS) model.

The structure of this article consists of 4 below sections. Sec. 1 describes pervious findings; Sec. 2 presents the study design, including methodology and variable determination; Sec. 3 presents analysis of changes in GS patterns; and Sec. 4 describes the effect of GS on air pollution.

MATERIALS AND METHODS

The study area. Isfahan is located in the center of Iran (33.38 N, 51.39 W) at an elevation 1550-1650 m and is Iran's third largest city after Tehran and Mashhad. The city of Isfahan had a population of 5,120,850 in the 2015 [19]. The city has 14 urban districts. This Isfahan mega-city is surrounded by the cities Khomeini Shahr and Najaf Abad to the west, Sofeh Mountain to the south, and Sepahan Shahr and Shahin Shahr to the North in addition to the Segzi fields. This mega city is ranked second in air pollution nationwide and is subject to a number of socio-economic and health problems. It is surrounded by industrial centers large and small, which constitute the main pollutant sources. In order to accomplish effective air pollution reduction measures, more serious studies with a focus on the contribution of urban GS to protection of the urban ecosystem and land use efficiency are necessary [20-21].

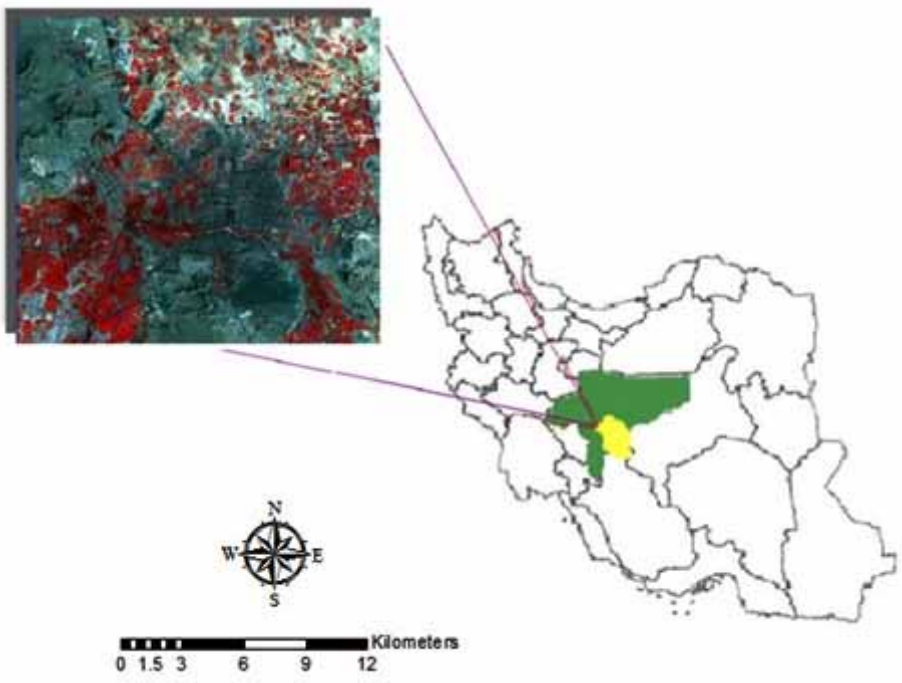


FIGURE 1
The geographic location of Isfahan City

TABLE 1
Description of land use categories

Land use categories	Description
Urban	Residential, industrial, commercial, in construction
River	Zayandeh Rood River
Road	Freeways, Blvds., Aves., Streets, Alleys, etc.
Barren	Zones with few or no plants
Farmland	Zones with landscape, like small urban agricultural lands
Landscape	Any landscape along the river banks, and parks

TABLE 2
The metrics applied in this study

Metrics	Symbol	Unit
Largest patch index	LPI	Percent
Percentage of landscape	PLAND	Percent
Number of patches	NP	NO Unit
Patch density	PD	Meter/ha

Land use classification. To diagnose changes in landscape patterns, land uses maps are prepared from Landsat TM Images from 2010 to 2016. In this supervised classification, for each phenomenon, a number of levels or regions are selected as sample or training sites to be applied in upcoming classifications. Here the maximum likelihood method is adopted as it is more accurate than its supervised counterparts [22]. In this method, supervised classification is applied to the false-color composite images from the TM bands during the experiment period. The six land use categories are tabulated in Table 1.

Quantifying landscape metrics and assessments of landscape pattern changes. Landscape metrics are measured at patch, class, and landscape levels at different scales. The landscape ecology emphasizes the interaction between spatial pattern, ecological process, and scale, and focuses on the structure, function, change, and management of landscape [1]. To study GS, some categorical indexes are not considered and applied in a direct manner. The 'patch' is the basic unit applied for assessing GS, and all indexes are obtained based on patch statistical data. In this study, the PD, NP, and LPI metrics are applied in describing the combination and spatial distribution of constituent elements at landscape level and the three NP, PLAND, and LPI metrics are applied at the class level, consistent with related literature (Table 2) [22].

Quantification of landscape metrics for a six-year period is made at both the landscape and class levels using FRAGSTATS software. This software contains a spatial pattern analysis program designed to compute different landscape metrics from land use maps [22].

Assessing the effect of green spaces on air pollution. The partial least square (PLS) model. The regressive PLS model is adopted herein to assess correlations between congestion, GS pattern formation, land use structural change patterns, and air pollution concentration reduction. PLS consists of the inner model, which describes correlations among latent variables, and the outer model, which describes correlations between latent and observed variables.

This model is capable of simultaneously accepting and assessing the reflective and formative structure, and is appropriate for analyzing small amounts of data, lost data, small sample data sizes, and independent co-linear variables. The sample size in this study is very small. The reflective analytic mode includes a series of latent and dependent variables for which correlations are assessed through the PLS mode. Adoption of the PLS model is appropriate for the objectives here, since the subject samples are quite small [1, 23].

Definitions of the latent and observed variables. Latent variables include the size and number of largest GS patches and particulate matter (PM), CO, NO_2, and SO_2 pollutant concentrations. Observed variables are obtained through measurement of the latent variables' rate of change and consist of changes in land use, fragmentation, largest patch size, and changes in pollution concentrations, which are in turn, obtained through the landscape metrics indices for the study period (Table 3).

1) Changes in landscape and land use consist of three latent or computed variables:
   a) Change of landscape
   b) Change of fragmentation
   c) Changes of largest patch percentage

2) The pollutant emission pattern change rate within the experiment period consists of only one latent variable which is the change in air pollution emissions.

The analysis of both latent and observed variables, their rate effects, and the manner in which they introduce pollution to the urban GS are tabulated in Table 3. This table contains two sections: 1) changes in urban GS and other land uses, and 2) changes in air pollution rates.

RESULTS AND DISCUSSION

Preparation of land use maps and accuracy assessment. After selecting the best training samples, the land use plans are executed through supervised classification implementation with regard to the six categories, where the maximum likelihood method is adopted on TM image bounds for the determined period (Figures. 2 and 3). To determine the accuracy of the classification, the false color composite images and GPS are applied; the accuracy percentages are 93.94% for the year 2010 and 92.08% for 2016. The use of multi-temporal images reduced possible errors and smoothed the results [24]. Changes in area allocated to a given land use are calculated for the study period according to the obtained efficiency plans (Tables 4 and 5).

Land use changes between 2010 and 2016. Within this period, the land use maps obtained from TM images are analyzed to reveal land use changes. According to these maps, the highest number of changes occurred in barren regions (that is, new landscapes), which constitute about 5% of the total and 10% of the urban barren region in the northern section. In the same period a 5% convergence of urban-agriculture land into urban expansion is evident. In general, land use change affects mostly urban agriculture and barren land. It is noteworthy that the river dimensions have remained constant.

Quantifying landscape metrics. The findings so far indicate that, due to population growth and an increase in city dwelling, man-made patches have increased in this period. This population growth and an increase in city dwelling have reduced the ideal land percentage.

TABLE 3
PLS model variables

Landscape	Latent Variable	Observed Variable
Change of green space	Change in landscape	Change in PLAND
	Change in fragmentation	Change in NP Change in PD
	Change in largest patch percentage	Change in LPI
Change of air pollution	Change in air pollution emission	Change in SO_2 emissions Change in NO_2 emissions Change in CO emissions Change in PM_{10} emission

TABLE 4
Land use classification error matrix for 2010

Land use classes	City	Road	River	Mountain	Agricultural land	Green space	Barren land	Sum	Commission error
City	3175	0	0	66	2	4	0	3247	0.0222
Road	40	26	0	0	0	0	0	66	0.6061
River	0	0	27	0	0	0	0	27	0.000
Mountain	37	0	0	4458	0	0	0	4495	0.0082
Agricultural Land	2	0	0	27	175	76	0	280	0.3750
Green space	43	0	0	0	16	448	0	507	0.1164
Barren land	0	0	0	9	0	0	244	253	0.0356
Sum	3297	26	27	4560	193	528	244	8875	0.0356
Commission error	0.0370	0.0000	0.0000	0.0224	0.0933	0.1515	0.0000		0.0363

Overall kappa: 93.94% Overall accuracy: 96.37%

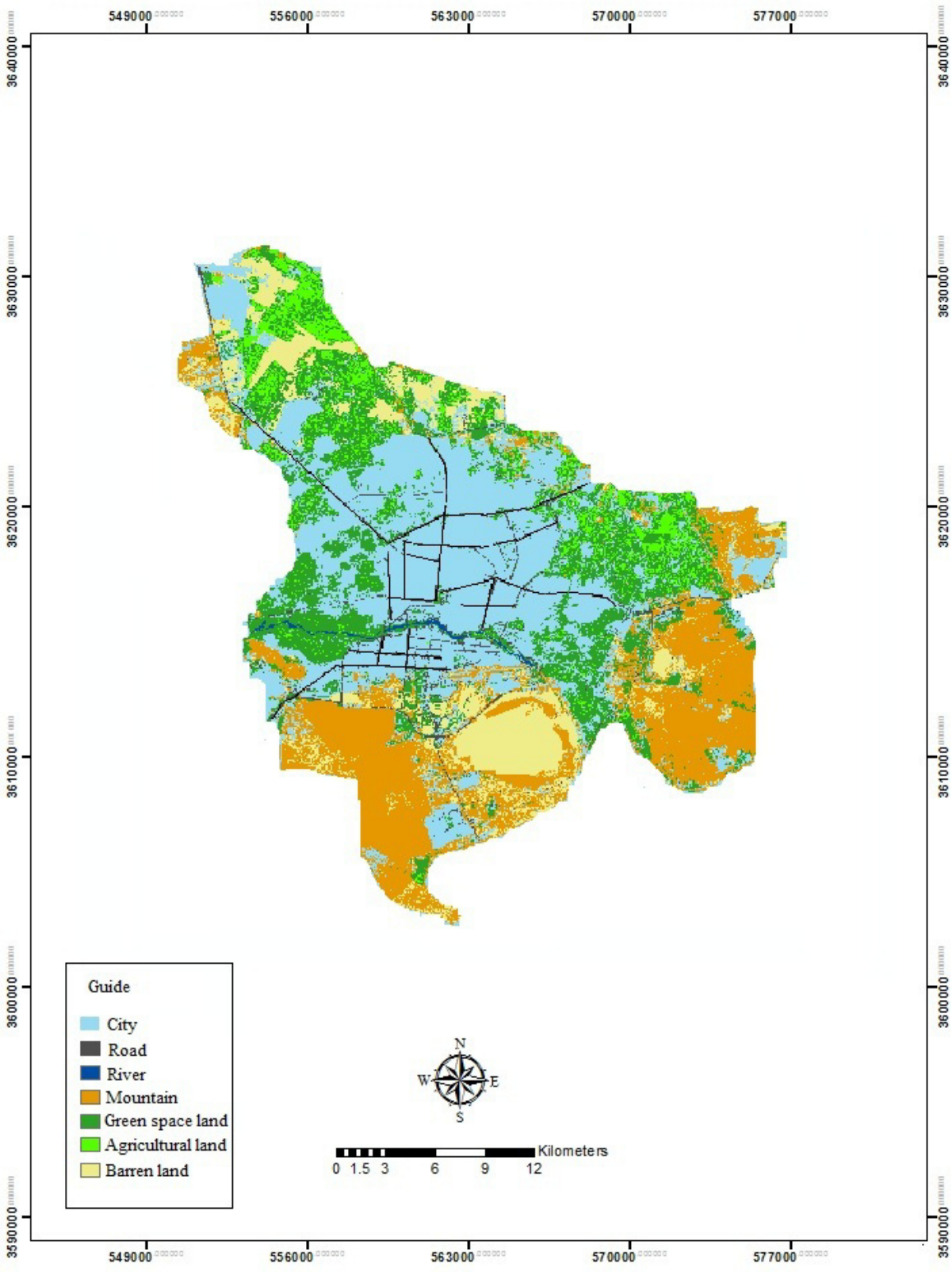


FIGURE 2
Land use map for 2010

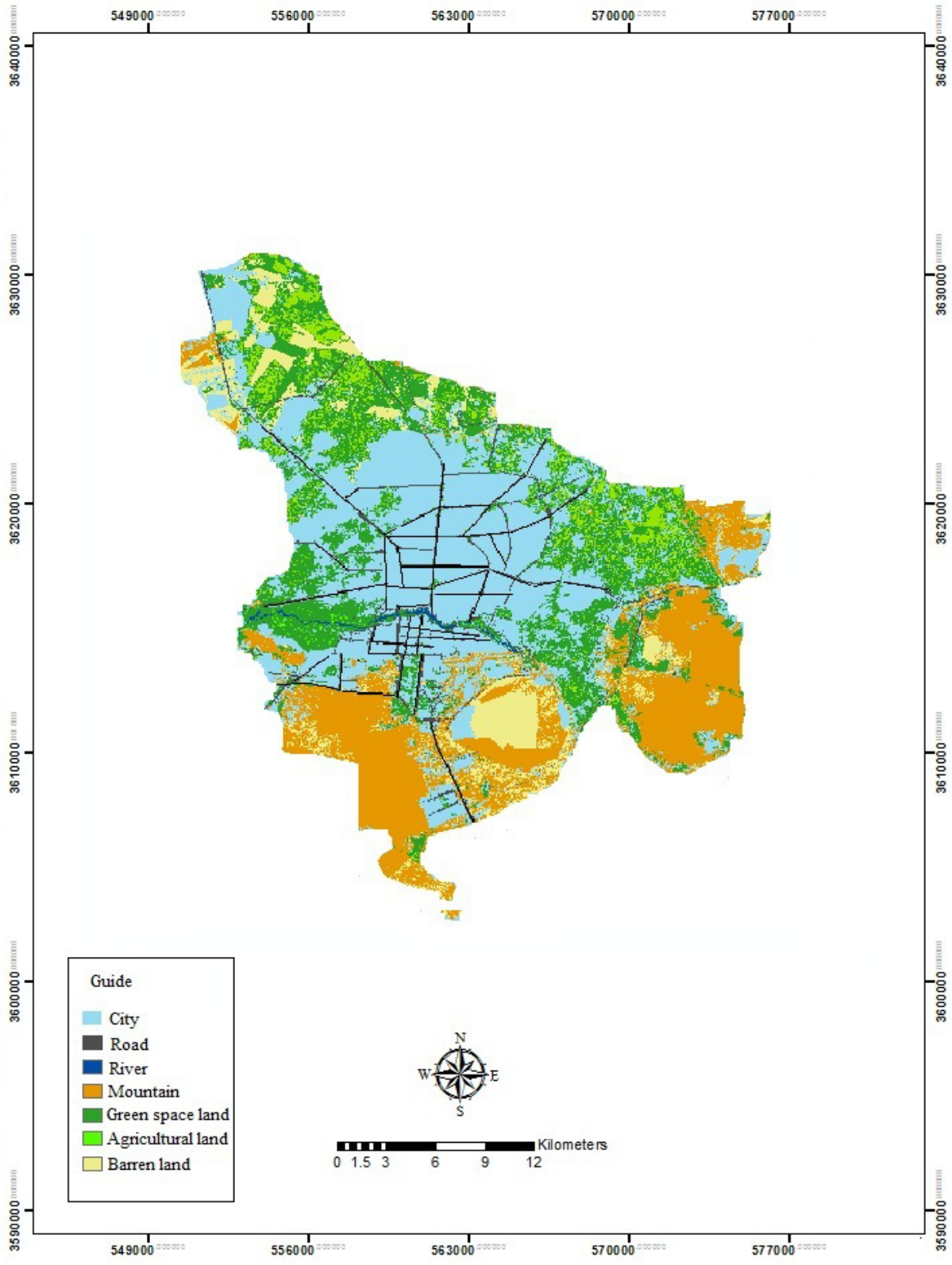


FIGURE 3
Land use map for 2016

TABLE 5
Land use classification error matrix for 2016

Land use classes	City	Road	River	Mountain	Agricultural Land	Green space	Barren land	Sum	Commission error
City	1268	1	0	71	0	2	0	1342	0.0551
Road	8	50	0	0	0	0	2	60	0.1667
River	0	0	32	0	0	0	0	32	0.000
Mountain	12	0	0	3253	0	5	32	3302	0.0148
Agricultural Land	0	0	0	0	311	117	0	428	0.2734
Green space	6	0	0	29	54	559	0	648	0.1373
Barren land	10	0	0	118	0	0	2326	2454	0.0552
Sum	1304	51	32	3471	365	683	2360	8266	0.0356
Commission error	0.0276	0.0196	0.0000	0.0628	0.01479	0.1816	0.0144	-	0.0565
Commission error	0.0276	0.0196	0.0000	0.0628	0.01479	0.1816	0.0144	-	0.0565

Overall kappa: 92.08% Overall accuracy: 94.35%

TABLE 6
Results of calculated landscape metrics

Landscape metrics			Year
LPI	PD	NP	
36	22	45877	2010
17	28	69231	2016

Landscape-level analysis. In this analysis, the whole span is considered a coherent ecology. As observed in Table 6, the patch volume metric and patch number have increased during the study period, and the biggest patch index matrix is reduced by 19%. The fragment concentration metric is applied as the patching index.

Class-level analysis. The PLAND reveals land use percentages at the class level and the combined landscape ecology percentage in general. Time variation can be applied to this matrix to achieve a general picture of changes in landscape ecology in a given study area [25]. In this study, the percentage of green space, man-made space, and road construction have increased during the study period; in 2010 barren land comprises the highest land use percentage, while urban and GS dominate in 2016.

Agricultural land use was reduced from 12.18% in 2010 to 9.65% in 2016. Man-made patches increased from 10.35% in 2010 to 14.90% in 2016, and barren land decreased due to urban development in the same period. The results obtained from the analysis are presented in Figures 4 and 5. The number of patches has increased in all categories. The increase in man-made patches indicates landscape ecology deterioration.

The results obtained from the analyses run on the urban coverage indicate that the change of spatial pattern, do reduce environment quality and introduce a number of problems including an increase in air pollution.

The effect of landscape on air pollution. Assessment of the PLS. (a) The Outer Model. The reliability of this model allows the inner path to be assessed. To verify outer model reliability, both the composite reliability (CR) and the average variance extracted (AVE) are assessed. The CR of all variables should be greater than 0.7 (CR>0.7); researchers prescribe a 0.5 or higher AVE for all variables (AVE>0.5) [26].

The findings here indicate CR values of 0.76-1.0 and AVE values of 0.62-1.0 for all latent variables, meeting the established standards and indicating good data quality (Table 8). All changes in landscape latent variables have direct, significant effects on changes in air pollutant concentrations (including CO_2, CO, NO_2, and SO_2), with either reduction or increase in the size of the biggest patch. Fragmented-patch data indicate indirect effects on pollution reduction, while largest-patch data indicate a direct effect on pollution reduction.

(b) The Inner Model. The necessary criteria for evaluating the structural model - coefficient of determination (R^2) and the paths of variable - are innate. In PLS model output, R^2 values of 33.67, 0.0, and 0.19 describe significant, medium, and weak states, respectively. The coefficient volume fluctuated within -1 and +1 in the standard state; higher effectiveness is indicated by values closer to either bound [26]. The coefficients of determination between latent GS variables and air pollution are tabulated in Table 8; these findings reveal that all

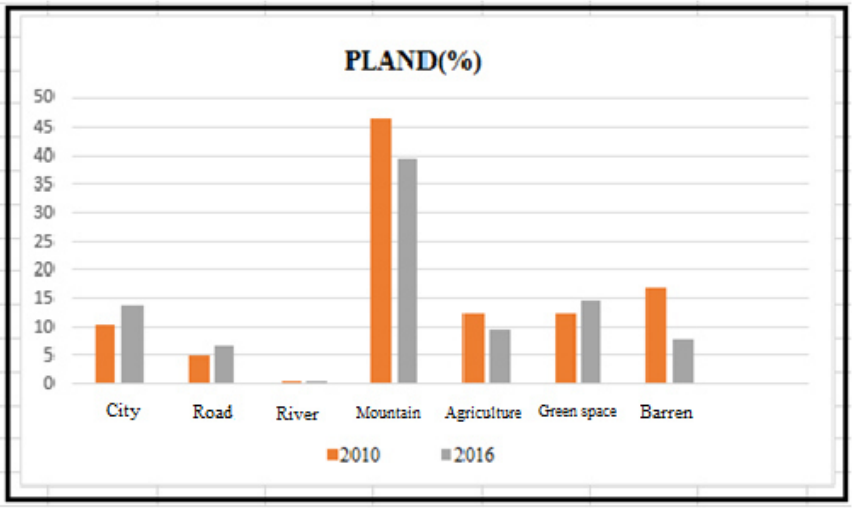


FIGURE 4
Values of PLAND during the study period

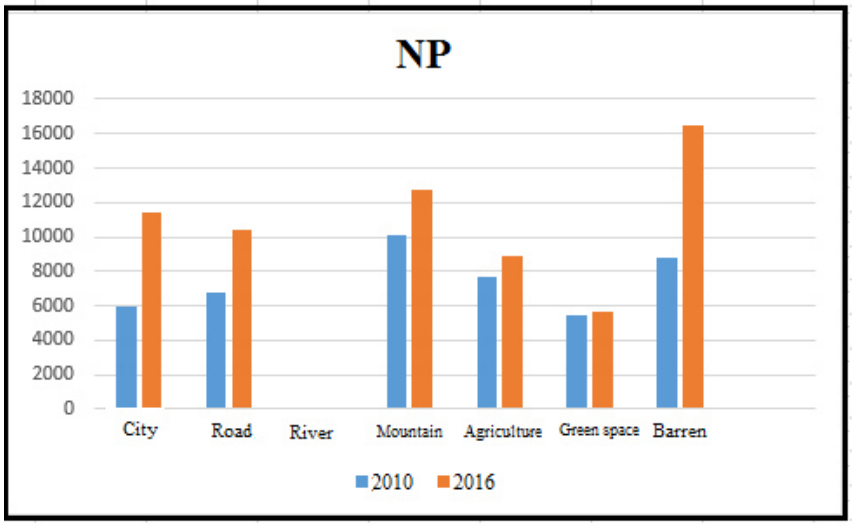


FIGURE 5
Comparison of the number of different patches

TABLE 7
Outer model assessment

Landscape	Latent variables	CR	Average
Change in green space	Change in fragmentation	0.764	0.624
	Change in landscape	1.000	1.000
	Change in largest patch percentage	1.000	1.000
Change in air pollution	Change in air pollution emission	0.973	0.900

TABLE 8
Path coefficient experimental results in the inner model.

Variables	Change in air pollution emission
change in fragmentation	0.475
change in landscape	-0.821
change in largest patch percentage	-0.427

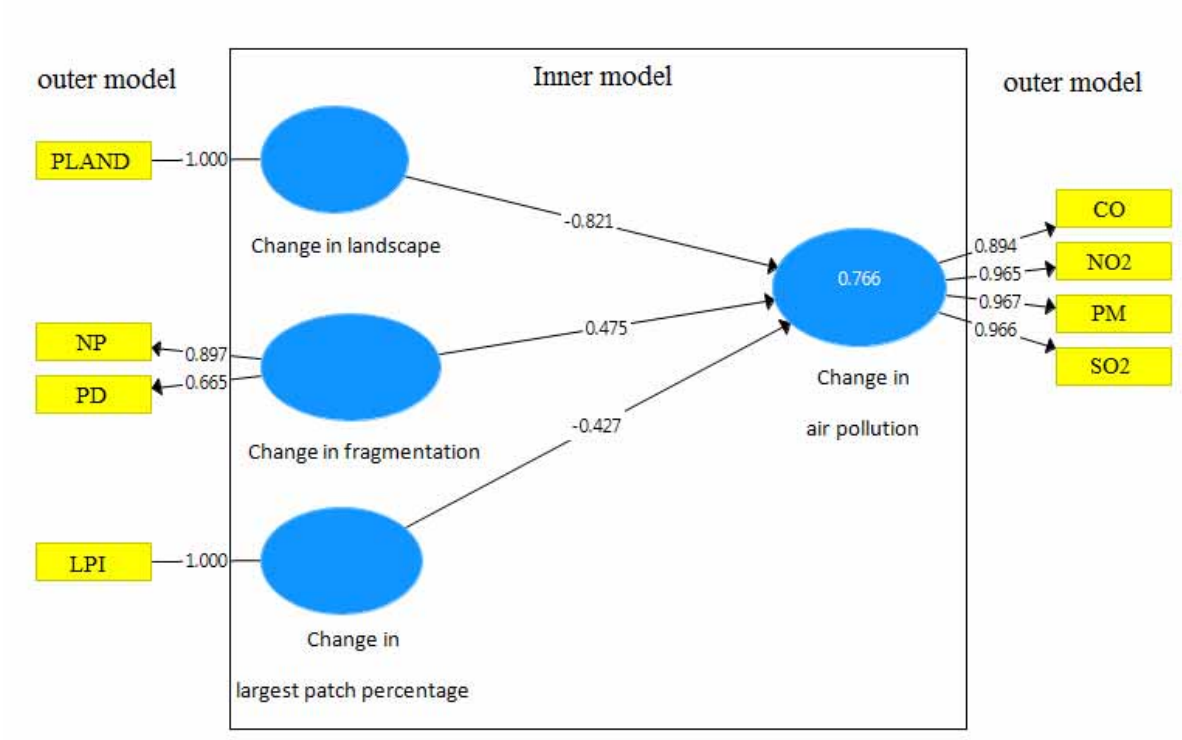


FIGURE 6
PLS model outcome

changes in latent GS variables have significant effects on pollutant emission. These findings are similar to those revealed in the outer model.

Analysis of results. The effect of changes in landscape and land uses categories on air pollution reduction. During this study period, area devoted to GS is decreased due to urban expansion, which has, together with increased fragmentation rate, led to a decrease in the largest patch size. This size change is considered to be a latent variable because of its negative effect on air pollution. As mentioned previously, the coefficient volume fluctuates within -1 and +1 in the standard state, where higher effectiveness is indicated by values closer to either bound. Thus, changes in landscape lead to changes in green space; that is, reduction in GS has a direct negative effect on air quality.

According to Figure 6, this study has verified the effects (direct, indirect, and total) of latent variables through PLS analysis. The effects of the latent variables are as follows:

The "change in landscape" latent variable: the number and area of GS changes affects changes in air pollution emission in a negative manner. The total effect of green space on air pollution change is -0.821, derived from the direct effect.

The "change in largest patch percentage" latent variable: changes in GS area and the largest patch percentage affect air quality in a negative manner. The total effect of changes in largest patch percentage on air pollution emission is -0.427, influenced by the direct effect.

The "change in fragmentation" latent variable: the fragmentation of GS affects air quality in a positive manner. The total effect on changes in air pollution emission is 0.475.

In general, it can be stated that air pollution is a major destructive force in urban settings, but can be confronted through one of the simplest and most common resolution patterns: an increase in urban GS area of any kind, shape, or form. Diagnosing changes in GS area and analyzing the effects thereof is necessary for determining air pollution rates in urban settings. In this study, land use plans were developed followed by analysis of green space structural pattern changes using landscape metrics. The consequences of these changes regarding air pollution concentrations are assessed using the PLS model.

The results obtained are as follows:

1. A reduction in urban landscape area is indicated by increases in city dwelling and GS structural pattern changes.
2. The assessments of landscape metrics during this study period indicate more fragmentation and reduction in the biggest green space patch. Due to changes in landscape area, GS configuration has become simpler while that of the larger patches has become more complex. Increases in the number and concentration patches and reductions in size of the

largest patches indicate disintegration of the landscape ecology. The same phenomenon is observed and addressed by Liu and Shen [1].

3. The results obtained using the PLS model reveal that changes in urban GS structural patterns have significant effects on air pollution. For example, a reduction in air pollution is experienced when the biggest patches grow in size in urban settings and when GS concentration is distributed in an appropriate manner. A decrease in the size of the largest patches due to a reduction in ecologically interconnected GS networks has a negative effect on air pollutants.

Increases in urban space and fragmented landscapes have negative effects on air pollution. Land use change due to human activities, urban area expansion, and lack of environmental restrictions have caused the development of fragmented landscapes, which in turn reduce the ability of landscapes to reduce pollution.

CONCLUSIONS

Air pollution is a major destructive force in urban settings, but can be confronted through one of the simplest and most common resolution patterns: an increase in urban GS area of any kind, shape, or form. The expansion of large cities and mega cities, particularly in in underdeveloped countries, intensifies the negative aspects of urban development, including, most notably, air pollution. Unsustainable urban development changes in land use patterns, and specifically green space, are assessed in this study, using the PLS model to determine the effects of green space changes on air pollution reduction. The spatial changes in green space and other land uses for the purpose of urban development have reduced environmental quality by increasing air pollution. Diagnosing changes in GS area and analyzing the effects thereof is necessary for determining air pollution rates in urban settings. Findings indicate that the size of the largest GS patches has decreased due to urban expansion, and this fragmentation ratio reveals an increase in GS degradation and air pollution increase. Through the PLS model, it is revealed that when the size of the largest green space patches becomes larger, air pollutant concentrations reduce, and an increase in the number of GS patches promotes pollutant emission rate reduction. Accordingly, as the number and area of parks, orchards, woods, and other protected natural landscapes in the city increase, the negative effects of air pollution will decrease.

ACKNOWLEDGEMENTS

The authors would like to thank the assistance and support of Islamic Azad University, Isfahan branch for funding this major research project.

REFERENCES

[1] Liu, H.L. and Shen, Y.S. (2014) The Impact of Green Space Changes on Air Pollution and Microclimates. Sustainability. 6, 8828-8854.
[2] Jayasooriya, V.M., Muthukumaran, S. and Perera, B.J.C. (2017) Green infrastructure practices for improvement of urban air quality. Urban Forestry & Urban Greening. 21, 34-47.
[3] Ozelkan, E., Karaman, M., Mostamandy, S., Avci, Z., Toros, H. (2015) Derivation of PM10 levels using OBRA on Landsat 5 TM images: a case study in Izmir, Turkey. Fresen. Environ. Bull. 24, 1585-1596.
[4] Janhall, S. (2015) Review on urban vegetation and particle air pollution - Deposition and dispersion. Atmospheric Environment. 105, 130-137.
[5] Tallis, M., Taylor, G., Sinnett, D. and Freer-Smith, P. (2011) Estimating the removal of atmospheric particulate pollution by the urban tree canopy of London, under current and future environments. Landscape and Urban Planning. 103, 129–138.
[6] Elbir, T., Kara, M., Simsi, S., Eren, T. and Ozdemir, S. (2010) Development of a GIS-based decision support system for urban air quality management in the city of Istanbul. Science of the Total Environment. 26, 547-566.
[7] Kocak, E., Kilavuz, S.A., Imamoglu, I., Tuncel, G. (2017) PM2.5 bound organic molecular marker speciation methods and observations from daily measurements in Ankara, Turkey. Fresen. Environ. Bull. 26, 263-272.
[8] Bencheikh, H. and Rchid, A. (2012) The effects of green spaces (Palme trees) on the microclimate in arides zones, case study: Ghardaia, Algeria. Energy Procedia. 18, 10-20.
[9] De Ridder, K., Adamec, V., Banuelos, A., Bruse, M., Burger, M., Damsgaard, O., Dufek, J., Hirsch, J., Lefebre, F., Perez-Lacorzana, J.M., Thierry, A. and Weber, C. (2011) An integrated methodology to assess the benefits of urban green space. Science of the Total Environment. 335, 489-495.
[10] Senanayake, I.P., Welivitiya, W.D.D.P. and Nadeeka, P.M. (2011) Urban green spaces analysis for development planning in Colombo, Sri Lanka, utilizing THEOS satellite imagery-A remote sensing and GIS approach. Urban Forestry & Urban Greening. 12, 307- 314.

[11] Han, L., Zhou, W., Li, W. and Li, L. (2014) Impact of urbanization level on urban air quality: A case of fine particles (PM2.5) in Chinese cities. Environmental Pollution. 194, 163–170.
[12] Dadvand, P., Rivas, I., Basagaña, X., Alvarez-Pedrerol, M., Su, J., Pascual, M., Amato, F., Jerret, M., Querol, X., Sunyer, J. and Nieuwenhuijsen M.J. (2015) The association between greenness and traffic-related air pollution at schools. Science of the Total Environment. 523, 59-63.
[13] Ramdhoni, S., Badriyah Rushayati, S. and Budi Prasetyo, L. (2012) Open green space development priority based on distribution of air temperature change in capital city of Indonesia, Jakarta. Procedia Environmental Sciences. 33, 204-213.
[14] Mavroidis, I. and Ilia, M. (2012) Trends of NOx, NO2 and O3 concentrations at three different types of air quality monitoring stations in Athens, Greece. Atmospheric Environment. 63, 135-147.
[15] Sezlmi, W., Weber, C., Riviere, E., Blond, N., Lotfi, M. and Nowak, D. (2012) Air pollution removal by trees in public green spaces in Strasbourg city, France. Urban Forestry & Urban Greening. 17, 192–201.
[16] Seker, D.Z., Kaya, S., Alkan, R.M., Tanik, A., Saroglu, E. (2008) 3D coastal erosion analysis of Kilyos - Karaburun region using multi-temporal satellite image data. Fresen. Environ. Bull. 17, 1977-1982.
[17] Sakellaris, I.A., Tolis, E., Saraga, D.E., Bartzis, J.G. (2017) VOCS, PAHS and ions measurements in an office environment in the vicinity of a small industry. Fresen. Environ. Bull. 26, 292-300.
[18] Sarigiannis, D., Nikolaki, S., Zikopoulos, D., Kermenidou, M. (2017) Determination of 19 PAHS in air samples using gas chromatography –mass spectrometry. Fresen. Environ. Bull. 26, 338-344.
[19] Hosseiniebalam, F. and Ghaffarpasand, O. (2015) The effects of emission sources and meteorological factors on sulphur dioxide concentration of Great Isfahan, Iran. Atmospheric Environment. 100, 94-101.
[20] Norouzi, A. and Mohammadi, Z. (2014) Zoning of air pollution by using GIS software and air quality index in Isfahan city of Iran. Proceedings of the first National Conference on Environment in Payam Noor University. Isfahan, Iran, 10-16.
[21] Atai, H. and Hashemi-Nasab, A. (2014) Evaluation and classification of air pollution using GIS in Isfahan city, Iran. Proceedings of the first National Conference on Environment in Payam Noor University. Isfahan, Iran, 1-9.
[22] Bihamta Tousi, N., Soffianian, A. and Fakheran, S. (2013) Quantifying landscape pattern changes using landscape metrics in Isfahan city, Iran. Planning and Environmental Management Conference. Tehran University, Iran, 1-8.
[23] Abdi, H. (2010) Partial least squares regression and projection on latent structure regression (PLS Regression). Computational statistics. 2(1), 97-106.
[24] Wicki, A. and Parlow, E. (2017) Attribution of local climate zones using a multi-temporal land use/land cover classification scheme. J. Appl. Remote Sens. 11(2), 1-16.
[25] Yousefi, A. and Salehi, A. (2010) Ecological analysis of green space in Birjand based on landscape metrics. Geographic space Journal. 14(46), 71-87.
[26] Amani, J., Khazri, H., Mahmodi, H. (2012) Introduction of modeling structural equations using partial least squares. Geographic space Journal. 1(1), 41-54.

Received: **24.07.2017**
Accepted: **02.10.2017**

CORRESPONDING AUTHOR

Mozhgan Ahmadi Nadoushan
Department of Environmental Science,
Isfahan (Khorasgan) Branch,
Islamic Azad University,
Isfahan – Iran

E-mail: m.ahmadi@khuisf.ac.ir
m.ahmadi1984@gmail.com

© by PSP Volume 26 – No. 12A/2017 pages 8146-8153 Fresenius Environmental Bulletin

EFFICIENCY OF PHEROMONE WATER TRAPS AND LIFE CYCLE OF *TUTA ABSOLUTA* (LEPIDOPTERA: GELECHIIDAE) IN DIYARBAKIR PROVINCE, TURKEY

Yunus Bayram[1], Mehmet Duman[2], Musa Buyuk[3], Cetin Mutlu[4,*]

[1]General Directorate of Food and Control, Ankara, Turkey
[2]Plant Protection Research Institute, Diyarbakir, Turkey
[3]Agricultural Vocational School of Dicle University, Diyarbakir, Turkey
[4]Abant Izzet Baysal University, Faculty of Agriculture and Natural Sciences, Department of Plant Protection, Bolu, Turkey

ABSTRACT

The first detection of Tomato leaf miner, [(*Tuta absoluta*) (Meyrick, 1917) (Lepidoptera: Gelechiidae)] in Turkey was in 2009 and it rapidly spread and became the major pest in the areas where tomato is cultivated, including Southeastern Anatolia Region of Turkey. The aim of this study was to investigate the infestation status, life cycle and efficiency of pheromone water traps of Tomato leaf miner in Diyarbakır province, Turkey.

The studies were conducted in farmers' fields and Diyarbakır Plant Protection Research Institute trial field between 2011-2013 years. Tomato leaf miners were subjected to trials in cages and the pheromone water traps were used for biotechnical control at open tomato fields. The infestation rate of *T. absoluta* was low in seedling stage and during ripening period of fruit and the infestation rate reached up to 100% and continued until the harvest in both years in the Central and Bismil districts of Diyarbakır. The pheromone water traps were not sufficient to control *T. absoluta* in spite of a large number of males caught. Adults of *T. absoluta* flying were recorded during at the end of March (8-12 °C and 62-75% relative humidity). Five generations were determined for *T. absoluta* with an average of 40 days for each generation and it was affected by extremely high temperatures and low humidity conditions.

KEYWORDS:
Tomato leaf miner, *Tuta absoluta*, infestation rate, life cycle, biotechnical control

INTRODUCTION

Tomato is one of the most produced and consumed products, and it plays a vital role in the global trade of agricultural products [2]. In Turkey, tomato is grown both in open fields and greenhouses in different regions, which are suitable in terms of climate. It can be consumed as fresh, dried, canned, frozen, pickled and as ketchup [4]. Turkey produces 7.2 % of the world's tomato and it is ranked 4th country in the world in terms of tomato production after China, India and USA [5]. In Diyarbakır province, tomato production has increased in recent years after the development of irrigation facilities and provision of state subsidies to farmers. Tomato production is curtailed by many serious pests and diseases [1].

The South American tomato leaf miner, *Tuta absoluta* (Meyrick), is a micro lepidopteran moth belonging to the Gelechiidae family and is considered one of the most devastating tomato pests. It is originated in South America has spread to other European countries and Mediterranean basin after first identification in Spain in 2006 [6, 15, 34]. The pest has a high reproductive potential and the larvae of *T. absoluta* feed voraciously on all parts of tomato plants except the root. The crop losses may increase from 80% to 100% in greenhouses and open field tomato crops [24]. Chemical control is difficult because the larvae live inside leaves, fruits and stems.

Tuta absoluta is a new pest for Turkey and the pest was found first in open tomato fields of Urla, İzmir in 2009 [20] and later in greenhouses of Kumluca, Antalya in 2010 [14]. Then the pest was spread very quickly and became the main pest of open fields tomato crops and greenhouses due to its high mobility and reproduction. After the establishment of tomato leaf miner in Turkey, studies on regarding distribution, population dynamics and some management aspects of *T.absoluta* were studied [10, 12, 21, 17, 19, 22, 32, 35, 25, 28, 30, 7].

Chemical agents are used as the primary means to control the pest in Southeast Anatolia Region as well as other parts of Turkey. However, intensive use of pesticides affects negatively environment and human health as well as natural enemies and causes pest resistance [23]. Regardless of this intensive use of different pesticides, high level of damage was recorded on tomatoes [27]. It is necessary to study biology, seasonal distribution as well as other effective and sustainable solutions to be able to control *T. absoluta* because it is a new harmful pest in Turkey.

The objective of this study was to determine the life cycle of the pest, its temporal distribution within the life span of the crop and to evaluation of biotech-

nical control method in reducing *T. absoluta* populations and leaf and fruit damage.

MATERIALS AND METHODS

Area of study and materials. This study was conducted at Central district (Ekinciler village (38° 08' 48,6" N and 39° 58' 55,4" E) and Bismil district (37° 50' 44.8" N and 40° 41' 08.8" E) of Diyarbakır province. The main materials of this study; tomato plants, tomato leaf miner, Delta-type pheromone traps (Russel IPM Tuta absoluta-500 PH-937-1RR Qlure-Tua 0.5 mg E3Z8Z11-14Ac+0.024 mg E3Z8-14Ac), blue color circular plastic water traps (54x17x15 cm), large cages (2x2x2 m) which was covered with thin muslin (40x70 mesh), small cages (100x70x70 cm), various branch muslin cages in different sizes (20x20 mesh, 5x5 cm and 10x10 cm), tomato planted pots (20x15 cm), plastic containers (30x50x10 cm), hand lenses, a stereo-binocular microscope.

Infestation level of *Tuta absoluta* on different growth stages of tomato plants. Studies to determine the infestation level of *T. absoluta* on different stages of tomato, samples were conducted weekly in two tomato fields (each selected field has an area of at least 0.3 ha) in Central and Bismil districts of Diyarbakır province during 2011 and 2012 by counting and recording infestation on leaves and fruits. The studies was initiated on 23 May, 12 June in 2011 and 2012, respectively and finished on 12 September, 18 September in 2011 and 2012, respectively in both districts (Central and Bismil).

The sampling method was totally randomized; 20 tomato plants were selected from each field from which three leaves (apical, middle and bottom) were cut. The leaves (total 60 for each field) were examined for the presence of different leaf miner stages and recorded weekly. Starting at the beginning of fruiting period, at least one fruit of randomly selected 20 tomato plants was examined for the presence of mining or existence of larvae until at the end of harvesting, The infestation level of tomato plants by *T. absoluta* was determined by using the number of infested leaves and fruits to the total number of examined leaves and fruits.

Efficiency of pheromone water traps on tomato fields of *Tuta absoluta*. Adults of *T. absoluta* were observed weekly on the same tomato cultivated fields and during the period as mentioned above in 2011 -2012 years. Before establishing trial, it was necessary for monitoring of the population of *T. absoluta* by setting up sticky traps during transplantation of tomato seedlings in fields at a rate of 1 trap/0,1 ha which were hanged on the top of seedlings (15-20 cm above the plants by using an iron rod).

After capturing of the first adults flying in sticky traps, trials were established as 6 traps /0.1 ha. Circular plastic containers (50 cm diameter) were used as traps and pheromone capsules were attached to the top of the middle of the plastic containers fastened with wires from both sides. The containers were filled with water and a thin layer of oil was added onto the surface of the water to avoid males to escape. The traps were each 30 m apart. Adults in the traps were counted and recorded weekly. Pheromone capsules were replaced every 6 weeks, pheromone water traps were cleaned and refilled with water, and drops of oil were added. During the first year of the studies in both districts no pesticides were used. The second year, growers applied the pesticide once in order to decrease the damage when the economic damage level had exceeded in both locations. Voliam Targo SC (45 g/l Chlorantraniliprole + 18 g/l Abamectin 80ml/100 liter of water) was used in August in both locations.

The Life cycle of *Tuta absoluta*. To determine the life cycle of *T. absoluta*, a stock culture has been established in a room under controlled climatic conditions (25 ± 1ºC temperature, 60 ± 5 % humidity, 16 Light:8 Dark) at the Plant Protection Research Institute in Diyarbakır province, and grown periodically on tomato seedlings that planted in pots to sustain foliage source for different stages of the pest. The larvae and pupae of leaf miners were collected from tomato fields and released on tomato seedlings and transferred into lattices to obtain adults. Recently emerged adults were given water with 15% sugar sprayed on seedlings (Patricia and Sánchez, 2006).

The badly damaged seedlings were replaced with new ones. The study of the biology of *T. absoluta* was initiated with the first catch by the traps, which were used to monitor the population in the field. Adults of *T. absoluta*, which were obtained from stock culture, were used to follow biological parameters of the pest from egg laying until the emergence of adults. An sucking tube was used to collect 20 pairs of adults (♂+♀) and the adults were released as five pairs in each lattice. The lattices were checked and tomato plants were examined daily to determine egg laying, first larval emergence stage the time of pupation and adulthood stage. The length of generation and the number of generations per year were also determined.

To complete life cycle of *T. absoluta* regardless of entering diapause during the winter seasons of December 2012 and November 2013, approximately 1-1.5 kg of soil was removed from 5-7 cm depth with some plant remains from different points of lattices and was brought to the laboratory. The soil samples were spread into plastic containers and covered with polyethylene bags to capture and ensure the date of adult emergence. During the study, weather data has been taken from Regional Meteorological Directorate of Diyarbakır province (Figure 3).

RESULTS

The weekly infestation rates of *Tuta absoluta* on tomato plants and fruits are shown in Figure 1.

According to the results, the infestation level was 25% in the first days of July, while it was 70% in the Mid-August of 2011 in both locations. The infestation level reached 100% on 29th August 2011 in Bismil district and 80% in the village of Ekinciler and the infestation rates increased up to 100% until the end of harvest (Figure 1). On the second year, the results from both locations showed that the infestation level varied between 30 to 35% at the end of July, while it increased 65-70% on the first week of August and reached 100% on 28th August and continued the same trend until the end of harvest (Figure 1). The average number of *T. absoluta* adults obtained from traps (Figure 2) and the level of infestation on leaves and fruits were similar as in Figure 1.

The population fluctuation of *T. absoluta*, which was observed weekly by using pheromone traps counting in tomato fields in Central and Bismil districts of Diyarbakır in 2011-2012 are shown in Figure 2.

The first peak point of the pest population was detected on 18th July as 34 adults/trap/week and the second peak point (the highest) was detected on 5th September as 105 adults/trap/week in both locations. Then the number of adults decreased as 87 adults/trap/week, which was recorded on 12th September (Figure 2). In the field of Bismil District, four peak points were detected. The first one was on 11th July as 78 adults/trap/week, the second one was on 25th July as 168 adults/trap/week, third one was on 15th August as 271 adults/trap/week and the last one was on 29th August which was the highest peak point among all as 311 adults/trap/week (Figure 2).

On the second year, during the sampling period of Ekinciler village, the population of *T. absoluta* increased continuously. The first peak point of *T. absoluta* was detected on 7th August as 235 adults/trap/week, the second one was detected on 21st August as 256 adults/trap/week, the third one was detected on 4th September as 303 adults/trap/week, while the fourth (the highest) one was detected on 18th September as 307 adults/trap/week (Figure 2). In Bismil district, the first peak point was detected on 17th July 36 adults/trap/week, the second one was detected on 7th August 134 adults/trap/week and the third one was detected on 28th August 165 adults/trap/week and the fourth one was detected on 4th September 200 adults/trap/week.

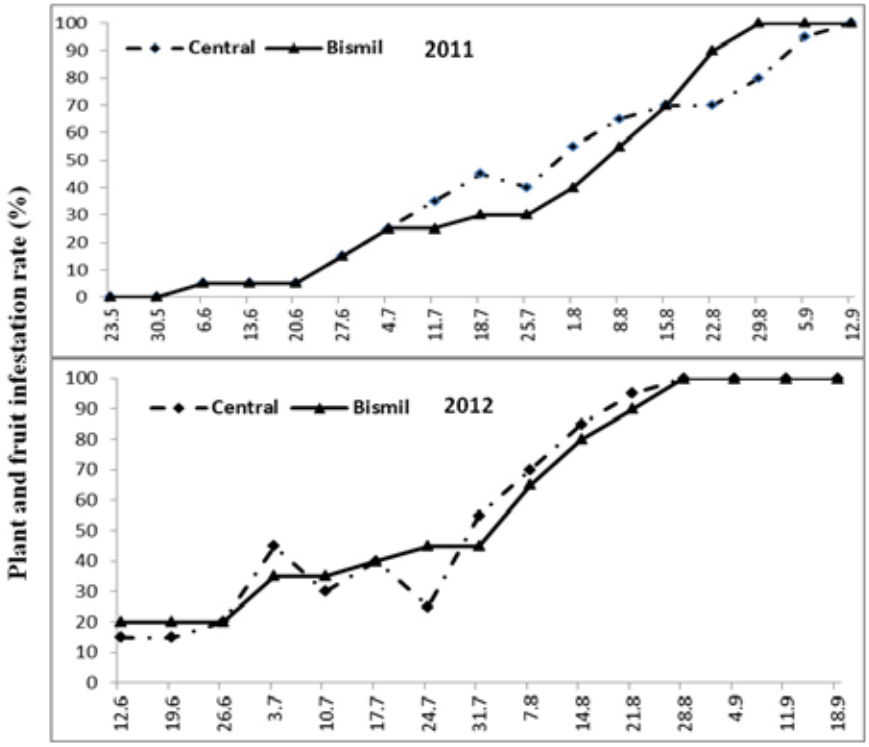


FIGURE 1
The infestation rate of *Tuta absoluta* on tomato plants and fruits in Central and Bismil districts of Diyarbakır in 2011-2012

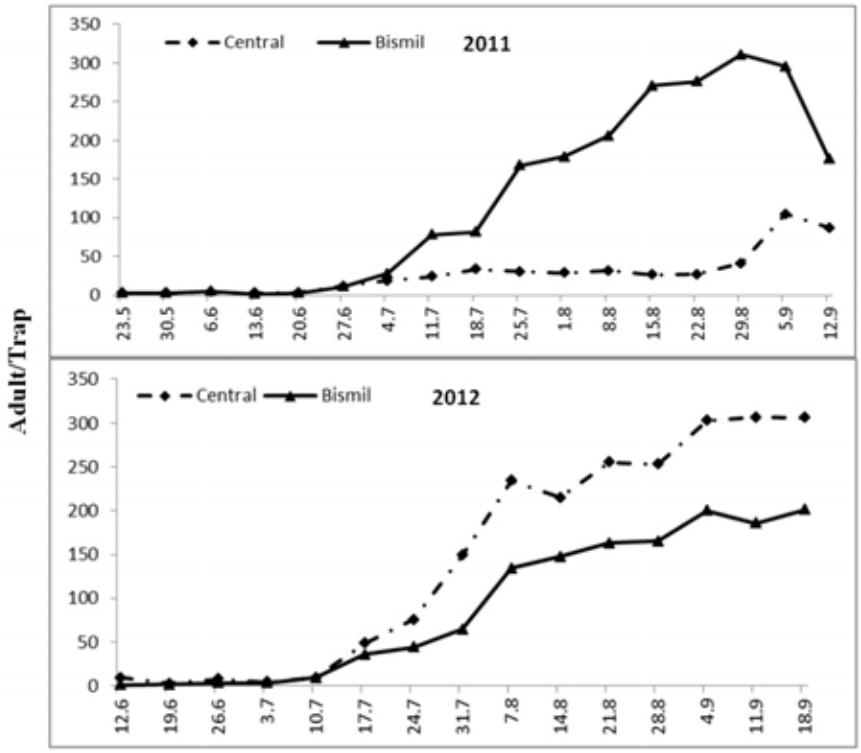


FIGURE 2
The weekly average numbers of *Tuta absoluta* adults in tomato fields in Central and Bismil districts of Diyarbakır in 2011-2012

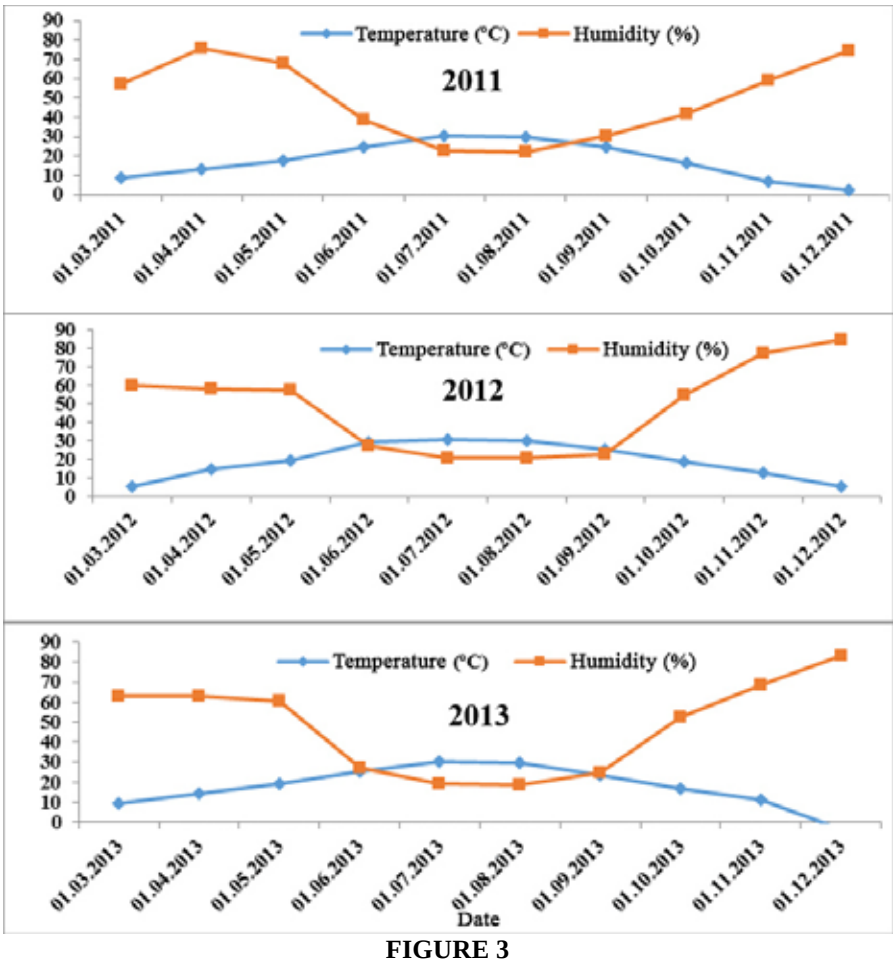


FIGURE 3
The temperatures and humidity in Diyarbakır province in 2011- 2013

TABLE 1
Duration of each biological stage, of Tuta absoluta in Diyarbakır province in 2012-2013

Biological stages	2012						2013					
	1. Gen.	2. Gen.	3. Gen.	4. Gen.	5. Gen.	6. Gen.	1. Gen.	2. Gen.	3. Gen.	4. Gen.	5. Gen.	6. Gen.
Egg date*	13.04.	30.05.	02.07.	03.08.	07.09	12.10.	09.04.	21.05.	25.06.	28.07.	03.09	21.10.
Number of days	5	5	4	4	7	4	4	5	4	5	8	12
Larva dates	18.04.	04.06.	06.07.	07.08.	14.09.	16.10.	13.04.	26.05.	29.06.	02.08.	11.09	02.11.
Number of days	24	13	14	14	15	32	21	14	15	16	15	23
Pupa dates	12.05.	17.06.	20.07.	21.08.	29.09.	17.11.	04.05.	09.06.	14.07.	18.08.	26.09	25.11.
Number of days	11	9	10	12	10	-	12	11	10	9	19	-
Adult exit	23.05.	26.06.	30.07.	02.09.	09.10.	-	16.05.	20.06.	24.07.	27.08.	15.10.	-
Number of days	7	6	4	5	3	-	5	5	4	7	6	-
Generation time (days)	47	35	32	35	35	-	42	35	33	37	48	-

*Elapsed time from egg to egg regarded as one generation.

In 2012 the first adults were observed in the trial fields on 3rd April (Average temperature was 11 ºC and relative humidity was 62%), while in 2013 they were detected on 7th April (the average temperature was 18 ºC and relative humidity was 57%). The findings obtained regarding the lifecycle of Tomato leaf miner are indicated in Table 1. The climatic data of Diyarbakır for 2012-2013 has been given in Figure 3.

The duration of biological stage of *T.absoluta* has shown in Table 1.

In 2012, 5 generations (from egg to egg) were obtained. The shortest duration of a generation was 32 days, which was observed in third generation, while the longest was 47 days in the first generation. Adult individuals emerged until 9th October when the 5th generation was completed. The development period of the eggs was 4-7 days, while the development period for larvae was 13-32 days, the development period for pupae was 9-12 days and the length of adult emergence was 3-7 days (Table 1). The last generation from egg to pupae lasted 32 days (16th October) due to decrease of temperature. After this date, even though the trial was controlled until 28th November, no adult emergence occurred. In addition, for possibility of obtaining adults or monitoring the diapause period of the pest, the remaining plant parts and soil were brought to the laboratory on 28th November and 6 adult individuals emerged after 10 days. As shown in, the remaining plant parts and soil samples were brought to the laboratory after the second year of the study and it was found out that the pest overwinters as pupa in the soil.

According to the results of the second year study (2013), the first adults were transferred to the cages on 7th April and the first eggs were collected on 9th April 2013. The shortest duration of a generation was 33 days in the third generation (30.4 ºC, 18.5% average humidity) and the longest was 48 days in fifth generation (20.5 ºC, 25.6% average humidity). Depending on the average temperature and relative humidity, the duration from egg to larva varied between 4-12 days, while the duration varied between 14-23 days from larva to pupa, between 9-19 days from pupa to adult and the emergence of adults lasted 4-7 days. But in the last generation, after 21st October 2013 the decrease of temperature (14ºC, 26 % humidity) changed, duration of transformation from larva stage to pupa stage occurred in 23 days (2nd November - 25th November) (Table 1).

DISCUSSION AND CONCLUSION

This study was conducted to evaluate the efficiency of pheromone water traps on *Tuta absoluta* and its life cycle on tomato fields. It is clear that the ratio of infestation obtained from this study was very high on tomato plants in both locations. Similarly [19] results displayed that the infestation rate of *T. absoluta* on tomato plants in greenhouses was low at the beginning of May, but this rate increased gradually at the end of May or at the beginning of June and the damaged fruit rate increased simultaneously until the highest rate as 38.4%. This study's results agree with [26], the damage of *T. absoluta* on tomato leaves and fruits increased towards the end of tomato growth due to increased temperature.

According to the climatic conditions of Diyarbakır, it is well understood that there is a close relationship between population increase and temperature. As low temperatures constitute limiting factors for *T. absoluta* survival [28], Diyarbakır which has hot climate condition will contribute positive effects to the tomato leaf miner population. Considering that "Economic Damage Threshold" for *T. absoluta* is 3% infestation of leaves and fruits according to available literature [3], therefore, climatic conditions

(temperature and humidity) should be taken into consideration for effective and sustainable control of the pest and for decision making with a strategic plan about necessary control methods.

According to the results of the biotechnical control in this study, the study revealed that the pest has four peak points. In the seedling period there was low infestation, then the infestation rate increases rapidly and reaches 100% in the period of fruit formation (the period of fruit set) until the end of harvest. Although the pesticide was applied in both fields, the number of male individuals collected from the traps was very high (Figure 2), the outcomes indicated that only biotechnical control itself was not sufficient for controlling *T. absoluta* and infestation rate increases continuously. Some previous studies verify results derived from this study [8, 16, 11, 37].

That is why, in the event that in a tomato fields where no control measures applied, this can cause an infestation source for the adherent tomato fields. Only biotechnical control itself is considered insufficient for the control of highly infested areas. Because there are many environmental factors, the pest cannot be controlled in wide areas. When these factors are in favor of the pest and the necessary measures are not taken, the pest can cause high damage, so in order to have an effective and successful pest management, biotechnical control as a method should be integrated with the other control methods (biological control, cultural methods and chemical control).

Comparing the studies carried out for 2 years on determining the biological criteria, the development durations of second, third and fourth generations were close to each other, the third generation (32-33 days) developed in the shortest time but the development durations of first and fifth generations were different (47 days for first generation in 2012, 48 days for fifth generation in 2013). The same results as the first year study were obtained on the second year for 5 generations and shifted to the pupa stage before completing the sixth generation. It is well known that the temperature and humidity dependent development an insect is a fundamental feature of its life history. In this study, one of the main factors affecting the emergence of adults from overwintered pupa is temperature. Since the number of individuals in the population of first generation affects potential occurrence of the later generations, the winter weather conditions with very low temperatures could restrict the activity of the pest throughout the year. By the higher population density and the higher infestation rate of the pest in spring and summer, the higher damage could be observed in all parts of the plant. However, since extremely high temperatures are observed in whole July and in the first half of August, an obvious stagnancy or decrease is observed in the activity of the pest. According to the results of two years, stagnation and lower activity of pest population have been observed at 40 °C or over 40 °C. Due to the beginning of temperature decrease in the second half of August in nighttime, the pest becomes active again and since these days coincide with the occurrence of fruit development stage of tomato production, the damage caused by the pest increases rapidly. The infestation rate of the pest in leaves and fruits was 85 % in the village of Ekinciler in Central District of Diyarbakır and 90% at Bismil district (Figure 1). Then all of the leaves of the plants dried rapidly and became dysfunctional. Consequently, the climatic conditions in spring and autumn are crucial for the development of the pest and population and effectiveness of other generations decrease when control measures are applied for the first generation. In order to cut down the effectiveness of the last generation at the end of harvesting (autumn season), the remaining plants with overwintering of the pest in fields should be destroyed by plowing. According to recent findings, there is a direct relation between the biology of *T.absoluta* and temperature, humidity; climatic and environmental conditions are very much influential on the population; infestation, reproductive capacity and the number of generations of the pest [32, 13, 9, 18].

As a result, the climatic conditions of Diyarbakır province, the first adult individuals of *T. absoluta* were observed active flying at temperatures between 8-12 °C and 62-75 % humidity. *T. absoluta* produces 5 generations from beginning of March until entering into diapause due to winter conditions of the region that some time below zero, snowy and extreme cold conditions. The shortest development time of a generation was 32 days. The durations of generations changed among generations depending on temperature and humidity. The pest overwinters as a pupa during winter. Extreme temperatures and low humidity affects the development from egg to adult stage of the pest. According to the biotechnical control study results, it was determined that in tomato production fields, mass trapping by pheromone traps was insufficient, although pesticides were applied the damage caused by the pest still continued, 4 peak points were detected on pheromone traps and the infestation of plants and fruits reached 80-100 % towards the end of harvest. Regarding this high-risk the pest which has recently been introduced to Turkey, more comprehensive measures should be implemented within the framework of integrated pest management, giving priority to biological control methods and cultural methods that are more environmentally friendly. Moreover, for a sustainable and effective control strategy, climatic conditions, pest bio-ecology, infestation rate and period, and IPM control plan should be taken into consideration.

ACKNOWLEDGEMENTS

This work was supported by the Republic of Turkey Ministry of Food, Agriculture and Livestock General Directorate of Agricultural Researches and Policies under Grant TAGEMBS-10/07-01/01-04.

REFERENCES

[1] Anonymous, (2008) Plant Protection Technical Instructions. Volume: 3. Ministry of Food, Agriculture and Livestock, General Directorate of Agricultural Research and Policy (TAGEM), Ankara, 332 p.

[2] Anonymous, (2011a) FAO. Web page: http://faostat.fao.org) (Access Date: January 2012).

[3] Anonymous, (2011b) Plant Protection Technical Instructions. *Tuta absoluta* (Meyrick) (Lepidoptera: Gelechiidae). Ministry of Food, Agriculture and Livestock, General Directorate of Agricultural Research and Policy, Ankara.

[4] Anonymous (2012) Tomato. Web page: http://tr.wikipedia.org/wiki/Domates) Access Date: January 2012).

[5] Anonymous (2014) Annual and official data of General Directorate of Plant Production. p 21.

[6] Baranieri, V., Cheraghian, A. (2011) The current status of *Tuta absoluta* in Iran and initial control strategies. In: EPPO/IOBC/FAO/ NEPPO Joint International Symposium on management of *Tuta absoluta* (tomato borer), 16-18 November 2011, Agadir, Morocco: 20.

[7] Bayram, Y., Bektaş, Ö, Büyük, M., Bayram, N., Duman, M., Mutlu, Ç. (2014) Determination of population dynamic of tomato leaf miner [*Tuta absoluta* (Meyrick) (Lepidoptera: Gelechiidae)] in tomato growing areas of Diyarbakır province. Plant Protection Bulletin. 54(4), 343-354.

[8] Cocco, A., Deliperi, S., Delrio, G. (2012) Potential of mass trapping for *Tuta absoluta* management in greenhouse tomato crops using light and pheromone traps. IOBC/WPRS Bulletin. 80, 319-324.

[9] Cuthbertson, A.G.S., Mathers, J.J., Blackburn, L.F., Korycinska, L.W., Jacobson, R.J., Northing, P. (2013) Population Development of *Tuta absoluta* (Meyrick) (Lepidoptera: Gelechiidae) under Simulated UK Glasshouse Conditions. Insects. 4, 185-197.

[10] Doğanlar, M., Yıldırım, A.E., Yiğit, A. (2011) The effect of some environmentally friendly pesticides on *Tuta absoluta* (Meyrick) (Lepidoptera: Gelechiidae) which harmful on greenhouse tomatoes. Turkey 4th Plant protection Congress (28-30 June 2011, Kahramanmaraş). 496 p.

[11] Duric, Z., Hmcic,´ S., Vujanovic,´ M., Đuric, B., Mitric, S. (2012) *Tuta absoluta* (Meyrick) (Lepidoptera, Gelechiidae) in the Republic of Srpska (Bosnia and Herzegovina). Bulletin OEPP/EPPO Bulletin. 42(2), 337-340.

[12] Durmuşoğlu, E., Hatipoğlu, A., Balcı, H., Sav, S. (2011) Efficiency of some plant extracts against *Tuta absoluta* (Meyrick, 1917) (Lepidoptera: Gelechiidae) under laboratory conditions 279. Turkey 4th Plant protection Congress (28-30 June 2011, Kahramanmaraş). 496 p.

[13] El Mahdy, I.A., Al Ansary, O. (2011) *Tuta absoluta* Pest Management. http://i3.makcdn. com/wp-content/blogs.dir//76492/files//2011/ 12/tuta–12–2011.pdf.

[14] Erler, F.C., Erdoğan, M., Ateş, A.O., Pradier, T. (2010) New record of *Tuta absoluta* (Meyrick) (Lepidoptera: Gelechiidae) on greenhouse-grown tomato in Southwestern Turkey (Antalya). Journal of Entomological Science. 45(4), 392-393.

[15] García, M.F., Espul, J.C. (1982) Bioecology of the tomato moth (*Scrobipalpula absoluta*) in Mendoza, Argentine Republic. Revista de Investigaciones Agropecuarias. 17, 135- 146.

[16] Hrncic, S., Radonjic,´ S. (2012) Tomato leaf miner - *Tuta absoluta* Meyrick (Lepidoptera, Gelechiidae) - current status in Montenegro. Bulletin OEPP/EPPO Bulletin. 42(2), 341-343.

[17] Karabüyük, F.S., Horuz, A.Y., Ulusoy, M.R. (2011) The studies on biological control of tomato leaf miner, *Tuta absoluta* (Meyrick). Turkey 4 th Plant Protection Congress (28-30 June 2011, Kahramanmaraş). 496 p.

[18] Karadjova, O., Ilieva, Z., Krumov, V., Petrova, E., Ventsislavov, V. (2013) *Tuta absoluta* (Meyrick) (Lepidoptera: Gelechiidae): Potential for Entry, Establishment and Spread in Bulgaria. Journal Agriculture Science. 19, 563-571.

[19] Karut, K., Kazak, C., Döker, I., Ulusoy, M.R. (2011) Pest status and prevalence of Tomato moth *Tuta absoluta* (Meyrick 1917) (Lepidoptera: Gelechiidae) in tomato growing greenhouses of Mersin. Turkish Journal of Entomology. 35(2), 339-347.

[20] Kılıç, T. (2010) First record of *Tuta absoluta* in Turkey. Phytoparasitica. 38(3), 243-244.

[21] Kılıç, T. (2011) The measures that taken against spread and control of Tomato moth [*Tuta absoluta* (Meyrick)] (Lepidoptera: Gelechiidae) in Turkey, 42". Turkey 4th Plant protection Congress (28-30 June 2011, Kahramanmaraş). 496 p.

[22] Konca, E., Pour, A.D., Erdoğan, T., Güz, N,, Gürkan, M.O. (2011) Characterization of detoxification enzymes of Tomato leaf miner [*Tuta absoluta* (Meyrick)] (Lepidoptera: Gelechiidae), 18". Turkey 4th Plant protection Congress (28-30 June 2011, Kahramanmaraş). 496 p.

[23] Lietti, M.M.M., Botto, E., Alzogaray, R.A. (2005) Insecticide resistance in Argentine populations of *Tuta absoluta* (Lep.: Gelechiidae). Neotropical Entomology. 34, 113-119.
[24] Lopez, E. (1991) Polilla del tomate: Problema cri'tico para la rentabilidad del cultivo de verano, Empresa y Avance Agricola. 1, 6-7.
[25] Mamay, M., Yanık, E. (2012) Adult population development of Tomato leaf miner [*Tuta absoluta* (Meyrick) (Lepidoptera: Gelechiidae)] in tomato growing fields of Şanliurfa province. Turkish Bulletin of Entomology. 2(3),189-198.
[26] Mollá, O., Montón, H., Vanaclocha, P., Beitia, F., Urbaneja, A. (2009) Predation by the mirids *Nesidiocoris tenuis* and *Macrolophus pygmaeus* on the tomato borer *Tuta absoluta*. IOBC/WPRS Bulletin. 49, 209-214.
[27] Moore, J.E. (1983) Control of tomato leaf miner (*Scrobipalpula absoluta*) in Bolivia. Tropical Pest Management. 29, 231-238.
[28] Notz, A.P. (1992) Distribution of eggs and larvae of *Scrobipalpula absoluta* in potato plants. Revista de la Facultad de Agronomía. 18, 425-432.
[29] Öztemiz, S. (2012) The Tomato Leaf miner [(*Tuta absoluta* Meyrick (Lepidoptera: Gelechiidae)] and its Biological Control. KSÜ Journal of Natural Science. 15 (4), 47-57.
[30] Patricia C P, Sánchez EN (2006) Effect of Two Solanaceous Plants on Developmental and Population Parameters of the Tomato Leaf miner, *Tuta absoluta* (Meyrick) (Lepidoptera: Gelechiidae) Neotropical Entomology. 35(5), 671-676.
[31] Portakaldalı, M., Öztemiz, S., Kütük, H. (2013) A New Host Plant for *Tuta absoluta* (Meyrick) (Lepidoptera: Gelechiidae) in Turkey. Journal Entomological Research Society. 15(3), 21-24/
[32] Robredo, J.F., Cardenoso, H.J.M., Alonso, J.J. (2008) *Tuta absoluta*, Meyrick: number of potential generations a year. Agricultura Revista Agropecuaria. 78, 474-480.
[33] Tatlı, E., Göçmen, H. (2011) Determination of Spread and Population Fluctuations of Tomato Leaf miner, *Tuta absoluta* (Meyrick) (Lepidoptera: Gelechiidae) in Tomato Production Fields of West Mediterranean Region". Turkey 4th Plant protection Congress. (28-30 June 2011, Kahramanmaraş), 496 p.
[34] Uchoa-Fernandes, M.A., Lucia, T., Della, M.C., Vilela, E.F. (1995) Mating, oviposition and pupation of *Scrobipalpuloides absoluta* (Meyr.) (Lepidoptera: Gelechiidae). Anais da Sociedade Entomológica do Brasil. 24(1), 159-164.
[35] Urbaneja, A., Vercher, R., Navarro, V., García, M.F., Porcuna, J.L. (2007) La polilla del tomate, *Tuta absoluta*. Phytoma España. 194, 16-23.
[36] Yükselbaba, U., Göçmen, H., İtken, C. (2011) Sequence Determination of Mitochondrial Cytochrome Oxidase Subunit I (mtCOI) Gene Region for *Tuta absoluta* (Meyrick) (Lepidoptera: Gelechiidae". Turkey 4th Plant protection Congress (28-30 June 2011, Kahramanmaraş). 496 p.
[37] Zhimerikin, V.N., Mironova, M.K. (2012) *Tuta absoluta*- a threat to tomato production. Zashchita i Karantin Rasteniĭ, 11, 32-34.

Received: **26.07.2017**
Accepted: **03.10.2017**

CORRESPONDING AUTHOR

Cetin Mutlu
Faculty of Agriculture and Nature Science,
Department of Plant Protection,
University of Abant İzzet Baysal,
14080, Bolu – Turkey

e-mail: cetinmutlu@hotmail.com

© by PSP Volume 26 – No. 12A/2017 pages 8154-8159 Fresenius Environmental Bulletin

MODEL PREDICTIVE CONTROL OF WIND TURBINE WITH DOUBLY FED INDUCTION GENERATOR

Jing Zhang[1,*], Peijia Yu[2], Bowen Li[1], Bangsong Shi[2]

[1]College of Electrical engineering, Guizhou University, Guizhou Province, China
[2]College of Computer Science and Information, Guizhou University, Guizhou Province, China

ABSTRACT

In this paper, a model predictive control (MPC) design method for the wind turbine (WT) with doubly fed induction generator (DFIG) is proposed. The WT with DFIG is represented by a third-order model where electromagnetic transients of the stator are neglected. Then the nonlinear model is linearized by using the Taylor series, which is considered as the predictive model. At the same time, in order to reduce the calculation cost of control strategy, the linear quadratic regulator (LQR) design method is introduced to design the optimal control for the linearized system. And the model mismatch is solved by using feedback of model prediction error. To illustrate the effectiveness of the model predictive controller proposed, simulations on the New England 39-bus power system is performed. Compared to the conventional linear quadratic regulator, the proposed MPC can improve the transient stability of the power systems and enhance the system damping.

KEYWORDS:
model predictive control, doubly fed induction generator, transient stability, wind power generation, power system

INTRODUCTION

With the shortage of electric energy and environmental problems become more and more serious, the use of wind energy as an important renewable clean alternative energy sources has a very important significance, which can reduce the cost and environmental pollution [1, 2]. Because of the with its low cost, small capacity of the rotor excitation converter, strong wind energy capture ability, and flexible control characteristics, doubly fed induction generator (DFIG) has been widely used in modern large scale wind farm [3]. However, wind is characterized with randomness and volatility, and the operating environment has a certain influence to parameters of the wind generator (such as reactance). With the growing integration of wind generators into power grids, the operation and control technology of the wind generator has been widely concerned. Especially when both the capacity of a single wind generator and the proportion of the total wind generators capacity in the power system have been increasing, how to improve the control performance of the wind generator to address the wind volatility and operating environment variety is more important. To design the advanced control strategy for DFIG is considerable focused.

The decoupling control technique is developed based on the traditional PID controller and this technique is widely used due to its' good reliability and simplicity. At present, the decoupling control technique for the active power and reactive power proposed in [4] has been widely used to design the controller of DFIG [5–7]. Though the PID controllers are widely adopted in many fields and successfully used in the power system, the parameters of the PID controllers are usually tuned with the approximately model linearized at the operating point. In this situation, the excellent dynamic control performance may not be maintained beyond the linear operating range of the DFIG, especially in the case of large disturbances in the power systems. Hence, in order to enhance the control performance, new methods used to design the controllers for the DFIG are proposed in references, such as fuzzy control [8, 9], adaptive control [10], nonlinear control [11, 12], Backstepping based control [13], and so on. However, because the parameters of the DFIG are affected by the operating environment and the prediction of the operating point is difficult to solve, the accurate model of the DFID is difficult to build for controller design. Therefore, the controllers designed with the hypothetically accurate model may not achieve to the excepted control performance in the practice.

With the rapid growth of computer technology, the model-based control strategy is introduced [14]. Such control strategy is frequently named as model predictive control (MPC) [15] and it is getting more and more interesting because the constraints on the states and control inputs can be systematically taken into account while operating the process optimally. MPC is based on the system behavior prediction from a priori model and selects the optimal control strategy according to the selective cost function. From the 70s of the last century when MPC is firstly invented [16], it becomes one of the key advanced control techniques and at present is widely and successfully used in practice [17-19].

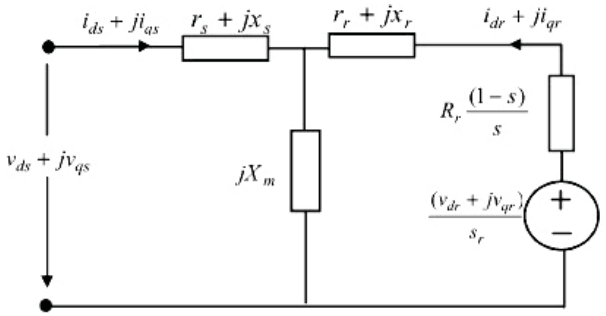


FIGURE 1
Equivalent circuit of DFIG

Recently the method of model predictive control is introduced to power system coordination control [20-22], excitation system control [23], power electronic equipment control [24], transient stability [25], and so on.

In this paper, a model predictive control method for a WT with DFIG will be investigated in the transient stability control of power systems where the electromechanical dynamics of DFIG are considered. Transient stability control performance of the nonlinear control will be examined.

The paper is arranged as follows. In Section 2, a third-order model of the WT with DFIG for stability studies is presented at first. A model predictive control design method using linear control theory is introduced in Section 3. Considering the model error, the model predictive control design method is applied to the control of the WT with DFIG where the WT with DFIG is integrated into the power system. In Section 4, simulations are performed on the New England 39-bus power system to verify the effectiveness of the proposed MPC controller for the WT with DFIG in the transient stability control, while conclusions are drawn in Section 5.

MATERIALS AND METHODS

Model of WT with DFIG. The WT system consists of a drive train and DFIG. The drivetrain of the WT system is represented with a one-mass model [18], while the DFIG is modeled by a second order model where the electromagnetic transients of the stator are neglected [19–22].

The equivalent circuit of DFIG is shown in Fig. 1. Hence, the model of the WT with DFIG used in this paper is a third-order model as follows.

Dynamic Equations:

$$\begin{cases} 2H\dfrac{ds}{dt} = P_s - P_m \\ \dfrac{dE_q^{'}}{dt} = -s\omega_s E_d^{'} + \omega_s \dfrac{L_m}{L_{rr}} V_{dr} - \dfrac{1}{T_0^{'}}[E_q^{'} - (X_s - X_s^{'})i_{ds}] \\ \dfrac{dE_d^{'}}{dt} = -s\omega_s E_q^{'} + \omega_s \dfrac{L_m}{L_{rr}} V_{qr} - \dfrac{1}{T_0^{'}}[E_d^{'} - (X_s - X_s^{'})i_{qs}] \end{cases} \quad (1)$$

Voltage Equations:

$$\begin{cases} E_d^{'} = -r_s i_{ds} + X_s^{'} i_{qs} + V_{ds} \\ E_q^{'} = -r_s i_{qs} - X_s^{'} i_{ds} + V_{qs} \end{cases} \quad (2)$$

Active and Reactive Power Equations:

$$\begin{cases} P_s = -E_d^{'} i_{ds} - E_q^{'} i_{qs} \\ Q_s = E_d^{'} i_{qs} - E_q^{'} i_{ds} \end{cases} \quad (3)$$

where *s* is the rotor slip. *H* is the total inertia constant of the turbine and the generator. P_s is the output active power of the stator of the DFIG. P_m is the mechanical power of the WT. L_{ss} is the stator self-inductance. L_{rr} is the rotor self-inductance. L_m is the mutual inductance. w_s=1-w_r is the synchronous angle speed, and w_r is the DFIG angle speed. X_s is the stator reactance. x_s is the stator leakage reactance. x_r is the rotor leakage reactance. $X_d^{'}$ is the stator transient reactance. $E_d^{'}$ and $E_q^{'}$ are the *d* and *q* axis voltages behind the transient reactance, respectively. $T_{d0}^{'}$ is the rotor circuit time constant. i_{ds} and i_{qs} are the *d* and *q* axis stator currents, respectively. v_{ds} and v_{qs} are the *d* and *q* axis stator terminal voltages, respectively. v_{dr} and v_{qr} are the *d* and *q* axis rotor voltages, respectively. Q_s is the reactive power of the stator of the DFIG. Equation (1) shows the third-order DFIG model and the voltage equations and the flux linkage equations of the DFIG are based on the motor convention. In the case of transient stability studies, it is common to reduce the fifth-order model to such a third-order model [17], [18]. From equation (1), the model of the WT with DFIG is a system with two inputs in the reference frame. The inputs are v_{dr} and v_{qr}, respectively. And

$$\begin{cases} X_s = \omega_s L_{ss} = x_s + X_m \\ X_s^{'} = \omega_s (L_{ss} - L_m^2 / L_{rr}) \\ T_0^{'} = L_{rr} / R_r \end{cases} \quad (4)$$

Model Predictive Control for the WT with DFIG. In order to simplify the introduction, without loss of generality, equation (1) is linearized near a chosen operating point using the first-order Taylor's series approximation and it can be written as follow.

$$\begin{cases} \dot{\boldsymbol{x}}(t) = \boldsymbol{A}\boldsymbol{x}(t) + \boldsymbol{B}\boldsymbol{u}(t) \\ \boldsymbol{y}(t) = \boldsymbol{C}\boldsymbol{x}(t) \end{cases} \quad (5)$$

where

$$\boldsymbol{x} = [\Delta\omega_r \quad \Delta E_d^{'} \quad \Delta E_q^{'}]^T \quad (6)$$

$$\boldsymbol{y} = [\Delta\omega_r \quad \Delta P_s \quad \Delta V_s]^T (7)$$

$$\boldsymbol{u} = [V_{dr} \quad V_{qr}]^T (8)$$

$$\boldsymbol{A} = \begin{bmatrix} 0 & i_{ds0} & i_{qs0} \\ \omega_s E_{q0}^{'} & (1-\omega_{r0})\omega_s & -1/T_0^{'} \\ \omega_s E_{d0}^{'} & -1/T_0^{'} & -(1-\omega_{r0})\omega_s \end{bmatrix} (9)$$

$$\boldsymbol{B} = \begin{bmatrix} 0 & 0 \\ \omega_s L_m / L_{rr} & 0 \\ 0 & -\omega_s L_m / L_{rr} \end{bmatrix} (10)$$

$$\boldsymbol{C} = \begin{bmatrix} 1 & 0 & 0 \\ 0 & -i_{ds0} & -i_{qs0} \\ 0 & \partial V_s / \partial E_d^{'} & \partial V_s / \partial E_q^{'} \end{bmatrix} (11)$$

The process of the MPC control is the optimization of the control selection process. In this paper, a cost function is defined in terms of the output variables and the control variables, and the cost function used is below.

$$J = \int_0^\infty (y^T \boldsymbol{Q}_1 y + u^T \boldsymbol{Q}_2 u) dt \quad (12)$$

where Q_1 and Q_2 are diagonal weighting matrices.

According to the linear quadratic regulator (LQR) method in the linear control theory [19], the optimal control law of the system shown in (5) can be obtained as follows.

$$\Delta \boldsymbol{u}^*(t) = -\boldsymbol{Q}_2^{-1} \boldsymbol{B}^T \boldsymbol{P} \boldsymbol{x}(t) (13)$$

where the matrix P can be solved by equation (14).

$$-\boldsymbol{PA} - \boldsymbol{A}^T \boldsymbol{P} + \boldsymbol{PBQ}_2^{-1} \boldsymbol{B}^T \boldsymbol{P} - \boldsymbol{C}^T \boldsymbol{Q}_1 \boldsymbol{C} = 0 (14)$$

Equation (13) is the conventional linear quadratic regulator. In the conventional linear control design method, the model of the nonlinear system is linearized near a chosen operating point using the first-order Taylor's series approximation. The accuracy of the approximate linearized model is acceptable only when the system is operating near the point chosen during design. Under large disturbances, the system operating point may be far away from the design point chosen. In this situation, the conventional linear quadratic regulator(13) may be greatly weakened in terms of large disturbance transient stability control. In order to reduce the influence caused by the simplified model, feedback is used to correct the optimal control law(13). The error caused by the simplified model is below.

$$e(t) = y(t) - \hat{y}(t) (15)$$

Where y are the practical outputs, and $\hat{y}$ are the predictive outputs by using the simplified model (5). Then, the optimal control law(13) can be corrected as follow.

$$\Delta u^*(t) = -Q_2^{-1} B^T P[x(t) + HC^{-1} e(t)] (16)$$

Where H is the correction matrix with constant elements. The model predictive control law is determined by the linear quadratic regulator and the feedback correction of the model error, so robust control performance can be guaranteed at any point where the system would operate.

RESULTS AND DISCUSSION

To analyze the proposed model predictive control presented above, the simulation was applied to the New England 39-bus power system shown in Fig. 2 to verify the effectiveness and control performances of the model predictive controller in improving the transient stability, the system damping and the fault ride-through capability of the WT with DFIG. The proposed model predictive control law, as given in (16), was implemented in MATLAB while the parameters of the WT with DFIG a given in Table 1.

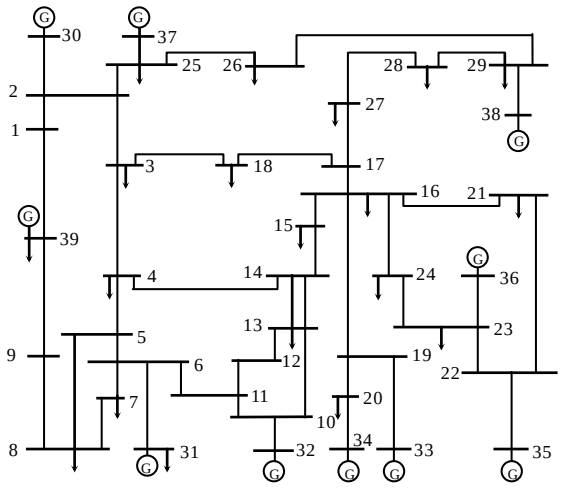


FIGURE 2
The New England 39-bus power system

TABLE 1
Parameters of the WT with DFIG

R_s (p.u.)	L_s (p.u.)	L_m (p.u.)	R_r (p.u.)	L_r (p.u.)	H (s)
0.00706	0.171	2.9	0.005	0.156	0.2

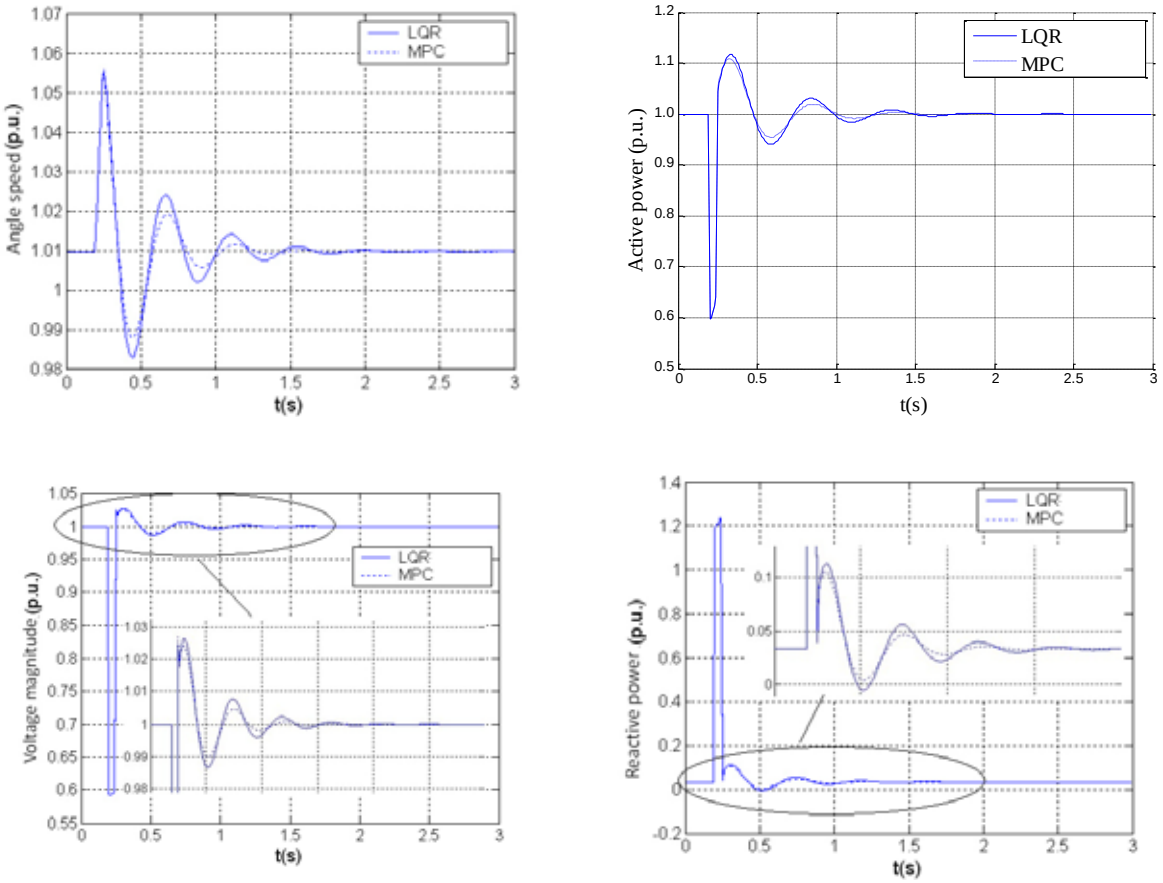


FIGURE 3
Dynamics of the WT with DFIG without parameter disturbance

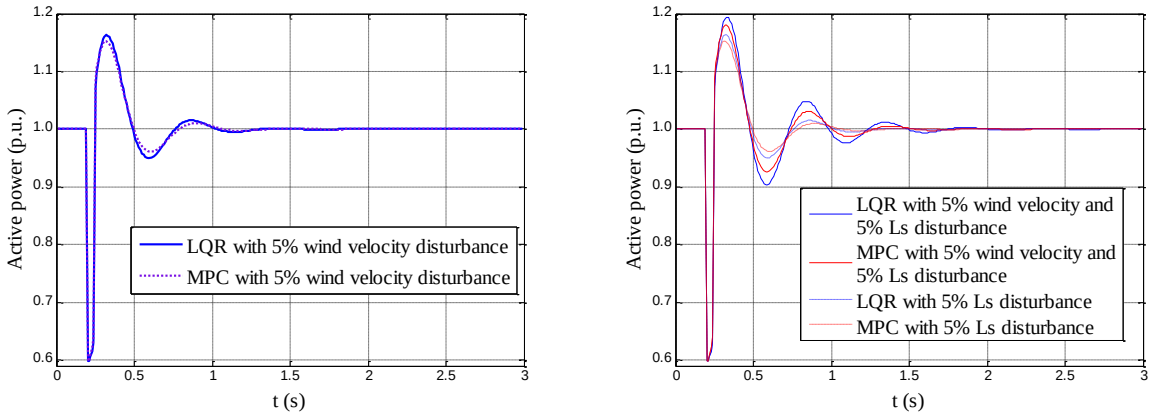


FIGURE 4
Active power dynamics of with parameter disturbance

The wind farm is connected to bus 36, and the wind farm active power is 1.0 p.u.. To make the comparison more accurately, the conventional linear quadratic regulator was applied to the WT with DFIG. The weight matrix in the cost function is the same as that of the model predictive controller.

A three phase ground fault with the ground resistance of 0.005 p.u. was applied at bus 36 at t=0.2 s, and the fault was cleared at t=0.25 s. Under this disturbance, the simulations were carried out to compare the damping of the WT with DFIG using the conventional linear quadratic regulator and the model predictive controller. The dynamics of the angle speed, active power, terminal voltage, reactive power of the WT with DFIG using the conventional linear quadratic regulator and the model predictive controller are illustrated in Fig. 3. It can be seen that applying the model predictive control, the system is stable and the damping of the WT system has been improved. The oscillations of the terminal voltage decayed very quickly after the fault was cleared.

During the transient process, the maximum active power of the WT with DFIG is about 1.1 p.u., but the magnitude by using model predictive controller is smaller than that by using conventional linear quadratic regulator. The oscillations of the active power with the proposed model predictive controller decayed at 1.5 s, while the oscillations of the active power with the conventional linear quadratic regulator decayed at almost 2.0 s. The maximum angle speed of the WT with DFIG with the model predictive controller is nearly 1.02 p.u., while the maximum angle speed of the WT with DFIG using the linear quadratic regulator is larger than 1.02 p.u.. The oscillations of the angle speed with the model predictive controller decayed at 1.5 s, while the oscillations of the angle speed with the linear quadratic regulator decayed at almost 2.0 s. This reveals that the WT with DFIG using the conventional linear quadratic regulator may lead to a worse transient stability problem of the power system. The trajectories of the voltage magnitude and the reactive power are similar when the two strategies are used, but the partial enlarged figure shows that the maximum deviation and the oscillation duration with the model predictive controller is less than those with linear quadratic regulator.

Moreover, the model parameters of the WT with DFIG always changes due to the actual operation situation. In order to test the robust performance of the proposed control strategy, 5% disturbance is added to the original wind velocity and parameter L_s. When the studied model is deferent from the actual model, the active power dynamics of the WT with DFIG are shown in Fig. 4.

Three situations are tested and the results are shown in Fig. 4. It can be seen that the performance by using model predictive controller is also better than that by using linear quadratic regulator. The model mismatch impact the performance of model predictive controller is little. Comparing to linear quadratic regulator, the control strategy proposed by this paper can reduce the effect brought by the model errors because the feedback of model prediction error is introduced.

CONCLUSIONS

In this paper a model predictive controller for WT with DFIG has been proposed, where the linear quadratic regulator (LQR) method is used and the model prediction error is considered. The calculation cost of control strategy is reduced much by using the linear quadratic regulator (LQR) method. And the model mismatch is solved by introducing the feedback of model prediction error. Therefore, robust control performance can be guaranteed at any point where the system would operate by using the proposed model predictive control. The dynamic simulation results on the New England 39-bus power system have shown that the damping and the maximum deviation have been improved using the proposed model predictive controller. The transient stability control benefit with the model predictive control is significant.

ACKNOWLEDGEMENTS

We would like to thank the project supported by National Natural Science Foundation of China (51007009). This work is also partially supported by the Science and Technology Foundation of Guizhou Province ([2016]1036), and Guizhou Province Reform Foundation for Postgraduate Education ([2016]02).

REFERENCES

[1] Chen, W.D., Fan, W.L., Zang, W.J. and Yu, G.Y. (2017) Optimal cost--reimbursement rules combining carbon emission reduction targets with power conversion efficiency for microgrid firms. Fresen. Environ. Bull. 26, 3182-3190.

[2] Zhou P., He, Y. and Sun, D. (2009) Improved direct power control of a DFIG-based wind turbine during network unbalance. IEEE Transactions on Power Electronics. 24, 2465-2474.

[3] Mohammad, E.K., Mohammad, S. and Wu, L. (2013) Enhancing the Dispatchability of Variable Wind Generation by Coordination with Pumped-Storage Hydro Units in Stochastic Power Systems. IEEE Transactions on Power Systems. 28, 2808-2818.

[4] Yamamoto, M. and Motoyoshi, O. (1991) Active and reactive power control for doubly-fed wound rotor induction generator. IEEE Trans. Power Electron. 6, 624–629.

[5] Pena, R., Clare, J.C. and Asher, G.M. (1996) Doubly fed induction generator using back-to-back PWM converters and its application to variable speed wind-energy generation. Proc. Inst. Elect. Eng., Elect. Power. 143, 231–241.
[6] Hughes, F.M., Anaya-Lara, O., Jenkins, N. and Strbac, G. (2005) Control of DFIG-based wind generation for power network support. IEEE Trans. Power Syst. 20, 1958–1966.
[7] Ekanayake, J.B., Holdsworth, L., Wu, X.G. and Jenkins, N. (2003) Dynamic modeling of doubly fed induction generator wind turbine. IEEE Trans. Power Syst. 18, 803–809.
[8] Vieira, J.P.A., Nunes, M.V.A., Bezerra, U.H. and Barra, W. (2007) New Fuzzy Control Strategies Applied to the DFIG Converter in Wind Generation Systems. IEEE Latin America Transactions. 5, 142-149.
[9] Liu, J.X., Gao, Y.B., Geng, S.J. and Wu, L.G. (2016) Nonlinear Control of Variable Speed Wind Turbines Via Fuzzy Techniques. IEEE Access. 99, 1-7.
[10] Kim, J., Seok, J.K., Muljadi, E. and Kang, Y.C. (2016) Adaptive Q–V Scheme for the Voltage Control of a DFIG-Based Wind Power Plant. IEEE Transactions on Power Electronics. 31, 3586-3599.
[11] Wu, F., Zhang, X.P., Ju, P. and Sterling, M.J.H. (2008) Decentralized Nonlinear Control of Wind Turbine with Doubly Fed Induction Generator. IEEE Trans. Power Syst. 23, 613–621.
[12] Liu, X.J. and Kong, X.B. (2014) Nonlinear Model Predictive Control for DFIG-Based Wind Power Generation. IEEE Transactions on Automation Science and Engineering. 11, 1046-1055.
[13] Xiong, P.H. and Sun, D. (2016) Backstepping-Based DPC Strategy of a Wind Turbine-Driven DFIG Under Normal and Harmonic Grid Voltage. IEEE Transactions on Power Electronics. 31, 4216-4225.
[14] Taylor, C.W. (2000) The future in on-line security assessment and wide-area stability control. Proc. IEEE Power Eng. Society Winter Meeting. 1, 78-83.
[15] Marinescu, B. and Bourlès, H. (1999) Robust predictive control for the flexible coordinated secondary voltage control of large-scale power system. IEEE Trans. Power System. 14, 1262–1268.
[16] Richalet, J., Rault, A., Testud, J.L. and Papon, J. (1978) Model predictive heuristic control: Applications to industrial processes. Automatica. 14, 413–428.
[17] Froisy, J.B. (1994) Model predictive control: Past, present and future. ISA Transactions. 33, 235-243.
[18] Qin, S.J. and Badgwell, T.A. (2000) An Overview of Nonlinear Model Predictive Control Applications. Nonlinear model predictive control: theory and application. 26, 369-392.
[19] Qin, S.J., and Badgwell, T.A. (2003) A survey of industrial model predictive control technology. Control Engineering Practice. 11, 733-764.
[20] Larsson, M., Hill, D.J. and Olsson, G. (2002) Emergency voltage control using search and predictive control. International Journal of Electrical Power and Energy Systems. 24, 121–130.
[21] Larsson, M. and Karlsson, D. (2003) Coordinated system protection scheme against voltage collapse using heuristic search and predictive control. IEEE Trans. Power System. 18, 1001-1006.
[22] Wen, J.Y., Wu, Q.H., Turner, D.R. and Cheng, S.J. (2004) Optimal coordinated voltage control for power system voltage stability. IEEE Trans. Power System. 19, 1115-1122.
[23] Liu, H., Li, X.C., Wei, H. and Wang, N. (2005) The design of nonlinear predictive excitation controller based on TSE. Proceedings of the CSEE. 25, 27-31.
[24] Xu, D., Han, M.X., Du, X. and Wang, H.W. (2015) Model Predictive Control for VSC With Wind Farm Connected in the Hybrid Three-terminal DC Grid. Proceedings of the CSEE. 35, 3195-3203.
[25] Ford, J., Ledwich, G. and Dong, Z.Y. (2008) Efficient and robust model predictive control for first swing transient stability of power systems using flexible AC transmission system devices. IET Generation, Transmission and Distribution. 2, 731-742.

Received: **26.07.2017**
Accepted: **08.10.2017**

CORRESPONDING AUTHOR

Jing Zhang
College of Electrical Engineering,
Guizhou University,
Guizhou Province – China

e-mail: zhangjing@gzu.edu.cn

© by PSP Volume 26 – No. 12A/2017 pages 8160-8165 Fresenius Environmental Bulletin

CONSUMER TRENDS FOR ORGANIC PRODUCTS: THE CASE OF THE MARMARA REGION IN TURKEY

Sule Turhan[1,*], Hasan Vural[1], Ibrahim Ak[2], Burcu Erdal[1]

[1]Uludag University, Faculty of Agriculture, Department of Agricultural Economics, Bursa, Turkey
[2]Uludag University, Faculty of Agriculture, Department of Animal Science, Bursa, Turkey

ABSTRACT

Organic agriculture, which is one of the prominent environmentally friendly alternative agriculture systems, aims to repair the environment's deteriorating balance with entirely natural methods and by using equity. Today, environmentally conscious consumers, whose numbers are increasing significantly every day, are turning to consumption of organic products for healthy living and clean land and water. Thus, the healthy and natural nutrition concept that entered our daily lives with the development of organic agriculture has increased in importance. This study aims to determine the organic product consumption trends of consumers and examine the marketing characteristics of organic producers. Therefore, data were collected from 240 consumers using questionnaires in the organic product markets in İstanbul and Bursa provinces. The data analyses show that there are slight differences between the preferences of female and male consumers, and most consumers of organic products are middle-aged and older with higher education and income levels. In organic product marketing, it is necessary to improve the product quality, regulate the marketplaces and decrease the marketing margins in favour of consumers.

KEYWORDS:
Organic, consumer trends, consumption, Marmara Region, Turkey.

INTRODUCTION

Since World War II, rapid industrialization based on new technologies and scientific innovations has occurred along with a free market-dominated globalized economy [13]. Arguments about the origin and the development of the organic movement are not competitive with this process but rather complementary. In fact, the idea of ecologic use of natural resources dates back to before the common era [11]. Organic agriculture, which developed in different countries and in different dimensions starting from the 1930s, reached a commercial dimension in the 1980s, and in 1985-86 this development began to be reflected in Turkey. According to data from 2012, organic production is carried out on approximately 703,000 ha by 55,000 producers, and the number of organic agriculture product types has increased to 204 [8- 23]. Organic agriculture in Turkey, compared to the European Union, is relatively new. However, because of factors such as climate, land and water resources; product variety; and the high percentage of the population that works in agriculture, Turkey has a favourable position for organic agriculture [24].

Currently, environmentally conscious consumers, whose numbers are increasing day by day, are moving to the consumption of organic products because of their desire for healthy living, healthy soil and clean water. This new and modern understanding directs connoisseurs of the organic philosophy [19- 20]. Every day, people observe that organic products are important both for their health and the health of the people around them; hence, they want to consume high-quality products for a healthier life for both their families and themselves [1]. Consumers who are concerned about such topics as healthy nutrition and safe food supply exhibit an especially positive attitude towards organic products [15]. However, the organic product market cannot achieve a sufficient quantity and variety because it faces some constraints and problems from the marketing point of view [14]. While manufacturers have difficulty finding a market for the products that they grow with great effort and expense, consumers complain about both the high prices of the products and lack of easy access to them [9-21].

To gain a better understanding of Turkish people's attitudes towards organic products and, as a result, to determine the demand for them will reveal the possibilities of marketing these products domestically. Therefore, this study examines the factors that affect the habits, attitudes towards the consumption of organic products, and buying behaviours of the consumers who use organic products. For this purpose, the factors affecting the habits, attitudes, and purchasing behaviour in the consumption of organic products of families living in Bursa and İstanbul have been determined by statistical methods.

TABLE 1
Demographic Characteristics of Survey Participants

Personal Characteristics	*Frequency*	*%*	Average	Standard Deviation	Standard Error
Sexuality			1,43	0,50	0,03
Female	137	57			
Male	103	43			
Age	***Frequency***	***%***	*3,44*	1,08	0,07
Less than 18	1	0.4			
18-29	44	18			
30-39	95	40			
40-49	61	25,4			
50-59	27	11,2			
60 and above	12	5			
Educational Attainment	***Frequency***	***%***	4,78	0,83	0,05
Primary school	5	2			
Secondary school	10	4			
High school	53	22			
University	136	57			
Graduate and above	36	15			
Income	***Frequency***	***%***	3,65	1,18	0,08
0-200 Euro	21	9			
201-400 Euro	17	7			
401-800 Euro	47	20			
801-1600 Euro	96	40			
1601 Euro and above	59	24			

MATERIALS AND METHODS

In this study, questionnaires were used as a data collection method. The survey questions were created in the light of the information obtained from a literature review. Some of the questions prepared for the survey are based on related research [15-2-12- 6] while others were created by the researchers based on the purpose of the study, the subject content and the characteristics of the main group in which the survey would be carried out.

The main target of the research is consumers who use organic products in Turkey. Due to the low consumption of organic products in Turkey, it can be said that the target group is limited. For this reason, based on an intentional sampling approach, the surveys were carried out in stores that offer organic products and open-air markets in İstanbul, where organic product markets concentrate, and in Bursa, which has shown development in organic product markets in recent years. The research was carried out with a 5% significance level, and the sample size was 240 consumers. The sample size was determined using proportional distribution based on the neighbourhood and household size in the 40 counties in İstanbul and 17 counties in Bursa where the survey was carried out. The number of consumers who participated in the survey was determined by the optimum sample size formula [7- 3-22]:

$n= Nt^2 pq / d^2 (N-1) + t^2 pq$

Field research was conducted between February and June 2013. Primarily, the descriptive statistics of the data were researched. Normality tests of each question were analysed using the Shapiro-Wilk (W statistics) test [19]. The chi-square test was used to test whether the relationships between variables were statistically significant [16- 5].

RESULTS AND DISCUSSION

This study aimed to determine organic product consumption trends in the Marmara region. For this purpose, 240 consumers were surveyed using a questionnaire. Based on the data normality test (W test), it was determined that the data were normally distributed. Of the participants, 57% are women, and 43% are men. Most of the participants are under 40 years old, and their education level is mostly university. In terms of income, 24% have an income of 1601 Euro or less, 40% have an income between 801 and 1600 Euro, and 24% have an income of more than 1600 Euro (Table 1).

The preferences of organic product consumers by gender are presented in Table 2. Chi-square tests show that gender has an effect on consumption. Organic product consumption is concentrated in the last five years (75.42%), and 18.98% of the consumers surveyed have used organic products for more than years. Female consumers have consumed organic products for a longer time than male consumers. There are no significant differences in the length of the consumption period between male and female consumers.

The trust factor for organic products is very high (62.92%). In addition, 32.91% of the consumers are uncertain or find organic products partially

trustworthy. The results show the importance of informing consumers about this issue. Producers and marketers should closely analyse why organic product consumption is not increasing. The type of packaging is very important in organic product marketing. Consumers' increasing awareness also affects organic product consumption. In packaging organic products, paper is preferred (72.50%). Male consumers prefer glass packaging. Other types of packaging are not highly preferred by consumers (Table 2).

In the chi-square (x^2) analysis conducted to determine the diversity between consumers' income level and the frequency of consumption of organic products, diversity was found at (x^(2)= 536.75, p<0,01) the 1% level. Thus, income level affects the frequency of consumption. When the consumption frequency of organic products was analysed based on consumer income, the consumption of organic products increased as income increased (Table 3).

TABLE 2
Consumption characteristics of consumers of organic products by gender

	Female		**Male**		**Total**	
	Number	**%**	**Number**	**%**	**Number**	**%**
Consumption history (year)						
0	4	2,92	9	8,74	13	5,42
1-5	107	78,10	74	71,85	181	75,42
6-10	17	12,41	14	13,59	31	12,92
11-20	3	2,19	3	2,91	6	2,50
21-+	6	4,38	3	2,91	9	3,74
	x^2 = 124,85	p < 0,01				
Trustworty in organic products						
Yes	87	63,50	64	62,14	151	62,92
No	4	2,92	6	5,83	10	4,17
Partially	46	33,58	33	32,03	79	32,91
	x^2 = 146,33	p < 0,01				
Packing type preference						
Plastic	12	8,76	4	3,88	16	6,67
Paper	102	74,45	72	69,91	174	72,58
Glass	20	14,60	23	22,33	43	17,92
Other	3	2,19	4	3,88	7	2,91
	x^2 = 98,67	p < 0,01				
Does the Difference in Price Should be	47	34,31	19	18,45	66	27,50
No	85	62,04	75	72,82	160	66,67
Yes	5	3,65	9	8,73	14	5,83
I have no idea	x^2 = 71,17	p < 0,01				
Purchase of site preferences						
Supermarket	17	12,41	9	8,74	26	10,83
Neighborhood market	68	49,63	47	45,63	115	47,92
Greengrocer	9	6,57	6	5,82	15	6,25
Organic product sales point	43	31,39	41	39,81	84	35,00
	x^2 = 18,09	p < 0,01				

TABLE 3
Consumption frequency of organic products based on consumers' income

Income Status (Euro)	Non-consumer Number	%	Weekly Number	%	Monthly Number	%	Yearly Number	%
0-200	1	0,12	18	8,49	1	5,88	1	50,00
201-400	-	-	16	7,55	1	5,88	-	-
401-800	-	-	44	20,75	3	17,65	-	-
801-1600	4	0,44	81	38,21	10	58,83	1	50,00
1601-+	4	0,44	53	25,00	2	11,76	-	-

x^2 = 536.75 p < 0.01

TABLE 4
Shopping days of organic product consumers

Days	Monday	Tuesday	Wednesday	Thursday	Friday	Saturday	Sunday
Number	43	37	56	24	39	134	143
%	17,92	15,42	23,33	10,00	16,25	55,83	59,58

The frequency of weekly consumption is also valid for the lower-income groups. We may say that the group with an income of 801-1600 Euro consumes the most organic products every week, once a month and once a year (38,21%, 58,83% and 50,0%). The highest-income group, in contrast to the expectations, has a lower level of organic product purchasing. When the shopping days of organic product consumers were examined (Table 4), it was found that weekends predominate. Many of the consumers stated that they may shop for food several days a week instead of only one day. While 55,83% of the consumers mentioned that they prefer to shop on Saturday, 59,58% mentioned Sunday, and approximately half mentioned that they may buy organic products on weekdays. This situation proves that opening an organic products market only on certain days of the week is not sufficient; permanent sales outlets must be established. The main factors that the studied consumers consider important in buying organic products are presented in Table 5.

TABLE 5
Important factors for consumers in buying organic products

Factors	%
Freshness	92,50
Cheapness	49,58
Hygiene	47,08
Brand	39,17
Taste and flavor	38,75
Packing type	38,75
Expiration date	38,33
Quality	37,50
Other	13,33

Generally, consumers stated that they consider more than one factor important. The most important factors are freshness of the products (92.50%), cheapness of the products (49.58%) and hygiene of the products (47.08%). Other factors that affect consumers' preferences are brand choices (39.17%) and quality (37.50%). These results show that by implementing developed methods in organic product marketing, the market volume can be increased.

Of the consumers surveyed, 66.67% expressed a positive opinion about the price difference between traditional and organic products. Thus, it can be said that as long as organic products meet certain quality specifications, selling them at a higher price is acceptable to consumers. Female consumers have a more positive approach to the price differences than male consumers (34.31%).

The first preference for the consumers in shopping outlets for organic products is neighbourhood markets (47.92%); the second is specialty shops (35.0%). Supermarkets and grocery stores were also preferred, albeit at lower rates. Some consumers stated that they shop at more than one type of place. In the ranking of importance, no differences were found between male and female consumers.

When the knowledge of the consumers about the definition of organic products was examined, 79.17% defined organic products as products for which synthetic pesticides and fertilizers are not used; 11.25% defined them as products for which hormones are not used. Only 3.75% defined organic products as certified products, which shows that consumers do not have accurate and adequate information about organic products. Thus, equipping consumers with accurate information emerges as an urgent need in terms of market growth for producers and marketers.

The preferences of consumers for more frequent use of organic products, in order of importance, are sales appeal, lower prices, higher durability, more sales areas and tastier products. While prices stand out as an important factor in this context, it can be seen that consumers also found other factors important.

Of the organic product consumers surveyed, 55.42% stated that their information sources were media and the Internet. While some consumers stated that they do not seek information about the subject, 14% stated that they use printed publications as information sources. Because lack of information among the general population appears to be a problem, there is a need for widespread, accurate information presented under public control.

CONCLUSION

At the beginning of the organic movement in the 1920s, the marketing of organic products occurred in small and often private networks between farmers and consumers. Organic production has evolved, and organic products have become a part of mainstream agricultural markets. It can be said that the organic movement is now on the threshold of changing from a niche to a mass market. It is argued that it is now becoming an increasingly visible element of the major food retailer chains [18] . Mainstream agricultural producers, manufacturers and supermarket chains have entered the organic market. Recent

developments in the market structure will inevitably lead to an organic market that increasingly resembles the conventional food industry [10].

Consumers are increasingly conscious about organic products. Studies have been conducted to investigate why more and more consumers prefer organic products. Consumer preferences related to work are less common. Mclver, in a study conducted in 2004, emphasized that consumers use organic products because they are healthy for themselves and the environment and because they do not have pesticide residues. Sarıkaya, in a study conducted in 2001, noted that consumers turn to organic products in a reaction against environmental pollution that they have observed [12]

Currently, for healthy nutrition purposes and as an alternative food source, the consumption of organic products is increasing in importance [4]. However, in spite of support (assistance), both production and consumption show slow growth. Among the reasons for this, the slow growth of the market and marketing problems are prominent. This research, in order to shed some light (solutions) on marketing problems, aimed to investigate the main factors.

In order to determine trends for consumption of organic products in the Marmara region, a questionnaire was administered to consumers via face-to-face interaction. The results showed that the consumers lacked knowledge about organic products. Because of this, first, consumers must be informed about the certification of organic products. Consumer demands must be taken into consideration for diversification of production. It is important to build special bazaar areas for these products. Excessively high prices decrease the demand and consumption. Government support is needed to reduce the production costs. In addition, because there is a lack of marketing services, specific marketing techniques must be applied so that organic product manufacturers and marketers can be informed about this issue.

REFERENCES

[1] Akbaba, U., Şahin, Y. and Türkez, H. (2011) Comparison Of Element Contents In Hazelnuts Grown Under Organic And Conventional Farming Regimes For Human Nutrition And Health. Fresen. Environ. Bull. 20(7), 1660-1665.

[2] Akdoğan, Ş.M., Güllü, K. and Babayiğit, S. (2005) Tüketicilerin Süpermarketleri Algılamalarına Yönelik Bir Çalışma. Sosyal Bilimler Enstitüsü Dergisi. Kayseri. 19(2), 37-70.

[3] Arıkan, R. (2004) Araştırma teknikleri ve rapor hazırlama. Ankara: Asil Yayın.

[4] Baran, F.B., Oğuz, H.İ. and Gökdoğan, O. (2017) Determination Of Energy Input-Output Analysis In Organic Strawberry Production, Fresen. Environ. Bull. 26(3), 2076-2081.

[5] Camilli, G. (1979) A Critique of the Chi-square Method for Assessing Item Bias. Unpublis Hed Paper Laboratory of Educational Research, University of Colorado.

[6] Crucefix, D. (1998) Organic Agriculture An Sustainable Rural Livelihoods İn Developing Countries, Soil Association, June.

[7] Düzgüneş, O., Kesici, T. and Gürbüz, F. (2015) İstatistik Metodları I, Ankara Üniversitesi Ziraat Fakültesi Yayınları: 861, Ankara Üniversitesi Yayınları, pp.218, Ankara.

[8] http://www.tarim.gov.tr (03.March.2017)

[9] Karabaş, S. and Gürler, A.Z. (2012) Organik Ürün Tercihinde Tüketici Davranışları Üzerine Etkili Faktörlerin Logit Regresyon Analizi İle Tahminlenmesi. Adıyaman Üniversitesi Sosyal Bilimler Enstitüsü Dergisi, ISSN: 1308–9196, 5(10), Adıyaman, 129-156.

[10] Klonosky, K. (2000) Forces Impacting the Production of Organic Foods, Agriculture and Human Values. 17, 233-243.

[11] Korcak, R. F. (1992) Early Roots of the Organic Movement: A Plant Nutrition Perspective. HortTechnology, American Society for Horticultural Science. 2(2), 263-267.

[12] Mclver, H. (2004) Organic Hip: Popular Picks at Health Food Stores. Better Nutrition. 66(2), 58.

[13] Rehber, E. (2009) Economics of Organic Farming, Published by IUP, ISBN:978-81-314-2326-4, India, 205.

[14] Rehber, E. (2011) Organik Tarım Ekonomisi, Ekin Yayınevi, Bursa, ISBN:978-605-5335-14-4, 293.

[15] Sarıkaya, N. (2007) Organik Ürün Tüketimini Etkileyen Faktörler ve Tutumlar Üzerine Bir Saha Çalışması Kocaeli Üniversitesi Sosyal Bilimler Enstitüsü Dergisi. Kocaeli. (14)2, 110-125.

[16] Scheuneman, J. (1979) A New Method fora SSESSİNG Bias in Test Items, Journal of Educational Measurement. 16, 143-152.

[17] Shapiro, S.S. and Wilk, M.B. (1965) An Analysis of variance Test for Normality. Biometrika. 52, 591-611.

[18] Shears, P. and Hillier, D. (2001) Retailing Organic Foods (Case Study). British Food Journal. 103(5), 358-365.

[19] Turhan, Ş. (2005) Tarımda Sürdürülebilirlik ve Organik Tarım, Tarım Ekonomisi Dergisi, İzmir. 11(1), 13-24.

[20] Turhan Ş. and Gürses, S. T. (2011) Organik Tarım Sektörünün Dış Satım Potansiyelinin SWOT Analizi İle Değerlendirilmesi, GAP VI. Tarım Kongresi, Şanlıurfa.

[21] Vural, H. (2010) Organik Hayvansal Ürün Pazarlaması, Türkiye 1. Organik Hayvancılık Kongresi 1-4 Temmuz 2010 Kelkit. Gümüşhane.

[22] Vural, H. (2012) Tarım ve Gıda Ekonomisi İstatistiği, Uludağ Üniversitesi Ziraat Fakültesi Ders Notları No:107, Bursa, 115.
[23] Vural H. and Turhan, Ş. (2013) Ekolojik-Organik Tarımda Hayvancılık, Ekolojik Hayvansal Ürünlerin Ekonomisi, Pazarlaması, Bursa. ISBN: 978-605-4798-46-9, s.343-363.
[24] Vural, H., Turhan, Ş., Ak, İ. and Erdal, B. (2013) Tüketicilerin Organik Ürün Tüketim Eğilimlerinin Belirlenmesi, Türkiye II. Organik Hayvancılık Kongresi, 24-26 Ekim 2013 Bursa.

Received: **27.07.2017**
Accepted: **03.10.2017**

CORRESPONDING AUTHOR

Sule Turhan
Uludag University,
Faculty of Agriculture,
Department of Agricultural Economics,
TR 16059 Bursa – Turkey

e-mail:sbudak@uludag.edu.tr

© by PSP Volume 26 – No. 12A/2017 pages 8166-8175 Fresenius Environmental Bulletin

EXPERIMENTAL STUDY ON THE MECHANICAL PROPERTIES OF ROCK SLOPE COLLAPSE

Qian Zhang, Weigang Zhao*, Yang Gao, Xinzhi Li, Yifang Li, Xiaoran He

Shijiazhuang Tiedao University, Shijiazhuang, 050043, China

ABSTRACT

The distinct geological and environmental characteristics in the Sichuan-Chongqing region of China are as follows: the crustal movements are very active; the terrain is steep and rugged, and the rainfall is abundant and strong; many bedding steep rock slopes exist in Sichuan-Chongqing region with relatively common failure mode of sliding - bending failure. The structural characteristics and failure modes of bedding steep slope were summarized based on the collection and analysis for destruction characteristic of slope instability in this paper, and the typical failure modes of bedding steep rock slope in seismic area considering seismic effect were proposed combined with the geological and environmental characteristics of Sichuan-Chongqing region. Then, the mechanical characteristics and deformation failure mechanism of bedding steep slope were studied by the geological mechanics model test for bending failure mechanism and control method of bedding steep slope. With the development of test bench composed by high strength composite steel structure and the adoption of servo hydraulic loading system and optical fiber grating real-time information monitoring system, deformation and mechanical characteristics were studied under different conditions of slide mass thickness and loading.

KEYWORDS:
bedding steep rock slope, bending failure, seismic effect, mechanics model test

INTRODUCTION

In the previous study, bedding steep rock slope was known as stable. In recent years, with continuous research, engineers gradually found that more and more collapse type of slope failure examples are appeared represented by southwest areas in china. Many scholars studied the bending landslide and failure mechanism by the way of traditional mechanics theory, the model experiment, the nonlinear theory, etc [1-9]. But till now systematic and mature analysis method have not formed.

In a series of research methods, the physical model experiment gets more and more attention because of its unique advantages: it can better simulate the actual project implementation process, external load action, time effect, etc. It can reflect the evolution of the slope rock mass's gradual deformation and destruction process. Meanwhile we can use the results to verify the theoretical analysis and numerical simulation results. Since the 1970s, slope geological mechanical model experiment has gotten rapid development in our country. Many scholar have gained a lot of satisfactory experimental results by using slope model experiment method. Xiu-wen Hu [10] studied the stability of the slope under the effect of four factors and the failure mechanism of instability in the Zhaoshuling of the three gorges reservoir though a small-scale physical model test; Wenkai Feng, et al. [11] studied on the instability mechanism of bedding slope and the possible deformation and failure process, using the method of bottom friction to analyze a layered slope, pointed out the typical failure mode of stratified side slop with gently inclined bedding; Jun Feng et al. [12] carried out the model test of layered slope in YuHuaiXian, slope excavation of relaxation zone was discussed. In order to study the stability of the bedding rock slope excavation characteristics under the condition of different strata dip angle, Congxin Chen [13] using the model test study, pointed out that the smaller formation dip Angle was, the greater the intensity of structural plane were, and the rock slope became more stable. The above achievements have promoted the research of layered slope stability problems.

EXPERIMENTAL

Summarize the failure modes of Sichuan-Chongqing Region. Southwest China's Sichuan Chongqing region of crustal movement is active, steep rugged terrain, abundant rainfall and great strength, there are many Bedding High Rock slope. The geological characteristics of the environment lead to the original stress field and strain field of rock slope should not stop internal change, the slope will gradually appear in different forms and the size of the slide and collapse, even in certain conditions evolve into a more serious loss of stability. The most common failure mode in this area is the sliding bending failure, which also is the focus of this paper.

Based on the previous research results and the cause of the disaster caused by the failure mode of the bedding failure, it can be divided into three types, namely, gravity instability, pressure instability and excavation unloading [14].

Gravity type failure loss stability: along the fissure structural plane layer on top of the slope the most exposed, vulnerable to rainfall or vegetation root erosion, the effect of slowly to the slope internal development, the structure of interlayer fissure gradually through the slope leading to the development of the main structural plane slip surface. At the same time, the method to crack rock slope will slide body is divided into several parts, the lower part of the sliding experience by gravity load of the upper sliding body, and the bending deformation, with the sustained effect of load that ultimately lead to buckling failure.

The characteristics of the failure of pressure instability are as follows: because the top of the bedding slope is usually covered with a relatively loose and large gap of the accumulation body, with the weathering of transport and accumulation and erosion of precipitation. The load on the bedding rock gradually become larger, resulting in the upper part of the layered rock slope along the level of creep deformation occurred, causing extrusion effect on rock slope, caused by buckling failure, finally the failure along with extrusion and cause the slope failure.

The characteristics of the excavation unloading damage type: the excavation slope Angle usually is that the slope angle and dip angle are equal. The main control structure tend not to be exposed on the cut slope. Slip surface decline blocked at the foot of the slope, which makes rock mass around slope toe get larger extrusion force. At the same time, because the excavation effect weakens the carrying capacity at the foot, it cannot withstand the sliding force from the upper slope. Unloading effect and weathering are obvious, which makes the slope front appear relaxation phenomenon, resulting in the slope instability.

Through the analysis of rock slope instability we can know that the buckling deformation of bedding steep rock slope will first appear in the top of the bedding slipping area. Because of the continuing role of external factors, the sliding body gravity stress perpendicular to the direction of tectonic rock formation component decreases, causing the overlying rock mass creep deformation along the tectonic rock surface, meanwhile it results a ripping faulting and deformation of the slope. With the continuous development of slope rock mass slip, slip plane occur cut through along the direction of tectonic rock formation, thus squeezing effects of the lower slope body. Lower pressure zone rock mass gotten the pressure along the direction of the slip plane is the maximum principal stress, while it's vertical force is the minimum principal stress. Both of them produce the tension fissure which mainly parallel to the sliding surface. It's lower side rock mass doesn't appear free face, resulting in integral slide tendency gets impede; rock stratum around slope toe happens upheaval or bending deflection together with interbedded crack. Finally it develop into sheared and distorted destroy of slope rock mass. The whole evolution process of bedding rock slope deformation can be roughly divided into four stages. The contents are as follows:

(1) The stress adjustment stage: when the slope rock mass under the influence of gravity, stack or excavation disturbance, rock mass will appear effect of unloading towards direction of free-face, leading to slope surface displacement and deformation and the emergence of the parallel to the surface tension tectonic strata cranny. Along with the continuously go deep into the effect of excavation unloading, tension crack develops slowly down, there will be a slippery slope block off, destroying the integrity of rock near the slope toe, making the strength of the rock mass falling fast.

(2) Shearing faulting stage: sliding surface of the bedding steep rock slope majority appears in soft rock strata or weak intensity structural surface. After the stress field of last stage redistributes, side slope appears stress concentration in lower-middle part, meanwhile with the effect of rainfall and other external forces, the rock mass strength gradually reduced. When the shear stress of rock mass in the slip surface part is more than the actual shear strength, rock mass damage. If plastic area expands unceasingly, the upper sliding will slide and deform, accompanied by faulting and deformation caused by cracking.

(3) Squeeze and bending stage: After cracking cracks appear, groundwater continuous infiltration, then in the back of the sliding mass become instability and it extruding compressive resistance, causing cracks on both sides of the sliding mass, and continuously extending makes the upper basic run-through slip plane. Resistance and smooth section upward bulge deformation due to compression, and has tension cracks in front of the slope. With the further development of slope deformation, tension crack extend slowly to the penetration, the front cut exports appear in succession, but the resistance of sliding surface is not completely through.

(4) Bending failure stage: When the slope deformation intensified, the front cut export extend continuously and inter-permeation slope landslide on either side of the border, the slope is in a state of instability and failure of the whole. Slip band of rock mass strength weakened gradually with the increase of sliding distance to the residual strength, at the same time, the sliding resistance also gradually decreases, and the slope sliding mass by uniform slip into acceleration slip.

For the bedding rock slope stability problem, considering the complexity of its own internal structure and its mechanical characteristics, in traditional analysis process of mathematical methods (such as limit equilibrium method), often on the basis of numerous engineering experience, the different slope failure mode is given many of the hypothetical conditions making it simplify. Abstract mechanics model may have big difference with the actual engineering. Among all kinds of analysis method, model test analytic method can largely simulate the actual working conditions of slope engineering similar, so it is widely applied at home and abroad in recent years, as a new trend of development of slope stability study. Model test method based on classical mechanics theory, use limited space and time, in the laboratory of large complex simulation of rock (soil) mass model, based on the similarity theory and dimensional theory, through direct solution, get the rock (soil) mass data such as strain, stress, displacement and failure mode and mutual relations, with a strong visual and reliability [14].

Therefore, carrying out the model test of bedding rock slope, not only for the bedding rock slope deformation and failure mechanism of research, but also for the slope engineering construction, monitoring and strengthening of provide effective guidance.

The determination of the basic mechanical parameters and selection of similar material.

(1) The basis of measurement process. This mechanical model test on the basis of soil test method and rock testing procedures as the main basis of highway construction. Measurement of slope rock mass of the elastic modulus, bulk density, Poisson's ratio, compressive strength, tensile strength, internal friction Angle and cohesive force of mechanical parameters.

(2) Block processing and saturation. ChengLan line D1K191 + 225 sample taken from the project, Ⅰ group sample taken from the bedrock region, Ⅱ group sample taken from area of the landslide mass and lithology are the phyllite of Jurassic-bonobo group in the Triassic system of, bedrock rock hard, weak weathering, weak joint fissure development, integrity is better; The soft rock of the landslide mass and weathering, joint fissure development, poor integrity. Two set of sample to make use of water drilling coring operation. Triangle compression test according to the relevant provisions of the relevant specification with a diameter of 50 mm and 100 mm cylindrical block, the Brazilian splitting test with a diameter of 50 mm, 50 mm height of cylindrical block, part of the sample is shown in figure 1.According to the model test procedures, remove dust and other particles on the surface of the specimen after clean, put it in the sink, water injection to the first block, a quarter of the high and intervals of two hours of water injection in order to block high 1/2 and 3/4 high, after 6 hours block was completely submerged. To block completely immersed in the water and free water absorption after 48 hours, forced to saturation.



FIGURE 1
Preparation of the sample



FIGURE 2
Triaxial compression test and brazilian splitting test

(3)Triaxial compression test and Brazilian splitting test. Conventional triaxial test with 5 MPa, 10 MPa, 15 MPa, 20 MPa and confining pressure load of 25 MPa. Brazilian split test adopts a continuous load method, loading speed is 0.12 mm/s, until the specimen. As shown in Figure 2.

The basic mechanical parameters of test were conducted five sample test. Test results are shown in Table 1.

TABLE 1
The test results of phyllite basic mechanical parameters

material	Unit weight γ/(KN·m^{-3})	Elasticity modulus E/GPa	Poisson ratio μ	Compressive strengthσ_c/MPa	Strength's extension σ_t /MPa	Cohesive force$C$/MPa	Internal friction angle/°
Irock sample	26.04	5.5	0.29	40.4	4.5	15	38
IIrock sample	25.5	3.5	0.31	14	1.3	7.8	36.3



FIGURE 3
Basic components of similar materials

Similar material preparation.

(1) Bedrock selection of raw materials. This experiment based on similar projects on site conditions, empirical research was carried out by a large number of similar material proportion, eventually developed the vaseline and as cementing agent. For cement strength regulator, with fine sand barite powder and talcum powder as the aggregate new similar material. Through proportioning, respectively used to simulate the actual engineering of bedrock and sliding body. At the same time, choose to find sand, talcum powder and silicon oil according to a certain proportion of fissure filling materials in the sliding surface of similar materials. Developed of two similar materials of good work-ability. Physical and chemical performance is stable, guarantee the similarity model test. In order to further reveal the suitable high steep slope instability mechanics have laid a solid foundation. The element of the similar material as shown in Figure 3.

(2)Preparation process of similar material

①Preparation process of the slope similar material can be divided into the following steps: we stir fine sand ,barite power, talcum powder and cement which have weighed in accordance with the provisions evenly, then we add silicone oil and Vaseline solution in order, at last we stir them fully;

②We put the mixed fully similar material into steel mold with certain pressure in order to make it quickly compaction;

③We remove the steel die down and take out the briquette which has been pressing forming block, at last we label on the surface used to group;

④We dry the briquette at room temperature for three to four days later. In this way, the briquette of similar material has finished. When making block using double open steel mould ,we can produce block size for Φ50m×l00mm.

(3)The determination of similar materials distribution ratio

①The change rule of material property with different proportion

Through the array test block, such as elastic modulus and compressive strength test, finally by matching test, we can rock similar material and similar basic mechanical parameters value and proportion, as shown in Table 2 to Table 3.

The high steep slope model test system. The model test system is made up by high strength steel structure test bench, servo hydraulic loading system and monitoring system of real-time information. The system has high strength, easy to assemble and the advantages of high degree of visualization, at the same time it can be realized in the process of test record and all the information real-time monitoring. Test mainly studied the mechanical characteristics of the slope deformation and stability characteristics in different load cases.

Three-dimensional sectional model test bench. This article through the analysis of the results, in combination with the practical situation of slope engineering, select appropriate section, designs the multifunctional high steep slope physical model test bench.

TABLE 2
Comparison of mechanical parameters of prototype and similar material

material	Unit weight γ /(KN·m^{-3})	Elastic modulus E/MPa	Poisson's ration μ	Cohesive force C/kPa	Frictional angle/°	Compressive strength σ_c /MPa	Strength of extension σ_t /kPa
bedrock	26.4	5500	0.29	1500	38	40.4	4500
Similar material	25.4	113	0.31	29.3	35	0.88	85.5
Sliding rock	25.5	3.5	0.31	780	36.3	14	1300
Similar material	25.1	2、5	0.3	15.7	34.4	0.41	29.1

TABLE 3
Similar material composition and proportion

	Fine sand	Blanc fixe	vaseline	Silicone oil	Talcum powder	cement
Rock similar material	1	0.1	0.1	0.1	0.06	0.04
Slip mass similar material	0.8	0.06	0.66	0.66	0.1	0.02

This test-bed's overall size: 2.5m (length)×1.7m(wide)×2m(high). This model test apparatus is made up of high-strength alloy steel and stalinite. Its advantages include strength and stiffness are larger; good impact resistance and corrosion resistance ability are strong; visualization operation can be achieved. Using high strength bolt and the flange, top beam, side beam and bottom beam can be connected together. Reaction wall made up of the long beam connected on the side of the beam. Meanwhile its bottom connects with baseboard of model. The entire model device is reasonable load and attractive appearance. Meanwhile it can ensure the whole stiffness and strength, which improving the accuracy of the test, as shown in figure 4.



FIGURE 4
Overall view of model framework



FIGURE 5

High pressure loading system

Uniform gradient loading system. High-pressure loading system made up of jack and pressing plate which connects with it, through coordinated control of the hydraulic oil cylinder pressure, which can realize the slope with uniform load, high pressure loading system is shown in figure 5.

Digital intelligent hydraulic automatic control system is composed of hydraulic control cabinet, high pressure oil pipe and pressure in composition. In the process of loading, if reach the set pressure value, the device will automatically stop the pressure. When the system pressure value is lower than the set pressure value, the device will automatically fill pressure, thus realize automatic pressure maintaining.

Multivariate information monitoring system.

(1) Fiber Bragg grating monitoring system. The basic characteristics of fiber grating can be expressed as a reflective optical filter. When an incident light into the grating, fiber Bragg grating will reflect specific wavelengths of light. If caused by outside conditions change grating axial or lateral strain, it will lead to changes in the center of the fiber Bragg grating wavelength. By monitoring the change of the center wavelength, we can estimate the changes of the surrounding environment. Fiber Bragg grating displacement sensor and strain sensor is relatively commonly used fiber Bragg grating sensor.

(2) Grating ruler multi-point displacement meter test system. The test system consists of the following parts: the measuring point, casing, wire rope, positioning frame, grating ruler, a heavy hammer, signal conversion system and data acquisition system. Its main advantages are high sensitivity, strong stability and weak influence, not easy to damage and convenient embedding and real-time display of displacement, etc. Grating ruler is measuring element, including indicating grating and the grating scale. We can measure the moire stripe to express scaleplate raster and the relative displacement of the grating.

(3) Resistance monitoring system. This system is made up of XL2101G static resistance strain gauge, brick of resistive strain components and pressure box components. Among them, the static resistance strain is mainly used for the connection and monitoring of bridge and half bridge. The size of resistive strain brick element and fiber bragg grating is same. This test uses three-way resistance strain gauge, which is bonded on the surface of a resistive strain brick. It also connects with inner diameter of 1.2mm. The pressure cell's boundary dimension is Φ17*7mm. Measurement range is 0~1.00Mpa.

Model test design.

Test scheme.

(1)The selection of model test of similar scale. The prototype of the test is bedding steep rock slope's instability process from chengdu in sichuan province to chuanzhusi of the lanzhou railway. According to the test schedule, find the geometric similarity scale model test is 1:50.

(2) The manufacturing flow of slope model. To meet the requirements of the model test is scientific. In the making process of the slope model, using "dry compaction method". It's concrete steps : scaling preparation materials in accordance with the provisions→mixing it well with mixer -paving material layered from top to the bottom within the test bed→ pressing the material artificially layer-by-layer then making it dry → Between the material and the bedrock sliding body laying talcum powder as a straight line of slope slip plane, according to the regulations of the design scheme in the layered slope parts embedded measuring element → In addition to places of element place to continue using artificial method

step by step a ramming material filling after the completion of the additional load to the end - model system.

Monitoring program and its measuring point embedding. In order to understand the slope's multivariate information under the deformation process [15]. The mainly monitor content is slope's stress, strain and displacement change under the stress. In addition, in order to study the different thickness of the sliding body condition, the changes of the displacement of the slope buckling critical load and buckling, this test sets respectively the sliding body thickness is 15 cm, 20 cm and 25 cm, meanwhile, we should analysis the monitoring data under different thickness. Each slide body thickness, each monitoring section were set up. We must arrange all kinds of monitor element in each monitoring section, including the displacement, strain and stress box components. Top-down adjacent element spacing is 5 cm. Each measuring point arrangement is shown in Figure 6.

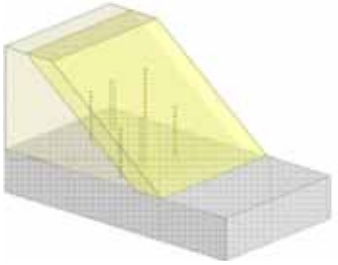


FIGURE 6

Monitoring sections and component layout

Monitoring device is mainly made up of fiber Bragg grating sensor and resistive sensor. The embedding process of the model's monitor element can be summarized as the following steps. Enact monitoring scheme→ensure the location of monitoring point→slotting and hole digging→back-fill materials→segmented compaction→lead to sidewall wires.

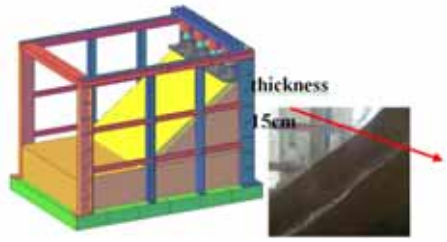
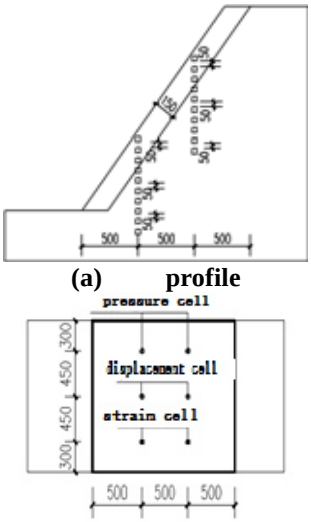


FIGURE 7
Diagram of Model loading

RESULTS AND DISCUSSION

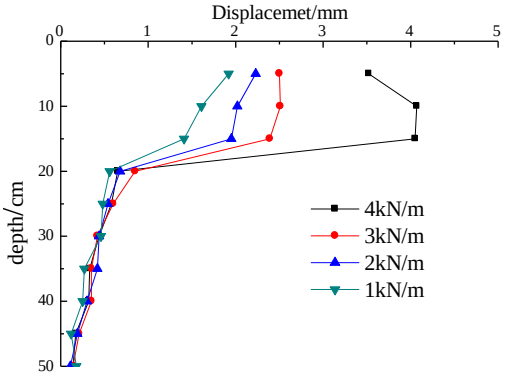
Data processing and analysis. Filling the first set of test models of slope sliding body thickness is 15 cm. The upper slope gets gradation loading by the upper slope model hydraulic loading system. Load per level, waiting for the displacement, stress and strain after stability, to the next level load (see Figure 7), monitoring the change of the data of the landslide mass. Monitoring position as shown in Figure 8.



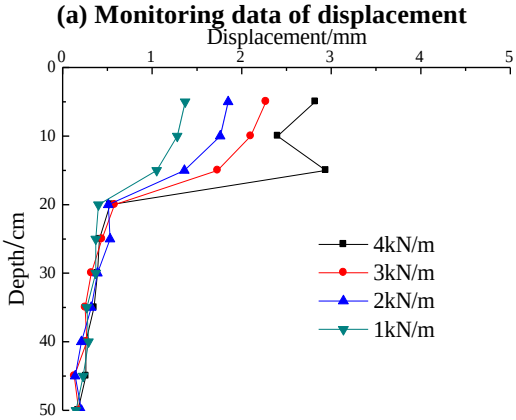
(a) profile

(b) Plan

FIGURE 8
Arrangement of measuring points with slide mass thickness of 15cm



(a) Monitoring data of displacement



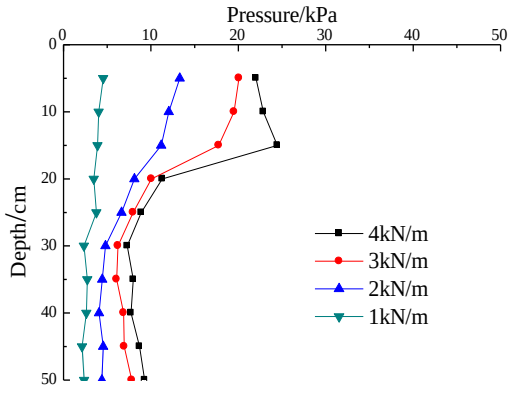
(b) Monitoring data of displacement

FIGURE 9
Curves of deep displacements

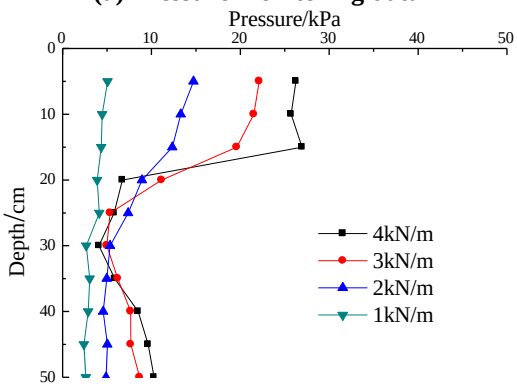
(1) Deep displacement. Along the depth direction of the slope of each measuring point displacement value as shown in Figure 9.

Deep displacement curve shows: the sliding body deep displacement of the high load level mutations and irregular fluctuations in displacement value. Slope surface uplift has been observed at this time, and accompanied by crack shows that layered buckling stage of sliding body. Record the pressure value is the critical load. Continue to monitor the displacement with the change of pressure until the crack appears as you can see obviously. Slope top load increase gradually, the displacement of the apparent increase. On the sliding surface of deep rock mass displacement curve mutations, and displacement of sliding body itself is continuous. Little change of deep rock mass displacement, high and steep slope of deep bedrock is often in a relatively stable state. The main research object of high and steep slope instability is the shallow rock mass. The shallow rock mass under the top load produce large changes in mechanical properties. The top load increase to level 4, with sliding collapse bend occur at the bottom of the landslide mass and accompanied by crack. I row (above) the displacement variation is greater than the variations in the displacement of row II (below).

(2) Pressure distribution. Along the depth direction of the slope of each measuring point pressure value is shown in Figure 10.



(a) Pressure monitoring data

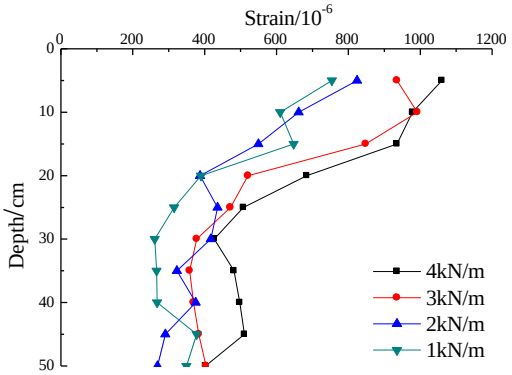


(b) Pressure monitoring data

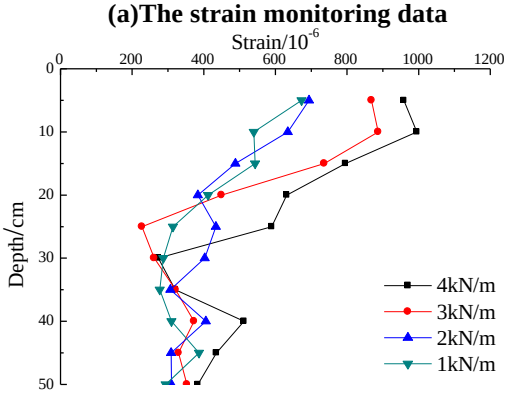
FIGURE 10
Curves of stresses

The curve shows: As the load grows, partial pressure of the landslide mass increases. Because with the sliding surface sliding of the landslide mass and slide body bottom rock mass by the traction effect, pressure also will increase. The part near the sliding surface, the pressure increases, the more obvious. This kind of phenomenon in the late loading becomes not obvious, is due to the collapse of the landslide mass bending deformation, related to the sliding surface from step by step. At the same time, the sliding body internal pressure not harmonious phenomenon also appears. This shows that the sliding body collapse occurred flexor leads to uneven distribution of inner stress of the landslide mass.

(3) The strain analysis. Along the depth direction of the slope strain values of measuring points is shown in Figure 11.



(a)The strain monitoring data

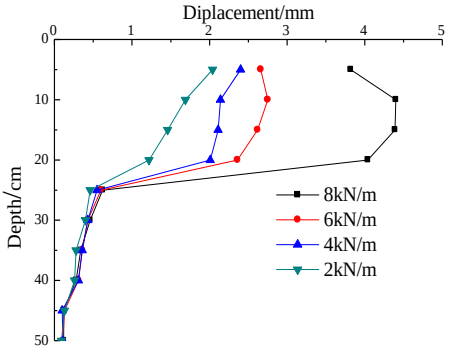


(b) The strain monitoring data

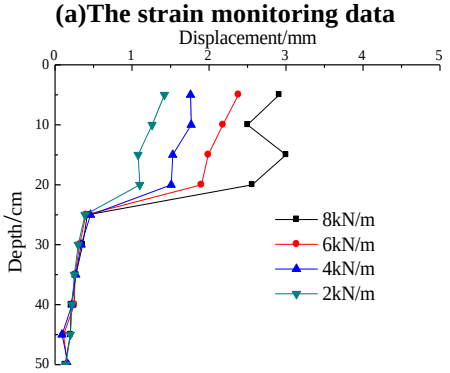
FIGURE 11
Curves of strain

The curve shows: Near the sliding surface, the bigger the strain, and the degree of loading at high load level increases. This shows the direction along the slip surface sliding of the landslide mass. The load level is high, the sliding body strain deformation not harmonious phenomenon in a significant increase in overall and at the same time. Thus we prove that under the condition of high load, slope is relatively easy to collapse bend failure happens.

When the thickness of the slip body fixed value respectively for 20 cm and 25 cm, deep displacement, stress distribution and strain data changes as shown in figure 12 -17 respectively.

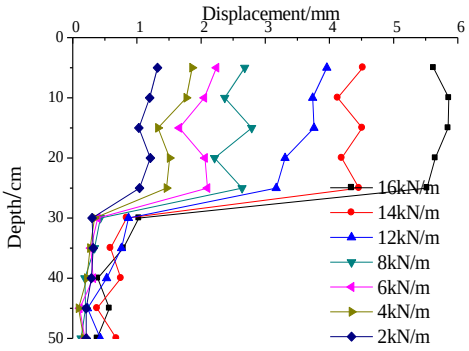


(a)The strain monitoring data

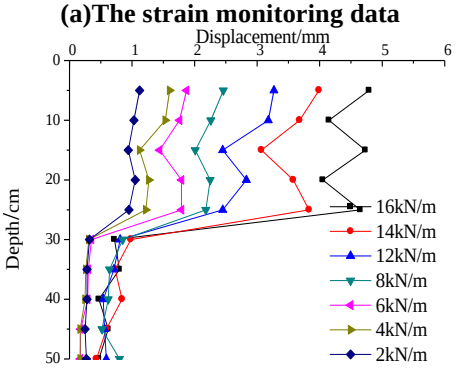


(b) The strain monitoring data

FIGURE 12
Curves of deep displacements with slide mass thickness of 20cm



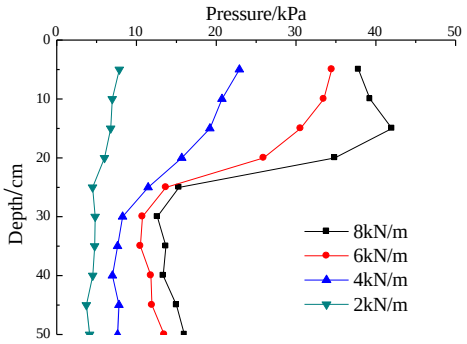
(a)The strain monitoring data



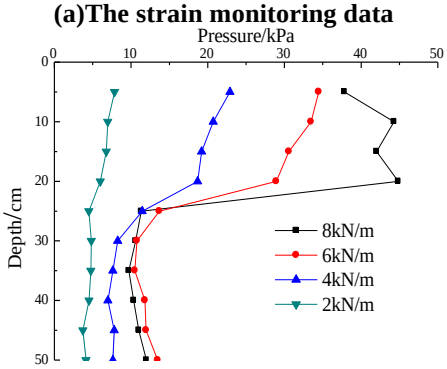
(b)The strain monitoring data

FIGURE 13
Curves of deep displacements with slide mass thickness of 25cm

Deep displacement curve shows: The different thicknesses of the sliding body case of deep displacement direction are basically identical. At the same level of loading conditions, the displacement value of the same location as the sliding body decreases with the increase of thickness. With the increase of thickness of sliding body, slide body can withstand the load level will gradually increase.

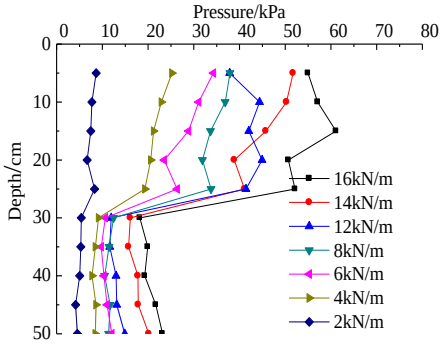


(a)The strain monitoring data

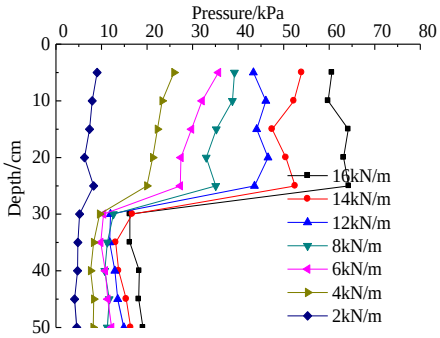


(b)The strain monitoring data

FIGURE 14
Curves of stresses with slide mass thickness of 20cm



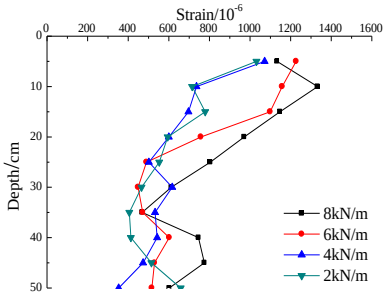
(a) The strain monitoring data



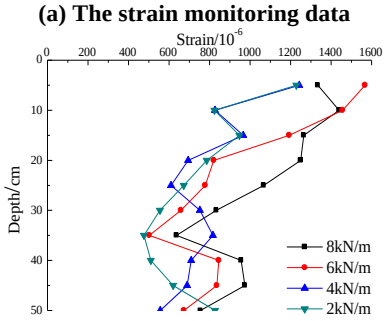
(b) The strain monitoring data

FIGURE 15
Curves of stresses with slide mass thickness of 25cm

The stress curve shows: Under the condition of different thickness of slide body, the stress curve with depth increasing trend. At the same level of loading conditions, the stress value of the same location with the increase of thickness of the sliding body and appear a little increase. With the increase of thickness of sliding body, slide body can withstand the load level will gradually increase. When loading the level reached a certain degree, II (below) the stress change gradually over I row (above) the stress variation.

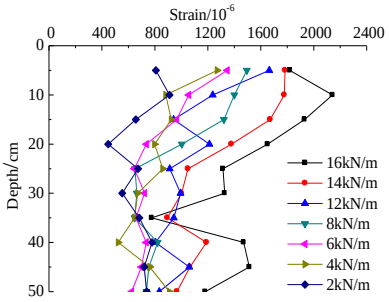


(a) The strain monitoring data

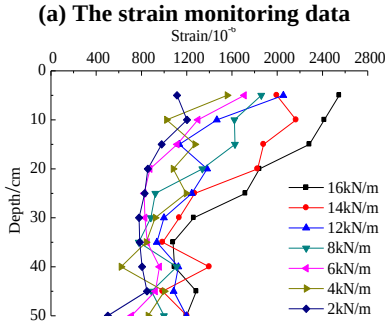


(b) The strain monitoring data

FIGURE 16
Curves of strain with slide mass thickness of 20cm



(a) The strain monitoring data



(b) The strain monitoring data

FIGURE17
Curves of strain with slide mass thickness of 25cm

As seen in the strain change curve, the different thickness of the sliding body case increase with depth, the direction of the strain curve rough approximation. At the same level of loading conditions, the same location with strain value increase with the increase of the thickness of the landslide mass. With the increase of thickness of sliding body, slide body can withstand the load level will gradually increase. When loading the level reached a certain degree, II (below) the strain change gradually over I row (above) the strain variation.

CONCLUSIONS

In this paper a high steep slope along ChengLan railway - was taken as the main research object. For the analysis of instability and failure of slope -- suitable structure characteristics and failure modes of high steep slope were summarized. Combining with the characteristics of the geological environment, along the typical high steep slope failure mode under the effect of earthquake region was put forward in consideration. Then, through suitable high steep slope collapse bend failure mechanism and mechanical model test. the stress characteristics and suitable high steep rock slope deformation failure mechanism were studied. Based on similarity theory, the three-dimensional high strength composite steel structure is developed with servo hydraulic loading system and the optical fiber grating real-time information monitoring system. It reveals the different thickness and loading conditions of the landslide mass along the high steep slope deformation and stress characteristics. The experimental results could provide reference for similar projects slop protection.

ACKNOWLEGDEMENTS

This work was supported by the natural science foundation of Hebei Province (E2017210147) and Collaborative Innovation Center for Disaster Prevention & Mitigation of large basic infrastructure in Hebei Provence. Great appreciation goes to the editorial board and the reviewers of this paper.

REFERENCES

[1] Zhang, Q. and Li, S.C. (2014) Stability analysis and evaluation of Zengziyan in Jinfo Mountain under seismic (vibration) action. Journal of Vibroengineering. 16(2), 575-583.

[2] Chen, J., Zhang, G. and Yuan, C.H. (2002) Analysis and Treatment of Bedding-slip Cut Slope. Chinese Journal of Rock Mechanics and Engineering. 21(l), 48-51.

[3] Sun, D.Y., Peng, Y.J. and Wang, X.Z. (2002) Application of DDA Method in Stability Analysis of Topple Rock Slope. Chinese Journal of Rock Mechanics and Engineering. 21(l), 39-42.
[4] Bai, Y.F. (2005) Study on Stability and Designing of Consequent Bedding Rock Cut Slope. Southwest Jiaotong University.
[5] Zhang, Q. and Li, S.C. (2014) Stability analysis of rock mass with sheet slope crack based on plates and shells theory. Polish Journal of Environmental Studies. 23(4), 1297-1306.
[6] Ma H.M., Wang, G.X. and Zhou, D.P. (2006) Disease control instance of Highway High Slopes in Mountainous Area. Beijing: China Communications Press.
[7] Liu, H., Song, J.B. and Xiang, X.Q. (2006) Failure Model and Stability Evaluation of Small Instable Rocks Distributed in Low-angled Stratofabric Rock Slope. Chinese Journal of Rock Mechanics and Engineering. 25(8), 1606-1611.
[8] Zhang, Q., Wang, J.C. and Zhang, H.X. (2017) Attribute recognition model and its application of risk assessment for slope stability at tunnel portal, Journal of Vibroengineering. 19(4), 2726-2738
[9] Zhou, D.P., Zhong, W. and Yang, T. (2008) Stability Analysis of Rocky Slope Based on Slope Structures. Chinese Journal of Rock Mechanics and Engineering. 27(4), 687-695.
[10] Hu, X.W. and Tang, H.M. (2005) Physical Model Studies on Stability of Zhaoshuiling Landslide in Area of Three Gorges Reservoir. Chinese Journal of Rock Mechanics and Engineering. 24(12), 2089-2095.
[11] Feng, W.K., Shi, Y.C. and Chai, H.J. (2004) Study of mechanism of deformation failure of a low-angle bedded high slope with physical simulation method. China Journal of Highway and Transport. 17(2), 32 – 36.
[12] Feng, J., Zhou, D.P. and Li, A.H. (2005) Physical Modeling Research on Relaxation Region of Consequent Rock Slope Induced by Road Cutting. China Journal of Highway and Transport. 24(5), 840 – 845.
[13] Chen, C.X., Huang, P.L. and Lu, Z.M. (2007) Study on Correlation between Stability of Consequent Rock Slope and Obliquity of Rock Layer by Simulation Experiment. Rock and Soil Mechanics. 28(3), 476 – 486.
[14] Zhang, Q. (2015) Instability Mechanism and Control Measures of Bedding Steep Slope in High Intensity Seismic Area. Shandong University.
[15] Lai, J.X., Fan, H.B. and Chen, J.X. (2015) Blasting vibration monitoring of undercrossing railway tunnel using wireless sensor network. International Journal of Distributed Sensor Networks. 2015(2), 6.

Received: **27.07.2017**
Accepted: **10.10.2017**

CORRESPONDING AUTHOR

Weigang Zhao
Shijiazhuang Tiedao University,
Shijiazhuang, 050043 – China

e-mail:935123166@qq.com

© by PSP Volume 26 – No. 12A/2017 pages 8176-8183 Fresenius Environmental Bulletin

RESERVOIR CHARACTERISTICS AND PORE STRUCTURE CLASSIFICATIONS OF CHANG 6 MEMBER OF YANCHANG FORMATION OF TRIASSIC IN JIYUAN OILFIELD OF ORDOS BASIN, CHINA

Ye Tao[1], Dazhong Ren[1,2,*], Shi Shi[3], Zhaohua Zhou[3], Shuwei Ma[1], Zhang Qian[1]

[1] State Key Laboratory of Continental Dynamics, Department of Geology, Northwest University, Xi'an, 710069, China
[2] School of Petroleum Engineering, Xi'an Shiyou University, Xi'an, 710065, China
[3] PetroChina Research Institute of Petroleum Exploration & Development, Beijing,100083, China

ABSTRACT

Methods such as conventional physical property, casting thin-section, scanning electron microscope (SEM), conventional mercury injection, nuclear magnetic resonance (NMR), etc. are used to analyze the classification of the microscopic pore structure and its influence on moveable fluid saturation in Chang 6 member of Yachang formation in Jiyuan area. The research shows that the accumulation space in this area are mainly primary interparticle pores followed by feldspar dissolution pore. According to capillary pressure curve and its corresponding parameters, the reservoir pore structure is classified into four types: Type Ⅰ, Ⅱ, Ⅲ and Ⅳ corresponding to different accumulation spaces, and the accumulation properties and permeability ability of these four types are turning worse from type Ⅰ to Ⅳ. It is tested from NMR that the distribution of T_2 spectrum is analogous to the distribution of the mercury saturation of its corresponding pore throat radius; the T_2 value is positively correlated with pore throat radius; pore throat radius is the main factor affecting the moveable fluid saturation; moveable fluid distribution is positively correlated with permeability which is the direct parameter characterizing the permeability ability of different pore structures.

KEYWORDS:
Jiyuan Area, Chang 6 member, Microscopic Pore Structure, Moveable Fluid Saturation, Pore Throat Radius, Permeability

INTRODUCTION

Jiyuan area is located at the centre of Tianhuan depression tectonic zone in Ordos Basin, in which Chang 6 member of Yanchang formation of Triassic is the main section for oil and gas exploration and development of Chang Qing oil field [1] (Fig. 1). Previous researchers have studied the provenance, sedimentation, diagenesis, physical properties, pore genesis and water flooding characteristics in Chang 6 member [2-4]. They believed that the target zone shows the listing characteristics: this zone is low porosity and ultra-low permeability; it was mainly affected by provenance from northeast and northwest; oil and gas mainly accumulated in subaquatic distributary channels in delta fronts; diagenetic evolution stage was from late diagenesis phase A period to early diagenesis phase B period; feldspar dissolution pore and interparticle pore are the main pore types; water flooding efficiency is low. Currently, very few researches have analyzed from micro-perspective the influence that the pore structure has on moveable fluid characteristics [5-8]. In this paper, casting thin-section, scanning electron microscope, conventional mercury injection and nuclear magnetic resonance have been used to analyze pore structure and moveable fluid characteristics, and to discuss the effects that the pore structure parameters have on moveable fluid, thus to summarize the effects the pore structure characteristics have on moveable fluid.

MATERIALS AND METHODS

Reservoir Petrological Characteristics. According to SY/T5368-2000 industry standard, sandstone types in Chang 6 member are mainly gray-dark gray arkose and a few fine arkose (Fig. 2). After analyzed the casting materials from samples, it is found that the average volume fraction of terrigenous clast is 78.1%, and that of quartz, feldspar and debris are 31.2%, 38.0% and 8.9% respectively; and that the feldspar is mainly plagioclase and the debris is mainly metamorphic debris (Fig. 3). According to microscopic identification, interstitial materials are mainly clay minerals, carbonate rocks and siliceous rocks; carbonates are mainly ferruginous calcite with a volume fraction of 4.3%; volume fraction of siliceous rocks is 1.13%.

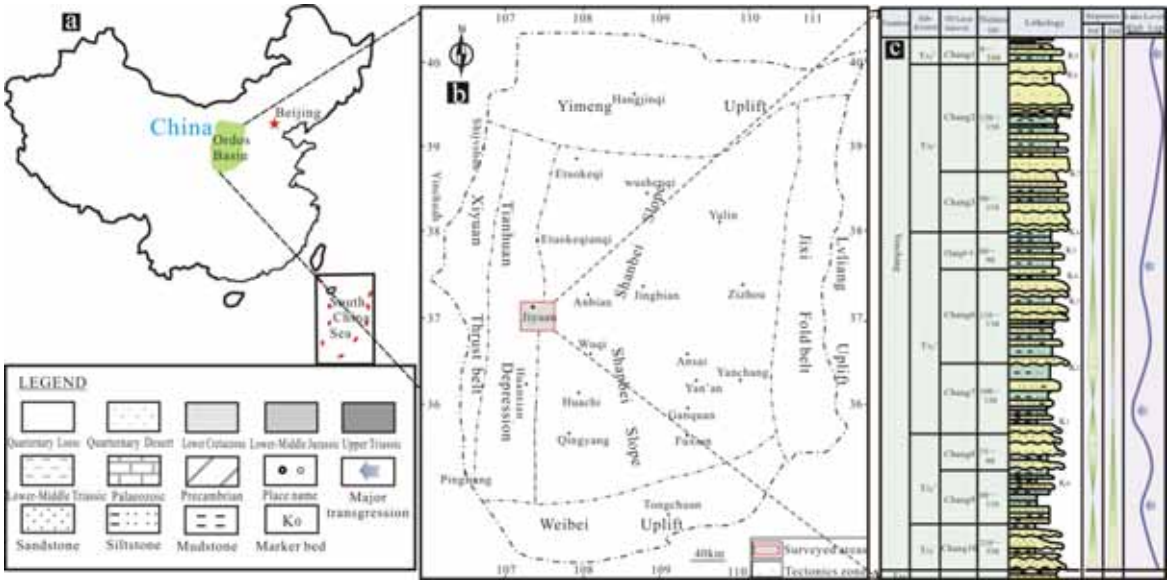
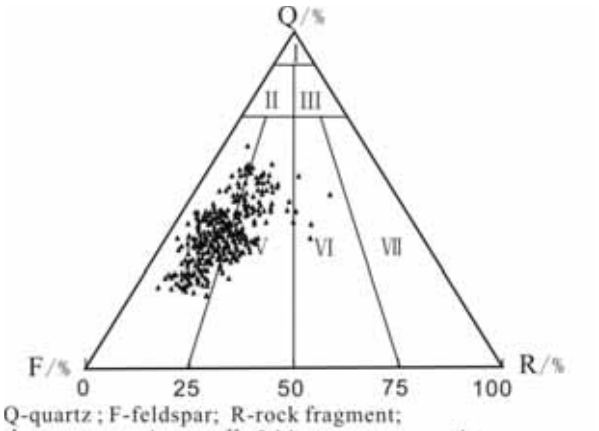


FIGURE 1
Tectonic location and Synthetical Stratum Histogram of Jiyuan Oilfield in Ordos basin China



Q-quartz ; F-feldspar; R-rock fragment;
I quartz sandstone; II feldspar quartz sandstone;
III lithic quartz sandstone; IV feldspar sandstone;
V lithic feldspar sandstone; VI feldspar lithic sandstone;
VII lithic sandstone

FIGURE 2
Characters and Types of Chang 6 Member in Jiyuan Oilfield

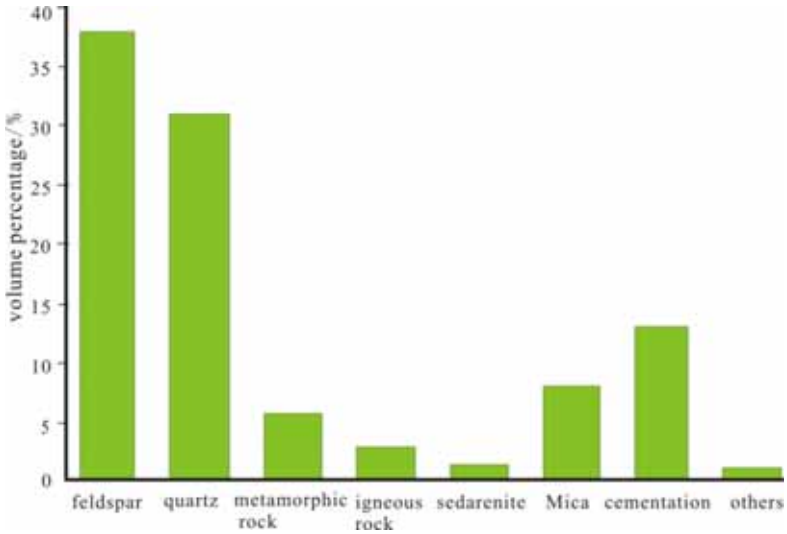
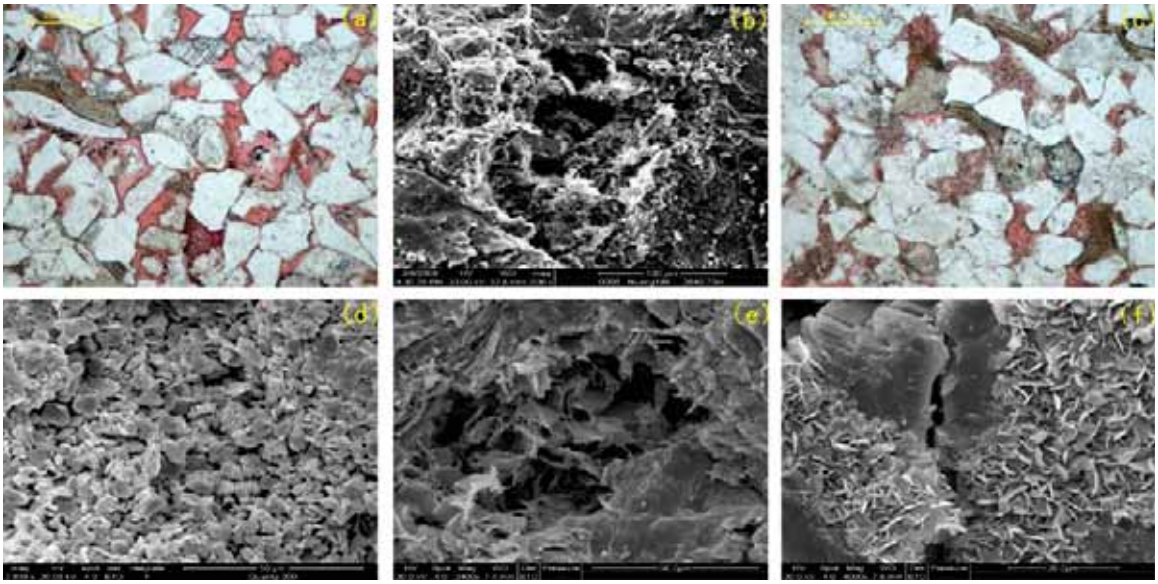


FIGURE 3
Clastic Rock Composition of Chang 6 Member in Jiyuan Oilfield



(a) Residual Interparticle Pore, L66 Well, 2394.6 m, Casting Thin Film; (b) Feldspar Dissolution Pore, H148 Well, 2640.74 m, Scanning Electron Microscope; (c) Rock Debris Dissolution Pore, L66 Well, 2394.6, Casting Thin Film; (d) Kaolin Intercrystal Pore, G63 Well, 2531.44 m, Scanning Electron Microscope; (e) Illite Intercrystal Pore, G46 Well, 2459.8 m, Scanning Electron Microscope; (f) Micro Fractures, H129 Well, 2359.9 m, Scanning Electron Microscope.

FIGURE 4
Photographs of Casting Thin Sections and SEM of Chang 6 Member in Jiyuan Oilfield

X-ray diffraction showed that interstitial matter volume fraction is relatively high in Chang 6 member in Jiyuan area with a big range of 1.5-35%, and the average fraction is 13.31%. The volume fraction of cements, a range of 1.0-35.0% and an average of 13.10%, is much higher than that of matrix. Among the cements, ferruginous calcite makes up 4.3%, kaolinite 3.45% and chlorite 3.89%. Besides of these minerals, small amount of reticular clay, feldspar, pyrite, siderite, etc. are also found among cements. Matrix volume fraction is low, the average of which is 2.29%. The diameters of clastic grains are mainly between 0.06-0.25mm. These grains are mainly subangular and medium sorting. Grain contact type is mainly point-line; contact and cementation types are mainly pore cementation and thin film cementation (Fig. 4).

RESULTS AND DISCUSSION

Microscopic Pore Structure Characteristics of Reservoir. Accumulation Space Types. Analysis from sandstone scanning electron microscope and casting thin film shows that pore types in target zone are mainly interparticle and dissolution pores transformed by compaction, cementation and dissolution progresses. Intercrystal pore and diagenetic fracture are not developed in this area, of which the total facial porosity is low with 3.81%; primary interparticle facial porosity is 2.3% and feldspar dissolution facial porosity is 1.22%. Pores appear mainly in types of combination. Dissolved pore-interparticle pore takes the dominate type filled mainly with autogenetic cement minerals and matrix. Pore coordination degree is medium-low, and the connectivity degree is medium (Fig. 4). Accumulation properties and permeability ability are directly affected by reservoir pore distribution characteristics and the materials filling in pores [9,10].

Pore Structure Types and Characteristics. Pore structure is a microphysical property that directly shows reservoir quality, and its evaluation characteristics affect the permeability of oil and gas [11-15]. Currently, variances of methods and basis have been used to study and classify reservoir pore structures [16,17]. In this paper, 32 samples from target zone have been under mercury injection experiment, and mercury injection parameters and their corresponding capillary pressure cures have been used to study pore structures. As a result, pores in research area have been classified into four types: Type Ⅰ, Ⅱ, Ⅲ and Ⅳ (Table 1, Fig. 5).

Type Ⅰ is mainly micro-medium throat of which capillary pressure curve usually tends to be at the left bottom of a diagram. The part of the curve of which value is less than $S_{Hg\text{-}50}$ is relatively gentle and displacement pressure is low (0.21-0.10 MPa) (Table 1, Fig. 5b); the values of mainstream pore throat radius mostly locate between 0.15-3.45 μm and its skewness is slightly bold (0.12-0.26); sorting coefficient of pore throat radius is 2.1-3.7 and its average is 2.5; the maximum mercury saturation locates between 85.0-94.0%, and its average is 91.6% (Table 1, Fig. 5a). Pores are mainly residual interparticle pores and feldspar dissolution pore etc. Chlorite and

TABLE 1
Different Structure Parameters of Mercury Injection of Chang 6 Member in Jiyuan Oilfield

Types		Ⅰ		Ⅱ		Ⅲ		Ⅳ	
Parameters		Range	Average	Range	Average	Range	Average	Range	Average
Physical Property	Porosity (%)	10.2-16.7	13.25	8.2-16.5	11.62	7.5-15.1	10.87	<11.0	7.65
	Permeability ($10^{-3}\mu m^2$)	0.18-2.3	0.92	0.09-1.3	0.47	0.07-1.0	0.25	<0.1	0.07
Conventional Mercury Injection	Displacement pressure (MPa)	0.21-1.0	0.52	0.51-2.84	1.19	0.95-5.72	3.06	>2.5	5.12
	Mainstream Throat Radius (μm)	0.15-3.54	0.46	0.07-1.24	0.15	0.04-0.61	0.08	<0.3	0.05
	Maximum Mercury Saturation (%)	85.0-94.0	91.6	70.0-91.0	85.3	60.0-88.0	75.2	<85.0	69.7
	Sorting Coefficient	2.1-3. 7	2.5	0.1-2.8	2.07	0.1-3.2	1.2	0.06-3.6	1.0
	throat Skewness	0.12—0.26		-0.15—0.16		-0.41—0.07		-0.61— -0.10	
Pore Types		Residual Interparticle Pore, Feldspar Dissolution Pore		Residual Interparticle Pore, Dissolution Pore, Intercrystal Pore, Mold Pore		Dissolution Pore, Intercrystal Micropore, A few Interparticle Pore		Matrix Micropore, Intercrystal Pore, Very few Diagenetic Fracture	
Sample Amount		5		15		9		3	

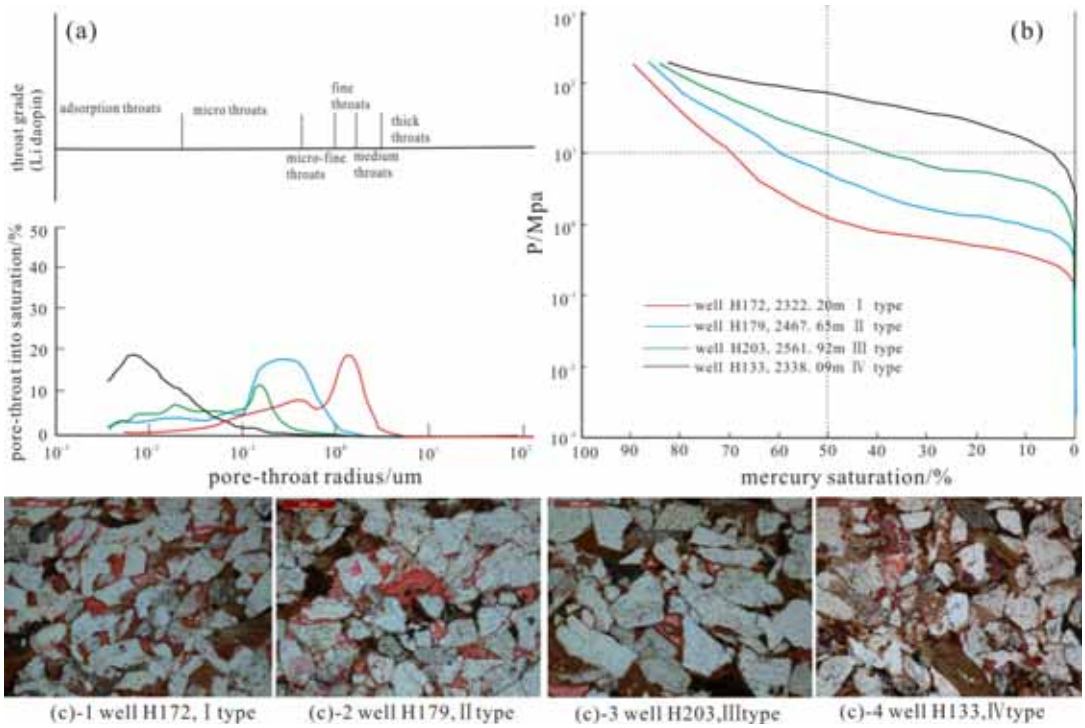


FIGURE 5
The Characteristic Parameters of Capillary Pressure Curves of Chang 6 Member in Jiyuan Oilfield

kaolinite are the main clay types in this pore (Table 1, Fig 5c-1). This type of pore is the highest in accumulation property and permearbility ability among the four types and it usually locates at underwater distributary channel with thick sand body (the center of a channel).

Type Ⅱ is mainly micro-fine throat. The capillary pressure curve of this one is similar to that of type Ⅰ but displacement pressure (0.51-2.84 MPa) is higher (Table 1, Fig. 5b). Mainstream pore throat radius are mostly between 0.07-1.24 μm; its skewness (-0.15-0.16) shows normal distribution and sorting coefficient is 0.1-2.8 of which the average is 2.07. The maximum mercury saturation is slightly high with a value of 70.0-91.0%, and the average is 85.3% (Table 1, Fig. 5a). Because of the increased levels of

mechanical compaction and cementation degree, compared to type Ⅰ, primary interparticle pore in this pore type decreased while secondary dissolution pore, mold pore and intercrystal pore are developed (Table 1, Fig. 5c-2). This type has good accumulation property and permeability ability and usually locates at underwater distributary channel or at both sides of a channel connected to the centre.

Type Ⅲ is mainly micro throat. Its capillary pressure curve tends to be at the right top of a diagram. The curve part whose value is less than S_{Hg-50} waves a lot. Displacement pressure (0.96-5.72 MPa) is higher than that of the above two types (Table 1, Fig. 5b). Mainstream pore throat radius is mostly between 0.04-0.61μm and skewness is gentle (-0.41-0.07); its sorting coefficient is between 0.10-3.2 and the average is 1.2; the maximum mercury saturation is lower than previous two types and its values are between 66.0%-88.0% with an average of 75.2% (Table 1, Fig.5a). Again, mechanical compaction and cementation degree increased compared to type Ⅱ, while losing primary interparticle pore at a high level. Dissolution and intercrystal pores are relatively developed. Interparticle facial porosity is slightly lower than dissolution facial porosity (Table 1, Fig. 5c-3). Compared to type Ⅰ and Ⅱ, single sand body of this type is thinner, and both sand layer and sand pore structure of this type are obviously heterogeneous. Accumulation property and permeability ability of this type are medium and worse than that of type Ⅰ and Ⅱ. This type of pore locates mainly at the top, bottom and boundary of a sand body of underwater distributary channel and at thin fluvial sands.

Type Ⅳ is mainly adsorbent-micro throat. Capillary pressure curve of this one is close to the right top of a diagram and barely has plateau. The part of the curve of which value is less than S_{Hg-50} increases smoothly and the displacement pressure (> 2.5 MPa) is the highest among these four types (Table 1, Fig. 5b); mainstream pore throat radius is less than 0.3 μm and skewness is gentle (-0.61-0.10). Sorting coefficient is between 0.06-3.6 with an average of 1.0; the maximum mercury saturation is 50.0-85.0% with an average of 69.7% (Table 1, Fig. 5a). This type is relatively strong in compaction and carbonate cementation; illite is the main cementation clay mineral and it contains relatively high amount of mica and matrix. Primary interparticle pore is almost lost while matrix micro pore and intercrystal micro pore are developed. Feldspar dissolution pore is slightly developed (Table 1, Fig. 5c-4). This type of pore is the lowest in accumulation property and permeability ability. It usually develops at the boundary of a distributary channel connected to interdistributary estuary or at estuary micro phases such as interdistributary estuary.

In conclusion, in Chang 6 member, pore structure of type Ⅰ is the best in accumulation property and permeability ability but development level is low; and the structures of type Ⅱ and Ⅲ are the most common while type Ⅳ is considered to be invalid reservoir.

The Influence on Moveable Fluid Saturation of Microscopic Pore Structure. Studies on Moveable Fluid Saturation Using Nuclear Magnetic Resonance (NMR). Based on the classifications of pore structures, NMR is used to test sandstone samples from research area. With references from previous research results moveable fluid saturation and T_2 parameters are used to qualitatively and quantitatively evaluate accumulation property and structure characteristics of microscopic pore [18]. For Chang 6 member of Jiyuan area, it is seen from NMR that the T_2 spectrogram shows three different shapes: high left peak with low right peak, low left peak with high right peak and single peak(Fig. 6a).

Three typical samples are selected for analysis from NMR test. Table 2 and Figure 6a show that the moveable fluid saturation tested from the sample of Well H172 is 63.52% of which T_2 spectrogram shape is low left peak with high right peak with main peak locating at the right of T_2 cut off value. These features indicate that interparticle pore developed better than dissolution and intercrystal pores; that throat radius is high; and that pore throat is good in connectivity but is medium in sorting. The moveable fluid saturation of the sample from Well H179 is 40.8%. T_2 spectrogram shape of this type is high left peak with low right peak and the main peak locates at the left of T_2 cut off value. These features indicate that secondary pore facial porosity is higher than that of interparticle pore; that feldspar is the highest in facial porosity; and that the amount of intercrystal pore has obviously increased. Compared to the previous sample, throat radius of this one is smaller both in its value and amount, and pore throat connectivity is worse. Sorting feature enhanced by micro pore is better. Moveable fluid saturation of Well H133 sample is 21.84% with a single peak T_2 spectrogram of which peak point locates at the right of T_2 cut off value indicating that pore structure of sample is relatively homogeneous with only micro pore and part of dissolution pore. Interparticle pore is not developed. Valid throat radius decreased both in value and amount. Pore throat connectivity is poor but the pore structure sorting dominated by micro pore has enhanced.

Combining analysis from both Figs. 5 and 6, it is concluded that moveable fluid is mainly distributed in large pores connected by valid throat; while throat and micro pores contain less moveable and thus mainly belong to irreducible fluid. The changes of T_2 value corresponded to moveable fluid is analogical to that of pore throat radius tested from mercury injection, and the shape of T_2 spectrogram is analogical to that of the distribution and saturation of corresponding mercury injection.

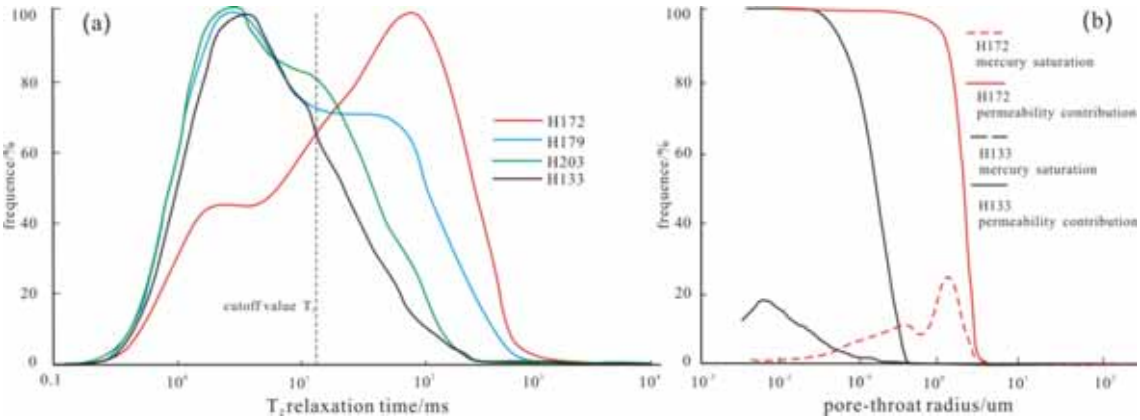


FIGURE 6
Movable Fluid Saturation of NMR and Parameters of Pores Structure of Chang 6 Member in Jiyuan Oilfield

TABLE 2
Parameters of Micro- pore Structure Characteristics of Different Moveable Fluid Distribution

Well NO.	H	φ	K	Pore Structure parameters				Experimental parameters From NMR	
	/m	/%	/mD	P_{cd} /Mpa	CS	R_{50}/μm	S_{max}/%	S_m/%	φ_i /%
H172	2322.20	12.5	0.62	0.57	2.41	0.13	89.82	63.52	7.67
H179	24.67.65	12.22	0.28	1.46	2.32	0.045	85.71	40.87	4.99
H203	2561.92	11.51	0.27	1.72	2.22	0.042	84.58	26.19	3.01
H133	2338.09	10.19	0.07	2.91	1.88	0.009	76.75	21.84	2.22

(H-depth, φ-porosity, k-permeability, P_{cd}-displacement pressure, CS-sorting coefficient, R_{50}-Median Radius, S_{max}-Maximum Mercury Saturation, W_e-Mercury Withdrawal Efficiency, S_m-Moveable Fluid Saturation, φ_i-Moveable Fluid Porosity)

TABLE 3
Correlation between Moveable Fluid Saturation of NMR and Parameters of Micro Pore Throat Structure from Data of Constant-Speed Mercury Injection in Chang 6 Reservoir

Parameters		Correlations with Moveable Fluid Saturation		
		Correlation Function	Correlation Type	R^2
Physical Property	Porosity/%	$S_m = 0.0328\varphi^{2.8123}$	Positive	0.2959
	Permeability/$10^{-3}\mu m^2$	$S_m = 80.131x + 14.689$	Positive	0.8073
High	Displacement Pressure/MPa	$S_m = 43.072P_{cd}^{-0.695}$	Negative	0.7114
Pressure	Sorting Coefficient	$S_m = 0.5573e^{1.8602CS}$	Positive	0.7518
Mercury	Maximum Mercury Saturation/%	$S_m = 0.284e^{0.056Smax}$	Positive	0.4680
Injection	Medium Radius/μm	$S_m = 20.172e^{9.1567R50}$	Positive	0.7742

After analyzing and comparing distributions of T_2 spectrogram tested from Well H172 and Well H133 samples and of pore throat radius of these samples (Fig. 6), it is concluded that the pore throat radius corresponded to T_2 cut off value is approximately 0.1μm, which is accordance with the conclusion saying that 0.1μm is the lower limit of pore throat radius through which fluid can move in nature state [19]. For the samples from Well H172, the mercury saturation of pore throat of which radius is higher than 0.1 μm is 61.31%, providing more than 90.71% of the whole permeability ability of these samples. And for the samples from Well H133, the mercury saturation of those pore throat of which radius is higher than 0.1μm is 14.87%, providing more than 78.55% of the whole permeability ability. It is indicated that moveable fluid saturation mainly locates in effectively connected pore throat spaces. Valid throat radius value and its distribution characteristics are the dominant factors affecting the moveable fluid saturation and distribution characteristics.

The Influence on Moveable Fluid Saturation of Pore Structure Parameters. By comparing and analyzing the relations between parameters of micro pore structure and NMR moveable fluid saturation (Table 3), it is found that moveable fluid saturation is positively correlated with median radius, sorting coefficient and maximum mercury saturation; and that correlation coefficient, R^2, are 0.7742, 0.7518, and 0.468, respectively; however, moveable fluid saturation is negatively correlated with displacement

pressure and correlation coefficient R^2 is 0.7114. Thus, it is deduced that the higher the sorting coefficient the higher the value and amount of pore throat radius, and the higher the validly connected pore throat volume, also, the higher the moveable fluid saturation in reservoir. Besides that, it is also found that moveable fluid saturation is positively correlated with physical property, and the correlation with permeability (R^2=8073) is much higher than that with porosity (R^2=2959). From the analysis above, it is found that the permeability is mainly provided by the throat in the pore net; throat radius is the key parameter for the evaluation of moveable fluid saturation in reservoir; throat radius value can be used to directly represent T_2 value from NMR (Fig. 6). For the development of tight reservoir, high permeable zones should be chosen preferentially or acidizing and fracturing may be applied to increase the value and amount of throat radius, thus to increase the permeability and moveable fluid saturation for the purpose of the improvement of ultimate oil recovery.

CONCLUSIONS

(1) Chang 6 member in Jiyuan area is tight reservoir. The effective sandbody of this reservoir is mainly fine-ultrafine arkose and the cement materials are mainly chlorite, kaolinite and ferrocalcite; the accumulation spaces are mainly primary interparticle pore and secondary the feldspar dissolution pore. Besides these, a few micro fractures caused by tectonism are developed. The pore combination form of this reservoir is mainly dissolution pore-interparticle pore.

(2) Based on the capillary pressure curve and its corresponding characterisation parameters, pore structures of target zone are classified into four types corresponding to different pore types of which the permeability ability and accumulation property turn worse in order of type Ⅰ, Ⅱ, Ⅲ and Ⅳ, in which, type Ⅱ and Ⅲ are the most developed in research area of Chang 6 member.

(3) Moveable fluid saturation in Chang 6 member is low, and T_2 spectrogram shows three shapes: low left peak with high right peak, high left peak with low right peak and single peak. The corresponding T_2 value of moveable fluid varies with the size of pore throat radius tested from mercury injection, which is the key factor for the evaluation of moveable fluid saturation in reservoir. The distribution of T_2 spectrogram is analogous to that of corresponding mercury saturation of pore throat radius; permeability has a good positive correlation with moveable fluid saturation and is a direct parameter representing the permeability ability of a pore structure.

(4) For the development of tight reservoir, high permeable zones should be chosen preferentially or acidizing and fracturing may be applied to increase the value and amount of throat radius, thus to increase the permeability and moveable fluid saturation for the purpose of the improvement of ultimate oil recovery.

ACKNOWLEDGEMENTS

The authors acknowledge the financial --project (2015M582699) supported by the China postdoctoral Science Foundation; project (2016JQ4022) supported by the Natural Science Foundation Research Project of Shaanxi Province, China; project (41702146) supported by the National Natural Science Foundation of China; project (2016ZX05047) supported by the National Science and Technology Major Project of China: Key Technology of the Tight Gas Enrichment Law and the Exploration and Development; Project supported by the postdoctoral Science Foundation of Shaanxi Province, China.

REFERENCES

[1] Wang, D.F. (2007) The Development of Extra-low Permeability Oilfield in Ordos Basin. Petroleum Industry Press, Beijing.

[2] Gong, F.H., Bao, Z.D., Ji, H.C., Fan, Z.P., Liu, L. and Wu, X. (2011) Study on the Reservoir Diagenesis Heterogeneity of Chang 6 Member of Upper Triassic in Jiyuan Area of Ordos Basin. Journal of Jilin University(Earth Science Edition). 41, 639-646.

[3] Gao, H. and Li, H.Z. (2015) Determination of movable fluid percentage and movable fluid porosityin ultra-low permeability sandstone using nuclear magnetic resonance(NMR) technique. Journal of Petroleum Science and Engineering. 133,258-267.

[4] Ren, D.H., Sun, W., Huang, H., Liu, D.K., Qu, X.F. and Lei, Q.H. (2016) Formation Mechanism of Chang6 Tight Sandstone Reservoir in Jiyuan Oilfield of Ordos Basin. Earth Science. 41, 1735-1744.

[5] Al-Mahrooqi, S.H., Grattoni, C.A., Muggeridge, A.H., Zimmerman, R.W. and Jing, X.D. (2006) Pore-scale modelling of NMR relaxation for the characterization of wettability. Journal of Petroleum Science and Engineering. 52, 172-186.

[6] Tan, M. and Zhao, W. (2006) Description of carbonate reservoirs with NMR log analysis method. Progress Geophys. 21, 489-493.

[7] Cai, Y., Liu, D., Pan, Z., Yao, Y., Li, J. and Qiu, Y. (2013) Petrophysical characterization of Chinese coal cores with heat treatment by nuclear magnetic resonance. Fuel. 108, 292-302.

[8] Eslami, M., Ilkhchi, A.K., Sharghi, Y. and Golsanami, N. (2013) Construction of synthetic capillary pressure curves from the joint use of NMR log data and conventional well logs. Journal of Petroleum Science and Engineering. 111, 50-58.
[9] Yang, H., Zhong, D.K., Yao, J.L., Liu, X.Y., Ma, S.Y. and Fan, L.L. (2013) Pore genetic types and their controlling factors in sandstone reservoir of Yanchang Formation in Longdong Area, Ordos Basin. Earth Science Fhrontiers. 20, 69-76.
[10] Di, S.X. (1991) pore textures in clastic reservoirs of China. Northwest University Press, Xi'an.
[11] Ren, D.H., Sun, W., Wei, H., Zhou, S.X., Zhang, Y.G., Zhang, X. (2014) Types of Sandstone Reservoir Diagenetic Facies and Microscopic Pore Structure Characteristics of Chang 81 Reservoir in Huaqing Oilfield of China. Geoscience. 28(2), 379-386.
[12] Liu, D.K., Sun, W., Ren, D.Z., Zhang, X., Ming, H.X., Chen, B. (2016) Features of pore-throat structures and movable fluid in tight gas reservoir: A case from the 8th member of Permian Xiashihezi Formation and the 1th member of Permian Shanxi Formation in the western area of Sulige Uasfield, Ordos Basin. Natural Gas Geoscience. 27(12), 2136-2146.
[13] Zhang, C., Sun, W., Yang, J.P., Gao, H., Hou, H.L., Qi, R., Luo, J.Y., Wei, X.W. (2012) Pore and Pore-Throat Size Distributions of Low Permeability SandstoneReservoir and Their Differential Origin. Acta Geological Sinica. 86, 335-348.
[14] Gao, H., Song, G., Gao, J., Sun, W., Lu, Y., Ren, G. (2008) The influences of microscopic pore structure on waterflooding effectiveness in Xifeng oilfield. J. Northwest University (Nat. Sci. Ed.) 38, 121-125.
[15] Luo, Z.T., Wang, Y.C. (1986) pore textures in Hydrocarbon reservoir of China. Science Press, Beijing.
[16] Bi, M.W., Chen, S.Y., Zhou, Z.H., (2015) Characteristics and significance of microscopic pore structure in tight sandstone reservoir of the 8th member of Lower Shihezi Formation in the Su 6 area of Sulige Gaslield . Natural Gas Geosciences. 26(10), 1851-1861.
[17] Clarkson, C.R., Freeman, M., He, L., Agamalian, M., Melnichenko, Y.B., Mastalerz, M., Bustin, R.M., Radlinski, A.P., Blach, T.P., (2012) Characterization of tight gas reservoir pore structure using USANS/SANS and gas adsorption analysis. Fuel. 95(1), 371-385.
[18] Yao, Y., Liu, D., Che, Y., Tang, D., Tang, S., Huang, W. (2010) Petrophysical characterization of coals by low-field nuclear magnetic resonance (NMR). Fuel. 89, 1371-1380.
[19] Peter, E., Peter, S.D., Atilla, A., John, W., Douglas, K.M. (2005) Structure, petrophysics, and diagenesis of shale entrained along a normal fault at Black Diamond Mines, California: Implications for fault sea. AAPG Bulletin. 89(9), 1113-1137.

Received: **31.07.2017**
Accepted: **06.10.2017**

CORRESPONDING AUTHOR

Dazhong Ren
State Key laboratory of continental Dynamics
Department of Geology,
Northwest University,
Xi'an, 710069 – China

e-mail: Petrogas999@163.com

© by PSP Volume 26 – No. 12A/2017 pages 8184-8198 Fresenius Environmental Bulletin

REACTIVE DYE DEGRADATION USING Fe-LOADED BENTONITE AS A FENTON-LIKE CATALYST: FROM PROCESS OPTIMIZATION TO EFFLUENT ACUTE TOXICITY

Milena Becelic Tomin[1], Aleksandra Kulic[1], Djurdja Kerkez[1], Miljana Prica[2,*], Sanja Rapajic[3], Dragana Tomasevic Pilipovic[1], Vesna Pesic[1]

[1]University of Novi Sad, Faculty of Sciences, Department of Chemistry, Biochemistry and Environmental Protection, Trg Dositeja Obradovica 3, Novi Sad, Serbia.
[2]University of Novi Sad, Faculty of Technical Sciences, Department of Graphic Engineering and Design, Trg Dositeja Obradovica 6, Novi Sad, Serbia.
[3]University of Novi Sad, Faculty of Sciences, Department of Mathematics and Informatics, Trg Dositeja Obradovica 4, 21000 Novi Sad, Serbia.

ABSTRACT

The present work demonstrates an application of the heterogeneous Fenton process in the degradation of aqueous solutions of Reactive Blue 4 (RB4) synthetic dye using Fe-loaded bentonite (Fe-Bt) as a catalyst. Characterizations of the Fe-Bt catalyst were performed using XRD, multipoint BET, BJH model, N_2 adsorption, FT-IR and SEM/EDS analysis. Effects of the operation conditions (catalyst loading, H_2O_2 concentration and pH) on decolourization efficiency are discussed with a selection of optimum parameters through response surface analysis. In terms of both decolourization efficiency (98.3%) and stability of the catalyst, optimum conditions for this Fenton process are pH = 3, minimum applied Fe-Bt load of 0.15 g L^{-1} and initial H_2O_2 of 3 mM. Samples obtained under optimum conditions described above were analysed to evaluate total organic carbon content within mineralization efficiency, toxicity, as well as ion concentrations (Cl^-, NO_3^-, NO_2^-, SO_4^{2-}). Organic degradation compounds of RB4 dye were detected by GC/MS. Acute toxicity was determined using an inhibitory test on bioluminescent bacterium *Vibrio fischeri*. According to the results, a Fenton-like process with Fe-Bt could be proposed as an appropriate process for decolourization with the possibility of multiple reuse of the catalyst (reuse of the catalyst was successful after the fifth run) but with an incomplete mineralization of the RB4 resulting in the generation of highly toxic effluent. This drawback of the applied process requires extended reaction time or combination with other methods to remove degradation products.

KEYWORDS:
decolourization, catalyst, Reactive Blue 4, heterogeneous Fenton process

INTRODUCTION

One of the major sources of water pollution is known to be the textile industry, and the quantity of wastewater from this industry has been increasing along with the growing demand for textile products. The wastewater contains organic dyes and their breakdown products, which may have toxic and/or mutagenic effects on life. The release of textile industry wastewater into the environment can cause serious health and environmental problems [1, 2].

The types of dyes used in the textile industry differ depending on the fabrics produced [3]. Reactive dyes are mainly used for dyeing cellulose fibres such as cotton and viscose [4, 5] but they are also increasingly gaining importance for wool [6] and polyamide [7]. Reactive dyes represent an increasing market share because they are used to dye cotton fibres, which make up about half of the world's fibre consumption [8] and account for 36% of overall dye consumption in the world.

Poor dye fixation has been a long-standing problem with reactive dyes [9]. Consequently, a significant amount of unfixed dyes through the second step (fabric washing) of the dying process may be released in wastewater. These wastewaters must be treated to meet the specifications for discharge or for recycling in the process [10].

Because both unfixed reactive dyes and their hydrolysed forms are readily soluble, they are difficult to eliminate in conventional biological wastewater treatment plants. The synthetic origin and complex aromatic structure of these agents make them more recalcitrant to biodegradation [11]. However, several other physical and chemical methods and hybrid techniques have been developed for removal of reactive dyes from wastewaters, including adsorption, membrane filtration, ion exchange, chemical oxidation, electrocoagulation, coagulation, photocatalysis and combinations of methods [12–25].

The Fenton process, from a group of advanced

oxidation processes, is one of the most studied and reported processes intended for the removal of organic dyes during the last decade. Investigations have focused on the use of Fenton-like processes and the synthesis of highly active and stable solid catalysts [26–28]. Various supports for iron ions such as activated carbon fibres [29], nafion [30] and silica [31] have been used as heterogeneous Fenton catalysts. Compared with the mentioned novel catalyst supports, the use of clay as a carrier of iron and other metal species is particularly stressed because it is a natural, abundant, inexpensive and accessible material [32–35].

In addition to the development of suitable catalysts, possible by-product formation during heterogeneous Fenton oxidation process of dye is still a top priority concern as they represent a source of secondary pollution [36]. Besides that, monitoring of the degradation products and their toxicity is essential for adjusting the reaction time and conditions to avoid the release of intermediates of higher toxicity than the original dye [37].

In cases when it is possible to choose more than one method for pollutants' removal in terms of their effectiveness, the cost of wastewater treatment has an important role. Overall, the costs of wastewater treatment include the benefits in terms of protecting human health and the recipient of wastewater and operating costs. The cost of the Fenton-like process, among other things, depends on the nature of the wastewater, dosage of H_2O_2, as well as of the source, modification, activity and stability of the catalyst [38]. These factors are considered in the optimization of the selected treatment process.

The objective of the present study was to apply and evaluate the effectiveness of the heterogeneous Fenton process for the degradation of Reactive Blue 4 (RB4) synthetic aqueous solution. To carry out the process in a cost-effective manner, impregnated clay mineral bentonite with Fe polycations was used as catalyst support. To reduce the time of synthesis, the impregnation procedure was improved with ultrasound. The research included 1) preparation and characterization of the catalyst, 2) evaluation of the effects of main operation conditions (catalyst loading, H_2O_2 concentration and pH) on decolourization; 3) selection of optimum parameters based on the results of the response surface analysis; 4) investigation of the possibility of the catalyst reuse and 5) assessment of mineralization, toxicity and degradation products of RB4 dye after Fenton treatment performed under the optimal conditions for decolourization.

MATERIALS AND METHODS

Materials. The catalyst support was Na^+-exchanged bentonite clay Claris-p70 (Bento product, Sipovo, Bosnia and Herzegovina). Cation exchange capacity (CEC) was found to be 0.90 mequiv g^{-1}. RB4 as model pollutant, H_2O_2 solution (30%, w/w), H_2SO_4, NaOH, Na_2CO_3, $Fe(NO)_3{\bullet}9H_2O$, NaCl and bovine liver catalase were purchased from Sigma-Aldrich Company. All chemicals used were analytical grade and used without further purification. All solutions were prepared with deionized water.

Preparation of bentonite catalyst. Treatment with Fe polycations was carried out by adapting the method reported by Iurascu et al. [33]. Before use, bentonite was washed several times with deionized water and dried in an oven at 100 °C for 12 h. A suspension of bentonite was prepared by adding 1 g of the clay to 50 mL of deionized H_2O under vigorous stirring for 30 min. In the meantime, Na_2CO_3 was added slowly in powder form into a vigorously stirred 0.2 mol L^{-1} solution of $Fe(NO_3)_3{\bullet}9H_2O$ with simultaneous application of ultrasound for 10 min, for achieving a mole ratio of 1:1 for $[Na^+]/[Fe^{3+}]$. The obtained solution was added very slowly to a suspension of bentonite in deionized water and the suspension was again subjected to ultrasonic irradiation for 10 min. The ratio Fe^{3+}/clay was 3 mmol g^{-1}. The resulting suspension was kept under stirring at room temperature for 12 h and then centrifuged and washed three times with deionized water. The material was then heated at 350 °C for 2 h. The sample was labelled Fe-Bt.

Characterization of prepared catalysts. The synthesized catalyst sample was analysed using different conventional techniques. Structural analysis was performed using 77 K N_2 adsorption–desorption isotherms by Autosorb iQ Surface Area Analyser (Quantachrome Instruments, USA). Samples were outgassed at 120 °C for 2 h before running isotherms. The multipoint BET (Brunauer–Emmett–Teller) method was used to determine the specific surface area. Mesopore volumes were derived from desorption isotherms using the BJH (Barrett–Joyner–Halenda) model and micropore volumes were calculated using the *t*-test method. X-ray diffraction (XRD) patterns of the sample were measured with a Rigaku MiniFlex II desktop X-ray diffractometer with Cu Kα radiation and recorded in the 2θ = 6–80° range (5°/min scan rate). FT-IR spectra were recorded on a NEXUS 670 (Nicolet, USA) in the 450–4000 cm^{-1} range. External morphology and surface elemental compositions were determined by scanning electron microscopy (SEM) (TM3030, Hitachi High-Technologies, Japan) and energy dispersive spectrometry (EDS) (Brucker Quantax 70 X-ray detector system, Brucker Nano, GmbH Germany).

Catalytic activity of impregnated bentonite in the Fenton process. The experiments were conducted on a jar test apparatus (FC6S Velp Scientific, Italy), where reactive mixtures with 0.25 L volumes were continually mixed in 1 L laboratory cups, at 150

rpm.

The experiments were performed in the following manner: first, the appropriate catalyst dosage (0.15–0.7 g L^{-1}) was added to the model dye solution (RB4 concentration 50 mg L^{-1}), which was followed by pH adjustment to the desired value (2.5–4), and the addition of the required amount of H_2O_2 (3.0–15 mM). Each experiment lasted 120 min. Samples were centrifuged at 10000 rpm for 5 min. This was followed by separation of the catalyst from the solution and its recovery for reuse.

Decolourization was monitored by absorbance (A) at λ_{max} = 594.78 nm (UV/vis spectrophotometer, Shimadzu, Japan). The analysis of iron in solution was done by atomic absorption, using a Perkin Elmer Analyst 700.

The efficiency of dye decolourization was obtained by the application of the following formula:

$$100 \cdot (A_0 - A) / A_0 = \text{dye removal (\%)} \quad (1)$$

where the A value was measured after a certain reaction time and A_0 is the initial absorbance.

Response surface analysis. In this study, response surface analysis was used for the optimization of the Fenton reaction catalysed by Fe-Bt. The effects of the three independent variables on the response are presented by the response surfaces. Numerical results and statistical analysis were obtained by using the software package *Mathematica 8.0*. The relationship between operating variables (H_2O_2 concentration, catalyst loading and pH) and the decolourization efficiency is described by a second-order polynomial model, so the experimental data are fitted with a quadratic polynomial function [39–41].

Mineralization and effluent toxicity. The aliquots after Fenton treatment performed under optimum conditions for decolourization were filtered through a 0.45 μm pore size membrane filter and immediately analysed for total organic carbon (TOC) content, evaluation of degradation products and overall toxicity.

TOC removal was followed by LiquiTOC II (Elementar, Germany), wherein the following formula is used:

$$100 \cdot (TOC_0 - TOC) / TOC_0 = \text{TOC removal (\%)} \quad (2)$$

where TOC value was measured after 120 min and TOC_0 is the initial value of Fe-Bt in deionized water at pH value 3.

Determination of ions (Cl^-, NO_3^-, NO_2^- and SO_4^{2-}) was conducted on Dionex ICS-3000, which was connected to the computer software Chromeleon 6.8 Chromatography Management Software.

Qualitative gas chromatography/mass spectrometry (GC/MS) analysis was included for determination of non-polar and semi-polar compounds in the effluent. The analysis was carried out in SCAN mode on the GC/MS, Agilent 7890A/5975C instrument, wherein the scanned ions were in the range 35–550 atomic mass units. Sample preparation and extraction was performed with hexane and methylene chloride according to the EPA 3510C. The manufacturer's original method was used for monitoring pesticides and 926 hormone-active substances in the prepared extract. Deconvolution software (Software Deconvolution Reporting-DRS) was used for evaluation and identification (Automated Mass Spectral Deconvolution and Identification System-AMDIS). In addition, identification of compounds was performed using the NIST and AMDIS libraries of mass spectra, all identified compounds are those recognized with a probability of >70%.

Afterwards, effluent toxicity was determined using an inhibitory test on bioluminescent bacteria *Vibrio fischeri* (NRRL B-11177) with a LUMIStox 300 instrument (Dr Lange GmbH, Germany), LUMISsoft IV software and according to the ISO 11348-1:2008 standard. The inhibitory effect (H_t) was measured in water samples, during 30-minute exposure to bacteria at 15 °C, and expressed in %. In addition, it is important to note that the sample after the Fenton process was treated with catalase solution (0.1 g L^{-1}) to scavenge the remains of H_2O_2 in solution [42]. Sample toxicity was calculated according to equation (3) with regard to non-contaminated control (2% solution of NaCl):

$$100 \cdot (I_{ct} - I_t) / I_t = H_t \text{ (\%)} \quad (3)$$

where I_{ct} was the luminescence of the control sample and I_t was the luminescence of the Fenton process effluent.

RESULTS AND DISCUSSION

Characterization of the catalyst. Textural characteristics of the original Bt as a catalyst support and impregnated bentonite (Fe-Bt) derived from N_2 adsorption–desorption isotherms are presented in Table 1. It can be seen that the surface area of the prepared material increased after impregnation. The effect of increasing surface area of modified clay has been observed by numerous authors [33, 43–45]. This phenomenon can be explained by the reduction of medium and large mesopores when inserting iron in bentonite, which causes a significant increase in surface area, which is also confirmed by the average pore size and pore volume of Fe-Bt. Namely, metal particles that penetrate larger pores lead to a decrease in average pore size and simultaneous increase in the pore volume. Besides that, addition of Na_2CO_3 at the catalyst synthesis stage is also capable of increasing both the surface area and pore volume [46].

The results of the FT-IR analysis are presented in Fig. 1. The spectrum of Bt revealed the characteristic absorptions. The band at 3625 cm^{-1} is due to the –OH stretching band for Al–OH. The interlamellar water molecules in the bentonite structure are resolved in the band at a wavenumber of 3443 cm^{-1}.

The wavenumber of 1638 cm^{-1} indicates the presence of adsorbed water in the first co-ordination sphere of the interlayer space [47]. The most intense peak at 1039 cm^{-1} is attributed to the Si–O stretching (in-plane) vibration for layered silicates. The bands at 915 and 876 cm^{-1} are attributed to AlAlOH and AlFeOH bending vibrations [48, 49].

For the Fe-Bt sample, reduced intensity peaks were observed that are due to the stretching vibration of the hydroxyl group linked to metal cations and water molecules and the cause may be the removal of hydroxyl groups in the calcination step [45, 47]. In addition, because of calcination, the peak detected at 1431 cm^{-1} in the Bt sample disappeared [50, 51]. However, no peaks due to Fe oxides or oxy-hydroxides were observed in the spectra.

The XRD was used for the investigation of the structural changes of Fe-Bt. Fig. 2 shows the XRD patterns of Bt and after loading with Fe. The diffractions at 2θ angle 6.8°, 19.8° and 61.9° are characteristic of clay mineral montmorillonite, while peaks originating from non-clay components (quartz, Q) are observed at 26.6 (2θ) [45, 52, 53]. After bentonite modification, the montmorillonite pattern at 6.8 (2θ) was no longer visible. However, on the Fe-Bt diffraction pattern, there are no additional peaks that would indicate the presence of the oxides or oxyhydroxides of iron, indicating that the various forms of metal oxides are finely dispersed in the particulate clay in a form of a very small crystallite size, thus not detected by XRD [52]. It is assumed that ultrasound applied in the phase of catalyst preparation has contributed to this occurrence due to its ability to produce non-agglomerated, crystalline particles in unique reaction conditions [54].

TABLE 1
Textural characteristics of original and prepared bentonite

Sample	Parameter BET (m^2/g)	Micropore *t*-test (cm^3/g)	BJH method mesopore (cm^3/g)	Total pore volume (cm^3/g)	Average pore diameter (Å)
Bt	97.30	0.029	0.092	0.040	22.763
Fe-Bt	180.198	0.028	0.068	0.071	14.683

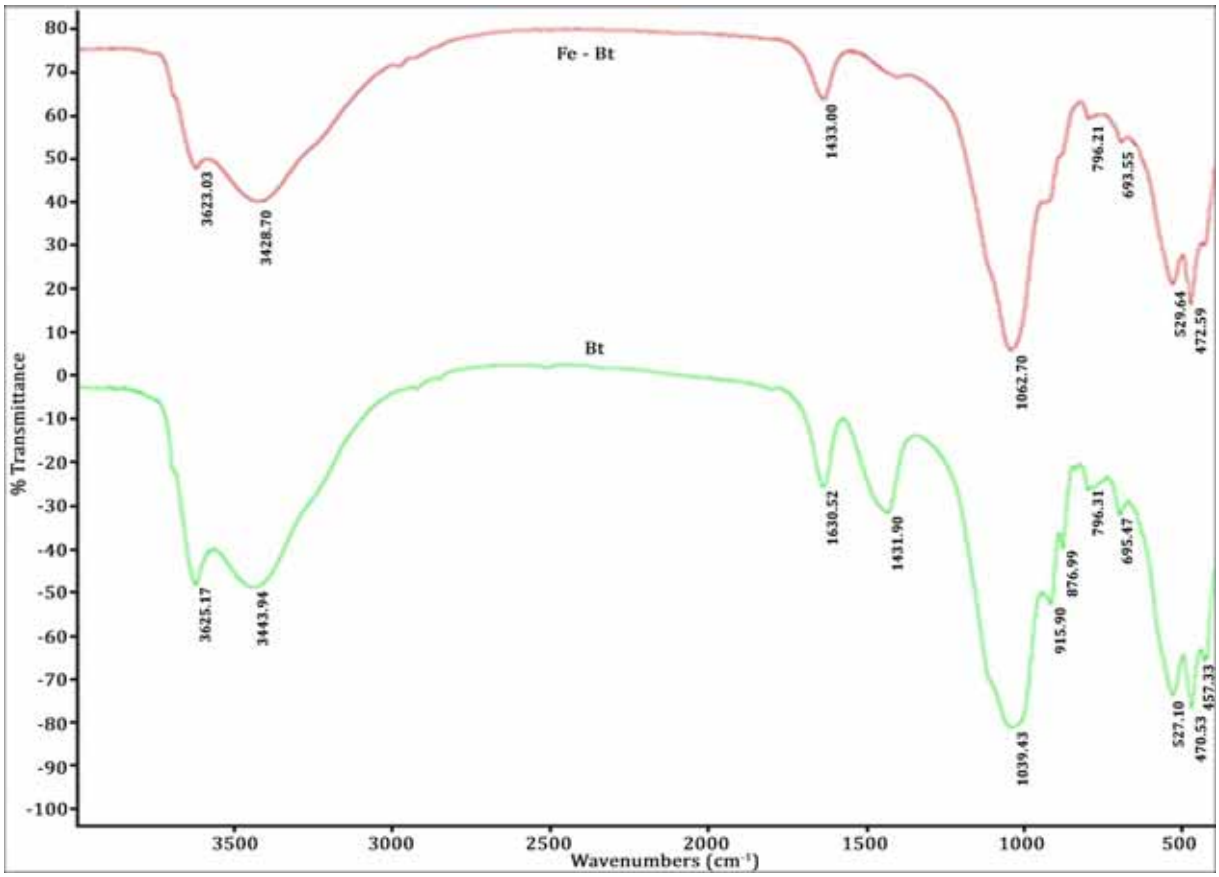


FIGURE 1
FT-IR spectra of Bt and Fe-Bt

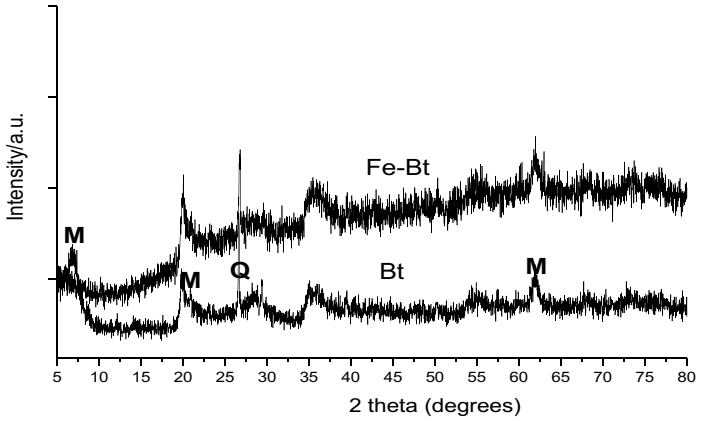
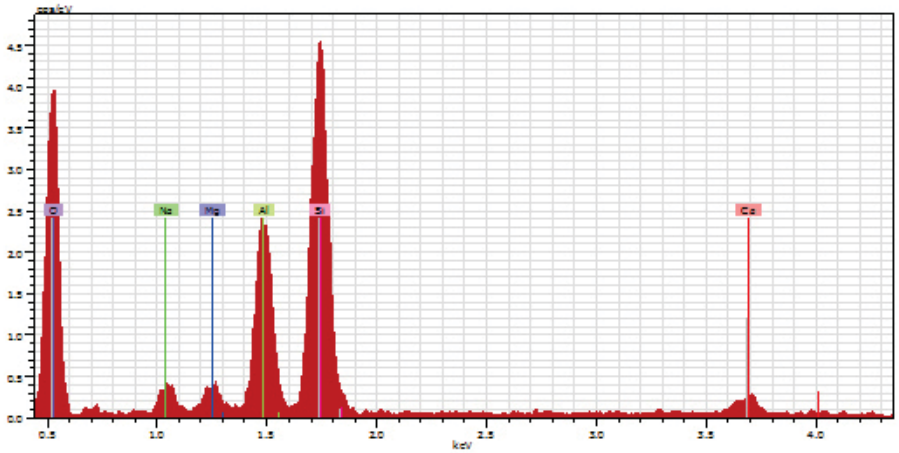


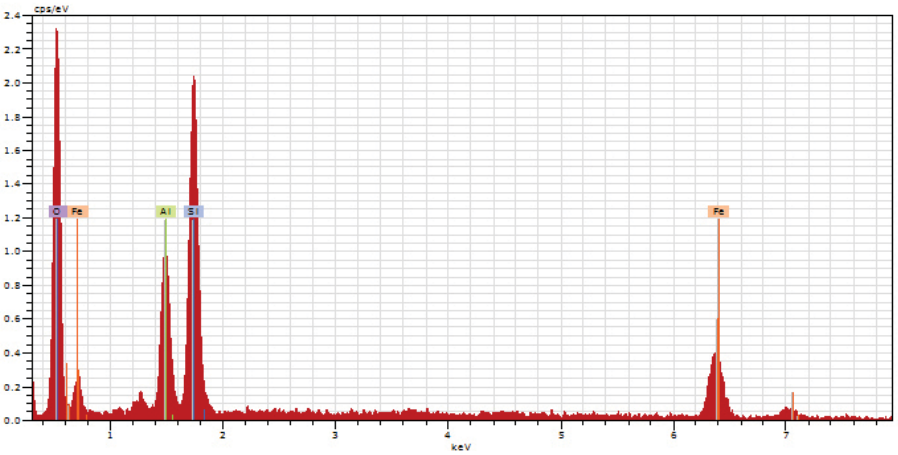
FIGURE 2
XRD diffractograms of Bt and Fe-Bt





Element	Wt. %
O	54,17
Si	26,81
Al	12,77
Na	2,66
Mg	1,93
Ca	1,67

A)



Element	Wt. %
O	44,76
Si	23,68
Fe	20,28
Al	11,27

B)

FIGURE 3
SEM/EDS analysis of a) Bt, b) Fe-Bt

Fig. 3 shows the morphology of the Bt and Fe-Bt samples. The structure of clay before impregnation is layered (Fig. 3a), with thin and thick slices that occur in the form of crystals with a fluffy appearance and pores of different sizes and shapes. After modification, there is an obvious increase in the number of pores and reduction in their radius (Fig. 3b). In addition, the presence of tiny iron aggregates can be observed. EDS analysis shows that O, Si, Al, Na, Mg and Ca are constitutive elements of Bt, with the most predominant being O, Si and Al, which are included in the composition of the clay layers. The impregnation process resulted in the replacement of the interlayer Na, Mg and Ca with Fe ions.

TABLE 2
Estimated regression coefficients

Term	Estimate	SE	*t* Stat	*P* Value
1	–187.879	39.812	–4.719	1.718×10^{-5}
x_1	–2.204	1.610	–1.369	0.177
x_2	–108.299	35.136	–3.082	0.003
x_3	236.191	23.530	10.038	5.995×10^{-14}
x_1x_2	2.691	0.920	2.924	0.005
x_1x_3	0.244	0.341	0.716	0.477
x_2x_3	17.644	7.664	2.302	0.025
x_1^2	–0.011	0.060	–0.182	0.856
x_2^2	21.773	27.174	0.801	0.426
x_3^2	–45.631	3.553	–12.845	4.743×10^{-13}

TABLE 3
ANOVA (quadratic model)

	DF	Sum of Squares	Mean Square	*F* Value	*P* Value
Model	9	61977.30	6886.36	136.41	0.00
Error	54	2726.02	50.48		
Total	63	64703.30			

Optimization of the Fenton reaction. The relationship between operating variables (H_2O_2 concentration, catalyst loading and pH) and the decolourization efficiency is described by a second-order polynomial model, so the experimental data were fitted with a quadratic polynomial function, where *Y* is the percentage of decolourization efficiency and x_1, x_2, x_3 are values of the H_2O_2 concentration, catalyst loading and pH, respectively (eq. 4):

$$Y=-187.879-2.20356\ x_1-0.0109948\ x_1^2-108.299\ x_2+2.69051\ x_1x_2+21.7729\ x_2^2+236.191\ x^3+0.244366\ x_1x_3+17.6441\ x_2x_3-45.6312\ x_3^2 \quad (4)$$

The adequacy and statistical significance of this quadratic model were analysed by analysis of variance (ANOVA) given in Tables 2 and 3.

High values of the coefficient of determination R^2 = 0.957869 and adjusted R^2 = 0.950847 and *P* value 0 indicate the statistical significance of the regression equation (3) and imply that this quadratic model fitted the experimental data well.

Diagnostic plots such as predicted versus actual values of decolourization efficiency, presented in Fig. 4, confirm the good agreement between actual and predicted values and point out that the quadratic model is appropriate. In addition, high values of R^2 and adjusted R^2 express a high correlation between the experimental data and data obtained from the model.

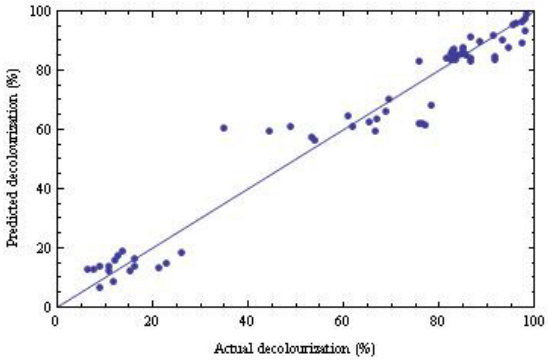


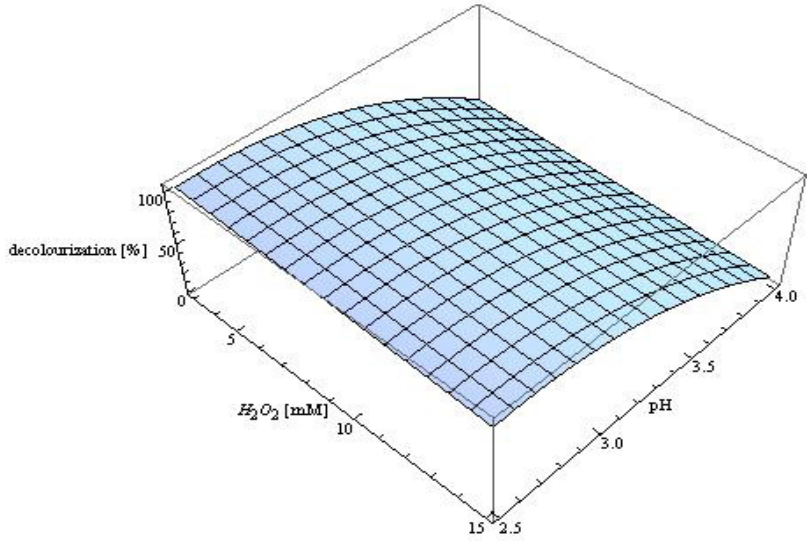
FIGURE 4
A comparison between the predicted values of decolourization efficiency and the experimental data

The interaction effects of the operating variables on the response were studied using response surface 3-D plots. The results indicate that the greatest impact on dye decolourization is the pH of the solution (Fig. 5a and 5b). The highest per cent of dye removal, 99.1% and 98.3% were obtained at pH ≤ 3. With increasing pH, there was a sharp decrease in the RB4 decolourization because of hydrolysis and precipitation processes of Fe(III) on the surface of the catalyst and a lower rate of HO• formation [52, 54–56]. In addition, as is evident from Fig. 4a, the RB4 removal rate is slightly decreased when H_2O_2 concentration increases from the minimum applied (3 mM). Higher H_2O_2 concentrations lead to scavenging of •OH [57–59], which results in a series of chain radical–radical or H_2O_2–radical reactions.

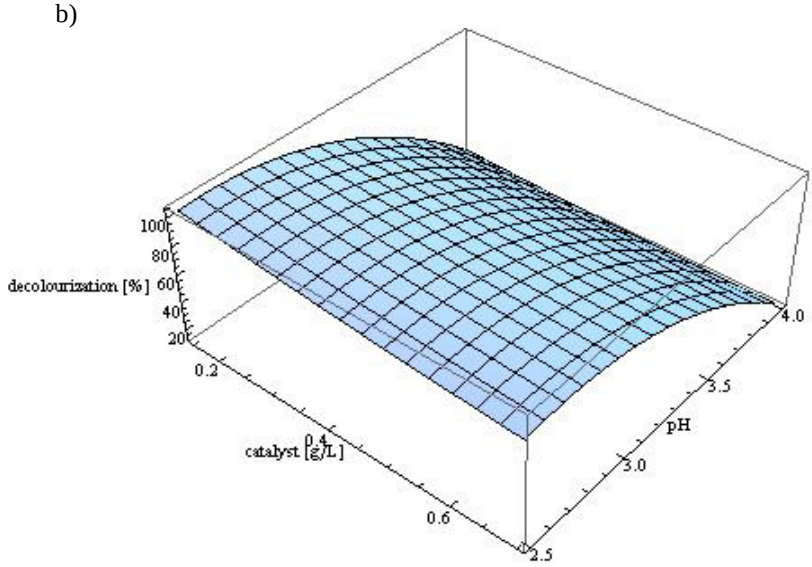
Fig. 5c shows the decolourization efficiency as a function of catalyst loading and H_2O_2 concentration at initial pH 2.5. Decolourization can occur through adsorption, catalytic reaction or both processes. To determine the influence of the adsorption processes on dye removal, experiments without H_2O_2 were carried out. Bt as a catalyst support has a low decolourization capacity (7.4%) in contrast to the Fe-Bt (23.6%) within 120 min of reaction. The reason for that is probably the larger surface area and pore volume of Fe-Bt (Table 1) [44].

The highest efficiency of RB4 removal is achieved at a minimum amount of added catalyst (0.15 g L^{-1}) and minimum initial concentration of H_2O_2 (3 mM). This is probably due to the good dispersion of a very small amount of Fe-Bt catalyst in the reaction medium making available all active sites on the catalyst for the adsorption and degradation of dye molecules [60]. Another reason for the limiting addition of catalyst above the optimum range might be consumption of •OH generated by the excess catalyst.

a)



b)



c)

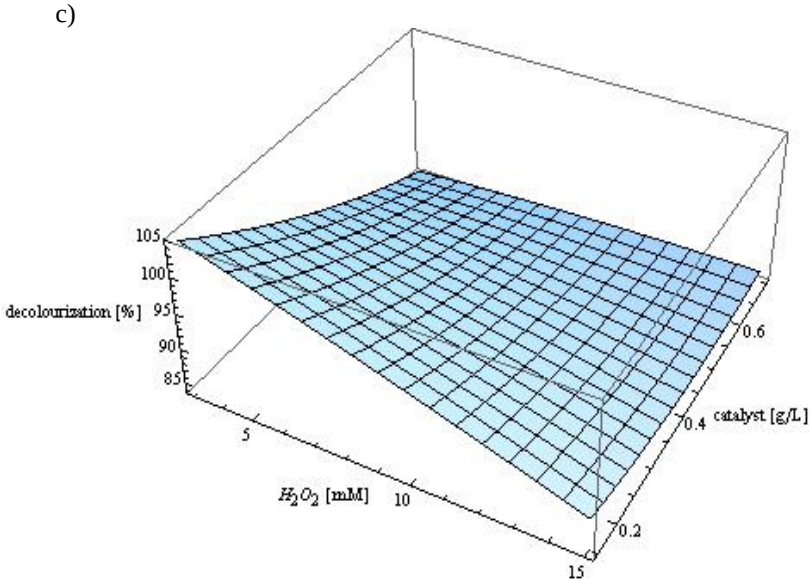


FIGURE 5
Effect of catalyst loading, H_2O_2 concentration and pH on decolourization efficiency: a) catalyst loading = 0.15 g L^{-1}; b) [H_2O_2] = 3 mM; c) pH = 2.5

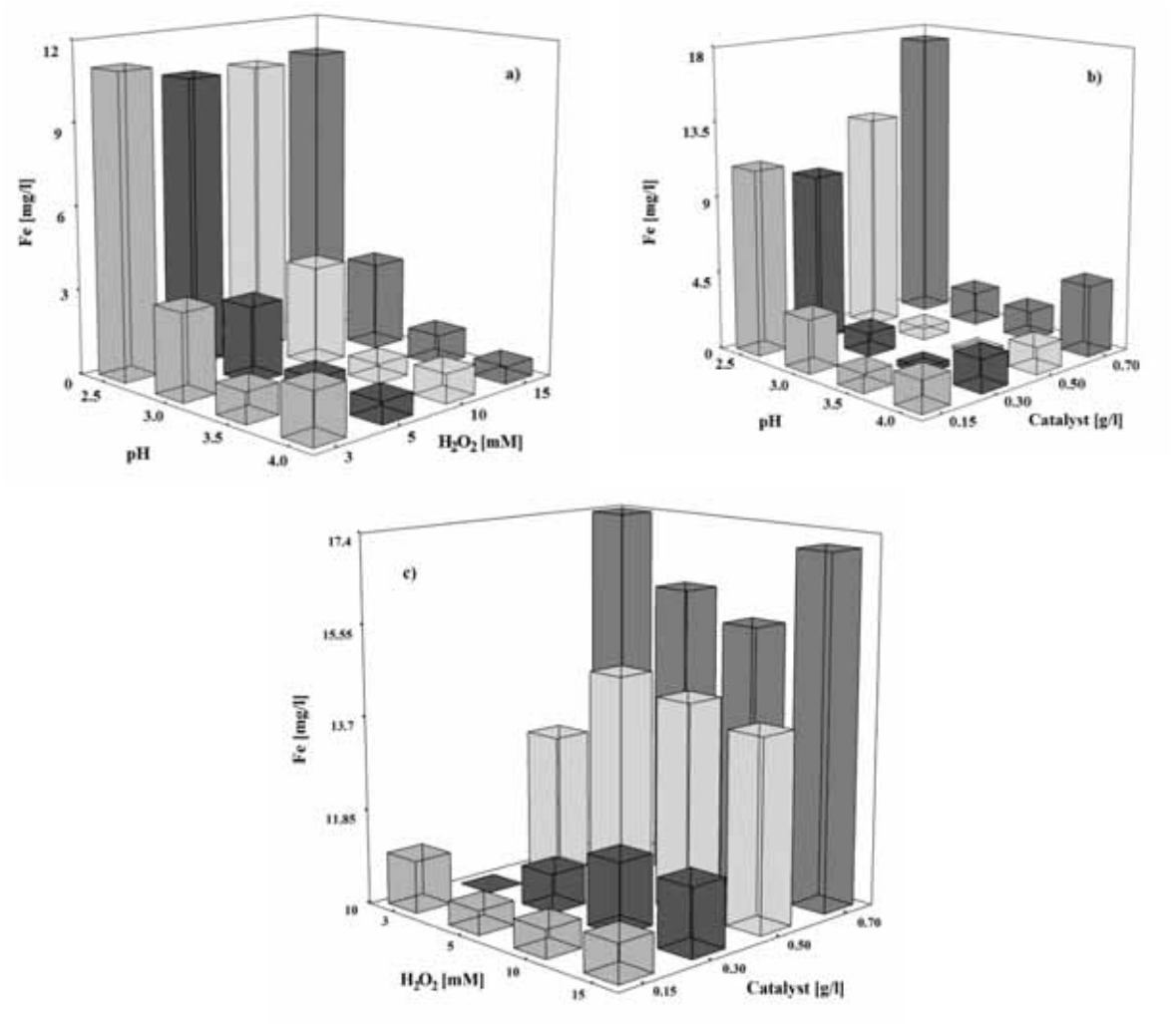


FIGURE 6
Effect of catalyst loading, H_2O_2 concentration and pH on iron leaching: a) catalyst loading=0.15 g L^{-1}; b) [H_2O_2] = 3 mM; c) pH = 2.5

Stability and reusability of the catalyst. Leaching tests of iron species from Fe-Bt catalyst during Fenton degradation of RB4 were performed to determine the stability of the catalyst. Fig. 6 shows the iron concentration dissolved in the aqueous solution after 120 min of reaction under different process conditions.

It is clear that dissolution of iron is more significant at pH 2.5 and with higher catalyst load (Fig. 6a and 6b). With the addition of 0.7 g L^{-1} of the catalyst in the solution, measured iron content was even 17.9 mg L^{-1} at the end of the reaction. Fig 6c illustrates the effect of initial H_2O_2 concentration and catalyst load upon Fe leaching. The change of Fe content in the reaction solution with the catalyst concentration up to 0.3 g L^{-1} is almost negligible for all initial H_2O_2 concentration. However, at higher concentrations of Fe-Bt and H_2O_2, leaching of Fe is increased. Therefore, it can be concluded that leaching of catalyst active species proceeds by a more complex mechanism than through a simple dissolution mediated by the acidic nature of aqueous solutions [61]. On the other hand, the leaching levels of metal are less than or equal to 0.3 ppm at pH > 2.5, which is an allowed value by national legislation for wastewater discharge into recipients [62]. In this condition, the concentration of dissolved iron in the solution is below 5% concerning the initial iron content in the catalyst.

Although the highest percentage of decolourization was achieved at pH 2.5, the stability of Fe-Bt was considered for the definition of the treatment optimum conditions. So, further experiments were done at the following conditions: pH = 3, minimum applied Fe-Bt load (0.15 g L^{-1}) and initial H_2O_2 (3 mM).

Possibility of catalyst reuse. The Fe-Bt catalyst was used for RB4 degradation in five consecutive runs. Between each run, the catalyst was separated from the solution by filtration, washed with deionized water, dried for 24 h at 100 °C and calcinated at 350 °C for 2 h. As seen in Fig. 7, catalytic activity slowly decreases to 92% after the fifth run.

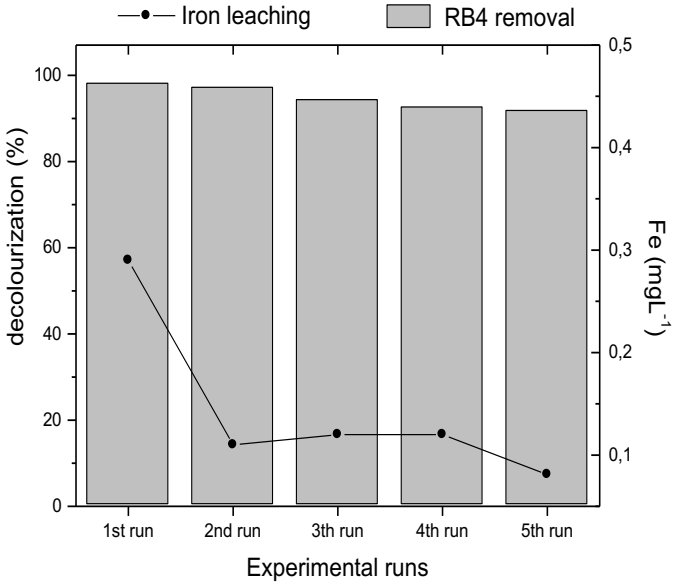


FIGURE 7
The decolourization efficiency and iron leaching after five successive runs

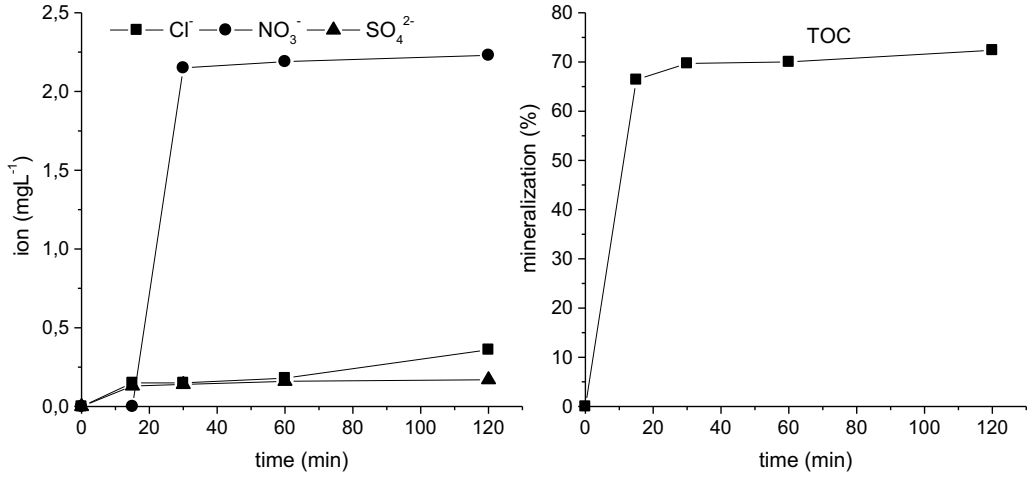


FIGURE 8
Mineralization of RB4: a) chloride, nitrate and sulfate ion concentrations; b) TOC removal efficiency

The content of leached iron is significantly lower and remains almost the same after the second cycle, and even decreases after the fifth run. Alwash et al. [63] have found the reason for this in the influence of the calcination step on material after each reuse run. Namely, calcination will enhance the stability of the remaining ions on the surface of the catalyst, thus reducing the leaching of Fe(III) from the surface of the catalyst and in this way maintaining the activity of the catalyst. Based on these results, the catalyst could be successfully reused five times.

Assessment of RB4 mineralization, degradation products and ion concentrations. The percentage of mineralization (TOC removal) after 15 min reaction was 66.4% and then increased gradually until the end of the reaction time, as shown in Fig. 8b (72%). Complete mineralization of the dye was not achieved, although UV-vis spectra (Fig. 9) indicated that almost no RB4 was present in the solution after 30 min of the Fenton process. This difference is due to the formation of persistent intermediate compounds, which are difficult to degrade.

SO_4^{2-} and Cl^- ions have a slightly rising trend in the solution from the beginning and onwards over time of the reaction (Fig. 8a). However, this trend of sulfate and chloride ion concentration in water solution indicates that desulfurization and dechlorination were not early stages of RB4 degradation. In contrast to that, nitrate ion concentration rapidly increased after 15 min of the beginning of the experiment and

remained almost stable to the end of reaction, which refers to the entire cleavage of the substituted triazine group [64]. Nitrite ion was not detected.

UV-vis absorption spectra of the dye solution were recorded to investigate the structural change of RB4 during reaction. Fig. 9 shows a comparison of the UV-vis spectra of the initial dye solutions and after the Fenton oxidation process with Fe-Bt. For the initial dye solution, absorption peaks at 594.78 nm, 370 nm and 296 nm are noted as characteristic of the anthraquinone group and the peak at 256 nm, which can be attributed to the aromatic structure of the dye and chlorotriazine group. As can be observed, peak intensities at all wavelengths significantly decrease after 30 min reaction time, extending anthraquinone and aromatic fragmentation of RB4 dye.

Intermediate organic degradation compounds of RB4 dye detected by GC/MS are summarized in Table 4.

The change in the RB4 structure is evident and the main identified compounds belong to the following groups: phenols, linear hydrocarbons, chlorinated hydrocarbons, organic acids, cyclic hydrocarbons, organic nitrogen compounds, phthalates and polycyclic aromatic hydrocarbons. Some of the compounds were detected by Gözmen et al. [65] (proposed reaction pathway A) after oxidative degradation of RB4 dye by wet air oxidation and wet peroxide oxidation, and these results confirm the authors' conclusions that hydrogen peroxide radicals attack the N-positions of RB4 molecules. Triazine groups were not identified after 120 min, which is consistent with the earlier assumption of their degradation at the beginning of the reaction.

Acute toxicity of effluent. An examination of the environmental impact of the Fenton process effluent can be performed by using bioluminescence inhibition assays. In this work, *V. fischeri* was used as a high sensitivity, fast (up to 30 minutes) and low-cost indicator of acute toxicity [66, 67]. The tests of inhibitory effect were conducted in the following water samples, (1) RB4 solution (50 mg L^{-1}), (2) Fe-Bt in deionized water at pH 3 and (3) effluent after Fenton oxidation. The results are presented in Figure 10, and as can be seen, the dye solution had a 13.21% and used catalyst in deionized water 25.58% inhibitory effect of the *V. fischeri* bacterium. After the Fenton process, the obtained toxicity value of the effluent rose to 97.41%. In their study, Lopez-Lopez et al. [68] have concluded that the toxicity of the effluent increases with the addition of H_2O_2, as an oxidant. Najjar et al. [69] evaluated acute toxicity of tyrosol solution after the heterogeneous Fenton process, where after 120 min of reaction comes the formation of phenolic by-products, which cause high inhibition effect, and as the reaction proceeded the toxicity decreased. A significant toxicity value in the sample after the Fenton process can be related to the results of GC/MS analysis, where the main detected compounds were phenolic, cyclic and polycyclic hydrocarbons, long-chain hydrocarbons and compounds containing Cl and N atoms [66, 70, 71].

CONCLUSION

The present work reports the efficiency of the heterogeneous Fenton process in degradation of RB4 synthetic aqueous solutions using the clay mineral bentonite impregnated with Fe polycations as a catalyst (Fe-Bt). It has been shown that use of Fenton chemistry in combination with Fe-Bt increased the decolourization of RB4 significantly. The advanced Fenton oxidation process is favoured under acidic condition and sensitive to the solution pH and the catalyst concentration, but an increase in H_2O_2 concentration decreases the extent of RB4 decolourization. The catalyst reusability study confirmed that the percentage of decolourization is still significant after the fifth run. However, the analysis of mineralization and also evaluation of the level of acute toxicity on the *Vibrio fischeri* bacterium indicated there has not been a complete degradation of RB4 dye, which may be the result of the short reaction time.

TABLE 4
GC/MS analyses of main degradation products

Retention time (min)	Intermediate	Formula
6.5	Phenol, *m-tert*-butyl-	$C_{10}H_{14}O$
8.2	Tetrachloroethylene	C_2Cl_4
8.8	Benzoic acid, *p-tert*-butyl-	$C_{11}H_{14}O_2$
12.1	Benzene, 1,3-diethyl-	$C_{10}H_{14}$
14.7	Pyridine, 5-ethenyl-2-methyl-	C_8H_9N
19.6	Dibutyl phthalate	$C_{16}H_{22}O_4$
20.1	9,10-Anthracenedione	$C_{14}H_8O_2$
21.0	Tridecane	$C_{13}H_{28}$
23.7	Dodecane	$C_{12}H_{26}$

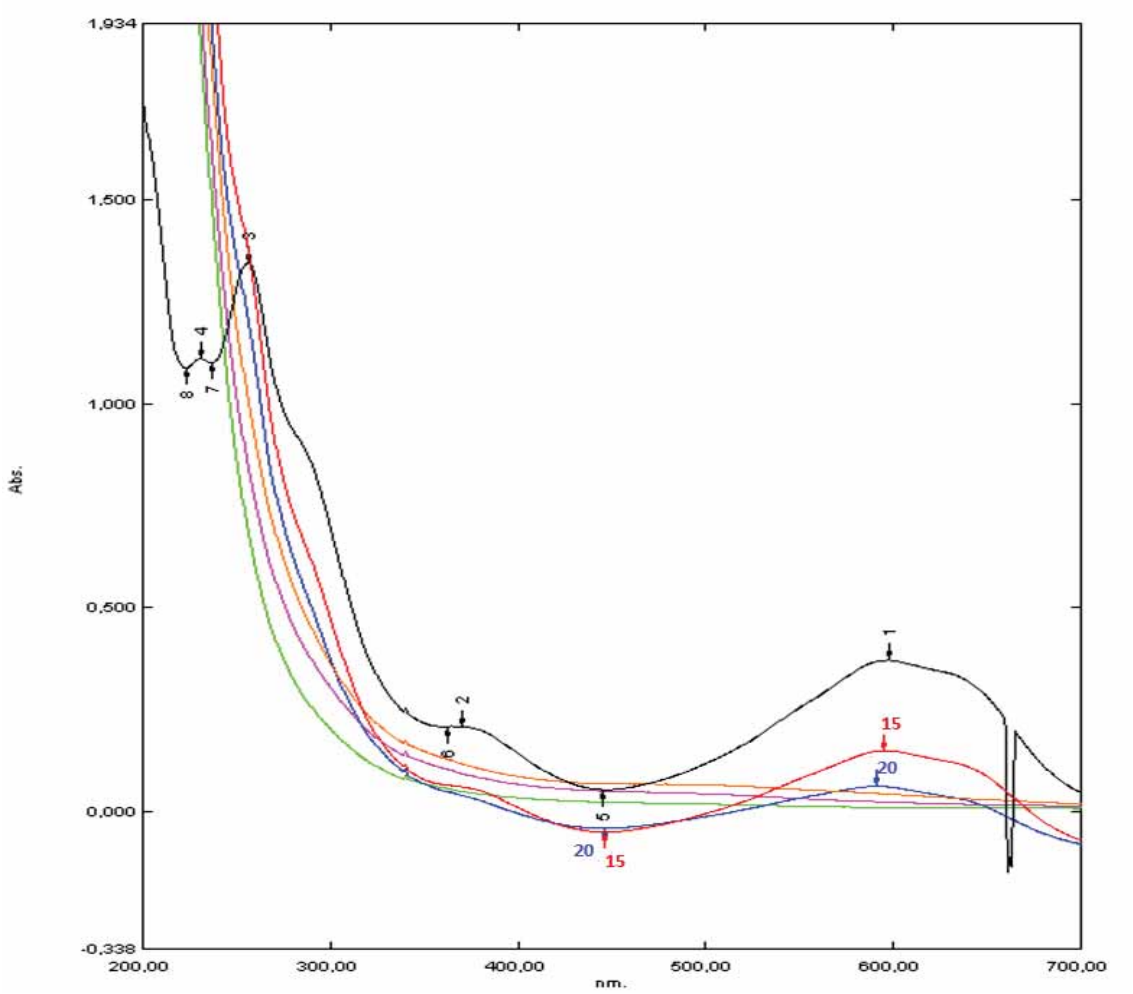


FIGURE 9
UV-vis spectra of an RB4 dye solution during reaction

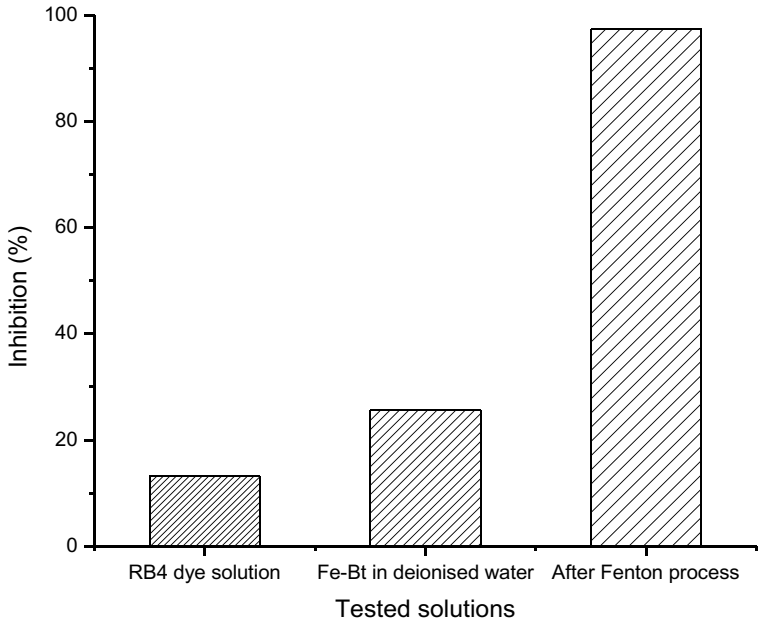


FIGURE 10
Inhibitory effect of different test solutions on *V. fischeri* bacterium

ACKNOWLEDGEMENTS

The research was funded by the Ministry of Education, Science and Technological Development (Project III_{43005} and TR_{37004}). The authors are grateful to the BioSense Institute (Novi Sad, Serbia) for conducting of analysis on SEM/EDS instrument and also Dr. Goran Kitić for kind support and assistance during the use and processing of data. Also, Bentoproduct (Šipovo, Bosnia and Herzegovina)

REFERENCES

[1] Veli, S., Öztürk, T. (2005) Kinetic modeling of adsorption of reactive azo dye on powdered activated carbon and pumice. Fresen. Environ. Bull.14(3), 212-218.

[2] Rahmani, A., Barjasteh Askari, F., Samadi, M.T., Asgari, Gh. (2012) Degradation of reactive red 198 dye by catalytic ozonation using pumice and copper coated pumice. Fresen. Environ. Bull. 21(9), 2810-2817.

[3] Kasikovic, N., Novakovic, D., Vladic, G., Klancnik, M. (2011) Influence Of Heat Treathment On Caracteristics Of Inkjet Prints On Textile Material. Journal of Graphic Engineering and Design. 2, 24-30.

[4] King, D. (2007) Dyeing of cotton and cotton products. In: Gordon, S. and Hsieh, Y.L. (Eds.) Cotton: Science and Technology, Woodhead Publishing, Cambridge. 353-377.

[5] Bhuiyan, M.A.R., Shaid, A., Bashar, M.M., Haque, P, Hannan, M.A. (2013) A Novel Approach of Dyeing Jute Fiber with Reactive Dye after Treating with Chitosan. Open Journal of Organic Polymer Materials. 3, 87-91.

[6] Lewis, D.M., Rippon, J.A. (2013) Dyeing wool blends, The Coloration of Wool and Other Keratin Fibres, John Wiley & Sons, Inc., New Jersey.

[7] Hunger, K. (2003) Industrial Dyes: Chemistry, Properties, Applications, LEY-VCH Verlag GmbH & Co. GaA, Weinheim.

[8] Kyzas, G.Z., Kostas, J.F., Matis, A. (2013) The Change from Past to Future for Adsorbent Materials in Treatment of Dyeing Wastewaters. Materials. 6, 5131-5158.

[9] Lewis, D.M. (2014) Developments in the chemistry of reactive dyes and their application processes. Coloration Technology. 130, 382-412.

[10] Levec, J., Pintar, A. (2007) Catalytic wet-air oxidation processes: A review. Catalysis Today. 124, 172-184.

[11] EC (European Commision) (2003) Integrated Pollution Prevention and Control (IPPC), Reference Document on Best Available Techniques for the Textiles Industry.

[12] Chiou, M.S., Li, H.Y. (2003) Adsorption behavior of reactive dye in aqueous solution on chemical cross-linked chitosan beads. Chemosphere. 50, 1095-1105.

[13] Konsowa, A.H. (2003) Decolorization of wastewater containing direct dye by ozonation in a batch bubble column reactor. Desalination. 158, 233-240.

[14] Libra, J.A., Sosath, F. (2003) Combination of biological and chemical processes for the treatment of textile wastewater containing reactive dyes. Journal of Chemical Technology and Biotechnology. 78, 1149-1156.

[15] Kim, T.H., Park, C., Yang, J., Kim, S. (2004) Comparison of disperse and reactive dye removals by chemical coagulation and Fenton oxidation. Journal of Hazardous Materials. 112, 95-103.

[16] Rajkumar, D., Kim, J.G. (2006) Oxidation of various reactive dyes with in situ electro-generated active chlorine for textile dyeing industry wastewater treatment. Journal of Hazardous Materials. 136, 203-212.

[17] Arslan-Alaton, I., Kabdas, I., Hanbaba, D., Kuybu, E. (2008) Electrocoagulation of a real reactive dye bath effluent using aluminum and stainless steel electrodes. Journal of Hazardous Materials. 150, 166-173.

[18] Alventosa-deLara, E., Barredo-Damas, S., Alcaina-Miranda, M.I., Iborra-Clar, M.I. (2012) Ultrafiltration technology with a ceramic membrane for reactive dye removal: Optimization of membrane performance. Journal of Hazardous Materials. 209-210, 492-500.

[19] Assadi, A., Nateghi, R., Bonyadinejad, G.R., Amin, M.M. (2013) Application of coagulation process reactive blue 19 dye removal from textile industry wastewater. Internationa Journal of Environmental Health Engineering. 2, 5.

[20] Greluk, M., Hubicki, Z. (2013) Evaluation of polystyrene anion exchange resin for removal of reactive dyes from aqueous solutions. Chemical Engineering Research and Design. 91, 1343-1351.

[21] Shokri, A., Salimi, M., Abmatin, T. (2017) Employing Photo Fenton and UV/ZnO processes for removing Reactive Red 175 from aqueous environment. Fresen. Environ. Bull. 26(2a), 1560-1565.

[22] Shokri, A., Mahanpoor, K., Soodbar, D. (2016) Degradation of 2-nitrophenol from petrochemical wastewater by UV/NiFe2O4/ clinoptilolite process. Fresen. Environ. Bull. 25(2), 500-508.

[23] Gao, A., Peng, Z., Wang, W., Li, F. (2017) Online monitoring of decolorization kinetics of reactive yellow B-4RFN in Fenton process. Fresen. Environ. Bull. 26(5), 3415-3421.

[24] Ayas N., Asci Y., Yurdakul M. (2016) Using of Fe/ZrO_2 catalyst to remove direct orange 26 from water by Fenton oxidation at wide pH values. Fresen. Environ. Bull. 25(8), 3272- 3279.
[25] Buyukada, M., Evrendilek, F. (2016) Modeling ultrasound-assisted decolorization efficiency of reactive blue 19 and reactive yellow 145 from aqueous solutions by cottonseed cake. Fresen. Environ. Bull. 25 (3), 692-705.
[26] Cao, Z., Zhang, J., Zhou, J., Ruan, X., Chen, D., Liu, J., Qian, G. (2017) Electroplating sludge derived zinc-ferrite catalyst for the efficient of dye. Journal of Environmental Management. 193, 146-153.
[27] Chen, S., Wu, Y., Li, G., Wu, J., Meng, G., Guo, X., Liu, Z. (2017) A novel strategy for preparation of an effective and stable heterogeneous photo-Fenton catalyst for the degradation of dye. Applied Clay Science. 136, 103-111.
[28] Fida, H., Zhang, G., Guo, S., Naeem, A. (2017) Heterogeneous Fenton degradation of organic dyes in batch and fixed bed using La-Fe montmorillonite as catalyst. Journal of Colloid and Interface Science. 490, 859–868.
[29] Sun, L., Yao, Y., Wang, L., Mao, Y., Huang, Z., Yao, D., Lu, W., Chen, W. (2014) Efficient removal of dyes using activated carbon fibers coupled with 8-hydroxyquinoline ferric as a reusable Fenton-like catalyst. Chemical Engineering Journal. 240, 413-419.
[30] Gumy, D., Fernandez-Ibanez, P., Malato, S., Pulgarin, C., Enea, O., Kiwi, J. (2005) Supported Fe/C and Fe/Nafion/C catalysts for the photo-Fenton degradation of Orange II under solar irradiation. Catalysis Today. 101, 375-382.
[31] Gan, P.P., Li, S.F.Y. (2013) Efficient removal of Rhodamine B using a rice hull-based silica supported iron catalyst by Fenton-like process. Chemical Engineering Journal. 229, 351-363.
[32] Feng, J., Hu, X., Yue, P.L. (2005) Discoloration and mineralization od Orange II by using a Bttonite clay-based Fe nanocomposite film as a heterogenous photo-Fenton catalyst. Water Research. 39, 89-96.
[33] Iurascu, B., Siminiceanu, I., Vione, D., Vicente, M.A., Gil, A. (2009) Phenol degradation in water through a heterogeneous photo-Fenton process catalyzed by Fe-treated laponite. Water Research. 43, 1313-1322.
[34] Garrido-Ramirez, E.G., Theng, B.K.T., Mora, M.L. (2010) Clays and oxide minerals as catalysts and nanocatalysts in Fenton-like reastions - A review. Applied Clay Science. 47, 182-192.
[35] Xu, T., Liu, Y., Ge, F., Liu, L., Ouang, Y. (2013) Application of response surface methodology for optimization of azorcamine B removal by heterogeneous photo-Fenton process. Applied Surface Science. 280, 926–932.
[36] Kerkez, Dj., Tomasevic, D., Kozma, G., Becelic-Tomin, M., Prica, M., Roncevic, S., Kukovecz, A., Dalmacija, B., Konya, Z. (2014) Three different clay-supported nanoscale zero-valent iron materials for industrial azo dye degradation: A comparative study. Journal of the Taiwan Institute of Chemical Engineers. 45(5), 2451-2461.
[37] da Silva Leite, L., de Souza Maselli, B., de Arag~ao Umbuzeiro, G., Pupo Nogueira, R.F. (2016) Monitoring ecotoxicity of disperse red 1 dye during photo-Fenton degradation. Chemosphere. 148, 511-517.
[38] Wang, N., Zheng, T., Zhang, G., Wang, P. (2016) A review on Fenton-like processes for organic wastewater treatment. Journal of Environmental Chemical Engineering. 4, 762-787.
[39] Behbahani, M., Alavi Moghaddam, M.R., Arami, M. (2011) Techno-economical evaluation of fluoride removal by electrocoagulation process: optimization through response surface methodology. Desalination. 271, 209-218.
[40] Chung, Y.T., Ng, L.N., Mohammad, A.W. (2014) Sulfonated-polysulfone membrane surface modification by employing methacrylic acid through UV-grafting: optimization through response surface methodology approach, Journal of Industrial and Engineering Chemistry. 20, 1549-1557.
[41] Elksibi, I., Haddar, W., Ticha, M.B., Gharbi, R., Mhenni, M. (2014) Development and optimization of a non conventional extraction process of natural dye from olive solid waste using response surface methodology (RSM). Food Chemistry. 161, 345-352.
[42] Trovo, A.G., Pupo Nogueira, R.F., Agüera, A., Fernandez-Alba, A.R., Malato, S. (2011) Degradation of the antibiotic amoxicillin by photo-Fenton process – Chemical and toxicological assessment, Water Research. 45, 1394-1402.
[43] Su, H., Zeng, S., Doing, H., Zhang, Y., Hu, R. (2009) Pillared montmorillonite supported cobalt catalysts for the Fisher-Tropsch. Applied Clay Science. 46, 325-329.
[44] Hou, M.F., Ma, C.X., Zhang, W.D., Tang, X.Y., Fan, Y.N., Wan, H.F. (2011) Removal of rhodamine B using iron pillared Bentonite. Journal of Hazardous Materials. 186, 1118-1123.
[45] Ayodele, O.D., Togunwa, O.S. (2014) Catalityc activity of copper modified Bttonite supported ferrioxalate on the aqueous degradation and kinetics of mineralization of Direct Blue 71, Acid Green 25 and Reactive Blue 4 in photo-Fenton process. Applied Catalysis A: General. 470, 285-293.
[46] Feng, J.Y., Hu, X.J., Yue, P.L. (2004) Discoloration and mineralization of orange II using different heterogeneous catalysts containing Fe: a comparative study. Environmental Science and Technology. 38, 5773–5778.

[47] Medejova, J. (2003) FTIR Techniques in clay mineral studies. Vibrational Spectroscopy. 31, 1-10.
[48] Patel, H.A., Somani, R.S., Bajaj, H.C., Jasra, R.V. (2007) Preparation and characterization of phosphonium montmorillonite with enhanced thermal stability. Applied Clay Science. 35, 194-200.
[49] Joshi, G.V., Kevadiya, B.D., Patel, H.A., Bajaj, H.C., Jasra, R.V. (2009) Montmorillonite as a drug delivery system: Intercalation and in vitro release of timolol maleate. International Journal of Pharmaceutics. 374, 53-57.
[50] Adams, S., Fordio, D. (2001) Monitoring of deposited particles in cultural properties the influence of visitors. Atmospheric Environment. 35, 4073-4080.
[51] Ndukwe, N.A., Jenmi, F.O. (2008) Effects of Vehicular Exhaust Fumes on urban Air Pollution in Lagos metropolis. Pollution Research. 27, 539-543.
[52] Herney Ramirez, J., Costa, C.A., Madeira, L.M., Mata, G., Vicente, M.A., Rojas-Cervantes, M.L., Lopez-Peinado, A.J., Martin-Aranda, R.M. (2007) Fenton-like oxidation of Orange II solutions using heterogeneous catalysts based on saponite clay. Applied Catalysis B: Environmental. 71, 44-56.
[53] Cotica, L.F., Freitas, V.F., Santos, L.A., Barabach, M., Anaissi, F.J., Miyahara, R.Y., Sarvezuk, P.W.C. (2011) Cobalt-modified Brazilian Bttonites: Preparation, characterisation nad thermal stability. Applied Clay Science. 51, 187-191.
[54] Bang, J.H., Suslick, K.S. (2010) Applications of Ultrasound to the Synthesis of Nanostructured Materials. Advanced Materials. 22, 1039-1059.
[55] Babuponnusami, A., Muthukumar, K. (2014) A review on Fenton and improvements to the Fenton process for wastewater treatment. Journal of Environmental Chemical Engineering. 2, 557-572.
[56] Shimizu, A., Tokumura, M., Nakajima, K., Kawase, Y. (2012) Phenol removal using zero-valent iron powder in the presence of dissolved oxygen: roles of decomposition by the Fenton reaction and adsorption/precipitation. Journal of Hazardous Materials. 201-202, 60-67.
[57] Behnajady, M.A., Modirshahla, N., Ghanbary, F. (2007) A kinetic model for the decolorization of C.I. Acid Yellow 23 by Fenton process. Journal of Hazardous Materials. 148, 98-102.
[58] Chen, Q., Wu, P., Li, Y., Zhu, N., Dang, Z. (2009) Heterogenous photo-Fenton photodegradation of reactive brilliant orange X-GN over iron-pillared montmorillonite under visible light. Journal of Hazardous Materials. 168, 901-908.
[59] Nidheesh, P., Gandhimathi, R., Ramesh, S.T. (2013) Degradation of dyes from aqueous solution by Fenton processes: a review. Environmental Science and Pollution Research. 20, 2099-2132.
[60] Zhu, M., Meng, D., Wang, C., Di, J., Diao, G. (2013) Degradation of methylene blue with H_2O_2 over a cupric oxide nanosheet catalyst. Chinese Journal of Catalysis. 34, 2125-2129.
[61] Sotelo, J.L., Ovejero G., Martınez F., Melero J.A., Milieni A. (2004) Catalytic wet peroxide oxidation of phenolic solutions over a LaTi1−x CuxO3 perovskite catalyst. Applied Catalysis B: Environmental. 47, 281-294.
[62] Official Gazette of RS, No. 67/2011, 48/2012. Regulation on emission limit values in waters and deadlines for their achievement.
[63] Alwash, A.H., Abdullah, A.Z., Ismail, N. (2013) Elucidation of Reaction Behaviors in Sonocatalytic Decolorization of Amaranth Dye in Water Using Zeolite Y Co-Incorporated with Fe and TiO_2. Advances in Chemical Engineering and Science. 3, 113-122.
[64] Pacchade, K., Sandhya, S., Swaminathan, K. (2009) Ozonation of reactive dye, Procion red MX-5B catalyzed by metal ions. Journal of Hazardous Materials. 167, 313–318.
[65] Gözmen, B., Kayan, B., Gizir, A.M., Hesenov, A. (2009) Oxidative degradations of reactive blue 4 dye by different advanced oxidation methods. Journal of Hazardous Materials. 168, 129– 136.
[66] Parvez, S., Venkataraman, C., Mukherji, S. (2006) A review on advantages of imple-menting luminescence inhibition test (*Vibrio fischeri*) for acute toxicity prediction of chemicals. Environment International. 32, 265-268.
[67] Halmi, M.I.E., Kai, I.P.R., Johari, W.L.W., Shukor, M.Y. (2014) Toxicity assessment of bioluminescent rapid bioassays (*Vibrio fischeri*) on selected DBPs. Journal of Environmental Microbiology and Toxicology. 2, 47-52.
[68] Lopez-Lopez, C., Purswani, J., Martín-Pascual, J., Martínez-Toledo, M.V., Muñío, M.M., Poyatos, J.M. (2015) Toxic effect of H_2O_2 in H_2O_2/UV, photo-Fenton and heterogeneous photocatalysis (TiO_2/H_2O_2/UV) systems to treat textile wastewater. Desalination and Water Treatment. 56, 3044-3053.
[69] Najjar, W., Azabou, S., Sayadi, S., Ghorbel, A. (2007) Catalytic wet peroxide photo-oxidation of phenolic olive oil mill wastewater contaminants, Part I. Reactivity of tyrosol over (Al-Fe)PILC. 74. 11-18.
[70] Choi, K., Sweet, L.I., Meier, P.G., Kim, P.G. (2004) Aquatic toxicity of four alkylphenols (3.tert-butylphenol, 2-isopropylphenol, 3-isopropylphenol, and 4-isopropylphenol) and their binary mixtures to microbes, invertebrates, and fish. Environmental Toxicology. 19, 45-50.

[71] Verbruggen, E. M. J. (2012) Environmental risk limits for polycyclic aromatic hydrocarbons (PAHs): For direct aquatic, benthic, and terrestrial toxicity. RIVM report 607711007/2012; 1-339.

Received: **01.08.2017**
Accepted: **08.10.2017**

CORRESPONDING AUTHOR

Miljana Prica
University of Novi Sad,
Faculty of Technical Sciences,
Department of Graphic Engineering and Design, Trg Dositeja Obradovica 6, Novi Sad – Serbia

e-mail: miljana@uns.ac.rs

© by PSP Volume 26 – No. 12A/2017 pages 8199-8206 Fresenius Environmental Bulletin

CONTAMINATION ASSESSMENT OF HEAVY METALS IN STREET DUST OF CHENGDU, SW CHINA

Bin Zhang[1,2], Jiao Yue[1], Jia Deng[1], Xinqiang Ning[3,*], Yanhua Cai[2], Di Wu[1]

[1]School of Food and Biotechnology of Xihua University, Chengdu 610039, China
[2]Chongqing Key Laboratory of Environmental Materials and Remediation Technology, Chongqing University of Arts and Sciences, Chongqing 402160, China
[3]School of Civil Engineering, Sichuan University of Science and Engineering, Zigong 643000, China

ABSTRACT

Street dusts of different functional areas from Chengdu, SW China are analyzed for Cu, Pb, Zn, Mn, Co, Ni, Cr and Cd. The results show that, in comparison with the background values of Chengdu and Chinese soils, the mean concentrations of all heavy metals are all higher than their corresponding background values of Chengdu soil and Chinese soil except Co and the street dusts from seven functional areas have different cumulative characteristics. Meanwhile, the value of I_{geo}, *PI*, *IPI* and *RI* are calculated. The results indicate that the order of I_{geo} is Cd>Pb>Cu>Zn>Ni>Cr>Mn>Co and the I_{geo} of heavy metals in the dust from TD and ID is higher than in other functional areas. The high I_{geo} for Cu, Pb, Zn, Ni and Cd in street dusts indicate that there is a moderate or strong Cu, Pb, Zn, Ni and Cd pollution. I_{geo} for Mn, Co and Cr are less than 0, indicating that the urban environment was scarcely contaminated by Mn, Co and Cr. The assessment results of *PI* also support Cu, Pb, Zn, Ni and Cd in street dusts presented serious pollution, and *IPI* indicates heavy metals of street dust polluted seriously. the *RI* values of heavy metals indicate the heavy metals of street dusts are considerable ecological risk or very high ecological risk and Cu, Pb and Cd are the main contributors to the potential ecological risk, especially Cd.

KEYWORDS:
Street dust, Heavy metals, Contamination assessment.

INTRODUCTION

Street dust, particles deposited on a road, originates from the interaction of solid, liquid and gaseous materials produced from different sources [1]. The components and quantity of street dust are also potential pollution indicators for urban environment [2]. Street dusts receives various heavy metal inputs from a variety of mobile or stationary sources, such as vehicular traffic, industrial plants, power generation facilities, residential oil burning, waste incineration, city construction and demolition activities and the re-suspension of surrounding contaminated soils [3, 4], and these dusts make a significant contribution to metal pollution in the urban environment. Because of a lack of bioavailability, biodegradability and persistence, heavy metals could accumulate and be enriched in urban environment. A previous study found that the contamination contents (e.g., heavy metals and other toxic trace elements) of road/street dusts are generally higher than those in other media (e.g. soils) [5]. Moreover, heavy metals in street dusts could easily enter human bodies through dust ingestion, inhalation and dermal contact under dynamic conditions such as wind, traffic and other human activities [6, 7].

Elevated levels of heavy metals are ubiquitous in urban settings as the result of a wide range of human activities, especially from industrial sources [8]. As a consequence, adverse effects on human health may occur in urban environments, particularly in metropolitan cities where urbanization, industrialization and rapid population growth have been taking place on an unprecedented scale. Although numerous studies on heavy metal contamination of street dusts have been performed in developed countries [9-11], only limited information is available for developing countries, especially for China. Over the last three decades, urbanization and industrialization have taken place at an unprecedented pace in China. Urban environmental pollution has become a very important issue for environmental researchers [12-14]. Chengdu, one of the most crowded cities in the world, has experienced a rapid urbanization and industrialization in the last decades. The rapid growth of industry, population and vehicle exerts a heavy pressure on its urban environment. The main goals of this study were to 1) determine and compare the concentrations of the heavy metals in urban street dusts collected from different functional areas in the city of Chengdu 2) investigate the differences between geo-chemical background values and metal levels, and 3) to evaluate and assess heavy meals pollution in street dusts using the Geo-accumulation (I_{geo}) and Ecological risk (*RI*) indices as a tool for urban sanitation decision-making.

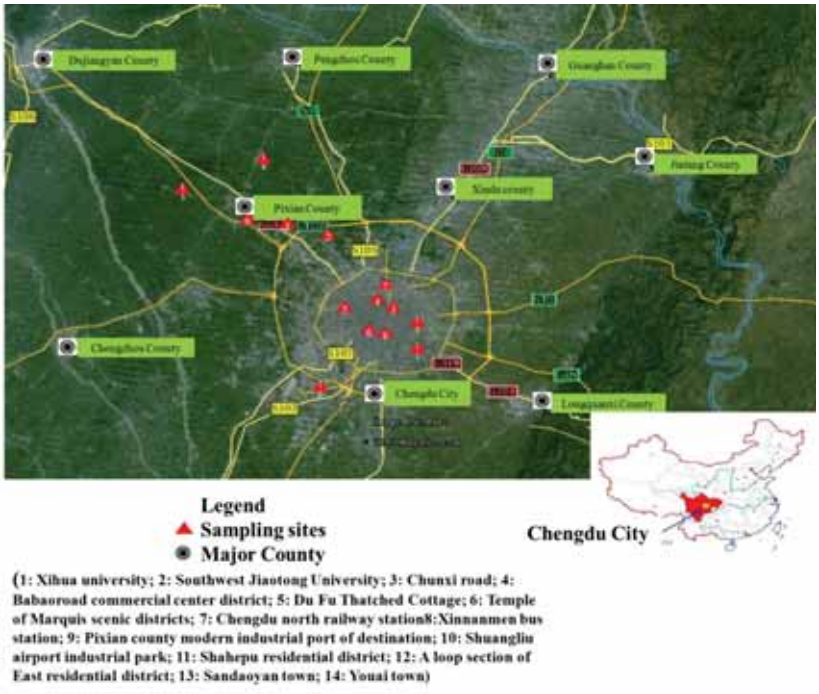


FIGURE 1
Location sketch of sampling sites

MATERIALS AND METHODS

Study area. Chengdu (30°05′-31°26′N, 102°54′-104°53′E), the capital of Sichuan province, is located in the southwest of China. Geomorphologically, it is high to the northwest and low to the southeast, not far from the western slopes of the Longmen Mountains. With a typical continental monsoon climate of northern temperate zone, there are four distinct seasons in Chengdu. The average temperature ranges from 5 °C in winter to 26 °C in summer. The average annual precipitation is 918 mm. Rainfall mainly concentrated from July to August. The least rainfall concentrated from December to March. In the present study, street dust samples were collected from various areas with different land uses (educational district, commercial district, scenic parks, traffic pivotal district, industrial district, residential district, and peri-urban district).

Sampling and analytical procedures. Although there was no strict functional classification in urban areas in Chengdu, forty-two samples were collected at different districts with different land use: Xihua university and Southwest Jiaotong University (educational district, abbreviation as ED, S1-S6), Chunxi road and Babaoroad commercial center district (commercial district, abbreviation as CD, S7-S12), Du Fu Thatched Cottage and Temple of Marquis scenic districts (scenic parks, abbreviation as SP, S13-S18), Chengdu north railway station and Xinnanmen bus station (traffic pivotal district, abbreviation as TD, S19-S24), Pixian county modern industrial port of destination and Shuangliu airport industrial park (industrial district, abbreviation as ID, S25-S30), Shahepu residential district and A loop section of East residential district (residential district, abbreviation as RD, S31-S36), and Sandaoyan town and Youai town (peri-urban district, abbreviation as PD, S37-S42) . Forty-two samples were collected on pavements next to roads at periods when no rain had occurred during the previous week in Chengdu. At every sampling site, more than 300 g of street dust composite sample was collected by sweeping using polyethylene brush and tray from three to five points of road/pavement edges within the scope of 10-20m^2. All the samples were stored in the sealed polyethylene bags, labeled and then transported to the laboratory. The samples were air-dried in the laboratory for 2 weeks. Dried samples were grinded by a porcelain mill and then passed through a 100-mesh sieve before analyzing. Sequential extraction was performed using a three-stage modified procedure recommended by BCR which has been used for several studies [14-16]. Detailed locations of sampling sites are shown in Figure 1.

Pollution assessment methodology of heavy metals in street dusts. Ecological risk (*RI*) [17] and geo-accumulation (I_{geo}) [18] indices are applied, which are established methodologies to assess the impact of heavy metals on the environment [19-21]. I_{geo} [18] is calculated as follows:

$$I_{geo}=Log_2[Cn/(1.5\times Bn)] \quad (1)$$

where *Cn* represents the measured concentration of

the element *n* and *Bn* is the geochemical background value of the element in fossil argillaceous sediment (average shale). In the study, *Bn* is the background content of element n in Chinese soil [22]. The constant 1.5 is introduced to minimize the effect of possible variations in the background values which may be attributed to lithologic variations in the sediments. The following classification is given for geo-accumulation index [18]: <0= practically unpolluted, 0-1= unpolluted to moderately polluted, 1-2= moderately polluted, 2-3= moderately to strongly polluted, 3-4= strongly polluted, 4-5= strongly to extremely polluted and >5 = extremely polluted.

Pollution index (*PI*) and integrated pollution index (*IPI*) are also commonly used to assess the environment quality [23]. The *PI* is defined as the ratio of element concentration in the study to the background content of the corresponding element of Chinese soil [22]. The *PI* of each element is calculated and classified as either low ($PI \leq 1$), middle ($1 < PI \leq 3$) or high ($PI > 3$). The *IPI* of all measured elements for each sample is defined as the mean value of the element's *PI*, and is then classified as low ($IPI \leq 1$), middle ($1 < IPI \leq 2$) or high ($IPI > 2$) [23].

The method of determining ecological risks of heavy metals originally introduced by Hakanson [17] has recently been used in dust contamination studies [24]. Hence, the potential ecological risk index (PERI) is calculated to assess the degree of metal pollution in Chengdu street dusts as follows:

$$RI=\sum Er^i;\ Er^i=Tr^i\times C_f^i;\ C_f^i=Cs/Cn \quad (2)$$

Where C_f^i corresponds to the pollution factor for each metal; *Cs* and *Cn* are heavy metal sample and background concentrations, respectively; Er^i is the ecological risk of each element and *RI* shows the ecological risk of multiple elements. Hakanson [17] defined Tr^i as a "toxic-response factor" for a given substance and demonstrated this value for Cu, Pb, Zn, Mn, Co, Ni, Cr, Cd to be 5, 5, 1, 1, 5, 5, 2, 30, respectively. The following terminologies are used to describe risk levels: C_f^i <1, clean; $1 \leqq C_f^i < 3$, Low pollution; $3 \leqq C_f^i < 6$, moderate pollution; $6 \leqq C_f^i < 9$, high pollution; $C_f^i \geq 9$, very high pollution. $Er^i < 40$, low potential ecological risk; $40 \leqq Er^i < 80$, moderate potential ecological risk; $80 \leqq Er^i < 160$, considerable potential ecological risk; $160 \leqq Er^i < 320$, high potential ecological risk; $Er^i \geq 320$, very high potential ecological risk. RI<150, low ecological risk; $150 \leqq RI < 300$, moderate ecological risk; $300 \leqq RI < 600$, considerable ecological risk; $RI \geq 600$, very high ecological risk.

RESULTS AND DISCUSSION

Heavy metal Concentrations in the street dusts of Chengdu. The concentrations of heavy metals in the street dust samples of Chengdu, as well as the background value of Chengdu soil [25] and Chinese soil [22] are shown in Table 1. It can be seen from Table 1, the mean concentrations of Cu, Pb, Zn, Mn, Co, Ni, Cr and Cd are all higher than their corresponding background values of Chengdu soil and Chinese soil except Co, which are 8.7, 14.3, 6.4, 2.3, 0.7, 3.0, 1.4, 15.6 times the background value of Chengdu soil and 10.9, 12.7, 6.9, 1.1, 0.8, 3.0, 1.6, 25.7 times the background value of Chinese soil, respectively. And their maximums are respectively 41.0, 61.5, 22.1, 8.7, 2.7, 18.7, 6.3, 112.6 times the background value of Chengdu soil and 51.5, 54.6, 23.8, 4.0, 2.7, 19.0, 7.1, 185.7 times the background value of Chinese soil. Whereas, contents of Cr and Co in this study are approximately the same as their background values, which indicates that Cr and Co may had mainly a natural source, while the other elements may come mainly from anthropogenic sources [2].

Table 1 shows that the analyzed metals presented diverse variation characteristics in street dust of seven functional areas. The mean concentrations of Cu, Pb, Zn, Mn in the dust from CD, TD and ID are higher than which from ED, RD and PD. The mean contents of Co, Ni, Cr, Cd in the dust from TD and ID are all higher than from other five functional areas. The order of the mean concentrations of the studied metals in street dust divided by the background value of Chengdu soil are various in seven functional areas, which is in the order of Pb>Cu>Zn>Cd>Ni>Mn>Cr>Co in ED and RD, Pb>Cu>Zn>Cd>Mn>Ni>Cr>Co in CD and PD, Pb>Cu>Cd>Zn>Mn>Ni>Cr>Co in CD in SP, Cd>Pb>Cu> Zn>Ni>Mn>Cr>Co in TD and ID. These results indicate that the street dusts from seven functional areas have different cumulative characteristics, which likely intimate the diversity of the anthropogenic activities and effects in seven functional areas of Chengdu.

The descriptive statistic results of heavy metal concentrations investigated in the studied samples are presented in Table 1. Table 1 shows the concentrations of Cu, Pb, Zn, Mn, Ni, Cr and Cd in street dusts of Chengdu are higher than the background values of Chinese soils [22]. The arithmetic mean of Cu, Pb, Zn, Mn, Co, Ni, Cr and Cd in street dusts is 246.47, 329.89, 511.16, 620.26, 9.57, 80.55, 97.16 and 2.5mg/kg, respectively. The geometric means of most studied metals are less than their arithmetic means, which are 196.10, 275.43, 465.56, 579.15, 8.04, 66.99, 85.59 and 1.30 mg/kg, respectively for Cu, Pb, Zn, Mn, Co, Ni, Cr and Cd. Table 1 also showed that CV value of Cu, Pb, Zn, Mn, Co, Ni, Cr and Cd is 81.1%, 69.8%, 51.4%, 49.3%, 64.1%, 92.7%, 76.8% and 141.8%, respectively. Otherwise, CV value of almost all heavy metal is more than 50% except Mn (49.3%), indicating significant heterogeneous distribution of heavy metal contents in street dusts corresponding to anthropogenic origins.

TABLE 1
Heavy metal concentrations (mg/kg) in street dust collected from Chengdu city (Chengdu B=background values in soil of Chengdu; China B= background values in soil of China; GM=geometric mean; CV= coefficients of variation)

Element	Cu	Pb	Zn	Mn	Co	Ni	Cr	Cd
			ED (n=6)					
Minimum	73.29	130.51	207.99	313.55	3.49	32.54	66.72	0.20
Maximum	248.23	255.71	548.26	654.73	6.78	59.82	81.30	1.17
Mean	149.43	174.57	409.36	444.04	4.96	45.07	73.00	0.62
S.D.	61.65	47.63	119.24	121.80	1.32	10.65	6.35	0.40
CV (%)	41.3	27.3	29.1	27.4	26.6	23.6	8.7	64.6
GM	138.54	169.64	391.87	431.24	4.82	44.02	72.77	0.51
Median	154.01	160.58	405.34	420.73	4.94	44.50	71.32	0.51
			CD (n=6)					
Minimum	206.20	217.48	320.81	619.55	6.32	51.15	79.40	0.78
Maximum	351.59	574.85	708.35	853.18	11.47	72.64	93.62	1.12
Mean	257.45	363.76	503.14	710.82	9.41	62.68	86.22	0.92
S.D.	59.17	130.09	143.23	80.15	1.76	8.34	5.24	0.13
CV(%)	23.0	35.8	28.5	11.3	18.8	13.3	6.1	14.2
GM	252.21	345.18	486.00	707.23	9.25	62.20	86.09	0.91
Median	235.55	353.35	483.14	707.98	9.64	64.12	85.68	0.87
			SP (n=6)					
Minimum	60.53	155.47	214.50	343.68	2.59	44.92	65.47	0.54
Maximum	277.88	301.76	634.14	698.20	9.34	54.64	81.24	1.12
Mean	157.39	201.95	382.75	554.50	5.35	50.33	73.43	0.83
S.D.	79.27	52.51	144.54	133.01	2.43	3.48	6.80	0.23
CV (%)	50.4	26.0	37.8	24.0	45.4	6.9	9.3	27.2
GM	139.48	197.05	361.61	539.41	4.89	50.23	73.17	0.81
Median	155.48	193.77	364.13	590.59	5.46	50.69	73.92	0.82
			TD (n=6)					
Minimum	187.18	387.24	542.21	556.48	7.72	89.63	87.30	3.26
Maximum	1164.30	1420.75	1763.07	769.49	20.88	510.38	435.92	18.02
Mean	442.91	653.20	839.75	670.56	12.95	177.28	154.86	6.59
S.D.	369.21	381.17	465.14	85.09	4.72	164.25	138.01	5.67
CV (%)	83.4	58.4	55.4	12.7	36.4	92.6	89.1	86.0
GM	356.11	590.54	763.98	665.98	12.29	141.14	125.90	5.38
Median	309.85	524.63	687.37	674.77	12.17	113.32	101.81	4.41
			ID (n=6)					
Minimum	232.85	372.05	423.93	594.27	13.75	94.33	84.92	4.21
Maximum	824.60	604.75	940.81	2347.05	34.85	140.75	402.73	12.93
Mean	404.73	495.21	687.31	951.41	19.45	115.63	148.19	6.88
S.D.	215.49	100.87	187.91	688.16	7.76	17.65	125.18	3.11
CV (%)	53.2	20.4	27.3	72.3	39.9	15.3	84.5	45.3
GM	369.12	486.46	664.61	823.65	18.47	114.50	122.65	6.42
Median	337.36	497.05	699.93	667.48	16.51	117.04	97.40	5.97
			RD (n=6)					
Minimum	50.88	197.24	322.39	512.52	7.94	68.31	68.36	0.79
Maximum	270.32	314.21	518.07	675.01	13.49	95.74	94.24	1.45
Mean	179.40	255.30	421.76	594.49	10.35	76.82	82.44	1.09
S.D.	88.57	50.77	75.55	62.70	1.99	10.13	9.14	0.29
CV (%)	49.4	19.9	17.9	10.5	19.2	13.2	11.1	27.0
GM	154.14	251.05	416.13	591.74	10.20	76.31	82.01	1.06
Median	206.26	255.58	405.28	585.10	10.47	73.11	82.06	1.03
			PD (n=6)					
Minimum	31.04	62.70	242.31	329.53	3.05	28.59	23.47	0.18
Maximum	258.41	284.68	485.73	510.29	7.37	43.01	80.75	1.08
Mean	133.96	165.22	334.05	416.01	4.55	36.02	62.00	0.55
S.D.	74.54	85.81	85.21	82.29	1.71	5.30	19.88	0.38
CV (%)	55.6	51.9	25.5	19.8	37.5	14.7	32.1	68.7
GM	112.94	144.51	325.80	409.24	4.30	35.69	57.96	0.45
Median	138.72	164.53	319.65	403.85	4.22	35.79	66.72	0.40
			Chengdu City (n=42)					
Minimum	31.04	62.70	207.99	313.55	2.59	28.59	23.47	0.18
Maximum	1164.30	1420.75	1763.07	2347.05	34.85	510.38	435.92	18.02
Mean	246.47	329.89	511.16	620.26	9.57	80.55	97.16	2.50
S.D.	199.90	230.26	262.86	306.08	6.14	74.66	74.65	3.54
CV (%)	81.1	69.8	51.4	49.3	64.1	92.7	76.8	141.8
GM	196.10	275.43	465.56	579.15	8.04	66.99	85.59	1.30
Median	207.51	274.33	424.32	596.32	8.67	64.12	81.27	1.03
Chengdu B [22]	28.4	23.1	79.7	271	12.8	27.3	69.5	0.16
China B [19]	22.6	26	74.2	583	12.7	26.9	61	0.097

TABLE 2
The I_{geo} of heavy metals in street dusts from Chengdu, China

Sampling sites	I_{geo}							
	Cu	Pb	Zn	Mn	Co	Ni	Cr	Cd
ED(n=6)	2.14	2.16	1.88	-0.98	-1.94	0.16	-0.33	2.10
CD (n=6)	2.92	3.22	2.18	-0.30	-1.02	0.64	-0.09	2.66
SP (n=6)	2.21	2.37	1.78	-0.66	-1.83	0.32	-0.32	2.52
TD (n=6)	3.71	4.07	2.92	-0.38	-0.56	2.14	0.76	5.50
ID (n=6)	3.58	3.67	2.63	0.12	0.03	1.52	0.70	5.56
RD (n=6)	2.40	2.71	1.92	-0.56	-0.88	0.93	-0.15	2.91
PD (n=6)	1.98	2.08	1.59	-1.07	-2.07	-0.16	-0.56	1.91
Study area (n=42)	2.53	2.82	2.06	-0.59	-1.24	0.73	-0.10	3.16
Minimum	-0.13	0.68	0.90	-1.48	-2.88	-0.50	-1.96	0.31
Maximum	5.10	5.19	3.99	1.42	0.87	3.66	2.25	6.95

TABLE 3
The *PI and IPI* for heavy metals in street dusts of Chengdu, China

Sampling sites	*PI*								*IPI*
	Cu	Pb	Zn	Mn	Co	Ni	Cr	Cd	
ED(n=6)	6.61	6.71	5.52	0.76	0.39	1.68	1.20	6.42	3.66
CD (n=6)	11.39	13.99	6.78	1.22	0.74	2.33	1.41	9.47	5.92
SP (n=6)	6.96	7.77	5.16	0.95	0.42	1.87	1.20	8.61	4.12
TD (n=6)	19.60	25.12	11.32	1.15	1.02	6.59	2.54	67.96	16.91
ID (n=6)	17.91	19.05	9.26	1.63	1.53	4.30	2.43	70.89	15.87
RD (n=6)	7.94	9.82	5.68	1.02	0.82	2.86	1.35	11.25	5.09
PD (n=6)	5.93	6.35	4.50	0.71	0.36	1.34	1.02	5.64	3.23
Study area (n=42)	10.91	12.69	6.89	1.06	0.75	2.99	1.59	25.75	7.83
Minimum	1.37	2.41	2.80	0.54	0.20	1.06	0.38	1.86	2.88
Maximum	51.52	54.64	23.76	4.03	2.74	18.97	7.15	185.73	31.92

Assessment results of the heavy metal contamination in street dusts. The I_{geo} values for the heavy metals in street dusts of Chengdu are presented in Table 2. The average I_{geo} values for heavy metals are 2.53 for Cu, 2.82 for Pb, 2.06 for Zn, -0.59 for Mn, -1.24 for Co, 0.73 for Ni, -0.10 for Cr and 3.16 for Cd. The order for the average I_{geo} values is follows: Cd>Pb>Cu>Zn>Ni>Cr>Mn>Co. The average I_{geo} values for Cd is 3.16, which is ranked as "strongly polluted", showing that the urban streeet dusts are obviously polluted by Cd, especially in the TD and ID area. Cu, Pb and Zn are ranked as "moderately to strongly polluted" levels. I_{geo} for Mn, Co and Cr are less than 0, indicating that the urban environment was scarcely contaminated by Mn, Co and Cr. The average I_{geo} for Ni (0.73) is 0 to 1, which is ranked as an "unpolluted to moderately polluted" level. In addition, Cu is moderately to strongly polluted in the dust from ED, CD, SP, RD and PD and strongly polluted from TD and ID; Pb is moderately to strongly polluted from ED, CD, SP, ID, RD and PD, strongly to extremely polluted from TD; Zn is moderately to strongly polluted from all functional areas; Mn, Co, and Cr is practically unpolluted in the dust from all functional areas except Mn, Co and Cr from TD or ID(unpolluted to moderately polluted); Ni is practically unpolluted to moderately polluted in the dust from all functional areas except from TD(moderately to stongly polluted) and ID(moderately polluted); Cd is moderately to strongly polluted in the dust from ED, CD, SP, RD and PD samples and extremely polluted from TD and ID.The I_{geo} of heavy metals in the dust from TD and ID is higher than in other functional areas. This could be associated with the industrial production and transportation activities that take place in these areas.

The *PIs*, calculated according to the background concentration of heavy metals in Chinese soil, vary greatly across the different metals (Table 3). Mn, Co and Cr exhibit lower values, raning from 0.54 to 4.03, from 0.20 to 2.74 and from 0.38 to 7.15. For Mn, the mean *PI* is 1.06 and all of the samples have low- or mid-level *PIs* except one sample, indicating that the concentration of Mn in the street dust samples are comparable with the background concentration of Chinese soil and there is no pollution of Mn in Chengdu street dust samples. The mean *PI* for Co is 0.75 and all of the samples are low- or mid-level *PIs*, showing that there is also no pollution of Co in street dusts from Chengdu. The average *PI* for Cr is 1.59, and only two samples are classified as high *PI* and forty samples are classified as low- or middle *PI*, indicating an absence of problematic Cr pollution of street dusts in Chengdu.

The *PIs* of Cu, Pb, Zn, Ni and Cd are much higher since all dust samples contained mid- or high *PIs*, ranging from 1.37 to 51.52, 2.41 to 54.64, 2.80

to 23.76, 1.06 to 18.97 and 1.86 to 185.73, with mean value of 10.91, 12.69, 6.89, 2.99 and 25.75 for Cu, Pb, Zn, Ni and Cd, respectively. These indicate that Cu, Pb, Zn, Ni and Cd in street dusts present serious pollution in Chengdu. The *IPIs* of street dust samples vary from 2.88 to 31.92 with an average of 7.83, indicating that all samples studied presented heavy metal pollution.

Potential ecological risk assessment results. The potential ecological risk assessment results of analyzed metals in street dusts from Chengdu are shown in Table 4 and Table 5. Table 4 shows that the Er^i value of that the Er^i value of Zn, Mn, Co, Ni and Cr in street dusts of all functional areas from Chengdu are <40, indicating low potential ecological risk. The Er^i value of Cu in ED, SP, RD and PD are <40, in CD are between 40 and 80, and in TD, ID are $80 \leqq Er^i < 160$, showing low potential ecological risk in ED, SP, RD, and PD, moderate potential ecological risk in CD, considerable potential ecological risk in TD and ID. The Er^i value of Pb in ED, SP and PD are <40, in CD and RD are $40 \leqq Er^i < 80$, in TD and ID are $80 \leqq Er^i < 160$, indicating low potential ecological risk in ED, SP and PD, moderate potential ecological risk in CD and RD, considerable potential ecological risk in TD and ID. The Er^i value of Cd in ED, CD, SP and PD are between 160 and 320, in TD, ID and RD are >320, showing high potential ecological risk in ED, CD, SP and PD, very high potential ecological risk in TD, ID and RD.

The potential ecological risk index (*RI*) of heavy metals in the dusts ranges from 142.47 to 5868.16 with an average of 920.30. Table 4 and Table 5 shows that the *RI* values of heavy metals in most dust samples (78.6%) are >300, showing considerable ecological risk or very high ecological risk in this study area. Table 4 and Table 5 also shows that Cu, Pb and Cd are the main contributors to the potential ecological risk, especially for Cd. Based on these results, most sampling locations show very high and considerable ecological risks, indicating that these elements pose a potentially high risk to the local ecosystem and management procedures should be adopted in those at-risk areas.

TABLE 4
The calculated values of C_f^i, Er^i and *RI* for heavy metals in street dusts of different functional areas from Chengdu, China

Heavy metals	Indices Value	ED(n=6)	CD(n=6)	SP(n=6)	TD(n=6)	ID(n=6)	RD(n=6)	PD(n=6)
Cu	C_f^i	6.61	11.39	6.96	19.60	17.91	7.94	5.93
	Er^i	33.06	56.96	34.82	97.99	89.54	39.69	29.64
Pb	C_f^i	6.71	13.99	7.77	25.12	19.05	9.82	6.35
	Er^i	33.57	69.95	38.84	125.61	95.23	49.10	31.77
Zn	C_f^i	5.52	6.78	5.16	11.32	9.26	5.68	4.50
	Er^i	5.52	6.78	5.16	11.32	9.26	5.68	4.50
Mn	C_f^i	0.76	1.22	0.95	1.15	1.63	1.02	0.71
	Er^i	0.76	1.22	0.95	1.15	1.63	1.02	0.71
Co	C_f^i	0.39	0.74	0.42	1.02	1.53	0.82	0.36
	Er^i	1.95	3.70	2.11	5.10	7.66	4.08	1.79
Ni	C_f^i	1.68	2.33	1.87	6.59	4.30	2.86	1.34
	Er^i	8.38	11.65	9.36	32.95	21.49	14.28	6.70
Cr	C_f^i	1.20	1.41	1.20	2.54	2.43	1.35	1.02
	Er^i	2.39	2.83	2.41	5.08	4.86	2.70	2.03
Cd	C_f^i	6.42	9.47	8.61	67.96	70.89	11.25	5.64
	Er^i	192.61	284.12	258.18	2038.67	2126.65	337.59	169.34
All elements	*RI*	278.24	437.21	351.82	2317.88	2356.33	454.14	246.49
	Ecological risk	moderate	considerable	considerable	Very high	Very high	considerable	moderate

TABLE 5
The calculated values of C_f^i, Er^i and *RI* for heavy metals in street dusts of Chengdu, China (n=42)

Sampling sites	Er^i								*RI*
	Cu	Pb	Zn	Mn	Co	Ni	Cr	Cd	
Study area (n=42)	54.53	63.44	6.89	1.06	3.77	14.97	3.19	772.45	920.30
Minumum	6.87	12.06	2.80	0.54	1.02	5.31	0.77	55.87	142.47
Maximum	257.59	273.22	23.76	4.03	13.72	94.87	14.29	5571.77	5868.16

CONCLUSION

1) The mean concentrations of all heavy metals are all higher than their corresponding background values of Chengdu soil and Chinese soil except Co. The order of the mean concentrations of the studied metals in street dust divided by the background value of Chengdu soil indicates the street dusts from seven functional areas have different cumulative characteristics, which likely intimate the diversity of the anthropogenic activities and effects in seven functional areas of Chengdu. CV value shows significant heterogeneous distribution of heavy metal contents in street dusts corresponding to anthropogenic origins.

2) The order of I_{geo} is Cd>Pb>Cu>Zn>Ni>Cr>Mn>Co and the I_{geo} of heavy metals in the dust from TD and ID is higher than in other functional areas. There is a moderate or strong Cu, Pb, Zn, Ni and Cd pollution. I_{geo} for Mn, Co and Cr are less than 0, indicating that the urban environment was scarcely contaminated by Mn, Co and Cr. The assessment results of *PI* also support Cu, Pb, Zn, Ni and Cd in street dusts presented serious pollution, and *IPI* indicates heavy metals of street dust polluted seriously.

3) The *RI* values of heavy metals indicate the heavy metals of street dusts are considerable ecological risk or very high ecological risk and Cu, Pb and Cd are the main contributors to the potential ecological risk, especially Cd.

4) These findings indicate that more attention should be paid to heavy metal contamination of street dust in Chengdu, especially Cd.

ACKNOWLEDGEMENTS

This work was Supported by the Open Research Subject of Key Laboratory of Food and Biotechnology (Grant No: szjj2017-108), the key scientific research fund of Chongqing Key Laboratory of Environmental Materials and Remediation Technology (Grant No: CEK1605), the National Science Foundation of China (51608339) and the Talent Introduction Project of Sichuan University of Science and Engineering(2015RC37) .

REFERENCES

[1] Banerjee, A.D.K. (2003) Heavy metal levels and solid phase speciation in street dusts of Delhi, India. Environ. Pollut. 123, 95-105.

[2] Han, Y.M., Du, P.X., Cao, J.J., Posmentier, E.S. (2006) Multivariate analysis of heavy metal contamination in urban dusts of Xi'an, Central China. Sci. Total Environ. 355, 176-186.

[3] Bilos, C., Colombo, J.C., Skorupka, C.N., Presa, M.J.R. (2001) Sources, distribution and variability of airborne trace metals in La Plata City area, Argentina. Environ. Pollut. 111, 149-158.

[4] Manno, E., Varrica, D., Dongarrà, G. (2006) Metal distribution in road dust samples collected in an urban area close to petrochemical plant at Gela, Sicily. Atmos. Environ. 40, 5929-5941.

[5] Shi, G.T., Chen, Z.L., Xu, S.Y., Zhang, J., Wang, L., Bi, C.J., Teng, J.Y. (2008) Potentially toxic metal contamination of urban soils and street dust in Shanghai, China. Environ. Pollut. 156, 251-260.

[6] Hou, W., Zhang, L., Wang, J., Zhang, C.X., Yang, C.L., Lu, Y.C. (2015) Health Risk Assessment of Heavy Metal Exposure to Surface Dust of Shenyang City, China. Fresen. Environ. Bull. 24(8), 2540-2548.

[7] Li, Q., Shan, Y.L., Zou, M.Y., Du, F.G. (2017) Health Risk Assessment of Heavy Metals in Road Dusts to The Population in Urban Parks and Squares: A Case Study from China. Fresen. Environ. Bull. 26(3), 2050-2057.

[8] Duzgoren-Aydin, N.S., Wong, C.S.C., Aydin, A., Song, Z., You, M., Li, X.D. (2006) Heavy metal Contamination and distribution in the urban environment of Guangzhou, SE China, Environ. Geochem. Health. 28, 375-391.

[9] Chon, H.T., Kim, K.W., Kim, J.Y. (1995) Metal contamination of soils and dusts in Seoul metropolitan city, Korea. Environ. Geochem. Health. 17, 139-146.

[10] De Miguel, E., Llamas, J.F., Chacón, E., Berg, T., Larssen, S., Røyset, O., Vadset, M. (1997) Origin and patterns of distribution of trace elements in street dust: Unleaded petrol and urban lead. Atmos. Environ. 31, 2733-2740.

[11] Charlesworth, S., Everett, M., Mccarthy, R., Ordóñez, A., de Miguel, E. (2003) A comparative study of heavy metal concentration and distribution in deposited street dusts in a large and a small urban area: Birmingham and Coventry, West Midlands, UK. Environ. Int. 29, 563-573.

[12] Qarri, F., Lazo, P., Bekteshi, L., Kane, S., Marku, E. (2015) A Study on Road Traffic Emissions of Heavy Metals in The Tirana-Elbasan Highway Tunnel Experiment in Albania By Using the Dust Samples. Fresen. Environ. Bull. 24(6), 2101-2112.

[13] Hercer, M., Wyszkowski, M., Modrzewska, B. (2016) Impact of Traffic on The Content of Trace Elements in Soils Along State Road 53 (Poland), Fresen. Environ. Bull. 25(3), 719-731.

[14] Zhang, B., Wu, D., He, Y., Niu, M., Zhang, G.F, Wang, S.M. (2017) Concentration Distribution of Heavy Metals Fractions in Street Dusts of Mega-City, Chengdu, Southwest China. Fresen. Environ. Bull. 26(2a), 1569-1578.

[15] Tokalio, L.S., Kartal, S. (2006) Multivariate analysis of the data and speciation of heavy metals in street dust samples from the Organized Industrial area in Kayseri (Turkey). Atmos. Environ. 40, 2797-2805.
[16] Li, H.M., Qian, X., Hu, W., Wang, Y.L., Gao, H.L. (2013) Chemical speciation and human health risk of trace metals in urban street dusts from a metropolitan city, Nanjing, SE China. Sci. Total. Environ. 456-457, 212-221.
[17] Hakanson, L. (1980) An ecological risk index for aquatic pollution control. A sedimentological approach. Water Res. 14, 975-1001.
[18] Müller, G. (1969) Index of geoaccumulation in sediments of the Rhine River. Geo. Journal. 2, 108-118.
[19] Atiemo, M.S., Ofosu, G.F., Kuranchie-Mensah, H., Tutu, A.O., Palm, N.D., Blankson, S.A. (2011) Contamination assessment of heavy metals in road dust from selected roads in Accra, Ghana. Res. J. Environ. Earth Sci. 3, 473-480.
[20] Wan, D.J., Han, Z.X., Liu, D.W., Yang, J.S. (2016) Pollution Levels and Spatial Distribution of Heavy Metals in House Dust from An Industrial Area in Xi'An, Central China. Fresen. Environ. Bull. 25(3): 719-731. 839-851.
[21] García-Martínez, L.L., Poleto, C. (2014) Assessment of diffuse pollution associated with metals in urban sediments using the geoaccumulation index (I_{geo}). J. Soils. Sediments. 14, 1251-1257.
[22] CNEMC (China National Environmental Monitoring, Centre). (1990) The Background Values of Chinese Soils, Environmental Science Press of China, Beijing, (in Chinese).
[23] Chen, T.B., Zheng, Y.M., Lei, M., Huang, Z.C., Wu, H.T., Chen, H., Fan, K.K., Yu, K., Wu, X., Tian, Q.Z. (2005) Assessment of heavy metal pollution in surface soils of urban parks in Beijing, China. Chemosphere. 60, 542-551.
[24] Tang, R., Ma, K., Zhang, Y., Mao, Q. (2013) The spatial characteristics and pollution levels of metals in urban street dust of Beijing, China. Appl. Geochem. 35, 88-98.
[25] Shi, W.G. (1991) Sediment on the Urban Street: Accumulation and Characteristics. Environment Science. 12, 18-23 (in Chinese).

Received: **02.08.2017**
Accepted: **14.10.2017**

CORRESPONDING AUTHOR

Xinqiang Ning
School of Civil Engineering
Sichuan University of Science and Engineering
Zigong 643000 - China

e-mail: 38096922@qq.com
ningxinqiang@126.com

© by PSP Volume 26 – No. 12A/2017 pages 8207-8210 Fresenius Environmental Bulletin

THE RETROSPECTIVE INVESTIGATION OF POISONING CASES APPLIED TO AN EDUCATIONAL RESEARCH HOSPITAL IN TURKEY

Gulten Kucukal[1], Itir Erkan[2,*]

[1]Saglik Bilimleri University, Istanbul Education and Research Hospital, Istanbul, Turkey
[2]Istanbul Yeni Yuzyil University, Faculty of Health Sciences, Istanbul, Turkey

ABSTRACT

In this study, the files of poisoning cases which were applied to an education and research hospital in Turkey between 01.01.2010-12.12.2016 were examined. In our study, it was determined that totally 679 cases of poisoning, of which 49.6% were male and 50.36% were female, were applied to health institutions between 2010-2016. 119 cases (17.53%) were due to pharmacological agents and; 560 cases (82.47%) were due to non-pharmacological agents. When analyzed according to the seasons, it was determined that 253 of the cases of poisoning occurred in winter, 167 in spring, 152 in autumn, and 107 in summer. Six cases (0.88%) were found to be poisoned after suicidal attempts and the other cases (99.11%) were found to be poisoned after the accident. It is stated that only for 19 numbers of 679 cases (examined in the study), forensic reports were held. Care should be taken that the anamnesis and judicial reports are thoroughly and correctly edited, since all poisonings will be judged as judicial cases. For 227 cases, no information was written on the symptom part of the system. However, a detailed anamnesis is very important both in terms of forensic and treatment.

KEYWORDS:
Poisoning, Hospital, Forensic sciences.

INTRODUCTION

Poisons have played an important role in the history of mankind for centuries, from the political assassinations in the times of Romans to the contemporary environmental health [1]. Contamination of consumed foodstuffs with disease-causing microorganisms or chemical substances or toxic substance in foodstuff causes food poisoning. Most food poisonings are caused by amount of bacteria or toxins produced by bacteria. Some bacteria may grow millions of, when the necessary humidity, nutrition, temperature and time conditions are established [2-4]. Today more than 200 diseases are transmitted to people through food. Food poisoning is the second one, following drug poisoning among the poisoning cases that have been applied to health institutions in the researchers conducted [5-9]. In developed countries, the annual incidence of intended suicide and accidental poisonings ranges from 0.02% to 0.93 % and it is known that the number of poisoning cases applied to the emergency service in our country constitutes 0.46-1.57% of all cases [10]. Although poisonings occur in all age groups, they are more frequent and more fatal in the childhood age group. In 1997, in a research conducted, basing on the data of 38 health institutions from each region of Turkey, 5077 cases of child poisoning were evaluated and found to be 0,9% rate in total emergency cases [11]. Prevalence, demographic and etiological characteristics of poisonings vary according to sociocultural and economic characteristics of societies [12].

In this study, the files of poisoning cases applied to an education and research hospital in Turkey between 2011-2016 were examined and the obtained data were interpreted in terms of public health and forensic sciences.

MATERIALS AND METHODS

In this study, the files of poisoning cases which were applied to an education and research hospital in Turkey between 01.01.2010-12.12.2016 were examined. In the case of poisoning, gender, age group, causative agents, and most frequently seen months and origin (suicide/accident) were evaluated. This study was approved by the Health Sciences University Ethics Committee (2017/11005).

RESULTS AND DISCUSSION

In our study, it was determined that totally 679 cases of poisoning, of which 49.6% were male and 50.36% were female, were applied to health institutions between 2010-2016. Because of the pharmacological agents, 119 cases (17.53%) were detected; but, 560 cases (82.47%) were due to non-pharmacological agents (Table 1).

TABLE 1
Agents and incidence of poisoning cases

Active substance	Number of case	%
Pharmacologicalagents	**119**	**17.53**
Analgesics (salicylate)	24	3.53
Antidepressants	19	2.80
Antiepileptic and sedative-hypnoticdrugs	42	6.19
Antipsychotics and neuroleptics	9	1.33
Cardiovascular system drugs	25	3.68
Non-pharmacologi-calagents	**560**	**82.47**
Aliphatic and aromatic hydrocarbons	11	1.62
Ethylalcohol	8	1.18
Insecticides and pesticides	13	1.91
Carbonmonoxide	333	49.04
Caustic / corrosive substances	74	10.90
Mushroom	39	5.74
Methylalcohol	33	4.86
Narcotic	18	2.65
Others*	31	4.57
Total	**679**	**100.00**

* Lead, metal, mercury, iron, arsenic, scorpion and snake poisoning

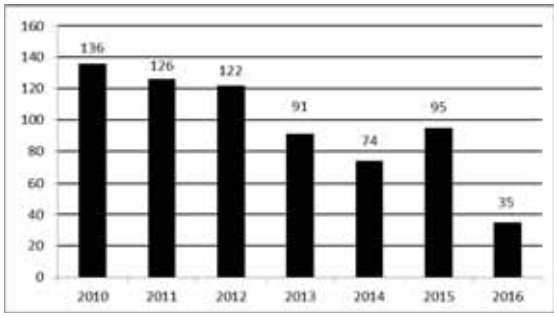


FIGURE 1
Distribution of the poisoning cases based on the year of diagnosis (n=679)

When Figure 1 is examined, it has been determined that the cases of poisoning applied to the health care institution occur mostly in 2010 and at least in 2016. When analyzed according to the seasons, it was determined that 253 of the cases of poisoning occurred in winter, 167 in spring, 152 in autumn, and 107 in summer. Carbon monoxide poisonings was detected in winter and autumn, pesticides poisoning (insecticide, pesticide) in spring, and food poisonings in summer, mostly.

In studies conducted in our country, among the poisoning cases applied to emergency services, food poisoning takes part with drug and chemical poisoning, as the most three common causes [13]. In the study conducted at Kirikkale, it was stated that 21% of the poisoning cases applied to emergency service were food poisoning [14], 14.6%, according to the study conducted in Bursa [15] and, 42.9% rate, according to the study conducted at Marmara University Hospital. A total of 80 cases (11.78%) of food poisoning were detected in our study from 679 applications; 8 cases due to ethyl alcohol, 33 cases due to methyl alcohol and 39 cases due to fungal intoxication. Epidemiological studies in this regard are very important [16, 17]. Thus, if which poisoning type are much in the area concerned, precautions can be taken for that root and new health policies can be developed. Food poisoning can lead to mild clinical tabulations, as well as lethal [6]. In the study of Sönmez et al., when they come to the health institution, patients' states of consciousness; 88.2% were open, 7.6% were confused and 4.1% were closed [7]. As to Kelebek et al. 11.8% of cases were confused, 4.8% were stupor, and 0.8% were coma, at the time of applying [8]. All poisonings are cases that should be evaluated as judicial [9].

Kirel et al. reported that [18] 29.1% of the poisonings were in the 15-18 age group, Onturk et al. [19] reported that 24.1% were in the 12-17 age group, while Aygün et al. [20] reported that 21.4% were in the 12-16 age group. In the study conducted by Sumer et al., 97% of the poisonings were found to be accidental, but in teenage girls, suicide attempts were found, mostly, causing poisoning [21]. In our study, poisonings were found to be mostly, among the group of 25-30 age (%11.34). 6 cases were as to, poisoned as a result of suicide attempt in total; 4 cases, high dose paracetamol, 1 case nitric acid and 1 case pesticide use. From intended suicide poisonings, 5 cases were found in 19-25 age group (4 female, 1 male) and 1 case was 44 years old (male). While, in 1996, in the UK, poisonings with paracetamol were coming first; as a result of limiting paracetamol usage, legally, it was seen that number of cases decreased in 2000 [22]. Similar results were found in other studies conducted in our country [23, 24]. 18 cases were poisoned after narcotic drug use and 3 cases were directed to drug abuse treatment center. 673 cases (%99.11) were found to be accidentally poisoned.

In our study, it was determined that there was chemical poisoning in 147 cases. 87 cases was identified due to pesticides (insecticide and pesticides) and caustic/corrosive substances. The occurrence of these incidents as an accident suggests that they are due to the fact that proper storage and usage conditions cannot be fulfilled. The number of cases can be reduced by making warnings about the usage instructions and risks, to the users. In addition, in a study conducted; lead, arsenic and mercury were detected in high proportion on toys [25]. This result shows that toys must be tested and checked before being presented to the market.

When symptoms of poisoning are suspected, findings that there is nausea-vomiting for 45 cases, dizziness for 15 cases, blurred consciousness in 1 case, and shortness of breath in 20 cases, after active substance ingestion, are observed in the system. More than one finding was recorded for 331 cases and no findings were reported for 227 cases in the

system. This situation will cause insufficient information to be obtained in the retrospective examinations on the patients in the system, as well as lack of information in the subsequent examinations of the same patient. However, a detailed anamnesis is very important both in terms of forensic and treatment.

It is stated that only for 19 numbers of 679 cases (examined in the study), forensic reports were held. Whatever the etiology, however, all cases of poisoning should be assessed within the context of a forensic case and the physician's legal responsibility [26]. To carry out an incorrect or incomplete judicial report, or not to carry out a judicial report for judicial cases is not to fulfill an important legal responsibility, at the same time. Thus, questions of judicial authorities can be answered about whether intoxication occurs intentionally or due to negligence [27-29].

CONCLUSION

Poisoning is an important public health problem. By taking the necessary legal precautions provision of food/drug safety, dissemination of control laboratories and raising awareness of users are required. Care should be taken that the anamnesis and judicial reports are thoroughly and correctly edited, since all poisonings will be judged as judicial cases.

ACKNOWLEDGEMENTS

We would also like to thank to the hospital for the use of data. Special thanks to Istanbul Yeni Yuzyil University for permission to study with in this period.

REFERENCES

[1] Wax, P.M. (2002) Historical principles and perspectives. In: Goldfrank, L.R., Flomenbaum, N.E., Lewin, N.A., Weisman, R.S., Howland, M.A., Hoffman, R.S. (eds.) Goldfrank's Toxicologic Emergencies, 7th edition, USA, The McGraw-Hill Companies. 1-17.

[2] Fry, A.M., Braden, C.R., Griffin, P.M and Hughes, J.M. (2005) Foodborn disease. In: Mandell, G.L, Bennet, J.E, Dolin, R. (eds.) Principles and practice of infectious diseases, Sixth ed. Phladelphia: Elsevier-Churchill Livingstone. 1286.

[3] Gunyar, O.A., Uztan, A.H, Ates, M., Yoltas, A. and Goker E. (2015) Airborne microfungus flora determined in the different units of the department of Tulay Aktas Oncology Hospital, Ege University. Fresen. Environ. Bull. 24(1b), 317-323.

[4] Sakartepe, E., Uztan, A.H. and Gunyar, O.A. (2016) Airborne mycobiota determined in the neonatal unit of the Ege University Hospital, Bornova, Turkey. Fresen. Environ. Bull. 25(8), 2833-2841.

[5] Ozkose, Z. and Ayoğlu, F. (1999) Etiological and demographical characteristics of acute adult poisoning in Ankara, Turkey. Human & Experimental Toxicology. 18,614-618.

[6] Sanaei-Zadeh, H. (2012) Can bacillus cereus food poisoning cause sudden death? Journal of Clinical Microbiology. 50, 3816.

[7] Sonmez, E., Karakuş, A., Çavuş, U.Y., Civelek, C., Ipek, G, and Zeren C. (2012) Evaluation of intoxication cases admitted to emergency department of a university hospital. Dicle Medical Journal. 39, 21-26.

[8] Kelebek, F., Satar, S., Kozacı, N., Acıkalın, A., Gulen, M. and Acehan, S. (2014) Emergency medicine admissions of pediatric intoxicated cases. The Journal of Academic Emergency Medicine. 13(2), 67-70.

[9] Ward, J., Kapadia, K., Brush, E. and Salhanick, S.D. (2013) Amatoxin poisoning: case reports and review of current therapies. Journal of Emergency Medicine. 44, 116–121.

[10] Ozayar, E., Degerli, S., Gulec, H., Sahin, S. and Dereli, N. (2011) Retrospective analysis of intoxication cases in the ICU. Yoğun Bakım Dergisi. 11(3), 59-62.

[11] Aji, D.Y. and Ilter, O. (1998) Childhood poisoning in Turkey. Türk Pediatri Arşivi. 33(3), 154-158.

[12] Goksu, S., Yildirim, C., Kocoglu, H., Tutak, A. and Oner, U. (2002) Characteristics of acute adult poisoning in Gaziantep, Turkey. Journal of toxicology. Clinical toxicology. 40(7), 833-837.

[13] Yesil, O., Akoglu, H., Onur, O. and Guneysel O. (2008) Retrospective evaluation poisoning patients in emergency department. Marmara Medical Journal. 21(1), 26-32.

[14] Deniz, T., Kandiş, H., Saygun, M., Buyukkocak, U., Ulger, H. and Karakus, A. (2009) Evaluation of intoxication cases applied to emergency department of Kirikkale University Hospital. Düzce Tıp Fakültesi Dergisi. 11(2), 15-20.

[15] Akköse, Ş, Fedakar, R., Bulut, M. and Çebiçci, H. (2003) Zehirlenme olgularının beş yıllık analizi. Acil Tıp Dergisi. 3, 8-10.

[16] Alharbi, N.S., Khaled, J.M., Kadaikunnan, S. Alkhotheri, O., Alobaidi, A.S., Mothana, R. and Salmen, S.H. (2016) In vitro susceptibility test for Bacillus species isolated from hands sterilized with instant waterless hand sanitizer. Fresen. Environ. Bull. 25(5), 1639-1646.

[17] Soltani, F., Ghomeishi, A., Mohammadi, M.J., Karimyan, A., Khoshgoftar, M., Darabpour, F., Afkar, A., Yari, A.R., Mahboubi, M., Rastegarimehr, B., Yusefzadeh, A., Salehi, S.Z., Vosoughi, M. and Geravandi, S. (2017) Association of toxic microbial and chemical water quality of hemodialysis instruments during 2016. Fresen. Environ. Bull. 26(8), 5357-5362.
[18] Kirel, B., Unluoglu, I., Dogruel, N. and Kocak, K. (2000) Retrospective analysis of childhood poisoning cases in the Eskişehir region. Türkiye Klinikleri Pediatrik Bilimler Dergisi. 9(3), 158-163.
[19] Onturk, Y.A. and Ucar, B. (2003) Retro-spective analysis of childhood poisoning cases in Eskişehir region. Çocuk Sağlığı ve Hasta-lıkları Dergisi. 46, 103-113.
[20] Aygun, A.D., Guvenc, H., Turkbay, D. and Kocabay, K. (1995) Hastanemizde izlenen zehirlenme olgularının değerlendirilmesi. Medical Network Klinik Bilimler Pediatride Yönelişler. 3, 48-51.
[21] Sumer, V., Guler, E., Karanfil, R., Dalkiran, T., Gursoy, H., Garipardic, M. and Davutoglu, M. (2011) Evaluation of the poisoning cases who applied to the pediatrics emergency unit. Türk Pediatri Arşivi. 46, 234-240.
[22] Turvill, J.L., Burroughs, A.K. and Moore, K.P. (2000) Change in occurrence of paracetamol overdose in UK after introduction of blisterpacks. Lancet. 355, 2048-2049.
[23] Ozdogan, H., Davutoglu, M., Bosnak, M., Tutanc, M. and Haspolat, K. (2008) Pediatric poisonings in southeast of Turkey: epidemiological and clinical aspects. Human and Experimental Toxicology. 27(1), 45-48.
[24] Hincal, F., Hincal, A.A., Muftu, Y., Sarikayalar, F., Ozer, Y., Cevik, N and Kinik E. (1987) Epidemiological aspects of childhood poisonings in Ankara: A 10-year survey. Human toxicology. 6(2), 147-152.
[25] Sogut, O. and Ezer, M. (2017) Determination of elemental composition of various children's play dough samples using XRF spectrometry. Fresen. Environ. Bull. 26(6), 4277-4282.
[26] Gurpinar, T. and Asirdizer, M. (2006) The responsibility of physician in intoxications. Turkiye Klinikleri J Surg Med Sci. 2(50), 56-62.
[27] Karbeyaz, K., Gündüz, T., Akkaya, H., Urazel, B. and Kokcuoglu, M.A. (2012) Watch out for judicial reports, Eskisehir experience. Sürekli Tıp Eğitimi Dergisi. 21(5), 292-296.
[28] Urazel, B., Celikel, A., Karbeyaz, K. and Akkaya, H. (2014) The evaluation of forensic cases reported due to food poisoning. Dicle Me dical Journal. 41(1), 113-117.
[29] Khaefi, M., Goudarzi, G., Yari, A.R., Geravandi, S. Dobaradaran, S., Idani E., Javanmardi, P., Youesfi, F., Hashemzadeh, B., Shahriari, A. and Mohammadi, M.J., (2016) An association between ambient pollutants and hospital admitted respiratory cases in Ahvaz, Iran. Fresen. Environ. Bull. 25(10), 3955-3961.

Received: **02.08.2017**
Accepted: **09.10.2017**

CORRESPONDING AUTHOR

Itir Erkan
Istanbul Yeni Yuzyil University,
Faculty of Health Sciences,
Istanbul, 34010 – Turkey

e-mail: itir.erkan@yeniyuzyil.edu.tr

© by PSP Volume 26 – No. 12A/2017 pages 8211-8220 Fresenius Environmental Bulletin

EFFECTS OF DIFFERENT IRRIGATION LEVELS ON MEDITERRANEAN CORN BORER (*SESAMIA NONAGRIOIDES* LEFEBVRE) POPULATIONS AND EFFECTS OF FATTY ACIDS IN CORN BORER PREFERENCES

Ali Beyhan Ucak[1,*], Cevdet Kaplan[2], Behcet Inal[3], Serpil Gencoglan[4]

[1]Siirt University, Faculty of Agriculture, Department of Biosystem Engineering, Siirt /Turkey
[2]Siirt University, Faculty of Agriculture, Department of Plant Protection, Siirt /Turkey
[3]Siirt University, Faculty of Agriculture, Department of Agricultural Biotechnology,Siirt /Turkey
[4]Kahramanmaraş Sütçü İmam University, Faculty of Agriculture, Department of Biosystem Engineering, Kahramanmaraş /Turkey

ABSTRACT

In this study, effects of different irrigation treatments (I_{100}, I_{70}, I_{35}) on Mediterranean corn borer (*Sesamia nonagrioides* Lefebvre) populations in different corn genotypes (31D24, ADASA16, P1429) and the effects of fatty acids on corn borer preferences were investigated. The lowest fatty acid content was observed in full irrigation (I_{100}) and the greatest fatty acid content was observed in excessive water deficit (I_{35}) treatment. As the average of two years, the greatest yield (10400 kg ha^{-1}), low number of alive larva + pupa per plant (3.34), tunnel length (9.44 cm) and fatty acid (2.03% ILE Eicosanoic acid, methyl ester (CAS)) were observed in I_{100}x31D24 interaction; the lowest yield (2853.3 kg ha^{-1}) and high fatty acid (46.03% İLE 9.12 Octadecadienoic acid (Z,Z), methyl ester (CAS)) values were observed in I_{35}xP1429 interaction. The greatest Mediterranean corn borer population was observed in full irrigation (I_{100}) and the lowest population was observed in excessive water deficit (I_{35}) treatment. Mediterranean corn borer preferred the genotypes (P1429) with high fatty acid contents. It was concluded that genotypes should be tested under water-stressed and non-water-stressed conditions for resistance to Mediterranean corn borer and alive larva, tunnel length and fatty acids could be used as screening parameters.

KEYWORDS:
Irrigation, Mediterranean corn borer (*Sesamia nonagrioides* Lefebvre), Fatty acid, Tolerance

INTRODUCTION

As it was in the world, there are several pests with negative impacts on corn culture in Turkey. Of these pests, European corn borer (*O.nubilalis* Hübner) and Mediterranean corn borer (*Sesamia nonagrioides* Lefebvre) are the most important ones. European corn borer is widespread in Europe, America and Turkey [1]. On the other hand, Mediterranean corn borer is widespread in Spain, France, Italy, Greece and Turkey, especially in Mediterranean countries [2, 1]. Therefore, it is called "Mediterranean Com Borer" in literature [3]. In Çukurova, European corn borer reproduces 3-4 times and Mediterranean corn borer reproduces 4-5 times in a year [4]. It was reported in previous researches that Mediterranean corn borer constituted 38.95% and European corn borer constituted 61.15% of corn pests in Çukurova [5]. Cerit et al. [5] indicated these ratios as 70% for Mediterranean corn borer and 30% for European corn borer based on infected number of plants; as 87% for Mediterranean corn borer and 13% for European corn borer based on alive larva plus pupa ratio per plant. Mediterranean corn borer creates damages in all organs of corn plants, except for roots. At harvest, about 95% infections were observed in untreated fields [6] and about 30% yields losses were experienced [7]. Tsitsipis [8] reported that Mediterranean corn borer resulted in 0-10% yield losses in the first crop and 80-100% yield losses in the second crop corn. Hunt et al. [9] carried out a study in Nebraska with irrigated and non-irrigated corn plots and reported greater European corn borer (*östrinia nubilalis* hübner) population in irrigated plots than in non-irrigated lots. Uçak et al. [10] investigated the effects of different irrigation treatments (I_{100}, I_{80}, I_{60}, I_{40}, I_{20}, I_0) on Mediterranean corn borer (*S.nonagrioides* Lefebvre) and European corn borer (*östrinia nubilalis* hübner) populations and reported greater population (27.167 per plant) in full irrigation treatments (I_{100}) than in non-irrigated treatments (I_0) (13.50 per plant).

Stressors stimulate the formation of reactive oxygen species in plants. These reactive species are usually called radicals and they attack to various surfaces in plant tissues and create damages. Free radicals mostly attack to polyunsaturated fatty acids in cell membranes. Interactions of unsaturated fatty acids with these radicals alter the saturated and unsaturated fatty acid ratios of cell membranes [11]. Salama et al. [12] reported increased total saturated fatty acid ratios with abiotic stressors.

TABLE 1
Climate data for the years 2015 and 2016 and long-term averages (1962-2014)

Years	Months	Mean max. temp. (°C)	Mean temp. (°C)	Mean min. temp. (°C)	Mean humidity (%)	Mean wind speed (m s^{-1})	Mean daily sunshine (h)	Total precipitation (mm)
Average 1962 - 2014	May	25.2	19.4	9.0	49.3	1.0	9.1	36.9
	June	27.2	26.0	17.8	34.9	1.1	11.6	11.5
	July	35.1	30.5	23.4	30.3	1.1	12.3	0.6
	August	34.5	30.3	27.0	29.5	1.0	11.4	2.7
	September	30.0	25.1	14.7	37.4	1.0	10.1	7.0
	October	24.5	17.9	12.7	42.0	1.0	7.2	50.9
2015	May	26.62	19.29	14.52	50.87	1.0	8.7	39.6
	June	26.09	28.16	20.0	35.50	1.1	11.5	10.6
	July	34.13	31.45	24.35	32.69	1.0	12.4	0.1
	August	33.92	31.19	24.23	32.95	1.0	11.3	0.4
	September	31.23	25.43	21.5	39.90	1.1	10.0	9.2
	October	24.3	16.8	11.5	42.3	1.1	7.0	55.1
2016	May	24.69	21.29	14.59	51.77	1.0	9.3	37.7
	June	28.19	28.41	20.25	34.40	1.1	12.0	9.3
	July	36.24	33.19	25.35	29.69	1.0	12.5	0.1
	August	35.92	32.45	24.73	29.95	1.0	11.5	0.0
	September	32.23	27.43	21.65	36.79	1.1	10.0	12.2
	October	21.1	19.7	12.0	44.2	1.0	7.3	69.20

Eicosapolyenoic acids (EP), which do not occur in higher plants, elicit a cascade of responses in plants, including an oxidative burst and the transcriptional activation of genes involved in phytoalexin synthesis, lignification, programmed cell death, and other responses typically associated with the hypersensitive response (HR) to pathogens [13]. Previous studies reported that common fatty acid in plant pathogenic oomycetes, and signals for immune responses and central nervous system development in mammals, function as conserved signaling molecules across eukaryotic kingdoms. Fatty acid released during infection of plants may serve as novel PAMPs that engage plant signaling networks to induce resistance to pathogens [13]. Levels of free fatty acids increase in response to various stresses and play a pivotal role in plant–microbe interactions. For example, fatty acid synthesis in the obligate biotrophism of arbuscular-mycorrhizal fungi is dependent on plant-derived C16 FAs [14]. Furthermore, eggplants with enhanced levels of palmitoleic acid (16:1) exhibited increased resistance to Verticillium dahlia, suggesting increasing the production of plant 16:1 as a viable approach to enhance crop resistance to fungal diseases [15].

Several studies were performed to determine quantitative sections in corn plants able to provide resistance to Mediterranean corn borer [16; 17; 18; 19; 20]. However, there are any studies in literature about the effects of different irrigation levels (I_{100}, I_{70}, I_{35}) on Mediterranean corn borer (*Sesamia nonagrioides* Lefebvre) population in corn plants, about determination of pest preferences with chemical analyses and effects of abiotic stress on fatty acid composition of the plants. Therefore, sufficient literature about present research topic was not able to be provided. This study was conducted to investigate the effects of different irrigation levels (I_{100}, I_{70}, I_{35}) on tunnel length and Mediterranean corn borer population in different corn genotypes (31D24, ADASA16, P1429) and to determine *Sesamia nonagrioides* Lefebvre preferences with chemical analyses. Another objective of this study was to investigate for the first time the effects of fatty acids on spread of Mediterranean corn borer in diverse corn genotypes with biotic stress screening parameters.

MATERIAL AND METHODS

Experiments were carried out over the experimental fields of Siirt Province during the maize growing seasons of 2015 and 2016. The research site has an altitude of 894 m and is located on 37° 58' N and 41° 50' E. The 31D24, ADASA16, P1429 corn genotypes were used as the plant material of the study. Long-term and annual climate data of the research site are provided in Table 1.

Soil samples were taken before sowing from 0-90 cm soil profile (from three depth segments as 0-30, 30-60 and 60-90 cm). Soil moisture content at field capacity (33 kPa) was determined in accordance with Klute [21] and bulk density with Blake & Hartge [22]. Disturbed samples were subjected to organic matter, texture and permanent wilting point analyses. Water holding capacity at permanent wilting point was determined in accordance Klute (21). Soil physico-chemical characteristics are provided in Table 2.

Experimental soils were classified as brown forest soil with low electrical conductivity and salinity, low phosphor content, high potassium

content and medium organic matter content. Lime levels were not posing any problems for plant growth.

TABLE 2
Some soil physical and chemical soil characteristics of the research site

Properties	Soil layer (cm)		
	0-30	30-60	60-90
Clay (%)	62.00	58.00	55.00
Silt (%)	20.00	25.00	32.00
Sand (%)	18.00	17.00	13.00
Texture	Clay	Clay	Clay
Field capacity (Pw)	33.52	36.04	35.38
Permanent wilting point (Pwp)	24.44	26.08	25.57
Bulk density (g cm^{-3})	1.42	1.39	1.41
pH (1.25 sw^{-1})	7.50	7.66	7.91
Electrical conductivity (dS m^{-1})	1.55	1.77	1.75
Organic matter (%)	3.09	2.06	1.80
$CaCO_3$ (%)	6.40	1.90	1.90

Irrigation water quality parameters were determined in accordance with the method specified by Tuzuner [23]. Irrigation water quality class was C_2S_1 with an average EC value of 0.34 dS m^{-1} and a pH value of 7.21. Experiments were conducted in randomized blocks-split plots experimental design with 3 replications with genotypes (P64 LE119, PR63 F73 and P64 LL62) on main plots and irrigation treatments (I_{100}, I_{70} and I_{35}) on sub-plots.

Irrigation program was scheduled as to have irrigations once a week. Treatments were selected as full irrigation (I_{100}) in which 100% of depleted moisture was supplied, water-stressed (WS) treatment (I_{70}) in which 70% of depleted moisture was supplied and excessive water stress treatment (I_{35}) in which 35% of depleted water was supplied. Therefore, one full irrigation and two deficit irrigation treatments were created.

Drip irrigation was used to perform irrigations. A lateral line (20 mm and 4 atm operational pressure, 0.33 m apart 4 L h^{-1} drippers) was placed along each plant row. Soil infiltration rate was measured as 7 mm h^{-1}. Deep percolation and surface runoff were not considered. Each plot has a size of 6 x 2.8 m (16.8 m^2) with 4 plant rows with 70 cm row spacing and 30 cm on-row plant spacing. A buffer zone of 2 m was placed between the experimental plots as to prevent interactions. All of the phosphor fertilizer (pure 90 kg ha^{-1} P_2O_5) and one third of nitrogen (280 kg ha^{-1} N) were supplied at sowing. Rest of the nitrogen was given when the plants were 40-50 cm tall.

Gravimetric moisture content of each layer (0-30, 30-60 and 60-90) was converted into depth with Equation 1.

$$d = (Pw\text{-}Pw_{AW})xAsxD/100 \quad (1)$$

Where; d, soil moisture content in depth (mm); Pw, field capacity (%); $Pw_{AW,}$ moisture content of each layer (%); As, soil unit weight (g cm^{-3}); D, layer depth (mm). Volume of water to be applied was calculated by using the following Equation 2.

$$d_{T\ 0\text{-}90}=d_{(0\text{-}30)}+ d_{(30\text{-}60)} + d_{(60\text{-}90)} \quad (2)$$

Where; $d_{T\ 0\text{-}90}$, Soil moisture at 0-90 cm soil profile (mm); $d_{(0\text{-}30),}$ Soil moisture at 0-30 cm soil profile (mm); $d_{(30\text{-}60),}$ Soil moisture at 30-60 cm soil profile (mm); $d_{(60\text{-}90)}$: Soil moisture at 60-90 cm soil profile (mm).

Volume of water to be applied to each plot was calculated by Equation 3.

$$V=d_TxAxU_oxP \quad (3)$$

Where; V, volume of water to be applied (L); A, plot size (m^2); Uo, deficit ratio (%) and P, cover ratio (%).

Plant canopy width was divided by row spacing to get cover ratios (CR). The ratio was taken as 0.30 and 0.80 for cover ratios of 30% and 80%. The principles specified in Gungor et al [2]) were used to find out the amount of water to be used in each plot.

Plant water consumptions were calculated by using Equation 4 [25].

$$ET_a= P + I – R_f – D_p \pm \Delta S \quad (4)$$

Where; $ET_{a,}$ evapotranspiration (mm); P, precipitation (mm); I, amount of irrigation water (mm); $R_{f,}$ surface flow (mm); $D_{p,}$ deep percolation (mm); ΔS, the change in soil moisture (mm).

Harvest was performed when the seed moisture content decreased to 15% to determine the yields. Side rows and 0.5 m space at top and bottom of inner two rows were omitted as to consider side effects.

Number of Alive Larva + Pupa: Effects of different irrigation levels on number of alive larva + pupa; 25 plants were splitted from mid-sections into two halves and then alive larva and pupas were counted [5].

Number of Alive Larva + Pupa per plant: Total number of larva and pupa was divided by number of plants to get number of alive larva + pupa per plant. Then, genotypes were compared with each other based on these numbers.

Number of holes / 100 internodes: To determine the effects of different irrigation levels on number of holes / 100 internodes ratio, 25 plants from two rows of each genotype were harvested 20 days before the harvested. Leaves were removed from the plants. Then, number of internodes and number of pest exit holes above and below the corn cobs were counted separately [26; 27].

Number of holes / 100 internodes method:

Below-cob section: Number of holes / 100 internodes = B/A x 100

(Below-cob total number of holes was divided by below-cob total number of internodes and the multiplied by 100). B: Below-cob total number of holes, A: Below-cob total number of internodes.

Above-cob section: Number of holes / 100 internodes = E/D x 100

(Above-cob total number of holes was divided by above-cob total number of internodes and the

multiplied by 100). E: Above-cob total number of holes, D: Above-cob total number of internodes.

Whole plant: Number of holes / 100 internodes = B+E/A+D x 100

(Below and above-cob total number of holes was divided by below and above-cob total number of internodes and the multiplied by 100).

Tunnel (gallery) Length / Plant: To determine the effects of different irrigation levels on tunnel (gallery) length / plant; 25 plants over which number of holes was counted were vertically splitted into two halves and the lengths of tunnels above and below the cobs were measured with a ruler [26, 27].

Tunnel length / Plant: The genotypes assessed for tunnel length / plant were then assessed for damage index; plants were assessed as highly resistant for tunnel lengths of less than 3 cm, resistant for tunnel lengths of between 3-7 cm, moderately resistant for tunnel legs of between 7-10 cm, sensitive for tunnel length of over 10 cm. The tunnels with a length of less than 2.5 cm were not assessed as tunnels, such holes was considered as entrance-exit of the pests and not fed from the plant [27].

Each plot had 4 rows, plot length was 6 m, row spacing was 70 cm and on-row plant spacing was 20 cm. Two rows were used for yield and other observations and the other two rows were used for European and Mediterranean corn borer damage assessments. Mediterranean corn borer inoculations were not performed and natural larva was considered in all calculations and assessments. Pesticides were not applied to control main pests (*s.nonagrioides* lef. and östrinia nubilalis hübner). Also the effects of different irrigation levels (I_{100}, I_{70}, I_{35}) on European corn borer (östrinia nubilalis hübner) populations were not found to be assessable because of quite small size of pest population.

Fatty acid contents. GS-MS device was used to determine the fatty acid composition of corn genotypes (31D24, ADASA16, P1429) at different irrigation levels (I_{100}, $I_{70,}$ I_{35}). Plant samples were grounded in a hand mill. Then, 5-7 grams of ground samples were extracted with petroleum ether at 110 °C for 45 minutes. Following the soxalate cartridge, extracts were kept in an over at 120 °C for 2 hours to fully volatilize the solvent. Then the samples was reweighted and placed again into the oven. This process was repeated until a constant weight. Sample with constant weight was weighted last time. Oil content was determined by using the following equation:

Amount of oil (%) = Amount of oil obtained / Amount of sample * 100

Esterification of oil sample and GC-MS process. About 3 mL oil samples were placed in tubes and then supplemented with 5 mL 1 M KOH solution (dissolved in methanol). Tubes were vortexed and thoroughly shaken. Esterified fatty acids formed an upper phase and this phase was filtered through 0.22 micron filter. Then, 0.5 mL of filtered sample was completed to 2 mL with methanol.

GC-MS conditions. For hydrocarbon analyses: Thermo-brand Trace 1310 GC and ISQ LT MS series. Column: Thermo-brand TG-WAXMS 250/260 ºC: 60 m x 250 µm x 0.25 µm. Carrier gas: Helium at 1.30 mL/min. Injection volume and temperature: 1µl, 250 ºC. Split ratio: 20:1. Ionization mode: EI, 50-550 amu mass, 53.36 minute program.

Analysis of variance (ANOVA) was performed in accordance with randomized blocks – split plots experimental design. Significant treatments were then subjected to LSD (Least Significant Difference) multiple comparison tests. A correlation analyses were carried out to identify the relationships between the traits. The directions of the relationships (positive or negative) were determined. Analyses were carried out with JUMP 5.0.1a statistical software [28].

RESULTS AND DISCUSSION

Sowing was performed on 30 May 2015 and 2016 in the first and second year of experiments. Irrigation treatments were initiated on 01.07.2015-2016 when 50% of available moisture in efficient root zone (0-90 cm) was depleted and treatments were terminated on 11.09.2015 and 19.09.2016. Harvest was performed on 30 September in I_{35} and on 03.October 2015 in I_{100} treatments of the first year; on 26 September in I_{35} and 30 September 2016 in I_{100} treatments of the second year. Because of drier conditions of the second year, harvests were performed 4 days earlier in I_{35} and 3 days earlier in I_{100} treatments of the second year (Table 2).

With regard to kernel yield, main plot (genotype) x sub-plot (irrigation) interactions were found to be significant ($P<0.01$). Kernel yields of the first varied between 10443.3-2916.6 $kgha^{-1}$ with the greatest yield from I_{100}x31D24 interaction (10443.3 $kgha^{-1}$) and the lowest yield from I_{35}xP1429 interaction (2916.6 $kgha^{-1}$). While I_{100}x31D24 interaction was placed in Group A, I_{35}xP1429 interaction was placed in Group I. According to variance analyses for yields, irrigation treatments and genotypes were also found to be significant ($P<0.01$). The greatest yield (10274.4) was obtained from I_{100} treatment and the lowest yield (3534.4 $kgha^{-1}$) was obtained from I_{35} treatment. With regard to genotypes, the greatest yield (7276.6 $kgha^{-1}$) was obtained from 31D24 genotype and the lowest yield (6678.8 $kgha^{-1}$) was obtained from P1429 genotype. The kernel yields of the second year varied between 10353.3-2800.0 $kgha^{-1}$ with the greatest yield from I_{100}x31D24 interaction (10353.3 $kgha^{-1}$) and the lowest yield from I_{35}xP1429 interaction (2800.0

TABLE 3
Changes in yield and physiological properties of corn genotypes depending on the amount of irrigation water

Treatments	Yield (kg ha^{-1}) **	NOH/100 (piece/plant) **	TL/P (cm) **	TNOAL+PP (piece/body) **	Irrigation water (mm)	ETa (mm)	WUE (kg da mm^{-1})
	2015 (First year)						
	Irrigation treatments						
I_{100} (FI)	1027.44 a	9.92 a	15.96 a	3.52 a	675.32	722.11	1.42
I_{70} (DI)	718.22b	7.93 b	14.13 b	2.25 b	518.77	565.77	1.27
I_{35} (DI)	353.44 c	5.73 c	7.13 c	2.23 b	297.77	358.22	0.99
LSD (0.05)	5.38	0.020	0.33	0.17			
	Varieties						
31D24	727.66 a	8.79 a	7.76 c	2.20 c			
ADASA16	703.55 b	7.54 b	10.66 b	2.64 b			
P1429	667.88 c	7.26 c	18.80 a	3.16 a			
LSD (0.05)	4.40	0.10	0.50	0.24			
	Iirrigation x genotype interactions						
I_{100}x31D24	1044.33 a	11.50 a	8.96 e	2.82 c	686.33	734.66	1.42
I_{100}xADASA16	1024.66 b	9.30 b	13.15 c	3.43 b	673.33	719.00	1.42
I_{100}xP1429	1013.33 c	8.98 c	25.79 a	4.32 a	666.32	712.66	1.42
I_{70}x 31D24	734.66 d	8.64 d	8.49 ef	1.98 fg	529.66	576.33	1.27
I_{70}x ADASA16	721.33 e	7.70 e	11.54 d	2.25 ef	515.67	561.33	1.28
I_{70}xP1429	698.66 f	7.47 f	22.37 b	2.70 cd	511.00	559.66	1.25
I_{35}x 31D24	404.00 g	6.24 g	5.85 h	1.80 g	304.00	360.33	1.12
I_{35X}ADASA16	364.66 h	5.62 h	7.30 g	2.25 ef	295.66	357.66	1.02
I_{35}xP1429	291.66 ı	5.34 ı	8.25 f	2.46 de	293.67	356.66	0.82
LSD (0.05)	9.33	0.17	0.58	0.30			
	2016 (Second year)						
	Irrigation treatments						
I_{100} (FI)	1018.00 a	11.10 a	16.97 a	4.55 a	675.33	722.10	1.41
I_{70} (DI)	709.22 b	8.98 b	15.15 b	3.24 b	522.66	565.77	1.25
I_{35}	341.66 c	6.78 c	8.09 c	2.37 c	295.67	358.22	0.95
LSD (0.05)	4.53	0.059	0.38	0.20			
	Varieties						
31D24	717.55 a	9.85 a	8.71 c	2.93 c			
ADASA16	692.88 b	8.62 b	11.67 b	3.38 b			
P1429	658.44 c	8.39 c	19.83 a	3.86 a			
LSD (0.05)	4.60	0.098	0.39	0.15			
	Iirrigation x genotype interactions						
I_{100}x31D24	1035.33 a	12.70 a	9.92 e	3.87 c	686.33	734.66	1.41
I_{100}xADASA16	1015.66 b	10.50 b	14.16 c	4.46 b	673.33	719.00	1.41
I_{100}xP1429	1003.00 c	10.10 c	26.83 a	5.33 a	666.33	712.66	1.40
I_{70}x 31D24	724.00 d	9.61 d	9.48 ef	2.70 e	529.66	576.33	1.26
I_{70}x ADASA16	711.33 e	8.71 e	12.55 d	3.33 d	515.66	561.33	1.27
I_{70}xP1429	692.33 f	8.62 e	23.41 b	3.70 c	511.00	559.66	1.24
I_{35}x 31D24	393.33 g	7.24 f	6.73 h	2.26.g	304.00	360.33	1.09
I_{35X}ADASA16	351.66 h	6.65 g	8.30 g	2.35 fg	295.66	357.66	0.98
I_{35}xP1429	280.00 ı	6.45 h	9.25 f	2.55 ef	293.66	356.67	0.79
LSD (0.05)	7.98	0.017	0.67	0.26	686.33	734.66	

* and **, significant at P≤0.05 and P≤ 0.01 level, respectively; ns, not significant; means in the same column with similar letter are not significantly different from each other; NOH/100, Number of holes /100 internodes; TL/P, Tunnel length/plant; TNOAL+PP, The number of alive larva+pupa in the plant; ETa, Plant water consumptions

kgha^{-1}). While I_{100}x31D24 interaction was placed in Group A, I_{35}xP1429 interaction was placed in Group I. The 31D24 genotype had greater yields in both full and deficit irrigation treatments (Table 3). Cerit et al. [5] reported the yields of fully irrigated non-chemical treated plots as between 3690.0-10955.0 kgha^{-1}; Turkay et al. [29] reported yields as between 2650-10524.0 kgha^{-1}; Turkay et al. [30] as between 3020.0-11020.0 kgha^{-1}; Turkay et al. [27] reported the yields of sensitive hybrids as between 386.0-2683.0 kgha^{-1} and the yields of resistant hybrids as between 6803.0-9984.0 kgha^{-1}. Present findings are somehow different from those earlier ones because of the differences in environmental factors, climates, irrigation programs, corn genotypes, cultural practices. With regard to corn borer population, main plot (genotype) x sub-plot (irrigation) interactions were found to be significant (P<0.01). In the first year (2015), Mediterranean corn borer populations varied between 4.32-1.80 pests plant^{-1} with the greatest population in I_{100}x P1429 interaction (4.32 pest plant^{-1}) and the lowest population in I_{35}x31D24 interaction (1.80 pest plant^{-1}). While P1429 genotype was placed in Group A, 31D24 genotype was placed in Group G. According to variance analyses on corn borer populations, irrigation treatments and genotypes were also found to be significant (P<0.01). The greatest corn borer population (3.52) was observed in I_{100}

TABLE 4
The correlation coefficients between irrigation and other parameters

a (2015)	NOH/100	TL/P	TNOAL+PP	Yield	ETa	Irrigation
NOH/100						
TL/P	0.263 ns					
TNOAL+PP	0.430 *	0.748 **				
Yield	0.933 **	0.510 **	0.643 **			
ETa	0.930 **	0.526 **	0.641 **	0.994 **		
Irrigation	0.928 **	0.528 **	0.633 **	0.995 **	0.999 **	
b (2016)	NOH/100	TL/P	TNOAL+PP	Yield	ETa	Irrigation
NOH/100						
TL/P	0.275 ns					
TNOAL+PP	0.673**	0.790**				
Yield	0.935**	0.512*	0.854**			
ETa	0.938**	0.496*	0.865**	0.994**		
Irrigation	0.942**	0.479*	0.856**	0.991**	0.999**	

* and **, significant at P≤0.05 and P≤ 0.01 level, respectively; ns, not significant; NOH/100, Number of holes /100 internodes; TL/P, Tunnel length/plant; TNOAL+PP, The number of alive larva+pupa in the plant; ETa, Plant water consumptions

and the lowest population (2.23) was observed in I_{35} treatment. Considering the genotypes, the greatest population (3.16) was observed in P1429 and the lowest population (2.20) was observed in 31D24 genotype. In the second year of the experiments (2016), Mediterranean corn borer populations varied between 5.33-2.26 pests plant^{-1} with the greatest value in I_{100}xP1429 interaction (5.33) and the lowest value in I_{35}x31D24 interaction (2.26). While P1429 genotype was placed in Group A, 31D24 genotype was placed in Group G. According to variance analyses, irrigation treatments and genotypes were also found to be significant in the second year (P<0.01). The greatest corn borer population (4.55 pests plant^{-1}) was observed in I_{100} and the lowest population (2.37 pests plant^{-1}) was observed in I_{35} treatments. Considering the corn borer populations of the genotypes, the greatest value (3.86) was observed in P1429 and the lowest value (2.93) was observed in 31D24 genotype. Cerit et al. [5] reported the number of alive larva + pupa in 33P67 Bt (transgenic) genotype in full irrigated and untreated plots as 0.037 and reported the value for isogenic (non-transgenic) 33P66 genotype as 2.220 pest plant^{-1}. Those values were partially similar with the present ones.

With regard to tunnel lengths, main plot (genotype) x sub-plot (irrigation) interactions were found to be significant (P<0.01). In the first year, tunnel lengths varied between 25.79-5.85 cm with the greatest value in I_{100}xP1429 interaction and the lowest value in I_{35}x31D24 interaction. While P1429 genotype was placed in Group A, 31D24 genotype was placed in Group H. According to variance analyses on tunnel lengths of the first year, irrigation treatments and genotypes were found to be significant. The greatest tunnel length (15.96 cm) was observed in I_{100} and the lowest tunnel length (7.13 cm) was observed in I_{35} treatment. Considering the tunnel lengths of the genotypes, the greatest value (18.80 cm) was observed in P1429 and the lowest value (7.76 cm) was observed in 31D24 genotype. In the second year of the experiments, tunnel lengths varied between 26.83-5.85 cm with the greatest value in I_{100}x P1429 interaction and the lowest value in I_{35}x31D24 interaction. While P1429 genotype was placed in Group A, 31D24 genotype was placed in Group H. Turkay et al. [31] reported tunnel lengths in full-irrigated untreated plots as between 0.2-56.9 cm plant^{-1}. Those values were different from the present ones because of differences in environmental factors, climates, cultural practices, irrigation programs, genotypes, inoculations and biotic stress factors.

With regard to number of holes 100 internodes^{-1} values, main plot (genotype) x sub-plot (irrigation) interactions were found to be significant (P<0.01). In the first year of the experiments (2015), number of holes 100 internodes^{-1} values varied between 11.50-5.31 with the greatest value in I_{100}x31D24 interaction (11.50) and the lowest value in I_{35}xP1429 interaction (5.31). While 31D24 genotype was placed in Group A, P1429 genotype was placed in Group I. According to variance analyses, irrigation treatments and genotypes were also found to be significant (P<0.01). The greatest number of holes 100 internodes^{-1} value (9.92) was observed in I_{100} and the lowest value (5.73) was observed in I_{35} treatment. Considering the number of holes 100 internodes^{-1} values of the genotypes, the greatest value (8.79) was observed in 31D24 and the lowest value (7.26) was observed in P1429 genotype. In the second year of the experiments (2016), number of holes 100 internodes^{-1} values varied between 12.70-6.45 with the greatest value in I_{100}x31D24 interaction and the lowest value in I_{35}xP1429 interaction. While 31D24 genotype was placed in Group A, P1429 genotype was placed in Group H. According to variance analyses in the second year, irrigation treatments and genotypes were also found to be significant (P<0.01). The greatest number of holes 100 internodes^{-1} value (11.10) was observed in I_{100} and the lowest value (6.78) was observed in I_{35} treatment (Figure 1). Considering the number of holes 100 internodes^{-1} values of the genotypes, the greatest value (9.85)



FIGURE 1
Images for Mediterranean corn borer counting

TABLE 5
Fatty acid contents of genotypes according to irrigation

RT	Bileşik ismi	I35-31D24 %Area	I35-ADASA16 %Area	I35-P1429 %Area	I70-31D24 %Area	I70-ADASA16 %Area	I70-P1429 %Area	I100-31D24 %Area	I100-ADASA16 %Area	I100-P1429 %Area
5.27	1Benzyloxymethyl1hydroxymethyl3.5cyclohexadıene		-	-	-	-	1.16	-	-	-
16.52	Hexadecanoic acid. methylester (CAS)	-	-	-	10.64	12.10	9.77	13.46	-	-
-+ 0/	Heptadecanoic acid. methylester (CAS)	12.42	15.77	14.51	-	-	-	-	13.30	-
17.44	7Hexadecenoic acid. methylester. (Z)	0.94	-	-	29.96	30.87	29.93	29.59	30.70	-
19.86	1.2.3 Propanetriol (CAS)	1.30	-	-	-	-	-	-	-	-
23.59	14Pentadecynoic acid. methylester (CAS)	-	-	-	-	-	2.71	-	-	-
23.81	Eicosanoicacid. methyl ester (CAS)	3.61	3.15	-	-	-	-	2.03	-	7.97
24.86	9Octadecenoic acid (Z).methyl ester CAS)	25.97	30.96	29.78	-	-	-	-	-	32.27
26.75	9.12Octadecadienoic Acid (Z.Z).methyl ester (CAS)	46.03	47.82	55.72	48.66	55.14	45.47	54.91	56.00	30.61
29.15	11.14.17Eicosatrienoic acid.methyl ester	3.50	2.29	-	-	-	-	-	-	-
30.02	9.12Octadecadienoic Acid (Z.Z).methyl ester (CAS)	0.96	-	-	-	-	-	-	-	-
30.49	9.12Octadecadienoic Acid (Z.Z). methyl ester (CAS)	0.40	-	-	-	-	-	-	-	-
31.67	Eicosanoicacid. methyl ester (CAS)	1.42	-	-	-	-	-	-	-	-
32.56	9Octadecenoic acid (Z).methyl ester (CAS)	1.75	-	-	-	-	-	-	-	-
39.56	Eicosanoicacid. methyl ester (CAS)	0.57	-	-	-	-	-	-	-	-
41.57	12Tridecynoic acid. methylester	0.61	-	-	-	-	-	-	-	-
48.84	Eicosanoic acid.methyl ester (CAS)	0.53	-	-	-	-	-	-	-	-

was observed in 31D24 and the lowest value (8.36) was observed in P1429 genotype. Cerit et al. [5] reported number of holes 100 internodes^{-1} value as 0.130 for 33P67 Bt (Transgenic) genotype, 8.350 for 33P66 genotype and 8.768 for TTM 815 genotype. Turkay et al. [29] reported the least number of holes 100 internodes^{-1} value of full-irrigated untreated plots as 6.1 for 9Bx24A genotype and the greatest as 80.1 for 7C2x9A genotype. Uçak et al. [10, 35] carried out a study about the effects of different irrigation treatments (I_0, I_{20}, I_{40}, I_{60}, I_{80}, I_{100}) on Mediterranean corn borer in second crop corn under Çukurova conditions and reported number of holes 100 internodes^{-1} value of ADA 9516 genotype as 13.50 in I_0 treatment and 27.167 in I_{100} treatment. Those findings were partially different from the present ones because of differences in irrigation programs, corn genotypes, cultural practices, climate conditions and resistance of genotypes to biotic stress.

The greatest values in number of alive larva + pupa, number of holes 100 internodes^{-1}, tunnel length and fatty acids were obtained from I_{100} (full irrigation) treatment and the lowest values were obtained from I_{35} (excessive water deficit) treatment. Corn borer population also decreased from I_{100} to I_{35} treatment. Larva preferred full-irrigated plants. As it was indicated in previous studies, fatty acids accumulated in cell membranes under deficit irrigations. These fatty acids were mostly anti-bacterial, anti-viral and anti-pathogenic. Higher Mediterranean corn borer incidences in I_{100} treatment than in fatty acid accumulated I_{35} treatment (Table 5) comply with the findings of earlier studies. The fatty acids accumulated in cell membranes provide membrane integrity and prevent cellular infection of the pest [32]. Increased fatty acid contents were reported in deficit irrigation treatments of previous studies [33]. It was reported in another study that fatty acids prevented cell membranes from negative environmental conditions, provided membrane flow and contributed to plant resistance and adaptation to adverse conditions [34].

Correlations of irrigations with yield, number of holes 100 internodes^{-1}, tunnel length, alive larva + pupa were also investigated in this study and significant correlations were observed ($p<0.01$) (Table 4). The correlations coefficients (r) for experimental years are provided in Table 4. Each year was assessed in itself to see the variations in correlations in years. In the first year, significant correlations were observed between all traits ($p<0.01$). Highly significant correlations were observed between irrigation and yield (r=0.995**), between irrigation and number of holes / 100 internodes (r=0.928**), between irrigation and tunnel length (r=0.528**), between irrigation and alive larva + pupa (r=0.663**). Similar significant correlations between all traits were also observed in the second year experiments ($p<0.01$). There were highly significant correlations between irrigation and yield (r=0.991**), between irrigation and number of holes 100 internodes^{-1} (r=0.942**), between irrigation and tunnel length (r=0.479*), between irrigation and alive larva + pupa (r=0.856**).

CONCLUSIONS

The present study was conducted to investigate the effects of different irrigation treatments on Mediterranean corn borer populations of three corn genotypes and to assess the pest preferences with chemical analyses. Another objective of the present study was to determine biotic stress screening parameters in identification of genotypes resistant to biotic stress. For determination of screening parameters, yield, tunnel length, alive larva + pupa and fatty acids at different irrigation treatments (I_{100}, I_{70} and I_{35}) were used. Mediterranean corn borer preferred full irrigation (I_{100}) treatment the most and excessive water stress treatment (I_{35}) the least. However, the pest did not prefer every genotype at the same level even in full irrigation treatment. They mostly preferred the genotypes with high fatty acid contents and did not prefer the genotypes with low fatty acid contents. The genotype sensitive to Mediterranean corn borer (P1429) had higher fatty acid contents and types than the genotype resistant to corn borer (P31D24). In this case, sensitive genotypes synthesized higher quantities of fatty acids than resistant genotypes under water deficit and biotic stress. Therefore, high fatty acid ratios can be thought as a defense mechanism against abiotic and biotic stressors. On the other hand, as compared to full irrigation treatment, genotypes had increasing fatty acid contents in their leaves in deficit irrigation treatments. It was also determined that the genotypes with the greatest number of holes had high yield levels and the genotypes with the greatest tunnel length, high number of alive larva + pupa and fatty acid contents had low yield levels. The genotype with the greatest number of holes (31D24) had low fatty acid contents and the pests used the holes only for in and out and not used for feeding purposes. Significant correlations were observed between all investigated traits ($P<0.01$). In other words, increasing yield, number of holes 100 internodes^{-1}, tunnel length and alive larva + pupa values were observed with increasing amount of irrigation water. Therefore, the genotypes with similar performance under both water-stressed and non-stressed conditions could be identified as resistant to corn borer. On the other hand, rather than number of holes 100 internodes^{-1}, tunnel length and fatty acid contents could yield more accurate outcomes in Mediterranean corn borer resistance studies. In this study, the genotype P31D24 with low fatty acid contents and tunnel lengths was identified as moderately resistant and the genotype P1429 with high fatty acid contents and tunnel lengths was identified as sensitive to biotic stress. Several stress screening parameters of the present study can be used in identification of genotype resistances to biotic stressors. Present findings can further be proved with field experiments in future studies.

ACKNOWLEDGEMENTS

The authors thank to Siirt University Scientific Research Projects Department for their financial support and to Fresenius Environmental Bulletin Journal for their technical supports.

REFERENCES

[1] Şimşek, N., Güllü, M. (1992) Akdeniz Bölgesi'nde Mısırda Zarar Yapan Mısır Koçankurdu (*Sesamia nonagrioides* Lef.) (Lepidoptera: Noctuidae) ve Mısırkurdu (*Ostrinia nubilalis* Hbn.) (Lepidoptera: Pyralidae)'nun Mücadelesine Esas Olabilecek Biyolojik Kriterlerin Araştırılması. Türkiye II. Entomoloji Kongresi Bildirileri 28-31 Ocak 1992, Adana. pp. 501- 512 (in Turkish)

[2] Kayapınar, A., Kornoşor, S. (1998) Çukurova Bölgesi'nde Mısır Koçankurdu'nun Mevsimsel Çıkışı ve Populasyon Gelişmesi. Proceedings Of A Symposium On Corn Borers And Control Measures, 1-3 November Adana. 87-91

[3] Castanera, P. (1986) Plagas del Maíz. IV Jornadas Técnicas sobre el Maíz, Líérida. Plagas:1-24. Ministerio de Agricultura Pesca y Alimentación, Madrid.

[4] Zeren, O., Güllü. M, Şimşek, N. (1988) Some Biological Investigations Relating To The Control of Stalk Borer (*Sesamia* spp.) And European Corn Borer (*Ostrinia nubilalis* Hbn.) on Corn in Mediterranean Region. Proceedings of a Symposium On Corn Borers And Control Measures, 1-3 November Adana. 1-19

[5] Cerit, İ., Sarıhan, H., Turkay, M.A., Uçak, A.B., Güllü, M., Kanat A.D. (2006) Mısır kurdu (*Ostrinia nubilalis* Hübner. Lepidoptera: Crambidae) ve Mısır Koçan kurdu (*Sesamia nonagrioides* Lefebvre. Lep doptera: Noctu dae) na Dayanıklı Transgen k Mısır Çeşid Pioneer 33P67 (MON 810) Bt'nin alan deneme Projesi Sonuç Raporu. 102 page Adana (in Turkish)

[6] Şimşek, N., Güllü, M., Zeren, O. (1988) Studies on Effectiveness of Some Agrochemicals Against Stem Borers, *Sesamia nonagrioides* Lef., S. cretica Led. , and European Corn Borer, *Ostrinia nubilalis* Hbn. İn Mediterranean Region of Turkey. Proceedings of a Symposium On Corn Borers And Control Measures, 1-3 November Adana. pp. 44-54.

[7] Larue, P. (1984) La Sésamie du maïs (*Sesamia nonagrioides* Lef.) dégâts et actualisation de la lutte. Phytoma. 227, 163-179

[8] Tsıtsıpıs, J.A. (1988) The corn stalk borer, *Sesamia nonagrioides* forecasting crop-loss assessment and pest management, "Integrated Pest Management in Cereals", Littlehampton, England, Ed. R. Cavallora, A. A. Balkema, Rotterdam, brookfield. pp.171-177

[9] Hunt, J.C.R., Auton, T.R., Sene, K., Thomas., H., Lower. (1988) Proc. Conf. Transient Phenomena in Multiphase Flow, Hemisphere

[10] Uçak, A., Değirmenci, H., Akyol, A., Aykanat, S (2011). İkinci ürün Mısırda Farklı Sulama Konularının Mısır Koçankurdu ve Sap Kurdu Populasyonu Üzerine Etkisi. GAP 6.Tarım Kongresi 09-12 Mayıs Şanlıurfa-Turkey Presentation. page 40-44 (in Turkish)

[11] Monteiro de Paula, F., Pham Thi, A.T., Zuily-Fodil, Y., Ferrari-Iliou, R., Vieira da Silva, J. and Mazliak, P. (1993) Effects of water stress on the biosynthesis and degradation of polyunsaturated lipid molecular species in leaves of *Vigna unguiculata*. Plant Physiol. Biochem. 31, 707-715.

[12] Salama, K.H.A., Mansour, M.M.F., Ali, F.Z.M. ve Abou-hadid, A. (2007) NaCl-induced changes in plasma membrane lipids and proteins of Zea mays L. cultivars differing in their response to salinity. Acta Physiol Plant. 29, 351-359.

[13] Savchenko, T., Walley, J.W., Chehab, E.W., Xiao, Y., Kaspi, R., Pye, M.F., Mohamed, M.E., Lazarus, C.M., Bostock, R.M., Dehesh, K. (2010) Arachidonic acid: an evolutionarily conserved signaling molecule modulates plant stress signaling networks. Plant Cell. 22, 3193-3205.

[14] Trepanier, M., Becard, G., Moutoglis, P., Willemot, C., Gagne, S., Avis, T.J., Rioux, J.A. (2005) Dependence of arbuscular-mycorrhizal fungi on their plant host for palmitic acid synthesis. Appl Environ Microbiol. 71, 5341-5347.

[15] Xing, J., Chin, C-K (2000) Modification of fatty acids in eggplant affects its resistance to Verticilliumdahliae. Physiol Mol Plant Pathol. 56, 217-225.77

[16] Suzuki, N., Miller, G., Salazar, C., Mondal, H.A., Shulaev, E., Cortes, D.F., Shuman,J.L., Luo, X., Shah, J., Schlauch, K., Shulaev, V., and Mittler, R (2013) Temporal-spatial interaction between reactive oxygen species and abscisic acid regulates rapid systemic acclimation in plants. Plant Cell. 25, 3553–3569

[17] Cardinal, A.J., Lee, M., Sharopova, N., Woodman-Clikeman, W.L., Long, M.J. (2001) Genetic mapping and analysis of quantitative trait loci for resistance to stalk tunneling by the European corn borer in maize. Crop Sci. 41, 835–845.

[18] Bohn, M., Schulz, B., Kreps, R., Klein, D., Melchinger, A.E. (2000). QTL mapping for resistance against the European corn borer (*Ostrinia nubilalis* H.) in early maturing European dent germplasm. Theor Appl Genet. 101, 907–917.

[19] Jampatong, C., Mcmullen, M.D., Barry, B.D., Darrah, L.L., Byrne, P.F., Kross, H. (2002). Quantitative trait loci for first and second generation European corn borer resistance derived from the maize inbred Mo47. Crop Sci. 42, 584–593

[20] Cardinal, A.J. and Lee, M. (2005). Genetic relationships between resistance to stalk-tunneling by the European corn borer and cell-wall components in maize population B739B52. Theor Appl Genet. 111, 1–7.
[21] Klute, A. (1986) Water retention: In: Klute, A. (Ed.), Methods of Soil Analysis. Part 2, Physical and Mineralogical Methods, 2nd Edition, Agronomy Monograph No.9, Soil Science Society of America, Madison, WI. pp. 635-653
[22] Blake, G.R. and Hartge, K.H. (1986) Bulk density. In: Methods of Soil Analysis, Part 1, Physical and Mineralogical Methods. (ed: A. Klute) Agr. Monogr. 9. ASA and SSSA, Madison WI. P. 363-375
[23] Tuzuner, A. (1990) Toprak ve Su Analiz Laboratuvarları El Kitabı, T.C. Tarım Orman ve Köyişleri Bakanlığı, Köy Hizmetleri Genel Müdürlüğü, Ankara/Turkey (in Turkish)
[24] Gungor, Y., Erozel, A.Z, Yildirim, O (2006). Sulama. Ankara Üniversitesi Ziraat Fakültesi Yayınları: 1592, Ders Kitabı: 424, Ankara (in Turkish)
[25] Sahin, U., Kiziloglu, F.M, Anapali, O. Okuroglu, M. (2007). Determining crop and pan coefficients for sugar beet and potato crops under cool season semiarid climatic conditions. Journal of Agronomy Crop Science. 193(2), 146-152
[26] Guthherie, W.D, Bary, B.D. (1987) Methodologies used for screening and determining resistance in maize to the European corn borer. In: Proceeding of the International Symposium on Methodologies for Developing Host Plant Rezistance to Maize İnsects, CIMMYT, Mexico. pp: 290-302.
[27] Turkay, M.A., Özkan, H., Serkaya, E., Güllü, M., Korkut, K.Z., Uçak, A.B., Sarıhan, H., Ülger, A.C., Bolat, A. (2011c). Mısır koçankurdu (Sesamia nonagrioides Lef.)'na dayanıklı Mısır Çeşidi Geliştirmek amacıyla Diallel Melezlemede Kullanılacak Hatların Seçilmesi ve melezlemenin Yapılması. Türkiye Tarla Bitkileri Kongresi Poster Bildiri. Page 538-542, 12-15 Eylül Bursa (in Turkish)
[28] Der, G. and Everitt, B.S. (2002) A Handbook Of Statistical Analyses Using SAS. Second Edition. CRC Press LLC, 2000 N.W. Corporate Blvd., Boca Raton, Florida 3431. USA.
[29] Turkay, M.A., Sarıhan, H., Uçak, A.B (2011a), Mısır koçankurdu (Sesamia nonagrioides Lef.) ve Mısırkurdu (ostrinia nubilalis Hübn.)'na dayanıklı Turkay mısır çeşidinin geliştirilmesi. Türkiye Tarla Bitkileri Kongresi Presentation Page 413-417, 12-15 Eylül Bursa (in Turkish)
[30] Turkay, M.A., Sarıhan, H., Uçak, A.B (2011b), Mısır koçankurdu (Sesamia nonagrioides Lef.) ve Mısırkurdu (ostrinia nubilalis Hübn.)'na dayanıklı Turkay mısır çeşidinin İlaçlı İlaçsız Şartlardaki Verim Kaybı ve Dayanıklılık Değerlerinin Belirlenmesi. Türkiye Tarla Bitkileri Kongresi Poster Bildiri Page 538-542, 12-15 Eylül Bursa (in Turkish)
[31] Turkay, M.A., Sarıhan, H., Uçak, A.B (2011d). Development and Evaluation of a Maize Variety With Resistance Against Pink Sem Borer (Sesamia nanogrioides) and European Corn Borer (Ostrinia nubilalis). Book of Extended Summaries for the 11. Asian Maize Conference. Presentation Page 18-21, 7-11 November Nanning,China (in Turkish)
[32] Toumi, I., Moschou, P. N., Paschalidis, K. A., Bouamama, B., Salem-Fnayou, A. B., Ghorbel, A. W., Mliki, A., Roubelakis-Angelakis, K. A (2010). Abscisic acid signals reorientation of polyamine metabolism to orchestrate stress responses via the polyamine exodus pathway in grapevine. Journal of plant physiology, 167, 519-525
[33] Zhang, G., Slaski, J.J., Archambault, D.J, Taylor, G.J. (2011) Alteration of plasma membrane lipids in aluminium-resistant and aluminium-sensitive wheat genotype in response to aluminium.-Physiol.Plant. 99, 302–308, 1997.
[34] Zepeda-Jazo, I., Velarde-Buendía, A. M., Enríquez-Figueroa, R., Bose, J., Shabala, S., Muñiz-Murguía, J., Pottosin, I. I., (2011). Polyamines interact with hydroxyl radicals in activating Ca 2+ and K+ transport across the root epidermal plasma membranes. Plant Physiology, 157, 2167-2180.
[35] Ucak, A.B., Bağdatli, M.C. (2017) Effect of Deficit Irrigation Treatments on Seed Yield, Oil Ratio And Water Use Efficiency of Sunflower (Helianthus annnnsL.) Fresen. Environ. Bull. 26, 2983-2991

Received: **03.08.2017**
Accepted: **13.10.2017**

CORRESPONDING AUTHOR

Ali Beyhan Ucak
Siirt University, Faculty of Agriculture, Department of Biosystem Engineering, Siirt /Turkey

e-mail:abucak@siirt.edu.tr

© by PSP Volume 26 – No. 12A/2017 pages 8221-8225 Fresenius Environmental Bulletin

PHYLOGENETIC ANALYSIS OF *URTICA* SPP. BY THE INTERNAL TRANSCRIBED SPACER (ITS) OF 18S-26S rDNA IN ORDU PROVINCE OF TURKEY

Onur Koloren*, Secil Eker

Department of Plant Protection, Faculty of Agriculture, Ordu University, Ordu, Turkey

ABSTRACT

Twenty *Urtica* spp. samples collected from different geographic locations in Ordu province of Turkey were examined by using 18S-26S rDNA the internal transcribed spacer (ITS) nucleotide sequences. Neighbor-Joining (NJ), Maximum-Parsimony (MP) and Maximum-Likelihood (ML) algorithms were conducted to evaluate the phylogenetic relationships between our samples and references from GenBank. The phylogenetic trees drawn with NJ, MP and ML algorithms showed similar topologies with minor differences. Two *Urtica* species within our samples (Ulubey-U5 and Fatsa-U6) were placed in the same lineage with *Urtica dioica* and *Urtica kioviensis.* Ulubey-U5 appeared as sister to *U. dioica* with 97.7% nucleotide sequence similarity and the pairwise genetic divergence was 0.0242. This relation was supported with 60% and 74% bootstrap values in the NJ and ML trees, respectively. The nucleotide sequence similarity and the pairwise genetic divergence between Fatsa-U6 and *U. kioviensis* were 98.7% and 0.0109. This relation was supported with 88%, 79% and 85% bootstrap values in the NJ, MP and ML trees, respectively. This study is the first report about phylogenetic relationships of *Urtica* species by rDNA-ITS molecular marker in investigated area.

KEYWORDS:
ITS (Internal Transcribed Spacer), *Urtica dioica, Urtica kioviensis,* Ordu

INTRODUCTION

The Urticaceae consist of 54 genera with more than 2000 species [1] and they have subcosmopolitan distribution with most genera and species found in the moist tropics. Sixty three *Urtica* spp. is the largest genus within the Urticeae. The plant is very rich in chemical content and they were used for pharmaceutical, food, fiber, paint and cosmetic industries since centuries. *Urtica* spp. is a single or perennial herbaceous plant found in fields, gardens and roads in our country. *Urtica* spp. reported in our country were *Urtica pilulifera, Urtica membranacea, Urtica urens, Urtica haussknechtii* and *Urtica dioica* [2].

The aim of this study was to investigate genetic diversity of *Urtica* spp. with using 18S-26S rDNA-ITS nucleotide sequences in Ordu province of Turkey. Besides, we aimed to determine different species apart from *Urtica* spp. that have been reported in our country previously and the relationships between them. It is also believed that the molecular level of *Urtica* spp. will help and guide the larger work to be done in the future.

MATERIALS AND METHODS

Plant materials. Twenty freshly plant samples of the *Urtica* species collected from different geographic locations in Ordu province of Turkey. Table 1 represented the *Urtica* spp. examined in this study with data locations and origins. The fresh *Urtica* leaves were collected from sampling sites and they were kept in fridge until using for DNA extraction.

DNA isolation and PCR. DNA was extracted by the CTAB method as previously described by Haymes [3] and by adding some modifications by Eker and Koloren [4]. Briefly, *Urtica* leaf tissues were quickly ground with a hand pestle under liquid nitrogen. The mixture was treated with chloroform/isoamylalcohol (24/1), ethanol/acetate (96/4), ethanol (70%) was reported by Haymes's [3] protocol, respectively. Then, RNase (Qiagen)100 mg/mL) was added to DNA to resuspended DNA and the samples were stored at 37°C. Then, DNA was saved at -20 °C for PCR. PCR reaction in 25 µL final volume was performed with 1×PCR buffer, 10 mM dNTPs, 2.5 mM $MgCl_2$, 10 mM of primers ITS1 and ITS4 [5], 5U Taq polymerase (Thermo Scientific, Maxima Hot Start). The reaction mixture was run in (PeqLab) thermal cycler including first denaturation at 95°C for 15 min, followed by 35 cycles of 95°C for 1 min, 48.7 °C for 2 min and 72 °C for 2 min, and final extension at 72°C for 7 min. PCR products were appeared under the QUANTUM ST5 (Vilber Lourmat) gel system.

TABLE 1
Locations and origin knowledge of *Urtica* species examined in the study

Number of samples	Locations	Latitude (°N)	Longitude (°E)
1	Ordu-Çamaş	45°30'33.26"	37°59'55.42"
2	Ordu-Çatalpınar	40°88'61.16"	37°45'87.28"
3	Ordu-Fatsa	41°02'07.65"	37°53'89.14"
4	Ordu-Fatsa	40°95'34.07"	37°33'20.97"
5	Ordu-Perşembe	41°08'25.38"	37°63'54.69"
6	Ordu-Perşembe	41°03'30.93"	37°75'77.09"
7	Ordu-Gülyalı	40°97'65.45"	38°00'66.06"
8	Ordu-Ünye	41°14'28.30"	37°23'24.65"
9	Ordu-Ünye	41°28'04.86"	37°00'09.92"
10	Ordu-Kumru	40°87'29.38"	37°26'36.94"
11	Ordu-Gölköy	40°37'45.63"	37°32'48.99"
12	Ordu-Gölköy	40°68'72.73"	37°61'93.71"
13	Ordu-Gölköy	40°41'47.51"	37°37'19.01"
14	Ordu-Gürgentepe	40°48'09.23"	37°36'47.07"
15	Ordu-Kabadüz	40°75'81.53"	37°93'78.89"
16	Ordu-Korgan	40°83'07.45"	37°34'66.99"
17	Ordu-Altınordu	40°97'69.91"	37°94'46.55"
18	Ordu-Altınordu	40°97'52.48"	37°96'67.69"
19	Ordu-Altınordu	40°98'26.41"	37°90'38.87"
20	Ordu-Ulubey	40°53'04.91"	37°43'21.22"

Sequence analysis and Phylogeny. PCR products were sequenced commercially by Macrogen Inc. (Amsterdam, the Netherlands) for forward and reverse with primer set ITS1/ITS4. BioEdit was used for combining the sequenced fragments [6]. BLAST (Basic Local Alignment Search Tool in NCBI) scores for multiple nucleotide alignments between our *Urtica* samples and the other references of *Urtica* from GenBank were applied with ClustalX [7] and set aright with MEGA 6.0 [8]. Neighbor-Joining (NJ), Maximum-Parsimony (MP) and Maximum-Likelihood (ML) algorithms were conducted to evaluate the phylogenetic relationships between our samples and references from GenBank. The nucleotide sequence similarity and the evolutionary divergence between haplotypes and references were calculated by BioEdit and MEGA version 6, respectively.

RESULTS AND DISCUSSION

Urtica species are wide taxons with different and similar morphological characteristics. Because of this, taxonomists still have problems with many different classifications. In response to this situation, molecular methods are used to determine phylogenetic relationships between different species. In molecular phylogenetic studies, the rDNA-ITS and ETS (external transcribed spacer) gene regions are among the most preferred molecular markers. ITS and ETS nucleotide sequences are an alternative molecular marker to Linnaean's plant classification. In recent years, lineage analysis of rDNA-ITS nucleotide sequences has been used to demonstrate genetic diversity among organisms. ITS and ETS markers still have common phylogenetic signals between data sets and the similar groups may appear at the end of multiple roads in ITS and ETS networks [9]. Phylogenetic association of closely related species can rapidly develop with rDNA-ITS regions [10, 11].

Grosse-Veldmann et al. [12] reported that the systematics of *Urtica* had been problematic for the long years and there had not reported understandable infrageneric relationships of them. The morphological diversity of the morphological characters is extremely limited, while they are found entirely together with different species. They were determined the first molecular phylogeny of 61 genus with 144 in group accessions and 14 outgroup taxa by ITS1–5.8S–ITS2 marker. They indicated that this marker and the others such as psbA–trnH intergenic spacer, trnL–trnF and trnS–trnG could be the solution to the phylogeny problem of *Urtica* spp.

A number of taxonomic problems of *Urtica* spp. in European and American have been solved by reporting many new taxonomic studies [13-16]. According to Henning et al., [15] the taxonomy of *Urtica dioica* was problematic and new florals describe the *U. dioica* which named subcommopolitan species extending from South Africa to New Zealand. *U. dioica* are identified primarily on two distinct clades which are the polygamous western Eurasian and African taxa and the monoecious American taxa by herbarium studies, molecular data and the experimental cultivation of them. Many species groups which have been quite similar to other species in the terms of morphological characters are solved by molecular phylogeny. The little radiations in *U. dioica* were found to be such as one in America, one in Australia-New Zealand, and one in northern Eurasia as previously reported by Henning et al. [15].

The studies reported about *Urtica* spp. in Turkey have been usually performed by microscopic analyses for the morphological characterization. Seçmen et al. [2] reported that *Urtica* species present

in our country are named *Urtica pilulifera*, *Urtica membranacea*, *Urtica urens*, *Urtica haussknechtii* and *U. dioica* by morphological characterization. Kav et al. [17] reported that *Urtica* species are the most commonly used plant for alternative treatment methods in cancer patients in Turkey between 2001-2007. Uzonur et al. [18] reported that *U. dioica* is an important complementary and alternative medicine plant in ethnobotany and medical care in Turkey. In their study, some preliminary experiments were carried out to reveal the strong ecotypes and genetic diversity of *U. dioica* from different phytogeographic regions of Turkey by Randomly amplified Polymorph DNA Polymerase Chain Reaction (RAPD-PCR) method. Hoşbaş ve ark. [19] represented *Urtica spp*. chlorogenic acid content by liquid chromatography. However, there are very few molecular studies on *Urtica* species according to the references information we have reached in Turkey. In addition, there has not been any molecular studies about *Urtica* species based on rDNA-ITS nucleotide sequence data in investigated area, so far. In this study, we used phylogenetic assays based on rDNA-ITS molecular marker data to better understand the genetic differences of *Urtica* spp. collected from Ordu province of Turkey. For this reason, we amplified the 18S-26S rDNA-ITS gene of *Urtica* spp. samples collected from Ordu province as shown in Figure 1. When examined at this gel image, two positive bands can be visible. One of them was from Ordu-Ulubey sample (Ulubey-U5) DNA in the 9th well and the other one was Ordu-Fatsa DNA (Fatsa-U6) in the 13th well (Figure 1).

We determined two *Urtica* species within our samples (Ulubey-U5 and Fatsa-U6). The phylogenetic trees drawn with NJ, MP and ML algorithms showed similar topologies with minor differences. In all of them, our species were placed in the same lineage with *U. dioica* and *U. kioviensis*. Ulubey-U5 appeared as sister to *U. dioica* with 97.7% nucleotide sequence similarity and the pairwise genetic divergence was 0.0242. This relation was supported with 60% and 74% bootstrap values in the NJ and ML trees, respectively. The nucleotide sequence similarity and the pairwise genetic divergence between Fatsa-U6 and *U. kioviensis* were 98.7% and 0.0109. This relation was supported with 88%, 79% and 85% bootstrap values in the NJ, MP and ML trees, respectively. Phylogenetic relationship between *Urtica* spp. from GenBank and our haplotypes was shown in Figure 2 and Pairwise genetic distance in Table 2.

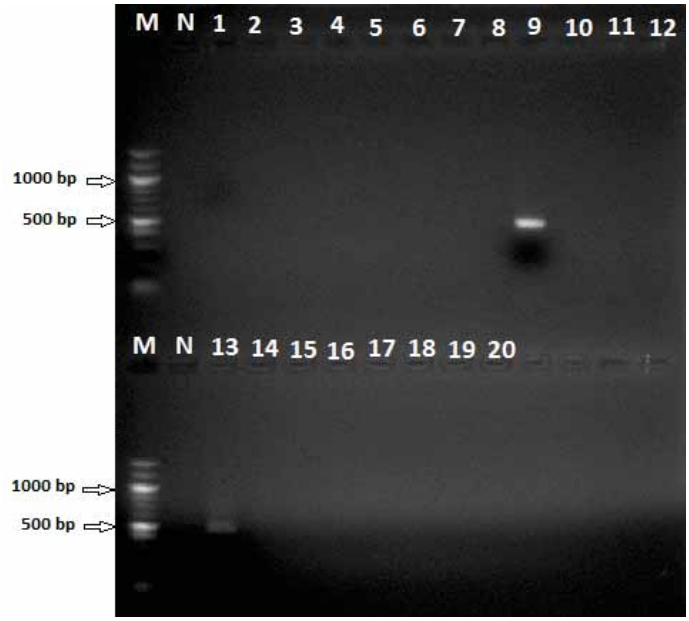


FIGURE 1
The agarose gel of rDNA-ITS gene in *Urtica* spp. collected from Ordu province of Turkey. lane M: 100bp ladder, lane N: Negative control (nuclease free water), lane 1: Ordu-Çamaş-DNA, lane 2: Ordu-Çatalpınar-DNA, lane 3: Ordu-Ünye-DNA, lane 4: Ordu-Altınordu-DNA, lane 5: Ordu-Güyalı-DNA, lane 6: Ordu-Perşembe-DNA, lane 7: Ordu-Kabadüz-DNA, lane 8: Ordu-Korgan-DNA, lane 9: Ordu-Ulubey-DNA, lane 10: Ordu-Gölköy-DNA, lane 11: Ordu-Gürgentepe-DNA, lane 12: Ordu-Gölköy-DNA, lane 13: Ordu-Fatsa-DNA, lane 14: Ordu-Fatsa-DNA, lane 15: Ordu-Gölköy-DNA, lane 16: Ordu-Altınordu-DNA, lane 17: Ordu-Kumru-DNA, lane 18: Ordu-Perşembe-DNA, lane 19: Ordu-Ünye-DNA, lane 20: Ordu-Altınordu-DNA.

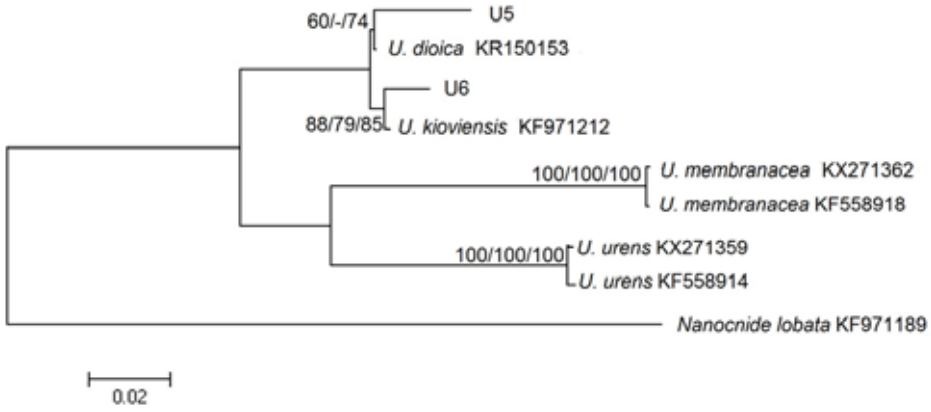


FIGURE 2
Phylogenetic relationship between *Urtica* spp. from GenBank and our haplotypes (Ulubey-U5 and Fatsa-U6)

TABLE 2
Pairwise genetic distance (marked with grey) and DNA sequence percentage similarities between rDNA-ITS haplotypes determined in our research (Ulubey-U5 and Fatsa-U6) and *Urtica* spp. references sequence from GenBank

	U5	***U. dioica***	**U6**	***U. kioviensis***	***U. membra-nacea***	***U. membra-nacea***	***U. urens***	***U. urens***	***Nanocnide lobata***
U5	ID	0,977	0,766	0,775	0,746	0,75	0,746	0,744	0,665
U. dioica	0,0242	ID	0,783	0,793	0,766	0,769	0,765	0,763	0,674
U6	0,0401	0,0153	ID	0,987	0,748	0,751	0,747	0,745	0,644
U. kioviensis	0,0287	0,0043	0,0109	ID	0,753	0,757	0,754	0,752	0,65
U. membranacea	0,1685	0,1388	0,1548	0,1442	ID	0,996	0,833	0,831	0,721
U. *membranacea*	0,1628	0,1334	0,1492	0,1388	0,0043	ID	0,833	0,831	0,72
U. urens	0,1388	0,1103	0,1203	0,1103	0,1379	0,1379	ID	0,998	0,713
U. urens	0,1415	0,1129	0,1230	0,1129	0,1405	0,1405	0,0022	ID	0,714
Nanocnide lobata	0,2702	0,2548	0,2670	0,2548	0,3067	0,3067	0,3162	0,3127	ID

As a result, we reported the phylogenetic relationships by rDNA ITS gene among the genus of *Urtica* in Black Sea of Turkey in here. We found two haplotypes by rDNA-ITS gene sequence and they were in the same lineage with *U. dioica and U. kioviensis*. Determining the phylogenic relationships between species is great importance in terms of genetic characterization, breeding studies and at the same time assessment of genetic material. In addition, the genetic identification of common species in the region can be very useful to more extensive work to be done in the future regarding the molecular level of *Urtica* spp.

ACKNOWLEDGEMENTS

This research was supported by the Ordu University Scientific Research Projects Coordination Unit (ODU BAP, Project Number: AR-1649).

REFERENCES

[1] Kim, C., Deng, T., Chase, M., Zhang, D.G., Nie, Z.L. and Sun, H. (2015) Generic phylogeny and character evolution in Urticeae (Urticaceae) inferred from nuclear and plastid DNA regions. Taxon. 64(1), 65–78.

[2] Seçmen, O., Gemici, Y., Görk, G., Bekat, L. and Leblebici, E. (2004) Tohumlu bitkiler sistematiği. Ege Üniversitesi Basımevi. 181–182.

[3] Haymes, K.M. (1996) Mini-prep method suitable for a plant breeding program. Plant Mol Biol Rep. 14(3), 280–284.

[4] Eker, S. and Koloren, O. (2016) Genetic diversity of *Artemisia* species in the Black Sea of Turkey. Fresen. Environ. Bull. 25(8), 3251–3257.

[5] White, T.J., Burns, T., Lee, S. and Taylor, J. (1990) Amplification and direct sequencing of fungal ribosomal RNA gene for phylogenetics. In: Innis, M.A., Gelfand, D.H., Sninsky, J.J. and White, T.J. (Eds.) PCR protocols: a guide to methods and applications, San Diego: Academic Press. 315–322.
[6] Hall, T.A. (1999) BioEdit: a user-friendly biological sequence alignment editor and analysis program for Windows 95/98/NT. Nucleic Acids Symposium Series. 41, 95–98.
[7] Thompson, J.D., Gibson, T.J., Plewniak, F., Jeanmougin, F. and Higgins, D.G. (1997) The ClustalX-Windows interface: Flexible strategies for multiple sequence alignment aided by quality analysis tools. Nucleic Acids Res. 25, 4876–4882.
[8] Tamura, K., Stecher, G., Peterson, D., Filipski, A. and Kumar, S. (2013) MEGA6: Molecular evolutionary genetics analysis version 6.0. Mol Biol Evol. 30, 2725–2729.
[9] Mitchell, A.D., Heenan, P.B. and Paterson, A.M. (2009) Phylogenetic relationships of *Geranium* species indigenous to New Zealand. New Zeal J Bot. 47, 21–31
[10] Schlötterer, C., Hauser, M.T., Von Haeseler, A. and Tautz, D. (1994) Comparative evolutionary analysis of rDNA ITS regions in *Drosophila*. Mol Biol Evol. 11(3), 513–522.
[11] Kolören, O. and Eker, S. (2016) Phylogenetic relationships of *Geranium* species in different regions of Turkey. Fresen. Environ. Bull. 25(12), 5467–5472.
[12] Grosse-Veldmann, B., Nürk, N.M, Smissen, R., Breitwieser, I., Quandt, D. and Weigend, M. (2016) Pulling the sting out of nettle systematics – A comprehensive phylogeny of the genus *Urtica* L. (Urticaceae). Mol Phylogenet Evol. 102, 9–19.
[13] Weigend, M. (2005) Die Erben Pokornys – Ein Beitrag zur Abgrenzung der enigmatischen Sippen *Urtica galeopsifolia* und *Urtica pubescens* in Mittel- und Osteuropa. Hoppea. 66, 101–117.
[14] Weigend, M. and Luebert, F. (2009) Weeding the nettles I: Clarifying species limits in perennial, rhizomatous *Urtica* (Urticaceae) from southern and central Chile and Argentina. Phytotaxa. 2, 1–12. http://dx.doi.org/10.11646/phytotaxa.2.1.1
[15] Henning, T., Quandt, D., Grosse-Veldmann, B., Monro, A. and Weigend, M. (2014) Weeding the nettles II: a delimitation of '*Urtica dioica* L.' (Urticaceae) based on morphological and molecular data, including a rehabilitation of *Urtica gracilis* ait. Phytotaxa. 162(2), 61-83.
[16] Weigend, M. and Monro, A.K. (2015) 104.17. *Urtica* L. (Urticaceae). In: Davidse, G., Sousa, Sanchez, M., Knapp, S. and Chiang Cabrera, F. (Ed.) Flora Mesoamericana. 2(3), 171–174.
[17] Kav, S., Hanoğlu Z. and Algıer L. (2008) Türkiye'de kanserli hastalarda tamamlayıcı ve alternatif tedavi yöntemlerinin kullanımı. literatür taraması. International Journal of Hematology and Oncology. 1, 18.
[18] Uzonur, I., Akdeniz, G., Katmer, Z. and Karaman Ersoy, S. (2013) RAPD-PCR and real-time PCR HRM based genetic variation evaluations of *Urtica dioica* parts, ecotypes and evaluations of morphotypes in Turkey. Afr J Tradit Complement Altern Med. 10(2), 232–245.
[19] Hoşbaş, S., Aslan, M. and Sezik, E. (2014) Quality assessment of *Urtica dioica* L. samples collected from different locations of Turkey. Turkey Journal Pharm Science. 11(2), 223–230.

Received: **04.08.2017**
Accepted: **13.10.2017**

CORRESPONDING AUTHOR

Onur Koloren
University of Ordu,
Faculty of Agriculture,
Department of Plant Protection,
Ordu - Turkey

e-mail: koloren@yahoo.com
koloren@odu.edu.tr

© by PSP Volume 26 – No. 12A/2017 pages 8226-8232 Fresenius Environmental Bulletin

ULTRASOUND EXTRACTION OF TOTAL FLAVONOIDS FROM TORREYA FARGESII FRANCH. AND ITS ANTIOXIDANT ACTIVITY BASED ON RESPONSE SURFACE METHODOLOGY (RSM)

Jin Shang, Jianhua Wang, Xianrong Zhou*, Bo Jiang, Mingyi Qin

College of Life Science and Technology, Yangtze Normal University, Fuling, 408100, China

ABSTRACT

Ultrasonic-assisted alcohol extraction process was applied to extract the total flavonoids of *Torreya fargesii* Franch., and the optimal extraction process was studied. Meanwhile, the extract solution was tested for its antioxidant activity. In this study, the extraction yield and antioxidant activity of TF from *T. fargesii* using ultrasound extraction (UE) is studied. Significant independent variables of the extraction, including ultrasonic power, ethanol concentration and extraction time, were optimized using the Box-Behnken (BB) method, and the optimal extraction conditions were obtained by response surface methodology (RSM). The extraction solution could effectively scavenge the two kinds of free radicals in a dose-dependent manner.

KEYWORDS:
Ultrasound, Total flavonoids, Box-Behnken (BB) method, *Torreya fargesii* Franch.

INTRODUCTION

Plants are vast repository of compounds with wide range of biological activities such as antinociceptive, anti-inflammation, antidiabetic, anticancer, antimicrobial and antioxidant etc. These properties are due to secondary metabolites including polyphenols, flavonoids, alkaloids, terpenoids, carotenoids, coumarins, curcumines, etc. which have also been confirmed by modern analytical techniques [1].

Torreya fargesii Franch. is up to 12 meters; bark dark gray, irregular longitudinal crack; annual branches green, two or three years old branches were yellow-green or yellow, thin brown. Leaf-shaped, thin striped lanceolate [2-4]. Seeds ovoid, globose or broadly elliptic, fleshy hypocotyls are slightly white powder, and the endosperm is deeply wrinkled inwardly. Flowering 4-5 months, seed 9-10 months mature [5-7]. For our unique species, produced in southern Shaanxi, western Hubei, eastern Sichuan, northeast and western Mount Emei 1000-1800 meters above sea level [8-10].

But its population density is small, habitat damage is serious, the species is in a state of crisis. According to the literature, there are 7 species and 2 varieties of the genus *Torreya*, which are distributed in East Asia and North America [11-13]. *T. taxifolia* and *T. califomica* are produced in North America. *T. nucifera* is distributed in Japan and the Korean Peninsula. *T. grandis*, *T. jackii*, *T. parvifolia*, *T. fargesii*, *T. fargesii* var. *yunnanensis* and *T. grandis* var. *Jiulongshanensis* are distributed in China. *Torreya* is a kind of ancient rare relict plant, has important economic, ecological and scientific research value, is the study of Taxaceae and gymnosperms system development of important groups [14, 15].

This study aims to evaluate the extraction yield and antioxidant activity of TF from *T. fargesii*. using ultrasound extraction (UE). First, the independent variables of the ultrasonic power (500–700 W), the ethanol concentration (50%–70%) and the extraction time (20–30 min) were optimized by using the Box-Behnken approach.

MATERIALS AND METHODS

Materials and reagents. *T. fargesii* were provided by Shuanghe town of Chengkou in Chongqing. Fresh seeds of *T fargesii* was washed, its aril was artificially stripped, was dried naturally. The aril was dried for 24 h at 60 °C to a constant weight. The drying aril was ground, passed through a 60-mesh sieve and kept in sealed polyethylene bags until further use.

Rutin (purity >99.9%) was purchased from Shifang Jubang Plant Material Co., Ltd China. DPPH was provided by Shanghai Dachen Chemical Reagent Factory. Tris (hydroxymethyl) methyl aminomethane was purchased from the Chinese Medicine Group Chemical Reagent Co. Ltd., China. Other analytical grade solvents (sodium nitrite, aluminium nitrate, sodium hydroxide, absolute ethyl alcohol, ferrous sulphate, hydrogen peroxide, concentrated hydrochloric acid and salicylic acid) were obtained from Beijing Dahua Co. Ltd.

UV-1810 UV Spectrophotometer: Beijing Yali Instrument Co., Ltd.; ZEALWAY type ultrasonic cleaning instrument: Nanjing Ultrasonic Instrument

Co., Ltd.; YSC-300 multi-functional Chinese medicine grinder: Beijing Yanshan Zhengde Chinese Medicine Machinery Co., Ltd.; EX35001ZH type of electronic DHG-9240A Digital Blowing Dryer: Beijing Qingyuan Industrial Co., Ltd. H · SWX-600BS Electric Heating Thermostatic Water Bath: Beijing Zhongji HSBC Technology Co., Ltd.; R-300 Rotary Evaporator: BUCHI Labortechnik AG.

Extraction of Total Flavonoids. The experiment was carried out by ultrasonic assisted extraction. Accurately weighed 2.0 g of the pseudo-seed powder in 100 mL Erlenmeyer flask, ethanol as solvent, placed in ultrasonic cleaner ultrasonic extraction, ultrasonic power of 250 W, repeat twice, the combined filtrate, filter, reduced to 100 mL volumetric flask, with the same volume fraction of ethanol constant volume to the scale, shake, put in the refrigerator to be measured.

Determination of total flavonoids content. Accurately weighed rutin standard 20 mg placed in 100 mL volumetric flask, add 60% ethanol, water bath dissolved, let cool, with 60% ethanol volume to the scale, shake, prepared into 0.2 mg / mL of the reed Standard solution.

Respectively, the precise absorption of rutin standard solution 0.0, 0.2 mL, 0.4 mL, 0.6 mL, 0.8 mL, 1.0 mL and 1.2 mL in 10 mL volumetric flask, add 5% $NaNO_2$ 0.5 mL solution, shake for 10min, add 10% Al $(NO_3)_3$ 0.5 mL, shake for 10 min, plus 1 mol / L NaOH 4.0 mL, with 60% ethanol solution volume, shake placed 20 min. At the wavelength of 510 nm, the first bottle solution was used as blank control. The absorbance at different concentrations was measured. The absorbance was the ordinate and the concentration was the abscissa. The standard curve was drawn.

Precision extraction of artificial flavonoids extract 5 mL, according to the steps of the determination of parallel 3 times. The total flavonoid content was calculated according to the standard curve.

TABLE 1
Factor level

Factor level	-1	0	1
A (ethanol concentration)/%	50	60	70
B (extraction time) /min	20	25	30
C (ultrasonic power) / W	500	600	700

Experimental design. The central composite design, an experimental design for RSM, was used to create a set of designed experiments by MINITAB software (version 17). In this paper, the central composite design is selected for 3 factors, i.e., ethanol concentration (A), extraction time (B) and ultrasonic power (C).

Table 1 shows the levels of original and coded factors using the Box-Behnken (BB) design. Table 2 shows the Box-Behnken (BB) design and response value.

TABLE 2
The Box-Behnken (BB) design and response value

Run Order	A	B	C	Extraction yield (%)
1	0	-1	-1	1.355
2	1	1	0	1.446
3	1	0	1	1.325
4	-1	1	0	1.323
5	0	1	1	1.373
6	-1	-1	0	1.481
7	-1	0	1	1.464
8	0	0	0	1.358
9	0	-1	1	1.376
10	-1	0	-1	1.413
11	0	1	-1	1.434
12	1	-1	0	1.426
13	0	0	0	1.315
14	1	0	-1	1.476
15	0	0	0	1.508

DPPH radical scavenging capacity. The DPPH radical scavenging capacity was measured by a previously described method [16] with some slight modification. The TF extracts was obtained under the optimal conditions obtained by RSM. DPPH powder (4 mg) was weighed and dissolved using 100 mL of 70% ethanol/water solution. 1 mL of the DPPH solution was added to 5 mL of TF samples solution at different concentration (0.6, 1.2, 1.8, 2.4, 3.0 μg/mL). The solution was then shaken and incubated in the dark at room temperature. After 30 min, the absorbance of the mixed solution, A1, at 517 nm was determined using pure ethanol as the blank. In total, 1 mL of the DPPH solution and 5 mL of 70% ethanol/water solution were used instead of the sample solution to determine Ax. Additionally, another group of TF sample solution was evaluated in this way, except 1 mL of ethanol replacing the 1 mL DPPH solution. The absorbance of these samples is denoted as A10.

The scavenging activity was calculated as follows:

$$\text{DPPH radical scavenging activity}(\%) = \left(1 - \frac{A_1 - A_{10}}{A_c}\right) \times 100\%$$

where A1 and A10 were the absorbance of the diluted extract solution at 517 nm after adding the DPPH solution and ethanol solution, respectively, and Ax is the absorbance of the DPPH solution without TF extracts.

Hydroxyl radical scavenging capacity. The ability of the extracts to scavenge hydroxyl radicals was determined according to a previously described method [17] with some slight modifications. The TF extracts was obtained under the optimal conditions

obtained by RSM. Firstly, 0.5 mL of 6 mmol/mL ferrous sulphate solution and 2 mL of 6 mmol/mL salicylic acid solution were successively added into each of 5 tubes numbered 1–5. Then, 5 mL of TF samples solution at different concentration (7, 14, 21, 28, 35 μg/mL) were added to each tube, respectively. Finally, 2 mL of 3% hydrogen peroxide was added. The absorbance of the mixed solution was designated as A2. Another group of TF samples solution was measured using 2 mL of distilled water in place of the 2 mL of 3% hydrogen peroxide; the absorbances of these samples solution were denoted as A20. Additionally, 0.5 mL of 6 mmol/mL ferrous sulphate solution, 2 mL of 6 mmol/mL salicylic acid solution, 5 mL of 70% ethanol/water solution and 2 mL of 3% hydrogen peroxide were mixed, and the absorbance of this samples solution was denoted as Ay. A blank sample was also prepared. All of the solution was mixed well and incubated for 40 min at 37 °C. The absorbance of all samples solution was determined at 510 nm using a UV spectrophotometer. The hydroxyl radical scavenging capacity was evaluated by the following equation:

$$\text{Hydrogen peroxide scavenging activity}(\%) = \left(1 - \frac{A_2 - A_{20}}{A_y}\right) \times 100\%$$

where A2 and A20 represent the test samples with and without hydrogen peroxide, respectively, at 510 nm, and Ay represents the absorbance value of the background solution.

RESULTS AND DISCUSSION

A positive ethanol concentration influence can be observed in Fig. 1, 2 and 3. In the same way, the negative effect of the quadratic terms of the ultrasonic power and extraction time can be viewed from Fig. 2 and 3.

To achieve the best extraction yield, it is essential to optimize the experimental conditions. Based on the model, three-dimensional surface plots were constructed to predict the relationship between the independent factors and the response by holding the other two variables at a fixed level. The visual inspection of the surface plots is in accordance with the multiple regression analysis.

The optimal conditions are as follows: ultrasonic power of 500W, ethanol concentration of 70% and extraction time of 30 min, and the maximum predicted extraction yield was 1.5389%. To validate the predicted value, the extraction of TF using UE was performed under the optimal conditions with some modification. A mean value for the extraction yield of 1.537% was obtained from these real experiments, and the relative error was less than 3%. Thus, there is a good correlation between the predicted results and the actual values, which validated the model.

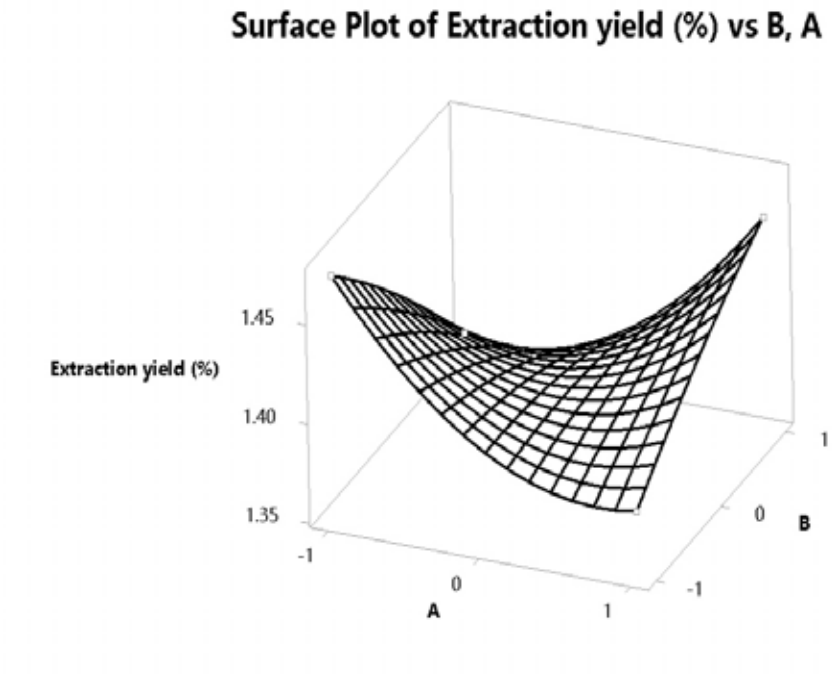


FIGURE 1
Effect of ethanol concentration and extraction time on the extraction yield of flavonoids

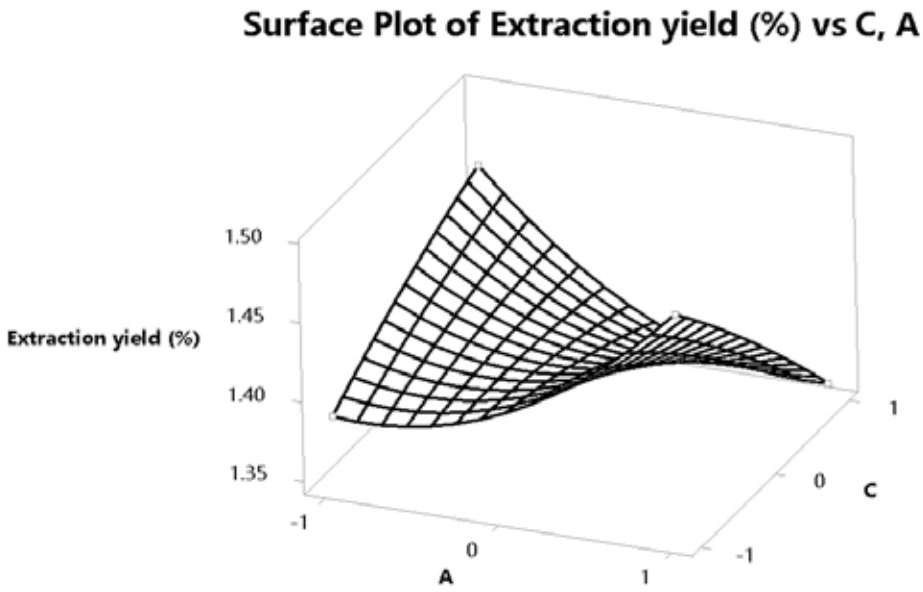


FIGURE 2
Effect of ethanol concentration and ultrasonic power on the extraction yield of flavonoids

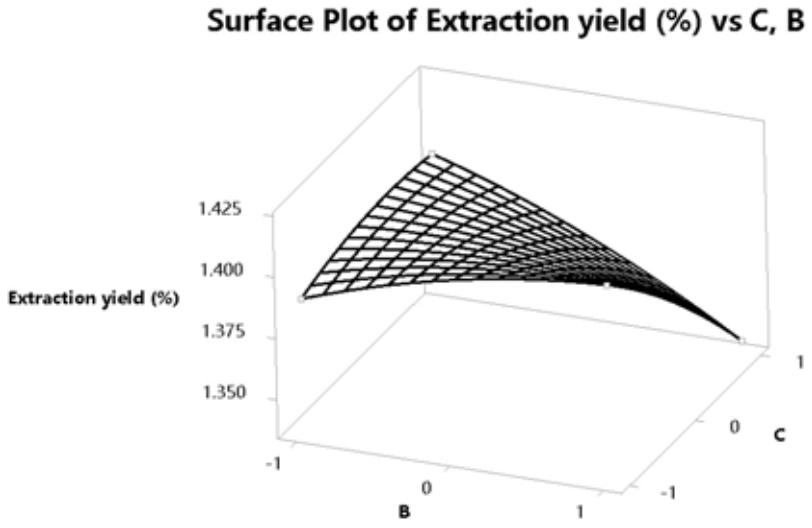


FIGURE 3
Effect of extraction time and ultrasonic power on the extraction yield of flavonoids

Antioxidant activities. DPPH radical scavenging activity. The DPPH radical scavenging activity of flavonoids from *T. fargesii* extracted by the UE method is shown in Fig. 5. These data show that the DPPH radical scavenging capacity increased with increasing TF concentration. For UE, the DPPH radical scavenging activity ranged from 30.81% to 76.24%.

Hydroxide radical scavenging activity. Fig. 6 shows that when the concentration of TF increased from 7 to 35 μg/mL, the values of the hydroxide radical scavenging activity of the TF extract ranged from 11.86% to 27.99% (UE). According to Fig. 6, the results indicated that TF extracted using UE exhibited significant hydroxide radical scavenging activity.

CONCLUSION

It can be concluded that the extraction yield and antioxidant capacities of DPPH, hydroxide radical scavenging activity were excellent for TF from *T. fargesii* using the UE method under the optimal conditions. The optimal conditions of UE method obtained using a response surface methodology for TF extraction from *T. fargesii*. These parameters were as follows: ultrasonic power of 500W, ethanol concentration of 70% and extraction time of 30 min.

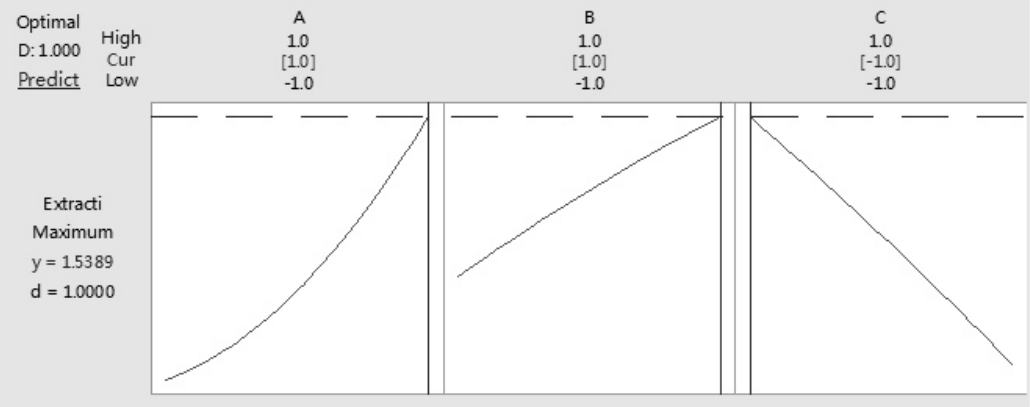


FIGURE 4
Optimal conditions of the extraction of TF

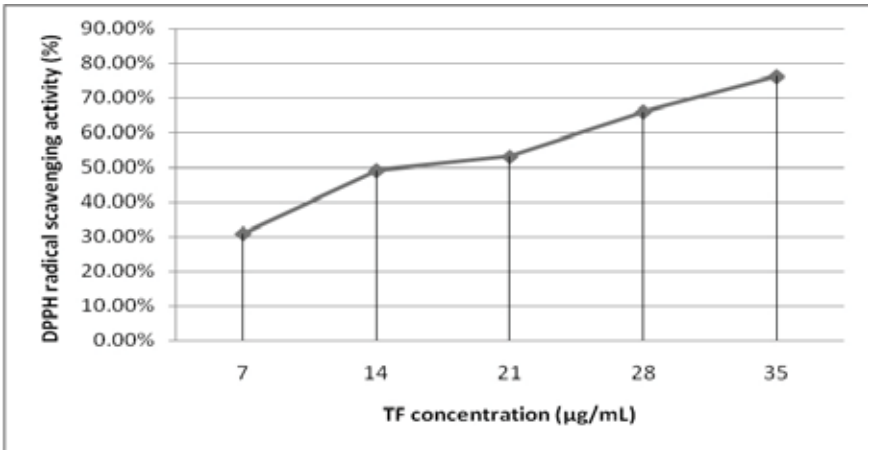


FIGURE 5
The DPPH radical scavenging activity of flavonoids of TF under UE treatment

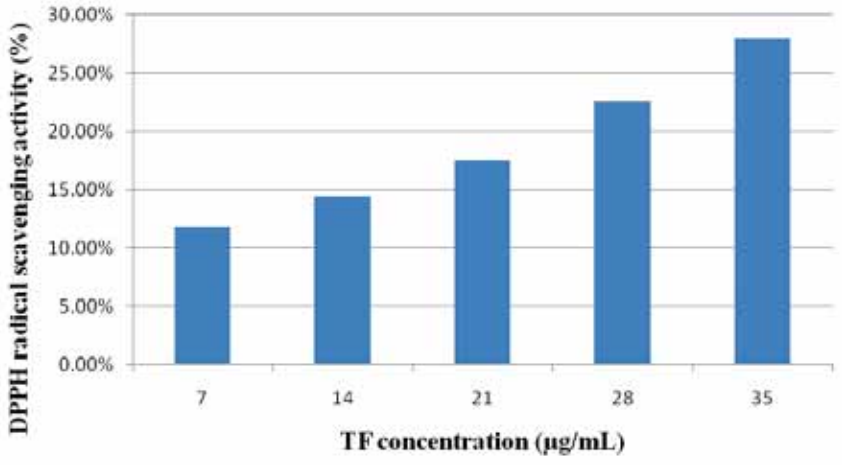


FIGURE 6
The Hydroxide radical scavenging activity of flavonoids of TF under UE treatment

ACKNOWLEDGEMENTS

The research was supported by the National Natural Science Foundation of China (31470568), the Spring Light Program of the Ministry of Education of China (Z2017), the Foundation of the Key Laboratory for Protection and Utilization of Wulingshan Region's Unique Plant Resources of Chongqing, China (2017), the Science and Technology Project of Fuling District, Chongqing, China (FLKJ,2017ABA).

The authors, Jin Shang and Jianhua Wang contributed equally to this work and should be considered co-first authors.

REFERENCES

[1] Singh, G., Maurya, S., Lampasona, M.P.D., and Catalan, C. (2006) Chemical constituents, antifungal and antioxidative potential of *Foeniculum vulgare* volatile oil and its acetone extract. Food Control. 17(9), 745-752.

[2] Ye, B., Chen, Y., Zhuang, Z., Lin, R., and Zhu, J. (2002) Study on isolation and characterization of total DNA and RAPD reaction condition in *Torreya fargesii* Franch. Journal of Xiamen University. 41(5), 683-686.

[3] Jiang, B., Wang, J.H., Shang, J., and Zhou, X.R. (2016) Characters and species diversity of *Torreya fargesii* Franch. community in the Jinfo Mountains. Journal of Landscape Research. 8(2), 71-74.

[4] Zhou, X.R., Wang, J.H., Shang, J., Jiang, B., and Wang, X. (2016) Interspecific relationships among dominant shrub populations of *Torreya fargesii* shrub community in karst mountain area of Jinfo Mountains. Journal of Southwest University (Natural Science Edition). 38(9), 88-94.

[5] Jiang, B., Zhou, X.R., Gong, L., Qin, M.Y., Sheng, Y.L., Zheng, Y.H., and Li, Z. (2016) Research on seed characteristics and seedling growth law of *Torreya fargesii*, an endangered plant in China. Seed. 35(10), 14-18.

[6] Zhou, X.R., Zhang, W., He, X.J., Zhou, S.D., Yu, Y., and Wang, J.H. (2012) Resources and conservation of *Torreya fargesii*. Journal of Northeast Forestry University. 40(2), 42-46.

[7] Fu, L.G., Li, N., and Mill, R.R. (1999) Taxaceae. In: Wu, Z.Y., and Raven, P.H. (eds.) Flora of China (vol.4) Beijing: Science Press & St. Louis: Missouri Botanical Garden Press.

[8] Farjon, A. (1998) World checklist and bibliography of conifers, 2nd ed. London: Royal Bot. Gard., Kew Publishing.

[9] Wang, J.H., Zhou, X.R., Shang, J., Jiang, B., and Yang, L.P. (2014) Niche characteristics of dominant woody plant populations in a *Torreya fargesii* shrub community in the Jinfo Mountains. Chinese Journal of Ecology. 33(5), 1135-1141.

[10] Ma, J., Chen, F.B., Zhou, X.R., Wang, J.H., and Song, X.H. (2014) Sequences analysis and comparison of *trn*L-*trn*F of geographical populations of *Torreya fargesii* (Taxaceae) and its closely related species. Genomics and Applied Biology. 33(5), 1053-1058.

[11] Wang, J.h., Zhou, X.R., He, X.J., Shang, J., and Jiang, B. (2013) Studies on species composition and structure of *Torreya fargesii* shrub community in the Jinfo Mountains. Journal of Southwest University (Natural Science Edition). 35(7), 32-38.

[12] Xie, X.L. Jiang, B., Zhou X.R., Zhao L.X., Wang, J.H., and Shang, J.. (2016) Allelopathic effects of aqueous extract of *Torreya fargesii* aril on seed germination and seedling growth of radish, mustard and cabbage. Agricultural Biotechnology. 5(4), 11-17.

[13] Zhou, X.R., Yu, Y., Zhou, S.D., and He, X.J. (2012) Geographic distribution and potential distribution of *Torreya fargesii*. Scientia Silvae Sinicae. 48(2),1-8.

[14] Zhou, X.R., Shang, J., Chen, F.B., Song, X.H.,and Jiang, B. (2015) *Psb*A-*trn*H sequence analysis of *Torreya fargesii* and its closely related species. Journal of West China Forestry Science. 44(1), 16-21.

[15] Li, J.H., Davis, C.C., Donoghue, M.J., Kelley S., and Tredici, P.D. (2001) Phylogenetic relationships of *Torreya* (Taxaceae) inferred from sequences of nuclear ribosomal DNA ITS region. Harvard Papers in Botany. 6(1): 275-281.

[16] Yang, T., Han, L., Feng, G.Q., Song, P.P., and Liu, P.H. (2015) Antioxidant activity of total flavonoids from *Sanicula astrantiifolia* Wolff. Modern Agricultural Science and Technology. (17), 311-313.

[17] Minjares-Fuentes,R., Femenia, A., Garau, M.C., Candelas-Cadillo, M.G., Simal, S., and Rosselló, C. (2016) Ultrasound-assisted extraction of hemicelluloses from grape pomace using response surface methodology. Carbohydrate Polymers 138, 180-191.

Received: **07.08.2017**
Accepted: **13.10.2017**

CORRESPONDING AUTHOR

Xianrong Zhou
College of Life Science and Technology,
Yangtze Normal University,
16 Juxian Road Lidu Fuling District
Chongqing – China

e-mail: zxrfsy@163.com

© by PSP Volume 26 – No. 12A/2017 pages 8233-8238 Fresenius Environmental Bulletin

GLUCOSINOLATES IN HEADS AND SPROUTS OF GREEN, WHITE AND ROMANESCO CAULIFLOWER

Golge Sarikamis*, Begum Aydin, Merve Yavuz

Ankara University, Faculty of Agriculture, Department of Horticulture, Ankara, Turkey

ABSTRACT

Brassicaceae vegetables synthesize sulfur containing glucosinolates that are related with health promoting activities due to the hyrolysis products such as isothiocyanates. However, the bioavailability may vary since the glucosinolate content is dependent on the genetic background, growing conditions or developmental stage of the plant. Recent studies suggest that brassica sprouts are rich sources of glucosinolates and can be considered as functional foods. In the present study, glucosinolate content of green, white and romanesco cauliflower cultivars were determined in heads and sprouts. The objective of the study was to identify whether variation exists in terms of glucosinolates among the varieties with different morphological features and to further elucidate whether sprouts or heads are better sources of bioactive compounds. Green, white and romanesco cauliflower were grown in field conditions. At the same time, sprouts of the cultivars were generated in climate controlled growth rooms. Individual and total glucosinolates of heads and sprouts were determined. The highest total glucosinolate content was found in green cauliflower followed by white and romanesco type both in heads and sprouts ($P<0.05$). Total glucosinolates were higher in sprouts compared to heads significantly in green cauliflower.

KEYWORDS:
brassica, cauliflower, glucosinolates, heads, sprouts

INTRODUCTION

Brassica vegetables are often associated with health promoting properties including anticancer activity, protection against diabetes and cardiovascular diseases [1, 2, 3]. These properties are generally attributed to the presence of sulfur containing glucosinolates that have important roles in plant defence as chemical defence compounds in the plant [4]. Glucosinolates are hydrolysed to a range of products by the activation of myrosinases that are also present in plant cells upon cellular damage. Glucosinolates can be hydrolysed to isothiocyanates, nitriles or indoles depending on the side chain structure each revealing different biological activities. Variation in the type of precursor glucosinolates and the hydrolysis products is present among different species within the *Brassicaceae*. While some products are toxic to a wide range of organisms working as defence compounds in plants, some are associated with antiproliferative activities providing anticancer properties. Among these hydrolysis products, isothiocyanates are reported to protect against various forms of cancers [5, 6, 7, 8]. The amount of precursor glucosinolates in brassicas is dependent on the genotype and is influenced by several factors such as growing conditions and different parts or developmental stages of the plant. Therefore, studies are mainly focused on the enhancement of glucosinolates in plants. The development of high glucosinolate broccoli lines through classical breeding approaches by introgressing wild genomic segments from *Brassica villosa* into a commercial genetic background was reported also demonstrating the influence of introgressing genomic segments from a wild brassica on glucosinolate content through genetic and molecular approaches [9].

Recent studies suggest that brassica sprouts are sources of bioactive compounds and may have a potential as functional foods [10]. Chaudhary et al. [11] reported the antioxidant and antiproliferative potential of brassica sprouts in vitro and the potential activity was correlated with the presence of organosulfur compounds such as glucosinolates in brassica sprouts. Broccoli and radish sprouts were evaluated for their postharvest quality including the microbiological and phytochemical content and reported as safe and rich sources of bioactive compounds [12]. The effect of germination temperature on the phytochemical content including total glucosinolates, ascorbic acid, phenolic content was determined in broccoli and rocket sprouts suggesting a positive association with increasing germination temperature and glucosinolate content [13]. Although there have been recent reports on the glucosinolate content of brassica sprouts mainly in broccoli, studies on the glucosinolate content of cauliflower sprouts is limitted.

In cauliflower (*Brassica oleracaea* var. *botrytis*) different varieties exist as a result of spontaneous mutations and selective breeding. Among these, Romanesco cauliflower with distinct head morphology revealing an intermediate form between broccoli and cauliflower originated in Lazio, Italy [14]. Green

head cauliflower is the result of a spontaneous mutation originating in Palermo, Italy [14]. While, these cultivars are grown and consumed particularly at places near the centre of origins, white head cauliflower is common worldwide.

In the present study, the aim was to determine health related glucosinolates in green, white and Romanesco cauliflower both in sprouts as well as in mature cauliflower heads of the same cultivars grown in field conditions in order to determine whether variation exists in terms of glucosinolates among the varieties with different morphological features and to further elucidate whether sprouts or heads are better sources of bioactive compounds in cauliflower varieties. Different from earlier stıudies, the present research reveals the results of two joint experiments demonstrating the response of cultivars at different experimental conditions.

MATERIALS AND METHODS

Plant Material. Green cauliflower *Brassica oleracea* var. *botrytis* cv.TiguanF1, Romanesco cauliflower cv.TouaregF1 (HM Clause Vegetable Seeds) and white cauliflower cv.Memphis F1 (Vilmorin seeds) commercial cultivars were used in the present study.

Field Experiment. The field experiment was conducted at the experimental plots of Ankara University Faculty of Agriculture Department of Horticulture during June-November 2015. Seeds were sown into plug trays on the first week of May and germinated in greenhouse conditions. Seedlings at four-five leaf stage were transplanted to the field conditions, planted in rows spaced as 60x60cm. Drip irrigation was used for watering plants. During the experimental period plants were not sprayed with any chemicals. Cauliflower heads were harvested at maturity beginning in October with Romanesco cauliflower, followed by white and green cauliflower in November 2015.

Generation of sprouts in climate controlled growth room. Seeds of each cultivar were sown in peatmoss (Plantaflor-Humus,Verkaufs-GmBH, Germany) and perlite (2:1) containing seedling trays (32 cmx 20 cmx6 cm) and irrigated with distilled water. Seedlings were generated in a growth room at 22°C±2°C. Light was provided at seedling level by cool fluorescent lamps (72 mMm-1 s-1) with a 16-h light/8-h dark cycle. The relative humidity in the growth room was maintained around 75%. Young seedlings were harvested from the surface two weeks upon sowing, weighed (fresh mass), frozen in liquid nitrogen, and stored at -80°C. Seedlings were lyophilized in a freeze drier (-84 °C, 0.02 mbar) prior to the analyses.

Analysis of Glucosinolates. Glucosinolate analysis was performed according to ISO 9167-1 developed for rapeseed with some modifications as described by [9]. Glucosinolates were extracted from lyophilized tissues that were ground to a fine powder, using 70% (v/v) methanol at 70°C. Extracts were desulfated using Type H-1 Sulfatase from *Helix pomatia* (Sigma®) in an ion exchange column (DEAE Sephadex™). The samples were then collected in vials and desulfoglucosinolates were analyzed by HPLC-UV detection (Shimadzu®) at Ankara University, Faculty of Agriculture, Department of Horticulture. A volume of 50 µl from the extract was injected into a Waters Spherisorb 5µM ODS 2, 4.6x250mm analytical cartridge. HPLC analysis was carried out on a gradient of 99% water and 1% acetonitrile at a flow rate of 1ml/min for 24 min. The detection was carried out at a wavelength of 229 nm. Glucotropaeolin (Applichem®) (16mM) a type of glucosinolate which is not synthesized by cauliflower was used as the internal standard for the quantification of the peaks.

The identity of peaks were determined using pure compounds sinigrin (2-propenyl glucosinolate) (Sigma®), glucoraphenin (4-methylsulsulfinyl-3-butenyl), progoitrin (2-hydroxy-3-butenyl), glucoerucin (4-methylthiobutyl) (PhytoLab® GmbH& Co.), and glucotropaeolin (benzyl glucosinolate) (Applichem®). The standards were desulfated prior to use and run in each sequence as external standards together with plant extracts. Quantification was performed according to [9] and expressed as µmolg^{-1} dry weight using correction factors for each compound [15].

Statistical Analysis. The experiment was conducted according to completely randomized design. Experimental data were expressed as the mean±standard error of the mean with four replications. Each replication consisted of four plants. One-way analysis of variance and Duncan's multiple range test was used to determine the significance of differences among cultivars and different developmental stages using Minitab®14 and MSTAT statistical software. Significant differences were evaluated at $P<0.05$ error level. Data were presented as mean values ± standart error (SE) of the mean.

RESULTS

The analysis of glucosinolates in cauliflower head tissues revealed that in green cauliflower, glucoiberin of the aliphatics was the predominant glucosinolate followed by 3-indolylmethyl of the indole group. In Romanesco cauliflower, 3-indolylmethyl was followed by glucoraphanin and glucoiberin of the aliphatics. In white cauliflower glucoiberin and sinigrin of the aliphatic group were predominant and were followed by 3-indolylmethyl

glucosinolates (Table 1, 2).

In terms of the aliphatic glucosinolates, white cauliflower heads had the highest content (8.39±0.85 μmolg^{-1}), followed by green cauliflower (7.23 ± 0.8 μmolg^{-1}) and Romanesco cauliflower (3.38±0.20 μmolg^{-1}) (P<0.05) (Table 1). However, total indole glucosinolates were not different in green cauliflower (6.84± 0.62 μmolg^{-1}), Romanesco cauliflower (6.66±0.75μmolg^{-1}) and white cauliflower 5.16±0.63μmolg^{-1} (P>0.05) (Table 2). In terms of total glucosinolates (aliphatics and indoles) green cauliflower and white cauliflower heads had the highest content (14.07 ± 0.74 μmolg^{-1} and 13.55 ± 0.74 μmolg^{-1} respectively) followed by Romanesco cauliflower (10.04±0.81 μmolg^{-1}) (P>0.05) (Table 5).

In sprouts, the glucosinolate profile was similar to heads. However, the amount of glucosinolates varied. In green cauliflower sprouts, glucoiberin was the predominant aliphatic glucosinolate (14.09±1.58 μmolg^{-1}), followed by 3-indolylmethyl (7.10 ± 1.19 μmolg^{-1}). In romanesco, glucoraphanin (5.37±1.95 μmolg^{-1}) and glucoiberin (2.17±0.77 μmolg^{-1}) of aliphatics and 3-indolyl-methyl (4.13± 0.99 μmolg^{-1}) of indoles were the predominant. In white cauliflower sprouts, sinigrin (5.86±0,44) and glucoiberin (2.80±0,25) of aliphatics and 3-indolylmethyl (3.48±0.22) of indoles were determined.

TABLE 1
Aliphatic glucosinolates in cauliflower heads (μmolg-1 DW)

Cauliflower	Progoitrin	Glucoiberin	Glucoraphanin	Sinigrin	Total Aliphatic
Green	0.06±0.05	5.83±0.88a	1.07 ± 0.22	0.28±0.08b	7.23 ± 0.80a
Romanesco	0.20±0.06	1.45±0.15b	1.57 ± 0.13	0.16 ± 0.04b	3.38 ± 0.20b
White	0.07± 0.07	4.57±0.62a	-	3.75±0.36a	8.39±0.85a

TABLE 2
Indole glucosinolates in cauliflower heads (μmolg-1 DW)

Cauliflower	3-indolylmethyl	4-methoxy-3-indolylmethyl	1-methoxy-3-indolylmethyl	4-hydroxy-3-indolylmethyl	Total Indoles
Green	4.28 ± 0.29	0.93 ± 0.07a	0.70 ± 0.09b	0.83 ± 0.08	6.84 ± 0.62
Romanesco	3.81 ± 0.47	0.65 ± 0.06b	1.56 ± 0.25a	0.64 ± 0.06	6.66 ± 0.75
White	2.99 ± 0.41	0.54 ± 0.06b	0.58 ± 0.05b	1.05 ± 0.24	5.16 ± 0.63

TABLE 3
Aliphatic glucosinolates of cauliflower sprouts (μmolg-1 DW)

Cauliflower	Progoitrin	Glucoiberin	Glucoraphanin	Sinigrin	Total Aliphatics
Green	-	14.09 ± 1.58a	0.05 ± 0.03b	-	14.14 ± 1.30a
Romanesco	-	2.17 ± 0.77b	5.37 ±1.95a	-	7.54 ± 0.82b
White	-	2.80 ± 0.25b	-	5.86±0.44	8.66 ± 0.64b

TABLE 4
Indole glucosinolates of cauliflower sprouts (μmolg-1 DW)

Cauliflower	3-indolylmethyl	4-methoxy-3-indolylmethyl	1-methoxy-3-indolylmethyl	4-hydroxy-3-indolylmethyl	Total Indoles μmolg-1
Green	7.10±1.19a	1.00±0.40	1.40±0.55	1.62±0.18a	11.12±1.09a
Romanesco	4.13±0.99ab	0.60±0.28	0.47±0.04	1.00±0.16ab	6.20±0.80b
White	3.48±0.22b	0.64±0.32	1.43±0.45	0.88±0.22b	6.43±0.87b

TABLE 5
Glucosinolates in heads and sprouts (μmolg-1 DW)

Cauliflower	Plant part	Total Aliphatic	Total Indole	Total Glucosinolates
Green	Head	7.23±0.80b	6.84±0.62b	14.07±0.74b
	Sprout	14.14±1.3a	11.12±1.09a	25.26±1.9a
Romanesco	Head	3.38±0.20b	6.66±0.75	10.04±0.81
	Sprout	7.54±0.82a	6.20±0.80	13.74±0.90
White	Head	8.39±0.85	5.16±0.63	13.55 ± 0.74
	Sprout	8.66±0.64	6.43±0.42	15.09±0.53

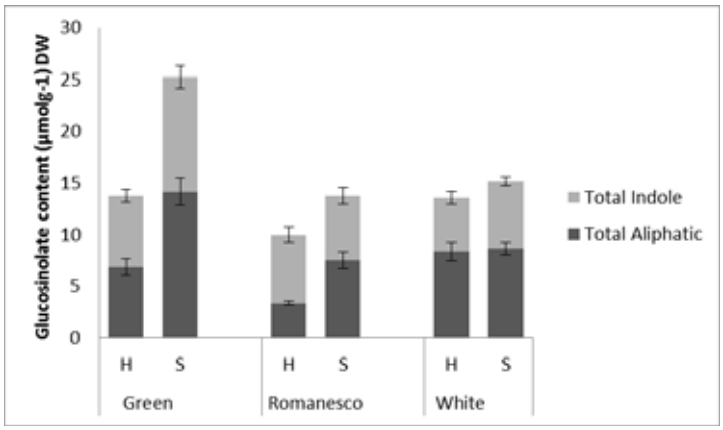


FIGURE 1
Aliphatic and indole glucosinolate content (µmolg-1 DW) of heads (H) and sprouts (S)

In terms of the aliphatic glucosinolate content of sprouts, the total aliphatic glucosinolates was highest in green cauliflower (14.14 ± 1.30 µmolg^{-1}), followed by white cauliflower (8.66 ± 0.64) and romanesco (7.54 ± 0.82 µmolg-1) ($P<0.05$) (Table 3). Indoles were highest in green (11.12±1.09 µmolg-1), white (6.43±0.87 µmolg-1) and romanesco (6.20 ±0.80 µmolg-1) ($P<0.05$) (Table 4). The highest total glucosinolates in sprouts was in green cauliflower (25.26 ± 1.9 µmolg-1), white (15.09±0.53) and romanesco (13.74±0.9 µmolg-1) and the difference among cultivars was significant ($P<0.05$) (Fig 1).

Comparing the glucosinolate content of heads and sprouts, the amount in sprouts was higher than heads (Fig 1). In green cauliflower, the difference among heads and sprouts in terms of aliphatic, indole and total glucosinolates was significant ($P<0.05$). In Romanesco while the difference in terms of aliphatics was significant ($P<0.05$), the difference in terms of indoles and total glucosinolates was not significant statistically ($P>0.05$). In white cauliflower, the difference among heads and sprouts was not significant ($P>0.05$) (Table 5).

DISCUSSION

Most research is focused on the health benefits of bioactive compound sulforaphane (1-isothiocyanato-4-methylsulphinylbutane), which is the hydrolysis product of aliphatic glucosinolate glucoraphanin (4-methylsulphinylbutyl) [2, 7, 8, 16, 17, 18, 19, 20]. Iberin (1-isothiocyanato-3-methylsulfinylpropane) derived from glucoiberin (3-methylsulphinylpropyl) is also reported to have similar activity to sulforaphane [21, 22]. A few research suggest that indole glucosinolates may have anticarcinogenic activities [23, 24]. In the light of these research findings, glucoiberin of the aliphatics was present among cultivars and the amount of total glucosinolates was higher in white and green cauliflower. Indoles, 3-indolylmethyl in particular were higher in green and Romanesco. Findings revealed that, green cauliflower sprouts had almost twice the amount of glucosinolates comapred to heads ($P<0.05$). Although white and romanesco sprouts had higher levels of glucosinolates compared to heads the difference was not significant ($P>0.05$). These are consistent with our previous findings with radish and cabbage seeds, sprouts and young seedlings revealing that the glucosinolate content was dependent on the developmental stage of the plant influencing health promoting properties as sources of bioactive compounds [25].

ACKNOWLEDGEMENTS

This Project was supported by Ankara University Scientific Research Project Office (BAP) Project number: 15H0447002

REFERENCES

[1] Bosetti, C., Filomeno, M., Riso, P., Polesel, J., Levi, F., Talamini, R., Montella, M., Negri, E., Franceschi, S. and La Vecchia, C. (2012) Cruciferous vegetables and cancer risk in a network of case-control studies. Annals of Oncology. 23, 2198–2203.

[2] Liu, X. and Lv, K. (2013) Cruciferous vegetables intake is inversely associated with risk of breast cancer: a meta-analysis. The Breast. 22(3), 309-313.

[3] Mewis, I., Glatt, H., Brigelius-Flohe, R., Blaut, M., Rohn, S., Kroh, L., Knorr, D., Wiesner, M. and Schreiner, M. (2016). Improving dietary glucosinolate production, processing and characterization of potential health effects for the prevention of colon cancer. Berichte aus dem Julius Kühn-Institut. 183, 36.

[4] Burow, M. And Halkier, B. A. (2017) How does a plant orchestrate defense in time and space? Using glucosinolates in Arabidopsis as case study. Current Opinion in Plant Biology. 38, 142-147.

[5] Sakao, K. and Singh, S.V. (2012) D,L-sulforaphane-induced apoptosis in human breast cancer cells is regulated by the adapter protein p66Shc. Journal of Cell Biochemistry. 113(2), 599-610.

[6] Li, Y. and Zhang, T. (2013) Targeting cancer stem cells with sulforaphane, a dietary component from broccoli and broccoli sprouts. Future Oncology. 9(8), 1097-1103.

[7] Tortorella, S.M., Royce, S.G., Licciardi, P.V. and Karagiannis, T.C. (2015) Dietary sulforaphane in cancer chemoprevention: the role of epigenetic regulation and HDAC inhibition. Antioxidants & redox signaling. 22(16), 1382-1424.

[8] Liu, C.M., Peng, C.Y., Liao, Y.W., Lu, M.Y., Tsai, M.L., Yeh, J.C., Yu, C.H. and Yu, C.C. (2016) Sulforaphane targets cancer stemness and tumor initiating properties in oral squamous cell carcinomas via miR-200c induction. Journal of the Formosan Medical Association. S0929-6646(16)00028-0. 10.1016/ j.jfma.2016.01.004. [Epub ahead of print]

[9] Sarıkamış, G., Marquez, J., Maccormack, A., Bennett, R., Roberts, J. and Mithen, R. (2006) High glucosinolate broccoli-A delivery system for sulforaphane. Molecular Breeding. 18, 219-228.

[10] Guo, L., Yang, R., Wang, Z., Guo, Q. and Gu, Z. (2014) Effect of NaCl stress on health-promoting compounds and antioxidant activity in the sprouts of three broccoli cultivars. International Journal of Food Science and Nutrition. 65(4), 476–481.

[11] Chaudhary, A., Choudhary, S., Sharma, U., Vig, A. P. and Arora, S. (2016) In vitro Evaluation of Brassica sprouts for its Antioxidant and Antiproliferative Potential. Indian Journal of Pharmaceutical Sciences. 78(5), 615-623.

[12] Baenas, N., Gómez-Jodar, I., Moreno, D.A., García-Viguera, C. and Periago, P.M. (2017) Broccoli and radish sprouts are safe and rich in bioactive phytochemicals. Postharvest Biology and Technology. 127, 60-67.

[13] Ragusa, L., Picchi, V., Tribulato, A., Cavallaro, C., Lo Scalzo, R. and Branca, F. (2017) The effect of the germination temperature on the phytochemical content of broccoli and rocket sprouts. International Journal of Food Sciences and Nutrition. 68(4), 411-420.

[14] Massie, I.H., Astley, D. and King, G.J. (1996) Patterns of genetic diversity and relationships between regional groups and population of Italian landrace cauliflower and broccoli (Brassica oleracea L. var. botrytis L. and var. italica Plenck. Proceedings of the International Symposium on Brassicas. Ninth crucifer genetics workshop. Acta Horticulture. 407, 45-53.

[15] Brown, P.D., Tokuhisa, J.G., Reichelt, M. and Gershenzon, J. (2003) Variation of glucosinolate accumulation among different organs and developmental stages of Arabidopsis thaliana. Phytochemistry. 62(3), 471-481.

[16] Melchini, A., Costa, C., Traka, M., Miceli, N., Mithen, R., De Pasquale, R. and Trovato, A. (2009) Erucin, a new promising cancer chemopreventive agent from rocket salads, shows antiproliferative activity on human lung carcinoma A549 cells. Food Chemical Toxicology. 47(7), 1430-1436.

[17] Verkerk, R., Schreiner, M., Krumbein, A., Ciska, E., Holst, B., Rowland, I., De Schrijver, R., Hansen, M., Gerhäuser, C., Mithen, R. and Dekker, M. (2009) Glucosinolates in Brassica vegetables: the influence of the food supply chain on intake, bioavailability and human health. Molecular Nutrition and Food Research. 53, Suppl 2:S219.

[18] Li, Y., Zhang, T., Korkaya, H., Liu, S., Lee, H.F., Newman, B., Yu, Y., Clouthier, S.G., Schwartz, S.J., Wicha, M.S. and Sun, D. (2010) Sulforaphane, a dietary component of broccoli/broccoli sprouts, inhibits breast cancer stem cells. Clinical Cancer Research. 16(9), 2580-2590.

[19] Moon, J.K., Kim, J.R., Ahn, Y.J. and Shibamoto, T. (2010) Analysis and anti-Helicobacter activity of sulforaphane and related compounds present in broccoli (Brassica oleracea L.) sprouts. Journal of Agricultural and Food Chemistry. 58 (11), 6672-7.

[20] Egner, P.A., Chen, J.G., Wang, J.B., Wu, Y., Sun, Y., Lu, J.H., Zhu, J., Zhang, Y.H., Chen, Y.S. and Friesen, M.D. (2011) Bioavailability of Sulforaphane from two broccoli sprout beverages: results of a short-term, cross-over clinical trial in Qidong, China. Cancer Preventive Research. 4(3), 384-395.

[21] Wang, W., Wang, S., Howie, A.F., Beckett, G.J., Mithen, R. and Bao, Y. (2005) Sulforaphane, erucin, and iberin up-regulate thioredoxin reductase 1 expression in human MCF-7 cells. Journal of Agricultural and Food Chemistry. 53(5), 1417-1421

[22] Chambers, K.F., Bacon, J.R., Kemsley, E.K., Mills, R.D., Ball, R.Y., Mithen, R.F. and Traka, M.H. (2009) Gene expression profile of primary prostate epithelial and stromal cells in response to sulforaphane or iberin exposure. The Prostate. 69(13), 1411-1421.
[23] Kim, Y.S. and Milner, J.A. (2005) Targets for indole-3-carbinol in cancer prevention. The Journal of Nutritional Biochemistry. 16(2), 65-73.
[24] Fujioka, N., Fritz, V., Upadhyaya, P., Kassie, F. and Hecht, S.S. (2016) Research on cruciferous vegetables, indole-3-carbinol, and cancer prevention: a tribute to lee w. wattenberg. Molecular Nutrition and Food Research 60(6), 1228-1238
[25] Sarıkamış, G., Yıldırım, A. and Alkan, D. (2015) Glucosinolates in seeds, sprouts and seedlings of cabbage and black radish as sources of bioactive compounds. Canadian Journal of Plant Science. 95(4), 681-687.

Received: **08.08.2017**
Accepted: **16.10.2017**

CORRESPONDING AUTHOR

Golge Sarikamis
Ankara University, Faculty of Agriculture,
Department of Horticulture,
Ankara – Turkey

e-mail: Golge.Sarikamis@agri.ankara.edu.tr

© by PSP Volume 26 – No. 12A/2017 pages 8239-8245 Fresenius Environmental Bulletin

THE EFFECTS OF CO-CULTIVATION IN WHEAT (TRITICUM SP.) AND FLAX (LINUM USITATISSIMUM L.) ON SHOOT REGENERATION CAPACITY OF EXPLANTS

Ramazan Beyaz[1,*], Mustafa Yildiz[2]

[1]Department of Soil Science and Plant Nutrition, Faculty of Agriculture, Ahi Evran University, 40100 Bagbasi, Kirsehir, Turkey
[2]Department of Field Crops, Faculty of Agriculture, University of Ankara, 06110 Diskapi, Ankara, Turkey

ABSTRACT

This study was carried out to investigate the relationship between explants from two different genotypes (wheat and flax) cultured together and determine the effects of co-cultivation on tissue culture response of mature embryo explants of wheat (*Triticum* sp.) and hypocotyl explants of flax (*Linum usitatissimum* L.). One winter bread wheat (*T. aestivum* L.) cv. 'Bezostaja 1', one winter durum wheat (*Triticum durum* Desf.) cv. 'Cakmak 79', and two flax cvs. 'Madaras' and '1886 Sel.' were used in the study. Mature embryos excised from sterilized seeds of wheat cultivars were placed scutellum downwards on a medium containing 3 mg l^{-1} 2,4-dichlorophenoxyacetic acid (2,4-D) and incubated at 24±1°C in total darkness for 14 days for callus induction. Hypocotyl segments in 5 mm length were excised from 7-day-old *in vitro*-grown seedlings of flax. Explants (callus for wheat and hypocotyl for flax) of both genotypes were cultured on MS medium supplemented with 0.20 mg l^{-1} 6-benzylaminopurine (BAP) and 0.01 mg l^{-1} naphthalene acetic acid (NAA) for regeneration at 24±1ºC under cool white fluorescent light (27 μmol m^{-2} s^{-1}) with a 16-h light/8-h dark photoperiod for 4 weeks. Sixteen explants were cultured in a 4 x 4 matrix in a Petri dish. Eight out of 16 explants for each genotype were cultured together for co-cultivation. 16 explants from each genotype were cultured alone as control. The results showed that co-cultivation between wheat and flax gave rise to the highest scores in comparison with culturing explants alone.

KEYWORDS:
Co-cultivation, flax, wheat, shoot regeneration

INTRODUCTION

Flax is an important crop all over the world in terms of its aspects as a source of natural fiber and industrial oil, and has the potential of meeting edible oil and protein deficiency [1]. Moreover, it has been used as a model system for genetic manipulation studies due to its small nuclear genome. Wheat (*Triticum aestivum* L.) is the main nutrition source for two thirds of the world population [2, 3]. Yield of wheat has gradually increased in the last century by using conventional breeding methods. However, these methods have some limitations such as long time requirement and limited gene pool [4]. It is well known that cereals' breeding depends on the use of tissue culture techniques which are used to overcome the problems of conventional breeding methods [5].

Flax regenerates more easily from hypocotyl explants *in vitro* [6, 7, 8, 9, 10]. Although the highest frequencies of callus and plant regeneration have been reported to be obtained from the culture of immature embryos in wheat [11, 12, 13] mature embryos which are readily available at all times have been successfully used in callus induction and plant regeneration [14, 15, 16, 17].

Plant tissue culture techniques help us propagate plants vegetatively in a large amount by using small parts of a tissue and by using the ability of cells to form a whole, fertile plant which is called totipotency. Explants regenerate shoots and roots, and consequently whole fertile plants under certain cultural conditions. Tissue culture studies aim to obtain high-frequency shoot regeneration, which is also a prerequisite for an efficient transformation system and clonal propagation of plants. Introduction of foreign genes coding agronomically important traits into plant cells has no meaning unless transgenic plants are regenerated from the genetically modified cell(s). The types and concentrations of plant growth regulators in plant cell culture significantly affect growth and morphogenesis. In order to obtain high frequency adventitious shoot regeneration for a related genotype, correct explant type, concentrations and combinations of auxins and cytokinins should be determined. However, determining the explant type, and correct concentrations and combinations of growth regulators is not enough for high-frequency shoot regeneration. Since every cell has an ability of forming a whole fertile plant under *in vitro* conditions, shoot regeneration frequency can always be higher than we obtain in theory. Many factors affecting the regeneration capacity of explants have not been found out yet. For instance, a recently reported technique utilizing competition among explants was

very effective in increasing shoot regeneration capacity [18]. Thus, this study was conducted to develop an efficient method to obtain higher shoot regeneration frequency via culturing explants together, which we called 'co-cultivation'. The method we described in this study was based on culturing explants from two different genotypes together and consequently increasing regeneration capacity of mature embryo explants of wheat (*Triticum* sp.) and hypocotyl explants of flax (*Linum usitatissimum* L.).

MATERIALS AND METHODS

Wheat. One winter bread wheat (*T. aestivum* L.) cv. 'Bezostaja 1' and one winter durum wheat (*Triticum durum* Desf.) cv. 'Cakmak 79' as sources of mature embryos were used in the study. Mature seeds of wheat cultivars were surface-sterilized with 70% (v/v) ethanol for 5 min, washed several times with sterile distilled water, immersed in commercial bleach (containing 5% sodium hypochlorite) for 25 min, and rinsed at least 7 times with sterile distilled water. Then, the seeds were imbibed in sterile distilled water for 24 h at 4ºC. For callus induction, mature embryos from imbibed and dehulled seeds were aseptically excised slightly with a scalpel. Excised embryos were placed scutellum downwards on a basal medium containing the mineral salts and vitamins of Murashige and Skoog (MS) [19], 3 mg l^{-1} 2,4-D, 2% (w/v) sucrose and 0.7% (w/v) agar. The Petri dishes were incubated at 24±1ºC in total darkness for 14 days. Developed calli were transferred to a shoot induction medium containing MS mineral salts and vitamins, 0.20 mg l^{-1} BAP and 0.01 mg l^{-1} NAA, glycine (2 mg l^{-1}), 2% (w/v) sucrose and 0.7% (w/v) agar at pH 5.8 in Petri dishes. The transferred callus cultures were incubated at 24±1ºC under cool white fluorescent light (27 μmol m^{-2} s^{-1}) with a 16-h light/8-h dark photoperiod for 4 weeks. At the end of the culture, culture efficiency in percentage, number of regenerated shoots and shoot lengths were determined.

Flax. Flax (*Linum usitatissimum* L. cvs. 'Madaras' and '1886 Sel.') seeds obtained from the Northern Crop Science Laboratories in North Dakota, USA were surface-sterilized with 40% commercial bleach containing 5% sodium hypochlorite at 10ºC for 20 min with continuous stirring and they were then washed three times with sterile distilled water at the same temperature according to the protocol described by Yildiz and Er [15]. Sterilized seeds were germinated on a basal Murashige and Skoog [19] medium containing the mineral salts and vitamins, 3% (w/v) sucrose and 0.7% (w/v) agar. All cultures were incubated at 25±1ºC under cool white fluorescent tubes (27 µmol m^{-2} s^{-1}) with a 16h light/8h dark photoperiod. The pH of the medium was adjusted to 5.8 prior to autoclaving. Hypocotyl segments in 5-mm lengths were excised from 7-d-old seedlings and imbibed in sterile distilled water with gentle shaking for 20 min. Then, the segments were cultured on an MS medium supplemented with 0.20 mg l^{-1} BAP and 0.01 mg l^{-1} NAA for regeneration. Shoot regeneration percentage, shoot number per explant, shoot length and total shoot number per petri dish were recorded 4 weeks after culture initiation. Sixteen explants were cultured in a 4 x 4 matrix in a Petri dish. Eight out of 16 explants for each genotype were cultured for co-cultivation. 16 explants from each genotype were cultured alone as control (Figure 1).

Statistical Analysis. Four replicates were tested. Petri dish was considered as the unit of replication. The number of explants per replication for co-cultivation was 8 for each genotype, and for cultivation alone, it was 16 for each genotype. All experiments were repeated two times. The data were statistically analyzed by Duncan's multiple range test using the 'SPSS for Windows' computer program [20].

RESULTS

The Effects of Co-cultivation on Tissue Culture Response of Wheat Cultivars. The culture efficiency of mature embryo-derived callus of wheat cvs. 'Cakmak 79' and 'Bezostaja 1' co-cultured with the hypocotyl explants of flax cvs. 'Madaras' and '1886 Sel.' was significantly higher ($P<0.01$) than that of callus cultured alone (Table 1). Culture efficiency of callus cultured alone was recorded as 59.38% and 53.13% while it was 96.88% and 100.00% in co-cultivation with 'Madaras'; 100.00% and 100.00% in co-cultivation with '1886 Sel.' in cv. 'Cakmak 79' and in cv. 'Bezostaja 1', respectively (Table 1). 9.50 and 8.50 shoots were regenerated out of 16 explants cultured alone in cv. 'Cakmak 79' and in cv. 'Bezostaja 1', respectively (Figure 2B and b). 7.75 and 8.00 shoots regenerated from 8 callus explants in cv. 'Cakmak 79' when callus was cultured together with hypocotyl explants of flax cvs. 'Madaras' and '1886 Sel.', respectively (Table 1) (Figure 2A, a1 and a2). In cv. 'Bezostaja 1', 8.00 and 8.00 shoots were regenerated from callus where they were cultured together with hypocotyls of both flax cultivars. The results clearly showed that co-cultivation between wheat and flax genotypes increased regeneration capacity significantly. Although only 8 explants from each cultivar were cultured in co-cultivation, the number of regenerated shoots was almost two times more than that in the explants cultured alone. Higher shoot lengths in co-cultivation could be attributed to the effect of explants from different genotypes on each other. The mean shoot length was recorded as 7.50 in callus cultured alone while it was about 10.50 in co-cultivation.

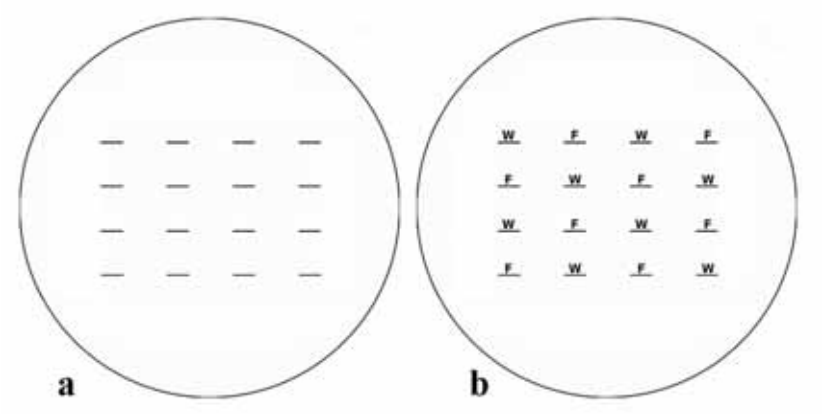


FIGURE 1
Schematic plan of explants cultured at '1.0 x1.0' distance for shoot regeneration. a) culture alone, b) co-cultivation between flax and wheat explants. F=Flax, W= Wheat

TABLE 1
Culture responses of mature embryo-derived callus of wheat (*Triticum* sp.) cvs. 'Cakmak 79' and 'Bezostaja 1' cultured alone and co-cultured with flax (*Linum usitatissimum* L.) cvs. 'Madaras' and '1886 Sel.'

Cultivars	Culture efficiency (%)[1]		
	Cultured alone	Co-cultured with 'Madaras'	Co-cultured with '1886 Sel.'
'Cakmak 79'	59.38 b±7.33	96.88 a±3.83	100.00 a±0.00
'Bezostaja 1'	53.13 b±4.94	100.00 a±0.00	100.00 a±0.00
Mean	**56.26**	**98.44**	**100.00**
Cultivars	**No. of regenerated shoots / No. of calli cultured**		
	Cultured alone	**Co-cultured with 'Madaras'**	**Co-Cultured with '1886 Sel.'**
'Cakmak 79'	9.50/16 b±0.07	7.75/8.00 a±0.04	8.00/8.00 a±0.00
'Bezostaja 1'	8.50/16 b±0.05	8.00/8.00 a±0.00	8.00/8.00 a±0.00
Mean	**9.00/16.00**	**7.88/8.00**	**8.00/8.00**
Cultivars	**Shoot length (cm)**		
	Cultured alone	**Co-cultured with 'Madaras'**	**Co-cultured with '1886 Sel.'**
'Cakmak 79'	7.21 b±0.45	10.24 a±1.58	10.94 a±1.10
'Bezostaja 1'	7.68 b±0.68	10.34 a±1.47	10.81 a±0.85
Mean	**7.45**	**10.29**	**10.88**

[1](Number of calli regenerated/Number of calli cultured) x 100
Means followed by different letters in a row for each cultivar are significantly different at 0.01 level

The Effects of Co-cultivation on Tissue Culture Response of Flax Cultivars. The culture efficiency of hypocotyl explants of flax cvs. 'Madaras' and '1886 Sel.' co-cultured with mature embryo-derived callus of wheat cvs. 'Cakmak 79' and 'Bezostaja 1' was significantly higher (P<0.01) than that of hypocotyls cultured alone (Table 2). Shoot regeneration percentage of hypocotyls cultured alone was 70.31% and 92.19% while it was 100.00% and 100.00% in co-cultivation with 'Cakmak 79' and with 'Bezostaja 1'. The data related to shoot number per explants was recorded as 1.64 and 2.00 in explants cultured alone in cv. 'Madaras' and in cv. '1996 Sel.', respectively (Figure 2C and c). 3.81 and 4.35 shoots regenerated from single explants in cv. 'Madaras' when hypocotyls were cultured together with callus of wheat cvs. 'Cakmak 79' and 'Bezostaja 1', respectively (Table 2) (Figure 2A, a1 and a2). 5.07 and 5.03 shoots regenerated from single explants when cv. '1886 Sel.' was cultured together with callus of both wheat cultivars. Shoot number per explant was significantly higher (P<0.01) in co-cultivation application than cultivation alone in both flax cultivars. The stimulatory effect of co-cultivation application could be seen in shoot length. The shoot lengths regenerated in hypocotyl explants cultured alone were lower than in the explants from two genotypes cultured together (Table 2). The mean shoot length in explants cultured alone was about 1.50 cm while it was approximately 3.50 cm in the co-cultivation application. The total shoot number per petri dish increased to 29.75 and 34.75 in hypocotyls of cv. 'Madaras' co-cultured with cv. 'Cakmak 79' and with cv. 'Bezostaja 1', respectively, while it was 22.75 in explants cultured alone. Similarly, total shoot number per petri dish increased to 40.50 and

40.25 in hypocotyls of cv. '1886 Sel.' cultured with cv. 'Cakmak 79' and with cv. 'Bezostaja 1' from 32.00 in explants cultured alone (Table 2).

DISCUSSION

High-frequency shoot regeneration is the main target of tissue culture studies. High-frequency shoot regeneration is also a prerequisite for an efficient transformation system. Shoot regeneration capacity of cells or tissues to be used in transformation studies affects the success of genetic transformation significantly [9, 21]. Viability and age of explant, and the tissue source from which the explant is excised are very important parameters for high-frequency shoot regeneration [22]. Fatima et al. [23] reported that growth and morphogenesis are controlled by the types and concentrations of plant growth regulators in plant cell culture. In order to obtain high frequency adventitious shoot regeneration for a related genotype, correct concentrations and combinations of auxins and cytokinins have been aimed to be determined.

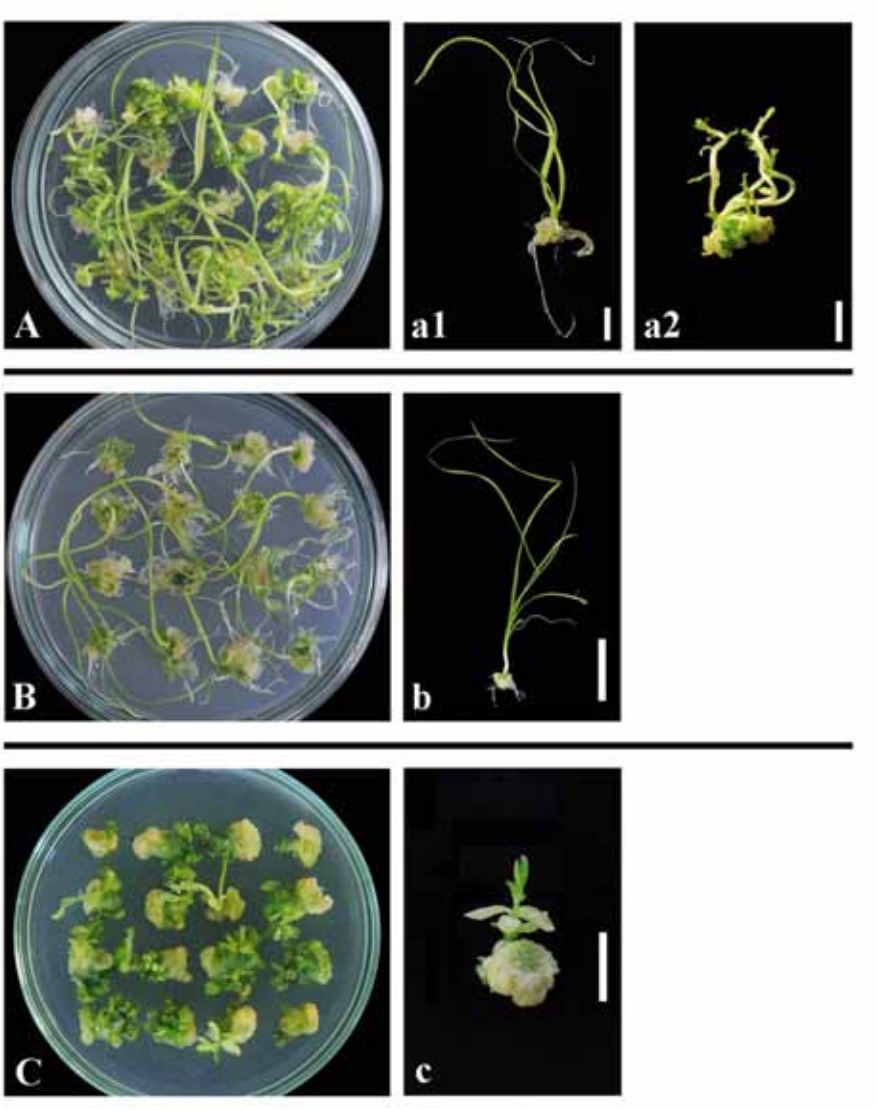


FIGURE 2
Shoot regeneration from flax hypocotyl and wheat callus explants 4 weeks after culture initiation. A) Tissue culture responses of flax hypocotyl and wheat callus explants cultured together, a1) Shoot formation from a wheat callus explant cultured together with flax hypocotyl explant, a2) Shoot development from flax hypocotyl explant cultured together with wheat callus explant, B-b) Tissue culture response of wheat callus explants cultured alone, C-c) Tissue culture response of flax hypocotyl explants cultured alone. Bars = 1.0 cm

TABLE 2
Culture responses of hypocotyl explants of flax (*Linum usitatissimum* L.) cvs. 'Madaras' and '1886 Sel.' cultured alone and co-cultured with mature embryo-derived callus of wheat (*Triticum* sp.) cvs. 'Cakmak 79' and 'Bezostaja 1'

Cultivars	Shoot regeneration (%)			Shoot number per explant		
	Cultured alone	Co-cultured with 'Cakmak 79'	Co-cultured with 'Bezostaja 1'	Cultured alone	Co-cultured with 'Cakmak 79'	Co-cultured with 'Bezostaja 1'
'Madaras'	70.31 b±6.54	100.00 a±0.00	100.00 a±0.00	1.64 b±0.29	3.81 a±0.32	4.35 a±0.49
'1886 Sel.'	92.19 b±7.25	100.00 a±0.00	100.00 a±0.00	2.00 b±0.17	5.07 a±0.13	5.03 a±0.25
Mean	**81.25**	**100.00**	**100.00**	**1.82**	**4.44**	**4.69**
Cultivars	**Shoot length (cm)**			**Total shoot number per petri dish**		
	Cultured alone	Co-cultured with 'Cakmak 79'	Co-cultured with 'Bezostaja 1'	Cultured alone	Co-cultured with 'Cakmak 79'	Co-cultured with 'Bezostaja 1'
'Madaras'	1.25 b±0.08	3.27 a±0.16	3.07 a±0.31	22.75 b±3.06	29.75 a±2.61	34.75 a±3.92
'1886 Sel.'	1.72 b±0.50	3.81 a±0.26	3.75 a±0.46	32.00 b±2.78	40.50 a±1.06	40.25 a±2.02
Mean	**1.49**	**3.54**	**3.41**	**27.38**	**35.13**	**37.50**

Means followed by different letters in a row for each cultivar are significantly different at 0.01 level

Plants compete each other with respect to water, nutrients and light. There are many studies reporting such competition among plants in field conditions [24, 25]. Plant density was reported as a biotic stress factor in natural conditions and this was one of the reasons for competition among plants [21]. Plant development and yield of many vegetable crops were affected significantly by plant density [26]. It was noted that fruit yield is increased by increasing plant density [28, 29, 30]. However, if plant density causes competition, plant yield starts to decrease. Early and total yield per pepper plant decreased by increasing plant density caused by higher interplant competition due to less spacing [31]. Abubaker [32] reported that the highest planting density caused the lowest yield in beans because of the high competition among plants for water and minerals. Asghari et al. [33] reported that the chicory plant had increased root diameter for increased absorption of water under high density due to high competition between plants.

Although many studies about the effects of plant density and competition have been conducted in field conditions, such competition has firstly been reported by Yildiz [10] regarding *in vitro* culture. In these studies, hypocotyl explants of different flax (*Linum usitatissimum* L.) cultivars were cultured at four different distances as '0.5 x 0.5', '1.0 x 1.0', '1.5 x 1.5' and '2.0 x 2.0' cm in order to determine the effects of competition among explants for constant amount of water and nutrients on shoot regeneration capacity. In all genotypes, the highest results with respect to tissue culture response were recorded at a culture distance of '1.0 x 1.0' cm. From the results, it could be concluded that 1.0 cm culture distance encouraged explants to compete each other for constant amount of water, sucrose and nutrients in the growth medium. Yildiz [10] showed that shoot regeneration capacity could be increased not only by determination of correct concentrations and combinations of auxins and cytokinins in the growth medium, but also by encouraging explants into competition. This is why, in this study, explants from both genotypes were cultured alone or together at a culture distance of '1.0 x 1.0' cm.

To our knowledge, this is the first study reporting that shoot regeneration frequency could be increased by culturing explants from two separate genotypes together. Finding two separate genotypes that could be cultured together is the main obstacle in front of the protocol described in this study.

REFERENCES

[1] Green, A.G., Marshall, D.R. (1984) Isolation of induced mutants in linseed (*Linum usitatissimum*) having reduced linolenic acid content. Euphytica. 33, 321-328.

[2] Barutcular, C., Yildirim, M., Koc, M., Dizlek, H., Akinci, C., El Sabagh, A., Saneoka, H., Ueda, A., Islam, M.S., Toptas, I., Albayrak, O., Tanrikulu, A. (2016) Quality traits performance of bread wheat genotypes under drought and heat stress conditions. Fresen. Environ. Bull. 25(12a), 6159-6155.

[3] Barutcular, C., El Sabagh, A., Koc, M., Ratnasekera, D. (2017) Relationships between grain yield and physiological traits of durum wheat varieties under drought and high temperature stress in Mediterranean environments. Fresen. Environ. Bull. 26(6), 4282-4291.
[4] Malik, S.T., Hamid, R., Tayyaba, Y., Minhas, N.M. (2003) Effects of 2,4-D on callus induction from mature wheat (Triticum aestivum L.) seeds. International Journal of Agriculture and Biology. 6(1), 156-159.
[5] Mendoza, M.G., Kaeppler, H.F. (2002) Auxin and sugar effects on callus induction and plant regeneration frequencies from mature embryos of wheat (*Triticum aestivum* L.). In Vitro Cellular & Developmental Biology-Plant. 38, 39-45.
[6] Gamborg, O.L., Shyluk, J.P. (1976) Tissue culture, protoplasts, and morphogenesis in flax. Botanical Gazette. 137, 301-306.
[7] Friedt, W. (1990) Biotechnology in breeding of industrial oil crops: the present status and future prospects. Fat Science Technology. 90, 51-55.
[8] Millam, S., Davidson, D., Powell, W. (1992) The use of flax (*Linum usitatissimum*) as a model system for studies on organogenesis in vitro: the effect of different carbonhydrates. Plant Cell, Tissue and Organ Culture. 28, 163-166.
[9] Dong, J., Mc Hughen, A. (1993) An improved procedure for production of transgenic flax plants using *Agrobacterium tumefaciens*. Plant Science. 88,61-71.
[10] Yildiz, M. (2000) Adventitious shoot regeneration and *Agrobacterium tumefaciens*-mediated gene transfer in flax (*Linum usitatissimum* L.). Ph.D. Thesis. Ankara University, Graduate School of Natural and Applied Sciences, Department of Field Crops, Ankara, Turkey.
[11] Maddock, S.E., Lanchester, V., Risiott, R., Franklin, J. (1983) Plant regeneration from cultured immature embryos and inflorescences of 25 cultivars of wheat (*Triticum aestivum* L.). Journal of Experimental Botany. 34, 915-926.
[12] Tuberosa, R.S., Ravaglia, S., Lucchese, C. (1988) Callus induction and plant regeneration in Italian cultivars of bread wheat. Agricoltura Mediterranea. 118, 361-365.
[13] Redway, F.A., Vasil, V., Lu, D., Vasil, I.K. (1990) Identification of callus types for long-term maintenance and regeneration from commercial cultivars of wheat (*Triticum aestivum* L.). Theoretical Applied Genetics. 79, 609-617.
[14] Bartok, T., Sagi, F. (1990) A new, endosperm-supported callus induction method for wheat (*Triticum aestivum* L.). Plant Cell, Tissue and Organ Culture. 22, 37-41.
[15] Ahmed, K., Bartok, T., Sagi, F. (1992) A modified method fro rapid callus induction by utilization of endosperm metabolites in mature and immature seeds of bread wheat (*Triticum aestivum* L.) and durum wheat (*Triticum durum* L.). Cereal Research Communications. 20, 81-86.
[16] Ozgen, M., Turet, M., Ozcan, S., Sancak, C. (1996) Callus induction and plant regeneration from immature and mature embryos of winter durum wheat genotypes. Plant Breeding. 115, 455-458.
[17] Pelit, S. (2011) The effect of *in vitro* competition on callus formation and shoot regeneration from mature embryos of wheat (*Triticum* sp.). M.Sc. Thesis, Ankara University, Graduate School of Natural and Applied Sciences, Department of Field Crops, Ankara, Turkey.
[18] Yıldız, M. (2011) Evaluation of the effect of *in vitro* stress and competition on tissue culture response of flax. Biologia Plantarum. 55(3), 541-544.
[19] Murashige, T., Skoog, F.A. (1962) Revised medium for rapid growth and bioassay with tobacco tissue culture. Physiologia Plantarum. 15, 473-497.
[20] Snedecor, G.W., Cochran, W.G. (1967) Statistical Methods. The Iowa State University Press, Iowa, USA.
[21] Jordan, M.C., Mc Hughen, A. (1988) Transformed callus does not necessarily regenerate transformed shoots. Plant Cell Reports. 7, 285-287.
[22] Yıldız, M., Er, C. (2002) The effect of sodium hypochlorite solutions on *in vitro* seedling growth and shoot regeneration of flax (*Linum usitatissimum*). Naturwissenschaften. 89, 259-261.
[23] Fatima, Z., Mujib, A., Fatima, S., Arshi, A., Umar, S. (2009) Callus induction, biomass growth, and plant regeneration in *Digitalis lanata* Ehrh.: influence of plant growth regulators and carbonhydrates. Turkish Journal of Botany. 33, 393-405.
[24] Wilson, J.B. (1988) Shoot competition and root competition. Journal of Applied Ecology. 25, 279-296.
[25] McPhee, C.S., Aarssen, L.W. (2001) The separation of above- and below-ground competition in plants. A review and critique of methodology. Plant Ecology. 152, 119-136.
[26] De Klerk, G.J. (2007) Stress in plants cultured *in vitro*. Propagation of Ornamental Plants. 7(3), 129-137.
[27] Stoffella, P.J., Bryan, H.H. (1988) Plant population influences growth and yields of bell pepper. Journal of the American Society for Horticultural Science. 113, 835-839.

[28] Decoteau, D.R., Grahan, H.A.H. (1994) Plant spatial arrangement affects growth, yield and pod distribution of cayenne peppers. HortScience. 29, 149-151.
[29] Jolliffe, P.A., Gaye, M.M. (1995) Dynamics of growth and yield component responses of bell peppers (*Capsicum annuum* L.) to row covers and population density. Scientia Horticulturae. 62, 153-164.
[30] Morgade, L., Willey, R. (2003) Effect of plant population and nitrogen fertilizer on yield and efficiency of maize/bean intercropping. Pesquisa Agropecuária Brasileira. 38, 1257-1264.
[31] Daşgan, H.Y., Abak, K. (2003) Effects of plant density and number of shoots on yield and fruit characteristics of peppers grown in glasshouses. Turkish Journal of Agriculture and Forestry. 27, 29-35.
[32] Abubaker, S. (2008) Effect of plant density on flowering date, yield and quality attribute of bush beans (*Phaseolus vulgaris* L.) under center pivot irrigation system. American Journal of Agricultural and Biological Sciences. 3, 666-668.
[33] Asghari, M.T., Daneshian, J., Farahani, A.A. (2009) Effects of drought stress and planting density on quantity and morphological characteristics of chicory (*Cichorium intybus* L.). Asian Journal of Agricultural Sciences. 1, 12-14.

Received: **09.08.2017**
Accepted: **25.09.2017**

CORRESPONDING AUTHOR

Ramazan Beyaz
Department of Soil Science and Plant Nutrition
Faculty of Agriculture
Ahi Evran University
40100 Bagbasi, Kirsehir – Turkey

e-mail: ramazanbeyaz@gmail.com

© by PSP Volume 26 – No. 12A/2017 pages 8246-8254 Fresenius Environmental Bulletin

ACCUMULATION CHARACTERISTICS AND HEALTH RISK OF HEAVY METALS IN SOIL AND PLANT: A CASE STUDY FROM HUAIBEI COALFIELD, CHINA

Dawei Huang[1,3], Herong Gui[2,3,*], Manli Lin[3], Weihua Peng[4]

[1]School of Earth and Environment, Anhui University of Science and Technology, Huainan 232001, China
[2]National Engineering Research Center of Coal Mine Water Hazard Controlling, Suzhou 234000, China
[3]School of Resources and Civil Engineering, Suzhou University, Suzhou 234000, China
[4]School of Space and Environment, Beihang University, Beijing 100191, China

ABSTRACT

Sunan mining area was selected as investigated area from Huaibei coalfield to study the accumulation and enrichment characteristics of heavy metals in soil and plant. This study focused on heavy metal content characteristics about surface and profile soil, maize plant bioconcentration transfer characteristics and health risk assessment of heavy metals. The results indicated that the mean content of heavy metals (Cd, Cr, Pb, Ni, Zn and Cu) were 0.26, 52.69, 24.09, 29.77, 57.00 and 26.09mg/kg in surface soil, respectively. Cr exceeded the secondary standard of national environment quality standard for soil in China with the proportion of 50%, while other heavy metals did not exceed the corresponding standard. Single factor pollution index showed that 8.33% of Ni and Cd samples belonged to the warning limit pollution level respectively, and other heavy metals were at clear. Profile heavy metal vertical migration characteristics revealed that except for Pb, other heavy metals showed an obvious trend of vertical migration in different degrees. Among organs of maize plant (e.g. roots, stems, leaves), Zn content was highest, while Cd content was lowest. The bioconcentration factor(BCF) and transfer factor (TF)of Cd were relatively larger, and maize plant root tended to absorb more Cd from the soil firstly, and then transferred to the upper part of the ground. Health risk assessment results suggested that the health risk of six heavy metals to children was much higher than that of adults, and Cr contribution were the largest among them.

KEYWORDS:
Huaibei coalfield, soil-plant system, heavy metals, accumulation characteristics, health risk assessment

INTRODUCTION

Heavy metal pollution is a worldwide environmental problem, and has attracted wide concerns in recent decades [1]. Heavy metal pollution also has many characteristics, such as concealment, hysteresis and long term. The waste water, coal dust and coal gangue discharged by coal mining activities go into the surrounding soil environment through surface runoff, atmospheric deposition and waste residue leaching, which result in soil heavy metal pollution of coal mine area [2-3]. The soil contaminated by heavy metals can not only cause direct harm to organisms, but also indirectly endanger people through dust intake, skin contact, food chain and other approaches [4-8]. It is not only difficult to be biodegraded, but also easily absorbed and accumulated by organisms (e.g. vegetables, maize, rice), and has a certain inhibitory effect [9]. Therefore, it is mounting necessary to monitor heavy metals in soil and plant to evaluate the status of heavy metal pollution in specific mining area.

In recent years, according to the status of heavy metal pollution in mining area farmland soil and crops, previous studies have mainly focused on the heavy metal pollution characteristics in surface soil, enrichment and migration laws, environmental effects and health risk assessment, and etc. For example, Qin et al. [10] found that the contents of As, Cu, Pb, Cd, Ni, Cr and Hg exceeded the soil background values of Guizhou Province, China. Xiong et al. [11]studied that the mean content of Cd, Cu, Pb and Zn were 0.26, 25.72, 29.71 and 62.71mg/kg from Huaibei coalfield in Linhuan mining area, and was 2.68, 1.16, 1.12 and 1.01 times of soil background value in Anhui Province, respectively. These heavy metals have shown a certain pollution accumulation in soil. Xiao et al. [12] researched on soil heavy metal contamination and health risks in Tongguan, indicating that Hg and Pb concentrations in grains and some vegetables exceeded tolerance limits, and heavy metal contents in wheat grains were higher than those in maize grains. In addition, Yu et al. [13] studied on the concentrations of As, Pb and Cd in soil, vegetables, maize, rice and road dust from Nandan mining area. It was final found that people were at a great health risk with intaking of local agricultural products, such as rice, vegetables

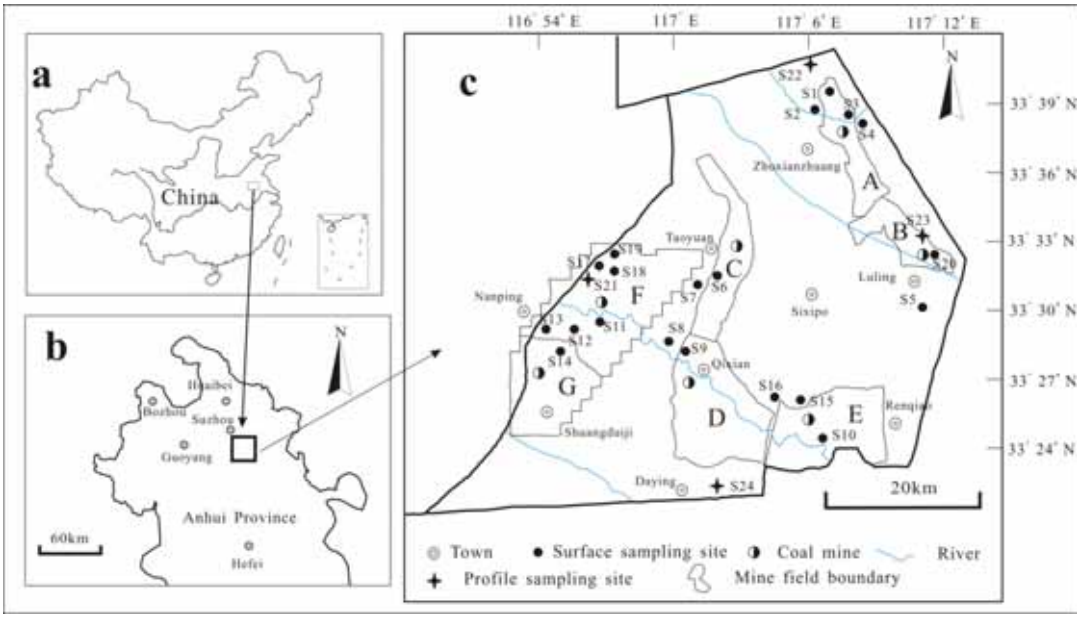


FIGURE 1
Location of the study area and sampling sites
(A Zhuxianzhuang; B Luling; C Taoyuan; D Qinan; E Qidong; F Qianyingzi; G Zouzhuang)

and corn, and children were more vulnerable than adults.

The Huaibei coalfield is part of North China coal field, which comprises 5 main mining areas and has abundant resources of coal [14]. In view of the fact that maize plants are the main food crops in this region, thus this paper takes maize plants as the research object, and collects the surface and deep soil on the farmland around the mining area. Specifically, a total of 44 soil samples and 24 maize plant samples have been collected from the Sunan mining area of Huaibei coalfield, Northern Anhui Province, China, and the concentrations of heavy metals in soil and maize organs, the single factor pollution index, enrichment characteristics as well as health risk assessment have been reported based on the content testing of Cd, Cr, Pb, Ni, Zn and Cu in this study. This paper provides reference for the further study of heavy metal pollution in soil and other food crops in other similar areas.

MATERIALS AND METHODS

Study area. Sunan mining area (33°21′-33°42′N,116°45′-117°12′E) is located in the north of Anhui Province, China (Figure 1), to be exactly, the study area includes seven coal mines, namely Luling, Taoyuan, Zhuxianzhuang, Qinan, Qidong, Qianyingzi and Zouzhuang mines. Besides, the district around is flat and has a relatively simple terrain as a whole. The soil types in the region are mainly fluvo aquic soil and sandy black soil. This region has four distinct seasons and a suitable climate. It has a warm temperate semi-humid monsoon climate with an average annual temperature of 14~14.5°C, the rainfall is concentrated in summer, and the annual rainfall is only 774~895mm [15]. The main rivers in this area are Huihe River and Tuohe River, which both belong to small seasonal rivers.

Soil sampling and chemical analysis. The preliminary sampling work was completed in August 2016. On the basis of the status quo of the investigation area, the collection of samples was concentrated in the farmland near the gangue hill. A total of 20 surface samples (0~20 cm) and 24 deep samples were collected, and the deep samples came from 4 soil profiles. The vertical direction was divided into 6 layers, namely, 0~10 cm, 10~20 cm, 20~30 cm, 30~40 cm, 40~50 cm, 50~60 cm. The maize cultivated in the mining area was selected as the research object of plant. At the same time, the maize plants were collected above the corresponding soil samples. Each sample point required a mixture of 3~5 samples, and the GPS locator was used to determine the coordinates.

After natural drying, crushing, and sieving of collected soil samples, the 0.25g prepared soil samples were digested by an acid mixture (HNO_3: HF: $HCLO_4$=5:4:2, in volume) in a graphite digester (SH230N). Every maize plant sample was separated by roots, stems and leaves. Firstly, the clay adhered on the surface of maize was washed with tap water, and then washed with deionized water several times, finally plant samples were dried to constant weight at 70 degrees, and crushed with a micro grinder

(FZ102). The certain weight plant samples were digested by an acid mixture (HNO_3: $HCLO_4$=9:1, in volume) in a graphite digester (SH230N).

Analytical processes were been performed in National Engineering Research Center of Coal Mine Water Hazard Controlling, China. Pb, Cr, Ni and Cd were determined by atomic absorption graphite furnace, while Zn and Cu were determined by atomic absorption flame photometry(TAS-990 Super). Under the same conditions, blanks, duplicates and standard reference materials (GBW07430, GSS-16) were analyzed to guarantee the quality assurance and quality control, and the recovery rate of each heavy metal was at the range from 75.4% to 131.8%. In addition, the relative deviations between the parallel samples were less than 5%.

Single factor pollution index. In order to analyze and evaluated the degree of soil heavy metal pollution in mining area, single factor pollution index was adopted. The method of single factor pollution index can be calculated by the following formula:

$$P_i = \frac{C_i}{S_i} \quad (1)$$

Where C_i is the actual measured concentration of the metal *i*(mg/kg), S_i is the evaluation standard of heavy metals (mg/kg), and the secondary standard values of National Environment Quality Standard for Soil(GB15618-1995) were used in this study[11]. The criteria for soil heavy metal pollution were listed in Table 1.

TABLE 1
Criteria for classification of soil heavy metal pollution

Classification	Single factor pollution index	Pollution level
Ⅰ	$P_i \leq 0.7$	Clean
Ⅱ	$0.7 < P_i \leq 1.0$	warning limit pollution
Ⅲ	$1.0 < P_i \leq 2.0$	Light pollution
Ⅳ	$2.0 < P_i \leq 3.0$	Medium pollution
Ⅴ	$P_i > 3.0$	Heavy pollution

Bioconcentration factor (BCF) and transfer factor(TF). Bioconcentration factor is the ratio of heavy metal content in plants and heavy metal content in soil, reflecting the ability of plant to enrich and absorb some heavy metals from soil under the same conditions [18]. while transfer factor is the ratio of some heavy metal content in the upper part of the plant to the heavy metal content of the roots, reflecting the migration ability of the heavy metals from the roots of plants [18, 19].

$$BCF = \frac{C_p}{C_s} \quad (2)$$

$$TF = \frac{C_{up}}{C_{down}} \quad (3)$$

Where C_p is the content of heavy metals in plants (mg/kg), C_s is the content of heavy metals in soil (mg/kg),

C_{up} is the heavy metal content in the upper part of the plant(mg/kg), C_{down} is the heavy metal content of the roots(mg/kg).

Health risk assessment method. Target hazard quotient (*THQ*) was used to evaluate the possible health risks of heavy metals through intaking. It represented the health risk of heavy metals according to the ratio of the heavy metal exposure dose to the reference dose proposed by the US Environmental Protection Agency (USEPA) [20]. The calculation formula of MMSOILS risk assessment model is as follows:

$$THQ = \frac{EF \times ED \times FI \times MC}{RfD \times BW \times AT} \quad (4)$$

$$TTHQ = \sum_{i=1}^{n} THQ_i \quad (5)$$

Where *MC* is heavy metal content in maize(mg/kg); *FI* is contact frequency(kg/d), FI_{adult}=0.15 kg/d, FI_{child}=0.1 kg/d [20-21]; *EF* is exposure frequency(d/a), *EF*=365d/a; *ED* is exposure time(a), ED_{adult}=70 a; *BW* is average individual weight(kg), BW_{adult}=70 kg, BW_{child}=16kg [22]; *AT* is average contact time of non-carcinogenic sources(d), *AT*=*ED*×365; *RfD* is heavy metal exposure reference dose(mg·(kg· d) $^{-1}$), the *RfD* of Cd, Ni, Pb, Cr, Zn and Cu are 0.001, 0.02, 0.0035, 0.003, 0.04 and 0.3 (mg·(kg· d) $^{-1}$) [23-24], respectively. When *TTHQ*< 1, there is no negative impact; 1<*TTHQ*<10 indicates that there may be a great negative impact; *TTHQ*>10 indicates the presence of chronic toxicological effects.

Statistical analysis. IBM SPSS Statistics 19.0 software was used to perform statistical analysis in this study. CorelDRAW 12 and OriginPro 9 were applied for mapping process.

RESULTS AND DISCUSSION

Surface soil heavy metals content characteristics. All analytical results are shown in Table 2. As can be seen from the Table 2, the mean content of heavy metals (Cd, Cr, Pb, Ni, Zn and Cu) were 0.26, 52.69, 24.09, 29.77, 57.00 and 26.09mg/kg, respectively. Moreover, the contents of Cd and Cu were relatively higher, which were 2.68 and 1.28 times of the soil background value in Anhui Province, and the other heavy metals were all lower than the soil background values in Anhui Province. Compared to the Grade II criterion of national environmental quality for soils in China [17], 50% of the Cr samples exceeded the corresponding limits. In general, the coefficient of variation(CV)can be characterized by the comparison of different dimensional data [25]. The CV of Pb, Zn, Cr and Cu ranged from 22.81% to 28.89% belonging to moderate variation level (15%

< CV < 36%), while Cd and Ni (46.15% and 59.79%, respectively) belonged to higher variation level (CV>36%). This indicated that the distribution of heavy metals in the study area was uneven, and it was more likely to be affected by human factors. According to the evaluation results of single factor pollution index, the pollution index range of Ni and Cd were 0.14~1.36, 0.23~0.92, respectively, and 8.33% of Ni and Cd samples belonged to the warning limit pollution level respectively. In addition, 8.33% Ni samples belonged to light pollution, while the single pollution index of other heavy metals was less than 0.7, belonging to the clean level. Therefore, there was a certain degree of pollution accumulation in soil Cd and Ni in the study area.

TABLE 2
Content statistical characteristics and single factor pollution indexes of heavy metals in soil

Element	Range（mg/kg）	Mean±standard deviation (mg/kg)	CV (%)[a]	Background value (mg/kg)[b]	Guide value (mg/kg)[c]	Single factor pollution index Pi
Cd	0.14~0.55	0.26±0.12	46.15	0.097	0.6	0.23~0.92
Cr	29.90~75.42	52.69±12.56	23.84	66.5	50	0.10~0.25
Pb	14.21~33.36	24.09±6.96	28.89	26.6	300	0.05~0.11
Ni	6.75~68.08	29.77±17.80	59.79	29.8	300	0.14~1.36
Zn	34.39~85.26	57.00±14.86	26.07	62	250	0.14~0.34
Cu	19.35~37.23	26.09±5.95	22.81	20.4	100	0.19~0.37

Note: [a]Coefficient of variation; [b]This paper selects the soil element content of A layer in Anhui Province as the reference background value; [c]takes "soil environmental quality standard" as the reference, in which the second grade standard selects the corresponding value when the soil pH value is 6.5 ~ 7.5.

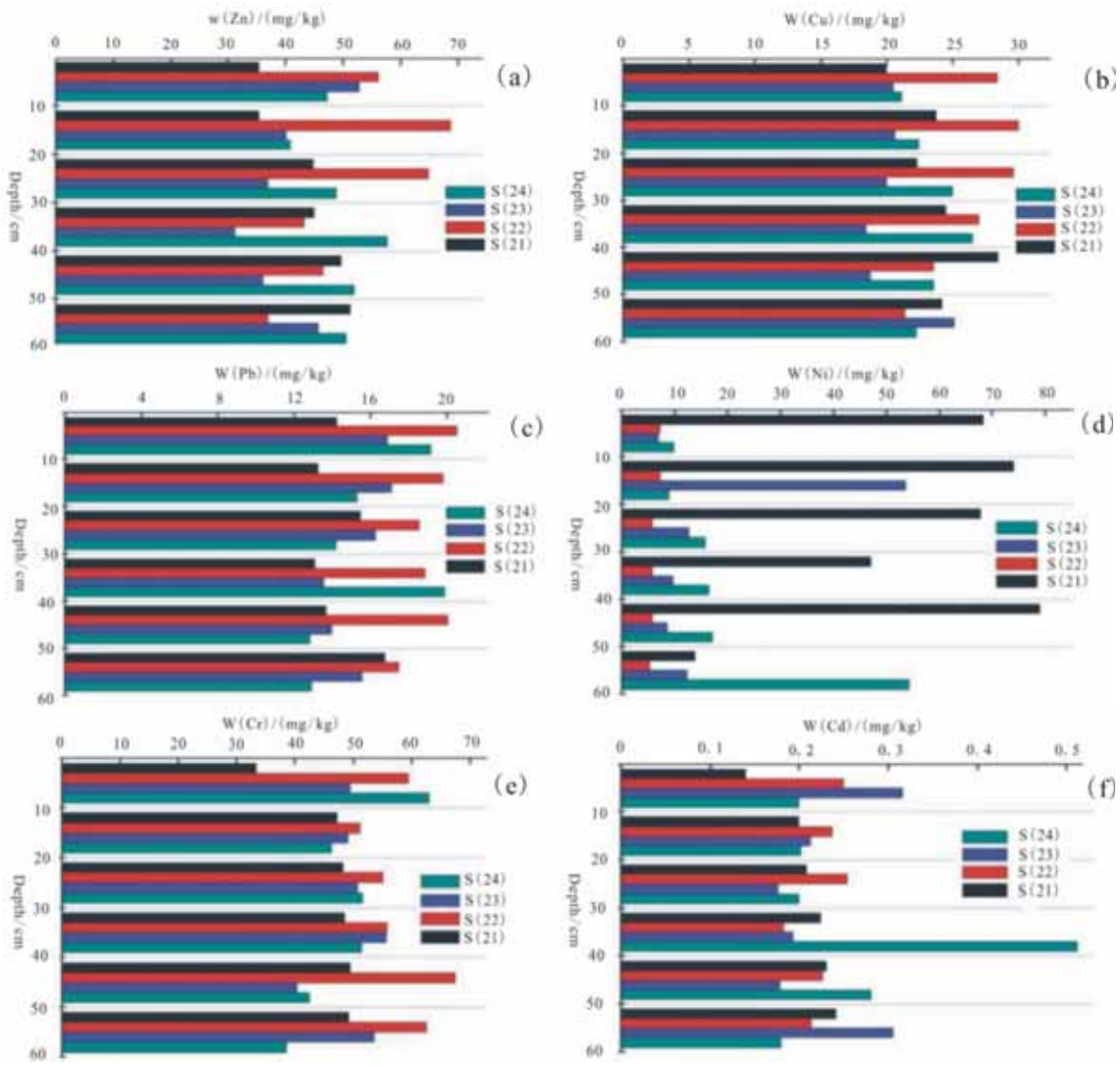


FIGURE 2
Distribution characteristics of heavy metals in the soil profile

Vertical migration characteristics of heavy metals in soil profile. To study the vertical migration characteristics of heavy metals in soil, stratified sampling of vertical soil profiles was carried out at 4 sampling points of 21, 22, 23 and 24, sample points 22 and 24 are non mining areas among them, the results of vertical migration characteristics of all heavy metals at different points are shown in figure 2. The concentrations of heavy metals (Cd, Cr, Pb, Ni, Zn and Cu) were in the ranges of 0.14~0.51, 5.18~78.87, 12.80~20.51, 33.17~67.39, 31.10~ 68.64 and 18.38~29.97 mg/kg, respectively. The Cr content of sample point S(22) was higher than other points, and all profile samples at point S(22) exceeded the Grade II criterion of national environmental quality for soils in China. Furthermore, the maximum value of its downward migration appeared at 40~50 cm.

As can be seen from the Figure 2, the contents of heavy metals in profile soil did not show a significant decrease with the increase of depth, which might be due to the influence of soil tillage, soil turnover and mining activities [26]. The distribution characteristics of heavy metals in vertical profile can be affected by changing the structure and hierarchy of the original soil.

From 10 cm vertical down to 60 cm, Zn and Cu content showed an overall trend of increasing firstly and then decreasing, and the concentration of them was basically stable with the downward migration to the depth of 40~60cm finally. It indicated that Zn and Cu content changed little in the depth direction, but had a downward migration trend. The change of Pb content in each sampling point was not significant, and was lower than the soil background values in Anhui Province. It showed that Pb was less disturbed by human activities than other elements, and the vertical migration was not obvious. The content of Ni was obviously different because of different sampling points, and it showed that the content of S (21) and S (23) samples in the mining area were obviously higher than those in the non mining area at 10~50 cm. However, the content of Ni had obvious downward migration in vertical section at non mining sample point S (24), and the content in 50~60 cm was 1.82 times of soil background value in Anhui Province. The content of Cr showed a cumulative trend with depth increasing, and three sampling points were all higher than the Grade II criterion of national environmental quality for soils in China at 20~40 cm section. Compared with surface soil, the content of Cd was higher at 50~60 cm section, and it may be disturbed by human factors [27]. In summary, the vertical migration characteristics of heavy metals at different sections were vary significantly, which may be related to human activities, heavy metal properties and morphological changes, soil physical and chemical properties, soil microorganisms or other factors [28].

Heavy metal content and accumulation characteristics of various organs in maize plant. The content of heavy metals(Cd, Ni, Pb, Cr, Cu and Zn) in roots, stems and leaves of maize plants are shown in Figure 3(a~f). The mean content of Zn in roots, stems and leaves of maize plants was 37.97, 34.25 and 36.23 mg/kg, respectively. The mean content of Cd was the lowest in roots, stems and leaves with 0.26, 0.30 and 0.19 mg/kg, respectively. The mean content of heavy metals in plant roots was Zn > Cu > Cr > Ni > Pb > Cd, the mean content of heavy metals in plant stems was Zn > Ni > Cu > Pb > Cr > Cd, while the mean content of heavy metals in plant leaves was Zn > Cu > Ni > Cr > Pb > Cd. It can also be obtained that except for Cd, Ni, Pb and Cr, the absorption and accumulation of Cu and Zn in the organs of maize plants were high relatively, and the content change of them was apparent.

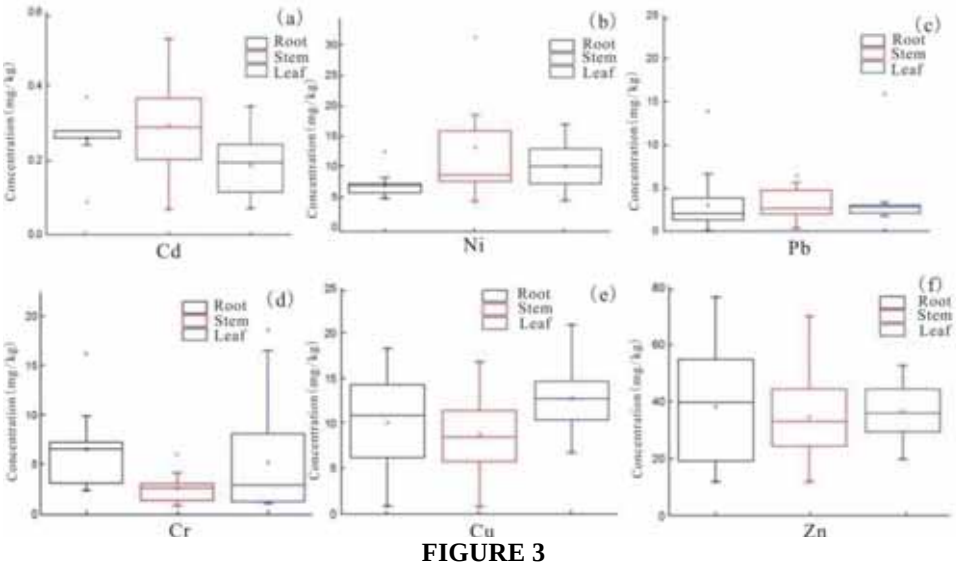


FIGURE 3
Distribution of heavy metals in different maize plant organs

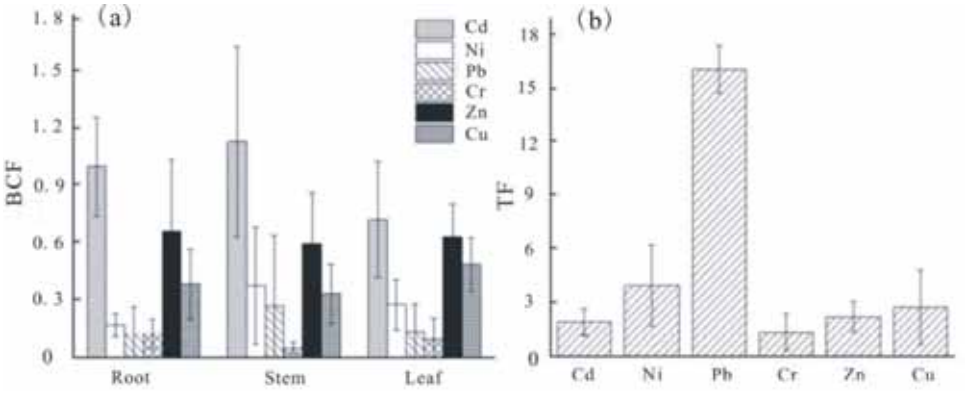


FIGURE 4
Bioconcentration and transfer factor of heavy metals in different maize plant organs

The bioconcentration factor (BCF) and transfer factor (TF) of heavy metals in different organs of maize plants are shown in Figure 4. The Figure 4 showed that the BCF size of heavy metals in the root and leaf was Cd > Zn > Cu > Ni > Pb > Cr, and the BCF size of that in the stem was Cd > Zn > Ni > Cu > Pb > Cr. The BCF of Cd is the largest, showing that the BCF of Cd of 81.25% root samples, 62.50% stem samples and 18.75% leaf samples was greater than one. These results indicated that Cd was more easily enriched in the root organs of maize plants, and had better migration ability in soil-maize system. The accumulation of Cr in maize plant is difficult relatively, and its BCF in the stem is only 0.05.

In addition, the mean value size of six heavy metals TF was Pb > Ni > Cu > Zn > Cd > Cr > 1, indicating that the tendency of these heavy metal migration from the root of maize to the upper part was larger. It was also showed that the potential ability for heavy metals to migrate from soil to their plant organs is stronger. In conclusion, the enrichment and migration characteristics of heavy metals in maize plants were different, and it may be related to many factors, such as the elemental valence states in the soil medium, element free ion activity, soil composition structure, ect [29]. The BCF and TF of Cd were relatively large, indicating that maize plant tended to absorb more Cd from soil, and transferred to the upper part of the ground. Moreover, Cd in mining area soil was in the warning limit pollution level, the subsequent monitoring of Cd in maize plants should be paid more attention to. Zn and Cu content in various organs of maize was higher, and had a stronger enrichment and migration ability. This was mainly due to the fact that Zn and Cu were essential elements of plant metabolism, and were important components of the tissues and organs of plants. Thus the maize plant depends on absorbing the large amount of these trace elements from the soil.

Correlation analysis of heavy metals in various organs of maize and soil. In order to explore the relationship between different organs of maize plant and soil heavy metal content, this study takes the low Zn content in soil relatively and the highest Zn mean content in the organs of maize plants as an example, and the results of the pearson correlation analysis are shown in Table 3. As can be seen from the Table 3, there was a significant positive correlation between root and stem (p<0.01). At 0.05 significant level, the soil and leaf were also significant, while other combinations were not obvious (p>0.05).

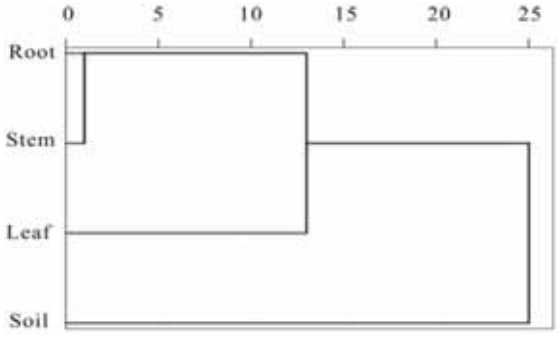


FIGURE 5
Cluster analysis results of Zn content in different maize organs and soil

As shown in Figure 5, when 15 was selected as the standard distance among these values, 2 distinct groups were obtained. The roots, stems and leaves were clustered into one class, indicating that Zn had the same or similar source route in the roots, stems and leaves, whereas the soil was classified as another class alone. This showed that the heavy metals in stems and leaves of maize mainly came from roots, and heavy metals in roots absorbed and accumulated from the soil [20], while Zn in soil may originate from automobile tire wear and combustion of engine oil [30-31]. It was easier to cause the accumulation of Zn in the soil with long term coal transportation activities in this area. Afterwards, the organs of maize plants can absorb and accumulate more Zn from the soil, thus completing this transfer process.

TABLE 3
Pearson correlation coefficient matrix of Zn content in different organs of maize plants and soil

	Soil	Root	Stem	Leaf
Soil	1			
Root	0.279	1		
Stem	0.160	0.857**	1	
Leaf	0.596*	0.473	0.393	1

Note:* *Correlation is significant at the 0.01 level(bilateral),* Correlation is significant at the 0.05 level (bilateral).

TABLE 4
Health risk assessment of heavy metals in maize plant

Index	Heavy metal elements	Adult	Children	Contribution of THQ to TTHQ (%)
	Cd	0.403	1.177	5.02
	Ni	0.890	2.597	11.09
THQ	Pb	2.013	5.872	25.08
value	Cr	3.776	11.012	47.05
	Zn	0.259	0.755	3.23
	Cu	0.685	2.000	8.53
TTHQ value	-	8.026	23.413	-

Health risk assessment. Maize was just in the panicle stage because of plant samples collected in the field. Studies had shown that the contents of heavy metals in various organs of maize were in the descending order of root, stem, leaf and grain [20, 32]. Therefore, the leaf segment, which is the closest part of the maize grain in heavy metal contents, is substituted for the grain as the edible part to evaluate the health risk in this paper.

From the results of maize health risk assessment of heavy metals in Table 4, for adults, Cr and Pb caused greater health risks, the THQ values were 3.776 and 2.013, respectively, while the THQ values of remaining heavy metals were all less than 1. Therefore, these heavy metals did not cause health risks for local adults. For children, the THQ values of heavy metals(Cr, Pb, Ni, Cu and Cd) were 11.012, 5.872, 2.597, 2.00 and 1.177, respectively, this indicated that those heavy metals had a certain degree of health risk.

As can be concluded from TTHQ value that the health risk of six heavy metals to children was higher than that of adults, and the findings were consistent with the study results of Yu et al. [13] and Sun et al. [16]. In addition, The TTHQ values of all heavy metals were in the descending order of Cr＞Pb＞Ni＞Cu＞Cd＞Zn. Further studies had found that the contribution of six heavy metals THQ to TTHQ in maize is different. The contribution degree of Cr and Pb was the largest, both above 25%, whereas Zn had the lowest degree of contribution. In the short run, maize grains can be consumed safely by human. However, we should pay more attention to the health risks of Cr and Pb, and strengthened the follow-up monitoring.

CONCLUSIONS

In this study area, a total of 20 surface soil samples (0~20 cm) and 24 profile samples (e.g. 0~10 cm, 10~20 cm, 20~30 cm, 30~40 cm, 40~50 cm and 50~60 cm) were collected from Sunan mining area, and analyzed for the content of heavy metals(Cd, Cr, Pb, Ni, Zn and Cu). The results of the investigation provided integrated information about soil and maize environment of this area. The heavy metal content characteristics indicated that the contents of Cd and Cu were relatively higher, and exceeded the soil background values in Anhui Province by 2.68- and 1.28-fold, respectively. The results of single factor pollution index indicated that there was a certain degree of pollution accumulation in soil Cd and Ni in the study area. Vertical migration characteristics of heavy metals in soil profiles revealed that heavy metals showed obvious vertical migration excluding Pb. Zn and Cu content in various organs of maize was higher, and had a stronger enrichment and migration ability. In addition, Cd was more easily enriched in the root organs of maize plants, and had better migration ability in maize plant. Health risk assessment results suggested that Cr and Pb had a higher negative effects among heavy metals, and the contributions of them were both above 25%.

ACKNOWLEDGEMENTS

This research project was supported by the National Natural Science Foundation of China (41773100,41373095); University Natural Science Research Project of Anhui Province (KJ2017A445);

and Excellent Youth Talent Support Program of Suzhou University (SZXYQNL2017002). We acknowledge editors and reviewers for polishing the language of the paper and further discussion sincerely.

REFERENCES

[1] Muhammad, S., Shah, M.T. and Khan, S. (2011) Health risk assessment of heavy metals and their source apportionment in drinking water of Kohistan region, northern Pakistan. Microchemical Journal. 98(2), 334-343.

[2] Yuan, X.T., Zhang, C.L., Sun, Q. and Wu, Y.C. (2011) Characteristics of heavy metal concentrations in soil around coal mining area in Suzhou city. Environmental Chemistry. 30(8), 1451-1455.

[3] Wu, Y., Yang, J., Zhou, X.Y., Lei, M., Gao, D., Qiao, P.W. and Du, G.D. (2015) Risk assessment of heavy metal contamination in farmland soil in Du'an autonomous county of Guangxi zhuang autonomous region, China. Environmental Science. 36(8), 2964-2971.

[4] Diatta, J.B., Komisarek, J. and Wiatrowska, K. (2012) Evaluation of heavy metals competitive sorption and potential mobility on the basis of Cu/Cd and Zn/Pb binary systems. Fresen. Environ. Bull. 21(5), 1105-1109.

[5] Symanowicz, B., Kalembasa, S. (2012) Effects of brown coal, sludge, their mixtures and mineral fertilisation on copper and zinc contents in soil and italian ryegrass (lolium multiflorum lam.). Fresen. Environ. Bull. 21(4), 802-807.

[6] Huang, Z., Pan, X.D., Wu, P.G., Han, J.L. and Chen, Q. (2014) Heavy metals in vegetables and the health risk to population in Zhejiang, China. Food Control. 36(1), 248-252.

[7] Mazur, Z., Radziemska, M., Maczuga, O. and Makuch, A. (2013) Heavy metal concentrations in soil and moss (Pleurozium schreberi) near railroad lines in Olsztyn (Poland). Fresen. Environ. Bull. 22(4), 955-961.

[8] Mishra S., Dwivedi S.P. and Singh R.B. (2010) A Review on Epigenetic Effect of Heavy Metal Carcinogens on Human Health. Open Nutraceuticals Journal. 3(1), 188-193.

[9] Yang, J., Wang, N. (2013) Assessment of potential ecological risk of heavy metal in soils from Jia-Pi-Gou gold mine area. Journal of Agro-Environment Science, 32(3), 595-600.

[10] Qin, F.X., Wei, C.F., Zhong, S.Q., Huang, X.F., Pang, W.P. and Jiang, X. (2016) Soil heavy metal(loid)s and risk assessment in vicinity of a coal mining area from southwest Guizhou, China. Journal of Central South University (English Edition). 23(9), 2205-2213.

[11] Xiong, S., Gui, H.R., Lin, M.L., Peng, W.H. (2017) Contents and pollution characteristics of heavy metals in soil from coal mining area: a case study in Linhuan mining district, northern Anhui province. Fresen. Environ. Bull. 26(3), 1989-1996.

[12] Xiao, R., Wang, S., Li, R., Wang, J.J. and Zhang, Z. (2017) Soil heavy metal contamination and health risks associated with artisanal gold mining in Tongguan, Shanxi, China. Ecotoxicology & Environmental Safety. 141, 17-24.

[13] Yu, Y.Y., Huang, Y.F., Song, B., Xu, T., Lu, S.F. and Yuan, Z.N. (2015) Investigation and health risk assessment of heavy metal content in soil and agricultural products in the surrounding areas of Nandan County. Environmental Chemistry. 34 (11), 2133-2135.

[14] Gui, H.R., Chen, L.W., Song, X.M., Tu, M. and Qin, Y. (2015) Research on water-proof and sand-proof technology for coal-mining in the shallow structure of thick loose-bed overlying area. China University of Mining and Technology Press, Xuzhou, China. 12-80.

[15] Sun, L. H, Peng, W.H. (2014) Groundwater in rural area of Suzhou, northern Anhui Province, China: Heavy metal concentrations and statistical analysis. Journal of Chemical & Pharmaceutical Research. 6(3), 1501-1505.

[16] Sun, Q.B., Yin, C.Q., Deng, J.F. and Zhang D.F. (2013) Characteristics of soil-vegetable pollution of heavy metals and health risk assessment in Daye mining area. Environmental Chemistry. 32(4), 671-677.

[17] Chinese National Environmental Protection Agency (CEPA) (1995) Environmental quality standard for soils (GB15618-1995) (in Chinese).

[18] Zhou, Y.Y., Yang, S.X., Yuan, Z.Z., Zhou, J.J. and Zhang, X.J. (2012) Assessment of heavy metal pollution in mine soil and bioaccumulation characteristics of dominant plants in a lead-zinc mineland, west Hunan. Earth and Environment. 40(3), 361-366.

[19] Padmavathiamma, P.K., Li, L.Y. (2012) Rhizosphere influence and seasonal impact on phytostabilisation of metals—a field study. Water Air & Soil Pollution. 223(1), 107-124.

[20] Ji, X.F., Zheng, N., Wang, Y., Liu, Q. and Zhang, J.J. (2015) Accumulation of mercury in soil-maize system of non-ferrous metals smelting area and its related risk assessment. Environmental Science. 36(10), 3845-3851.

[21] Gang, Y., Fei, S., Zhong, G., Xie, L., Wang, Y. and Jun, W.U. (2011) Concentration and health risk of heavy metals in crops and soils in zinc-lead mining area in southwest mountainous regions. Acta Scientiae Circumstantiae. 31(9), 2014-2021.

[22] Shi, G.L., Lou, L.Q., Zhang, S., Xia, X.W. and Cai, Q.S. (2013) Arsenic, copper, and Zinc contamination in soil and wheat during coal mining,with assessment of health risks for the inhabitants of Huaibei, China. Environmental Science and Pollution Research. 20(12), 8435-8445.
[23] US Environmental Protection Agency (USEPA). (1997) Exposure factors handbook—general factors. Office of Research and Development, National Center for Environmental Assessment, Washington, America.
[24] Phillips, L., Moya, J. (2012) The evolution of EPA's Exposure Factors Handbook and its future as an exposure assessment resource. Journal of Exposure Science & Environmental Epidemiology. 23(1), 13-21.
[25] Wilding, L.P. (1985) Spatial variability: its documentation, accommodation and implication to soil survey. Pudoc, Wageningen, Netherlands:Soil Spatial Variations. 166-193.
[26] Ji, Y.F., Li, Y.H., Yang, L.S., Sun, H.F. and Wang, W.Y. (2009) Distribution characteristics and environmental significance of heavy metals in typical soil profiles of Fenghuang lead zinc mining area of China. Acta Scientiae Circumstantiae. 29(5), 1094-1102.
[27] Zhang, A.X., Nie, Y.N., Ji, H.B., Feng, J.G. and Qin, F. (2014) Vertical distribution, morphological characteristics of heavy metals in soils of Wan Zhuang Gold mine field. Environmental Science & Technology. 37(120), 1-8.
[28] Blaha, U., Appel, E. and Stanjek, H. (2008) Determination of anthropogenic boundary depth in industrially polluted soil and semi-quantification of heavy metal loads using magnetic susceptibility. Environmental Pollution. 156(2), 278-289.
[29] Chen, C.S., Xie, Z.X. and Liu, X.J. (2009) Interactive effects of drought and salt stresses on winter wheat seedlings growth and physiological characteristics of stress-resistance. Chinese Journal of Applied Ecology. 20(4), 811-816.
[30] Han, Y.L., Qiu, E.F., Wang, Y.F., Tang, L.Q. (2015) Study on heavy metals distribution and correlation in soil and TSP of Beijing, Ecological and Environment, 24(1), 146-155.
[31] Wilcke, W., Müller, S., Kanchanakool, N. and Zech, W. (1998) Urban soil contamination in Bangkok: heavy metal and aluminium partitioning in topsoils. Geoderma. 86(3–4), 211-228.
[32] Carbonell, G., de Imperial, R.M., Torrijos, M., Delgado, M. and Rodriguez, J.A. (2011) Effects of municipal solid waste compost and mineral fertilizer amendments on soil properties and heavy metals distribution in maize plants. Chemosphere. 85(10), 1614-1623.

Received: **10.08.2017**
Accepted: **09.10.2017**

CORRESPONDING AUTHOR

Herong Gui
National Engineering Research Center of Coal Mine Water Hazard Controlling,
Suzhou 234000 – China

e-mail: hrgui@163.com

© by PSP Volume 26 – No. 12A/2017 pages 8255-8262 Fresenius Environmental Bulletin

EFFECTS OF LOW TEMPERATURE STRESS ON THE PHYSIOLOGICAL PROPERTIES OF 'DAWUXING' YOUNG LOQUAT FRUIT

Ronggao Gong*, Wei Yang, Mingan Liao, Zhihui Wang, Qunxian Deng, Yong Zhang

College of Horticulture, Sichuan Agricultural University, Chengdu, Sichuan, 611130, China

ABSTRACT

The young loquat fruits of 'Dawuxing' cultivar were selected as the materials, and semi-lethal temperature (LT_{50}), MDA content, antioxidant enzyme activities and physiological properties in pulp and seeds under different low temperatures and times were investigated to explore the response mechanism of fruit to chilling injury. The semi-lethal temperature was -6.1 ℃ and -4.9 ℃ in pulp and seeds, respectively. The activities of the SOD, CAT and POD increased, while the relative electric conductivity (REC) and MDA content maintained at low levels in pulp and seeds at 3 ℃ and 0 ℃, respectively. The activities of SOD, CAT and POD gradually decreased, and the REC and MDA content increased in pulp and seeds at -3 ℃ and 0 ℃, respectively. Microstructure diagrams showed that the loquat fruit was firstly destroyed at 0℃ for the exocarp and-3 ℃for the mesocarp the, then it happened freeze injury. And the firstly destroyed part was testa, followed by the leaf primordium or leaf again, and finally to the cell rupture. The soluble sugars, organic acids and soluble protein in pulp increased under low-temperature stress while the vitamin c content changed little. The expressions of genes (*Unigene25620* and *CL8135*) related to stress resistance in fruit were up-regulated. This study provide theory basis for the for thehigh quality and high yield cultivation in loquat industry.

KEYWORDS:
Low temperature stress, Young loquat fruit, Antioxidant enzyme, Microstructure

INTRODUCTION

The loquat (*Eriobotrya japonica Lindl)* isan evergreen tree in the family Rosaceae with origins in subtropical China, and it has been one of the most economic plants in south and marginal zones of China.However, the loquat frequently suffer from freezing injury due to its flowering period in the winter cold. Therefore, low temperature stress has become the important limiting factorto the healthy and sustainable development of loquat industry in Sichuan province, China [1].

Low temperature has a significant influence in plant growth affecting metabolism enzyme system, uptake of water, nutrients level and others. Compared to the leaves, the young loquat fruits, especially those with diameters of about 1 cm, suffered from cold infection more easily, which usually caused the seeds cold death [2]. The seed of loquat turned browning initially and then the young fruit pulp was frozen to death when suffering from low-temperature damage [3]. found that the young loquat fruit of cultivar 'Jiefangzhong' suffered from freezing injury under low temperature stress of 0 ℃, and the plasma membranes and tonoplast structure were broken in pulp under the temperature stress of -3℃. Under 0 ℃ chilling stress, the chloroplast and mitochondria structure were damaged in young loquat fruit pulp of cultivar 'Zaozhong No. 6' [4]. In general, low temperature stress could cause the plant membrane lipid peroxidation and the increase of malondialdehyde (MDA) content, which consequently led to the low-temperature damage of plants [5].

The antioxidation enzyme system, consists of superoxide dismutase (SOD) and catalase (CAT) and peroxidase (POD), is the main active oxygen scavenger in plant, which can effectively reduce the membrane lipid peroxidation [5, 6]. Huang et al. (2011) reported that the increase of cold-resistant ability of young loquat fruit by saclic acid (SA) was due to its positive effect on the antioxidationenzyme of young fruit. Wu et al. (2010) found that exogenous nitric oxide (NO)decreased the membrane lipid peroxidation by increasing the activities of SOD, CAT and POD of loquat pulp. The study on the loquat leaf envidenced that the antioxidation enzyme activity increased under mild low-temperature stress, but it was severely inhibited while the malondialdehyde (MDA) content increased significantly with the extension of time and decrease of temperature [9].

Previous studies on the cold resistance of loquat focused on the leaves and pulps, however, the effects of semilethal and low temperature stress on the oxidation enzyme system and tissue structure of the young fruit pulp and seed have not been reported [1, 2, 3, 9, 10]. This paper mainly investigated the physiological characteristics and organelle changes of young fruit pulp and seed of loquat under the low

temperature stress. The changes in related gene expressions were also analyzed to investigate the mechanisms of the young loquat fruit response to low-temperature damage.

MATERIALS AND METHODS

Sample preparation. Ten-year-old loquat cultivar 'Dawuxing' were grown at Longquanyi district horticultural field, Chengdu city, Sichuan province, China.

The three-year-old *E. japonica* Lindl. cv. Jiefangzhong was used as rootstock. Young loquat fruits were handpicked at 75 days after full bloom-from trees planted in well-spaced rows growing in a regularly maintained orchard. After clipping and sorting, the fruit was washed with distilled water and cultivated in the modified Hoagland's.

Determination of the relative electric conductivity (REC). The young loquat fruits were treated at 6 ℃, 3 ℃, 0 ℃, -3 ℃ and -6 ℃ for 12 h, 24 h, 36 h and 48 h, respectively. The culturation with relative humidity 70 %, light time 9 h/d and light intensity 3000 Lx was carried out in climatic cabinate for treatments at temperature above 0 ℃ (including 0 ℃) and in refrigerating cabinate for treatments at temperature below 0 ℃, respectively. Each treatment was equlibrated at room temperature for 12 h and then the pulp and seed were sampled and suspended in distilled water before analysis. The conductivities of fruit soak solutions were determined by a conductivity meter (DDS-11A) and the relative electric conductivity (REC) was calculated according to the method described by Li et al. (2000),

$$REC=\frac{\text{the conductivity of the treatment at room temperature}}{\text{the conductivity of the treatment after boiling}}\times 100\%$$

Determination of the Lethal temperature 50 (LT_{50}). The young loquat fruits were treated at 8 ℃,6 ℃, 4℃, 2℃,0 ℃, -2℃, -4℃ and -6 ℃ for 12 h, respectively. The culturation with relative humidity 70 %, light time 9 h/d and light intensity 3000 Lx was carried out in climatic cabinate for treatments at temperature above 0 ℃(including 0 ℃) and refrigerating cabinate for treatments at temperature below 0 ℃, respectively. Each treatment was equlibrated at room temperature for 12 h and then the pulp and seed were sampled and suspended in distilled water for REC analysis. The LT_{50} is calculated by logistic regressing analysis. The logistic regression equation was Y=, where y represents the REC, k represents the maximum rate of cell damage saturation capacity, a and b are the equation parameters. According to the regression analysis, the turning point of temperature (X = ln) in the equation is precisely the lethal temperature LT_{50} [12].

Determination of the enzyme activities. Samples of 0.25 g were homogenized in 5 mL of 50 mM phosphate buffer (pH 7.0) containing 1.0 N NaCl, 1% PVP (Sigma) M.W. 40 000, 1 mM ascorbate (Sigma) at 4 °C. After centrifugation at 15 000 × g for 15 min the supernatant was collected. The MDA activity was recorded by the method of Li et al. (2011). The specific activity of SOD was assayed by measuring its ability to inhibit the photochemical reduction of NBT [1]. PPO was assayed by using photochemical method and CAT activity was determined as described by Li et al. (2000).

Determination of physiological properties. Determination of soluble sugars, soluble protein , organic acids and vitamin C. Samples of 0.15g were homogenized and extracted in 5 mL 80 % ethanol, and heated for 45 min in boiling water. After cooling to room temperature, the extraction was centrifuged at 3,000 rpm for 10 min. The supernatant was collected to determine the amount of soluble sugars by the colorimetric method with anthrone-sulfuric acid at 620 nm with glucose as a standard.

The protein content was determined by the Coomassie Brilliant Blue G-250 method with bovine serum albumin as the standard. Soluble proteins were extracted from 0.2 g of fresh tissue at 4 °C with 5 mL of extracting solution containing 93.7 % 0.2 M Na2HPO4, 5.2 % 0.2 M NaH2PO4, 2 % PVP, and 0.1 % (v/v) β-mercaptoethanol for 60 min. After centrifugation at 4,000 rpm for 10 min, the supernatant was used for protein determination.

The organic acids and vitamin C were determined by HPLC using a C18 column and an RP-18 precolumn for the stationary phase. High-performance-liquid-chromatographic-(HPLC-)grade water is brought to pH 2.2 with sulphuric acid for the mobile phase. The flow rate is 0.4 mL/min, and UV detection is at 254 nm for vitamin C and 214 nm for organic acids.

Observation of the tissue structure of young fruit pulp. The structure slice was made according to the method described by Yu et al. (2010). The loquat pulp and loquat seed were sampled and sliced by longitudinal section. The observation was carried out by the optical microscope (steREO Discovery. V8, zeiss)

Quantitative reverse-transcription RCR (qRT-PCR). Thirty fruit spurs which were taken from the crown with young fruit, of which 10 placed in artificial climate box at 12℃ as a control, another 10 under 6℃ processing low temperature stress as a treatment, and another 10 under 3℃ processing low temperature stress as another treatment , dealt with 12 hours.

Total RNA from loquat fruit pulp was isolated as previously described by Reid et al. (2006). Pedicel

and seeds of each loquat were removed before grinding in liquid nitrogen. Total RNA was subjected to DNA digestion with 5 units of RNase-free DNase I (Promega) for 1h at 37°C. RNA content was measured at 260 mm with a spectrophotometer (GeneQuant™ Pro, GE Healthcare, Pessac alouette, France) and visualized by electrophoresison 1.5% agarose gels.

cDNA was synthesised using 1 μg of RNA using the SuperScript III first-strand cDNA synthesis kit (Invitrogen, San Diego, CA, USA) in a final volume of 20μL, and this was diluted to 200 μL before use in the qPCRreaction mixes. The PCR was performed on 1 μL cDNA from each sample, using a model 7300 Sequence Detection System (Applied Biosystems, Warrington, UK) and the Power SYBR-GreenPCR Master kit (Applied Biosystems Applera France, Courtaboeuf, France). PCR conditions used consited of an initial denaturation step at 50°C for 2 min, 95°C for10 min followed by 40 cycles of 95°C for 15 sec, 60°Cfor 1 min. The PCR primer combinations for each gene were listed in Fig 1.Relative quantification of the target expression level was performed using the comparative Ct method.

Reid KE, Olsson N, Schlosser J, Peng F, Lund ST: An optimized grapevineRNA isolation procedure and statistical determination of reference genes for real-time RT-PCR during berry development. BMC Plant Biol2006, 6:27.

Statistical analysis. Each experiment was conducted in triplicates and an average value was obtained for data analysis. Data were compared by Duncan's multiple range test (DMRT) at the 5% level of probability using SPSS 15.0 software.

RESULTS AND DISCUSSION

Effects of low-temperature stress on the REC and LT_{50} of the young loquat fruit pulp and seeds. The results of REC in the pulp and seeds of young loquat fruit were shown in Fig. 1. The REC results (RECs) of young loquat fruit pulp and seeds increased along with the decrease of temperature, and they increased rapidly at the temperature below -3℃.Under low-temperature stress at -3℃, there were no significant differences between the treatments except the treatment after48 h, while the RECs of seeds were significantly higher than those of pulp, indicating that the cell membranes of seeds damaged more seriously than pulp. The RECs of fruit pulp and seed were significantly higher than other treatments under low-temperature stress at -6 ℃. As can be seen in Table 1, the LT_{50} of the young loquat pulp (-6.1 ℃) was lower than that of the seeds (-4.9 ℃), meaning that the pulp has higher low-temperature resistance than the seeds.

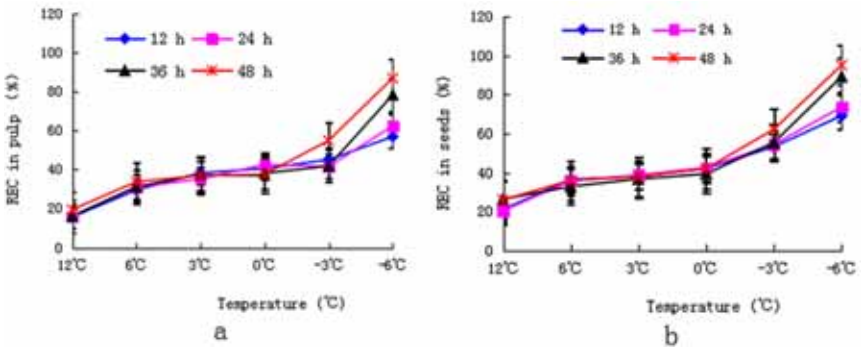


FIGURE 1
Changes of REC in pulp (a) and seeds (b) of young fruit under low-temperature stress.

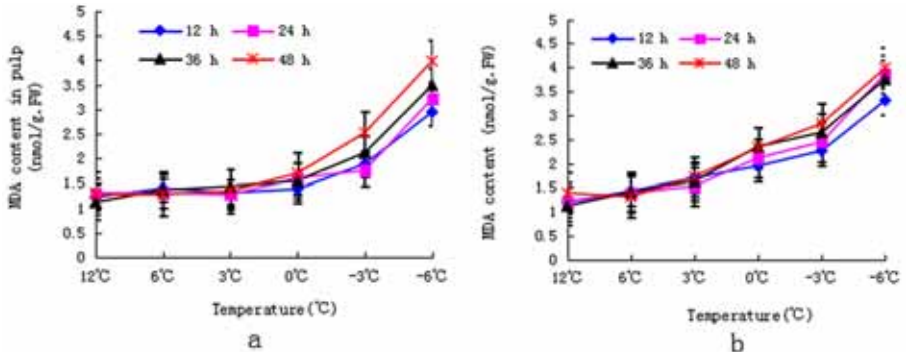


FIGURE 2
Changes of MDA content in pulp (a) and seeds (b) of young fruit under low-temperature stress.

TABLE 1
Semi-lethal temperature and parameters of yang loquat fruit

Part	Parameters of equation		LT_{50} (℃) Semi-lethal temperature	Relational coefficient
	a	b		
Pulp of young fruit	12.49	-0.54	-6.1	0.915
Seed embryo of young fruit	14.53	-0.42	-4.9	0.913

TABLE 2
Changes of the soluble sugars, organic acids ,Vc and soluble protein in young fruit under low-temperature stress

Treatment stress	Organic acid ($mg.g^{-1}FM$)	Soluble sugar ($mg.g^{-1}FM$)	Vc ($mg.100g^{-1}FM$)	Soluble protein ($mg.100g^{-1}FM$)
12℃ for 12h (CK)	10.648 c	2.467 b	5.381 a	0.164 b
6℃ for 12h	12.561 b	3.113 b	4.997 a	0.207 b
3℃ for 12h	18.213 a	5.371 a	6.011 a	0.413 a

Notes: Different letters behind data mean significant difference ($P<0.05$).

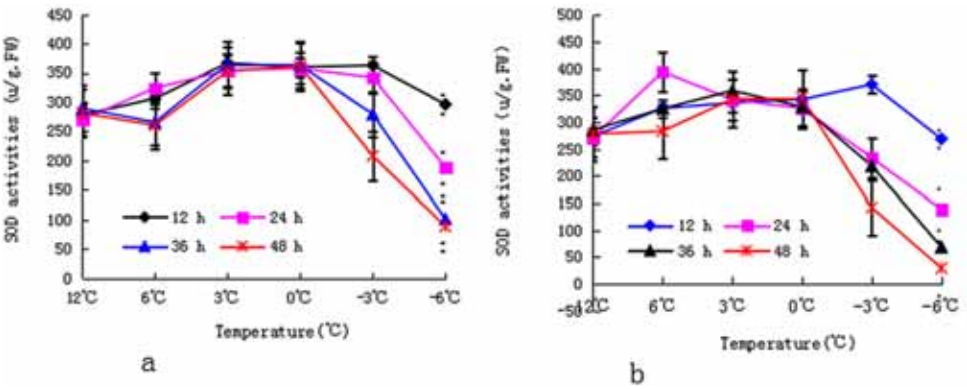


FIGURE 3
Changes of SOD activities in pulp (a) and seeds (b) of young fruit under low-temperature stress

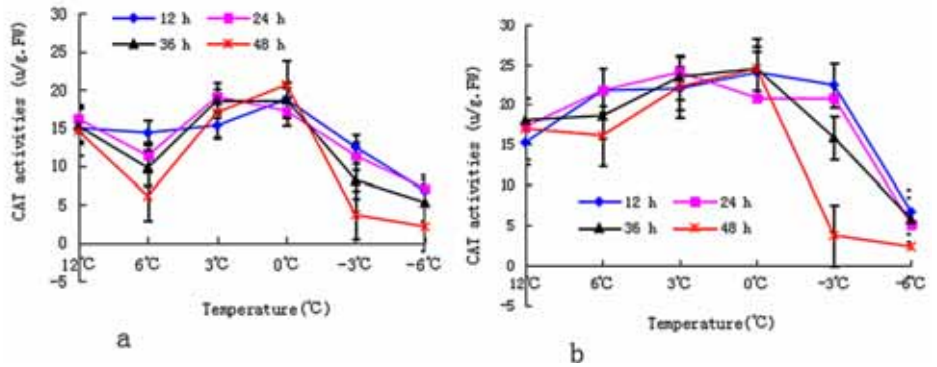


FIGURE 4
Changes of CAT activities in pulp (a) and seeds (b) of young fruit under low-temperature stress

The effects of low-temperature stress on the enzyme activities of the young loquat fruit pulp and seeds. Effect on MDA activity. MDA is one of the final products of polyunsaturated fatty acids peroxidation in the cells and its content reflects the level of lipid peroxidation and the status of impaired cells indirectly. The MDA content of young fruit pulp showed no obvious change under low-temperature stress at 0 ℃and above (Fig.2a). Under the low-temperature stress at 3℃and below, the MDA content of loquat pulp increased rapidly and there were significant differences between the treatments. In other words, the lipid peroxidation of young loquat pulp increased under low-temperature stress at 3℃and below. Figure 2b showed that the MDA content of young loquat seeds increased with the decrease of temperature, and the differences between treatments were not significant under low-temperature stress at 3℃and above, while the differences became significant under under low-temperature stress at 0 ℃ and below, indicating that the lipid peroxidation of seeds started to increase at 0 ℃.

Effect on SOD activity. SOD is the first line of defense from damages caused by oxygen radicals (Mittler, 2002) and its activity has been linked to physiological stresses such as low temperature, high intensity light, water stress and oxidative stress (Bowler et al., 1992). From Fig.3a, it can be seen that the SOD activities of young loquat pulp and seeds under low-temperature stress both increased during the earlier stage and then decreased fast along with time at the temperature below 0 ℃. There were significant difference between treatments under low-temperature stress at temperature below 0 ℃. Under low-temperature stress at -3℃ and below, the SOD activities of loquat seeds decreased faster than those of young loquat pulp (Fig. 3b). It was noted that the antioxidation capability of young loquat seeds was weaker than that of pulp.

Effect on CAT activity. CAT is a very important enzyme in protecting the cell from oxidative damage by reactive oxygen species. The overall CAT activities of young loquat pulp and seeds increased under the low-temperature stress at 0 ℃ and above. And under the low-temperature stress below 0 ℃, the CAT activities decreased along with the time.

Effect on POD activity. Increased POD activity is considered as an indicator of oxidative stress in plants. Figure 5 showed that the POD activities of young fruit pulp and seeds increased under mild low-temperature stress and decreased with the lower of the temperature. Additionally, the POD activities increased rapidly under low-temperature stress at 3 ℃ and below. The POD activity of young fruit pulp increased under low-temperature stress at 0℃ and above and decreased thereafter while the POD activity of seeds decreased under low-temperature stress at 6℃and below. Low-temperature stress reduced the enzymes capabilities of defensing the reaction oxygen species (ROS) in plants, and increased the concentration of fress radicals in fruit pulp and seeds.

Effect of low-temperature stress on the nutrient contents and tissue structure of young fruit pulp. Effect on soluble sugars, soluble protein, organic acids and vitamin C. The results of soluble sugars, soluble protein, organic acids and vitamin C changes under low-temperature stress in pulp were listed in Table 1. It was shown that the contents of soluble sugars, soluble protein and organic acids increased with the decrease of temperature, while the vitamin C content remained relatively stable in fruit pulp under low-temperature stress.

Effect on the tissue structure. Figure 6 shows the changes of tissue structure in pulp under different low-temperature stresses. The exocarp began to rupture under low-temperature stress at 6 ℃, and the cells turned to autolyze at 0 ℃. The pulp began to rupture under low-temperature stress at -3 ℃, and the cells turn to autolyze at -6 ℃.

Figure 7 shows the changes of tissue structure in seeds under different low-temperature stresses. The embryo began to rupture and autolyze under low-temperature stress at 3 ℃. The testa and embryo turned to separate at 3℃. The separation and rupture became more apparent with the decrease of temperature.

Effect on the genes expression. *Unigene25620* and *CL8135* are two important enzyme genes responsible for the early C-6 oxidation pathway and late C-6 oxidation pathway during the biosynthesis of brassinolide. The Plant brassinolide is considered as a key index reflecting the plant stress resistance to low-temperature, salinity and so on. Compared with the treatment at 12 ℃, the expression of *Unigene25620* increased by 2.9 times at 6 ℃and 1277 times at 3 ℃, respectively (Fig. 7). The expression of *CL8135*in fruit pulp increased by about 6 times under low-temperature stress at 3 ℃ as contrast to the treatment at 12℃ and 6 ℃.

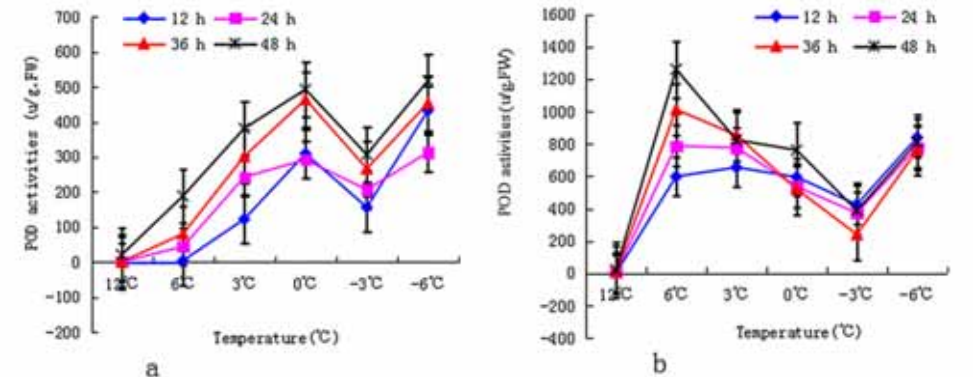


FIGURE 5
Changes of POD activities in pulp (a) and seeds (b) of young fruit under low-temperature stress

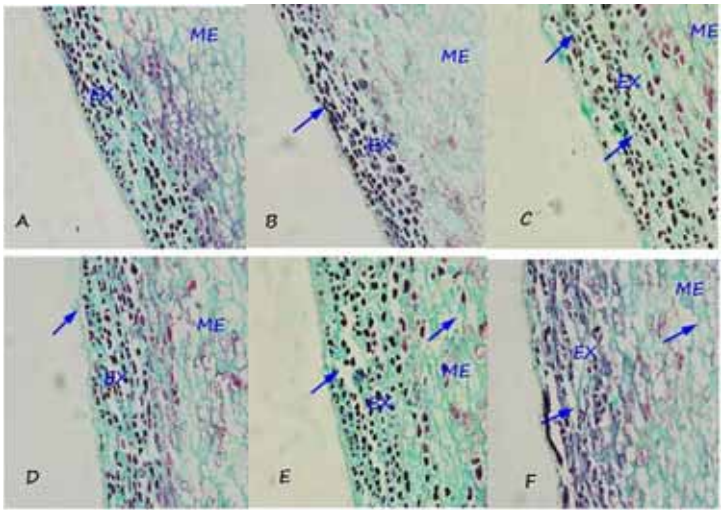


FIGURE 6
Microstructure of exocarp and pulp under different temperature (20X)
(A: Microstructure of control; B: Micro-structure of 6 ℃, the arrow marked exocarp; C: Microstructure of 3 ℃, the arrows markedexocarp; D: Microstructure of 0 ℃, the arrow markedexocarp; E: Microstructure of -3 ℃, the arrows markedexocarp; F: Microstructure of -6℃, the arrows markedexocarp and mesocarp; EX: Exocarp; ME: Mesocarp.)

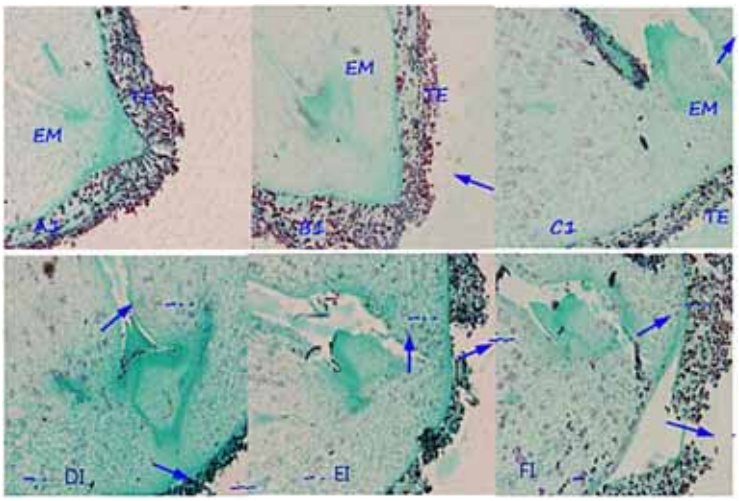


FIGURE 7
Seed microstructure under different temperature (20X)
(A1: Microstructure of control; B1: Microstructure of 6 ℃, the arrow marked testa; C1: Microstructure of 3 ℃, the arrow markedembryo; D1: Microstructure of0 ℃, the arrows markedtesta and embryo; E1: Microstructure of -3 ℃, the arrows markedtesta and embryo; F1: Microstructure of-6℃, the arrows markedtesta and embryo; TE: Testa; EM: Embryo.)

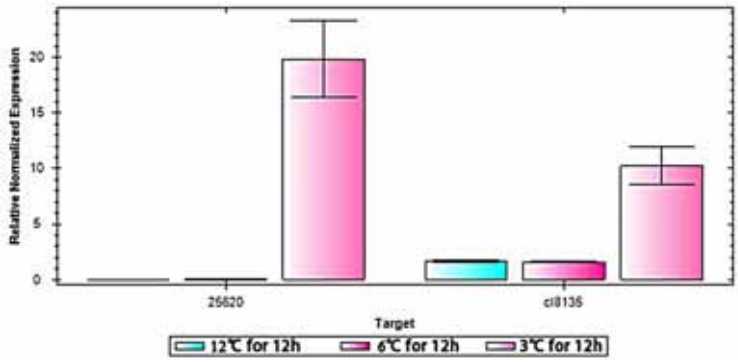


FIGURE 8
The expression pattern of gene 25620 and CL8135

DISCUSSION

The RECs of the loquat pulp and seeds increased under low-temperature stress, meaning that the pulp and seeds cells began to lose activity with the decrease of temperature.$LT_{50}$is an important physiological and ecological index to reflect the plant cold resistance [14,15]. The results in this study showed that the LT_{50} of the young loquat pulp and seeds were -6.1℃ and -4.9℃, respectively, which demonstrated that the seeds was weaker and frozen to death more easily than the fruit pulp [2].

Growth at low temperature may increase the concentration of reactive oxygen species (ROS), which may cause damage to membrane lipids, proteins and nucleic acids, leading to the death of the cells. The antioxidation enzymes including MPD, SOD, CAT and POD can scarvage ROS through their synergistic effects, which protect the plants from membrane lipid peroxidation [16, 17]. Under mild low-temperature stress (above 0 ℃ for the pulp and above 3 ℃ for the seeds), the activities of SOD, CAT and POD in young loquat fruit increased and the REC and MDA content were relatively low, showing that the antioxidation enzyme system of the young fruit did work under such stress. As the temperature decreased, the SOD activity of young fruit was relatively high which catalyzed the ROS to form H_2O_2, meanwhile the activities of CAT and POD decreased rapidly, causing the H_2O_2 accumulation and toxication to the young fruit. In other words, the antioxidation enzyme systems of young loquat fruit lost the protection function at -3℃ for the pulp and 0℃ for the seeds.

POD was thought as a key enzyme during the biosynthesis of lignin and it participated in the polymerization of lignin with H_2O_2. Thus, POD was found effective to improve the degress of tissue lignin [18]. It was noted that the phenomenon of rapid recovery appeared in POD activities of young loquat fruit under low-temperature stress at -3℃and below. The reason might be related to the fruit cell suberification after low-temperature damage [16]. The inner mechanism needs to be further investigated.

The exocarp cells and mesocarp cells were significantly changed under low-temperature stress (Figure 7 and Figure 8). Under mild low-temperature damage, the wax layer of epidermis wrinkled, and the pulp cells autolyzed and cell structure destroyed with the aggravation of low-temperature stress. These results were agreed with Chen et al. (2001). Low-temperature stress was found to increase the metabolism of soluble sugars, organic acids and soluble protein in pulp, which would improve the quality of loquat fruit in some degree and could be explained by the fact that loquat ripening period in winter. In other words, low temperature was important for the quality and mature of loquat fruit. The low-temperature stress also induced the expressions of *Unigene25620* and *CL8135*, indicating the enhanced biosynthesis of brassinolide in young fruit response to the cold damage.

CONCLUSION

The antioxidant enzyme activities increased at moderate low temperature stress, whereas declined significantly when the temperature attained certain critical temperature stress. The low-temperature resistance of young fruit pulp was highest, followed by the exocarp, and the seeds owned the weakest level. The soluble sugars, organic acids and soluble pprotein got increased under low-temperature stress. But the vitamin C content did not change much. The expression of genes related to brassinolide was induced as a result of the young fruit to the cold environment.

ACKNOWLEDGEMENTS

The project is supported by Scientific Research Fund of Sichuan Provincial Education Department, No. 2009ZA071.

The authors declare no conflict of interest.

REFERENCES

[1] Li, J., Sun, S.X., Xie, H.J., Chen, D., Tu, M.Y. (2011) The relationship between freezing injury and physiological indexes of loquat (*Eriobotrya japonica*) flowers and fruits. Journal of Fruit Science. 28(3), 453-457 (in Chinese).

[2] Chen, G.Z., Hu, B. (2001) Physiology of loquat frost and freezing measures. News of Citrus and Subtropical Fruit. (9), 26-27 (in Chinese).

[3] Zheng, G.H, Zhang, H.Y. (2008) Effects of chilling stress on cell ultrastructure and membrane permeability and protective enzyme activity in young loquat fruits. Chinese Journal of Tropical Crops. 29(6), 730-735 (in Chinese).

[4] Zheng, G.H., Zhang, H.Y. (2008) Changes in ultrastructure of loquat young fruits under different lower temperature stress. Journal of Fujian Agriculture and Forestry University(Natural Science Edition). 5(37), 474-476 (in Chinese).

[5] Li, J., Yan, X.F., Zhu, Y.G. (2000) Generation of activated oxygen and change of cell defense enzyme activity in leaves of Korean pine seedling under low temperature. Chinese Bulletin of Botany. 42(2), 148- 152 (in Chinese).

[6] Wu, N.B., Wu, J.Y., Zhu, L.Q., Wang, A. (2003) Effects of low temperature stress on physiological index and protein phosphorylation in brassica oleracea L. Acta Horticulturae Sinica. 30(5), 530-534 (in Chinese).

[7] Huang, Z.M., Wu, J.C., Chen, W.J. (2011) Effects of SA on enzymes of ascorbate-glutathione cycle in young loquat fruits after low temperature stress. Scientia Silvae Sinicae. 47(9), 36-42(in Chinese).
[8] Liu, L.Y, Zhao, D.Y., Zheng, Y., Shen, L., Sheng, J.P. (2009) Hydrogen peroxide metabolism and signal transduction under cold Stress in plants. Acta Horticulturae Sinica, 36(11), 1701-1708 (in Chinese).
[9] Zheng, G.H., Zhang, H.Y, Zhong X.R. (2009) Changes in cell ultra-structure, membrane permeability and protective enzyme activity in *Eriobotrya japonica* Lindl. Leaves under cold stress. Chinese Journal of Eco-Agricultre. 17(4), 739-745(in Chinese).
[10] Wu, J.C., Chen, W.J., Cai, L.Q., Xie, C.P., Huang, S.J. (2010) Effects of exogenous nitric oxide on anti-oxidation capacities in young loquat fruits under low temperature stress. Scientia Silvae Sinicae. 46(9), 73-78 (in Chinese).
[11] Li, H.S., Sun, Q., Zhao, S.J. (2000) Theory and technique of plant physiological and biochemical experiments. Beijing: Higher Education Press. 167-169, 195, 258-263.
[12] Zhu, G.H., Liu, Z.Q., Zhu, P.R. (1986) A study on determination of lethal temperature with logistic function. Journal of Nanjing Agricultural University. (3), 12-16 (in Chinese).
[13] Yu, J., Zhou, Z.S., Mu, Y.C., Zhang, Y., Jing, C. (2010) Comparison of leaf tissue structure of different cold hardiness winter wheat varieties under low temperature. Journal of Northeast Agricultural University. 41(4), 7-11 (in Chinese).
[14] Su, A., Mi, R.Q., Wang, W.Y. (1987) The study on the quantification of plant resistance. Science in China, Ser.B. 10, 1058-1067. (in Chinese).
[15] Yan, H.J., Tan, F. (2000) The relation between the membrane protective system and semilethal temperature of gardenia jasminoides ellis leaves as temperature fell. Acta Phytoecologica Sinica. 24(1), 91-95 (in Chinese), .
[16] Yang, S.C., Xie, C.T., Zhang, P., Chen, D., Ding, Y. (2003) Changes in membrane lipid peroxidation and activities of cell defense Enzyme in leaves of butia capitata becc seedling under low temperature stress. Acta Horticulturae Sinica. 30(1),104-106. (in Chinese).
[17] Fu, J.M., Huang, B.R. (2001) Involvement of antioxidants and lipid peroxidation in the adaptation of two cool-Season grasses to localized drought stress. Environmental and Experimental Botany. 45, 105-114.
[18] Wang, Y.S., Tian, S.P., Xu, Y. (2005) Effects of high oxygen concentration on por-and anti-oxidant enzymes in peach fruits during postharvest periods. Food Chemistry. (91), 99-104.
[19] Chen, X.W., Yang, L., Zhang, Y. (2006) Changes in ultrastructure of hypocotyl cells in phaseolus radiatus linn. under Low Temperature Condition. Plant Physiology Communications. 42 (6), 1099-1102. (in Chinese)
[20] Mittler, R. (2002) Oxidative stress, antioxidants and stress tolerance. Trends Plant Sci. 7, 405-410.
[21] Bowler, C., Montague, M.V. and Inze, D. (1992) Superoxide dismutases and stress tolerance. Ann. Rev. of Plant. Physiol. and Plant Mol. Bio. 43, 83-116.

Received: **12.08.2017**
Accepted: **11.10.2017**

CORRESPONDING AUTHOR

Ronggao Gong
College of Horticulture,
Sichuan Agricultural University,
No.211, Huimin Road,
Wenjiang District, Chengdu City,
Sichuan Province, 611130 – China

e-mail: rggong016@sohu.com

© by PSP Volume 26 – No. 12A/2017 pages 8263-8269 Fresenius Environmental Bulletin

SOIL CARBON SEQUESTRATION POTENTIAL OF DIFFERENT LAND USE AND LAND COVER SYSTEMS IN EASTERN PLATEAU AND HILLS AGROCLIMATIC ZONE OF INDIA

Anita Mohanty[1], Chandan Sahu[1], Hemendra Nath Nayak[2], Sanjat Kumar Sahu[1,*]

[1]P.G. Department of Environmental Sciences, Sambalpur University, Odisha, India
[2]Regional Office, State Pollution Control Board, Sambalpur

ABSTRACT

With the advent of industrialization and the rapid progress in developmental activities, the emission of carbon dioxide in to the atmosphere has amplified and with it has increased the demand of carbon sequestration. Soil is considered as a major carbon pool and hence is considered very strongly as a potent system for carbon sequestration. The purpose of this study was to examine the potential for carbon sequestration in the soil as a means of reducing carbon dioxide (CO_2) in the atmosphere. The study was taken up inside the Sambalpur University campus in four land use systems viz. pasture land, forest land, agricultural land and garden soil at three soil depths (0 – 10, 10 – 20 and 20 – 30 cm) to analyze for the organic carbon content, bulk density and Soil Organic Carbon (SOC) stock of the respective land uses. The result indicated that the OC varied with different depths in various land use system and was found to be in following sequence: forest land > garden soil > pasture land > agricultural land. Bulk density was also found to be negatively correlated with the OC and hence had a following sequence: agricultural land > pasture land > forest land > garden soil. The calculated SOC stock was found to be highest in forest land (38.97 t/ha) followed by pasture land (32.15 t/ha), garden soil (28.17 t/ha) and agricultural land (27.91 t/ha). From the above result it can be inferred that natural forest land plays an important role in sequestering atmospheric carbon and helps in mitigating climate change than the other man engineered land use systems.

KEYWORDS:
Soil, Carbon Sequestration, SOC, Forest, Pasture, Garden, Agricultural Land, Land Use

INTRODUCTION

Soil carbon represents the largest carbon pool of terrestrial ecosystems, and has been estimated to have one of the largest potentials to sequester carbon. Worldwide the responses of soil carbon stocks to forestry and agriculture activities are complex and need careful attention [1]. Agro-climatic conditions, land-use changes and forest/soil degradation not only affect carbon pools significantly [2]but also causes rapid depletion in carbon storage capacity of the soil and have important implications for CO_2 emissions and global climatic change[3].Whereas, integrated combination of land-management strategies shows considerable potential for carbon mitigation [4]. There is much variability in rates of carbon addition when conditions increases soil organic carbon during the conversion of cultivated soils to perennial vegetation, such as forest, grassland etc or when cultivated land loses its potential for crops generation [5]. Further, changed agricultural practices and future land-use change such as urbanization or abandonment of agricultural fields, exert significant influence on the potential of SOC sequestration at country-scale [6, 7].

When amount of carbon entering the soil exceeds that is lost to the atmosphere by oxidation, SOC increases. Such an increase can result from practices like improved: (i) tillage management and cropping systems, (ii) management to increase land cover, (iii) efficient use of production inputs, e.g. nutrients and water [8]. Grazing lands account for about one-fourth of potential carbon (C) sequestration in world soils. Relevant combinations of land use and managements like afforestation of cropland, conversion of grassland to cropland, soil tillage, and inputs from crop residue and organic fertilizers etc are expected to be most conducive to C stock changes within forestry and agriculture [9].

Based on the above facts a study was carried out to assess the soil carbon sequestration potential of four land use systems in Eastern Plateau and Hills agro-climatic zone of India and to make a comparison between the various classes of natural and man intervened land use system with respect to their soil carbon sequestration potential.

MATERIALS AND METHODS

Geographical Location of the study area. The study was carried out in Sambalpur University campus which is situated in the state of Odisha and falls in the eastern plateau and hills agro-climatic zone of India. Geographically, it lies between the co-ordinates of $21^0$28'50.03'' N and $83^0$53'01.88'' E with an elevation of 177 m above MSL.

Sampling of soil. In the present study,8 sites covering four different land use/ land cover systems, namely forest, pasture; agricultural and garden were chosen in the Sambalpur University campus for assessing the soil carbon sequestration potential. The soil of the area belongs to red and lateritic type. Ten numbers of samples at each sampling site was collected at three different soil depths: 0-10 cm, 10-20 cm and 20-30 cm using a soil core sampler. A total of 120 (4 x 10 x 3) soil samples were collected for SOC estimation. The soil samples collected were packed in zip lock polythene bags and quickly transported to laboratory for the analysis of various soil parameters.

Analysis of Bulk Density, Stones and Gravel, Soil Organic Carbon and Total SOC Stock. Bulk density of the soil was estimated using the standard core method [10]. The upper vegetation of the soil was gently cleaned and the soil samples of the particular land use were dug in the dimension of (10×10×10) cm of l×b×h with the help of a soil core sampler. It was brought to the laboratory and weighed over a digital balance to note its initial weight. The soil sample was then sieved using a 2 mm size sieve and the left out coarse material was measured to determine stones and gravel content. The sieved soil on the other hand was kept in hot air oven at 105^0 C for 24 hours to measure final weight of the dried sample of the soil. The dried soil was also put in a measuring cylinder to note the volume of the dried soil excluding pore spaces. The bulk density of the soil was measured using the formula as given below and expressed as g/cm^3.

Bulk Density (g/cm^3) = Weight of the oven dry soil/Volume of soil including solids and pores

Soil Organic Carbon was estimated by rapid titration method [11]. 0.5 – 1.0 g of sieved soil sample was taken in a 500 ml conical flask and 10 ml of 1N potassium dichromate was added to it followed by 20 ml of sulphuric acid – silver sulphate mixture solution. The mixture was gently stirred, allowed to stand for half an hour for digestion and diluted to 250 ml using distilled water. After adding 10 ml of orthophosphoric acid, the mixture was finally titrated against standard ferrous ammonium sulphate (FAS) solution using di-phenyl ammine indicator and the OC (%) was calculated using the following formula:

OC (%) = ((A – B) x 0.003 x 100)/ Weight of the soil sample taken

Where, A = Volume of FAS consumed in control and B = Volume of FAS consumed in experimental setup.

The total Soil Organic Carbon (SOC) stock was calculated as per the following formula given below [12, 13]:

SOC stock (t/ha) = Soil Depth (cm) x Bulk Density (g/cm^3) x OC (%) x CFst

Where, CFst (correction factor for stones and gravels) = (1 – {(% stone + % gravel)/100}).

After determining the total SOC stocks of different depths under different land use and land cover systems, the total carbon sequestration potential (t/ha) was calculated taking all the depths into consideration.

RESULTS AND DISCUSSION

The bulk density of soils at different depths of various land use systems in Eastern Plateau and Hills agro-climatic zone of India is presented in Table 1 and Figure 1. From the table, it is evident that, in the pasture land, the bulk density value ranged from 0.83 – 1.11 g/cm^3, 0.88 – 1.09 g/cm^3 and 0.98 – 1.14 g/cm^3 with a mean value of 1.00 ± 0.08, 0.99 ± 0.07, 1.06 ± 0.06 g/cm^3 at 0 - 10, 10 - 20, 20 – 30cm depth respectively while that in the garden land was found to be 0.31 – 0.58 g/cm^3, 0.12 – 0.51 g/cm^3, 0.43 – 0.63 g/cm^3 with a mean value of 0.44 ± 0.08, 0.38 ± 0.11 and 0.52 ± 0.06 g/cm^3 at a depth of 0 – 10, 10 – 20 and 20 – 30 cm respectively. However, in the forest land bulk density was found to be in the range of 0.52 – 0.83 g/cm^3, 0.57 – 0.74 g/cm^3, 0.52 – 0.79 g/cm^3 with a mean of 0.67 ± 0.11, 0.65 ± 0.06 and 0.67 ± 0.08 g/cm^3 at a depth of 0 – 10, 10 – 20 and 20 – 30 cm respectively while that in agricultural land was found to be in the range of 0.97 – 1.26 g/cm^3, 1.03 –1.48 g/cm^3, 1.24 – 1.62 g/cm^3 with a mean of 1.12 ± 0.10, 1.16 ± 0.15 and 1.41 ± 0.12 g/cm^3 at depths of 0 – 10, 10 – 20 and 20 – 30 cm respectively.

Bulk density is the property of soil that ultimately regulates the amount of soil carbon sequestration. The present study reported lowest soil bulk density in the garden and forest soil which might have been due to the presence of high organic matter. Presence of organic matter in soil tends to make the soil loose and porous thereby decreases the bulk density of the soil [14]. Excepting the agricultural land, the soil bulk density was at reduced level at 10 – 20 cm depth with a subsequent increase in bulk density with further depths which might have also been due to greater organic matter content in the middle zone. Moreover, compaction of soil increases the bulk density and hence a subsequent increase of bulk density in depth 20 – 30 cm is observed in our study as well. Bulk density of the soil showed a significant difference with respect to land use only

TABLE 1
Range and Mean ± S.D. values of various parameters at different depths in various land use systems in Eastern Plateau and Hills agro-climatic zone of India

Land use	Depths (cm)		OC (%)	BD (gm/cm^3)	SOC (t/ha)
Pasture	0 - 10	Range	0.12 - 3.0	0.83 - 1.11	0.63 - 21.35
		Mean ± S.D.	1.43 ± 0.87	1.00 ± 0.08	10.06 ± 6.15
	10 - 20	Range	0.66 - 2.7	0.88 - 1.09	3.48 - 17.75
		Mean ± S.D.	1.63 ± 0.71	0.99 ± 0.07	11.15 ± 5.24
	20 - 30	Range	0.48 - 3.72	0.98 - 1.14	3.23 - 24.98
		Mean ± S.D.	1.58 ± 1.06	1.06 ± 0.06	10.94 ± 7.22
Garden	0 - 10	Range	1.5 - 4.56	0.31 - 0.58	4.31 - 14.26
		Mean ± S.D.	2.96 ± 1.06	0.44 ± 0.08	10.06 ± 3.53
	10 - 20	Range	1.62 - 4.56	0.12 - 0.51	4.22 - 10.67
		Mean ± S.D.	2.98 ± 1.05	0.38 ± 0.11	7.61 ± 2.42
	20 - 30	Range	1.5 - 4.44	0.43 - 0.63	4.80 - 15.55
		Mean ± S.D.	2.77 ± 1.01	0.52 ± 0.06	10.50 ± 3.76
Forest	0 - 10	Range	0.84 - 5.52	0.52 - 0.83	4.61 - 23.51
		Mean ± S.D.	3.09 ± 1.55	0.67 ± 0.11	14.47 ± 6.53
	10 - 20	Range	0.48 - 5.46	0.57 - 0.74	2.73 - 26.73
		Mean ± S.D.	3.09 ± 1.64	0.65 ± 0.06	14.72 ± 8.03
	20 - 30	Range	0.06 - 4.26	0.52 - 0.79	0.29 - 20.79
		Mean ± S.D.	2.02 ± 1.44	0.67 ± 0.08	9.78 ± 7.08
Agriculture	0 - 10	Range	0.12 - 1.96	0.97 - 1.26	1.12 - 16.82
		Mean ± S.D.	1.08 ± 0.57	1.12 ± 0.10	9.50 ± 5.39
	10 - 20	Range	0.48 - 1.74	1.03 - 1.42	4.54 - 14.81
		Mean ± S.D.	0.92 ± 0.35	1.16 ± 0.15	9.00 ± 3.03
	20 - 30	Range	0.48 - 1.26	1.24 - 1.62	4.70 - 14.62
		Mean ± S.D.	0.86 ± 0.26	1.41 ± 0.12	9.41 ± 3.91

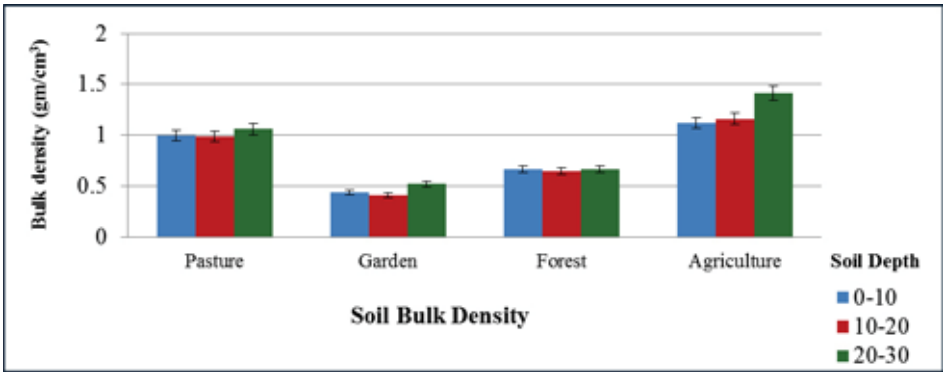


FIGURE 1
Bulk Density (g/cm^3) of soils at different depths of various land use systems in Eastern Plateau and Hills agro-climatic zone of India

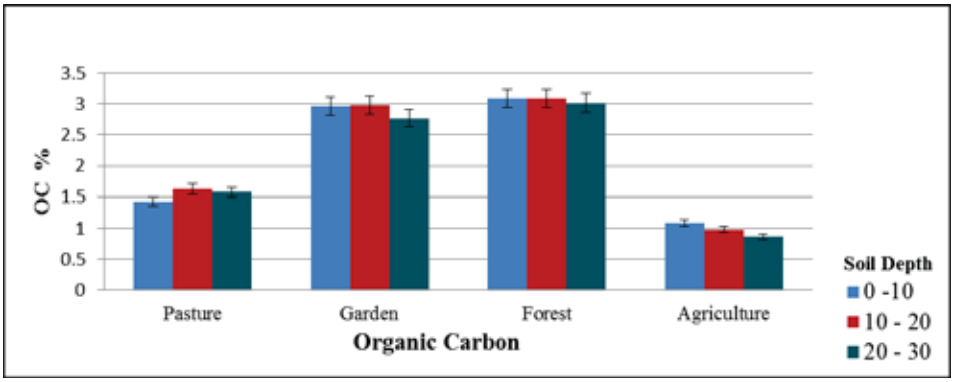


FIGURE 2
Soil Organic Carbon (%) of soils at different depths of various land use systems in Eastern Plateau and Hills agro-climatic zone of India

(F_1 = 81.27, $p < 0.05$). Significant negative correlation of bulk density with organic carbon ($r = -0.991$, $p < 0.05$) was obtained in the present study that also confirms the influence of organic carbon over the bulk density of the soil. This result corroborates the findings of [15] and [16].

The Organic carbon content of soils at different depths of various land use systems in Eastern Plateau and Hills agro-climatic zone of India is presented in Table 1 and Figure 2. It can be clearly seen that, in the pasture land, the organic carbon content ranged from 0.12 – 3.0 %, 0.66 – 2.70 % and 0.48 – 3.72 % with a mean value of 1.43 ± 0.87, 1.63 ± 0.71 and 1.58 ± 1.06 % at 0 – 10, 10 – 20 and 20 – 30 cm depth respectively while that in the garden land was found to be 1.5 – 4.56 %, 1.62 – 4.56 %, 1.5 – 4.44 % with a mean value of 2.96 ± 1.06 , 2.98 ± 1.05 and 2.77 ± 1.01 % at a depth of 0 – 10, 10 – 20 and 20 – 30 cm respectively. However, the forest land had the organic carbon content in the range of 0.84 – 5.52 %, 0.48 – 5.46 % and 0.06 – 4.26 % with a mean of 3.09 ± 1.55, 3.09 ± 1.64 and 2.02 ± 1.44 % at a depth of 0 – 10, 10 – 20 and 20 – 30 cm respectively and the agricultural land had the organic carbon content in the range of 0.12 – 1.96 %, 0.48 – 1.74 %, 0.48 – 1.26 % with a mean of 1.08 ± 0.57, 0.92 ± 0.35 and 0.86 ± 0.26 % at depths of 0 – 10, 10 – 20 and 20 – 30 cm respectively.

Organic matter content in soil directs the fertility status and biological activity in soil [17]. Greater microbial activity in soil with large organic matter content has direct influence over the soil carbon storage [18]. The present results of the organic carbon in soil suggested high organic carbon in forest land and garden soil which might have been sourced from the litter deposition from the thick vegetation cover. However, a relatively low organic carbon was found in the pasture land followed by the agricultural land. This suggests that the transformation of a forest land into other land use forms through slashing of thick vegetation ultimately might have resulted in the decline of the organic matter and in consequence organic carbon content, in the animal interfered pasture and human engineered agricultural soil. Organic carbon content showed a significant difference with respect to land use only (F_1 = 13.77, $p < 0.05$). When correlated with the overall SOC stock of the soil irrespective of the land use pattern, a significant positive correlation ($r = 0.767$, $p < 0.05$) suggested that organic carbon content in soil also has an influence over the carbon sequestration potential of soil. This result was in agreement with the findings of [19] who reported that as the land is converted from natural forest to other land use forms, there is a considerable decline in the organic carbon content of the soil. Similar results were also reported by other workers like [20] and [21]. However, excepting the agricultural land, all other land uses had greater organic carbon content in the middle zone (10 – 20 cm) than the surface zone (0 – 10 cm). This might have been due to the fact that the surface organic matter is likely to be decomposed faster by the microorganism resulting in the loss of organic carbon in the form of surface carbon dioxide emission. On the other hand, the subsurface zone is a safer area for the accumulation of the organic carbon because they remain stable for a longer duration of time [22].

The SOC stock content of different land use from various depths of the soil is given in Table 1 and Figure 3. It can be clearly seen that, in the pasture land, the SOC stock value ranged from 0.63 – 21.35 t/ha, 3.48 – 17.75 t/ha and 3.23 – 24.98 t/ha with a mean value of 10.06 ± 6.15 , 11.15 ± 5.24,10.94 ± 7.22 t/ha at 0 - 10, 10 - 20, 20 – 30cm depth respectively while that in the garden land was found to be 4.31 – 14.26 t/ha, 4.22 – 10.67 t/ha, 4.80 – 15.55 t/ha with a mean value of 10.06 ± 3.53, 7.61 ± 2.42 and 10.50 ± 3.76 t/ha at a depth of 0 – 10, 10 – 20 and 20 – 30 cm respectively. However, in the forest land SOC stock was found to be in the range of 4.61 – 23.51 t/ha, 2.73 – 26.73 t/ha, 0.29 – 20.79 t/ha with a mean of 14.47 ± 6.53, 14.72 ± 8.03 and

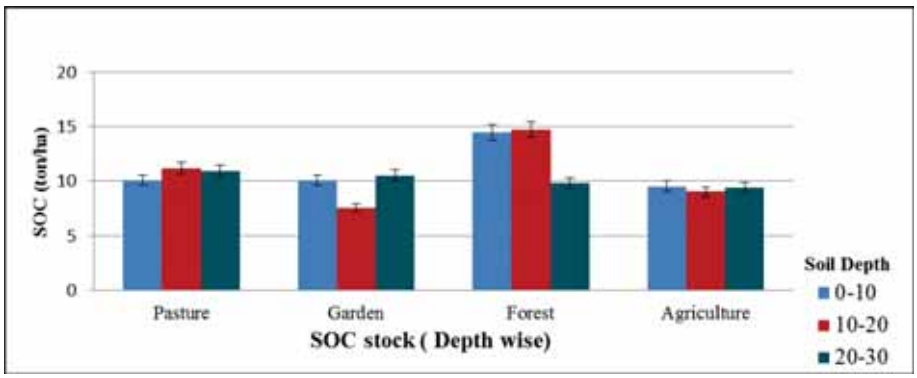


FIGURE 3
SOC Stock (t/ha) of soils at different depths of various land use systems in Eastern Plateau and Hills agro-climatic zone of India

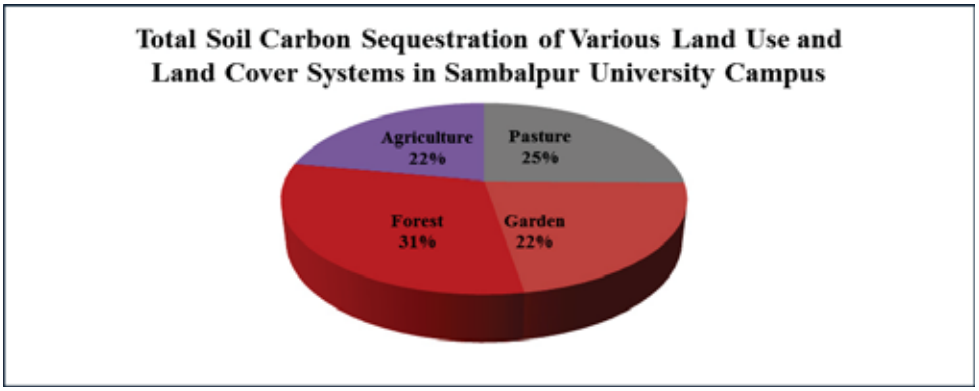


FIGURE 4
Soil carbon sequestration of various land use in Sambalpur University campus

9.78 ± 7.08 t/ha at a depth of 0 – 10, 10 – 20 and 20 – 30 cm respectively while that in agricultural land was found to be in the range of 1.12 – 16.82 t/ha, 4.54 – 14.81 t/ha, 4.70 – 14.62 t/ha with a mean of 9.50 ± 5.39, 9.00 ± 3.03 and 9.41 ± 3.91 t/ha at depths of 0 – 10, 10 – 20 and 20 – 30 cm respectively.

In the present study the total SOC stock of soils in different land use systems was calculated taking all the depths into consideration and has been presented in Table 2. The soil carbon sequestration (SOC stock) value was found highest in forest land (38.97 t/ha) followed by pasture land (32.15 t/ha), garden soil (28.17 t/ha) and agricultural land (27.91 t/ha).

TABLE 2
Total SOC stock (t/ha) of various land use systems in Eastern Plateau and Hills agro-climatic zone of India

Land use	0 - 10 cm	10 - 20 cm	20 - 30 cm	0 - 30 cm
Pasture	10.06	11.15	10.94	32.15
Garden	10.06	7.61	10.50	28.17
Forest	14.47	14.72	9.78	38.97
Agriculture	9.50	9.00	9.41	27.91

Soil carbon sequestration potential is a dependent parameter of soil that is directly governed by the soil physical properties [23]. The present study showed highest soil carbon sequestration potential in case of natural forest land and as the natural system is transformed into pasture land for grazing by the remnants and subsequently to maintained land like garden and human engineered land like agricultural field, there is a gradual decline in the overall carbon sequestration potential of the soil. The main reason for this might have been the high organic carbon content in forest land through litter deposition than the other land use forms. The result corroborates the previous research findings of [19]. This justifies the fact that carbon sequestration is highest in virgin soils and nature directs every phenomenon towards a balance. This balance is disturbed only when there is a human intervention. However, [24] reported that the soil carbon sequestration is a function of activities of the decomposers rather than carbon inputs. This might have been the main reason for the current observation of low soil carbon sequestration potential in garden land as compared to pasture land although the organic matter content in the former is more than the later.

The total Soil Carbon Sequestration in the four land use in Sambalpur University campus is represented in Figure 4. The highest soil carbon sequestration was achieved by Forest land (31 %) followed by Pasture land (25 %), Garden soil (22 %) and Agriculture soil (22 %). This result clearly suggests that the natural land have greater potential to sequester soil carbon than the intervened land use.

CONCLUSION

The present study focused on the estimation of Soil Carbon Sequestration of various land use and land cover systems inside the campus of Sambalpur University. The findings of our research showed the following trend of carbon sequestration potential of various land use and land cover systems inside Sambalpur University campus: Forest land (38.97 t/ha or 31 %) > Pasture land (32.15 t/ha or 25 %) > Garden soil (28.17 t/ha or 22 %) > Agricultural land (27.91 t/ha or 22 %). The result clearly suggests that the natural forest land has the maximum capacity of soil carbon sequestration than the other man engineered land use systems.

ACKNOWLEDGEMENTS

The author (AM) would like to thank the HOD, P.G. Department of Environmental Sciences, for providing the laboratory facilities to carry out this research work.

REFERENCES

[1] Oliva, F.G. and Masera, O.R. (2004) Assessment and measurement issues related to soil-carbon sequestration in land-use, land-use change, and forestry (lulucf) projects under the kyoto protocol. Climatic Change. 65, 347 – 364.

[2] Upadhyay, T.P., Sankhayan, P.L. and Solberg, B. (2004) A review of carbon sequestration dynamics in the Himalayan region as a function of land-use change and forest/soil degradation with special reference to Nepal. Agriculture, Ecosystems and Environment. 05, 449 – 465.

[3] Lal, R. (2005) Forest soils and carbon sequestration. Forest Ecology and Management. 220, 242 – 258.

[4] Smith, P., Powlson, D.S., Smith, J., Falloon, P. and Coleman, K. (2000) Meeting Europe's climate change commitments: quantitative potential for carbon mitigation by agriculture. Global change biology. 6, 525 - 539.

[5] Post, W.M. and Kwon, K.C. (2000) Soil Carbon Sequestration and Land-Use Change Processes and Potential. Global Change Biology. 6, 317 – 328.

[6] Akpalu, W. and Ekbom, A. (2010) The Bioeconomics of Conservation Agriculture and Soil Carbon Sequestration in Developing Countries. Environment for Development Discussion paper series. 20, 165 - 186.

[7] Yagasaki, Y. and Shirato, Y. (2014) Assessment on the rates and potentials of soil organic carbon sequestration in agricultural lands in Japan using a process-based model and spatially explicit land-use change inventories – Part 2: Future potentials. Bio geosciences. 11, 4443 – 4457.

[8] Follett, R.F. (2001) Soil management concepts and carbon sequestration zin crop land soils. Soil and Tillage Research. 61, 77 - 92.

[9] Vesterdal, L. and Leifeld, J. (2010) Land-use change and management effects on soil carbon sequestration: Forestry and agriculture. Greenhouse-gas budget of soils under changing climate and land use (BurnOut). 25 - 32.

[10] Mckenzie, N.J., Jacquier D.J., Isbell. R.F. and Brown, K.L. (2004) Australian Soils and Landscapes: An Illustrated Compendium. CSIRO Publishing: Collingwood, Victoria.

[11] Walkley, A. and Black, I.A. (1934) An examination of Degtjareff method for determining soil organic matter and a proposed modification of the chromic acid titration method. Soil Science. 37, 29 - 37.

[12] Qin, Z., Dunn, J.B., Kwon, H., Mueller, S. and Wander, M.M. (2015) Soil carbon sequestration and land use change associated with biofuel production: empirical evidence. GCB Bioenergy. 1 - 15.

[13] Koppad, A.G. and Janagoudar, B.S. (2016) Vegetation Analysis and Carbon Sequestration in Forest Soils of Different Zones in Uttara Kannada District through Geo-informatics Approach. International Journal of Research in Management & Technology. 6(1), 16 - 20.

[14] Yihenew, G.S. and Getachew, A. (2013) Effects of different land use systems on selected physicochemical properties of soils in North-western Ethiopia. 5(4), 112 – 120.

[15] Michel, K.Y., Pascal, K.T.A., Souleymane, K., Jerome, E.T., Yao, T., Luc, A. and Daniele, B. (2010) Effects of landuse types on soil organic carbon and nitrogen dynamics in Mid-West cote d'lvoire. European Journal scientific research. 40(2), 211 - 222.

[16] Islam, K.R. and Weil, R.R. (2000) Land use effects on soil quality in a tropical forest ecosystem of Bangladesh. Agricultural Ecosystems and Environment. 79, 9 – 16.

[17] Sahu, C., Basti, S. and Sahu, S.K. (2016) Carbon dioxide evolution and enzymatic activities of soil different land use practices located near Bhawanipatna town in Odisha, India. Fresen. Environ. Bull. 25(12), 5432 – 5439.

[18] Sahu, C., Basti, S., Pradhan, R.P. and Sahu, S.K. (2016) Physicochemical properties of soil under different land use practices located near Bhawanipatna town in Odisha, India. International Journal of Environmental Sciences. 6(6), 941 – 953.

[19] Ahukemere, C.M., Akamigbo, F.O.R., Onweremdu, E.U., Ndukwu, B.N. and Osisi, F.A. (2015) Carbon and nitrogen forms and sequestration in relation to agricultural land use types in a humid agro-ecosystem. Global Biosciences. 4(3), 1655 - 1665.

[20] Lemenih, M., Karltun, E., Olsson, M. (2005) Assessing soil chemical and physical property responses to deforestation and subsequent cultivation in smallholders farming system in Ethiopia. Agriculture, Ecosystems & Environment. 105, 373 - 386.

[21] Martinez-Mena, M., Lopez, J., Almagro, M., Boix-Fayos, V. and Albaladejo, J. (2008) Effect of Water Erosion and Cultivation on the Soil Carbon Stock in a Semiarid Area of South-East Spain. Soil and Tillage Research. 99, 119 - 129.

[22] Mbah, C.N. and Idike, F.I. (2011) Carbon storage in tropical agricultural soils of south eastern Nigeria under different management practices. International Research Journal of Agricultural Science. 1(2), 53 - 57.

[23] Batjes, N.H. (1996) Total carbon and nitrogen in the soils of the world. International soil reference and information center (ISRIC). European journal of soil science. 47, 151 – 163.

[24] Schlesinger, W.H., and Andrews, J.A. (2000) Soil respiration and the global carbon cycle. Biogeochemistry, 48, 7 – 20.

Received: **14.08.2017**
Accepted: **21.09.2017**

CORRESPONDING AUTHOR

Sanjat Kumar Sahu
P.G. Department of Environmental Sciences,
Sambalpur University,
Jyoti Vihar, Burla,
Odisha – India

e-mail: sahusanjat@rediffmail.com

© by PSP Volume 26 – No. 12A/2017 pages 8270-8277 Fresenius Environmental Bulletin

INFLUENCE OF Al^{3+} DOSAGE ON THE FLOCCULATION PERFORMANCE OF ACTIVATED SLUDGE AND ITS MECHANISM

Haisong Li[1], Jia Zhou[2], Xiaolei Chen[3], Dongjin Wan[4,*], Wenning Mai[5]

[1]Zhengzhou University, School of Chemical Engineering and Energy, Zhengzhou 450001 China
[2]Zhengzhou University, School of Public Health, Zhengzhou 450001, China
[3]ZhiHe Environmental Science and Technology Co., Ltd, Zhengzhou 450001, China
[4]Henan University of Technology, School of Chemistry and Chemical Engineering, Zhengzhou 450001, China
[5]Zhengzhou University, School of Water Conservancy and Environment, Zhengzhou 450001, China

ABSTRACT

Aluminum flocculants can improve the flocculation performance of activated sludge (AS). This study systematically investigated the influence of Al^{3+} dosage on AS flocculation and explored its underlying mechanism by total interaction energy (W_{tot}) and loosely-bound extracellular polymeric substances (LB-EPS) content. AS samples cultivated in a sequencing batch reactor (SBR) were added a range of Al^{3+} dosages: 0, 0.0625, 0.125, 0.25, 0.5, 1, 2, and 4 mEq·L^{-1}. As Al^{3+} dosage increased from 0 to 2 mEq·L^{-1}, W_{tot}, LB-EPS content and supernatant turbidity all decreased, which appeared as better AS flocculation. However, when Al^{3+} dosage further increased to 4 mEq·L^{-1}, W_{tot} and LB-EPS content decreased, whereas supernatant turbidity tended to increase and AS flocculation deteriorated. Most of the added Al^{3+} distributed within the pellet at all Al^{3+} dosages, which is the core element governing the differences in AS flocculation performance. This study together with our previous findings are the first time to uncover that W_{tot}, LB-EPS content, supernatant turbidity decreased in two-phases: 0–0.25 VS. 0.25–2 mEq·L^{-1} Al^{3+} dosages as the concentration of added Al^{3+} in the pellet increased, whereas high dosage (4 mEq·L^{-1}) deviated from the tendency.

KEYWORDS:
Activated sludge, Al^{3+}, Flocculation, Extracellular polymeric substances, Interaction energy.

INTRODUCTION

AS is widely used in wastewater treatment, owing to its simple operation, reasonable cost, and no secondary pollution, among other features [1]. AS flocculation performance is an important factor influencing wastewater treatment plant operation. It has been reported that 70–90% of AS systems experience assorted solid-liquid separation issues in settling tanks [2]. Therefore, improvement of AS flocculation would have a profound impact in effluent quality. Al^{3+}, a common coagulant, can bridge between negative charge functional groups within the EPS, and promote AS flocculation [3].

The Derjaguin-Landau-VerweyOverbeek (DLVO) and multivalent cation bridging theories have been proposed to explain the role of cations in AS flocculation performance [4]. Classical DLVO theory elaborates the stability of colloidal particles, and the extended DLVO theory brings in the Lewis acid-base interactions (W_{AB}); thus, W_{tot}= electric double layer (W_R) + van der Waals force (W_A) + W_{AB} [5]. The DLVO theories are based on the assumption that surfaces of particles are smooth and shapes are uniform. In fact, AS is not ideal colloid; surface properties of AS particles are extremely complicated owing to the existence of EPS.

AS flocs consist of various microorganisms (mainly bacteria) and EPS [6], the latter being the dominating factor affecting AS flocculation performance [7]. EPS contains carboxyl, hydroxyl, phosphate group, sulfonic group and other functional groups, so its surface is always with a large number of negative charges, which produce electrostatic repulsion between AS flocs [8–10]. Metal ions, such as Al^{3+}, Fe^{3+} and Zn^{2+}, could facilitate AS flocculation through neutralizing the surface negative charges and continuous compressing electric double layer [11, 12]. Due to the complicacy of EPS, the binding properties and interaction mechanisms between cations and EPS are yet to be elucidated [6].

Our previous studies reported different flocculation-promoting additives (Ca^{2+}, Al^{3+} and Fe^{3+}) [13] and the influence of multivalent cations on the AS flocculation with different sludge retention times (SRT) [14]. We deduced that Al^{3+} which possess a higher binding affinity for AS would promote larger AS flocs formation, so to improve AS flocculation and dewaterability. However, the influence

of Al^{3+} dosage on AS flocculation had not been systematically studied yet, and the underlying mechanism remained obscure. This study intended to further determine the influence of Al^{3+} dosage on AS flocculation performance, track the distribution of added Al^{3+} in AS, and explore the underlying mechanism by W_{tot} and EPS content at various Al^{3+} dosages, thereby provide a theoretical basis for engineering applications.

MATERIALS AND METHODS

AS cultivation. The AS obtained from Qu Yang wastewater treatment plant (Shanghai, China) was cultivated in a 4L SBR. Glucose, NH_4Cl, and KH_2PO_4 were used as carbon, nitrogen, and phosphorus sources respectively, and relative proportion of chemical oxygen demand (COD), N and P (COD:N: P ratio) in influent was maintained at 100: 7.5: 1.5. Micronutrient concentrations were maintained according to Liao et al [2]. Mixed liquor suspended solids (MLSS) were kept at 2300 $mg \cdot L^{-1}$ by adjusting influent COD concentration at 327.5 ± 22.2 $mg \cdot L^{-1}$. The reactor was equipped with a paddle mixer operating at 100 rpm; temperature was maintained at 20±1 °C. Air was introduced to maintain the dissolved oxygen (DO) in the range of 2–3 $mg \cdot L^{-1}$. Influent pH was controlled between 6.8–7.2 by $NaHCO_3$. The SBR was operated 4 h a cycle, six cycles per day; the specific operation details of each cycle were consistent with our previous studies [14]. AS samples was collected at 15 d to be further analyzed.

Al^{3+} dosing test. 800 mL collected AS was mixed and decanted into 8 identical 250 mL beakers, 100 mL AS each. Al^{3+} ($AlCl_3$) solutions with various concentrations (0, 0.0625, 0.125, 0.250, 0.50, 1, 2, and 4 $mEq \cdot L^{-1}$) were added to these beakers respectively, and the beaker without Al^{3+} (0 $mEq \cdot L^{-1}$) was used as control. The samples were mixed rapidly at 117 rpm for 5 min, then slowly at 50 rpm for 5 min.

The supernatant of AS was taken by a 0.45 μm PTFE membrane to avoid multiple scattering; the size of AS flocs was determined by the Eyetech particle size and shape analyzer (KS-100, ANKERSMID, Holland). The supernatant of AS was carefully taken after settling for 30 min, and turbidity was measured using a turbidity meter (2100P, HACH, USA). 100 mL AS suspension was collected, and Sludge Volume Index (SVI) was measured by a graduated cylinder. The dewaterability of AS flocs was determined by capillary suction time (CST) using a CST measuring instrument (model 319, Triton, UK). MLSS, SS and COD were analyzed by standard laboratory method of 2540 D [15]. The EPS extraction protocol used herein was same as our previously published methods [14].

Analyses. The total organic carbon (TOC) contents of bulk solution, LB-EPS, and tightly-bound extracellular polymeric substances (TB-EPS) were determined by TOC/TN analyzer (TMM-1, SHIMADZU, Japan). Cationic concentrations in the bulk solution, LB-EPS, TB-EPS, and pellet were analyzed by inductively coupled plasma optical emission spectrometry (ICP-AES, Optima 2100 DV, Perkin Elmer, USA). Aqua regia digestion was employed to digest the pellet following the standard method (USEPA method 3051a) before its cation concentrations were determined. The interaction energy curves were determined by contact angle approach; the contact angle was measured by contact angle analyzer (JC2000 D, Powereach Co., Shanghai, China) and Zeta potential of AS flocs was quantified using a Zetasizer (Nano Z, Malvern, United Kingdom). W_{tot} of AS was measured and calculated according to Liu et al. [16]. All measurements in this paper were repeated for five times.

RESULTS AND DISCUSSION

Influence of Al^{3+} on flocculation-related characteristics of AS. The effects of Al^{3+} dosage on flocculation, sedimentation, and dewaterability of AS were shown in Table 1. There was no significant difference in AS flocs size at Al^{3+} dosages below 1 $mEq \cdot L^{-1}$; yet, compared with control, flocs size of AS at Al^{3+} dosages of 1, 2, and 4 $mEq \cdot L^{-1}$ increased by 14%, 36% and 66% respectively. Variations of Al^{3+} dosage were seemed to affect supernatant turbidity in two phases: first, supernatant turbidity decreased as Al^{3+} dosage increased up to 2 $mEq \cdot L^{-1}$; then, when Al^{3+} dosage was increased to 4 $mEq \cdot L^{-1}$, supernatant turbidity increased by 36% compared with that of 2 $mEq \cdot L^{-1}$. This is likely due to over-adsorption and chelation of Al^{3+}. AS surface tend to bring positive charges, which increased electrostatic repulsion of AS [3]. Poor supernatant turbidity may cause a build up of COD, total nitrogen (TN), and total phosphate (TP), heavy metals, potential pathogens and other pollutants, hence, supernatant turbidity is the main indicator of AS flocculation.

Contrary to supernatant turbidity, SVI tended to increase as Al^{3+} dosages increased, achieving a maximum value at 2 $mEq \cdot L^{-1}$, then markedly decreased at 4 $mEq \cdot L^{-1}$. AS flocs size became larger with the increase of Al^{3+} dosages, which led to larger interspace between flocs particles and higher SVI. As a result, AS flocculation performance deteriorated. Meanwhile, CST decreased by approximately 8% at 0.5 $mEq \cdot L^{-1}$, and decreased to the

TABLE 1
Influence of different Al^{3+} dosage on AS characteristics

Al^{3+} dosage ($mEq \cdot L^{-1}$)	Mean floc size [D(1,0)] (μm)	Supernatant turbidity (NTU)	SVI ($mL \cdot g^{-1}$)	CST (s)
0	78.8±9.4	9.77±0.54	76.6±4.5	8.50±0.30
0.0625	82.8±5.6	5.52±0.23	80.0±2.4	8.37±0.10
0.125	80.1±2.1	4.41±0.68	83.6±3.5	8.36±0.15
0.25	80.6±3.4	4.14±0.24	84.1±6.4	8.30±0.54
0.5	80.7±5.3	3.83±0.12	84.3±2.3	7.80±0.84
1	89.6±7.3	3.61±0.22	92.0±28.3	7.90±0.43
2	107.5±3.2	2.72±0.23	111.1±1.3	7.40±0.24
4	130.5±2.5	3.69±0.13	95.8±9.2	7.20±0.10

minimum value at 4 $mEq \cdot L^{-1}$. These findings suggested that low Al^{3+} dosages (0-2 $mEq \cdot L^{-1}$) were beneficial for AS flocculation, whereas AS settling and compressing performances deteriorated. Integrated the above four indicators, Al^{3+} dosage can be divided as low Al^{3+} dosages (0–2 $mEq \cdot L^{-1}$) and high Al^{3+} dosage (4 $mEq \cdot L^{-1}$).

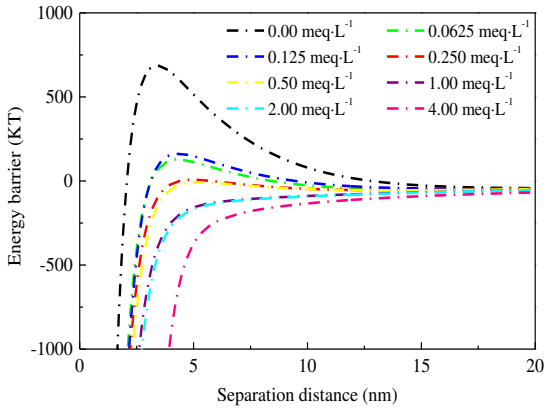


FIGURE 1
W_{tot} curves of AS at various Al^{3+} dosages.

Influence of Al^{3+} on AS interaction energy. Interaction energy variations at various Al^{3+} dosages. W_{tot} was investigated in order to further explore how Al^{3+} dosage promote AS flocculation. Energy barrier was gradually reduced as Al^{3+} dosage increased (Figure 1). When Al^{3+} dosages exceeded 1 $mEq \cdot L^{-1}$, the energy barrier disappeared and total interaction energy acquired negative values at all separation distances (≤ 20 nm). As Al^{3+} dosages increased, negative charges in the surface of AS particles decreased. This phenomenon could be satisfactorily explained by extended DLVO theory and multivalent cation bridging theory, indicating that Al^{3+} could neutralize the negative charges on the surface of AS particles, reduced the electrostatic repulsion, thereby W_{tot} reduced.

Influence of W_{tot} on AS flocculation. W_{tot} was closely related to AS flocculation. As Al^{3+} dosage increased (≤ 2 $mEq \cdot L^{-1}$), both W_{tot} and supernatant turbidity gradually reduced (Figure 2). When W_{tot} was negative, AS can overcome the energy barrier to flocculate. The lower the energy barrier, the easier it was for AS to polymerize. The reduction in energy barrier was so significant that an irreversible adhesion of AS flocs occurred. Al^{3+} compressed the electric double layer effectively and decreased the Zeta potential on AS particle surface. Supernatant turbidity declined as suspended particles decreased, which explains W_{tot} was beneficial for AS flocculation at low Al^{3+} dosages.

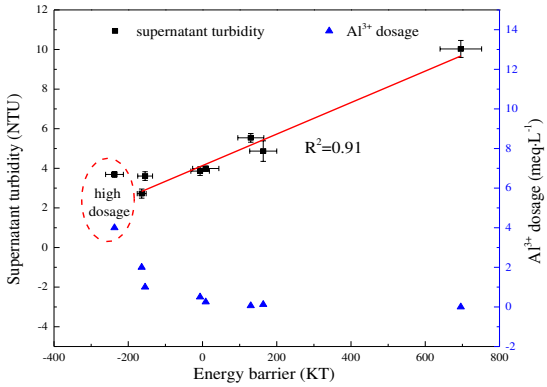


FIGURE 2
The relations among Al^{3+} dosage, W_{tot}, and supernatant turbidity. Error bars represent mean values ± one standard deviation.

However, W_{tot} continued to decrease at high Al^{3+} dosage, but supernatant turbidity increased. This observation was consistent with Higgins's study [17]. We deduced that the phenomenon may be beyond the application range of extended DLVO theory. There might be several other factors accounting for the influence of W_{tot} on AS flocculation. AS, which consists of various microorganisms and EPS, is different from general colloid. There is

close relationship between EPS and W_{tot}. The influence of W_{tot} on AS flocculation cannot be restricted to W_{tot} alone, and EPS should be taken into consideration and shed some light on the analysis.

Influence of Al^{3+} on EPS content. Variations in EPS content at various Al^{3+} dosages. AS are divided into four fractions: bulk solution, LB-EPS, TB-EPS and pellet [18]. It was necessary to further investigate which one (or more) of these four played the crucial role in AS flocculation at various Al^{3+} dosages. The content of the organic substances (in terms of TOC) in different parts of AS at various Al^{3+} dosages varied obviously (Figure 3). TOC concentration in the bulk solution decreased as Al^{3+} dosages increased (≤ 2 mEq·L^{-1}), but increased 184% at 4 mEq·L^{-1} compared with control, consistent with the changes observed in supernatant turbidity. These results indicated that high Al^{3+} dosage would promote electrostatic repulsion among AS flocs. AS was re-dissolving due to flocs destabilization, therefore, TOC content in the bulk solution increased.

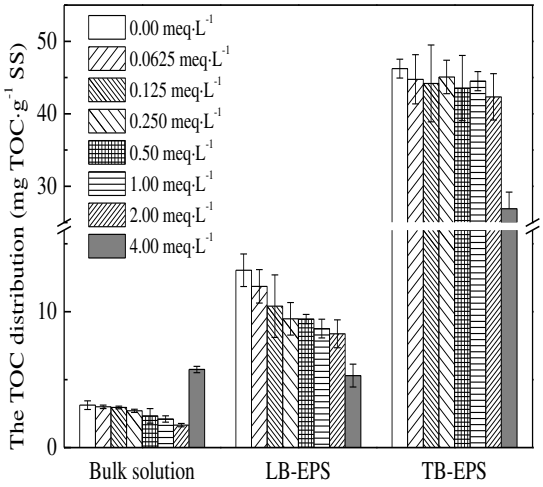


FIGURE 3
Influence of Al^{3+} dosage on the TOC contents in different parts of the AS.

The LB-EPS and TB-EPS content decreased as Al^{3+} dosages increased. At 2 mEq·L^{-1}, LB-EPS decreased by 36%, whereas TB-EPS decreased by 8.4% compared with control. This phenomenon was consist with previous studies [19–20]. LB-EPS content showed more variable than TB-EPS content. These differences were attributed to the location of LB-EPS on the sludge surface, which was more easily affected by the environmental changes [21]. Al^{3+} could combine with the negatively-charged sites in the EPS surface and form salt bridges, strengthen the binding capacity between EPS and pellet, eventually result in LB-EPS and TB-EPS content reduction.

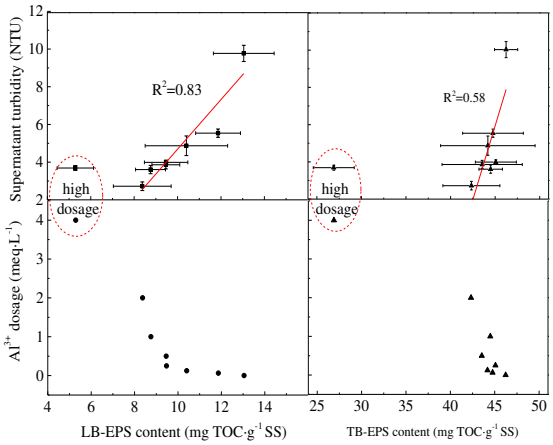


FIGURE 4
Relations between supernatant turbidity and LB-EPS (a) and TB-EPS (b) at various Al^{3+} dosages. Error bars represent mean values ± one standard deviation.

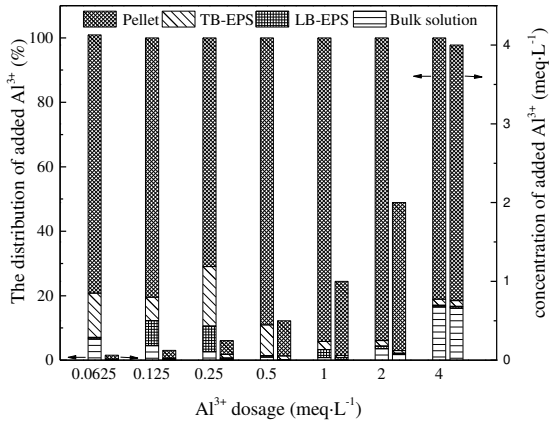


FIGURE 5
The distribution of Al^{3+} added in different AS components at various Al^{3+} dosages.

Influence of EPS content on AS flocculation. EPS is the main factor influencing AS flocculation performance. On one hand, EPS is a major composition of the organic matter in AS; on the other, EPS locates on the periphery of AS, which is the reaction site between AS particles [12]. Both LB-EPS and TB-EPS content positively correlated to the supernatant turbidity, but the correlation coefficient between supernatant turbidity and LB-EPS content was remarkablely higher (Figure 4). Li and Yang [20] had shown that the content of bound water became higher with the increase of LB-EPS content, generated the low density structure of AS, thereby the AS flocculation deteriorated; our results showed the same phenomenon. Al^{3+} added would hydrolyze in water and produce hydroxyl complexes to bridge with each other, then, form polymeric networks to seize the suspended small particles, cut down the EPS content and eventually improve supernatant turbidity. However, at high Al^{3+} dosage,

LB-EPS and TB-EPS content decreased significantly, but supernatant turbidity increased, showing a deviation from the tendency at low Al^{3+} dosages. We concluded that there may be other factors involved in the AS flocculation.

Al^{3+} distribution characteristics in AS. The distribution characteristics of added Al^{3+} in AS. In order to track the distribution of added Al^{3+} in AS, Al^{3+} concentration in different parts was measured, and the added Al^{3+} concentration was calculated accordingly. Most of the added Al^{3+} (≥70%) distributed within the pellet at all Al^{3+} dosages, with the maximum of 94% at 2 mEq·L^{-1} (Figure 5), suggesting that Al^{3+} has a strong affinity with the AS. This observation was in accordance with our previous results. Li et al. [13] found that added Ca^{2+} was primarily existed freely in the bulk solution, whereas Al^{3+} and Fe^{3+} added were found to concentrate in the pellet. Al^{3+} can bound with AS through ion exchange, adsorption, and chelation [22], thus be able to pass through LB-EPS and TB-EPS, and combine with pellet of AS, which is the core of AS, and is the most negatively charged to provide the most bonding sites for Al^{3+}. However, percentage of added Al^{3+} in the pellet decreased to 81% at high Al^{3+} dosage. We inferred that at this point, binding sites of pellet were saturated; excessive binding caused repulsion and Al^{3+} bounded to pellet dissociated out. Accordingly, the concentration of added Al^{3+} in the bulk solution increased.

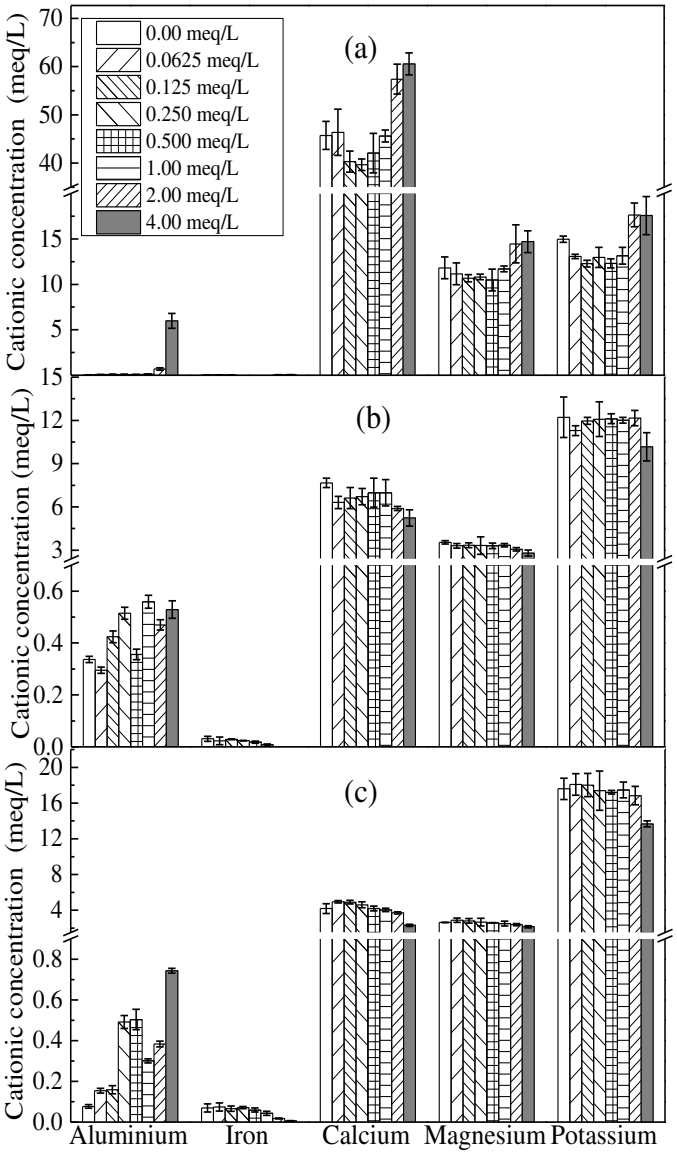


FIGURE S1
Influence of Al^{3+} dosage on the distribution of other cations in the bulk solution (a), LB-EPS (b), and TB-EPS (c)

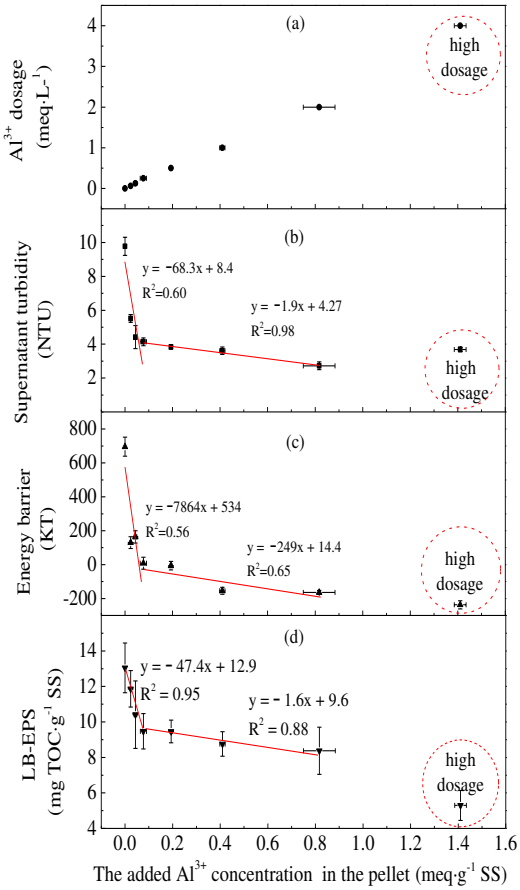


FIGURE 6
Influence of added Al^{3+} concentration in the pellet on supernatant turbidity (b), W_{tot} (c), and LB-EPS content (d) at various Al^{3+} dosages. Error bars represent mean values ± one standard deviation.

TABLE S1
Comparison with our previous study

X	Y	Correlation curve	Al^{3+} dosage (mEq/L)	R^2	References
pellet Al^{3+} concentration	supernatant turbidity	Y= -68.3X+8.4	0-0.25	0.60	This study
		Y= -1.9X+4.27	0.5-2	0.98	
		Y= -52.3X+24.1	2	0.90	[14]
	W_{tot}	Y= -7864X+534	0-0.25	0.56	This study
		Y= -249X+14.4	0.5-2	0.65	
		Y= -8729.6X+3330.3	2	0.82	[14]
	LB-EPS content	Y= -47.4X+12.9	0-0.25	0.95	This study
		Y= -1.6X+9.6	0.5-2	0.88	
		Y=-54.7X+29.5	2	0.88	[14]

The distribution characteristics of different cations in AS. With the increasing Al^{3+} dosages, concentration of other cations in the bulk solution initially decreased then gradually increased (Figure S1). It was speculated that other cations were closely bound to AS particles in the bulk solution at Al^{3+} dosages lower than 0.5 mEq·L^{-1}. As Al^{3+} dosages went up, the limited cationic binding sites were gradually occupied by Al^{3+}, resulting in the release of other cations into the bulk solution [23]. Influence of Al^{3+} dosage on the concentration of other cations in LB-EPS and TB-EPS fraction was much lower than that in the bulk solution, but still exhibited a decreasing trend as Al^{3+} dosage increased.

Influence of added Al^{3+} concentration in the pellet on supernatant turbidity, W_{tot}, and LB-EPS content. The supernatant turbidity, W_{tot}, and LB-EPS content showed a similar decline tendency as the concentration of added Al^{3+} in the pellet increased at low Al^{3+} dosages (Figure 6). This decline tendency seemed to be divided into two stages, so two curves were fitted: supernatant turbidity, W_{tot}, and LB-EPS content first at decreased rapidly (Al^{3+} dosages 0–0.25 mEq·L^{-1}), then the descent slowed down when Al^{3+} dosages grew to 0.25–2 mEq·L^{-1}. Supernatant turbidity, W_{tot}, and LB-EPS content were negatively correlated to the concentration of added Al^{3+} in the pellet. Correlation coefficient (R^2) between added Al^{3+} concentration in the pellet and LB-EPS content were as high as 0.95 and 0.88 at low Al^{3+} dosages, indicating that added Al^{3+} in the pellet had a significantly greater influence on LB-EPS content than on W_{tot} and supernatant turbidity. This was due to that Al^{3+} can flocculate the EPS and bind them to the AS pellet closely, so to make EPS more difficult to extract, which manifested as less EPS content. Thus, the concentration of added Al^{3+} in the pellet was an important parameter indicating LB-EPS content. At the same time, the Al^{3+} accumulation in the pellet can effectively reduce the Zeta potential of AS according to the DLVO theory, which led to W_{tot} reduction. The more Al^{3+} bound tightly with AS, the more W_{tot} was reduced. Our previous study [14] also proved that the increasing concentration of trivalent cations in the AS pellet significantly contributed to the reduction in W_{tot} (R^2 = 0.82) and LB-EPS content (R^2 = 0.88), demonstrating that the concentration of added Al^{3+} in the pellet played a vital role in AS flocculation performance.

W_{tot} and LB-EPS content further decreased at high Al^{3+} dosage, however, supernatant turbidity tended to increase, so the result deviated from the tendency exhibited at low Al^{3+} dosages. These results indicated that although our original theory still applied to low Al^{3+} dosages (Table S1), this cloud not fit the case at high Al^{3+} dosage.

CONCLUSIONS

The influences of Al^{3+} dosage on AS flocculation performance (indicated by supernatant turbidity) were divided into two phases: low Al^{3+} dosages improved AS flocculation, whereas high Al^{3+} dosage had the opposite effect. Both W_{tot} and LB-EPS content were correlated to AS flocculation performance, which explains the promoting mechanism of Al^{3+} dosage on AS flocculation performance. Most of the added Al^{3+} distributed within the pellet at all Al^{3+} dosages due to its remarkable binding capacity onto the AS surface, and this part of Al^{3+} was closely related to supernatant turbidity, W_{tot} and LB-EPS content. Hence, it is proposed that the concentration of added Al^{3+} in the pellet is a fundamental element governing the differences in AS flocculation performance at various Al^{3+} dosages.

ACKNOWLEDGEMENTS

This research was supported by the National Natural Science Foundation of China (NO.51508517) and (NO.51208179). The authors are grateful for the technical assistance provided by ZhiHe Environmental Science and Technology Co., Ltd.

REFERENCES

[1] Lan, H.X., Chen, R., Ma, P., Zhang, H., Lan, S.H., Wang, Y.D. (2015) Cultivation and characteristics of microaerobic activated sludge with weak magnetic field. Desalin. Water Treat. 53, 27–35.

[2] Liao, B.Q., Allen, D.G., Droppo, I.G., Leppard, G.G., Liss, S.N. (2001) Surface properties of sludge and their role in bioflocculation and settleability. Water Res. 35, 339–350.

[3] Subramanian, S.B., Yan, S., Tyagi, R.D., Surampalli, R.Y. (2010) Extracellular polymeric substances (EPS) producing bacterial strains of municipal wastewater sludge: Isolation, molecular identification, EPS characterization and performance for sludge settling and dewatering. Water Res. 44, 2253–2266.

[4] Zhang, H.F., Wang, Z.P., Zhang, L.H., Song, L.F. (2014) Impact of sludge cation distribution pattern on its filterability in membrane bioreactor. Bioresour. Technol. 171, 16–21.

[5] Wu, W., Giese, R.F., Van Oss, C.J. (1999) Stability versus flocculation of particle suspensions in water-correlation with the extended DLVO approach for aqueous systems, compared with classical DLVO theory. Coll. Surf. B-Biointerf. 14, 47–55.

[6] Ruan, X., Li, L., Liu, J. (2013) Flocculating characteristic of activated sludge flocs: Interaction between Al^{3+} and extracellular polymeric substances. J. Environ. Sci. 25, 916–924.

[7] Wang, B.B., Chang, Q., Peng, D.C., Hou, Y.P., Li, H.J., Pei, L.Y. (2015) A new classification paradigm of extracellular polymeric substances (EPS) in activated sludge: Separation and characterization of exopolymers between floc level and microcolony level. Water Res. 64, 53–60.

[8] Yan, L., Liu, Y., Wen, Y., Ren, Y., Hao, G., Zhang, Y. (2015) Role and significance of extracellular polymeric substances from granular sludge for simultaneous removal of organic matter and ammonia nitrogen. Bioresour. Technol. 179, 460–466.
[9] Park, C., Fang, Y., Murthy, S.N., Novak, J.T. (2010) Effects of floc aluminum on activated sludge characteristics and removal of 17-alpha-ethinylestradiol in wastewater systems. Water Res. 44, 1335–1340.
[10] Ji, B., Yang, K., Wang, H.Y. (2015) Impacts of poly-aluminum chloride addition on activated sludge and the treatment efficiency of SBR. Desalin. Water Treat. 54, 2376–2381.
[11] Sheng, G.P., Yu, H.Q., Li, X.Y. (2010) Extracellular polymeric substances (EPS) of microbial aggregates in biological wastewater treatment systems: A review. Biotechnol. Adv. 28, 882–894.
[12] Park, C., Novak, J.T. (2007) Characterization of activated sludge exocellular polymers using several cation-associated extraction methods. Water Res. 41, 1679–1688.
[13] Li, H.S., Wen, Y., Cao, A.S., Huang, J.S., Zhou, Q., Somasundaran, P. (2012) The influence of additives (Ca^{2+}, Al^{3+}, and Fe^{3+}) on the interaction energy and loosely bound extracellular polymeric substances (EPS) of activated sludge and their flocculation mechanisms. Bioresour. Technol. 114, 188–194.
[14] Li, H.S., Wen, Y., Cao, A.S., Huang, J.S., Zhou, Q. (2014) The influence of multivalent cations on the flocculation of activated sludge with different sludge retention times. Water Res. 55, 225–232.
[15] APHA. (2012) Standard methods for the examination of water and wastewater. American Public Health Association, Washington.
[16] Liu, X.M., Sheng, G.P., Yu, H.Q. (2007) DLVO approach to the flocculability of a photosynthetic H-2-producing bacterium, Rhodopseudomonas acidophila. Environ. Sci. Technol. 41, 4620–4625.
[17] Higgins, M.J., Novak, J.T. (1997) The effect of cations on the settling and dewatering of activated sludges: laboratory results. Water Environ. Res. 69, 215–224.
[18] Shao, L.M., Wang, G.Z., Xu, H.C., Yu, G.H., He, P.J. (2010) Effects of ultrasonic pretreatment on sludge dewaterability and extracellular polymeric substances distribution in mesophilic anaerobic digestion. J. Environ. Sci. 22, 474–480.
[19] Yang, S.F., Li, X.Y. (2009) Influences of extracellular polymeric substances (EPS) on the characteristics of activated sludge under non-steady-state conditions. Process Biochem. 44, 91–96.
[20] Li, X.Y., Yang, S.F. (2007) Influence of loosely bound extracellular polymeric substances (EPS) on the flocculation, sedimentation and dewaterability of activated sludge. Water Res. 41, 1022–1030.
[21] Zhang, W.J., Cao, B.D., Wang, D.S., Ma, T., Xia, H., Yu, D.H. (2016) Influence of wastewater sludge treatment using combined peroxyacetic acid oxidation and inorganic coagulants re-flocculation on characteristics of extracellular polymeric substances (EPS). Water Res. 88, 728–739.
[22] Masion, A., Vilge-Ritter, A., Rose, J., Stone, W.E., Teppen, B.J., Rybacki, D. Bottero, J.Y. (2000) Coagulation-flocculation of natural organic matter with Al salts: Speciation and structure of the aggregates. Environ. Sci. Technol. 34, 3242–3246.
[23] Lawson, P.S., Sterritt, R.M., Lester, J.N. (1984) Factors affecting the removal of metals during activated sludge wastewater treatment I. The role of soluble ligands. Arch. Environ. Con. Tox. 13, 383–390.

Received: **15.08.2017**
Accepted: **20.08.2017**

CORRESPONDING AUTHOR

Dongjin Wan
School of Chemistry and Chemical Engineering
Henan University of Technology
Zhengzhou – China

e-mail: dongjinwan@126.com

© by PSP Volume 26 – No. 12A/2017 pages 8278-8285 Fresenius Environmental Bulletin

USE OF PERMEABLE REACTIVE BARRIER FOR GROUNDWATER REMEDIATION AT ONE WASTEWATER TREATMENT PLANT SITE

Qingshan Ma, Zujiang Luo*

School of Earth Sciences and Engineering, Hohai University, Nanjing, Jiangsu 211100, P.R. China

ABSTRACT

The remediation of a nitrobenzene contaminated aquifer at a wastewater treatment plant by a permeable reactive barrier (PRB) filled with Zero-valent iron (ZVI) was presented as a case study. Based on fully analyzing the hydrogeological conditions of aquifer and groundwater contaminant characterization of the wastewater treatment plant site, a 2-D numerical model, solved using a finite difference method via MODFLOW·MT3DMS software, was established to describe the pollutant transport within groundwater and the pollutant degradation occurring inside PRB. Then the effect of decreasing nitrobenzene concentration was simulated with the model by ZVI-PRB in rehabilitating groundwater contaminant. Model results showed that PRB is an effective tool for the remediation of the aquifer under analysis, since the nitrobenzene concentration downstream the barrier reduced effectively and met the regulatory limit set for groundwater.

KEYWORDS:
Permeable reactive barrier, Zero-valent iron, Nitrobenzene, Groundwater contaminant remediation, MODFLOW·MT3DMS

INTRODUCTION

Groundwater pollution due to contaminant leakage from the disposal sites is a widespread concern in many countries [1, 2]. Organic compounds such as BTEX (benzene, toluene, etc.) are among the most frequently detected groundwater contaminants, and also defined as priority pollutants by USEPA [3, 4]. Especially, Nitrobenzene has been considered as a significant groundwater contaminant due to its wide usage in explosives, insecticides, herbicides, pharmaceuticals and dyes [5]. In recent years, environmental pollution accidents occurred frequently, such as Songhua River accident, China, over 100 tons of nitrobenzene and related compounds were released into the Songhua River and formed an 80 km pollution slick belt flowing downstream [6], and resulting in underground drinking water sources near the Songhua River contaminated. Therefore, how to remediate the polluted groundwater has aroused great public concern.

Groundwater pollution remediation technology most commonly used include: Pump and Treat, PRBs situ processing technology. Pump and Treat consists in pumping the contaminated water out of the aquifer, then performing an ex situ treatment and finally re-injecting the treated water downstream into the aquifer [7]. However, Pump-and-treat systems often take a very long time (e.g., 50-100 years) to meet cleanup goals, and in many cases they are never expected to ever achieve those goals. PRB is a very promising groundwater remediation technique, which can be adopted also in case of multiple contaminations [8]. It has gained acceptance as an effective passive remediation strategy for treating organic and inorganic contaminants in groundwater [9, 10].

Biochemical degradation can effectively remove organic matter from groundwater; and natural attenuation often degrades organic contaminants to more innocuous compounds. Enhanced natural attenuation, where natural processes are accelerated, is becoming a preferred option [11]. In recent years, ZVI-based PRB has been studied intensively to treat groundwater contaminated by nitrobenzene as well as other chlorinated organic compounds. Vesela et al. (2006) studied BTEX and naphthalene degradation using a ZVI free biological permeable reactive barrier (bio-PRB). They achieved BTEX and naphthalene removal rates of 57.3% and 99.9%, respectively [12]. Biodegradation of BTEX has been investigated widely and deemed an efficient and environmentally compatible way to treat contaminated groundwater [13, 14, 15]. Reactions between ZVI and groundwater constituents can cause ZVI corrosion and subsequent secondary mineral precipitations contribute to reduction in performance of ZVI-based PRB in the long term [16]. The reduction kinetics has often been reported to follow a pseudo first order kinetics in term of the concentration of nitrobenzene [17, 18].

The objective of this work is to investigate the removal effect of aqueous-phase nitrobenzene by PRB in MODFLOW·MT3DMS environment. A nitrobenzene contaminated aquifer of the wastewater treatment plant was taken as a case study and (ZVI) was considered as barrier built material. Starting from a complete hydraulic characterization of the

TABLE 1
Parameter values for each zone of the model

Aquifer	Zone number	K (m/d)	μ	α_L (m)	α_T (m)	θ
Unconfined aquifer	1	0.10	0.06	10	1	0.09
	2	0.30	0.076	10	1	0.08
	3	0.41	0.083	10	1	0.07
	4	0.2	0.06	10	1	0.09

site, 2-D coupled model of groundwater seepage and contaminant transport was established, which takes into account the specific dynamics of the aquifer under analysis. Finally, the influence of width and parameters of PRB on the removal efficiency of nitrobenzene contamination was evaluated, respectively.

MATERIALS AND METHODS

Site description and generalization. The wastewater treatment plant site is located in the southeast of Tianjing city, about 45 km from the Tianjin downtown, 40 km from Tianjin Airport, and 20 km from the Tianjin Port. It is with an area of 1.62×10^3 m^2. As a result of accident, the bottom impervious layer of wastewater treatment plant was broken, which resulting in the wastewater leaked into groundwater, and the scope of the nitrobenzene contaminant plume is 160 m^2, according to the requirement of the national standards for drinking water quality [19]. Considering the pollution characteristics and local hydrogeological conditions, the depth of within 20 m in Quaternary loose rock pore unconfined aquifer is chosen as the aimed layer, which is mainly composed of plain fill, silty clay, silt and clay and generalized into homogeneous isotropic.



FIGURE 1
Schematic diagram of the conceptual model

Based on analyzing the hydrogeological conditions of the study area, the state of groundwater was generalized into a two-dimensional transient flow. The south and northeast of the study area are sea, set as the drainage boundary. The eastern boundary is parallel to the water table, set as the lateral inflow boundary, and the northwest, southeast and west boundary were generalized as zero flux boundary (Fig.1). The top of the model system was a recharge boundary to receive precipitation infiltration, and also a drainage boundary to evaporate the groundwater. The bottom of the model system is an impervious layer, so it was generalized as the zero flux boundary. For the purpose of tracking contaminant transport, the lateral boundaries of the model were set as no dispersive mass flux boundary. Unconfined aquifer was divided into four zones based on the soil types. The values of soil property (hydraulic conductivity K and specific yield μ) for each zone were obtained from a variety of sources including pumping tests, soil tests and the literature. The value of longitudinal dispersity of aquifer was assigned as 10 m, and the ratio of transverse to longitudinal dispersity α_L was 1.0. The parameter values for each zoning are presented in Table 1.

Methodology. In this work, groundwater flow through a PRB and the transport phenomenon describing the degradation occurring inside the barrier were modelled using MODFLOW·MT3DMS.

Groundwater flow model. According to the continuity principle and the Darcy's law，with the coordinates in the principal permeability directions of the isotropic porous media，the 2-D transient flow equation for the porous media can be expressed as:

$$\frac{\partial}{\partial x}(K(h-z)\frac{\partial h}{\partial x})+\frac{\partial}{\partial y}(K(h-z)\frac{\partial h}{\partial y})+W=\mu\frac{\partial h}{\partial t}\quad (x,y)\in\Omega \qquad (1)$$

where K is the hydraulic conductivity, h is the water head at point (x,y) and at the instant t, W is the source and sink terms, μ is specific yield, t is time, z is the bottom elevation of aquifer, Ω is the computational domain.

The initial and boundary conditions for the transient seepage calculation are as follows：

(1) Initial condition:

$$h(x,y,t)\big|_{t=0}=h_0(x,y) \qquad (2)$$

where $h_0(x,y)$ is the initial water head at the point (x,y).

(2) Boundary conditions:

$$\begin{cases} h(x,y,t)\big|_{\Gamma_1} = h_1(x,y,t) & t>0,\ (x,y)\in\Gamma_1 \\ K(h-z)\dfrac{\partial h}{\partial n}\Big|_{\Gamma_2} = q(x,y,t) & t>0,\ (x,y)\in\Gamma_2 \end{cases} \quad (3)$$

where $h_1(x,y,t)$ is the known-head at the Dirichlet boundary, $q(x,y,t)$ is the normal unit flux of the Neumann boundary Γ_2 ;for no flow boundaries, q equals zero; n is the outward normal direction of the boundary.

Contaminant transport model. The solute transport in groundwater is a comparable complex physical chemistry process, mainly involving the convection, dispersion, adsorption, physical and chemical function [20, 21]. In this work, the convection-dispersion process and chemical function were considered, the assumptions are as follows: (a) effective porosity keeps constant; (b) the biological/chemical reaction follows first-order kinetics model in PRB and the first order reaction rate keep constant; Thereby, the governing equation describing the fate and transport of contaminant in groundwater and PRB can be represented by:

$$\frac{\partial C}{\partial t} = \frac{\partial}{\partial x_i}\left(D_{ij}\frac{\partial C}{\partial x_j}\right) - \frac{\partial}{\partial x_i}(v_i C) + \frac{q_s^*}{\theta}C_s - \lambda\left(C + \frac{\rho_b}{\theta}\overline{C}\right) \quad (4)$$

where C is the dissolved concentration of contaminant; $\overline{C}$ is the concentration sorbed on the subsurface solids; v_i is the seepage velocity; q_s^* represents the source and sink terms of fluid; C_s represents the source and sink terms of concentration; λ is the first-order reaction rate; θ is the porosity; ρ_b is the bulk density of the subsurface medium. D_{ij} is the hydrodynamic dispersion coefficient tensor, expressed as follows [22]:

$$\begin{cases} D_{xx} = \alpha_L\dfrac{v_x^2}{v} + \alpha_T\dfrac{v_y^2}{v} + D_d^* \\ D_{yy} = \alpha_L\dfrac{v_y^2}{v} + \alpha_T\dfrac{v_x^2}{v} + D_d^* \\ D_{xy} = D_{yx} = (\alpha_L - \alpha_T)\dfrac{v_x v_y}{v} + D_d^* \end{cases} \quad (5)$$

where D_{xx}, D_{yy} are the diagonal entries of the dispersion tensor in a 2-D system, D_d^* is the coefficient of molecular diffusion (a scalar), v_x and v_y refer to the seepage velocity along the two direction axes (x,y), respectively, while α_L and α_T are the longitudinal and transverse dispersity, and $v=\sqrt{v_x^2+v_y^2}$ .The transverse dispersity is generally related to the longitudinal one by the following equation [23]:

$$\alpha_L = 10\alpha_T \quad (6)$$

The initial and boundary conditions for contaminant transport calculation are as follows：

(1) Initial concentration condition

$$C(x,y,t)\big|_{t=0} = C_0(x,y) \quad (7)$$

where $C_0(x,y)$ is the initial concentration of the study area.

(2) Boundary conditions:

$$\begin{cases} C(x,y,t)\big|_{\Gamma_1} = C_1(x,y,t) & t>0,(x,y)\in\Gamma_1 \\ \theta D_{ij}\dfrac{\partial C}{\partial x_j}\Big|_{\Gamma_2} = g(x,y,t) & t>0,(x,y)\in\Gamma_2 \end{cases} \quad (8)$$

where Γ_1 denotes the specified-concentration boundary, and $C_1(x,y,t)$ is the specified concentration along Γ_1. $g(x,y,t)$ is a known function representing the dispersive flux normal to the boundary Γ_2 .

Kinetic of nitrobenzene reduction model. Previous studies have shown that the reduction of nitrobenzene by ZVI particles could be described by a pseudo first-order kinetic model, the reduction rate is changed linearly, pseudo first-order kinetic reaction equation is as follows [17, 18, 24]:

$$\frac{-dC_{NB}}{dt} = k_{obs}C_{NB} \quad (9)$$

where C_{NB} is nitrobenzene concentration, k_{obs} (min^{-1}) is the observed first-order rate constant. The integration of Eq. (9) results in Eq. (10):

$$C_{NB} = C_{NB}^0 e^{-k_{obs}t} \quad (10)$$

where C_{NB}^0 is the initial nitrobenzene concentration, and t is the residence time. Therefore, k_{obs} can be calculated from the regression of $ln\,C_{NB}$ versus residence time, and the half-life, $t_{1/2}$, of nitrobenzene can be calculated by Eq. (11):

$$t_{1/2} = \frac{1}{k_{obs}}\ln 2 \quad (11)$$

Design of PRB. Before designing a barrier it is necessary to consider the characteristics of hydraulic conductivity, site soil mechanics, contaminant concentration and distribution, selected reaction medium and the factors of chemical reaction processes. The barrier width is depended on the repair time which should be long enough for degradation process to take place [25]. Therefore, the barrier width (W) must satisfy the following inequality:

$$\frac{W}{u} > (k_{obs}\cdot\alpha)^{-1} \quad (12)$$

In the above equation u represents groundwater flow velocity through the barrier, k_{obs} is the overall mass transfer coefficient for degradation reactions and α represents the external specific surface of particles. The conceptual model and parameters of PRB is shown in Fig.2 and Table 2, respectively.

The numerical solution with the related initial and boundary conditions was performed by MODFLOWMT3DMS, which accounted for both transport and the degradation phenomena occurring inside the PRB, in a unique framework.

TABLE 2
Summary of PRB characteristics

	Reactive media	ZVI
PRB parameters	Porosity, n_b	0.45
	Hydraulic conductivity, K_{PAB}	0.32m/d
	Longitudinal dispersivity, α_L	10m
	Transverse dispersivity, α_T	1m
	Quasi-first order reaction rate constant, k_{obs}	0.006min^{-1}
	PRB Width, W	150cm
	PRB Width, L	53m

Note: Length and width are enough to allow a thorough remediation of the plume, avoiding any polluted water overflow.

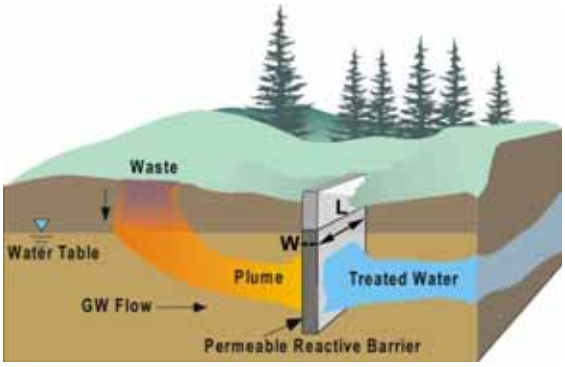


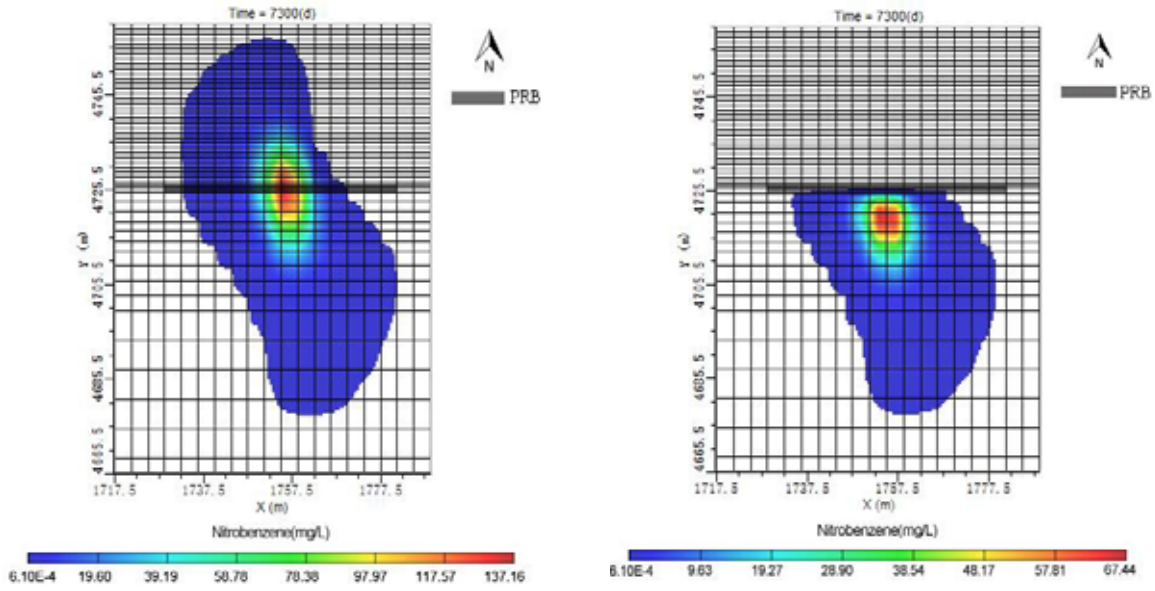
FIGURE 2
PRB design conceptual model (modified by [26])

RESULTS AND DISCUSSION

Groundwater remediation simulation. The standard concentration limit of nitrobenzene in water is 0.00061 mg/L, according to American water quality criteria for human health. Here, the contaminant plume is defined as the area that groundwater concentration exceeds the water quality criteria. Nitrobenzene concentration distribution of 20 years in the absence and presence of PRB is shown in Fig.3a and Fig.3b, respectively.

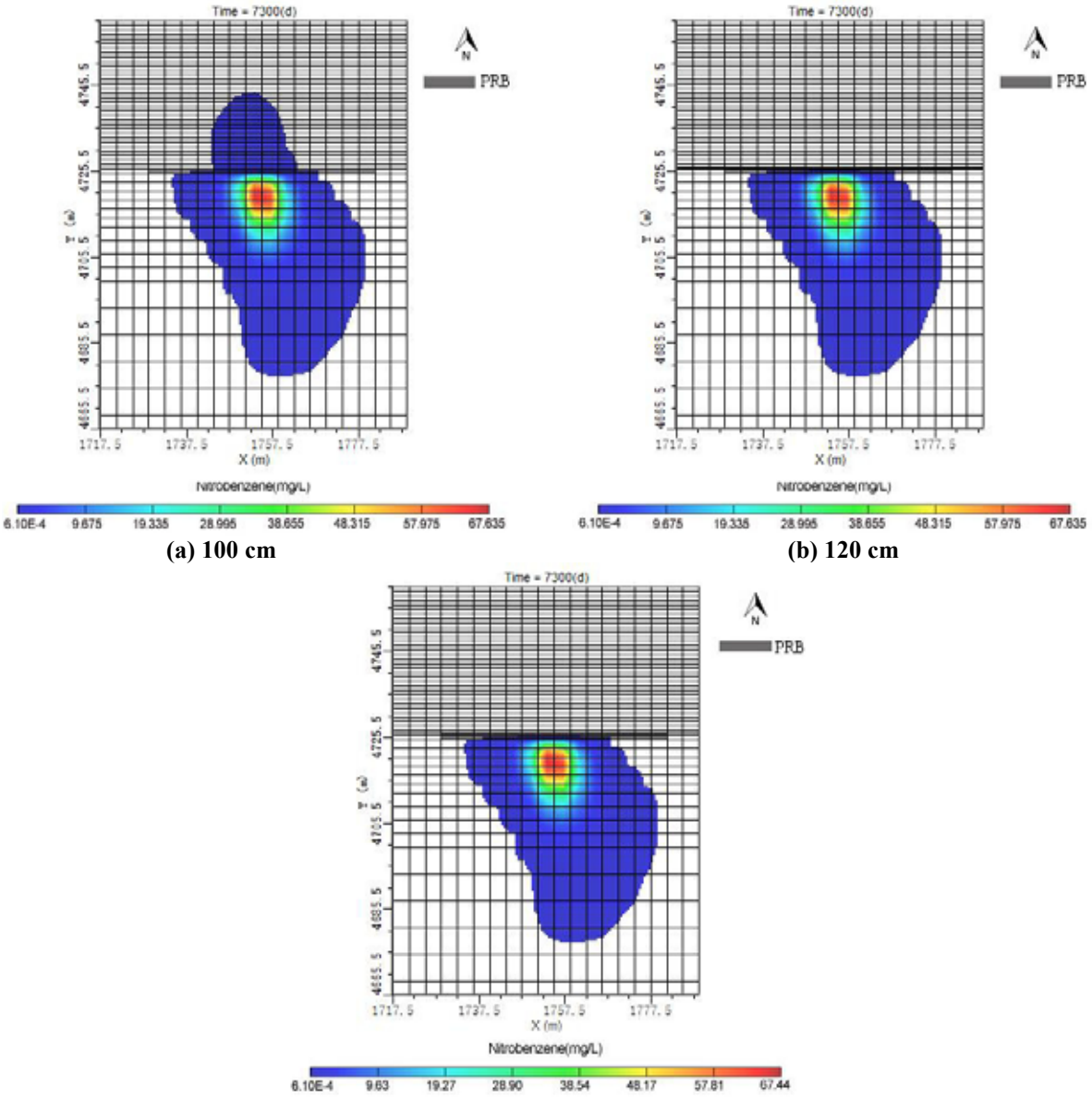
Fig. 3 shows the range of contaminant plume expanded constantly due to the effect of convection and dispersion. While, the concentration of the center decreased gradually, and it is obviously lower than the original concentration. Fig 3b shows that the removal efficiency of contaminant is significant, the contaminant plume area has been effectively controlled, and contaminant is difficult to diffuse into the PRB downstream aquifer. This is because that nitrobenzene in groundwater could go through the downstream barrier, and contact fully with the barrier material.

Response of removal efficiency to change in width of PRB. The width of a PRB has a significant effect on the success of remediation. Nitrobenzene removal efficiency is influenced by varying PRB width. The response of removal efficiency related to the change in widths of PRB, are shown in Fig. 4.



(a) absence of PRB **(b) presence of PRB**

FIGURE 3
Nitrobenzene concentration distribution in the absence and presence of PRB



(a) 100 cm **(b) 120 cm**

(c) 150 cm

FIGURE 4

The response of removal efficiency to the change in widths of PRB

Fig. 4 shows that with a runtime of 20 years, the outflowing concentration of nitrobenzene varies significantly using different barrier widths. As shown by Fig. 4, the barrier with a width of 100 cm cannot be effectively capturing the contaminant relative to the barrier width of 120 cm and 150 cm. It can be concluded in this simulation that a barrier with a width of 100 cm will not be sufficient in retarding the contaminant. The water quality downstream of a barrier with 100 cm width would not meet American water quality standards for nitrobenzene concentration criteria. The explanation for the results is related to the time, which takes for the contaminant to pass through the PRB. A width of 100 cm reduces the duration of action in contact with zero-valent iron, and the reaction is not complete when a short barrier width is used. The barrier width of 120 cm and 150 cm have a good performance on removal effect of nitrobenzene in groundwater, the out-flowing concentration are always lower than the regulatory limit.

Fig.5 better illustrates the effects of different barrier widths on the effect of removing the nitrobenzene through observing the change in concentration over time. It can be seen that the change of concentration showed a similar trend with the three kinds of barrier width. The concentration initially increased and then went decreased as time progressed. This is because high concentrations of the contaminant plume area transport to the wall as the direction of flow, and caused the out-flowing concentrations increasing.

For the barrier width of 100 cm, the concentration reached a maximum of 0.0174 mg/L in 4015 days, and reduced to 0.01 mg/L in 7300 days. Nitrobenzene concentration is higher than the permitted limits. For the barrier width of 120 cm and 150 cm, the concentration reached the maximum of 4.58E-5 mg/L and 1.50E-5 mg/L in 4380 days, and reduces to 3.57E-5 mg/L and 1.16E-5 mg/L in 7300 days, respectively. The outlet nitrobenzene concentration was always lower than the American water quality criteria for nitrobenzene limit.

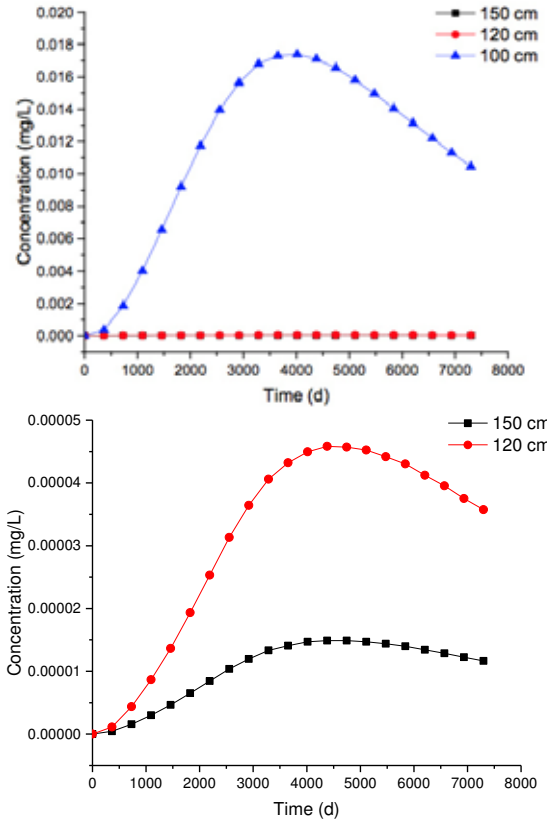


FIGURE 5
Variation of nitrobenzene concentration with time for the observation well under different widths of PRB

Response of removal efficiency to change in parameters of PRB. In order to study the influence of different parameters of the PRB on the removal of nitrobenzene contamination, the hydraulic conductivity and the first-order rate constant were chosen to illustrate the variation of nitrobenzene concentration.

Under the effect of convection and dispersion, the contaminant plume moved to the barrier and the concentration at the observation well initially increased and then went decreased. From Fig. 6, it can be seen that the first order reaction constant has an obvious effect on the removal of pollutants. However, the hydraulic conductivity has a little effect on the results. By increased the first order reaction constant of the barrier material, it will lead to an increase in the degradation rate of nitrobenzene and a decrease in the outlet nitrobenzene concentration. When first-order rate constant increased by 20% (k_{obs} =10.34 (d^{-1})), the outlet nitrobenzene concentration decreased by 30.53% (Fig. 6a). Increased the hydraulic conductivity of the barrier material, it will lead to an increase in the velocity of groundwater and a decrease in the retention time of nitrobenzene in the barrier, and resulting in the outlet nitrobenzene concentration increased. When hydraulic conductivity increased by 20% (K =0.38 ($m \cdot d^{-1}$)), the outlet nitrobenzene concentration increased by about 0.77% (Fig. 6b).

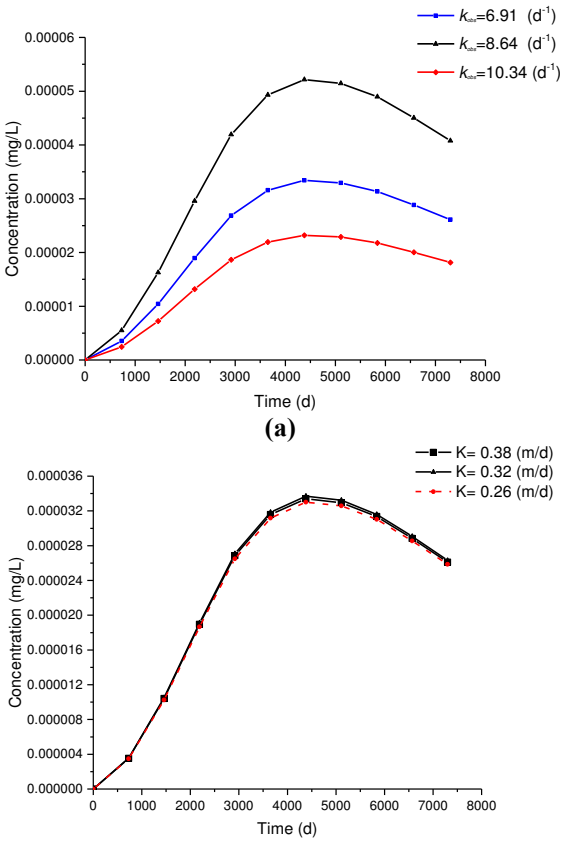


FIGURE 6
Variation of nitrobenzene concentration with time for the observation well under different parameters of PRB

CONCLUSIONS

In this study, a 2-D numerical model was developed and implemented in MODFLOW·MT3DMS environment to describe the pollutant transport in the aquifer and the degradation occurs in PRB. The model was applied to a case study represented by a wastewater treatment plant in which a nitrobenzene contamination is present. According to above discussions, the following conclusions can be drawn from the study results: (1) the results shows that ZVI could be a potential reactive media for nitrobenzene-contaminated groundwater, and the width of PRB has a

significant effect on remediation's success and the outlet nitrobenzene concentration can always be maintained lower than the regulatory limit. (2) taking into account the effect of groundwater remediation and engineering costs, it is recommended to use the PRB with the width of 120 cm. (3) compared to hydraulic conductivity of barrier material, the first order reaction constant has an obvious effect on the removal of pollutants.

ACKNOWLEDGEMENTS

The research work described herein was funded by the Special Fund of Jiangsu Geology and Mineral Exploration Bureau (No: 2014-KY-12).

REFERENCES

[1] Mouser, P.J., Rizzo, D.M., Druschel, G.K., Morales, S.E., Hayden, N., O'Grady, P., Stevens, L. (2010) Enhanced detection of groundwater contamination from a leaking waste disposal site by microbial community profiles. Water Resources Research. 46(12).

[2] Nagaraju, A., Veeeraswamy, G., Sreedhar, Y. and Thejaswi, A. (2017) Assessment of groundwater quality in Gudur area of Andhra Pradesh, South India. Fresen. Environ. Bull. 26(5), 3597-3606.

[3] Phelps, C.D., Young, L.Y. (1999) Anaerobic biodegradation of BTEX and gasoline in various aquatic sediments. Biodegradation. 10(1), 15-25.

[4] USEPA, Integrated Risk Information System Benzene. (2003) Available from: http://cfpub.epa.gov/iris/quick view.cfm? substance_nmbr=0276.

[5] Dong, J., Zhao, Y., Zhao, R., Zhou, R. (2010) Effects of pH and particle size on kinetics of nitrobenzene reduction by zero-valent iron. Journal of environmental sciences. 22(11), 1741-1747.

[6] Zhu, Y.G., Wang, L., Wang, Z.J., Christie, P., Bell, J.N.B. (2007) China steps up its efforts in research and development to combat environmental pollution.

[7] Cohen, R.M., Mercer, J.W., Greenwald, R.M., Beljin, M.S. (1997) Design guidelines for conventional pump-and-treat systems. United States Environmental Protection Agency, Office of Research and Development, Office of Solid Waste and Emergency Response.

[8] Erto, A., Bortone, I., Di Nardo, A., Di Natale, M., Musmarra, D. (2014) Permeable Adsorptive Barrier (PAB) for the remediation of groundwater simultaneously contaminated by some chlorinated organic compounds. Journal of environmental management. 140, 111-119.

[9] Yang, Y., Wu, P. (2016) Remediation of nitrate pollution of groundwater with straw compost humus PRB. Water resources protection. 6(32), 93-97.

[10] Liu, L., Xu, W., Gan, S. (2006) Study on permeable reactive barrier for remediation of groundwater contamination. Water resources protection. 6(22), 76-80.

[11] Barry, D.A., Prommer, H., Miller, C.T., Engesgaard, P., Brun, A., Zheng, C. (2002). Modelling the fate of oxidisable organic contaminants in groundwater. Advances in Water Resources. 25(8), 945-983.

[12] Vesela, L., Nemecek, J., Siglova, M., Kubal, M. (2006) The biofiltration permeable reactive barrier: practical experience from Synthesia. International biodeterioration & biodegradation. 58(3), 224-230.

[13] Farhadian, M., Vachelard, C., Duchez, D., Larroche, C. (2008) In situ bioremediation of monoaromatic pollutants in groundwater: a review. Bio-resource technology. 99(13), 5296-5308.

[14] Mackay, D.M., de Sieyes, N.R., Einarson, M. D., Feris, K.P., Pappas, A.A., Wood, I.A., Wilson, J.T. (2006) Impact of ethanol on the natural attenuation of benzene, toluene, and oxylene in a normally sulfate-reducing aquifer. Environmental science & technology. 40(19), 6123-6130.

[15] Maliyekkal, S.M., Rene, E.R., Philip, L., Swaminathan, T. (2004) Performance of BTX degraders under substrate versatility conditions. Journal of hazardous materials. 109(1), 201-211.

[16] Jeen, S.W., Gillham, R.W., Gui, L. (2009) Effects of initial iron corrosion rate on long-term performance of iron permeable reactive barriers: Column experiments and numerical simulation. Journal of contaminant Hydrology. 103(3), 145-156.

[17] Jafarpour, B., Imhoff, P.T., Chiu, P.C. (2005) Quantification and modelling of 2, 4-dinitrotoluene reduction with high purity and cast iron. Journal of contaminant hydrology. 76(1), 87-107.

[18] Mu, Y., Yu, H.Q., Zheng, J.C., Zhang, S.J., Sheng, G.P. (2004) Reductive degradation of nitrobenzene in aqueous solution by zero-valent iron. Chemosphere. 54(7), 789-794.

[19] Jin, Y.L., EXL, C.C., Chen, S.J., Xing, D.R., Chen, X.P., Wang, Z.H., Zhuang, L. (2007) GB5749-2006 Standards for Drinking Water Quality.

[20] Li, Y., Zhang, Q., Wang, D., Yang, B., Zhi, X., Fan, S. and Sun, G. (2015) The performance of a predictive risk model for arsenic contamination in groundwater throughout China at the county level. Fresen. Environ. Bull. 24(9a), 3057-3062.

[21] Ma, Q., Luo. Z., Wang. Q. (2017) Evaluation of groundwater environmental capacity in Nantong, China. Fresen. Environ. Bull. 26(8), 5236-5250.

[22] Konikow, L.F., Grove, D.B. (1977) Derivation of equations describing solute transport in ground water (No. 77-19). US Geological Survey, Water Resources Division.
[23] Gelhar, L.W., Welty, C., Rehfeldt, K.R. (1992) A critical review of data on field‐scale dispersion in aquifers. Water resources research. 28(7), 1955-1974.
[24] Bandstra, J.Z., Tratnyek, P.G. (2004) Applicability of single-site rate equations for reactions on inhomogeneous surfaces. Industrial & engineering chemistry research. 43(7), 1615-1622.
[25] Di Nardo, A., Di Natale, M., Erto, A., Musmarra, D., Bortonea, I. (2010) Permeable reactive barrier for groundwater PCE remediation: the case study of a solid waste landfill pollution. Computer Aided Chemical Engineering. 28, 1015-1020.
[26] Barrier, P.R., Table, W. (1998) Permeable reactive barrier technologies for contaminant remediation. 600R98125.

Received: **29.08.2017**
Accepted: **01.10.2017**

CORRESPONDING AUTHOR

Zujiang Luo
School earth sciences and engineering,
Hohai University
No.8 Focheng West Road,
Jiangning District, 211100, Nanjing – China

e-mail: luozujiang@sina.com

© by PSP Volume 26 – No. 12A/2017 pages 8286-8297 Fresenius Environmental Bulletin

ESTIMATING RECOVERABLE FUEL WOOD BIOMASS FROM SMALL DIAMETER TREES IN BRUTIAN PINE (*PINUS BRUTIA* TEN.) STANDS

Mehmet Eker*, Ramazan Ozcelik

Süleyman Demirel University, Faculty of Forestry, Forest Engineering Department., Isparta, Turkey

ABSTRACT

Accurate estimation of recoverable energy wood potential from small sized trees during first thinning is very important for forest managers and renewable energy sectors for feasibility. Reliable and accurate biomass equations for individual tree and tree components like that fuel wood are still lacking for small diameter trees from Brutian pine (*Pinus brutia* Ten.) stands. The aim of the study was to provide biomass models allowing estimating tree level fuel wood biomass. It was harvested 108 individuals selected randomly from brutian pine stands at sapling stage (average dbh < 8 cm) across different site conditions in Mediterranean Region of Turkey covering different sizes (1.5 to 11 cm diameter at breast height (*dbh*)), ages (10 to 20 years) and stand densities (1600 to 3100 trees ha^{-1}). Using linear and nonlinear regression models were exposed for estimation of fuel wood biomass, and total tree biomass based on *dbh* or diameter at stump height (*dsh*), or with tree height (*h*) as predictors. Results showed that *dsh* had high effects on model performance, depending on highly correlation between fuel wood biomass and *dsh* (R:0.837; p<0.001). In the models developed for fuel wood, the coefficient of determination (R^2) of the *dsh* allometric equations ranged from 0.658 to 0.828. Statistical result revealed that these models with single or two variable can be used for small diameter brutian pine trees in similar sites.

KEYWORDS:
Fuel wood, biomass model, small diameter trees, biomass recovery, first thinning, *Pinus brutia*

INTRODUCTION

The growing interests on the climate change and sustainable development have increased to use of renewable energy resources such as woody biomass from forest trees [1,2] . However, the amount of wood raw material obtained from forest is low and has a supply shortage across the sharing of the limited sources among other sectors [3], which precludes the utilization of the merchantable wood in bio-energy. Therefore, the energy biomass should be supplied from minimal or low value forest products. The one of most candidate source of extra bio-energy is small diameter trees [4, 5].

The general source of small diameter trees is thinning operations in the young stands. The current need for first thinning in Turkish forests has been reported to be over 215000 ha per annum, 50000-100000 ha of which has been applied in brutian pine (*Pinus brutia* Ten.) forests [6]. Brutian pine is commercially one of the most important species in Turkey [7], occupying an area of about 5.9 million ha with growing stock volume of approximately 270.1 million m^3 [8]. Therefore, General Directorate of Forestry (GDF) recommended that the unutilized woody biomass from brutian pine stands could be used to promote bioenergy and to reduce fire hazard [9]. Currently, at least one or two fiber wood (chip wood for particleboard industry) stick is conventionally produced from stem section of a small diameter tree, small end diameter of which should be higher than 4 cm with at least 0.5 m in length. Then, the rest of the stem, and branches were left in stands. As well, the small sized tree with *dbh* is less than 8 cm is usually unutilized also completely left in forest floor. It is argued that there may be a considerable potential of the biomass feedstock depending on first thinning in fast growing brutian pine stands.

So, utilization of woody sections of small sized trees has created an increasing interest among bioenergy investors, fuel/fire wood suppliers, and also chip-board industry [10]. The increasing concern requires a better understanding of what section of a tree can be recovered for sustainable biomass supply and how many biomass as fuel wood can be recovered from the allowed forest stands.

Fuel wood for energy (FW) is defined that is a low value or minimal value woody biomass, which is available as source of both conventional directly firing and also modern converting to bioenergy. FW can be produced from underutilized full stem biomass of small sized trees, *dsh* of which is smaller than 8 cm. It also can be supplied from unmerchantable section (tree top to 2 cm diameter) of stem biomass after fiber wood utilization. FW biomass doesn't contain residual slash material composed of branches, twigs, cones, needles, and tree tops, large end diameter of which less than 2 cm.

Accurate quantification of the biomass of total tree and tree components is critical for estimating biomass [11]. The estimation of recoverable aboveground biomass potential is focused on theoretical coefficients and rates that may not always overlap with operational realities [12-14]. The estimation procedures for recoverable biomass are based on above-ground biomass equations for individual tree, which involves allometric equations using the measurements of a given tree species [15]. The most common procedure to estimate total tree biomass and its component by fitting models is to measure tree variables, where *dbh* and *h* are the most commonly used variables for this purpose. Recently, many attempts have been undertaken to produce species-specific allometric equations to facilitate biomass estimation [16]. The allometric models using local inventory data allows for estimating accurate biomass [17, 18]. Some studies exerted substantial variability and some difficulties on biomass estimations because of discrepancy in methodology and variation on site-specific factors changing tree and stand characteristics between regional and national level [19]. The differences among estimation strengthen the need to develop species or site-specific biomass equations to fortify more precise predictions of recoverable biomass under local conditions [15].

However, little effort has been made to develop aboveground biomass models for brutian pine except of several studies in localized areas of Turkey [20, 21, 22], Greece [23], and Syria and Lebanon [24]. The majority of the equations and models predicting biomass for medium and large size trees (*dbh* ≥ 12 cm) are not usually applicable for young or small diameter trees (0.1 cm-11.9 cm *dbh*), therefore; it is necessary to develop small tree biomass equations in the initial stages of their growth. Applying various equations without considering stand development stage may lead to misprediction of tree component biomass [11].

Additionaly, in literature, most of developed equations for large-scale application couldn't match closely to site specific application. So, it was recommended developing and applying site specific equations [19]. As well, previous studies on biomass equation have not been related to the small diameter trees and its components in first thinning stage. However, estimating available biomass for tree components such as stem, branch or FW may need to different allometric equations depending on tree variables. The available information about biomass estimation may not be sufficient when increasing use of weight of recoverable biomass as a measure of energy potential for feasibility studies. Moreover, there is still a lack of knowledge and uncertainty on the recoverable FW biomass potential from small diameter trees from first thinning of brutian pine stands at the less favorable forest conditions.

The assumption is based on that small diameter trees from first thinning operations in brutian pine forest with nearly 6 million ha may have a great potential for energy wood biomass feedstock. It can be possible to estimate the recoverable FW biomass potential if any biomass equation is to be consistently developed by measured data at the species-specific level. If the bioenergy sector is developed, biomass estimators for predicting quantities of energy wood will be needed in order to recoverable potential can be estimated accurately for feasibility. Therefore, the objectives of this study were to (i) develop recoverable biomass equations for FW potential for small brutian pine trees in the young stands and (ii) examine biomass equations for FW potential to diameter or both diameter and tree height using linear or nonlinear regression. Thus, it was intented to develop a stratum at tree-level biomass equations for brutian pine in Mediterrnean Region. The equations for both FW and total tree biomass (TB) were considered so that it can be used in verification of biomass quantity per tree and comparison with literature.

TABLE 1
Descriptives on study site and material characteristics

Characteristics	Description
Forest Region	Bucak Forest District in Isparta
Location	37°14'- 37°38' N, 30°40' - 30°50' E
Silvicultural Prescription	FirstThinning
Development Stage	Seedling to Sapling
Ground Conditions	Mountainous and undulating
Elevation above sea level (m)	400-900
Age (year)	17 (10-20)
Number of trees per ha	2282 (1600-3067)
Number of removal trees per ha	1520 (933-2222)
Moisture Content (%)	63 (42-75)
Mean Removed Tree Volume (dm^3 $tree^{-1}$)	6.4 (0.2-34.4)
Logging removal (m^3 ha^{-1})	9.7 (0.2-76.4)

MATERIALS AND METHOD

Site. The study area is in state-owned forests of Isparta Regional Directorate of Forestry at the mountainous forest part of Mediterranean Region of Turkey (Table 1). The natural pure brutain pine (*Pinus brutia* Ten.) stands managed to multi-functional forestry practices were studied during the first thinning operations. The stands are placed on cracked limestone, marly and flysch deposits with alternating sandy, silt and limey layers. Brutian pine trees grow on primarily on rendzina soils in karstic areas of study site. Redbrown Mediterranean soils [25] and brown forest soils were appeared in the stands [7]. In the studied region, the mean annual temperature varies from 15 C° to 20 C°, while the annual precipitation ranges from 400 mm -900 mm, with climates ranging from semi-arid to humid zone.

TABLE 2
Summary statistics of the removed trees for aboveground biomass estimations

Statistics	Tree characteristics			Biomass (dry kg)				
	dsh	dbh	h	Tree	Stem	Branch	Fiber wood	Fuel wood
Mean	9.50	4.94	4.25	5.71	3.33	2.38	1.63	1.69
Minimum	3.80	1.50	1.30	0.42	0.12	0.27	0.00	0.12
Maximum	15.80	11.00	9.00	18.61	12.93	6.87	9.10	4.74
Std. Error of Mean	0.322	0.234	0.199	0.449	0.306	0.159	0.216	0.114
Std. Deviation	3.284	2.392	2.032	4.581	3.121	1.630	2.203	1.166

dsh: diameter at stump height (cm), dbh: diameter at breast height (cm), h: tree height (m),

The stands consist of young trees, age of which was between 10 and 20 year-old. The felling operations were conducted between 2013-2015 years in the context of ordinary silvicultural prescriptions. The study sites were randomly selected among the stands having different site quality and located in different forest conditions so that it can be have the capacity to represent ability. The mean removed tree intensity, for trees with *dbh* (1.3 m above the ground) nearly 4.9 cm was 1368 (± 310) trees ha^{-1}. Mean tree height was 4.3 (± 1.6) m, as well.

Data. The determining the amount of FW biomass was based on site-specific real data provided by measurement of tree and stand characteristics before and after harvesting via destructive tree sampling. It was applied an observational design [26] for first thinning in the randomized 6 sampling stands. Each stand was divided into three sampling plots, which were subjectively selected to represent the existing range of ages, stand density, tree diameter, and site quality throughout the area of distribution of brutian pine. The trees both to be removed and also left in each stand were separately counted using either in 10x10 m^2 or 15x15 m^2 square shaped plots. Data from 108 only felled small diameter trees that were to be removed from 18 plots installed in natural stands of this species were used. In each plot, six sampling trees from different sizes were randomly selected among the eligible trees to cover the variations in tree biomass and stand characteristics for developing above-ground biomass equation.

dbh was measured to the nearest 0.1 cm in each tree with a digital calliper. The selected trees were felled from above the root collar nearest to ground level, where stump height was below 10 cm. Diameter at stump height (*dsh*) and tree height (*h*) were measured and verified (Table 2). Subsequently, fresh weight of the total tree biomass was weighed by a portable weighbridge at stump side. Then, the felled tree was sorted into two sections; merchantable stem wood and entire crown. If the large-end diameter of the stem was higher than 8 cm throughout at least 0.5 m in length, it was apportioned for merchantable fiber wood. Afterward, the crown mass was motor-manually or manually delimbed to tree top, and then the rest of stem in the crown section was stripped off their branches. Thus, the unutilized stem section which called fuel wood in the study, was recovered. Tree components were separately weighed to be used in biomass quantification. The branches including needles and twigs were left in stand as logging residues, as well. After weighing the biomass, a sample mass to scale moisture content of all components were randomly taken by the sampling methods. So, subsamples were taken from the stem and fuel wood was weighed again.

The total aboveground dry biomass of sample trees from removal stands in first thinning operation varied between 0.42 and 18.6 kg $tree^{-1}$, the stem biomass ranging from 0.12 to 12.9 kg $tree^{-1}$. The recoverable FW ranged from 0.12 to 4.74 kg $tree^{-1}$ (Table 2). The overbarked stem biomass represented the most important fraction of the total tree biomass (average 58.3 %) and rest of which was branch biomass.

Method. Moisture content, in wet basis, was determined by the gravimetric method; the samples were weighed before and after drying in an oven in the laboratory conditions to a constant weight at 65 C° to obtain oven dry weight. Oven-dried biomass of a tree or tree components such as FW was calculated by multiplying the ratio of dry weight/fresh weight with the whole fresh biomass [10]. The fresh weight of all parts of a small diameter tree were separately scaled in unit of kg and converted to green metric tons, t.

Various models have been produced to estimate the biomass of different tree components. The predictors used in the models may range from one single variable (*dbh* or *dsh*) to multiple (e.g., tree height, age, etc.). The aim was to fit models for the FW components of aboveground tree biomass. Therefore, the tree-level information was *dbh*, *dsh*, and *h* was tested with different models dealing with biomass prediction and including different combinations of the above-mentioned predictors. Since alternative models were sequentially provided for FW and also TB for the best possible combination of the available predictors and the best equation when using single or multiple predictor. It was attempted to reveal the best equation for FW biomass estimation so that it can be simplistic and practical. It was gradually implemented two methods to expose the best fit model, where the first was the conventional linear regression model and the second was nonlinear regression.

The variables were appeared to be related linearly, and then the simple linear regression models were used to determine which model to use. In this concept, two type linear model that are common biomass equations were evaluated for their accuracy in predicting only FW and TB biomass (kg/tree). In the first type linear model, biomass equation was fitted as function of *dbh* or *dsh* as single input variable (Model-1 in Table 3). With the Model-1, the relationship between biomass and *dbh* or *dsh* was linear. This was a common technique that was used effectively in many other biomass studies [16, 27, 28].

In the second type, *dbh* or *dsh* was used as first variable, and tree height (*h*, in m) were also added to the model as second variables (Model-2). Then, multivariate linear models performed in the study were fitted by using regression analysis. The Model-2 used an additional variable of *h* along with *dbh* or *dsh* to estimate FW biomass and TB. In this model, multiple regression procedure was used to determine when the added variable of *h* significantly improved the accuracy of predicting biomass. When the predicted values of Model-1 and Model-2 were compared with, it was found a minor difference between them on the expressiveness of the equations. Because transformations procedure or correction factors were needed to improve the equations as stated by Baskerville [29], to avoid the additional treatments, nonlinear regression models were implemented as second way.

Before developing the nonlinear regression models, the scatter-plots were primarily implemented to show relationship between dry biomass and tree diameter (*dbh* and *dsh*). Since it was recognized that the plots resembled a mathematical function, it was fitted data to that type of model. Then, the equations were produced by curve-estimation method using different models [30] which was compared for the relationship between biomass quantity and tree characteristics. In the event that the model was to be inadequate because its coefficients didn't make practical sense, the other curve-estimation models were evaluated for the fit values. Thus, depending on R^2, *StdE*, and *p* values, it was chosen one or more curve estimation regression models that were power function (Model-3), cubic (Model-4), and S-curve functions (Model-5) as respectively.

The models (3-5) used non-linear regression to estimate biomass like that in many studies [31], which was useful because the data didn't need to transform [32]. However, in order to explore an alternative model that may be appropriate rather than previous and to show the effects of adding *h* to estimation model, nonlinear regression procedure was implemented via ordinary least squares (OLS) method, this time [22]. Thus, it was avoided the additivity problem arising from the mismatch between the sum of component-based predictions and total biomass estimates [33, 34]. Then, 22 well-known models [27] were fitted for FW and TB biomass using combined tree characteristics (Table 3).

TABLE 3
The candidate models for FW and TB

Model ID	Expression
Model-1	$y = b_0+b_1d$
Model-2	$y = b_0+b_1d+b_2h$
Model-3	$y = b_0d^{b1}$
Model-4	$y = b_0+b_1d+ b_2d^2+b_3d^3$
Model-5	$y = exp(b_0+(b_1/d)$
Model-6	$y = b_0+b_1d^2$
Model-7	$y = b_0+b_1d^2+b_2h$
Model-8	$y = b_0+b_1d+b_2h^2$
Model-9	$y = b_0+b_1d^{b2}$
Model-10	$y = b_0+b_1d^{b2}+b_3h$
Model-11	$y = b_0+b_1d+b_2h^{a3}$
Model-12	$y = b_0+b_1d^2h$
Model-13	$y = b_0+b_1d^{b2}h$
Model-14	$y = exp(b_0+b_1d)$
Model-15	$y = b_0d^{b1}h$
Model-16	$y = b_0dh^{b1}$
Model-17	$y = b_0d^{b1}h^{b2}$
Model-18	$y = exp(b_0+b_1d+b_2h)$
Model-19	$y = exp(b_0+b_1d^2)$
Model-20	$y = exp(b_0+b_1d^2+b_2h)$
Model-21	$y = exp(b_0+b_1d+b_2h^2)$
Model-22	$y = exp(b_0+b_1d^{b2})$

Where, *y* was the dry biomass in kg of a tree or tree component such as FW; b_0 was the constant; b_1 was model parameters; *d* was tree diameter (*dbh* or *dsh*) in cm; and *h* was total tree height in m, as well.

In producing linear and curve estimation equations, statistical software preferred for that analysis was IBM SPSS statistics 20 package. Nonlinear regression analysis was carried out by SAS software for model fitting. All analysis was performed at an alpha level of 0.05. The results of the study were usually presented in tree level on average of all samplings.

Evaluation. Many evaluation criteria could be used when selecting the best biomass model for tree components [24]. The best model was chosen based on goodness-of-fit statistics for the prediction of FW and also TB. For the linear equations, goodness of fit for all regression equations was achieved by examining the lowest *p*-values and standard error of the estimate, and also the highest coefficient of determination (R^2) through SPSS software which was used for all model fitting [35]. To fit equations and to select the best one, the simplistic models especially linear and curve-estimation equations were evaluated by R^2 and *StdE*. The R^2 statistic is a measure of the strength of association between the observed and model-predicted values of the dependent variable. The large R^2 values indicate strong relationships, where R^2 for a model is larger, though it is not clear whether this is due to the model capitalizing on chance with an extra parameter [30].

TABLE 4
Single input linear model for aboveground FW and TB biomass

Model ID	Biomass	*d*	b_0	b_1	*p*	R^2	StdE
Model-1	TB	dsh	-6.394	1.274	0.000	0.834	1.876
		dbh	-2.903	1.743	0.000	0.829	1.904
	FW	dsh	-1.128	0.297	0.000	0.701	0.640
		dbh	-0.256	0.395	0.000	0.658	0.685

TABLE 5
Biomass models with two variable for FW and TB

Model ID	Biomass	*d*	*h*	b_0	b_1	b_2	*p*	R^2	StdE
Model-2	TB	dsh	h	-6.073	1.062	0.397	0.000	0.842	1.839
		dbh	h	-2.938	1.683	0.078	0.000	0.829	1.916
	FW	dsh	h	-0.841	0.107	0.356	0.000	0.801	0.525
		dbh	h	-0.468	0.032	0.472	0.000	0.778	0.554

Four statistical criteria obtained from the residuals were examined to compare the performance of the developed linear and nonlinear models in Table 3: the root mean square error (*RMSE*) (Eq. 1), which indicates the accuracy of the estimates; the coefficient of determination (R^2) (Eq. 2), which is a measure used to determine the relationship and the goodness-of-fit between the estimated and the measured data; the mean bias (*E*) (Eq. 3), which indicates an overall indication of the error variance of the model; and Akaike's information criterion (*AIC*) (Eq. 4), which is an index used to select the best model from a group of candidate models [36]. The expressions of the statistics are summarized as follows [22]:

$$\mathrm{RMSE} = \sqrt{\frac{\sum_{i=1}^{i=n}\left(y_i - \hat{y}_i\right)^2}{n-p}} \quad (1)$$

$$R^2 = 1 - \left[\frac{\sum_{i=1}^{n}\left(Y_i - \hat{Y}_i\right)^2}{\sum_{i=1}^{n}\left(Y_i - \bar{Y}\right)^2}\right] \quad (2)$$

$$E = \frac{\sum_{i=1}^{i=n}\left(y_i - \hat{y}_i\right)}{n} \quad (3)$$

$$\mathrm{AIC} = n\ln\left(RMSE\right) + 2p \quad (4)$$

where y_i , $\hat{y}_i$ and $\overline{y}$ are the measured, estimated and average values of the dependent variable, respectively; *n* is the total number of observations used for fitting the model; and *p* is the number of model parameters to be estimated.

RESULTS

Parameters and evaluation statistics are given in Table 4 for tested models from the removed trees to estimate tree-based dry biomass potential for FW recovery. The FW biomass was firstly correlated with *dbh* (*R*: 0.811; $p<0.001$) and *dsh* (*R*:0.837; $p<0.001$) due to the fact that they were the easily measurable variable. Therefore, the single entry model fit was tested to predict FW and also TB dry biomass. The result of the linear equation (Model-1) was presented in Table 4, where it was accounted more than 82 % of the variability of the total tree biomass. However, single entry linear model with *dbh* and *dsh* variables could explain at least 65 and 70 % of FW biomass, respectively. Overall validation statistics with simultaneous fitting were better for TB but relatively decreased for FW component of a tree.

The R^2 values of Model-1 fitting with both *dsh* and also *dbh* was relatively lower. However, explaination capacities of the equation using *dsh* were more powerful than *dbh* because of having higher R^2 and relatively lower *StdE* values. The linear model stated that the expected dry FW biomass was equal to -1.128 + 0.297**dsh* inTable 4.

However, when tree height inserted to the single entry linear equations as secondary explaining variable, they increased the equation fit compared to equations with *dsh* or *dbh* as a single input variable (Table 5). The general regression models in the pooled equations with three input variables (diameter and height) were relatively more powerful than diameter specific regression models for especially FW estimation, because their R^2 values were considerably higher and *StdE* values were relatively weaker. The addition of tree height to TB equations slightly improved the R^2 values of the equation fit with *dsh* and *h* whereas didn't get it on the equation fitting with *dbh* and *h*. However, the equations for FW biomass using *dsh* and *h* had a higher R^2 value then ones the *dbh* and *h* as input variable, in the linear models.

To figure out the correlation and to identify the direction of the relationship, and then to compare them, the scatter-plots were developed. It showed relationship between dry TB and FW biomass and both *dbh*, and also *dsh*, in Figure 1. A separate model could be produced for each variable. The curve fit

chart gave a quick visual assessment of the fit of each model to the observed values. From this plot, it appeared that the power functioned model (Model-3 in Table 3) was better to explain the relationship between TB and *dsh*, and polynomial model (Model-4) was fitted by using of *dbh*. The power models (Model-3) were the best-fitted for estimation FW biomass respect to both *dsh* and also *dbh* in Figure 1.

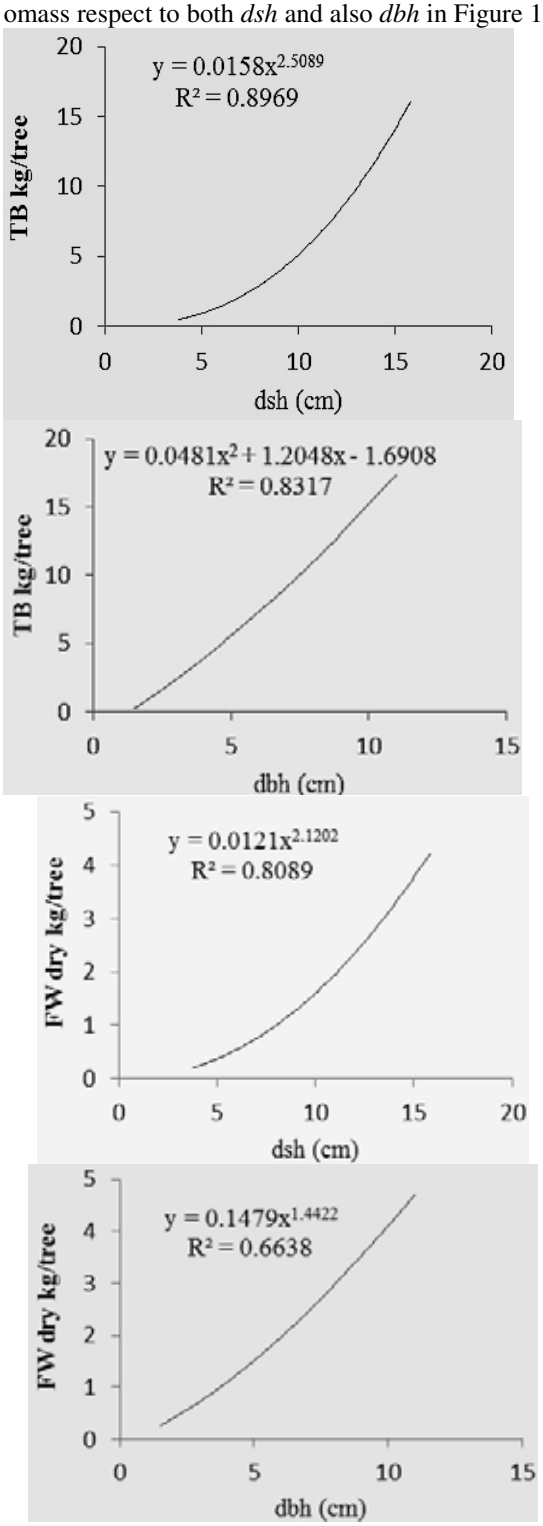


FIGURE 1
The scatter-plots for total aboveground TB and FW to tree level variables

To strength the consistency curve-estimation models and to improve best fitted model with single variable, it was produced curve estimation regression statistics for more different regression models in Table 3, as well. The best fitted equations for TB and FW biomass was summarized in Table 6.

Power function was the best equation fit for aboveground total TB using of *dsh* and whereas cubic function presented the best model when *dbh* was used. Biomass equation of TB was the highest R^2 while *dsh* was being used as predictor. FW biomass was predicted more accurately by S-curved functions by using of *dsh* and cubic function with *dbh*, as well. In order to be able to fortify representation capacity of the equation, it was substituted *dbh* with *dsh*. But, FW biomass was strongly predicted by *dsh* as independent variable by means of higher R^2 and weaker *StdE* (Table 6).

The nonlinear (multivariable) regression equations were developed to get more explanatory models by means of Table 3. So, it was experienced to see what happened when the second variable, *h*, was added to the equations. The result of the nonlinear biomasss equations with two variable was presented in Table 7.

The equations for aboveground tree biomass were derived from 22 models in Table 3. The model fitted TB, with higher R^2 (0.881) value and lower *StdE*. As well, *RMSE* value (1.597) and *AIC* were the minimal value among 22 models. So, Model-17 in Table 3 was fitted as the best equation for TB estimation. This model used *dsh* and h *to* develop the equation.

The best fit was obtained for the equation of FW by using of *dsh* and *h* as independent variables within the nonlinear models. The model fitted the FW, with higher R^2 value and lower *StdE*. As well, *RMSE* value of FW was equal to 0.5116 which were the minimal value among other models with two variables. Among the 22 models, most coud be eliminated from consideration because of high values of *AIC*. Off the a lot of with minimal value *AIC*, the Model-8 in Table 3 had the lowest value equation for FW biomass. The 22 models was tested by both *dbh* and *dsh* with together *h*, as well. But, the equation with *dsh* gave the most available results. The greatest degree of pattern was betwen FW biomass and *dsh* supported the relationship. Based on the assumption, it was shown that an incerase on FW biomass per tree from smallest diameter to smaller one, like that in Figure 1. All the predictors in the models were significant ($p<0.001$). So, *dsh* was a significant predictor, in all cases, the biomas equations fitted by *dsh* for FW presented higher R^2 value than the equations fitted by *dbh*.

TABLE 6
Parameter estimations for tested models in Table 3

Model ID	Biomass	*d*	b_0	b_1	b_2	b_3	*p*	R^2	StdE
Model-3	TB	dsh	0.016	2.509	-	-	0.000	0.897	0.319
Model-4		dbh	-0.126	0.170	0.244	-0.011	0.000	0.833	1.902
Model-5	FW	dsh	2.238	-16.714	-	-	0.000	0.828	0.367
Model-4		dbh	-0.048	1.162	0.064	-0.005	0.000	0.666	0.684

TABLE 7
Available nonlinear biomass models with goodness-of-fit statistics

Model ID	Var.	Cfc.	Estimate	StdE	Approx Pr.>|t|	R^2	RMSE	E	AIC
Model-17 for TB	dsh; h	b_0	0.0234	0.0086	0.0075	0.881	1.5975	0.0096	103.44
		b_1	2.2396	0.1889	<0.0001				
		b_2	0.1819	0.1046	0.0850				
Model-8 for FW		b_0	-0.3158	0.1870	0.0943	0.811	0.5116	-7.046E-16	-133.37
		b_1	0.1364	0.0260	<0.0001				
		b_2	0.0322	0.0042	<0.0001				

TB: Total tree biomass (kg/tree), FW: Energy wood biomass (kg/tree), *dsh*: Diameter at stump height (cm), *h*: Tree height (m), Var.: Varibles, Cfc.: Coefficients, StdE: Standard error of the estimate, RMSE: Root mean square error, E: Bias, and AIC: Akaike's Information criteria.

When the models developed for FW prediction was compared to each other, with constant and model parameters in Model-5, gave the best fitted solution because of higher R^2 value and relatively lower error indice (Table 8). *dsh* was the most effective variable because it placed in all models for fitting.

TABLE 8
Comparison of the equations for FW biomass estimation

Model ID	Variables	R^2	StdE
Model-1	*dsh*	0.701	0.640
Model-2	*dsh, h*	0.801	0.525
Model-8	*dsh, h*	0.811	0.187
Model-5	*dsh*	0.828	0.367

Discussion. The estimation of total tree biomass and its components are essential for bioenergy feasibility studies [37]. Previous studies [25,38] illustrated that estimation models (equations) and choice the best fitted one may have a substantial impact on the defining the amount of biomass. It can be argued that biomass estimation models for all tree species and site-specific conditions is not studied, yet

Biomass equations and above ground biomass estimation of small trees have not received much attention in the literature except for recently published a few studies as Nelson et al. [39] and Schuler et al. [40]. There is increasing national and international interest in accurately estimating forest biomass for potential bioenergy purposes and others. The uncertainties of brutian pine forest areas in Turkey have been driven partly by high portion of small tree dominant stands in the Meditrrenean Region and the unknown performance of the small tree biomass models.

Even though one study was also completed on determination of the amount of energy wood from young trees in first thinning of brutain pine [2], it was not included any study on FW biomass estimation. So, this is the first time this study could present a biomass model for FW depending on different tree variable with different model structure. There was a few study has focused on developing equations of tree or tree component biomass for small diameter trees in brutian pine stands [20,41]. The estimates of FW biomass may differ relatively from estimates made with more regionally representative models in literature, and the privilege of the biomass estimation study may depend on these differences [15]. Therefore, the directly comparison of our model with those in the literature was not possible without similar product-specific partition strategy, such as FW biomass, was applied. Moreover, the differences on tree characteristics resourced from local growing conditions causes the variation on models, which complicates use of the models to refit [19]. However, when total aboveground biomass equations in literature for brutian pine trees [21,23,24] were compared with the study, it was illustrated that the range of biomass estimates in the literature gave higher results more than this study because their biomass equations fit had been produced from the higher diameter tree variables.

We wanted to understand the implications of using a particular equation for predicting FW biomass from first thinning. It was tested several models to the same tree for quantifying the differences among the results and to show the reaction when it

was used one equation instead of another. In previous studies, it was usually performed dimensional analysis approach using regression model to estimate the relationship between one or more tree dimension and component weight [19, 42]. In this study the aboveground TB and available FW biomass was estimated using the equation containing *dsh* or *dbh*, and *h* as predictors, like that in other studies for mature trees [21, 43]. Estimating recoverable FW biomass was successfully accomplished using standard *dbh* or *dsh* -based biomass equations, like that in literature [16]. The results showed that increasing *dsh* and also *dbh* is followed by an increase in FW biomass. This finding is similar with the previous studies [44, 45].

It was tested two different equation types as linear and nonlinear, for biomass estimation from at tree-level data in young stands. The results showed that the relationship between dry FW biomass and tree diameter (*dbh* or *dsh*) was a generic to an extent that the single variable equation across the all trees in the stands. Model fit and individual parameter estimates of recoverable FW biomass, based on tree *db*h, were highly significant in literature [15]. Although reliable significance ($p<0.01$), the equations setting with *dbh* were significantly lower R^2 and had a higher *StdE* for TB and FW biomass in both linear and nonlinear models. This suggested that the relationship between TB or FW biomass and *dbh* was less accurate. This showed that predicting FW biomass with equations based on *dsh* without considering *h* even so may give consistent result, which result similar with Peichl and Arain (2007). However, when adding *h* as second input variable, the equation fit may be considerably improved for prediction FW biomass in the linear models, but this may be less frequently used in practice [46]. The single variable nonlinear models using *dsh* had a higher R^2 and lower error indices values. However, TB and FW biomass were strongly correlated to *dsh*, whereas the correlation of TB and FW biomass to *dbh* were slightly weaker, which result is similar with Peichl and Arain [11]. This explains why the adding of tree height as second variable doesn't result in any major improvement of equations for FW and TB. The regression models including only tree diameter (*dsh*) estimated aboveground biomass for tree components such as FW biomass are better than the model containing *dbh* and *h*. These results are in accordance with previous studies [47]. Moreover, the tree variables *dsh* or *dbh* and *h* had a significant impact on the relationships for dry biomass, in agreement with literature [48]. On the other hand, it should be noted that simplified biomass models dependent on commonly measured variables like diameter (*dsh* or *dbh*) and *h*, offers some advantageous from the application point of view [49].

The models for estimating FW biomass were considerable and had higher R^2 and lower error indices for nonlinear models. However, linear models have relatively lower R^2 and higher error indices. It is expected that this can be resulted from different incremental growth curve. The most of the equations for FW biomass requires estimates of *dsh* rather than *dbh*. If there is only *dbh* data, it can be used linear or nonlinear equations from Table 4 and 6, and Figure 1 that corresponds to the diameter range of interest and use all of them to quantify aboveground TB and FW biomass. The differences between models can be omitted in terms of results from one equation are higher than the average of all of the appropriate equations [19].

Since estimation capability of linear models was lower, curve-estimation regression was tested for predicting the available amount of FW biomass. The curve estimation procedure allowed us to quickly estimate regression statistics and produced related plots for different models. Curve estimation is most appropriate when the relationship between the dependent variable(s) and the independent variable is not necessarily linear. In particular, the linear model seems to underestimate FW and also TB biomass for cases with small values of tree diameters. The regression sum of squares was considerably larger than the residual sum of squares, which indicated that most of the variation in the estimation of FW or TB biomass was explained by the models.

More than 22 initial models were tested; there was significantly difference between goodness-of-fit measures. R^2 value of only few values of 22 equations exceeded 0.80, suggesting a high proportion of the variation in the data was explained by the models [44]. According to other conventional interpretation of test statistics (bias, AIC, and RMSE) only one of the 22 equations had suitable score that met threshold value in Table 7. The test statistics are more helpful in defining the most suitable subset of models [50]. Moreover, the best model for FW biomass estimation should exhibit a balance between accuracy, simplicity and practical application [51]. The equation for dry FW biomass using *dsh* with S-curved function had a 24% higher R^2 value (R^2: 0.828) and smaller *StdE* than using *dbh* (R^2: 0.666) with as single input variable, which is similar with Peichl and Arain [11]. So, it was dedicated S-curve model (Model-5) to be most suitable for the prediction of FW biomass, possibly due to the fact that the fuel wood biomass slowly increases at the initial stage but becomes more increased with age and increasing diameter at the thinning stage before a certain maturity stage. However, power function is the best model for aboveground total tree biomass which is compatible with the previous studies [24, 52, 53]. In the equations mentioned in Table 4-7 and Figure 1, the R^2 values are different among equations for FW biomass. The difference between lowest and highest R^2 values of single entry biomass equations was 0.127 for *dsh*. However, the difference between two variable linear and nonlinear equations decreases to

0.010 when *dsh* and *h* is used, as well. The error indices values of FW model decreased by approximately 28 % from two variables (*dsh* and *h*) model to one-variable (*dsh*) model.

The product and species-specific recoverable FW biomass estimations from the model were unbiased across the entire range of small diameter tree *dsh* below 10 cm on average. The estimates of FW biomass may differ relatively from estimates made with more regionally representative models [22, 24] for wide range tree diameters, and the success of a biomass estimation in the future may depends on these differences.

Often, the results obtained from equations produced specifically for a product or wood components are faced with the problem of not reflecting the total biomass of the tree. In this study it was fitted the equations for the tree component, FW, simultaneously with the total tree biomass depending on the sum of the components to guarantee that the total biomass estimation is equal to the total aboveground estimated by the aboveground biomass equation [49]. However, it is noted that the differences between the biomass measured and estimated may be explained by the fact that these equations only used as an explanatory variable [54].

Depending on the study results, in Mediterranean region, observations of recovery rates of FW from unutilized tops of small diameter trees (4.5-11 cm at *dbh*) revealed that approximately 30% of the total tree biomass of brutain pine. It should be taken into consideration that the inclusion of larger trees and branches may increase the additional biomass and warranted the inclusion of additional biomass parameters. In addition to tree size and tree species, it is possible that the rate of FW biomass recovery could be affected by the site quality, age classes, and thinning intensity [11, 15, 55]. Further research of the factors that may contribute to recoverable biomass, due to operational constraints may be needed.

CONCLUSION

Biomass harvesting for a significant supply of bioenergy remains the ability to precisely estimate the amount of wood biomass that can be recovered from various forest resources such as small diameter trees. Therefore, determining of the recoverable biomass potential from a tree is the first step for revealing feedstock capacity in modern and classic bioenergy utilization. This study exposed product-specific biomass model to predict the amount of fuel wood and total tree biomass on small diameter trees in even-aged young brutian pine stands of west Mediterranean Region. It was examined well known linear and nonlinear models with data collected from destructively sampled small dimeter trees. These models was generally simple in form and produced highly significant estimates of recoverable FW biomass from in oven-dry basis for individual tree, based on diameter (*dsh* or *dbh*) alone, and with tree height as predictor variables. Even though single variable nonlinear equation was reasonably fit the actual data, the multiple models with the conventional goodness-of-fit tests for predicting FW biomass across the range of diameters were gave a reasonable solution.

The presented recoverable biomass models for small diameter trees will assist stand-level prediction of available biomass potential for utilization in the bio-economy. The equations can be used in conjunction with stand inventory for removal tree intensity to refine accurately estimation of available FW biomass in Mediterranean sites. This tree-level study sets the stage to complete stand-level surveys that will allow for the local and regional-scale consistently prediction of the biomass potential for small diameter trees. These models can also be used by biomass harvesting scientists, forest managers, bioenergy investors, and by ecologist to study on biomass potential. Moreover, the presented models for available biomass are sensitive to ecosystem requirements because the models are established to give the results that the residues (at least1/3 of removing tree total biomass) will be left on site. However, since site-specific conditions are more important factors in estimating biomass, more work is required to establish this range of allometric relationships across sites of varying geographic locations in different regions. Additionally, intensified removal for producing fiber wood may have more serious effect in first thinning as studied here, so future work is needed related to logging intensity of removing small diameter trees.

ACKNOWLEDGEMENTS

This article was carried out by using of a minor part of data collected in the project, “Investigation on Supply Possibilities of Logging Residues” (No:110O435) funded by TUBITAK (Scientific and Technological Research Council of Turkey). The Authors thank to TUBİTAK for their financial support.

REFERENCES

[1] Björheden, R. (2008) Optimal point of comminution in the biomass supply chain. The Nordic-Baltic Conference on Forest Operations, Copenhagen, September 23-25. Forest and Landscape Working Papers 30, Denmark.

[2] Eker, M., Spinelli, R., Gurlevik, N. (2017) Recovering energy biomass from sustainable forestry using local labor resources. J Clean Prod. 157, 57-64.

[3] Eker, M. (2014) Trends in Woody Biomass Utilization in Turkish Forestry. Croat J For Eng. 35, 255-270.
[4] Gullberg, T., Johansson, J. (2006) A method for integrated extraction of logging residues and soil scarification on a small scale. Biomass and Bioenergy. 30,1035-1042.
[5] Roser D, Asikainen A, Rasmussen KR, Stupak I (2008). Sustainable Use of Forest Biomass for Energy: A Synthesis with Focus on The Baltic And Nordic Countries. Managing Forest Ecosystem. Volume-II, 232 p. Netherlands.
[6] GDF (2017) The Administrative Activity Report of 2016. General Directorate of Forestry, Ministry of Forestry and Water Affairs. 110 p., Ankara (In Turkish) https://www.ogm.gov.tr/ekutuphane/FaaliyetRaporu/ (Accessed 22 January 2017)
[7] Boydak, M. (2004) Silvicultural characteristics and natural regeneration of *Pinus brutia* Ten. – a review. Plant Ecology. 171, 153–163.
[8] GDF (2017) Total forest area by tree species in 2016, Forestry Statistics. General Directorate of Forestry. http://www.ogm.gov.tr/ ekutuphane/ Istatistikler/ (Accessed 13 April 2017)
[9] GDF (2009) The Status of Forest Biomass in Renewable Energy. Report of Bioenergy Working Group, General Directorate of Forestry, 154 p., Ankara (In Turkish).
[10] Eker, M., Acar, H.H., Özçelik, R., Alkan, H., Gürlevik, N., Çoban, H.O., Korkmaz, M., Yılmaztürk, A. (2013) Investigation on supply possibilities of logging residues in forestry – Final Report, TUBITAK, Project No:110O435, Ankara (In Turkish).
[11] Peichl, M., Arain, M.A. (2007) Allometry and partitioning of above –and belowground tree biomass in an age-sequence of white pine forests. Forest Ecology and Management. 253, 68-80.
[12] Smeets, E., Faaij, A. (2007) Bioenergy potentials from forestry in 2050 – An assessment of the drivers that determine the potentials. Climatic Change, 81(3–4), 353–390.
[13] Demirbaş, A. (2008) Importance of biomass energy sources for Turkey. Energy Policy. 36(2), 834–842.
[14] Pare, D., Bernier, P., Thiffault, E., Titus, B.D. (2011) The potential of forest biomass as an energy supply for Canada. For. Chron. 87(1), 71–76.
[15] Thiel, M., Basiliko, N., Caspersen, J., Fera, J., Jones, T. (2015) Operational biomass recovery of small trees: equations for six central Ontario tree species. Can J For Res. 45, 372-377.
[16] Ter-Mikaelian, M.T., Korzukhin, M.D. (1997) Biomass equations for sixty-five North American tree species. Forest Ecology and Management. 97, 1–24.
[17] Ketterings, Q.M., Coe, R., van Noordwijk, M., Palm, C.A. (2001) Reducing uncertainty in the use of allometric biomass equations for predicting above-ground tree biomass in mixed secondary forests. Forest Ecology and management. 146(1), 199-209.
[18] Durkaya B, Varol, T., Durkaya. A. (2014) Determination of carbon stock changes: Biomass models or biomass expansion factors. Fresen. Environ. Bull. 23(3), 774-781.
[19] Jenkins, J.C., Chojnacky, D.C., Heath, L.S., Birdsey. R.A. (2003) National scale biomass estimators for United States tree species. For. Sci. 49(1), 12-35.
[20] Sun, O., Uğurlu, S., Özer, E. (1980) Determination of Red Pine Biomass, Forestry Research Institute Publications, Technical Bulletin. No:104, p. 32, Ankara.
[21] Durkaya, A., Durkaya, B., Ünsal, A. (2009) Predicting the above ground biomass of calabrian pine (*Pinus brutia* Ten.) stands in Turkey. Afr J Biotechnol. 8(11), 2483-2488.
[22] Özçelik, R., Diamantopoulou, M. J., Eker, M., Gürlevik, N. (2017) Artificial Neural Network Models: An Alternative Approach for Reliable Aboveground Pine Tree Biomass Prediction. For. Sci. 63(3), 291–302.
[23] Zianis, D., Xanthopoulos, G., Kalabokidis, K., Kazakis, G., Ghosn, D., Roussou, O. (2011) Allometric equations for aboveground biomass estimation by size class for *Pinus brutia* Ten. trees growing in North and South Aegean Islands, Greece. European Journal of Forest Research. 130(2), 145-160.
[24] de--Miguel, S., Pukkala, T., Assaf, N., Shater, Z. (2014) Intra-specific differences in allometric equations for aboveground biomass of eastern Mediterranean Pinus brutia. Annals of Forest Science. 71(1), 101-112.
[25] Neyişçi, T. (1987) Kızılçamın ekolojisi. Kızılçam.Ormancılık Araştırma Enstitüsü Yayınları, El Kitabı Dizisi 2 (Muhtelif Yayınlar Serisi 52), Ankara, 23–56 (In Turkish).
[26] Magagnotti, N., Spinelli, R. (2012) Good Practice Guidelines for Biomass Production Studies, COST Action FP-0902, WG-2 Operations Research and Measurement Methodologies. 52 p., Italy.
[27] Zianis, D., Muukkonen, P., Mäkipää, R. and Mencuccini, M. (2005) Biomass and stem volume equations for tree species in Europe. Silva Fennica Monograph. (4), 63 p.
[28] Dong, L., Zhang, L. and Li, F. (2016) Developing Two Additive Biomass Equations for Three Coniferous Plantation Species in Northeast China. Forests. 7(136), 21.
[29] Baskerville, G.L. (1972) Use of logarithmic regression in the estimation of plant biomass. Can J For Res. 2, 49–53.

[30] SPSS (2014) SPSS Professional Statistics, 13.0, SPSS Inc., Chicago.
[31] Barclay, H., Pang, P., Pollard, D. (1985) Aboveground biomass distribution within trees and stands in thinned and fertilized Douglas-fir. Can. J. For. Res. 16, 438- 442.
[32] Coltrin, W.R. (2010) Biomass Quantification of Live Trees in A Mixed Evergreen Forest Using Diameter-Based Allometric Equations. Ms Thesis, The Faculty of Humboldt State University. 59 p.
[33] Snowdon, P., Eamus, D., Gibbons, P., Khanna, P.K., Keith, H., Raison, R.J., Kirschbaum, M.U.F. (2000) Synthesis of allometrics, review of root biomass and design of future woody biomass sampling strategies. National Carbon Accounting System Technical Report 17. Australian Greenhouse Office, Canberra. 114 p.
[34] Parresol, B.R. (2001) Additivity of non-linear biomass equations. Can J For Res. 31, 865–878.
[35] Güner, Ş.T., Çömez, A. (2017) Biomass equations and changes in carbon stock in afforested black pine (*Pinus nigra* Arnold. subsp. *pallasiana* (Lamb.) Holmboe) stands in Turkey. Fresen. Environ. Bull. 26(3), 2368-2379.
[36] Akaike, H. (1981) Citation classic-a new look at the statistical-model identification. Current Contents/ Engineering Technology & Applied Sciences. (51), 22-22.
[37] Zhou, X., Hemstrom, M.A. (2009) Estimating aboveground tree biomass on forest land in the Pacific Northwest: a comparison of approaches. Res. Pap. PNW-RP-584. Portland, OR: U.S. Department of Agriculture, Forest Service, Pacific Northwest Research Station. 18 p.
[38] Chave, J., Condit, R., Aguilar, S., Hernandez, A., Lao, S., Perez, R. (2004) Error propagation and scaling for tropical forest biomass estimates. Philosophical Transactions of the Royal Society of London B: Biological Sciences. 359(1443), 409-420.
[39] Nelson, A.S., Weiskittel, A.R., Wagner, R.G., Saunders, M.R. (2014) Development and evaluation of aboveground small tree biomass models for naturally regenerated and planted species in eastern Maine, U.S.A. Biomass and Bioenergy. 68, 215-227.
[40] Schuler, J., Bragg, D. C., McElligott, K. (2017) Biomass estimates of small diameter planted and natural–origin Loblolly pines show major departures from the National biomass estimator equations. For Sci. 63, 319-330.
[41] Küçük, Ö., Bilgili, E. (2007) Crown fuel load for young calabrian pine (Pinus brutia Ten.) trees. J For Fac Kastamonu Uni-Kastamonu. 7, 180–189.
[42] Whittaker, R.H., Woodwell, G.M. (1968) Dimension and production relations of trees and shrubs in the Brookhaven Forest, New York. Journal of Ecology. 56, 1-25.
[43] de-Miguel, S., Pukkala, T., Assaf, N., Bonet, J.A. (2012) Even-aged or uneven-aged modelling approach? A case for Pinus brutia. Ann For Sci. 69, 455–465.
[44] McElligott, K.M., Bragg, D.C. (2013) Deriving biomass models for small-diameter loblolly pine on the crossett experimental forest. Journal of the Arkansas Academy of Science. 67, 94-102.
[45] Daryaei, A., Sohrabi, H. (2015) Additive biomass equations for small diameter trees of temperate mixed deciduous forests, Scandinavian Journal of Forest Research. 31(4), 394-398.
[46] Gómez-García, E., Biging, G., García-Villabrille, J.D., Crecente-Campo, F., Castedo-Dorado, F., Rojo-Alboreca, A. (2015) Cumulative continuous predictions for bole and aboveground woody biomass in Eucalyptus globulus plantations in northwestern Spain.Biomass and Bioenergy. 77, 155-164.
[47] Chaturvedi, R.K., Raghubanshi, A.S. (2013) Aboveground biomass estimation of small diameter woody species of tropical dry forest. New Forests. 44, 509-519.
[48] Calama, R., Montero, G. (2006) Stand and tree-level variability on stem form and tree volume in *Pinus pinea* L.: a multilevel random components approach. Invest Agrar: Sist Recur For. 15, 24-41.
[49] Correia A.C., Tome, M., Pacheco, C.A., Faias, S., Dias, A.C., Freire J., Carvalho P.O., Pereira J.S. (2010) Biomass allometry and carbon factors for a Mediterranean pine (*Pinus pinea* L.) in Portugal. Forest Systems. 19(3), 418-433.
[50] Burnham, K.P., Anderson, D.R., (2004) Multimodel inference: understanding AIC and BIC in Model Selection. Sociological Methods and Research. 33, 261–304.
[51] Wang, L., Xing, Y. (2008) Remote sensing estimation of natural forest biomass based on an artificial neural network. The journal of applied ecology/Zhongguo sheng tai xue xue hui. 19(2), 261-266.
[52] Muukkonen, P. (2007) Generalized allometric volume and biomass equations for some tree species in Europe. European Journal of Forest Research. 126, 157-166.
[53] Küçük, Ö., Bilgili, E., Saglam, B. (2008) Estimating crown fuel loading for Calabrian pine and Anatolian black pine. Int J Wildland Fire. 17, 147–154.
[54] Montero, G., Ruiz-Peinado, R., Muñoz, M. (2005) Producción de biomasa y fijación de CO_2 por los bosques españoles. Instituto Nacional de Investigación y Tecnología Agraria y Alimentaria.
[55] Heth, D., Spetter, E. (1993) Growth of *Pinus brutia* Ten.as affected by thinning intensity. Commonw For Rev. 72, 57-60.

Received: **07.09.2017**
Accepted: **06.10.2017**

CORRESPONDING AUTHOR

Mehmet Eker
Süleyman Demirel University,
Faculty of Forestry,
Forest Engineering Department,
Isparta – Turkey

e-mail: mehmeteker@sdu.edu.tr

© by PSP Volume 26 – No. 12A/2017 pages 8298-8303 Fresenius Environmental Bulletin

EVALUATION OF ECO-FRIENDLY LEMON OIL AGAINST THE GREEN PEACH APHID *MYZUS PERSICAE* SULZER (HOMOPTERA: APHIDIDAE) USING FOUR SOLVENTS

Tawfiq M Al-Antary*, Idres H Belghasem, Salah Eddin A Araj

School of Agriculture, Department of Plant Protection, University of Jordan, Amman 11942, Jordan

ABSTRACT

Efficacy of lemon essential oil with four different solvents namely: acetone, ethanol, n-hexane and chloroform, was screened against the green peach aphid *Myzus persicae*, for their aphicidal effects under lab conditions. The aphid was reared in a special insectary until reaching sensitive strain after ten generations, bioassay was then applied to find lethal concentration, after three different times; 24, 48 and 72 hours, and between four solvents. Results have shown that, lemon oil with chloroform was the most effective against 1st and 2nd nymphal instars (early nymphal instars) of *M. persicae*. Also, lemon oil with Acetone oil had the highest significant mortality on the late nymphal instars. Lemon oil has shown effectiveness on early nymphal instars with LC50 of 0.0008, and 0.001 (v/v) with chloroform and ethanol, respectively. Lemon oil have shown the highest effectiveness on late nymphal instars with LC50 of 0.0009 v/v for both Acetone and n- hexane. Results indicated significant differences in mean percentage mortalities after 24, 48, and 72 hours of the exposure at 10% concentration. Lemon oil showed highest mortality which ranged between 94.25 to 97.75%. This study indicated the essential oil as promising insecticide and may be used effectively in the management of *M. persicae* to provide safe environment and high quality crops.

KEYWORDS:
Bioassay, Essential oil, Green peach aphid, Lemon oil.

INTRODUCTION

The green peach aphid is an important pest. It causes an economic damage to vegetables and fruit trees in the world [1, 2, 3]. Many of cultivated vegetables in mountainous regions and Jordan Valley is considered hosts for the GPA [4, 5]. This aphid is able to transmit several viral diseases to planted vegetables [6, 7]. Direct feeding damage by low numbers of GPA causes little damage to plants. However, this aphid is considered as a serious pest when associated with virus diseases. GPA is capable of becoming resistant to a wide range of insecticides groups. Therefore, pest management strategies aimed at preventing or minimizing resistance [8, 9]. The GPA is distributed worldwide and several resistant strains have been identified using molecular techniques. A form with a chromosome translocation is wide spread in glass houses and has been shown to have very high levels of resistance. It is difficult to be controlled with insecticides because of their small sizes and hidden habits [10, 11]. Crops differ in their susceptibility to green peach aphid, but it is actively growing plants, or the youngest plant tissue, that most often harbors large aphid populations [12, 13]. Contamination of harvestable plant material with aphids, or with aphid honeydew, also causes great losses. In Arkansas (USA), mild winters allow good overwintering survival of the green peach aphid on spinach, thereby leading to contamination problems [3, 14, 34]. The serious damage caused by the green peach aphid is through transmission of plant viruses. Indeed, this aphid is considered by many to be the most important vector of plant viruses throughout the world. Nymphs and adults are equally capable of virus transmission [4, 15]. Moreover, 100 viruses transmitted by this species were listed [14]. Specific environmental chemicals, including pesticides have been described as endocrine disruptors, as known elicit their adverse effects by mimicking or antagonizing natural hormones in the body. It has been supposed that their long-term, low-dose exposure is increasingly linked to human health effects like immune repression, hormone disturbance, diminished cleverness, reproductive abnormalities and cancer [5, 16, 17, 18].

The heavy use of insecticides to control *M. persicae* over many years had led to population that are now resistant to several classes of insecticides including the organophosphates, carbamates, pyrethroids, cyclodienes, and neonicotinoids. This resistance had made the GPA one of the most widely and strongly resistant species worldwide [6, 19]. The GPA populations have high levels of esterase resistance for organophosphates. Many members of this main group of insecticides have excellent selectivity as aphicides [7, 20]. Most citrus peel oils are expressed mechanically or cold pressed.

Due to the relatively large quantities of oil in citrus peel and low cost to grow and harvest the raw materials, citrus-fruit oils are cheaper than most other essential oils [9]. Citrus essential oils showed a broad spectrum of biological activities, mainly antimicrobial [13, 21, 22]. Lemons have many important natural chemical components, including citric acid, ascorbic acid, minerals, flavonoids and essential oil [3, 23].

MATERIALS AND METHODS

Rearing of the aphid. *M. persicae* adults reared in the laboratory at 22±2°C. The aphid was identified by Prof. Tawfiq Al-Antary, of the University of Jordan according to Blackman and Eastop [24]. The GPA was collected from unsprayed area in Ghore Al Safi region. A colony of GPA was established from apterous individuals obtained from a continuously maintained culture in an insectary in the Department of Plant Protection at the School of Agriculture, the University of Jordan. *M. persicae* kept in cages with a wooden frame of (60 × 40 × 45) dimension, with four (20x30cm) fine mesh doors. A continuous supply of new plants of sweet pepper was provided as needed for the colony replenishment. Sweet pepper seeds Super Lamuyo (Scanttin seed company) were pre-germinated for three days in plastic Petri dish (9 x1.5 cm) lined on the bottom with wet filter paper before being planted in plastic seedling trays (50 × 30 × 60 cm, 50 seeds/tray) containing commercial potting soil peat moss (Kasvuturvas). After growing for 10 days under greenhouse conditions, seedlings in the primary leaf stage individually transplanted into a plastic pot (15 cm diameter) filled with the soil.

Plants kept in a greenhouse at 22 ± 4°C in the campus of the University of Jordan. These plants were regularly irrigated. The pots of plants were placed on eight plastic cages in the insectary. Each cage contained twelve plant pots, supplemented with 16: 8 L: D average of temperature 22±2°C regime and irrigated as needed.

Oil content active ingredients (essential oil) in oil extracts. The oil was bought from Talya Bitkisel Company (Amman-Jordan). Used oil were analyzed to determine the active ingredient percentage in the Laboratory of Fruits and Vegetables Processing at Department of Nutrition and Food Technology the University of Jordan as shown in (Table 1). The quantity of essential oil was carried out as following. Five milliliters of oil was taken in triplicates and placed into a previously weighed glass Petri dishes (12cm). Thereafter, they were placed in an oven for 2 hours at 75°C. After that they were taken from the oven, placed in a desiccator to cool down for15 minutes and weighed. The difference between the first weight and the second was calculated and considered to be the essential oil weight in grams. To determine the water contained in oil, the glass Petri dish with the oil was again placed in the oven at 105°C for 3hr. Calculations for the water content % was done for oil. There were three replications for oil each time.

Bioassays. In order to test the toxicity of the essential oil against *M. persicae*, first, second, third and fourth nymphal instars of apterous aphid were placed on a sweet pepper leaves in (9cm in diameter) Petri dishes. Essential oil was diluted with distilled water and Tween 20 (0.005 ml) (adjuvant). There were four concentrations for lemon oil used. There were four solvents for oil. The used solvents were: n- hexane (purity 99.5%), chloroform (purity 99.5%), ethanol (purity 99.9%), and acetone (purity 99.5%) and distilled water with Tween 20 as control. Each treatment was replicated four times. Oil was diluted separately with the four solvents in four replicates. In addition, each solvent (four replicates) in each treatment was tested separately against the green peach aphid. Each replicate has 35 to 50 aphids. The diluted oil with solvent was shaken for 5 minutes by hand. Each replicate was sprayed with the diluted oil with a sprayer on the placed aphids on the sweet pepper leaf in the Petri dish. The sprayer was consisted of 18 ml glass container. It was provided with an atomizer. One sprayer was separately used for each concentration. Petri dishes were kept open to dry for 15 minutes of spraying. Mortality rate of the aphids was assessed after exposure for 24, 48, and 72h. Petri dishes provided with sterile water and Tween 20 was served as a negative control, and Calypso (neonicotinoid) insecticide at the recommended rate of the application as a positive control. Four replicates for each concentration were used. Each treatment was tested to find the lowest concentration which gave around 30% mortality, and the highest concentration which gave around 95% mortality. The concentrations for lemon were 0.1, 0.01, 0.001, 0.0001and 0.00001. The LC50 and LC90 for oil were obtained after repeating the experimental work several times. Slope and confidence of limits were also reported.

Statistical analysis. Data were analyzed using Statistical Analysis Software [25] for LC50, LC90 and finding differences between means.

RESULTS

The lethal concentrations for LC50s and LC90s of the aphid population of green peach aphid (GPA), were determined and shown in Tables 2 and 3 for lemon essential oil, with four different solvents: ethanol, acetone, n-hexane, and chloroform after 24 hours. The software version SAS program (SAS 2014) was used to estimate parameters of toxicity,

95% confidence limits (CL) for the concentrations used and the slope. In addition, Pearson's Chi- square test was used. The comparison between effect of the lemon oil with different solvents against early nymphal (1st and 2nd) instars and late (3rd and 4th) of *M. persicae* are found in Tables 4 and 5 after 24, 48 and 72 hours.

Lethal concentrations of lemon oil. Lemon oil with different solvents showed significantly the highest toxicity with chloroform; the LC50 was (0.0008 v/v) followed by ethanol and acetone solvents; the LC50 was 0.001v/v for each. On the other hand, the lowest in toxicity was n-hexane with LC50 of 0.006v/v against early nymphal instar of the GPA. The LC90 for all solvents were not significantly different (Table 2).

TABLE 1
Means of essential oil% and water content% for lemon oil

Oil	Name	Part of the plant	Essential oil %	Water content%
Lemon oil	*Citrus lemon* peel oil	Peel	5.44	0.57

TABLE 2
Concentration (v/v)-mortality data for the different solvents of lemon oil on early nymphal instars of *M. persicae* after 24 hours of treatment.

Solvent	Slope	LC50*	95%CL***	LC90**	95%CL***	Chi-Square	Pr > Chi-Square
Ethanol	28.52	0.001b	-0.021 - 0.018	0.078b	0.049 - 0.195	12.21	<.0001
Acetone	28.14	0.001b	-0.019 - 0.016	0.079b	0.052 - 0.157	17.29	<.0001
n-hexane	31.21	0.006c	-0.011 - 0.020	0.076a	0.057 - 0.113	34.90	<.0001
Chloroform	28.88	0.0008a	-0.016 - 0.013	0.076a	0.056 - 0.119	33.30	<.0001

*LC50 values sharing the same letters do not differ significantly (95%of CL aren't overlapping).
**LC90 values sharing the same letters do not differ significantly (95%of CL aren't overlapping).
***95% confidence limit for LC50, LC90.

TABLE 3
Concentration (v/v)-mortality data for the different solvents of lemon oil on late nymphal instars of *M. persicae* after 24 hours of treatment.

Solvent	Slope	LC50*	95%CL***	LC90**	95%CL***	Chi-Square	Pr > Chi-Square
Ethanol	27.86	0.004b	-0.021 - 0.025	0.083b	0.050 - 0.237	10.35	0.0013
Acetone	27.88	0.0009a	-0.016 - 0.012	0.079b	0.054 - 0.146	19.08	<.0001
n-hexane	30.57	0.0009a	-0.007 - 0.008	0.072a	0.060 - 0.091	101.59	<.0001
Chloroform	29.22	0.005b	-0.003 - 0.014	0.081b	0.062 - 0.114	48.01	<.0001

LC50 values sharing the same letters do not differ significantly (95%of CL aren't overlapping).
**LC90 values sharing the same letters do not differ significantly (95%of CL aren't overlapping).
***95% confidence limit for LC50, LC90.

TABLE 4
Effect of different solvents on efficacy of lemon oil against early nymphs of *M. persicae* using 10% (0.1) concentration at three times.

Solvents	% mortality, ±SE		
	After 24hours	After 48hours	After 72hours
Ethanol	95.50a ± 0.64	96.25ab ± 0.47	97.00a ± 0
Acetone	94.50a ± 0.64	97.00a ± 0.57	97.00a ± 0.57
Chloroform	93.50ab ± 1.19	95.00ab ± 0.91	95.75a± 0.85
n-Hexane	95.50a ± 0.64	96.00ab ± 0.70	96.00a ± 0.70
Calypso	91.25b ± 1.25	94.50b± 0.50	96.00a ± 1.22
Control	4.00c ± 0.70	4.50c± 1.19	06.75b`± 0.75

Means within the same column sharing the same letters do not differ significantly at 5% level using LSD test.

TABLE 5
Effect of different solvent on efficacy of lemon oil against late nymphs of *M. persicae* using 10% (0.1) concentration at three times.

Solvents	% mortality, ±SE		
	After 24hours	After 48hours	After 72hours
Ethanol	94.25ab ± 0.85	95.00ab ± 1.08	95.75ab ± 1.31
Acetone	95.50a± 0.95	97.75a± 0.62	97.75a ± 0.62
Chloroform	92.25b± 1.18	93.75b ± 1.18	94.00b ± 1.41
n-Hexane	92.75b ± 0.94	93.00b ± 0.70	94.50ab ± 1.44
Calypso	94.00ab ± 0.57	94.00b ± 0.57	96.00ab ± 1.22
Control	04.00c± 0.70	04.50c ± 1.19	06.75c ± 0.75

Means within the same column sharing the same letters do not differ significantly at 5% level using LSD test.

Among the lemon oil with different solvents tested against the late nymphal instars of *M. persicae*, the most significant toxic ones were with acetone and n- hexane; LC50 was 0.0009 v/v for both followed by ethanol (0.004v/v) and chloroform (0.005v/v) (Table 3). The lemon oil showed significantly the least activity with LC90 with ethanol and chloroform solvents (0.083 and 0.081v/v), respectively. The most toxic were significantly with acetone and n-hexane (0.078 and 0.079v/v), respectively.

Lemon with different solvents on oil extraction. Table 4 showed the results of the effect of the different solvents on efficacy of lemon oil against early nymphal instars on *M. periscae* at 24, 48 and 72 hours of the treatment using 10% (0.1) concentration. Ethanol acetone, chloroform and n- hexane extracts caused significant high level of mortality against early nymphal instars with lemon oil rather than Calypso insecticide at 24 and 48h, but without significant difference after 72h. All treatments had significant difference with control.

Table 5 shows that acetone oil had the highest significant mortality on the late nymphal instars; Mortality ranged between 95.50 to 97.75%. Ethanol and Calypso ranked the second and caused 94-96% mortality. Chloroform and n- hexane ranked the third and caused 92.25-96% mortality. All treatments had significant difference with control.

DISCUSSION

Increased use of the insecticides in public health and agriculture for the control of vector and pest species has created different problems, such as the development of physiological resistance in major insect species, environmental pollution and toxic hazards to human and other non- target organisms due to their broad spectrum of activity [26, 27].The use of natural plant products is considered more sustainable, cheaper and safer. Natural pesticides are preferred for many reasons. Of these, they are cheaper compared with the chemical pesticides. In addition, they are made from local resources and safer to humans than chemical pesticides [28]. They concluded that essential oil of garlic plant and mint oil could be used as effective natural products and to be included in the integrated pest management programs**.** However, essential oils may be effective when used in pest management practices against several insect pests [3, 5, 13, 29]. Lemon oil has demonstrated strong toxic effect against *M. persicae*. It caused the highest mortality taking in consideration the LC50 and LC90 (Table 3). This oil was proved to be the most effective against the two spotted spider mite (≥90% mortality) [30]. These significant results given in this study shared indication of the insecticidal activity of many Eos which has been reported by Regnault-Roger et al. [31]. Manimaran et al. [32] have tested 25 essential oil against mosquitoes, they observed that lemon oil recorded LC50 value of 43.79 ppm and orange oil LC50 values of 54.97 ppm, after 24 h of the exposure. They also observed that lemon oil, mint oil and orange oil acted as100% larvicidal. These oils have also knockdown activities which agreed with the present results. They reported that anise oil extracts were potential as an eco-friendly biopesticide in integrated pest management against *M. persicae.* Furthermore, orange oil extracted from citrus peel caused 68 and 96% mortality to *Coptotermes formosanus* Shiraki (Isoptera: Rhinotermitidae). There was a significant reduction in feeding as compared to control [33].

ACKNOWLEDGEMENTS

The authors would like to thank the Deanship of Scientific Research at the University of Jordan, Agriculture Research Center of Libya and ICARDA.

We declare that none of the authors have any competing interests in the manuscript.

REFERENCES

[1] Lecrone, S. and Smilowitz, Z. (1980) Selective toxicity of primicarb carboryl and methamidophose to green peach aphid, *Myzus persicae* (Sulzer), Coleomogills maculula (Lenai) (Temberlake) and *Chrysopa occulata* (Say). Environmental Entomology. 9, 752-755.

[2] Parker, B.L., Booth, R.H. and Brayns, J. (1983) Methamidophos, solelhion, phenthoate and R & H 0994 for control of *Myzus persicae* (Sulzer) on potato tubers in Peru. American Potato Journal. 60, 55-59.

[3] Madanat, H.M., Al-Antary, T.M., Abu Zarga, M. (2016) Toxicity of Six Ethanol Plant Extracts against the Green Peach Aphid Myzus persicae Sulzer (Homoptera: Aphididae). Fresen. Environ. Bull. 25(3), 706-718.

[4] Al-Momany, A. and Al-Antary, T.M. (2008) Pests of Garden and Home. Publications of University of Jordan, Amman.

[5] Al-Antary, T.M., Belghasem, I.H. and Araj, S.E.A. (2017) Toxicity of anise oil against the green peach aphid *Myzus persicae* Sulzer using four solvents (Homoptera: Aphididae). Fresen. Environ. Bull. 26(5), 3705-3710.

[6] Al-Antary, T.M. and Al-Momany, A. (1990) Pests of Garden and Home. Dar Al- Arabiah for Publications and Distributions, Cairo.

[7] Madanat, H.M., Al-Antary, T.M. and Abu Zarqa, M. (2011) Toxicity of six acetone plant extract against the green peach aphid *Myzus persicae* Sulzer (Homoptera: Aphididae). Fresen. Environ. Bull. 26(5), 3340-3349.

[8] Cameron, P.J. (1996) Green Peach Aphid Resistance Management Strategy. In Pesticide Resistance: Prevention and Management, eds. G. W. Bourdot and D. M. Suckling, 207-209. New Zealand Plant Protection Society. Lincoln, New Zealand.

[9] Al-Antary, T.M., Belghasem, I.H. and Araj, S.E.A. (2017) Effect of mint oil against the green peach aphid *Myzus persicae* Sulzer using four solvents (Homoptera: Aphididae). Advances in Environmental Biology. 11(1), 61-67.

[10] Lewis, M. (1997) Altering fate: Why the past does not predict the future. Guilford Press, New York.

[11] Al-Antary, T.M and Khadir, B. (2017) Susceptibility of three strains of green peach aphid *Myzus Persicae* Sulzer (Homoptera: Aphididae) for four pesticides. Advances in Environmental Biology. 11(1), 3399 -3404.

[12] Heathcote, G.D. (1962) The suitability of some plant hosts for the development of the peach-potato aphid, *Myzus persicae* (Sulzer). Entomologia Experimental at Applicata. 5(2), 114-118.

[13] Madanat, H.M., Al-Antary, T.M. and Abu Zarqa, M. (2016) Toxicity of six ethanol plant extracts against the green peach aphid *Myzus persicae*Sulzer (Homoptera: Aphididae). Fresen. Environ. Bull. 25(3), 706-718 .

[14] Kennedy, J.S., Day, M.F. and Eastop, V.F. (1962) A Conspectus of Aphids as Vectors of Plant Viruses. Common Wealth Institute of Entomology, London.

[15] Namba, R. and Sylvester, E.S. (1981) Transmission of cauliflower mosaic virus by the green peach, turnip, cabbage, and pea aphids. Journal of Economic Entomology. 74(5), 546-551.

[16] Crisp, T.M.C., Clegg, E.D., Cooper, R.L., Wood, W.P., Anderson, D.G., Baeteke, K., K.P., Hoffmann, J., Morrow, M., Rodier, D.J., Schaeffer, J.E., Touart, L.W., Zeeman, M.G and Patel, Y.M. (1998) Environmental endocrine disruption: An effects assessment and analysis.Environ Health Perspect. 106(1), 11–56.

[17] Hurley, P.M., Hill, R.N. and Whiting, R.J. (1998) Mode of carcinogenic action of pesticides inducing thyroid follicular cell tumours in rodents. Environ Health Perspect. 106(8), 437-445.

[18] Brouwer, A., Longnecker, M. P., Birnbaum, L. S., Cogliano, J., Kostyniak, P., Moore, J., Schantz, S. and Winneke, G. (1999) Characterization of potential endocrine related health effects at low dose levels of exposure to PCBs. Environ Health Perspect.107(4), 639-449.

[19] Chris, B., Alin, M.P., Christoph, T.Z., Ian, D., Linda, M.F., Stephen, P.F. and Oliver, G. (2014) The evolution of insecticide resistance in the peach potato aphid, *Myzus persicae*. Insect Biochemistry and Molecular Biology. 51(8), 41–51.

[20] Foster, D.R., Clayden, S., Orwig, D.A., Hall, B. and Barry, S. (2002) Oak, chestnut and fire: climatic and cultural controls of long-term forest dynamics in New England. Journal of Biogeography. 29, 1359–1379.

[21] Tako, E., Ferket, P.R. and Uni, Z. (2004) Effects of in ovo feeding of carbohydrates and β-hydroxy-β-methylbutyrate on the development of chicken intestine.Poult Sci. 83(12), 2023–2028.

[22] Gutierrez, J., Barry-Ryan, C. and Bourke, P. (2008) The anti-microbial efficacy of plant essential oil combinations and interactions with food ingredients. Int J Food Microbiol. 124(1), 91–97.

[23] Poiana, M., Attanasio, G., Albanese, D. and Di Matteo, M. (2006) Alcoholic extracts composition from lemon fruits of the Amalfi-Sorrento peninsula. Journal of Essential Oil Research. 18(4), 432-437.

[24] Blackman, R.L. and Eastop, V.F. (1984) Aphids on the World's Crops: An Identification and Information Guide. John Wiley & Sons, Chichester, England.

[25] Finney, D. (1971) Probit analysis. Cambridge University Press., Cambridge, UK. 333pp.
[26] WHO. (1992) Vector Resistance for Pesticides. World Health Organization Technical Report. Geneva. 62pp.
[27] Koul, O., Walia, S. and Dhliwal, G. (2008) Essential oils as green pesticides: potential and constraints. Biopestic. Int. 4(1), 63–84.
[28] Sharaby, A., Montasser, S.A., Mahmoud, Y.A. and Ibrahim, S.A. (2011) Plant extracts as alternative botanical insecticides for control the grasshopper *Heteracris littoralis* Ramb. (Orthoptera: Acrididae) with reference to histological changes on the reproductive system. J. Basic Appl Sci Res. 1(9), 1031–1038.
[29] Siskos, E.P., Konstantopoulou, M.A., Mazomenos, B.E. and Jervis, A.M. (2007) Insecticidal activity of *citrus aurantium* fruit, leaf, and shoot extracts against adult olive fruit flies (Diptera: Tephritidae). J. Economic Entomology. 100(4), 1215-1220.
[30] Cloyd, R.A., Galle, C.L., Keith, S.R., Kalscheur, N.A. and Kemp, K.E. (2009) Effect of commercially available plant-derived essential oil products on arthropod pests. J Econ Entomol. 102(4), 1567–1579.
[31] Regnault-Roger, C., Vincent, C. and Arnason, J.T. (2012) Essential oils in insect control: low-risk products in a high-stakes world.Annu Rev Entomol. 57, 405-424.
[32] Manimaran, A., Mary, M., Cruz, J.J., Muthu, C., Vincent, S. and Ignacimuthu, S. (2012) Larvicidal and knockdown effect of some essential oils against *Culex quinquefasciatue* Say, *Aedes aegypti* (L) and *Anopheles stephensi* (Liston). International Journal of Mosquito Research. 3(3), 06-11.
[33] Raina, A., Bland, J., Doolittle, M., Lax, A., Boopathy, R. and Folkins, M. (2007) Effect of orange oil extract on the Formosan subterranean termite (Isoptera: Rhinotermitidae). Journal of Economic Entomology. 100(3), 880-885.
[34] McLeod, P. (1991) Influence of temperature on translaminar and systemic toxicities of aphicides for green peach aphid (Homoptera: Aphididae) suppression on spinach. Journal of Economic Entomology. 84, 1558-1561.

Received: **05.10.2017**
Accepted: **10.10.2017**

CORRESPONDING AUTHOR

Tawfiq M Al-Antary
School of Agriculture
Department of Plant Protection
University of Jordan
Amman 11942 – Jordan

e-mail: tawfiqalantary@yahoo.com

© by PSP Volume 26 – No. 12A/2017 pages 8304-8315 Fresenius Environmental Bulletin

DETERMINATION OF THE VISUAL PREFERENCE LEVELS AND PERCEPTUAL DIFFERENCES IN THE APPEARANCE OF CERTAIN TAXA IN DIFFERENT SEASONS

Emine Tarakci-Eren*, Tugba Duzenli

Department of Landscape Architecture Karadeniz Technical University, Trabzon, Turkey

ABSTRACT

The most important elements of open spaces are plants. Also plants are important elements perception and preferences of an environment. The plants are divided into two groups based on seed properties: Angiosperms and gymnosperms. In the present study, angiosperm plants were selected. Because angiosperms are more developed when compared to gymnosperms and their seasonal differences are more effective. Angiosperms have seasonal colour, texture, size and form changes. The most distinctive feature of Angiosperms is the differentiated flowers and fruits in different season. The identification of these changes and clarification of the effects on people are quite important for landscape architecture. The aim of the present study is to reveal differences in preference levels and perceptions about certain taxa in Karadeniz Technical University (KTU) campus, located in Trabzon province, based on their seasonal differences. To accomplish this objective, trees that belong to the designated Angiosperm taxa were photographed in different seasons during 2015 and 2016. These photographs were presented to KTU, Landscape Architecture, architecture, interior architecture, forest engineer, city and regional planning students in a survey to determine which appearance of these taxa were liked, i.e. preferred, out of the four seasonal outlooks, and their visual preference levels were determined. Differences in visual perception were attempted to be determined with the semantic differential technique. The results of the semantic differential test were evaluated, and the analysis of the obtained data was interpreted based on the differences in visual perception after the evaluation. As a result of the study, it was observed that different seasonal appearances of certain taxa found on KTU campus affected the preference of the users and there were concurrent perceptual differences.

KEYWORDS:
Semantic differential, Visual preference, Perceptual difference, Taxon, Seasonal appearance, Trabzon-Turkey

INTRODUCTION

The primary goal of landscape architecture is to be able to respond to the physiological, psychological, aesthetic needs and liking of individuals. According to psychology, which seeks to find the underlying causes for the behavior of individuals, these needs and tastes differ between the individuals and communities [1]. Thus, psychology is important for landscape architecture as it is important for all occupational disciplines directly serving people. The traits of an individual such as emotions, age, gender, fears, anxieties, and profession, affect the psychology of the individual, thus influencing the individual's visual perception and preferences [2, 3, 4].

Among the materials used in landscape architecture, plants occupy a special place. Plants play an important role especially in the design of aesthetic and functional spaces. Thus, hard, solid, dull and lifeless aspects of the materials such as stone, wood, concrete, iron, etc. could be rendered more natural and human-friendly through the use of vibrant, nice, soft and warm material such as plants. The plants provide these activities with their dynamism in time and they only grow and develop in a certain period of time and exhibit their own character and provide the fourth dimension to the landscape [5, 6, 7, 8].

Seasonal change of the appearance of angiosperm plants are observed [9, 10, 11]. It has been suggested that seasonal aspects are an important component of landscape perception and aesthetic valuation [11, 12, 13, 14]. However, seasonal landscape changes, e.g. in colours and texture, have rarely been investigated in landscape preference research.

The field in which the plants are mainly scrutinized in landscape design is plant appearance and composition [15, 16, 17, 18]. To create composition, it is necessary to know the relations of the plants with their environment and conditions of coexistence, as well as the structural and visual characteristics of plants [16, 19, 20, 21]. Indeed, plants are elements that grow and develop in a landscape, and assume different appearances in different seasons [22]. There are several different characteristics of plants such as evergreens, deciduous trees,

as well as those that change color in autumn, with influential flowers, with effective tree trunks during the leafless period, and with calligraphic qualities, etc. [23]. Within all these variations, creating a composition using the main principles of plant design could reveal difficult to accomplish but successful landscape work [24]. Using colours is the best way to show the differences in plant compositions depending on seasons because people can mostly realize the differences from the colours [25, 19].

The visual preferences about a landscape are the effect of the landscape and its elements on the observer [26, 27, 28]. In other words, the preference of an element that belongs to to the landscape or the landscape as a whole is an inquiry about how many criteria were met with the element. The landscape, which is described as environment, could be anything from macro scale to micro scale. In other words, the abovementioned environment or landscape may be a city park, and the landscape element may be a plant [29]. Criteria that affect the visual preference are grouped into two; those that affect individuals and the environment. Problems, desires, expectations, needs and perceptual processes are those related to individuals. Formal / aesthetic and functional / functional criteria are those related to the environment. Within the context of the present study, environmental components are the differentiating appearance patterns of certain taxa in the winter, spring, summer and autumn seasons, and perceptual processes are the human components.

How people perceive the aesthetic value of a landscape or plant depends on both physical characteristics of the landscape or plant and the perceptual continuums that those characteristics remind of the observer [30, 31]. The aesthetic evaluation of a landscape or plant is thus consolidated with thoughtsand feelings people affiliate with a landscape [26, 32]. Therefore, socio-demographic variables like age, gender orprofessional background [33, 34, 28].

Semantic difference techniques are often used in visual perception studies [35, 36, 37, 38, 39, 40, 41, 42, 43, 44]. In this study, seasonal changes in plant views were thought to have an important effect on the perceiving of them. Therefore, our aims were; to define effects of seasonal variance on visual preference and perception, to identify which season influence perception of people, to determine which plants is effectual as seasonal changing in planting design.

METHOD

A wide variety of methods have been used to determine the effect of visual perception on individuals' preferences. These methods were based on the assessment of images presented to the participant using identified scales [27, 45, 46, 47, 48]. Photographs and computer simulations were used for visual assessment in various studies [45, 49, 50, 51]. In the present study, photographs of certain taxa taken in winter, spring, summer and autumn seasons were used for the participants to evaluate these. The plants in the campus of KTU, Trabzon were the main material of this study. Thus, it was aimed to determine which of the views that reflect the four seasons are more liked, preferred and thus, to evaluate the level of visual preferences. It was aimed to determine the differences in visual perception using adjective pairs in the semantic differential scale. In Particular, woody plants were selected for taking photos due to the human eye perception grade and above. In plants as a basis, 1 m and 20–30 m lengths were selected for low and high limit, respectively. The Delphi technique is used to obtain systematic expert opinion in scientific research. The photographs were sent to the academicians, specialized in this subject in the Turkish Universities together with the evaluation questionnaire by e-mail. Evaluation questionnaire was prepared as a Word document. In the questionnaire, they were asked to evaluate the photograph groups as follows: inappropriate – appropriate – most appropriate for the subject. In the first stage, 9 out of the 15 specialists responded to the questionnaires. In the second stage, photographs were sent to the specialist group of 10 people for the eliminations and only five of the specialists responded. The photograph groups that were evaluated as appropriate and most appropriate were chosen according to the responses. After this determination, the number of the photograph groups, which was 20, was decreased to 10.

Study Area. Karadeniz Technical University, Kanuni campus, located within the borders of Trabzon province in the Eastern Black Sea region in Turkey, was selected as the research area (40 ° 33'N- 41 ° 07 'N, 37 ° 07' E 40 ° 30 'E). Trabzon, the third largest province in the region, has a population of 250,000 and a surface area of 190 km2. The altitude is 37 m, the annual precipitation is 760 mm and the average temperature is 14.6 ° C. The study area is presented in Figure 1.

One of the reasons for the selection of the KTU campus was the high variety of available plant species. Thus, it was important for the present study to select plant taxa that would demonstrate great structural variations such as fruit, leaf, flower, etc. with the changing seasons. Another reason was the fact that the specialist group with which the questionnaire was conducted was using the campus. It was important that the participants experienced the variations in the seasonal views of the plants that were used in the questionnaire. Trabzon is located in the Colchis section of the Euro-Siberian flora geography region, one of the three flora regions in

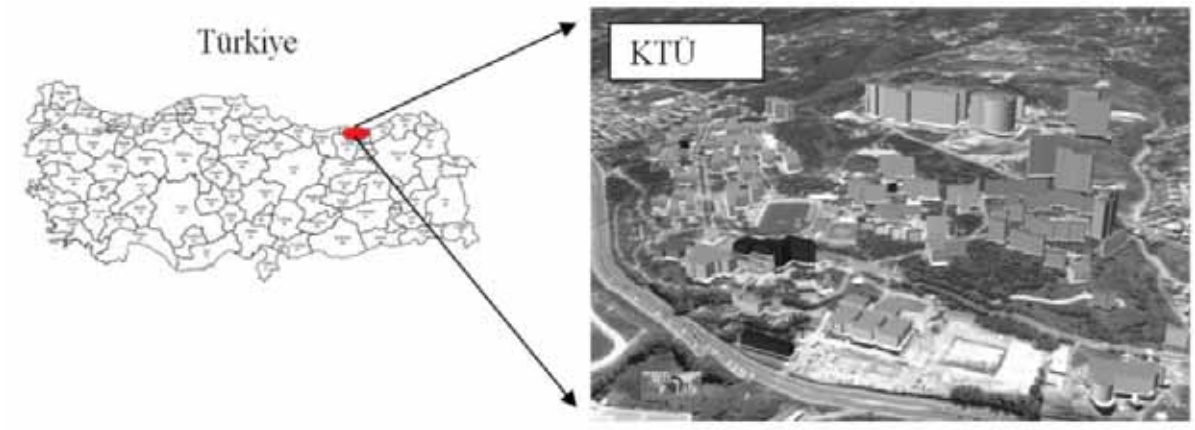


FIGURE 1
Study area KTU Kanuni campus (KTU Gis Lab, 2016)

TABLE 1
Plants that were the subject of visual assessment

	Latin nomenclature	English name
1	Acer buergerianum	Trident maple
2	Acer palmatum	Japanese maple
3	Parthenocissus quinquefolia	Virginia creeper
4	Albizia julibrissin	Persian silk tree
5	Cornus kousa	Korean dogwood
6	Euonymus alatus 'Compactus'	Winged spindle
7	Koelreutaria paniculata	Goldenrain
8	Quercus pontica	Pontine oak
9	Liriodendron tulipifera	Tulip poplar
10	Photinia x fraseri	Red robin

Turkey. Based on the climate and topography, the region has resulted in three prime vegetation types, namely "pseudo-maquis, forest and alpine (high mountain) vegetation" along with a diverse vegetation cover [52].

Photographs. Photographs submitted for the evaluation of the participants in this study included photographs of certain taxa taken in winter, spring, summer and autumn at Kanuni Campus in Karadeniz Technical University. Photos were taken with a digital camera with a resolution of 8 Megapixels. Four similar images of the same tree were taken from the same spot and at the same time of the day in the seasons of winter, spring, summer and autumn.

Selection of plant species. In the present study, broad-leaved trees were used. The species, height and diameters of these trees are shown in Table 1. The reason for the selection of broad-leaved species in the study was the change in their colors forms, flower, fruit, leaf, size and texture throughout the four seasons. Thus, the effects of the visual change that occurred during four seasons were assessed by the participants clearly.

Assessment of photographs. In the study, 40 photographs of 10 plants were evaluated for four different seasons. Photographs were evaluated by 620 KTU landscape architecture, architecture, urban planning, interior architecture and forestry engineering students. The photographs were evaluated with a three-step visual questionnaire. In the first stage, participants were asked to choose the most favorite image among the 40 photographs presented.

To measure perceptual differences in the study, "Semantic Differential" technique was used [54]. According to this technique, eleven opposite adjective pairs were chosen to assess the photographs. The method designed by Summit and Sommer (1999) was used to create and group these pairs in the present study [51]. Based on the abovementioned study, determined pairs of adjectives were *liked / disliked, beautiful / ugly, repellent / attractive, disturbing / relaxing, ineffective / effective*, and in determination of visual perception and quality of the trees, these were *boring / interesting, monotonous / animated, irregular / regular, plain / ostentatious, legible / illegible, and complex / simple*. Evaluators were asked to assign a score of "-2, -1, 0, 1, 2" for each adjective pair related to each. To facilitate the assessment when transferring the questionnaires to the computer environment the scores of "-2, -1, 0, 1, 2" were translated into "1: negative higher, 2: negative lesser, 3: neutral, 4:

positive lesser, 5: positive higher.

The data were analysed using the SPSS (Statistical Package for Social Science) 23.0 statistical package.

At the third and final stage, participants were asked to conduct a general assessment using a 5-point scale (5: best, 1: none) to determine which seasonal view they preferred the most among the images taken in four different seasons, regardless of the plant type.

RESULTS AND DISCUSSION

Demographical characteristics. The survey was conducted with 620 KTU landscape architecture, architecture, interior architecture, forest engineer, city and regional planning students to reveal the differences between the preferences and perceptions of certain taxa due to seasonal changes (Table, 2).

Visual Liking ratios based on seasonal appearance of the taxa. In the present section, four seasonal appearances of the species of *Acer buergerianum, Acer palmatum, Parthenocissus quinquefolia, Albizia julibrissin, Cornus kousa, Euonymus alatus 'Compactus', Koelreutaria paniculata, Quercus pontica, Liriodendron tulipifera* and *Photinia x fraseri* were presented to the participants to determine liking levels for seasonal appearance of plants. As a result, it was determined that the most liked appearances were those taken in the summer for 8 out of 10 plants (Figure 2).

TABLE 2
Demografic structures of participants

		Department							
Demografic Structure		Landscape Architecture	Architecture	Interior architecture	City and regional planning	Forest engineering	Total	$\chi 2$	df
		217	90	125	102	86	620	**64.890[a]**	**3**
Gender	Male	94	38	59	64	42	297		
	Female	123	52	66	38	44	323	**1.090[a]**	**1**
Living Area	City	86	46	56	48	40	276		
	Town	16	4	22	20	9	71	**208.452[b]**	**3**
	Village	115	40	47	34	37	273		

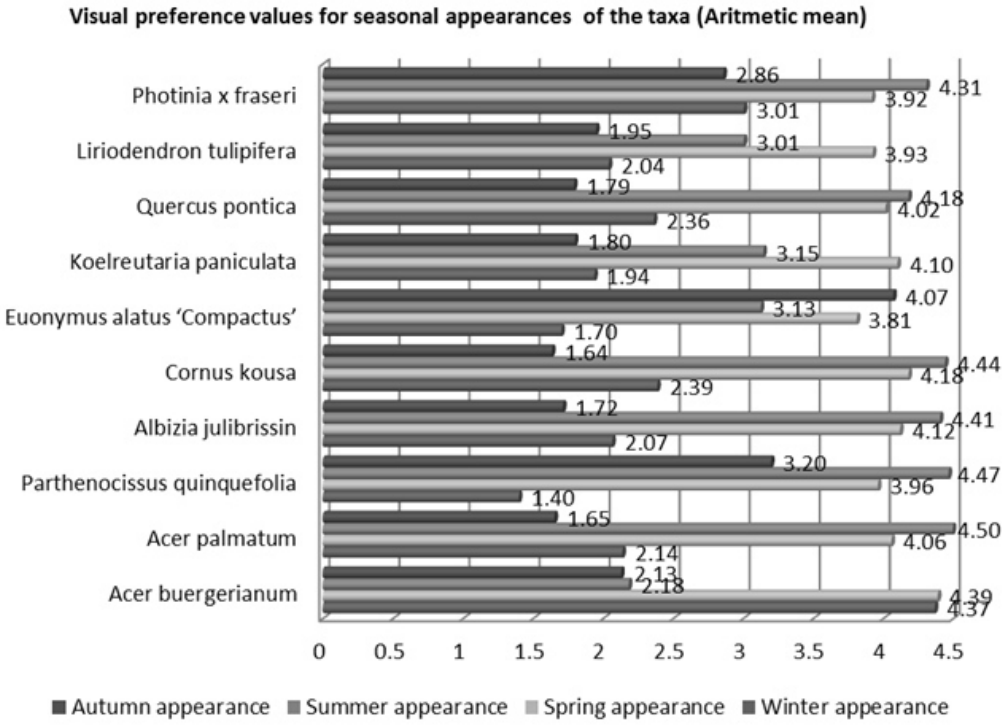


FIGURE 2
Liking levels for the seasonal appearances of the taxa (Arithmetic mean)

TABLE 3
Visual evaluation of plant

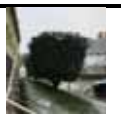
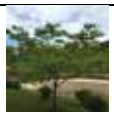
	Acer buergeria num	*Acer palma-tum*	*Parthenoci ssus quinquefol ia*	*Albizia julibrissin*	*Cornus kousa*	*Euonymus alatus 'Compac-tus'*	*Koelreu-taria paniculata*	*Quercus pontica*	*Liriodendr on tulipifera*	*Photinia x fraseri*
Winter										
Spring										
Summer										
Autumn										

TABLE 4
Observed change in plant

No	Plant Name in Latin	Season	Observed changes in plant
1	*Acer buergerianum*	Winter	Leaves, flowers and fruit leaves are fallen.
		Spring	Leaves, flowers and fruit leaves are green.
		Summer	Leaves are orange-red, fruit leaves are brown-like.
		Autumn	Leaves are orange.
2	*Acer palmatum*	Winter	Leaves, flowers and fruit leaves are fallen.
		Spring	The sprouting leaves are light green in spring. Flowers are reddish purple. Fruit leaves are green and red.
		Summer	Leaves and fruit leaves are burgundy-red.
		Autumn	Leaves and fruit leaves are orange.
3	*Parthenocissus quinquefolia*	Winter	Leaves are fallen.
		Spring	Leaves are green.
		Summer	Leaves turn red. Fruits are dark smoke color.
		Autumn	Leaves are orange. Fruits are dark smoke color.
4	*Albizia julibrissin*	Winter	Leaves are fallen.
		Spring	Leaves are green.
		Summer	Leaves are green and flowers are pink.
		Autumn	Leaves turn yellow and are about to fall.
5	*Cornus kousa*	Winter	Leaves are fallen.
		Spring	Leaves are green and flowers are white.
		Summer	Leaves and fruits are red.
		Autumn	Leaves turn yellow and are about to fall.
6	*Euonymus alatus 'Compactus'*	Winter	Leaves are fallen.
		Spring	Leaves are green.
		Summer	Leaves and fruits are red.
		Autumn	Leaves are about to fall.
7	*Koelreutaria paniculata*	Winter	Leaves are fallen.
		Spring	The sprouting leaves are very light green.
		Summer	Leaves are green, flowers are yellow.
		Autumn	Leaves and fruits take on a brown-orange hue.
8	*Quercus pontica*	Winter	Leaves are fallen.
		Spring	Leaves and fruits are green.
		Summer	Leaves and fruits start to turn yellow.
		Autumn	Fruits are brown, leaves are yellow.
9	*Liriodendron tulipifera*	Winter	Leaves are fallen.
		Spring	Leaves are light green. Flowers are green and ineffective.
		Summer	Leaves are green, flowers are at full bloom and green.
		Autumn	Leaves turn yellow and start to fall.
10	*Photinia x fraseri*	Winter	Leaves are green.
		Spring	Leaves are red and green.
		Summer	Leaves are red and flowers are cream colored.
		Autumn	Leaves are green.

TABLE 5
Semantic differential of Plants seasonal appearances

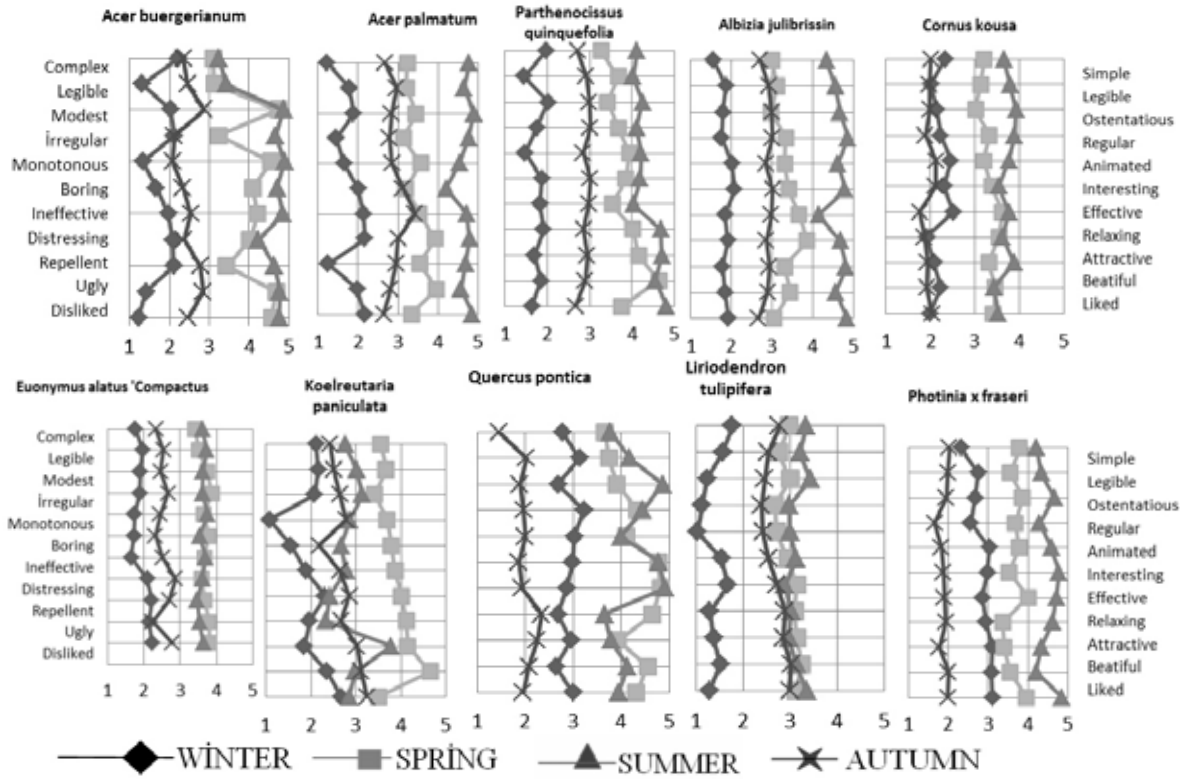


TABLE 6
Variance analysis

		Sum of Squares	df	Mean Square	F	Sig.
Ostentatious	Between Groups	29,480	3	9,827	35,792	,000
	Within Groups	9,884	36	,275		
	Total	39,364	39			
Legible	Between Groups	21,601	3	7,200	32,213	,000
	Within Groups	8,047	36	,224		
	Total	29,648	39			
Simple	Between Groups	20,627	3	6,876	34,279	,000
	Within Groups	7,221	36	,201		
	Total	27,848	39			
Regular	Between Groups	28,329	3	9,443	27,260	,000
	Within Groups	12,471	36	,346		
	Total	40,800	39			
Animated	Between Groups	29,776	3	9,925	27,986	,000
	Within Groups	12,768	36	,355		
	Total	42,544	39			
Interesting	Between Groups	25,944	3	8,648	26,375	,000
	Within Groups	11,804	36	,328		
	Total	37,747	39			
Effective	Between Groups	25,119	3	8,373	23,180	,000
	Within Groups	13,004	36	,361		
	Total	38,123	39			
Relaxing	Between Groups	24,811	3	8,270	26,478	,000
	Within Groups	11,244	36	,312		
	Total	36,055	39			
Attractive	Between Groups	26,284	3	8,761	31,857	,000
	Within Groups	9,901	36	,275		
	Total	36,184	39			
Beatiful	Between Groups	28,243	3	9,414	30,086	,000
	Within Groups	11,265	36	,313		
	Total	39,507	39			
Liked	Between Groups	25,868	3	8,623	21,078	,000
	Within Groups	14,727	36	,409		
	Total	40,594	39			

Differences between the perceptions of the taxa based on seasonal appearances. In this sec-

tion, arithmetic means of adjective pairs were used to evaluate the seasonal appearance of plants based on the perceptual processes of the participants (Table 5).

The *Acer buergerianum* spring appearance received the highest positive value in the "beautiful-ugly" adjective pair. In other words, the most beautiful appearance among the plants was that of the *Acer buergerianum* species in the spring.

The summer image of *Parthenocissus quinquefolia* received the highest positive score for the like-dislike adjective pair. The winter image of the species received the lowest negative score in legible-illiterate adjective pair.

The *Albizia julibrissin* summer appearance received the highest positive value in the "repulsive / attractive" adjective pair. Thus, the most attractive among the plants was *Albizia julibrissin* summer appearance.

The *Euonymus alatus 'Compactus'* winter appearance received the highest negative value in the "effective-ineffective" adjective pair. In other words, the most ineffective appearance among plants was that of the *Euonymus alatus 'Compactus'* in winter.

The *Koelreutaria paniculata* winter appearance received the highest negative value in the "regular-irregular" adjective pair. Thus, the most irregular appearance among the plants was the winter appearance of *Koelreutaria paniculata*.

The *Quercus pontica* summer appearance received the highest positive value in the "effective-ineffective" adjective pair. Thus, the most effective among the plants was the *Quercus pontica* summer appearance. Summer appearances of *Albizia julibrissin* and *Quercus pontica* species received the highest positive values in the boring-interesting adjective pair. Thus, the most interesting appearances among the plants were the summer appearances of *Quercus pontica* and *Albizia julibrissin*.

The *Liriodendron tulipifera* winter appearance received the highest negative value in the "repulsive / attractive" adjective pair. Thus, the most repulsive appearance among the plants was that of the *Liriodendron tulipifera* in winter. The Liriodendron tulipifera winter appearance received the highest negative value in the the distressing-relaxing adjective pair. Thus the most distressing among the plants was the *Liriodendron tulipifera* winter appearance.

The *Photinia x fraseri* summer appearance received the highest positive value in the "liked-disliked" adjective pair. Thus, the most liked appearance among plants was the summer appearance of the *Photinia x fraseri* (Table 5, 6).

The relationships between the seasonal photograph groups and the adjective pairs. In addition, variance analysis was conducted on mean values for the previously determined 11 adjective pairs. The winter, spring, summer and winter appearances of the plants were assigned as variance groups. One of the hypotheses of the study was that 'perceptual differences are the result of the assessment of different seasonal appearances of the plants by the users'. Accordingly, it can be observed that p values (sig) are less than 0.05 in Table 6. In other words, statistical differences between seasonal appearances for all adjective pairs were significant. For each photograph, there was a statistically significant difference for each adjective pair between seasonal groups of users ($p < 0.05$, $N = 620$). The results obtained in the variance analysis are presented in Table 9.

Since the plants selected in this study were particularly broad-leaved plants, the differences in the perceptual processes of the individuals were reflected by the change in the colors of the leaves or defoliation. While the summer appearance of the plants was predominantly preferred, the highest visual quality and perception was associated with the summer appearance of *Acer palmatum*. Because this species has very effective seasonal leaf coloration. Similarly, *Albizia julibrissin* summer appearance had the second highest value. This species has quite effective form, leaf and flower. It has an umbrella-shaped scattered top and gray-brown trunk. Its flowers are pink and very effective in the form of vertical clusters. Its flowers open in June and August. Thus, the summer appearance of this species received the second highest score as a result of the perceptual evaluations of the participants. Following these plants, *Photinia x fraseri,* and *Parthenocissus quinquefolia* summer appearances also scored high assessments in perceptual evaluations. A look at the photo that contains the summer appearance of *Photinia x fraseri* would demonstrate that red leaves and cream-colored flowers provide an effective image. Thus, when the seasonal appearances was examined, the summer appearances received high perceptual values. The abovementioned findings demonstrated that there were perceptual differences between the seasonal appearances of plants. This influences the visual preference (Table 7, 8).

Another result of the study was that the winter appearances of the plants used in the present study were the least preferred and received the lowest scores in the perceptual assessment. *Liriodendron tulipifera* winter appearance was the species that received the lowest values in the assessments. Among the seasonal appearances of the species, the winter appearance was rather weak. Because this species is a high cone-shaped deciduous tree. In the spring, it has green leaves which turn to a dark yellow color in the autumn. Thus, this species received the lowest scores in participant evaluations among the species. When seasonal appearances are considered, it could be observed that the winter appearances received the lowest scores. In general,

winter appearances were less preferred because the winter appearance of plants is leafless and without flowers. They also received lower perceptual evaluations. Several studies demonstrated that the perceptions of individuals affected their experiences [55, 34]. This shows that the fact that our experiences throughout the life affect our visual perceptions is an undeniable fact. Thus, it is necessary to study how the evaluators' experiences lead to changes in the outcome. Furthermore, the examination of the determined visual values of the specified trees would provide more precise information about whether the results obtained in this study could be generalized.

TABLE 7
The arithmetic mean values of responses about adjective pairs for the most favored and preferred seasonal appearances are presented below

	Seasonal appearance of plants	Visual perception											The arithmetic mean of Visual perception
		Liked Disliked	Beautiful Ugly	Repellent Attractive	Distressing Relaxing	Ineffective Effective	Boring Interesting	Monotonous Animated	Irregular Regular	Plain Ostentatious	Legible Illegible	Complex Plain	
1	*Acer buergerianum* spring appearance	4,57	4,68	3,43	4,02	4,21	4,09	4,56	3,24	4,73	3,12	3,10	3,97
2	*Acer palmatum* summer appearance	4,85	4,58	4,69	4,79	4,72	4,21	4,53	4,76	4,89	4,65	4,78	4,67
3	*Parthenocissus quinquefolia* summer appearance	4,81	4,55	4,71	4,68	4,04	4,19	4,21	4,11	4,25	4,02	4,12	4,33
4	*Albizia julibrissin* summer appearance	4,85	4,58	4,82	4,69	4,15	4,79	4,62	4,87	4,67	4,56	4,34	4,63
5	*Cornus kousa* summer appearance	3,52	3,42	3,88	3,61	3,76	3,54	3,76	3,89	3,92	3,79	3,65	3,70
6	*Euonymus alatus* 'Compactus' summer appearance	3,64	3,53	3,47	3,59	3,71	3,52	3,74	3,61	3,62	3,73	3,61	3,61
7	*Koelreutaria paniculata* spring appearance	3,51	4,64	4,15	4,12	4,01	3,86	3,78	3,69	3,42	3,67	3,55	3,85
8	*Quercus pontica* summer appearance	3,95	4,14	3,79	3,66	4,91	4,79	3,99	4,45	4,87	4,18	3,78	4,22
9	*Liriodendron tulipifera* summer appearance	3,35	3,12	2,97	3,01	2,88	3,12	2,99	2,98	3,42	3,21	3,34	3,12
10	*Photinia x fraseri* summer appearance	4,86	4,21	4,34	4,62	4,71	4,78	4,59	4,29	4,67	4,34	4,22	4,51

TABLE 8
The arithmetic mean values of responses to the adjective pairs related to the least favored and least preferred seasonal appearances are as follows

	Seasonal appearance of plants	Visual perception											The arithmetic mean of Visual perception
		Liked Disliked	Beautiful Ugly	Repellent Attractive	Distressing Relaxing	Ineffective Effective	Boring Interesting	Monotonous Animated	Irregular Regular	Plain Ostentatious	Legible Illegible	Complex Plain	
1	*Acer buergerianum* winter appearance	1,23	1,42	2,11	2,09	1,98	1,67	1,34	2,13	2,03	1,32	2,23	1,77
2	*Acer palmatum* winter appearance	2,16	1,98	1,26	2,17	2,13	2,01	1,65	1,46	1,89	1,78	1,23	1,79
3	*Parthenocissus quinquefolia* winter appearance	1,64	1,85	1,69	1,91	1,83	1,87	1,48	1,76	2,02	1,45	1,97	1,77
4	*Albizia julibrissin* winter appearance	1,93	1,73	1,78	1,92	1,84	2,08	2,02	1,67	1,79	1,87	1,56	1,83
5	*Cornus kousa* autumn appearance	2,03	1,92	1,93	1,86	1,76	2,11	2,12	1,89	1,99	1,98	2,01	1,96
6	*Euonymus alatus 'Compactus* winter appearance	2,22	2,14	2,21	2,09	1,65	1,73	1,74	1,88	1,89	1,96	1,77	1,93
7	*Koelreutaria paniculata* winter appearance	2,67	2,36	1,85	1,97	2,32	1,89	1,56	1,09	2,09	2,16	2,12	2
8	*Quercus pontica* autumn appearance	1,96	2,08	2,25	2,34	1,94	1,87	2,01	1,97	1,89	2,03	1,45	1,98
9	*Liriodendron tulipifera* winter appearance	1,27	1,51	1,37	1,29	1,67	1,54	1,02	1,12	1,23	1,56	1,76	1,39
10	*Photinia x fraseri* autumn appearance	1,99	2,01	1,78	1,95	1,91	1,88	1,83	1,67	1,96	1,99	2,03	1,90

TABLE 9
Correlation between the preference for seasonal views and perceptual evaluations.

	1	2	3	4	5	6	7	8	9	10	11
(1)Liked-Dısliked	-	,945**	,906**	,922**	,888**	,892**	,893**	,896**	,909**	,864**	,869**
(2)Beautiful-Ugly		-	,916**	,940**	,929**	,933**	,908**	,914**	,932**	,898**	,907**
(3)Attractive-Repellent			-	,931**	,949**	,948**	,940**	,900**	,909**	,915**	,925**
(4)Relaxing-Dıstressing				-	,945**	,955**	,930**	,925**	,946**	,890**	,889**
(5)Effective-Ineffectıve					-	,966**	,942**	,943**	,924**	,942**	,925**
(6)İnteresting-Borrıng						-	,969**	,936**	,914**	,940**	,926**
(7)Animated- Monot-onous							-	,932**	,882**	,926**	,902**
(8)Regular-Irregular								-	,926**	,945**	,904**
(9)Ostentatious-Modest									-	,930**	,894**
(10)Legıble-İllegible										-	,915**
(11)Simple-Complex Preference	,033	,746**	,795**	,692**	,770**	,710**	,742**	,742**	,733**	,785**	- ,701**

**. Correlation is significant at the 0.01 level (2-taile)

Determination of the correlation between seasonal preference and adjectives. In the final stage, preference scores for seasonal views were evaluated using the 5-point scale, regardless of the plant type. In the photographs, regardless of the species, summer view (4.2 mean) was preferred at the highest level; it was determined that preference levels for autumn (2.8 mean) and spring (3.4 mean) views were moderate and winter (1.9 mean) views were the less preferred images. Correlation analysis was then performed to determine the relationship between preferred seasonal views and adjectives used to describe the photographs (Table 9). Based on the findings, the most effective perceptual characteristics in the preference of seasonal views were "Attractive", "legible" and "effective" adjectives. All perceptive features, except "liked-disliked", were influential in the preference of seasonal views.

DISCUSSION AND CONCLUSION

The present study examined the changes in visual perceptions about certain taxa in the city center of Trabzon due to the seasonal changes. For this purpose, the perceptions of the KTU Landscape Architecture, architecture, interior architecture, city and regional planning and forest engineer students were used. It was considered that their assessments would be more educated since they have knowledge on plant use. However, although there are studies that support this opinion, there are also other that suggest assessments should be conducted by non-experts. Hess and King (2001) argued that expert assessments improved the reliability of their study [56], while Misgav (2000) argued that evaluations by simple users were more realistic [57]. KTU Landscape architecture, architecture, interior architecture, city and regional planning and forest engineer students fit both views since they are both experts and users who live in Trabzon area. In the present study, wide leaf trees with 10 different textures were used. The findings of the present study clearly demonstrated that there were differences between the visual perceptions based on all adjective pairs and groups. This finding supported the fact that selected plants had different compositional values. As shown by Summit and Sommer (1999) in their study, the individual visual values of the plants could be identified using these pairs and groups of adjectives [51]. Summit and Sommer (1999) have shown that *column* and *conical* form plants have superior visual characteristics than others [51]. On the other hand, *scattered* form trees have the lowest visual characteristics. The most effective change that was observed in the present study was the changes that occured in the leaf and flower colors.

As a result, in the present study, the most popular seasonal views were the summer views. When the changes in the summer views of the plants are examined, it was observed that features such as form, branches, leaves, flowers, fruits were very effective in summer views. In the winter months, except the evergreen and partially-evergreen plants completely defoliate. In this season, the only aesthetic feature of the plants is the calligraphy formed by their branches. However, compared to other seasons, the level of appreciation was lower in winter.

The perceptual differences in the seasonal views of plants were determined based on the differences in the mean scores for the adjective pairs for the most favored seasonal view and the least appreciated seasonal view (Tables 5, 6). Accordingly, the most favored season view and least favored season view were interpreted by looking at the difference between the highest mean and the lowest mean scores obtained for the adjective pairs. Ac-

cordingly, the most perceptual difference score was between summer and winter seasons. The highest perceptual difference was found in the *Acer palmatum* taxon, followed by *Albizia julibrissin*. The lowest perceptual difference was found between the winter and fall views. Based on the variance analysis results conducted with the mean scores for 11 adjective pairs, the statistical differences between the seasonal views for all adjective pairs were significant. That is, there was significant differences between the evaluations of the participants for different seasonal views of the plants. In the present study, when the correlation between preferred seasonal views and adjectives used to evaluate these views was investigated, the adjectives "attractive", "legible" and "effective" adjectives were found to be the most effective adjectives. It was determined that all adjective pairs except "liked-disliked" were also effective in the preference of seasonal views.

Ariaza et al. (2004) presented a methodology for assessing the visual quality of agricultural landscapes in a study they conducted on the visual quality of rural landscapes [27]. In the surveys conducted, 16 photographs of the grain and olive farmlands in Andalucía in southern Spain were assessed by 226 participants by stating the most and least liked photographs. As a result, they found that the degree of naturalness increased with the perceived visual quality. Lamb and Purcell investigated the correlation between the perception of naturalness and plant cover in landscapes. Seventy-one different landscapes depicting the vegetation structure were presented to 81 subjects with different socio-demographic traits [58]. The naturalness of the landscapes was analyzed based the vegetation structure classification by Specht. The naturalness classification was determined based on the level of human intervention. The thick and dense vegetation was considered as more natural when compared to shorter and less dense vegetation. Scrubs or dwarf plant cover was considered as less natural by the subjects when compared to other areas. In a study by Lindemann-Matthies et al. (2010) that investigated the effect of agricultural land use with different biodiversity on aesthetic preference of alpine landscapes, the participants were asked to evaluate simulated color photographs of 16 different agricultural areas [59]. They were asked to rank the photographs on a descending order based on their liking. The areas that contained the highest species diversity and were preserved were appreciated the most. It was determined that agricultural areas had a positive effect on aesthetics and tourism. In a Dutch study [60] on beauty assessment of agricultural and nature landscapes, it was found that biodiversity was effective on perceived complexity level and there was a positive correlation between the two [61].

The views of landscapes or the plants vary based on the season [62]. This variation is particularly apparent during harvest times in agricultural areas [12, 13]. Plant taxa views or the views of plant compositions could be observed in different seasons. It was suggested that seasonal variations are a very important component in the perception and aesthetic evaluation of landscapes [63, 13, 14]. Seasonal landscape variations, however, were seldom explored in the landscape preference studies. Hence, the present study is rather significant.

REFERENCES

[1] Gibb, C.L. (2001) An exploratory study of the landscape preferences of normally aging seniors. Graduate Thesis, The University of Guelph, Canada.

[2] Ulrich, R.S. (1983). Aesthetic and Affective Response to Natural Environment. In: Irwin Altman, Joachim F. Wohlwill (Eds.), Behavior and the Natural Environment, Plenum Press, New York, 85-125.

[3] Kaplan, R., Kaplan, S. (1989) The experience of nature: A psychological perspective. CUP Archive.

[4] Ronnberg. L. (1998) Qualrty of Life in Nursing Home Residents: An Intervention Study of the Effect of Mental Stimulation Through an Audiovisual Programme. Age and Aging. 27(3), 393-397.

[5] Acar, C., Demirbaş, E., Dinçer, P., Acar, H. (2003) Anlamsal Farklılaşım Tekniğinin Bitki Kompozisyonu Örneklerinde Değerlendirilmesi. Turkish Journal of Forestry. A(1), 15-28.

[6] Müderrisoğlu, H., Eroğlu, E. (2006) Bazı İbreli Ağaçların Kar Yükü Altında Görsel Algılanmasındaki Farklılıklar. Turkish Journal of Forestry. A (1), 136-146.

[7] Müderrisoğlu, H., Eroğlu, E., Özkan, Ş., Ak, K. (2006) Visual perception of tree forms. Building and Environment. 41(6), 796-806.

[8] Acar, C., Güneroğlu, N.A. (2009) Trabzon Kentindeki Çizgisel Bitki Kompozisyonlarının Tür Çeşitliliği ile İşlevsel ve Görsel Değerleri Üzerine Bir Araştırma. Ekoloji Dergisi. 18(72), 65-73.

[9] Yang, L.H., Rudolf, V.H.W. (2010) Phenology, ontogeny and the effects of climate change on the timing of species interactions. Ecology letters. 13(1), 1-10.

[10] Sparks, T.H., Menzel, A. (2002) Observed changes in seasons: an overview. International Journal of Climatology. 22(14), 1715-1725.

[11] Fry, G., Tveit, M.S., Ode, Å., Velarde, M.D. (2009) The ecology of visual landscapes: Exploring the conceptual common ground of visual and ecological landscape indicators. Ecological indicators. 9(5), 933-947.

[12] Coeterier, J.F. (1996) Dominant attributes in the perception and evaluation of the Dutch landscape. Landscape and urban planning. 34(1), 27-44.
[13] Brassley, P. (1998) On the unrecognized significance of the ephemeral landscape. Land-scape research. 23(2), 119-132.
[14] Stobbelaar, D.J., Hendriks, K. (2007) Seasonality of agricultural landscapes: reading time and place by colours and shapes. In: Seasonal landscapes. Springer Netherlands, 103-126.
[15] Nutt, N., Nurme, S., Hiob, M., Salmistu, S., Kotval, Z. (2013) Restoring Manor Parks: exploring and specifying original design and character through the study of dendrologous plants in estonian historical Manor Parks. Baltic Forestry. 19(2), 280-288.
[16] Bell, S. (2004) Elements of visual design in the landscape.London and New York: Spon Press Taylor & Francis Group. 65.
[17] Altman, I., Wohlwill, J.F. (Eds.) (2012) Behavior and the natural environment (Vol. 6). Springer Science & Business Media.
[18] Nasar, J.L. (1989) Perception, cognition, and evaluation of urban places. In Public places and spaces. Springer US., 31-56.
[19] Robinson, T.L. (2004) Recent advances and future directions in orchard planting systems. In VIII International Symposium on Canopy, Rootstocks and Environmental Physiology in Orchard Systems 732, 367-381.
[20] Bello, F.D., Lavorel, S., Lavergne, S., Albert, C.H., Boulangeat, I., Mazel, F., Thuiller, W. (2013) Hierarchical effects of environmental filters on the functional structure of plant communities: a case study in the French Alps. Ecography. 36(3), 393-402.
[21] Kress, G.R., Van Leeuwen, T. (1996) Reading images: The grammar of visual design. London and New York. Routledge, Taylor & Francis Group Psychology Press. 36.
[22] Grime, J.P., Hillier, S.H. (2000) The contribution of seedling regeneration to the structure and dynamics of plant communities, ecosystems and larger units of the landscape. Seeds. The ecology of regeneration in plant communities, 2nd edn. CABI Publishing, Wallingford. 361-374.
[23] Bernhardt, P. (2003) Wily violets and underground orchids: revelations of a botanist. Chicago: University of Chicago Press. 51.
[24] Gültekin, E. (1990) Bitki Kompozisyonu. ÇÜ Ziraat Fakültesi, Ders Kitabı, (10), 70.
[25] Nelson, K.C., Monroe, M.C., Johnson, J.F., Bowers, A. (2005) Living with fire: homeowner assessment of landscape values and defensible space in Minnesota and Florida, USA. International Journal of Wildland Fire. 13(4), 413-425.
[26] Kahn, P.H. (1999) The human relationship with nature: Development and culture. MIT Press.
[27] Arriaza, M., Cañas-Ortega, J.F., Cañas-Madueño, J.A., Ruiz-Aviles, P. (2004) Assessing the visual quality of rural landscapes. Landscape and urban planning. 69(1), 115-125.
[28] Dramstad, W.E., Tveit, M.S., Fjellstad, W.J., Fry, G.L. (2006) Relationships between visual landscape preferences and map-based indicators of landscape structure. Landscape and urban planning. 78(4), 465-474.
[29] Naveh, Z., and Lieberman, A.S. (2013) Landscape ecology: theory and application. Springer Science & Business Media.
[30] Steffen, W., Sanderson, R.A., Tyson, P.D., Jäger, J., Matson, P.A., Moore III, B., Wasson, R.J. (2006) Global change and the earth system: a planet under pressure. Springer Science & Business Media. 311.
[31] Daniel, T.C. (2001) Whither scenic beauty? Visual landscape quality assessment in the 21st century. Landscape and urban planning. 54(1), 267-281.
[32] Greider, T., Garkovich, L. (1994) Landscapes: The social construction of nature and the environment. Rural sociology. 59(1), 1-24.
[33] Lyons, E. (1983) Demographic correlates of landscape preference. Environment and behavior. 15(4), 487-511.
[34] Strumse, E. (1996) Demographic differences in the visual preferences for agrarian land-scapes in western Norway. Journal of Environmental Psychology. 16(1), 17-31.
[35] Lohse, G.L., Biolsi, K., Walker, N., Rueter, H.H. (1994) A classification of visual representations. Communications of the ACM. 37(12), 36-50.
[36] Litton Jr, R.B. (1979) Descriptive approaches to landscape analysis.
[37] Bruce, V., Green, P.R., Georgeson, M.A. (2003) Visual perception: Physiology, psychology, & ecology. Hove and New York: Taylor & Francis Group Psychology Press. 475.
[38] Kaplan, R. (1979) Visual resources and the public: An empirical approach.
[39] Daniel, T.C., Vining, J. (1983) Methodological issues in the assessment of landscape quality. In Behavior and the natural environment. Springer US., 39-84.
[40] Özgen, Y. (1984) Eastern Black Sea coastal region between the Ordu-Rize road landscape features, reveal landscape architecture in terms of research on the problems and solutions, İ.Ü. Journal of Faculty of Forestry. 34 (2), 20–27
[41] Ulrich, R.S. (1986) Human responses to vegetation and landscapes. Landscape and urban planning. 13, 29-44.

[42] Tahvanainen, L., Tyrväinen, L., Ihalainen, M., Vuorela, N., Kolehmainen, O. (2001) Forest management and public perceptions—visual versus verbal information. Landscape and urban planning. 53(1), 53-70.
[43] Daniel, T.C., Meitner, M.M. (2001) Representational validity of landscape visualizations: the effects of graphical realism on perceived scenic beauty of forest vistas. Journal of Environmental Psychology. 21(1), 61-72.
[44] Müderrisoğlu, H., Eroğlu, E., Özkan, Ş., Ak, K. (2006). Visual perception of tree forms. Building and environment, 41 (6), 796-806.
[45] Sanoff, H. (2016) Visual Research Methods in Design (Routledge Revivals). Routledge.
[46] Shelby, B., Harris, R. (1985) Comparing methods for determining visitor evaluations of ecological impacts: Site visits, photographs, and written descriptions. Journal of leisure research. 17(1), 57-67.
[47] Anderson, L.M. (1981) Land use designations affect perception of scenic beauty in forest landscapes. Forest Science. 27(2), 392-400.
[48] Hull, R.B., Stewart, W.P. (1992) Validity of photo-based scenic beauty judgments. Journal of environmental psychology. 12(2), 101-114.
[49] Habron, D. (1988) Vissual Perception of Wildland in Scotland. Landscape and Urban Planning. 42(1), 45-56.
[50] Tyrväinen, L., Tahvanainen, L. (1999) Using computer graphics for assessing the aesthetic value of large-scale rural landscapes. Scandinavian Journal of Forest Research. 14(3), 282-288.
[51] Summit, J., Sommer, R. (1999) Further studies of preferred tree shapes. Environment and Behavior. 31(4), 550-576.
[52] Anşin, R. (1980) Doğu Karadeniz Bölgesi florası ve asal vejetasyon tiplerinin floristik içerikleri. Doctoral Thesis. Karadeniz Technical University, Faculty of Forestry, Trabzon, 220.
[53] Ktü, Gıs Lab, (2016) Karadeniz Technical University, Geographic Information Systems Laboratory Raports, Trabzon.
[54] Osgood, C.E., May, W.H., Miron, M.S. (1975) Cross-cultural universals of affective meaning (Vol. 1). University of Illinois Press.
[55] Fleischer, A., Tsur, Y. (2000) Measuring the recreational value of agricultural landscape. European review of agricultural economics. 27(3), 385-398.
[56] Hess, G.R., King, T.J. (2002) Planning open spaces for wildlife: I. Selecting focal species using a Delphi survey approach. Landscape and Urban Planning. 58(1), 25-40.
[57] Misgav, A., Amir, S. (2001) Integration of visual quality considerations in development of Israeli vegetation management policy. Environmental Management. 27(6), 845-857.
[58] Lamb, R.J., Purcell, A.T. (1990) Perception of naturalness in landscape and its relationship to vegetation structure. Landscape and Urban Planning. 19(4), 333-352.
[59] Lindemann-Matthies, P., Briegel, R., Schüpbach, B., Junge, X. (2010) Aesthetic preference for a Swiss alpine landscape: The impact of different agricultural land-use with different biodiversity. Landscape and Urban Planning. 98(2), 99-109.
[60] Van den Berg, A.E., Vlek, C.A., Coeterier, J.F. (1998) Group differences in the aesthetic evaluation of nature development plans: a multilevel approach. Journal of environmental psychology. 18(2), 141-157.
[61] Stilma, E.S.C., Smit, A.B., Geerling-Eiff, F.A., Struik, P.C., Vosman, B., Korevaar, H. (2009) Perception of biodiversity in arable production systems in the Netherlands. NJAS-Wageningen Journal of Life Sciences. 56(4), 391-404.
[62] Palang, H., Fry, G., Jauhiainen, J.S., Jones, M., Sooväli, H. (2005) Landscape and seasonality-seasonal landscapes. Landscape Research. 30(2), 165-172.
[63] Hull, R.B., McCarthy, M.M. (1988) Change in the landscape. Landscape and Urban Planning. 15(3-4), 265-278.

Received: **23.06.2017**
Accepted: **01.10.2017**

CORRESPONDING AUTHOR

Emine Tarakci-Eren
Department of Landscape Architecture
Karadeniz Technical University,
Trabzon – Turkey

e-mail: eminemtarakci@gmail.com

© by PSP Volume 26 – No. 12A/2017 pages 8316-8320 Fresenius Environmental Bulletin

ANTIBIOTIC RESISTANCE RATIO OF *ACINETOBACTER BAUMANNII* AGAINST TO TEN ANTIBIOTICS AND MULTIDRUG RESISTANCE INDEX

Nur Ceyhan-Guvensen[1,*], Dilek Keskin[2], Funda Sankur[3]

[1]Mugla Sitki Kocman University, Faculty of Sciences, Department of Biology, Mugla, Turkey
[2]Cine Vocational High School, Adnan Menderes University, Aydin, Turkey
[3]Mugla Sitki Kocman University Research Hospital, Mugla, Turkey

ABSTRACT

To assignation the grade of resistance to the widely used antibiotics in 50 clinical isolates of *Acinetobacter baumannii* were collected from special hospital in Muğla and recorded at specimens. The new BD PHOENIX automated microbiology system (Becton Dickinson Diagnostic Systems, Sparks, Md.) is designed for automated rapid antimicrobial susceptibility testing and identification of clinically relevant bacteria. MIC results previously obtained in recent clinical isolates with well-defined in isolates with well-characterized resistance mechanisms with the microdilution method were re-interpreted for the susceptible, intermediate and resistant categories using the 2012 EUCAST breakpoints. Clinical samples are most commonly isolated from tracheal aspirates, wound site, blood, mucus, abscess, catheter, urine samples, throat and nose cultures. All isolates were defined as Cefoperazone/Sulbactam and Colistin resistant. The resistance rates for Meropenem, Imipenem, Ampicillin/Sulbactam, and Ciprofloxacin were 96%, 96%, 94% and 94% respectively. All of 50 isolates (100%) isolates showed Multiple Antibiotic Resistance (MAR) four to ten antibiotics. These resistance rates are considered indicators of a gradual increase in difficulties treating *Acinetobacter* infections. This would facilitate the active monitoring of resistance frequency and distinguish antibiotic resistance trends and prevalence, all of which would be effective tools in antibiotic treatment programs.

KEYWORDS:
Acinetobacter baumannii, antibiotic resistance, Multiple Antibiotic Resistance (MAR)

INTRODUCTION

Acinetobacter species, non-fermenting gram-negative bacilli that are ubiquitous in the environment, have emerged as important nosocomial pathogens [1]. Resistance to drying and to many commonly used antimicrobial agents are the key factors that enable these organisms to survive and spread in nosocomial environments [2]. Its ability to form biofilm and survive in the environment for extended periods in adverse conditions and in the presence of antibiotics are the factors contributing to its successful colonization in hospital environment and on medical devices [3]. Chromosomally encoded cephalosporinase, high level of efflux pump expression combined with a minimally permeable cell membrane confer intrinsic resistance to several commonly used antimicrobial agents [4]. It can cause different infection such as respiratory tract, bloodstream, urinary tract infections, meningitis, endocarditis, and wound infections [5]. *A. baumannii* often associated with epidemic outbreaks of infections. These infections are becoming harder to treat due to the rising number of nosocomial infections having the ability to resist all antimicrobials in use including Colistin [6]. Several studies also demonstrated in Turkey that *A. baumannii* have a high resistance to most antibiotics [7-12].

The aim of this study was to determine the characteristics and patterns of antibiotic resistance among isolates of *A. baumannii* recovered from clinical specimens in Muğla.

MATERIALS AND METHODS

Bacterial Isolates. Fifty *A. baumannii* were isolated from clinical samples in Muğla. Bacterial isolates were identified to level of species and subspecies by using the morphological and traditional biochemical tests and automatic diagnostic systems currently present in the market and commonly used for AST (Antimicrobial Susceptibility Testing) in clinical laboratories will therefore have to incorporate these criteria in their instruments to meet the needs of European microbiology laboratories according to standard methods [13]. All isolates were obtained from patients at intensive care units. In total, 50 *A. baumannii* were isolated from various clinical samples and detected by the PHOENIX (Becton Dickinson, USA) at the microbiology laboratory of our hospital between from January to December 2015. The PhoenixTM Automated Microbiology

System (BD Diagnostics, Sparks, MD, USA) is designed for the rapid bacterial identification at the species level and determination of AST of clinically significant human bacterial pathogens [14].

Antibiogram Profile of *A. baumannii*. MIC results previously obtained in recent clinical isolates with well-defined in isolates with well-characterized resistance mechanisms with microdilution method were re-interpreted for the susceptible, intermediate and resistant categories using the 2012 EUCAST breakpoints. Ten different antibiotics were used [15].

Multiple Antibiotic Resistance Index (MAR Index). For all isolates, we calculated the MAR index values (a/b, where a represents the number of antibiotics the isolate was resistant to, b represents the total number of antibiotics the isolate tested against). A MAR index value ≥ 0.2 is observed when isolates are exposed to high risk sources of human or animal contamination, where antibiotics use is common; in contrast a MAR index value <or = 0.2 observed when antibiotics are seldom or never used [16, 17].

RESULTS AND DISCUSSION

Nowadays antibiotic resistance of microorganisms is the most important problem in the infectious diseases [18, 19, 20]. *Acinetobacter* infections are isolated from various samples. Acinetobacter infections are most commonly isolated from tracheal aspirates, wound site, blood and urine samples [21]. Aral and his friends reported tracheal aspirate 30%, wound site 29% and blood 25% [22]. Kurtoğlu and his friends have determined tracheal aspirate 42%, wound site 28%, urine 12% and blood 10% [23]. Similarly, in our study, the bacteria was most commonly isolated in tracheal aspirate blood and mucus samples.

The results of the antibiotic susceptibility of the isolates are shown in Table 1. The numbers of isolates are shown in Table 1.

All of the *A. baumannii* strains, 50 (100%) isolates showed Multiple Antibiotic Resistance four to ten antibiotics (Table 2).

TABLE 1
Antibiotic suspectibility pattern of *A. baumannii* isolated from clinical samples.

Antibiotics	Resistance	Intermediate	Sensitive
SCP	50(100%)	0(0%)	0(0%)
CL	50(100%)	0(0%)	0(0%)
MEM	48(96%)	0(0%)	2(4%)
IPM	48(96%)	0(0%)	2(4%)
SAM	47(%94)	1(%2)	2(4%)
CIP	47(%94)	1(%2)	2(4%)
TZP	46(92%)	0(0%)	4(8%)
GM	43(86%)	0(0%)	7(14%)
AN	41(82%)	7(14%)	2(4%)
TGC	0(0%)	6(12%)	44(88%)

Abbreviation; SCP: Cefoperazone/Sulbactam CL: Colistin, MEM: Meropenem, IPM: Imipenem, SAM: Ampicillin/Sulbactam, CIP: Ciprofloxacin, TZP: Piperacillin tazobactam, GM: Gentamicin, AN; Amikacin, TGC: Tigecyline

TABLE 2
Number of clinical samples and Multiple Antibiotic Resistance Index 50 *A. baumannii* strains.

Source of isolates	Number of isolates and Percentage	Multiple Antibiotic Resistance Index (MAR)
Tracheal aspirate	17(34%)	0.7 (3isl), 0.8(13 isl), 1(1isl)
Blood	12(24%)	0.7(4isl), 0,8(6isl) 0,6(1isl) 1(1isl)
Wound	3(6%)	0.8(3isl)
Mucus	6(12%)	0.8(5isl), 1(1isl)
Urine	4(%8)	0,7(1 isl) 0,8(3isl)
Throat Cultures	3(6%)	0,4(1 isl) 0,8(2isl)
Catheter	2(4%)	0.7(1 isl), 0.8(1 isl)
Nose Cultures	1(2%)	0,8(1isl)
Abscess	2(4%)	0,8(1isl) 1(1isl)
Total	50	

Cefoperazone/Sulbactam (SCP) resistance was seen in 100% isolates in our study. Some researchers have reported SCP resistance rate to *A. baumannii* in clinical samples% [12,22, 23]. Our results were similar to El-Kholy et al. (2015) who also reported resistance to SCP was 100% [24].

Our rate of Colistin (CL) resistance was 100%. Dogan and his friends determined a resistance rate of 1.4%[25]. Advance of resistance to CL is probably connected to changes in *A. baumannii* lipopolysaccharide (e.g. acidification, acylation or the existence of intermediary antigens in connecting antibiotic to cell membrane [26].

We found that 96% isolates were resistance to Meropenem (MEM) in our study. Several investigators have informed MEM resistance rate to *A. baumannii* in clinical samples [9, 10, 12, 13, 27, 28]. Our results were similar to Evren and his friends who also reported resistance to MEM was 96% [29].

Our rate of Imipenem (IPM) resistance was 96%. Some scientists have notified IPM resistance rate to *A. baumannii* in different specimens [9, 10, 11, 12, 27, 28, 29, 30]. Similarly, the results of Sanal and Kilic (2014), who also reported resistance to IPM was 94% [31].

The rate of Ampicillin/Sulbactam (SAM) resistance was 94%. The other studies have reported (SAM) resistance rate to *A. baumannii* [10, 11, 27]. The results of Guven and his friends who also declared resistance to Ampicillin/Sulbactam resistance was 95,7% [10].

Ciprofloxacin (CIP) resistance was seen 94%. Several searchers have reported CIP resistance rate to *A. baumannii* in medical specimens [8, 9, 10, 13, 27, 30]. The data of our work were similiar to Guven et al. (2014), who also reported resistance to CIP resistance was 96,2% [10].

Our rate of Piperacillin/Tazobactam (TZP) resistance was 92%. In other studies, it declared TZP resistance rate to *A. baumannii* in clinical samples [10, 11, 12, 27, 28]. Similarly, the data of Direkel and his friens who also reported resistance to TZP was 92,8% [11].

We found that 86% isolates were Gentamycin (GM) resistance to in our study. Some scientists have informed GM resistance rate to *A. baumannii* [10, 11, 12, 27, 28]. The GM resistance rate was also in line with the results from Islamic Republic of Iran and India [29]. Our results were similar to Safari and his friends who also notified resistance to GM was 88% [33].

Amikacin (AN) resistance was seen 82%. Several searchers have reported AN resistance rate to *A. baumannii* in different clinical materials [12, 13, 15-19, 31, 34, 38]. Our results were similar to Safari et al. (2013) who also declared resistance to AN was 84% [33].

The rate of Tigecyline (TGC) resistance was 0%. In other works, it has been reported TGC resistance rate to *A. baumannii* in clinical samples [10, 11, 13, 28]. TGC is effective against *Acinetobacter* sp. [34, 35, 36], but the rates of resistance continue to increase [34].

It is commonly known that MDR (Multidrug Resistance) and PDR (Pan Drug Resistance) strain rates are high in nosocomial *A. baumannii* infections [38]. Some researchers have informed MDR and PDR from 4.7% to 15.5% [39, 40, 41].

CONCLUSION

In conclusion, results of this study demonstrate the need for effective surveillance of antimicrobial resistance in *A. baumannii* in Turkey and suggest that it is essential to use antibiotics with the most caution to prevent the emergence of drug-resistant strains. According to our results, TGC is used for *A. baumannii* infections. Furthermore, these findings indicate that the prevalence of antibiotic-resistant *A. baumannii* is high in Turkey, especially for the antibiotics of choice. This is an emerging concern to public health, particularly in the clinical management of persons with life-threatening *A. baumannii* infections. We strongly suggest the implementation of a countrywide surveillance system.

REFERENCES

[1] Dijkshoorn, L., Nemec, A., Seifert, H. (2007) An increasing threat in hospitals: multidrug-resistant *Acinetobacter baumannii.* Nature Reviews Microbiology. 5, 939–951.

[2] Peleg, A.Y., Seifert, H., Paterson, D.L. (2008) *Acinetobacter baumannii*: emergence of a successful pathogen. Clinical Microbiology Reviews. 21, 538–82.

[3] Pour, N.K., Dusane, D.H., Dhakephalkar, P.K., Zamin, F.R., Zinjarde, S.S., Chopade, B.A. (2011) Biofilm formation by *Acinetobacter baumannii* strains isolated from urinary tract infection and urinary catheters. FEMS Immunology and Medical Microbiology. 62(3), 328-338.

[4] Coyne, S., Courvalin, P., Périchon, B. (2011) Efflux-mediated antibiotic resistance in *Acinetobacter spp.* Antimicrobial Agents and Chemotherapy. 55(3), 947-53

[5] Thom, K., Hsiao, W., Harris, A., Stine, O., Rasko, D., Johnson, J. (2010). Patients with *Acinetobacter baumannii* bloodstream infections are colonized in the gastrointestinal tract with identical strains. American Journal of Infection Control. 38, 751- 753.

[6] Mc Connell, M., Actisand, L., Pachon, J. (2013) *Acinetobacter baumannii*: human infections, factors contributing to pathogenesis and animal models. FEMS Microbiology Reviews. 37, 130-155.

[7] Ece, G., Samlioglu, P., Atalay, S., Kose, S. (2014) Evaluation of the in vitro colistin susceptibility of *Pseudomonas aeruginosa* and *Acinetobacter baumannii* strains at a tertiary care centre in Western Turkey. Le Infezioni in Medici. 1, 36-40.

[8] Celik, C., Gözel, M.G., Dayı, F., Bakıcı, M.Z., Elaldı, N., Gültürk, E. (2014) Increasing antimicrobial resistance in nosocomial pathogens; multidrug-resistant extensively drug-resistant and pandrug-resistant *Acinetobacter baumannii.* Journal of Microbiology and Infectious Diseases. 4(1), 7-12.

[9] Atasoy, A.R., Karakeçe, E., Terzi, H.A., Çiftçi, I.H. (2014) Antibiotic resistance of *Acinetobacter baumannii* strains isolated from clinical samples. J Surg Arts. 7(1), 7-10.

[10] Guven, T., Yilmaz, G., Guner, H.R., Kaya-Kalem, A., Eser, F., Tasyaran, M.A. (2014) Increasing resistance of nosocomial *Acinetobacter baumannii*: are we going to be defeated? Turkish Journal of Medical Science. 44, 73-78.

[11] Direkel, S., Uzunoglu, E., Keles, S., Yapar, K. (2015) Antibiotic resistance rates of *Acinetobacter baumannii* strains isolated from various clinical samples in Giresun, Dr. Atilla Ilhan Ozdemir State Hospital. GMJ. 26, 92-96.

[12] Ahmed, A., Zeb, M., Jilani, M., Tanvir, S.B. (2015) Susceptibility Pattern of *Acinetobacter* Isolates in quantitative tracheal aspirates. European Journal of Biotechnology and Bioscience. 3(8), 22-275.

[13] Macfaddin, J.F. (2000) Biochemical Tests for Identification of Medical Bacteria. 3rd ed. Lippincott Williams and Wilkins, USA.

[14] Holt, J.R., Krieg, N.R., Sneath, H.A., Stanley, J.T., Williams, S.T. (1994) Bergeys Manual of Determinative Bacteriology. (9th ed.), Baltimore; Wiliams and Wilkins, USA. 120-134.

[15] O'Hara, C.M. (2002) Manual and automated instrumentation for identification of *Enterobacteriaceae* and other aerobic gram-negative bacilli. Clinical Microbiology Reviews. 18, 147-162.

[16] Krumperman, P.H. (1985) Multiple antibiotic resistance indexing of *Escherichia coli* to identify high-risk sources of fecal contamination of foods. Applied and Environmental Microbiology. 46, 165–170.

[17] Matyar, F., Kaya, A., Dinçer, S. (2008) Antibacterial agents and heavy metal resistance in Gram-negative bacteria isolated from seawater, shrimp and sediment in Iskenderun Bay, Turkey. Science Total and Environment. 407, 279-285.

[18] Ozcan, B., Esen, M., Coleri, A., Yolcu, H., Caliskan, M. (2009) In vitro antimicrobial and antioxidant activities of various extracts od Salvia microstegia (Boiss.) Et. Bal. From Antakya, Turkey. Fresen. Environ. Bull. 18(5a), 658-662.

[19] Gulhan, T., Boynukara, B., Durmuş, A., Kizirоğlu, I., Sancak, Y.C. (2012) Enteric bacteria and some pathogenic properties of *Enterococcus faecalis*, *Enterococcus faecium* and *Escherichia coli* strains isolated from wild ducks and gulls. Fresen. Environ. Bull. 21(7a), 1966-1971.

[20] Ye, Q., Lu, G., Yan, Z., Liu, J. (2013) In vitro effects of pharmaceuticals on hepatocytes from the Crucian carp, *Carassius auratus*. Fresen. Environ. Bull. 22(10), 2878-2881.

[21] Colpan, A., Güngör, S., Baykam, N., Dokuzoğuz, B. (2002) Investigation of *Acinetobacter* species resistance profile of isolated from intensive care unit. Turkish Journal of Infectious. 16, 5.

[22] Aral, M., Doğan, S., Paköz, N.I.E. (2010) Investigations of antibiotic resistance of *Acinetobacter baumannii* strains isolated from various clinical samples. Ankem Journal. 24, 215.

[23] Kurtoglu, M.G., Opuş, A., Meral, K., Kesli, R., Güzelant, A., Yüksekkaya, S. (2011) Antimicrobial resistance of *Acinetobacter baumannii* strains isolated from clinical samples in an education and research hospital (2008-2010). Ankem Journal. 25, 35-41.

[24] El-Kholy Iman, M.A., Abdo, A., Abdel Aziz, H.M. (2015) High prevalence and multidrug resistance of *Acinetobacter baumannii* among patients after liver transplantation. Issues Bioligal Science and Pharmaceutical Research. 3(7), 71-77.

[25] Dogan, M., Tasbent, F.E., Feyzioglu, B., Baykan, M. (2014) Investigation of colistin, tigecycline and other antibiotic resistance profiles of Acinetobacter species isolated from several clinical specimens. Ankem Journal. 28, 138-143.

[26] Peterson, A., Fesik, S., McGroarty, E. (1987) Decreased binding of antibiotics to lipopolysaccharides from polymyxin-resistant strains of *Escherichia coli and Salmonella typhimurium.* Antimicrobial Agents and Chemotherapy. 31(2), 230-237.

[27] He, R., Luo, B., Hu, C.L.Y., Niu, R. (2014) Differences in distribution and drug sensitivity of pathogens in lower respiratory tract infections between general wards and RICU. J Thorac Dis. 6(10), 1403–1410.

[28] Atasoy, A.R., Karakeçe, E., Terzi, H.A., Çiftçi, I.H. (2014) Antibiotic resistance of *Acinetobacter baumannii* strains isolated from clinical samples. J Surgic Arts. 7(1), 7-10.

[29] Evren, E., Göçmen, S.J., Demirbilek, M., Alışkan, H.E. (2013) Imipenem, meropenem, colistin, amikacin and fosfomycin susceptibilities of multidrug resistant *Acinetobacter baumannii* different clinical isolates. GMJ. 24, 1-4.

[30] Gozutok, F., Sariguzel, F.M., Celik, I., Berk, E., Aydin, B., Güzel D. (2013) Investigation of antimicrobial resistance rates of *Acinetobacter baumannii* strains from nosocomial infections. Ankem Journal. 27, 7-12.

[31] Mughsis, U.A., Farooq, R., Hawashim, N.A., Ahmed, M., Yiannakou, N. (2015) Sensitive, resistant and multi-drug resistant *Acinetobacter baumannii* at Saudi Arabia hospital eastern region. Pakistan Journal of Pharmaceutical Science. 28(3), 825-832.

[32] Yadegarynia, D., Khalili, A.M., Gachkar, L., Rahmati, L.R., Arab-Mazar, Z. (2015) Drug resistance of *Acinetobacter* in selected hospitals. Novel Biomed. 3(3), 103-110.

[33] Safari, M., Saidijam, M., Bahador, A., Jafari, R. (2013) High prevalence of multidrug resistance and metallo-beta-lactamase (MβL) producing *Acinetobacter baumannii* isolated from patients in ICU Wards, Hamadan, Iran. Journal of Research Health Science. 13(2), 162-167.

[34] Sanal, L., Kilic, H. (2014) Antimicrobial resistance of *Acinetobacter baumannii* strains isolated from blood cultures of inpatients in intensive care unit. Mediter Med J. 6(3), 105- 110.

[35] Dong, X., Chen, F., Zhang, Y. Liu, H.,,Liu Y., Ma, L. (2014) In vitro activities of rifampin, colistin, sulbactam and tigecycline tested alone and in combination against extensively drug-resistant *Acinetobacter baumannii*. J Antibiot (Tokyo). 67, 677-680.

[36] Kehl, S.C., Dowzicky, M.J. (2015) Global assessment of antimicrobial susceptibility among Gram-negative organisms collected from pediatric patients between 2004 and 2012: results from the Tigecycline Evaluation and Surveillance Trial. Journal of Clinical Microbiology. 53, 1286-1293.

[37] Deng, M., Zhu, M.H., Li, J.J. (2014) Molecular epidemiology and mechanisms of tigecycline resistance in clinical isolates of *Acinetobacter baumannii* from a Chinese university hospital. Ant*i*microbial Agents and Chemotherapy. 58, 297-303.

[38] Zhang, Y., Chen, F., Sun, E. (2013) In vitro antibacterial activity of combinations of fosfomycin, minocycline and polymyxin B on pan-drug-resistant *Acinetobacter baumannii*. Exp Ther Med. 5, 1737-1739.

[39] Joung, M.K., Kwon, K.J., Kong, C.I. (2010). Impact of in appropriate antimicrobial therapy on outcome in patients with hospital acquired pneumoniae caused by *Acinetobacter baumannii*. Journal of Infectious. 61, 212-218.

[40] Aimsaad, L., Diraphat, P., Utrarachkij, F. (2009) Epidemiological characteristics of *Acinetobacter baumannii* infections at Phramongkutklao Hospital. J Med Assoc Thai. 92, 164- 172.

[41] Eser, Ö.K., Ergin, A., Hasçelik, G. (2009) Antimicrobial resistance and existence of metallo-beta-lactamase in Acinetobacter species isolated from adult patients. Microbiology Bulletin. 43, 383- 390.

Received: **31.05.2017**
Accepted: **29.09.2017**

CORRESPONDING AUTHOR

Nur Ceyhan-Guvensen
Mugla Sitki Kocman University
Faculty of Sciences
Department of Biology
Mugla – Turkey

E-mail: nurceyhan@msn.com

© by PSP Volume 26 – No. 12A/2017 pages 8321-8327 Fresenius Environmental Bulletin

THE SEASONAL VARIATIONS OF HEAVY METAL ACCUMULATION IN THE TENCH (*TINCA TINCA*, L., 1758) AND PIKE (*ESOX LUCIUS*, L., 1758) OF ASARTEPE DAM LAKE, TURKEY

Pınar Karacakaya*, M Borga Ergonul, Sibel Atasagun

Ankara University, Faculty of Science, Department of Biology, Besevler 06100, Ankara, Turkey

ABSTRACT

The concentration of heavy metals (Cd, Cr, Cu, Fe, Mn, Pb, Zn) was determined by ICP-OES) in two fish samples (*Esox lucius*, L., 1758 and *Tinca tinca* L., 1758) in Asartepe Dam Lake which is an important irrigation source. The dam lake is within the Canıllı village boundaries and as a result, the sewage from the village has affected the water quality and aquatic life. This study was investigated during one year study period as seasonally. Seasonal changes in mean and SD values of the tested heavy metals in liver, gill and muscle of *Esox lucius* and *Tinca tinca*. The accumulation orders of heavy metals for pike as follow Zn>Fe>Cu>Mn>Cd>Pb>Cr for summer, for autumn Fe>Zn>Cu>Mn>Cd>Pb>Cr, for winter Fe>Zn>Cu>Mn>Cd>Cr>Pb and for spring Zn>Fe>Cu>Mn>Cd>Pb>Cr. Distribution of heavy metals in tissues for all heavy metals, the lowest accumulation was determined in muscle tissue. Cu and Zn had the highest concentration in gill and Cd, Cr, Fe, Mn and Pb had the highest concentration in liver. The accumulation orders of heavy metals for tench as follows Fe>Cu>Zn>Mn>Pb>Cr>Cd for summer, for autumn Fe>Cu>Zn>Mn>Cd>Cr>Pb, for winter Fe>Cu>Zn>Mn>Cd>Pb>Cr and for spring Fe>Cu>Zn>Pb>Mn>Cr>Cd was determined. Distribution of heavy metals in tissues for all heavy metals, the lowest accumulation was determined in muscle tissue, Mn had the highest concentration in gill and Cd, Cr, Cu, Fe, Pb and Zn had the highest concentration in liver.

KEYWORDS:
Asartepe Dam Lake, Heavy Metal, Seasonal Variation, *Esox lucius, Tinca tinca*

INTRODUCTION

Heavy metals are one of the most important environmental pollutants [1]. They discharged into the aquatic environment from various anthropogenic sources. Their levels have increased day by day, due to domestic, industrial, mining, agricultural activities, etc. Most heavy metals released into the environment find their way into the aquatic phase as a result of direct input and atmospheric deposition [2]. Because of their toxicity, long persistence, bioaccumulation and biomagnification in the food chain, the contamination of fresh water by heavy metals cause to damage of aquatic life [3-4-5]. The aim of this study was to determine the accumulation of heavy metals (Cd, Cr, Cu, Fe, Mn, Pb, Zn) in the water and some tissues of pike (*Esox lucius*, L., 1758) and tench (*Tinca tinca*, L., 1758) of Asartepe Dam Lake, Turkey.

MATERIALS AND METHODS

Study Area. Asartepe Dam Lake (Ankara) was built on Ilhan Stream, a tributary of Kirmir Stream between 1975-1980 for irrigation. The location of Asartepe Dam Lake 40º 08'- 41º 76' N, 32º 23'- 49º 82' E is shown in Fig. 1. The Dam Lake is 825 m above the sea level, maximum depth is 36 m and body filler type is soil. The Dam Lake is within the Canıllı village boundaries because of that the sewage from the village is effect the water quality and aquatic life [6].

Sampling Procedure. Water and fish samples were collected from three different stations of Asartepe Dam Lake between August 2013 and May 2014. Water samples were obtained by means of a Nansen Sampler 0.5 m below the water surface in one-liter bottles precleaned with polyethylene and acidified by adding 0.5% concentrated nitric acid. Also, some physico-chemical parameters (Temperature, pH, EC, DO, Secchi depth) measured in the Asartepe Dam Lake. Fish samples were collected using a standard skimmer at selected stations. Totally 40 fish were collected. The fish samples were held in the bags with ice to the laboratory on the same day and kept at -20 ºC until analyzed.

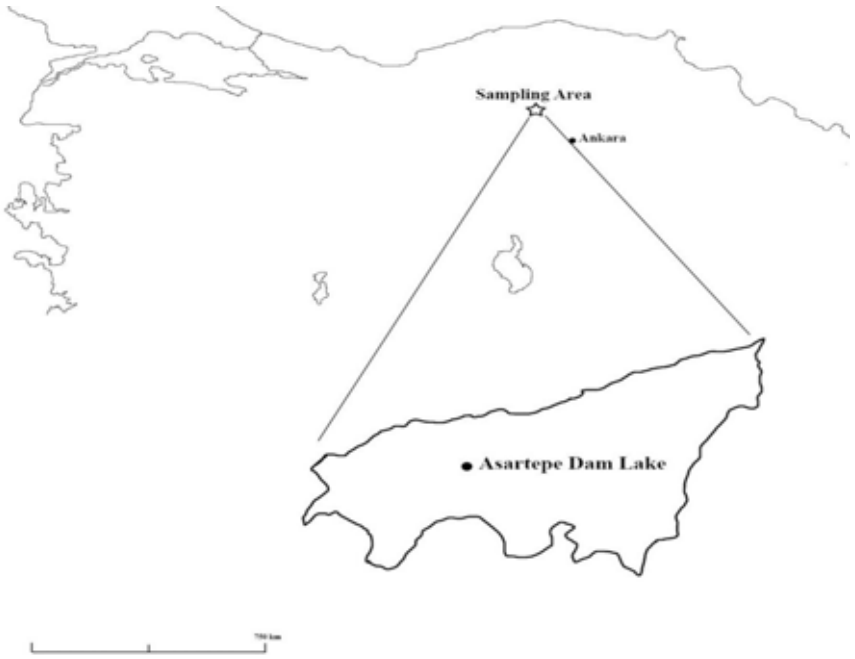


FIGURE 1
The Map of Asartepe Dam Lake (Ankara)

Analysis of Heavy Metals. Fish samples, specimens with total body lengths mean for *Esox lucius* 42.8 cm and for *Tinca tinca* 28.7 cm. Approximately 1 g of muscle, gill and liver tissue samples were recovered from each specimen. Tissue samples were digested with 2mL HNO_3 and 1mL $HClO_4$ at 80ºC for 20 min. Following digestion, samples were resuspended in 5mL distilled water and acidified as above with 65% nitric acid prior to analysis. All measurements were performed in YEBIM (Ankara University, Turkey). Tissue and water samples were analyzed by inductively coupled plasma optical emission spectrometry (ICP-OES). [7-8].

Statistical Analysis. SPSS 23.0 (International Business Machines Corporation, USA) was utilized for statistical analysis. Normality of distribution was evaluated by 'Shapiro–Wilk's and 'Kolmogorov-Smirnov' test. All data is within the normal distribution. Statistical analysis showed that parametric tests were not applicable and Kruskal-Wallis test was used for the investigation of accumulation. (Tests are 95 % confidence interval)

RESULTS AND DISCUSSION

The physico-chemical parameters determined in Asartepe Dam Lake are given in Table 1.

According to these parameters, the temperature varied between 25.6°C and 26.8 °C in the summer, 11.6°C and 12.3°C in the autumn, 5.3°C and 6.4 °C in the winter, 17.0 °C and 17.6°C in the spring; the pH varied between 8.86 and 9.19 in the summer, 8.49 and 9.40 in the autumn, 9.05 and 9.76 in the winter, 9.15 and 9.41 in the spring; the dissolved oxygen between 3.78 mg/L and 6.78 mg/L in the summer, 6.24 mg/L and 12.02 mg/L in the autumn, 10.31 mg/L and 13.56 mg/L in the winter, 10.72 mg/L and 12.34 mg/L in the spring; the electrical conductivity between 378 µS/cm and 395 µS/cm in the summer, 436 µS/cm and 448 µS/cm in the autumn, 466 µS/cm and 481 µS/cm in the winter, 349 µS/cm and 380 µS/cm in the spring; the secchi depth 54 cm and 72 cm in the summer, 32 cm and 86 cm in autumn, 28 cm and 42 cm in the winter, 56 cm and 72 cm in the spring.

The concentrations of heavy metals in the fish samples are given in Table 2 and Table3.

All heavy metal concentrations were determined on a wet weight basis. Seasonal changes in mean and SD values of the tested heavy metals in liver, gill and muscle of *Esox lucius* are shown in Table1. The accumulation orders of heavy metals Zn>Fe>Cu>Mn>Cd>Pb>Cr for summer, for autumn Fe>Zn>Cu>Mn>Cd>Pb>Cr, for winter Fe>Zn>Cu>Mn>Cd>Cr>Pb and for spring Zn>Fe>Cu>Mn>Cd>Pb>Cr. When examined, the seasonal variation changes between *Esox lucius* tissues were statistically variable. For Cd, Cu and Mn, muscle tissues were statistically significant (Kruskal-Wallis test $p<0.05$), gill and liver tissues were statistically not significant (Kruskal-Wallis test $p>0.05$). For Fe and Pb, muscle and liver tissues were statistically significant (Kruskal-Wallis test $p<0.05$), gill tissues were statistically not significant (Kruskal-Wallis test $p>0.05$). For Zn, muscle and gill tissues were statistically significant (Kruskal-Wallis test $p<0.05$), liver tissues were statistically not significant (Kruskal-Wallis test $p>0.05$). For Cr,

TABLE 1
Some physico-chemical parameters of Asartepe Dam Lake

Physico-Chemical Parameters	Summer	Autumn	Winter	Spring
	Min.-Max. Mean±SD	Min.-Max. Mean±SD	Min.-Max. Mean±SD	Min.-Max. Mean±SD
Water Temperature(°C)	25.6-26.8 26.26±0.61	11.1-12.3 11.63±0.61	5.3-6.4 5.96±0.58	17.0-17.6 17.33±0.30
pH	8.86-9.19 9.00±0.16	8.49-9.40 8.90±0.46	9.05-9.76 9.33±0.37	9.15-9.41 9.32±0.14
Dissolved Oxygen (mg/L)	3.78-6.78 4.98±1.58	6.24-12.02 8.98±2.90	10.31-13.56 12.18±1.67	10.72-12.34 11.74±0.89
Electrical Conductivity (µS/cm)	378-395 385±8.88	436-448 442±6.0	466-481 471.33±8.38	349-380 364.66±15.50
Secchi Depth (cm)	54-72 64.66±9.45	32-86 54.66±28.02	28-42 34.66±7.02	56-72 65.33±8.32

TABLE 2
Seasonal changes in heavy metal concentrations in *Esox lucius* tissues (µg/g wet weight)

Species	Season	Tissue	Cd	Cr	Cu	Fe	Mn	Pb	Zn
Esox lucius	Summer	Muscle	0.003±0.001	0.016±0.015	0.811±0.491	0.720±0.555	0.034±0.026	0.008±0.007	0.550±0.132
		Gill	0.017±0.012	0.018±0.011	2.525±1.647	2.814±0.425	0.320±0.146	0.025±0.011	8.405±3.900
		Liver	0.051±0.030	0.030±0.032	1.353±0.889	4.349±2.125	0.369±0.216	0.034±0.028	2.361±1.681
	Autumn	Muscle	0.035±0.002	0.014±0.011	2.189±0.255	3.484±1.992	0.144±0.032	0.012±0.004	1.544±0.564
		Gill	0.035±0.015	0.020±0.007	3.190±1.204	4.771±2.802	0.377±0.117	0.043±0.038	9.732±4.943
		Liver	0.091±0.022	0.047±0.005	2.372±1.146	23.531±14.463	0.382±0.103	0.053±0.028	8.394±4.709
	Winter	Muscle	0.033±0.001	0.023±0.018	1.669±0.789	1.609±0.529	0.063±0.059	0.010±0.002	1.263±0.452
		Gill	0.037±0.005	0.024±0.030	2.099±0.843	10.600±7.412	0.278±0.112	0.018±0.003	19.137±7.904
		Liver	0.115±0.080	0.032±0.028	2.029±1.814	14.282±6.749	0.370±0.307	0.028±0.015	6.163±6.653
	Spring	Muscle	0.035±0.002	0.020±0.009	1.398±0.527	1.481±1.007	0.081±0.064	0.021±0.001	0.854±0.446
		Gill	0.034±0.002	0.030±0.023	4.054±1.318	5.379±1.924	0.226±0.081	0.021±0.001	24.941±8.055
		Liver	0.056±0.009	0.031±0.003	1.719±0.806	15.892±12.495	0.178±0.075	0.007±0.002	6.478±2.773

TABLE 3
Seasonal changes in heavy metal concentrations in *Tinca tinca* tissues (µg/g wet weight)

Species	Season	Tissue	Cd	Cr	Cu	Fe	Mn	Pb	Zn
Tinca tinca	Summer	Muscle	0.009±0.007	0.031±0.005	1.690±0.258	2.055±1.523	0.088±0.081	0.046±0.034	0.982±0.519
		Gill	0.023±0.007	0.035±0.007	2.813±0.41	8.434±2.246	0.438±0.111	0.086±0.021	1.368±0.181
		Liver	0.031±0.006	0.036±0.029	4.588±1.393	12.266±9.029	0.254±0.102	0.108±0.06	1.895±1.009
	Autumn	Muscle	0.033±0.007	0.015±0.002	1.505±0.252	6.170±9.163	0.058±0.011	0.013±0.007	0.908±0.208
		Gill	0.038±0.005	0.026±0.014	1.715±2.224	7.635±6.643	0.589±0.545	0.014±0.003	0.919±0.841
		Liver	0.144±0.109	0.070±0.124	1.959±1.389	27.695±10.213	0.231±0.120	0.064±0.069	1.106±0.462
	Winter	Muscle	0.033±0.001	0.021±0.007	1.563±0.403	1.505±0.990	0.043±0.015	0.018±0.003	0.745±0.100
		Gill	0.039±0.005	0.021±0.003	1.446±0.296	7.173±1.530	0.578±0.209	0.025±0.009	1.247±0.029
		Liver	0.114±0.028	0.046±0.02	1.724±0.417	26.008±7.331	0.233±0.053	0.049±0.015	1.429±0.147
	Spring	Muscle	0.048±0.018	0.103±0.054	1.468±0.138	1.798±1.189	0.025±0.024	0.099±0.008	0.754±0.266
		Gill	0.048±0.017	0.138±0.157	1.502±0.600	15.019±8.942	0.590±0.402	0.300±0.292	1.503±0.347
		Liver	0.152±0.09	0.268±0.257	2.539±0.371	17.063±3.99	0.161±0.141	0.391±0.281	1.876±0.705

all tissues were statistically not significant. Distribution of heavy metals in tissues for all heavy metals, the lowest accumulation was determined in muscle tissue. Cu and Zn had the highest concentration in gill and Cd, Cr, Fe, Mn and Pb had the highest concentration in liver.

Seasonal changes in mean and SD values of the tested heavy metals in liver, gill and muscle *Tinca tinca* are shown in Table 3. The heavy metal accumulation in *Tinca tinca* as follows Fe>Cu>Zn>Mn>Pb>Cr>Cd for summer, for autumn Fe>Cu>>Zn>Mn>Cd>Cr>Pb, for winter Fe>Cu>Zn>Mn>Cd>Pb>Cr and for spring Fe>Cu>Zn>Pb>Mn>Cr>Cd was determined. When examined, the seasonal variation changes between *Tinca tinca* tissues were statistically variable. For Cr and Pb, muscle and gill tissues were statistically significant (Kruskal-Wallis test $p<0.05$), liver tissues were statistically not significant (Kruskal-Wallis test $p>0.05$). For Cu, gill and liver tissues were statistically significant (Kruskal-Wallis test $p<0.05$), muscle tissues were statistically not significant (Kruskal-

Wallis test $p>0.05$). For Fe, liver tissues were statistically significant (Kruskal-Wallis test $p<0.05$), muscle and gill tissues were statistically not significant (Kruskal-Wallis test $p>0.05$). Zn and Mn, for all tissues were statistically not significant ($p>0.05$). For Cd, all tissues were statistically significant (Kruskal-Wallis test $p<0.05$). Distribution of heavy metals in tissues for all heavy metals, the lowest accumulation was determined in muscle tissue, Mn had the highest concentration in gill and Cd, Cr, Cu, Fe, Pb and Zn had the highest concentration in liver.

Copper is an essential trace element, but at high concentrations it can be toxic. For *Esox lucius* the minimum concentration of Cu recorded in summer in the muscle tissue (0.811±0.419). The maximum concentration of Cu recorded in spring in the gill tissue (4.054±1.318). For *Tinca tinca* the minimum concentration of Cu recorded in spring in the muscle tissue (0.468±0.138). The maximum concentration of Cu recorded in summer in the liver tissue (4.588±1.393).

Cadmium is so toxic for all living organisms and it is widely distributed in the earth's crust and is used in many industries and in agriculture. [9]. Fish are very sensitive to cadmium. High amounts of cadmium cause hyperglycemia, cardiovascular disorders and hormonal irregularities [10-11-12]. For *Esox lucius* the minimum concentration of Cd recorded in summer in muscle tissue (0.003±0.001) and the maximum concentration of Cd recorded in winter in the liver tissue (0.115±0.080). For *Tinca tinca* the minimum concentration of Cd recorded in summer in the muscle tissue (0.009±0.007). The maximum concentration of Cd recorded in spring in the liver tissue (0.152±0.090).

Chromium is a naturally occurring compound found in rocks, soil and plants. Chromium has two major forms trivalent and hexavalent. Hexavalent form is very toxic [13-14]. Seasonal variation in the distribution of heavy metals in surface waters from Pulicat lake, Tamil Nadu, India.) for *Esox lucius* the minimum concentration of Cr was recorded in autumn in the muscle tissue (0.014±0.011). The maximum concentration of Cr was recorded in autumn season in the liver tissue (0.047±0.005). For *Tinca tinca* the minimum concentration of Cr was recorded in autumn in the muscle tissue (0.015±0.002) and the maximum concentration of Cr was recorded in spring in the liver tissue (0.268±0.257).

Iron is an important metal for organisms. Iron plays an important role in cellular processes and the absence of iron it is almost not possible to live [15]. but in high concentrations iron can be toxic. Iron toxcity can cause liver and kidney diseases [16-17]. For *Esox lucius* the minimum concentration of Fe was recorded in summer in the muscle tissue (0.720±0.555). The maximum concentration of Fe was recorded in autumn season in the liver tissue (27.695±10.213). For *Tinca tinca* the minimum concentration of Fe was recorded in winter in the muscle tissue (1.505±0.990) and the maximum concentration of Fe was recorded in autumn in the liver tissue (23.531±14.463).

Manganese is toxic when it is in high amount but at low amount it is considered as micro-nutrient [18]. For *Esox lucius* the minimum concentration of Mn was recorded in summer in the muscle tissue (0.034±0.026). The maximum concentration of Mn was recorded in autumn season in the liver tissue (0.382±0.103). For *Tinca tinca* the minimum concentration of Mn was recorded in spring in the muscle tissue (0.025±0.024) and the maximum concentration of Mn was recorded in summer in the gill tissue (0.438±0.111).

Lead is a highly toxic metal substance which cause of adverse health effects in living organisms. [13] For *Esox lucius* the minimum concentration of Pb was recorded in spring in the liver tissue (0.007±0.002). The maximum concentration of Pb was recorded in autumn season in the liver tissue (0.053±0.028). For *Tinca tinca* the minimum concentration of Pb was recorded in autumn in the muscle tissue (0.013±0.007) and the maximum concentration of Pb was recorded in spring in the liver tissue (0.341±0.281).

Zinc is an essential nutrient and has an importance for health but like other metals, it can be toxic in high concentrations. [19]. Zinc toxicity can cause slow reflex, anemia and metabolic effects. [20]. For *Esox lucius* the minimum concentration of Zn was recorded in summer in the muscle tissue (0.555±0.132). The maximum concentration of Zn was recorded in spring season in the gill tissue (24.941±8.055). For *Tinca tinca* the minimum concentration of Zn was recorded in winter in the muscle tissue (0.745±0.100) and the maximum concentration of Zn was recorded in summer in the liver tissue (1.895±1.009).

For both species, the highest concentrations were detected in liver and gills and the lowest concentration was found in the muscles. High concentration of heavy metals in the liver and gills has been notified for a number of fish species. These instances were reported in *Leuciscus cephalus* and *Tinca tinca* from Yeniçağa [5]. and in *Tinca tinca* from Beyşehir Lake [21]. Also in the *Leuciscus cephalus* and *Lepomis gibbosus* from Sarıçay, high concentrations of heavy metals have been notified in the liver and gills [22]. Studies showing that heavy metals accumulated in liver and gills usually at high level and in muscle at low levels. [23-34].

The reason why non-lethal heavy metal accumulation occurs in liver and gills more than the muscles can be explained by the higher metabolic activity of these organs [35-36]. Another explanation for that is muscles do not directly contact with metals [37].

In the study which was made in Işıklı Lake, it was found that the ratio of Fe and Zn in the liver of pike was higher than the other metals. In this study,

Fe and Zn quantity in the pike was generally found high amount. The seasonal heavy metal accumulation was examined of *Tinca tinca* tissues, the highest accumulation was in autumn for Fe in liver while the lowest accumulation was in summer for Cd in muscle tissue.

In fish, different heavy metals are accumulated from different tissues at different rates and it changes according to the species [35-40].

CONCLUSION

In Asartepe Dam Lake, the concentrations of heavy metals in two fish tissue were high, possibly due to direct contamination of the water by metals or the geochemical structures of the basin.

As a result, it would be possible to take necessary steps against to harmful effect of metals to the aquatic system, by assessing the pollution indicator.

ACKNOWLEDGEMENTS

This research was a part of the project financed by the Ankara University, Coordinatorship of Scientific Research Projects 13B4240003

REFERENCES

[1] Schüürmann, G., Markert, B.A. (Eds.) (1998) Ecotoxicology: ecological fundamentals, chemical exposure, and biological effects. New York: Wiley. 900p.

[2] Veena, K.B., Radhakrishnan, C.K., Chacko, J. (1997) Heavy metal induced biochemical effects in an estuarine teleost. Indian J. Mar. Sci. 26, 74-78

[3] Yigit, S., Altindag, A. (2006) Concentration of heavy metals in the food web of Lake Egirdir, Turkey. Journal of environmental biology. 27(3), 475-478.

[4] Malik, N., Biswas, A.K., Qureshi, T.A., Borana, K., Virha, R. (2010) Bioaccumulation of heavy metals in fish tissues of a freshwater lake of Bhopal. Environmental Monitoring and Assessment. 160(1), 267-276.

[5] Saygı, Y., Yiğit, S.A. (2012) Assessment of Metal Concentrations in Two Cyprinid Fish Species (*Leuciscus cephalus* and *Tinca tinca*) Captured from Yeniçağa Lake, Turkey. Bulletin of environmental contamination and toxicology. 89(1), 86-90.

[6] Atici, T., Obali, E.O. (2010) The diatoms of Asartepe Dam Lake (Ankara), with environmental and some physicochemical properties. Turkish Journal of Botany. 34(6), 541-548.

[7] Bernhard, M. (1976) Manual of methods in aquatic environment research, FAO, Fisheries Technical Paper Rome, 58.

[8] Dybern, B.I. (1983) Manuel of methods in aquatic environment research. Analyses of Metals in Fish: FAO Technical paper, p 221

[9] Roberts, J.R. (1999) Metal toxicity in children. Training Manual on Pediatric Environmental Health: Putting it into Practice. Emeryville, CA: Children's Environmental Health Network.

[10] Gill, T.S., Pant, J.C. (1983) Cadmium toxicity: Inducement of changes in blood and tissue metabolites in fish. Toxicology letters. 18(3), 195-200.

[11] Jureša, D., Blanuša, M. (2003) Mercury, arsenic, lead and cadmium in fish and shellfish from the Adriatic Sea. Food Additives & Contaminants. 20(3), 241-246.

[12] Godt, J., Scheidig, F., Grosse-Siestrup, C., Esche, V., Brandenburg, P., Reich, A., Groneberg, D.A. (2006) The toxicity of cadmium and resulting hazards for human health. Journal of occupational medicine and toxicology. 1(1), 22.

[13] Gopinathan, K.M., Amma, R.S. (2006) Bioaccumulation of toxic heavy metals in the edible soft tissues of green mussel (*Perna viridis* L.) of Mahe region. Project report submitted to the Department of Science, Technology and Environment (DSTE), Government of Pondicherry.

[14] Dhinamala, K., Pushpalatha, M., Samuel, T., Raveen, R. (2015) Spatial and temporal variations in the water quality parameters of Pulicat Lake, Tamil Nadu, India. International Journal of Fisheries and Aquatic Studies. 3(2), 255-259.

[15] Jagadevan, S., Jayamurthy, M., Dobson, P., Thompson, I.P. (2012) A novel hybrid nano zerovalent iron initiated oxidation–Biological degradation approach for remediation of recalcitrant waste metalworking fluids. Water research. 46(7), 2395-2404.

[16] Meroño, T., Sorroche, P., Rosso, L.A.G., Casañas, L., Boero, L.E., Arbelbide, J.A., Brites, F.D. (2010) Proatherogenic disturbances in lipoprotein profile, associated enzymes and transfer proteins in women with iron deficiency anemia. Clinical biochemistry. 43(4), 416-423.

[17] Lee, T.W., Kolber, M.R., Fedorak, R.N., van Zanten, S.V. (2012) Iron replacement therapy in inflammatory bowel disease patients with iron deficiency anemia: a systematic review and meta-analysis. Journal of Crohn's and Colitis. 6(3), 267-275.

[18] Osman, A.G., Kloas, W. (2010) Water quality and heavy metal monitoring in water, sediments, and tissues of the African catfish *Clarias gariepinus* (Burchell, 1822) from the river Nile, Egypt. Journal of Environmental Protection. 1(04), 389.

[19] Hotz, C., Lowe, N.M., Araya, M., Brown, K.H. (2003) Assessment of the trace element status of individuals and populations: the example of zinc and copper. The Journal of Nutrition. 133(5), 1563S-1568S.

[20] Klaassen, C.D., Amdur, M.O. (Eds.) (1996) Casarett and Doull's toxicology: the basic science of poisons (Vol. 5). New York: McGraw-Hill.

[21] Tekin-Özan, S., Kir, İ. (2008) Seasonal variations of heavy metals in some organs of carp (*Cyprinus carpio* L., 1758) from Beyşehir Lake (Turkey). Environmental monitoring and assessment. 138(1), 201-206.

[22] Yılmaz, A.B., Doğan, M. (2007) Heavy metals in water and in tissues of Himri (*Carasobarbus luteus*) from Orontes (Asi) River. Environmental Monitoring and Assessment. 144, 437-444.

[23] Kargin, E., Erdem, C. (1992) Bakır-Çinko Etkileşiminde Tilapia nilotica'nın karaciğer, kas ve solungaç dokularındaki Metal Birikimi. Turkish Journal of Zoology. 16, 343-348.

[24] Gümgüm, B., Ünlü, E., Akba, O., Yıldız, A., Namlı, O. (2001) Copper and zinc contamination of the Tigris River (Turkey) and its wetlands. Archiv fūr Naturschutz und Landschaftsforschung. 40, 233-239.

[25] Canli, M., Ay, Ö., Kalay, M. (1998) Levels of Heavy Metals (Cd, Pb, Cu, Cr and Ni) in Tissue of *Cyprinus carpio*, *Barbus capito* and *Chondrostoma regium* from the Seyhan River, Turkey. Turkish Journal of Zoology. 22(2), 149-158.

[26] Karadede, H., Ünlü, E. (2000) Concentrations of some heavy metals in water, sediment and fish species from the Atatürk Dam Lake (Euphrates), Turkey. Chemosphere. 41(9), 1371-1376.

[27] Özkurt, S. (2000) Çatören ve Kunduzlar (Kırka-Eskişehir) Baraj Göletlerindeki Sazanların (*Cyprinus carpio* L., 1758) Dokularında Bor Birikimi. Turkish Journal of Biology. 24, 663-676.

[28] Alam, M.G.M., Tanaka, A., Allinson, G., Laurenson, L.J.B., Stagnitti, F., Snow, E.T. (2002) A comparison of trace element concentrations in cultured and wild carp (*Cyprinus carpio*) of Lake Kasumigaura, Japan. Ecotoxicology and Environmental Safety. 53(3), 348-354.

[29] Cicik, B. (2003) Bakır-çinko etkileşiminin sazan (*Cyprinus carpio* L.)'nın karaciğer, solungaç ve kas dokularındaki metal birikimi üzerine etkileri. Ekoloji. 12(48), 32-36.

[30] Köse, E. (2007) Enne Barajı'nda yaşayan balıklarda ağır metal birikiminin araştırılması (in Turkish). Master Thesis, Dumlupınar University, Institute of Science, Kutahya (Turkey). p. 50-70.

[31] Köse, E., Uysal, K. (2008) Cinsi Olgunluğa Erişmemiş Pullu Sazan (*Cyprinus carpio* L., 1758)'Larin Kas, Deri Ve Solungaçlarindaki Ağir Metal Akümülasyon Oranlarının Karşılaştırılması (in Turkish). Dumlupınar University, Institue of Science Journal. 17, 19-26.

[32] Tekin-Özan, S., Kir, İ. (2007) Accumulation of some heavy metals in *Raphidascaris acus* (Bloch, 1779) and its host (*Esox lucius* L., 1758). Türkiye Parazitoloji Dergisi. 31(4), 327-329.

[33] Türkoğlu, M. (2008) Van Gölünden alınan su, sediment ve İnci Kefali (*Chalcalburnus tarichi*, Pallas, 1811) örneklerinde bazı ağır metal düzeylerinin araştırılması (in Turkish). Master Thesis, Yüzüncü Yıl University, Institute of Science, Van (Turkey). p. 59-60.

[34] Alhas, E., Oymak, S.A., Akin, H.K. (2009) Heavy metal concentrations in two barb, *Barbus xanthopterus* and *Barbus rajanorum mystaceus* from Atatürk Dam Lake, Turkey. Environmental Monitoring and Assessment. 148(1-4), 11-18.

[35] Karadede, H. (1997) Atatürk Baraj Gölü'nde su, sediment ve balık türlerinde ağır metal birikiminin araştırılması (in Turkish). Master Thesis, Dicle University, Institute of Science, Diyarbakır (Turkey). p. 72.

[36] Yang, R., Yao, T., Xu, B., Jiang, G., Xin, X. (2007) Accumulation features of organochlorine pesticides and heavy metals in fish from high mountain lakes and Lhasa River in the Tibetan Plateau. Environment International. 33(2), 151-156.

[37] Uysal, K., Köse, E., Bülbül, M., Dönmez, M., Erdoğan, Y., Koyun, M., Özmal, F. (2009) The comparison of heavy metal accumulation ratios of some fish species in Enne Dame Lake (Kütahya/Turkey). Environmental Monitoring and Assessment. 157(1), 355-362.

[38] Singh, K.P., Mohan, D., Singh, V.K., Malik, A. (2005) Studies on distribution and fractionation of heavy metals in Gomti river sediments—a tributary of the Ganges, India. Journal of Hydrology. 312(1), 14-27.

[39] Erdoğrul, Ö., Ateş, D.A. (2006) Determination of cadmium and copper in fish samples from Sir and Menzelet Dam Lake Kahramanmaraş, Turkey. Environmental monitoring and assessment. 117(1), 281-290.

[40] Tekin-Özan, S. (2008) Determination of heavy metal levels in water, sediment and tissues of tench (*Tinca tinca* L., 1758) from Beyşehir Lake (Turkey). Environmental Monitoring and Assessment. 145(1), 295-30.

Received: **21.06.2017**
Accepted: **23.09.2017**

CORRESPONDING AUTHOR

Pinar Karacakaya
Biology Department,
Faculty of Science,
Ankara University,
Beşevler 06100, Ankara – Turkey

e-mail: pinarkaracakaya@gmail.com

© by PSP Volume 26 – No. 12A/2017 pages 8328-8336 Fresenius Environmental Bulletin

THE IMPACTS OF THE BIOCHAR ADDITION IN DIFFERENT DOSES ON YIELD AND NUTRIENT UPTAKE OF THE CHICKPEA PLANT (CICER *ARIETINUM* L.) UNDER THE CONDITIONS WITH AND WITHOUT INCUBATION

Ahmet Demirbas[1,*], Tolga Karakoy[1], Hasan Durukan[1], Halil Erdem[2]

[1]Cumhuriyet University, Vocational School of Sivas, Department of Crop and Animal Production, Sivas, Turkey
[2]Gaziosmanpasa University, Faculty of Agriculture, Soil Science and Plant Nutrition Department, 60240 Tokat, Turkey

ABSTRACT

Biochar which is intensively used in the issue of the struggle against global warming in recent years also enhances the physical, chemical and biological properties of the soil when it is added to the soil. With this study; the impact of the biochar applications (0%, 0.5%, 1%, 2%, 3%, 4% and 5% (v/v)) in different doses under the conditions with and without incubation on the yield of the chickpea plant and nutrient concentrations has been examined. The study has been carried out with three repetitions according to the experimental pattern of randomized blocks in the plastic pots with the capacity of 3 kg under the greenhouse conditions. The addition of biochar was made 60 days before the plantation of the herbs to the pots with incubation and watering has been made with pure water for 60 days. The dry matter production and nutrient concentrations have been determined in the plants harvested in the broad bean bonding period. The results of the study have shown that the application that increases the dry matter production of the chickpea plant most is the application of 3% biochar dose under the conditions with incubation (10.02 g pot^{-1}). In addition; the biochar applications have decreased the uptake of other nutrient except for K and Zn under both the conditions with and without incubation. While 3% biochar application under the conditions with incubation and 4% biochar application without incubation have been the applications having the most significant impact on the Zn concentration of the chickpea plant respectively with 67.2 mg Zn kg^{-1} and 60.5 mg Zn kg^{-1}, 2% biochar application has been the application which has had the most significant impact on the K concentration of the chickpea with respectively 2.81% K and 2.37% K under the conditions both with and without incubation. In addition; when the general averages in the study have been assessed, it has been determined that the biochar applications have more impact on the dry matter production of the chickpea plant and the concentrations of N, P, K, Zn and Mn according to the conditions without incubation.

KEYWORDS:
Biochar, chickpea, macro-element, micro-element, incubation.

INTRODUCTION

Chickpea is the *Cicer arietinum* L. from Cicer genus bound to the subfamily of Viceae which includes the most important species of Papilionacea (butterfly flowered ones) family taking place in Leguminosae kind [1]. It is the third edible legume which is grown most after bean and pea in the world [2].

Biochar is an organic substance rich in carbon attained by pyrolyzing of the plant and animal-based biomasses in an environment with no or little oxygen [3]. The similar and superior properties of biochar when compared to other organic materials are its physical and chemical properties such as high load intensity [4] and high nutrient uptake capacity depending on this [5] and its resistance [6] to microbial degradation due to its specific chemical [7] and colloidal structure when compared to other organic materials. There are many data in the literature as to the fact that it could remain for centuries without any degradation in the soil due to the resistance of biochar rich in carbon against microbial degradation [8].

The process of pyrolysis used while giving the definition of biochar is called as the event of the burning of the organic substance in high temperatures in the oxygen-free environments [9]. The nutrient element content of biochar attained as a result of the pyrolysis of the organic material is dependent on the composition of the organic material [10,11], content of humidity [12], the conditions in which the process of pyrolysis has been conducted [13] and the conditions to which the product attained as a result of pyrolysis has been subjected [14]. The application of biochar to the soil has shown positive impacts in terms of the fertility of the soil and product [15, 16], because biochar improves the change of the soil nutrient, capacity of the uptake of organic carbon and water and the physico-chemical properties of the soil infiltration [17]. Alaboz et al [18] also indicated that the biochar doses and incubation time significantly

effective on field capacity of the soil.

The special purpose of the application of biochar to the soil is to increase its biochemical and agricultural quality [19, 20, 21, 22, 23, 24, 25, 26, 27, 28, 29, 30, 31] and the storage of carbon [32]. The use of biochar could be an efficient tool for the long-term sustainable agriculture by increasing the storage of carbon in the soil (C decreasing strategy), fertility and productivity (soil quality) and by decreasing the greenhouse gas emissions [33].

The addition of biochar to the soil ensures the regeneration of most of the nutrient terminated by the plants due to their property of intaking the nutrient and humidity. Due to the high surface area and high surface load intensity [4], biochar increases the ability of the soils to protect their nutrient and humidity and decreases the leaching of the nutrient and agricultural chemicals [26, 34, 35, 36].

As aforementioned; the addition of biochar to the soil provides many benefits, but there is little information about the interaction of the biochar-plant-nutrient [37]. In this study; it has been aimed to determine the impacts of the biochar applications in different doses on the yield of the incubated and non-incubated chickpea plant and the concentrations of the macro and micro nutrient.

MATERIALS AND METHODS

The study has been conducted with three repetitions according to the experiment pattern of randomized blocks in the greenhouses of Cumhuriyet University, Vocational School of Sivas, Department of Crop and Animal Production. 2 mm sieved air dry 3 kg soil has been put in each pot. Some physical and chemical properties belonging to the test soil are given in Table 1. The soil used in the study is silty clayed loam, light alkaline (pH 7.28), with so much lime (19.6%), saltless (0.033%) and its useful phosphor concentration is low (34.0 kg P_2O_5 ha^{-1}). In the study; 50 mg kg^{-1} N (in $CaNO_3.4H_2O$ form), 100 mg kg^{-1} P and 125 mg kg^{-1} K (in KH_2PO_4 form), 2.5 mg kg^{-1} Zn (in $ZnSO_4.7H_2O$ form) and 2.5 mg kg^{-1} Fe (in Fe-EDTA form) has been applied to each pot as the basic fertilization. 7 different doses of the biochar attained from rosehip seed has been applied in the study. The doses of biochar has been applied as 0% (control), 0.5% (15 g pot^{-1}), 1% (30 g pot^{-1}), 2% (60 g pot^{-1}), 3% (90 g pot^{-1}), 4% (120 g pot^{-1}) and 5% (150 g pot^{-1}). Experiment has been established as incubated and non-incubated and watering has been made to the incubated pots for 60 days with pure water after the addition of biochar before the plantation. Hasanbey has been used as the chickpea species in the study, 5 seeds have been planted to each pot at the beginning and the number of the plants has been thinned down to 2 after germination. The chickpea has been harvested in the broad bean bonding period (when the plants are 60 days old) and the dry weight has been determined by firstly washing the leaf samples with tap water, then HCl of 0.1% and then tap water again and pure water for 2 times and by drying them for 48 hours at 65 °C until they have a stable weight [38] and after that, they have been grinded.

TABLE 1
Physical and chemical properties of experimental soil

Soil Property	Depth (0-30cm)
pH	7.28
Lime (%)	19.6
Salt (%)	0.033
Organic matter (%)	1.71
Texture	SiCL
Available P (kg ha^{-1})	34.0
Available K (kg ha^{-1})	635.5
Available Fe (mg kg^{-1})	3.99
Available Mn (mg kg^{-1})	2.91
Available Zn (mg kg^{-1})	0.42
Available Cu (mg kg^{-1})	1.23

TABLE 2
Physical and chemical properties of the biochar

Biochar Yield %	32.65
Field Capacity %	17.41
Wilting Point %	16.29
Cation Exchange Capacity cmol kg^{-1}	6.08
Specific Surface Area m^2 g^{-1}	278.03
Carbon %	87.18
Nitrogen %	1.01
C/N	86.31
pH	8.46
EC mS cm^{-1}	1.73
P g kg^{-1}	3.61
K g kg^{-1}	1.56
Ca g kg^{-1}	10.53
Mg g kg^{-1}	3.64
Fe mg kg^{-1}	593.5
Zm mg kg^{-1}	47.9
Mn mg kg^{-1}	51.4
Cu mg kg^{-1}	15.4

The Production of Biochar. The seed of rosehip (Rosa canina) taking place in Sivas region in a wide area and consumed as marmelade has been used as the biochar material. Biochars have been produced by slow pyrolysis of feedstocks at 500°C in an ingeniously developed reactor. Thus; biochars have been grinded to maximum size 2 mm before mixing to soil. Slow pyrolysis process has been characterized by slow heating rates (a rate of approximately 10°C min^{-1}) and long residence times of biomass. The pyrolysis temperature has been kept constant at 500°C and biochar has been held in the unit until pyrolysis gas has disappeared. After heating for almost 4 to 6 hours, the biochars have been allowed to cool to room temperature [39].

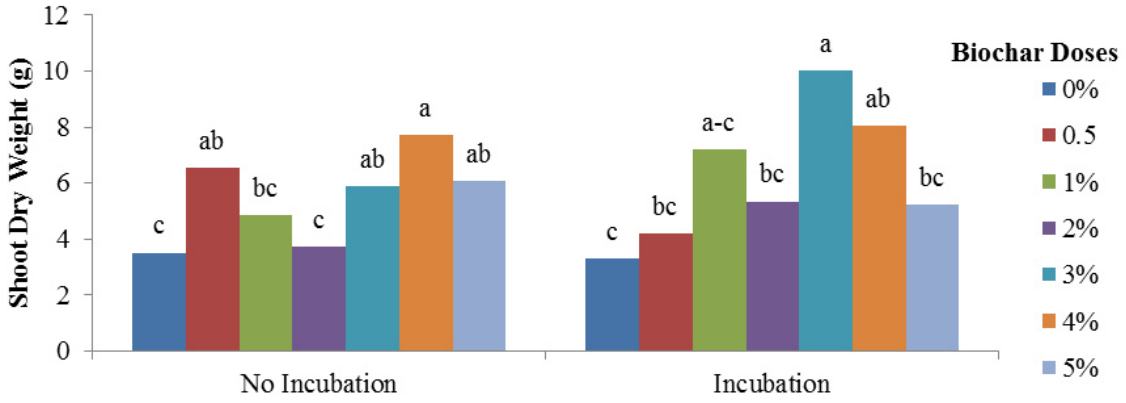


FIGURE 1
Effects of biochar application on shoot dry matter of chickpea plant

Some physical and chemical properties of the produced biochar have been determined and are given in Table 2. pH of biochar is 8.46, cation change capacity is 6.08 cmol kg^{-1}, specific surface area is 278.03 m^2 g^{-1}, carbon and nitrogen concentration is respectively 87.18% and 1.01, C/N ratio is 86.31, electrical conductivity is 1.73 mS cm^{-1}, P, K, Ca and Mg are respectively 3.61, 1.56, 10.53 and 3.64 g kg^{-1}.

Macro-Micro Nutrients Analysis. Harvested plants have been ashed in a microwave oven by using 2 ml of 35% H_2O_2 and 5 ml of 65% HNO_3. Following the digestions P concentration has been colorimetrically measured at 882 nm in a spectrophotometer [40] and K, Fe, Zn, Cu and Mn have been analyzed by using an inductively coupled plasma optical emission (ICP-OES; Thermo ICAP7000) spectrometer [41]. Total nitrogen was measured by Kjeldahl method [42].

Statistical Analyses. The data attained as a result of the study have been subjected to ANOVA variance analysis with the use of SPSS 22.0 for Windows package program. The smallest differences between the applications have been determined in a way that they will be <P0.05 with Tukey test.

RESULTS AND DISCUSSION

Shoot dry matter yield. In the study; the impacts of biochar applications in different doses on the shoot dry matter production of chickpea plant grown in incubated and non-incubated environment have been examined and given in Figure 1.

Dry matter production has changed between 3.51-7.70 g $plant^{-1}$ in the chickpea plant grown under the incubation conditions. While the highest dry matter production has been determined in 4% biochar application with 7.70 g $plant^{-1}$, the lowest dry matter production has been determined in 0% biochar dose being the control application (3.51 g $plant^{-1}$). Dry matter production has changed between 3.30-10.02 g $plant^{-1}$ in the chickpea plant grown under the conditions without incubation. While the highest dry matter production has been determined in 3% biochar application with 10.02 g $plant^{-1}$, the lowest dry matter production has been determined in 0% biochar dose being the control application (3.30 g $plant^{-1}$). It has been determined that there is a statistical difference when the average dry matter productions of the chickpea plant grown under the conditions with and without incubation. While the dry matter production is 6.19 g $plant^{-1}$ in the chickpea plant grown in incubated environment, it has been seen that this value is 5.49 g $plant^{-1}$ in the chickpea plant grown in non-incubated environment (Figure 1). When Erdem et al. [39] have applied the biochar produced from mahleb to the tobacco plant grown in Cd contaminated soil, they have specified that biochar application generally increases the dry matter production of the tobacco plant and the highest dry matter production is in 2% biochar dose with 3.15 g $plant^{-1}$. Biederman et al [43] have reported that biochar made of oak plant increases the yield of the plants by 5.2%. Similarly; Arif et al [44] have reported that 5-tons biochar application per decare has increased the yield of bean plant under the field conditions in Pakistan.

Shoot N, P and K concentrations. The results of the study have shown that biochar applications do not have any impact on the nitrogen concentration of the chickpea plant grown in the environments both with and without incubation (Table 3). The highest N concentration of the chickpea plant has been attained at 0% dose of biochar under both incubated (1.68% N) and non-incubated (1.72% N) conditions with biochar applications.

It has been observed that there has been a decrease in the nitrogen concentrations of chickpea plant with the increasing biochar applications under non-incubated conditions. Similarly; it has been detected that nitrogen concentration decreases with the biochar application (0%, 1%, 2% and 3%) in increasing doses for the tobacco plant grown in Cd contaminated soils [39]. In another conducted study; the

TABLE 3
Effects of biochar application on N, P and K concentrations of chickpea plant

	Biochar Doses %	N		P %		K	
	0	1.68	±0.01a	0.25	±0.01a	2.11	±0.07bc
	0.5	1.09	±0.11d	0.23	±0.03ab	2.13	±0.16bc
Incubation	1	1.35	±0.09c	0.20	±0.01bc	1.91	±0.43c
	2	1.44	±0.05bc	0.22	±0.00a-c	2.81	±0.02a
	3	1.11	±0.01d	0.22	±0.04a-c	2.37	±0.02b
	4	1.36	±0.13c	0.14	±0.02d	2.08	±0.04bc
	5	1.57	±0.00ab	0.19	±0.02c	2.12	±0.24bc
	Mean	**1.37A**		**0.21A**		**2.22A**	
	0	1.72	±0.11a	0.22	±0.00a	1.45	±0.58cd
	0.5	1.61	±0.35ab	0.20	±0.02a	2.26	±0.14ab
	1	1.35	±0.30a-c	0.16	±0.02c	1.62	±0.10cd
Non-incubation	2	1.15	±0.14bc	0.21	±0.04a	2.37	±0.06a
	3	1.12	±0.02bc	0.16	±0.00c	1.79	±0.01bc
	4	1.12	±0.09bc	0.16	±0.00bc	1.20	±0.01d
	5	1.10	±0.46c	0.20	±0.01ab	1.64	±0.39cd
	Mean	**1.31B**		**0.19 B**		**1.77B**	

P<0.05

application of rice husk biochar has caused to the decrease in the nitrogen concentration of lettuce plant and the increasing biochar applications have decreased the growth of the plant [45]. As in the nitrogen concentrations of chickpea plant; it has been observed that the highest shoot phosphor concentration is in the control applications both under incubated (0.25% P) and non-incubated (0.22% P) conditions. The reason for this may stem from the biochar to bond some essential nutrient on their surfaces and decrease the bio-usefulness [46]. Similarly; Liu et al [47] have specified that biochar made of woody material decreases the P and N uptake of the potato plant and it may release phytotoxin. When the shoot potassium concentrations of the plants have been considered, it has been observed that both incubated (2.81% K) and non-incubated (2.37%) conditions have the highest K concentration at 2% biochar dose. Puga et al [48] have applied the biochar attained from sugar cane straw to Jack bean (*Canavalia ensiformis*) and *Mucuna aterrima* plants and they have attained similar results. They have expressed that K concentration being respectively 27 mg kg^{-1} and 39 mg kg^{-1} in the control applications of Jack bean (*Canavalia ensiformis*) and *Mucuna aterrima* plants has increased to respectively 312 mg kg^{-1} and 382 mg kg^{-1} at 5% dose of biochar. Rees et al [49] have taken soil from two different depths in Cd, Pb and Zn contaminated soils and they have expressed that Ca and Na concentration have decreased generally with the increasing biochar addition in the root and shoot in *L. perrenne*, K concentration has increased in *L. perrenne* grown in soil A and P concentration has decreased with biochar doses in the shoot. When the average nitrogen, phosphor and potassium concentrations have been examined, it has been detected that incubated chickpea plant is statistically much more important with its respectively 1.37% N, 0.21% P and 2.22% K content than non-incubated chickpea plant.

Shoot microemelent concentrations. In Table 4; the impacts of biochar applications in different doses on Fe, Zn, Cu and Mn concentrations of chickpea plant grown in incubated and non-incubated environment are given. According to the results; Fe results show great similarity with the results of N and P. It has been observed that the concentration of Fe plant has changed between 139.3 mg kg^{-1} and 260.6 mg kg^{-1}. It has been seen that control plants have the highest Fe concentration under incubated and non-incubated conditions respectively with 260.6 mg kg^{-1} and 259.8 mg kg^{-1}. In addition; it has been seen that shoot Fe concentration of the plant has decreased under both incubated and non-incubated conditions as the biochar dose increases. Lowest Fe concentration has been observed in both applications under 5% biochar dose conditions (respectively 142.6 mg kg^{-1} and 139.3 mg kg^{-1}). In a study conducted by Al Wabel et al [50] in which they have applied biochar application in four different doses (0, 1, 3 and 5 g kg^{-1}) to the maize plant; they have expressed that while shoot Fe concentration of maize plant is 624 mg kg^{-1} in control application, it is 890 in 1 dose, 957 in 3 doses and 757 mg kg^{-1} in 5 doses. When considered generally, it has been observed that biochar applications increase the shoot Zn concentration both in incubated and non-incubated conditions on the chickpea plant. It has been observed that while Zn concentration of the control application is 49.8 mg kg^{-1} under incubated conditions, this value has risen to 67.2 mg kg^{-1} in 3% biochar dose. Lucchini et al [51] have conducted biochar to the soil in three different doses (0, 25 and 50 t ha^{-1}) and they have grown the plant of wheat in this soil. According to the results they have attained; they have expressed that there have been increases and decreases in the shoot Zn concentrations of the plant as the dose of biochar increases. Researchers have found that while Zn concentration of the plants to which biochar application has not been made is 65.1 mg kg^{-1}, this value has risen to

67.1 mg kg^{-1} at 25 doses and decreased to 49.1 mg kg^{-1} at 50 t ha^{-1} dose.

As in Fe concentrations; a decrease has been observed with the increasing biochar applications under both the incubated and non-incubated conditions in shoot Cu and Mn concentrations. While the highest Cu concentration has been determined in the control application with 12.8 mg Cu kg^{-1} under incubated conditions and with 12.9 mg Cu kg^{-1} under non-incubated conditions, the highest Mn concentration has again been determined in the control application with 91.0 mg Mn kg^{-1} under incubated conditions and with 92.2 mg Mn kg^{-1} under non-incubated conditions in Mn concentrations. Karami et al [52] have expressed that the addition of biochar to the soil decreases the usefulness of Pb and Cu. Coumar et al [53] have reported that the copper uptake of the plant decreases with the biochar application depending on the pH of the soil. Fellet et al [54] have specified that biochar increases the adsorption of the nutrient due to the width of its surface area and cause to the lowness of their bio-usefulness. Other researchers express that biochar applications may decrease the usefulness of the metals due to the fact that they bond the heavy metals directly in the soil or they indirectly increase the pH of the soil [55] and they may be the reason for the decrease of metal transfer to the plant [56, 57]. In the study conducted by Nzanza et al [58]; they have expressed that the eucalyptus biochar and mycorrhiza fungus applications do not have any impact on N, Ca, B, Cu, Mn and Zn concentrations in the tissues of the plant if the tomato is worn out. In the studies conducted by other researchers, it is often reported that biochar tightly keeps the nutrient and limits the intake [59, 60, 61].

In this study; a positive correlation has been determined while a negative significant relation has been found between the dry weight and N, P, Fe, Mn and Cu in the chickpea plant grown with the application of biochar and incubation (Table 5). While a positive relation has been determined between N and Fe, P and Fe, Zn, Mn and Cu, Fe and Mn and Cu, Mn and Cu; a negative significant relation has been detected between Fe and Zn, Zn and Mn, Mn and Cu. A negative significant relation has been determined between the dry weight and N, P and Fe in the chickpea plant grown with the application of biochar, but without the application of incubation (Table 6). In addition; a positive significant relation has been determined between N and Fe and Cu, P and Fe, Fe and Mn and Zn and Cu.

TABLE 4
Effects of biochar application on Fe, Zn, Mn and Cu concentrations of chickpea plant

	Biochar Doses %	Fe		Zn		Cu		Mn	
		mg kg^{-1}							
Incubation	0	260.6	±7.99a	49.8	±1.94c	12.8	±0.57a	91.0	±2.62a
	0.5	174.2	±19.45c	50.1	±8.16c	11.3	±0.28b	69.9	±9.18cd
	1	165.0	±0.92cd	60.2	±0.53ab	10.8	±0.57b	74.9	±8.06bc
	2	199.1	±2.47b	55.9	±8.37bc	12.8	±0.14a	85.7	±2.33ab
	3	145.8	±12.66de	67.2	±0.28a	10.9	±1.27b	74.4	±2.33bc
	4	144.2	±0.14e	63.9	±2.46ab	10.8	±0.07b	59.3	±8.06d
	5	142.6	±8.34e	60.7	±1.99ab	8.6	±0.28c	59.0	±0.85d
	Mean	**175.9B**		**58.2A**		**11.1A**		**73.5A**	
Non-incubation	0	259.8	±19.09a	43.2	±2.17c	12.9	±0.14a	92.2	±2.69a
	0.5	196.7	±13.58b	57.7	±0.35ab	12.4	±0.28ab	54.7	±6.51c
	1	152.7	±25.88cd	54.8	±0.01ab	11.6	±0.14b	70.1	±4.10b
	2	163.5	±6.36b-d	49.0	±0.48bc	10.3	±0.28c	59.5	±0.78c
	3	188.7	±24.11bc	51.7	±0.11a-c	9.1	±0.71d	63.4	±5.80bc
	4	148.6	±9.83d	60.5	±11.04a	11.4	±0.14b	68.8	±4.24b
	5	139.3	±20.44d	54.6	±3.66ab	9.1	±0.07d	57.5	±4.24c
	Mean	**178.5A**		**53.1B**		**10.9B**		**66.7B**	

P<0.05

TABLE 5
Correlations between the parameters that obtained from incubated variants

	Dry Matter	N	P	K	Fe	Zn	Mn
N	-0.454*						
P	-0.624**	0.044					
K	-0.355	-0.014	0.203				
Fe	-0.752**	0.519*	0.666**	0.140			
Zn	0.494*	-0.224	0.601**	0.016	-0.730**		
Mn	-0.842**	0.266	0.746**	0.398	0.837**	-0.491*	
Cu	-0.800**	0.305	0.850**	0.406	0.751**	-0.589**	0.787**

* Significiant at P<0.05
** Significant at P<0.01

TABLE 6
Correlations between the parameters that obtained from non-incubated variants

	Dry Matter	N	P	K	Fe	Zn	Mn
N	-0.535*						
P	-0.767**	0.353					
K	-0.196	0.110	0.286				
Fe	-0.444*	0.649**	0.482*	0.038			
Zn	0.059	0.379	-0.244	-0.184	0.121		
Mn	-0.399	0.414	0.395	-0.421	0.640**	-0.129	
Cu	-0.357	0.503*	0.056	0.057	0.101	0.711**	-0.126

* Significiant at P<0.05
** Significant at P<0.01

CONCLUSIONS

The results revealed that biochar application and incubation were significantly increased dry matter yield of chickpea (P<0.05). However, there has been a decrease in the nitrogen, phosphorus, iron, copper and manganese concentrations of chickpea plant with the increasing biochar applications under incubated and non-incubated conditions. When considered generally, biochar applications increased only potassium and zinc concentrations both in incubated and non-incubated conditions on the chickpea plant.

REFERENCES

[1] Şehirali, S. (1988) Yemeklik dane baklagiller [pulses]. Ankara, Turkey. Ankara University Press.

[2] FAOSTAT. http://faostat.fao.org

[3] Ahmad, M., Rajapaksha, A.U., Lim, J.E., Zhang, M., Bolan, N., Mohan, D., Vithanage, M., Lee, S.S. and Ok, Y.S. (2014) Biochar as a sorbent for contaminant management in soil and water: A review. Chemosphere. 99, 19-33.

[4] Liang, B., Lehmann, J., Solomon, D., Kinyangi, J., Grossman, J. and O'Neill, B. (2006) Black Carbon Increases Cation Exchange Capacity in Soils. Soil Sci. Soc. Am. J. 70, 1719-1730.

[5] Lehmann, J., da Silva, Jr., J.P., Steiner, C., Nehls, T., Zech, W. and Glaser, B. (2003) Nutrient availability and leaching in an archaeological Anthrosol and a Ferralsol of the Central Amazon basin: fertilizer, manure and charcoal amendments, Plant and Soil. 249, 343–357.

[6] Cheng, C.H., Lehmann, J., Thies, J.E., Burton, S.D. and Engelhard, M.H. (2006) Oxidation of black carbon by biotic and abiotic processes. Organic Geochemistry. 37(11), 1477-1488.

[7] Baldock, J.A. and Smernik, R.J. (2002) Chemical composition and bioavailability of thermally altered Pinus resinosa (Red pine) wood'. Organic Geochemistry. 33, 1093–1109.

[8] Lehmann, J. (2007) Bio-energy in the black. Frontiers in Ecology and the Environment. 5(7), 381-387.

[9] Bridgwater, A.V. (1994) Catalysis in thermal biomass conversion. Appl. Catal. A Gen. 116, 5–47.

[10] Abdullah, H., Mediaswanti, K.A. and Wu, H.W. (2010) Biochar as a fuel: 2. Significant differences in fuel quality and ash properties of biochars from various biomass components of Mallee trees. Energy Fuels. 24, 1972–1979.

[11] Yip, K., Tian, F.J., Hayashi, J. and Wu, H.W. (2010) Effect of alkali and alkaline earth metallic species on biochar reactivity and syngas compositions during steam gasification. Energy Fuels. 24, 173–181.

[12] Yip, K., Wu, H. and Zhang, D.K. (2007) Effect of inherent moisture in collie coal during pyrolysis due to in-situ steam gasification. Energy Fuels. 21, 2883–2891.

[13] Hossain, M.K., Strezov, V., Chan, K.Y., Ziolkowski, A. and Nelson, P.F. (2011) Influence of pyrolysis temperature on production and nutrient properties of wastewater sludge biochar. J. Environ. Manage. 92, 223–228.

[14] Azargohar, R. and Dalai, A.K. (2008) Steam and KOH activation of biochar: Experimental and modeling studies. Microporous Mesoporous Mater. 110, 413–421.

[15] Chan, K.Y., Zweiten, L.V., Meszaros, I., Downie, A. and Joseph, S. (2007) Agronomic Values of Green waste Biochar as a Soil Amendment. Australian J. Soil Res. 45, 629-634.

[16] Zhang, J., Cai, H., Zhang, C., Ren, J. and Wang, L. (2015) First Characterization of Humic-Like Substances Isolated from Maize Straw Biochar. Fresen. Environ. Bull. 24(5a), 1815-1821.S

[17] Clough, T.J. and Condron, L.M. (2010) Biochar and the nitrogen cycle: introduction. Journal of Environmental Quality, 39(4), 1218-1223.

[18] Alaboz, P., Coskan, A. and Isildar, A.A. (2017) Effects of Saw-Dust Biochar on Some Soil Moisture Constants. Fresen. Environ. Bull. 26(6), 4033-1038.

[19] Glaser, B., Lehmann, J. and Zech, W. (2002) Ameliorating physical and chemical properties of highly weathered soils in the tropics with charcoals a review. Biology and Fertility of Soils, 35, 219-230.
[20] Steiner, C., Teixeira, W.G., Lehmann, J., Nehls, T. and Vasconcelos de Macêdo, J.L. (2007) Long Term Effects of Manure, Charcoal and Mineral Fertilizer application on Crop Production and Fertility on a Highly Weathered Central Amazonian Upland Soil. Plant and Soil. 291, 275-290.
[21] Chan, K.Y. and Xu, Z. (2009) Biochar: Nutrient Properties and Their Enhancement. In: Lehmann, J., and Joseph, S. (Eds.) Biochar for Environmental Management, Science and Technology. Earthscan, London. 67-81.
[22] Asai, H., Samson, B.K., Stephan, H.M., Songyikhangauthor, K., Homma, K., Kiyono, Y., Inoue, Y., Shiraiwa, T. and Horie, T. (2009) Biochar Amendment Techniques for Upland Rice Production in Northern Laos 1. Soil Physical Properties, Leaf SPAD and Grain Yield, Field Crops Research. 111, 81-84.
[23] Brown, R.A. (2009) Biochar Production Technology. In: Lehmann, J., and Joseph, S. (Eds.) Biochar for Environmental Management, Science and Technology. Earthscan, UK. 127-139.
[24] Atkinson, C.J., Fitzgerald, J.D. and Hipps, N.A. (2010) Potential Mechanisms for Achieving Agricultural Benefits from Biochar Application to Temperate Soils: A Review. Plant Soil. 337, 1-18.
[25] Singh, B.P., Hatton, B.J., Singh, B., Cowie, A.L. and Kthuria, A. (2010) Influence of Biochars on Nitrous Oxide Emission and Nitrogen Leaching from Two Contrasting Soils. J. Environ. Qual. 39, 1224-1235.
[26] Laird, D.A., Fleming, P., Davis, D.D., Horton, R., Wang, B. and Karlen, D.L. (2010) Impact of Biochar Amendments on the Quality of a Typical Midwestern Agricultural Soil. Geoderma. 158, 443-449.
[27] Major, J., Lehmann, J., Rondon, M. and Goodale, C. (2010) Fate of Soil-Applied Black Carbon: Downward Migration, Leaching and Soil Respiration. Global Change Biology. 16, 1366-1379.
[28] Schulz, H. and Glaser, B. (2012) Effects of Biochar Compared to Organic and Inorganic Fertilizers on Soil Quality and Plant Growth in a Greenhouse Experiment. J. Plant Nutr. Soil Sci. 175, 410-422.
[29] Liu, C., Lu, M., Cui, J., Li, B. and Fang, C. (2014) Effects of Straw Carbon Input on Carbon Dynamics in Agricultural Soils: A Meta-Analysis. Global Change Biology. 20, 1366-1381.
[30] Sun, F. and Lu, S. (2014) Biochars Improve Aggregate Stability, Water Retention, and Pore-Space Properties Of Clayey Soil. J. Plant Nutr. Soil Sci. 177, 26-33.
[31] Zhang, W., Xiu, L., Chen, W. (2016) Remediation Effects Of Maize-Straw-Derived Biochar On Rice Grown In Cadmium-Contaminated Soil In North China. Fresen. Environ. Bull. 25(2), 602-611.
[32] Lehmann, J., Liang, B., Solomon, D., Lerotic, M., Luizão, F., Kinyangi, F., Schäfer, T., Wirick, S. and Jacobsen, C. (2005) Near-edge X-ray absorption fine structure (NEXAFS) spectroscopy for mapping nano-scale distribution of organic carbon forms in soil: Application to black carbon particles. Global Biogeochemical Cycles. 19, pGB1013.
[33] Jeffery, S., Bezemer, T.M., Cornelissen, G., Kuyper, T.W., Lehmann, J., Mommer, L., Sohi, S.P., Van de Voorde, T.F.J., Wardle, D.A. and Groenigen, J.W.V. (2014) The Way Forward in Biochar Research: Targeting Trade-Offs Between The Potential Wins. Global Change Biology. 7(1), 1-13.
[34] Rogovska, N.P., Fleming, P., Laird, D.A., Cruse, R.M., Parkin, T. and Meek, D. (2010) Biochar Influences on Greenhouse Gas Emissions from a Midwestern Agricultural Soil. Submitted to Soil Sci. Soc. Am. J.
[35] Krishnakumar S., Rajalakshmi, A.G., Balaganesh, B., Manikandan, P., Vinoth, C. and Rajendran, V. (2014) Impact of Biochar on Soil Health. Review Article. International Journal of Advanced Research. 2(4), 933-950.
[36] Wang, C., Du, S., Nishimura, O., Wu, L., Zhang, F., Cui, J. and Liu, N. (2017) Effects Of Wheat Straw-Derived Biochar On Water Retention And Inorganic Nitrogen Leaching In Calcareous Clay Soil. Fresen. Environ. Bull. 26(5), 3365-3373.
[37] Günes, A., İnal, A., Taskın, M.B., Sahin, O., Kaya, C.E. and Atakol, A. (2014) Effect of phosphorus-enriched biochar and poultry manure on growth and mineral composition of lettuce (*Lactuca sativa* L. cv.) grown in alkaline soil. Soil Use and Management. 30, 182-188.
[38] Kacar, B. and Inal, A. (2008) Plant analysis. Nobel Pres. 1241, 891.
[39] Erdem, H., Kınay, A., Gunal, E., Yaban, H. and Tutus, Y. (2017) The effects of biochar application on cadmium uptake of tobacco. Carpathian Journal of Earth and Environmental Sciences. 12(2), 447 – 456.
[40] Murphy, J. and Riley, J.P. (1962) A modified single solution for the determination of phosphate in natural waters. Analtica Chemica Acta. 27, 31-36.

[41] Bataglia, O.C., Furlani, A.M.C., Teixeira, J.P.F., Furlani, P.R. and Gallo, J.R. (1983) Metodos de analise química de plantas. Instituto Agronomico, Campinas. p. 48.
[42] Bremner, J. M. (1965) Total nitrogen. Methods of soil analysis. Part 2. Chemical and microbiological properties. (methodsofsoilanb), 1149-1178.
[43] Biederman, L.A., Phelps, J., Ross, B., Polzin, M. and Harpole, W.S. (2017) Biochar and manure alter few aspects of prairie development: A field test. Agriculture Ecosystems & Environment. 236, 78-87.
[44] Arif, M., Jalal, F., Jan, M.T., Muhammad, D. and Quilliam, R.S. (2015) Incorporation of Biochar and Legumes into the Summer Gap: Improving Productivity of Cereal-Based Cropping Systems in Pakistan. Agroecology and Sustainable Food Systems. 39, 391-398.
[45] Kim, H.S., Kim, K.R., Kim, H.J., Yoon J.H., Yang, J.E., Ok, Y.S., Owens, G. and Kim, K.H. (2015) Effect of biochar on heavy metal immobilization and uptake by lettuce (Lactuca sativa L.) in agricultural soil. Environ Earth Sci. 74, 1249–1259.
[46] Beesley, L., Moreno-Jiménez, E., Gomez-Eyles, J.L., Harris, E., Robinson, B. and Sizmur, T. (2011) A review of biochars' potential role in the remediation, revegetation andrestoration of contaminated soils. Environ. Pollut. 159, 3269–3282.
[47] Liu, C., Liu, F., Ravnskov, S., Rubaek, G.H., Sun, Z. and Andersen, M.N. (2017) Impact of Wood Biochar and Its Interactions with Mycorrhizal Fungi, Phosphorus Fertilization and Irrigation Strategies on Potato Growth. Journal of Agronomy and Crop Science. 203, 131-145.
[48] Puga, A.P., Abreu, C.A., Melo, L.C.A. and Beesley, L. (2015) Biochar application to a contaminated soil reduces the availability and plant uptake of zinc, lead and cadmium. Journal of environmental management. 159, 86-93.
[49] Rees, F., Germain, C., Sterckeman, T. and Morel, J.L. (2015) Plant growth and metal uptake by a non-hyperaccumulatingspecies (Lolium perenne) and a Cd-Zn hyperaccumulator (Noccaea caerulescens) in contaminated soils amendedwith biochar. Plant Soil. 395, 57-73.
[50] Al-Wabel, M.I., Usman, A.R.A., El-Naggar, A.H., Aly, A.A., Ibrahim, H.M., Elmaghraby, S.and Al-Omran, A. (2015) *Conocarpus* biochar as a soil amendment for reducing heavy metal availability and uptake by maize plants. Saudi Journal Of Biological Sciences. 22(4), 503-511.
[51] Lucchini, P., Quilliam, R.S., DeLuca, T.H., Vamerali, T. and Jones, D.L. (2014) Does biochar application alter heavy metal dynamics in agricultural soil? Agriculture, Ecosystems & Environment. 184, 149-157.
[52] Karami, N., Clemente, R., Moreno-Jiménez, E., Lepp, N.W. and Beesley, L. (2011) Efficiency of green waste compost and biochar soil amendments for reducing lead and copper mobility and uptake to ryegrass. Journal of Hazardous Materials. (191), 41–48.
[53] Coumar, M.V., Parihar, R.S., Dwivedi, A.K., Saha, J.K., Lakaria, B.L., Biswas, A.K., Rajendiran, S., Dotaniya, M.L. and Kundu, S. (2016) Pigeon Pea Biochar as a Soil Amendment to Repress Copper Mobility in Soil and Its Uptake by Spinach. Bioresources. 11, 1585-1595.
[54] Fellet, G., Marmiroli, M. and Marchiol, L. (2014) Elements uptake by metal accumulator species grown on mine tailings amended with three types of biochar. Sci. Total Environ. 468-469, 598-608.
[55] Rees, F., Simonnot, M.O. and Morel, J.L. (2014) Short-term effects of biochar on soil heavy metal mobility are controlled by intra-particle diffusion and soil pH increase. Eur J Soil Sci. 65, 149–161.
[56] Cui, L., Li, L., Zhang, A., Pan, G., Bao, D. and Chang, A. (2011) Biochar amendment greatly reduces rice Cd uptake in a contaminated paddy soil: a two-year field experiment. Bioresources. 6, 2605–2618.
[57] Houben, D., Evrard, L. and Sonnet, P. (2013) Beneficial effects of biochar application to contaminated soils on the bioavailability of Cd, Pb and Zn and the biomass production of rapeseed (Brassica napus L.). Biomass Bioenergy. 57, 196–204.
[58] Nzanza, B., Marais, D. and Soundy, P. (2012) Effect of Arbuscular Mycorrhizal Fungal Inoculation and Biochar Amendment on Growth and Yield of Tomato. International Journal of Agriculture and Biology. 14, 965-969.
[59] Warnock, D.D., Mummey, D.L., McBride, B., Major, J., Lehmann, J. and Rillig, M.C. (2010) Influences of non-herbaceous biochar on arbuscular mycorrhizal fungal abundances in roots and soils: Results from growth-chamber and field experiments. Applied Soil Ecology. 46, 450-456.
[60] Lehmann, J., Rillig, M.C., Thies, J., Masiello, C.A., Hockaday, W.C. and Crowley, D. (2011) Biochar effects on soil biota - A review. Soil Biology & Biochemistry. 43, 1812-1836.
[61] Zama, E.F., Zhu, Y.G., Reid, B.J. and Sun, G.X. (2017) The role of biochar properties in influencing the sorption and desorption of Pb(II), Cd(II) and As(III) in aqueous solution. J. Clean Prod. 148, 127-136.

Received: **17.06.2017**
Accepted: **19.10.2017**

CORRESPONDING AUTHOR

Ahmet Demirbas
Cumhuriyet University,
Vocational School of Sivas,
Department of Crop and Animal Production,
58140 Sivas – Turkey

e-mail: ademirbas@cumhuriyet.edu.tr

© by PSP Volume 26 – No. 12A/2017 pages 8337-8344 Fresenius Environmental Bulletin

BARLEY POWDERY MILDEW (*BLUMERIA GRAMINIS* F. SP. *HORDEI*) VIRULENCE GENE SPECTRUM IN THE SOUTHAEGEAN REGION OF TURKEY

Ahmet Zeybek*, Elif Dalgic

Muğla Sıtkı Koçman University, Department of Biology, 48000, Muğla, Turkey

ABSTRACT

In this study, *Blumeria graminis* f. sp. *hordei* populations taken from barley cultivation areas in 3 different periods have been analysed in terms of virulence gen frequency, virulence gen complexity, changes in pathotype frequencies, and the reactions between some of the single spore isolates and Turkish barley varieties. As plant material, susceptible Bülbül-89 barley variety and powdery mildew isogenic test genotypes, transferred through back-ross hybridization into Pallas and Siri varieties, each one having a separate resistance gene, have been used. During the harvest period of *B. graminis* f. sp. *hordei*, *cleistothecia* samples have been taken, and the single spore isolates taken from conidies, asexual period, and *cleistothecias,* sexual period, have been used as a disease material. In the *B. graminis* f. sp. *hordei* populations acquired from powdery mildew samples, first spore collection time determined 24, second sampling time determined 23 and harvest period determined 22 virulence genes. Highest virulence gene frequency has been observed in Va8 (100.00 %) gene, and lowest virulence gene frequency was observed in Vro and Vr1 (0.00 %) virulence genes. Average virulence gene complexity values was found to be between 11.88-14.94 %. Differences were observed during vegetation period and harvest time in aggression gene's complexity values. Against powdery mildew disease, the most resistant barley varieties were Kaya (91.14 %) and Bayrak (88.97 %), while the most susceptible were Bülbül-89 (0.00 %) and Hilal (8.68 %).

KEYWORDS:
Barley, *Blumeria graminis* f. sp. *hordei,* Virulence gene, Resistance

INTRODUCTION

Among all grains, barley is an important cultivated plant being used in both food industry and forage industry, has widespread planting areas and production in the world and in Turkey. In Turkey, barley cultivation area is 2.8 million ha, production is 8 million ton and productivity is 2.200 kg ha^{-1} [1] and in the world, barley cultivation area is 49 million ha, production is 148 million ton and productivity is 2.300 kg ha^{-1} [2]. Regarding the 100 % increase in yield; 60 % is thought to be the result of highly yield new breeding varieties, and 40 % is thought to be the result of advances in cultural methods [3]. Among the leading diseases causing productivity and quality losses in Europe and Turkey, powdery mildew factor *B. graminis* f. sp. *hordei* is significant. In the studies related to race formation and virulence gene quantity and conducted in accordance with powdery mildew's economic significance, a low polymorphism, in terms of virulence genes were observed in the powdery mildew populations [4, 5, 6, 7, 8, 9, 10]. Researchers were explained this by the selection pressure that occurs through the varieties that are heavily cultivated in these areas. A change in the barley variety spectrum was always led to a change in the genetic structure of the pathogen population. The mutual interaction between cultivated barley and barley powdery mildew at the barley production zones was ended in the formation of a proportionally homogeneous pathogen population. Due to *Erysiphe graminis* f. sp. *hordei*'s adaptation ability, powdery mildew resistance of new production varieties are mostly low according to experience. Multiple line varieties were proposed as a means of control off powdery mildew. Variety mixtures were clearly reduced powdery mildew rates in summer barley [11]. In host-parasite systems it was often observed that host population carry a low number of resistance gene, while pathogen population carry a great number of aggression gene [12]. The purpose in this study was to determine the virulence gene frequency distribution, virulence gen complexity of *B. graminis* f. sp. *hordei* pathogen in cultivated barley and the reactions of 12 Turkish barley varieties.

MATERIALS AND METHODS

Plant materials. As a plant material, susceptible Bülbül-89 barley variety and powdery mildew isogenic test genotypes that were transferred by introgressive hybridization to Pallas and Siri varieties acquired from ICARDA (The International Centre for Agricultural Research in the Dry Areas)

and each one having a separate resistance gene (Table 1). Barley leaves were collected from the Adnan Menderes University Farm's barley field in three different periods and preserved at +4ºC.

***In vitro* assays.** Pathogen isolates were obtained by stimulating ascospore formations on each leaf of the susceptible variety, Bülbül-89, in laboratory conditions. Each isolate was purified from a single spore [13]. The leaves of isogenic lines were cut in a 3 cm length, placed in 9 cm in diameter petri dishes containing BA (Benzimidazole Agar-5 ppm) in the counterclockwise direction with the order in Table 1, where the bottom surface of the leaves were in contact with the feeding environment. As a control, susceptible variety Bülbül-89 leaf particles were placed at the center of the petri dishes.

Inoculation of single spore isolates on test varieties was implemented with the aid of home-made inoculation tower in a sterile cabinet. Inoculated pieces of leaves on petri dishes were incubated at 17ºC / 14-hour dark and 10-hour light periods in a climate chamber for 8-10 days. The test plates were assessed for full inoculation and sufficient colony formation and on the Bülbül-89 susceptible variety according to the 0-4 scale developed by Welz [14]. Following the tests determining the genetic composition of pathotypes, the virulence gene frequencies and the level of complexities in virulence genes were determined using MS-Excel version 5.0 developed by Habgood [15]. The identification of powdery mildew isolates were determined using the software by Hermann et al. [16]. According to this method, the 0-4 scale results in evaluating the test sets were turned into a binary code system. As a result, two-type outcomes were obtained; the scale values of 0, 1, 2, were translated as 0 (resistant), the values of 3 and 4 were translated as 1 (susceptible). The following formula by Habgood [15] was used to determine the pathotypes.

$$PTi = \sum_{nr=1}^{25} 2^{(nr-1)} . \ kpi \qquad (1)$$

Pti: pathotype index, *nr*: order # of differential lines (Table 1), *kpi*: binary code # of differentil lines (0 or 1).

The values of the gene frequency aggression were divided into 5 different groups according to this style of grouping, if virulence gene frequency in population is bigger than 90 %, the population is considered fixed. If it is between 60 % and 90 %, it is high; if it ranges between 30 % to 60 %, it is medium; if the frequency is between 10 % and 30 %, it is very low degree and if it is smaller than 10 %, it is called recessive. Virulence complexity is a number of genes in a single isolate. The number of virulence genes was determined per isolate. Afterwards, the number isolates having the same complexity values as percentages are determined as complexity frequencies. Tarm-92, Akhisar-98, Erginel-90, Sancak Hilal, Vamık Hoca, Hamidiye, Kaya, Sancak, Akhisar, Hilal, Bayrak, Bülbül-89 (Control) 12 Turkish barley varieties were cultivated in climate chamber until reaching 1-2 leaf period. Then from these varieties, barley leaf pieces have been cut 3 cm long, their lower parts have been placed anticlockwise on BA, ensuring contact with agar. For control purposes, leaf particle of Bülbül-89 variety was placed at the centre of petri dishes. Inoculation procedure to the test varieties of the 64 single spore isolates were done by tin cylinders (10 cm diameter, 20 cm height, covered and a 1 cm hole). The inoculed petri dishes were left at the climate chamber for 8-10 days for incubation. Then, by considering whether the control group was completely inoculed or not, the leaves of 11 barley and Bülbül-89 varieties placed inside the petri dishes were evaluated as per 0-4 scale [14].

TABLE 1
Differential test genotypes for the virulence of *B. graminis* f. sp. *hordei* collected in the Aegean Region.

No	Isogenic Lines*	Resistance Gene	No	Isogenic Lines*	Resistance Gene
01	Siri-01	Mla1	14	Siri-19	Mlp
02	Siri-02	Mla3	15	Pallas-20	Mlat
03	Siri-03	Mla6	16	Pallas-22	Ml-05
04	Siri-04	Mla7	17	Pallas-23	Ml(la)
05	Pallas-08B	Mla9	18	Pallas-24	Mlh
06	Siri-10	Mla12	19	Lotta	Ml(AB)
07	Siri-11	Mla13	20	Hellas	Ml(He)
08	Siri-12	Mlc	21	Union	Mlg
09	Pallas-13	Mla23	22	Alexis	Mlo
10	Pallas-14	Mlra	23	Siri	Mla8
11	Pallas-15	Ml(Ru2)	24	Gunnar	Ml(tu)
12	Siri-17	Mlk	25	Ogra	Ml(wo)
13	Siri-18	Mlnn	26	Bülbül-89	none known genes

*obtained from ICARDA

TABLE 2
Virulence gene frequency values (%) in *B. graminis* f. sp. *hordei* populations.

Virulence Genes	Virulence Gene Frequencies (%)		
	1th Population	2th Population	*Cleistothecia*
Vr1	3.36	0.00	0.00
Vr3	22.68	90.16	24.86
Vr6	10.92	59.57	10.17
Vr7	8.40	11.27	6.78
Vr9	4.20	0.00	1.13
Vr12	65.52	48.30	6.78
Vr13	4.20	0.00	1.13
Vrc	63.00	30.59	59.89
Vra23	84,00	96.60	81.36
Vrra	19.32	45.08	15.82
Vr(Ru2)	96.60	94.99	94.92
Vrk	95.76	94.99	94.92
Vrn	99.12	99.82	98.31
Vrp	99.12	91.77	98.31
Vrat	96.60	96.60	94.92
Vr-05	0.00	93.38	4.52
Vr(La)	96.60	91.77	94.92
Vrh	99.12	99.82	98.31
Vr(AB)	72.24	96.6	81.36
Vr(He)	21.84	99.82	99.44
Vrg	22.68	72.45	24.86
Vro	0.00	0.00	2.26
Vra8	97.44	99.82	98.31
Vr(Tu)	20.16	19.32	19.21
Vr(wo)	12.60	43.47	9.04
Bülbül-89	100.00	100.00	100.00

RESULTS AND DISCUSSION

In the *B. graminis* f. sp. *hordei* populations acquired from the powdery mildew samples, it was observed that during the first spore collection time there were 24 virulence genes and during the second sampling time there were 23, while in the population acquired from the *cleistothecia* samples there were 22. The virulence genes from the powdery mildew populations collected in all three periods were different in quantity and in frequency. The frequencies of virulence genes of the *B. graminis* f. sp. *hordei* populations were observed to be between 0.00 % and 100 %. The frequency of the Va8 gene in the populations acquired during the vegetation period and the powdery mildew populations acquired from the *cleistothecia* samples collected during harvest, was defined as 100 %. It was observed that during the first spore collection time virulence gen frequencies ranged between 0.00 % and 100 %, Vr-05 and Vro virulence genes were low and Vra8 gene was the highest virulence frequency. During the second spore collection time, it was observed that virulence gene frequencies ranged between 0.00 % and 100 %, highest virulence gene frequency was in Vra8 gene (100 %) and lowest virulence gene frequency was in Vro, Vr-05, Vr13, Vr9 genes. It was observed that in both spore collection periods, Va8 virulence gene frequency was 100 % in powdery mildew populations and there were no changes. It was observed that Vr3, Vr6, Vr7, Vr23, Vrra, Vr(AB), Vr(He), Vrg, Vr(wo), frequencies increased when moved from first spore collection time to second spore collection time in the populations. Frequency reductions were observed in Vr9, Vr12, Vr13, Vrc, Vr(Ru2), Vrk, Vrp, Vr(La) virulence genes when moved from first spore collection time to the second spore collection time (Table 2). The frequencies of Vro-5 and Vro virulence genes, the pathogen counterpart of Ml-05, which is a significant source of resistance against powdery mildew, and mlo resistance genes, acquired through mutation, were observed to be 0.00 % at the first and second spore collection times. Vr-05 virulence gene is the counterpart of Mlo-5 resistance gene and it's frequency was a similar with the value acquired by Hovmoller et al. [17] from the powdery mildew populations they were collected from the European barley cultivation areas. In a 2011 study in Australia conducted to determine the 86 barley varieties, 9 forward line and pathogen's 40 reference isolates and powdery mildew disease's resistance genes, a total of 22 known resistance genes were determined, while in only one variety was a non-specific mlo recessive gene. Researchers were recommended that in order to improve resistance against powdery mildew disease in new varieties, mlo gene could be used in Australia barley improvement programs and also to improve European varieties [18].

TABLE 3
Virulence gene frequencies distribution in *B. graminis* f. sp. *hordei* populations.

Exchange interval	Virulence Genes		
	1th Population	2th Population	*Cleistothecia*
More than 90%	Vr(Ru2), Vrk, Vrn, Vrp, Vrat, Vrh, Vr(La)	Vr3, Vra23, Vr(Ru2), Vrk, Vrn, Vrp, Vrat, Vr(La), Vrh, Vr(AB), Vr(He), Vra8	Vr(Ru2), Vrk, Vrn, Vrp, Vrat, Vr(La), Vrh, Vra8, Vr(He)
Between 60-90 %	Vr12, Vrc, Vra23, Vr(AB)	Vrg	Vr12, Vra23, Vr(AB)
Between 30-60 %	-	Vr12, Vrc, Vrra, Vr(wo), Vr6	Vrc
Between 10-30 %	Vr3, Vr6, Vra, Vr(He), Vr(Tu), Vrg, Vr(wo)	Vr7, Vr(Tu)	Vr6, Vr3, Vr(Tu), Vrg, Vra
Less than 10%	Vr1, Vr7, Vr13, Vr-05, Vr9, Vro	Vr0-5, Vr1, Vr9, Vr13, Vro	Vr1, Vr9, Vr13, Vr-05, Vro, Vr(wo)

During the first population collection time; it was found that Vr(Ru2), Vra8, Vrk, Vrn, Vrp, Vrat, Vrh, Vr(La) virulence genes were frequencies over 90 % and fixed in population,Vr12, Vrc, Vra23, Vr(AB) virulence genes were frequencies ranging between 60-90 %,Vr3, Vr6, Vra, Vr(He), Vr(Tu) virulence genes were frequencies ranging between 10-30 %, Vr1, Vr7, Vr13, Vr-05, Vr9, Vro, Vr(wo) virulence genes frequencies in population were lower than 10 % and recessive. During the second population collection time; it was observed that frequency of Vr3, Vra23, Vr(Ru2), Vrk, Vrn, Vrp, Vrat, Vr(La), Vrh, Vr(AB), Vr(He) genes was higher than 90 % and fixed in population, frequency of Vrg virulence gene ranged between 60-90 %, frequency of Vr12, Vrc, Vra, Vr(wo) genes ranged between 30-60 %, while the frequency of Vr6, Vr7, Vr(Tu) genes ranged between 10-30 %, frequency of Vr1, Vro, Vr13, Vro, Vr-05 virulence genes was lower than 10 % and recessive in population. During the *cleistothecia* period; it was observed that Vr (Ru2), Vrk, Vrn, Vrp, Vrat, Vr(La), Vrh, Vra8, Vr(He) virulence genes are fixed in population, Vr12, Vra23, Vra(AB) genes were a frequency ranging between 60-90 % , Vrc virulence gene frequency ranges between 30-60 %, Vr3, Vr6, Vr7, Vr(Tu), Vrg, Vra virulence genes were a frequency ranging between 10-30 %, Vr1, Vr9, Vr13, Vr-05, Vr(wo), Vro genes were a frequency lower than 10 % and recessive in population (Table 3). The 25 isogenic lines used in the study were a different resistance gene and the pathogen counterpart of each resistance was found to be virulency, which is an indication that there is a very dynamic change in the pathogen population. In the study, the virulence gene frequency analysis findings acquired in the population taken from powdery mildew samples were similar to Kokina and Rashal [8], Yahyaoui et al. [19], Dreiseilt and Rashal [20]'s findings. The values acquired by Wachter and Fristste [21] from the powdery mildew population collected from the European barley cultivation areas indicated differences in terms of some virulence genes and Vrn, Vrk, Vrc, Vrg, Vra7 and Vra12 virulence genes were frequency values ranging between 40-60 %. In France, *E. graminis* f. sp. *hordei* populations were collected from barley cultivation areas carrying Mlg resistance gene, and Vrg virulence gene's frequency was ranged between 40-80 %, Vrg virulence gene's frequency at the first spore collection time was observed as 22.68 %, at second spore collection time it was observed as 72.45 % and during the cleistothecia period it was observed as 24.86 % [22]. These differences could be related to different powdery mildew resistance genes of barley varieties cultivated in Turkey and also to different environmental conditions**.**

Throughout the vegetation period, *cleistothecia* were collected from the trial zone in two different periods and in harvest period, and their samples were virulence gene complexities with average respective frequency values of 11.88 %, 14.94 % and 12.67 %. At the first period population, complexity values ranged between 7 and 18, and from the collected single spore isolates, 84 % of them were the lowest, and 1.68 % of them were the highest virulence complexity values. During the second period population, virulence gene complexity values ranged between 11 and 19, and from the collected single spore isolates, 3.22 % were the lowest, and 3.22 % of them were the highest virulence gene complexity. During the c*leistothecia* period, the average virulence gene complexity was observed to be 12.67, and the virulence gene complexity value was ranged between 8 and 17. From the collected single spore isolates, 1.13 % was the lowest and 1.13 % was the highest virulence gene complexity (Table 4). The findings acquired in the study are higher than the study conducted by Caffier et al. [23] in France, where airborne powdery mildew populations were analysed by 12 discriminative test varieties. This difference could be related to having a higher number of discriminative test variety in the study, resistance genes of the barley varieties commonly grown in the two spore collection areas and to different environmental conditions.

In the first spore collection time 109 pathotypes were observed, in the second spore collection time 62 were observed, and in the population of the *cleistothecia* samples 53 pathotypes were observed. No similarities were found among the populations in terms of pathotypes. At the first spore collection period, 2325920 pathotypes was the highest frequency (3.36 %), at the second spore collection

period, 6258054 and 14645126 pathotypes was the highest frequency (1.61 %) and at the *cleistothecia* period 040776720 and 004676320 pathotypes was the highest frequency (6.78 %) (Table 5). The findings related to pathotype values are similar to Andrivan et al. [22]'s findings. It is interesting to see that the pathotypes acquired in the study was differences in all three populations. The total powdery mildew populations were different pathotypes, from the same trial parcel at different times, where same genotype was effective. This is an indication that there was a time-related rapid change among populations.

Against the 46 powdery mildew isolates implemented, the most resistant variety was Kaya (91.14 %) and Bayrak (88.97 %), most susceptible was control Bülbül-89 (0.00 %) and Hilal (8.68 %). Resistance levels of other varieties were variable (Table 6). The findings are found to be similar to those of Czembor and Czembor [24] and Naghavi et al. [25].

TABLE 4
The virulence gene complexity values (%) in *B. graminis* f. sp. *hordei* populations.

	Virulence Gene Complexities (%)		
Virulence Genes	**1th Population**	**2th Population**	***Cleistothecia***
7	0.84	0.00	0.00
8	0.84	0.00	1.13
9	3.36	0.00	1.13
10	10.92	0.00	3.39
11	31.92	3.22	10.17
12	20.16	9.66	27.12
13	20.16	11.27	24.86
14	4.20	16.10	19.21
15	3.36	24.15	6.78
16	0.84	14.49	4.52
17	1.68	9.66	0.00
18	1.68	8.05	0.00
19	0.00	3.22	0.00
Average	11.88	14.94	12.67

TABLE 5
The pathotype frequencies in *B. graminis* f. sp. *hordei* populations.

	Pathotypes			
No	**Habgood number**	**1th Population**	**2th Population**	***Cleistothecia***
1	040776720	0.00	0.00	6.78
2	004676320	0.00	0.00	6.78
3	246676320	0.00	0.00	5.65
4	044676320	0.00	0.00	4.52
5	046676320	0.00	0.00	3.39
6	006676320	0.00	0.00	3.39
7	2325920	3.36	0.00	0.00
8	3112352	1.68	0.00	0.00
9	2588066	1.68	0.00	0.00
10	2587936	1.68	0.00	0.00
11	2588032	1.68	0.00	0.00
12	2588064	1.68	0.00	0.00
13	11501565	1.68	0.00	0.00
14	11501533	1.68	0.00	0.00
15	6519810	1.68	0.00	0.00
16	6520226	1.68	0.00	0.00
17	10977152	0.00	0.00	0.00
18	246676360	0.00	0.00	2.26
19	244676760	0.00	0.00	2.26
20	6258054	0.00	1.61	0.00
21	14645126	0.00	1.61	0.00
Total frequencies of other pathotypes (%)		81.52	96.2	64.97
Number of pathotypes		109	62	53
Number of isolates tested		119	62	88

TABLE 6
Reactions of Turkish barley cultivars against powdery mildew isolates.

İsolate no	Tarm-92	Akhisar 98 (İzmir)	Erginel 90	Sancak Hilal	Hilal	Vamık hova	Hamidiye	Kaya (İzmir)	Sancak	Akhisar	Bayrak	Bülbül-89 (control)
1	4	4	4	0	4	2	4	1	4	4	3	4
2	4	4	4	4	0	0	4	0	4	4	0	4
3	4	3	4	3	0	3	3	0	4	3	0	4
4	4	3	4	4	0	4	4	0	4	4	1	4
5	4	4	4	4	0	0	4	0	0	4	3	4
6	4	4	4	4	0	3	4	0	4	3	1	4
7	4	4	4	4	0	1	4	0	4	3	1	4
8	4	4	4	4	0	1	4	0	4	4	0	4
9	4	4	4	4	0	0	3	0	4	3	0	4
10	4	4	4	4	0	3	4	0	4	4	0	4
11	2	3	2	2	0	4	3	0	0	2	0	4
12	2	3	3	2	0	0	3	0	2	2	0	4
13	4	3	4	2	0	0	3	0	4	4	0	4
14	1	2	1	0	0	0	0	0	2	0	4	4
15	3	0	4	4	0	4	4	0	3	3	0	4
16	4	3	4	4	0	4	4	0	4	2	0	4
17	2	0	3	3	0	3	3	0	3	2	0	4
18	4	4	4	4	0	3	3	0	4	4	0	4
19	4	3	4	0	1	0	4	4	2	0	4	4
20	3	3	3	3	0	0	3	0	1	2	0	4
21	3	4	4	0	0	0	4	0	3	2	0	4
22	4	4	4	4	0	3	3	0	4	4	3	4
23	4	0	4	3	0	0	2	0	4	4	0	4
24	4	4	3	4	0	2	4	0	1	4	0	4
25	4	4	4	4	0	0	4	0	4	4	1	4
26	4	4	4	0	0	2	1	4	4	4	1	4
27	4	4	0	0	0	0	1	0	4	0	0	4
28	4	4	4	4	4	0	4	4	4	0	0	4
29	3	0	2	1	0	2	1	3	0	2	1	4
30	3	3	3	0	0	3	4	4	4	4	0	4
31	4	4	4	4	0	4	3	4	4	0	0	4
32	4	4	4	0	3	4	3	0	3	4	0	4
33	3	3	3	3	0	0	2	0	3	3	0	4
34	4	4	4	4	0	0	4	0	4	4	0	4
35	0	0	3	2	0	1	2	0	2	2	0	4
36	3	4	4	4	0	4	2	0	4	4	0	4
37	4	4	0	4	0	0	4	0	4	4	0	4
38	4	4	4	4	0	0	4	0	0	3	0	4
39	4	4	4	4	0	0	4	0	4	4	0	4
40	3	3	4	4	0	1	1	0	4	4	1	4
41	4	4	4	4	4	0	4	4	4	0	0	4
42	4	3	4	3	0	0	3	0	4	3	0	4
43	3	2	3	3	0	0	3	0	3	4	0	4
44	4	4	3	2	0	2	2	0	4	4	0	4
45	4	3	4	3	0	0	3	0	4	4	0	4
46	4	3	3	0	0	0	2	0	3	0	0	4
Virulence gene	88.97	84.63	88.97	65.1	91.14	30.38	75.95	15.9	78.12	67.27	10.85	1.00
Resistance	10.85	13.02	10.85	32.55	8.68	69.44	23.87	84.63	21.7	32.55	88.97	0.00

CONCLUSION

In the powdery mildew populations, it was determined that at the first spore collection time there were 24 virulence genes, in the second sampling time there were 23 and at the *cleistothecia* period there were 22 virulence genes. In the acquired powdery mildew populations, the virulence gene frequencies ranged between 0.00 % and 100 %, the lowest virulence gene was found in Vr-05 and Vro; and the highest virulence gene was found in the Vra8 virulence gene. Powdery mildew samples were respective virulence gene complexities of 11.88 %, 14.94 % and 12.67 %. Aggression gene complexity values also displayed differences through vegetation period and harvest period. In all three populations, increases or decreases occurred in some virulence gene frequencies, while in some populations no virulence gene frequency change was observed. The acquired pathotypes varied in all three populations, but the fact that *B. graminis* f. sp. *hordei* populations were different pathotypes is an indication that there is a time related rapid change between populations. Whether this change is caused by migration needs to be tested with a further, detailed study. From the Turkish barley varieties, the most resistant to powdery mildew was found to be Kaya (91.14 %) and Bayrak (88.97 %) varieties, while the most susceptible was found to be control Bülbül-89 (0.00 %) and Hilal (8.68 %) varieties. We have reached the conclusion that in the control against powdery mildew disease in barley, determining a virulence gene spectrum and using the varieties that are resistant against these genes in production would contribute to prevent loss of productivity.

REFERENCES

[1] TSI (Turkish Statistical Institute) (2016). Agricultural structure and production. Government Statistic Institute of Prime Minister Publ. Online located at: http://www.tuik.gov.tr (in Turkish)

[2] FAO (Food and Agriculture Organization of the United Nations) (2016). Statistical database. Online located at: http://fao.org/statisitcs/en

[3] Roth, G.W., Marshall, H.G., Hatley, O.E. and Hill, R.R. (1984). Effect management practices on grain yield, test weight, and lodging of soft red winter wheat. Agronomy Journal. 76, 379-383.

[4] Limpert, E., Andrivon, D., Knittel, R. and Fischbeck, G. (1991). Barley mildew in Europe: patterns of composition of the pathogen population during the period 1985-1988.? In: Jørgensen JH ed. Integrated control of cereal mildews: Virulence Patterns and Their Change, 1991. Roskilde, Denmark, 87-103.

[5] Kokina, I. and Rashal, I. (2002). Genetic structure peculiarities of the *Blumeria graminis* f. sp. *hordei* population in the north-eastern part of Lithuania. Biologia, 3, 47-49.

[6] Zeybek, A. and Yiğit, F. (2003). Assessment of powdery mildew resistance in wild barley (*Hordeum spontaneum* L.) populations in the aegean region of Turkey. Phytoprotection, 83, 125-130.

[7] Dreiseitl, A. (2004). Virulence frequencies to powdery mildew rezsistance genes of winter barley cultivars. Plant Protection Science. 40(4), 135-140.

[8] Kokina, I. and Rashal, I. (2008). Results oft he monitoring oft he population of *Blumeria graminis* f. sp. *hordei* in the Latgale region of Latvia in 2007. Zemdirbyste-Agriculture. 3, 320-326.

[9] Parks, R., Carbon, I., Murphy, J.P., Marshal, D. and Cowger, C. (2008). Virulence structure of the Eastern U.S. Wheat Powdery Mildew Population. Plant Disease. 92, 1074–1082.

[10] Zeybek, A., Khan, M.K., Pandey, A., Gunel, A., Erdogan, O. and Akkaya, M.S. (2017). Genetic structure of powdery mildew disease pathogen *Blumeria graminis* f. sp. *hordei* in the barley fields of Cukurova in Turkey. Fresen. Environ. Bull. 26(1a), 906-912.

[11] Gabler, J. and Fritshe, H. (1991). Results (1987-1989) of virulence analysis in barley mildew in the former GDR. Integrated control of cereal mildews: virulence patterns and their change Ed. J. Helms Jorgensen. Riso National Laboratory, Roskilde, Denmark.

[12] Frank, A.S. (1992). Ecological and genetic models of host-pathogen convolution. Heredity. 67,73-83.

[13] Winzeler, M., Streckeisen, P. and Fried, P.M. (1991). Virulence analysis of the wheat powdery mildew population in Switzerland between 1980 and 1989. In J. Helms Jorgensen, ed (Roskilde). 15-21.

[14] Welz, G. (1986). Struktur und dynamik der virulenz in populationen von *Erysiphe graminis* f sp. *hordei* marchal. Ph.D Thesis.

[15] Habgood, R.M. (1970). Designation of physiological races of plant pathogens. Nature. 227, 1268-1269.

[16] Herrmann, A., Löwer, C.F. and Schachtel, G.A. (1999). A new tool for entry and analysis of virulence data for plant pathogens. Plant Pathology. 48, 154–158.

[17] Hovmøller, M.S., Caffier, V., Jalli, M., Andersen, O., Besenhofer, G., Czembor, J.H., Dreiseitl, A., Felsenstein, F., Fleck, A., Heinrics, F., Jonsson, R., Limpert, E., Mercer, P., Plesnik, S., Rashal, I., Skinnes, H., Slater, S. and Vronska, O. (2000). The European barley powdery mildew virulence survey and disease nursery 1993-1999. Agronomie. 20, 729-743.
[18] Dreitseitl, A., Platz, G. (2012). Powdery mildew resistance genes in barley varieties grown in Australia. Crop and Pasture Science. 63(10), 997-1006.
[19] Yahyaoui, A.H., Reinhold, M. and Scharen, A.L. (1997). Virulence spectrum in populations of the barley powdery mildew pathogen, *Erysiphe graminis* f. sp. *hordei* in Tunisia and Morocco in 1992. Plant Pathology. 46, 139-146.
[20] Dreiseitl, A. and Rashal, I. (2004). Powdery mildew resistance genes in Latvian barley varieties. Euphytica. 135, 325-332.
[21] Wachter, V. and Fritsche, H. (1991). The composition of virulence genes in powdery mildew populations from wheat and barley in the from 1978 to 1988 using race analyses. Integrated Control of Cereal Mildews: Virulence Patterns and Their Change.
[22] Andrivon, D.E.L. and Vallavieille-Pope, C. (1991). Evolution of barley mildew populations in France, 1986-1989. In: Integrated Control of Cereal Mildews: Virulence Patterns and Their Change Ed. J. Helms Jorgensen. Riso National Laboraty, Roskilde, Denmark. 43-52.
[23] Caffier, V., Hoffstadt, T. and Leconte, M. (1996). Seasonal changes in pathotype complexity in French populations of barley powdery mildew. Plant Pathology. 45, 454-468.
[24] Czembor, J.H. and Czembor, H.J. (2000). Powdery mildew resistance in selections from Moroccan barley landraces. Phytoparasitica. 28, 1.
[25] Naghavi, M.R., Yazdi-Samadi, B. and Ghannadha, M.R. (2008). Genetics of powdery mildew resistance in barley cultivars. Plant Breeding Dept., Faculty of Agriculture, Univ. of Tehran, Iran. 33.

Received: **24.04.2017**
Accepted: **15.10.2017**

CORRESPONDING AUTHOR

Ahmet Zeybek
Muğla Sıtkı Koçman University
Department of Biology
48000 Muğla-Turkey

e-mail: ahmetzeybek@hotmail.com

© by PSP Volume 26 – No. 12A/2017 pages 8345-8552 Fresenius Environmental Bulletin

HOT SPOTS OF NO_X EMISSION FROM THE CEMENT FACTORY MAIN STACKS

Majid Farhadi[1], Pierre Sicard[2], Alessandra De Marco[3], Mohammad Khoshgoftar[4], Adewale M. Taiwo[5], Mohammad Javad Mohammadi[6,7], Shahram Sadeghi[8], Shirin Esmaeili[9], Abdeltif Amrane[10], Bahram Kamarehie[1], Yusef Omidi Khaniabadi[11,*]

[1]Nutrition Health Research Center, Department of Environmental Health, School of Health and Nutrition, Lorestan University of Medical Sciences, Khorramabad, Iran.
[2]ACRI-HE, Sophia-Antipolis, France.
[3]Department of Territorial and Production Systems Sustainability, SSPT-MET-INAT, ENEA, Via Anguillarese 301, 00123, Rome, Italy.
[4]Vice-chancellery of Health, Shahroud University of Medical Sciences, Shahroud, Iran.
[5]Department of Environmental Management & Toxicology, Federal University of Agriculture, Abeokuta, Nigeria.
[6]Abadan School of Medical Sciences, Abadan, Iran
[7]Asadabad School of Medical Sciences, Asadabad, Iran
[8]Environmental Health Research Center, Kurdistan University of Medical Sciences, Sanandaj, Iran
[9]Department of Environmental Health Engineering, School of Public Health, Ahvaz Jundishapur University of Medical Sciences, Ahvaz, Iran.
[10]Ecole Nationale Supérieure de Chimie de Rennes, CNRS, UMR 6226, 11 allée de Beaulieu, CS 50837, 35708 Rennes Cedex 7, France.
[11]Health Care System of Karoon, Ahvaz Jundishapur University of Medical Sciences, Ahvaz, Iran.

ABSTRACT

The aim of this study was to assess nitrogen oxides (NO_x) dispersion from the main stacks of a cement factory in Doroud, Iran. The SCREEN3 software and Gaussian plume model were applied to predict and to compare the on-site NO_x concentrations to provide relevant information on its emissions and dispersion. The results showed that within a radius of 400-650 m from the source, the estimated NO_x concentrations were higher than the National Ambient Air Quality Standards for human health protection. Therefore, a distance higher than 650 m at downwind direction of the source was recommended for human settling and activities.

KEYWORDS:
NO_x, Cement plant, Dispersion, SCREEN3, Gaussian plume model

INTRODUCTION

The deterioration of ambient air quality by industrial and related emission sources of air pollutants (e.g. traffic, biomass burning, incineration of wastes, refineries, etc.) is one of the important problems in the world, especially in developing countries [1-3]. Exposure to air pollutants is associated with chronic and acute adverse effects on human health [3-5].

In 2012, around 7 million global prematurely deaths were linked to air pollution of which one in eight deaths was from lung cancer, strokes and heart diseases [6-10]. In the last decades, the effects of long-term exposure to air pollutants and their impacts on human health were deeply investigated [2].

Air pollution is associated with problems such as exacerbated asthma, hospital admissions and increased medication use. The epidemiological studies had focused on ozone (O_3), particulate matter (PM), sulfur dioxide (SO_2), carbon monoxide (CO), nitrogen dioxide (NO_2), particulate lead and other atmospheric chemical toxicants due to their proven health outcomes [11-13]. NOx is one of the specific groups responsible for secondary formation of PM through reaction between O_3 and VOCs. Due to the well documented concerns about NO_x, the United States Environmental Protection Agency (USEPA) had established standards for NOx emissions in the air. NO_x emissions depend on several factors such as wind speed and direction, relative air humidity, ambient air temperature, wet and dry depositions of NO_2 and the reactions of NO_2 with O_3 and VOCs to form secondary PM. Exposure to high NO_2 high concentrations can result in rapid and severe lung damage. Some evidence suggested that exposure to NO_x may result in both acute and chronic health effects in vulnerable population such as people with asthma and the elderly. The airways may become acutely inflamed and even short-term exposure to NO_2 may predispose towards an increased risk for respiratory diseases [12, 14]. A prolonged NO_2 exposure may reduce lung host defenses and significantly change lung structure.

Cement is one of the most widely used man-made substances on the planet. The annual mean consumption in cement is 450 kg per capita in the World. However, making cement is an energy and resource intensive process with negative impacts on local and global environment. Air pollutants due to industrial activities from Doroud Cement Factory affect cities located in the southwest of Iran. Around

this factory, people are exposed to high nitrogen oxides (NO_x) levels from major sources including fuel-burning process at temperatures higher than 1250 ˚C and road traffic. The largely emitted pollutants during the production of cement are PM, NO_x, SO_2, carbon dioxide (CO_2) and CO. Trace quantities of volatile organic compounds (VOCs), and trace metals.

To reduce the adverse effects of air pollutants, it is important to identify how pollutants are dispersed in the troposphere [1, 15-17]. Parameters that impact the dispersion of air pollutants and downwind concentrations are wind speed and direction, air temperature lapse rates, elevation, release height and the atmospheric stability [18-20]. There is a requirement to quantify, identify and distribute these pollutants with appropriate management strategies [16]. To overcome these issues, software tools based on Gaussian dispersion equation are usually used to estimate air pollutant concentrations away from their different sources. Many models are available for dispersion studies i.e., gross screening, intermediate and advance models. The gross screening models require only a hand-held calculator or spreadsheet, while the intermediate models (computed-based e.g. the SCREEN3) incorporates meteorological parameters (wind speed and stability classes) and more sophisticated source information. Advanced models require a workstation and extensive datasets for meteorology and emission sources including multiple source type points, area and volume, and also additional features such as flow around buildings and layered atmospheric structure. Some examples of advanced models are ISC3, AERMOD, CALPUFF and ADMS. The main objective of this study is to assess the NO_x emissions from the stack of Doroud Cement factory using the SCREEN3 and Gaussian plume models during four season in 2013-2014.

EXPERIMENTAL SECTION

Study area. Doroud cement factory (33˚29′N; 49˚4′E) is one of the most productive industries in the Doroud City (Lorestan Province) located in the southwestern Iran (Fig. 1). The factory (capacity of 300 tons per day) was established in 1959. It is located in vicinity of the residential areas. Figure 1 shows the location of the study area in Iran.

***In situ* measurements of NO_x.** Four sampling campaigns were conducted to measure NO_x mass flow (mass per unit of time) and concentrations at three stacks in the cement plant in May, August, November 2013 and February in 2014. The samples were taken from the stack gas flow based on standard of ASTMD5522-EPACTM-030 using Testo (XL350) instrument. The mass flow and concentrations of NO and NO_2 were measured separately. The sum of NO and NO_2 ($NO+NO_2$) mass flow was considered as NO_X emissions.

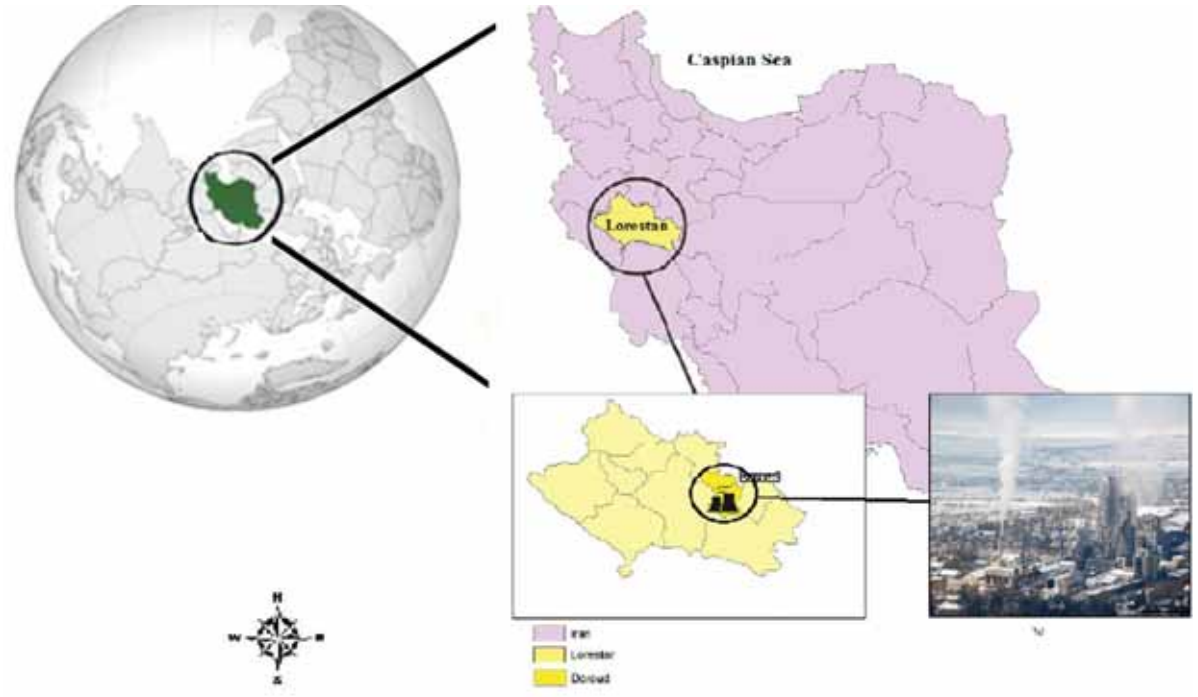


FIGURE 1
The map of the study location (Doroud Factory) in Iran

TABLE 1
Stability classes over four sampling periods for the three stacks: Electro filter 1, Electro filter 2 and Kiln

Fuel characteristics	Season	Stability class
Natural gas +Fuel-oil	Spring	C
Natural gas	Summer	B
Natural gas	Fall	D
Fuel-oil	Winter	F

TABLE 2
Physical factors related to the three stack of cement factory

Physical factors of stacks	Electro filter 1	Kiln	Electro filter 2
Stack height (m)	54	70	90
Stack inside diameter (m)	2.8	2.8	4.0
Temperature of gas flow (˚K)	356.0 ± 9.9	403.0 ± 13.0	435.0 ± 9.9
Exit gas velocity (m/s)	7.77 ± 0.52	14.77 ± 3.22	11.62 ± 1.79

Measurement of Meteorological data. The required meteorological data were obtained from the meteorological station located at the Doroud's airport, close to the cement factory. The relative humidity (RH), air temperature, and surface wind speed and directions at attitude 10m above the ground-level were used in the meteorological analysis to estimate and simulate the NO_X emissions and dispersion from the cement factory stack. Monthly averages of air temperature, wind speed and RH were applied for trends in meteorological parameters. The 3-month results of wind speed and direction were used to produce the seasonal wind roses. For short time period, a constant representative of atmospheric stability was assumed. In this study, four stability classes were considered: slightly unstable (C), unstable (B), neutral (D) and stable (F); for each season, a stability class was selected. Table 1 illustrates the stability classes over the sampling periods from the three stacks (Electro filter 1, 2 and Kiln) and fuel characteristics.

The seasonal nitrogen oxides measured from the three stacks of the cement plant were applied for calibration of the model. The temperature of the gas flow and exit velocity was measured during the sampling period while the stack height and stack inside diameter were used to model the dispersion of NO_x (Table 2).

Modeling. (1) Gaussian model. Gaussian dispersion model combines source-linked factors and meteorological parameters to assess pollutant concentration from different sources. The model assumes that the pollutant does not undergo chemical reactions or do not undergo elimination through other processes including dry or wet deposition. The ground-level NO_x concentrations are calculated by a Gaussian model in the downwind direction [18].

For the calculation of the wind speed at the stack height, it is necessary to convert the wind speed at 10 m height (measured by the meteorological station) to the wind speed at the stack nozzle (Eq.1).

$$u = u_0\left(\frac{H_s}{Z_0}\right)^n \quad (1)$$

Where, u and u_0 (m/s) are the wind speed at the stack height (H_s, m) and the measured wind speed at 10 m height (Z_0, m), respectively. Parameter n, i.e. the wind profile exponent, is a function of the atmospheric stability.

The standard theory assumes that a rising buoyant plume entrains ambient air at a rate proportional to both its cross-sectional area and its speed relative to the surrounding air. For the calculation of rising buoyant plume (dh), the parameters of initial velocity of gas flow (w_0), the inside stack radius (R_0), and temperature are needed. Initial buoyancy flux (F_b) can be obtained by Eq. 2.

$$F_b = \frac{W_0 R_0^2 g}{T_{p0}(T_{p0} - T_{a0})} \quad (2)$$

where T_{p0} and T_{a0} are the initial plume temperature and the ambient temperature at the stack height, respectively. For amount of $F_b \geq 55$ m^4 s^{-3} in the Pasquill categories of A-D, buoyant rise was obtained by Eq. 3. In this study, the amount of F_b for classes of A-D was lower than 55 m^4 s^{-3}.

$$dh = 38.71\frac{F_b^{0.6}}{u_s} \quad (3)$$

Where, u_s is the wind speed at the stack height.

In a stable atmosphere (class E and F), the final plume rise dh is given by Eq. 4.

$$dh = 2.6\left(\frac{F_b}{u_s}\right)^{\frac{1}{3}} \quad (4)$$

The final effective plume height (H, m) is the stack height (h_s) plus the plume rise (dh) given by Eq. 5.

$$H = h_s + dh \quad (5)$$

Equations that approximately fit the Pasquill-Gifford curves are used to estimate δy and δz for the rural mode. The equations (6-8) were used to calculate of δy and δz.

$$\delta_y = 465.11628(x)\tan(TH) \quad (6)$$

$$\delta_z = ax^b \quad (7)$$

Where, *TH* was computed by Eq. 9.

$$TH = 0.017452393[c - d\ln(x)] \quad (8)$$

In Eqs. 6-8, *x* is the downwind distance and the coefficients *a, b, c* and *d* were calculated according to the Pasquill stability category.

(2) The SCREEN3. The SCREEN3 is a software (Likes Environmental Software, Waterloo, Ontario, Canada), developed by the EPA based on Gaussian model. It is a screening version of the Industrial Source Complex Dispersion Models (ISC3) and can be used for dispersion modeling at distances lower than 100 km from the emission source. To estimate the air pollutant concentrations, SCREEN3 incorporates different factors related to emitted source and meteorological parameters. The requested information to run the SCREEN3 software includes source type, emission rate (g/s), source stack height (m), stack inner diameter (m), stack exit velocity (m/s), temperature of exit gas (˚K), outdoor air temperature (˚K), receptor height from ground level (m), wind direction, and urban or rural option.

RESULTS AND DISCUSSION

Atmospheric conditions are the driving force in the dispersion and air pollutant plumes transport [18-21]. The variation of meteorological parameters such as including RH, temperature and surface wind speeds are presented in Fig. 2. The average wind speed increased from July to October and then decreased till February. The highest and the lowest wind speed occurred in spring (May) and winter (February), respectively, due to unstable meteorological conditions during different time intervals, which have an important role in the formation of powerful winds [21-23]. A minimum hourly temperature of - 9.6 ˚C was recorded during the study period in January 2014. The temperature gradually increased from April to August (spring, summer) and decreased from September to January (autumn, winter). The maximum mean air temperature (39°C) and minimum RH (23%) were observed in August. The RH decreased from April to August.

Fig. 3 (a-d) show the seasonal wind rose plots of wind directions from the daily data recorded by meteorological station. Generally, seasonal winds and mountain-valley breezes influenced the diurnal climate. The easterly winds were prevalent during the spring season; but as temperature increases from spring to winter, the wind directions changed from south-easterly to southeasterly. The maximum percentage of time the winds were blowing from the prevalent southerly winds during spring, summer, fall, and winter were 27.5, 17.4, 26.1 and 38.5%, respectively. A similar study by Seangkiatiyuth et al. [23] from *in-situ* measurement and model estimation using the American Meteorological Society-Environmental Protection Agency Regulatory Model (AERMOD) at a cement plant in Bangkok (Thailand) showed that the percentage of time of wind change as 6.9%, 17.7%, and 47.8%, respectively. Sari et al. [21] reported that the prevailing direction of NO_x dispersion from the palm oil mill stack in Indonesian was southerly, with a maximum concentration of 90.1 µg/m^3. In addition, the changes of wind directions in Figure 3 (a-d) were more pronounced in warm season (spring and summer) than during the cold season (autumn and winter). Therefore, there were fewer episodes of calm periods in cold season compared to the warm season.

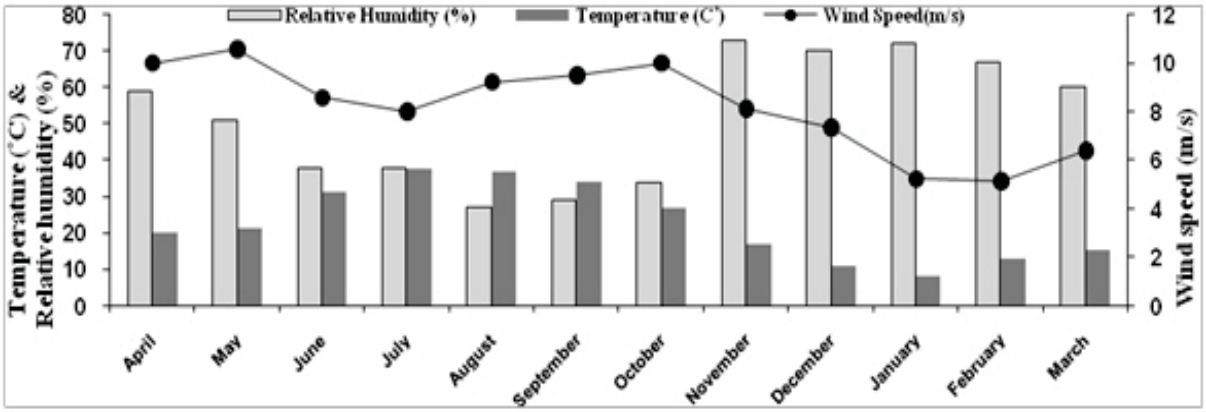


FIGURE 2
Seasonal pattern of wind speed, RH and temperature from April 2013 to March 2014

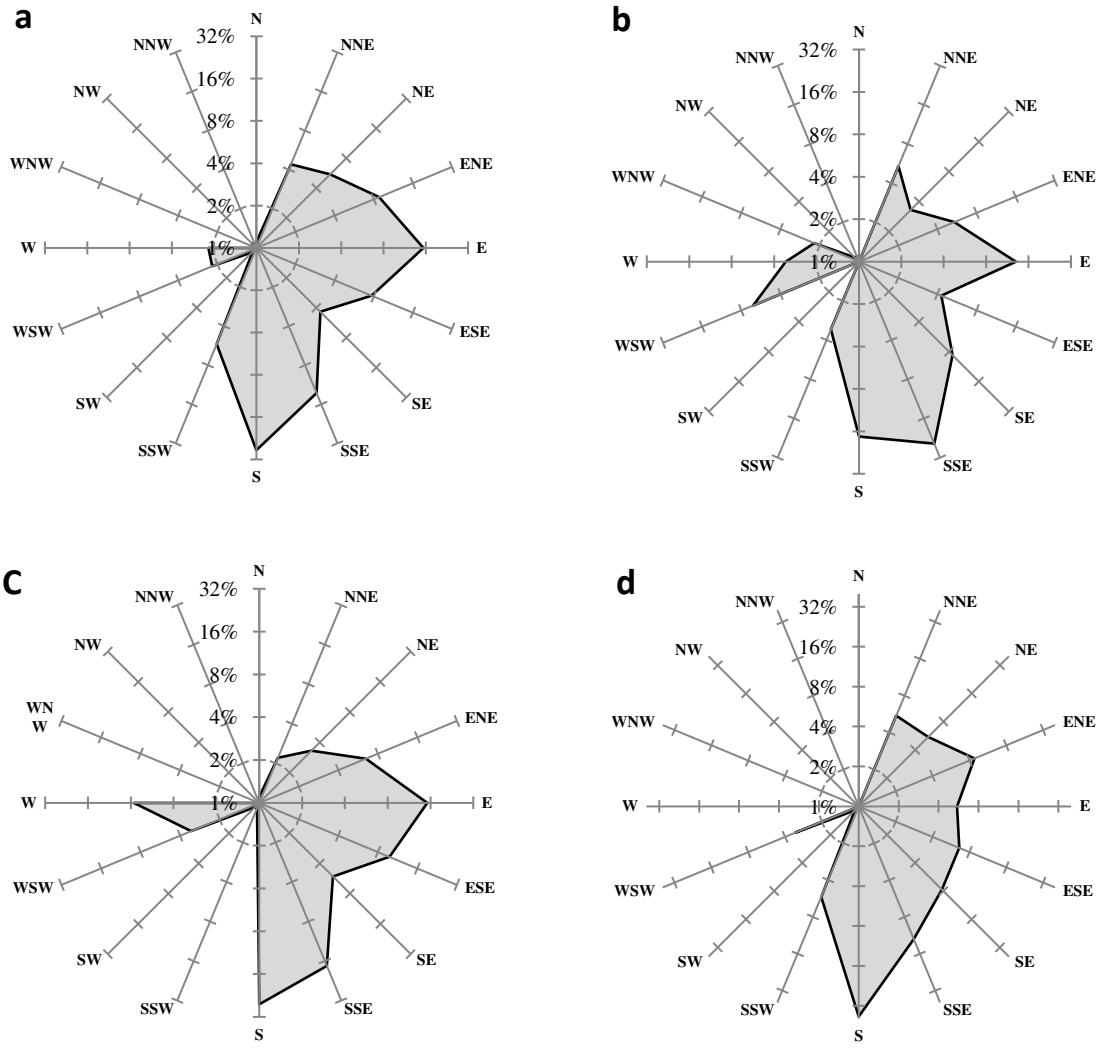


FIGURE 3
Wind rose plots (a) spring, (b) summer, (c) fall, and (d) winter during the study period

The comparison between NO_x dispersion simulated by the SCREEN3 and Gaussian plume models for the four stability classes at spring, summer, fall and winter seasons are presented in Fig. 4 (a-d). The maximum predicted NO_x concentrations under the stability classes of C, B, D, and F by the SCREEN3 at the downwind of the source were 344.9, 213.2, 114.1, and 195.7 µg/m^3, respectively, while the Gaussian model estimations were 273.8, 176.9, 109.8, and 187.6 µg/m^3, respectively. The ratios of maximum predicted levels by Gaussian plume to SCREEN3 in four stability classes of C, B, D, and F were 0.79, 0.83, 0.96, and 0.96, respectively. The previous study [1] showed that, the maximum 1-hour predicted level of NO_x by AERMOD from the stack of a Jordanian cement plant was 85.1 µg/m^3 within 2000 meter from the source.

The seasonal variation of distances where the maximum concentrations of NOx were measured is 526 m (spring), 584 m (summer), 960 m (autumn) and 2647 m (winter) downwind. Close to the source within the radius of 200-500 m (at summer and winter) from the NO_x concentrations (8.6, 0.3, 0.4 and 0.1 µg/m^3) were low, but from, the, distance of 526, 584, 960, and 2647 m from the source; the NO_x levels increased rapidly to 345, 213, 115 and 196 µg/m^3, respectively. The present study is consistent with those of Mohebbi and Baroutian [19] who demonstrated that the point of maximum concentration of PM_{10} was 750 m downwind of a cement plant in Kerman, Iran. The study also revealed good agreement among the predicted concentrations of PM_{10} by the Eulerian, Gaussian plume and ANNs models. Seangkiatiyuth et al. [23] showed that NO_2 concentration peaks were found within 1 to 5 km by the AERMOD applied at a Cement complex located about 108 km northeast of Bangkok.

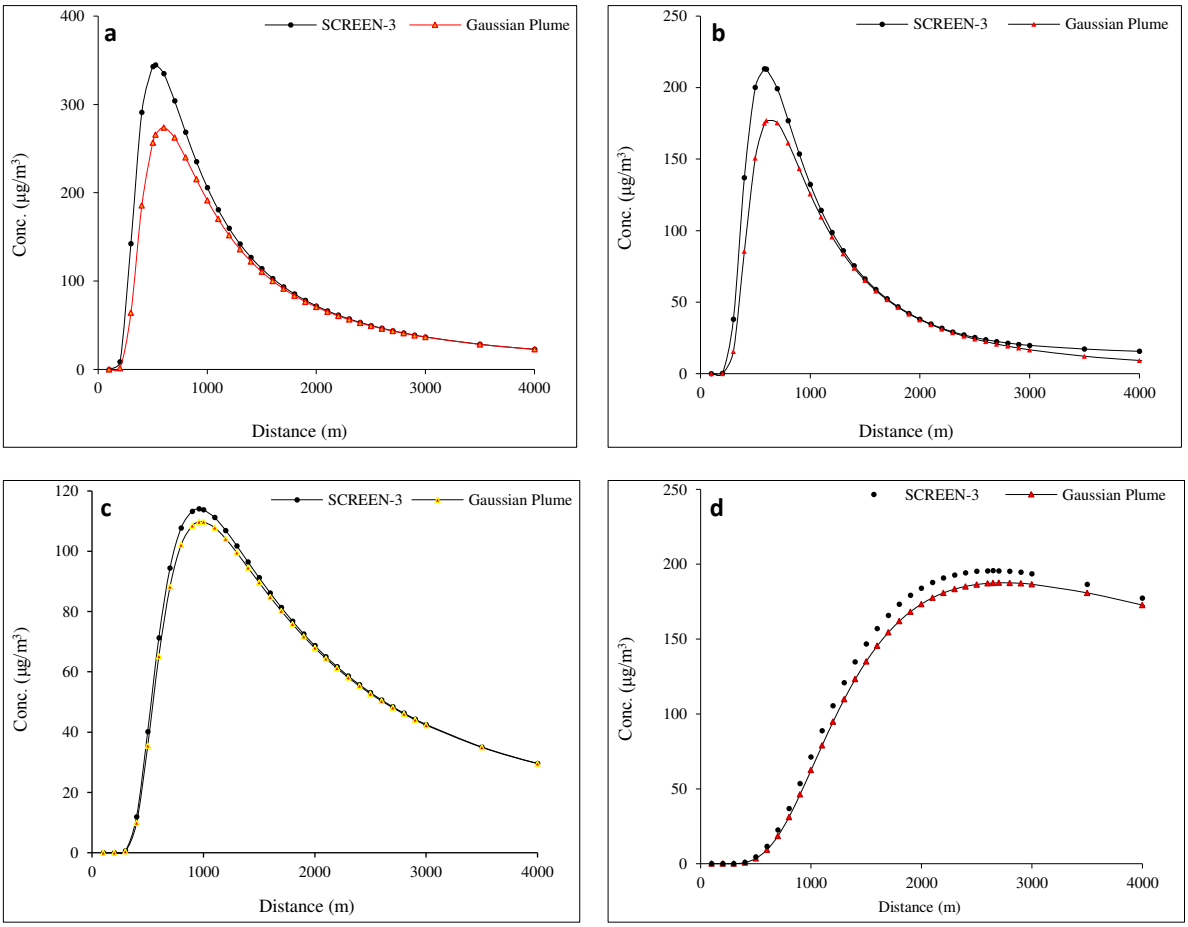


FIGURE 4
Comparison of estimated concentrations by the SCREEN3 and Gaussian plume model at (a) spring, (b) summer, (c) autumn and (d) winter over the study period

The highest concentrations of NO_x were obtained in winter with a stability class of F for both models. The worst atmospheric condition was obtained in slightly unstable class during spring season, where pollution concentrations increased rapidly. The comparison between the results of the SCREEN3 and the Gaussian plume showed that there is a good agreement between the two models, especially for D and F stability classes. The amounts of NO were very low, and sometime close to zero. Considering NO_2 as representative of NO_X emissions, during spring the NO_2 concentrations of 320 µg/m^3 (1-hour average value) at stability class of C were higher than the Nation Ambient Air Quality Standard (NAAQS). Therefore, at a distance of 400-650 m from the source, the NO_x concentrations estimated by the SCREEN3 were higher than the NAAQS. Our NO_x results were higher than emissions reported values from European cement kilns in 2010 [24]. The concentrations of NO_x as NO concentrations ranged from 145 to 2040 mg/m^3 with an average concentration of 785 mg/m^3 [25]. Exposure to high concentration of NO_x and other air pollutants from the cement factory is dangerous to public health. Schuhmacher et al. [22] indicated that NO_2 has not been considered as a causal predictor of mortality, but has increased the risk of asthma by 0.2%. Otaru et al. [20] reported that due to the emissions from cement plants; a simulated safety distance of 7000 m from the source is recommended for human settlement and their activities.

CONCLUSION

In this study, two different models were used find out the patterns of NO_x dispersion from Doroud Cement Factory in Iran. The dominant direction of NO_x dispersion was toward the southern parts of the cement plant. The highest and the lowest concentration were predicted under the stability classes of C and D, respectively. There was a good agreement between the results from the SCREEN3 software and the Gaussian plume model. At a distance of 400-650 m from the source, the estimated NO_x concentrations were higher than the NAAQ standards. This indicates that NO_x emissions from the cement plant can negatively impact the health of the residents living

around the vicinity of the industry. Therefore, a distance farther than 650 m downwind of the cement plant is recommended for human settlement and activities. The method proposed to quantify emissions with field experience in the cement industry, and model dispersion had produced good results. Both models adopted in this study provided useful information to determine pollution hotspots for NOx dispersion. It is important to emphasize that application of atmospheric dispersion models can be useful when applied together with measured data to permit more robust and improved predictive atmospheric studies [20, 27].

ACKNOWLEDGEMENTS

This study was supported by Lorestan University of Medical Sciences (Grant no: 1143).

The authors do not have conflict of interest.

REFERENCES

[1] Abu-Allaban, M., Abu-Qudais, H. (2011) Impact Assessment of Ambient Air Quality by Cement Industry: A Case Study in Jordan. Aerosol and Air Quality Research. 11, 802-810.

[2] Taiwo, A.M., Harrison, R.M., Shi, Z. (2014b) A review of receptor modelling of industrially emitted particulate matter. Atmospheric Environment. 97, 109-120.

[3] Dobaradaran, S., Geravandi, S., Goudarzi, G., Idani, E., Salmanzadeh, S., Soltani, F. (2016) Determination of Cardiovascular and Respiratory Diseases Caused by PM_{10} Exposure in Bushehr, 2013. Journal of Mazandaran University of Medical Sciences. 26, 42-52.

[4] Daryanoosh, M., Goudarzi, G., Rashidi, R., Keishams, F., Hopke, P.K., Mohammadi, M.J., Nourmoradi, H., Sicard, P., Takdastan, A., Vosoughi, M., Veysi, M., Kianizadeh, M., Khaniabadi, Y.O. (2017) Risk of morbidity attributed to ambient PM10in the western cities of Iran. Toxin Reviews.

[5] Geravandi, S., Sicard, P., Khaniabadi, Y.O., De Marco, A., Ghomeishi, A., Goudarzi, G. (2017) A comparative study of hospital admissions for respiratory diseases during normal and dusty days in Iran. Environmental Science and Pollution Research. 24, 18152-9.

[6] Khaefi, M., Goudarzi, G., Yari, A.R., Geravandi, S., Dobaradaran, S., Idani, E. (2016) An association between ambient pollutants and hospital admitted respiratory cases in Ahvaz, Iran. Fresen. Environ. Bull. 25, 3955-61.

[7] Goudarzi, G., Daryanoosh, S., Godini, H., Hopke, P., Sicard, P., De Marco, A., Rad, H., Harbizadeh, A., Jahedi, F., Mohammadi, M. (2017) Health risk assessment of exposure to the Middle-Eastern Dust storms in the Iranian megacity of Kermanshah. Public Health. 148, 109-116.

[8] Hess, G. (1989) Simulation of Photochemical Smog in the Melbourne Air shed: Worst Case Studies. Atmospheric Environment. 23, 661-669.

[9] Jeong, S. (2013) The Impact of Air Pollution on Human Health in Suwon City. Asian J Atmos Environ. 7, 227-33.

[10] Kahforoshan, D., Fatehifar, E., Babalou, A., Ebrahimin, A., Elkamel, A., Soltanmohammadzadeh, J. (2008) Modeling and Evaluation of Air pollution from a Gaseous Flare in an Oil and Gas Processing Area, WSEAS Conferences Santander, Cantabria, Spain, 23-25.

[11] Zajac, G., Szyszlak, J., Wasilewski, J., Kuranc, A. (2017) Emission characteristics of biomass combustion in a domestic heating boiler fed with wood and virginia mallow pellets. Fresen. Environ. Bull. 26, 4663-4670.

[12] Khaniabadi YO, Daryanoosh SM, Amrane A, Polosa R, Hopke PK, Goudarzi G, Mohammadi MJ, Sicard P, Armin H (2017a): Impact of Middle Eastern Dust storms on human health. Atmospheric Pollution Research 8, 606-613.

[13] Khaniabadi, Y.O., Daryanoosh, S.M., Hopke, P.K., Ferrante, M., De Marco, A., Sicard, P., Conti, G.O., Goudarzi, G., Basiri, H., Mohammadi, M.J. (2017b) Acute myocardial infarction and COPD attributed to ambient SO2 in Iran. Environmental Research. 156, 683-687.

[14] Khaniabadi, Y.O., Fanelli, R., De Marco, A., Daryanoosh, S.M., Kloog, I., Hopke, P.K., Conti, G.O., Ferrante, M., Mohammadi, M.J., Babaei, A.A. (2017c) Hospital admissions in Iran for cardiovascular and respiratory diseases attributed to the Middle Eastern Dust storms. Environmental Science and Pollution Research. 1-9.

[15] Khaniabadi, Y.O., Goudarzi, G., Daryanoosh, S.M., Borgini, A., Tittarelli, A., De Marco, A. (2017d) Exposure to PM10, NO2, and O3 and impacts on human health. Environmental Science and Pollution Research 24, 2781-2789.

[16] Khaniabadi, Y.O., Hopke, P.K., Goudarzi, G., Daryanoosh, S.M., Jourvand, M., Basiri, H. (2017e) Cardiopulmonary mortality and COPD attributed to ambient ozone. Environmental research. 152, 336-341.

[17] Khaniabadi, Y.O., Polosa, R., Chuturkova, R.Z., Daryanoosh, M., Goudarzi, G., Borgini, A., Tittarelli, A., Basiri, H., Armin, H., Nourmoradi, H., Babaei, A.A., Naserian, P. (2017f) Human health risk assessment due to ambient PM10 and SO2 by an air quality modeling technique. Process Safety and Environmental Protection. 111, 346-354.
[18] Wan, D., Han, Z., Liu, D., Yang, J. (2016) Pollution levels and spatial distribution of heavy metals in house dust from an industrial area in xi'an, central China. Fresen. Environ. Bull. 25, 839-51.
[19] Mohebbi, A., Baroutian, S. (2007) Numerical Modeling of Particulate Matter Dispersion from Kerman Cement Plant, Iran. Environ Monit Assess. 130, 73–82.
[20] Otaru, A., Odigure, J., Okafor, J., Abdulkareem, A. (2013) Model prediction of particulate dispersion from a Cement Mill Stack: Case study of a Cement Plant in Nigeria. IOSR Journal Of Environmental Science, Toxicology And Food Technology. 3, 97-110.
[21] Sari, N., Tarumum, S., Saryono, S. (2014) Pollutant dispersion modelling (Dust, CO, NOx, and SOx) from palm oil mill stack. Indonesian Journal of Environmental Science and Technology. 1, 28-34.
[22] Schuhmacher, M., Domingo, J.L., Garreta, J. (2004) Pollutants emitted by a cement plant: health risks for the population living in the neighborhood. Environmental Research. 95 198-206.
[23] Seangkiatiyuth, K., Surapipith, V., Tantrakarnapa, K., Lothongkum, A.W. (2011) Application of the AERMOD modeling system for environmental impact assessment of NO2 emissions from a cement complex. Journal of Environmental Sciences. 23, 931–940.
[24] Taiwo, A., Beddows, D., Calzolai, G., Harrison, R.M., Lucarelli, F., Nava, S., Shi, Z., Valli, G., Vecchi, R. (2014a) Receptor modelling of airborne particulate matter in the vicinity of a major steelworks site. Science of the Total Environment 490 488-500.
[25] U.S. Environment Protection Agency RTP, NC, USA (1995) SCREEN3 Model User's Guide. EPA-454/B-95-004.
[26] Zhong, S., Zhou, L., Wang, Z. (2011) Software for Environmental Impact Assessment of Air Pollution Dispersion Based on ArcGIS. Procedia Environmental Sciences. 10, 2792 - 2797.
[27] Zhou, M., Liu, Y., Wang, L., Kuang, X., Xu, X., Kan, H. (2014) Particulate air pollution and mortality in a cohort of Chinese men. Environmental Pollution. 186 1-6.

Received: **25.06.2017**
Accepted: **13.10.2017**

CORRESPONDING AUTHOR

Yusef Omidi Khaniabadi
Health Care System of Karoon, Ahvaz Jundishapur University of Medical Sciences, Ahvaz, Iran

E-mail: yusefomidi@yahoo.com

AUTHOR INDEX

A

Abari, M. F. 8135
Abbas, T. 7643
Ahmad, K. 7643, 7838
Ak, I. 8160
Akhtar, M. 7838
Aksoy, H. S. 7626
Aksoy, L. 7893
Al Khushman, M. 7806
Al Sahli, A. 7643, 7838
Alansi, S. 7780
Al-Antary, T. M. 8298
Al-Najjar, T. 7806
Alpaslan, M. N. 7634
Al-Qurainy, F. 7780
Alshameri, A. 7780
Altikatoglu, M. 7832
Amrane, A. 8345
Araj, S. E. A. 8298
Arikan, S. 7634
Asikoglu, O. L. 7874
Atasagun, S. 8321
Attar, A. 7832
Aydın, B. 8233
Ayub, M. 7643, 7838

B

Bagheri, Z. 8135
Bakopoulos, V. 7849
Bashir, H. 7838
Batool, A. I. 7838
Batool, F. 7838
Bayram, Y. 8146
Belghasem, I. H. 8298
Benzeden, E. 7874
Beyaz, A. 7717
Beyaz, R. 8239
Bilgin, A. 8093
Buyuk, M. 8146
Buyukben, A. 7893
Buyukdeveci, F. 8109

C

Cai, Y. 8199
Caldirak, H. 8047
Canoglu, M. C. 8047
Cao, J. 7769
Celik, B. 7931
Celik, L. 7750
Celik, M. 7750
Cenkseven, S. 7992
Cetin, A. K. 7974
Ceyhan-Guvensen, N. 7957, 8316
Chalazas, T. 7849
Chan, K. C. C. 7906
Chen, M. 7734
Chen, X. 8270
Chunwang, L. 8078
Ciftci, H. 7740
Cilingir, I. 7717
Cooper, D. 7849
Coruhlu, Y. E. 8008
Cristache, C. M. 7832

D

Dagtekin, M. 7717
Dalgic, E. 8337
Darici, C. 7992
De Marco, A. 8345
Demir, B. 7651
Demirbas, A. 8328
Deng, J. 8199
Deng, Q. 8255
Devetakovic, J. 7925
Diken, M. E. 8023
Dincer, D. 7789
Dogan, S. 8023
Dogan, Y. 7838
Dogan, M. 8023
Dolgen, D. 7634
Dong, G. 7687
Dong, G.-T. 8131
Duman, M. 8146
Durukan, H. 8328
Duzenli, T. 7789, 8304

E

Efstratiou, M. A. 7849
Eker, M. 8286
Eker, S. 8221
Elshikh, M. S. 7643, 7838
El-Zaidy, M. 7643, 7838
Emdad, M. R. 7885
Er, C. 7740
Erci, F. 7832
Erdal, B. 8160
Erdem, H. 8328
Erdogan, M. A. 7760
Erdogan, O. 7695
Ergonul, M. B. 8321
Eris, E. 8001
Erkan, I. 8207
Esmaeili, S. 8345

F
Fang, F. 7769
Farhadi, M. 8345
Farivar, A. 7750

G
Gaafar, A.-R. Z. 7780
Gao, Y. 8166
Gencoglan, S. 8211
Gerdan, D. 7717
Gong, R. 8255
Gor, M. 7626
Gore, M. E. 7695
Guanfang, Z. 8078
Gui, H. 8246
Gulcin,, D. 7941
Guo, J.-X. 7724

H
Han, Y. 7914
Hazman, O. 7893
He, X. 8166
Huang, D. 8246
Huang, L. 8069

I
Inal, B. 8211
Iqbal, S. 7838
Isildak, I. 7832

J
Jiang, B. 8226
Jing, L. 8078
Jokanovic, D. 7925

K
Kadak, A. E. 7750
Kamarehie, B. 8345
Kang, Y. 7667
Kanmaz, E. 7710
Kaplan, C. 8211
Karacakaya, P. 8321
Karakoy, T. 8328
Kariptas, E. 7740
Katsoulis, K. 7825
Kaukab, R. 7643
Kaynas, B. Y. 8041
Kendirlioglu, G. 7974
Kerkez, D. 8184
Keskin, D. 8316
Khadra, K. A. 7806
Khalaf, M. 7806
Khan, S. 7780
Khan, Z. I. 7643, 7838
Khaniabadi, Y. O. 8345
Khoshgoftar, M. 8345
Kiray, E. 7740
Kiyaga, V. B. 8109
Kocak, B. 7992
Koloren, O. 8221
Korkmaz-Guvenmez, H. 7992
Kucharski, J. 7658
Kucukal, G. 8207
Kucukgulmez, A. 7750
Kulic, A. 8184
Kurtulus, B. 8047
Kuzu, S. B. 7992

L
Li, B. 7981, 8154
Li, C. 7769
Li, G.-Q. 7906
Li, H. 8270
Li, J.-Z. 8100
Li, M. 7667
Li, Q. 7914, 7756
Li, W. 8131
Li, X. 8166
Li, Y. 8131, 8166
Li, Z.-D. 8131
Liao, F.-M. 7724
Liao, M. 8255
Lin, M. 8246
Liu, C. 7681
Liu, H. 8084
Liu, J. 7914
Liu, N. 7914
Liu, X. 7815, 7860
Liu, Z. 7681
Luan, J. 7981
Luo, D.-M. 7724
Luo, Z. 8278

M
Ma, Q. 8278
Ma, S. 8176
Mahpara, S. 7643, 7838
Mai, W. 8270
Mehmood, N. 7643, 7838
Mohammadi, M. J. 8345
Mohanty, A. 8263
Muneeb, A. 7838
Muqaddas, H. 7643, 7838
Mutlu,, C. 8146

N
Nadeem, M. 7780
Nadoushan, M. A. 8135
Nayak, H. N. 8263
Nikolic, V. 7925
Ning, X. 8199
Nonic, M. 7925
Noorka, I. R. 7643, 7838

O
Ozcelik, R. 8286
Ozgonen-Ozkaya, H. 7695
Ozgoren, Y. O. 7900
Ozyurt, C. E. 8109

P
Peng, M. 7860
Peng, W. 8246
Pengpeng, G. 8078
Pesic, V. 8184
Phanpadith, P. 7667
Pilipovic, D. T. 8184
Prica, M. 8184

Q
Qi, L. 7769, 8125
Qian, Z. 8176
Qiao, S. 7815
Qin, M. 8226

R
Rapajic, S. 8184
Ren, D. 8176
Ruan, R. 7769

S
Sadeghi, S. 8345
Sahu, C. 8263
Sahu, S. K. 8263
Sanin, S. L. 8093
Sankur, F. 8316
Sarikamis, G. 8233
Shad, H. A. 7643, 7838
Shang, J. 8226
Sher, M. 7838
Shi, B. 8154
Shi, K. 7681
Shi, S. 8176
Sicard, P. 8345
Sirin, U. 7710
Stankovic, D. 7925
Sume, V. 7674
Sun, L. 7681
Sun, Y. 7967

T
Taemthong, W. 7951
Tafteh, A. 7885
Taiwo, A. M. 8345
Tang, L. 7967
Tao, Y. 8176
Tarakci-Eren, E. 8304
Tarroum, M. 7780
Tomin, M. B. 8184
Tunca, E. 8047
Turhan, S. 8160
Turhan, Y. 8023
Turkmen, H. 7957
Tzoraki, O. 7849

U
Ucak, A. B. 8211
Ullah, M. F. 7643
Ustunturk-Onan, M. 7651

V
Valdivieso, A. L. 8062
Vilotic, D. 7925
Vural, H. 8160

W

Wahsha, M. 7806
Wajid, K. 7643
Wan, D. 8270
Wang, G. 8069
Wang, H. 7801, 8062
Wang, J. 7681
Wang, J. 8226
Wang, L. 7681
Wang, P. 8131
Wang, Y. 7756
Wang, Z. 8255
Wei, X. 7734, 7914
Weijun, N. 8125
Wieczorek, K. 7658
Wu, D. 8199
Wu, L. 7815, 7860
Wyszkowska, J. 7658

X

Xia, Z. 8069
Xiaomei, S. 8125
Xie, K. 8119
Xiong, X. 8030
Xu, L.-Z. 7906

Y

Yang, D.-N. 7724
Yang, W. 8255
Yao, Z. 8084
Yavuz, M. 8233
Yesil, P. 7703
Yifan, K. 8078
Yildirim, V. 7931
Yildiz, M. 8239
Yildiz, O. 8008
Yilmaz, K. T. 7941
Yilmaz, S. 7789
Yin, H.-Q. 7724
Yu, D. 7667
Yu, P. 8154
Yu, Z. 7667
Yuan, A.-Y. 8100
Yuan, X. K. 7687
Yue, J. 8199

Z

Zeybek, A. 8337
Zeybek, Z. 7651
Zhang, A. 7801
Zhang, B. 8199
Zhang, H.-X. 8131
Zhang, J. 8154
Zhang, L. 7906, 7801
Zhang, Q. 8166
Zhang, S. 7667
Zhang, Y. 8255
Zhang, Z. 8030
Zhang, Z. M. 7687
Zhao, C. 7769
Zhao, H. 7687
Zhao, W. 8166
Zhao, Y. 7687, 8119
Zhongping, Z. 8078
Zhou, J. 8270
Zhou, X. 8226
Zhou, Z. 8062, 8176
Zhu, C.-Q. 8100
Zhu, H. 8062
Zhu, J. 8062, 8119
Zou, J. N. 7906

SUBJECT INDEX

A

Acanthamoeba 7651
accumulation characteristics 8246
Acid Red B 7756
Acid-freezing rain 7967
Acinetobacter baumannii 8316
Activated sludge 8270
Adsorption 7634
Adsorption/Belebungsverfahren 7769
aesthetic of landscape 7703
age 7925
Agent 8030
Agricultural Land 8263
agricultural landscape 7941
air pollution 7681, 8135
Al^{3+} 8270
antibacterial activity 7832
anti-biofilm activities 7957
antibiotic resistance 8316
Antioxidant 7893
antioxidant activities 7957
Antioxidant enzyme 8255
Aqaba 7806
aquatic ecosystem 7825
Araneae 8041
arsenic 7634
Asartepe Dam Lake 8321
astaxanthin 7974
Astragalus 7626
Atmospheric dust 7914

B

Bacillus cereus 8119
Bacteria 7849
Bald cypress 7925
Barley 8337
bedding steep rock slope 8166
bending failure 8166
beta type 7900
Bioassay 8298
Bioavailability 7914
Biochar 8328
Biochar-morel agent 7667
Biodegradation 8119
biomass model 8286
biomass recovery 8286
biopolymer 7626
biotechnical control 8146
Biothic indices 7931
Blattodea 8041
Blumeria graminis f. sp. hordei 8337
border strip irrigation 7885
Box-Behnken (BB) method 8226
brassica 8233
Brutia pine 8041
bulblet formation 7710
β-glucosidase 7658

C

calcium hydroxide 7801
CAPE 7893
Carbon dioxide 7951
Carbon Sequestration 8263
Catalase (CAT) 7780
Catalyst 7724, 8184
cauliflower 8233
Cellulase 7992
Cement plant 8345
Chang 6 member 8176
Chelonia mydas 8109
chickpea 8328
Chitosan 7750
Chlorella vulgaris 7974
chlorophylls 7974
Circulating fluidized bed boiler (CFBB) 7906
Classroom 7951
Coal mines 8100
Coal mining area 7914
Coastal protection 7674
Co-cultivation 8239
Co-digestion 7769
Collembola 8041
colonial M. Aeruginosa 7801
compressive property 7967
Concentrations 7806
concrete 7967
consumer trends 8160
consumption 8160
Contamination 7838
Contamination assessment. 8199
copper nanoparticles 7832
cotton 7695
cyanobacteria blooms 7801

D

Deacetylation degree 7750
decolourization 8184
Degradation efficiency 7734
depth treatment 8131
Desulfurization 7724
disease intensity 7695
Distributed coupling effects 7815
domestic sewagewater 7838
dose 8062
doubly fed induction generator 8154
Droplet size 7717
Dust content in flue gas 7906

disinfection. 7651
Dispersion 8345
Dynamic model 7860

E
Eastern Black Sea 7674
ecosystem services 7941
efficiency 8100
Electrochemical oxidation 7756
Electroplating Wastewater 8069
Enthusiasm of farmers 7981
Environmental Consciousness 8093
Environmental protection 7674
Environmental Risk 8093
environmental toxicity 8023
epicotyl 7710
Epilithic algae 7931
Epinephelus marginatus 8109
Esox lucius 8321
Essential oil 8298
Extracellular polymeric 8270
Extreme Learning Machine 7906

F
Farming loads 7849
Fatty acid 8211
Fe-based ionic liquids 7724
fertile islands 7687
filter feeder 7825
first thinning 8286
Fishes 7806
flax 8239
flocculant 8062
Flocculation 8270
Food safety 7981
Forensic sciences 8207
Forest 8263
Forest fires 8041
Fragmentation 7941
free- living amoeba 7651
Frequency of use 7789
Fuel wood 8286

G
Garden 8263
Gaussian plume model 8345
Generalized Depth–Duration–Frequency (DDF) relationships 7874
Generalized Extreme Value (GEV) 7874
ghost fishing 8109
glucosinolates 8233
Glutathione S-transferase 8023
Gossypol 7695
Graphene-TiO_2 hydrogels 7734
green method 7832
Green peach aphid 8298
Groundwater contaminant remediation 8278
Growth 7667
growth rings 7925

H
heads 8233
Health risk assessment 7914, 8246
health risk index 7643
Heavy Metal 8069, 8321
heavy metals 7643, 7658, 7806, 7838, 7914, 8047, 8199, 8246
hedge network 7941
heterogeneous Fenton process 8184
Hexahydroimidazo [1,5-a] pyridinium bromides 7957
horizontal and vertical distances 7687
Hospital 8207
Huaibei coalfield 8246
Hydrolysis 8069
hypocotyl 7710

I
illite 7801
Image J 7717
Image processing 7717
imidazolinium salts 7957
incubation 8328
Indoor air quality 7951
infestation rate 8146
inhibition 8023
Interaction energy. 8270
intergranular suction 7967
iron oxide coating 7634
Iron tailing 8062
Irrigation 8211
Iskenderun Bay 8109
ITS (Internal Transcribed Spacer) 8221

J
Jiyuan Area 8176

K
Kinematic hardening plastic constitutive model 8078
Kitchen Waste 7769

L

Lake Salda 8047
Land Use 8263
Land use change 7860
land use selection 7760
Landsat TM images 8135
landscape metrics 7941
landscape metrics 8135
Landslide 8001
Lanzhou 7681
latewood proportion 7925
Lead 7740
Lemon oil 8298
Levels 7806
licensed surveying engineering office 8008
life cycle 8146
Lipid peroxidation 7893
Loess Plateau 7815
long-range correlation 7681
Lost net 8109
low temperature difference 7900
Low temperature stress 8255
low-cost adsorbent 7634

M

macro-element 8328
Malathion 7893
Marmara Region 8160
MATLAB 7981
MBR 8069
mechanics model test 8166
Medical waste 8084
Mediterranean corn borer (Sesamia nonagrioides Lefebvre) 8211
Mediterranean ecosystems 8041
metalloid 8047
Methane Yield 7769
micro-element 8328
Microscopic Pore Structure 8176
Microstructure 8255
Model 7951
model predictive control 8154
Modern Life. 8093
MODFLOW MT3DMS 8278
Modified dynamic model 7815
Moveable Fluid Saturation 8176
Multiple Antibiotic Resistance (MAR) 8316
multi-scale 7681
mussel excretion 7825
mussel tank 7825
Mytilus galloprovinciallis 7825

N

NaClO 7651
Nickel 7740
Niksar 7703
Nitrobenzene 8278
NO_x 8345
NOx emissions 7906
nutrient dynamic 7825
Nutrients 7849

O

Ocimum basilicum leaf extract. 7832
OLS correlation 7981
Ordu 8221
Organic 8160
Oxidant 7893

P

Parapenaeus longirostris 7750
Pasture 8263
pathogenic microorganisms 7957
Perceptual difference 8304
Permeability 8176
Permeable reactive barrier 8278
pesticides 8023
petrochemical oily wastewater 8131
Phytohormones 7667
Pinus brutia 8286
Poisoning 8207
Pollution 7931, 8047
Pore Throat Radius 8176
Posidonia shale 8125
power laws 7681
power system 8154
Preconcentration 7740
Probability Weighted Moments (PWM) 7874
proline 7780
protein 7974
Proximity 7789

R

Railway embankment design 7626
rainfall threshold 8001
Reactive Blue 4 8184
Red Sea 7806
regeneration 7900
regenerative displacer 7900
resilience modulus 7626
resistance 7658, 8337
reuse 8131
Reverse logistics 8084
RFID 8084
Rhodococcus ruber. 7740

S

Safety management 8084
Salt stress 7667, 7780
sand shock 8078
Satisfaction 7789
SCREEN3 8345
Seasonal appearance 8304
Seasonal Variation 8321
Sediment 7674
sediment assessment methods 8047
sediment concentration 8062
Sediment yield 7860
seed germination 7710
seismic effect 8166
Self-organizing network 8030
Semantic differential 8304
Separation 7740
sepiolite 7634
Sesbania sesban (L.) Merril 7780
settle velocity 8062
settlement 7760
shoot regeneration 8239
small diameter trees 8286
SOC 8263
Social Risk 8093
soil 7643,
Soil and water 7815
Soil microbial activity 7992
soil nutrient 7687
soil-plant system 8246
sprouts 8233
SRFR model 7885
Steel ball 8078
stem height 7925
Stirling engine 7900
Stream 7931
Streams 7849
Street dust 8199
strength parameters 7626
Stress distribution 8125
Sub-catchment 7860
superoxide dismutase (SOD) 7780
surveying activities 8008
Surveying private sector 8008
Swimming pool 7651
SWOT Analysis 8008

T

Taxon 8304
technological breakthrough 8100
the aeroengine blader damage 8078
T-head groin 7674
Tinca tinca 8321
Tissue culture 7710
TOC removal 7756
Tolerance 8211
Tomato leaf miner 8146
Torreya fargesii Franch. 8226
Total aerobic bacteria and fungi counts 7992
Total flavonoids 8226
Trabzon 8001
Trabzon-Turkey 8304
transient stability 8154
Triclopyr 8119
Turkey 7703, 8160
Tuta absoluta 8146

U

Urban park 7142
urea 7539

V

Ultrasonic heating circumfluence method 7724
Ultrasound 8226
unconfined compression test 7626
unicellular M. aeruginosa 7801
Urban expansion 8135
Urban green space 7789
Urtica dioica 8221
Urtica kioviensis 8221
UV−vis absorption spectra 7734
Ventilation 7951
Verticillium dahliae Kleb. 7695
viewshed 7760
Virulence gene 8337
visibility 7760
visual perception 7703
Visual preference 8304
Visual quality 7703
visual quality assessment 7703
Vitex negundo 7687
Volumetric Productivity 7769

W

wastewater irrigation 7643
wastewater treatment 7756
water bodies 7760
Water Purification 7849
Water quality 7931
Water use productivity 7885
Water-sediment-adsorbed NPS 7815
Water-sensitive card 7717
well wall stability 8125
Well-being 7789
wheat 8239
wheat (Millat-2011) 7838
wind power generation 8154
Winter wheat 7667
Wisdom agriculture 8030
working face 8100

wavelength 7974

X
Xylanase Nerium oleander L 7992

Y
Yanhe River watershed 7860 Young loquat fruit 8255

Z
Zero-valent iron 8278 Zigbee 8030

FEB – GUIDE FOR AUTHORS

General

FEB accepts original papers, review articles, short communications, research abstracts from the entire sphere of environmental-chemistry,-biology,-microbiology,- technology, -biotechnology and-management, furthermore, about residue analysis/ and ecotoxicology of contaminants.

Acceptance or no acceptance of a contribution will be decided, as in the case of other scientific journals, by a board of reviewers. Papers are processed with the understanding that they have not been published before (except in form of an abstract or as a part of a published lecture, review or thesis);that they are not under consideration for publication elsewhere; that their publication has been approved by all co-authors, if any, as well as-tacitly or explicitly- by the responsible authorities at the institute where the work has been carried out and that, if accepted, it will not be published elsewhere in the same form, in either the same or another language, without the consent of the copyright holders.

Language

Papers must be written in English. Spelling may either follow American (Webster) or British (Oxford) usage but must be consistent. Authors who are less familiar with the English language should seek assistance from proficient colleagues in order to produce manuscripts that are grammatically and linguistically correct.

Size of manuscript

Review articles should not exceed 30 typewritten pages. In addition up to 5 figures may be included.

Original papers must not exceed 14 typewritten pages. In addition up to 5 figures may be included.

Short-Communications should be limited to 4 typewritten pages plus not more than 1 illustration.

Short descriptions of the authors, presentation of their groups and their research activities (with photo) should together not exceed I typewritten page. Short research abstracts should report in a few brief sentences (one-fourth to one page) particularly significant findings. Short articles by relative newcomers to the chemical innovation arena highlight the key elements of their Master and PhD-works in about I page.

Book Reviews are normally written in-house, but suggestions for books to review are welcome.

Preparation of manuscript

Dear authors,

FEB is available both as printed journal and as online journal on the web. You can now e-mail your manuscripts with an attached file. Save both time and money. To avoid any problems handling your text please follow the instructions given below:

When preparing your manuscripts have the formula K/SS (Keep It Simple and Stupid) in mind. Most word processing programs such as MS-Word offer a lot of features. Some of them can do serious harm to our layout. So please do not insert hyperlinks and/or automatic cross-references, tables of contents, references, footnotes, etc.

1. Please use the standard format features of your word processor (such as standard.dot for MS Word).
2. Please do not insert automatisms or secret link-ups between your text and your figures or tables. These features will drive our graphic department sometimes mad.
3. Please only use two fonts for text or tables "Times New Roman" and for graphical presentations "Arial".
4. Stylesheets, text, tables and graphics in shade of grey
5. Turn on the automatic language detection in English (American or British)
6. Please - check your files for viruses before you send them to us!!

Manuscripts should send to:parlar@wzw.tum.de
or:parlar@prt-parlar.de

Thank you very much!

STRUCTURE OF THE MANUSCRIPT

Title page: The first page of the manuscript should contain the following items in the sequence given: A concise title of the paper (no abbreviations). The names of all authors with at least one first name spelled out for every author. The names of Universities with Faculty, City and Country of all authors.

Abstracts: The second page of the manuscript should start with an abstract that summarizes briefly the contents of the paper (except short communications). Its length should not exceed 150-200 words. The abstract should be as informative as possible. An extended repetition of the paper's title is not considered to be an abstract.

Keywords: Below the Summary up to 6 key words have to be provided which will assist indexers in cross-indexing your article.

Introduction: This should define the problem and, if possible, the frame of existing knowledge. Please ensure that people not working in that particular field will be able to understand the intention. The word length of the introduction should be 150 to 300 words.

Materials and methods:
Please be as precise as possible to enable other scientists to repeat the work.

Results: Only material pertinent to the subject must be included. Data must not be repeated in figures and tables.

Acknowledgements: Acknowledgements of financial support, advice or other kind of assistance should be given at the end of the text under the heading "Acknowledgements". The names of funding organisations should be written in full.

References: Responsibility for the accuracy of references rests with the authors. References are to be limited in number to those absolutely necessary. References should appear in numerical order in brackets and in order of their citation in the text. They should be grouped at the end of the paper in numerical order of appearance. Abbreviated titles of periodicals are to be used according to Chemical or Biological Abstracts, but names of lesser known journals should be typed in full. References should be styled and punctuated according to the following examples:

ORIGINALPAPERS:
l. Author, N.N. and Author, N.N. (Year) Full title of the article. Journal and Volume, first and last page.
BOOK OR PROCEEDING:
2. Author, N.N. and Author, N.N. (Year) Title of the contribution. In: Title of the book or proceeding. Volume (Edition of klitor-s, ed-s) Publisher, City, first and last page

DOCTORAL THESIS:
3. Author, N.N. (Year) Title of the thesis, University and Faculty, City

UNPUBLISHED WORK:
Papers that are unpublished but have been submitted to a journal may be cited with the journal's name followed by "in press". However, this practice is acceptable only if the author has at least received galley proofs of his paper. In all other cases reference must be made to “unpublished work" or "personal communication".

Discussion and Conclusion: This part should interpret the results in reference to the problem outlined in the introduction and of related observations by the author/s or others. Implications for further studies or application may be discussed. A conclusion should be added if results and discussion are combined.

Corresponding author: The name of the corresponding author with complete postal address

Precondition for publishing:
A minimum number of 25 reprints must be ordered and prepaid.
1 - 4 pp.: 200,- EURO + postage/handling
5 - 8 pp.: 250,- EURO + postage/ handling
More than 8pp: 1.50 EURO/page x number of reprints +postage/ handling.
The prices are based upon the number of pages in our journal layout (not on the page numbers of the submitted manuscript).
Postage/ Handling: The current freight rate is Germany 10 €, Europe 18,00 €, International 30 €.
VAT: In certain circumstances (if no VAT registration number exists) we may be obliged to charge 7% VAT on sales to other EU member countries.MESAEP and SECOTOX members get a further discountof 20% (postage/ handling full).